

Prestressed Concrete Structures

@Seismicisolation

Prestressed Concrete Structures

Michael P. Collins

*Department of Civil Engineering
University of Toronto*

Denis Mitchell

*Department of Civil Engineering
and Applied Mechanics
McGill University*

Response Publications, Canada

@Seismicisolation

To
Judy and Barbara

The authors and publisher of this book have used their best efforts in preparing this book. These efforts include the development, research, and testing of the theories and programs to determine their effectiveness. The authors and publisher make no warranty of any kind, expressed or implied, with regard to these programs or the documentation contained in this book. The authors and publisher shall not be liable in any event for incidental or consequential damages in connection with, or arising out of, the furnishing, performance, or use of these programs.

© 1997 by Response Publications, Canada

All rights reserved. No part of this book may be reproduced, in any form or by any means, without permission in writing from the publisher.

Printed in Canada by Copywell, Ontario

10 9 8 7 6 5 4 3 2 1

ISBN 0-9681958-0-6

Response Publications, Toronto and Montreal

@Seismicisolation

Contents

Preface	xvii	
Chapter 1	Introduction	
1.1	Prestressed Concrete	1
1.2	Basic Concepts of Prestressing	5
1.3	Typical Prestressed Concrete Structures	7
1.4	Design of Prestressed Concrete Structures	15
1.5	Additional Introductory Reading	18
	References	23
Chapter 2	Pretensioning and Post-Tensioning Technology	
2.1	Introduction	25
2.2	Prestressing Tendons	25
2.3	Pretensioning Operations	27
2.4	Standard Precast Pretensioned Members	30
2.5	Post-Tensioning Operations	31
2.6	Post-Tensioning Systems	33
2.7	Grouting of Ducts	38
2.8	Profiles of Post-Tensioned Tendons	42
2.9	Losses during Post-Tensioning	46
2.10	Example of Friction Loss Calculations	51
	References	54
	Demonstration Problems	55
Chapter 3	Material Properties	
3.1	Introduction	57
3.2	Concrete Material Technology	57
3.3	Concrete in Uniaxial Compression	61

3.4	Cyclic Loading of Concrete	65	Chapter 5	Response of Members Subjected to Flexure	
3.5	Influence of Rate of Loading and Concrete Strength	66	5.1	Introduction	168
3.6	Creep of Concrete	67	5.2	Compatibility Conditions	170
3.7	Example Calculation of Creep Strain	71	5.3	Equilibrium Conditions	171
3.8	Concrete in Uniaxial Tension	72	5.4	Predicting Response of Flexural Members	171
3.9	Shrinkage of Concrete	74	5.5	Tensile Stresses in the Concrete	172
3.10	Thermal Properties of Concrete	76	5.6	Layer-by-Layer Evaluation of the Section Forces	173
3.11	Weight of Concrete	79	5.7	Evaluation of Section Forces Using Stress-Block Factors	175
3.12	Stress-Strain Response of Confined Concrete	79	5.8	Calculation of Moment-Curvature Using Stress-Block Factors	177
3.13	Types of Reinforcement	80	5.9	Calculation of Moment-Curvature Using Layer-by-Layer Approach	182
3.14	Stress-Strain Response of Reinforcement	87	5.10	Determination of Long-Term Moment-Curvature Response	187
3.15	Relaxation of Prestressing Steel	90	5.11	Elastic Uncracked Response	190
3.16	Fatigue Characteristics of Reinforcement	92	5.12	Example Calculations Assuming Uncracked Response	195
3.17	Thermal Properties of Reinforcement	93	5.13	Estimation of Camber and Deflections	201
3.18	Bond Characteristics of Reinforcement	96	5.14	Examples of Calculating Camber and Deflection	204
3.19	Durability Considerations	105	5.15	Crack Widths and Crack Spacing	208
	References	116	5.16	Example Calculations of Crack Widths	210
	Demonstration Problems	120	5.17	Accounting for Construction Stages – Composite Construction	213
Chapter 4	Response of Members Subjected to Axial Load		5.18	Accounting for Nonuniform Thermal and Shrinkage Strains	221
4.1	Introduction	124	5.19	Evaluation of Fatigue Resistance	227
4.2	Compatibility Conditions	124	5.20	Members with Unbonded Tendons	229
4.3	Equilibrium Conditions	126	5.21	Example of a Beam with Unbonded Tendons	229
4.4	Predicting Response of Axially Loaded Members	127	5.22	Members Subjected to Combined Axial Load and Flexure	235
4.5	Accounting for Relaxation, Creep, Shrinkage, and Thermal Effects	131	5.23	Examples of Calculating $M-N$ Interaction Diagrams	237
4.6	Predicting Long-Term Response of Member C	133	5.24	Examples of Calculating $M-\phi-N$ Relationships	241
4.7	Comparison of Short-Term and Long-Term Responses	135	5.25	Slender Columns – The $P\Delta$ Effect	242
4.8	Linear Elastic Uncracked Response	137	5.26	Example of a Slender Column	245
4.9	Example Calculations Assuming Elastic Uncracked Response	139	References	249	
4.10	Tensile Stresses in the Concrete after Cracking	142	Demonstration Problems	250	
4.11	Example Using Average Tensile Stresses in the Concrete	147	Chapter 6	Design for Flexure	
4.12	Tension Stiffening in Prestressed Concrete Members	150	6.1	Introduction	256
4.13	Crack Widths and Crack Spacings	152	6.2	General Design Considerations	256
4.14	CEB-FIP Code Expressions for Crack Spacing and Crack Widths	152	6.3	Permissible Stresses in Tendons	258
4.15	Gergely-Lutz Expression for Crack Widths	154	6.4	Permissible Stresses in Concrete	258
4.16	Example of Crack Width Calculations	157	6.5	Calculation of Stresses in the Concrete	259
4.17	Minimum Reinforcement for Crack Control	159	6.6	Example of Calculating Stresses in the Concrete	266
	References	163	6.7	Control of Crack Widths	270
	Demonstration Problems	164			

6.8	Camber and Deflections	270	Chapter 9	Design of Disturbed Regions	
6.9	Design for Flexural Strength and Ductility	273	9.1	Introduction	412
6.10	The Design Process	278	9.2	Behavior Prior to Cracking – Elastic Analysis	413
6.11	Additional Considerations for Composite Construction	286	9.3	Example Design of Anchorage Zone Reinforcement Using Elastic Analysis	418
6.12	Example Design of Double-Tee Floor Member	289	9.4	Deep Beam Analogy for Design of End Zones	422
6.13	Example Design of Post-Tensioned, One-Way Floor Slab	296	9.5	Behavior after Cracking	424
	References	305	9.6	Strut and Tie Models	426
	Demonstration Problems	305	9.7	Example Design of Anchorage Zone Using Strut and Tie Model	444
Chapter 7	Members Subjected to Shear		9.8	Example Design of Corbel Using Strut and Tie Model	449
7.1	Introduction	309	9.9	Example Design of Deep Beam Using Strut and Tie Model	453
7.2	Diagonal Cracking	309	9.10	Example Design of Post-Tensioned Deep Beam	459
7.3	Example of Estimating Diagonal Cracking Shears	317	9.11	Special Considerations for Bearing Areas	462
7.4	Behavior after Diagonal Cracking	320	9.12	Special Considerations Where Tendons Change Direction	463
7.5	The 45° Truss Model	323	9.13	Shear Transfer across Planes of Weakness – The Shear Friction Concept	466
7.6	Traditional ACI Approach	325	9.14	Design of Shear Interface of Composite Beams	468
7.7	Design Example Using ACI Shear Provisions	330		References	471
7.8	Variable-Angle Truss Models	334		Demonstration Problems	473
7.9	Compression Field Theory	338	Chapter 10	Statically Indeterminate Structures	
7.10	The Modified Compression Field Theory	343	10.1	Introduction	476
7.11	Example of Predicting Response in Shear	353	10.2	Restraint Actions in Prestressed Concrete Structures	478
7.12	Design Using Modified Compression Field Theory	359	10.3	Calculation of Deformations	479
7.13	Design Example Using Modified Compression Field Theory	368	10.4	Use of Virtual Work to Calculate Deflection	481
	References	375	10.5	Calculation of Restraint Actions – Flexibility Approach	484
	Demonstration Problems	377	10.6	Finding Restraint Actions by Moment Distribution	488
Chapter 8	Design for Torsion		10.7	Calculation of Fixed-End Moments Due to Prestress	489
8.1	Introduction	380	10.8	Example of Finding Restraint Moments	491
8.2	Thin-Walled Tubes in Torsion	380	10.9	Restraint of Axial Deformations	495
8.3	Torsional Response Prior to Cracking	383	10.10	Example Involving Restraint of Axial Deformation	495
8.4	Example of Calculating Pre-Cracking Response	385	10.11	Finding Restraint Actions Using Standard Computer Programs	502
8.5	Torsional Response after Cracking	386	10.12	Calculating Restraint Actions Using Elastic Plane-Frame Program	503
8.6	Example of Calculating Torsional Strength	391	10.13	Influence of Creep on Restraint Actions	506
8.7	Combined Torsion and Flexure	394	10.14	Example Design of a Statically Indeterminate Structure	509
8.8	Variable-Angle Truss Model for Combined Torsion, Shear, and Flexure	396	10.15	Influence of Restraint Moments on Load Distribution at Ultimate	517
8.9	Design Approach for Combined Torsion, Shear, and Flexure	398		References	519
8.10	Detailing Considerations	400		Demonstration Problems	519
8.11	Redistribution of Torsion in Statically Indeterminate Structures	401			
8.12	Design of Guideway Girder for Torsion, Shear, and Moment	405			
	References	410			
	Demonstration Problems	411			

Chapter	11	Post-Tensioned Slabs		14.7	Tests of Complex Structures		
	11.1	Introduction	523		References	660	
	11.2	Factors Influencing Choice of Slab Thickness	525			667	
	11.3	Corrosion Protection of Unbonded Tendons	527				
	11.4	Load Balancing	528	Chapter	15	Evaluation and Rehabilitation	
	11.5	Distribution of Tendons in Two-Way Slabs	533		15.1	Introduction	668
	11.6	Analysis Using the Equivalent Frame Method	535		15.2	Symptoms of Distress	669
	11.7	Stress Checks and Control of Cracking	539		15.3	Testing Techniques	672
	11.8	Special Considerations for Edge and Corner Panels	542		15.4	Analytical Assessment	684
	11.9	Investigation of the Flexural Capacity of Slabs	542		15.5	Rehabilitation and Upgrading Measures	686
	11.10	Shear Design of Slabs	545			References	705
	11.11	Estimation of Deflections of Slabs	552	Appendix A		Computer Program RESPONSE	
	11.12	Example Design of Post-Tensioned Flat Plate	554				707
		References	579	Appendix B		Computer Program SHEAR	745
		Demonstration Problems	580			Computer Program MEMBRANE	747
Chapter	12	Buildings		Index			
	12.1	Introduction	581				753
	12.2	Typical Framing of Precast Concrete Buildings	581				
	12.3	Structural Integrity of Precast Concrete Buildings	582				
	12.4	Parking Structures	590				
	12.5	Special Applications of Post-Tensioning to Building Structures	598				
	12.6	Post-Tensioned Foundations	600				
		References	607				
Chapter	13	Bridges					
	13.1	Introduction	608				
	13.2	Types of Prestressed Concrete Bridges	609				
	13.3	Economic Considerations	609				
	13.4	Special Construction Techniques	613				
	13.5	Loads	616				
	13.6	Analysis	620				
	13.7	Membrane Action in Deck Slabs	622				
	13.8	Dimensioning and Detailing	625				
	13.9	Example Design of Precast Bridge Girder	625				
		References	639				
Chapter	14	Design of Complex Structures					
	14.1	Introduction	640				
	14.2	Linear vs. Nonlinear Analysis	641				
	14.3	Types of Elements	644				
	14.4	Membrane Elements	646				
	14.5	Example of Calculating Stresses in a Membrane Element	650				
	14.6	Shell Elements	656				

Preface

The primary objective of this book is to explain the basic concepts necessary to understand and predict the response of prestressed concrete members and to design prestressed concrete structures. The approach taken reflects the authors' strong belief that the engineer needs to develop a solid understanding of fundamental principles rather than relying upon a large collection of restricted, empirical equations for design.

Chapters 1 and 2 introduce the basic concepts of prestressing, give a brief history of its development, and explain the technology involved in pretensioning and post-tensioning. A comprehensive summary of the material properties of concrete, prestressing steel, and reinforcing bars, which are of particular significance in the design of prestressed concrete structures, is given in Chapter 3.

Chapter 4 provides a basic understanding of prestressed concrete behavior, upon which all other chapters build. In a major departure from the traditional approach, the basic principles of prestressed concrete behavior are presented first for the simplest case of members subjected to pure axial load. The principles are then extended to members subjected to flexure and axial load in Chapter 5. The basic concepts involved in designing prestressed concrete members for flexure are explained in Chapter 6.

Innovative rational design procedures for shear and torsion are explained in Chapters 7 and 8. Chapter 9 introduces the powerful, yet simple, strut and tie models which can be used to design deep beams, corbels, anchorage zones, and other regions characterized by a complex flow of internal stress.

While Chapters 4 through 9 are concerned with the response of prestressed concrete members, Chapter 10 begins the discussion of prestressed concrete structures. In this chapter the additional considerations involved in designing statically indeterminate prestressed concrete structures are explained. Chapters 11, 12, and 13 highlight the important aspects of the design of prestressed concrete two-way slabs, buildings, and bridges.

Chapter 14 demonstrates how the basic principles can be applied in the design of complex prestressed concrete structures such as offshore platforms and nuclear containment structures. Chapter 15 illustrates how the behavioral tools developed in the text can be applied in the evaluation and rehabilitation of existing prestressed concrete structures.

Most of the chapters contain detailed design examples and conclude with a set of "demonstration problems" chosen to illustrate that the concepts can be applied to a wide range of practical problems.

Included with the text is a diskette containing three computer programs, RESPONSE, SHEAR and MEMBRANE. Program RESPONSE is a menu-driven, user-friendly program capable of predicting the response of prestressed concrete sections subjected to any combination of axial load, moment and shear. SHEAR is a very short, simple program for the special case of prestressed concrete sections subjected to shear. Program MEMBRANE is used to predict the load-deformation response of prestressed concrete elements subjected to in-plane shear and normal forces.

This book is intended for advanced undergraduate students, graduate students, and practicing structural engineers. The text contains sufficient material for a sequence of two one-semester courses, the first dealing primarily with member behavior and the second emphasizing the design of prestressed concrete structures. Alternatively, a judicious selection of material would enable a one-semester course to introduce the basic concepts and give examples of applications.

The "back-to-basics" approach, the realistic detailed worked examples, and the emphasis on behavioral predictions employing "simple-to-use" computer programs should all appeal to the practicing engineer. In addition, the coverage of recent advances in shear, torsion, and detailing as well as the comprehensive treatment of other topics, including high-strength concrete and rehabilitation of existing structures, makes this text an up-to-date guide for the design of prestressed concrete structures.

While much of the text is independent of specific code provisions, the essential features of the American Concrete Institute's "Building Code Requirements for Reinforced Concrete" are described and, where appropriate, used in detailed design examples.

The authors would like to thank Professor Peter Gergely of Cornell University, Professor Kurt Gerstle of the University of Colorado, and Professor Richard Spencer of the University of British Columbia for their helpful review comments, which strengthened the value of the text.

This text is the result of 20 years of collaborative research by the authors. The authors wish to gratefully acknowledge the financial support of the Natural Sciences and Engineering Research Council of Canada for this research.

We would like to thank a number of people who helped in the preparation of this book. In particular, we would like to acknowledge the significant contributions of the late Agnes Kaneko, who in her elegant style typed numerous earlier drafts of this text. Lucile Lo expertly prepared the final manuscript. Alain Dandurand displayed his artistic flair in a number of the figures. Andreas Felber and Daniel Kuchma contributed their computer expertise in preparing programs RESPONSE and MEMBRANE. The authors are particularly indebted to Angela Cellini, who carefully prepared the numerous figures and led the drafting team, and to Peter Leesti, who capably managed the intricate task of preparing the camera-ready copy.

Michael P. Collins
Denis Mitchell

Introduction

The author ... has succeeded in creating ... an entire new material.

Eugene Freyssinet, 1936

1.1 PRESTRESSED CONCRETE

Prestressed concrete is a type of reinforced concrete in which the steel reinforcement has been tensioned against the concrete. This tensioning operation results in a self-equilibrating system of internal stresses (tensile stresses in the steel and compressive stresses in the concrete) which improves the response of the concrete to external loads. While concrete is strong and ductile in compression it is weak and brittle in tension, and hence its response to external loads is improved by applying a precompression.

If a plain concrete member made from concrete with a compressive strength of 5000 psi (35 MPa) were subjected to axial tension, the concrete would crack when the average applied stress (axial tension divided by cross-sectional area) reaches about 300 psi (2 MPa) (see Fig. 1-1a). As well as being low, the concrete tensile strength is rather unpredictable and is associated with very small deformations prior to failure.

If longitudinal reinforcing bars were cast into the concrete member, its tensile performance would be much improved. For example, if 1.5% of 60 ksi (400 MPa) reinforcement were used (i.e., about 200 lb of reinforcing bars per cubic yard of concrete, or about 120 kg/m³), the response shown in Fig. 1-1b could be achieved. Instead of failing when the first crack forms, the member can now continue to resist loads until the reinforcement crossing the cracks yields. Because it now requires a substantial energy input (the work

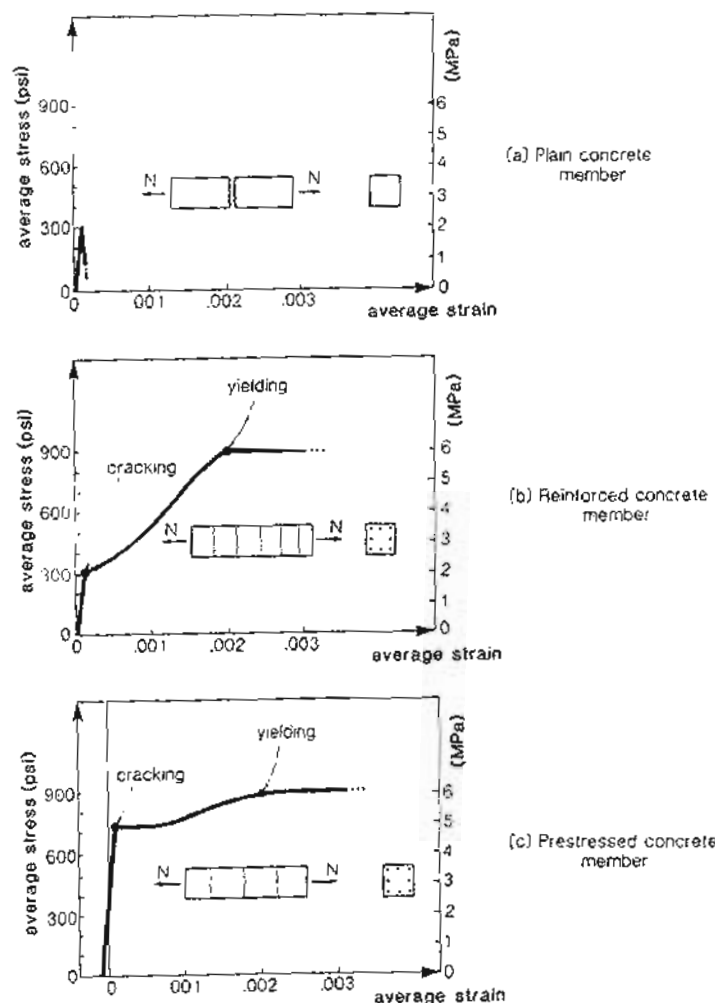


Figure 1-1 Response of plain concrete, reinforced concrete, and prestressed concrete.

done is the area under the curve) to fail the member, we can classify it as a tough, ductile member. There is, however, a substantial loss in stiffness after cracking.

If the member contained about 70 lb/yd^3 (about 40 kg/m^3) of reinforcing bars and

35 lb/yd^3 (about 20 kg/m^3) of high-strength prestressed steel, the response shown in Fig. 1-1c could be achieved. The 0.25% of longitudinal prestressing tendons will pre-compress the concrete prior to the application of the external load. This precompression substantially increases the external load required to crack the concrete, resulting in a member that is strong, tough, and stiff.

The originator of practical prestressed concrete was Eugene Freyssinet of France (see Fig. 1-2), who in 1928 began to use high-strength steel wire for prestressing concrete. Earlier attempts at producing prestressed concrete using normal-strength reinforcement had been unsuccessful.



Figure 1-2 Eugène Freyssinet, the father of prestressing. Photograph courtesy of Freyssinet International. "More than any other person it was the relentless pioneering efforts of this courageous French engineer-builder who converted the concept of prestressing into a practical reality" (Ref. 1-1).

After being precompressed, concrete continues to shorten with time in a process called creep. Loss of moisture with time also causes shortening of the concrete by shrinkage. Creep and shrinkage together may cause a total shortening of the concrete of nearly 1 part per thousand. With normal-strength reinforcement it was not possible to elongate the steel in the prestressing operation by more than about 1.5 parts per thousand. Thus in the early attempts to prestress concrete about two-thirds of the prestressing in the reinforcement was lost due to creep and shrinkage. High-strength steel wire, on the other hand, can be elongated about 7 parts per thousand in the prestressing operation. Even with a loss of 1 part per thousand, six-sevenths of the prestressing would remain.

To reduce losses due to creep and shrinkage and to make possible much higher levels of precompression, Freyssinet recommended the use not only of higher-strength steel but

also of higher-strength concrete. In a dramatic demonstration of the potential of prestressed concrete, Freyssinet commenced his 1936 lecture in London (Ref. 1-2) by applying an internal pressure of 2000 psi (14 MPa), equivalent to a head of water of 4600 ft (1400 m), to a water-filled prestressed concrete pipe. The pipe had been prestressed "to induce in the reinforcement a permanent tension of about 170,000 to 185,000 psi, counteracted by a permanent compression of the concrete amounting to something like 7000 psi." The pipe could withstand "before leaking, internal pressure ten times greater than that which caused the above-mentioned pipe of ordinary reinforced concrete of highest quality and of same dimensions to give way." Freyssinet was justified in titling his lecture "A Revolution in the Technique of the Utilisation of Concrete."

After Freyssinet's original work, prestressed concrete was increasingly utilized in both Europe and North America. By the time of the First United States Conference on Prestressed Concrete in 1951, it was reported that about 175 prestressed concrete bridges and 50 prestressed concrete building frames had been constructed in Europe and about 700 prestressed concrete water tanks had been built in North America (Ref. 1-3).

Two different procedures for prestressing concrete were developed: post-tensioning and pretensioning. Figure 1-3 illustrates the post-tensioning procedure in which the steel is tensioned after the concrete has been cast. This was the procedure used by Freyssinet. Figure 1-4 illustrates the pretensioning procedure in which the steel is tensioned prior to casting of the concrete. The German engineer, E. Hoyer, developed pretensioning as a practical technique in 1938 (Ref. 1-4).

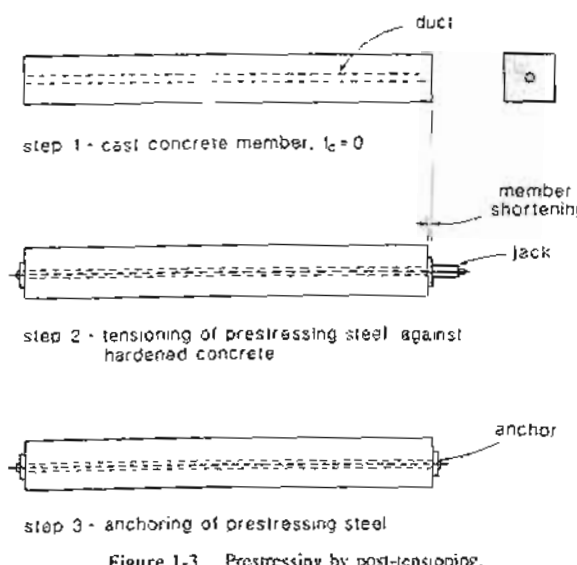
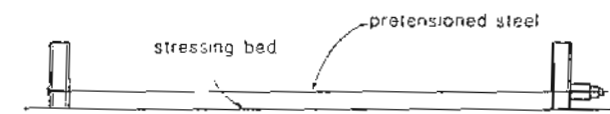


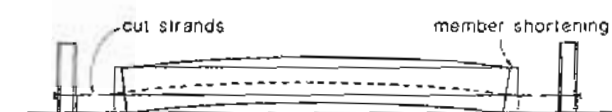
Figure 1-3 Prestressing by post-tensioning.



step 1 - tensioning of prestressing steel in stressing bed before casting concrete



step 2 - casting of concrete around tensioned steel, $t_c = 0$



step 3 - release of strands from stressing bed causing shortening of member

Figure 1-4 Prestressing by pretensioning.

Since these early developments, prestressed concrete has grown to be a multibillion-dollar industry in North America (see Fig. 1-5). Currently, about 200,000 tons of prestressing steel is used in North America each year, which is about one-quarter of the total world consumption. In North America, about two-thirds of the prestressing steel is used to manufacture precast, pretensioned products, with the remaining one-third being used for post-tensioning. Figure 1-6 shows that about 65% of precast products are structural elements for buildings and bridges, with the rest being architectural precast elements. This figure also shows that in the United States and Canada, about 59% of post-tensioning steel is used in the construction of buildings, while about 26% is used in bridges. In the rest of the world, a somewhat different pattern exists, with about 66% of post-tensioning steel being used in bridge construction.

1.2 BASIC CONCEPTS OF PRESTRESSING

The basic concept of reinforced concrete, for both prestressed and non-prestressed construction, is that steel reinforcement is placed in those locations of a structure where tensile stresses will occur. In prestressed concrete construction, high-strength reinforcement is used, and this reinforcement is tensioned prior to the application of external loads. This

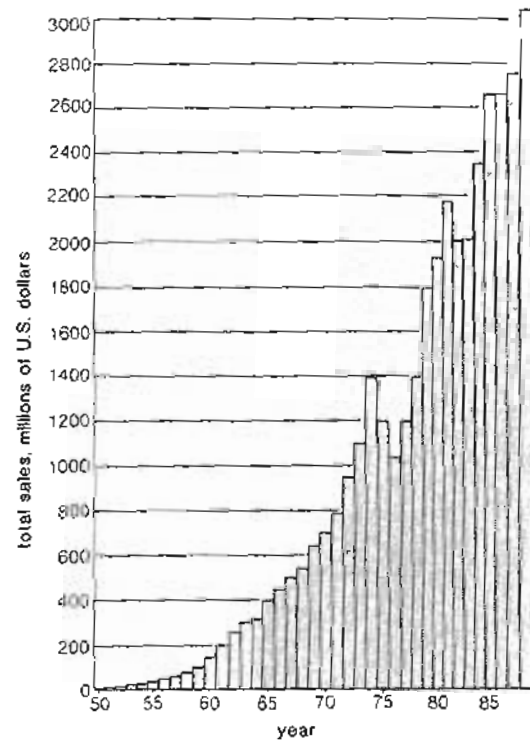


Figure 1-5 Growth of prestressed concrete industry in United States and Canada. Data from Prestressed Concrete Institute

initial tensioning of the reinforcement precompresses the surrounding concrete, giving it the ability to resist higher loads prior to cracking.

Figure 1-7 compares the behavior of two reinforced concrete beams, one of which is prestressed. For the non-prestressed beam there are no strains and no stresses in either the concrete or the reinforcement prior to the application of external loads. Only a relatively small external load can be applied to the non-prestressed beam before the concrete cracks and hence, prior to cracking, the tensile stresses developed in the reinforcement and the compressive stresses in the concrete will be very small. After cracks form, the tensile stresses in the reinforcement will substantially increase and will continue to increase as the load is increased. At failure the moment will be resisted by high tensile stresses in the reinforcement and high compressive stresses in the concrete.

As shown in Fig. 1-7, the prestressing operation results in a self-equilibrating system of stresses. These self-equilibrating stresses consist of high tensile stresses in the prestressing steel, which result in a tensile force P , and counterbalancing compressive stresses in

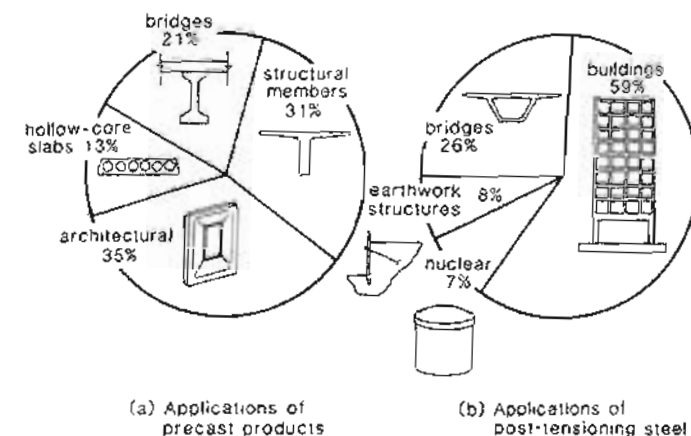


Figure 1-6 Applications of prestressed concrete in North America.

the concrete, which result in a compressive force of magnitude P . It must be recognized that as these two force resultants cancel each other out, prestressing causes neither axial load nor bending moment. Although there is no axial load or moment, the member shortens and curves due to the prestressing. Because large compressive stresses exist in the concrete prior to the application of external load, the member can resist substantial loads before the bottom fiber of concrete reaches its cracking stress. Once again at failure the moment will be resisted by high tensile stresses in the reinforcement and high compressive stresses in the concrete.

The non-prestressed reinforcement undergoes strain only when the surrounding concrete is strained. Thus it can develop high tensile strains only when the surrounding concrete is severely cracked. On the other hand, the strain in prestressed reinforcement is considerably higher than the strain in the surrounding concrete (see Fig. 1-7). Because of this, the prestressed reinforcement can have high tensile stresses even before the concrete has cracked. Non-prestressed reinforcement can be considered as passively accepting imposed strains. By prestressing the reinforcement the engineer can actively control the stress in the reinforcement and the deformations of the structure.

1.3 TYPICAL PRESTRESSED CONCRETE STRUCTURES

Since prestressing can be used to minimize or eliminate cracking at service loads and to control deflections, it results in more slender structures. Thus, a prestressed one-way floor slab can have a span-to-depth ratio of 45 to 1 which is about 60% more than the ratio

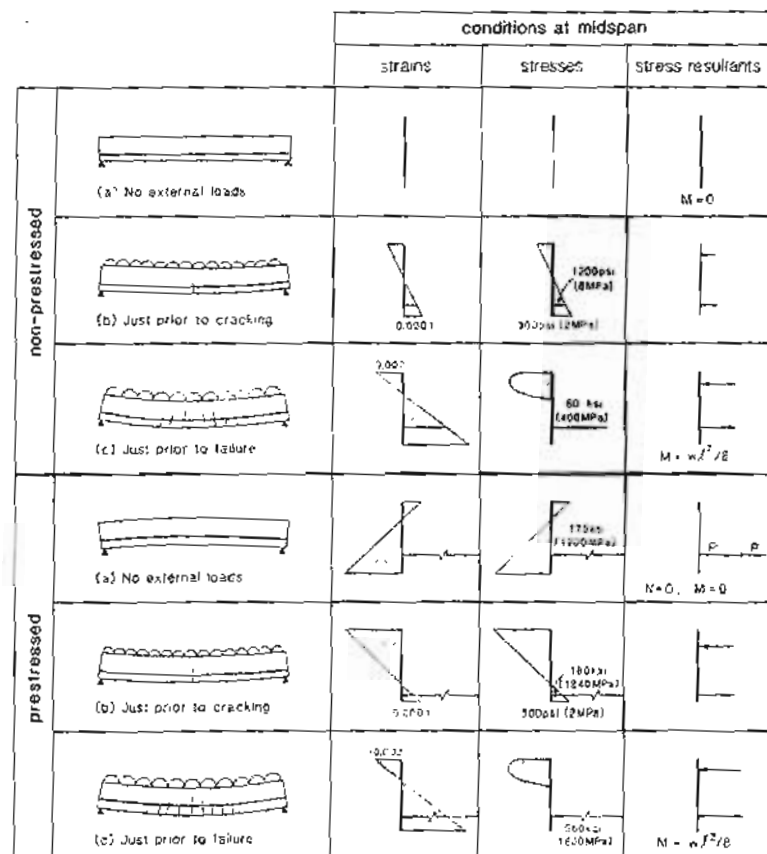


Figure 1-7 Behavior of non-prestressed and prestressed concrete beams.

possible with a non-prestressed one-way floor slab (see Fig. 1-8). For a given span, the amount of concrete in the prestressed slab will be less than two-thirds of the concrete in the non-prestressed slab. A few examples of typical prestressed concrete structures are given below.

More than 50% of bridges are now constructed of prestressed concrete. Prestressed concrete bridges range from simple highway overpasses constructed from precast, pretensioned I-girders (see Figs. 1-9 and 1-10), to cast-in-place post-tensioned box-girder bridges

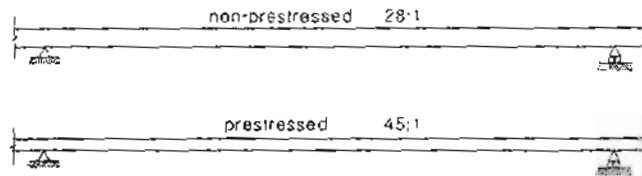


Figure 1-8 Typical span-to-depth ratios of prestressed and non-prestressed one-way slabs.

with spans of about 500 ft or 150 m (see Fig. 1-11) to cable-stayed bridges with spans of about 1000 ft or 300 m (see Fig. 1-12).

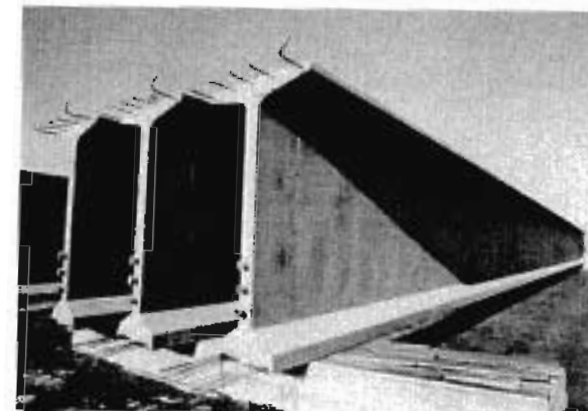


Figure 1-9 These 90 in. (2300 mm) deep pretensioned precast I-girders will be post-tensioned after erection. Photograph courtesy of Con-Force Structures Ltd.

In North America there are over 500 plants that produce precast, pretensioned building elements. The repetitive nature of the production process together with the controlled environment of the plant results in elements with high-quality concrete whose dimensions are closely controlled.

Because many parking structures are subjected to a very corrosive environment, the use of high-quality concrete, prestressed to control cracking, is advisable. Figure 1-13 illustrates a typical parking structure constructed from precast, pretensioned components. More than 35% of parking structures are now constructed using precast, pretensioned concrete while about 40% are constructed using post-tensioned, cast-in-place construction.

About 20,000 tons of prestressing strand is used in North America each year to post-tension floor slabs, with up to 100 million square feet ($10 \times 10^6 \text{ m}^2$) of slabs being post-tensioned in some years. Post-tensioning enables thinner slabs to be used resulting

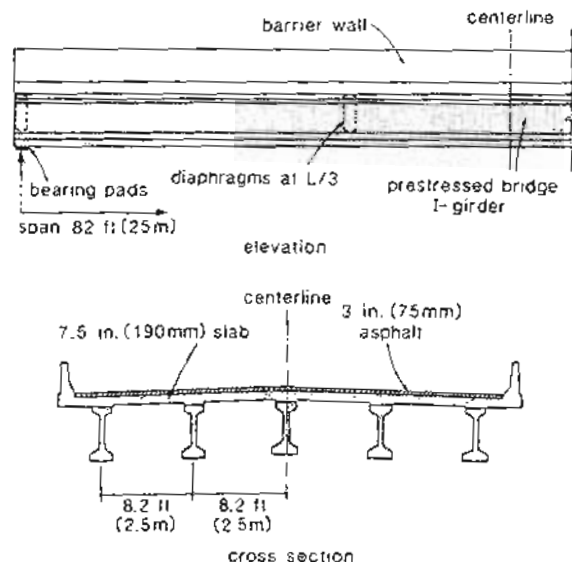


Figure 1-10 Typical highway overpass with span of 82 ft (25 m).

in reductions in overall building height, dead weight, and in cladding, heating, and air conditioning costs (see Figs. 1-14 and 1-15).

While non-prestressed structures must deform significantly before they can resist large loads, prestressing can actively resist applied loads without significant deformations. Because prestressing permits the engineer active control of load distribution and deformations, it has been widely used to solve difficult foundation problems (see Fig. 1-16).

In 1936, Freyssinet demonstrated that prestressed concrete cylindrical structures can resist considerable internal pressure without leakage. This principle was put into practice by the Preload Company of New York, which developed special wire-winding machines to circumferentially post-tension prestressed concrete tanks (Ref. 1-6). Over 2000 prestressed concrete tanks have been constructed. Recently, water tanks have been constructed by circumferentially post-tensioning precast, pretensioned elements (see Fig. 1-17).

The ability of prestressed concrete to contain great pressure makes it suitable for use in the containment structures of nuclear power plants. These structures provide the last line of defense in the event of a nuclear accident (see Figs. 1-18 and 1-19).

Tall, slender towers for television, microwave, and radio transmission are another class of structure frequently constructed of prestressed concrete. Post-tensioning the 1500 ft (450 m) long tendons of the CN Tower in Toronto (see Fig. 1-20) involved elongating these cables by about 10 ft (3 m) (Ref. 1-8). This structure contains about 1000 tons of post-tensioned steel.



Figure 1-11 Construction of Burlington Skyway, cast-in-place segmental box-girder bridge with 495 ft (151 m) main span. Photograph courtesy of Stelco Steel.

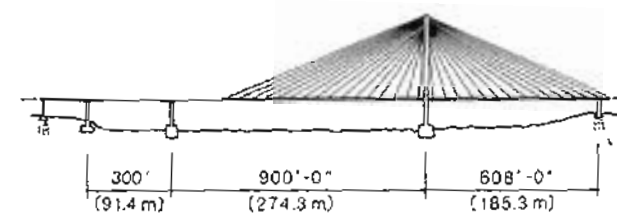


Figure 1-12 East Huntington Bridge over the Ohio River. Adapted from Grant (Ref. 1-5).

Also shown in Fig. 1-20 is the SkyDome, a 550-million-dollar sports stadium with a retractable roof spanning 670 ft (205 m). The post-tensioned concrete frames which support the roof contain about 700 tons of prestressing steel. The seating for the stadium is supported by 215,000 ft² (20 000 m²) of precast, pretensioned bleacher units, while over 900,000 ft² (84 000 m²) of pretensioned double tees were used as floor units.

Exploiting the oil and gas reserves that lie under the ocean requires large offshore production platforms. In the North Sea there are about 40 such platforms standing in

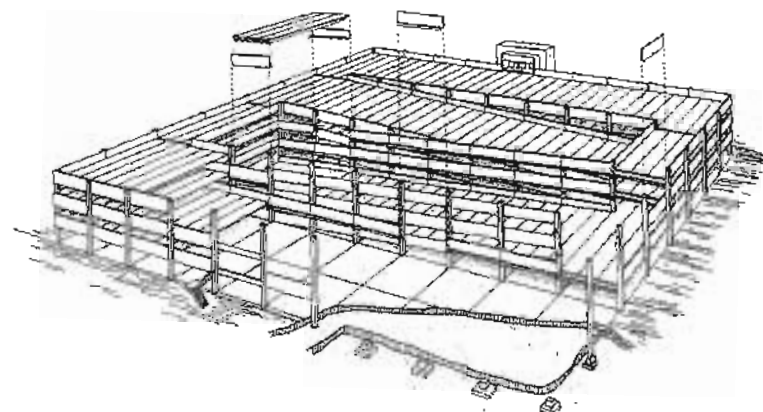


Figure 1-13 Typical parking structure.

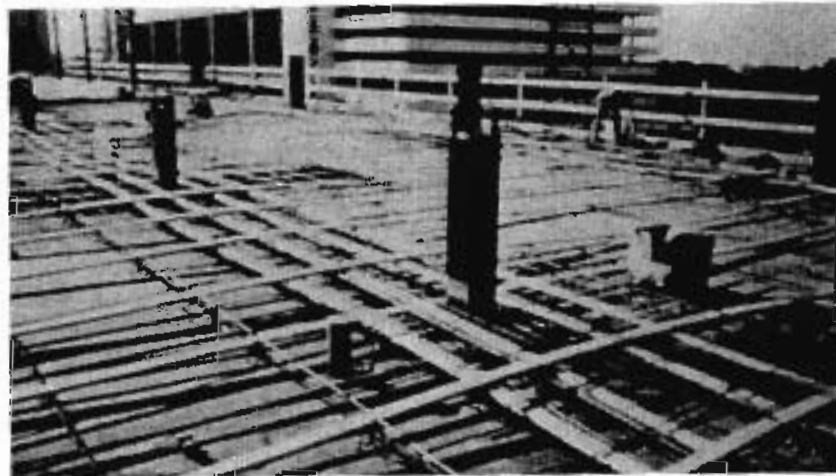


Figure 1-14 Post-tensioned slab with banded tendon arrangement. Photograph courtesy of VSL International Ltd.



Figure 1-15 Galtier Plaza, Minneapolis, a 30-story apartment tower, a 46-story condominium tower, and parking and commercial areas totalling 1,500,000 ft² (150 000 m²) of post-tensioned floor slabs. Photograph courtesy of VSL International Ltd.

water depths greater than 325 ft (100 m), with about 15 of these being prestressed concrete platforms (see Fig. 1-21). Such platforms have been designed for water depths of up to 1100 ft (330 m) (see Fig. 1-22). As these platforms must be floated to location, there is a great premium on weight. Hence high-strength concrete and "thin" heavily reinforced sections are used.

Although only a relatively small number of platforms have been built, each platform involves a very considerable expenditure. For example, the 24 lower domes that support Gullfaks C, one of which is shown in Fig. 1-23, each contain 2000 yd³ (1500 m³) of concrete, 600 tons of reinforcing bars, and 70 tons of prestressing steel. The total platform contains 320,000 yd³ (250 000 m³) of concrete and displaces about 1.5 million tons of water.

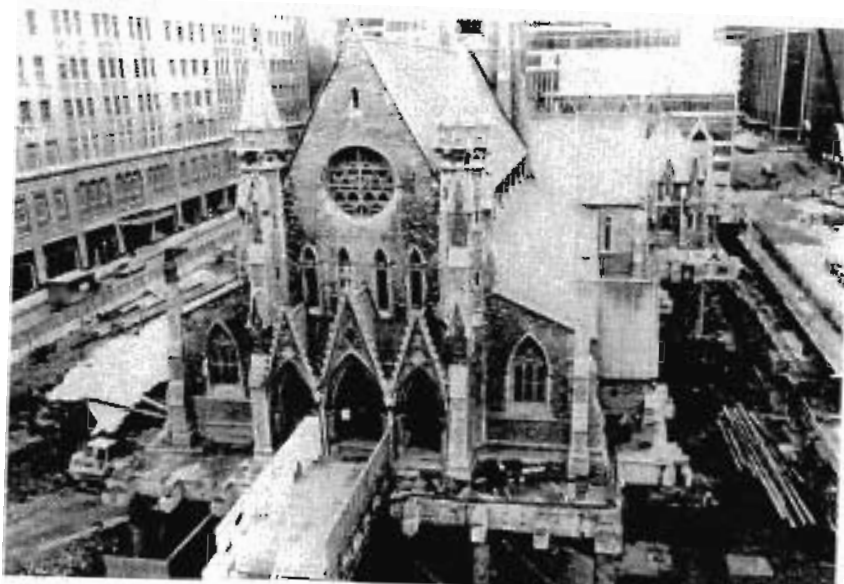


Figure 1-16 Grid of post-tensioned beams used to underpin Christ Church Cathedral, Montreal.

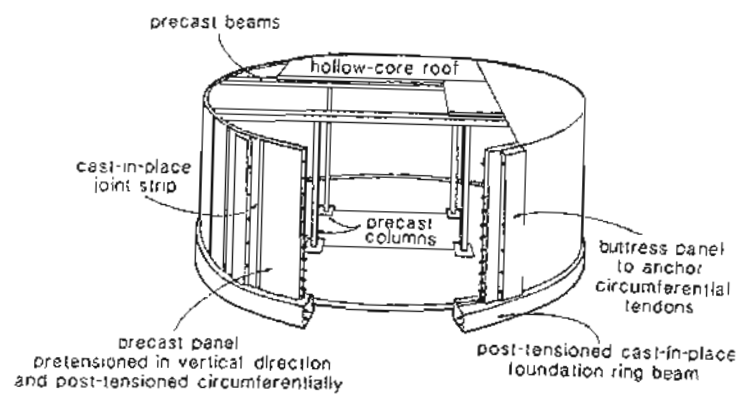


Figure 1-17 Water storage tank constructed of prestressed precast concrete.

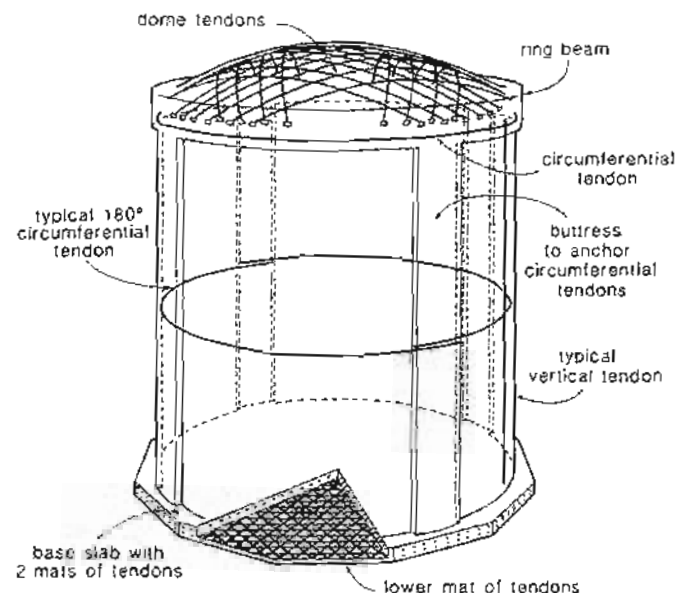


Figure 1-18 Prestressed concrete containment structure for nuclear power plant. Adapted from Mamat and Moselhi (Ref. 1-7).

1.4 DESIGN OF PRESTRESSED CONCRETE STRUCTURES

The designer of a prestressed concrete structure aims to produce a safe, serviceable, durable, economical, and aesthetically pleasing structure. To achieve these aims, the structural engineer must master the basic principles that govern the behavior of prestressed concrete.

Design can be thought of as consisting of three rather distinct but interrelated phases: conceptual design, analysis, and dimensioning and detailing (see Fig. 1-24). Conceptual design is the most critical and creative part of the design process. Here the form of the structure is chosen, preliminary dimensions and prestressing profiles are assigned, and design loadings are decided upon. Considering the required function of the structure, a design is evolved using art, experience, knowledge of construction techniques, intuition, and creativity. In most cases the engineer relies strongly upon past experience as a guide to what will be the most economical solution in a particular set of circumstances.

In the analysis phase the actual structure is idealized as an assemblage of elements and the manner in which the applied loads are distributed among these elements is determined. The stress resultants or sectional forces throughout the structure are found. For the analysis phase we typically assume linear elastic behavior and then use the elegant,

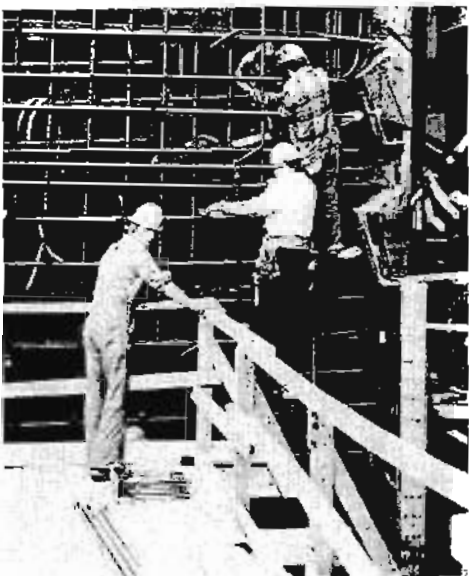


Figure 1-19 Installing post-tensioning tendons in the walls of Bruce B nuclear power station, Ontario, Canada.

powerful techniques of modern structural analysis. Standard computer programs (plane frame, space frame, finite elements) can be of considerable use in this analysis phase.

In the dimensioning and detailing phase, the response of the individual elements of the structure to their calculated stress resultants is investigated, the elements' dimensions are checked, the required amounts of reinforcing bars and prestressing tendons are determined, and the specific details of how this reinforcement will be placed are decided upon. In this phase of the design the engineer must account for the complex, real behavior of prestressed concrete. The techniques traditionally used in this phase of the design are a mixture of empirical equations (e.g., for crack widths and for shear strength), approximate procedures (e.g., calculating stresses assuming linear elastic, uncracked response), and rational models (e.g., plane-sections theory for flexure). The recent availability and power of microcomputers have considerably increased the usefulness of rational models for this phase of the design. Much of this book will be devoted to explaining these dimensioning and detailing procedures.

Apart from employing basic principles of structural mechanics, the designer of prestressed concrete structures also obtains guidance from codes of practice and industry handbooks. These documents summarize design procedures which in the past have produced satisfactory structures. In this book, we will use provisions from the American Concrete Institute's building code, ACI 318-89 (Ref. 1-9), and the design manual of the Prestressed Concrete Institute (Ref. 1-10). In addition, where appropriate, reference will be made to the Canadian Standards Association's design code, CSA A23.3-M84 (Ref. 1-11), and the European concrete code, CEB-FIP Model Code (Ref. 1-12).



Figure 1-20 The 1815 ft (553 m) high CN Tower and the 55,000-seat SkyDome stadium in Toronto. Photograph by the Kalloon Company Inc.

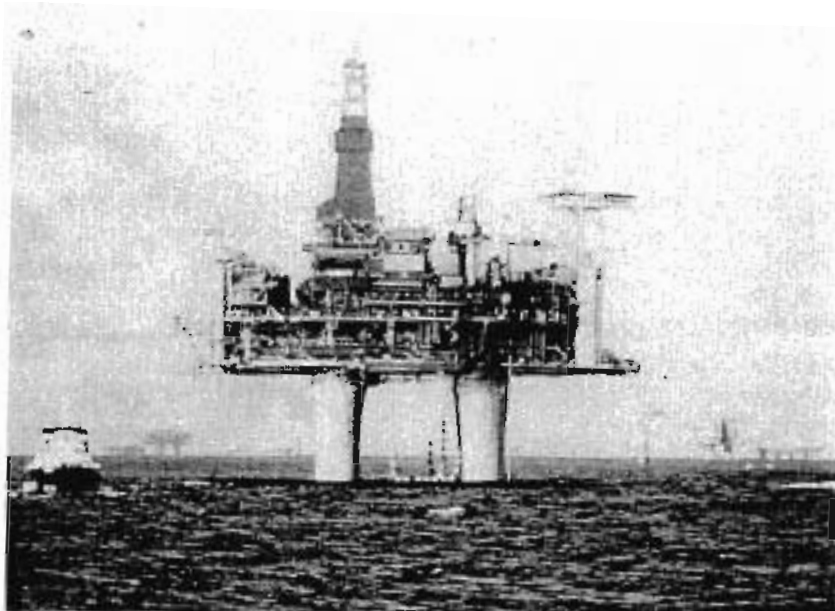


Figure 1-21 Condeep oil-production platforms on site in the North Sea. Photograph courtesy of Husmo Foto, Norway.

1.5 ADDITIONAL INTRODUCTORY READING

The development of prestressed concrete was strongly influenced by a number of significant technical papers, conference proceedings, and books. A study of some of these important documents will help the engineer to understand the background of modern prestressed concrete.

We have already mentioned Freyssinet's inspiring 1936 London lecture (Ref. 1-2), which marked the beginning of significant interest in prestressed concrete in the English-speaking world. The 1949 Freyssinet paper "Prestressed Concrete: Principles and Applications" (Ref. 1-13) summarizes Freyssinet's approach to prestressed concrete. The papers and books of Freyssinet's colleague, Yves Guyon, explained in considerable detail the French analytical procedures for investigating prestressed concrete structures (Refs. 1-14 and 1-15). Freyssinet's entertaining 1954 speech, "The Birth of Prestressing" (Ref. 1-16) gives a strong impression of the "father of prestressing."

Another individual who strongly influenced the early development of prestressed concrete was Prof. Gustave Magnel of Belgium. This dynamic individual was an excellent

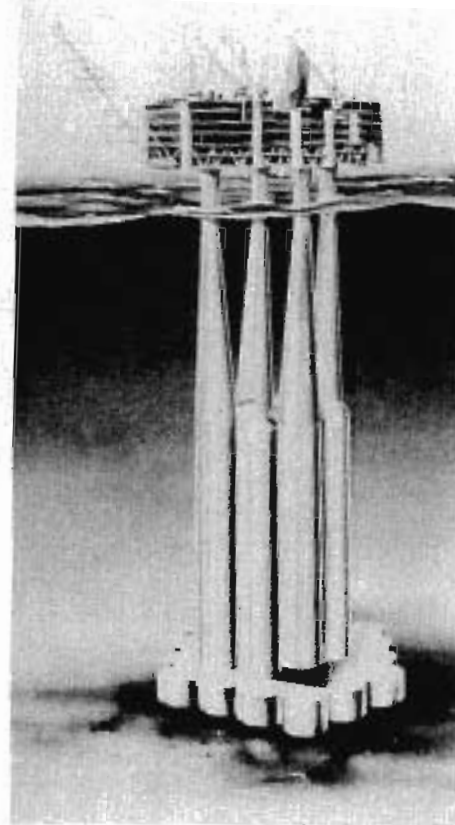


Figure 1-22 Prestressed concrete offshore production platform for a water depth of 1100 ft (330 m). Illustration courtesy of Norwegian Contractors.

teacher and lecturer and a prolific author. His 1948 book *Prestressed Concrete* (Ref. 1-17) introduced many English-speaking engineers to the details of prestressed concrete design. The construction of the Walnut Lane Bridge in Philadelphia in 1950, for which Prof. Magnel acted as a consultant, introduced European techniques for prestressed concrete to North America (Ref. 1-18). See also Refs. 1-19 and 1-20.

The techniques for constructing prestressed concrete tanks economically were developed by the Preload Company of New York. J.M. Crom, who was one of the founders of the Preload Company, described the design procedures for these circular tanks in a 1950 paper entitled "Design of Prestressed Tanks" (Ref. 1-21).

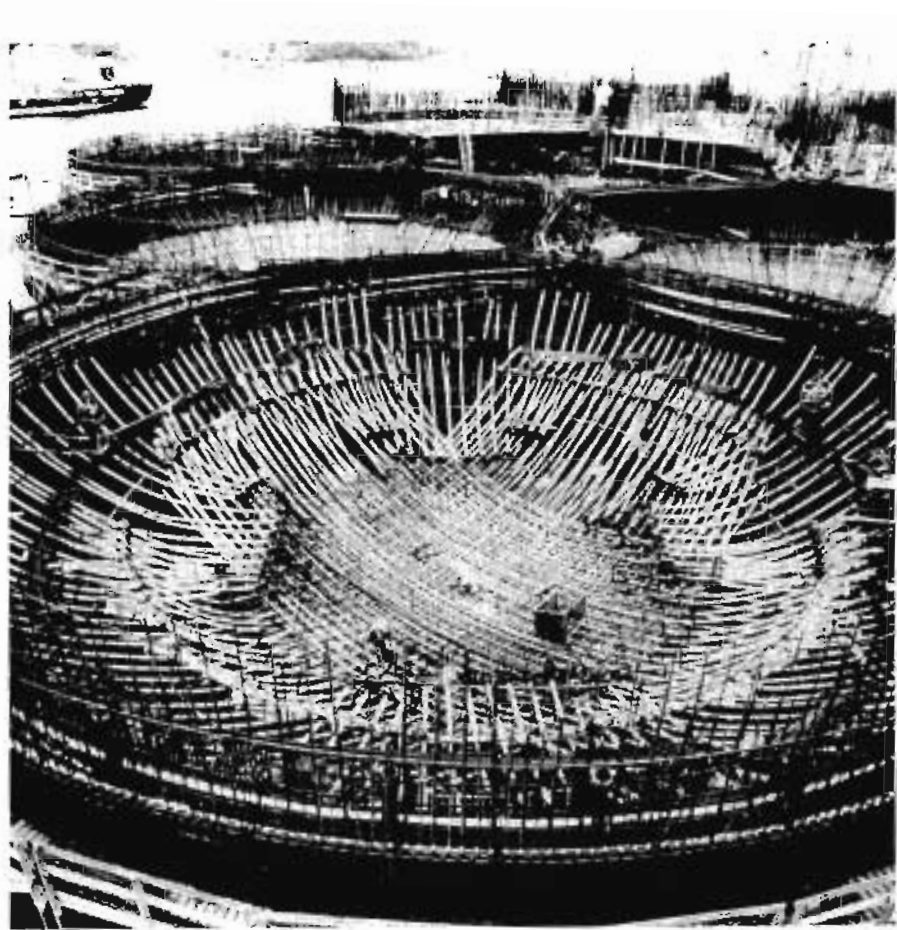


Figure 1-23 Construction of one of the lower domes for Gullfaks C, an offshore production platform for a water depth of 710 ft (216 m). Photograph courtesy of Norwegian Contractors.

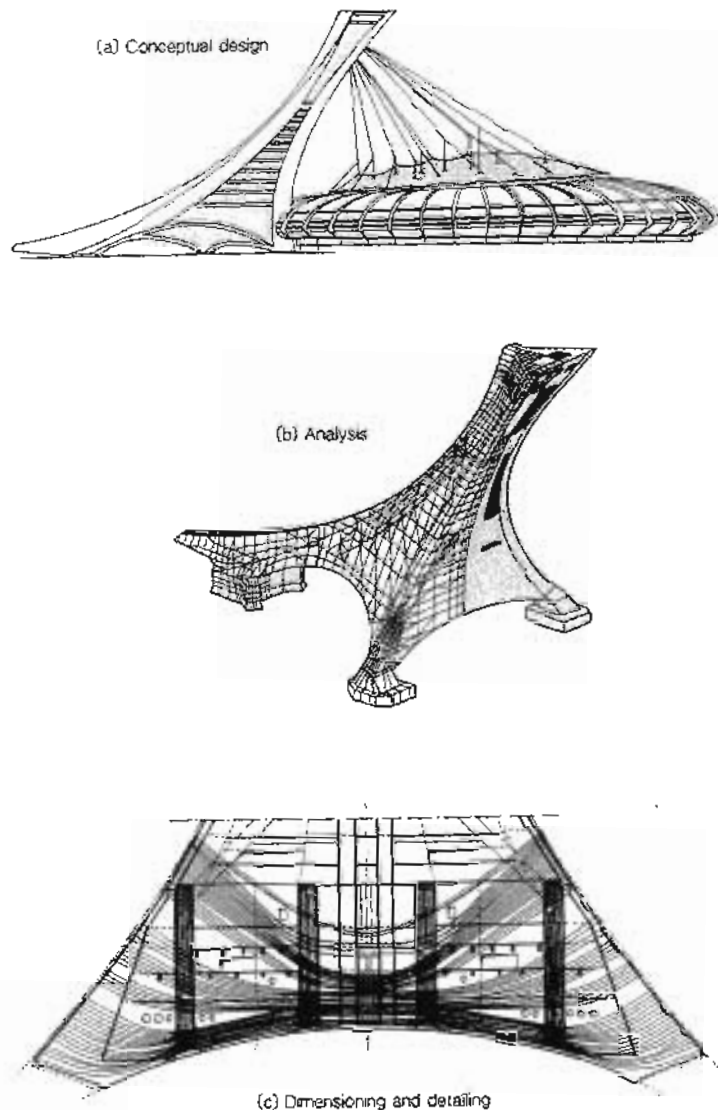


Figure 1-24 Design phases for the Montreal Olympic Tower.

Another significant, early paper on prestressed concrete was the 1943 American Concrete Institute paper by Herman Shorer entitled "Prestressed Concrete. Design Principles and Reinforcing Units" (Ref. 1-22).

Many of these early designers believed that prestressed concrete should not be allowed to crack under working loads. At the First United States Conference on Prestressed Concrete in 1951, the 600 participants heard considerable discussion as to the importance of cracking. W. Dean, the Bridge Engineer for the Florida State Road Department, stated "It is my belief that the cracking point in a prestressed concrete beam should be accorded a respect similar to that shown for the yield point in structural steel design." M. Formerod, the Chief Engineer for the Preload Company, advocated calling the cracking load the "transformation load" since, at this load, he believed "a normal prestressed girder is transformed into an ordinary reinforced concrete girder." On the other hand, L.H. Corning, of the Portland Cement Association, pointed out that "a completely crackless concrete member is only better for a specific purpose if the presence of minute cracks is detrimental to its use." He drew attention to the work of Abeles (Refs. 1-23 and 1-24) who had shown that improved ductility and controllable warning of failure were possible if partial prestressing was used. On the same side of the debate, T. Germundson, also of the Portland Cement Association, stated that the "cracking load computed for prestressed concrete has practically no real significance except that it marks the spot where the stress and deflection curves begin to change their slope."

T.Y. Lin's 1955 book, *Design of Prestressed Concrete Structures* (Ref. 1-25), was dedicated "to engineers who, rather than blindly following the codes of practice, seek to apply the laws of nature." This book, which made prestressed concrete design look simple, was responsible for a large increase in the number of American engineers prepared to design prestressed concrete.

The year 1955 also saw the publication of the first edition of F. Leonhardt's book *Spannbeton für die Praxis* (Ref. 1-26). The second edition of this standard work is available in English translation as *Prestressed Concrete - Design and Construction* (Ref. 1-27). It is probably still the most comprehensive reference book available for detailed information on prestressed concrete construction.

The progress of prestressed concrete structures since 1955 is well documented in the *Journal of the Prestressed Concrete Institute*. The series of nine articles entitled "Reflections on the Beginnings of Prestressed Concrete in America," published from May-June 1978 to May-June 1980, is particularly recommended.

References

- 1-1 Bilington, D.P., "Historical Perspective on Prestressed Concrete," *PCI Journal*, Vol. 21, No. 5, Sept.-Oct. 1976, pp. 48-71.
- 1-2 Freyssinet, E., "A Revolution in the Technique of the Utilisation of Concrete," paper read at a joint meeting of the British Section of the Société des Ingénieurs Civils de France and the Institution of Structural Engineers, London, Mar. 19, 1936, 23 pp.
- 1-3 Dobell, C., "Prestressed Concrete Tanks," *Proceedings of the First United States Conference on Prestressed Concrete*, Massachusetts Institute of Technology, Cambridge, Mass., Aug. 1951, pp. 9-20.
- 1-4 Hoyer, E., *Der Stahlsaitenbeton (Piano-Wire Concrete)*, Elsner, Berlin, 1939.
- 1-5 Grant, A., "Design and Construction of East Huntington Bridge," *PCI Journal*, Vol. 32, No. 1, Jan.-Feb. 1987, pp. 20-29.
- 1-6 Crom, J.M., "Design of Prestressed Tanks," *Proceedings ASCE*, Vol. 76, Separate No. 37, Oct. 1950, 19 pp.
- 1-7 Mamet, J.C., and Moselhi, O., "Outline of Current Analysis Procedure for CANDU 600 MW Reactor Buildings," *Canadian Journal of Civil Engineering*, Vol. 12, No. 4, Dec. 1985, pp. 796-804.
- 1-8 Knoll, F., Prosser, M.J., and Outer, J., "Prestressing the CN Tower," *PCI Journal*, Vol. 21, No. 3, May-June 1976, pp. 84-111.
- 1-9 ACI Committee 318, "Building Code Requirements for Reinforced Concrete (ACI 318-89) and Commentary - ACI 318 R-89," American Concrete Institute, Detroit, 1989, 360 pp.
- 1-10 Prestressed Concrete Institute, *PCI Design Handbook: Precast and Prestressed Concrete*, 3rd ed., PCI, Chicago, 1985.
- 1-11 CSA Committee A23.3, *Design of Concrete Structures for Buildings*, CAN3-A23.3-M84, Canadian Standards Association, Rexdale, Canada, 1984, 281 pp.
- 1-12 CEB-FIP, *Model Code for Concrete Structures: CEB-FIP International Recommendations*, 3rd ed., Comité Euro-International du Béton, Paris, 1978, 348 pp.
- 1-13 Freyssinet, E., "Prestressed Concrete: Principles and Applications," *Journal of Institute of Civil Engineers*, Vol. 33, Nov. 1949, pp. 331-380.
- 1-14 Guyon, Y., "Etude sur les Poutres Continues et sur Certains Systèmes Hyperstatiques en Béton Précontraint," Institut Technique du Bâtiment et des Travaux Publics, Circulaire Série No. 8, Sept. 1945.
- 1-15 Guyon, Y., *Prestressed Concrete*, John Wiley and Sons, New York, Vol. 1, 1953, Vol. 2, 1960.
- 1-16 Freyssinet, E., "The Birth of Prestressing," speech made by Eugene Freyssinet on the occasion of his Jubilee as an Engineer, May 1954. Published in *Travaux*, Paris, July-Aug. 1954, (in French).
- 1-17 Magnel, G., *Prestressed Concrete*, Concrete Publications, London, 1948.
- 1-18 Magnel, G., "Prototype Prestressed Beam Justifies Walnut Lane Bridge Design," *ACI Journal*, Vol. 24, No. 4, Dec. 1950, pp. 301-316.
- 1-19 Magnel, G., "Creep of Steel and Concrete in Relation to Prestressed Concrete," *ACI Journal*, Vol. 19, No. 6, Feb. 1948, pp. 485-500.

- 1-20 Zollman, C.C., "Magnell's Impact on the Advent of Prestressed Concrete," *PCI Journal*, Vol. 23, No. 3, May-June 1978, pp. 22-48.
- 1-21 Crom, J.M., "Design of Prestressed Tanks," *Proceedings ASCE*, Vol. 76, No. 37, Oct. 1950, pp. 1-19.
- 1-22 Shore, H., "Prestressed Concrete, Design Principles and Reinforcing Units," *ACI Journal*, Vol. 14, No. 6, June 1943, pp. 493-528.
- 1-23 Abeles, P.W., "How Much Prestress?" *Engineering News-Record*, July 5, 1951.
- 1-24 Abeles, P.W., *The Principles and Practice of Prestressed Concrete*, Crosby Lockwood and Sons, London, 1949.
- 1-25 Lin, T.Y., *Design of Prestressed Concrete Structures*, John Wiley and Sons, New York, 1955.
- 1-26 Leonhardt, F., *Spannbeton für die Praxis*, Wilhelm Ernst und Sohn, Berlin, 1953.
- 1-27 Leonhardt, F., *Prestressed Concrete - Design and Construction*, English translation 2nd ed., Wilhelm Ernst und Sohn, Berlin, 1964, 677 pp.

2

Pretensioning and Post-Tensioning Technology

I believe that one of the greatest retardants to prestressed concrete construction is the lack of a simple, practical, inexpensive method of applying and anchoring the prestressing force

W.E. Dean, 1951

2.1 INTRODUCTION

The designer of prestressed concrete structures must be knowledgeable about the techniques and the technology associated with prestressing and must be familiar with the terminology. In this chapter we briefly review the basic techniques of prestressing, give details of some of the more widely used prestressing systems, and introduce prestressing terminology.

The information on prestressing operations is subdivided into two classifications: pretensioning and post-tensioning. In pretensioning the tendon is tensioned prior to casting the concrete, while in post-tensioning the tendon is tensioned after the concrete has been cast.

2.2 PRESTRESSING TENDONS

The term "tendon" is used to describe either an individual wire, strand, or bar or a group of wires, strands, or bars (see Fig. 2-1). The most widely used type of prestressed

reinforcement is seven-wire strand. Because the seven-wire strand was developed in the United States, the standard nominal diameters used worldwide are given in inches, with 3/8 in. (9.53 mm), 1/2 in. (12.70 mm), and 0.6 in. (15.24 mm) being the most popular diameters. These strands are used in both pretensioned and post-tensioned construction. The ultimate tensile strength of these strands ranges from 250 to 270 ksi (1720 to 1860 MPa).

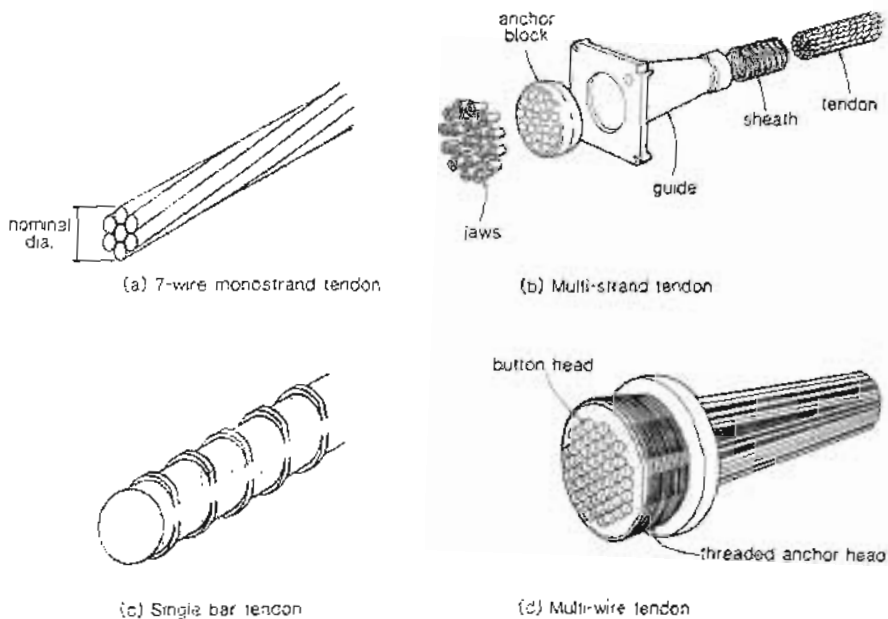


Figure 2-1 Typical tendons

Deformed prestressing bars are a more specialized type of reinforcement which are useful in some types of post-tensioned construction. Their nominal diameters vary from 5/8 in. (15 mm) to 1 3/8 in. (36 mm), and their ultimate tensile strengths are about 150 ksi (1030 MPa).

Individual wires were the first successful form of prestressed reinforcement and are still used today for special applications such as railway ties. The wires typically have 0.196 in. (5 mm) or 0.276 in. (7 mm) diameters and have ultimate strengths ranging from 235 to 250 ksi (1620 to 1720 MPa).

2.3 PRETENSIONING OPERATIONS

The first step in pretensioning is the stressing of high-strength steel tendons (usually seven-wire strands) between the abutments of a pretensioning bed (see Fig. 2-2a). The concrete is then placed in the formwork. After the desired concrete strength has been reached, the tendons are detensioned and the member becomes prestressed (see Fig. 2-2b).

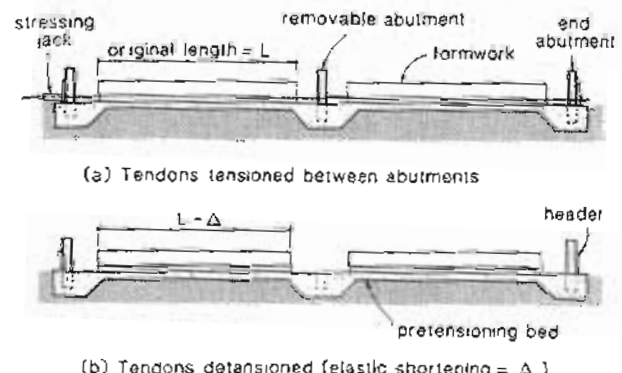


Figure 2-2 Pretensioning on a stressing bed.

An excellent summary of pretensioning technology has been given by Scott in Ref. 2-1. The stressing beds, which also serve as casting and curing beds, must typically allow a daily production cycle using minimum labor. A typical layout for a stressing bed is shown in Fig. 2-2a, with an abutment at each end for stressing and anchoring the tendons. Very long stressing beds can be subdivided into shorter beds by the use of removable abutments as shown in Fig. 2-2a. The length of stressing and casting beds varies from about 80 ft (25 m) to about 650 ft (200 m), depending on the product. Single-strand jacking is the most common form of tensioning the strand. Special long-stroke jacks which react against the fixed abutments are used (see Fig. 2-3).

Strands that have been tensioned individually are typically released by flame-cutting or sawing. The sequence of cutting should be such that the stresses are kept as symmetrical as possible. The cutting should be done gradually and as close to the member as possible to minimize the amount of energy transferred dynamically by bond stresses upon release. The use of headers that allow multiple-strand detensioning using hydraulic rams reduces damage to the bond near the end of the member.

To achieve a more favorable profile, pretensioned tendons are often "draped" or "harped" as shown in Fig. 2-4. Shallow members such as double tees are usually draped at the center of the span, while deep sections such as bridge girders usually have two harping points. Strands are either first tensioned straight and then deflected using a hydraulic ram, or tensioned in the draped position, in which case the hold-down device must allow for the longitudinal movement of the strands during the tensioning operation.

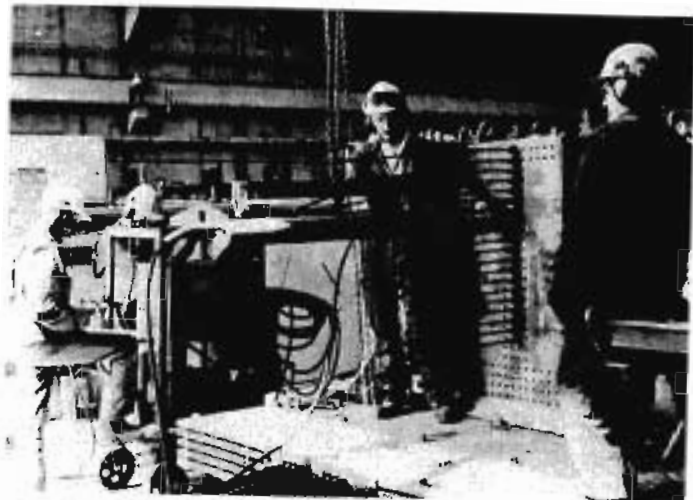


Figure 2-3 Jacking of single strand with long-stroke jack against abutment. Photograph courtesy of Con-Force Structures Ltd.

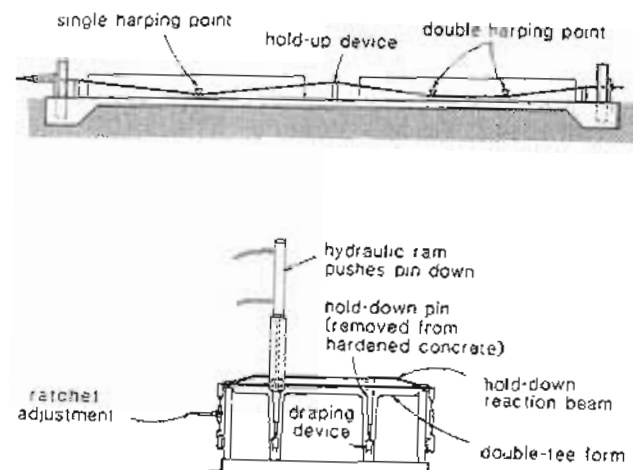


Figure 2-4 Draping or harping of tendons. Adapted from Ref. 2-1.

Draping of the tendons decreases their end eccentricity, which should prevent cracking of the concrete at the top surface near the ends. An alternative way of achieving this objective is to reduce the effective prestressing force in this region by debonding some of the strands to produce so-called "blanketed strands" (Ref. 2-2) (see Fig. 2-5).

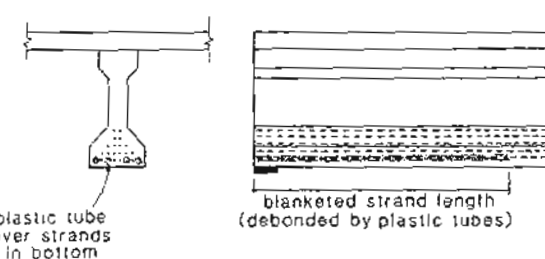


Figure 2-5 Blanketing of strands.

The steel molds that are used for standard cross-sectional shapes are usually 20 to 50 ft (6 to 15 m) in length and can be interconnected for long members. Figure 2-6 illustrates a bridge girder mold with demountable side forms and an external vibrator. Figure 2-7 shows a precast double-tee beam being lifted out of the mold.

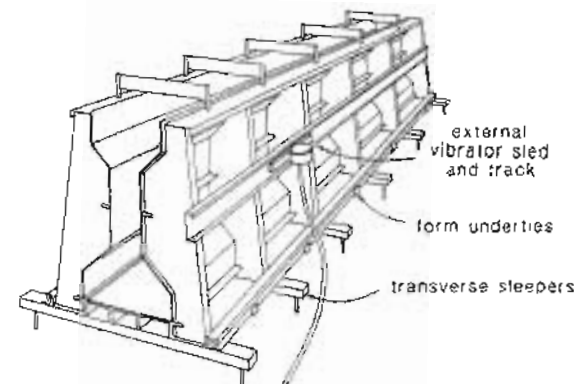


Figure 2-6 Detail of steel mold for bridge I-girder. Adapted from Ref. 2-1.

External and/or internal vibration is used for compacting the concrete in the molds. Superplasticizers are commonly used to reduce the water/cement ratio while maintaining workability. Vibrating screeds are used to strike-off and to compact pretensioned products

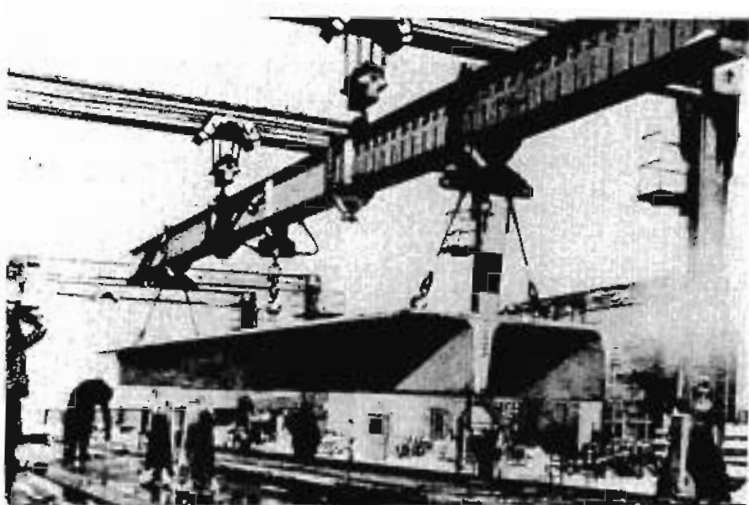


Figure 2-7 Long-span, double-tee beam being lifted from mold. Photograph courtesy of CPCL.

with wide top surfaces. A rake may be used to provide surface roughening for those surfaces that will become interfaces between the pretensioned member and cast-in-place concrete.

To achieve a daily production cycle, the concrete must reach a strength sufficient to permit release of the strands in about 16 hours. This can be achieved either by heating the concrete or by using high early strength concrete in insulated forms. The heating can be achieved either by electrical-resistance heating, steam curing (wet system), or by circulating hot fluid (dry system).

2.4 STANDARD PRECAST PRETENSIONED MEMBERS

Details of cross-sectional shapes that are recommended standards in the precast, prestressed concrete industry in North America are provided by the Prestressed Concrete Institute (Ref. 2-3) and the Canadian Prestressed Concrete Institute (Ref. 2-4). Some of these cross sections are shown in Fig. 2-8.

The standard shapes include: stemmed deck elements (double-tee and single-tee members); flat deck elements (solid flat slabs and hollow-core slabs); wall panel elements (solid wall panels, double-tee wall panels, and hollow-core wall panels); framing members (rectangular beams, L-beams, inverted-tee beams and columns); foundation elements (piles and sheet piles); and bridge I-girders.

The hollow-core slab elements shown in Fig. 2-8 are typically produced by an extrusion process on a "long line" pretensioning bed. Low-slump concrete is delivered to

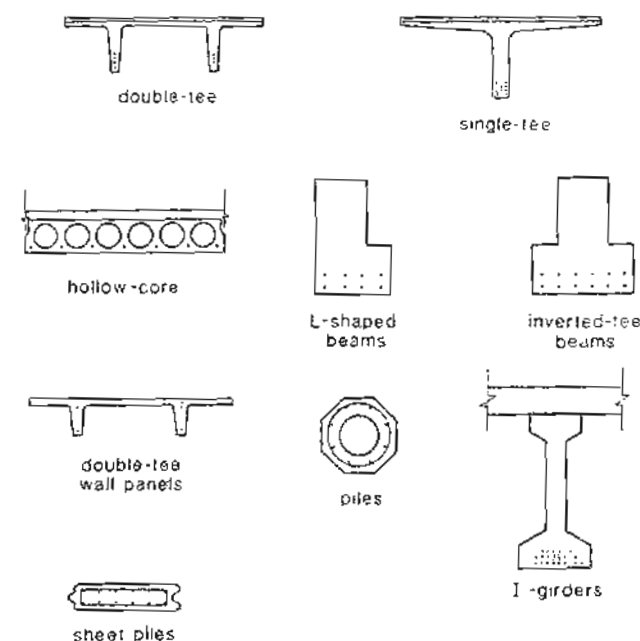


Figure 2-8 Standard precast pretensioned elements.

the hopper of an extruding machine which moves on rails along the bed and extrudes the concrete around the pretensioned tendons (see Fig. 2-9). Tapered mandrels or augers shape the cores as the extruder moves along the track. After the concrete has cured, the strands are released from the abutments and the hollow-core slab is cut into the desired lengths.

While there are recommended standard cross sections, there is a considerable range in the specific sections produced in different precast plants. Hence the engineer should investigate the specific sections available from local precasters in the early stages of the design. Some sectional properties of the PCI double-tee and single-tee cross sections are given in Fig. 2-10. These include the cross-sectional area, A , the moment of inertia, I_y , the distance from the bottom face to the centroid, y_c , and the volume-to-surface area ratio, V/S .

2.5 POST-TENSIONING OPERATIONS

The first step in producing a post-tensioned member is to place the reinforcing cage and the post-tensioning ducts in the formwork. After the casting and curing of the concrete, the

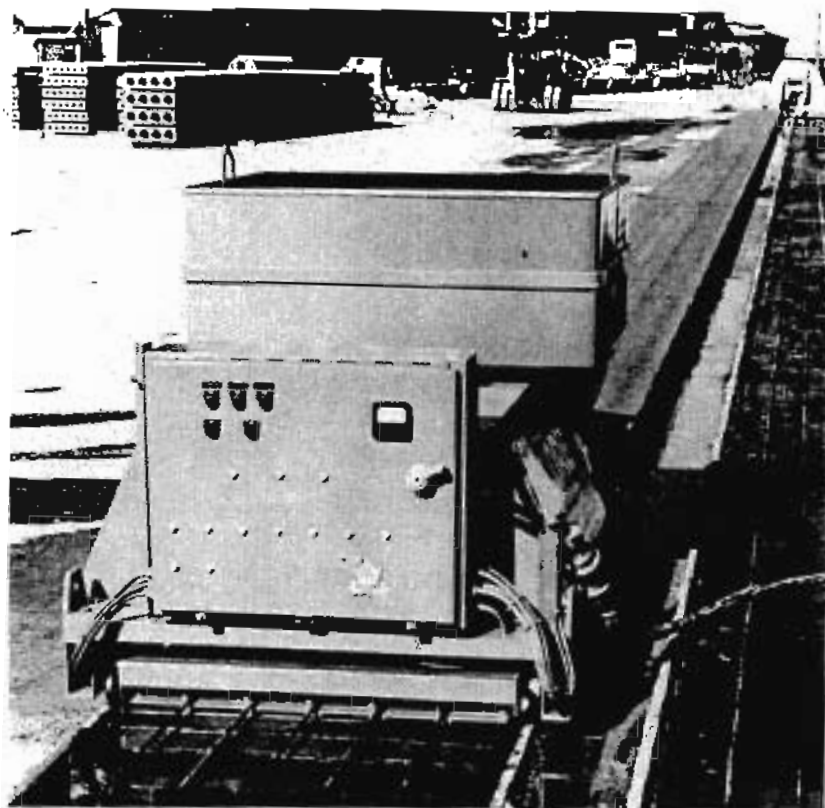


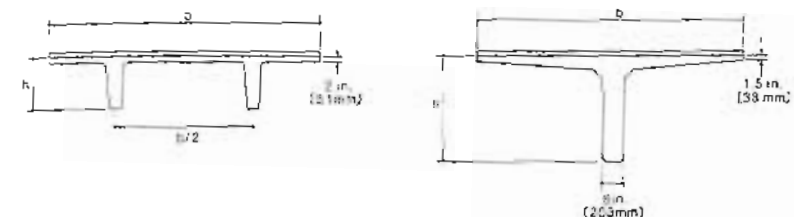
Figure 2-9 Manufacturing hollow-core slabs. From Ref. 2-5, courtesy of Dy-Core Systems Inc.

tendons are tensioned and anchored using special post-tensioning jacks that react against the member. Unless unbonded tendons are being used, the duct is then grouted to complete the post-tensioning operation (see Fig. 2-11).

Figure 2-12 shows a typical bonded and a typical unbonded tendon. In the bonded tendon the grout bonds the tendon to the surrounding concrete and provides corrosion protection for the tendon. The unbonded tendon is attached to the concrete only at its end anchors. Corrosion protection for the unbonded tendon is provided by grease-filled plastic tubes and by special details at the anchorages.

Unbonded tendons are often used in applications such as post-tensioned two-way slabs where the small duct diameter, the low friction between the strand and the greased duct, and the elimination of the grouting operation all offer considerable economies. With

Sec. 2.6 Post-Tensioning Systems



double-tee sections single-tee sections

Type	b in. (mm)	h in. (mm)	A in^2 (mm^2)	y_b in. (mm)	I in^4 (mm^4)	v/S in. (mm)
BDT12	8 (243)	12 (305)	197×10^3 (1.195×10^5)	9.12 (229)	1879 (1.195×10^7)	1.22 (21)
BDT14	8 (243)	14 (356)	216×10^3 (1.475×10^5)	10.51 (267)	2509 (1.605×10^7)	1.28 (23)
BDT16	8 (243)	16 (406)	325×10^3 (2.115×10^5)	11.93 (303)	4034 (2.615×10^7)	1.23 (22)
BDT18	8 (243)	18 (457)	344×10^3 (2.225×10^5)	12.37 (327)	4984 (3.025×10^7)	1.22 (22)
BDT20	8 (243)	20 (508)	363×10^3 (2.335×10^5)	14.59 (370)	10211 (6.224×10^7)	1.15 (19)
BDT24	8 (243)	24 (610)	461×10^3 (3.005×10^5)	17.16 (438)	28965 (1.875×10^8)	1.41 (26)
BDT32	8 (243)	32 (813)	567×10^3 (3.665×10^5)	21.21 (539)	58404 (3.225×10^8)	1.79 (45)
10DT24	10 (254)	24 (610)	660×10^3 (4.351×10^5)	11.77 (294)	22469 (1.555×10^8)	1.39 (34)
10DT32	10 (254)	32 (813)	615×10^3 (4.051×10^5)	21.98 (558)	59728 (3.465×10^8)	1.89 (47)

Figure 2-10 Sectional properties of PCI stemmed deck elements.

unbonded tendons, special attention is required to ensure that the strand is protected from corrosion, where it enters the end anchorages. Further, it may be necessary to place additional reinforcing bars to provide adequate crack control.

2.6 POST-TENSIONING SYSTEMS

Various proprietary post-tensioning systems are available. These systems differ in the type of tendon that they employ, in the manner in which the tendons are tensioned, and in the anchorage devices which are used.

There are four common types of tendon systems: monostrand tendons, single-bar tendons, multi-wire tendons, and multi-strand tendons. Figure 2-13 compares the tendon forces that can be achieved with these different types of tendon systems. Apart from tendon force, other considerations that may influence the choice of tendon type include (1) the compactness of the monostrand jacking and anchorage systems; (2) the ease of coupling and anchoring threaded bars; (3) the positive anchorage and low friction of smooth

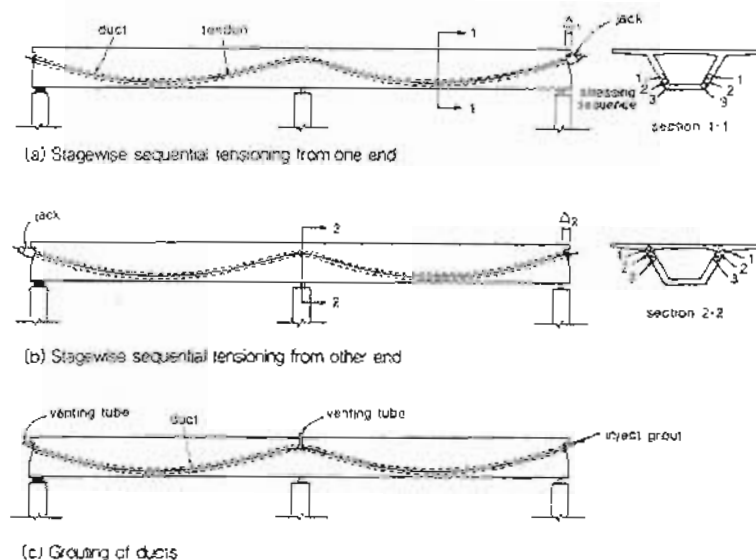


Figure 2-11 Post-tensioning operations.

button-headed wires; and (4) the versatility and economy of multi-strand systems. A brief summary of the details of some of the more widely used post-tensioning systems is given below.

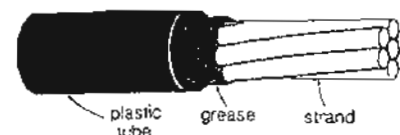
The Freyssinet K-Range System (Ref. 2-6) is illustrated in Fig. 2-14. In this multi-strand system, each strand is individually gripped by three-piece conical jaws that seat into tapered holes inside the anchorage block. The stressing is performed by a center-hole jack which simultaneously tensions all the strands in a tendon (see Fig. 2-14b). Upon release of the jack, pull-in of the strand engages the wedge-like jaws that anchor the strands. The loss of tendon elongation associated with this seating of the anchorage (anchorage set loss) must be accounted for in design. Details useful in design such as minimum tendon spacing, minimum free edge distances, minimum dimensions for anchorage recesses, and clearances required for different jack capacities are given in Fig. 2-14.

Figure 2-15 summarizes useful design details of the VSL multi-strand system (Ref. 2-7). The jacking and anchoring devices for this system are similar to those described previously for the Freyssinet System. Multi-strand tendons can be jacked from both ends to reduce frictional losses (see Fig. 2-11) or can be jacked from one end with the other end of the tendon terminating in a dead-end anchor. Both the Freyssinet and the VSL systems utilize seven-wire strand with nominal diameters of 0.5 and 0.6 in. (13 and 15 mm) having cross-sectional areas of 0.153 and 0.215 in² (99 and 140 mm²), respectively.

The Dwydak post-tensioning system, summarized in Fig. 2-16, uses high-strength alloy bars with rolled threads (Ref. 2-8). These threaded bars, which are available in lengths



(a) Grouted, corrugated metal sheath containing bonded multi-strand tendon



(b) Plastic sheath filled with grease containing unbonded monostrand

Figure 2-12 Bonded and unbonded tendons.

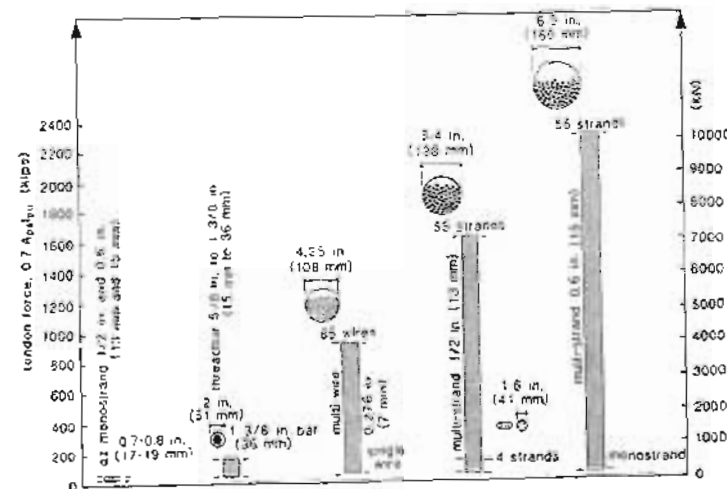
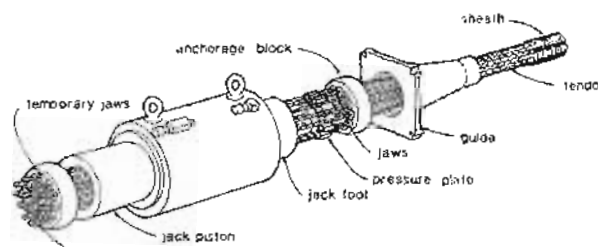
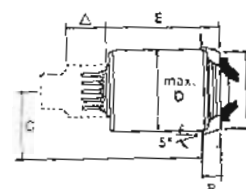


Figure 2-13 Tendon forces for different tendon types.



(a) Jacking and anchorage components



(b) Jacking details

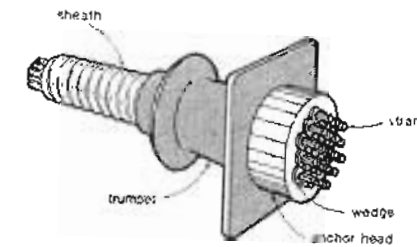
Jack type	A in. (mm)	B in. (mm)	C in. (mm)	D in. (mm)	E in. (mm)
4/5	5.0 (125)	4.5 (110)	4.5 (110)	1.0 (25)	2.5 (65)
7/5	6.25 (160)	4.5 (110)	6.0 (150)	1.0 (25)	2.5 (65)
12/5	7.25 (185)	4.5 (110)	7.0 (175)	1.0 (25)	2.5 (65)
12/6	8.00 (200)	4.5 (110)	8.0 (200)	1.5 (38)	2.5 (65)
19/6	11.00 (280)	5.0 (125)	9.0 (225)	2.0 (50)	3.5 (90)

unit	range in no. of strands	sheath inside dia. in. (mm)	tendon force kips (kN) 0.7 Apf _{pu}
17/5	1	1.0 (25)	29.0 (129)
7/5	2	2.1 (54)	87.8 (395)
		300.4 (900)	
12/5	3	3.8 (98)	251.3 (1120)
	5	345.9 (1540)	
19/5	12	3.3 (84)	375.6 (1671)
	19	549.1 (2443)	
27/5	20	3.7 (94)	578.0 (2572)
	27	780.5 (3472)	
37/5	28	4.4 (113)	909.4 (4000)
	37	1009.5 (4475)	
65/5	35	6.0 (126)	1009.5 (4466)
	35	1160.0 (5072)	

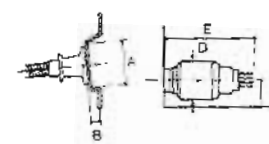
(c) 1/2 in. (13mm)-270K series

unit	range in no. of strands	sheath inside dia. in. (mm)	tendon force kips (kN) 0.7 Apf _{pu}
17/6	1	5.4 (138)	41.0 (182)
4/6	2	8.1 (203)	82.0 (368)
	4	16.0 (380)	164.0 (730)
7/6	5	11.5 (270)	205.0 (910)
	7	267.0 (1177)	
12/6	8	12.2 (306)	308.0 (1465)
	12	492.0 (2169)	
19/6	12	14.3 (360)	632.2 (2871)
	19	778.0 (3460)	
27/6	20	16.7 (397)	805.0 (3645)
	27	1107.0 (4924)	
37/6	28	19.1 (492)	1142.0 (5107)
	37	1517.0 (6748)	

(d) 0.6 in. (15mm)-270K series



(a) Stressing anchorage details



(b) Jacking details

Jack type	A in. (mm)	B in. (mm)	C in. (mm)	D in. (mm)	E in. (mm)
ES-3	1.4 (35.1)	3.1 (78.7)	7.1 (178)	1.8 (33.0)	5.1 (129.1)
ES-7	1.6 (40.6)	3.1 (78.7)	2.1 (52.9)	1.8 (40.0)	5.2 (132.1)
ES-10	1.8 (46.7)	3.1 (78.7)	3.1 (78.7)	1.8 (40.0)	5.2 (132.1)
ES-19	2.2 (56.1)	3.1 (78.7)	7.1 (178)	1.0 (25.4)	5.2 (132.1)
ES-31	2.7 (68.6)	7.1 (178)	11.1 (273)	2.0 (45.0)	5.7 (144.0)
ES-55	3.6 (91.4)	10.0 (249)	18.0 (45.7)	3.0 (70.0)	7.0 (177.0)

unit	range in no. of strands	sheath inside dia. in. (mm)	tendon force kips (kN) 0.7 Apf _{pu}
ES-3	2	1.25 (31.1)	37.8 (167)
	3	1.52 (39.0)	98.7 (438)
ES-4	4	1.63 (41.2)	115.8 (514)
ES-7	5	1.79 (44.4)	144.8 (643)
	7	1.80 (50.0)	202.4 (900)
ES-12	8	2.08 (51.0)	232.0 (1129)
	12	2.56 (63.0)	346.8 (1548)
ES-19	12	2.83 (68.6)	315.8 (1427)
	19	3.19 (79.0)	549.3 (2442)
ES-22	19	3.25 (89.1)	378.2 (1671)
	22	3.38 (95.0)	626.9 (2870)
ES-31	23	3.50 (98.6)	664.9 (2947)
	31	4.00 (110.0)	996.2 (4360)
ES-55	31	5.49 (136.0)	1086.4 (4707)

(c) VSL 1/2 in. (13mm)-270K 'E' series

unit	range in no. of strands	sheath inside dia. in. (mm)	tendon force kips (kN) 0.7 Apf _{pu}
ED-3	2	1.50 (38.1)	80.0 (363.5)
	3	1.50 (38.0)	123.5 (547.5)
ED-4	4	2.00 (50.0)	164.1 (716.0)
ED-7	5	2.25 (57.5)	205.1 (870.1)
	7	2.25 (57.0)	267.1 (1127.1)
ED-12	8	2.85 (71.1)	320.2 (1429.2)
	12	3.00 (75.0)	481.7 (2189.7)
ED-19	13	3.25 (85.5)	532.3 (2371.3)
	19	3.75 (95.5)	779.4 (3493.2)
ED-22	20	4.00 (100.0)	825.6 (3864.6)
	22	4.00 (100.0)	902.4 (4041.2)
ED-31	25	4.50 (114.0)	945.9 (4186.5)
	31	5.00 (125.0)	1271.6 (5562.4)
ED-55	31	6.50 (160.0)	2256.1 (10021.1)

(d) VSL 0.6 in. (15mm)-270K 'E' series

Figure 2-14 Freyssinet multi-strand system. From Ref. 2-6.

Figure 2-15 VSL multi-strand system. From Ref. 2-7.

@Seismicisolation

up to 60 ft (18 m), can be coupled conveniently at any location and are positively anchored by means of a nut with a conical nose that seats into a plate anchor or a bell-shaped anchor (see Fig. 2-16). This anchorage system typically has negligibly small anchorage set losses.

The basic concept of the BBR System (Ref. 2-9), which is summarized in Fig. 2-17, is the use of smooth, high-strength steel wires anchored at each end by cold-formed "button heads." The wires are 0.276 in. (7 mm) in diameter and have a cross-sectional area of 0.060 in² (38.5 mm²). The parallel wires of a tendon all pass through a common anchor head (see Fig. 2-17b and c). Before detensioning, shim plates are inserted between the anchor head and the bearing plate, locking the tendon elongation into place.

Monostands, which are usually unbonded (see Fig. 2-18), offer an economical and versatile means of post-tensioning thin slabs and narrow members. The monostands can be arranged in a single horizontal layer which, together with the small-diameter ducts, provides maximum possible eccentricity. Monostrand post-tensioning systems also utilize compact anchorages and grommets together with small, lightweight stressing jacks, thus permitting the stressing operation to be carried out by one person.

Figure 2-19 illustrates a number of different dead-end anchorages for different pre-stressing systems. It is sometimes necessary to couple tendons together. For example, in the construction of a segmental box-girder bridge it is necessary to couple the tendons stressed during phase 1 of the construction to the tendons that are to be stressed in phase 2. Figure 2-20 illustrates typical couplers.

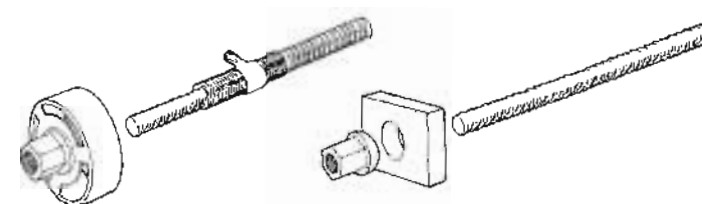
2.7 GROUTING OF DUCTS

In bonded post-tensioned construction the ducts are grouted as soon as possible after stressing the tendons. The objective of the grouting operation is to fill the duct completely with material that provides an alkaline environment for corrosion protection of the pre-stressing steel and has sufficient strength to bond the tendons to the surrounding concrete. To minimize the time that the ungrouted tendons are exposed to corrosive conditions, it is advisable to insert the tendons into the ducts just prior to stressing the tendon.

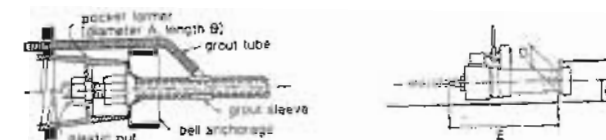
Grout usually consists of a mixture of cement and water (water/cement ratio of about 0.50) together with a water-reducing admixture and an expansive agent. Grout for larger-diameter ducts may also contain filler materials such as sand, fly ash, or pozzolans. A satisfactory grout should maintain sufficient fluidity during the grouting operation, should exhibit minimum bleeding and segregation, should not shrink, should have adequate strength, and should not contain detrimental amounts of chlorides, nitrates, sulfides, or other compounds that contribute to corrosion.

The grout is injected at the low points of the tendon or at the ends of the member. Venting tubes are provided at the high points of the tendon, as shown in Fig. 2-11c. If the duct is not properly vented, pockets of air may be trapped at high points of the duct (see Fig. 2-21). Freezing of water that may collect in these air pockets can result in serious deterioration of the structure and may lead to corrosion of the tendon.

It is not usually possible to grout the ducts successfully if the temperature of the surrounding concrete is less than about 40°F (5°C). Hence it may be necessary to leave



(a) Bell and plate anchorage



nominal bar dia. in. (mm)	bell anchor size in. (mm)	anchor plate size in. (mm)	A in. (mm)	B in. (mm)	C in. (mm)	D in. (mm)	E in. (mm)
5/8 (15)	3.25 x 1.50 (83 x 38)	3 x 3 x 0.75 (76 x 76 x 19)	7.12 (180)	4.75 (121)	3.25 (82)	2 (52)	26 (65)
1 (25)	8.50 x 1.85 (216 x 47)	5 x 5.50 x 1.25 (127 x 140 x 32)	5.12 (130)	7 (178)	4 (102)	4.18 (106)	36 (90)
5/8 (15)	6.75 x 2.60 (171 x 67)	6 x 7 x 1.25 (153 x 178 x 32)	9.32 (240)	8 (205)	4 (102)	4.13 (106)	36 (90)
1 1/8 (30)	11.75 x 3.13 (297 x 79)	7 x 7.00 x 1.75 (178 x 197 x 44)	9.32 (240)	9.63 (244)	9 (229)	4.75 (120)	46 (115)

(b) Jacking and anchorage details

nominal bar dia. in. (mm)	area in. ² (mm ²)	sheath inside dia. in. (mm)	ultimate stress, f _u kg/mm ² (psi)	bar force size (kN) 0.7 A _s f _u
5/8 (15)	0.471 (17)	0.75 (19)	167 (1080)	30.5 (124)
1 (25)	1.02 (54)	1.25 (32)	150 (1030)	69.3 (304)
1 1/8 (30)	1.75 (76)	1.50 (38)	160 (1100)	121.3 (540)
1 3/8 (38)	2.08 (84)	1.75 (44)	150 (1030)	163.9 (720)

(c) Bar sizes and properties

Figure 2-16 Dywidag threadbar post-tensioning system. From Ref. 2-8.

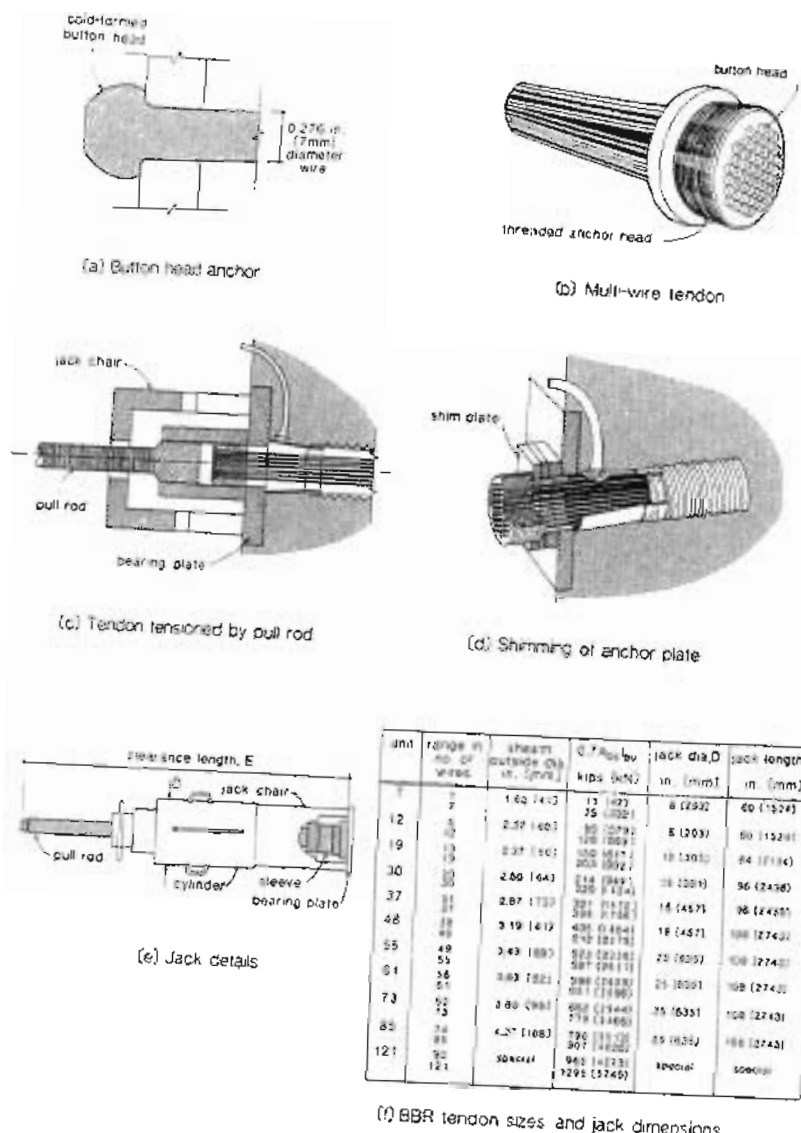


Figure 2-17 BBR multi-wire system. From Ref. 2-9.

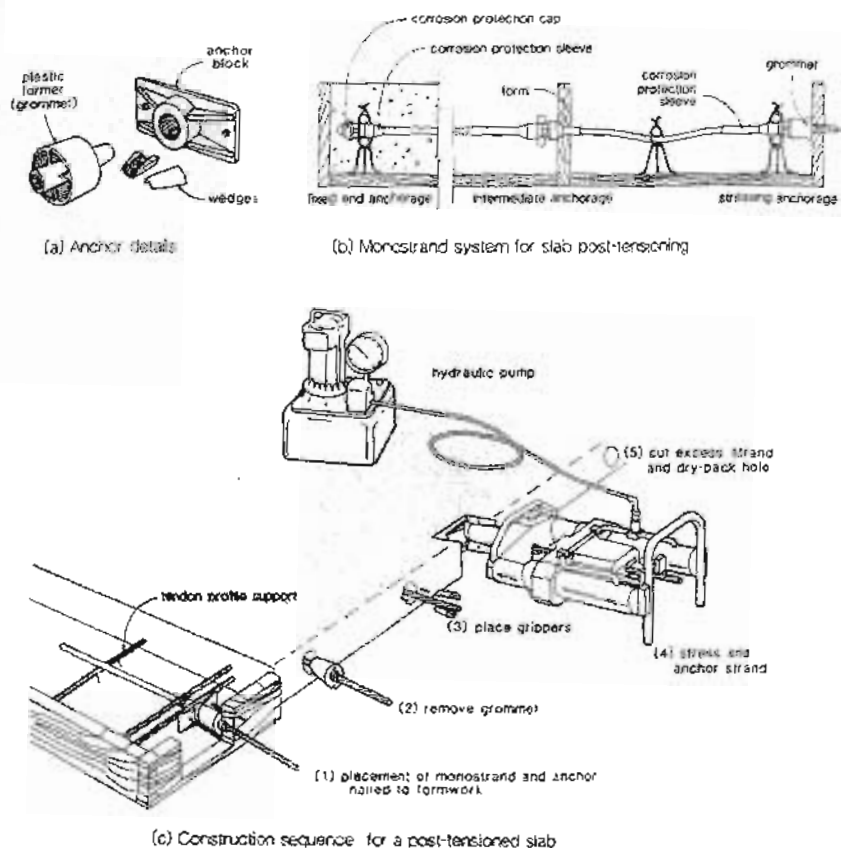


Figure 2-18 Monostrand post-tensioning system. From Refs. 2-7 and 2-10.

ducts ungrouted for some period of time if the temperature stays near freezing. In such cases, particular care must be taken to prevent water from entering the ducts and to ensure that all low points in the ducts are properly drained.

Prior to grouting, the ducts should be blown out using oil-free compressed air to remove debris from the ducts. Sometimes the ducts are flushed out with water prior to grouting. If blockage of a duct occurs during grouting, the duct needs to be flushed out immediately by injecting water into the closest air vent, against the direction of grouting.

Records of the grouting pressures, volume of grout used, temperatures, and other details of the grouting operation need to be kept. High grouting pressures (e.g., over 200 psi or 1.5 MPa) may indicate blockage in the duct and may cause segregation of the grout or splitting of the concrete surrounding the duct.

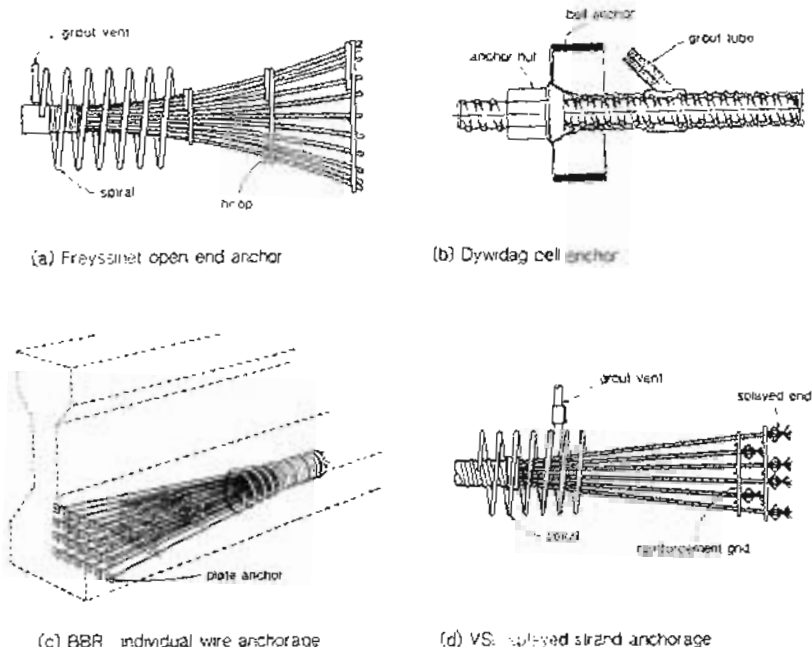


Figure 2-19 Examples of dead-end anchorages. From Refs. 2-6 to 2-9.

The long-term durability of a bonded, post-tensioned structure depends on the success of the grouting operation. Specifications for this highly specialized and critical procedure are given by the Post-Tensioning Institute in Ref. 2-11. Further details on grouting are given in Ref. 2-12.

2.8 PROFILES OF POST-TENSIONED TENDONS

In post-tensioned construction, tendon profiles are usually of parabolic shape. The tendon profile for a simply supported beam usually consists of one parabolic curve with the maximum eccentricity being located at midspan (see Fig. 2-22a). Tendon profiles in continuous beams can be described as a series of parabolic segments with concave segments in the spans and convex segments over the supports (see Fig. 2-22b).

Sec. 2.8 Profiles of Post-Tensioned Tendons

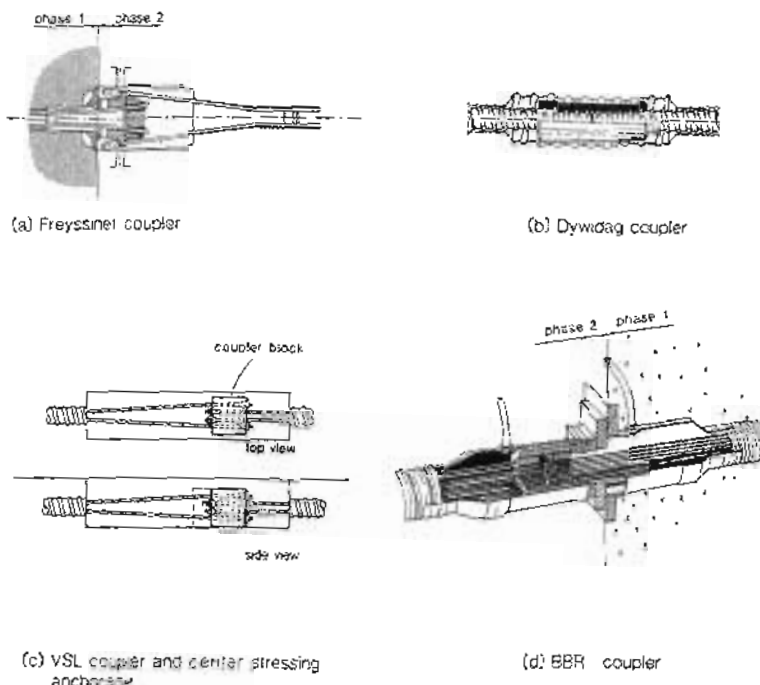


Figure 2-20 Tendon couplers and center-stressing anchorages. From Refs. 2-6 to 2-9.

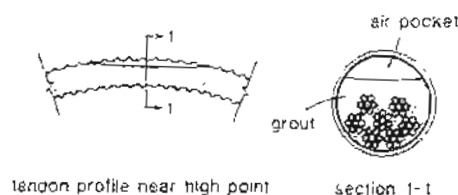


Figure 2-21 Air pocket formed at tendon high point due to inadequate venting.

Useful geometric relationships for a parabolic segment are given in Fig. 2-23a. Figure 2-23b illustrates how a series of parabolic segments fit together. At the location of maximum eccentricity, e_1 , parabols 1 and parabola 2 both have zero slopes and hence are

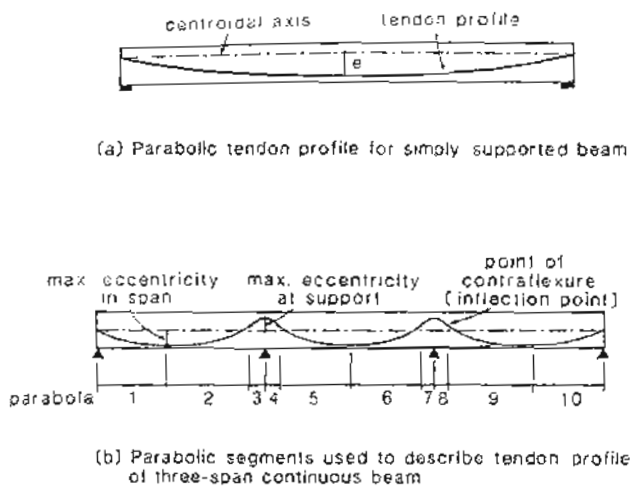


Figure 2-22 Parabolic tendon profiles

compatible. In order that parabola 2 and parabola 3 are compatible, their slopes at the inflection point must be equal and hence

$$\frac{2(e_1 + e_2 - h_2)}{(\lambda - \beta)\ell} = \frac{2h_2}{\beta\ell}$$

Thus the inflection point must be located a distance, h_2 below the high point, where

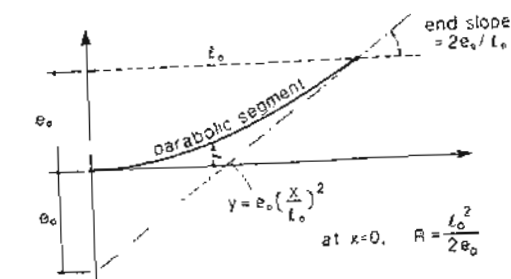
$$h_2 = \frac{\beta}{\lambda}(e_1 + e_2) \quad (2-1)$$

The inflection point must therefore lie on a straight line connecting the points of maximum eccentricities as shown in Fig. 2-23b.

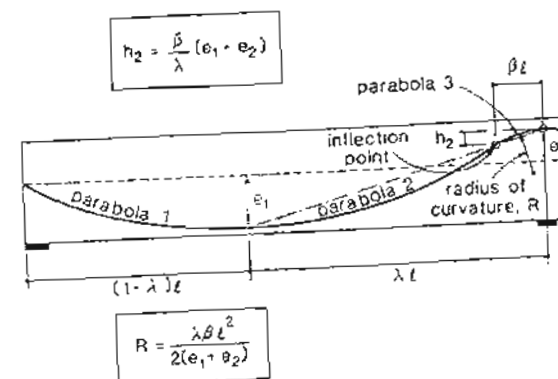
Note that the common slope of the two parabolas meeting at the inflection point is given by

$$\text{slope} = \frac{2(e_1 + e_2)}{\lambda\ell} \quad (2-2)$$

The convex segment over the support is required in order to avoid a kink in the tendon at this location. The length of the convex segment, $\beta\ell$, in Fig. 2-23b, needs to be chosen such that over the support the radius of curvature, R , of the tendon is not less than the minimum radius of curvature recommended for the particular tendon. Examples of recommended minimum radii for a multi-strand tendon system are given in Table 2-1.



(a) Geometry of parabolic segment



(b) Parabolic segments with compatible slopes

Figure 2-23 Geometry of parabolic profiles.

For monostrand systems, Ref. 2-14 recommends a minimum radius of curvature of 8 ft (2.5 m) for 1/2 in. (13 mm) and 0.6 in. (15 mm) diameter strands.

In determining duct locations it is important to recognize that the centroid of the tendon, called the center of gravity of steel (c.g.s.) will not always coincide with the center of the duct. When the tendon is stressed it will be pulled toward the inside wall of curved ducts (see Fig. 2-24). The resulting eccentricities of the tendon inside the duct for one post-tensioning system (Ref. 2-7) are given in Fig. 2-24. It can be seen that for large tendons these eccentricities can be significant.

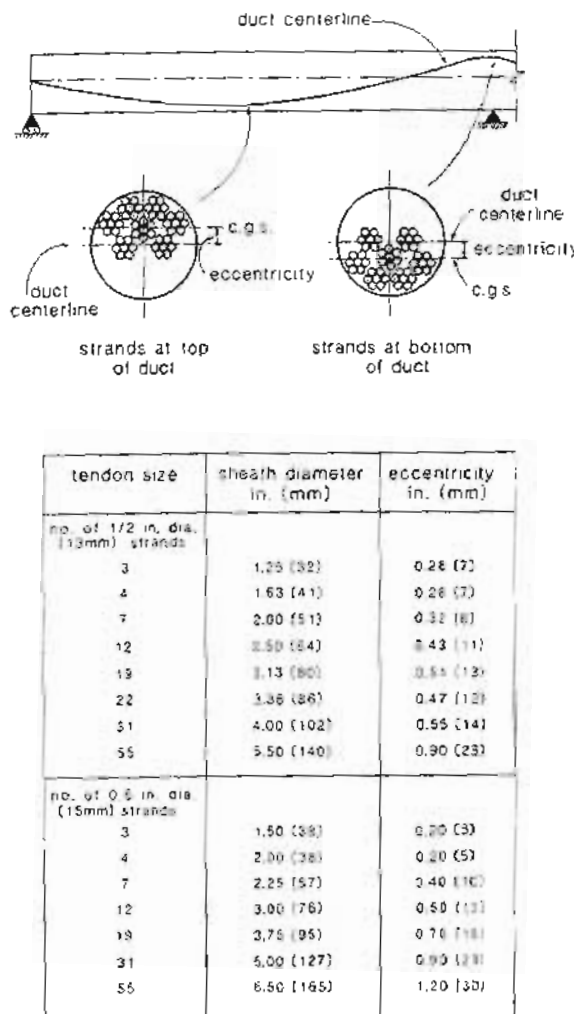


Figure 2-24 Location and eccentricity of tendon in duct after stressing. From Ref. 2-7.

2.9 LOSSES DURING POST-TENSIONING

When a tendon is tensioned by a jack, the force produced is not constant along the length of the tendon due to friction between the tendon and the duct. It is customary to consider

Sec. 2.9 Losses during Post-Tensioning

Table 2-1 Recommended minimum radius of curvature.
From Ref. 2-13.

Sheath inside diameter	in. (mm)	1.8–2.2 (45–55)	2.6–3.2 (65–80)	3.3–3.7 (85–95)	3.9–4.3 (100–110)
Minimum radius of curvature	ft (m)	12 (3.5)	15 (4.5)	16 (5.0)	23 (7.0)

the frictional loss as consisting of two components: the curvature and the wobble frictional losses.

Curvature frictional loss results from the intended change of angle of the tendon profile. If over a tendon length of dx the tendon direction changes by angle $d\alpha$, a normal force, N , equal to $2P \sin(d\alpha/2)$ results (see Fig. 2-25). If the coefficient of friction between the tendon and the duct is μ , then the friction loss in length dx will be μN . As the angles involved are typically small, $2 \sin(d\alpha/2)$ can be taken equal to $d\alpha$ and hence the friction loss becomes $\mu P d\alpha$.

Additional frictional losses result from unintended angle changes of the tendon along its length (see Fig. 2-26). The magnitude of these wobble losses depends on the rigidity of the sheathing, the diameter of the sheathing (larger sheaths have lower losses), the spacing of the sheath supports, the tendon type, and the sheath type, as well as the form of construction. Wobble losses over the tendon length, dx , are expressed as $K P dx$, where K is the empirical wobble coefficient.

The total friction loss over length dx is thus

$$dP = \mu P d\alpha + K P dx$$

The change in tendon force between point A and point B can be found as follows:

$$\int_{P_A}^{P_B} \frac{dP}{P} = \mu \int_0^\alpha d\alpha + K \int_0^x dx$$

Solving this equation gives

$$P_B = P_A e^{-\mu \alpha + Kx} \quad (2-3)$$

where P_A = tendon force at location A

P_B = tendon force at location B

μ = friction coefficient

α = total intended, cumulative angle change between A and B, radians

K = wobble friction coefficient per foot or per meter of tendon

x = tendon length between A and B, feet or meters

The range of friction coefficients recommended by ACI Committee 343 (Ref. 2-15) is given in Table 2-2. Representative friction coefficients recommended in the CEB-FIP Model Code (Ref. 2-16) are given in Table 2-3. From these tables it can be seen that the coefficient of friction, μ , depends on the surface characteristics of the tendon and of the duct and may vary between 0.05 and 0.50. It can be seen that the wobble coefficient, K , is a function of both the coefficient of friction, μ , and the sheath rigidity, and may

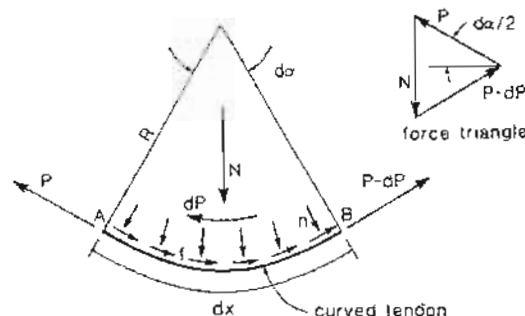


Figure 2-25 Curvature frictional loss.

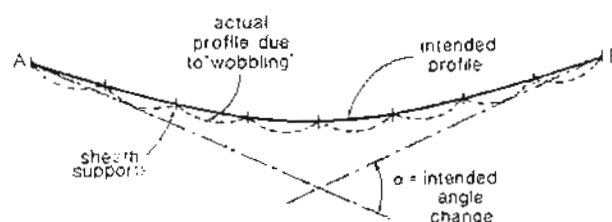


Figure 2-26 Wobble frictional loss.

Table 2-2 Range of friction coefficients recommended by ACI. From Ref. 2-15.

Type of Tendon	Curvature Coefficient, μ	Wobble Coefficient, K^1	
		per foot	per meter
Tendons in flexible metal sheathing			
Wire tendons	0.15–0.25	0.0010–0.0015	0.0033–0.0049
7-wire strand	0.15–0.25	0.0005–0.0020	0.0016–0.0066
High-strength bars	0.08–0.30	0.0001–0.0006	0.0003–0.0021
Tendons in rigid metal duct – 7-wire strand	0.15–0.25	0.0002	0.00066
Unbonded pregreased tendons – wires and 7-wire strand	0.03–0.15	0.0003–0.0020	0.0010–0.0066
Unbonded mastic-coated tendons – wires and 7-wire strand	0.05–0.15	0.0010–0.0020	0.0033–0.0066

vary between 0.0001 and 0.002 per foot (0.0003 and 0.0066 per meter). Since both of these friction coefficients can vary over an order of magnitude, it is clear that in order to calculate frictional losses accurately, information on the specific system being used is needed. As well as obtaining the friction coefficients for the specific post-tensioning system

being employed, it is also necessary to take into account the influence of workmanship and construction type. For example, segmental construction results in additional unintended curvatures at the locations of the segment interfaces. The FIP recommendations (Ref. 2-17) suggest doubling the K coefficients given in Table 2-3 for this type of construction. A study (Ref. 2-18) of a variety of tendons in eight segmentally constructed bridges resulted in a mean μ of 0.36 and a mean K of 0.001 per foot (0.003 per meter). For multi-stage construction having complex tendon geometry, the actual friction losses should be determined during stressing and empty ducts for supplementary tendons should be provided in case the friction losses are greater than expected. Additional considerations are that the friction coefficients increase with decreasing radius of curvature, increase with increasing force, and increase when surface corrosion is present.

Table 2-3 Representative friction values* recommended by CEB-FIP for tendons with radii of curvature not less than 6 m (20 ft). From Ref. 2-16.

Type of Tendon	Curvature Coefficient, μ	Wobble Coefficient, K^1	
		per foot	per meter
Cables in concrete ducts	0.50	0.0015	0.0050
Tendons in metal sheathing			
Drawn wires	0.20	0.0006	0.0020
Strand	0.20	0.0006	0.0020
Smooth rolled wires	0.25	0.0008	0.0025
Deformed wire	0.30	0.0009	0.0030

*Multiply values by 0.90 if tendon is slightly lubricated.

¹In the CEB-FIP Model Code, K is expressed as 0.01μ per meter (0.003 μ per foot).

Figure 2-27 illustrates the manner in which frictional losses influence the variation in tendon force along the length of the member. In using Eq. (2-3) to determine frictional losses, it is sufficiently accurate to calculate the tendon force only at the ends of each parabolic segment and then assume that the force varies linearly between these points, as shown in Fig. 2-27b.

If a reasonably long tendon, such as that shown in Fig. 2-27, is stressed from only one end, there may be a considerable loss in force along the member length. The influence of frictional losses is reduced if the member is stressed from both ends. Temporary overstressing of the tendon followed by release and subsequent restressing will also reduce the variation in tendon force caused by friction (see Fig. 2-27c). Additional measures need to be taken if this overstressing technique is to be used for post-tensioning systems with self-anchoring wedges such as multi-strand tendons. During post-tensioning it is usually permitted to stress the tendon temporarily to a maximum of about 80% of the specified tensile strength of the tendon. After anchoring, the stress in the tendon at anchorages and couplers is usually limited to 70% of the specified tensile strength (Ref. 2-19).

During the tensioning of the tendon, both the jack force and the corresponding tendon elongation are recorded. The elongation readings are compared to the calculated elongation

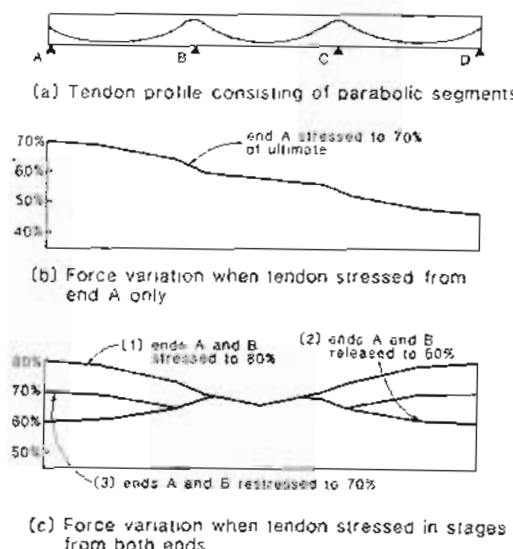


Figure 2-27 Tendon force variation due to frictional losses.

and must agree within specified tolerances ($\pm 5\%$ is usually acceptable). Smaller than expected elongations may indicate that the tendon is jammed in the duct and hence only a portion of the tendon length is being stressed or it may indicate higher than normal frictional losses. The elongation of the tendon can be calculated as follows:

$$\Delta = \frac{P_{av}\ell}{A_{ps}E_p} \quad (2-4)$$

where Δ = expected tendon elongation

P_{av} = average force in tendon determined from calculated force variation along tendon

ℓ = total length of tendon

A_{ps} = cross-sectional area of tendon

E_p = Young's modulus of tendon

It is useful to recognize that the term $P_{av}\ell$ in Eq. (2-4) is equal to the area under the curve which shows the variation of tendon force along the length of the tendon.

After the stressing operation is completed it is necessary to anchor the tendons. For most post-tensioning systems the anchoring operation will result in an additional loss of tendon force due either to seating of the wedges or to deformation of the shims. The anchorage set for strand tendons anchored by wedges is usually about 0.25 in. (6 mm).

Figure 2-28 shows the influence of anchorage set on the force variation near the end of the tendon. The length of tendon affected by anchorage set is a function of the

frictional losses. If friction is low (e.g., for unbonded tendons), the length affected may be very large. The anchorage set is equal to the shortening of the tendon which results from the force change in the tendon. As this shortening is proportional to the shaded area in Fig. 2-28, the length affected by anchorage set can be calculated in the following manner:

$$\Delta_{set} = \frac{0.5\Delta P\ell_{set}}{A_{ps}E_p} \quad (2-5)$$

Assuming a constant frictional loss per unit length, p , we obtain

$$\Delta P = 2p\ell_{set} \quad (2-6)$$

where p is the friction loss expressed as a change in force per unit length calculated from a tendon force variation diagram. Substituting for ΔP in Eq. (2-5) gives

$$\ell_{set} = \sqrt{\frac{\Delta_{set}A_{ps}E_p}{p}} \quad (2-7)$$

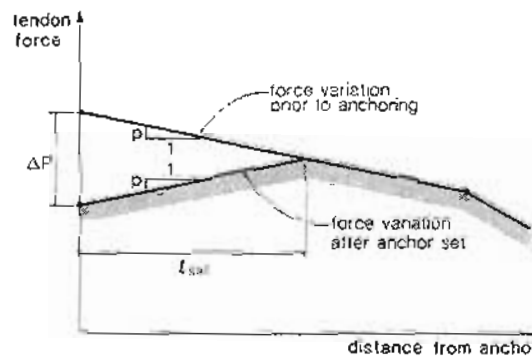


Figure 2-28 Influence of anchorage set on force variation.

2.10 EXAMPLE OF FRICTION LOSS CALCULATIONS

The four-span continuous bridge girder shown in Fig. 2-29 is post-tensioned with tendons consisting of twenty 0.6 in. (15 mm) diameter strands with $f_{pu} = 270$ ksi (1860 MPa). The symmetrical tendons are simultaneously stressed to 75% f_{pu} , that is, 871 kips (3870 kN), from both ends and then anchored.

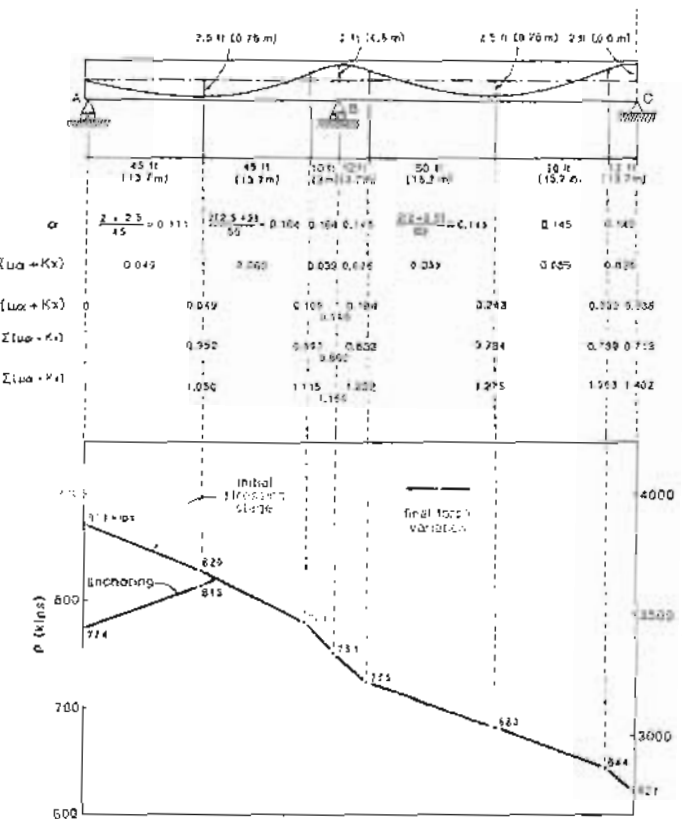


Figure 2-29 Example of frictional loss calculation.

For this application the tendon properties are:

$$\begin{aligned}
 A_{p,t} &= 4.30 \text{ in}^2 \quad (2800 \text{ mm}^2) \\
 E_p &= 28,200 \text{ ksi} \quad (195,000 \text{ MPa}) \\
 \mu &= 0.20 \\
 K &= 0.0006/\text{ft} \quad (0.0020/\text{m}) \\
 \Delta_{act} &= 0.25 \text{ in.} \quad (6 \text{ mm})
 \end{aligned}$$

- Calculate the expected elongation due to the stressing operation.

- Calculate the tendon force variation after anchorage.

(a) Determination of Tendon Force Variation

The $\mu\alpha + Kx$ values for each parabolic segment are first determined. Since each parabolic segment has one end which is horizontal (zero slope) the angular change, α , within each segment is equal to the slope at the inclined end. The equation in Fig. 2-23a and Eq. (2-2) are used to find these slopes.

During stressing, the force at location x along the tendon is given by

$$P_x = P_A e^{-\sum(\mu\alpha + Kx)}$$

The tendon force variation after jacking is shown in Fig. 2-29.

(b) Calculation of Elongation

The average force in the tendon can be approximated as

$$\begin{aligned}
 P_{av} &= \left[\frac{1}{2}(871 + 829) \times 45 + \frac{1}{2}(829 + 781) \times 45 \right. \\
 &\quad + \frac{1}{2}(781 + 751) \times 10 + \frac{1}{2}(751 + 725) \times 12 \\
 &\quad + \frac{1}{2}(725 + 683) \times 50 + \frac{1}{2}(683 + 644) \times 50 \\
 &\quad \left. + \frac{1}{2}(644 + 621) \times 12 \right] / 224 = 745 \text{ kips (3315 kN)}
 \end{aligned}$$

The calculation above assumes a linear force variation between the ends of each parabolic segment. From Eq. (2-4), the expected elongation is

$$\Delta = \frac{745 \times 224 \times 12}{4.30 \times 28,200} = 16.5 \text{ in. (419 mm)}$$

(c) Anchorage Set

Within the first 45 ft (13.7 m) of the tendon the friction loss per inch is $(871 - 829)/(45 \times 12) = 0.078 \text{ kips/in. (13.6 N/mm)}$.

The length of tendon affected by anchorage set is given by Eq. (2-7):

$$\ell_{set} = \sqrt{\frac{0.25 \times 4.30 \times 28,200}{0.078}} = 623 \text{ in.} = 52 \text{ ft (15.8 m)}$$

Because ℓ_{set} exceeds 45 ft (13.7 m), the friction loss per inch, p , could be recalculated if a more accurate answer is desired. However, in this case the small difference will be neglected.

From Eq. (2-6),

$$\Delta P = 2 \times 0.078 \times 623 = 97.2 \text{ kips (432 kN)}$$

Hence after anchoring, the force at the end of the tendon is

$$871 - 97.2 = 773.8 \text{ kips (3442 kN)}$$

This force in the tendon corresponds to a stress of $0.67f_{pu}$, which is less than the stress limit of $0.70f_{pu}$ permitted by the ACI Code (Ref. 2-19) at end anchorages. The force variation after anchoring is shown in Fig. 2-29.

References

- 2-1 Scott, Norman L., "The Long Line Pretensioning Method," *Proceedings of the FIP/PCI Symposia*, Vol. 3, Canadian Prestressed Concrete Institute, Ottawa, Aug. 1984, pp. 7-24.
- 2-2 Kaar, P.H., and Magura, D.D., "Effect of Strand Blanketing on Performance of Pretensioned Girders," *PCI Journal*, Vol. 10, No. 6, Dec. 1965, pp. 20-34.
- 2-3 Prestressed Concrete Institute, *PCI Design Handbook: Precast and Prestressed Concrete*, 3rd ed., PCI, Chicago, 1985.
- 2-4 Canadian Prestressed Concrete Institute, *Metric Design Manual - Precast and Prestressed Concrete*, 2nd ed., CPCI, Ottawa, 1987.
- 2-5 Dy-Core Integrated Building Systems, a product brochure of Dy-Core Systems, a Division of Dy-Form Engineering Ltd., Vancouver, Canada.
- 2-6 The K-Range System, a product brochure of Freyssinet International Ltd., Paris, France.
- 2-7 Post-Tensioning Systems, a product manual of VSL Corporation, Los Gatos, Calif.
- 2-8 Dywidag Threadbar Post-Tensioning System, a product brochure of Dywidag Systems International, Lincoln Park, N.J.
- 2-9 BBR Cona Multi Prestressing Systems, a product brochure of Bureau BBR Ltd., Zurich, Switzerland.
- 2-10 VSL Monostand Post-Tensioning System, a product brochure of VSL Corporation, Campbell, Calif., 1989, 16 pp.
- 2-11 Post-Tensioning Institute, *Post-Tensioning Manual*, Post-Tensioning Institute, Phoenix, Ariz., 1976.
- 2-12 PCI Committee on Post-Tensioning, "Recommended Practice for Grouting of Post-Tensioned Prestressed Concrete," *PCI Journal*, Vol. 17, No. 6, Nov.-Dec. 1972, pp. 18-25.
- 2-13 TESIT Post-Tensioning Systems: Technical Information and Data, TESIT Spa, Milan, Italy.
- 2-14 Ritz, P., Matt, P., Tellenbach, Ch., Schlub, P., and Aeberhard, H.U., *Post-Tensioned Slabs*, Losinger Ltd.-VSL International, Berne, Switzerland, Jan. 1981, 41 pp.
- 2-15 ACI Committee 343, "Analysis and Design of Reinforced Concrete Bridge Structures," ACI 343R-88, American Concrete Institute, Detroit, 1988.
- 2-16 CEB-FIP, *Model Code for Concrete Structures: CEB-FIP International Recommendations*, 3rd ed., Comité Euro-International du Béton, Paris, 1978, 348 pp.
- 2-17 FIP Commission on Practical Design, *FIP Recommendations - Practical Design of Reinforced and Prestressed Concrete Structures Based on the CEB-FIP Model Code (MC78)*, Thomas Telford Ltd., London, 1984, 36 pp.
- 2-18 Virlogeux, M., and Jaeger, D., *Pertes de Précontrainte par frottement, dans le cas des poutres construites par encorbellements successifs* (Prestressing Friction Losses in Segmental Bridge Construction), Technique Française du Béton Précontrainte, FIP Congress, Stockholm, Sweden, 1982, pp. 251-272.
- 2-19 ACI Committee 318, "Building Code Requirements for Reinforced Concrete (ACI 318-89) and Commentary - ACI 318 R-89," American Concrete Institute, Detroit, 1989, 360 pp.

Demonstration Problems

- 2-1 Define the following terms: anchorage block, anchorage set, blanketed strand, button head, center-hole jack, composite topping, coupler block, dead-end anchor, duct, grommet, harped strand, hold-down device, jack chair, monostrand, multiple strand detensioning, pretensioning bed, removable abutment, sheath, splayed strand, stemmed deck elements, stressing bed, tendon, trumpet, venting tubes, and wobble.
- 2-2 The inside diameter of a sheath for a post-tensioned tendon must be sufficiently large to ensure adequate space around the tendon for grout. Prepare a plot that shows the relationship between the ratio of the duct area to the tendon area (A_{duct}/A_{tend}) and the inside diameters of the sheaths for the VSL 1/2 in. (13 mm) multi-strand system. Comment on the variation observed.
- 2-3 In constructing the four-span continuous bridge girder described in Fig. 2-29, it is necessary to support the tendon sheaths at 3 ft (0.9 m) centers along the length of the girder. If the concrete centroidal axis shown in Fig. 2-29 is 3 ft (0.9 m) above the bottom surface of the girder, prepare a table giving the elevations of the sheath centerline relative to the bottom surface of the girder at the sheath support locations in span AB. The eccentricities given in Fig. 2-29 are to the centroid of the tendon. Allow for the fact that the tendon centroid will not coincide with the sheath centroid.
- 2-4 A four-span post-tensioned one-way floor slab is described in Fig. 2-30. The tendons are stressed from both ends and the stressing procedure is: jack to 80% of the ultimate tensile strength (UTS), release to 60% UTS, rejack to 70% UTS, and anchor. Assuming that $\mu = 0.25$, $K = 0.0015/\text{ft}$ (0.005/m), calculate (a) the tendon force at 1.44, 2.0, 2.5, and 3.0 and (b) the average tendon force in each span. Express the forces as a ratio of the UTS of the tendon. Assume that the anchor set is negligibly small.

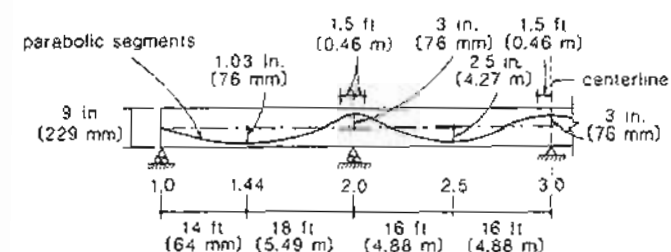


Figure 2-30 Post-tensioned one-way floor slab.

- 2-5 A straight post-tensioning tendon has a wobble factor, K , of 0.001/\text{ft} (0.0033/m). The tendon is stressed to 200 ksi (1400 MPa) at the jacking end and then anchored. Due to wedge draw-in, the tendon slips back a distance of 0.25 in. (6 mm) during anchoring. Over what length of tendon will the stress be reduced because of wedge draw-in? What will be the highest stress in the tendon immediately after anchoring? What will be the stress in the tendon at the anchor? Assume that $E_p = 29,000 \text{ ksi}$ (200,000 MPa).
- 2-6 A cylindrical tank is to be post-tensioned with strands in small semi-rigid ducts [$K = 0.0015/\text{ft}$ (0.005/m), $\mu = 0.20$]. The tendons will be anchored in buttresses and will be stressed from both ends. The stressing procedure will be to stress to 80% UTS, release to 60%, restress to

70%, and then anchor. If the tank size is such that the tendon radius is 65 ft (19.8 m), how far apart can the buttresses be if the average force in the tendon is not to be less than 66% UTS? Neglect anchor set losses.

- 2-7 A post-tensioning supplier has devised a testing system in order to determine experimentally the frictional loss coefficients for different tendon systems. Two concrete elements have been cast, one being straight and the other being a circular arc with a radius of 75 ft (see Fig. 2-31). The losses in prestress force measured were 4.3% in the case of the straight tendon and 10.1% in the case of the curved tendon. Find the frictional loss coefficients, μ and K .

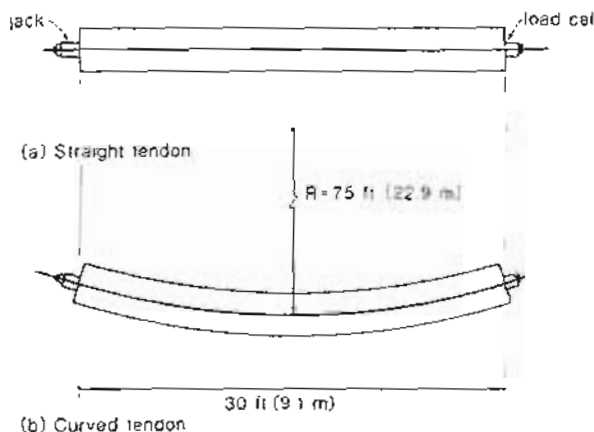


Figure 2-31 Experimental determination of μ and K .

3

Material Properties

There is also a kind of powder which from natural causes produces astonishing results. ... This substance, when mixed with lime and rubble, not only lends strength to buildings of other kinds, but even when piers of it are constructed in the sea, they set hard under water. ... The water taken in makes them cohere, and the moisture quickly hardens them so that they set into a mass which neither the waves nor the force of water can dissolve.

Vitruvius, c. 30 B.C.

3.1 INTRODUCTION

The designer needs to be knowledgeable about the properties of the concrete, the pre-stressing steel, and the reinforcing bars used in the construction of prestressed concrete structures. In this chapter we summarize those material properties of particular importance to the designer.

3.2 CONCRETE MATERIAL TECHNOLOGY

The techniques involved in producing concrete and the complex chemical processes that occur during hydration are described in textbooks on concrete materials (e.g., Refs. 3-1 and 3-2). A brief summary of some aspects particularly relevant to predicting the structural response of prestressed concrete is given in this section.

The principal components of concrete are portland cement, water, and aggregates. Figure 3-1 illustrates the typical composition of concrete used in prestressed concrete construction. Concrete hardens due to the chemical reactions that occur between the portland

cement and water. Portland cement consists largely of calcium silicates. These silicates react with water to produce calcium silicate hydrate which provides most of the strength, and calcium hydroxide which makes the concrete alkaline. Portland cement also contains tricalcium aluminate (C_3A), which contributes to the alkalinity of the concrete and helps to bind chemically any chloride ions that may be present. Figure 3-2 shows hydrate products at different times after the addition of water to the cement. Portland cements can have widely differing chemical compositions. The five standard types of portland cement used in North America are described in Table 3-1.

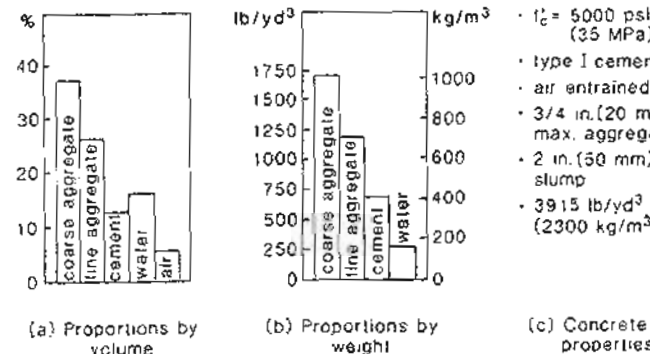


Figure 3-1 Composition of typical concrete.

Table 3-1 Standard types of portland cement as specified by ASTM (Ref. 3-3)

Type	Characteristic	Application
I	"Normal" cement	General purpose
II	Lower C_3A content	Moderate sulfate resistance Moderate heat of hydration
III	More finely ground and/or higher C_3S content	High early strength Low-temperature concreting
IV	Lower C_3S and C_3A content	Low heat of hydration Concreting massive sections
V	Low C_3A	Sulfate resistant

To hydrate the cement completely requires a minimum amount of water equal to about 25% of the weight of the cement. Although it is desirable to minimize the amount of water in the mix, a water/cement ratio of about 0.30 is the lowest value that can be achieved in

practice. Water in excess of that used in the hydration process causes small voids to form in the resulting cement paste, weakening the paste and making it more porous. Increasing the water/cement ratio thus reduces the strength and increases the permeability of the concrete. In prestressed concrete construction, where the concrete strengths are typically 4500 to 9000 psi (30 to 60 MPa), reasonably low water/cement ratios are required.

Superplasticizers are linear polymers containing sulfonic acid groups which temporarily increase the workability of the concrete. The use of these admixtures enables low water/cement ratios (0.30 to 0.40) to be used while maintaining workability with slumps of 7 to 9 in. (175 to 225 mm), resulting in high-strength, low-permeability concrete.

Natural pozzolans, fly ash, condensed silica fume, and blast furnace slag are all supplementary cementitious materials which are sometimes used to partially replace portland cement and/or to enhance the characteristics of the resulting concrete. Condensed silica fume or "microsilica," which is a by-product from the manufacture of ferrosilicon, is about two orders of magnitude finer than portland cement (Ref. 3-4). When used to replace 5 to 10% of the portland cement, it can result in very high strength concretes such as the concrete described in Table 3-2.

Aggregates for use in prestressed concrete should be inert, hard, nonporous, non-expansive, clean, and should have appropriate size, shape, and grading. In addition, they should not contain deleterious amounts of substances such as salts, sulfates, or organic compounds. It is especially important that the aggregate not react in the alkaline environment of the cement paste. In addition to influencing the strength and durability, the aggregate also affects the creep, shrinkage, and thermal properties of the concrete.

High-quality lightweight aggregates are available which make it possible to produce lightweight concretes having strengths appropriate for prestressed concrete construction.

Table 3-2 Representative mix proportions for high-strength silica fume concrete. From Moksnes and Jakobsen (Ref. 3-5).

Components	Quantities
Cement	420 kg/m ³ (708 lb/yd ³)
Silica fume	30 kg/m ³ (51 lb/yd ³)
Sand (0-5 mm)	875 kg/m ³ (1475 lb/yd ³)
Aggregate (5-20 mm)	945 kg/m ³ (1593 lb/yd ³)
Water	153 l/m ³ (258 lb/yd ³)
Plasticizing admixtures	8.5 l/m ³ (14.3 lb/yd ³)
Water/cement ratio	= 153/420 + 30 = 0.34
Slump	= 260 mm (10.2 in.)
Cube strength	= 74.8 MPa (10,800 psi) at 7 days = 98.4 MPa (14,300 psi) at 28 days = 113.3 MPa (16,400 psi) at 90 days
Density	= 2430 kg/m ³ (152 lb/ft ³)



Figure 3-2 Surface scanning micrographs showing stages in the hydration of portland cement. Photographs courtesy of R.H. Mills.

3.3 CONCRETE IN UNIAXIAL COMPRESSION

While the compressive stress-strain responses of the constituents of the concrete, that is the aggregate and the cement paste, are linear the stress-strain response of the resulting concrete is nonlinear (see Fig. 3-3). Usually, the aggregates are stiffer and stronger (14,000 to 30,000 psi or 100 to 200 MPa are typical strengths) than the paste.

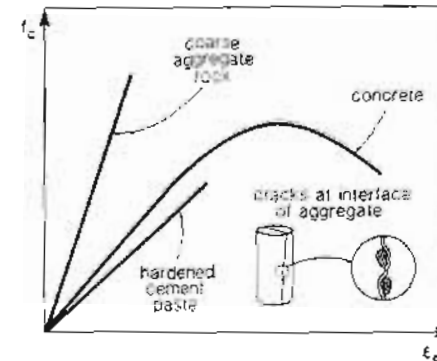


Figure 3-3 Stress-strain responses of concrete and its constituent materials

The nonlinearity of the concrete stress-strain response is caused by the interaction between the paste and the aggregate. Microcracks occur at the aggregate-paste interfaces at relatively low stress levels. The development and propagation of these cracks soften the concrete, resulting in a "rounded" stress-strain curve. Prior to failure, significant longitudinal cracking develops and considerable lateral expansion of the concrete occurs.

The response of concrete in uniaxial compression is usually determined by loading a cylinder of concrete 6 in. (150 mm) in diameter and 12 in. (300 mm) long so that the maximum stress, f'_c , is reached in 2 to 3 minutes. Typical stress-strain curves for a range of concrete strengths are shown in Fig. 3-4. It can be seen that as the concrete strength increases, the concrete stress-strain curves exhibit increased initial stiffness, greater linearity, and decreased ductility.

Several expressions to represent the compressive stress-strain response of concrete have been reviewed by Popovics (Ref. 3-7). A generalization of two of the expressions given by Popovics has been found by Thorenfeldt, Tomasewicz, and Jensen (Ref. 3-8) to represent well the family of stress-strain curves for concretes of different strengths. This expression relating the stress, f_c , and the strain caused by this stress, ϵ_{cf} , is

$$\frac{f_c}{f'_c} = \frac{n (\epsilon_{cf}/\epsilon'_c)}{n - 1 + (\epsilon_{cf}/\epsilon'_c)^{nk}} \quad (3-1)$$

where f'_c = peak stress obtained from a cylinder test

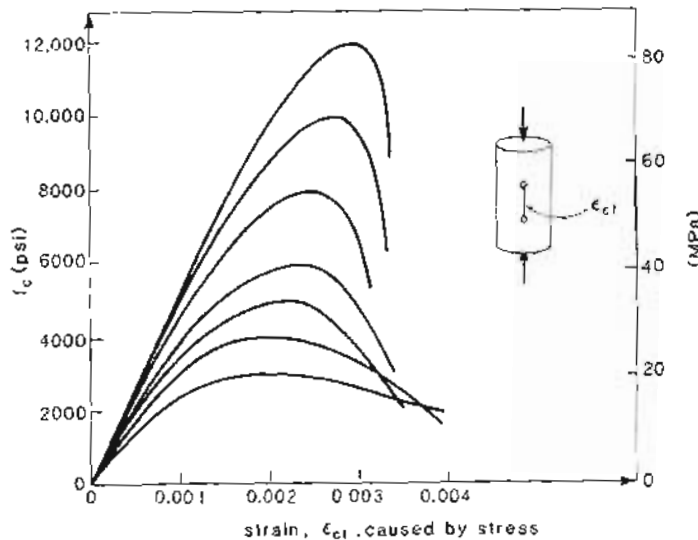


Figure 3-4 Typical compressive stress-strain curves. Adapted from Nilson (Ref. 3-6).

ϵ'_c = strain when f'_c reaches f'_c

n = curve-fitting factor equal to $E_c/(E_c - E'_c)$

E_c = tangent stiffness when ϵ_{cf} equals zero

$E'_c = f'_c/\epsilon'_c$

k = factor to increase the postpeak decay in stress, taken as 1.0 for $(\epsilon_{cf}/\epsilon'_c)$ less than 1.0 and as a number greater than 1.0 for $(\epsilon_{cf}/\epsilon'_c)$ greater than 1.0

In order to use Eq. (3-1) to predict the relationship between ϵ_{cf} and f'_c , four constants are required (e.g., f'_c , ϵ'_c , E_c , and k). These four constants can be derived directly if the actual stress-strain curve has been determined experimentally. However, in many design situations only the compressive strength, f'_c , is known and it is then necessary to estimate the other three parameters.

The initial tangent stiffness of the concrete, E_c , lies between the stiffness of the aggregate and the stiffness of the paste (see Fig. 3-3). Its value can be estimated from these stiffnesses using composite material modeling laws (e.g., Mills and Ono, Ref. 3-9). If only the strength and the unit weight of the concrete are known, E_c , can be estimated from the equation recommended by the ACI Code (Ref. 3-10), which is based on the work of Pauw (Ref. 3-11). That is,

$$E_c = w_c^{1.5} 33 \sqrt{f'_c} \quad \text{lb/in}^2 \text{ and psi} \quad (3-2)$$

$$E_c = w_c^{1.5} 0.043 \sqrt{f'_c} \quad \text{kg/m}^3 \text{ and MPa}$$

Table 3-3 Compressive stress-strain coefficients for normal-weight concrete.

f'_c psi (MPa)	3000 (20.7)	3500 (24.1)	4000 (27.6)	5000 (34.5)	6000 (41.4)	8000 (55.2)	10,000 (69.0)	12,000 (82.7)	16,000 (110.3)
E_c ksi (MPa)	3191 (22,000)	3366 (23,200)	3530 (24,300)	3828 (26,400)	4098 (28,300)	4578 (31,600)	5000 (34,500)	5382 (37,100)	6060 (41,800)
$\epsilon'_c \times 1000$	1.88	1.91	1.94	2.03	2.13	2.33	2.53	2.71	3.07
n	2.00	2.20	2.40	2.80	3.20	4.00	4.80	5.60	7.20
k	1.00	1.06	1.11	1.23	1.34	1.56	1.78	2.00	2.45

where w_c is the unit weight of concrete.

Equation (3-2) was derived to represent the slope of a line passing through the stress-strain curve at $0.4/\epsilon'_c$. However, for the concrete strengths used in prestressed concrete, the difference between this secant modulus and the initial tangent modulus is negligible. For normal-weight concretes Eq. (3-2) gives a value of $57,000 \sqrt{f'_c}$ psi ($4,730 \sqrt{f'_c}$ MPa) for E_c .

It has been pointed out by Carrasquillo, Nilson, and Slatte (Ref. 3-12) that Eq. (3-2) overestimates the stiffness of concretes with strengths greater than 6000 psi (41 MPa). They recommend that the stiffness of normal-weight concrete be calculated as

$$E_c = 40,000 \sqrt{f'_c} + 1,000,000 \quad \text{psi} \quad (3-3)$$

$$E_c = 3320 \sqrt{f'_c} + 6900 \quad \text{MPa}$$

For normal-weight concretes we will use Eq. (3-3) to estimate E_c . To use Eq. (3-1), two more constants remain to be determined. Popovics (Ref. 3-7) noted that the E_c/E'_c ratio, which determines n , varies from about 4 for low-strength concretes (f'_c about 1000 psi or 7 MPa) to about 1.3 for high-strength concretes (f'_c about 10,000 psi or 70 MPa). A suitable expression for n for normal-weight concrete is

$$n = 0.8 + \frac{f'_c}{2500} \quad \text{psi} \quad (3-4)$$

$$n = 0.8 + \frac{f'_c}{17} \quad \text{MPa}$$

Knowing n , f'_c , and E_c , the term ϵ'_c can be calculated from

$$\epsilon'_c = \frac{f'_c}{E_c} \frac{n}{n-1} \quad (3-5)$$

The decay factor, k , increases with increasing concrete strength going from about 1.0 at f'_c equal to or less than 3000 psi (21 MPa) to about 2.0 at f'_c equal to 12,000 psi (83 MPa). A suitable expression for k is

$$k = 0.67 + \frac{f'_c}{9000} \quad \text{psi} \quad (3-6)$$

$$k = 0.67 + \frac{f'_c}{62} \quad \text{MPa}$$

However, k must not be less than unity.

The values of E_c , n , ϵ'_c , and k given by Eqs. (3-3) to (3-6) are given in Table 3-3. The resulting stress-strain relationships predicted by Eq. (3-1) for a range of concrete strengths are shown in Fig. 3-5.

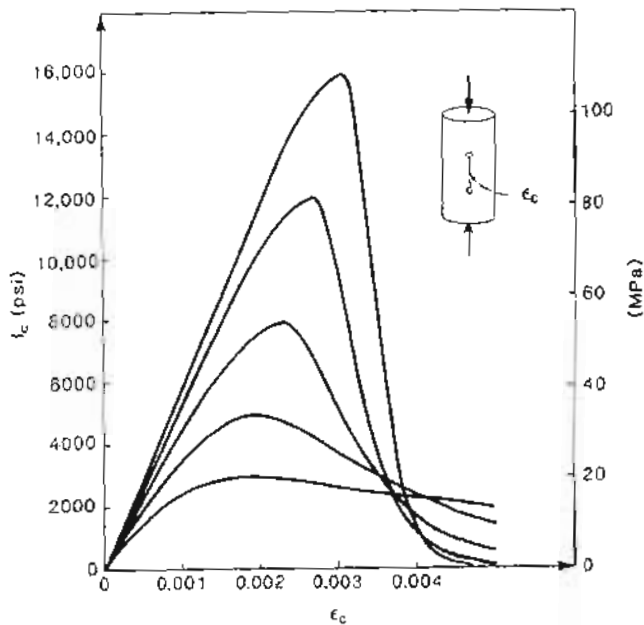


Figure 3-5 Predicted stress-strain relationships for normal-weight concretes.

For concrete strengths less than about 6000 psi (41 MPa) the stress-strain relationship can be reasonably described by a simple parabola rather than the more complex function given by Eq. (3-1). That is,

$$\frac{f_c}{f'_c} = 2 \frac{\epsilon_{cf}}{\epsilon'_c} - \left(\frac{\epsilon_{cf}}{\epsilon'_c} \right)^2 \quad (3-7)$$

Although Eq. (3-1) is a better representation of the stress-strain response, the simple parabola of Eq. (3-7) has some advantages. For example, if we wish to find the strain, ϵ_{cf} , caused by a certain stress, Eq. (3-7) can be solved to give

$$\epsilon_{cf} = \epsilon'_c \left(1 - \sqrt{1 - \frac{f_c}{f'_c}} \right) \quad (3-8)$$

Equation (3-8) is valid for the loading portion (i.e., prepeak) of the stress-strain curve. After the peak the minus sign before the radical becomes a plus. For relatively low compressive

stresses (say, $f_c < 0.6f'_c$) an even simpler stress-strain relationship can be used, namely the linear elastic relationship

$$f_c = E_c \epsilon_{cf} \quad (3-9)$$

3.4 CYCLIC LOADING OF CONCRETE

If the concrete is unloaded prior to reaching its peak stress, the unloading response will be approximately linear, with a slope equal to about E_{cl} (line AB in Fig. 3-6). Upon reloading, the stress-strain response will approximately follow the unloading line until the original curve is rejoined at A. Unloading after the peak results in unloading and reloading "lines" which are less stiff and demonstrate more pronounced hysteresis. The envelope curve to the cyclic loading response is typically almost identical to the stress-strain curve obtained from a single continuous load application (Ref. 3-13).

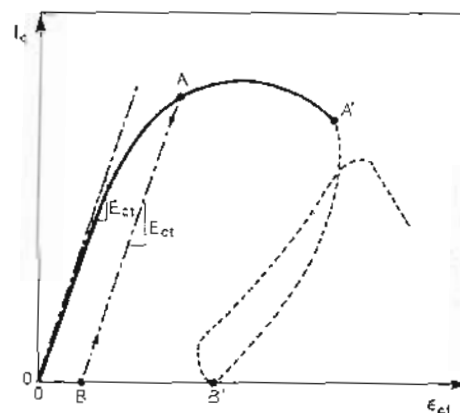


Figure 3-6 Cyclic loading response of concrete.

Concrete has a very substantial ability to resist many cycles of repeated loading. Consequently, the fatigue resistance of prestressed concrete structures will typically be governed by the fatigue of the reinforcement rather than the fatigue of the concrete.

The possibility of concrete fatigue can be checked from the Goodman-Johnson diagram shown in Fig. 3-7, which comes from the work of Warner (Refs. 3-14 and 3-15). It can be seen from this diagram that concrete can be cycled from zero stress to 60% of f'_c for about 1 million cycles before failure occurs. Notice that the stress range ($f_{c,max} - f_{c,min}$) required to cause failure decreases as $f_{c,min}$ increases.

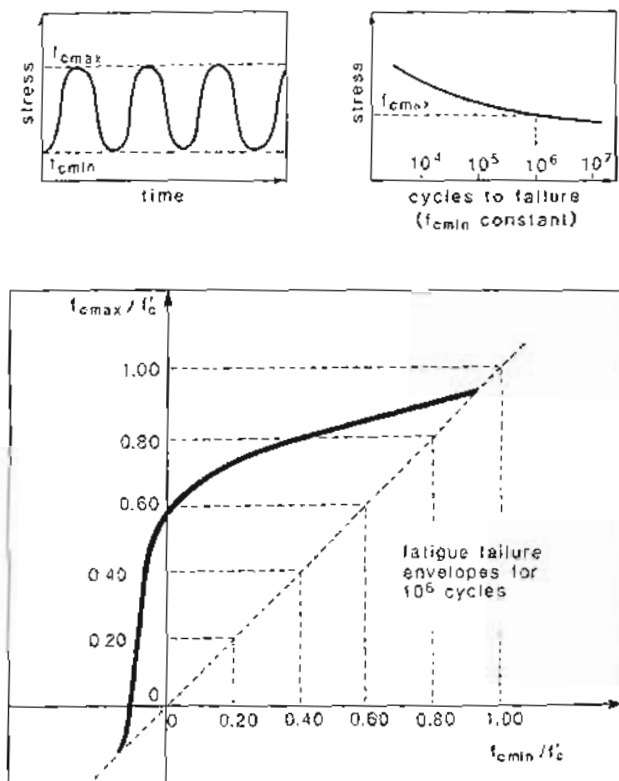


Figure 3-7 Fatigue resistance of concrete. From Warner and Faulkes (Ref. 3-15).

3.5 INFLUENCE OF RATE OF LOADING AND CONCRETE STRENGTH

If three cylinders that had all been cast from the same batch of concrete were allowed to mature for, say, one year and then were loaded at three very different loading rates, the observed stress-strain responses would be as shown in Fig. 3-8. That is, fast loading increases the strength by about 20%, while slow loading reduces the strength by about 20% (see Ref. 3-16).

In design we usually neglect the decrease in strength caused by long-term loading. However, we also typically neglect the gain in concrete strength that occurs with time and base our designs on the 28-day strength of the concrete. As the concrete will typically gain 20 to 40% in strength due to the hydration that occurs after 28 days, these two assumptions together make a conservative set.

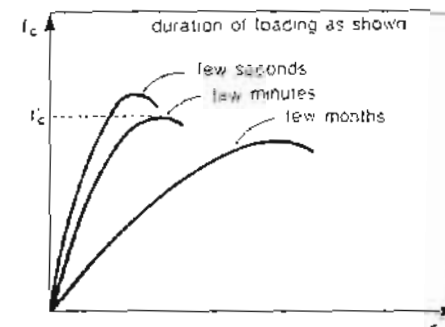


Figure 3-8 Influence of loading rate.

3.6 CREEP OF CONCRETE

The stress-strain response of concrete depends upon the rate of loading and the time history of loading. If the stress is held constant for some length of time, the strain increases—a phenomenon referred to as creep. If the strain is held constant for some length of time, the stress will decrease—a phenomenon referred to as relaxation (see Fig. 3-9).

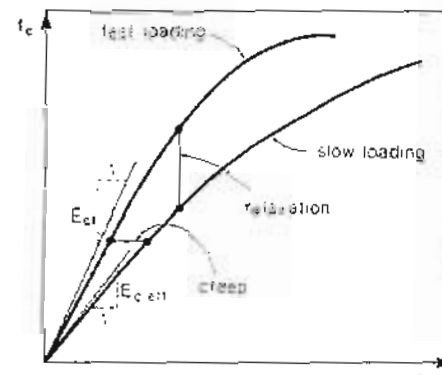


Figure 3-9 Creep of concrete.

We will account for creep by using a reduced initial stiffness, $E_{cl,eff}$, to define the stress-strain curve. That is, the strain, ϵ_c , at which the stress peaks will be increased when dealing with long-term loads (see Fig. 3-10).

The amount of creep that a particular concrete will exhibit is difficult to estimate accurately unless tests are conducted to determine the creep characteristics. Without specific tests, accuracies of better than $\pm 30\%$ should not be expected. In view of this scatter it is reasonable to use simple, approximate procedures for estimating creep deformations.

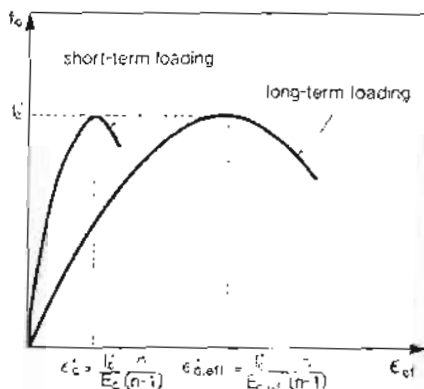


Figure 3-10 Short-term and long-term stress-strain curves.

In a typical creep experiment, a stress is applied to the concrete some days after the concrete has been cast (t_i , days) and is then held constant over time. The strain that occurs upon initial loading is called the "elastic strain" while the additional strain that develops with time is called "creep strain" (see Fig. 3-11). The ratio of creep strain to elastic strain t days after casting for concrete loaded t_i days after casting is called the creep coefficient, $\phi(t, t_i)$.

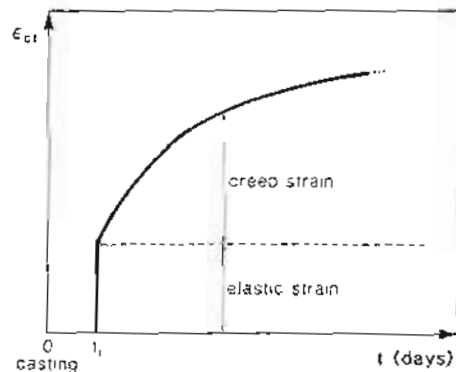


Figure 3-11 Development of creep with time.

In lieu of data for the specific concrete, the following simplified expression for the creep coefficient, which is based on the data published in Refs. 3-17 to 3-21 and Ref. 3-6, may be used:

$$\phi(t, t_i) = 3.5 k_c k_f \left(1.58 - \frac{H}{120} \right) t_i^{-0.118} \frac{(t - t_i)^{0.6}}{10 + (t - t_i)^{0.6}} \quad (3-10)$$

Sec. 3.6 Creep of Concrete

where H is the relative humidity in percent, k_c is a factor that accounts for the influence of the volume-to-surface ratio of the member, and k_f is a factor accounting for the influence of concrete strength. Values of k_c are given in Fig. 3-12. The factor k_f accounts for the lower creep of high-strength concrete and is given in Eq. (3-11), where f'_c is the 28-day compressive strength of the concrete.

$$k_f = \frac{1}{0.67 + (f'_c/9\,000)} \quad \text{psi} \quad (3-11)$$

$$k_f = \frac{1}{0.67 + (f'_c/62)} \quad \text{MPa}$$

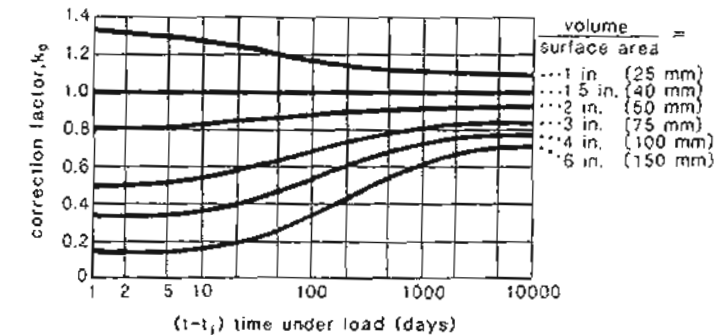


Figure 3-12 Correction factor for volume/surface ratio, based on data given in Refs. 3-20 and 3-21.

In determining the age of concrete at initial loading, t_i , for use in Eq. (3-10), one day of accelerated curing can be regarded as adding 7 days to the age of concrete.

To calculate $E_{c,eff}$, the following equation may be used:

$$E_{c,eff} = \frac{E_{ci}}{1 + \phi(t, t_i)} \quad (3-12)$$

where $E_{ci} = E_c$ at time t_i .

To calculate the strain at t days after casting, caused by a stress of f_c , applied t_i days after casting and then held constant, we could use the following linear approximation:

$$\epsilon_{cf}(t, t_i) = \frac{f_{ci}}{E_{c,eff}} \quad (3-13)$$

If, rather than remaining constant, the stress varies gradually with time (see Fig. 3-13), then the strain at t days after casting, when the initial stress f_{ci} is applied t_i days after

Table 3-4 Values of coefficient, χ .

$t - t_i$ days	$\phi(\text{sec. 7})$	t_i , days		
		10	100	1000
10	1.5	0.720	0.826	0.825
	2.5	0.774	0.843	0.837
	3.5	0.806	0.856	0.848
100	1.5	0.739	0.919	0.932
	2.5	0.804	0.935	0.943
	3.5	0.839	0.948	0.951
1000	1.5	0.732	0.943	0.981
	2.5	0.795	0.956	0.983
	3.5	0.830	0.964	0.981
10,000	1.5	0.717	0.934	0.983
	2.5	0.781	0.949	0.986
	3.5	0.818	0.958	0.989

casting can be expressed as

$$\epsilon_{cf}(t, t_i) = \frac{f_c}{E_{c,adj}} + \frac{\Delta f_c}{E_{c,adj}} \quad (3-14)$$

where Δf_c is the change in stress between t_i and t . The adjusted effective modulus, $E_{c,adj}$, is

$$E_{c,adj} = \frac{E_c}{1 + \chi \phi(t, t_i)} \quad (3-15)$$

The factor χ , called the relaxation coefficient by Trost (Ref. 3-22), accounts for the reduction in creep that occurs because not all of the stress is applied at the initial time, t_i .

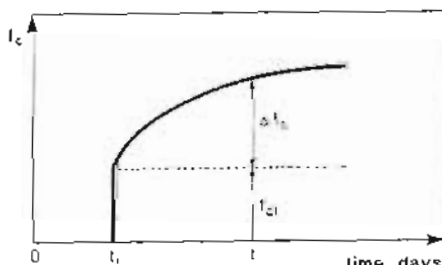


Figure 3-13 Variation of stress with time.

In most situations, χ can be taken as 0.8. The factor χ has been determined more precisely by Bazant (Ref. 3-23). Table 3-4 gives some of Bazant's values.

3.7 EXAMPLE CALCULATION OF CREEP STRAIN

The plain concrete prism shown in Fig. 3-14 was subjected to a compressive stress of 2000 psi (13.8 MPa) 10 days after casting the concrete, at which time the concrete strength was 5000 psi (34.5 MPa). The prism had been steam-cured for 1 day. Estimate the initial strain caused by the stress and the magnitude of this strain after the prism has been loaded for 100 days in an environment where the relative humidity was 70%. As the concrete strength at the time of first loading was 5000 psi (34.5 MPa), then from Table 3-3, $E_c = 3828 \text{ ksi}$ (26 400 MPa) and $c'_c = 2.03 \times 10^{-3}$.

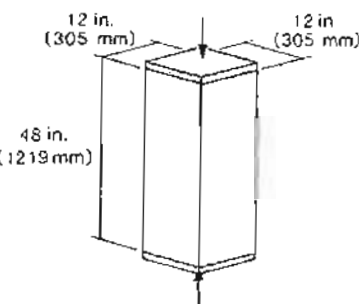


Figure 3-14 Concrete prism subjected to compression.

For a compressive stress of 2000 psi (13.8 MPa), the linear approximation of Eq. (3-9) would predict an initial compressive strain of

$$\epsilon_{cf} = \frac{2}{3828} = 0.52 \times 10^{-3}$$

while Eq. (3-1) can be solved by trial and error to give

$$\epsilon_{cf} = 0.53 \times 10^{-3}$$

To estimate the long-term strain we need to first calculate the creep coefficient. For this calculation we need the volume/surface area ratio for the prism. In determining this ratio, only that portion of the surface area which is exposed to the environment is counted. Thus,

$$\frac{\text{volume}}{\text{surface area}} = \frac{12 \times 12 \times 48}{4 \times 12 \times 48} = 3 \text{ in. (76 mm)}$$

Hence from Fig. 3-12, the correction factor for shape and size, k_c , is 0.68 while from Eq. (3-11), the correction factor for concrete strength, k_f , is 0.82.

The creep coefficient given by Eq. (3-10), with an effective age at initial loading of $7 + 9 = 16$ days, is

$$\phi(116, 16) = 3.5 \times 0.68 \times 0.82 \left(1.58 - \frac{70}{120} \right) \times 16^{-0.018} \frac{100^{0.6}}{10 + 100^{0.6}} = 0.86$$

The effective stiffness, $E_{c,eff}$, from Eq. (3-12), is

$$E_{c,eff} = \frac{3828}{1 + 0.86} = 2058 \text{ ksi (14 200 MPa)}$$

From Fig. 3-10 it can be seen that the stress-strain relationship, which includes the creep deformations, would peak at a compressive strain of

$$\epsilon'_{c,eff} = 2.03 \times 10^{-3} \times \frac{3828}{2058} = 3.78 \times 10^{-3}$$

If the approximate linear expression of Eq. (3-13) were used, then

$$\epsilon_{cf}(116, 16) = \frac{2}{2058} = 0.97 \times 10^{-3}$$

whereas if the more accurate Eq. (3-1) were employed, the predicted compressive strain would be

$$\epsilon_{cf}(116, 16) = 0.98 \times 10^{-3}$$

3.8 CONCRETE IN UNIAXIAL TENSION

The stress-strain response of concrete in uniaxial tension is nearly linear up to cracking, which occurs at a relatively low stress. With a stiff testing machine it is possible to detect post-cracking tensile resistance at very small crack widths (see Fig. 3-15).

In trying to understand how tensile stresses can be transmitted across a crack it is important to recognize that the crack surfaces are locally very rough and that the crack widths are extremely small in comparison to the irregularities on the surfaces of the crack. The jamming of the rough surfaces of the crack still makes it possible to transmit some tension for crack widths less than about 0.002 in. (0.05 mm).

Because it is difficult to test concrete in pure axial tension (see Fig. 3-16a), the cracking strength is usually determined from an indirect test. Typically, either the modulus of rupture, f_r , is determined from a bending test (see Fig. 3-16b), or the splitting strength, f_{sp} , is determined by splitting a concrete cylinder with a line load as shown in Fig. 3-16c. The double-punch test (see Fig. 3-16d) is one more indirect test method for determining concrete cracking strength.

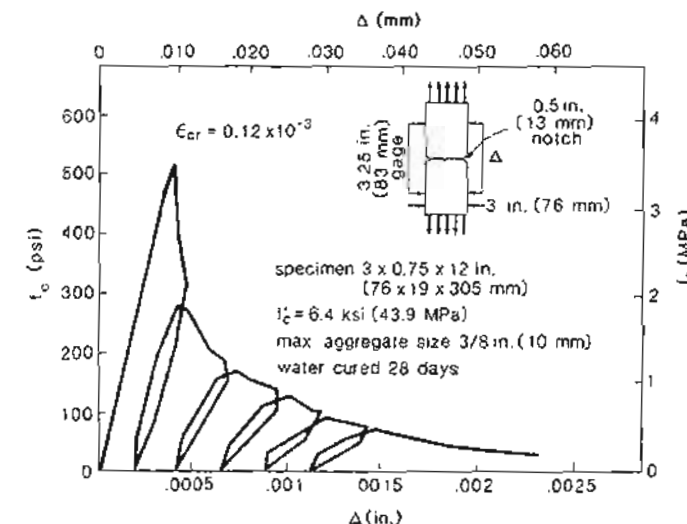


Figure 3-15 Stress-strain response of concrete in tension. Adapted from Gopalaratnam and Shah (Ref. 3-24).

The tensile stress at which concrete cracks is not constant for a particular concrete but varies with a number of parameters. Increasing the volume of concrete subjected to high tensile stress lowers the cracking stress. Hence larger members crack at lower stresses. The cracking stress is inversely proportional to about the fourth root of the size. Thus doubling the depth of a beam decreases the cracking stress by a factor of $0.5^{0.25} = 0.84$. Members with large strain gradients can resist high local tensile stresses prior to cracking. Additional factors such as the presence of restrained shrinkage stresses can greatly reduce the apparent cracking stress.

In view of the factors noted above, it is not surprising that the cracking stresses determined from the various test methods shown in Fig. 3-16 differ. Figure 3-16 gives some approximate relationships that can be used to correlate the values obtained from the different test methods.

If only the cylinder crushing strength, f'_c , of the concrete is known, then an estimate of the direct cracking strength can be made from

$$f_{cr} = 4.00\lambda \sqrt{f'_c} \quad \text{psi} \quad (3-16)$$

$$f_{cr} = 0.33\lambda \sqrt{f'_c} \quad \text{MPa}$$

where λ = factor accounting for the density of the concrete

$\lambda = 1.00$ for normal-weight concrete

$\lambda = 0.85$ for sand-lightweight concrete

$\lambda = 0.75$ for all-lightweight concrete

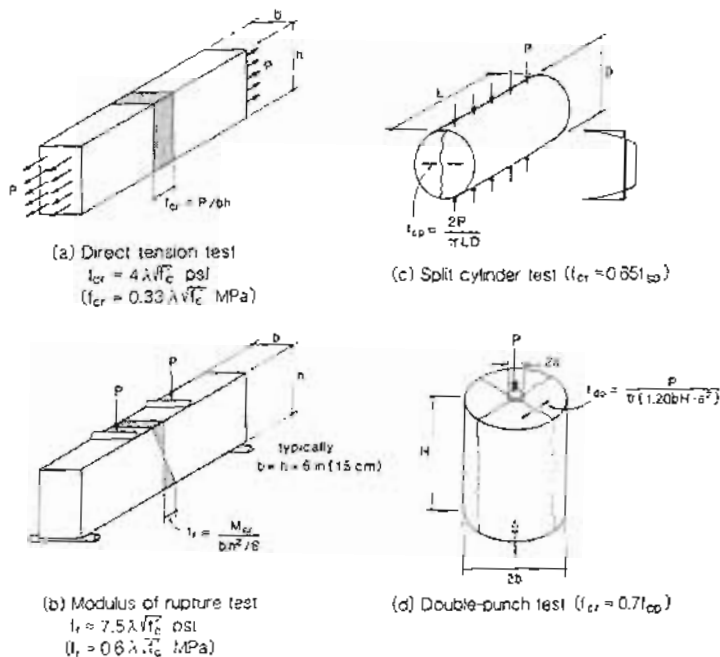


Figure 3-16 Methods of estimating cracking strength of concrete.

In estimating flexural cracking loads for typical building elements, the use of the modulus of rupture, f_r (see Fig. 3-16b) will lead to more accurate predictions. The ACI Code (Ref. 3-10) recommends the following relationship for estimating f_r :

$$\begin{aligned} f_r &= 7.5\lambda \sqrt{f'_c} \quad \text{psi} \\ f_r &= 0.63\lambda \sqrt{f'_c} \quad \text{MPa} \end{aligned} \quad (3-17)$$

The stress-strain response of concrete in tension can be assumed to be linear prior to cracking. That is,

$$f_c = E_c \epsilon_{cf} \quad (3-18)$$

3.9 SHRINKAGE OF CONCRETE

Unless kept under water or in air at 100% relative humidity, concrete loses moisture with time and decreases in volume, a process known as shrinkage. The amount of shrinkage

depends strongly upon the composition of the concrete, with the total amount of water in the mix being especially important. This can be seen in Fig. 3-17. The quality of the aggregate is also important with hard, dense, stiff aggregates of low absorption (e.g., hard limestone or granite), resulting in less shrinkage.

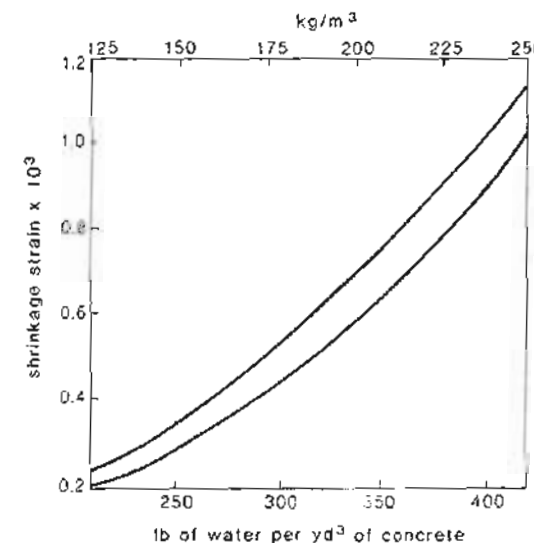


Figure 3-17 Influence of amount of water on shrinkage. Adapted from Blanks (Ref. 3-25).

In lieu of specific information on the shrinkage properties of the concrete, the following approximate expressions for shrinkage can be used. These expressions are based on the information in Refs. 3-17 to 3-21. For moist-cured concrete,

$$\epsilon_{sh} = -k_s k_h \left(\frac{t}{35+t} \right) 0.51 \times 10^{-3} \quad (3-19)$$

For steam-cured concrete,

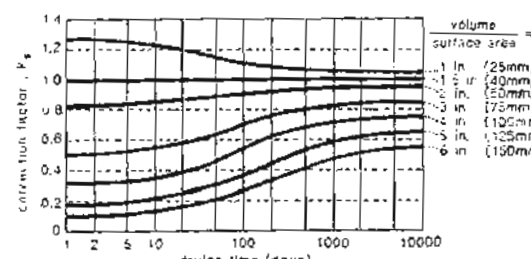
$$\epsilon_{sh} = -k_s k_h \left(\frac{t}{55+t} \right) 0.56 \times 10^{-3} \quad (3-20)$$

where t is the time in days that the concrete has been exposed to drying. If the moist-cured concrete is exposed to drying before 5 days of curing, the shrinkage from Eq. (3-19) should be increased by about 20%.

The two factors k_s and k_h , which account for size and relative humidity, are given in Fig. 3-18. Note that the relative humidity in the interior of buildings will typically be lower than the ambient humidity.



(a) Annual average ambient relative humidity

(b) Factor k_s

Avg. ambient rel. hum.	k_s
40 %	1.43
50 %	1.29
60 %	1.14
70 %	1.00
80 %	0.86
90 %	0.43
100 %	0.00

(c) Factor k_s

Figure 3-18 Correction factors for relative humidity, based on data given in Ref. 3-20.

3.10 THERMAL PROPERTIES OF CONCRETE

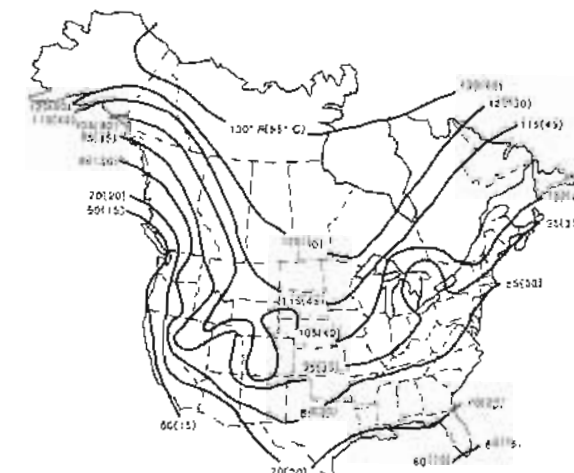
Like most materials, concrete expands when it is heated and contracts when it is cooled. The thermal strain, ϵ_{cth} , is given by

$$\epsilon_{cth} = \alpha_c \Delta T \quad (3-21)$$

Sec. 3.10 Thermal Properties of Concrete

where the coefficient of thermal expansion, α_c , depends strongly on the aggregate type. Typical values for moist-cured concrete are given in Fig. 3-19. These values are from Ref. 3-26.

type of aggregate	$\alpha_c (10^{-6}/^{\circ}\text{F})$	$(10^{-6}/^{\circ}\text{C})$
basalt	5.9	(9.5)
silicate	4.7	(8.5)
foamed slag	9.0	(19)
granite	5.0	(8)
gravel	6.7	(12)
limestone	3.2	(6)
Portland stone	3.3	(6)
slate	3.9	(7)
quartzite	7.2	(13)
sandstone	5.8	(10)

(d) Coefficient of thermal expansion, α_c 

(b) Maximum seasonal climatic temperature change

Figure 3-19 Information for determining thermal strains. From Refs. 3-20 and 3-26.

The value of α_c stays reasonably constant over a wide range of temperatures, although by the time the temperature reaches 900°F (500°C), there is usually an increase of about 50% in α_c . If the aggregate type is not known, it is customary to use $6 \times 10^{-6}/^{\circ}\text{F}$ ($10 \times 10^{-6}/^{\circ}\text{C}$) for α_c . The most common cause of temperature change is the climate.

The map shown in Fig. 3-19 can be used to estimate likely values of ΔT . If the concrete is in a heated building, the ΔT from the map can be reduced by 50% (see Ref. 3-20).

Concrete is also heated during the hydration process (it is an exothermic reaction) and for thick concrete members, temperature rises of up to 110°F (60°C) have been observed. The heat generated during the first 7 days of hydration varies from about 200 joules/gram for type IV cement to 500 joules/gram for type III cement. For the typically rather thin sections used in prestressed concrete structures, the high surface area-to-volume ratio usually dissipates the heat released by hydration fast enough to avoid large temperature increases.

In some accident situations such as fire or loss of coolant in a nuclear power plant, concrete may be subjected to very significant temperature increases. Once again the response will be highly dependent upon the aggregate type.

Significant reduction in concrete strength can occur for temperatures in excess of 750°F (400°C). Significant reductions in stiffness can occur for temperatures in excess of 212°F (100°C), with E_r at 750°F (400°C) being about one-third of the 70°F (20°C) value (see Fig. 3-20). Creep and shrinkage are both significantly increased by high temperatures, with the creep at 140°F (60°C) being about three times greater than that at 70°F (20°C).

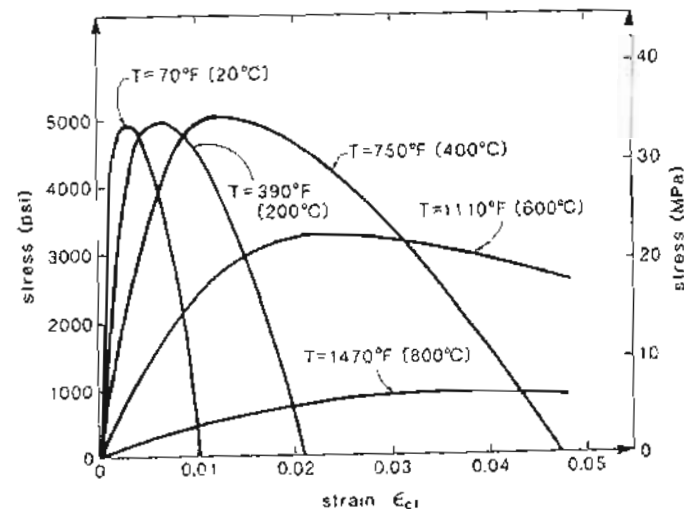


Figure 3-20 Strength reduction at high temperatures. Adapted from Lie, Rowe, and Lin (Ref. 3-27).

In cases where it is desired to conduct a heat flow analysis, it is necessary to know the conductivity and the specific heat of the concrete. Both parameters depend strongly on the aggregate type. Values for conductivity usually lie between 1 and 2.6 W/(m·°C), while specific heat usually varies between 800 and 1200 J/kg·°C.

3.11 WEIGHT OF CONCRETE

Depending primarily on the density of the aggregate, normal-density plain concrete has a density of between 135 and 170 lb/ft³ (2150 and 2700 kg/m³). A typical value for normal-weight plain concrete is 145 lb/ft³ (2400 kg/m³ or 23.5 kN/m³).

As steel weighs about 490 lb/ft³ (77 kN/m³), the weight per unit volume of a prestressed concrete element depends upon the percentage of reinforcement (see Table 3-5). For elements containing the usual amount of reinforcement, an assumed weight of 150 lb/ft³ (24 kN/m³) is reasonable. To reduce the weight of concrete, aggregates having a porous structure (lightweight aggregates) are sometimes used. Expanded shale, which is produced by firing shale in a rotary kiln, is one such aggregate. Concrete made with lightweight aggregates is not as stiff as normal-density concrete [see Eq. (3-2)].

Table 3-5 Weight of reinforced concrete.

Volumetric reinforcement ratio, %	0	1	2	3	4
Weight per unit volume, lb/ft ³	145	148	152	155	159
kN/m ³	(23.5)	(24.0)	(24.6)	(25.1)	(25.6)

Because the aggregate is relatively weak in comparison to the cement paste, cracks in low-density concrete tend to pass through the aggregate. These relatively "smooth-faced" cracks will form at somewhat lower tensile stresses and will propagate more easily than cracks in normal-density concrete [see Eqs. (3-16) and (3-17)].

3.12 STRESS-STRAIN RESPONSE OF CONFINED CONCRETE

In a classic study at the University of Illinois, Richart, Brandzaeg, and Brown (Ref. 3-28) found that lateral confining pressures greatly increased the strength and stiffness of concrete cylinders and dramatically increased the strain at which the peak stress was reached (see Fig. 3-21). Based on this work, it was suggested that the peak compressive strength for confined concrete, $f'_{c,con}$, be taken as

$$f'_{c,con} = f'_c + 4.1 f_{cer} \quad (3-22)$$

where f_{cer} is the confining pressure.

Later tests (Ref. 3-25) showed that Eq. (3-22) overestimated the strength gain for very high confining pressures, and underestimated the gain for lower confining pressures. Confined concrete strengths as high as 80 ksi (550 MPa) are reported in Ref. 3-25.

The very large increase in energy-absorbing capacity (i.e., the area under the stress-strain curve) provided by even small confining pressure is useful in increasing the ductility of reinforced concrete. Thus in seismic regions, appropriately detailed transverse reinforcement is provided to confine the concrete and hence increase the ductility of columns and beams (see Refs. 3-29 and 3-30).

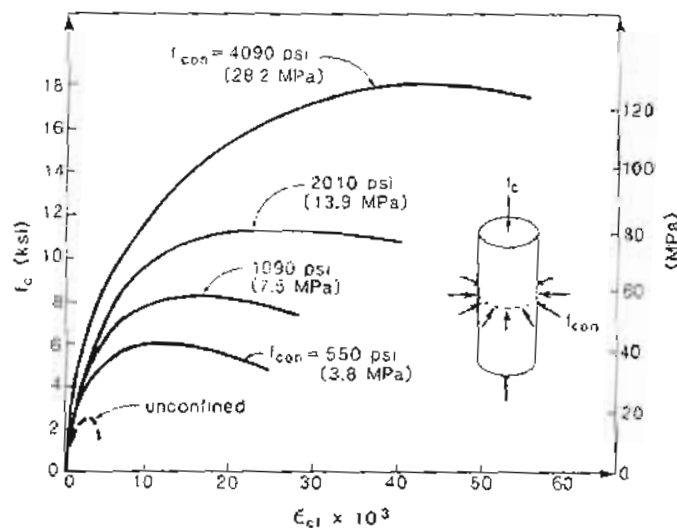


Figure 3-21 Effect of lateral confining pressure on stress-strain response.
Adapted from Richart, Brandlzaeg, and Brown (Ref. 3-28).

3.13 TYPES OF REINFORCEMENT

Prestressed concrete structures can be reinforced with prestressing tendons, deformed reinforcing bars, and welded wire fabric. As discussed in Chapter 2, prestressing tendons consist of strands, wires, or high-strength bars (see Fig. 2-1). The properties of standard prestressing strands, wires, and bars conforming to ASTM Standards A416 (Ref. 3-31), A421 (Ref. 3-32), and A722 (Ref. 3-33), or to CSA Standard G279 (Ref. 3-34), are given in Table 3-6. The required characteristics of prestressing tendons as specified by the ASTM Standards are summarized in Table 3-7.

The most commonly used type of prestressing steel is seven-wire strand. The process used in manufacturing seven-wire strand is summarized in Fig. 3-22. As can be seen, two different types of strand are produced: stress-relieved strand and low-relaxation strand. The cold-drawing and stranding operations result in significant residual stresses in the strand. These residual stresses cause the stress-strain response of the strand to be very rounded (see Fig. 3-23). Stress relieving removes residual stresses and results in a strand with a much higher proportional limit. Strain tempering is even more effective in improving the stress-strain characteristics and has the additional advantage of substantially reducing the time-dependent losses due to relaxation of the strand.

Table 3-6 Standard prestressing strands, wires, and bars.

(a) Common types from PCI Design Handbook (Ref. 3-20)

Tendon Type	Grade f_{pu} ksi	Nominal Dimension		Weight plf
		Diameter in.	Area in. ²	
Seven-wire strand	250	1/4	0.036	0.12
	270	5/8	0.085	0.29
	250	3/8	0.060	0.27
	270	1/2	0.153	0.53
	250	1/2	0.144	0.49
	270	0.6	0.215	0.74
Prestressing wire	250	0.196	0.0302	0.10
	240	0.250	0.0491	0.17
	235	0.276	0.0598	0.20
Deformed prestressing bars	157	5/8	0.28	0.98
	150	1	0.85	3.01
	130	1 1/4	1.25	4.39
	130	1 3/8	1.58	5.56

(b) Common types from CPC Metric Design Manual (Ref. 3-21)

Tendon Type	Grade f_{pu} MPa	Size Design ration	Nominal Dimension		Mass kg/m
			Diameter mm	Area mm ²	
Seven-wire strand	1860	9	9.13	55	0.432
	1860	11	11.13	74	0.582
	1860	13	12.70	99	0.775
	1860	15	15.24	140	1.109
	1760	16	15.47	148	1.173
	1550	5*	5.00	19.6	0.154
Prestressing wire	1720	5	5.00	19.6	0.154
	1620	7	7.00	38.5	0.302
	1760	7	7.00	38.5	0.302
Deformed prestressing bars	1080	15	15.0	177	1.44
	1030	26	26.5	551	4.48
	1100†	26	26.5	551	4.48
	1030	32	32.0	804	6.53
	1100†	32	32.0	804	6.53
	1030	36	36.0	1018	8.27

* Available with surface indentation.

† Available on special order.

Table 3-7 Requirements for prestressing tendons specified by ASTM (Refs. 3-31 to 3-33).

Tendon Type	Minimum Tensile Strength	Minimum "Yield" Strength	Minimum Elongation at Rupture	Gage Length
	ksi	ksi		
0.5 and 0.6 in. stress-relieved strand	270	230	3.5	24 in.
0.5 and 0.6 in. low-relaxation strand	270	245	3.5	24 in.
.276 in. wire	235	200	4.0	10 in.
1, 1 1/4, and 1 3/8 in. deformed prestressing bar	150	120	4.0	20 d_b [†]

* Yield strength taken as the stress at an elongation of 1.0% for strand and wire and as the 0.2% offset stress for bars.

[†] d_b , nominal diameter of reinforcing bar

In North America the most frequently used type of deformed reinforcing bars has a specified yield stress of 60 ksi (400 MPa), and conforms to ASTM Standard A615 (Ref. 3-35) or to CSA Standard G30.12 (Ref. 3-36). These standards are of a performance type and do not control the chemical composition of the bars, which can thus vary widely. Bars manufactured to conform to ASTM Standard A706 (Ref. 3-37) or to CSA Standard G30.16 (Ref. 3-38) on the other hand, have a controlled chemical composition (they are weldable), which results in a more predictable and a more ductile stress-strain response. Geometric properties of standard reinforcing bars are summarized in Table 3-8. The requirements for reinforcing bars specified by ASTM Standards A615 and A706 are compared in Table 3-9.

Welded wire fabric (WWF) consists of a grid of cold-drawn wires welded together at their intersections. The wires may be either smooth or deformed and are fused together at their intersections by automatic, electrical-resistance welding. Welded wire fabric used in North America conforms to ASTM Standards A185 and A497 (Refs. 3-39 and 3-40) or to CSA Standards G30.5 and G30.15 (Refs. 3-41 and 3-42). Table 3-10 illustrates the industry method of designating welded wire fabric and lists some common stock styles.

It is important for the designer to recognize that the ASTM and CSA Standards do not currently require that welded wire fabric be stress-relieved after fabrication, as is required in some European standards. Non-stress-relieved welded wire fabric, particularly for the smaller wire sizes, may fail near the welded intersections at relatively small strains (see Fig. 3-24) and hence such reinforcement may not be suitable where significant ductility is required.

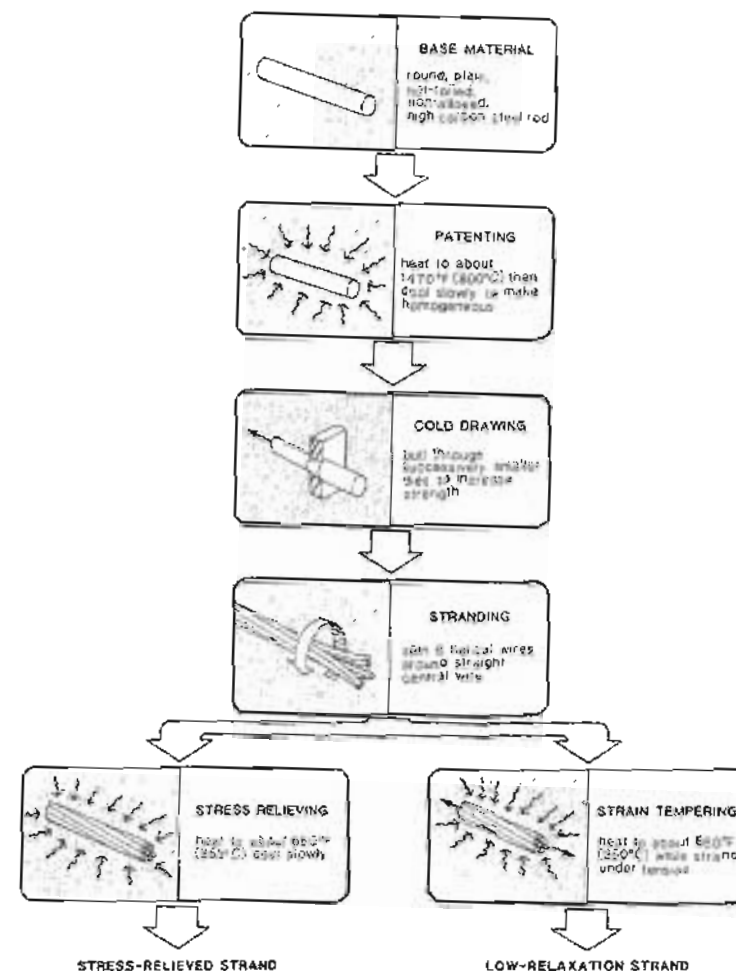


Figure 3-22 Production of seven-wire strand.

Table 3-8 Geometric properties of deformed reinforcing bars.

(a) ASTM standard reinforcing bars

Bar Size	Nominal Diameter in.	Nominal Area in. ²	Weight plf
#3	0.373	0.11	0.376
#4	0.500	0.20	0.668
#5	0.625	0.31	1.043
#6	0.750	0.44	1.502
#7	0.875	0.60	2.044
#8	1.000	0.79	2.670
#9	1.128	1.00	3.400
#10	1.270	1.27	4.303
#11	1.410	1.56	5.313
#14	1.693	2.25	7.650
#18	2.257	4.00	13.600

(b) CSA standard reinforcing bars

Bar No.	Nominal Diameter mm	Nominal Area mm ²	Mass kg/m
10	11.3	100	0.785
15	16.0	200	1.570
20	19.5	300	2.355
25	25.2	500	3.925
30	29.9	700	5.495
35	35.7	1000	7.850
45	43.7	1500	11.775
55	56.4	2500	19.625

Table 3-9 ASTM requirements for reinforcing bars *

	A615		A706
	Grade 40	Grade 60	
Minimum yield, ksi	40	60	60
Maximum yield, ksi	—	—	78
Minimum ultimate, ksi	70	90	80 $\times 1.25/\gamma_e$
Minimum elongation in 8 in. gage length, %			
# 3	11	9	14
# 4, 5, 6	12	9	14
# 7, 8	—	8	12
# 9, 10, 11	—	7	12
# 14, 18	—	7	10
Pin diameter for 180° bond test			
# 3, 4, 5	3.5d _b	3.5d _b	3d _b
# 6	5d _b	5d _b	4d _b
# 7, 8	—	5d _b	4d _b
# 9, 10, 11	—	7d _b	6d _b
# 14, 18	—	9d _b	8d _b

* f_y , yield stress; d_b , nominal diameter of reinforcing bar.

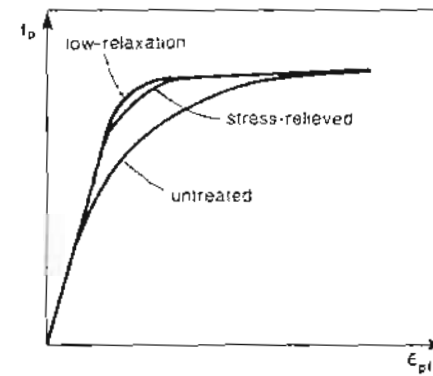


Figure 3-23 Improvement of stress-strain response of seven-wire strand.

Table 3-10 Typical types of welded wire fabric.

Designation*	Wire Diameter in.	Wire Area in. ²	Cross-Sectional Steel Area per Foot Width		Approximate Weight lb/ft ²
			Long. in. ²	Transv. in. ²	
6x6-W1.4xW1.4	0.135	0.014	0.029	0.029	0.21
6x6-W2.1xW2.1	0.162	0.021	0.041	0.041	0.30
6x6-W2.9xW2.9	0.192	0.029	0.058	0.058	0.42
6x6-W4.0xW4.0	0.225	0.040	0.080	0.080	0.58
6x6-W5.5xW5.5	0.264	0.055	0.110	0.110	0.80
4x4-W1.4xW1.4	0.135	0.014	0.043	0.043	0.31
4x4-W2.1xW2.1	0.162	0.021	0.062	0.062	0.44
4x4-W2.9xW2.9	0.192	0.029	0.087	0.087	0.62
4x4-W4.0xW4.0	0.225	0.040	0.120	0.120	0.85
4x4-W4.7xW4.7	0.244	0.047	0.141	0.141	1.02
4x4-W5.5xW5.5	0.264	0.055	0.165	0.165	1.19

*The first number is the longitudinal wire spacing and the second number is the transverse wire spacing. The third and the fourth numbers are the areas of the longitudinal and transverse wires in hundredths of a square inch, respectively.

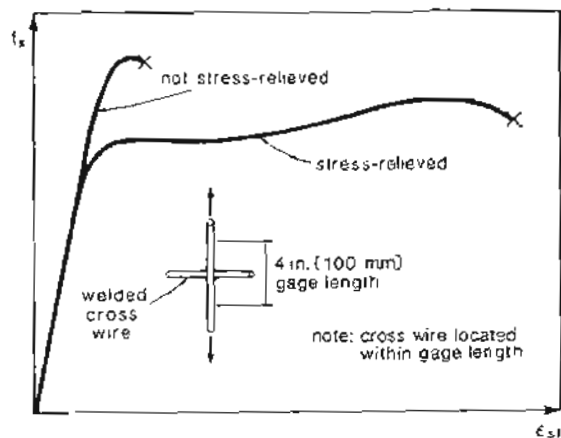


Figure 3-24 Improved ductility of stress-relieved welded wire fabric.

3.14 STRESS-STRAIN RESPONSE OF REINFORCEMENT

Figure 3-25 compares the stress-strain response of three different types of reinforcement. While all reinforcements have essentially the same initial stiffness, the strength of the steels used for prestressing is substantially greater than those used for non-prestressed reinforcement.

For non-prestressed reinforcement, the relationship between the stress in the steel, f_s , and the strain caused by this stress, ϵ_{sf} , is usually assumed to be bilinear, as shown in Fig. 3-26. That is,

$$f_s = E_s \epsilon_{sf} \leq f_y \quad (3-23)$$

The same relationship is assumed to be valid for both tension and compression. The Young's modulus of the reinforcement, E_s , can be taken as 29,000 ksi (200,000 MPa).

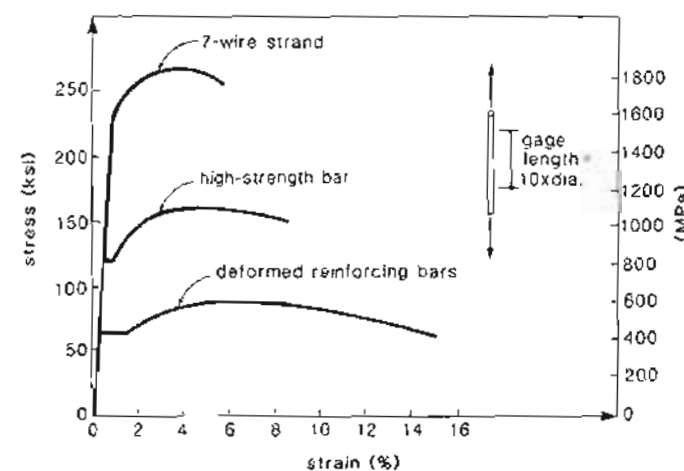


Figure 3-25 Stress-strain response of different types of reinforcements.

The stress-strain response of prestressed reinforcement can be approximated by the bilinear relationships of Eq. (3-24):

$$f_p = E_p \epsilon_{pf} \leq f_{py} \quad (3-24)$$

For strands and wire that do not exhibit a yield plateau, an equivalent "yield stress" is defined as the stress at a strain of 1% (see Fig. 3-27). The ratios of the yield stress, f_{py} , to the ultimate stress, f_{pu} , for different types of prestressing steel, are given in Table 3-11.

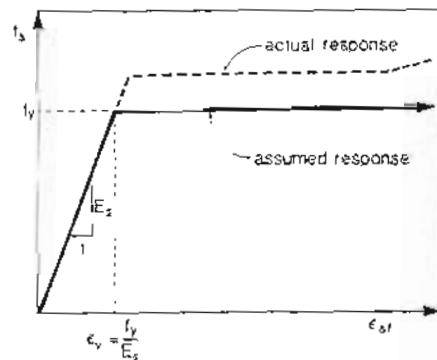


Figure 3-26 Assumed stress-strain response of non-prestressed reinforcement.

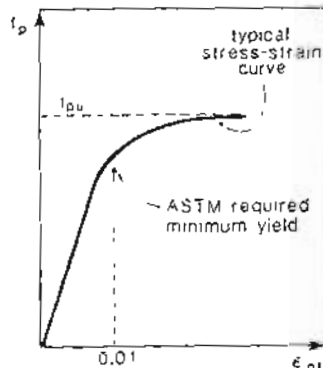


Figure 3-27 Equivalent yield stress for prestressing steel.

A more accurate representation of the stress-strain response of prestressing strand can be obtained by using the modified Ramberg-Osgood function recommended by Mattock (Ref. 3-43) and given below.

$$f_p = E_p \epsilon_{pf} \left\{ A + \frac{1-A}{\{1+(B\epsilon_{pf})^C\}^{1/C}} \right\} \leq f_{pu} \quad (3-25)$$

As can be seen from Fig. 3-28, this function, which consists of two straight lines joined by a curve, is defined by four constants. If an actual stress-strain curve for the strand in question is available, then the four coefficients for Eq. (3-25) can be found as follows:

1. Represent the actual stress-strain relationship as two straight lines connected by a curve.
2. Determine E_p from the slope of the first line.
3. Determine A from the slope of the second line. The slope is AE_p .
4. Determine B from the intersection of the second line and the f_p axis. The value of f_p at the intersection is $E_p(1-A)/B$.
5. Determine C by trial and error to give an appropriate transition curve. A high value of C gives an abrupt transition.

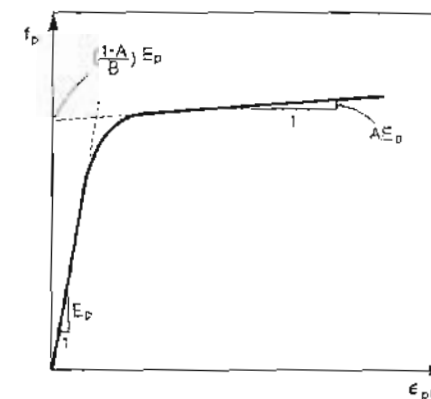


Figure 3-28 Modified Ramberg-Osgood function.

For low-relaxation strand with $f_{pu} = 270$ ksi (1860 MPa), an appropriate formulation is

$$f_p = 29 \times 10^3 \epsilon_{pf} \left\{ 0.025 + \frac{0.975}{[1 + (118\epsilon_{pf})^{10}]^{0.10}} \right\} \leq 270 \text{ ksi} \quad (3-26)$$

$$f_p = 200 \times 10^3 \epsilon_{pf} \left\{ 0.025 + \frac{0.975}{[1 + (118\epsilon_{pf})^{10}]^{0.10}} \right\} \leq 1860 \text{ MPa}$$

while for stress-relieved strands with $f_{pu} = 270$ ksi (1860 MPa), an appropriate formulation is

$$f_p = 29 \times 10^3 \epsilon_{pf} \left\{ 0.03 + \frac{0.97}{[1 + (121\epsilon_{pf})^6]^{0.167}} \right\} \leq 270 \text{ ksi} \quad (3-27)$$

$$f_p = 200 \times 10^3 \epsilon_{pf} \left\{ 0.03 + \frac{0.97}{[1 + (121\epsilon_{pf})^6]^{0.167}} \right\} \leq 1860 \text{ MPa}$$

The coefficients of Eqs. (3-26) and (3-27) have been chosen so that the curves pass through the minimum specified "yield strengths" at a strain of 1%. The stress-strain response of actual strands will typically lie somewhat above these curves.

Table 3-11 Typical values of f_{py}/f_{pu} .

Tendon Type	f_{py}/f_{pu}
Low-relaxation strand	0.90
Stress-relieved strand	0.85
Plain prestressing bars	0.85
Deformed prestressing bars	0.80

3.15 RELAXATION OF PRESTRESSING STEEL

The force required to hold a highly stressed steel tendon at a given elongation will reduce with time—a phenomenon referred to as relaxation (see Fig. 3-29). Relaxation is negligibly small if the initial stress, f_{p1} , applied to the steel is less than $0.55f_{py}$. Relaxation of steel is analogous in many ways to creep of concrete and, like creep, relaxation can be accurately predicted only if information for the specific material under the specific conditions is available.

Tests by Magura, Sozen, and Siess (Ref. 3-44) showed that the relaxation of stress-relieved wires or strands varied in an approximately linear fashion with the log of the time under stress (see Fig. 3-29). Based on their tests, Magura, Sozen, and Siess recommended the following expression:

$$\frac{f_p}{f_{p1}} = 1 - \frac{\log t}{10} \left(\frac{f_{p1}}{f_{py}} - 0.55 \right) \quad (3-28)$$

where t is the time under load in hours. Note that this equation implies that a large part of the loss occurs in the first few hours under stress. For example, after 10 hours ($\log t = 1$) the loss is one-sixth of the loss that will occur after 1 million hours (i.e., 114 years).

For low-relaxation strand or prestressing bars, the Ontario Highway Bridge Design Code (Ref. 3-45) recommends the use of the following modified version of Eq. (3-28):

$$\frac{f_p}{f_{p1}} = 1 - \frac{\log t}{45} \left(\frac{f_{p1}}{f_{py}} - 0.55 \right) \quad (3-29)$$

The temperature of the steel strongly influences the magnitude of the relaxation. Equations (3-28) and (3-29) were determined for the standard temperature of 70°F (20°C) but can be conservatively applied for lower temperatures. For temperatures significantly higher than 70°F (20°C), allowance should be made for increases in relaxation. For example, relaxation losses at 100°F (40°C) will be about twice as large as those at 70°F (20°C).

In the same way that we can account for creep of concrete by using a reduced stiffness of the concrete, $E_{c,eff}$, we can account for relaxation of the steel by using a reduced stiffness of the steel, $E_{p,eff}$ (see Fig. 3-30).

The reduced stiffness, $E_{p,eff}$, can be calculated from

$$E_{p,eff} = \frac{f_p}{f_{p1}} E_p \quad (3-30)$$

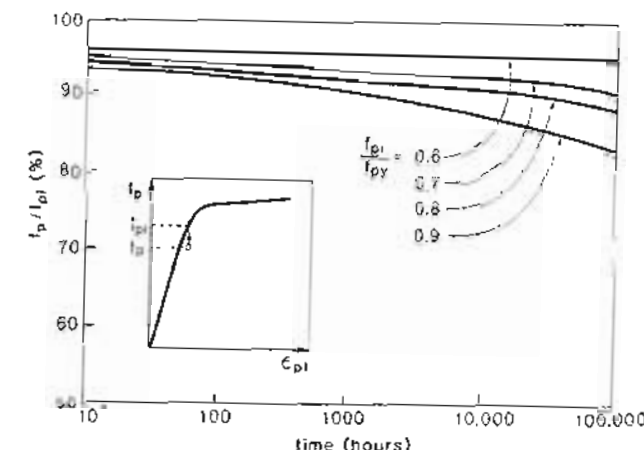


Figure 3-29 Variation of relaxation with time. From Magura, Sozen, and Siess (Ref. 3-44).

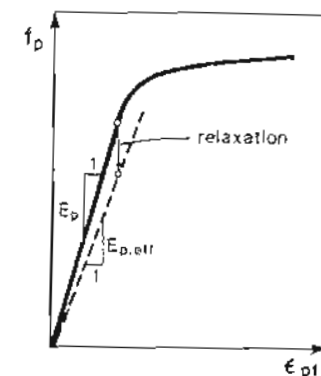


Figure 3-30 Effective stiffness of prestressing steel.

where f_p/f_{p1} is given by either Eq. (3-28) or (3-29)

In a prestressed concrete member the strain in the prestressing tendon does not typically stay constant. Rather, due to creep and shrinkage of the concrete, ϵ_{p1} will decrease with time. This will have the effect of reducing the relaxation loss. It is as if we started with a lower value of f_{p1}/f_{py} . This reduction of relaxation caused by the shortening of

the tendon can be expressed in terms of a reduction coefficient, χ_r . Figure 3-31 shows the values for χ_r given by Ghali and Trevino (Ref. 3-46). In many practical cases, χ_r can be taken as 0.8 (i.e., a 20% reduction in the loss due to relaxation).

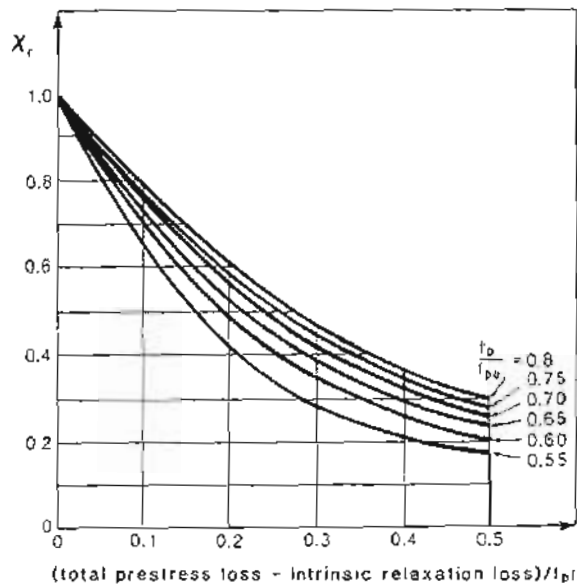


Figure 3-31 Relaxation reduction coefficient, χ_r , where intrinsic relaxation loss may be determined from Eq. (3-28) or (3-29). From Ghali and Trevino (Ref. 3-46).

Allowing for χ_r , the effective steel stiffness becomes

$$E_{p,eff} = \left[1 - \chi_r \left(1 - \frac{f_p}{f_{pu}} \right) \right] E_p \quad (3-31)$$

where again f_p/f_{pu} is given by either Eq. (3-28) or (3-29).

3.16 FATIGUE CHARACTERISTICS OF REINFORCEMENT

The fatigue characteristics of reinforcement are usually defined in terms of the relationship between the stress range ($f_{s,max} - f_{s,min}$) and the number of cycles of such loading required to cause failure (i.e., S-N curves or Wöhler diagrams). Figure 3-32 compares a number of S-N curves for deformed reinforcing bars obtained by different investigators.

seen that after about 1 or 2 million cycles the S-N curves become nearly horizontal. The stress range at which the S-N curve becomes horizontal is called the fatigue limit or the endurance limit. It is assumed that cycles of stress which have a stress range smaller than the fatigue limit can be endured indefinitely.

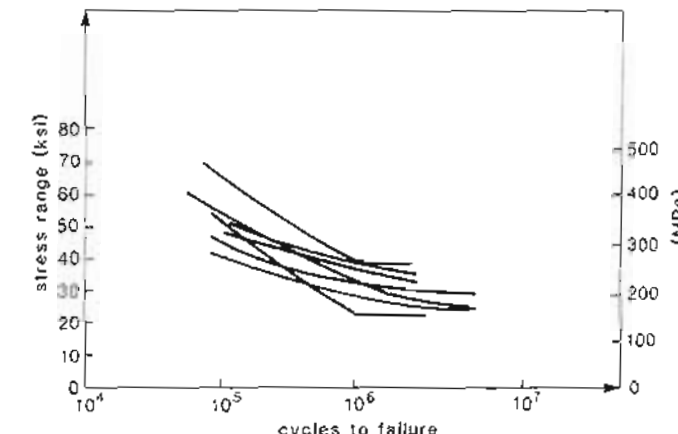


Figure 3-32 S-N curves for reinforcing bars. Adapted from Hanson, Somes, and Helgason (Ref. 3-48).

The fatigue failure of a reinforcing bar usually starts with the formation of a small crack at the surface of the bar. As the load is cycled, this initial crack will propagate until eventually the remaining area of the bar cannot carry the load and failure occurs. The deformations on the reinforcing bar act as stress raisers and hence are usually the location where the fatigue failure is initiated.

The CEB-FIP Code (Ref. 3-47) defines the characteristic fatigue strength of reinforcing bars as the stress range which can be resisted 2×10^6 times (with the maximum stress going to $0.7f_y$), by nine bars out of ten. This code recommends that in the absence of specific test results the characteristic fatigue strength may be taken as 36 ksi (250 MPa) for smooth bars and 22 ksi (150 MPa) for deformed bars. If the bar is spot-welded these values should be multiplied by 0.4, while if the bar is bent, the values should be multiplied by $(1 - 3d_b/D)$, where d_b is the diameter of the bar and D is the diameter of the bend.

As part of a major study at Lehigh University on the fatigue characteristics of prestressed concrete, Warner and Hulsbos investigated the fatigue properties of prestressing strand (Ref. 3-49). Using 7/16 in. (11 mm) diameter seven-wire strand, they determined that a stress range of about 34 ksi (235 MPa) or about $0.13f_{pu}$, with a minimum stress of $0.6f_{pu}$, could be resisted for 2×10^6 cycles before a fatigue failure occurred. They noted that: "One of the six outside wires was always the first to fail in fatigue. Successive failures occurred in other outside wires until the remaining wires were so overstressed that they

failed statically. Those wires which had failed in fatigue could be clearly distinguished by a typical fracture surface containing a crescent-shaped fatigue crack." Later investigators (e.g., Rabbat, Kaar, Russell, and Bruce, Ref. 3-50) also commented on the appearance of strands that have failed in fatigue, noting that wires failing in fatigue lack the distinctive necked-down, cup-and-cone appearance of wires failing statically (see Fig. 3-33).

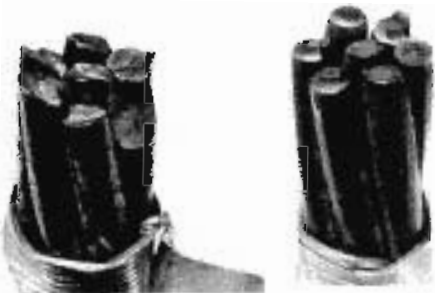


Figure 3-33 Fatigue and tension fracture surfaces of strands: left, fatigue fractures; right, cup-and-cone tension fractures. From Rabbat, Kaar, Russell, and Bruce (Ref. 3-50). Photographs courtesy of the Portland Cement Association.

Based on the Lehigh tests, Tide and Van Horn (Ref. 3-51) suggested the following relationship between the stress range, Δf_p , and the mean fatigue life for prestressing strand:

$$\log N = 10 - 3.6 \log \left(\frac{100 \Delta f_p}{f_{pu}} \right) \quad (3-32)$$

Thus for a stress range of 36 ksi (250 MPa) and $f_{pu} = 270$ ksi (1860 MPa), a mean fatigue life of 892,000 cycles could be expected (i.e., the probability of failure would be 0.50).

It is important to recognize that fatigue properties, which are governed by the presence of small flaws, are inherently highly variable and hence mean values, such as those given by Eq. (3-32), need to be treated very cautiously.

The FIP Recommendations (Ref. 3-52) define the characteristic fatigue strength of prestressing steel as the stress range that can be resisted 2×10^6 times (with the maximum stress going to $0.85 f_{py}$) with a probability of failure of 0.10. This document recommends that in the absence of specific test results, the characteristic fatigue strength may be taken as 29 ksi (200 MPa) for wires and strands and 12 ksi (80 MPa) for high-strength bars. It cautions that "the above values are valid for exposed tendons; lower values may be necessary for tendons in grouted or ungrouted ducts."

Even for beams with pretensioned tendons, it has been observed that the fatigue life of tendons in beams is shorter than for comparable tendons tested in air. Thus in one of

the Lehigh tests (Ref. 3-53) a strand subjected to a measured stress range of 20 ksi (142 MPa) failed after only 0.57×10^6 cycles. More alarmingly, in the PCA tests of Rabbat et al. (Ref. 3-50), pretensioned strands subjected to a calculated stress range of only about 9 ksi (60 MPa) fractured in fatigue after about 3×10^5 cycles.

Rigon and Thürlimann (Ref. 3-54) tested 15 large post-tensioned beams in which the prestressing tendons consisted of either 16 parallel 0.276 in. (7 mm) wires or four 0.6 in. (15 mm) grade 250 seven-wire strands. The tendon profile in these beams consisted of three straight sections joined by curves with a minimum radius of curvature of 11.5 ft (3.5 m).

The $S-N$ curves deduced from the beam fatigue tests of Rigon and Thürlimann are shown in Fig. 3-34. On the basis of this figure, it can be deduced that the characteristic fatigue strength of the parallel-wire tendons in the metal sheaths was about 13 ksi (90 MPa) while for the tendons with seven-wire strands it was about 10 ksi (70 MPa). These values are considerably below the values obtained when prestressing steels of the same types were tested in air. The tests in air gave characteristic fatigue strengths of about 41 ksi (280 MPa) for the wire and 38 ksi (260 MPa) for the seven-wire strand.

As about 80% of the wire breaks occurred within the regions where the tendon was curving, it is reasonable to assume that the curves in the tendon profile were the principal cause for the low fatigue strengths.

When a tendon inside a curved duct is post-tensioned, it will be pulled against the inside face of the sheath. Under cyclic loads of a magnitude large enough to open cracks, the tendon will move with respect to the surrounding grout and the sheath. This rubbing of the tendon against the metal sheath will cause a premature failure, particularly if oxygen can reach the location being rubbed, by a process described as fretting fatigue (Ref. 3-55). It is characteristic of this type of failure that corrosion will start on the surface being rubbed.

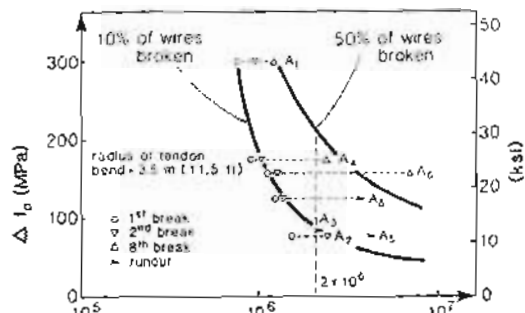
Based on the lower fatigue life of tendons in actual beams, it would seem prudent to use values for the characteristic fatigue strength lower than those given in the FIP Recommendations. Values of 14 ksi (100 MPa) for wires and strands, 9 ksi (60 MPa) for high-strength bars, and 10 ksi (70 MPa) for wires or strands in curved ducts would seem to be conservative.

In investigating the fatigue resistance of prestressed concrete members, special attention should be paid to stress fluctuations at the locations of anchorages or couplings. While such devices can usually develop the full static strength of the tendon, they typically have less than half the fatigue strength (Ref. 3-56).

3.17 THERMAL PROPERTIES OF REINFORCEMENT

While the coefficient of thermal expansion for steel is actually about $6.5 \times 10^{-6}/^\circ\text{F}$ ($11.5 \times 10^{-6}/^\circ\text{C}$), it is conventional to use a value of $6 \times 10^{-6}/^\circ\text{F}$ ($10 \times 10^{-6}/^\circ\text{C}$) for both the concrete and the reinforcement.

Above about 400°F (200°C) there is a substantial decrease in both the stiffness and the strength of reinforcement. By 750°F (400°C), the tensile strength of wires or strand



(a) 16 - 7 mm (0.276 in) wire tendons in steel sheaths

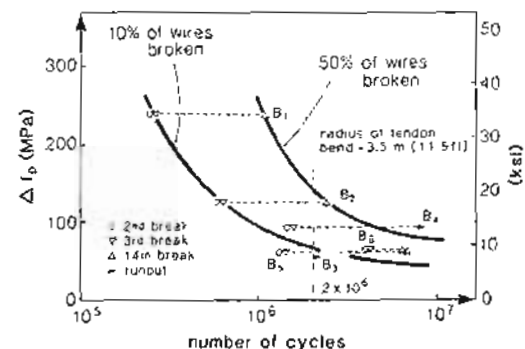


Figure 3-34 S-N curves deduced from fatigue tests of Rigon and Taillmann (Ref. 3-54).

will be only about 50% of its value at room temperature (see Fig. 3-35). The specific heat of reinforcement may be taken as $480 \text{ J/kg}^{\circ}\text{C}$ while the conductivity may be taken as $180 \text{ W}/(\text{m}^{\circ}\text{C})$.

3.18 BOND CHARACTERISTICS OF REINFORCEMENT

The force required to pull a deformed reinforcing bar out of a block of concrete increases as the length of the bar cast into the block (the embedment length) increases (see Fig. 3-36). When the embedment length becomes long enough, the bar will yield in tension before

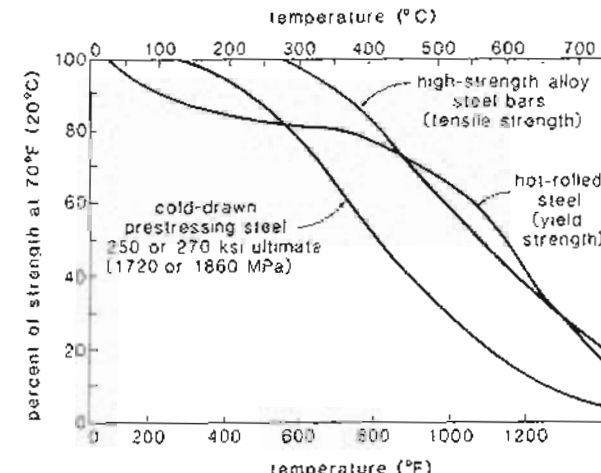


Figure 3-35 Strength reduction of reinforcement at high temperatures. From Ref. 3-20.

it pulls out of the block. The minimum embedment length required to develop the yield force of the bar is called the development length. This development length, l_d , is used as an indicator of the bond characteristics of the reinforcing bar.

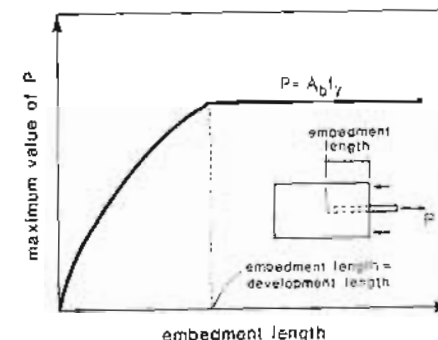


Figure 3-36 Concept of development length.

Forces are transferred from the reinforcing bar to the concrete primarily by inclined compressive forces radiating out from the bar. This was recognized by Abrams (Ref. 3-57)

in 1913 (see Fig. 3-37). The radial components of these inclined compressive forces are balanced by circumferential tensile stresses in the concrete surrounding the bar (see Fig. 3-38). The ability of a deformed bar to transfer its load into the surrounding concrete is typically limited by the failure of this ring of tension when the concrete cover (the thinnest part of the ring) splits (see Fig. 3-39a). However, if a relatively small diameter bar is embedded in a large block of concrete, the bar might pull out prior to the splitting of the concrete (see Fig. 3-39b).

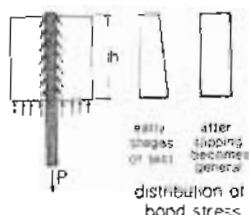


Figure 3-37 Stress in a pull-out specimen. From Abrams (Ref. 3-57).

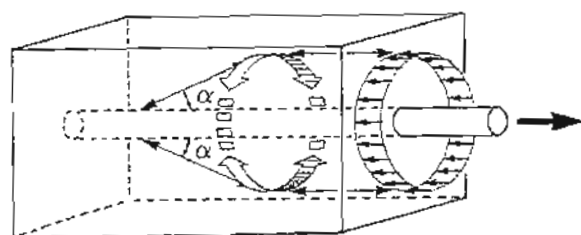


Figure 3-38 Tensile stress rings in the concrete balance radial components of inclined compressive forces. From Tepfers (Ref. 3-58).

The ACI Code (Ref. 3-10) assumes that the basic development length required to prevent splitting failures, $\ell_{db,sp}$, is a function of the area of the bar, while the length required to prevent pull-out, $\ell_{dp,po}$, is a function of the diameter of the bar. The equations for these basic development lengths are as follows: For #11 (No. 35) and smaller bars,

$$\ell_{db,sp} = 0.04 A_b f_y / \sqrt{f'_c} \quad \text{in., psi} \quad (3-33)$$

$$\ell_{db,sp} = 0.02 A_b f_y / \sqrt{f'_c} \quad \text{mm., MPa} \quad (3-33)$$

$$\ell_{dp,po} = 0.03 d_b f_y / \sqrt{f'_c} \quad \text{in., psi} \quad (3-34)$$

$$\ell_{dp,po} = 0.375 d_b f_y / \sqrt{f'_c} \quad \text{mm., MPa} \quad (3-34)$$

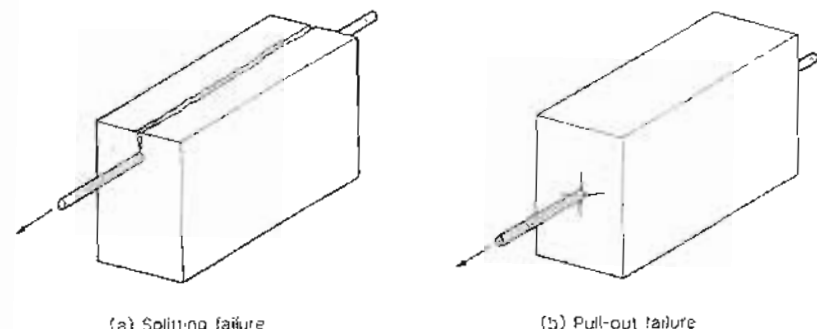


Figure 3-39 Splitting failures and pull-out failures.

Equations (3-33) and (3-34) imply that as the concrete strength increases the development lengths become smaller. However, the Code does not permit development lengths to decrease for concrete strengths greater than 10,000 psi (70 MPa), and hence the term $\sqrt{f'_c}$ is not to be taken greater than 100 psi (8.37 MPa in metric version).

Tables 3-12 and 3-13 give these basic tension development lengths for standard reinforcing bars and typical material strengths. It can be seen that for smaller reinforcing bars pull-out is more critical, while for larger reinforcing bars splitting is more critical.

The development length required to prevent a splitting failure will decrease as the clear cover over the bar increases, as the clear spacing between adjacent bars increases and as the amount of confining reinforcement increases. To account for these parameters the ACI Code requires that the basic development lengths to prevent splitting given in Table 3-12(a) be multiplied by a modification factor, k_1 , as given in Fig. 3-40.

Both the development length required to prevent splitting and the development length required to prevent pull-out will increase for "top bars," for bars with high yield strength, for bars cast in lightweight concrete, and for epoxy-coated bars. On the other hand, a smaller development length can be used if extra reinforcement has been provided at the section. To account for these parameters the ACI Code requires that the calculated development lengths required to prevent splitting and pull-out be multiplied by a modification factor, k_2 , as given in Table 3-14.

The development length to prevent splitting, $\ell_{d,sp}$, is thus

$$\ell_{d,sp} = k_1 k_2 \ell_{db,sp} \quad (3-35)$$

while the development length to prevent pull-out, $\ell_{d,po}$, is

$$\ell_{d,po} = k_2 \ell_{dp,po} \quad (3-36)$$

The development length, ℓ_d , required by the ACI Code is the larger of the two lengths calculated above but is not to be taken as less than 12 in. (300 mm).

Table 3-12 Basic tension development lengths for ASTM standard reinforcing bars, according to ACI 318-89.

(a) Basic splitting development length, $\ell_{db,p}$, inches

Bar Size	f'_c , psi					
	3000	4000	5000	6000	8000	$\geq 10,000$
# 3	4.8	4.2	3.7	3.4	3.0	2.6
# 4	8.8	7.6	6.8	6.2	5.4	4.8
# 5	13.6	11.8	10.5	9.6	8.3	7.4
# 6	19.3	16.7	14.9	13.6	11.8	10.6
# 7	26.3	22.8	20.4	18.6	16.1	14.4
# 8	34.6	30.0	26.8	24.5	21.2	19.0
# 9	43.8	37.9	33.9	31.0	26.8	24.0
# 10	53.6	48.2	43.1	39.4	34.1	30.5
# 11	66.4	59.2	52.9	48.3	41.9	37.4
# 12	93.1	80.6	72.1	65.8	57.0	51.0
# 13	137	119	106	96.8	83.9	75.0

(b) Basic pull-out development length, $\ell_{db,po}$, inches

Bar Size	f'_c , psi					
	3000	4000	5000	6000	8000	$\geq 10,000$
# 3	12.3	10.7	9.5	8.7	7.5	6.8
# 4	16.4	14.2	12.7	11.6	10.1	9.0
# 5	20.5	17.8	15.9	14.5	12.6	11.3
# 6	24.6	21.3	19.1	17.4	15.1	13.5
# 7	28.8	24.9	22.3	20.3	17.6	15.8
# 8	32.9	28.5	25.5	23.2	20.1	18.0
# 9	37.1	32.1	28.7	26.2	22.7	20.3
# 10	41.7	36.1	32.3	29.5	25.6	22.9
# 11	46.3	40.1	35.9	32.8	28.1	25.4
# 12	55.6	48.2	43.1	39.3	34.1	30.5
# 13	74.2	64.2	57.5	52.4	45.4	40.6

If a bar subjected to its yield force is embedded for a length equal to the development length, then the average bond stress, u , on the surface of the bar is

$$u = \frac{A_b f_y}{\pi d_b \ell_d} = \frac{\pi d_b^2 f_y}{4\pi d_b \ell_d} = \frac{d_b f_y}{4\ell_d} \quad (3-37)$$

By using Eq. (3-37) to convert the development lengths into equivalent bond strengths, Fig. 3-41 was obtained. It can be seen that for concrete strengths typically used in prestressed concrete (f'_c about 5000 psi or 35 MPa), the bond strength for bars smaller than #8 (No. 25) is about 590 psi (4 MPa).

The CEB-FIP Code (Ref. 3-47) gives bond strengths for both deformed and smooth reinforcing bars (see Fig. 3-42). Unlike the ACI Code, the CEB-FIP Code does not make

Table 3-13 Basic tension development lengths for ASTM standard metric reinforcing bars, according to ACI 318-89

(a) Basic splitting development length, $\ell_{db,p}$, mm

Bar No.	f'_c , MPa					
	25	31	35	40	60	≥ 70
10	160	146	135	126	103	96
15	320	292	270	253	207	191
20	480	433	406	379	310	287
25	800	730	676	632	516	478
30	1120	1022	947	885	723	669
35	1600	1461	1352	1265	1033	956
45	2000	1826	1690	1581	1291	1195
55	3200	2921	2704	2530	2066	1912

(b) Basic pull-out development length, $\ell_{db,po}$, mm

Bar No.	f'_c , MPa					
	25	30	35	40	60	≥ 70
10	339	309	287	268	219	203
15	480	438	406	379	310	287
20	585	534	494	462	378	350
25	756	690	639	598	488	453
30	897	819	758	709	579	536
35	1071	978	905	847	691	640
45	1311	1197	1108	1036	846	783
55	1692	1545	1430	1338	1092	1011

the bond strength a function of the bar diameter. With $f'_c = 5000$ psi (35 MPa), this code gives a bond strength of 535 psi (3.7 MPa) for deformed bars with diameters less than 1.26 in. (32 mm).

It should be appreciated that the bond strengths given in the codes are conservative values applicable for use over the entire development length. If a short length of bar is subjected to a pull-out test, considerably higher values of bond stress can be resisted (see Fig. 3-43).

The bond characteristics of prestressing tendons are of particular importance in pretensioned members where the tendon is anchored by bond alone. The length of tendon at the end of a pretensioned member over which the prestress in the tendon develops is called the transfer length.

Kaar, La Fraugh, and Mass (Ref. 3-60) studied the effects of concrete strength and method of strand release on the transfer length of seven-wire strand ranging in size from 1/4 in. (6.4 mm) diameter up to 0.6 in. (15 mm) diameter. The pretensioned members were designed to have a compressive stress in the concrete of about $0.6f'_c$, with f'_c ranging from about 1660 to 5000 psi (11 to 35 MPa). The stress in the prestressing steel after transfer

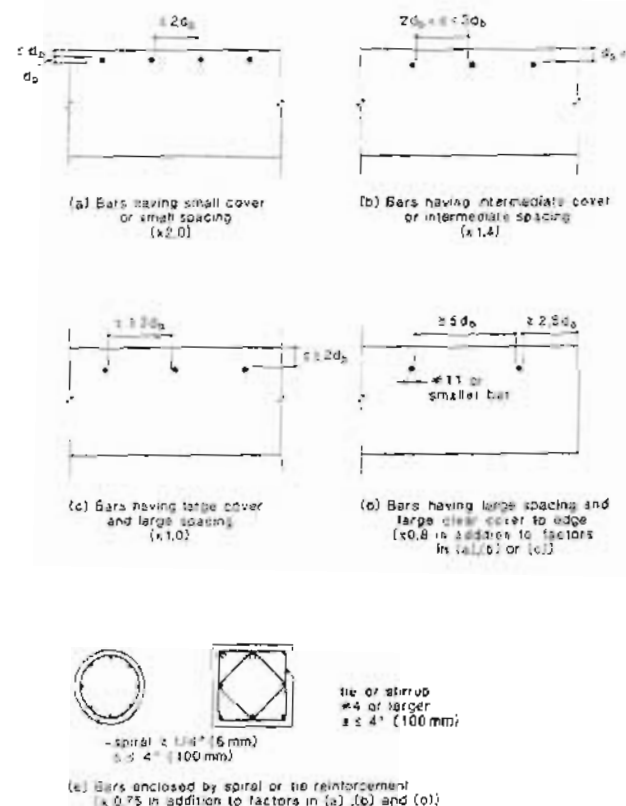


Figure 3-40 Values of factor k_1 modifying basic development length required to prevent bond-splitting failures. From Ref. 3-10.

was $0.7f_{pu} = 175$ ksi (1207 MPa). Compressive strains measured on the surface of the concrete and along the length of the specimens enabled the buildup of prestress from the ends of the members to be estimated. The transfer length was then taken as the length required to build up the full prestress in the concrete. Figure 3-44 illustrates the measured compressive strains along the length of one member. From this diagram the transfer length can be seen to be about 39 in. (1000 mm) at the end of the strand that was flame-cut, while the end with more gradual release has a transfer length of only about 32 in. (825 mm). The observed variation in transfer lengths for different concrete strengths is shown in Fig. 3-45.

Table 3-14 Values of modification factor k_2 for development length. From Ref. 3-10.

(a) Top reinforcement — horizontal reinforcement with more than 12 in. (300 mm) of fresh concrete cast below reinforcement	1.3
(b) Lightweight aggregate concrete Or if f_{ct} is specified — psi units MPa units	$6.7\sqrt{f'_c/f_{ct}}$ $0.556\sqrt{f'_c/f_{ct}}$
(c) Epoxy-coated reinforcement* Bars with cover $< 3d_b$ or clear spacing $< 6d_b$ All other conditions	1.5 1.2
(d) Excess reinforcement (A_s required/ A_s provided)	

*The product of top bar factor and factor for epoxy coating need not be taken greater than 1.7.

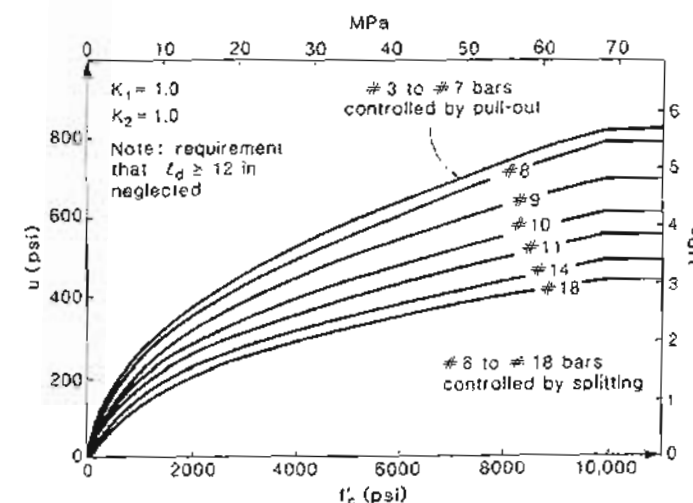


Figure 3-41 Bond strengths for deformed bars implied by ACI Code.

The ACI Code suggests that the transfer length can be taken as 50 strand diameters for strands and 100 wire diameters for individual wires. The CEB-FIP Code, on the other hand, suggests that transfer lengths may vary between 45 and 90 strand diameters for strands and between 100 and 140 wire diameters for individual wires.

When a prestressing tendon is stretched between the abutments on a pretensioning bed the diameter of the tendon is reduced (Poisson's effect). After the concrete has hardened,

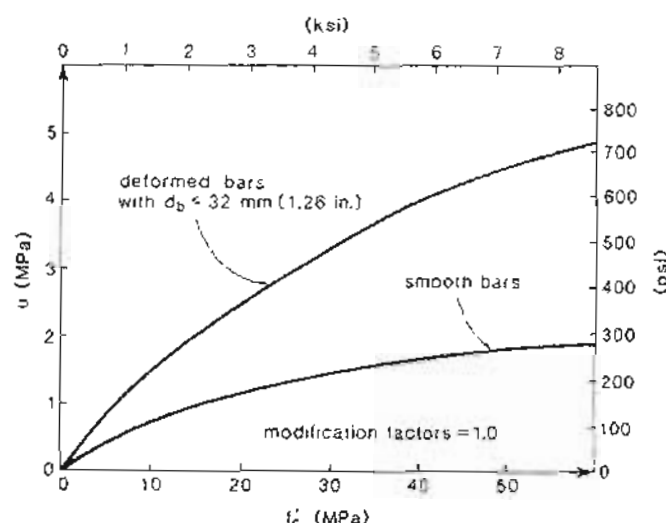


Figure 3-42 Bond strengths for deformed bars and smooth bars given in the CEB-FIP Code.

the tendons are released from the abutments, and at the free ends of the beams the stress in the tendons returns to zero. As the tendon stress goes back to zero, the diameter of the tendon expands and pushes against the surrounding concrete, which improves the bond strength at the ends of the beam. This improvement in bond caused by the lateral expansion of the released tendon is sometimes referred to as the Hoyer effect (Ref. 3-61).

The better bond conditions at the free end of the beam indicate that it is inappropriate to use a constant bond stress along the length of the tendon. The ACI Code requires that a pretensioned strand have a development length beyond the critical section equal to

$$\begin{aligned}\ell_d &\approx 0.333f_{sc}d_b + (f_{ps} - f_{sc})d_b && \text{ksi and inches} \\ \ell_d &= 0.048f_{sc}d_b + 0.145(f_{ps} - f_{sc})d_b && \text{MPa and mm}\end{aligned}\quad (3-38)$$

where f_{sc} is the effective prestress in the strand and f_{ps} is the stress in the strand at the critical section. Equation (3-38) implies a bond strength of 750 psi (5.21 MPa) within the transfer length and then 250 psi (1.72 MPa) for the interior portion of the strand (see Fig. 3-46), where the bond stress is calculated on the basis of the nominal circumference of the strand (i.e., πd_b).

Once again, with short specimen lengths, it is possible to obtain local bond stresses higher than the code values given above. For example, Fig. 3-47 shows the bond stress-slip curves obtained by Stocker and Sozen (Ref. 3-62) using 1 in. (25 mm) bonded lengths. As their test specimens did not benefit from the Hoyer effect, the appropriate bond stress from

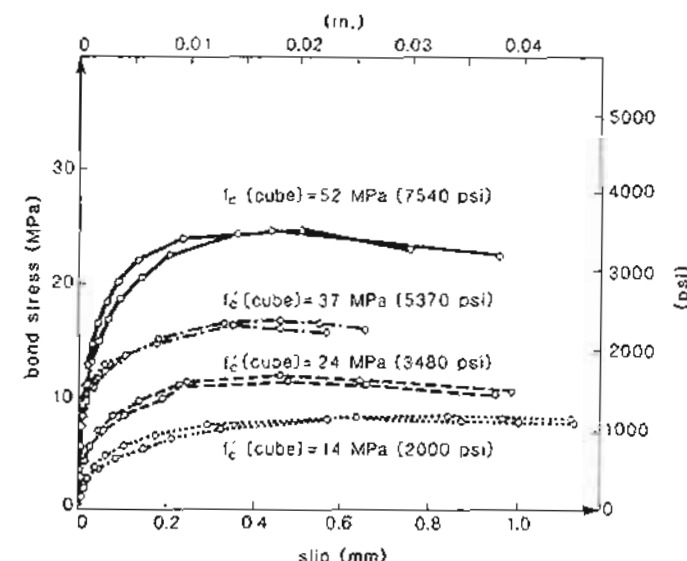


Figure 3-43 Experimental bond stress-slip curves for 0.47 in. (12 mm) diameter deformed bars with short anchorage length. From Berggren (Ref. 3-59)

the code would be 250 psi (1.72 MPa). It can be seen from Fig. 3-47 that bond stresses of between 400 psi (3 MPa) and 720 psi (5 MPa) were determined from these tests.

3.19 DURABILITY CONSIDERATIONS

The greatest threat to the durability of a prestressed concrete structure is corrosion of the reinforcement. Corrosion of reinforcing bars may cause the cover concrete to spall. The resulting unsightly damage is difficult and expensive to repair. Corrosion of prestressing tendons is of even greater concern, for it may trigger the collapse of the structure. For example, in May 1980 the roof of the Berlin Congress Hall collapsed as a result of corrosion and fatigue of the post-tensioned tendons (Ref. 3-63).

Corrosion of steel embedded in concrete is an electrochemical process (see Fig. 3-48), similar to the action that takes place in a battery (Ref. 3-64). One area of the reinforcement acts as the anode, and it is here that the steel corrodes, with the iron being oxidized to ferrous ions and electrons being given off. Other areas of the reinforcement, which have a higher electrochemical potential, act as the cathodes, consuming oxygen, water, and electrons to form hydroxyl ions. To complete the electrochemical cell, the bar itself acts as the electrical conductor and the concrete pore water containing dissolved salts acts as the electrolyte (Ref. 3-65).

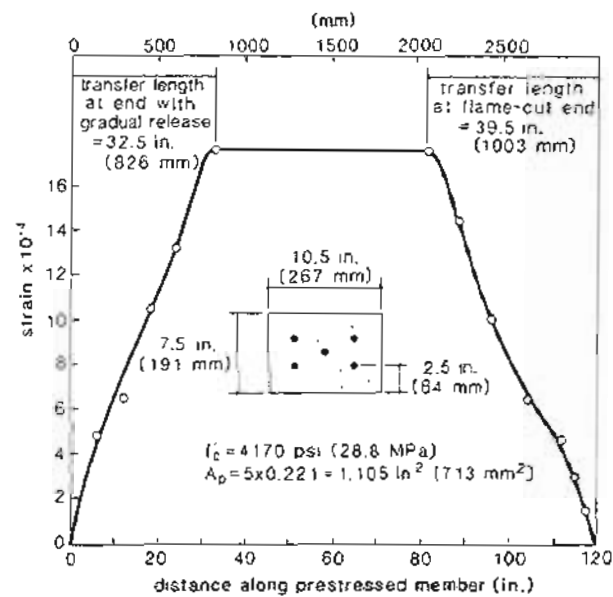


Figure 3-44 Determination of transfer length in a 10 ft (3 m) long specimen pretensioned with 0.6 in. (15 mm) diameter strand. From Kaar, La Fraugh, and Mass (Ref. 3-60).

Portland cement concrete is typically a highly alkaline environment. The hydration of the portland cement produces large quantities of calcium hydroxide, which buffers the system at a pH level of about 12.5. For the range of typical potentials for concrete and at this level of alkalinity, the steel will typically be passive. The passivity of the steel is characterized by a thin and tightly adherent oxide film on the surface of the steel which protects the reinforcement from further corrosion. This is similar to the oxide films that form on the surface of aluminum or zinc under normal atmospheric conditions and prevent further corrosion. While the oxide film remains unbroken, the reinforcement will not corrode.

The natural alkalinity of concrete can be reduced by the chemical reactions that occur between the hardened portland cement paste and carbon dioxide. This process, which is called carbonation, can lower the pH of the concrete to about 8, destroying the passivity of the embedded reinforcement and permitting corrosion to start.

Fortunately, carbonation is a very slow process, particularly in high-quality concretes. Thus for a concrete where $f'_c = 5000 \text{ psi}$ (35 MPa), the depth of carbonation would probably be less than 0.4 in. (10 mm) after 20 years (Ref. 3-66). Hence, in uncracked concrete, carbonation will not typically penetrate the concrete cover. If the concrete contains cracks,

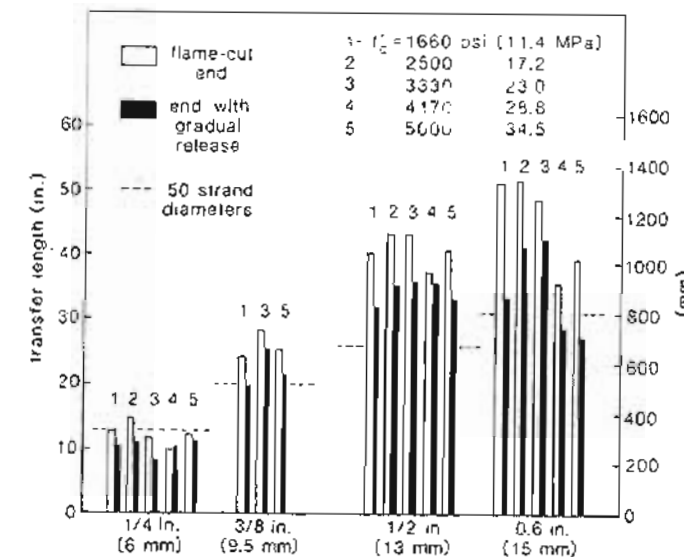


Figure 3-45 Experimentally determined prestress transfer lengths. From Kaar, La Fraugh, and Mass (Ref. 3-60).

the carbon dioxide can reach further into the concrete and hence the depth of carbonation will be increased.

The presence of chlorides can endanger the passivity of the reinforcement even at high pH levels. Very small concentrations of chlorides in the liquid phase of the concrete can destroy the protective oxide film on the embedded reinforcement (Ref. 3-67). The chlorides in concrete come from many sources. Typically, the cement itself will contain about 50 to 100 parts per million (ppm) by weight of chlorides. Potable water usually has less than 250 ppm of chlorides, with city water supplies generally having less than 50 ppm. In comparison, seawater contains about 20,000 ppm (i.e., 2%) of chlorides. The chloride content of the aggregates will generally fall in the range 10 to 400 ppm, although some dolomites can contain 1000 ppm of chlorides. Nonchloride water-reducing admixtures generally contain between 100 and 800 ppm of chlorides, while calcium chloride accelerating admixtures might contain as much as 200,000 ppm (i.e., 20%) of chloride (Ref. 3-68). The way in which the chlorides present in the different mix ingredients contribute to the total chloride content of the concrete is illustrated by an example in Table 3-15.

As might be expected, not all of these chlorides will contribute equally to corrosion of the reinforcement. Thus 100 g of chlorides in the water is more likely to cause problems

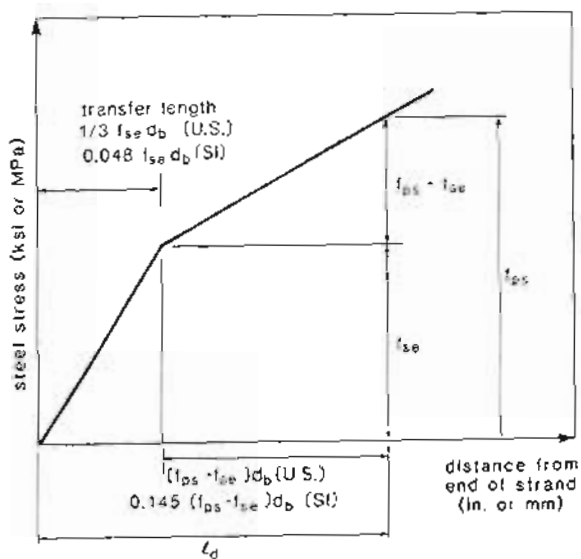


Figure 3-46 Development of stress in pretensioned strands.

than is 100 g of chlorides inside the coarse aggregate particles. Furthermore, only about one-half to three-quarters of the total chlorides in the concrete are soluble in water, and it is believed that only the soluble chlorides influence corrosion. It has been reported (Ref. 3-64) that corrosion can start if the water-soluble chlorides exceed 0.15% of the weight of the cement.

Perhaps more important than the chlorides in the mix ingredients are the chlorides that may penetrate the concrete during its service life. Structures in or near the sea will be subjected to saltwater or windborne spray. In regions that use deicing chemicals, parking garages, bridges, and structures near roads will all be subjected to highly concentrated chloride solutions.

While the rate of chloride penetration into the concrete will depend on many factors, one of the most important factors will be the quality of the concrete. Thus in Fig. 3-49 we see that concrete with a water/cement ratio of 0.40 is much more resistant to the ingress of chlorides than is concrete with a water/cement ratio of 0.60.

Once the passivity of the embedded reinforcement has been destroyed, either by carbonation of the concrete or penetration of chlorides, corrosion will start and the remaining life of the structure will then depend upon how fast the corrosion proceeds. The rate of corrosion depends on how efficiently the electrochemical cell can operate. In most situations, it will be the electrical resistivity of the concrete and the availability of oxygen at

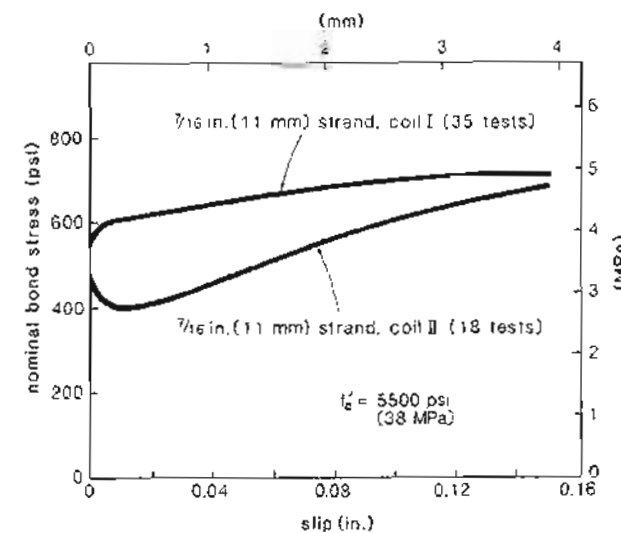


Figure 3-47 Experimental bond force-slip curves for 7/16 in. strand. From Stocker and Sozen (Ref. 3-62).

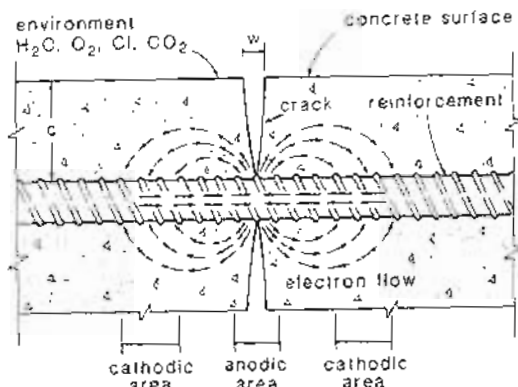
the cathode that will control the rate of corrosion (Ref. 3-67).

If the electrical resistivity of the concrete is high enough (say 50×10^3 ohm-cm) not enough current can flow to generate significant corrosion. While the quality of the concrete will influence the resistivity, it is the moisture content of the concrete that is the most dominant parameter determining resistivity. If the degree of water saturation is less than about 40%, the resistivity will be high enough to prevent significant corrosion.

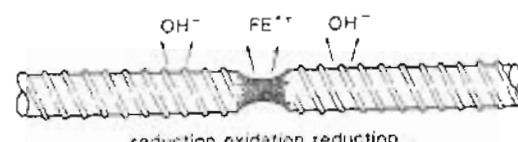
The permeability of the concrete and the thickness of the concrete cover over the reinforcement are the most important factors governing the availability of oxygen. Because the permeability of high-quality, uncracked concrete is so low, Gerwick and Mehta (Ref. 3-70) have postulated that significant corrosion of the reinforcement occurs only after significant microcracking has increased the permeability of the concrete enough "to permit access of oxygen to large areas of the reinforcement."

The strong influence of concrete cover and chloride content on the durability of concrete structures was demonstrated in a study by Rasheeduzzafar, Dakhil, and Gahtani (Ref. 3-71). They surveyed 62 reinforced concrete structures, 10 to 15 years old, located along the Arabian Gulf seacoast in eastern Saudi Arabia.

In this hot (corrosion rates increase with temperature), humid, salty environment, they found "an alarming degree of concrete deterioration." By analyzing samples of concrete taken from around corroding reinforcing bars, they found that there was "an almost direct relationship between chloride content and loss of metal." However, even for the same



(a) Flow of electrons



(b) Corrosion at the anode

Figure 3-48 Corrosion of reinforcement – an electrochemical process.

Table 3-15 Example calculation of total chloride ion content. Adapted from Gaynor (Ref. 3-68).

Component	Quantity lb/yd ³	Chloride Content, ppm	Total Chloride lb/yd ³
Cement	600	50	0.03
Sand	1150	100	0.115
Coarse aggregate	1800	1060	1.908
Water	280	250	0.07
Admixture	1.9	800	0.0015
Total chloride content = 2.1245 lb/yd ³			
Total chloride = 0.354% of weight of cement			

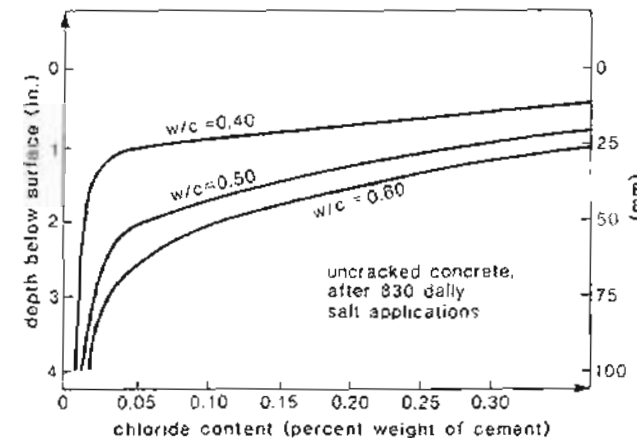


Figure 3-49 Variation of chloride content with depth below surface after 830 daily salt applications. From Clear (Ref. 3-69).

chloride content at the concrete-steel interface, corrosion was substantially decreased if the concrete cover was increased (see Fig. 3-50).

In view of the strong influence of concrete cover on corrosion, it is not surprising that most concrete codes relate the required amount of cover to the severity of the environment. While there is general agreement that larger covers are required in aggressive environments, there is a wide divergence of opinion as to the actual magnitude of the required cover. For example, the required cover for severe climatic conditions varies from about 3/4 in. (20 mm) to about 2 1/2 in. (60 mm) in different national codes, suggesting that the actual numerical limits are rather arbitrary (see Fig. 3-51).

In the ACI Code the required concrete cover is a function of the exposure condition, the member type, the concrete type, and the reinforcement size. The ACI requirements are summarized in Table 3-16. The values given are for the specified cover (i.e., the nominal cover), and it is understood that the cover may be decreased somewhat by construction tolerances.

The ACI Code does not give specific values for the cover required to protect the reinforcement when deicing chemicals are to be applied to the concrete. The ACI Commentary (Ref. 3-10) suggests that in such cases the water/cement ratio of the concrete should not exceed 0.40 and that the concrete cover should be at least 2 in. (50 mm) for walls and slabs and 2 1/2 in. (60 mm) for other members. It suggests further that the water-soluble chloride ions in the concrete not exceed 0.15% of the weight of cement for reinforced concrete and 0.06% for prestressed concrete.

One "protective treatment" that can be employed to resist corrosion is the use of epoxy-coated reinforcing bars. In this procedure, cleaned reinforcing bars are passed through an electronic oven where an epoxy coating is applied and fused to the steel.

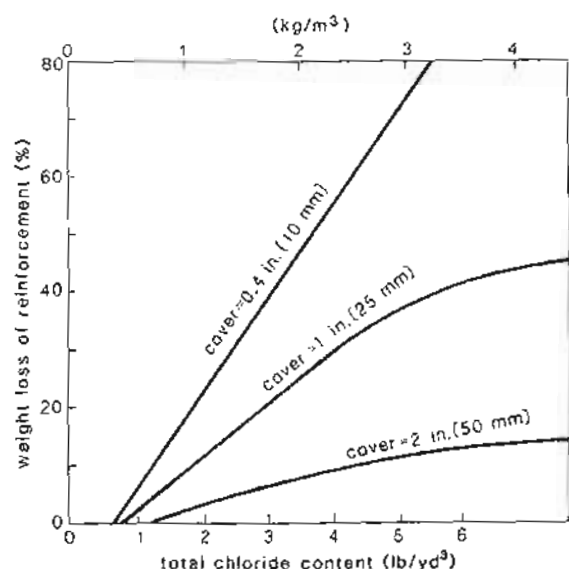


Figure 3-50 Relationship between concrete cover, chloride content, and amount of corrosion. Adapted from Rasheeduzzafar, Dakhil, and Gahtani (Ref. 3-71).

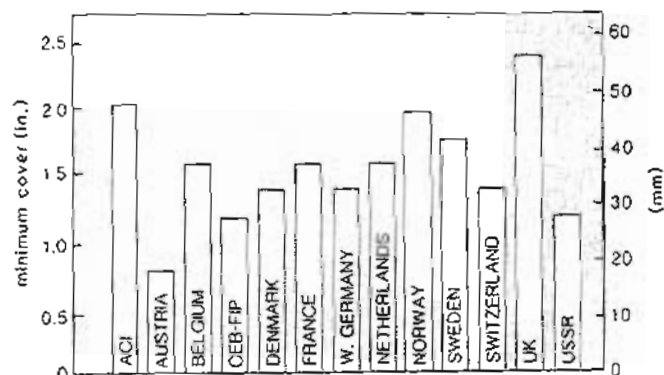


Figure 3-51 Required minimum concrete cover over reinforcing bars for members exposed to severe climatic conditions. From Beeby (Ref. 3-72).

Table 3-16 Concrete cover required by ACI Code. From Ref. 3-10.

Exposure Conditions	Member Type	Reinforcement Size	Cover, ^a in.		
			Non-prestressed Cast-in-Place Concrete	Precast Concrete	Prestressed Concrete ^b
Cast against and permanently exposed to earth	All	All	3	—	3
Exposed to earth or weather	Wall panels	# 14, 18 ≤ # 14	— —	1 1/2 3/4	1 1
	Prestressed slabs and joists	All	—	—	1
	Other members	# 14, 18 # 6 to # 11 # 3, 4, 5	2 2 1 1/2	2 1 1/2 1 1/4	1 1/2 1 1/2 1 1/2
Not exposed to earth or weather	Slabs, walls, and joists	# 14, 18 ≤ # 14	1 1/2 3/4	1 1/2 5/8	3/4 3/4
	Beams and columns	Principal reinforcement Ties, stirrups, and spirals	1 1/2	d _b ^c 3/8	1 1/2 1
	Shells and folded plates	> # 5 # 3, 4, 5	3/4 1/2	5/8 3/8	d _b ^c 3/8
Exposed to deicing salts, seawater, salt spray, or other corrosive environments	Amount of cover shall be "suitably increased" and "denseness and non-porosity of protecting concrete shall be considered."				

^a d_b, nominal diameter of bar, wire, or strand

^b Cover for prestressed concrete members exposed to earth, weather, or corrosive environments should be increased by 50% if these members crack at service loads.

^c Cover in this case shall not be less than 5/8 in. and need not be more than 1 1/2 in.

^d Cover in this case shall not be less than 3/4 in.

The fusion-bonded epoxy coating isolates the steel from contact with oxygen, moisture, and chlorides and hence protects the bar from corrosion. This passive protection is similar to the coatings used on major home appliances, such as refrigerators. While epoxy-coated bars need to be handled with some additional care, local breaks in the coating will not result in excessively accelerated corrosion. With the more widespread use of these bars, the large cost premium which they initially required has been substantially reduced.

Because structural cracks will considerably increase the "porosity" and "permeability" of the concrete cover, it would seem logical to relate the corrosion protection to the crack width at the surface of the concrete (see Fig. 3-48). The CEB-FIP Code has adopted

this approach and recommends the limits for the characteristic crack width at the surface of the concrete given in Table 3-17. The characteristic crack width is defined as 1.7 times the average crack width and is regarded as being that width which only one crack in twenty will exceed.

Table 3-17 CEB-FIP crack width limits for durability.* From Ref. 3-47.

Exposure Conditions	Load to Be Considered	Limits for Reinforcement Highly Sensitive to Corrosion [†]	Limits for Reinforcement Moderately Sensitive to Corrosion [†]
Mild Usual interior exposure Low-humidity exterior exposure	Frequent (dead load plus frequently occurring live load)	0.2 → 0.3 mm (0.008 → 0.012 in.)	0.4 → 0.6 mm (0.016 → 0.024 in.)
	Permanent (dead load plus sustained live load)	0.1 → 0.15 mm (0.004 → 0.006 in.)	need not be checked
Moderate High humidity or slightly corrosive interior exposure Running water Ordinary soil exposure Usual exterior exposure	Frequent	0.1 → 0.15 mm (0.004 → 0.006 in.)	0.2 → 0.3 mm (0.008 → 0.012 in.)
	Permanent	No tension in concrete	need not be checked
Severe Seawater exposure Slightly acidic liquids Deicing chemicals Corrosive gases Corrosive soils	Rare (dead load plus maximum possible live load)	0.1 → 0.15 mm (0.004 → 0.006 in.)	0.2 → 0.3 mm (0.008 → 0.012 in.)
	Frequent	No tension in concrete	0.1 → 0.15 mm (0.004 → 0.006 in.)

*The limits given refer to the characteristic crack widths, w_c . The lower limit is for a cover equal to the minimum required by CEB, while the upper limit is for a cover at least 1.5 times the minimum cover.

[†]Reinforcement considered to be highly sensitive to corrosion includes prestressing steel, small diameter (< 5 mm or 0.2 in.) bars or wires, and treated steels (heat treated or cold worked). Normal reinforcing bars are considered to be moderately sensitive to corrosion.

While it would seem logical that wider cracks would lead to more corrosion, Beeby (Ref. 3-72) has pointed out that numerous experimental investigations have indicated "no reasons to believe in a relationship between crack width and corrosion." Typically, the results of such tests show that while any crack acts as a path for chlorides to reach the

reinforcement, there is very little difference between the corrosion caused by a 0.004 in. (0.1 mm) wide crack and that caused by a 0.020 in. (0.5 mm) wide crack.

In studying the influence of crack widths on corrosion rates, it is important to recognize that for corrosion to proceed, oxygen must reach the cathodic area of the reinforcing bar (see Fig. 3-48). Further, for corrosion to proceed rapidly, the cathodic area must greatly exceed the anodic area (the corrosion rate is approximately proportional to the cathode-to-anode area ratio). Hence a crack that crosses the bar, such as that shown in Fig. 3-48, is much less dangerous than a secondary crack that runs parallel to the bar.

To prevent significant quantities of oxygen reaching large areas of the bar, it is probably more efficient to control the stress in the bar rather than the crack width at the surface of the concrete. This is because at high steel stresses a system of microcracks will develop in the concrete near each bar deformation as the bar stretches in the surrounding concrete. This system of cracks will provide pathways for the oxygen to reach large areas of the bar.

To ensure the durability of our prestressed concrete structures, we should ensure that the reinforcement is covered by an adequate thickness of high-quality concrete. Further, we should ensure that excessive quantities of chlorides are not contained in the concrete mix ingredients or in the grout. Calculating and controlling crack widths will certainly not hurt the structure but we should realize that these calculated crack widths are not very good indicators of possible corrosion. Careful attention to details such as drainage is much more important, as this can reduce the severity of the exposure conditions the structure has to endure, while conscientious maintenance can substantially increase the life of the structure.

While corrosion of the reinforcement is the greatest threat to the durability of prestressed concrete structures, other types of chemical attack can also occur. For example, solutions containing sulfates (SO_4^{2-}) attack concrete made from normal portland cement, and certain types of aggregates chemically react in the alkaline environment of the concrete. The resulting expansion of the aggregate, which can reach one part per thousand, may severely damage the structure.

References

- 3-1 Neville, A.M., *Properties of Concrete*, 2nd ed., McGraw-Hill Book Company, New York, 1968.
- 3-2 Mindess, S., and Young, J.F., *Concrete*, Prentice-Hall, Inc., Englewood Cliffs, N.J., 1981.
- 3-3 American Society for Testing and Materials, "Standard Specification for Portland Cement," ASTM C150-81, ASTM, Philadelphia, 1981.
- 3-4 ACI Committee 357, "Offshore Concrete Structures for the Arctic," *Concrete International-Design and Construction*, Vol. 7, No. 8, Aug. 1985, pp. 23-33.
- 3-5 Moksnes, J., and Jakobsen, B., "High-Strength Concrete Development and Potentials for Platform Design," *Offshore Technology Conference*, Houston, Paper No. SOT3, May 1985.
- 3-6 Nilson, A.H., "High Strength Concrete — An Overview of Cornell Research," *Proceedings of the Symposium "Utilization of High Strength Concrete,"* Stavanger, Norway, June 1987, Tapir, Trondheim, pp. 27-38.
- 3-7 Popovics, S., "A Review of Stress-Strain Relationships for Concrete," *ACI Journal*, Vol. 67, No. 3, Mar. 1970, pp. 243-248.
- 3-8 Thorenfeldt, E., Tomaszewicz, A., and Jensen, J.J., "Mechanical Properties of High-Strength Concrete and Application in Design," *Proceedings of the Symposium "Utilization of High Strength Concrete,"* Stavanger, Norway, June 1987, Tapir, Trondheim, pp. 149-159.
- 3-9 Mills, R.H., and Ono, K., "Elastic Modulus of Close-Packed Randomly Oriented Maxwell Elements," *Journal Matériaux et Constructions*, Vol. 5, No. 27, 1972, pp. 127-133.
- 3-10 ACI Committee 318, "Building Code Requirements for Reinforced Concrete (ACI 318-89) and Commentary — ACI 318 R-89," American Concrete Institute, Detroit, 1989, 360 pp.
- 3-11 Pauw, A., "Static Modulus of Elasticity of Concrete as Affected by Density," *ACI Journal*, Vol. 57, No. 6, Dec. 1960, pp. 679-688.
- 3-12 Carrasquillo, R.L., Nilson, A.H., and slate, F.O., "Properties of High Strength Concrete Subject to Short-Term Loads," *ACI Journal*, Vol. 78, No. 3, May-June 1981, pp. 171-178.
- 3-13 Sinha, B.P., Gerstle, K.H., and Tulin, L.G., "Stress-Strain Relationships for Concrete under Cyclic Loading," *ACI Journal*, Vol. 61, No. 2, Feb. 1964, pp. 195-211.
- 3-14 Warner, R.F., and Hulsbos, C.L., "Probable Fatigue Life of Prestressed Concrete Beams," *PCI Journal*, Vol. 11, No. 2, Mar.-Apr. 1966, pp. 16-39.
- 3-15 Warner, R.F., and Faulkes, K.A., *Prestressed Concrete*, Putman Publishing Pty. Ltd., South Melbourne, Australia, 1979.
- 3-16 Rüsch, H., "Researches toward a General Flexural Theory for Structural Concrete," *ACI Journal, Proceedings* Vol. 57, No. 1, July 1960, pp. 1-28.
- 3-17 Meyers, B.L., Branson, D.E., Schumann, C.G., and Christianson, M.L., "The Prediction of Creep and Shrinkage Properties of Concrete," Final Report No. 70-5, Iowa Highway Commission, Des Moines, Aug. 1970, pp. 1-140.
- 3-18 ACI Committee 209, "Prediction of Creep, Shrinkage, and Temperature Effects in Concrete Structures," *ACI 209R-82, Designing for the Effects of Creep, Shrinkage and Temperature in Concrete Structures*, SP-27, American Concrete Institute, Detroit, 1971, pp. 51-93.
- 3-19 PCI Committee on Design Handbook, "Volume Changes in Precast, Prestressed Concrete Structures," *PCI Journal*, Vol. 22, No. 5, Sept.-Oct. 1977, pp. 39-53.

- 3-20 Prestressed Concrete Institute, *PCI Design Handbook: Precast and Prestressed Concrete*, 3rd ed., PCI, Chicago, 1985.
- 3-21 Canadian Prestressed Concrete Institute, *Metric Design Manual — Precast and Prestressed Concrete*, 2nd ed., CPC1, Ottawa, 1987.
- 3-22 Trost, H., "Auswirkungen des Superpositionsprinzips auf Kriech- und Relaxationsprobleme bei Beton und Spannbeton" (Effects of the Principle of Superposition on Creep and Relaxation Problems in Concrete and Prestressed Concrete), *Beton- und Stahlbetonbau*, Vol. 62, No. 10, Oct. 1967, pp. 230-238; No. 11, Nov. 1967, pp. 261-269.
- 3-23 Bazant, Z.P., "Prediction of Concrete Creep Effects Using Age-Adjusted Effective Modulus Method," *ACI Journal*, Vol. 69, No. 4, Apr. 1972, pp. 212-217.
- 3-24 Gopalaratnam, V.S., and Shah, S.P., "Softening Response of Plain Concrete in Direct Tension," *ACI Journal*, Vol. 82, No. 3, May-June 1985, pp. 310-323.
- 3-25 Blanks, Robert F., "Concrete for Prestressing," *Proceedings of the First United States Conference on Prestressed Concrete*, Massachusetts Institute of Technology, Cambridge, Mass., Aug. 1951, pp. 136-149.
- 3-26 Priestley, M.J.N., "Thermal Stresses in Concrete Structures," *Proceedings of the Canadian Structural Concrete Conference*, Toronto, Sept. 1981, pp. 255-283.
- 3-27 Lie, T.T., Rowe, T.J., and Lin, T.D., "Residual Strength of Fire-Exposed Reinforced Concrete Columns," *Evaluation and Repair of Fire Damage to Concrete*, SP-92, American Concrete Institute, Detroit, 1986, pp. 153-174.
- 3-28 Richart, F.E., Brandtzæg, A., and Brown, R.L., "A Study of the Failure of Concrete under Combined Compressive Stresses," Bulletin No. 185, Engineering Experimental Station, University of Illinois, 1928, 104 pp.
- 3-29 Kent, D.C., and Park, R., "Flexural Members with Confined Concrete," *Journal of the Structural Division, ASCE*, Vol. 97, No. ST7, July 1971, pp. 1969-1990.
- 3-30 Sheikb, S., and Uzumeri, S.M., "Strength and Ductility of Tied Concrete Columns," *Journal of the Structural Division, ASCE*, Vol. 106, No. ST5, May 1980, pp. 1079-1102.
- 3-31 American Society for Testing and Materials, "Specification for Uncoated 7-Wire Stress-Relieved Steel Strand for Prestressed Concrete," ASTM A416-85, ASTM, Philadelphia, 1985.
- 3-32 American Society for Testing and Materials, "Standard Specification for Uncoated Stress-Relieved Steel Wire for Prestressed Concrete," ASTM A421-80, ASTM, Philadelphia, 1980.
- 3-33 American Society for Testing and Materials, "Standard Specification for High-Strength Steel Bar for Prestressing Concrete," ASTM A722-75, ASTM, Philadelphia, 1981.
- 3-34 Canadian Standards Association, "Steel for Prestressed Concrete Tendons," CSA G279-M82, CSA, Rexdale, Canada, 1982.
- 3-35 American Society for Testing and Materials, "Standard Specification for Deformed and Plain Billet-Steel Bars for Concrete Reinforcement (Metric)," ASTM A615-87, ASTM, Philadelphia, 1987.
- 3-36 Canadian Standards Association, "Billet-Steel Bars for Concrete Reinforcement," CSA G30.12-M77, CSA, Rexdale, Canada, 1977.
- 3-37 American Society for Testing and Materials, "Specification for Low-Alloy Steel Deformed Bars for Concrete Reinforcement," ASTM A706/A706M-86, ASTM, Philadelphia, 1986.
- 3-38 Canadian Standards Association, "Weldable Low Alloy Steel Deformed Bars for Concrete Reinforcement," CSA G30.16-M77, CSA, Rexdale, Canada, 1977.

- 3-39 American Society for Testing and Materials. "Standard Specification for Welded Steel Wire Fabric for Concrete Reinforcement." ASTM A185-85. ASTM, Philadelphia, 1985.
- 3-40 American Society for Testing and Materials. "Standard Specification for Welded Deformed Steel Wire Fabric for Concrete Reinforcement." ASTM A497-79. ASTM, Philadelphia, 1979.
- 3-41 Canadian Standards Association. "Welded Steel Wire Fabric Concrete Reinforcement." CSA G30.5-M83. CSA, Rexdale, Canada, 1983.
- 3-42 Canadian Standards Association. "Welded Deformed Steel Wire Fabric for Concrete Reinforcement." CSA G30.15-M83. CSA, Rexdale, Canada, 1983.
- 3-43 Mattock, Alan H., "Flexural Strength of Prestressed Concrete Sections by Programmable Calculator," *PCI Journal*, Vol. 24, No. 1, Jan.-Feb. 1979, pp. 32-54.
- 3-44 Magura, D., Sozen, M.A., and Siess, C.P., "A Study of Stress Relaxation in Prestressing Reinforcement," *PCI Journal*, Vol. 9, No. 2, Mar.-Apr. 1964, pp. 13-57.
- 3-45 OHBDC. *Ontario Highway Bridge Design Code*. 2nd ed., Ontario Ministry of Transportation and Communications, Toronto, 1983, 357 pp.
- 3-46 Ghali, Amin, and Trevino, Jose, "Relaxation of Steel in Prestressed Concrete," *PCI Journal*, Vol. 30, No. 5, Sept.-Oct. 1985, pp. 82-90.
- 3-47 CEB-FIP. *Model Code for Concrete Structures: CEB-FIP International Recommendations*, 3rd ed., Comité Euro-International du Béton, Paris, 1978, 348 pp.
- 3-48 Hanson, J.M., Somes, N.F., and Helgason, Th., "Investigation of Design Factors Affecting Fatigue Strength of Reinforcing Bars," *Abelès Symposium on Fatigue of Concrete*, SP-41, American Concrete Institute, Detroit, 1974, pp. 71-106.
- 3-49 Warner, R.F., and Hulsbos, C.L., "Fatigue Properties of Prestressing Strand," *PCI Journal*, Vol. 11, No. 1, Jan.-Feb. 1966, pp. 32-52.
- 3-50 Rabbat, B.G., Kaar, P.H., Russell, H.G., and Bruce, R.N., "Fatigue Tests of Pretensioned Girders with Blanketed and Draped Strands," *PCI Journal*, Vol. 24, No. 4, July-Aug. 1979, pp. 88-114.
- 3-51 Tide, R.H.R., and Van Horn, D.A., "A Statistical Study of the Static and Fatigue Properties of High Strength Prestressing Strand," Laboratory Report No. 309.2, Fritz Engineering Laboratory, Lehigh University, Bethlehem, Pa., June 1966.
- 3-52 FIP Commission on Practical Design. *FIP Recommendations—Practical Design of Reinforced and Prestressed Concrete Structures*. Thomas Telford Ltd., London, 1984, 36 pp.
- 3-53 Hanson, John M., Hulsbos, Cornel L., and Van Horn, David A., "Fatigue Tests of Prestressed Concrete I-Beams," *Journal of the Structural Division, ASCE*, Vol. 96, No. ST11, Nov. 1970, pp. 2443-2464.
- 3-54 Rigan, Claudio, and Thürlmann, Bruno, "Fatigue Tests on Post-Tensioned Concrete Beams," Bericht Nr. 8101-1, Institut für Baustatik und Konstruktion, Eidgenössische Technische Hochschule, Zürich, Aug. 1984, 74 pp.
- 3-55 Waterhouse, R.B., *Fretting Fatigue*, Applied Science Publishers Ltd., Barking, Essex, UK, 1981.
- 3-56 ACI Committee 215, "Considerations for Design of Concrete Structures Subjected to Fatigue Loading," *ACI Journal*, Vol. 71, No. 3, Mar. 1974, pp. 97-121.
- 3-57 Abrams, Duff A., "Tests of Bond between Concrete and Steel," Bulletin No. 71, Engineering Experiment Station, University of Illinois, Champaign, 1913.

- 3-58 Tepfers, Ralejs, "A Theory of Bond Applied to Overlapped Tensile Reinforcement Splices for Deformed Bars," Publication 73.2, Division of Concrete Structures, Chalmers University of Technology, Göteborg, Sweden, 1973, 328 pp.
- 3-59 Berggren, L., "Utdragsprov med kör vidhäftningsplattan," Publication 686, Division of Concrete Structures, Chalmers University of Technology, Göteborg, Sweden, 1965.
- 3-60 Kaar, P.H., La Frangh, R.W., and Mass, M.A., "Influence of Concrete Strength on Strand Transfer Length," *PCI Journal*, Vol. 8, No. 5, Oct. 1963, pp. 47-67.
- 3-61 Hoyer, E., and Friedrich, E., "Beitrag zur Frage der Haftspannung in Eisenbetonbauteilen" (Contribution towards the Question of Bond Strength in Reinforced Concrete Members), *Beton und Eisen*, Berlin, Vol. 38, No. 6, 1939, pp. 107-110.
- 3-62 Stocker, M.F., and Sozen, M.A., "Bond Characteristics of Prestressing Strand," Bulletin No. 503, Engineering Experiment Station, University of Illinois, Champaign, 1970, 263 pp.
- 3-63 Schlaich, J., Kordina, K., and Engell, H.-J., "Teileinsturz der Kongresshalle Berlin-Schadensursachen zusammenfassendes Gutachten" (Partial Collapse of the Berlin Congress Hall—Summary of the Investigation into the Causes of the Collapse), *Beton- und Stahlbetonbau*, Vol. 75, No. 12, Dec. 1980, pp. 281-294.
- 3-64 ACI Committee 222, "Corrosion of Metals in Concrete," *ACI Journal*, Vol. 82, No. 1, Jan.-Feb. 1985, pp. 3-32.
- 3-65 Manning, David G., "Corrosion Resistant Design of Concrete Structures," *Proceedings of the Canadian Structural Concrete Conference*, Toronto, 1981, pp. 199-223.
- 3-66 Schiessl, Peter, "Zur Frage der zulässigen Rissbreite und der erforderlichen Betondeckung im Stahlbetonbau unter besonderer Berücksichtigung der Karbonatisierung des Betons" (A Contribution towards the Question of Allowable Crack Widths, Required Concrete Cover with Special Consideration of the Carbonization of Concrete), Bulletin No. 255, Deutscher Ausschuss für Stahlbeton, Berlin, 1976, 175 pp.
- 3-67 Gjørv, O.E., "Steel Corrosion in Reinforced and Prestressed Concrete Structures," *Nordisk Betong, Journal of the Nordic Concrete Federation*, No. 2-4, 1982, pp. 147-151.
- 3-68 Gaynor, R.D., "Understanding Chloride Percentages," *Concrete International: Design and Construction*, Vol. 7, No. 9, Sept. 1985, pp. 26-27.
- 3-69 Clear, K.C., *Time-to-Corrosion of Reinforcing Steel in Concrete Slabs, Vol. 3: Performance after 830 Daily Salt Applications*, Report No. FHWA-RD-76-70, Federal Highway Administration, Washington, D.C., 1976, 64 pp.
- 3-70 Gerwick, B.C., and Mehta, P.K., "Cracking-Corrosion Interaction in Concrete Exposed to Marine Environment," *Concrete International: Design and Construction*, Vol. 4, No. 10, Oct. 1982, pp. 45-51.
- 3-71 Rasheeduzzafar, Dakhil, Fahd H., and Gahtam, Ahmad S., "Corrosion of Reinforcement in Concrete Structures in the Middle East," *Concrete International: Design and Construction*, Vol. 7, No. 9, Sept. 1985, pp. 48-55.
- 3-72 Beeby, A.W., "Cracking, Cover, and Corrosion of Reinforcement," *Concrete International: Design and Construction*, Vol. 5, No. 2, Feb. 1983, pp. 35-40.

Demonstration Problems

- 3-1 Write brief notes on the following topics
- Influence of water/cement ratio on concrete performance.
 - Factors that will cause the strain of concrete to vary.
 - Differences in the properties of stress-relieved and low-relaxation strand.
 - Factors that influence the fatigue strength of post-tensioned tendons.
 - Influence of concrete cover and crack widths on corrosion of reinforcement
- 3-2 A normal-weight concrete has a cylinder strength of 6000 psi (41 MPa). Prepare a predicted compressive stress-compressive strain curve for this concrete using Eq. (3-1). Also plot the parabolic stress-strain curve using Eq. (3-7). Comment on the differences between the two curves. If the concrete is subjected to a short-term load of 4000 psi (27.6 MPa), determine the resulting strain.
- Use the linear elastic relationship of Eq. (3-9).
 - Use the parabolic stress-strain relationship of Eq. (3-8).
 - Use the stress-strain relationship of Eq. (3-1). Use trial and error.
- 3-3 The measured stress-strain response for a lightweight concrete ($w_c = 116 \text{ lb}/\text{ft}^3$ or $1860 \text{ kg}/\text{m}^3$) is shown in Fig. 3-52. Use this response to calculate values of E_c , n , and k appropriate for this concrete. Using these fixed parameters, draw a stress-strain curve using Eq. (3-1) and compare it with the measured response. Using Eq. (3-1) plot the stress-strain response of a normal-weight concrete having the same strength. Comment on the influence of concrete density on the shape of the stress-strain curve.
- 3-4 A normal-density concrete has a compressive strength of 4000 psi (27.6 MPa). A compressive stress is applied to the concrete. This stress is increased in value from zero to 3500 (24.1 MPa) over a short period of time and is then reduced to zero again. Calculate the residual compressive strain that remains in the concrete after the compressive stress has been removed. For simplicity use the parabolic stress-strain relationship.
- 3-5 The normal-density concrete panel shown in Fig. 3-53 was moist cured for 7 days and was then subjected to a compressive stress of 1700 psi (11.7 MPa). At this time the concrete strength was 4500 psi (31 MPa). Estimate the total concrete strain after the panel had been loaded for 50 days in an environment where the relative humidity was 50%. Include both creep and shrinkage when calculating the strains. For the short-term response use the linear elastic relationship of Eq. (3-9).
- 3-6 A large plain concrete beam has a cross section of 36×36 in. (914×914 mm). The simply supported beam spans 18 ft (5.49 m) and is subjected to a point load at midspan. The crushing strength of a standard cylinder cast from the same concrete as the beam was 3600 psi (24.8 MPa). Estimate the magnitude of the point load required to crack the beam. Assume that the concrete weighs $150 \text{ lb}/\text{ft}^3$ (23.5 kN/m³). Account for the influence of size on the tensile strength of concrete.
- 3-7 A plain concrete prism has a cross section of 6×6 in. (152×152 mm) and is 36 in. (914 mm) long. The ends of the prism are attached to rigid abutments that prevent the prism from changing length. The concrete prism is then subjected to rapid cooling. If the normal-weight concrete has a compressive strength of 5000 psi (34.5 MPa), estimate the drop in temperature required to crack the concrete.

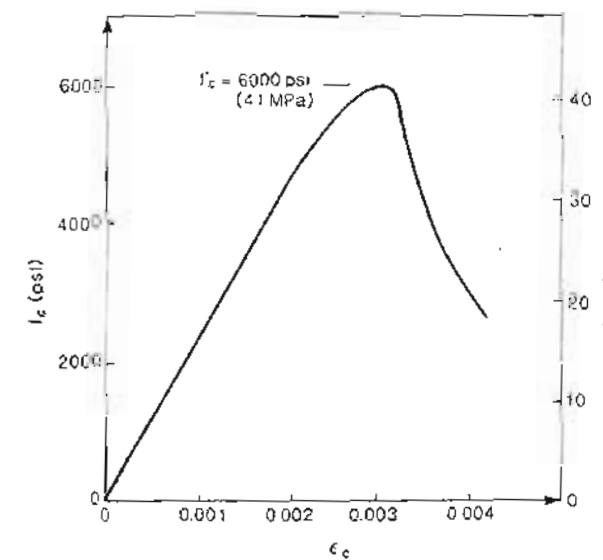


Figure 3-52 Measured stress-strain response of lightweight concrete.

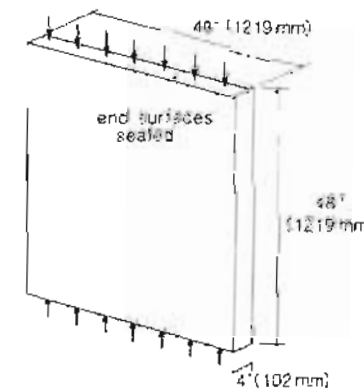


Figure 3-53 Plain concrete panel.

- 3-8 The measured stress-strain response of a 0.276 in. (7 mm) wire is shown in Fig. 3-54. Using this plot, develop an appropriate modified Ramberg-Osgood function to represent the response of this wire.

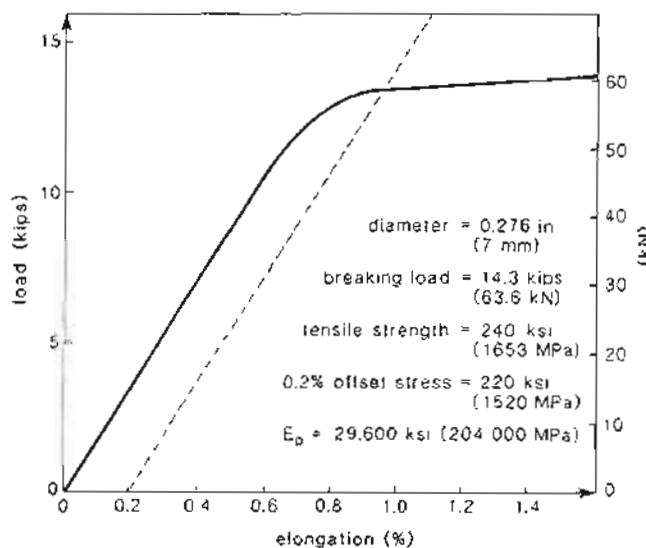


Figure 3-54 Stress-strain response of 0.276 in. (7 mm) wire.

- 3-9 Use Tide and Van Horn's suggested relationship to plot an *S-N* curve for prestressing strand tested in air. On the same plot show points representing the observed fatigue life of strands tested in pretensioned and post-tensioned beams. Comment on the resulting diagram.

- 3-10 A force is applied to the end of a cantilever such that the end deflection is Δ (see Fig. 3-55). If the system were elastic, then

$$F_{\text{elastic}} = \frac{3E_c I}{L^3} \Delta$$

- (a) Plot the force required to hold Δ constant if Δ is suddenly imposed at 28 days and then held constant.
- (b) Plot the force (as a ratio of the elastic force required to produce the deflection existing at any time) if the deflection is gradually imposed starting at 28 days.

- 3-11 A #8 bar (25 mm diameter) with a yield strength of 60,000 psi (414 MPa) is cast along the centroidal axis of a prism of concrete with a square cross section. The normal-weight concrete has a cylinder crushing strength of 5000 psi (34.5 MPa). Prepare a plot showing how the development length, ℓ_d , required by the ACI Code changes as the width of the square increases.

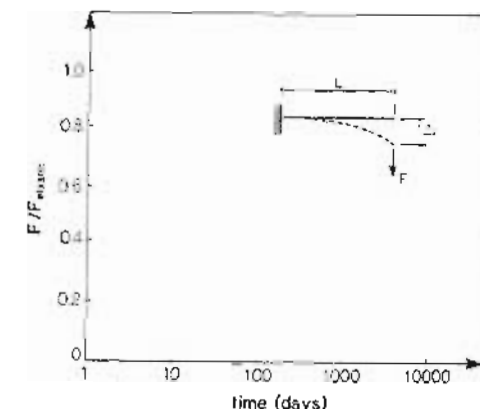


Figure 3-55 Variation of force with time.

Response of Members Subjected to Axial Load

... the demand is not so much for the mastering of difficult techniques as for a clear and thorough understanding of fundamental principles.

A.S. Hall and R.W. Woodhead, 1961

4.1 INTRODUCTION

While prestressed concrete members subjected to pure axial load do not often occur in practice, we will study this simple case in some detail because it enables us to introduce the basic principles governing prestressed concrete behavior. Figure 4-1 illustrates the type of axially loaded member that we will study in this chapter. The member has a symmetrical cross section and may contain both prestressed reinforcement (area A_p) and non-prestressed reinforcement (area A_s). It will be assumed that the concrete (area A_c) is subjected to strains in only the axial direction and that these concrete strains are uniform over the section.

4.2 COMPATIBILITY CONDITIONS

The concrete strain is taken to be zero when the concrete is cast. Thus the length of the member at the time of casting is defined as the undeformed length of the member, L . The axial deformation measured from this undeformed condition will be called Δ .

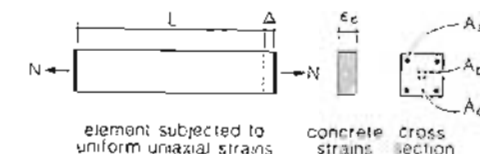


Figure 4-1 Member subjected to axial load.

The concrete strain, which is assumed to be uniform both over the cross section and along the length of the member, is given by

$$\epsilon_c = \frac{\Delta}{L} \quad (4-1)$$

We will assume that the concrete, the reinforcing bars, and the prestressing tendons are all rigidly anchored together at the ends of the member. Hence any change in length of the concrete must be accompanied by an identical change in length of the reinforcement.

The non-prestressed reinforcement and the concrete both have zero strain at the time the concrete is cast. As these two materials start with the same strain, have the same undeformed length, and undergo identical deformations, their strains must always be equal. Hence

$$\epsilon_s = \epsilon_c \quad (4-2)$$

Because prestressing involves stretching the reinforcement, the prestressed reinforcement does not start with the same strain as the surrounding concrete. Furthermore, the prestressed reinforcement will have a somewhat shorter (by about 1%) undeformed length than the surrounding concrete. While the two materials start with different strains they will subsequently be subjected to identical changes in deformation. Hence the subsequent changes in strain (i.e., changes in deformation divided by undeformed length) can be considered to be identical (i.e., the small difference in undeformed lengths is ignored). Thus the difference in strain between the prestressing steel and the surrounding concrete will remain essentially constant throughout the life of the member. This strain difference, which we will call $\Delta\epsilon_p$, is the basic "signature" of the prestressing operation. Hence at any stage in the life of a prestressed member, the strain in the prestressed reinforcement can be found from the strain in the surrounding concrete as

$$\epsilon_p = \epsilon_c + \Delta\epsilon_p \quad (4-3)$$

The strain difference, $\Delta\epsilon_p$, can be determined from the specific details of the prestressing operation. For pretensioned members (see Fig. 4-2) the concrete strain is zero, while the strain in the prestressing tendons, ϵ_{pbet} , has a high tensile value when the two

materials are bonded together. Hence for pretensioned members the strain difference is equal to the tensile strain in the tendons at the time the concrete is placed. For post-tensioned members there is a small compressive strain in the concrete and a large tensile strain in the tendons at the time the two materials are bonded together. In this case $\Delta\epsilon_p$ is found from the difference between these two strains (see Fig. 4-2).

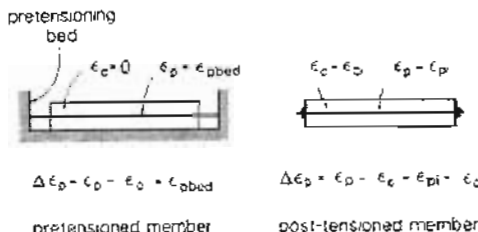


Figure 4-2 Calculation of strain difference, $\Delta\epsilon_p$.

4.3 EQUILIBRIUM CONDITIONS

For this simple case the equilibrium conditions reduce to the requirement that the internal stresses balance the applied load (see Fig. 4-3). That is,

$$\int_A f dA = N \quad (4-4)$$

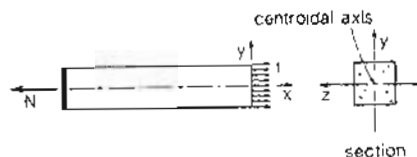


Figure 4-3 Free-body diagram of member subjected to axial load.

As the total concrete strain is uniform and assuming that temperature and shrinkage strains are also uniform, the stress in the concrete will be uniform over the section. Similarly, the reinforcing bars will all be at the same stress and any prestressing tendons will all have the same stress. Hence Eq. (4-4) becomes

$$A_c f_c + A_s f_s + A_p f_p = N \quad (4-5)$$

4.4 PREDICTING RESPONSE OF AXIALLY LOADED MEMBERS

The response of uniformly strained elements can be predicted by using the equilibrium and compatibility conditions described above, together with the material stress-strain relationships described in Chapter 3.

To illustrate the calculation procedures and to study the influence of prestressing, we will calculate the load-deformation response of the four members described in Fig. 4-4. These four members all have the same concrete dimensions but are reinforced in different ways. Member A is a non-prestressed member which contains eight #5 reinforcing bars with a yield strength of 60 ksi (414 MPa). Pretensioned member B contains only prestressed reinforcement, namely four 1/2 in. (13 mm) strands with a yield strength of 240 ksi (1655 MPa); in this example the stress-strain response of the strand is assumed to be bilinear. Partially prestressed member C contains both prestressed and non-prestressed reinforcement: two 1/2 in. (13 mm) strands and four #5 bars. Member D is reinforced with four 1/2 in. (13 mm) strands, but these strands have not been prestressed. The reinforcing of the four members described in Fig. 4-4 was chosen so that the yield force of the reinforcement in each member was essentially the same.

In calculating the response of these members we will assume short-term loading (i.e., negligible creep effects) and that shrinkage strains and temperature strains are zero. We will calculate the response of the members in both tension and compression. For this 5000 psi (34.5 MPa) concrete we will use the simple parabola of Eq. (3-7) for the compressive stress-strain relationship and a linear relationship in tension.

To determine the complete load-deformation response, we shall determine the axial load, N , which corresponds to various values of ϵ_c . The procedure is to choose a value of ϵ_c , to find the corresponding strains in the reinforcing bars and the prestressing tendons, to use the stress-strain relationships to find the stresses corresponding to these strains, and then to calculate the corresponding axial load, N .

Throughout these calculations we will use the convention that tensile stresses and tensile strains are positive while compressive stresses and compressive strains are negative.

(a) Predicting Response of Member A

1. Choose a value of ϵ_c .
Choose $\epsilon_c = -1.0 \times 10^{-3}$.
2. Find the corresponding strains in reinforcement.
From compatibility equation (4-2),

$$\epsilon_s = \epsilon_c = -1.0 \times 10^{-3}$$

3. Find the concrete stress, f_c .
As there are no shrinkage strains or thermal strains, all of the strain is caused by stress. Hence

$$\epsilon_{cf} = \epsilon_c = -1.0 \times 10^{-3}$$

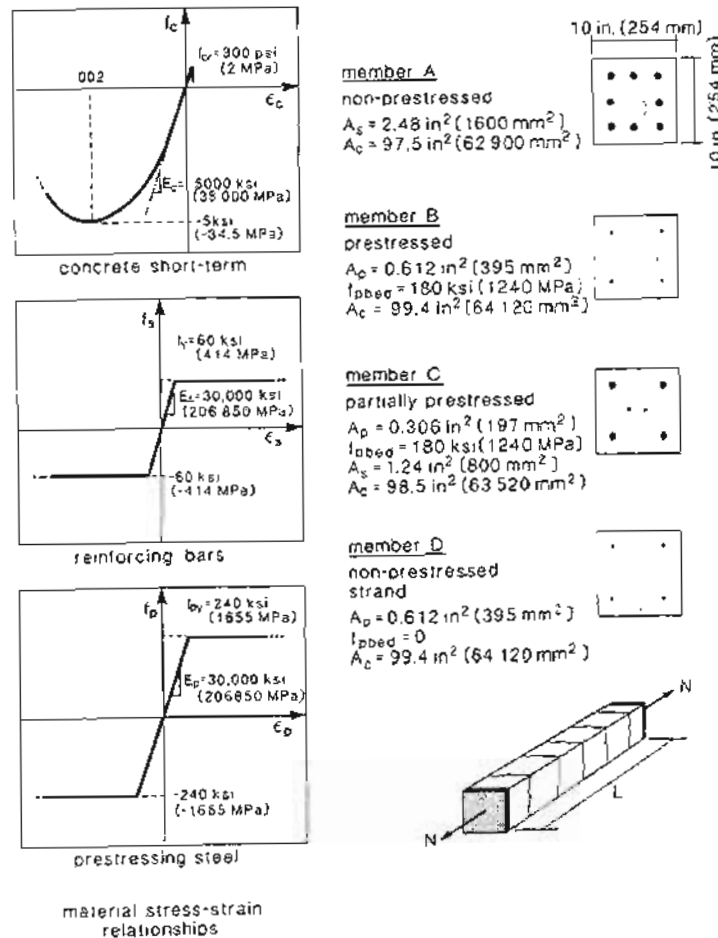


Figure 4-4 Details of example members.

Sec. 4.4 Predicting Response of Axially Loaded Members

From the stress-strain relationship of Eq. (3-7),

$$f_c = -5 \left[2 \left(\frac{-0.001}{-0.002} \right) - \left(\frac{-0.001}{-0.002} \right)^2 \right] = -3.75 \text{ ksi} (-25.9 \text{ MPa})$$

4. Find the reinforcing bar stress, f_s .

As there is no thermal strain, all of the strain in the reinforcing bars is caused by stress. Hence

$$\epsilon_{sf} = \epsilon_s = -1.0 \times 10^{-3}$$

From the stress-strain relationship of Eq. (3-23),

$$f_s = 30 \times 10^3 \times (-1.0 \times 10^{-3}) = -30 \text{ ksi} (-207 \text{ MPa})$$

Note that the steel has not yielded.

5. Find the applied axial load, N .

From equilibrium equation (4-5),

$$N = A_c f_c + A_s f_s = 97.5(-3.75) + 2.48(-30) = -440 \text{ kips} (-1957 \text{ kN})$$

Thus when the concrete strain is -0.001 , the member is subjected to an axial compression of 440 kips (1957 kN).

Repeating the calculations above for different values of ϵ_c enables the values shown in Table 4-1 to be obtained. Note that for concrete tensile strains higher than the strain to cause cracking, it is assumed that the stress in the concrete is zero.

(b) Predicting Response of Member B

1. Choose a value of ϵ_c .

Choose $\epsilon_c = -1.0 \times 10^{-3}$.

2. Find the corresponding strains in reinforcement.

The strand was stressed to 180 ksi (1240 MPa) prior to casting of the concrete. Hence, from Fig. 4-2,

$$\Delta \epsilon_p = \epsilon_{p,bed} = \frac{180}{30,000} = 6.0 \times 10^{-3}$$

From compatibility equation (4-3),

$$\epsilon_p = \epsilon_c + \Delta \epsilon_p = -1.0 \times 10^{-3} + 6.0 \times 10^{-3} = 5.0 \times 10^{-3}$$

3. Find the concrete stress, f_c .

$$\epsilon_{cf} = \epsilon_c = -1.0 \times 10^{-3}$$

Hence from the stress-strain relationship of Eq. (3-7),

$$f_c = -3.75 \text{ ksi} (-25.9 \text{ MPa})$$

4. Find the stress in prestressed reinforcement.

$$\epsilon_{pf} = \epsilon_p = 5.0 \times 10^{-3}$$

From the stress-strain relationship of Eq. (3-24),

$$f_p = 30 \times 10^3 \times 5.0 \times 10^{-3} = 150 \text{ ksi} (1034 \text{ MPa}) < f_{py}$$

5. Find the applied axial load, N .

From equilibrium equation (4-5),

$$N = A_c f_c + A_p f_p = 99.4(-3.75) + 0.612 \times 150 = -281 \text{ kips} (-1250 \text{ kN})$$

Thus when the concrete strain is -0.001 , the member is subjected to an axial compression of 281 kips (1250 kN).

Repeating the calculations above for different values of ϵ_c gives the values listed in Table 4-1. Note that for this prestressed member a significant axial tension is required to produce zero strain in the concrete.

(c) Predicting Response of Members C and D

The response of member C and the response of member D can be predicted using the same procedure already explained for member A and member B. The results of these calculations are summarized in Table 4-1. Note that member D must undergo very substantial elongations before the non-prestressed high-strength reinforcement yields in tension.

(d) Influence of Prestressing on Response

The calculated responses of the four members are compared in Figs. 4-5 and 4-6. From these figures the following observations can be made:

- Prestressing does not influence the tensile capacity of the members, this capacity being equal to the area of reinforcement times the yield strength of the reinforcement.
- Prestressing increases the load at which the concrete cracks.
- Prestressing results in the load-deformation curve being offset from the origin. That is, for the prestressed members, when N equals zero, ϵ_c is not zero.
- Prestressing reduces the concrete tensile strains at service load levels.
- Prestressing is detrimental to compressive response, causing reduced capacities and increased deformations.
- Prestressing enables high-strength reinforcement to be used efficiently in resisting tension. Figure 4-6 shows that high-strength, non-prestressed reinforcement would exhibit excessive deformations at service loads.

Table 4-1 Response values for members A, B, C, and D.

	Strain, ϵ_c	Stress, ksi			Axial load, N , kips	Stress, MPa			Axial load, N , kN	Comments
		f_c	f_s	f_p		f_c	f_s	f_p		
A	-0.003	-3.75	-60	—	-514.4	-25.9	-414	—	-2288	
	-0.002	-5.00	-60	—	-636.3	-34.5	-414	—	-2830	$f_c = f'_c$
	-0.001	-3.75	-30	—	-440.0	-25.9	-207	—	-1957	
	0.000	0.00	0	—	0.0	0.0	0	—	0	
	+0.00006	+0.30	+2	—	+33.7	+2.0	+12	—	+150	$f_c = f_{cr}$
	+0.002	0.00	60	—	+148.8	0.0	+414	—	+662	$f_s = f_{sy}$
	+0.003	0.00	60	—	+148.8	0.0	-414	—	+662	
B	-0.003	-3.75	—	+90	-317.7	-25.9	—	+621	-1413	
	-0.002	-5.00	—	+120	-423.6	-34.5	—	+827	-1884	$f_s = f'_c$
	-0.001	-3.75	—	+150	-281.0	-25.9	—	+1034	-1250	
	0.000	0.00	—	+180	+110.2	0.0	—	+1240	+490	
	+0.00006	+0.30	—	+182	+141.2	+2.0	—	+1254	+628	$f_c = f_{cr}$
	+0.002	0.00	—	+240	+146.9	0.0	—	+1655	+653	$f_p = f_{py}$
	+0.003	0.00	—	+240	+146.9	0.0	—	+1655	+653	
C	-0.003	-3.75	-60	+90	-416.2	-25.9	-414	+621	-1851	
	-0.002	-5.00	-60	+120	-530.2	-34.5	-414	+827	-2358	$f_c = f'_c$
	-0.001	-3.75	-30	+150	-360.7	-25.9	-207	+1034	-1604	
	0.000	0.00	0	+180	+55.1	0.0	0	+1240	+245	
	+0.00006	+0.30	+2	+182	+87.5	+2.0	+12	+1254	+389	$f_c = f_{cr}$
	+0.002	0.00	+60	+240	+147.8	0.0	-414	+1655	+568	steel yields
	+0.003	0.00	+60	+240	+147.8	0.0	+414	+1655	+568	
D	-0.003	-3.75	—	-90	-427.8	-25.9	—	-621	-1903	
	-0.002	-5.00	—	-60	-533.7	-34.5	—	-414	-2374	$f_c = f'_c$
	-0.001	-3.75	—	-30	-391.1	-25.9	—	-207	-1740	
	0.000	0.00	—	0	0.0	0.0	—	0	0	
	+0.00006	+0.30	—	+2	+30.9	+2.0	—	+12	+138	$f_c = f_{cr}$
	+0.002	0.0	—	+60	+36.7	0.0	—	+414	+163	
	+0.003	0.0	—	+240	+146.9	0.0	—	+1655	+653	$f_p = f_{py}$

4.5 ACCOUNTING FOR RELAXATION, CREEP, SHRINKAGE, AND THERMAL EFFECTS

The response predictions illustrated in Figs. 4-5 and 4-6 can be regarded as showing "short-term" response, for they did not consider the time-related effects of creep, shrinkage, relaxation, and temperature change. As discussed in Chapter 3, we can account for creep by using a modified stress-strain relationship for the concrete and can account for relaxation by using a reduced, effective modulus for the prestressing steel. Shrinkage strains and thermal strains can be taken into account by identifying the component parts of the total strain.

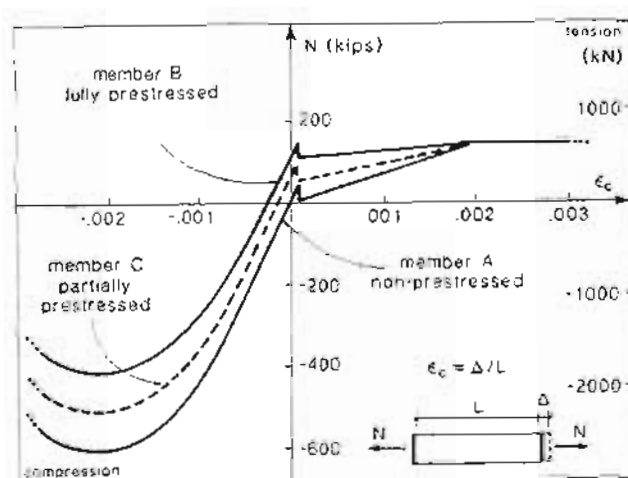


Figure 4-5 Influence of prestressing on load-deformation response.

Thus the total strain in the concrete, ϵ_c , is given by

$$\epsilon_c = \epsilon_{cf} + \epsilon_{sh} + \epsilon_{sth} \quad (4-6)$$

where ϵ_{cf} is the strain caused by stress, ϵ_{sh} is the unrestrained shrinkage strain (see Section 3.9), and ϵ_{sth} is the strain caused by temperature change (i.e., $\alpha_c \Delta T$ – see Section 3.10).

The total strain in the non-prestressed reinforcement, ϵ_s , is given by

$$\epsilon_s = \epsilon_{sf} + \epsilon_{sth} \quad (4-7)$$

where ϵ_{sf} is the strain caused by stress and ϵ_{sth} is the strain caused by temperature change (i.e., $\alpha_s \Delta T$ – see Section 3.17).

The total strain in the prestressed reinforcement, ϵ_p , is given by

$$\epsilon_p = \epsilon_{pf} + \epsilon_{pth} \quad (4-8)$$

where ϵ_{pf} is the strain caused by stress and ϵ_{pth} is the strain caused by temperature change (i.e., $\alpha_p \Delta T$ – see Section 3.17).

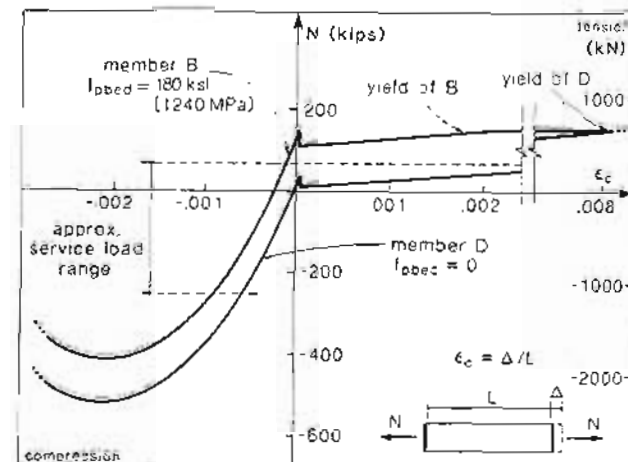


Figure 4-6 Need to prestress high-strength reinforcement.

4.6 PREDICTING LONG-TERM RESPONSE OF MEMBER C

To illustrate how we account for time-related effects, we will calculate the long-term response of member C (see Fig. 4-4) assuming that:

1. The creep coefficient, ϕ , is 2.7. The resulting long-term stress-strain relationship for the concrete is shown in Fig. 4-7.
2. The concrete unrestrained shrinkage strain, ϵ_{sh} , is -0.4×10^{-3} .
3. The prestressing strand has a loss of stress due to relaxation of 5%. Hence, from Eq. (3-30),

$$E_{p,eff} = 0.95 \times 30.000 = 28,500 \text{ ksi (197000 MPa)}$$

4. A temperature drop of 50°F (28°C) has occurred and the coefficients of thermal expansion, α_c , α_s , and α_p , are all equal to $6 \times 10^{-6}/^{\circ}\text{F}$ ($10 \times 10^{-6}/^{\circ}\text{C}$).

Rather than considering in detail the actual history of loading and deformation that might occur, we will calculate a limiting long-term response. Thus it will be considered that the shrinkage and thermal strains have occurred first and then the axial load has been very slowly applied so that the creep and relaxation have had time to occur.

Once again, we will determine the axial load, N , which corresponds to various chosen values of concrete strain, ϵ_c .

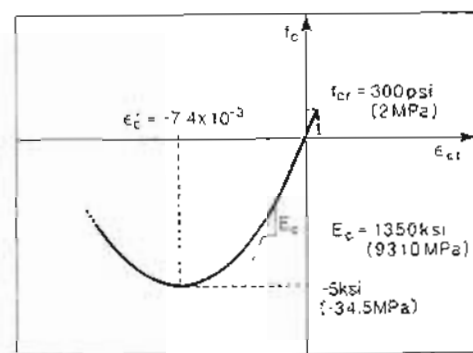


Figure 4-7 Long-term stress-strain response of concrete.

1. Choose a value of ϵ_c .
Choose $\epsilon_c = -1.0 \times 10^{-3}$

2. Find the corresponding strains in reinforcement.
For reinforcing bars,

$$\epsilon_s = \epsilon_c = -1.0 \times 10^{-3}$$

For prestressed strand,

$$\epsilon_p = \epsilon_c + \Delta\epsilon_p = -1.0 \times 10^{-3} + 6.0 \times 10^{-3} = 5.0 \times 10^{-3}$$

3. Find the concrete stress, f_c .

Only part of the total concrete strain, ϵ_c , is caused by stress. From Eq. (4-6).

$$\begin{aligned}\epsilon_{cf} &= \epsilon_c - \epsilon_{sth} - \epsilon_{eth} = -1.0 \times 10^{-3} - (-0.4 \times 10^{-3}) \\ &\quad - (-50 \times 6 \times 10^{-6}) \\ &= -0.3 \times 10^{-3}\end{aligned}$$

From the concrete long-term stress-strain relationship shown in Fig. 4-7.

$$f_c = -5 \left[2 \left(\frac{-0.3}{-7.4} \right) - \left(\frac{-0.3}{-7.4} \right)^2 \right] = -0.40 \text{ ksi } (-2.7 \text{ MPa})$$

4. Find the stresses in reinforcement, f_s and f_p .
From Eq. (4-7),

$$\epsilon_{sf} = \epsilon_s - \epsilon_{sth} = -1.0 \times 10^{-3} - (-50 \times 6 \times 10^{-6}) = -0.7 \times 10^{-3}$$

From the stress-strain relationship for the reinforcement,

$$f_s = E_s \epsilon_{sf} = 30,000 \times (-0.7 \times 10^{-3}) = -21 \text{ ksi } (-145 \text{ MPa})$$

From Eq. (4-8),

$$\epsilon_{pf} = \epsilon_p - \epsilon_{pth} = 5.0 \times 10^{-3} - (-50 \times 6 \times 10^{-6}) = 5.3 \times 10^{-3}$$

From the long-term stress-strain relationship for the prestressed reinforcement,

$$f_p = E_{p,eff} \epsilon_{pf} = 28.5 \times 10^3 \times 5.3 \times 10^{-3} = 151 \text{ ksi } (1042 \text{ MPa})$$

5. Find the applied axial load, N .

$$\begin{aligned}N &= A_c f_c + A_s f_s + A_p f_p \\ &= 98.5 \times (-0.40) + 1.24 \times (-21) + 0.306 \times 151 \\ &= -19.2 \text{ kips } (-85 \text{ kN})\end{aligned}$$

Hence for the long-term conditions given, a concrete strain of -0.001 occurs when only a small compressive force of 19.2 kips (85 kN) acts on the member.

Repeating the calculations above for different values of ϵ_c gives the values listed in Table 4-2.

Table 4-2 Long-term response values for member C.

ϵ_c	Strains $\times 1000$			Stresses, ksi			N kips	Stresses, MPa			N kN
	ϵ_{cf}	ϵ_{sf}	ϵ_{pf}	f_c	f_s	f_p		f_c	f_s	f_p	
-10.00	-9.30	-9.70	-3.70	-4.67	-60	-105	-567	-32.2	-414	-724	-2518
-8.10	-7.40	-7.80	-1.80	-5.00	-60	-51	-583	-34.5	-414	-352	-2589
-6.00	-5.30	-5.70	+0.30	-4.60	-60	+ 9	-524	-31.7	-414	+ 62	-2332
-4.00	-3.30	-3.70	+2.30	-3.47	-60	+ 66	-397	-23.9	-414	+ 455	-1760
-2.30	-1.60	-2.00	+4.00	-1.93	-60	+114	-230	-13.3	-414	+ 786	-1021
-0.478	+0.222	-0.178	+5.822	+0.30	+ 5.34	+168	+ 74	+ 2.0	+ 36.8	+1145	+ 328
0	+0.70	+0.30	+6.30	0.0	+ 9	+180	+ 66	0.0	+ 62.0	+1241	+ 294
+1.00	+1.70	+1.30	+7.30	0.0	+39	+208	+112	0.0	+ 269	+1434	+ 498
+1.70	+2.40	+2.00	+8.00	0.0	+60	+228	+144	0.0	+ 414	+1572	+ 641
+2.12	+2.82	+2.42	+8.42	0.0	+60	+240	+148	0.0	+ 414	+1655	+ 657
+3.00	+3.70	+3.30	+9.30	0.0	+60	+240	+148	0.0	+ 414	+1655	+ 657

4.7 COMPARISON OF SHORT-TERM AND LONG-TERM RESPONSES

Figure 4-8 compares the predicted long-term response for the prestressed concrete member with the predicted short-term response.

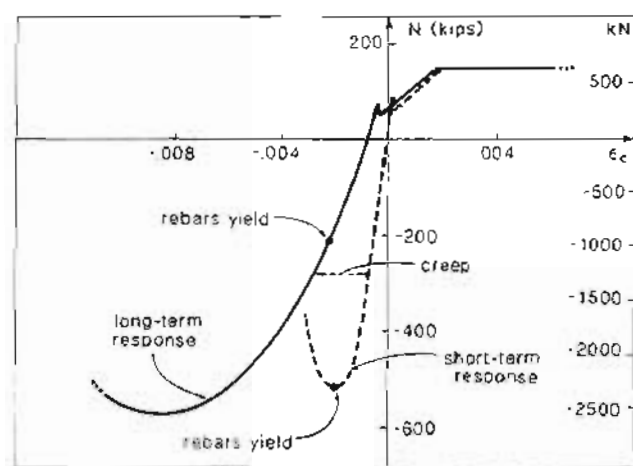


Figure 4-8 Short-term and long-term responses.

The "short-term" response and the "long-term" response are intended to be bounds on the possible response. "Short-term" implies no shrinkage or thermal strains, no creep of the concrete, and no relaxation of the prestressing steel. "Long-term" implies that all of the creep, shrinkage, and relaxation have taken place and the member has undergone the maximum temperature decrease. Hence "long-term" will give the greatest shortening possible.

The actual response will lie between these two extreme cases. Thus, if the member were loaded to 280 kips (1250 kN) compression and then the load held constant, the deformation would gradually increase from the short-term value toward the long-term value (see Fig. 4-8).

By comparing the two responses shown in Fig. 4-8, the following observations can be made:

- Under zero applied load ($N = 0$) there is a substantial change in length with time. This substantial shortening, which is about 1 part per thousand, must be accounted for in design.
- Under long-term loading the reinforcing bars yield in compression at a surprisingly small load. Creep and shrinkage cause the compression load to be transferred to the reinforcing bars.
- The long-term compressive capacity is a little larger than the short-term compressive capacity. For short-term loading the prestressing tendons are still in tension when

the concrete reaches its maximum compressive stress.

- For long-term loading the concrete cracks while the total concrete strain is still "compressive." While the total concrete strain is compressive, the strain caused by stress is tensile. Thus it is possible for cracks to form even in parts of prestressed concrete structures that are undergoing significant shortening.

4.8 LINEAR ELASTIC UNCRACKED RESPONSE

The procedures described above enable the axial load, N , corresponding to a given concrete strain, ϵ_c , to be conveniently calculated. While simple to calculate, the relationship between N and ϵ_c is highly nonlinear (see Fig. 4-9). Because of this, trial and error must be used to find the strain corresponding to a given axial load.

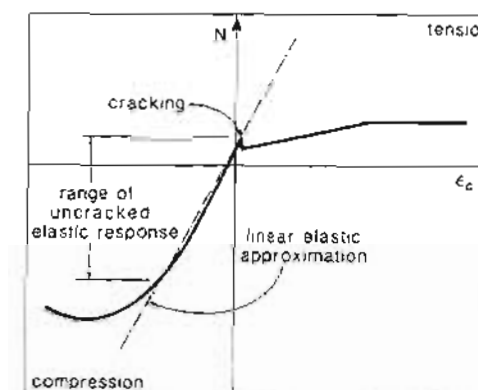


Figure 4-9 Range of applicability of linear elastic response.

While the concrete remains uncracked and while the stresses in the concrete and the reinforcement remain in the "elastic range," the relationship between N and ϵ_c is essentially linear (see Fig. 4-9). For this range of loads it is possible to derive closed-form expressions that enable us to predict the member response at a given axial load without resorting to trial and error.

The relationships used in determining this response are summarized below. Equilibrium relationships:

$$N = A_c f_c + A_s f_s + A_p f_p \quad (4-5)$$

Compatibility relationships:

$$\epsilon_s = \epsilon_c \quad (4-2)$$

$$\epsilon_p = \epsilon_c + \Delta\epsilon_p \quad (4-3)$$

Stress-strain relationships:

$$f_c = E_c \epsilon_{cf} \quad (4-9)$$

$$f_s = E_s \epsilon_{sf} \quad (4-10)$$

$$f_p = E_p \epsilon_{pf} \quad (4-11)$$

Strain relationships:

$$\epsilon_c = \epsilon_{cf} + \epsilon_{sth} + \epsilon_{cth} \quad (4-6)$$

$$\epsilon_s = \epsilon_{sf} + \epsilon_{sth} \quad (4-7)$$

$$\epsilon_p = \epsilon_{pf} + \epsilon_{pth} \quad (4-8)$$

Substituting the compatibility and stress-strain relationships into equilibrium equation (4-5) gives

$$\begin{aligned} N &= A_c E_c (\epsilon_c - \epsilon_{sth} - \epsilon_{cth}) + A_s E_s (\epsilon_s - \epsilon_{sth}) + A_p E_p (\epsilon_p + \Delta\epsilon_p - \epsilon_{pth}) \\ &= (A_c E_c + A_s E_s + A_p E_p) \epsilon_c + A_p E_p \Delta\epsilon_p \\ &\quad - (A_c E_c \epsilon_{sth} + A_c E_c \epsilon_{cth} + A_s E_s \epsilon_{sth} + A_p E_p \epsilon_{pth}) \end{aligned} \quad (4-12)$$

For convenience, call

$$N_0 = A_p E_p \Delta\epsilon_p - (A_c E_c \epsilon_{sth} + A_c E_c \epsilon_{cth} + A_s E_s \epsilon_{sth} + A_p E_p \epsilon_{pth}) \quad (4-13)$$

The term N_0 can be referred to as the decompression force, that is, the force required to produce zero strain in the concrete. The term A_{trans} is defined as

$$A_{trans} = A_c + \frac{E_s}{E_c} A_s + \frac{E_p}{E_c} A_p \quad (4-14)$$

where A_{trans} is the transformed area.

With this notation, Eq. (4-12) can be written as

$$\epsilon_c = \frac{N - N_0}{E_c A_{trans}} \quad (4-15)$$

The linear relationship above, between the applied axial load, N , and the total concrete strain, ϵ_c , is an approximation to the more complex relationship shown in Fig. 4-9.

It is, of course, only appropriate to apply this linear relationship for tensile loads less than the cracking load and for compressive loads less than those causing significant nonlinearity.

4.9 EXAMPLE CALCULATIONS ASSUMING ELASTIC UNCRACKED RESPONSE

For member C described in Fig. 4-4, calculate the stress in the concrete, f_c , the stress, f_p , in the prestressed strand, and the stress, f_s , in the reinforcing bars, for short-term response and long-term response when the axial load, N , is zero. Use the conditions and the material properties from Section 4.6 for the long-term calculation. That is, $\phi = 2.7$, $\epsilon_{sth} = -0.4 \times 10^{-3}$, $\epsilon_{cth} = \epsilon_{sth} = \epsilon_{pth} = -0.3 \times 10^{-3}$, and $E_{p,eff} = 28,500$ ksi (197 000 MPa). Assume that $E_c = 5000$ ksi (35 000 MPa).

(a) Calculation of Short-Term Stresses

$$\begin{aligned} N_0 &= A_p E_p \Delta\epsilon_p - (A_c E_c \epsilon_{sth} + A_c E_c \epsilon_{cth} + A_s E_s \epsilon_{sth} + A_p E_p \epsilon_{pth}) \\ &= 0.306 \times 30,000 \times 0.006 - 0 \\ &= 55.1 \text{ kips (245 kN)} \\ A_{trans} &= A_c + \frac{E_s}{E_c} A_s + \frac{E_p}{E_c} A_p \\ &= 98.5 + \frac{30}{5} \times 1.24 + \frac{30}{5} \times 0.306 \\ &= 107.8 \text{ in}^2 (69 530 \text{ mm}^2) \end{aligned}$$

The total strain when N equals zero, under short-term conditions, can then be found from Eq. (4-15) as

$$\begin{aligned} \epsilon_c &= \frac{N - N_0}{E_c A_{trans}} \\ &= \frac{0 - 55.1}{5000 \times 107.8} \\ &= -0.102 \times 10^{-3} \end{aligned}$$

For this short-term response, ϵ_{cf} equals ϵ_c , and hence the concrete stress is

$$\begin{aligned} f_c &= E_c \epsilon_{cf} \\ &= 5000 \times (-0.102 \times 10^{-3}) \\ &= -510 \text{ psi} (-3.52 \text{ MPa}) \end{aligned}$$

From Eq. (4-3),

$$\begin{aligned} \epsilon_p &= \epsilon_c + \Delta\epsilon_p \\ &= -0.102 \times 10^{-3} + 6.0 \times 10^{-3} \\ &= 5.898 \times 10^{-3} \end{aligned}$$

For this short-term response, ϵ_{pf} equals ϵ_p , and hence the stress in the strand is

$$\begin{aligned} f_p &= E_p \epsilon_{pf} \\ &= 30,000 \times 5.898 \times 10^{-3} \\ &= 176.9 \text{ ksi (1220 MPa)} \end{aligned}$$

Recalling that in the stressing bed the stress in the strand was 180 ksi (1241 MPa), we can see that the elastic shortening of the member when released from the bed has resulted in about a 2% loss of presress.

The strain, ϵ_{sf} , caused by stress, for this short-term response, is equal to the total strain, ϵ_s , which in turn equals ϵ_c , and hence the stress in the reinforcing bars is

$$\begin{aligned} f_s &= E_s \epsilon_{sf} \\ &= 30,000 \times (-0.102 \times 10^{-3}) \\ &= -3.06 \text{ ksi } (-21 \text{ MPa}) \end{aligned}$$

(b) Calculation of Long-Term Stresses

For long-term elastic calculations we will use Eqs. (4-13), (4-14), and (4-15) except that in these equations we will substitute $E_{c,eff}$ for E_c and $E_{p,eff}$ for E_p , where

$$\begin{aligned} E_{c,eff} &= \frac{E_c}{1 + \phi} = \frac{5000}{1 + 2.7} = 1351 \text{ ksi } (9318 \text{ MPa}) \\ E_{p,eff} &= 28,500 \text{ ksi } (197,000 \text{ MPa}) \end{aligned}$$

From Eq. (4-13),

$$\begin{aligned} N_o &= A_p E_{p,eff} \Delta \epsilon_p - A_c E_{c,eff} (\epsilon_{sth} + \epsilon_{cth}) - A_s E_s \epsilon_{sth} - A_p E_{p,eff} \epsilon_{pth} \\ &= 0.306 \times 28,500 \times 6 \times 10^{-3} - 98.5 \times 1351(-0.7 \times 10^{-3}) \\ &\quad - 1.24 \times 30,000(-0.3 \times 10^{-3}) - 0.306 \times 28,500 \times (-0.3 \times 10^{-3}) \\ &\approx 159.3 \text{ kips } (709 \text{ kN}) \end{aligned}$$

From Eq. (4-14),

$$\begin{aligned} A_{trans} &= A_c + \frac{E_s}{E_{c,eff}} A_s + \frac{E_{p,eff}}{E_{c,eff}} A_p \\ &= 98.5 + \frac{30}{1.351} \times 1.24 + \frac{28.5}{1.351} \times 0.306 \\ &\approx 132.5 \text{ in}^2 (85,480 \text{ mm}^2) \end{aligned}$$

Hence from Eq. (4-15), the total concrete strain, ϵ_c , under long-term conditions for the case when $N = 0$ is

$$\begin{aligned} \epsilon_c &= \frac{N - N_o}{E_{c,eff} A_{trans}} \\ &= \frac{0 - 159.3}{1351 \times 132.5} \\ &= -0.890 \times 10^{-3} \end{aligned}$$

Note that the long-term shortening under zero axial load is nearly 1 part per thousand.

Only part of the total concrete strain is caused by stress. From Eq. (4-6),

$$\begin{aligned} \epsilon_{sf} &= \epsilon_c - \epsilon_{sh} - \epsilon_{cth} \\ &= -0.890 \times 10^{-3} - (-0.4 \times 10^{-3}) - (-0.3 \times 10^{-3}) \\ &= -0.190 \times 10^{-3} \end{aligned}$$

Hence the long-term concrete stress when the axial load is zero is

$$\begin{aligned} f_c &= E_c \epsilon_{sf} \\ &= 1351 \times (-0.190 \times 10^{-3}) \\ &= -257 \text{ psi } (-1.77 \text{ MPa}) \end{aligned}$$

Note that due to creep, shrinkage, and relaxation the compressive stress in the concrete has been reduced from 510 psi to 257 psi (3.52 MPa to 1.77 MPa), a loss of about 50%. From Eq. (4-3),

$$\begin{aligned} \epsilon_p &= \epsilon_c + \Delta \epsilon_p \\ &= -0.890 \times 10^{-3} + 6 \times 10^{-3} \\ &= 5.110 \times 10^{-3} \end{aligned}$$

From Eq. (4-8),

$$\begin{aligned} \epsilon_{pf} &= \epsilon_p - \epsilon_{pth} \\ &= 5.110 \times 10^{-3} - (-0.3 \times 10^{-3}) \\ &= 5.410 \times 10^{-3} \end{aligned}$$

Hence the long-term stress in the prestressing strand when the axial load is zero, is

$$\begin{aligned} f_p &= E_{p,eff} \epsilon_{pf} \\ &= 28,500 \times 5.410 \times 10^{-3} \\ &= 154.2 \text{ ksi } (1063 \text{ MPa}) \end{aligned}$$

Hence due to creep, shrinkage, and relaxation, the tensile stress in the prestressing strand has been reduced from 176.9 ksi to 154.2 ksi (1220 MPa to 1063 MPa), a loss of 13%. From Eq. (4-2),

$$\begin{aligned} \epsilon_s &= \epsilon_c \\ &= -0.890 \times 10^{-3} \end{aligned}$$

From Eq. (4-7),

$$\begin{aligned} \epsilon_{sf} &= \epsilon_s - \epsilon_{sth} \\ &= -0.890 \times 10^{-3} - (-0.3 \times 10^{-3}) \\ &= -0.590 \times 10^{-3} \end{aligned}$$

Hence the long-term stress in the reinforcing bars is

$$\begin{aligned} f_s &= E_s \epsilon_{sf} \\ &= 30,000 \times (-0.590 \times 10^{-3}) \\ &= -17.7 \text{ ksi} (-122 \text{ MPa}) \end{aligned}$$

Hence due to creep, shrinkage, and relaxation, the compressive stress in the reinforcing bars increases from 3.06 ksi to 17.7 ksi (21 MPa to 122 MPa), an increase of 478%. This example demonstrates that the presence of non-prestressed reinforcing bars results in a significant redistribution of compressive stresses, increasing the compressive stress in the reinforcing bars and reducing the compressive stress in the concrete.

The short-term and long-term load-deformation responses for member C predicted assuming linear elastic uncracked response are compared in Fig. 4-10. Note that due to creep, shrinkage and relaxation, the stiffness of the member is greatly reduced, the deformation at zero axial load is greatly increased, and the axial load required to cause zero concrete strain is increased.

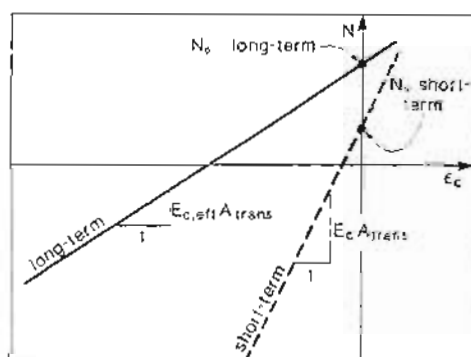


Figure 4-10 Comparison of short-term and long-term linear elastic response.

4.10 TENSILE STRESSES IN THE CONCRETE AFTER CRACKING

In the previous calculations we have assumed that when ϵ_{cf} exceeds the cracking strain, ϵ_{cr} , the tensile stress in the concrete will be zero. This assumption is equivalent to neglecting the presence of the concrete after cracking. Thus once the concrete has cracked, the load-deformation response of a bar encased in concrete is assumed to be exactly the same as that of a bare bar.

As early as 1899, it was known that this was not the case. Considère (Ref. 4-1) tested small mortar prisms reinforced with steel wires. When he subjected the prisms to tension he observed that their load-deformation response was almost parallel to the bare steel response but remained well above it.

In 1908, Mörsch (Ref. 4-2) explained this phenomenon in the following way:

Because of friction against the reinforcement, and of the tensile strength which still exists in the pieces lying between the cracks, even cracked concrete decreases to some extent the stretch of the reinforcement.

This effect came to be called "tension stiffening."

The results from a typical test of a bar encased in concrete are shown in Fig. 4-11.

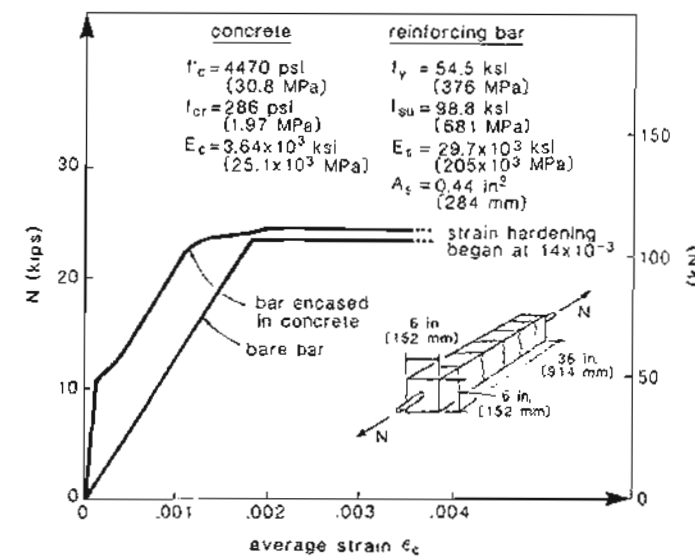


Figure 4-11 Observed response of bar encased in concrete. Adapted from Ref. 4-3.

To help us model the postcracking response of such a member, let us consider the manner in which the axial load is shared between the concrete and the reinforcement along the length of the member. The bond between the reinforcement and the concrete will enable some tension to be transferred from the bar to the concrete. Forces are transferred from the bar to the concrete by inclined compressive forces radiating out from the bar. As shown

by Goto (Ref. 4-4), these forces cause internal secondary cracks to form in addition to the primary cracks that are visible on the surface of the member (see Fig. 4-12).

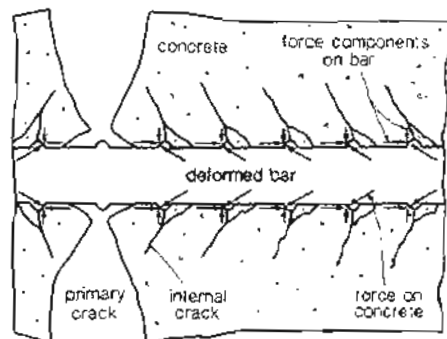


Figure 4-12 Formation of internal cracks. Adapted from Goto (Ref. 4-4).

Figure 4-13 illustrates the manner in which the axial load is shared between the concrete and the reinforcement and how this load sharing is influenced by the formation of cracks. Prior to cracking (see Fig. 4-13a) the load carried by the concrete, N_c , and the load carried by the steel remain constant along the length of the member. The applied load corresponding to a given elongation is $N_c + N_s$ (see Fig. 4-14). After the first primary crack forms, N_c and N_s are no longer constant along the member (see Fig. 4-13). At the crack, a short length of the bar will be debonded from the concrete and over this length all of the applied load must be carried by the bar. At primary cracks the concrete will be unstressed and a certain distance, the transfer length, will be required to build up the tensile stresses in all of the concrete surrounding the bar. At no section of the member can the load carried by the concrete exceed the area of concrete times the cracking stress of the concrete, $A_c f_{cr}$, for when this value is reached, a new primary crack will form. When there is no longer sufficient length between adjacent primary cracks for the load in the concrete to build up to the cracking load, no further primary cracks will form. The load sharing along the length of the member for this fully developed crack pattern is shown in Fig. 4-13c.

Figure 4-15 illustrates the variation of steel strain in a heavily instrumented reinforced concrete tension specimen tested by Scott and Gill (Ref. 4-5). It can be seen that the strain in the reinforcing bar rises to a peak at a crack location. After yielding of the bar at a crack location, the concentration of the straining at the crack will become even more pronounced.

If the variation of the tensile force in the bar along the length of the member is known, the variation of the strain along the member length can be calculated. The deformation

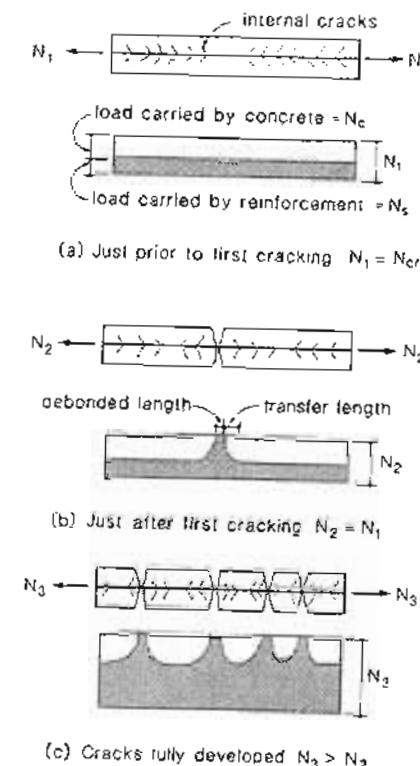


Figure 4-13 Load sharing between concrete and reinforcement.

of the member can then be found by integrating these strains along the length. This integration is equivalent to finding the average strain along the length of the bar. Because of the presence of the concrete, the average steel strain is, of course, somewhat smaller than the maximum strain in the steel which occurs at the cracks. Provided that the steel has not yielded, the steel strain at the cracks equals $N/A_s E_s$, while the average strain in the steel equals $N_s/A_s E_s$, where N_s is the average force in the bar.

The average force in the bar, N_s , can be found by subtracting the average force in the concrete, N_c , from the applied load, N . Thus the member deformation can be found from

$$\Delta = \epsilon_c L \quad (4-16)$$

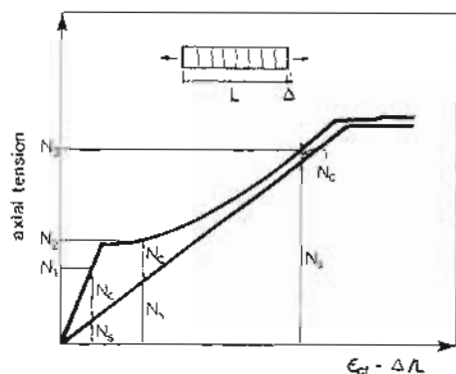


Figure 4-14 Influence of tension in concrete on load-deformation response.

$$\epsilon_c = \epsilon_s = \frac{N_s}{A_s E_s} \quad (4-17)$$

$$N_s = N - N_c \quad (4-18)$$

$$N_c = A_c f_c \quad (4-19)$$

where f_c is the average tensile stress in the concrete, which must be less than the cracking stress, f_{cr} .

When the first primary crack forms, the average stress in the concrete, f_c , will equal the cracking stress, f_{cr} . After the formation of the first crack, the average stress in the concrete will be reduced and as further cracks develop, the average stress will be further reduced. The decrease in average concrete stress observed by a number of different investigators is illustrated in Fig. 4-16. Also shown in this plot is a suggested average stress vs. average strain relationship, which is a modification of that suggested by Vecchio and Collins (Ref. 4-12). This suggested relationship is

If $\epsilon_{cf} > \epsilon_{cr}$, then

$$f_c = \frac{\alpha_1 \alpha_2 f_{cr}}{1 + \sqrt{500 \epsilon_{cf}}} \quad (4-20)$$

where α_1 = factor accounting for bond characteristics of reinforcement

$\alpha_1 = 1.0$ for deformed reinforcing bars

$\alpha_1 = 0.7$ for plain bars, wires, or bonded strands

$\alpha_1 = 0$ for unbonded reinforcement

α_2 = factor accounting for sustained or repeated loading

$\alpha_2 = 1.0$ for short-term monotonic loading

$\alpha_2 = 0.7$ for sustained and/or repeated loads

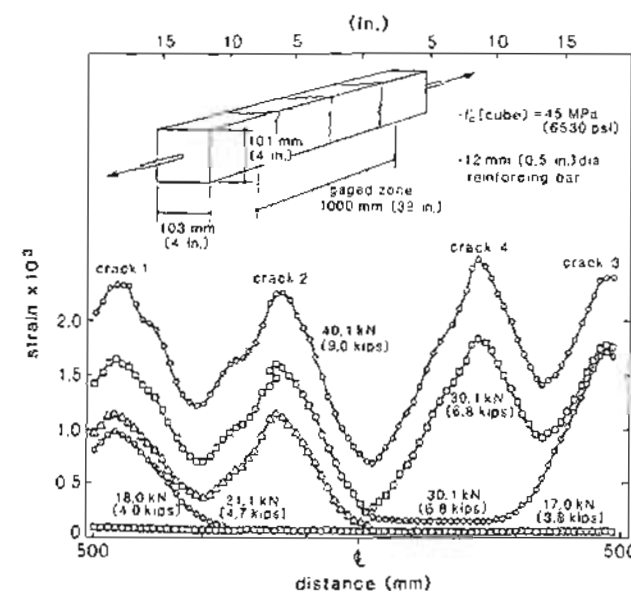


Figure 4-15 Variation of steel strain along the length of a tension specimen tested by Scott and Gill (Ref. 4-5).

Figure 4-17 illustrates the suggested average stress vs. average strain response for concrete in tension.

Using average stresses in the concrete is merely a convenient way of estimating the load corresponding to a particular member deformation. It is important to realize that at the crack no tensile stresses exist in the concrete and hence all of the applied axial tension must be carried by the reinforcement. The yield force of the reinforcement at the crack location will thus determine the maximum load that a member can carry.

4.11 EXAMPLE USING AVERAGE TENSILE STRESSES IN THE CONCRETE

Calculate the short-term tensile response of the member described in Fig. 4-11, accounting for the tensile stresses in the concrete after cracking. Once again the procedure will be to find N for a range of values of ϵ_c . For example, if $\epsilon_c = 1 \times 10^{-3}$, then the strain causing stress is also 1×10^{-3} since there are no shrinkage strains or thermal strains. As 1×10^{-3} greatly exceeds the concrete cracking strain, the concrete will be cracked. Hence

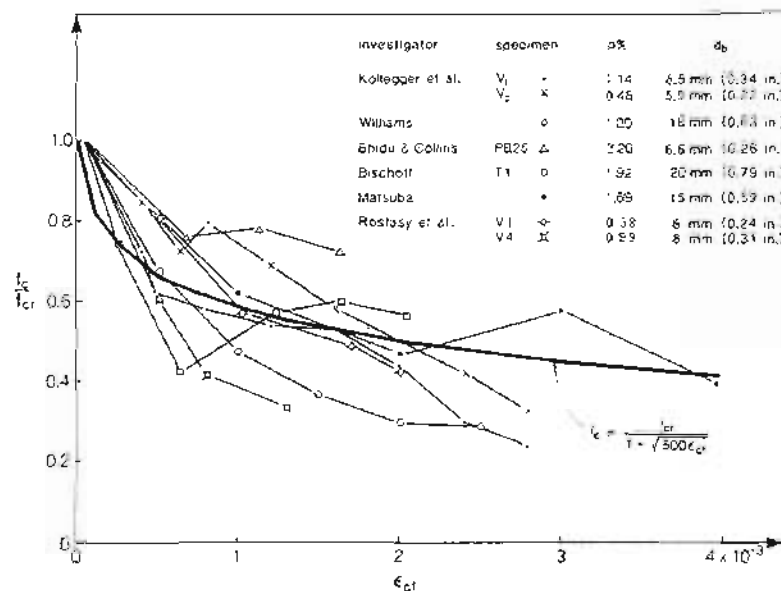


Figure 4-16 Average stress in concrete after cracking. Experimental data from Refs. 4-6 to 4-11.

from Eq. (4-20), for this short-term monotonic loading of a member containing a deformed reinforcing bar, the average tensile stress in the cracked concrete is

$$\begin{aligned} f_c &= \frac{\sigma_1 \alpha_2 f_{cr}}{1 + \sqrt{500 \epsilon_{cf}}} \\ &= \frac{1.0 \times 1.0 \times 286}{1 + \sqrt{500} \times 1 \times 10^{-3}} \\ &\approx 168 \text{ psi (1.16 MPa)} \end{aligned}$$

If the total concrete strain, ϵ_c , equals 1×10^{-3} , the total strain in the reinforcing bar also equals 1×10^{-3} . Since there is no thermal strain, the strain in the reinforcing bar due to stress, ϵ_{sf} , is also equal to 1×10^{-3} . Hence from the stress-strain relationship for the reinforcing steel, the average stress in the reinforcing bar is

$$\begin{aligned} f_s &= E_s \epsilon_{sf} \\ &= 29.7 \times 10^3 \times 1 \times 10^{-3} \\ &= 29.7 \text{ ksi (205 MPa)} \end{aligned}$$

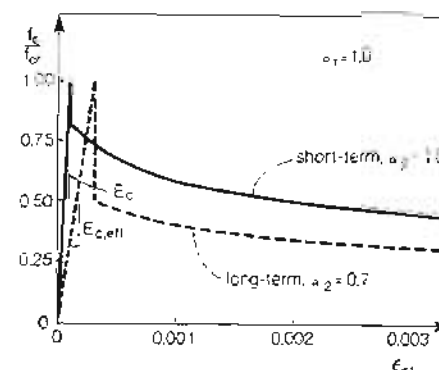


Figure 4-17 Average stress vs. average strain relationship for concrete in tension.

The axial load, N , corresponding to a concrete strain of 1×10^{-3} is thus

$$\begin{aligned} N &= A_c f_c + A_s f_s \\ &= 35.56 \times 0.168 + 0.44 \times 29.7 \\ &= 19.0 \text{ kips (84.5 kN)} \end{aligned}$$

The ability of the reinforcing bar to transmit this tensile load across the cracks must be checked. The stress in the reinforcement at a crack is given by

$$\begin{aligned} f_{scr} &= \frac{N}{A_s} \\ &= \frac{19.0}{0.44} \\ &= 43 \text{ ksi (298 MPa)} \end{aligned}$$

As this stress is less than the yield stress of the bar, $f_y = 54.5 \text{ ksi (376 MPa)}$, the reinforcement is capable of transmitting the tension across the cracks. At higher loads, yielding of the reinforcement at the cracks will govern the maximum load.

The calculations above have been repeated for a number of values of ϵ_c and the results of these calculations are summarized in Table 4-3. If this predicted response is compared with the experimental response shown in Fig. 4-11, it will be found that there is good agreement.

Table 4-3 Predicted response of bar encased in concrete.

$\epsilon_c \times 1000$	f_c ksi (MPa)	f_s ksi (MPa)	N kips (kN)	$f_{s,r}$ ksi (MPa)	Remarks
0.05	0.182 (1.25)	1.5 (10)	7.13 (32)	16.2 (112)	Un-cracked response
0.079	0.286 (1.97)	2.4 (16)	11.23 (50)	25.5 (176)	Cracking of concrete
0.10	0.234 (1.63)	3.0 (21)	9.6 (43)	21.9 (151)	
0.30	0.191 (1.31)	14.9 (102)	13.3 (59)	30.3 (209)	
1.00	0.168 (1.16)	29.7 (205)	19.0 (85)	43.2 (298)	
1.50	0.153 (1.06)	44.6 (307)	24* (107)	54.5 (376)	
2.00	0.143 (0.99)	54.5 (376)	24* (107)	54.5 (376)	
2.50	0.135 (0.93)	54.5 (376)	24* (107)	54.5 (376)	

* N controlled by yielding of reinforcement crossing crack

4.12 TENSION STIFFENING IN PRESTRESSED CONCRETE MEMBERS

Tension stiffening of prestressed concrete members can be accounted for by using the average concrete stress vs. average concrete strain relationship of Eq. (4-20). Once again we estimate the load corresponding to a given member deformation by adding a concrete load, N_c , to the bare steel load.

Figure 4-18 gives the load-deformation responses for a series of axially loaded members tested by Bischoff (Ref. 4-9). The specimens differed from each other in the type of longitudinal reinforcement used.

Specimen T1 contained four non-prestressed reinforcing bars which had a well-defined yield plateau. Note that there is a significant influence of the tensile stresses in the concrete up to the load at which the bars yield. Because the specimen was not loaded until 95 days after casting, an appreciable shortening of the member due to concrete shrinkage occurred before loading. In each of the three prestressed specimens, tensile stresses in the concrete contributed significantly to the load-deformation response. Note that because the specimens were prestressed, the bare steel responses do not pass through the origins. Specimen T3, in which the longitudinal reinforcement consisted of bonded post-tensioned strands with a rounded stress-strain response, did not exhibit any significant decay in tension stiffening. On the other hand, for specimen T6, which contained both reinforcing bars and unbonded post-tensioned strands, the member response approached the bare steel response as the load increased.

In specimens containing reinforcement with different bond characteristics, such as specimen T6, it is appropriate to calculate the tension-stiffening factor, α_1 , as the weighted average of the α_1 values for the different types of reinforcement. Thus, for specimen T6, which contained 1.24 in^2 (800 mm^2) of deformed reinforcing bars ($\alpha_1 = 1.0$) and 0.306 in^2 (198 mm^2) of unbonded strands ($\alpha_1 = 0.0$),

$$\alpha_1 = \frac{1.24 \times 1.0 + 0.306 \times 0.0}{1.24 + 0.306} = 0.80$$

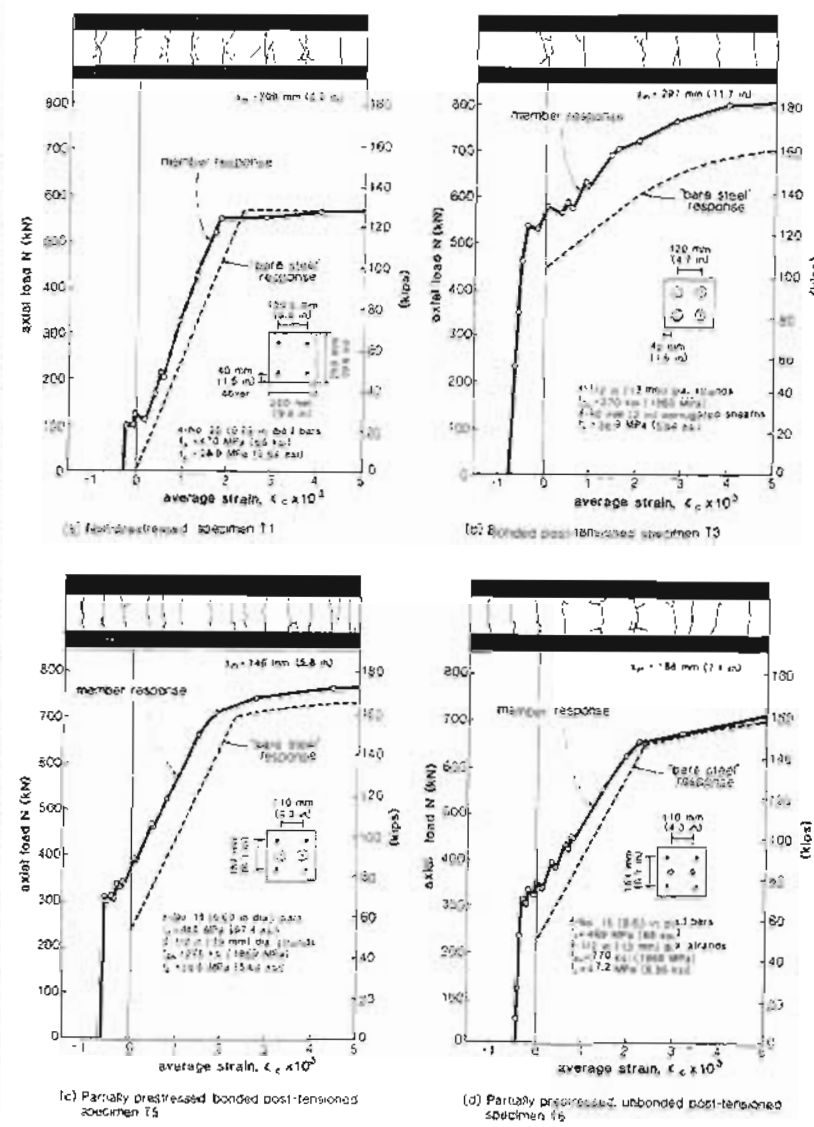


Figure 4-18 Influence of reinforcement type on tension stiffening and crack pattern. Adapted from Bischoff (Ref. 4-9)

In accounting for tension stiffening in prestressed concrete members, it is again necessary to limit the axial tensile load on the member so that it does not exceed the tensile capacity of the reinforcement.

4.13 CRACK WIDTHS AND CRACK SPACINGS

Concrete can tolerate only a small tensile strain due to stress before it cracks. After cracking, the concrete elongates by widening of the cracks and by formation of new cracks. Ignoring the small elastic strain in the concrete between the cracks, we can relate the crack width to the strain of the member by

$$w_m = \epsilon_{cf} s_m \quad (4-21)$$

where w_m is the mean crack width and s_m is the mean crack spacing.

For a primary crack (see Fig. 4-12) to form, the tensile stress at the outer surface of the concrete must reach the tensile strength of the concrete. When a crack forms, the concrete in the vicinity of the crack is relieved of any tension, resulting in a stress-free zone near the crack. The effect of these stress-free zones on the formation of primary cracks is illustrated in Fig. 4-19. From this figure it can be seen that a simple approximation for the average spacing of the primary cracks is twice the length of the stress-free zones. Using the assumed angle of dispersion shown in Fig. 4-19 gives

$$s_m = 3c_{max} \quad (4-22)$$

where c_{max} is the maximum distance that a point on the surface of the concrete can be away from a reinforcing bar (see Fig. 4-20).

4.14 CEB-FIP CODE EXPRESSIONS FOR CRACK SPACING AND CRACK WIDTHS

The CEB-FIP Code (Ref. 4-13) expression for the average crack spacing accounts for the influence of several variables in the following manner:

$$s_m = 2 \left(c + \frac{s}{10} \right) + k_1 k_2 \frac{d_b}{\rho_{ef}} \quad (4-23)$$

where c = clear concrete cover

s = maximum spacing between longitudinal reinforcing bars but shall not be taken greater than $15d_b$

d_b = bar diameter

$\rho_{ef} = A_s / A_{eff}$

A_{eff} = area of steel considered to be effectively bonded to the concrete

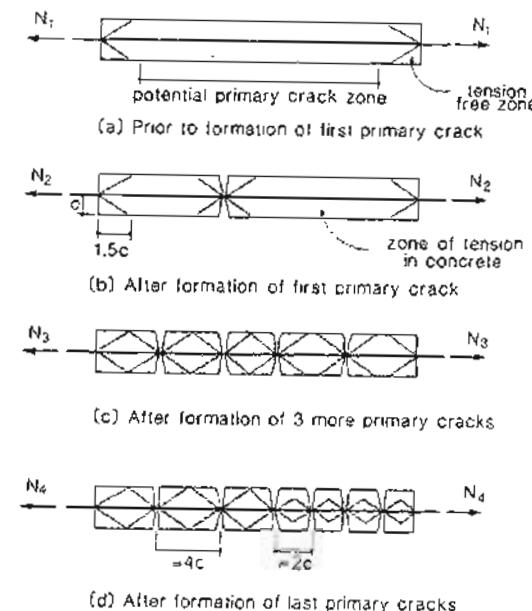


Figure 4-19 Formation of primary cracks.

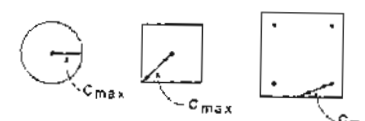


Figure 4-20 Definition of c_{max} .

A_{eff} = area of effective embedment zone of the concrete where the reinforcing bars can influence the crack widths (see Fig. 4-21)

k_1 = coefficient that characterizes bond properties of bars

$k_1 = 0.4$ for deformed bars

$k_1 = 0.8$ for plain bars

k_2 = coefficient to account for strain gradient

$k_2 = 0.25(\epsilon_1 + \epsilon_2)/2\epsilon_1$

(ϵ_1 and ϵ_2 = the largest and the smallest tensile strains in the effective embedment zone)

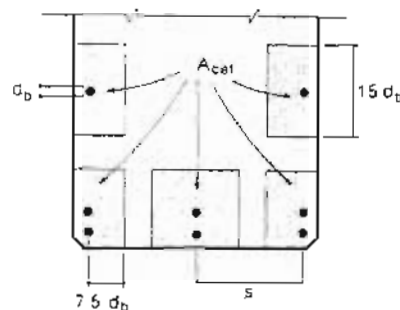


Figure 4-21 Definition of A_{eff} .

It is important to realize that the distance between cracks will vary randomly over a very wide range, with the maximum crack spacing being about twice the minimum crack spacing (see Fig. 4-19). The crack spacings will be influenced by additional variables not accounted for in Eq. (4-23). For example, transverse reinforcing bars act as crack initiators and hence, influence the crack spacings. Figure 4-22 compares three specimens, with different spacings of transverse reinforcement, tested by Rizkalla, Hwang, and El Shahawi (Ref. 4-14). It can be seen that if the spacing of the transverse reinforcement is close to the average crack spacing that would form in the absence of transverse bars, a very uniform pattern of cracks will form.

Due to the wide variation in crack spacings, there will also be a wide variation in crack widths. To account for this variation, the CEB-FIP Code defines the characteristic crack width, w_k , as the width that only 5% of the cracks will exceed. This characteristic width is taken as

$$w_k = 1.7 w_m \quad (4-24)$$

The limits that these characteristic crack widths must satisfy are given in Table 3-17.

4.15 GERGELY-LUTZ EXPRESSION FOR CRACK WIDTHS

The ACI Code (Ref. 4-15) bases its crack control requirements on the Gergely-Lutz expression (Ref. 4-16) for crack widths. While the CEB-FIP approach is to calculate crack widths by first estimating average steel strains and average crack spacings, the Gergely-Lutz approach is to use a simple empirical equation that relates maximum crack widths to

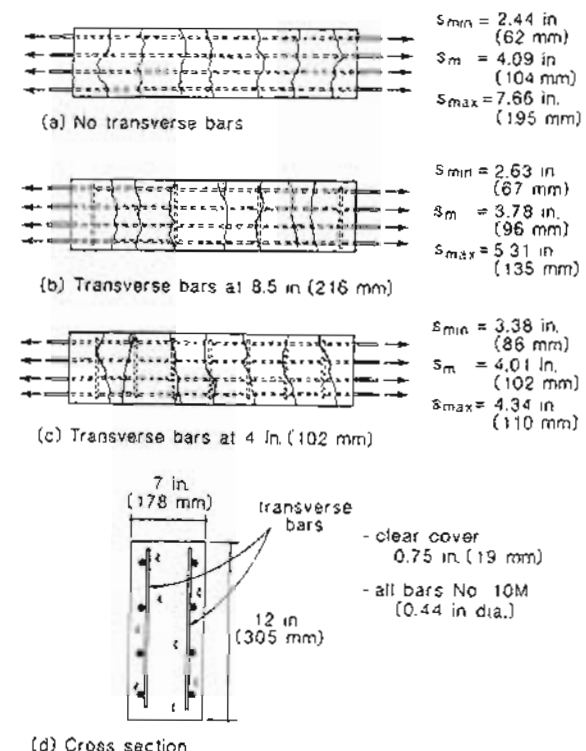


Figure 4-22 Influence of transverse bars on crack spacings. Adapted from Rizkalla, Hwang, and El Shahawi (Ref. 4-14).

three variables: steel stress at the crack, concrete cover, and area of concrete around each bar. This expression is as follows:

$$w_{max} = 2.2 \beta \epsilon_{scr} \sqrt{d_c A} \quad (4-25)$$

where w_{max} = maximum crack width

β = factor accounting for strain gradient

= 1.0 for uniform strains

= h_2/h_1 for varying strains, where h_1 is the distance from the tension steel to the neutral axis and h_2 is the distance from the extreme tension fiber to the neutral axis

ϵ_{scr} = strain in reinforcing bar at crack location

d_c = distance from extreme tension fiber to center of the closest bar (see Fig. 4-23)

A = effective area of concrete surrounding each bar taken as the total area of concrete in tension which has the same centroid as the tension reinforcement. When the reinforcement consists of different sizes of bars, the number of bars used to compute A is found by dividing the total area of reinforcement by the area of the largest bar (see Fig. 4-23).

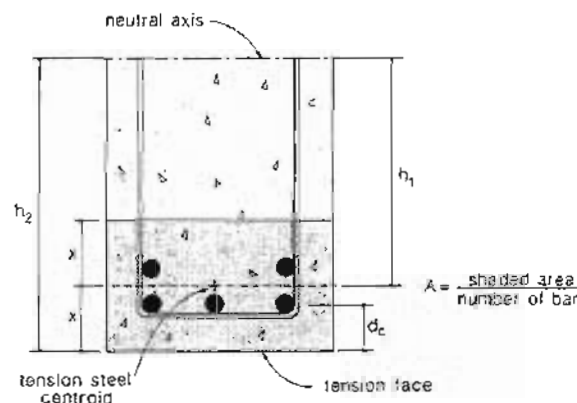


Figure 4-23 Crack width parameters in Gergely-Lutz expression.

In applying the Gergely-Lutz approach, it is necessary to calculate the strain in the reinforcement at a crack location. For a non-prestressed axially loaded member, this is given by

$$\epsilon_{scr} = \frac{N}{E_s A_s} \quad (4-26)$$

For a prestressed member a somewhat more complex calculation is required. At a crack

$$\begin{aligned} N &= A_p f_{per} + A_s f_{scr} \\ &= A_p E_p \epsilon_{per} + A_s E_s \epsilon_{scr} \\ &= A_p E_p (\epsilon_{scr} + \Delta \epsilon_p) + A_s E_s \epsilon_{scr} \end{aligned}$$

Thus

$$\epsilon_{scr} = \frac{N - A_p E_p \Delta \epsilon_p}{A_p E_p + A_s E_s} \quad (4-27)$$

In determining the effective area of concrete, A , for prestressed members, unbonded tendons should be neglected while a bonded post-tensioned tendon should be treated as a single bar with an area equal to the area of the steel in the tendon (see Refs. 4-17 and 4-18).

4.16 EXAMPLE OF CRACK WIDTH CALCULATIONS

Estimate the maximum crack width that will occur when the partially prestressed member described in Figs. 4-24 and 4-4 (member C) is subjected to a short-term axial tension load of 100 kips (445 kN).

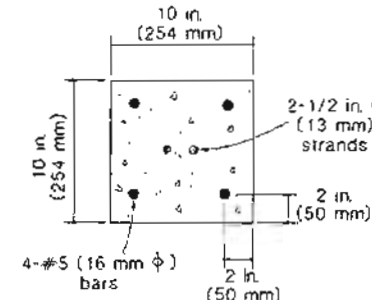


Figure 4-24 Cross section details for member C.

(a) Using Average Tensile Stress in Cracked Concrete Approach

Find ϵ_c corresponding to a short-term load of 100 kips (445 kN). Try $\epsilon_c = 1 \times 10^{-3}$. Hence

$$\begin{aligned} \epsilon_{cf} &= \epsilon_c - \epsilon_{sh} - \epsilon_{ctf} \\ &\approx 1 \times 10^{-3} - 0 - 0 = 1 \times 10^{-3} \end{aligned}$$

As ϵ_{cf} exceeds ϵ_{cr} , use Eq. (4-20), where

$$\alpha_1 = \frac{1.24 \times 1.0 + 0.306 \times 0.7}{1.24 + 0.306} = 0.94$$

Thus

$$\begin{aligned} f_c &= \frac{\alpha_1 \alpha_2 f_{cr}}{1 + \sqrt{500 \epsilon_{cf}}} \\ &= \frac{0.94 \times 1.0 \times 300}{1 + \sqrt{500 \times 0.001}} \\ &= 165 \text{ psi (1.14 MPa)} \end{aligned}$$

$$\epsilon_{sf} = \epsilon_s = \epsilon_c = 1 \times 10^{-3}$$

Therefore,

$$f_s = 30 \times 10^3 \times 1 \times 10^{-3} = 30 \text{ ksi (207 MPa)}$$

$$\epsilon_p = \epsilon_c + \Delta\epsilon_p = 1 \times 10^{-3} + 6 \times 10^{-3}$$

$$= 7 \times 10^{-3}$$

$$\epsilon_{pf} = \epsilon_p = 7 \times 10^{-3}$$

Hence

$$f_p = E_p \epsilon_p = 30 \times 10^3 \times 7 \times 10^{-3} = 210 \text{ ksi (1448 MPa)}$$

From equilibrium,

$$\begin{aligned} N &= A_c f_c + A_s f_s + A_p f_p \\ &= 98.5 \times 0.165 + 1.24 \times 30 + 0.306 \times 210 \\ &= 117.7 \text{ kips (523 kN)} \end{aligned}$$

Hence ϵ_c must be less than 1×10^{-3} . By trial and error we find that for $N = 100$ kips (445 kN), ϵ_c must equal 0.58×10^{-3} .

Using the CEB-FIP expression for crack spacing, Eq. (4-23), and using a k_1 value of 0.8 for the strands:

$$\begin{aligned} k_1 &= \frac{1.24 \times 0.4 + 0.306 \times 0.8}{1.24 + 0.306} = 0.48 \\ s_m &= 2 \left(c + \frac{s}{10} \right) + k_1 k_2 \frac{d_b}{\rho_{ef}} \\ &= 2 \left(1.69 + \frac{6}{10} \right) + 0.48 \times 0.25 \times \frac{0.625}{1.546/100} \\ &= 8.6 \text{ in. (219 mm)} \end{aligned}$$

Thus, from Eq. (4-21), the average crack width is

$$\begin{aligned} w_m &= \epsilon_{ef} s_m \\ &= 0.58 \times 10^{-3} \times 8.6 = 0.0050 \text{ in. (0.13 mm)} \end{aligned}$$

assuming that

$$\begin{aligned} w_{max} &= 1.7 w_m \\ &= 1.7 \times 0.0050 = 0.0085 \text{ in. (0.22 mm)} \end{aligned}$$

(b) Using Gergely-Lutz Approach

From Eq. (4-27),

$$\begin{aligned} \epsilon_{scr} &= \frac{N - A_p E_p \Delta\epsilon_p}{A_p E_p + A_s E_s} \\ &= \frac{100 - 0.306 \times 30 \times 10^3 \times 6 \times 10^{-3}}{0.306 \times 30 \times 10^3 + 1.24 \times 30 \times 10^3} \\ &= 0.97 \times 10^{-3} \end{aligned}$$

The effective area of concrete surrounding each bar, A_c , is found by dividing the total concrete area, 100 in² (64500 mm²) by the equivalent number, n , of #5 bars, where

$$n = \frac{1.24 + 0.306}{0.31} = 4.99$$

Hence

$$A_c = \frac{100}{4.99} = 20 \text{ in}^2 (12900 \text{ mm}^2)$$

Hence, from Eq. (4-25),

$$\begin{aligned} w_{max} &= 2.2 \delta \epsilon_{scr} \sqrt{d_c A} \\ &= 2.2 \times 1.0 \times 0.97 \times 10^{-3} \times \sqrt{2 \times 20} \\ &= 0.0073 \text{ in. (0.19 mm)} \end{aligned}$$

4.17 MINIMUM REINFORCEMENT FOR CRACK CONTROL

If a reinforced concrete member that is subjected to tension contains only a very small amount of reinforcement, this reinforcement may not be capable of providing crack control. When the first crack forms, the reinforcement crossing the crack will yield and all further deformations will occur at this single crack. To avoid this undesirable response it is necessary to provide enough reinforcement to resist loads in excess of the first cracking load. This will ensure that several cracks will form before failure.

A series of tests on large reinforced concrete members subjected to tension conducted by Williams (Ref. 4-7) demonstrated well the need for a minimum amount of reinforcement if cracks are to be controlled. The 250 mm × 1500 mm (9.8 in. × 59.1 in.) specimens shown in Fig. 4-25 each contained 18 deformed reinforcing bars, with the diameter of these bars varying from 25 to 8 mm (1 to 0.31 in.). The resulting steel percentages ranged from 2.36 to 0.24%. It can be seen that 0.24% of reinforcement was not capable of providing crack control while a reinforcement amount of 0.38% provided only marginal crack control. A well developed pattern of cracks developed over the full test length in the four specimens containing larger amounts of reinforcement. Also shown in Fig. 4-25 is the stress in the

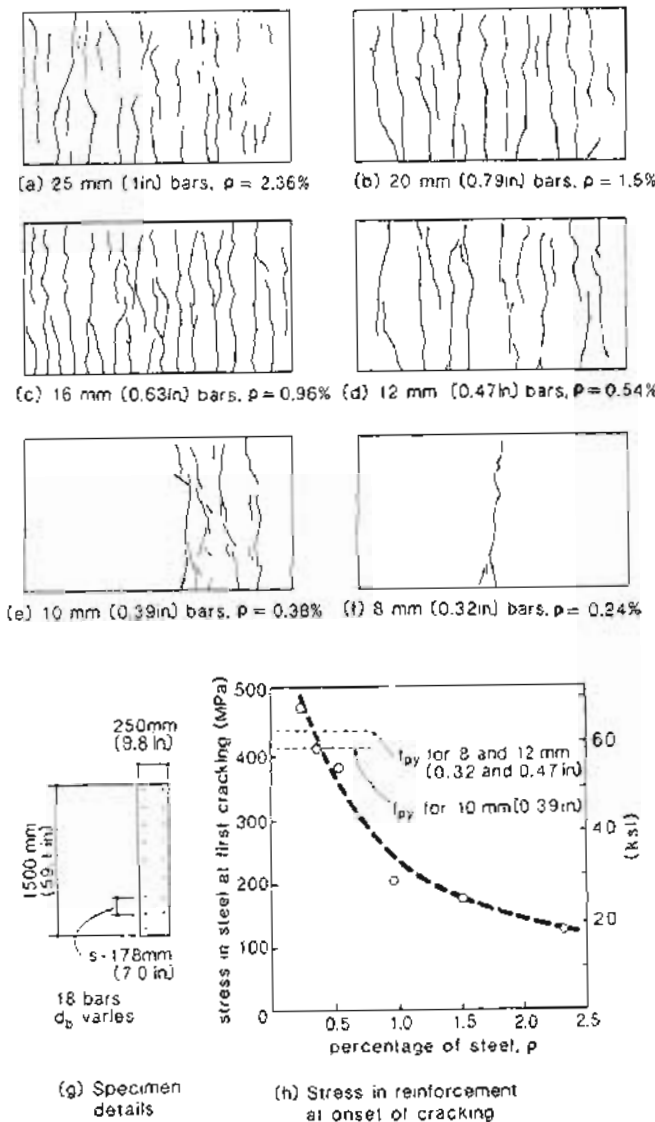


Figure 4-25 Influence of percentage of reinforcement on crack pattern and steel stress at cracking. Adapted from Williams (Ref. 4-7).

Sec. 4.17 Minimum Reinforcement for Crack Control

161

reinforcement at a crack when cracking was first observed. It can be seen that if yielding of the reinforcement occurred at the first cracking of the concrete, adequate crack control was not obtained.

When the first crack occurs, a tensile force ($A_s f_{cr}$) must be transferred from the concrete to the reinforcement, resulting in an increase of steel stress at the crack. For non-prestressed members there will only be a small stress in the reinforcement when the concrete first cracks and hence the stress increase that can be tolerated will be about equal to the yield strength of the reinforcement. Hence the minimum reinforcement required to prevent yielding of the reinforcement at first cracking can be found from the requirement that $A_s f_y$ equal or exceed $A_s f_{cr}$, and hence

$$\rho_{min} = \frac{f_{cr}}{f_y} \quad (4-28)$$

Thus, for a case where $f_{cr} = 300$ psi (2 MPa) and the yield stress of the reinforcement is 60 ksi (400 MPa), at least 0.5% of reinforcement would be required to control cracking in members subjected to tension.

The need for at least 0.5% of reinforcement if cracking is to be controlled was also demonstrated by Falkner (Ref. 4-19). Falkner subjected reinforced concrete members fully restrained against shortening to temperature drops of 60°C (108°F), causing significant cracking. He found that the average crack widths stayed less than 0.20 mm (0.008 in.) for reinforcement ratios as low as 0.5% provided that small-diameter, closely spaced reinforcing bars were used (see Fig. 4-26).

For a member in which the reinforcement is prestressed, the minimum percentage of prestressing steel, $\rho_{p,min}$, to control cracking can be found from

$$\rho_{p,min} = \frac{f_{cr}}{f_{py} - f_{pcr}} \quad (4-29)$$

where f_{pcr} is the stress in prestressing steel just prior to cracking of concrete.

For example, if a member has been reinforced with low-relaxation strand pretensioned to a strain of 6.5×10^{-3} , then the strain in the strand just prior to cracking of the concrete, under short-term conditions, will be about 6.5×10^{-3} . Hence f_{pcr} is about 190 ksi (1300 MPa). Thus, if the concrete cracks at about 300 psi (2 MPa) and the strand yields at 245 ksi (1675 MPa), the minimum percentage of prestressing reinforcement required for crack control is

$$\rho_{p,min} = \frac{0.300}{245 - 190} \approx 0.55\%$$

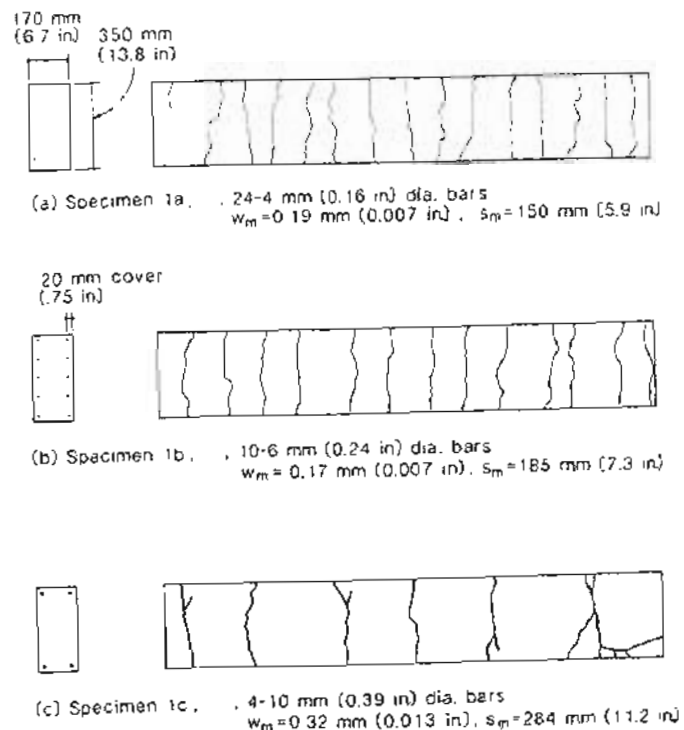


Figure 4-26 Influence of distribution of reinforcement on crack patterns for members with 0.5% reinforcement. Adapted from Falkner (Ref. 4-19).

References

- 4-1 Considère, "Influence des armatures métalliques sur les propriétés des mortiers et bétons" (Influence of Metal Reinforcement on the Properties of Mortar and Concrete), *Le Génie Civil*, Vol. 34, No. 15, 1899, pp. 229-233.
- 4-2 Mörsch, E., *Concrete-Steel Construction*, English translation by E.P. Goodrich, The Engineering News Publishing Company, New York, 1909, 368 pp. [Translation from 3rd ed (1908) of *Der Eisenbetonbau*, 1st ed., 1902.]
- 4-3 U.W., "Tension Stiffening in Structural Concrete," B.A.Sc. thesis, Department of Civil Engineering, University of Toronto, 1974, 58 pp.
- 4-4 Goto, Y., "Cracks Formed in Concrete around Deformed Tension Bars," *ACI Journal*, Vol. 68, No 4, Apr. 1971, pp. 224-251.
- 4-5 Scott, R.H., and Gill, P.A.T., "Short-Term Distributions of Strain and Bond Stress along Tension Reinforcement," *Structural Engineer*, Vol. 65B, No. 2, June 1987, pp. 39-48.
- 4-6 Kollegger, J., Günther, G., and Mehlihorn, G., "Zug und Zug-Druckversuche an Stahlbetonscheiben" (Tension and Tension-Compression Tests on Reinforced Concrete Panels), *Forschungsberichte aus dem Fachgebiet Massivbau*, No. 1, Gesamthochschule Kassel, Kassel, West Germany, 1986.
- 4-7 Williams, A., "Tests on Large Reinforced Concrete Elements Subjected to Direct Tension," Technical Report No. 562, Cement and Concrete Association, Wexham Springs, UK, Apr. 1986, 56 pp.
- 4-8 Bhinde, S.B., and Collins, M.P., "Reinforced Concrete Elements in Shear and Tension," Publication No. 87-02, Department of Civil Engineering, University of Toronto, Jan 1987, 308 pp.
- 4-9 Bischoff, Peter H., "Response of Prestressed Concrete Tension Members," M.Eng. thesis, McGill University, Montreal, Jan. 1983, 161 pp.
- 4-10 Rostasy, F.S., Koch, R., and Leonhardt, F., "Zur Mindestbewehrung von Zwang von Außenwänden aus Stahlleichtbeton" (On the Minimum Reinforcement of External Lightweight Concrete Walls for Restraining Actions), Bulletin No. 267, Deutscher Ausschuss für Stahlbeton, Berlin, 1976, 83 pp.
- 4-11 Matsuba, P., "Crack Width Prediction and Tension Stiffening of Prestressed Concrete," B.A.Sc. thesis, Department of Civil Engineering, University of Toronto, 1981, 142 pp.
- 4-12 Vecchio, F.J., and Collins, M.P., "The Modified Compression Field Theory for Reinforced Concrete Elements Subjected to Shear," *ACI Journal*, Vol. 83, No. 2, Mar.-Apr. 1986, pp. 219-231.
- 4-13 CEB-FIP, *Model Code for Concrete Structures: CEB-FIP International Recommendations*, 3rd ed., Comité Euro-International du Béton, Paris, 1978, 348 pp.
- 4-14 Rizkalla, S.H., Hwang, L.S. and El Shahawi, M., "Transverse Reinforcement Effect on Cracking Behaviour of R.C. Members," *Canadian Journal of Civil Engineering*, Vol. 10, No. 4, Dec. 1983, pp. 566-581.
- 4-15 ACI Committee 318, "Building Code Requirements for Reinforced Concrete (ACI 318-89) and Commentary - ACI 318 R-89," American Concrete Institute, Detroit, 1989, 360 pp.
- 4-16 Gergely, P., and Lutz, L.A., "Maximum Crack Width in Reinforced Concrete Flexural Members," *Causes, Mechanisms, and Control of Cracking in Concrete*, SP-20, American Concrete Institute, Detroit, 1968, pp. 87-117.

- 4-17 CSA Committee A23.3, *Design of Concrete Structures for Buildings*, CAN3-A23.3-M84, Canadian Standards Association, Rexdale, Canada, 1984, 281 pp.
- 4-18 Thormählen, Uwe "Zum Einfluss von Spanngliedern mit nachträglichem Verbund auf Rissbildung und rissbreiten Beschränkung bei teilweise vorgespannten Konstruktionen" (Influence of Bonded Prestressing Tendons on Crack Development and Crack Width Control in Partially Prestressed Structures). Doktor-Ingenieurs (Ph.D.) thesis, Fakultät für Bauwesen der Rheinisch-Westfälischen Technischen Hochschule, Aachen, West Germany, Feb. 1978.
- 4-19 Falkner, H., "Zur Frage der Rissbildung durch Eigen- und Zwangsspannungen infolge Temperatur in Stahlbetonbauteilen" (Cracking of Reinforced Concrete Members Due to Residual and Restraining Stresses Caused by Temperature), Deutscher Ausschuss für Stahlbeton, No. 208, 1969, 99 pp.

Demonstration Problems

- 4-1 In Section 4.4 the response of member B to axial load was calculated on the assumption that the concrete compressive strength was 5000 psi (34.5 MPa) and that the concrete stress-strain curve was parabolic, peaking at a compressive strain of 0.002. Compute the short-term response of member B if the concrete compressive strength is 12,000 psi (82.7 MPa). For the concrete compressive stress-compressive strain relationship, use Eq. (3-1). Comment on the influence of concrete strength on the load-deformation response of the member.
- 4-2 At about the turn of the century, a number of people attempted to produce prestressed concrete by pretensioning ordinary reinforcing bars with f_y about equal to 40 ksi (300 MPa) and casting low-quality concrete around the reinforcement. For the pretensioned member shown in Fig. 4-27.

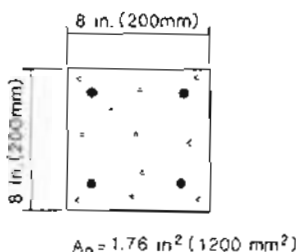


Figure 4-27 Pretensioned member.

- (a) Calculate the stress in the concrete immediately after release of the bars assuming that $E_c = 2000 \text{ ksi}$ (14000 MPa) and also assuming the steel was stressed to 32 ksi (250 MPa) at the time the concrete was cast.
- (b) Calculate the stress in the concrete after creep and shrinkage have occurred assuming that in this case $E_{c,eff} = 600 \text{ ksi}$ (4000 MPa) and the free shrinkage strain is -0.6×10^{-3} . Comment on why these early attempts to produce prestressed concrete failed.
- 4-3 In Section 4.9 it was shown that for the partially prestressed member (member C in Fig. 4-4) creep, shrinkage, and relaxation resulted in a 50% loss of compressive stress in the concrete.

Determine what percentage loss in compressive stress will occur in the fully prestressed member (member B in Fig. 4-4) due to creep, shrinkage, and relaxation. Comment on why the percentage loss is substantially different in the two members.

- 4-4 It is possible to produce precast, prestressed concrete elements without ever mechanically stressing the steel. The process involves electrically heating the prestressing steel and then casting concrete around the steel while it is still hot. After the concrete has hardened, the heating current is switched off and the steel cools down, compressing the concrete. The precast roof slab shown in Fig. 4-28 has been produced by this thermal process. If, after creep, shrinkage, and relaxation losses have occurred, the compressive stress in the concrete is still 300 psi (2 MPa) under no external loads, what was the rise in temperature of the steel due to the electrical heating? Assume that thermal strains in the concrete are negligible. Assume that $A_p = 9 \times 0.215 \text{ in}^2$ (140 mm^2), $E_{p,eff} = 27,500 \text{ ksi}$ ($190,000 \text{ MPa}$), $\alpha_p = 6 \times 10^{-6}/^\circ\text{F}$ ($10 \times 10^{-6}/^\circ\text{C}$), $E_{s,eff} = 1350 \text{ ksi}$ (9310 MPa), $\epsilon_{sh} = -0.3 \times 10^{-3}$.

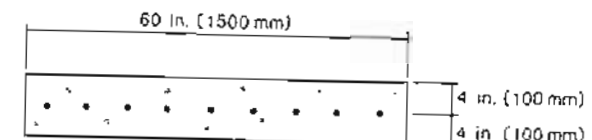


Figure 4-28 Precast roof slab.

- 4-5 A precast, pretensioned 8 in. \times 8 in. ($200 \text{ mm} \times 200 \text{ mm}$) column supports a water tank (see Fig. 4-29). The strands were stressed to 210 ksi (1450 MPa) at the time the concrete was cast

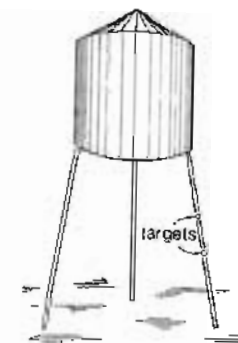


Figure 4-29 Columns supporting water tank.

Just prior to release of the low-relaxation strands, two targets exactly 80 in. (2032 mm) apart were glued to the surface of the concrete. The temperature at this time was 68°F (20°C). About five years after construction, when the temperature was 14°F (-10°C), the distance between the two targets was measured to be 79.84 in. (2028 mm). Estimate the axial load on the column. Cross-sectional properties of column: $A_p = 0.612 \text{ in}^2$ (395 mm²), $A_s = 1.24 \text{ in}^2$ (800 mm²), $f_y = 60 \text{ ksi}$ (414 MPa), $E_p = E_c = 29,000 \text{ ksi}$ ($200 \times 10^3 \text{ MPa}$), $f'_c = 5000 \text{ psi}$ (35 MPa), $f_{py} = 240 \text{ ksi}$ (1650 MPa), $\alpha_s = \alpha_p = 6 \times 10^{-6}/^\circ\text{F}$ ($10 \times 10^{-6}/^\circ\text{C}$), $\alpha_c = 5 \times 10^{-6}/^\circ\text{F}$ ($9 \times 10^{-6}/^\circ\text{C}$), $\epsilon_{sh} = -0.4 \times 10^{-3}$.

- 4-6 The 50 ft (15 m) long beam shown in Fig. 4-30 has been axially post-tensioned by means of eight 0.6 in. (15 mm) diameter strands. The stress in the concrete after anchoring and grouting the strands was 1000 psi (6.9 MPa) uniform compression.

- (a) Calculate $\Delta\epsilon_p$ assuming that $E_c = 4530 \text{ ksi}$ ($30 \times 10^3 \text{ MPa}$).
- (b) How far did the bearing at B move during the post-tensioning?
- (c) What will be the total movement at B after creep shrinkage and relaxation have occurred? Assume that $\epsilon_{sh} = -0.4 \times 10^{-3}$, $E_{c,eff} = 0.27E_c$, and $E_{p,eff} = 0.95E_p$.
- (d) If the bearing at B is prevented from moving immediately after tensioning of the strands, what will be the stress in the concrete after creep, shrinkage, and relaxation have occurred?
- (e) What will be the force in the jammed bearing?

Section properties: $A_c = 300 \text{ in}^2$ ($194 \times 10^3 \text{ mm}^2$), $A_p = 1.72 \text{ in}^2$ (110 mm²), $E_p = 30,000 \text{ ksi}$ ($200 \times 10^3 \text{ MPa}$).

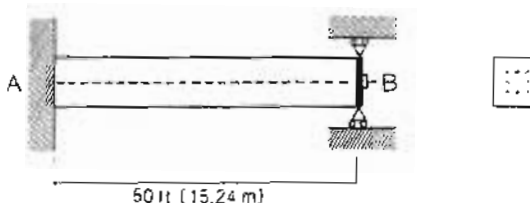


Figure 4-30 Post-tensioned beam.

- 4-7 After the partially prestressed member described in Fig. 4-4 (member C) has been released from the stressing bed, it is fixed between rigid abutments and then the temperature is varied. Ignoring the influence of temperature on the material stress-strain characteristics, plot the relationship between the temperature change and the force in the member for both short- and long-term response for temperature changes from -700°F to +1000°F (-400°C to +600°C) (see Fig. 4-31).

- 4-8 Shown in Fig. 4-32 is the observed response of a partially prestressed member subjected to axial tension. The member was post-tensioned at 30 days to produce a strain difference $\Delta\epsilon_p = 4.2 \times 10^{-3}$. At 68 days it was loaded in tension. The material properties were: $f'_c = 47.2 \text{ MPa}$ (6.85 ksi), $\epsilon_{sh} = -0.3 \times 10^{-3}$, $E_c = 26.6 \times 10^3 \text{ MPa}$ (3860 ksi), $f_y = 404 \text{ MPa}$ (58.6 ksi), and $f_{sr} = 3.2 \text{ MPa}$ (464 psi). Use Eq. (3-26) for the stress-strain relationship of the

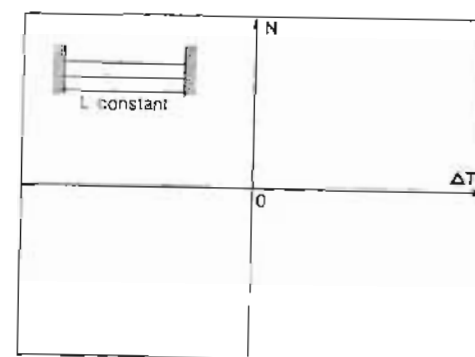


Figure 4-31 Variation of axial load with temperature change.

prestressing strand. Predict the load-deformation response and compare it with the observed response.

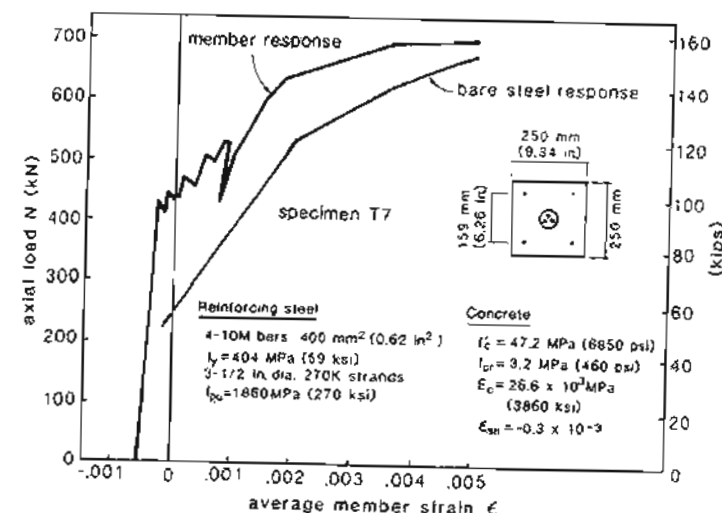
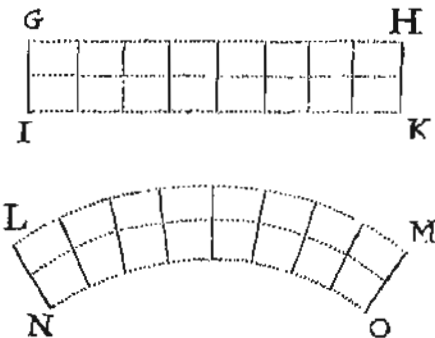


Figure 4-32 Load-deformation response of partially prestressed member. From Ref. 4-9.

- 4-9 Estimate the average crack width when the member described in Fig. 4-32 was subjected to an axial tension of 510 kN (115 kips).

Response of Members Subjected to Flexure



LM will be extended, and NO will be diminished in proportion to the flexure.

Robert Hooke, 1678

5.1 INTRODUCTION

Since flexural members such as beams and slabs are the most widely used prestressed concrete elements, it is appropriate to study their response in some detail. While flexural members will typically have zero axial load, it is convenient to develop the calculation procedures for the more general case of combined flexure and axial load.

Figure 5-1 illustrates the type of member that we will study in this chapter. It is assumed that the cross section of the member is symmetrical about the vertical axis and

contains both prestressed (area A_p) and non-prestressed (area A_s) reinforcement. It will be assumed that the concrete is subjected to strains in only the axial direction and that these strains are uniform over the width of the section but vary linearly over the depth of the section (i.e., plane sections remain plane).

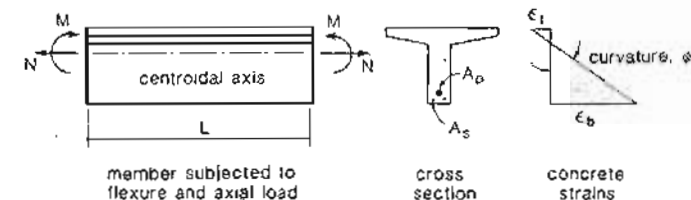


Figure 5-1 Section subjected to flexure and axial load

The sectional forces, M and N , are determined from structural analysis. In this procedure the actual structure is idealized by a line model with each member being represented by a line (see Fig. 5-2). It is important to recognize that the values of M and N depend on the location of the line chosen to represent the member. Because the reinforcement details are often unknown at the time of analysis, we typically use the centroidal axis of the gross concrete section as the line to represent the member.

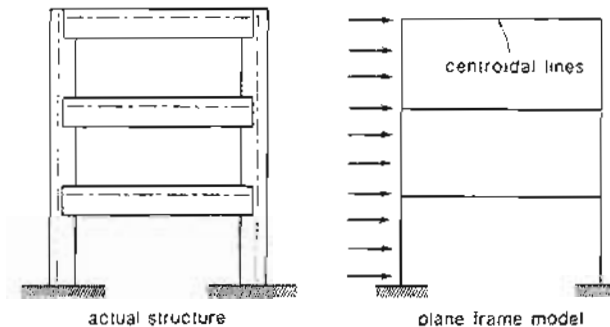


Figure 5-2 Calculation of sectional forces M and N .

5.2 COMPATIBILITY CONDITIONS

The hypothesis that "plane sections remain plane" is often credited to Navier (1826, Ref. 5-1) or Bernoulli (1705, Ref. 5-2). In fact, Hooke in his 1678 paper (Ref. 5-3) not only proposed what became known as Hooke's law but also demonstrated a clear understanding of the "plane-sections" hypothesis. This geometric assumption still forms the basis of engineering beam theory.

Because of the plane-sections assumption, the concrete strain distribution can be defined by just two variables (e.g., the strain at the top face and the strain at the bottom face). The two variables that we will choose to define the linear strain distribution are the strain at the centroid, ϵ_{cen} , and the curvature, ϕ (see Fig. 5-3). The curvature is equal to the change in slope per unit length along the member and is also equal to the strain gradient over the depth of the member.

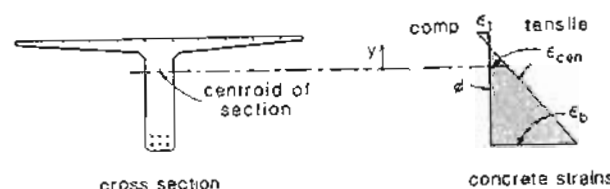


Figure 5-3 Concrete strain distribution.

Thus the concrete strain at any level y is given by

$$\epsilon_c = \epsilon_{cen} - \phi y \quad (5-1)$$

The strain in the reinforcing bars at any level y is equal to the strain in the surrounding concrete; hence

$$\epsilon_s = \epsilon_{cen} - \phi y \quad (5-2)$$

The strain in the prestressing tendons at any level y is equal to the strain in the surrounding concrete plus the strain difference, $\Delta\epsilon_p$, at this level; thus

$$\epsilon_p = \epsilon_{cen} - \phi y + \Delta\epsilon_p \quad (5-3)$$

In the equations above, it has been assumed that tensile strains are positive and compressive strains are negative. Further, it has been assumed that a positive curvature is associated with the bottom face having an algebraically larger strain than the top face (see Fig. 5-3).

5.3 EQUILIBRIUM CONDITIONS

At any section the stresses, when integrated over the section, must add up to the required sectional forces M and N (see Fig. 5-4). Hence

$$\int_{A_c} f_c dA_c + \int_{A_s} f_s dA_s + \int_{A_p} f_p dA_p = N \quad (5-4)$$

and

$$\int_{A_c} f_c y dA_c + \int_{A_s} f_s y dA_s + \int_{A_p} f_p y dA_p = -M \quad (5-5)$$

In these equations tensile stresses are taken as positive and compressive stresses are taken as negative. The axial load, N , is positive if tensile and negative if compressive. The moment, M , is positive if it causes tensile stresses on the bottom face (see Fig. 5-4).

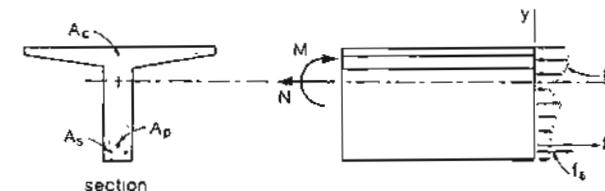


Figure 5-4 Stresses and stress resultants

5.4 PREDICTING RESPONSE OF FLEXURAL MEMBERS

The response of flexural members can be predicted by using the equilibrium and compatibility conditions described above together with the material stress-strain relationships described in Chapters 3 and 4.

As we have seen, the concrete strain distribution is defined by two variables, say the strain at the top face and the strain at the bottom face. If the strain distribution across the section is known, then the stress-strain relationships can be used to find the distribution of stresses across the section. If the stresses are known, then the moment and axial load acting at the section can be determined from the equilibrium equations. Thus if we know the strain at the top face and the bottom face of a section, we can calculate the axial load and moment that caused these strains.

In investigating the pure flexural response of beams (i.e., axial load zero) it is useful to determine the moment-curvature response of the section. A convenient approach is to choose a value of top concrete strain and then find, by trial and error, the corresponding bottom concrete strain that will result in zero axial load. The moment and curvature associated with this strain distribution can then be determined. If these calculations are repeated for different values of top concrete strains, the complete moment-curvature response of the section can be predicted (see Fig. 5-5).

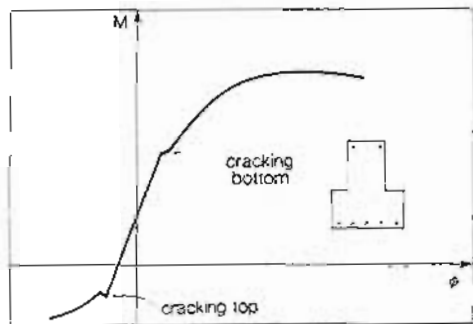


Figure 5-5 Moment-curvature response.

5.5 TENSILE STRESSES IN THE CONCRETE

Prior to cracking, the concrete is fully effective in resisting tensile stresses. After cracks have formed, the situation becomes more complex. At a crack there are no tensile stresses, while between the cracks, tensile stresses are introduced into the concrete by the bonded reinforcement (see Fig. 5-6).

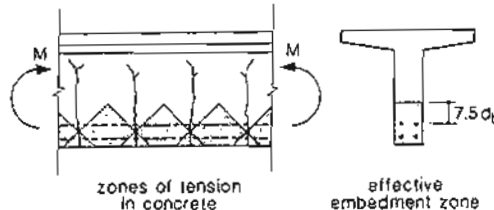


Figure 5-6 Tensile stress in cracked concrete.

Before cracks have formed, a length of beam subjected to a constant moment will have a constant curvature along the length. After cracks have formed, the local curvatures will vary along the length with higher curvatures occurring at crack locations (see Fig. 5-7). The tensile stress in the reinforcement will be highest at a crack location where the tension in the concrete is zero. Because of this, flexural failure of a member will typically occur at a section that contains a crack (see Fig. 5-7). Hence, in investigating the flexural capacity of a section it is appropriate to neglect tensile stresses in the concrete.

The presence of the tensile stresses in the concrete between the cracks stiffens the member. To account for this "tension stiffening" we can use the average tensile stress-

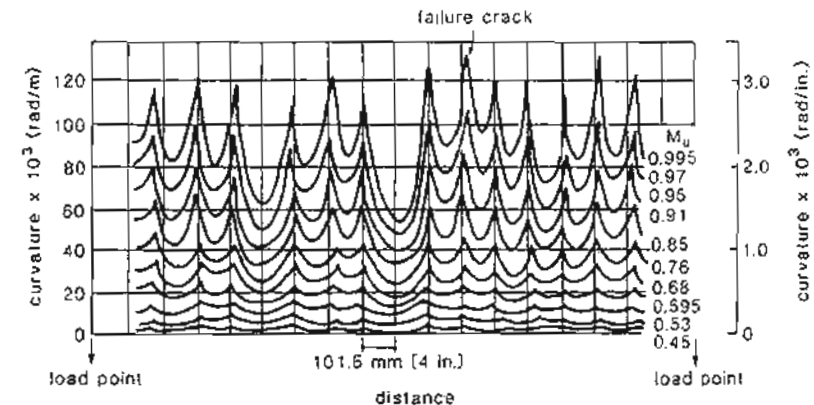


Figure 5-7 Measured curvature distribution in constant-moment zone. Adapted from Priestley, Park, and Lo (Ref. 5-4).

average tensile strain relationship of Eq. (4-20) to estimate the average tensile stress in the concrete after cracking.

The tensile stresses in the concrete between the cracks will be concentrated in a zone of concrete around the reinforcement called the "effective embedment zone" (see Fig. 5-6). The CEB-FIP effective embedment zone defined in Fig. 4-21 will be used. That is, we will ignore average tensile stresses in the cracked concrete that is outside this effective embedment zone.

5.6 LAYER-BY-LAYER EVALUATION OF THE SECTION FORCES

The only feature that makes evaluating the response of a flexural member a more difficult task than evaluating the response of an axially loaded member is that now the stresses and strains vary over the depth of the member. Rather than simply multiplying the areas by the stresses when evaluating the section forces, we must now evaluate the integrals of Eqs. (5-4) and (5-5).

As the reinforcing bars and prestressing tendons consist of a number of discrete elements, the integrals involving the forces in the bars and the tendons can be replaced by summations. The force in each bar and each tendon is assumed to be equal to the stress at the center of the bar or the tendon times the area of the bar or the tendon. The problem then remaining is to evaluate the integrals involving stresses in the concrete.

One simple procedure for evaluating the integrals is to idealize the cross section as a series of rectangular layers, and to assume that the strain in each layer is uniform and equal to the actual strain at the center of the layer (see Fig. 5-8). If the strain is uniform over the layer, the concrete stress will also be uniform over the layer. The force in each layer

can then be found by multiplying the stress in the layer by the area of the layer, while the moment contribution can be found by multiplying the layer force by the distance between the middle of the layer and the reference axis.

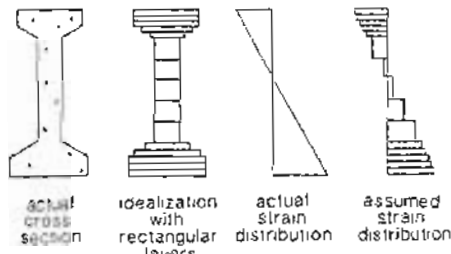


Figure 5-8 Layer-by-layer section idealization.

The manner in which this layer-by-layer procedure is used to evaluate the sectional forces corresponding to a given strain distribution is illustrated in Fig. 5-9. As can be seen, the stress resultants are determined by evaluating the forces in each layer of concrete and each layer of reinforcement.

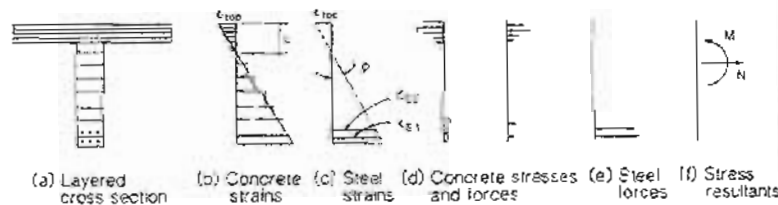


Figure 5-9 Determining sectional forces using layer-by-layer evaluation.

Obviously the idealization will become more accurate, but will require more computational effort as the layers become thinner. Figure 5-10 illustrates how the values of the integrals change as more refined discretizations of the cross section are employed. It is perhaps surprising to note that for the rather complex cross section used in the example, accurate estimates of both the compressive resultant and its moment about the reference axis are obtained by using a fairly coarse discretization, involving only four layers to represent the compression zone.

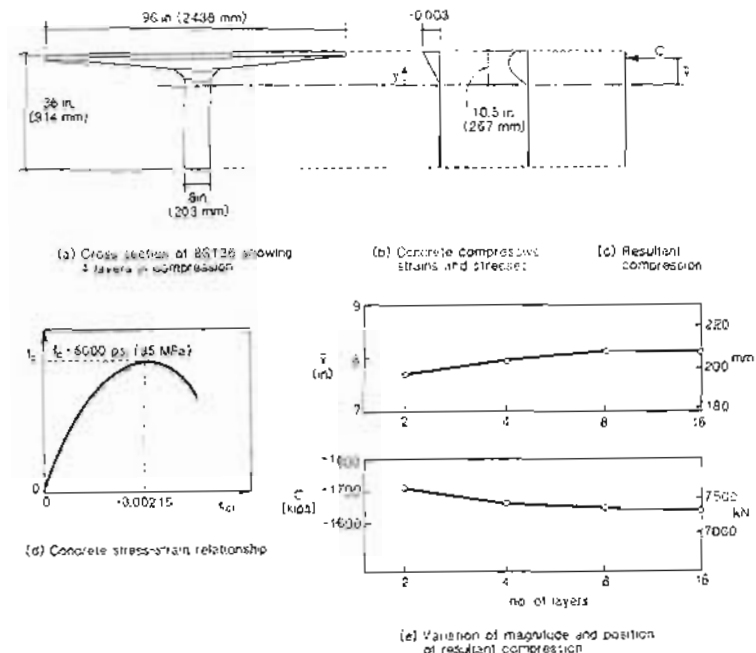


Figure 5-10 Sensitivity of calculated values to degree of discretization.

A somewhat more refined procedure for evaluating the concrete stress integrals is to assume a parabolic stress variation over each layer rather than a constant stress over each layer. Further, instead of using rectangular layers more general trapezoidal layers which can have different widths at the top and bottom of the layer may be used. A computer program for evaluating the moment-curvature response of prestressed concrete members using this approach is described in Appendix A. The program is called RESPONSE.

5.7 EVALUATION OF SECTION FORCES USING STRESS-BLOCK FACTORS

While the layer-by-layer integral evaluation approach is appropriate if a microcomputer is being used, it is quite a time-consuming procedure if only a programmable calculator is available. For cross sections having essentially constant widths, the concrete stress integrals of Eqs. (5-4) and (5-5) can be efficiently evaluated with the aid of stress-block factors. Instead of using the actual nonlinear stress distributions, equivalent uniform stress distributions, whose integrals can be evaluated by inspection, are employed (see Fig. 5-11).

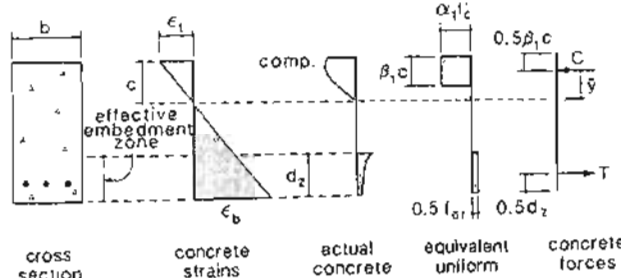


Figure 5-11 Stress-block factors.

For a given compressive stress distribution, the stress-block factors α_1 and β_1 are determined so that the magnitude and location of the resultant force are the same in the equivalent uniform stress distribution as in the actual distribution. The requirement that the magnitude of the resultant force remains the same is

$$\int_0^c f_c b dy = \alpha_1 f'_c \beta_1 c b \quad (5-6)$$

- For a parabolic stress-strain curve and a constant width, b , Eq. (5-6) reduces to

$$\alpha_1 \beta_1 = \frac{\epsilon_b}{\epsilon'_c} - \frac{1}{3} \left(\frac{\epsilon_b}{\epsilon'_c} \right)^2 \quad (5-7)$$

- The requirement that the location of the resultant force remain the same is

$$\bar{y} = \frac{\int_0^c f_c b y dy}{\int_0^c f_c b dy} = c - 0.5\beta_1 c \quad (5-8)$$

where y in this case is measured from the neutral axis (see Fig. 5-11).

For a parabolic stress-strain curve and a constant width, b , Eq. (5-8) reduces to

$$\beta_1 = \frac{4 - \epsilon_b/\epsilon'_c}{6 - 2\epsilon_b/\epsilon'_c} \quad (5-9)$$

where ϵ_b is the extreme compressive fiber strain. Values of the stress-block factors for a parabolic stress-strain curve are given in Table 5-1.

The stress-block factors for the more general concrete stress-strain relationship of Eq. (3-1) can be obtained by numerically integrating Eqs. (5-6) and (5-8). The resulting stress-block factors for different concrete strengths are given in Table 5-2.

Table 5-1 Stress-block factors for parabolic stress-strain curve.

ϵ_b/ϵ'_c	0.25	0.50	0.75	1.00	1.25	1.50	1.75	2.00
α_1	0.336	0.595	0.779	0.888	0.928	0.900	0.810	0.667
β_1	0.682	0.700	0.722	0.750	0.786	0.833	0.900	1.000

Table 5-2 Stress-block factors for more general stress-strain relationship.

f'_c psi (MPa)	0.25	0.50	0.75	1.00	1.25	1.50	1.75	2.00	
(20.7)	α_1	0.359	0.641	0.818	0.910	0.945	0.947	0.930	0.904
	β_1	0.675	0.697	0.727	0.762	0.796	0.830	0.861	0.890
(24.1)	α_1	0.335	0.614	0.801	0.902	0.937	0.929	0.899	0.839
	β_1	0.672	0.689	0.717	0.750	0.788	0.827	0.864	0.900
(27.6)	α_1	0.316	0.591	0.787	0.895	0.929	0.911	0.869	0.817
	β_1	0.670	0.684	0.709	0.741	0.781	0.825	0.869	0.911
(34.5)	α_1	0.290	0.556	0.762	0.884	0.912	0.871	0.801	0.724
	β_1	0.668	0.677	0.691	0.728	0.772	0.827	0.886	0.943
(41.4)	α_1	0.272	0.530	0.742	0.874	0.896	0.830	0.735	0.641
	β_1	0.667	0.673	0.689	0.717	0.767	0.834	0.908	0.980
(55.2)	α_1	0.250	0.495	0.712	0.859	0.863	0.744	0.610	0.501
	β_1	0.667	0.669	0.679	0.704	0.763	0.859	0.963	1.061
(69.0)	α_1	0.237	0.472	0.689	0.847	0.826	0.659	0.511	0.408
	β_1	0.667	0.668	0.674	0.695	0.767	0.893	1.022	1.132
(82.7)	α_1	0.228	0.456	0.672	0.838	0.786	0.585	0.441	0.350
	β_1	0.667	0.667	0.672	0.689	0.776	0.930	1.071	1.184
(110.3)	α_1	0.218	0.435	0.648	0.824	0.702	0.484	0.363	0.290
	β_1	0.667	0.667	0.669	0.682	0.804	0.990	1.134	1.242

If it is desired to account for the stiffening effect of the tension in the concrete between the cracks, then the small tensile stresses in the concrete can be approximated by a uniform stress of $0.5f_{cr}$ acting over that part of the effective embedment zone which is in tension (see Fig. 5-11).

5.8 CALCULATION OF MOMENT-CURVATURE USING STRESS-BLOCK FACTORS

To illustrate the use of stress-block factors, we will calculate the short-term moment-curvature response of the pretensioned member described in Fig. 5-12. This beam, which was one of the specimens tested by Priestley, Park, and Lu (Ref. 5-4), was made from concrete with the following properties: $f'_c = 6510$ psi (44.9 MPa), $\epsilon'_c = -0.0025$, and $f_{cr} = 420$ psi (2.9 MPa). The member was pretensioned using two 0.276 in. (7 mm) diameter wires with a total area of 0.120 in^2 (77 mm^2). The wires had a rounded stress-strain curve that could be represented by the following modified Ramberg-Osgood function (see

Section 3.14):

$$f_p = 29 \times 10^3 c_{pf} \left\{ 0.032 + \frac{0.968}{[1 + (135c_{pf})^6]^{1/6}} \right\} \text{ ksi}$$

The prestressing of the member was such that $\Delta\epsilon_p = 4.24 \times 10^{-3}$.

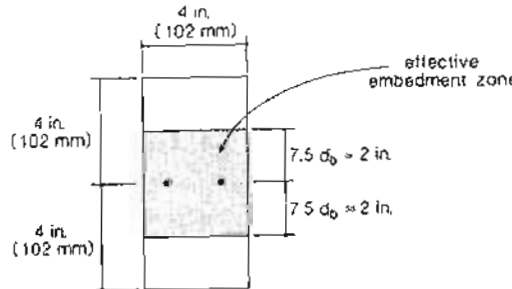


Figure 5-12 Cross section of pretensioned member.

To determine the complete moment-curvature response, we shall determine the moments and curvatures that correspond to various values of top concrete strain, ϵ_t . The procedure is to choose a value of ϵ_t and then find by trial and error the associated bottom fiber strain, ϵ_b , which results in zero axial load. In the calculations given below, the compressive stress-strain relationship for the concrete is assumed to be parabolic.

For example, for the choice of $\epsilon_t = -0.001$, the calculations would be as follows:

Step 1: Determine stress-block factors.

From Eq. (5-7),

$$\alpha_1 \beta_1 = \frac{1}{2.5} - \frac{1}{3} \left(\frac{1}{2.5} \right)^2 = 0.347$$

From Eq. (5-9),

$$\beta_1 = \frac{4 - (1/2.5)}{6 - 2(1/2.5)} = 0.692$$

Hence $\alpha_1 = 0.347/0.692 = 0.501$.

Step 2: Find ϵ_b so that $N = 0$.

Guess that $\epsilon_t = 0.002$. From the linear strain distribution (see Fig. 5-13) the neutral axis depth, c , is

$$c = \frac{0.001}{0.001 + 0.002} \times 8 = 2.67 \text{ in. (68 mm)}$$

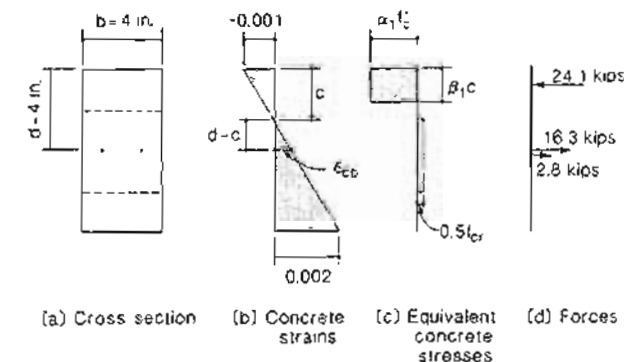


Figure 5-13 Calculation of sectional forces.

The concrete strain at the location of the prestressing steel, ϵ_{cp} , is

$$\begin{aligned} \epsilon_{cp} &= \frac{c - d}{c} \times \epsilon_t \\ &= \frac{2.67 - 4}{2.67} \times (-0.001) \\ &= 0.498 \times 10^{-3} \end{aligned}$$

The strain in the prestressing steel is thus

$$\begin{aligned} \epsilon_p &= \epsilon_{cp} + \Delta\epsilon_p \\ &= 0.498 \times 10^{-3} + 4.240 \times 10^{-3} \\ &= 4.738 \times 10^{-3} = \epsilon_{pf} \end{aligned}$$

This strain corresponds to a stress of 135.9 ksi (937 MPa) and hence the tensile force in the prestressing steel is $135.9 \times 0.120 = 16.3$ kips (72 kN).

The resultant compressive force in the concrete is equal to

$$\begin{aligned} \alpha_1 f'_c \beta_1 c b &= 0.501 \times 6.51 \times 0.692 \times 2.67 \times 4 \\ &= 24.1 \text{ kips (107 kN)} \end{aligned}$$

The resultant tensile force in the concrete is equal to $0.5 f_{cr}$ times the area of the effective embedment zone that is in tension, which equals $0.5 \times 0.420 \times 4 \times (2 + 1.33) = 2.8$ kips (12 kN). Hence the resultant axial load corresponding to the assumed strain distribution is

$$\begin{aligned} N &= 16.3 + 2.8 - 24.1 \\ &= -5.0 \text{ kips (-22 kN)} \end{aligned}$$

As the axial load should be zero, the bottom strain should be somewhat larger than 0.002. The axial loads corresponding to different trial values of ϵ_b are shown in Table 5-3, where it can be seen that the correct value of ϵ_b is 0.00255.

The trial-and-error procedure for determining ϵ_b can be performed conveniently with the aid of a programmable calculator.

Table 5-3 Determination of ϵ_b
for $\epsilon_t = -0.001$.

$\epsilon_b \times 10^3$	2.0	2.5	2.6	2.55
N. kips	-5.0	-0.4	+0.4	0.00
(kN)	(-22)	(-2)	(+2)	(0)

Step 3: Determine moment and curvature corresponding to the strain distribution.

Using the strain distribution corresponding to zero axial load, we can calculate the forces in the concrete and the reinforcement and the resulting moment and curvature (see Fig. 5-14).

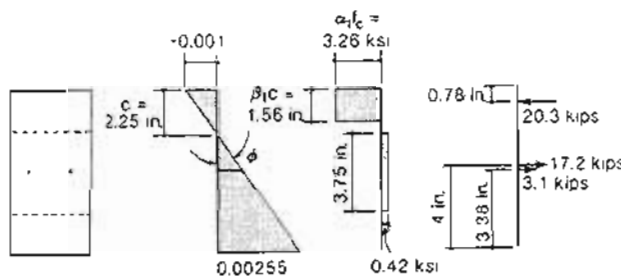


Figure 5-14 Calculation of sectional forces, moment, and curvature.

From the strain distribution the curvature, ϕ , is

$$\phi = \frac{0.001}{2.25} = 0.444 \times 10^{-3} \text{ rad/in.}$$

From the section forces acting at the locations shown in Fig. 5-14, the moment, M , acting on the section is

$$\begin{aligned} M &= 20.3(4 - 0.78) + 3.1(4 - 3.88) \\ &= 65.7 \text{ in.-kips (7.43 kNm)} \end{aligned}$$

Repeating Steps 1 to 3 for different values of ϵ_t results in the values given in Table 5-4.

Table 5-4 Calculated response accounting for tension in concrete.

$\epsilon_t \times 10^3$	$\epsilon_b \times 10^3$	$\phi \times 10^3$		M	
		rad/in.	rad/m	in.-kips	kNm
-0.25	0.096	0.043	1.70	30.1	3.40
-0.50	0.643	0.143	5.63	49.4	5.58
-1.00	2.55	0.444	17.5	65.9	7.45
-1.50	4.93	0.802	31.6	78.3	8.85
-2.00	7.51	1.189	46.8	87.1	9.85
-2.50	10.19	1.586	62.5	93.3	10.54
-3.00	12.88	1.985	78.1	96.7	10.92
-4.00	17.35	2.667	105.0	97.9	11.06
-5.00	18.77	2.971	117.0	92.3	10.43

So that we can check the ability of a section at a crack to transmit the moment, we recalculate the moment-curvature response neglecting tensile stresses in the concrete. The values calculated assuming no tension in the concrete will represent the response of a section at a crack. These values are summarized in Table 5-5, where it can be seen that the predicted failure moment of the section is 89.6 in.-kips (10.12 kNm).

Table 5-5 Calculated response of a section at a crack.

$\epsilon_t \times 10^3$	$\epsilon_b \times 10^3$	$\phi \times 10^3$		M	
		rad/in.	rad/m	in.-kips	kNm
-0.25	0.100	0.044	1.72	29.8	3.36
-0.50	0.784	0.161	6.32	44.6	5.03
-0.75	1.82	0.32	12.7	52.5	5.93
-1.25	4.33	0.70	27.5	65.5	7.40
-1.75	7.08	1.10	43.5	76.0	8.59
-2.25	10.03	1.54	60.4	83.2	9.40
-3.25	16.15	2.43	95.5	89.1	10.07
-3.75	18.78	2.82	110.9	89.6	10.12
-4.25	20.68	3.12	122.7	88.8	10.03
-4.75	21.36	3.29	129.5	86.8	9.80

The predicted response of the beam is shown in Fig. 5-15. The predicted response follows the calculated values, which include tension in the concrete up to a moment of 89.6 in.-kips (10.12 kNm), at which point it is predicted that the section will fail at a crack. The average curvature values measured by Priestley, Park, and Lu at various values of moment are also shown in Fig. 5-15. It can be seen that the predicted and observed responses agree very well.

For a given value of moment, the predicted curvature, assuming zero tension in the concrete, corresponds to the curvature at a section containing a flexural crack which should

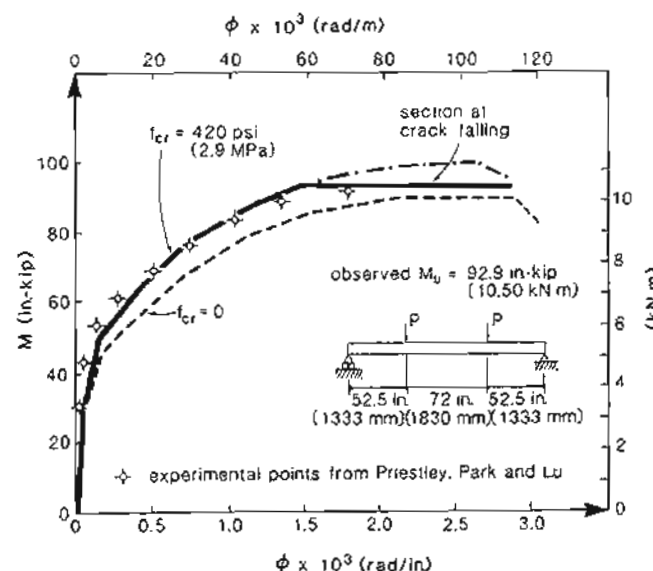


Figure 5-15 Comparison of calculated and observed moment-curvature responses.

be the maximum curvature associated with this moment. The curvature calculated taking into account tension stiffening, that is, using the average tensile stresses in the cracked concrete, will be the average curvature associated with a given moment.

The local curvatures measured by Priestley, Park, and Lu (Ref. 5-4), when the moment was 76 in.-kips (8.6 kNm), are compared with the predicted maximum curvature and the predicted average curvature at this moment in Fig. 5-16. It can be seen that the predicted maximum curvature agrees well with the curvatures measured at crack locations.

The distribution of local curvatures along the length of the beam will become more "peaked" at the cracks as the moment approaches the failure value (see Fig. 5-7). For this beam, failure is predicted to occur by crushing of the concrete in the compression zone above a crack after very large tensile strains have occurred in the prestressing. At the crack location, the local strain in the prestressing steel when the moment reaches its maximum value is predicted to be 11.8×10^{-3} , corresponding to a stress of 217 ksi (1495 MPa).

5.9 CALCULATION OF MOMENT-CURVATURE USING LAYER-BY-LAYER APPROACH

To illustrate the layer-by-layer approach for determining moment-curvature response, we will calculate the short-term response of the precast, pretensioned single-tee beam described in Fig. 5-17, using the program RESPONSE, described in Appendix A.

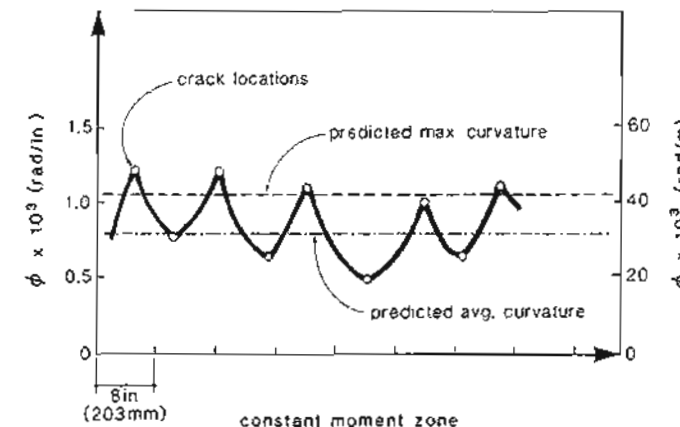


Figure 5-16 Comparison of predicted average and maximum curvatures measured by Priestley, Park, and Lu (Ref. 5-4).

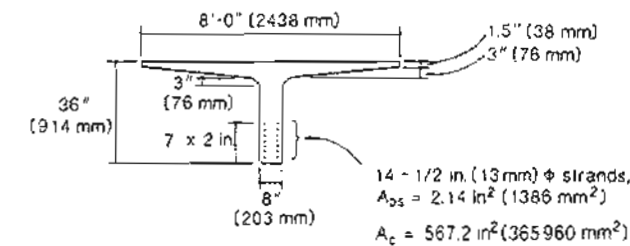


Figure 5-17 Cross-sectional properties of single-tee beam.

The discretization of the concrete cross section into five concrete layers and seven steel layers is shown in Fig. 5-18a. Note that in performing the numerical integration, RESPONSE further subdivides the concrete layers. The concrete in the shaded zone in Fig. 5-18a is assumed to have average tensile stresses after cracking and hence will contribute to tension stiffening. In determining the effective embedment zones, we should keep in mind the approximate nature of the "7.5 times the bar diameter" rule illustrated in Fig. 4-21. Hence some adjustments in the embedment zones can be made if they simplify the idealization.

The low-relaxation prestressing strands were tensioned to a stress of 200 ksi (1379 MPa) in the pretensioning bed, prior to casting of the concrete (i.e., $\Delta\epsilon_p$ is about $200/29,000 = 0.00690$). The stress-strain curve of these strands is given by Eq. (3-26)

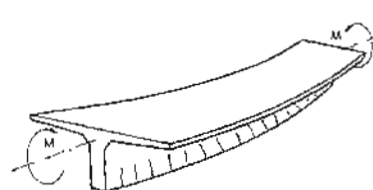
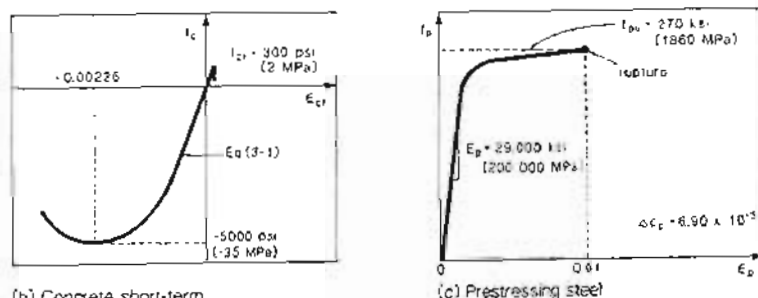
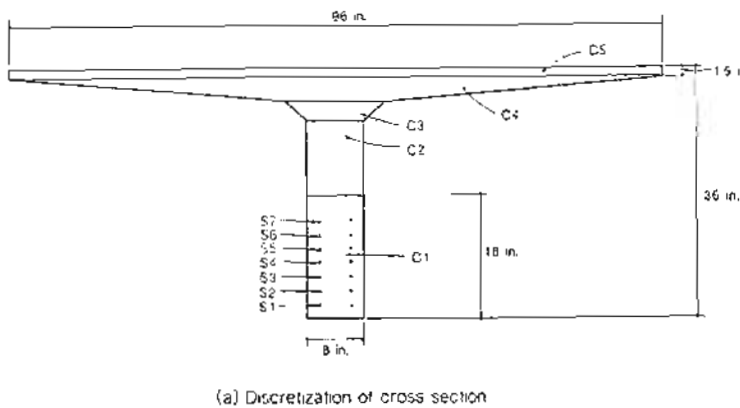


Figure 5-18 Details of single-tee member.

except that the strands are assumed to rupture at a strain of 0.040 (i.e., 4%). The stress-strain response of the concrete was calculated using Eq. (3-1), which is called the "high-strength concrete model" in RESPONSE.

After the section properties have been defined we can analyze the section in several different modes using RESPONSE. For a section subjected to only moment and axial load, with a constant axial load (zero in our case) we can either have the program calculate the complete response of the section or we can calculate just one point on the response corresponding to a given concrete strain at a given location. For this example we will use this point-by-point mode. As discussed in Section 5.8, when we calculate the moment-curvature response of a member we can either account for the tensile stresses in the concrete between the cracks, which will give us a good estimate of the average curvature at a given moment, or we can neglect the postcracking concrete tensile stresses, which will give us a good estimate of the maximum curvature at a given moment. We will conduct two analyses, one accounting for tension stiffening and the other neglecting tension stiffening.

The calculated response of our single tee when tension stiffening is taken into account is summarized in Table 5-6 and illustrated in Fig. 5-19. The first three sets of values listed in Table 5-6 show what happens when the section is subjected to negative moments. Because the section contains no reinforcement near the top face, it takes only a small negative moment to fail the section. Obviously, if such a member were turned upside down, it would fail under its own weight.

Table 5-6 Calculated response accounting for tension in concrete

$\epsilon_c \times 10^3$	$\epsilon_b \times 10^3$	$\phi \times 10^3$		M		Comments
		rad/in.	rad/m	ft-kips	kNm	
7.51	-4.00	-0.320	-12.58	-89	-121	Bottom concrete crushing
4.84	-2.70	-0.210	-8.27	-109	-148	Maximum negative moment
0.52	-1.10	-0.044	-1.73	0	0	Zero moment
0.20	-0.88	-0.030	-1.18	47	63	
0.077	-0.85	-0.026	-1.01	22	30	Top concrete cracking
-0.19	-0.19	0	0	620	841	Zero curvature
-0.30	0.077	0.010	0.41	866	1174	Bottom concrete cracking
-0.50	1.60	0.058	2.30	1083	1469	
-0.75	5.28	0.168	6.60	1198	1624	
-1.00	10.33	0.315	12.39	1228	1665	
-1.25	16.30	0.488	19.20	1249	1694	
-1.50	22.87	0.677	26.65	1269	1721	
-1.95	35.15	1.031	40.57	1305	1769	
-1.76	35.16	1.026	40.38	1079	1463	Bottom strands ruptured

We assumed that the tensile strength of the concrete was 300 psi (2.07 MPa). With a concrete stiffness of 3889 ksi (26800 MPa) the concrete will crack when the concrete strain due to stress reaches 0.077×10^{-3} . We find that the top fibers of concrete will reach this strain at a moment of 22 ft-kips (30 kNm) while the bottom fibers of concrete will crack when the moment reaches 866 ft-kips (1174 kNm). In between these two moments the section will be uncracked and a reasonable prediction of response could be made using the assumption of linear elastic, uncracked behavior. Methods for calculating the response in this uncracked range are given in Section 5.11.

From Fig. 5-19 it can be seen that when the top face cracks there is a sudden change in the moment-curvature response. The loss of stiffness of the large, unreinforced top flange causes a cusp in the moment-curvature curve.

For moments higher than 866 ft-kips (1174 kNm) flexural cracks will form near the bottom face and it becomes important to distinguish between the response at a crack (calculated by ignoring tension in the concrete) and the average response (calculated by accounting for tension stiffening). Table 5-7 summarizes the calculated response of a section at a crack. For this section, which has a relatively small area of concrete in the flexural tension zone, tension stiffening has only a small effect.

Table 5-7 Calculated response of a section at a crack.

$\epsilon_t \times 10^3$	$\epsilon_b \times 10^3$	$\phi \times 10^3$		M		Comments
		rad/in.	rad/m	ft-kips	kNm	
-0.50	1.76	0.063	2.47	1059	1436	
-0.75	5.50	0.174	6.84	1174	1591	
-1.00	10.39	0.322	12.67	1208	1637	
-1.25	16.61	0.496	19.53	1231	1670	
-1.50	23.22	0.687	27.03	1254	1700	
-1.93	35.15	1.030	40.58	1290	1750	Maximum moment
-1.75	35.16	1.025	40.36	1065	1444	2 strands ruptured
-1.83	37.45	1.091	42.95	1071	1451	
-1.62	37.45	1.085	42.73	858	1163	4 strands ruptured
-1.69	40.05	1.159	45.65	863	1170	
-1.48	40.03	1.153	45.40	663	899	6 strands ruptured
-1.55	42.99	1.237	48.70	667	904	
-1.31	42.94	1.229	48.40	479	650	8 strands ruptured
-1.37	46.34	1.325	52.18	483	654	

From Fig. 5-19 it can be seen that after cracks form on the bottom face, the moment-curvature relationship begins to change its slope, with the initial change in slope immediately after cracking being rather small. The rounded nature of the post-cracking moment-curvature response reflects, in part, the rounded nature of the stress-strain response of the prestressing strand. A strain of 1% is sometimes regarded as defining the "yield point" of the strand. The points at which the lowest and the highest layers of strands reach this strain have been shown on the moment-curvature response in Fig. 5-19. It can be seen that after all the strands have "yielded" the stiffness of the member deteriorates significantly.

At a moment of 1290 ft-kips (1750 kNm) the strain in the lowest layer of strands is predicted to be 0.040 (i.e., the strain in the surrounding concrete is $40 \times 10^{-3} - 6.90 \times 10^{-3} = 33.10 \times 10^{-3}$) at a crack location. At this strain the strands are about to rupture, defining the maximum moment capacity of the member. When the two strands in the lowest layer rupture the section unloads to a moment of 1065 ft-kips (1444 kNm). A small increase in moment to 1071 ft-kips (1451 kNm) will then cause the next layer of strands to rupture. The resulting "sawtooth" postpeak response caused by the rupturing of successive layers of strands is shown in Fig. 5-19. The points defining this postpeak response were calculated

by setting the strain at the various tendon layers to a value just below that causing rupture (e.g., 33.09×10^{-3}) and then setting it just above the rupture strain (e.g., 33.11×10^{-3}).

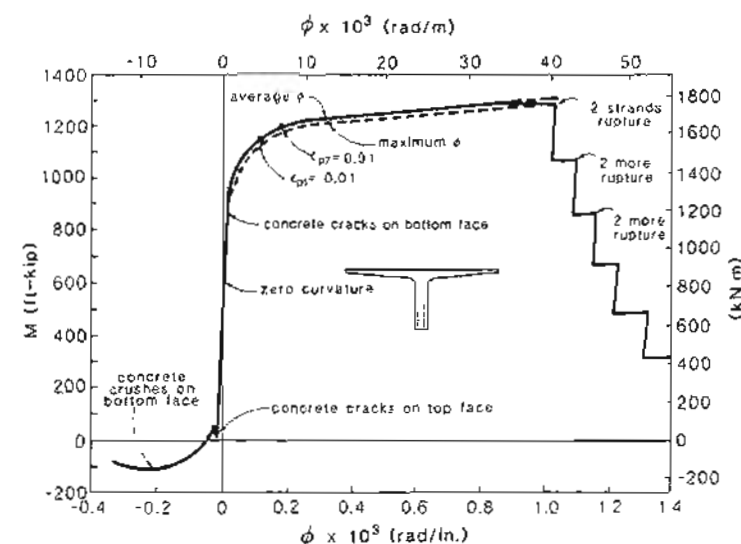


Figure 5-19 Short-term moment-curvature response of single-tee beam.

Note that in drawing the moment-curvature response shown in Fig. 5-19 we have "cut off" the predicted average response at the maximum moment that can be resisted at a crack. As the bond will be severely deteriorated at failure, we have assumed that the postpeak response will follow the response predicted by ignoring tension stiffening.

Because of the large area of concrete in the wide top flange of the single tee, the flexural capacity of the section is governed by failure of the strands in tension rather than by crushing of the concrete in compression. When the most highly stressed strands are just about to rupture, the highest compressive strain in the concrete is -1.93×10^{-3} , which is just below the strain required to cause a stress of f'_c .

5.10 DETERMINATION OF LONG-TERM MOMENT-CURVATURE RESPONSE

To illustrate how the long-term, moment-curvature response of a section can be determined, we will recalculate the response of the single-tee beam described in Fig. 5-17, accounting for creep, shrinkage, and relaxation.

We will assume that the creep coefficient of the concrete is 2.7 and that the concrete was first loaded when its compressive strength was 3500 psi (24.1 MPa), which from

Table 3-3 gives an initial modulus of 3366 ksi (23 200 MPa). The long-term modulus is thus $3366/(1 + 2.7) = 910$ ksi (6273 MPa). It is assumed that under slowly applied long-term loading the compressive strength of the concrete will be 5000 psi (34.5 MPa).

Thus the long-term stress-strain curve will peak at a strain of $2.8 \times 5000/(910,000 \times 1.8) = 8.55 \times 10^{-3}$ (see Fig. 3-10). The cracking stress is assumed to be 300 psi (2.1 MPa). The resulting long-term stress-strain curve for the concrete is shown in Fig. 5-20a.

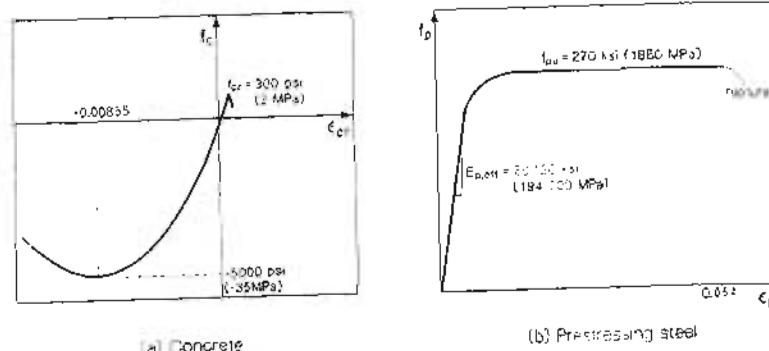


Figure 5-20 Long-term stress-strain relationships.

It will be assumed that the prestressing strands lose 3% of their initial stress due to relaxation, resulting in an effective modulus, $E_{p,eff}$, of $0.97 \times 29,000 = 28,130$ ksi (194,000 MPa). We will use the modified Ramberg-Osgood function of Eq. (3-26) for the long-term stress-strain relationship for the strand except that the coefficient of 29×10^3 will be replaced by 28,130. It will further be assumed that under long-term loading the strand will rupture at a strain of 0.054 (i.e., 5.4%). The resulting long-term stress-strain curve for the strand is shown in Fig. 5-20b. In addition to the creep and relaxation, it is assumed that a concrete shrinkage strain of -0.48×10^{-3} occurs.

In determining flexural response we assume that the total concrete strains vary linearly over the depth of the cross section. If the total concrete strain, ϵ_c , in a given layer is known and the shrinkage strain, ϵ_{sh} , in this layer is known, the concrete strain caused by stress, ϵ_{cf} , can be found from Eq. (4-6) as

$$\epsilon_{cf} = \epsilon_c - \epsilon_{sh} \quad (5-10)$$

In the present example, it is assumed that the shrinkage strain is uniform over the section.

The long-term moment-curvature response for the single tee was again obtained using the computer program RESPONSE, which is described in Appendix A. The cross section was represented by the five concrete layers and the seven steel layers shown in Fig. 5-18a. The results of these calculations are summarized in Tables 5-8 and 5-9.

Table 5-8 Long-term response calculated accounting for tension in concrete.

ϵ_t $\times 10^3$	ϵ_b $\times 10^3$	$\phi \times 10^3$		M		Comments
		rad/in.	rad/m	ft-kips	kNm	
16.39	-8.00	-0.678	-26.67	-142	-193	
12.35	-7.00	-0.538	-21.16	-126	-171	
5.05	-5.00	-0.279	-10.99	-77	-103	
0.32	-3.25	-0.099	-3.90	12	16	
-0.15	-3.22	-0.085	-3.36	-45	-61	Top concrete cracking
-0.23	-3.05	-0.078	-3.09	0	0	Zero moment
-1.15	-1.15	0	0	522	708	Zero curvature
-1.64	-0.15	0.041	1.62	797	1080	Bottom concrete cracking
-2.00	1.10	0.086	3.39	946	1283	
-2.50	4.18	0.186	7.31	1104	1497	
-3.00	10.58	0.377	14.85	1160	1573	
-4.00	27.73	0.891	34.70	1218	1651	
-5.00	47.12	1.448	57.00	1276	1730	

Note that under this long-term loading, the concrete will crack when the total strain in the concrete is

$$\epsilon_c = \frac{f_{cr}}{E_{c,eff}} + \epsilon_{sh} = \frac{300}{910,000} - 0.48 \times 10^{-3} = -0.150 \times 10^{-3}$$

Table 5-9 Long-term response calculated neglecting tension in concrete.

ϵ_t $\times 10^3$	ϵ_b $\times 10^3$	$\phi \times 10^3$		M		Comments
		rad/in.	rad/m	ft-kips	kNm	
-2.00	1.24	0.090	3.54	937	1270	
-3.00	10.98	0.388	15.29	1147	1556	
-4.00	28.11	0.892	35.11	1208	1639	
-5.00	47.53	1.459	57.45	1269	1721	
-5.13	50.16	1.536	60.46	1276	1730	Maximum moment
-4.71	50.16	1.524	60.01	1052	1426	2 strands ruptured
-4.86	53.58	1.624	63.92	1060	1437	
-4.42	53.55	1.610	63.40	848	1150	4 strands ruptured
-4.57	57.42	1.722	67.80	855	1159	
-4.09	57.35	1.707	67.19	656	889	6 strands ruptured

This long-term moment-curvature response is compared with the short-term response predicted in Fig. 5-21. From this figure it can be seen that creep, shrinkage, and relaxation have caused a "lowering" of the moment-curvature response. The moments required to fail the section, to crack the bottom-face concrete, to cause zero curvature, and to crack

the top-face concrete have all been lowered. The substantial decrease in flexural stiffness of the uncracked section is particularly worthy of note. It is also important to observe that under long-term loading the strands will rupture at a slightly lower (about 1% smaller) moment but at a considerably larger curvature than in the case of short-term loading.

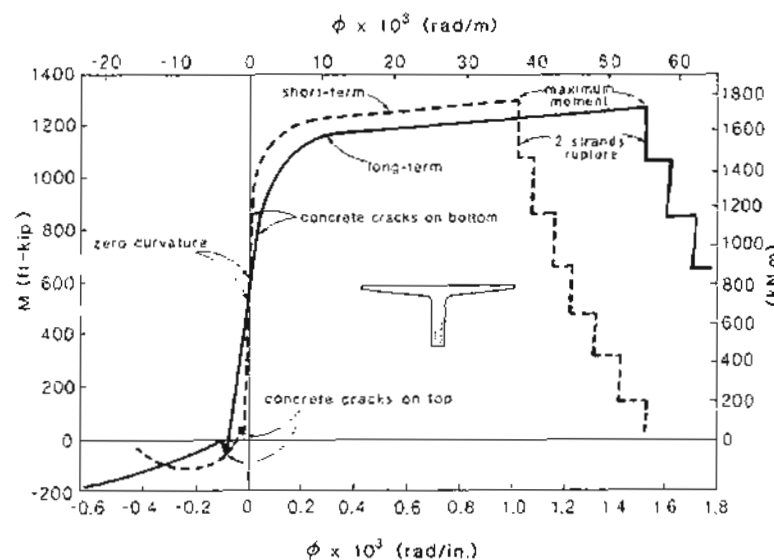


Figure 5-21 Comparison of short-term and long-term moment-curvature responses.

As discussed in Chapter 4, "short term" and "long term" are intended to represent bounds on the actual response of a prestressed concrete member. It is also possible, by making somewhat more detailed calculations, to predict the response for a specific load history.

5.11 ELASTIC UNCRACKED RESPONSE

Prestressed concrete members typically remain uncracked over a large range of moments (see Fig. 5-21). Within this range, reasonable predictions of response can be made by assuming that the material stress-strain relationships are all linearly elastic and by assuming that the concrete is uncracked. With these assumptions, simple closed-form expressions can be derived which enable behavioral predictions to be made conveniently. These closed-form expressions can be derived by considering the compatibility, the stress-strain, and the equilibrium relationships, as follows:

(a) Compatibility

Once again we assume that plane sections remain plane, as shown in Fig. 5-22. For these calculations it is convenient to use the centroidal axis of the transformed cross section as the origin.

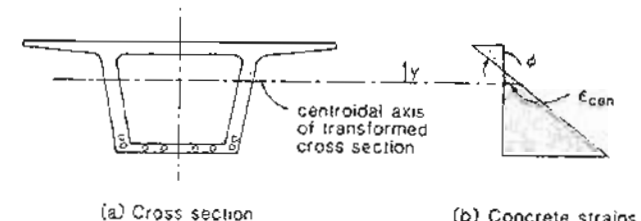


Figure 5-22 Variation of concrete strain over cross section.

The strains at level y , in the concrete, reinforcing steel, and prestressing steel are

$$\epsilon_c = \epsilon_{cen} - \phi y \quad (5-11)$$

$$\epsilon_s = \epsilon_{cen} - \phi y \quad (5-12)$$

$$\epsilon_p = \epsilon_{cen} - \phi y + \Delta\epsilon_p \quad (5-13)$$

(b) Stress-Strain Relationships

It is assumed that there is a linear relationship between the stress and the strain caused by the stress (see Fig. 5-23). In addition, strains not caused by stress, such as thermal strains and shrinkage strains, are taken into account. These strains, which have no stress associated with them, are for uniformity called ϵ_{co} , ϵ_{so} , and ϵ_{po} (see Fig. 5-23). The term ϵ_{co} equals the concrete shrinkage strain, ϵ_{sh} , plus the thermal strain, ϵ_{sth} , while ϵ_{so} equals ϵ_{sth} and ϵ_{po} equals ϵ_{pth} .

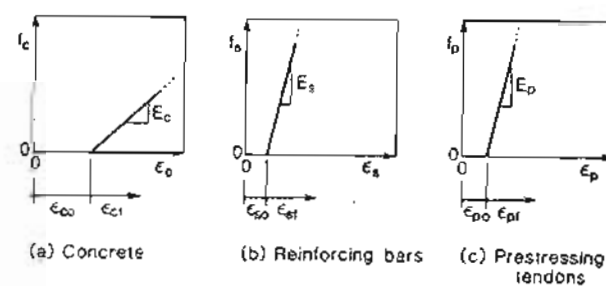


Figure 5-23 Relationship between stresses and strain.

The stresses at level y thus become

$$f_c = E_c \epsilon_{cf} \quad (5-14)$$

$$f_s = E_s \epsilon_{sf} \quad (5-15)$$

$$f_p = E_p \epsilon_{pf} \quad (5-16)$$

where

$$\epsilon_{cf} = \epsilon_c - \epsilon_{co} \quad (5-17)$$

$$\epsilon_{sf} = \epsilon_s - \epsilon_{so} \quad (5-18)$$

$$\epsilon_{pf} = \epsilon_p - \epsilon_{po} \quad (5-19)$$

(c) Equilibrium

The integral of the stress over the area must equal the applied axial load, N ; thus

$$N = \int_{A_c} f_c dA_c + \int_{A_s} f_s dA_s + \int_{A_p} f_p dA_p \quad (5-20)$$

Substituting the compatibility and stress-strain expressions into this equilibrium equation gives

$$\begin{aligned} N &= \int_{A_c} E_c [\epsilon_{cen} - \phi y - \epsilon_{co}] dA_c + \int_{A_s} E_s [\epsilon_{cen} - \phi y - \epsilon_{so}] dA_s \\ &\quad + \int_{A_p} E_p [\epsilon_{cen} - \phi y + \Delta \epsilon_p - \epsilon_{po}] dA_p \\ &= E_c \epsilon_{cen} \left[A_c + \frac{E_s}{E_c} A_s + \frac{E_p}{E_c} A_p \right] + \int_{A_p} E_p \Delta \epsilon_p dA_p \\ &\quad - E_c \phi \left[\int_{A_c} y dA_c + \frac{E_s}{E_c} \int_{A_s} y dA_s + \frac{E_p}{E_c} \int_{A_p} y dA_p \right] \\ &\quad - \left[\int_{A_c} E_c \epsilon_{co} dA_c + \int_{A_s} E_s \epsilon_{so} dA_s + \int_{A_p} E_p \epsilon_{po} dA_p \right] \quad (5-21) \end{aligned}$$

Recognizing that the transformed area of the cross section is

$$A_{trans} = A_c + \frac{E_s}{E_c} A_s + \frac{E_p}{E_c} A_p \quad (5-22)$$

and that the third term in Eq. (5-21) equals zero (i.e., the first moment of area about the centroidal axis is, by definition, zero), Eq. (5-21) can be written as

$$\epsilon_{cen} = \frac{N - N_o}{E_c A_{trans}} \quad (5-23)$$

where

$$N_o = \int_{A_p} E_p \Delta \epsilon_p dA_p - \int_{A_c} E_c \epsilon_{co} dA_c - \int_{A_s} E_s \epsilon_{so} dA_s - \int_{A_p} E_p \epsilon_{po} dA_p \quad (5-24)$$

The second equilibrium requirement is that the integral of the stresses times the distance from the centroidal axis must balance the applied moment and hence

$$\int_{A_c} f_c y dA_c + \int_{A_s} f_s y dA_s + \int_{A_p} f_p y dA_p = -M \quad (5-25)$$

which can be rearranged to give

$$\phi = \frac{M - M_o}{E_c I_{trans}} \quad (5-26)$$

where

$$M_o = - \int_{A_p} E_p \Delta \epsilon_p y dA_p + \int_{A_c} E_c \epsilon_{co} y dA_c + \int_{A_s} E_s \epsilon_{so} y dA_s + \int_{A_p} E_p \epsilon_{po} y dA_p \quad (5-27)$$

Figure 5-24 illustrates the predicted response of a prestressed concrete beam subjected to applied load, N , and moment, M . As would be expected, straight-line responses are predicted. Prestressing causes the lines to be offset from the origins. Shrinkage strains and thermal strains also contribute to these offsets.

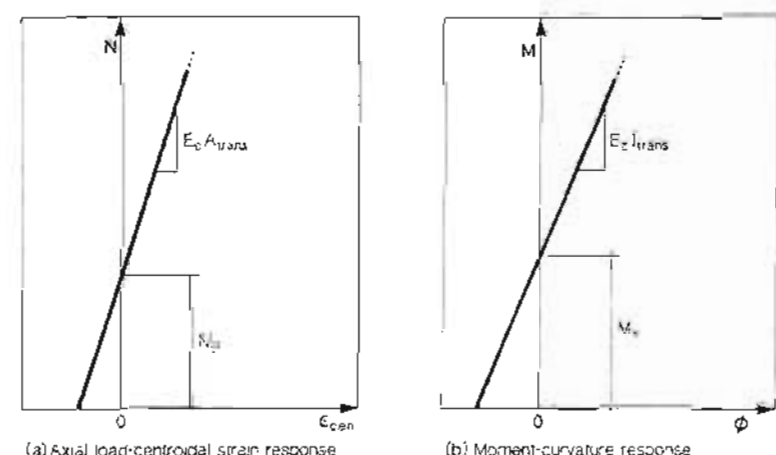


Figure 5-24 Elastic uncracked response predictions.

Note that if a section is subjected to an axial load of N_o and a moment of M_o , both ϵ_{con} and ϕ will equal zero (see Fig. 5-24). Thus under the combined action of these two loads the concrete strain will be zero over the complete section. Hence N_o and M_o can be thought of as the actions required to produce zero concrete strains.

(d) Calculation of Transformed Section Properties

Before the closed-form expressions based on the assumption of elastic uncracked response can be calculated, it is necessary to calculate the transformed section properties. That is, we need to know the location of the centroid of the transformed section, the area of the transformed section, A_{trans} , and the second moment of area about the centroidal axis, I_{trans} . These properties can be conveniently calculated using either a programmable calculator or a microcomputer.

An appropriate solution technique for calculating these section properties is to build the section up piece by piece, calculating the new section properties from the old section properties by using the equations of the parallel axis theorem (see Fig. 5-25) as follows:

$$A_{new} = A_{old} + A_i \quad (5-28)$$

$$y_{new} = \frac{A_{old}y_{old} + A_iy_i}{A_{new}} \quad (5-29)$$

$$I_{new} = I_{old} + A_{old}(y_{new} - y_{old})^2 + I_i + A_i(y_{new} - y_i)^2 \quad (5-30)$$

where A_{old} = area of old section

I_{old} = second moment of area of old section about its own centroidal axis

y_{old} = distance from arbitrary reference axis to centroid of old section

A_i = area of piece being added to previous section

I_i = second moment of area of piece being added, about its own centroidal axis

y_i = distance from reference axis to centroid of piece being added

A_{new} = area of new section formed by adding piece to previous section

I_{new} = second moment of area of new section about its own centroidal axis

y_{new} = distance from reference axis to centroid of new section.

It is usually convenient to input the concrete section as a series of component rectangles and triangles ignoring the "holes" caused by the reinforcement. The resulting section properties are referred to as the gross section properties.

Before inputting the steel areas they are transformed to equivalently stiff areas of concrete by multiplying their areas by the term $(n - 1)$, where n equals the modular ratio E_s/E_c or E_p/E_c , and the 1 allows for the hole in the concrete caused by the reinforcement. The transformed reinforcement areas are then added to the gross section with the I_r for the reinforcement typically taken as zero. The resulting section properties are referred to as the transformed section properties.

For standard precast sections the gross section properties are usually known (see Fig. 2-10 and Ref. 5-5). Further, in calculating the transformed section properties the

reinforcement can be considered as "lumped" at its centroid (see Fig. 5-26). In such cases the transformed section properties can be calculated as follows:

$$A_{trans} = A_{gross} + (n - 1)A_p \quad (5-31)$$

$$y_{bt} = \frac{A_{gross}y_{bg} + (n - 1)A_p y_{bs}}{A_{trans}} \quad (5-32)$$

$$I_{trans} = I_{gross} + A_{gross}(y_{bg} - y_{bt})^2 + (n - 1)A_p(y_{bt} - y_{bs})^2 \quad (5-33)$$

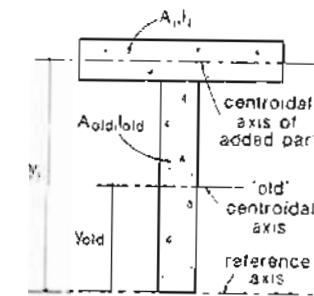


Figure 5-25 Calculation of section properties

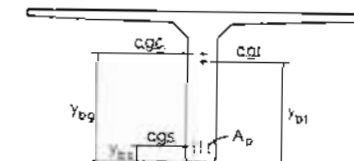


Figure 5-26 Calculation of transformed section properties.

5.12 EXAMPLE CALCULATIONS ASSUMING UNCRACKED RESPONSE

As a demonstration of the use of the equations for elastic uncracked response, we will use them to predict some aspects of short-term response and long-term response of the precast, pretensioned single-tec beam described in Figs. 5-17 and 5-18.

(a) Prediction of Short-Term Response

We will calculate the stresses in the concrete and in the prestressing strands immediately after transfer for external loads of $N = 0$ and $M = 475$ ft-kips (644 kNm). This moment is the dead-load moment at midspan for an 80 ft (24.4 m) span. We will assume that no creep, shrinkage, relaxation or thermal strains have occurred. Assume that at release, f'_c equals 3500 psi (24.1 MPa) and that the modulus, E_c , from Table 3-3 is 3366 ksi (23 200 MPa).

Step 1: Calculate the transformed section properties.

The modular ratio, n , is equal to $29,000/3366 = 8.62$ and hence $(n - 1)$ equals 7.62. The dimensions required are shown in Fig. 5-27. The transformed section properties from Eqs. (5-31), (5-32), and (5-33) are

$$A_{trans} = 570 + 7.62 \times 2.14 = 586.3 \text{ in}^2 (378,250 \text{ mm}^2)$$

$$y_{bt} = \frac{570 \times 26.01 + 7.62 \times 2.14 \times 8.0}{586.3} = 25.51 \text{ in. (648 mm)}$$

$$I_{trans} = 68,917 + 570(26.01 - 25.51)^2 + 7.62 \times 2.14(25.51 - 8.0)^2 = 74,059 \text{ in}^4 (30,830 \times 10 \text{ mm}^4)$$

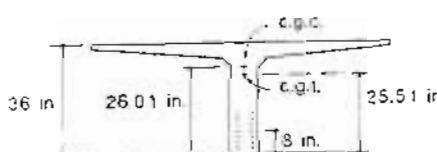


Figure 5-27 Dimensions required in calculating short-term response.

Step 2: Calculate N_o and M_o .

The strain components, ϵ_{co} , ϵ_{so} and ϵ_{po} are all zero. The prestressing strands were all tensioned to a stress of 1400 MPa prior to casting the concrete, giving a strain difference of

$$\Delta\epsilon_p = \frac{200}{29,000} = 6.90 \times 10^{-3}$$

Hence, from Eq. (5-24),

$$N_o = E_p \Delta\epsilon_p A_p$$

$$= 29,000 \times 6.90 \times 10^{-3} \times 14 \times 0.153$$

$$= 428 \text{ kips (1904 kN)}$$

As ϵ_{co} , ϵ_{so} and ϵ_{po} are zero and $\Delta\epsilon_p$ is constant, Eq. (5-27) reduces to

Sec. 5.12 Example Calculations Assuming Uncracked Response

$$M_o = E_p \Delta\epsilon_p A_p (y_{bt} - y_{bs})$$

$$= N_o (y_{bt} - y_{bs}) \quad (5-34)$$

From Fig. 5-27 and Eq. (5-34),

$$M_o = 428(25.51 - 8.0)$$

$$= 7494 \text{ in.-kips (847 kNm)}$$

Note that this moment, 624 ft-kips (847 kNm), is very close to the 622 ft-kips (843 kNm) listed in Table 5-6 as the moment required to cause zero curvature under short-term loading.

Step 3: Determine concrete strains and stresses.

The strain at the centroid can be determined from Eq. (5-23) as

$$\epsilon_{cen} = \frac{N - N_o}{E_c A_{trans}}$$

$$= \frac{0 - 428}{3366 \times 586.3} = -0.217 \times 10^{-3}$$

The curvature can be determined from Eq. (5-26) as

$$\phi = \frac{M - M_o}{E_c I_{trans}}$$

$$= \frac{475 \times 12 - 7494}{3366 \times 74,059} = -7.20 \times 10^{-6} \text{ rad/in.}$$

Knowing ϵ_{cen} and ϕ , the concrete strain at any location in the beam can be determined using Eq. (5-11). The resulting distribution of concrete strains is shown in Fig. 5-28a. As ϵ_{eo} is zero, the concrete stresses are found by multiplying the concrete strains by E_c , resulting in the stress distribution shown in Fig. 5-28b.

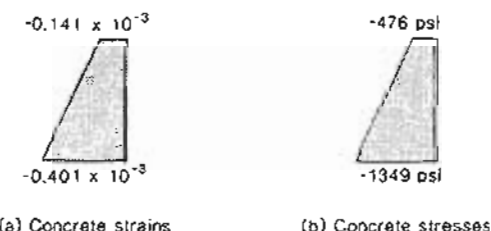


Figure 5-28 Concrete strains and stresses immediately after transfer.

Step 4: Determine the stress in prestressing.

From Eq. (5-13) the strain at the centroid of the prestressing is

$$\begin{aligned}\epsilon_p &= \epsilon_{cen} - \phi y + \Delta\epsilon_p \\ &= -0.217 \times 10^{-3} - (-7.20 \times 10^{-6}) \times (-17.51) + 6.9 \times 10^{-3} \\ &= 6.557 \times 10^{-3}\end{aligned}$$

As $\epsilon_{po} = 0$, the stress in the prestressing at its centroid is

$$\begin{aligned}f_p &= 29,000 \times 6.557 \times 10^{-3} \\ &= 190 \text{ ksi (1311 MPa)}\end{aligned}$$

Note that elastic shortening of the beam has caused the stress in the strands to drop 10 ksi (69 MPa), which corresponds to 5% of the initial stress in the strands.

(b) Prediction of Long-Term Response

We will calculate the stresses in the concrete and in the prestressing strands after creep, shrinkage, and relaxation have occurred for external loads of $N = 0$ and $M = 475$ ft-kips (644 kNm).

We will assume that the creep coefficient is 2.7, that the concrete shrinkage strain is -0.48×10^{-3} , and that the relaxation loss in the prestressing strand is 3%.

Step 1: Calculate the transformed section properties.

From Eq. (3-12) the effective modulus of the concrete is

$$E_{c,eff} = \frac{3366}{1 + 2.7} = 910 \text{ ksi (6273 MPa)}$$

From Eq. (3-30) the effective modulus of the prestressing strand is

$$E_{p,eff} = 0.970 \times 29,000 = 28,130 \text{ ksi (194,000 MPa)}$$

Hence $(n - 1) = 29.91$. The transformed section properties from Eqs. (5-31), (5-32), and (5-33) are

$$\begin{aligned}A_{trans} &= 570 + 29.91 \times 2.14 = 634.0 \text{ in}^2 (409,000 \text{ mm}^2) \\ y_{bt} &= \frac{570 \times 26.01 + 29.91 \times 2.14 \times 8.0}{634.0} = 24.19 \text{ in. (614 mm)} \\ I_{trans} &= 68,917 + 570(26.01 - 24.19)^2 + 29.91 \times 2.14(24.19 - 8.0)^2 \\ &= 87,582 \text{ in}^4 (36,450 \times 10^6 \text{ mm}^4)\end{aligned}$$

Sec. 5.12 Example Calculations Assuming Uncracked Response**Step 2:** Calculate N_o and M_o .

For this case, where $\Delta\epsilon_p$ and ϵ_{co} are constant, and ϵ_{sg} and ϵ_{po} are zero, Eq. (5-24) reduces to

$$\begin{aligned}N_o &= E_{p,eff} \Delta\epsilon_p A_p - E_{c,eff} \epsilon_{co} A_c \\ &= 28,130 \times 6.9 \times 10^{-3} \times 2.14 - 910 \times (-0.48 \times 10^{-3}) \times 570 \\ &= 415.4 + 249.0 \\ &= 664.3 \text{ kips (2955 kN)}\end{aligned} \quad (5-35)$$

Note that in evaluating Eq. (5-35) we have approximated A_c by the gross concrete area.

For uniform values of $\Delta\epsilon_p$ and ϵ_{co} over the section and with ϵ_{sg} and ϵ_{po} equal to zero, Eq. (5-27) reduces to

$$M_o = E_{p,eff} \Delta\epsilon_p A_p (y_{bt} - y_{bs}) + E_{c,eff} \epsilon_{co} A_c (y_{bg} - y_{bt}) \quad (5-36)$$

Hence, from Fig. 5-29 and Eq. (5-36),

$$\begin{aligned}M_o &= 28,130 \times 6.9 \times 10^{-3} \times 2.14(24.19 - 8.0) \\ &+ 910 \times (-0.48 \times 10^{-3}) \times 570 \times (26.01 - 24.19) \\ &= 6725 - 453 \\ &= 6272 \text{ in.-kips (709 kNm)}\end{aligned}$$

Note that this moment, 523 ft-kips (709 kNm), is quite close to the 519 ft-kips (704 kNm) listed in Table 5-8 as the moment required to produce zero curvature under long-term loading.

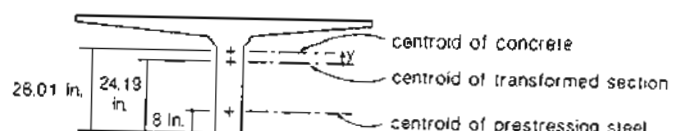


Figure 5-29 Dimensions required in calculating long-term response.

Step 3: Determine concrete strains and stresses.

From Eq. (5-23),

$$\begin{aligned}\epsilon_{cen} &= \frac{N - N_o}{E_{c,eff} A_{trans}} \\ &= \frac{0 - 664.3}{910 \times 634.0} = -1.151 \times 10^{-3}\end{aligned} \quad (5-37)$$

From Eq. (5-26),

$$\phi = \frac{M - M_g}{E_{c,eff} I_{trans}} \quad (5-38)$$

$$= \frac{475 \times 12 - 6272}{910 \times 87.582}$$

$$= -7.18 \times 10^{-6} \text{ rad/in.}$$

From Eq. (5-11) the total concrete strain at the top of the member is

$$\epsilon_c = -1.151 \times 10^{-3} - (-7.18 \times 10^{-6}) \times (36 - 24.19) = -1.066 \times 10^{-3}$$

and the total concrete strain at the bottom is

$$\epsilon_c = -1.151 \times 10^{-3} - (-7.18 \times 10^{-6}) \times (-24.19) = -1.325 \times 10^{-3}$$

As the concrete shrinkage strain is -0.48×10^{-3} , the strain due to stress in the top fiber of concrete is

$$\epsilon_{cf} = \epsilon_c - \epsilon_{co} = -1.066 \times 10^{-3} - (-0.48 \times 10^{-3})$$

$$= -0.586 \times 10^{-3}$$

Hence the stress in the top fiber of concrete is

$$f_c = E_{c,eff} \epsilon_{cf} = 910 \times (-0.586 \times 10^{-3}) = -533 \text{ psi} (-3.68 \text{ MPa})$$

The strain due to stress in the bottom fiber of concrete is

$$\epsilon_{cf} = -1.325 \times 10^{-3} - (-0.48 \times 10^{-3})$$

$$= -0.845 \times 10^{-3}$$

Hence the stress in the bottom fiber of concrete is

$$f_c = 910 \times (-0.845 \times 10^{-3}) = -769 \text{ psi} (-5.30 \text{ MPa})$$

Figure 5-30 compares the concrete stresses immediately after transfer with the long-term concrete stresses. It can be seen that creep, shrinkage, and relaxation have substantially changed the concrete stresses. The compressive stress in the top fiber of the beam has increased by 12%, while the compressive stress in the bottom fiber has been reduced to 57% of its initial value.

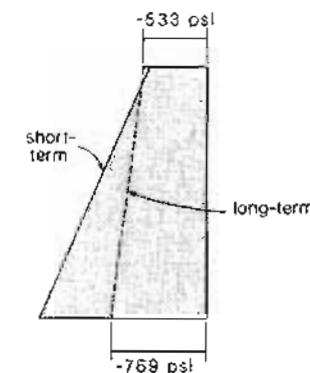


Figure 5-30 Comparison of short-term and long-term concrete stresses.

Step 4: Determine stress in prestressing.

From Eq. (5-13) the strain at the centroid of the prestressing is

$$\epsilon_p = \epsilon_{con} - \phi y + \Delta \epsilon_p$$

$$= -1.151 \times 10^{-3} - (-7.18 \times 10^{-6}) \times (-16.19) + 6.90 \times 10^{-3}$$

$$= 5.633 \times 10^{-3}$$

As $\epsilon_{po} = 0$, the stress in the prestressing at its centroid is

$$f_p = 28,130 \times 5.633 \times 10^{-3}$$

$$= 158 \text{ ksi (1093 MPa)}$$

Note that the creep, shrinkage and relaxation have caused the stress in the strand to drop an additional 32 ksi (220 MPa), which corresponds to 16% of the initial stress in the strands. Thus the total loss in tendon stress (i.e., elastic shortening loss plus creep, shrinkage, and relaxation losses) is 21%.

5.13 ESTIMATION OF CAMBER AND DEFLECTIONS

Due to eccentric prestressing, prestressed concrete beams typically are curved upward when the applied moments are low. The resulting upward deflection is called camber. This camber may increase or decrease with time, depending on the stress distribution across the member under sustained loads. Additional superimposed load will, of course, cause downward deflections of the member.

In design it is necessary to check that the upward cambers and the downward deflections do not exceed allowable limits. Moment-curvature relationships can be used to estimate the curvatures along a member corresponding to a given distribution of moments. Deflections can then be determined from these curvatures. This procedure is illustrated in Fig. 5-31 for a uniformly loaded prestressed concrete beam.

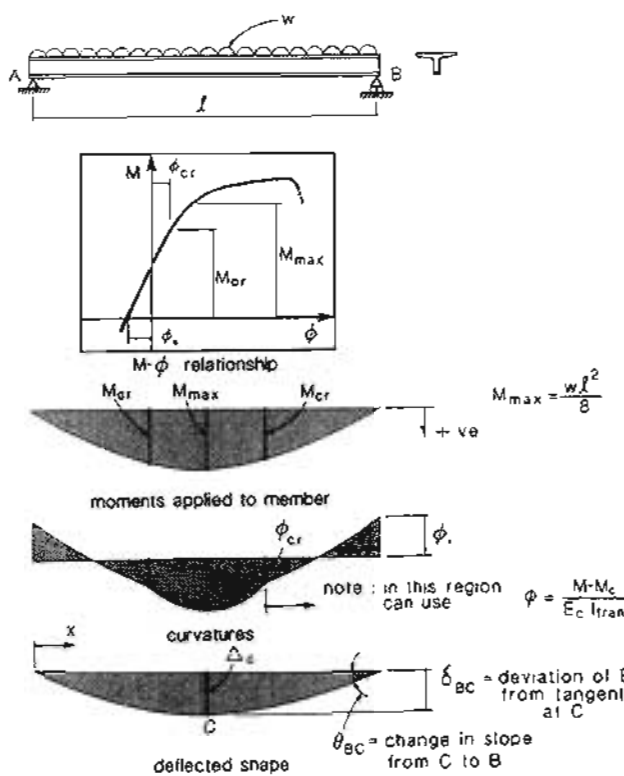


Figure 5-31 Calculating deflections from curvature.

The change of slope between any two points along the beam is equal to the area under the curvature diagram between these two points. That is,

$$\theta_{BC} = \int_{x_c}^{x_b} \phi \, dx \quad (5-39)$$

The deviation of point B from a tangent drawn at point C is equal to the first moment of area of the area under the curvature diagram between B and C taken about point B.

$$\delta_{BC} = \int_{x_c}^{x_b} \phi(x_b - x) \, dx \quad (5-40)$$

For a uniformly loaded, simply supported beam, the deflection at midspan can be found from Eq. (5-40) as

$$\Delta = \int_0^{0.5l} \phi x \, dx \quad (5-41)$$

In order to find the deflection it is convenient to perform the integration numerically (see Fig. 5-32). Thus Eq. (5-41) can be approximated as

$$\Delta = \left(\frac{\phi_1 x_1 + \phi_2 x_2}{2} \right) \Delta x_1 + \left(\frac{\phi_2 x_2 + \phi_3 x_3}{2} \right) \Delta x_2 + \dots \quad (5-42)$$

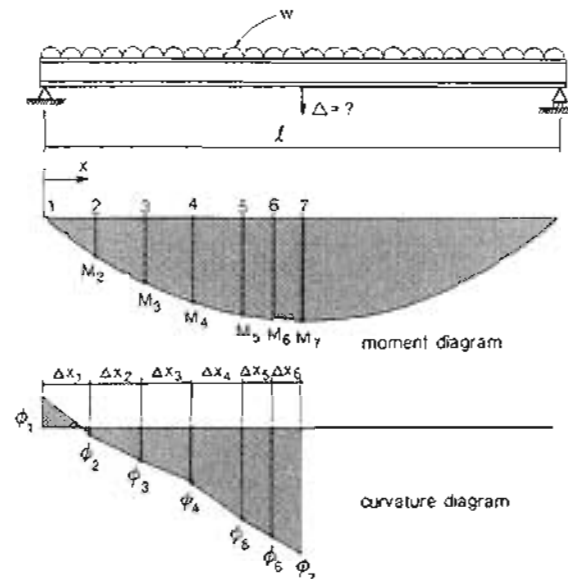


Figure 5-32 Numerically integrating curvatures to find midspan deflection.

When estimating deflections at service load levels it will often be appropriate to calculate curvatures assuming elastic uncracked response. Thus from Eq. (5-26),

$$\phi = \frac{M - M_o}{E_c I_{trans}}$$

5.14 EXAMPLES OF CALCULATING CAMBER AND DEFLECTION

In order to demonstrate the use of the procedures for calculating camber and deflections, we will use them to estimate cambers and deflections for the precast, pretensioned single-tee beam described in Fig. 5-17. We will calculate the short-term and long-term cambers for an 80 ft (24.4 m) span with only self-weight acting. Additionally, we will estimate the midspan deflection at failure if the beam is subjected to severe overloads. We will assume a constant eccentricity of prestress along the member length. The member self-weight is 594 lb/ft (8.76 kN/m).

(a) Calculation of Short-Term Camber

Assuming elastic uncracked response, it is convenient to express the curvature as

$$\phi = \frac{M}{E_c I_{trans}} - \frac{M_o}{E_c I_{trans}} \quad (5-43)$$

For the tee-beam under short-term loading, the following values were calculated in Section 5.12(a):

$$E_c = 3366 \text{ ksi} (23200 \text{ MPa})$$

$$I_{trans} = 74,059 \text{ in}^4 (30830 \times 10^6 \text{ mm}^4)$$

$$M_o = 7494 \text{ in.-kips} (847 \text{ kNm})$$

The dead-load moment at midspan is 475 ft-kips (644 kNm). The resulting curvatures along the beam are shown in Fig. 5-33.

From the first moment of area of these curvature diagrams, the camber (upward deflection) at midspan immediately after release is

$$\begin{aligned} \Delta &= 480 \times 30.06 \times 10^{-6} \times 0.5 \times 480 \\ &\quad - \frac{2}{3} \times 480 \times 22.87 \times 10^{-6} \times \frac{5}{8} \times 480 \\ &= 3.463 - 2.196 \\ &= 1.27 \text{ in. (32 mm) upward} \end{aligned}$$

(b) Calculation of Long-Term Camber

For the tee-beam under long-term loading the following values were calculated in Section 5.12(b):

$$E_{c,eff} = 910 \text{ ksi} (6273 \text{ MPa})$$

$$I_{trans} = 87,582 \text{ in}^4 (36450 \times 10^6 \text{ mm}^4)$$

$$M_o = 6272 \text{ in.-kips} (709 \text{ kNm})$$

Hence after creep, shrinkage, and relaxation have occurred,

$$\begin{aligned} \frac{M}{E_{c,eff} I_{trans}} &= \frac{475 \times 12}{910 \times 87,582} \\ &= 71.52 \times 10^{-6} \text{ rad/in.} \end{aligned}$$

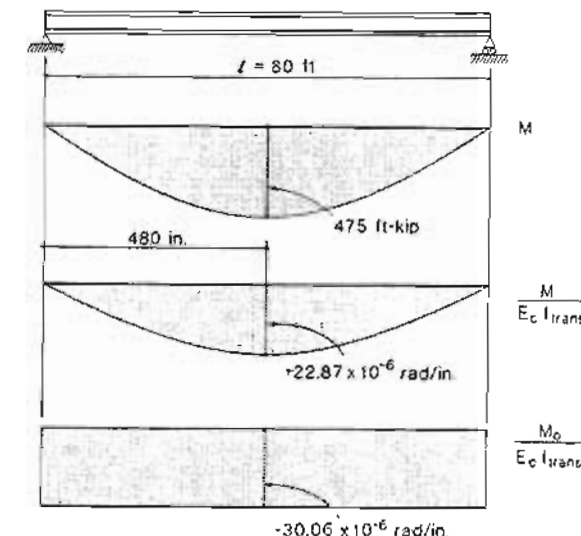


Figure 5-33 Curvatures used in calculation of short-term camber.

while

$$\begin{aligned} \frac{M_o}{E_{c,eff} I_{trans}} &= \frac{6272}{910 \times 87,582} \\ &= 78.70 \times 10^{-6} \text{ rad/in.} \end{aligned}$$

Thus the long-term camber at midspan is

$$\begin{aligned} \Delta &= 480 \times 78.70 \times 10^{-6} \times 0.5 \times 480 \\ &\quad - \frac{2}{3} \times 480 \times 71.52 \times 10^{-6} \times \frac{5}{8} \times 480 \\ &= 9.066 - 6.866 \\ &= 2.20 \text{ in. (56 mm) upward} \end{aligned}$$

It is important to realize that the actual long-term camber may vary somewhat from the calculated camber. The camber will be influenced by a large number of factors, such as the actual load history, the actual shrinkage, creep, and relaxation, and the change of concrete properties with time. Hence calculated cambers should always be treated as estimates.

It is interesting to note that in our example the downward deflections due to the member weight increased by a factor of $6.866/2.196 = 3.13$, while the upward deflection component due to prestress increased by a factor of $9.066/3.463 = 2.62$.

The *PCI Design Handbook* (Ref. 5-5) provides "suggested multipliers which can be used as a guide in estimating long-time cambers and deflections for typical members." These multipliers, which are based on work by Martin (Ref. 5-6), are reproduced in Table 5-10. It can be seen from this table that the long-term multipliers calculated above are a little higher than the typical values suggested by PCI (i.e., 2.70 and 2.45).

Table 5-10 Suggested multipliers to be used as a guide in estimating long-time cambers and deflections for typical members. From Ref. 5-5.

	Without Composite Topping	With Composite Topping
At erection:		
(1) Deflection (downward) component – apply to the elastic deflection due to the member weight at release of prestress	1.85	1.85
(2) Camber (upward) component – apply to the elastic camber due to prestress at the time of release of prestress	1.80	1.80
Final:		
(3) Deflection (downward) component – apply to the elastic deflection due to the member weight at release of prestress	2.70	2.40
(4) Camber (upward) component – apply to the elastic camber due to prestress at the time of release of prestress	2.45	2.20
(5) Deflection (downward) – apply to elastic deflection due to superimposed dead load only	3.00	3.00
(6) Deflection (downward) – apply to elastic deflection caused by the composite topping	—	2.30

(c) Calculation of Deflection at Failure

In order to estimate the deflection of the tee-beam at failure, we will utilize the short-term moment-curvature response determined in Section 5.9. Figure 5-34 shows the moment diagram when the beam is subjected to a uniformly distributed load large enough to cause failure at midspan. In order to produce the failure moment of 1290 ft-kips (1750 kNm) at midspan, a uniformly distributed superimposed load of 127 psf (6.10 kN/m²) is required. The curvatures corresponding to the moments at failure are also shown in Fig. 5-34 and are listed in Table 5-11. These values were determined from program RESPONSE using the option of finding the strains associated with fixed values of axial load and moment.

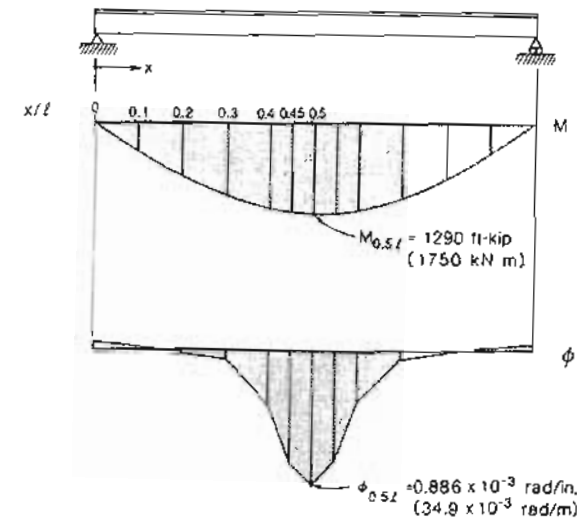


Figure 5-34 Distribution of moments and curvatures at failure

From Eq. (5-42) the deflection at midspan is

$$\begin{aligned}\Delta \times 10^3 &= \left(\frac{-0.045 \times 0 - 0.007 \times 96}{2} \right) \times 96 \\ &+ \left(\frac{-0.007 \times 96 + 0.009 \times 192}{2} \right) \times 96 \\ &+ \left(\frac{0.009 \times 192 + 0.059 \times 288}{2} \right) \times 96 \\ &+ \left(\frac{0.059 \times 288 + 0.397 \times 384}{2} \right) \times 96 \\ &+ \left(\frac{0.397 \times 384 + 0.757 \times 432}{2} \right) \times 48 \\ &+ \left(\frac{0.757 \times 432 + 0.886 \times 480}{2} \right) \times 48 \\ &= -32.3 + 50.7 + 899 + 8133 + 11,507 + 18,055\end{aligned}$$

Hence at failure,

$$\Delta = 38.6 \text{ in. (981 mm)}$$

Table 5-11 Moments and curvatures along the beam at failure load.

x/L	0	0.1	0.2	0.3	0.4	0.45	0.50
$M/(w^2/8)$	0	0.360	0.640	0.840	0.960	0.990	1.000
M	ft-kips	0	464	826	1084	1238	1277
	kNm	0	630	1119	1464	1679	1731
$\phi \times 10^3$	rad/in.	-0.045	-0.007	0.009	0.059	0.397	0.757
	rad/m	-1.76	-0.26	0.35	2.32	15.6	29.8
							34.9

Thus at failure of this beam, the deflection-to-span ratio is 1/25.

Figure 5-35 shows a pretensioned beam under simulated uniform loading. This member deflected a distance equal to the span divided by 29.4 when subjected to the maximum load. The concentration of large positive curvatures at midspan and the occurrence of small negative curvatures near the ends of the beam are visible in Fig. 5-35.

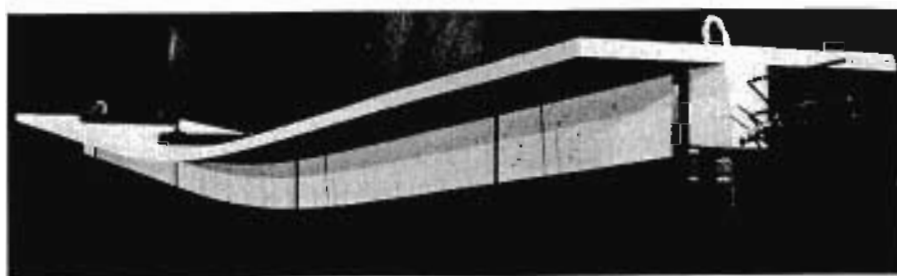


Figure 5-35 Pretensioned T-beam subjected to simulated uniform loading. Tested by Cellini (Ref. 5-7).

5.15 CRACK WIDTHS AND CRACK SPACING

Many prestressed concrete members are designed so that they remain uncracked under service loads. Such members are called fully prestressed members. In some situations it may be appropriate to provide less prestressing and to permit the members to crack under service loads. For these partially prestressed members, it is necessary to check that the crack widths are not unacceptably wide.

Ignoring the small elastic tensile strains in the concrete between the cracks, the mean crack widths, w_m , at any level, y , can be estimated from

$$w_m = \epsilon_{cf} \times s_m \quad (5-44)$$

where ϵ_{cf} is the average concrete strain caused by stress at level y and s_m is the mean crack spacing at level y .

The spacing of the cracks is influenced by many parameters and will typically vary over the depth of the beam. As shown in Fig. 5-36, the crack spacing will decrease near the compression zone of the beam and in the vicinity of bonded reinforcement.

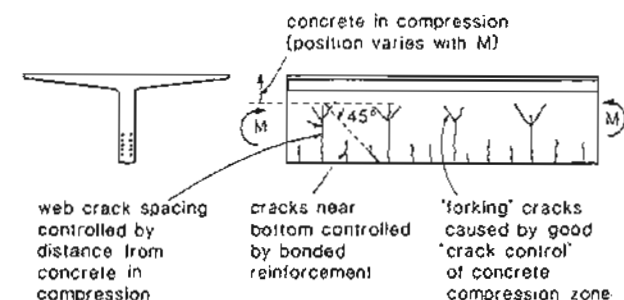


Figure 5-36 Control of crack spacing in different regions of typical beams.

Figure 5-37 shows the crack pattern in a pretensioned double-tee beam at a load close to failure. The influence of the compression zone and the local influence of the strand on the crack pattern can be seen.

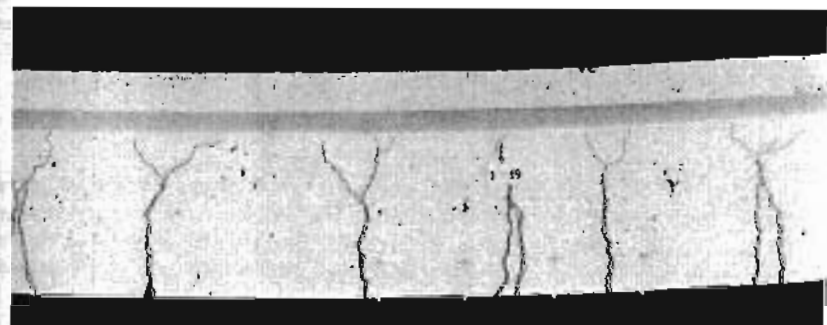


Figure 5-37 Crack pattern near failure in pretensioned double-tee beam. Tested by Cellini (Ref. 5-7).

The manner in which the compression zone influences crack formation is illustrated in Fig. 5-38. This figure shows a piece of unreinforced concrete that has been forced to curve by the application of eccentric compressive forces. As the compressive forces increase, the compression zone will be curved into a circular arc. To follow this curve, the tension zone must develop a relatively closely spaced pattern of cracks (see Fig. 5-38). As the curvature increases, the tensile cracks typically bifurcate, producing the characteristic "forking" cracks.

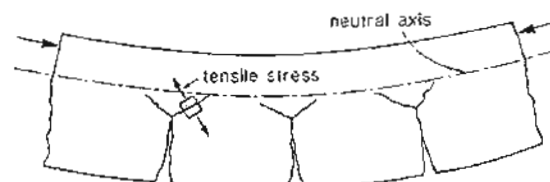


Figure 5-38 Influence of compression zone on crack pattern.

In the CEB-FIP Code (Ref. 5-8) the factor k_2 in the crack spacing expression [see Eq. (4-23)] reflects the beneficial influence of the uncracked compression zone. The expression for k_2 is such that more highly curved beams are predicted to have smaller crack spacings. The influence of bonded reinforcement on crack spacing is accounted for in the CEB-FIP expression, in terms of cover, spacing, bar diameter, bond characteristics, and percentage of reinforcement.

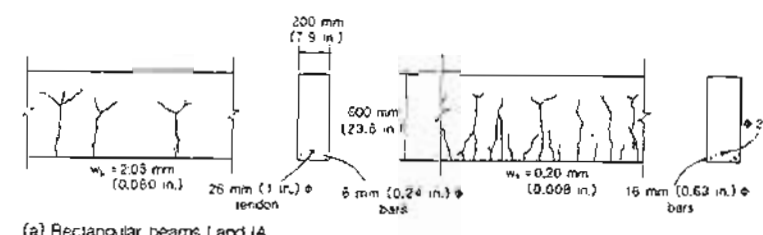
The way in which the reinforcement details influence crack spacings in prestressed concrete beams was convincingly demonstrated in a test series by Trost, Cordes, and Thormählen (Ref. 5-9). Each of the beams in the series was post-tensioned with a single 26 mm (1.02 in.) diameter Dywidag bar (see Fig. 5-39). Each pair of beams differed only in the size of the reinforcing bars in the tension zone, with one beam having 6 mm (0.24 in.) diameter bars, while the other had 16 mm (0.63 in.) diameter bars. It can be seen that increasing the amount of bonded reinforcing in the tension zone significantly improves the crack control characteristics.

5.16 EXAMPLE CALCULATIONS OF CRACK WIDTHS

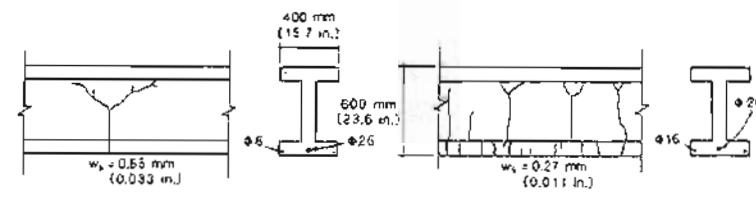
To demonstrate the procedures for calculating crack widths, we will calculate the crack width on the bottom face of the single-tec beam described in Fig. 5-17. We will assume that the beam spans 80 ft (24.4 m) and carries a superimposed load of 75 psf (3.6 kN/m^2). We will determine the maximum crack width expected for this load under both short-term and long-term loading.

Due to the applied loading, the moment at midspan is

$$\begin{aligned} M &= \frac{w t^2}{8} \\ &= \frac{(594 + 8 \times 75) \times 80^2}{8} \\ &= 955 \text{ ft-kips (1295 kNm)} \end{aligned}$$



(a) Rectangular beams I and IA



(b) I-beams III and IIIA

Figure 5-39 Influence of reinforcement details on crack width and spacings.
Adapted from Trost, Cordes, and Thormählen (Ref. 5-9).

(a) Short-Term

To determine the short-term concrete strains corresponding to the applied moment we again use the program RESPONSE, with the section properties defined as in Fig. 5-18. Because we are interested in finding average strains, we account for tension stiffening. Using the "Fixed Loads" mode of the program we find that for a moment of 955 ft-kips (1295 kNm) the concrete strains are 0.322×10^{-3} on the bottom face and -0.339×10^{-3} on the top face. Note that for this short-term condition all of the concrete strains are caused by stress.

We will estimate the average crack spacing using Eq. (4-23):

$$s_{in} = 2 \left(c + \frac{s}{10} \right) + k_1 k_2 \frac{d_b}{\rho_{ef}}$$

From Fig. 5-40 it can be seen that

$$\rho_{ef} = \frac{14 \times 0.153}{8 \times 17.75} = 0.0151$$

The factor k_2 is calculated from the largest and smallest tensile strains in the embedment zone. Hence

$$k_2 = 0.25 \times \frac{0.322 + 0}{2 \times 0.322} = 0.125$$

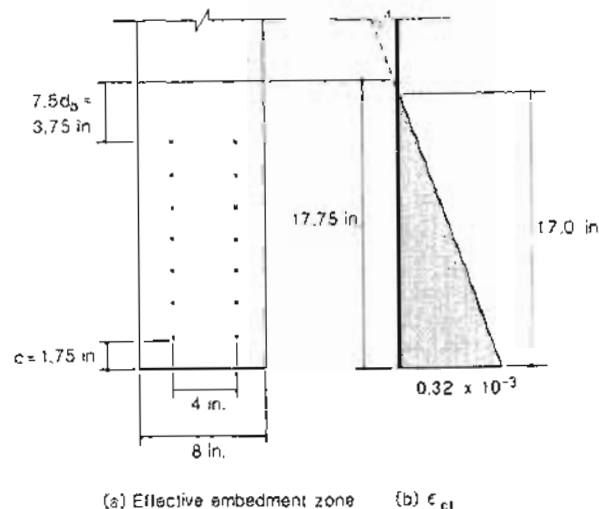


Figure 5-40 Parameters influencing short-term cracking.

Assuming that the bond properties of the pretensioned strand are equivalent to those of a plain bar gives $k_1 = 0.8$. Hence Eq. (4-23) becomes

$$\begin{aligned} \delta_m &= 2 \left(1.75 + \frac{4}{10} \right) + 0.8 \times 0.125 \times \frac{0.50}{0.0151} \\ &\approx 7.61 \text{ in. (193 mm)} \end{aligned}$$

Thus from Eq. (5-44) the average crack width on the bottom face is

$$\begin{aligned} w_m &= \epsilon_{cf} \delta_m \\ &= 0.322 \times 10^{-3} \times 7.61 \\ &= 2.45 \times 10^{-3} \text{ in. (0.062 mm)} \end{aligned}$$

Hence the "maximum" crack width is about

$$\begin{aligned} w_k &= 1.7w_m \\ &= 1.7 \times 2.45 \times 10^{-3} \\ &= 4.17 \times 10^{-3} \text{ in. (0.106 mm)} \end{aligned}$$

(b) Long-Term

Using the long-term section properties described in Section 5.10 we find that for a moment of 955 ft-kips (1295 kNm) the program RESPONSE predicts that the total concrete strains are 1.203×10^{-3} on the bottom face and -2.023×10^{-3} on the top face. To find the strains due to stress, we must subtract the shrinkage strain, $\epsilon_{sh} = -0.48 \times 10^{-3}$, from the total concrete strains. Hence on the bottom face,

$$\begin{aligned} \epsilon_{cf} &= \epsilon_c - \epsilon_{sh} \\ &= 1.203 \times 10^{-3} - (-0.48 \times 10^{-3}) \\ &= 1.683 \times 10^{-3} \end{aligned}$$

At the top of the embedment zone,

$$\begin{aligned} \epsilon_c &= 1.203 \times 10^{-3} - (2.023 \times 10^{-3} + 1.203 \times 10^{-3}) \times \frac{17.75}{36} \\ &= -0.388 \times 10^{-3} \end{aligned}$$

and

$$\epsilon_{cf} = -0.388 \times 10^{-3} - (-0.48 \times 10^{-3}) = 0.092 \times 10^{-3}$$

Thus

$$k_2 = 0.25 \times \frac{1.683 + 0.092}{2 \times 1.683} = 0.132$$

For long-term loading,

$$\delta_m = 2 \left(1.75 + \frac{4}{10} \right) + 0.8 \times 0.132 \times \frac{0.50}{0.0151} = 7.80 \text{ in. (198 mm)}$$

Hence the "maximum" crack width is about

$$\begin{aligned} w_k &= 1.7 \times \epsilon_{cf} \delta_m = 1.7 \times 1.683 \times 10^{-3} \times 7.80 \\ &= 0.022 \text{ in. (0.57 mm)} \end{aligned}$$

It is evident that under this heavy loading, the crack widths under long-term conditions would be unacceptably wide.

5.17 ACCOUNTING FOR CONSTRUCTION STAGES – COMPOSITE CONSTRUCTION

In the previous discussions we have assumed that all of the concrete in a given member was cast at the same time. However, many prestressed concrete members are constructed in stages. For example, single-tee and double-tee precast beams often have a cast-in-place topping which acts compositely with the beams.

Figure 5-41 illustrates the strain compatibility conditions for a composite beam. At the time when the topping concrete is cast there will be substantial strains in the precast member, but of course, zero strains in the topping. Hence a strain discontinuity at the interface of the two concretes will be produced. After the topping concrete has hardened, the two concretes at the interface will undergo the same changes in strain and hence the strain discontinuity will remain constant throughout the life of the member.

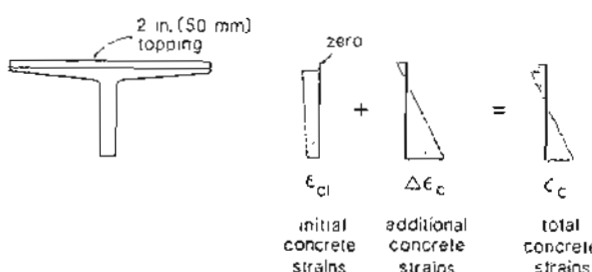


Figure 5-41 Precast single-tee beam with cast-in-place topping slab.

The total concrete strain can be expressed as the sum of the initial strain and the additional strains. Hence at a given level, y ,

$$\epsilon_c = \epsilon_{ci} + \Delta\epsilon_c \quad (5-45)$$

where ϵ_c = total concrete strain at level y

ϵ_{ci} = initial concrete strain at level y when topping concrete is cast

$\Delta\epsilon_c$ = additional strains occurring after topping concrete is cast

As the initial strains are assumed to be linearly distributed over the initial cross section, it will take two variables to describe this initial strain distribution. The additional concrete strains are assumed to be linearly distributed over the total composite cross section. Hence two additional variables are required to describe these additional concrete strains. In other words, the distribution of total concrete strains can be described in terms of four variables (e.g., the strain at the top face, the strain at the bottom of the topping, the strain at the top of the precast member, and the strain at the bottom face).

In analyzing the response of composite beams, it is necessary to account for load history, that is, it is first necessary to determine the initial concrete strains, ϵ_{ci} , in the precast member at the time the topping concrete is cast. In analyzing the member for later stages in its life, these initial concrete strains are taken into account in determining the total concrete strain distribution (see Fig. 5-41). Once again, when calculating concrete stresses from concrete strains, we must use only those components of concrete strain, ϵ_{cf} , which are caused by stress. As an example of how the response of a composite member can be determined, we will consider the following case.

The precast, pretensioned single-tee beam described in Fig. 5-17 had a concrete strength at transfer, f'_c , of 3500 psi (24.1 MPa) and a specified 28-day strength of 5000 psi (34.5 MPa). The precast beam is used to span 80 ft (24.4 m). After installing the beam a 2 in. (51 mm) cast-in-place concrete topping is added. The topping concrete had a specified 28-day strength of 3000 psi (20.7 MPa). We will calculate the long-term moment-curvature response of this composite member.

Step 1: Determine the stresses and strains just prior to placing the topping.

We will assume that the topping is to be placed 50 days after prestress transfer. The precast single tee was given accelerated curing resulting in an effective age, t_e , of 7 days at transfer.

(a) *Creep, shrinkage, and relaxation at 50 days.* From Fig. 2-10, the volume-to-surface area ratio for the single tee is 2.16 in. (55 mm). Hence from Fig. 3-12 the creep correction factor for volume-to-surface area ratio after 50 days under load is 0.83. The correction factor for concrete strength is 0.82. Assuming that the ambient relative humidity is 70%, the creep coefficient from Eq. (3-10) is $\phi(57, 7) = 0.96$. The modulus of the precast concrete at transfer from Table 3-3 is 3366 ksi (23 200 MPa), and hence

$$E_{c,eff} = \frac{3366}{1 + 0.96} = 1717 \text{ ksi (11 840 MPa)}$$

From Fig. 3-18 the shrinkage correction factor for volume-to-surface area ratio after 50 days of drying is 0.87. The shrinkage strain from Eq. (3-20) is thus

$$\epsilon_{sh} = -0.23 \times 10^{-3}$$

To allow for relaxation losses in the prestressing strand an effective modulus will be calculated using Eqs. (3-31) and (3-29). Assuming a reduction coefficient χ_r of 0.8 gives

$$\begin{aligned} E_{p,eff} &= [1 - 0.8(1 - 0.98)]29,000 \\ &= 28,536 \text{ ksi (197 000 MPa)} \end{aligned}$$

(b) *Transformed section properties for 50-day loading.* The transformed section properties are calculated from Eqs. (5-31) to (5-33) with $(n - 1)$ equal to 15.62.

$$\begin{aligned} A_{trans} &= 603.4 \text{ in}^2 (389 300 \text{ MPa}) \\ y_{bt} &= 25.01 \text{ in. (635 mm)} \\ I_{trans} &= 79,159 \text{ in}^4 (32 950 \times 10^6 \text{ mm}^4) \end{aligned}$$

(c) *Stresses and strains at midspan.* From Eqs. (5-35) and (5-36), $N_o = 646$ kips (2880 kN) and $M_o = 6942$ in.-kips (784 kNm). As the axial load, N , is zero, the concrete strain at the centroid, from Eq. (5-37), is

$$\epsilon_{con} = -0.624 \times 10^{-3}$$

The midspan moment due to the self-weight of the precast tee is 5702 in.-kips (644 kNm). Hence the curvature of the precast tee just prior to placing the topping concrete, from Eq. (5-38), is

$$\phi = -0.00912 \times 10^{-3} \text{ rad/in. } (-0.36 \times 10^{-3} \text{ rad/m})$$

The resulting total concrete strains are shown in Fig. 5-42.

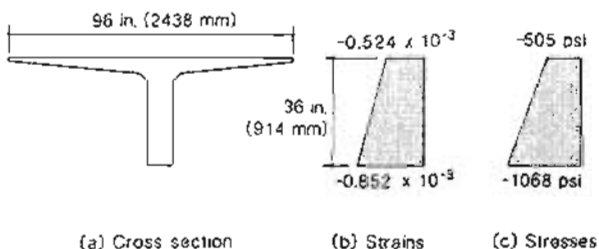


Figure 5-42 Strains and stresses at 50 days prior to placement of topping.

As the concrete shrinkage strain is -0.23×10^{-3} the strain due to stress in the top fiber of concrete is

$$\begin{aligned}\epsilon_{cf} &= \epsilon_c - \epsilon_{co} \\ &= -0.524 \times 10^{-3} - (-0.23 \times 10^{-3}) \\ &= -0.294 \times 10^{-3}\end{aligned}$$

Hence the stress in the top fiber of concrete is

$$\begin{aligned}f_c &= E_{c,eff} \epsilon_{cf} \\ &= 1717 \times (-0.294 \times 10^{-3}) \\ &= -505 \text{ psi } (-3.48 \text{ MPa})\end{aligned}$$

From similar calculations the stress in the bottom fiber of concrete is -1068 psi (-7.36 MPa). The stresses and strains in the precast tee just prior to placing the topping are shown in Fig. 5-42.

Step 2: Determine the additional stresses and strains caused by the self-weight of the topping.

We will assume that at the time of placing the topping the precast concrete has a strength of 5000 psi (34.5 MPa) and a short-term modulus, E_c , of 3828 ksi (26400 MPa) (see Table 3-3). For this short-term loading, E_p equals 29,000 ksi (200000 MPa) and hence $(n - 1)$ is 6.58. The transformed section properties calculated from Eqs. (5-31) to (5-33) are thus

$$\begin{aligned}A_{trans} &= 584.1 \text{ in}^2 (377000 \text{ mm}^2) \\ y_{bc} &= 25.57 \text{ in. (650 mm)} \\ I_{trans} &= 73,374 \text{ in}^4 (30540 \times 10^6 \text{ mm}^4)\end{aligned}$$

The normal-weight concrete topping weighs $(2/12) \times 8 \times 150 = 200 \text{ lb}/\text{ft}$ (2.90 kN/m). Hence the additional midspan moment that the precast beam carries due to the weight of

the fresh concrete topping is

$$\begin{aligned}M &= \frac{wl^2}{8} \\ &= \frac{0.200 \times 80^2}{8} \\ &= 160 \text{ ft-kips} = 1920 \text{ in.-kips (217 kNm)}$$

This additional moment will cause the curvature of the beam to change by

$$\frac{M}{E_c I_{trans}} = \frac{1920}{3828 \times 73,374} = 0.00684 \times 10^{-3} \text{ rad/in. (} 0.27 \times 10^{-3} \text{ rad/m)}$$

From Eq. (5-1) the change in curvature will cause a change in the bottom fiber strain equal to

$$-\phi_y = -0.00684 \times 10^{-3} \times (-25.57) = 0.175 \times 10^{-3}$$

This change in strain corresponds to a stress change of

$$0.175 \times 10^{-3} \times 3828 = +669 \text{ psi (4.61 MPa)}$$

Similarly, the change in top fiber strain is

$$-0.00684 \times 10^{-3} \times (36 - 25.57) = -0.071 \times 10^{-3}$$

corresponding to a stress change of

$$-0.071 \times 10^{-3} \times 3828 = -272 \text{ psi } (-1.87 \text{ MPa})$$

The total strains in the precast member just after the topping is placed are shown in Fig. 5-43b. These strains correspond to the initial strains, $\epsilon_{ci}(y)$ in Eq. (5-45) and in Fig. 5-41. Note that the initial curvature, ϕ_i , of the beam is $-0.00912 \times 10^{-3} + 0.00684 \times 10^{-3} = -0.00228 \times 10^{-3} \text{ rad/in. } (-0.090 \times 10^{-3} \text{ rad/m})$. The concrete stresses in the cross section at this time are shown in Fig. 5-43c. Note that at this time the strains and the stresses in the topping concrete are assumed to be zero.

Step 3: Determine the material parameters for long-term loading.

Assume that the beam is under load for 10,000 days (about 27 years).

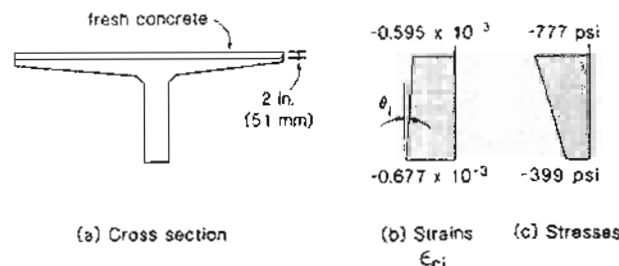


Figure 5-43 Strains and stresses just after fresh concrete topping is placed.

(a) *Precast beam*. Due to the addition of the concrete topping the volume-to-exposed-surface-area ratio of the tee-beam has changed to 3.59 in. (91 mm). Hence, from Eq. (3-10), $\phi(10007, 7) = 1.76$ and the effective modulus is

$$E_{e,eff} = \frac{3366}{1 + 1.76} = 1220 \text{ ksi (8410 MPa)}$$

From Fig. 3-10 and Table 3-3, the strain at which the long-term stress-strain curve will reach its peak stress of 5000 psi (34.5 MPa) is

$$\epsilon' = \frac{5000 \times 2.80}{1,220,000 \times (2.80 - 1)} \\ = -6.38 \times 10^{-3}$$

From Eq. (3-20) the shrinkage strain is $\epsilon_{sh} = -0.43 \times 10^{-3}$. We will assume that the cracking stress of the concrete in the precast beam is 300 psi (2.07 MPa).

(b) *Cast-in-place concrete topping*. The volume-to-exposed-surface-area ratio of the topping is 2 in. (51 mm). The topping concrete is 50 days younger than the precast beam and we will assume that the topping concrete starts picking up load soon after casting, say after 1 day. Thus the creep coefficient from Eq. (3-10) is

$$\phi(9957, 1) = 3.11$$

Assume that the elastic stiffness of the topping concrete when 1 day old is 70% of the 28-day stiffness given in Table 3-3. Since all of the stress in the topping concrete develops gradually with time, it is appropriate to use the adjusted effective modulus, $E_{e,adj}$. From Eq. (3-15),

$$E_{e,adj} = \frac{0.7 \times 3191}{1 + 0.8 \times 3.11} = 640 \text{ ksi (4420 MPa)}$$

From Fig. 3-10 and Table 3-3 the strain at which the long-term stress-strain curve will reach its peak stress of 3000 psi (20.7 MPa) is

$$\epsilon' = -9.38 \times 10^{-3}$$

Assume that the topping is moist cured for 3 days. From Fig. 3-18 the shrinkage correction factor for volume-to-surface-area ratio of 2 in. (51 mm) after 9954 days of drying is 0.95. The shrinkage strain from Eq. (3-19) is

$$\epsilon_{sh} = -0.48 \times 10^{-3}$$

We will assume that the topping concrete cracks at a tensile stress of 220 psi (1.52 MPa)

(c) *Prestressing steel*. From Eqs. (3-31) and (3-29) the effective modulus of the strands is

$$E_{p,eff} = 28,437 \text{ ksi (196 000 MPa)}$$

It is assumed that under long-term loading the strands will rupture at a strain of 0.054.

Step 4: Calculate the long-term, moment-curvature response.

The long-term, moment-curvature response for the composite beam with initial strains as shown in Fig. 5-43b was obtained using computer program RESPONSE described in Appendix A. The cross section of the precast tee was represented by the five concrete layers and the seven steel layers shown in Fig. 5-18, while the concrete topping was represented by one additional concrete layer.

In the program RESPONSE, composite sections with strain discontinuities are treated by first entering the distribution of initial concrete strains (see Fig. 5-41). The program then calculates the additional concrete strains, $\Delta\epsilon_c$ in Fig. 5-41, required to produce the specified condition. The strains and curvatures reported by the program all refer to these additional strains. That is, to find the total concrete strains the initial strains, ϵ_{ci} , must be added to the additional concrete strains, $\Delta\epsilon_c$.

The calculated response for the topped single tee is summarized in Tables 5-12 and 5-13. The values in these tables were calculated using the "specified strain" mode of program RESPONSE. Thus to find the moment at which the bottom face of the precast beam cracks, we specified that the additional strain at the bottom face is 0.493×10^{-3} . This value is calculated as follows:

Strain due to cracking stress:

$$\epsilon_{cr} = \frac{f_{cr}}{E_{e,eff}} = \frac{300}{1220 \times 10^3} = 0.246 \times 10^{-3}$$

The total concrete strain at cracking is found by adding the shrinkage strain to the strain due to stress:

$$\begin{aligned}\epsilon_c &= \epsilon_{ci} + \epsilon_{sh} \\ &= 0.246 \times 10^{-3} - 0.430 \times 10^{-3} \\ &= -0.184 \times 10^{-3}\end{aligned}$$

However, the initial concrete strain on the bottom face of the beam was -0.677×10^{-3} . Hence, from Eq. (5-45),

$$\begin{aligned}\Delta\epsilon_c &= \epsilon_c - \epsilon_{ci} \\ &= -0.184 \times 10^{-3} - (-0.677 \times 10^{-3}) \\ &= 0.493 \times 10^{-3}\end{aligned}$$

Table 5-12 Long-term response of composite section, calculated accounting for tension in concrete.

$\Delta\epsilon_t \times 10^3$	$\Delta\epsilon_b \times 10^3$	$\Delta\phi \times 10^3$		$\phi \times 10^3$		M		Comments
		rad/in.	rad/m	rad/in.	rad/m	ft-kips	kNm	
18.98	-7.00	-0.684	-26.92	-0.686	-27.00	-150	-204	
10.76	-5.00	-0.415	-16.32	-0.417	-16.41	-120	-162	
2.06	-2.50	-0.120	-4.72	-0.122	-4.81	-23	-32	
0.54	-1.96	-0.066	-2.59	-0.068	-2.68	-27	-36	Top-face precast cracks
-0.136	-0.85	-0.019	-0.74	-0.021	-0.83	326	442	Topping cracks
-0.38	-0.29	0.002	0.09	0	0	533	722	Zero curvature
-0.72	0.493	0.032	1.26	0.030	1.17	824	1118	Bottom face cracks
-1.00	1.54	0.067	2.63	0.065	2.54	974	1320	
-1.50	4.73	0.164	6.45	0.162	6.36	1152	1562	
-2.00	9.57	0.304	12.00	0.302	11.91	1207	1637	
-3.00	20.91	0.629	24.77	0.627	24.68	1262	1711	
-4.00	33.83	0.995	39.19	0.993	39.10	1311	1778	
-5.00	47.89	1.392	54.80	1.390	54.71	1359	1842	Fails at crack

Table 5-13 Long-term response of composite section, calculated neglecting tension in concrete.

$\Delta\epsilon_t \times 10^3$	$\Delta\epsilon_b \times 10^3$	$\Delta\phi \times 10^3$		$\phi \times 10^3$		M		Comments
		rad/in.	rad/m	rad/in.	rad/m	ft-kips	kNm	
-4.00	34.04	1.001	39.40	0.999	39.31	1302	1763	
-5.17	50.71	1.471	57.90	1.469	57.82	1356	1839	Maximum moment
-4.84	30.70	1.461	57.54	1.459	57.45	1123	1523	2 strands ruptured
-5.04	53.98	1.553	61.15	1.551	61.06	1130	1532	
-4.67	53.94	1.542	60.72	1.540	60.63	910	1234	4 strands ruptured
-4.87	57.63	1.645	64.76	1.643	64.67	915	1241	
-4.45	57.56	1.632	64.25	1.630	64.15	707	959	6 strands ruptured

The predicted long-term moment-curvature response of the composite beam is shown in Fig. 5-44. Also shown in this figure is the long-term response of the untopped tee beam calculated in Section 5.10. The following observations can be made:

1. The addition of the topping has increased the flexural capacity by about 6%, which is about the same as the percentage increase in the overall depth.
2. The addition of the topping significantly increases the stiffness of the member in the uncracked range.
3. There is a relatively small moment range over which the topped beam will be uncracked. The precast beam restrains the shrinkage of the cast-in-place topping and the resulting restraint stresses will crack the topping, particularly in regions of low moment.
4. The cracking of the topping reduces the stiffness of the composite member to the stiffness of the precast beam, which remains uncracked.

5. A significant change in behavior occurs when the unreinforced top flange of the precast beam cracks.

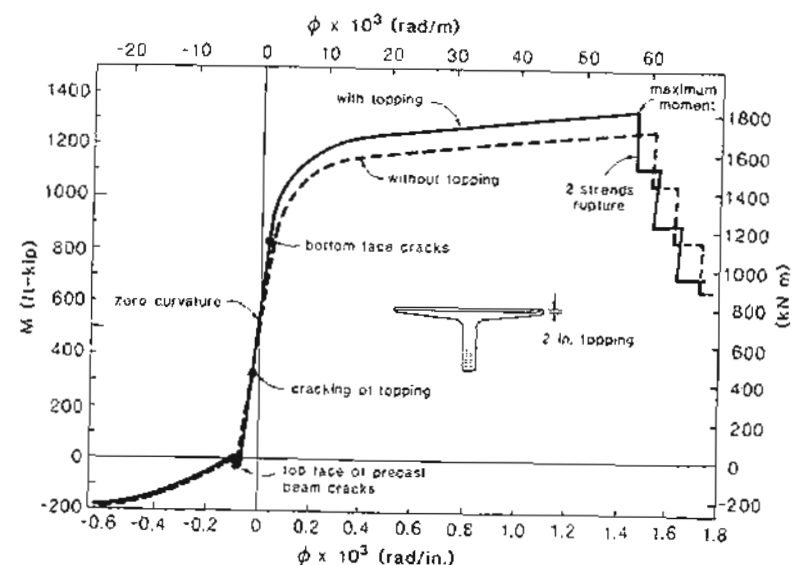


Figure 5-44 Long-term, moment-curvature response of composite beam.

5.18 ACCOUNTING FOR NONUNIFORM THERMAL AND SHRINKAGE STRAINS

Cracks in concrete structures are often caused by the restraint of thermal and shrinkage strains. For some prestressed concrete bridge structures, the change of stress at the deck surface caused by the sun going behind a cloud will be greater than that caused by a truck passing over the bridge. As stated by Leonhardt (Ref. 5-10), "temperature plays a much more important role in causing stresses than most engineers are aware of."

If a simply supported beam, such as that shown in Fig. 5-45, increases uniformly in temperature, no restraint stresses will be caused, the beam will merely become longer. If this member is subjected to temperature changes that vary linearly over the depth of the beam, again no restraint stresses will be caused. The beam would merely curve upward or downward in addition to changing length. If the beam were not on simple supports, as it tried to elongate or curve it would be restrained by the supports. The way in which the resulting restraint actions are treated in such statically indeterminate structures is discussed in Chapter 10. In this section we treat only statically determinate members, that is, members that are not subjected to external restraint.

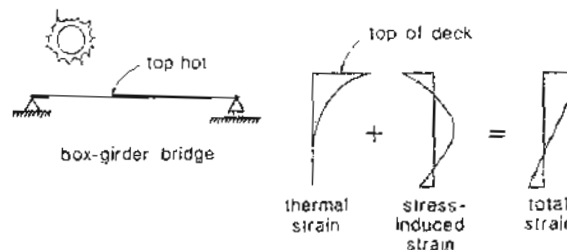


Figure 5-45 Thermal stresses in box-girder bridge.

If the thermal strains vary in a nonlinear fashion over the cross section, restraint stresses will develop even in statically determinate members. If the individual fibers of the cross section were not connected, they would be free to undergo their individual thermal strains arising from the nonlinear temperature distribution. The resulting strains would distort the cross section (i.e., plane sections would not remain plane). Experiments have shown that such nonuniform thermal strains do not, in fact, distort the cross section (Ref. 5-11). Rather, additional strains due to self-equilibrating stresses are developed which result in a linear distribution of the total concrete strains (see Fig. 5-45).

The actual values of temperature in the cross section are important when determining the thermal elongation of the member. However, when determining thermally-induced stresses, it is the distribution of thermal strains that is important rather than their actual values. A suggested temperature distribution for checking thermal stresses due to solar radiation in bridge cross sections is given in Fig. 5-46. The temperature variation shown in this figure can be represented by

$$T = (58 - 9h) \left(\frac{y}{48} \right)^5 \text{ in. and } ^\circ\text{F}$$

$$T = (32 - 0.2h) \left(\frac{y}{1200} \right)^5 \text{ mm and } ^\circ\text{C}$$
(5-4)

where h = asphalt thickness, in. or mm

T = temperature, $^{\circ}\text{F}$ or $^\circ\text{C}$

y = distance measured up from a point 48 in. or 1200 mm below the top of the concrete

In addition to temperature variations caused by solar radiation, the heat produced during the hydration of the cement can also result in highly nonlinear thermal distributions, particularly during winter concreting. Figure 5-47 shows the local temperatures measured in different parts of a box-girder bridge during the first few days after the top portion of the section had been cast. It can be seen that the thermal gradients reached their highest values about 1 day after casting.

Shrinkage strains will typically exhibit nonlinear distributions over the depth of the section because the moisture loss occurs near the surfaces. The nonlinear shrinkage strain will induce self-equilibrating restraint stresses similar to those produced by nonlinear thermal strains. Thus rapid drying of the surface of young concrete can produce high tensile

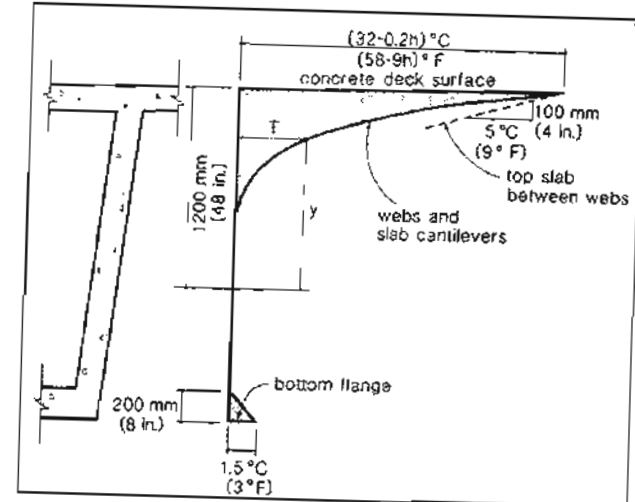


Figure 5-46 Suggested temperature variation for bridge sections. Adapted from Priestley (Ref. 5-12).

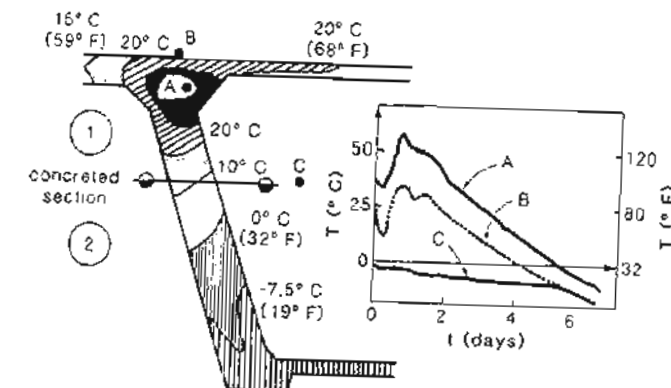


Figure 5-47 Large temperature gradients due to heat of hydration. Adapted from Pauser (Ref. 5-13).

stresses at the surface. As the tensile strength of the young concrete will be low, these tensile stresses may crack the concrete.

The presence of thermal and shrinkage strains was accounted for in the derivations of the expressions for elastic uncracked response. These strains, which are not caused by stress (ϵ_{co} , ϵ_{so} , and ϵ_{po}), were accounted for by offsetting the stress-strain relationships (see Fig. 5-23). The presence of these strains, in addition to the prestress, causes the resulting load-deformation relationships to be offset from the origin (see Fig. 5-24). For uniform distributions of thermal and shrinkage strains, the integrals involving these terms (see Eqs. (5-24) and (5-27)) can easily be calculated. For nonuniform distributions, numerical integration may have to be used to determine the terms N_a and M_a .

In evaluating the flexural response of members, using the layer-by-layer approach, it is a straightforward task to account for the presence of nonuniform thermal or shrinkage strains. The thermal and shrinkage strain values are entered for each layer, and these strain offsets (ϵ_{co} , ϵ_{so} , and ϵ_{po}) are deducted from the total strains (ϵ_c , ϵ_s , and ϵ_p) in order to calculate the strains in each layer caused by stress (ϵ_{cf} , ϵ_{sf} , and ϵ_{pf}).

As an example of accounting for nonuniform thermal strains, we will calculate the response of the post-tensioned, box-girder highway bridge described in Fig. 5-48. The bridge is simply supported over a span of 200 ft (61 m). We will calculate the influence on the response of the temperature changes shown in Fig. 5-46. We will assume that there is no asphalt topping (i.e., $h = 0$).

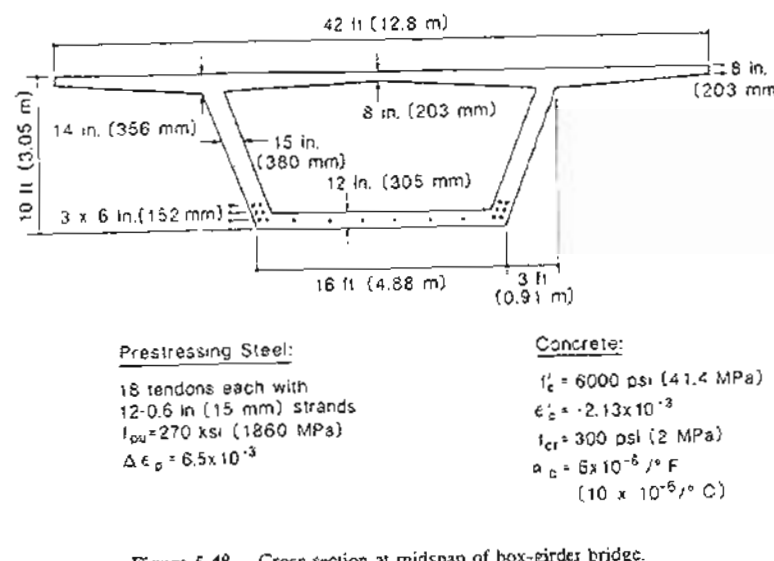


Figure 5-48 Cross section at midspan of box-girder bridge.

The response of the box girder was calculated using the RESPONSE program described in Appendix A. Table 5-14 summarizes the predicted response assuming there were no thermal strains, while Table 5-15 gives the predicted response when thermal strains are

Table 5-14 Response of box-girder bridge section calculated neglecting thermal strains.

$\epsilon_l \times 10^3$	$\epsilon_b \times 10^3$	$\phi \times 10^3$		M		Tens. Suff.	Comments
		rad/in.	rad/m	ft-kips	kNm		
0.068	-0.61	-0.006	-0.22	0	0	Yes	Zero moment
-0.24	-0.10	0.001	0.05	56,290	76,320	Yes	Dead-load moment
-0.35	0.073	0.004	0.14	75,580	102,890	Yes	Bottom face cracks
-0.50	1.13	0.014	0.54	87,950	119,250	Yes	
-0.75	4.41	0.043	1.69	101,470	137,590	Yes	
-1.00	9.11	0.084	3.32	104,310	141,450	Yes	
-1.50	20.80	0.182	7.15	108,050	146,500	Yes	
-2.08	35.37	0.312	12.28	111,540	151,240	No	Maximum moment
-1.30	35.33	0.305	12.02	47,480	64,380	No	10 tendons ruptured
-1.34	37.37	0.323	12.70	47,730	64,720	No	

accounted for. From these tables and from Fig. 5-49 it can be seen that thermal strains have very little influence on the overall moment-curvature response of the box girder.

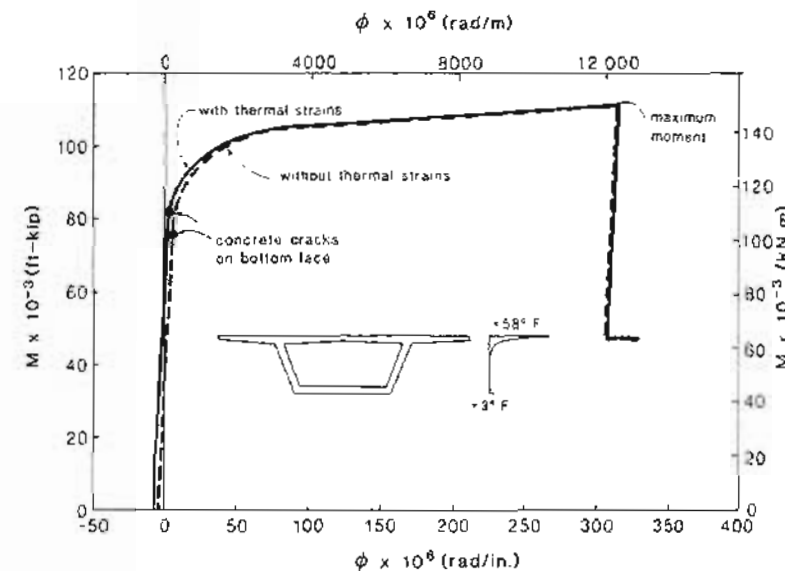


Figure 5-49 Influence of thermal strains on moment-curvature response.

Table 5-15 Response of box-girder bridge section calculated accounting for thermal strains.

$\epsilon_t \times 10^3$	$\epsilon_b \times 10^3$	$\phi \times 10^3$ rad/in.	M ft-kips	Tens. kNm	Stress. Stuff.	Comments
-0.31	-0.66	-0.008	-0.32	0	0	Yes Zero moment
-0.06	-0.14	-0.001	-0.03	56,290	76,320	Yes Dead-load moment
-0.20	0.09	0.002	0.09	81,750	110,850	Yes Bottom face cracks
-0.30	3.61	0.034	1.35	100,700	136,550	Yes
-0.75	8.28	0.075	2.96	104,340	141,490	Yes
-1.00	13.73	0.123	4.84	106,210	144,020	Yes
-1.25	19.76	0.173	6.90	108,030	146,480	Yes
-1.50	26.14	0.230	9.08	109,900	149,010	Yes
-1.70	31.32	0.275	10.84	111,370	151,010	Yes
-1.85	35.36	0.310	12.20	111,560	151,270	No Maximum moment
-1.02	35.32	0.303	11.92	47,520	64,440	No 10 tendons ruptured
-1.06	37.34	0.320	12.60	47,770	64,770	No

While thermal strains have little influence on the overall response and the failure moment of the box girder, they do influence the concrete stresses at service loads. Figure 5-50a shows the concrete stresses at midspan due to dead-load moment and prestress. Figure 5-50b shows the concrete stresses at midspan due to dead-load moment, prestress, and the thermal strains. It can be seen that the thermal strains have considerably reduced the compressive stresses in the web of the bridge while increasing the compressive stresses in the flanges. Vertical cracks in the webs of box-girder bridges have been observed in practice, and these cracks have been attributed to solar radiation (Ref. 5-12).

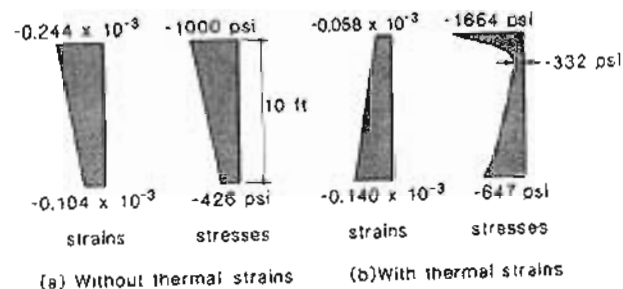
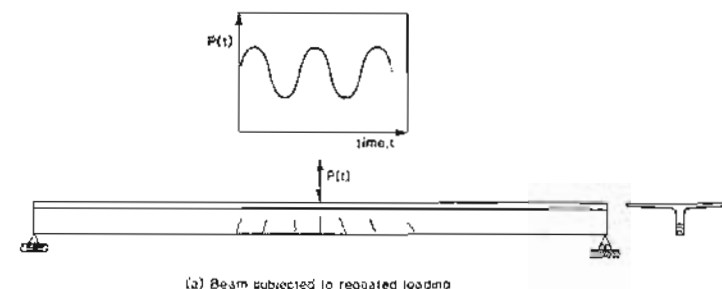


Figure 5-50 Effect of thermal strains on concrete stresses in box-girder section subjected to dead-load moment.

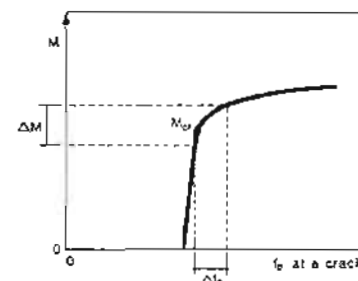
5.19 EVALUATION OF FATIGUE RESISTANCE

If a member is subjected to repeated applications of load and if this load exceeds the cracking load, there is a possibility that a fatigue failure of the tendon may occur.

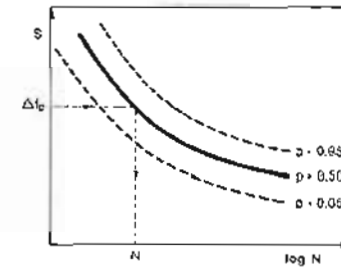
We investigate fatigue resistance by calculating the stress range, Δf_p , produced in the prestressing tendon by the cyclic load and comparing this stress range with that obtained from the S-N curve for the particular prestressing system. Because fatigue failures will always occur at crack locations, we determine Δf_p using the moment-curvature response for a cracked section (see Fig. 5-51).



(a) Beam subjected to repeated loading



(b) Determination of stress range



(c) Estimating fatigue life from S-N curve

Figure 5-51 Investigation of fatigue resistance.

In evaluating the fatigue resistance of a member, the following aspects should be considered:

1. Most of our knowledge of fatigue performance is based on experiments using constant-amplitude cyclic loading as shown in Fig. 5-51a. Actual loadings will be considerably more complex. To evaluate the fatigue life of a member subjected to complex loading, we typically employ Miner's rule (Ref. 5-14). We determine

the number of cycles of different amplitudes that will occur in the actual loading. For each amplitude range we compute the ratio of the actual number of cycles at this stress range, N_i , to the number of cycles, $N_{f,i}$, required to cause failure in a constant-amplitude test using this stress range. Miner's hypothesis is that under complex loading a fatigue failure will not occur if

$$\sum \frac{N_i}{N_{f,i}} < 1.00 \quad (5-47)$$

2. *S-N* curves are not precise limits but rather represent probabilities of failure. There is a great scatter in the experimental data on which they are based. Reported *S-N* relationships, such as that given in Eq. (3-32), usually represent the mean fatigue life (i.e., the number of cycles at which the probability of failure is 50%). For use in design these experimental *S-N* curves should be reduced by a factor of safety. The FIP Recommendations (Ref. 5-15) suggest that a design *S-N* curve be obtained by dividing the experimental stress ranges by a factor of 1.5.
3. Strands in a prestressed concrete beam when subjected to a given stress range fail at a lower number of cycles than the same strands tested in air (see Section 3.16). A suggested *S-N* curve for the mean fatigue life of straight strands in prestressed concrete beams is given in Fig. 5-52. Also shown in this figure is the *S-N* curve for strands in air suggested by Tide and Van Horn (Ref. 5-16). The maximum stress range of the experimental data used by Tide and Van Horn was about $0.4 f_{pu}$.

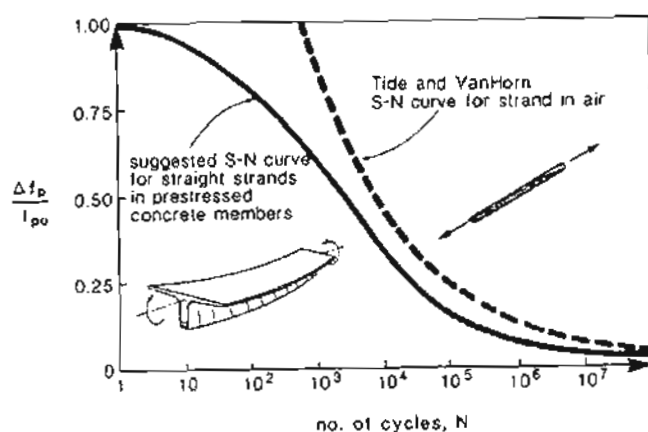


Figure 5-52 Suggested *S-N* curve for straight strands in prestressed concrete members, compared with *S-N* curve suggested by Tide and Van Horn (Ref. 5-16) for strands in air.

4. If the concrete cracks at any stage during the loading history, the ability of the concrete to resist tension at this location will be destroyed. Hence in determining the stress range, Δf_p , for a given moment range, ΔM , it is appropriate to neglect the tensile strength of the concrete.
5. While an individual load cycle may be applied at "short-term" loading rates, the loading continues for a "long term." During this time creep, shrinkage and relaxation will increase the stress range, Δf_p , for a given moment range. Because of these effects, it is appropriate to use the long-term response of the member when calculating the stress range, Δf_p , corresponding to a given moment range, ΔM .
6. Care should be exercised when choosing an appropriate *S-N* curve for curved post-tensioned tendons. Fretting can considerably reduce the fatigue life of such elements (see Section 3.16).

5.20 MEMBERS WITH UNBONDED TENDONS

So far all of the examples that we have dealt with in this chapter have involved members in which the tendons were bonded to the surrounding concrete. Our basic assumption has been that the change in strain in the prestressing steel is equal to the change in strain in the surrounding concrete. Thus

$$\epsilon_p = \bar{\epsilon}_{cp} + \Delta \epsilon_p \quad (5-48)$$

This approach will have to be modified for a beam with unbonded tendons. In such a beam the strain in the unbonded tendon will be constant along the length of the tendon, while the strain in the surrounding concrete, ϵ_{cp} , will vary along the length of the beam. The compatibility condition will now be that the change in overall length of the tendon between the anchorages, must equal the total change in length of the surrounding concrete from one end anchorage to the other, that is

$$\epsilon_p = \bar{\epsilon}_{cp} + \Delta \epsilon_p \quad (5-49)$$

where $\bar{\epsilon}_{cp}$ is the average strain of the fiber of concrete at the level of the tendon, averaged over the total length between the anchorages of the unbonded tendon (see Fig. 5-53).

Figure 5-54 illustrates the variation of the stress in a bonded tendon and an unbonded tendon in a heavily loaded beam. Bonded tendons exhibit large stress increases in regions of high moment (particularly at crack locations) while unbonded tendons exhibit stresses which are averaged out over the total length between anchorages.

5.21 EXAMPLE OF A BEAM WITH UNBONDED TENDONS

Janney, Hognessad, and McHenry (Ref. 5-17), of the Portland Cement Association, tested a number of beams to compare the flexural behavior of pretensioned beams, post-tensioned bonded beams, post-tensioned unbonded beams, as well as conventionally reinforced beams. The details of one of their unbonded beams are shown in Fig. 5-55.

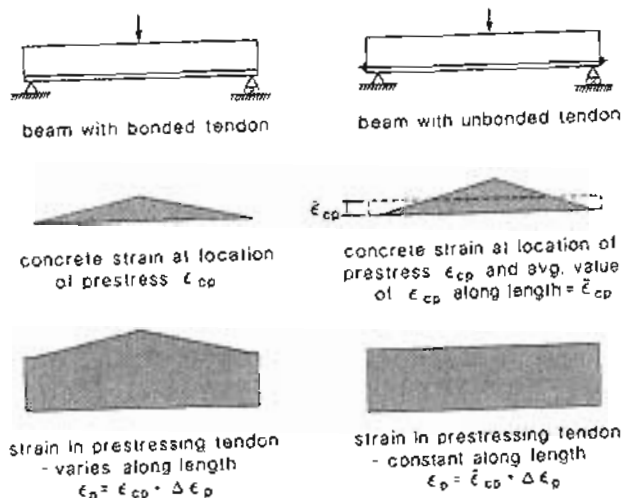


Figure 5-53 Compatibility conditions for bonded and unbonded beams.

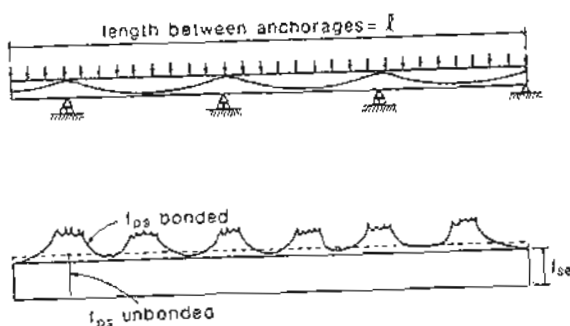


Figure 5-54 Tendon stress variation for unbonded and bonded tendons.

The beam was made from concrete which had a cylinder strength of 4930 psi (34 MPa). The 3/8 in. (9.5 mm) diameter strand was not stress-relieved and hence had a very rounded stress-strain curve, which is well represented by the following Ramberg-Osgood function:

$$f_p = \frac{E_p \epsilon_p}{[1 + (106 \epsilon_p)^2]^{0.5}}$$

where $E_p = 27.85 \times 10^3$ ksi (192×10^3 MPa). The ultimate strength of the strands, f_{pu} ,

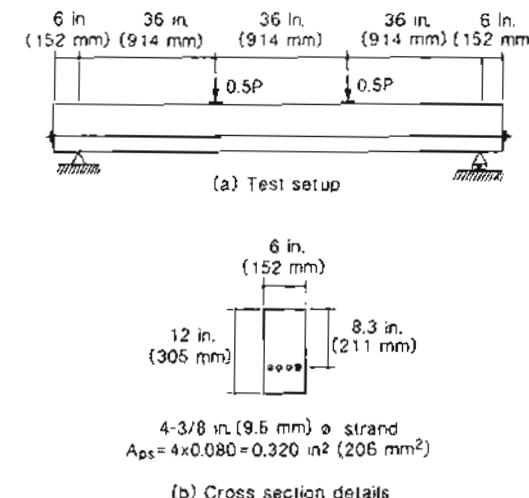


Figure 5-55 Unbonded post-tensioned beams tested by Janney, Hognesiad, and McHenry (Ref. 5-17).

was 240 ksi (1655 MPa). Prior to loading the beams, the unbonded strands were tensioned to a stress of 130 ksi (897 MPa).

We will calculate the relationship between the total applied load, P , and the midspan deflection, Δ . Because the load was applied reasonably quickly, we will calculate the "short-term" response of the member.

Step 1: Determine the initial conditions.

Due to the post-tensioning operation, the tensile force in the tendon is 41.6 kips (185 kN) and the concrete compressive stress on the bottom face will be 1242 psi (8.57 MPa), while on the top face a tensile stress of 66 psi (0.46 MPa) will occur.

As the modulus of the concrete was about 4000 ksi (27 600 MPa), the concrete strain on the bottom surface will be -0.311×10^{-3} , while the concrete strain on the top surface will be 0.017×10^{-3} . Thus the strain in the concrete at the level of the prestress is -0.21×10^{-3} .

The strain in the prestressing due to the post-tensioning stress of 130 ksi (897 MPa) is 5.35×10^{-3} . Hence

$$\Delta\epsilon_p = 5.56 \times 10^{-3}$$

At this stage, when the applied load, P , is zero, the curvature of the beam is

$$\phi = \frac{-0.311 \times 10^{-3} - 0.017 \times 10^{-3}}{12}$$

$$= -0.027 \times 10^{-3} \text{ rad/in. } (-1.08 \times 10^{-3} \text{ rad/m})$$

which corresponds to a midspan deflection of

$$\Delta = \frac{\phi l^2}{8} = -\frac{0.027 \times 10^{-3} \times (108)^2}{8}$$

$$= -0.039 \text{ in. } (-1.0 \text{ mm}). \text{ (i.e., upward)}$$

Step 2: Find the load P and deflection Δ when the tendon stress equals 137.5 ksi (948 MPa).

We will analyze the behavior of the beam by finding the loads and deflections that correspond to chosen values of stress in the tendon.

When the stress in the tendon reaches 137.5 ksi (948 MPa), the tensile strain in the tendon corresponding to this stress is

$$\epsilon_{pf} = 5.80 \times 10^{-3}$$

As there is no thermal strain, $\epsilon_p = \epsilon_{pf}$.

The average strain in the concrete at the level of the tendon is thus

$$\bar{\epsilon}_{cp} = \epsilon_p - \Delta \epsilon_p$$

$$= 5.80 \times 10^{-3} - 5.56 \times 10^{-3}$$

$$= 0.24 \times 10^{-3}$$

The tensile force in the tendon is

$$F = A_{ps} f_p = 0.320 \times 137.5 = 44 \text{ kips (196 kN)}$$

This tensile force must be balanced by an equal but opposite compressive force in the concrete (see Fig. 5-56). The external moment, M , is balanced by the couple consisting of the tension in the tendon and the compression in the concrete. Hence as the moment changes along the length of the beam, the distance between these two forces must change. Hence the strain in the concrete at the level of the tendon will change as the moment changes.

To find the relationship between ϵ_{cp} and M , we will use the following procedure:

1. Choose a value of ϵ_t .
2. Determine the stress-block factors α_1 and β_1 from Eqs. (5-7) and (5-9) using $\epsilon'_c = -2.1 \times 10^{-3}$.
3. Find ϵ_b such that $\int_{A_c} f_c dA_c = 44 \text{ kips (196 kN)}$.
4. Determine ϵ_{cp} and M .

The results of these calculations are summarized in Table 5-16.

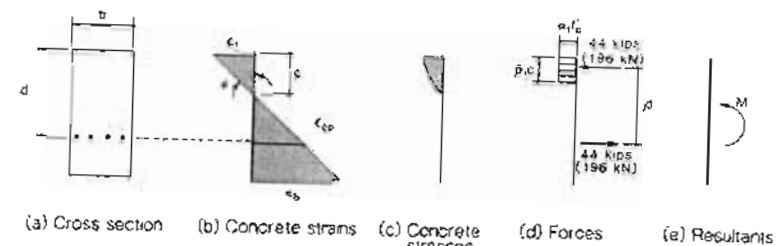


Figure 5-56 Influence of moment on strain, ϵ_{cp} .

Table 5-16 Response values for prestressing force = 44 kips (196 kN).

$\epsilon_t \times 10^3$	$\epsilon_b \times 10^3$	$\epsilon_{cp} \times 10^3$	M		$\phi \times 10^3$	
			m-kips	kNm	rad/in.	rad/m
-1.25	3.57	2.09	316	35.7	0.400	15.80
-1.00	2.24	1.24	308	34.8	0.270	10.63
-0.75	1.16	0.57	293	33.1	0.159	6.25
-0.50	0.39	0.11	263	29.7	0.074	2.90
-0.30	0.03	-0.07	203	22.9	0.027	1.08
-0.27	0	-0.08	186	21.0	0.022	0.88
-0.13	-0.13	-0.13	102	11.5	0	0
0	-0.27	-0.19	16	1.8	-0.022	-0.88

Recall that the average value of ϵ_{cp} over the length between the anchorages must equal 0.24×10^{-3} . Hence if the moment were constant between the anchorages, it would need to have a value between 263 (29.7) and 293 in.-kips (33.1 kNm). The moments will, in fact, vary along the length of the beam, as shown in Fig. 5-57. For this variation in moments, we must find by trial and error the value of the moment at midspan which gives the required value of ϵ_{cp} .

Try a midspan moment of 300 in.-kips (34 kNm). With this value of the midspan moment, we can determine the values of ϵ_{cp} at different sections along the beam from the values given in Table 5-16. These interpolated values are given in Table 5-17.

Table 5-17 Values of ϵ_{cp} corresponding to a midspan moment of 300 in.-kips (34 kNm).

Section	1	2	3	4	5	6	7
M, kNm	0	0	10	20	31	34	34
$\epsilon_{cp} \times 10^3$	-0.20	-0.20	-0.14	-0.08	0.22	0.91	0.91

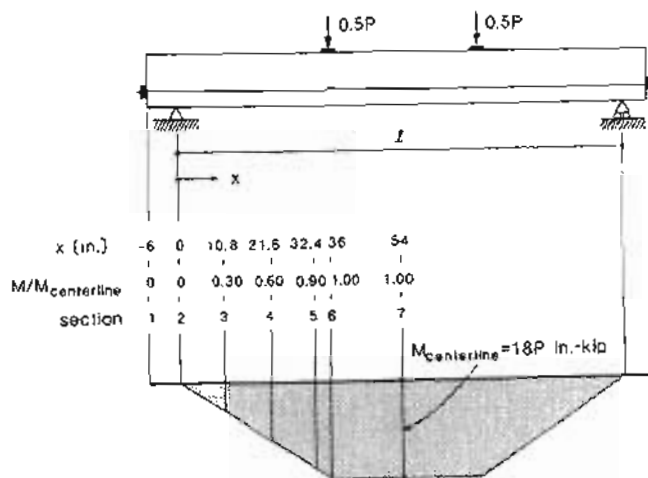


Figure 5-57 Moment variation between anchorages and sections used in numerical integration.

Knowing the values of $\bar{\epsilon}_{cp}$ at the seven sections along the span, we can numerically integrate to find the average strain, $\bar{\epsilon}_{cp}$, as

$$\bar{\epsilon}_{cp} = 0.249 \times 10^{-3}$$

The midspan moment should thus be a little less than 300 in.-kips (34 kNm) to give a value of $\bar{\epsilon}_{cp} = 0.24 \times 10^{-3}$, but we will accept this result as being accurate enough.

Hence the total applied load, P , when the tendon stress reaches 137.5 ksi (948 MPa), is

$$P = \frac{300}{18} = 16.7 \text{ kips (74.1 kN)}$$

The deflection corresponding to this load can be found by numerically integrating the beam curvature from the support to the midspan. The resulting deflection is

$$\Delta = 0.21 \text{ in. (5.4 mm)}$$

Step 3: Repeat Step 2 for different values of tendon stress.

By repeating the calculations given in Step 2 for different choices of stress in the tendon, we obtain the values listed in Table 5-18.

Table 5-18 Response predictions for beam with unbonded tendons

Tendon Stress ksi	$\bar{\epsilon}_{cp} \times 10^3$	P		Δ	
		kips	kN	in.	mm
137.5	0.24	16.7	74.1	0.21	5.4
144	0.64	18.4	81.8	0.39	10.0
151	1.09	19.6	87.1	0.57	14.5
165.5	2.09*	21.6*	95.9*	1.02	25.9

*Predicted failure load.

At a tendon stress of 165.5 ksi (1141 MPa), the beam is very close to failure. The top fiber concrete strain, ϵ_t , in the central region of the beam is -2.70×10^{-3} , and the bottom fiber strain, ϵ_b , is 10.61×10^{-3} . At midspan the strain in the concrete at the level of the prestress, $\bar{\epsilon}_{cp}$, is 6.50×10^{-3} . Note that the average strain, $\bar{\epsilon}_{cp}$, is about one-third of the ϵ_{cp} value at midspan. This ratio remains reasonably constant throughout the life of the member and is indicative of the shape of the moment diagram.

The response predictions are compared with the response observed by Janney, Hognestad, and McHenry in Fig. 5-58. From strain gages on the strands, Janney, Hognestad, and McHenry calculated that the stress in the strand increased by 37.4 ksi (258 MPa) during loading of the beam. It can be seen from Table 5-18 that the predicted stress in the strands at failure is 165.5 ksi (1141 MPa), which corresponds to a stress increase of 35.5 ksi (244 MPa).

5.22 MEMBERS SUBJECTED TO COMBINED AXIAL LOAD AND FLEXURE

In this chapter we have developed procedures capable of predicting the response of prestressed concrete members subjected to combined flexure and axial load. While the examples discussed so far have concentrated on the common case of flexural members with zero axial load, the more general case of a nonzero axial load can be treated using the same procedures.

The basic assumption, on which the calculation procedures depend, is that the concrete strain varies linearly over the depth of the section. With this assumption, the concrete strain distribution can be defined by just two variables, say the strain at the top face, ϵ_t , and the strain at the bottom face, ϵ_b (see Fig. 5-59). If the strains are known, the stress-strain relationship can be used to find the stresses. Integrating the stresses and the turning effect of the stresses then results in the axial load, N , and the moment, M [see Eqs. (5-4) and (5-5)].

For a given cross section the calculated values of N and M , for a particular choice of the strain values ϵ_t and ϵ_b , could be plotted as a point on a diagram such as that shown in Fig. 5-60. Repeating the calculations for many different values of ϵ_t and ϵ_b would then define a "feasible region" of possible combinations of N and M . The boundary of this feasible region can be called the "failure envelope" or the "interaction curve." Values of N and M , which lie outside the failure envelope, cannot be resisted by the cross section being considered. That is, such loads would cause failure of the section.

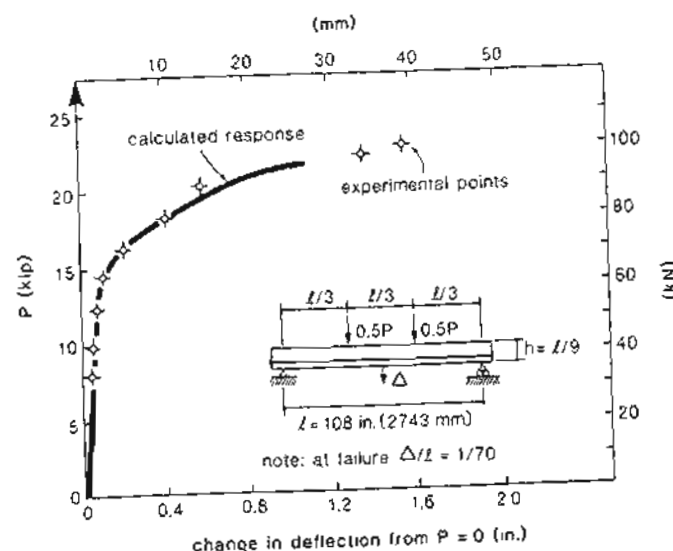


Figure 5-58 Comparison of predicted response with observed response for a beam with unbonded tendons tested by Janney, Hognestad, and McHenry (Ref. 5-17).

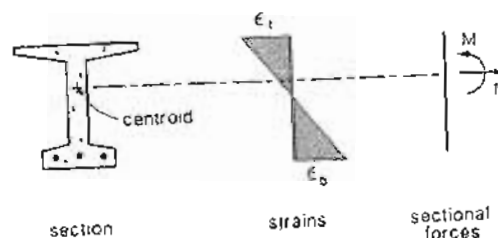


Figure 5-59 Section subjected to combined axial load and flexure.

One convenient procedure for determining the failure envelope is to fix the value of the axial load, N , and then find the highest and the lowest moments that can be resisted in the presence of this chosen axial load (see Fig. 5-60). Because the strength of a section will be controlled by the response at a crack, we neglect postcracking tensile stresses in the concrete when calculating failure envelopes.

In addition to determining the range of axial loads and moments that can be resisted by a given section, we sometimes wish to find the load-deformation response of members.

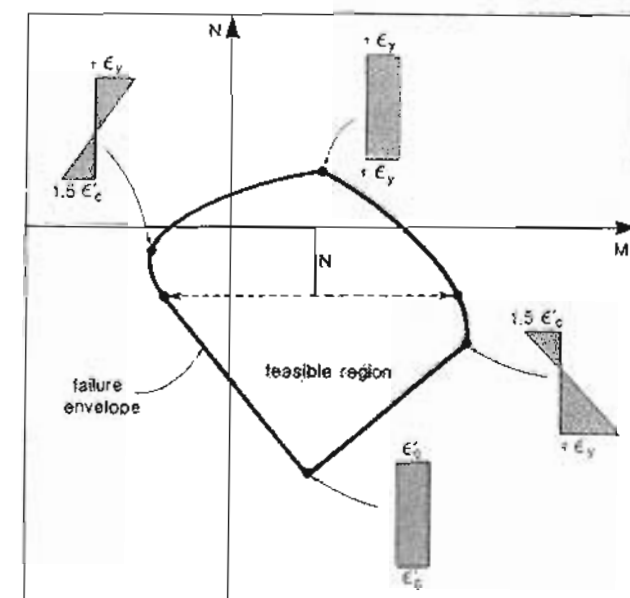


Figure 5-60 Axial load-moment interaction diagram.

subjected to axial load and moment. Thus we may wish to determine how the moment-curvature response of a section changes as the axial load changes (see Fig. 5-61). Because deflections of a member are influenced by the tensile stresses in the concrete between the cracks (i.e., tension stiffening), we should account for postcracking tensile stresses in the concrete when calculating the load-deformation response.

5.23 EXAMPLES OF CALCULATING $M-N$ INTERACTION DIAGRAMS

We will determine the range of axial compressions and flexural moments that can be resisted by the symmetrical, precast, pretensioned wall panel shown in Fig. 5-62. This panel contains three 1/2 in. (13 mm) low-relaxation strands with $f_{pu} = 270$ ksi (1860 MPa). The stress-strain curve of the strands can be represented by Eq. (3-26). The strands were pretensioned to 189 ksi (1303 MPa), which results in a strain difference, $\Delta\epsilon_p$, of 6.52×10^{-3} . The concrete has a 28-day cylinder strength, f'_c , of 5000 psi (34.5 MPa).

We will calculate the interaction diagrams for short-term loads and for long-term loads.

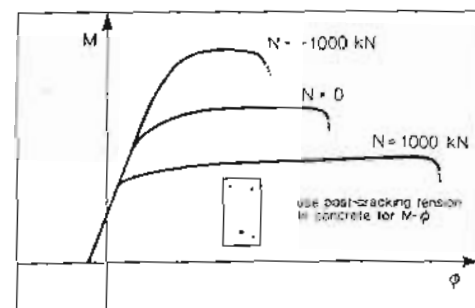


Figure 5-61 Influence of axial load on moment-curvature response.

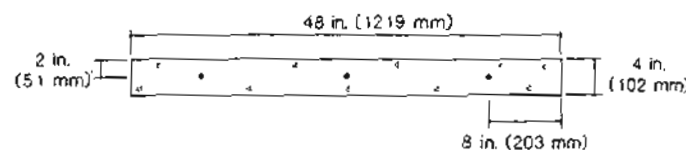


Figure 5-62 Precast, pretensioned wall panel.

(a) Short-Term Loads

Using the program RESPONSE, which is described in Appendix A, the maximum moments that can be resisted for different chosen values of axial compression were determined. These values, which are summarized in Table 5-19, were used to construct the $M-N$ interaction diagram illustrated in Fig. 5-63. Note that increasing the axial compression applied to the panel first causes an increase in flexural capacity and then, at higher values of compression, causes a decrease in flexural capacity. This is because the flexural capacity is governed by tensile "yielding" of the prestressing strands at low levels of compression and compressive crushing of the concrete at high levels of compression.

It is of interest to note that for a wide range of values of axial compression the maximum flexural capacity is reached at about the same value of compressive strain. The values in Table 5-19 were computed using the high-strength concrete model contained in the program RESPONSE, which assumes that the concrete reaches its peak compressive stress at a strain, ϵ'_c , of -2.03×10^{-3} (see Table 3-3). As can be seen in Table 5-19, the maximum flexural capacity is reached when the maximum compressive strain in the section is somewhat higher than ϵ'_c . The ACI Code (Ref. 5-18) suggests that the maximum capacity of the section be taken as the loads associated with a maximum compressive strain of 0.003. The loads corresponding to this strain have been plotted in Fig. 5-63. It can

5.23 Examples of Calculating $M-N$ Interaction Diagrams

Table 5-19 Maximum loads that can be resisted by wall panel under short-term loading.

N kips	M ft-kips	ϵ_c	ϵ_b
		$\times 10^3$	$\times 10^3$
0	0	16.49	22.34
-100	-445	26.09	35.35
-200	-890	32.43	43.97
-300	-1335	35.99	48.78
-400	-1780	36.32	49.26
-500	-2225	33.18	44.99
-600	-2670	26.37	35.77
-700	-3115	17.61	23.89
-800	-3560	8.63	11.70
-900	-4005	0	0
		-2.45	-2.45
		-2.35	-0.41
		-2.22	-0.91
		-2.03	-2.03

be seen that these loads provide a very accurate estimate of the failure envelope for low values of axial compression and a somewhat conservative estimate for high values of axial compression.

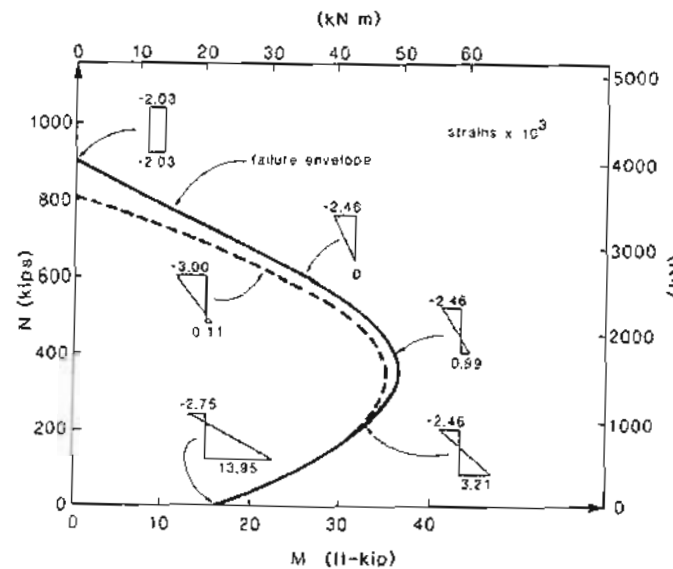


Figure 5-63 Axial compression-flexure interaction diagram for wall panel subjected to short-term loads.

(b) Long-Term Loads

We will assume that the creep coefficient of the concrete is 2.1 and that the concrete was first loaded when its compressive strength was 3500 psi (24.1 MPa). From Table 3-3 the initial modulus of the concrete was 3366 ksi (23 200 MPa). The creep-adjusted effective modulus from Eq. (3-12) is thus $3366/(1 + 2.1) = 1086$ ksi (7487 MPa). It is assumed that under slowly applied, long-term loading the compressive strength of the concrete will be 5000 psi (34.5 MPa). Hence, from Fig. 3-10 the strain, ϵ'_c , at which the concrete will reach its peak compressive stress is

$$\epsilon'_c = -\frac{f'_c}{E_{c,eff}} \left(\frac{n}{n-1} \right) = -\frac{5000}{1086,000} \left(\frac{2.80}{2.80-1} \right)$$

$$= -7.16 \times 10^{-3}$$

Further, we will assume that the concrete shrinkage strain, ϵ_{sh} , is -0.40×10^{-3} and that the strands have an effective modulus of 28 130 ksi (193 960 MPa) and rupture at a long-term strain of 0.054.

With the material properties above, the maximum moments that can be resisted, for different chosen values of axial compression, were determined and are given in Table 5-20. The resulting long-term interaction diagram is shown in Fig. 5-64, where it is compared with the interaction diagram for short-term loads. Note that for high values of axial compression, the long-term capacity is predicted to be higher than the short-term capacity. From Fig. 5-63 it can be seen that the maximum compressive capacity, under short-term loads, is reached at a uniform concrete strain of -2.03×10^{-3} . At this concrete strain, the prestressing strands still have a tensile strain of 4.49×10^{-3} . Hence the strands are in tension and do not help in carrying the external compression load. For the long-term loads, the maximum compressive capacity is reached at a strain of -7.56×10^{-3} . At this concrete strain, the strands are in compression and help to carry the external load.

Table 5-20 Maximum loads that can be resisted by wall panel under long-term loading.

<i>N</i>		<i>M</i>		ϵ_c	ϵ_a
kips	kN	ft-kips	kNm	$\times 10^3$	$\times 10^3$
0	0	16.64	22.55	-10.18	48.20
-100	-445	26.64	36.12	-9.38	19.50
-200	-890	32.58	44.16	-9.30	11.12
-300	-1335	35.66	48.33	-9.05	6.64
-400	-1780	36.57	49.58	-9.05	3.80
-500	-2225	34.78	47.14	-9.00	1.69
-600	-2670	29.93	40.57	-9.09	0.20
-700	-3115	22.03	29.90	-9.05	-1.05
-800	-3560	13.59	18.43	-8.60	-2.54
-900	-4005	5.20	7.01	-8.08	-4.45
-973	-4330	0	0	-7.56	-7.56

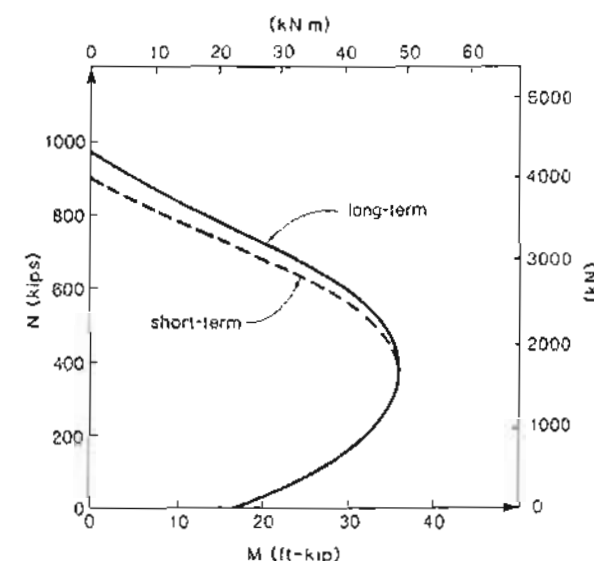
5.24 Examples of Calculating $M-\phi-N$ Relationships

Figure 5-64 Comparison of long-term and short-term $M-N$ interaction diagrams.

5.24 EXAMPLES OF CALCULATING $M-\phi-N$ RELATIONSHIPS

To illustrate the influence of axial load on moment-curvature response, we will calculate the short-term, moment-curvature response of the wall panel described in Fig. 5-62 for axial compression loads of 50 kips (222 kN) and 200 kips (890 kN).

We will assume that the cracking strength of the concrete is 300 psi (2.1 MPa). To account for tension stiffening, we will use the average tensile stress-average tensile strain relationship of Eq. (4-20) for the concrete in the effective embedment zone. This zone will extend to a distance of 7.5 times the strand diameter from the strand (see Figs. 4-21 and 5-65). Thus the total width of concrete contributing to tension stiffening will be $3 \times 2 \times 7.5 \times 0.5 = 22.5$ in. (572 mm).

The moment-curvature response calculations for the wall panel subjected to 50 kips (222 kN) compression are summarized in Table 5-21, while the calculations for the panel subjected to 200 kips (890 kN) compression are summarized in Table 5-22. The resulting moment-curvature predictions are illustrated in Fig. 5-65. Note that increasing the axial compression increases the cracking load and the maximum flexural capacity but reduces the ductility of the section. Also note that for both of these sections the concrete "fails" in compression before the prestressing strands rupture in tension.

Table 5-21 Moment-curvature response of wall panel subjected to 50 kips (222 kN) compression.

$\epsilon_1 \times 10^3$	$\epsilon_b \times 10^3$	$\phi \times 10^3$		M		Tens. Stiff.	Comments
		rad/in.	rad/m	ft-kips	kNm		
-0.25	-0.11	0.034	1.33	2.75	3.73	Yes	
-0.44	0.078	0.130	5.13	10.57	14.33	Yes	Concrete cracking
-0.50	0.16	0.164	6.46	12.09	16.39	Yes	
-0.75	0.67	0.356	14.01	15.99	21.68	Yes	
-1.00	1.43	0.608	23.94	18.04	24.46	Yes	
-1.25	2.36	0.902	35.55	19.46	26.38	Yes	
-1.50	3.39	1.223	48.15	20.52	27.82	Yes	
-1.75	4.47	1.556	61.26	21.35	28.95	Yes	
-2.00	5.58	1.896	74.65	21.94	29.76	Yes	Fails at crack
-2.00	5.87	1.967	77.44	21.13	28.65	No	
-2.50	8.04	2.636	103.78	21.75	29.49	No	
-2.80	9.18	2.995	117.91	21.80	29.56	No	Maximum moment
-3.00	9.85	3.214	126.54	21.75	29.49	No	
-3.50	11.24	3.685	145.08	21.40	29.02	No	
-4.00	12.24	4.060	159.84	20.85	28.27	No	

Table 5-22 Moment-curvature response of wall panel subjected to 200 kips (890 kN) compression.

$\epsilon_1 \times 10^3$	$\epsilon_b \times 10^3$	$\phi \times 10^3$		M		Tens. Stiff.	Comments
		rad/in.	rad/m	ft-kips	kNm		
-0.50	-0.27	0.057	2.26	4.59	6.22	Yes	
-0.75	-0.03	0.181	7.12	14.27	19.33	Yes	
-0.86	0.078	0.234	9.23	18.47	25.04	Yes	Concrete cracking
-1.00	0.25	0.312	12.30	22.30	30.23	Yes	
-1.25	0.64	0.472	18.58	26.73	36.24	Yes	
-1.50	1.11	0.652	25.69	29.47	39.96	Yes	
-1.75	1.63	0.844	33.24	31.22	42.33	Yes	
-2.00	2.17	1.043	41.05	32.32	43.82	Yes	Fails at crack
-2.00	2.25	1.062	41.79	31.62	42.87	No	
-2.50	3.28	1.446	56.92	32.41	43.94	No	Maximum moment
-3.00	4.09	1.773	69.81	31.83	43.16	No	
-3.50	4.66	2.040	80.31	30.44	41.27	No	
-4.00	5.03	2.258	88.88	28.55	38.71	No	

5.25 SLENDER COLUMNS – THE $P\Delta$ EFFECT

The sectional forces, M and N to which a particular cross section is subjected, are determined from an analysis of the structure (see Fig. 5-2). Usually, such an analysis is based on the geometry of the undeformed structure. For slender columns subjected to high axial

5.25 Slender Columns – The $P\Delta$ Effect

compression, this is not a conservative procedure. Account must be taken of the change in geometry caused by the deformations of the structure and of the resulting changes in the magnitudes of the sectional forces.

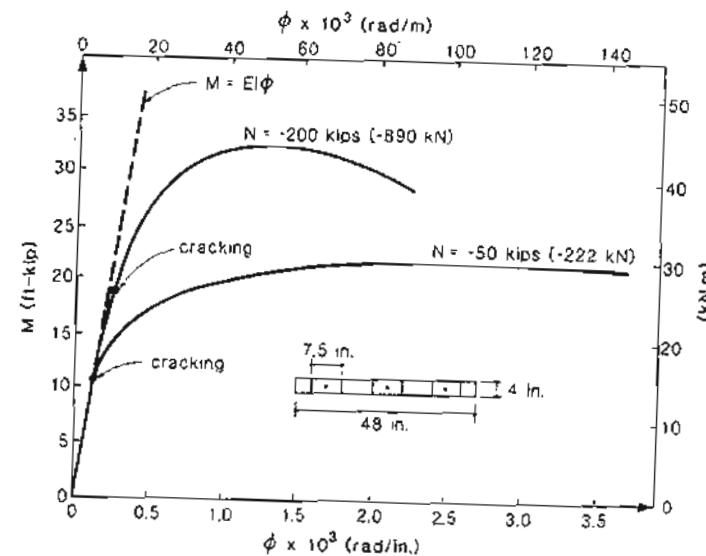
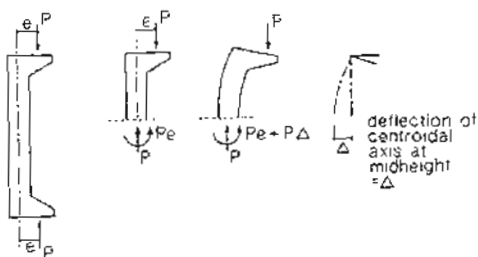


Figure 5-65 Moment-curvature response of wall panel subjected to axial compression.

The column shown in Fig. 5-66 is subjected to an eccentric compression force P . If we calculate the sectional forces at midheight of the column using the undeformed geometry of the column, we would find an axial compression of P and a moment of Pe . However, if we account for the deflection, Δ , we would calculate an axial compression of P but a moment of $Pe + P\Delta$. Thus the moment has been increased by the term $P\Delta$. This magnification of the moment caused by deflection is sometimes referred to as the " $P\Delta$ effect."

Figure 5-67 illustrates how the slenderness of a column influences the failure load. The figure shows how the axial load and moment at midheight of the column will increase as the magnitude of the eccentric end loads, P are increased. For a short column, M will remain equal to Pe (i.e., the $P\Delta$ term will be negligibly small). For a longer column the $P\Delta$ term will cause the moment to increase faster than the axial load. Because the moment is bigger, the axial load required to cause failure will be reduced (see Fig. 5-67). For very long columns, the maximum load capacity of the column may be reached before

Figure 5-66 The $P\Delta$ effect.

the sectional forces at midheight reach the failure envelope of the section (see Fig. 5-67). Such failures can be called "stability failures."

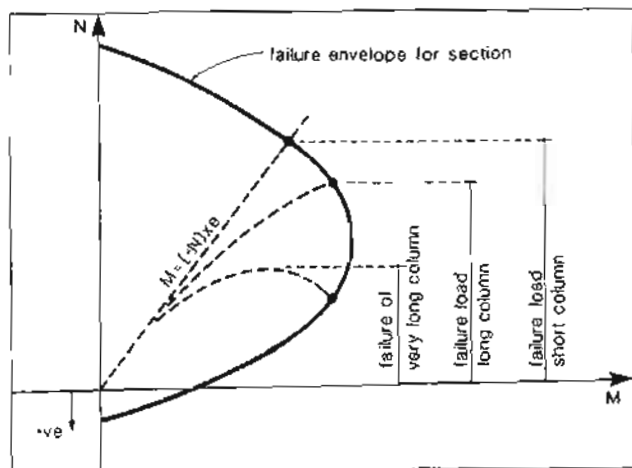


Figure 5-67 Axial load and moment at midheight of column.

A structural analysis in which account is taken of the change in geometry caused by the deformations of the structure is called a "second-order analysis." It typically involves an interactive procedure which goes through the following steps:

Step 1: Use the undeformed geometry of the structure to find the sectional forces.

Step 2: Use the sectional forces to calculate the deformations of the structures.

Step 3: Modify the geometry of the structure to account for the deformations.

Step 4: Use the new geometry of the structure to recalculate the sectional forces.

If there is a significant change in section forces, return to Step 2 and repeat the process.

5.26 EXAMPLE OF A SLENDER COLUMN

The precast, pretensioned wall panel described in Fig. 5-62 carries an axial compression of 200 kips (890 kN) and has an effective length of 10 ft (3.05 m). Find the maximum eccentricity of the load that the panel can tolerate. Assume short-term loading.

At the ends of the column the moment is

$$M_{end} = Pe \quad (5-50)$$

while at midheight of the column the moment is

$$M_{mid} = Pe + P\Delta_{mid}$$

Hence

$$M_{mid} = M_{end} + P\Delta_{mid} \quad (5-51)$$

The curvature at midheight, ϕ_{mid} , can be related to the moment at midheight, M_{mid} , by using the moment-curvature relationship for the section. Because the moments change over the height of the column, the curvatures will also change over the height of the column (see Fig. 5-68).

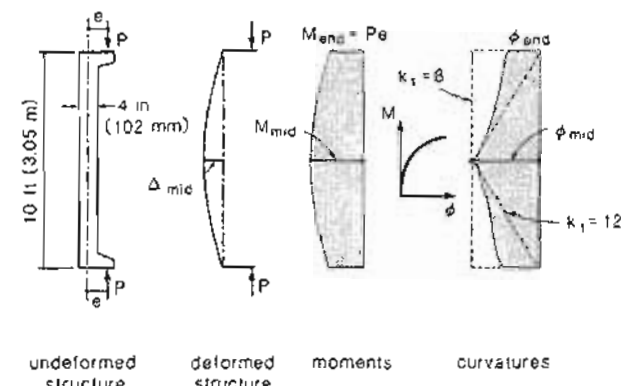


Figure 5-68 Moments, curvatures, and deformations of slender wall panel.

The deflection at midheight, Δ_{mid} , can be related to the curvature at midheight, ϕ_{mid} , by

$$\Delta_{mid} = \frac{\phi_{mid} L^2}{k_1} \quad (5-52)$$

where k_1 is a coefficient that depends on the shape of the curvature diagram. If the curvature is constant over the height of the column k_1 equals 8. If the curvature linearly decreases to zero at the ends, then k_1 equals 12 (see Fig. 5-68). In most cases it will be sufficiently accurate to assume that k_1 equals 10.

The maximum end eccentricity that the wall panel can tolerate can be determined using the following procedure:

Step 1: Plot the moment-curvature response of the section for the given axial load. This has already been done in Fig. 5-65 but is replotted to a more convenient scale in Fig. 5-69. This figure will be used to relate ϕ_{mid} to M_{mid} .

Step 2: For each value of ϕ_{mid} , calculate Δ_{mid} from Eq. (5-52). Use a k_1 value of 10.

Step 3: For each value of ϕ_{mid} , calculate M_{end} using the moment-curvature response and Eq. (5-51).

Step 4: Find the maximum value of M_{end} .

Step 5: Find the maximum eccentricity as

$$e_{max} = \frac{(M_{end})_{max}}{P}$$

Thus when ϕ_{mid} is 0.472×10^{-3} rad/in. (18.58×10^{-3} rad/m), M_{mid} is 26.73 ft-kips (36.24 kNm) (see Table 5-22). For this curvature

$$\begin{aligned} \Delta_{mid} &= \frac{\phi_{mid} L^2}{k_1} \\ &= \frac{0.472 \times 10^{-3} \times 120^2}{10} \\ &= 0.680 \text{ in. (17 mm)} \end{aligned}$$

From Eq. (5-51),

$$\begin{aligned} M_{end} &= M_{mid} - P\Delta_{mid} \\ &= 26.74 - 200 \times \frac{0.680}{12} \\ &= 15.41 \text{ ft-kips (20.90 kNm)} \end{aligned}$$

It can be seen from Fig. 5-69 that this is about the highest end moment that can be resisted by the wall panel. Hence the maximum eccentricity of the load that the panel can tolerate is

$$\begin{aligned} e_{max} &= 15.41 \times \frac{12}{200} \\ &= 0.93 \text{ in. (23 mm)} \end{aligned}$$

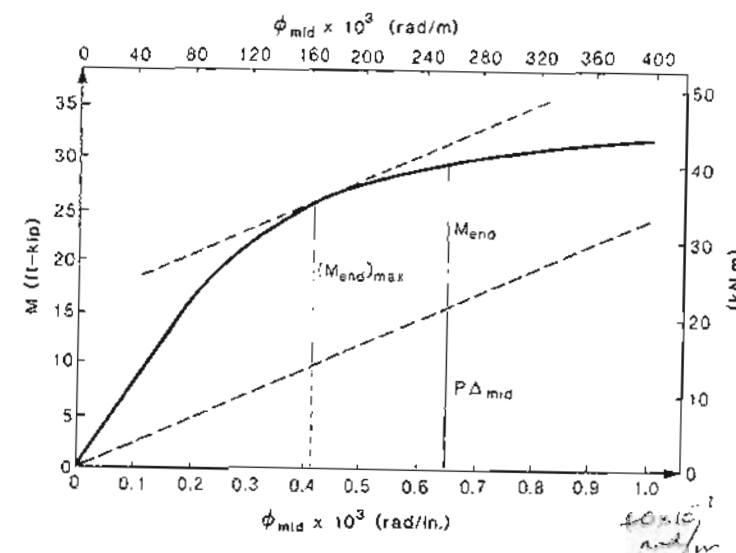


Figure 5-69 Determination of maximum end moment the panel can tolerate.

By repeating the calculations above for different values of axial compression, N , and different column lengths, L , interaction diagrams relating N , M_{end} , and L can be produced. An example of such a diagram, computed by Nathan (Ref. 5-19), is shown in Fig. 5-70. Because tension stiffening of concrete was neglected by Nathan, his predicted maximum end moments will be somewhat more conservative than those that we would calculate

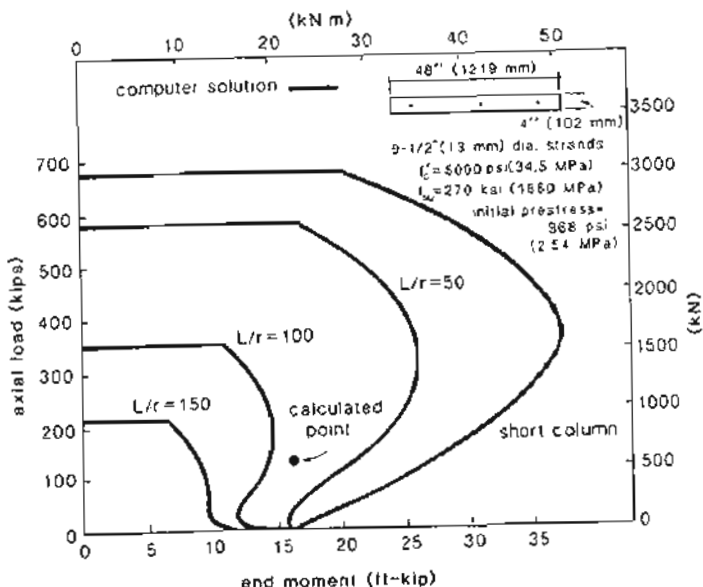


Figure 5-70 Axial load-end moment interaction diagram for wall panel.
Adapted from Nathan (Ref. 5-19).

References

- 5-1 Navier, "Résumé des leçons ... de la résistance des corps solides," Paris, 1826.
- 5-2 Bernoulli, Jacob, "Histoire de l'Académie des Sciences de Paris," Paris, 1705.
- 5-3 Hooke, Robert, "Lectures De Potentia Restitutiva, or of Spring Explaining the Power of Springing Bodies," printed for John Martyn Printer to The Royal Society, at the Bell in St. Paul's Church-Yard, 1678, 24 pp.
- 5-4 Priestley, M.J.N., Park, R., and Lu, F., "Moment Curvature Relationships for Prestressed Concrete in Constant Moment Zones," *Magazine of Concrete Research*, Vol. 23, No. 75-76, June-Sept. 1971, pp. 69-78.
- 5-5 Prestressed Concrete Institute, *PCI Design Handbook: Precast and Prestressed Concrete*, 3rd ed., PCI, Chicago, 1985.
- 5-6 Martin, L.D., "A Rational Method of Estimating Camber and Deflections of Precast, Prestressed Concrete Members," *PCI Journal*, Vol. 22, No. 1, Jan.-Feb. 1977, pp. 100-108.
- 5-7 Cellini, A., "Influence of Concrete Strength on Response of Pretensioned Members," M.Eng. thesis, McGill University, Montreal, May 1990.
- 5-8 CEB-FIP, *Model Code for Concrete Structures: CEB-FIP International Recommendations*, 3rd ed., Comité Euro-International du Béton, Paris, 1978, 348 pp.
- 5-9 Trost, H., Cordes, H., and Thormählen, U., "Sinnvolle Begrenzung der schlaffen Bewehrung zur Aufnahme der Zugkräfte für die Rissbeschränkung im Spannbeton" (Limiting the Non-Prestressed Reinforcement for Crack Control in Prestressed Concrete), Institut für Massivbau, Rheinisch-Westfälischen Technischen Hochschule, Aachen, West Germany, Jan. 1976.
- 5-10 Leonhardt, F., "Crack Control in Concrete Structures," IABSE Surveys No. S-4/77, International Association for Bridge and Structural Engineering, Zurich, 1977, 26 pp.
- 5-11 Thurston, S.T., and Priestley, M.J.N., "Thermal Stresses in Concrete Structures," Research Report 78.21, Department of Civil Engineering, University of Canterbury, Christchurch, New Zealand, 1978.
- 5-12 Priestley, M.J.N., "Design of Concrete Bridges for Temperature Gradients," *ACI Journal*, Vol. 75, No. 5, May 1978, pp. 209-217.
- 5-13 Pauser, A., "Grundsätze für die bauliche Durchbildung" (Principles for Structural Detailing), *Zement und Beton*, No. 3, Vienna, 1976.
- 5-14 Miner, M.A., "Cumulative Damage in Fatigue," *Journal of Applied Mechanics*, Vol. 12, No. 3, Sept. 1945, pp. A-159-A-164.
- 5-15 FIP Commission on Practical Design, *FIP Recommendations—Practical Design of Reinforced and Prestressed Concrete Structures Based on the CEB-FIP Model Code (MC78)*, Thomas Telford Ltd., London, 1984, 36 pp.
- 5-16 Tide, R.M.R., and Van Horn, D.A., "A Statistical Study of the Static and Fatigue Properties of High Strength Prestressing Strand," Report No. 309.2, Fritz Engineering Laboratory Lehigh University, Bethlehem, Pa., June 1966.
- 5-17 Janney, Jack R., Hognestad, Eivind, and McHenry, Douglas, "Ultimate Flexural Strength of Prestressed and Conventionally Reinforced Concrete Beams," *ACI Journal*, Vol. 52, No. 6, Feb. 1956, pp. 601-620.
- 5-18 ACI Committee 318, "Building Code Requirements for Reinforced Concrete (ACI 318-89) and Commentary – ACI 318 R-89," American Concrete Institute, Detroit, 1989, 353 pp.

- 5-19 Nathan, Noel D., "Slenderness of Prestressed Concrete Columns," *PCI Journal*, Vol. 28, No. 2, Mar.-Apr. 1983, pp. 50-77.
- 5-20 Hanson, John M., Hulsbos, Corrie L., and Van Horn, David A., "Fatigue Tests of Prestressed Concrete I Beams," *Journal of the Structural Division, ASCE*, Vol. 96, No. ST11, Nov. 1970, pp. 2443-2464.

Demonstration Problems

5-1 Calculate the short-term moment-curvature response of the rectangular, pretensioned beam shown in Fig. 5-71. Assume that $b = 12$ in. (300 mm), $h = 24$ in. (600 mm), $d = 20$ in. (500 mm), and $A_p = 1.5 \text{ in}^2$ (1000 mm 2). For simplicity, use a bilinear stress-strain curve for the prestressing steel, with $f_{py} = 240$ ksi (1650 MPa), and $E_p = 29,000$ ksi (200 000 MPa). Assume that the strands were tensioned to 190 ksi (1300 MPa) prior to casting the concrete. Assume that the concrete has a parabolic stress-strain curve, with $f'_c = 5000$ psi (35 MPa), and $\epsilon'_c = -0.002$. Neglect the tensile strength of the concrete (i.e., $f_{cr} = 0$). For this section, the applied moment is resisted by an internal couple consisting of a tensile force, T , in the reinforcement, and an equal but opposite compressive force, C , in the concrete. Thus $M = Tjd$, where jd is the "lever arm" of the internal couple. On a plot of the moment-curvature response, sketch this internal couple for a number of representative points. That is, draw arrows representing the forces C and T , separated by the lever arm jd . Comment on how T and jd change in magnitude as the moment increases.

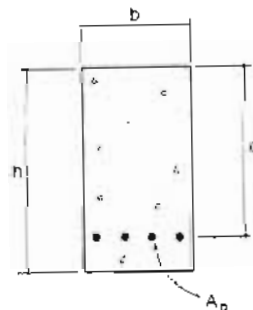


Figure 5-71 Rectangular, pretensioned beam.

5-2 Repeat Prob. 5-1 for a non-prestressed rectangular beam which contains 7.2 in^2 (4700 mm 2) of reinforcing bars with $f_y = 50$ ksi (350 MPa) and $E_s = 29,000$ ksi (200 000 MPa). All other section properties are identical to those given in Prob. 5-1. Contrast the manner in which T and jd increase for a non-prestressed section with that for a prestressed section. Also comment on the similarities and differences of the two moment-curvature responses.

5-3 In North American practice, failure of a section in flexure is assumed to occur when the "top" concrete strain reaches -0.003. Further, usually no upper limit is placed on the strain which can

occur in the prestressing tendons (i.e., ϵ_p is allowed to exceed the rupture strain of 0.04). Use this procedure to calculate the flexural capacity of the single tee described in Figs. 5-17 and 5-18. Compare this capacity with that calculated in Section 5.9. Comment on the magnitude of the increase in flexural capacity that results from permitting the tendon strain to exceed 0.04.

5-4 The determination of the flexural capacity of a prestressed concrete beam, using the North American approach of assuming a concrete strain of -0.003 is made considerably simpler if the stress in the prestressing steel at the time of flexural failure is known. The rectangular, pretensioned beam, shown in Fig. 5-71, contains low-relaxation strand whose stress-strain response is given by Eq. (3-26). The strands were pretensioned to 200 ksi (1380 MPa) prior to casting the concrete. Prepare a plot that relates the stress in the strand at flexural failure, f_{psf} , to the reinforcing index ω , where

$$\omega = \frac{A_p f_{py}}{bd f'_c}$$

Assume a parabolic stress-strain curve for the concrete and $\epsilon'_c = -0.002$; thus use the rectangular stress-block factors, α_1 and β_1 , for ϵ_t/ϵ'_c equal to 1.50. Hint: Assume a value of f_{psf} and find the corresponding ω .

5-5 If a beam contains a very small amount of reinforcement, it may fail in a brittle manner as soon as the first crack forms. By equating the flexural capacity to the cracking load, determine the reinforcement ratio, $p_p = A_p/(bd)$, below which such brittle failures will occur for the beam shown in Fig. 5-71. Assume that $f'_c = 5000$ psi (34.5 MPa), $f_{cr} = 300$ psi (2.07 MPa), $d/h = 0.8$, and $\Delta\epsilon_p = 6.90 \times 10^{-3}$.

5-6 The rectangular stress-block factors given in Table 5-1 were derived for a triangular strain distribution acting on a zone of constant width. However, with some modifications they can be used either exactly or approximately in other situations. Use the factors to determine the magnitude and position of the resultant concrete force for the three situations shown in Fig. 5-72. In each case assume that $f'_c = 5000$ psi (34.5 MPa), $\epsilon'_c = -0.002$, and $\epsilon_{sh} = 0$. For case (a) and case (b) determine the resultant by adding fictitious areas to the cross section to obtain a constant-width area with a triangular strain distribution [e.g., add an area 10 in. (250 mm) wide and 12 in. (300 mm) deep to the bottom of the section in case (a)]. Find the resultants by subtracting the resultants on the fictitious areas from the resultants for the total area. For case (c) use the same α_1 and β_1 factors as for a constant-width section. Compare the approximate results so obtained with the actual values obtained by integration.

5-7 The single tee described in Fig. 5-17 spans 80 ft (24.4 m) and is supported by a ledger beam as shown in Fig. 5-73. Choose an appropriate thickness of the neoprene pad on which the beam sits if the maximum horizontal deformation of the pad under dead loads is to be limited to 0.50 times the thickness of the pad. Hint: The horizontal movement of the bottom face of the beam can be found by integrating the bottom face strains. Table 5-6 can be used to calculate the movement under short-term loads, while Table 5-8 can be used to calculate the movement under long-term loads.

5-8 Using the expressions for elastic, uncracked response derived in Section 5.11, calculate the moments required to crack the bottom face of the single tee, which is described in Fig. 5-17, under short-term loads and under long-term loads. Assume that $f_{cr} = 300$ psi (2.07 MPa), $E_c = 3828$ ksi (26 400 MPa), $E_{s,eff} = 910$ ksi (6273 MPa), $E_p = E_s = 29,000$ ksi (200 000 MPa), $E_{p,eff} = 28,130$ ksi (194 000 MPa), and $\epsilon_{sh} = -0.48 \times 10^{-3}$.

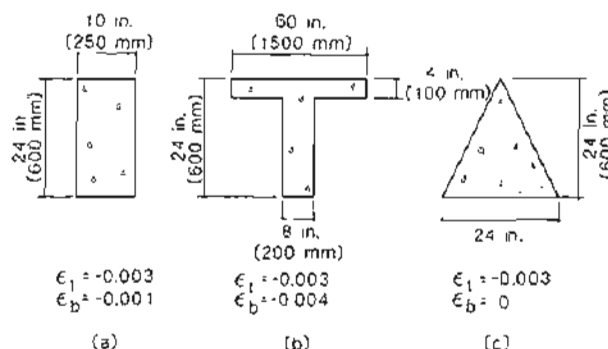


Figure 5-72 Strain distributions on cross sections.

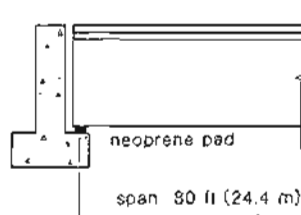


Figure 5-73 Single tee sitting on neoprene pad.

5-9 A precast concrete plant manufactures pretensioned panels. The panels are 10 in. (250 mm) thick, 6 ft (1800 mm) wide and contain twelve 0.5 in. (13 mm) strands, six near each face located 1 in. (25 mm) from the face. The strands are pretensioned to 175 ksi (1200 MPa). The panels are cast and cured in a factory at 72°F (22°C). When taken outside in the winter they cool down substantially, with the top and bottom surfaces cooling more rapidly than the interior of the panel. Some time after being taken outside, the temperature distribution across the thickness of the slab is as shown in Fig. 5-74. Calculate the concrete stress distribution at this time. Assume that $\alpha_c = \alpha_p = 6 \times 10^{-6}/^{\circ}\text{F}$ ($10 \times 10^{-6}/^{\circ}\text{C}$), $E_c = 3828$ ksi (26400 MPa), and $E_p = 29,000$ ksi (200000 MPa).

5-10 The floor system of a low-rise industrial building consists of single tees which are described in Fig. 5-17, spanning 80 ft (24.4 m). A new tenant installs a metal stamping machine directly over one of the tee-beams and located at midspan (see Fig. 5-75). The dead load of the machine is 14 kips (62.2 kN) but due to impact it exerts an equivalent load (dead load plus impact) of 28 kips (124.6 kN) each time it stamps. It stamps once every 2 minutes, for 8 hours a day, 6 days a week. Estimate how long it will take before the beam fails in fatigue. The self-weight of the beam can be taken as 594 lb/ft (8.76 kN/m).

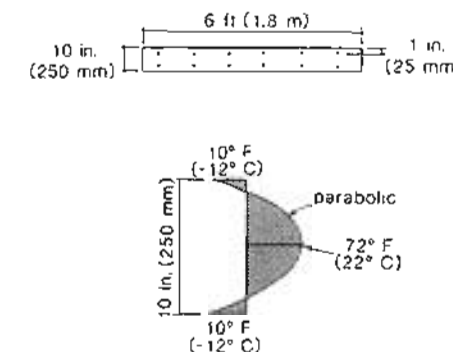


Figure 5-74 Temperature distribution across thickness of panel.

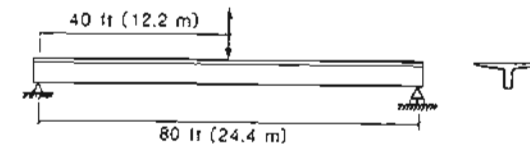


Figure 5-75 Loading of single tee.

5-11 Hanson, Hulbos, and Van Horn (Ref. 5-20) tested the beam shown in Fig. 5-76 in order to study its fatigue resistance. The beam was made from a concrete that had a cylinder strength at 50 days of 7120 psi (49.1 MPa). The stress-relieved 7/16 in. (11 mm) diameter strands had a stress-strain curve which could be represented by the following modified Ramberg-Osgood function:

$$f_p = E_p \epsilon_{pf} \left\{ 0.020 + \frac{0.980}{[1 + (103\epsilon_{pf})^{7.3}]^{0.137}} \right\}$$

where $E_p = 27,850$ ksi (192000 MPa). The breaking stress of the strands, f_{pu} , was about 283 ksi (1950 MPa). The strands were pretensioned to a stress of 162 ksi (1115 MPa) in the stressing bed. The concrete was moist cured for 4 days and the strands were released from the bed on the fifth day. Cyclic loading began on about the 30th day using a loading rate of 250 cycles per minute and the loading arrangement shown in Fig. 5-76. The loads P were varied between 7 and 18.9 kips (31 and 84 kN) two million times. In addition to the two million cycles described above, the member was subjected to one cycle of a peak load of 34 kips (151 kN). The loads were then cycled between 7 and 21 kips (31 and 93 kN) with fatigue failure taking place after 570,000 cycles. Accounting for the loading history described above, estimate the number of cycles required to cause fatigue failure and compare your result with the 570,000 cycles determined by Hanson, Hulbos, and Van Horn.

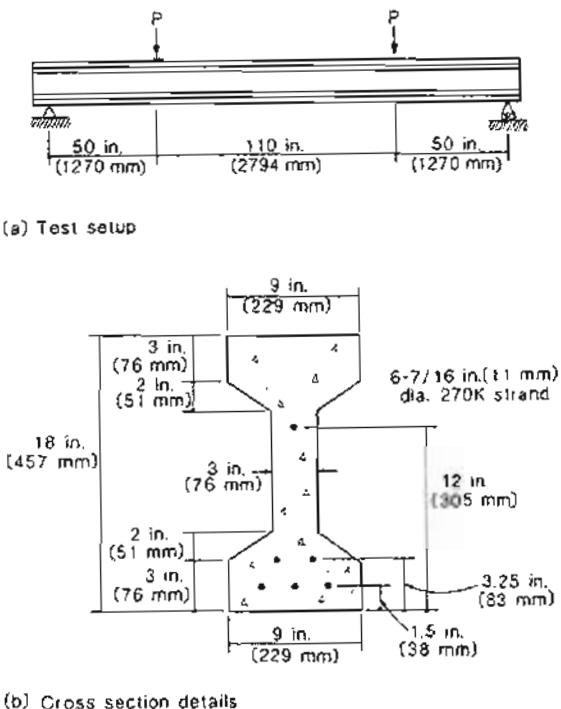


Figure 5-76 Details of beam tested by Hanson, Hulbos, and Van Horn (Ref. 5-20).

5-12 The unbonded beam whose load-deflection response was calculated in Section 5.21 had a companion beam with grouted tendons. Apart from the bonded tendons, the only significant difference between the two beams was that the strands in this second beam were post-tensioned to 118 ksi (814 MPa) rather than 130 ksi (897 MPa). Calculate the load-deformation response and compare your predictions with the observed response given in Table 5-23. Comment on the effect of bonding the tendons.

Table 5-23 Observed response of beam with bonded tendons. From Ref. 5-17.

P	kips	0	6.3	8.3	12.0	15.0	16.5	27.0
	kN	0	28	57	83	103	114	120
Δ	in.	0	0.04	0.08	0.32	0.80	1.18	Fails
	mm	0	1	2	8	20	30	Fails

5-13 A 12 by 12 in. (300 by 300 mm) pretensioned column contains four 0.5 in. (13 mm) low-relaxation strands. The strands are located near each corner of the section, with the center of each strand being 2 in. (50 mm) from the face of the column. The strands were pretensioned to 200 ksi (1400 MPa) prior to casting the concrete. Calculate the range of axial compressions and flexural moments that can be resisted by the section if the concrete compressive strength is 10,000 psi (70 MPa). Calculate the interaction diagram in two ways. First, assume that the stress-strain response of the concrete is given by Eq. (3-1), and then, assume that the stress-strain response of the concrete is given by Eq. (3-7). Comment on the influence of the shape of the concrete stress-strain curve upon the axial load-moment interaction diagram. Use Eq. (3-26) for the stress-strain curve of the strands.

5-14 The precast, pretensioned wall panel described in Fig. 5-62 carries an axial compression of 200 kips (890 kN) and has an effective length of 10 ft (3.05 m). Find the maximum eccentricity of the load that the panel can tolerate, assuming long-term loading. Comment on the influence of creep, shrinkage, and relaxation on the failure load. Use the assumed material properties given in Section 5.23(b).

5-15 Produce an interaction diagram for the precast, pretensioned wall described in Fig. 5-62, relating axial load and end moment for L/r values of 50, 100, and 150. Assume short-term loading.

5-16 The precast pretensioned rectangular wall panels described in Fig. 5-62 have been used as the bearing elements in a precast multistory apartment building. The concentric load supported by a ground-floor panel is 200 kips (890 kN). A fire occurs in a ground-floor apartment. Calculate the temperature difference through the wall thickness that the panel can tolerate prior to collapse. Ignore changes of material characteristics with the temperature and assume the panel to be pinned at each floor level. Assume a linear distribution of temperature through the wall. Floor-to-floor height = 10 ft (3.05 m). $\alpha_c = \alpha_p = 6 \times 10^{-6}/^{\circ}\text{F}$ ($10 \times 10^{-6}/^{\circ}\text{C}$). Hint: The curvature at midheight will be partly due to the temperature gradient and partly due to the $P\Delta$ moment. Look at Fig. 5-69. It contains the answer!

Design for Flexure

To engineers who, rather than blindly following the codes of practice, seek to apply the laws of nature.

T.Y. Lin, 1955

6.1 INTRODUCTION

Prestressed concrete construction requires high-quality materials, precise workmanship, and careful design. The decision to use prestressing imposes on the design engineer the responsibility to check behavior carefully at all critical stages in the life of the structure. To fulfill this responsibility the engineer must understand the basic behavior of prestressed concrete structures.

In this chapter we explain how our knowledge of prestressed concrete behavior can be applied to the flexural design of prestressed concrete beams. In introducing the basic concepts of design, we will restrict our attention to simply supported beams. The additional considerations required in the design of statically indeterminate structures will be presented in Chapter 10.

6.2 GENERAL DESIGN CONSIDERATIONS

The purpose of prestressing is to improve the response of the member to external loads and to utilize high-strength materials efficiently. Prestressing produces a self-equilibrating system of internal stresses consisting of very high tensile stresses in the prestressing tendons and compressive stresses in the concrete. Because of these self-equilibrating stresses the

design process for prestressed concrete is different from that used for other construction materials. In prestressed concrete it is necessary to consider all the critical stages in the life of the member while properly accounting for the presence of the self-equilibrating stresses. It is, for example, possible to fail the prestressed concrete member during the prestressing operation. Thus a prestressed member can fail when the external moment and the external axial load are both zero. To check the safety during the prestressing operation we calculate stresses in the prestressing tendon and the concrete and compare these to acceptable limits rather than comparing a factored external moment with a factored flexural capacity.

Figure 6-1 illustrates some important stages in the life of a pretensioned beam. In order to ensure safety during the tensioning operation, we must limit the tensile stress in the strands (see Fig. 6-1a). We must check that when the pretensioned strands are released from the abutments the young concrete is not crushed or severely cracked (see Fig. 6-1b).

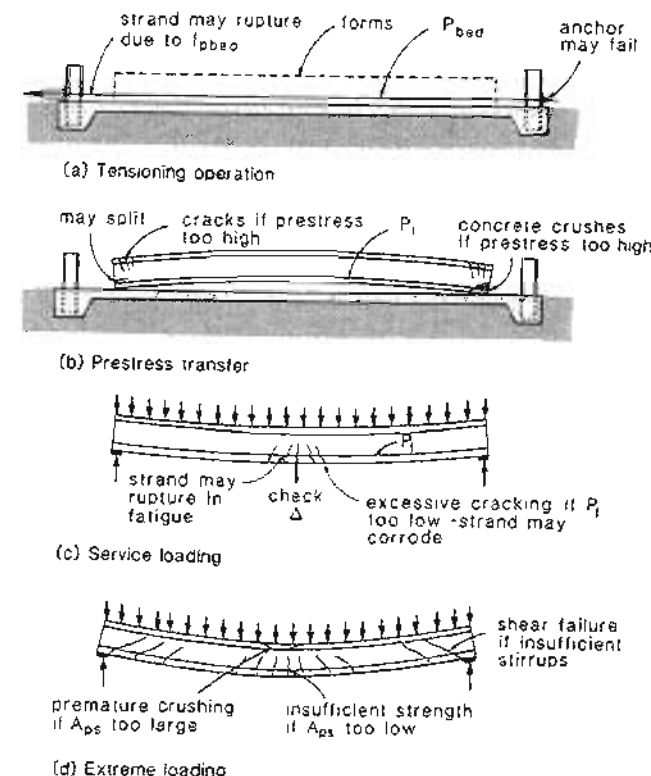


Figure 6-1 Design considerations for simply supported beams.

We must check that even after creep, shrinkage, and relaxation losses have occurred, the beam can still resist the expected service loads without exhibiting excessive deflections or excessive cracking (see Fig. 6-1c). Finally we must ensure that the beam can tolerate significant overloads prior to failure (see Fig. 6-1d).

The limits and procedures which are used in investigating the stages described above are summarized in the sections below. The methods given are those recommended by the ACI Code, "Building Code Requirements for Reinforced Concrete (ACI 318-89) and Commentary - ACI 318 R-89" (Ref. 6-1).

6.3 PERMISSIBLE STRESSES IN TENDONS

The maximum tensile stress in tendons at jacking and after transfer is limited in order to provide a margin of safety against tendon fracture or end-anchororage failures, to avoid inelastic tendon deformation and to limit relaxation losses. The ACI Code (Ref. 6-1) limits for tendon stresses are given in Table 6-1.

Table 6-1 ACI Code (Ref. 6-1) tendon stress limits in terms of f_{pu} .

Tendon Type	f_{py}	At Jacking	After Transfer
Low-relaxation strand or wire	0.9	0.80	0.74*
Normal stress-relieved strand or wire	0.85	0.80	0.70
Plain prestressing bars	0.85	0.80	0.70
Deformed prestressing bars	0.80	0.75	0.66

* Post-tensioned tendons limited to $0.70 f_{pu}$ at anchorages and couplers.

If there is a significant drop in temperature of pretensioning tendons while in the stressing bed, this will give rise to larger tendon stresses which must be accounted for in checking the stress limits.

6.4 PERMISSIBLE STRESSES IN CONCRETE

The stresses in the concrete are investigated at different stages in the life of a member. These stresses are calculated on the basis of the materials exhibiting an elastic, uncracked response.

(a) Initial Stage

The stresses in the concrete immediately after prestress transfer (i.e., before time-dependent losses have occurred) are limited to prevent crushing or cracking of the young

Sec. 6.5 Calculation of Stresses in the Concrete

concrete due to the high prestress force (see Table 6-2). Simply supported beams pretensioned with straight strands will initially have high tensile stresses in the top concrete fibers near the ends of the beams. Experience has shown that a small amount of cracking in these zones can be tolerated and hence higher tensile stresses are permitted.

The tensile stress limits can be exceeded if appropriate reinforcement is provided to control the resulting cracking. This crack control reinforcement should consist of a well-distributed array of small bars (see Fig. 6-2).

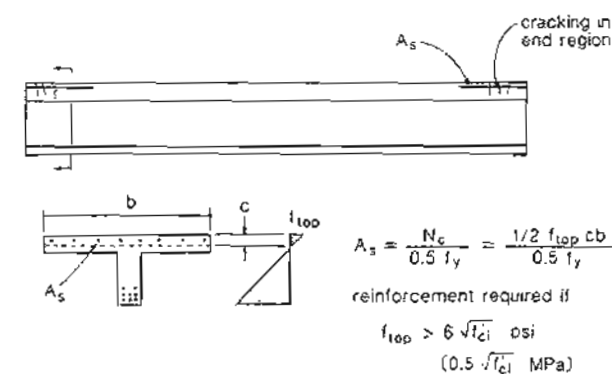


Figure 6-2 Control of cracking occurring at transfer.

(b) Final Stage

The stresses in the concrete are also investigated at a stage when all prestress losses have occurred and the full service loads are applied. The tensile zones being investigated are those regions of the member where the prestress causes compressive stresses (pre-compressed) but are in tension under service loads.

The consequences of cracking for a structure in a corrosive environment (e.g., a parking garage) are much more severe, and hence lower tensile stress limits and larger concrete covers should be used.

6.5 CALCULATION OF STRESSES IN THE CONCRETE

(a) The Strain Compatibility Approach

As the stresses are calculated on the basis of the concrete remaining uncracked and material stress-strain relationships being linear, the strain compatibility procedure of Section 5.11 can be used provided that the tendons are bonded to the concrete. In these procedures the total strains in the concrete are found by calculating the strain, ϵ_{con} , at the

Table 6-2 Concrete stress limits from the ACI Code (Ref. 6-1) and the CSA Code (Ref. 6-2).

	ACI Code		CSA Code*	
	Compressive Stress Limit	Tensile Stress Limit, psi	Compressive Stress Limit	Tensile Stress Limit, MPa
Initial stage At prestress transfer Concrete strength = f'_c	$0.6f'_c$	(a) $3\sqrt{f'_c}$ (b) $6\sqrt{f'_c}$ at simply supported ends (c) If values above exceeded, provide bonded reinforcement. $A_s = N_c/0.5f_y$ to resist tensile stress resultant, N_c	$0.6f'_c$	(a) $0.25\lambda\sqrt{f'_c}$ (b) $0.50\lambda\sqrt{f'_c}$ at simply supported ends (c) If values above exceeded, provide bonded reinforcement, $A_s = N_c/0.5f_y$ to resist tensile stress resultant, N_c
Final stage After all prestress losses Concrete strength assumed $\approx f'_c$	$0.45f'_c$	(a) $6\sqrt{f'_c}$ in precompressed tensile zone (b) $12\sqrt{f'_c}$ in precompressed tensile zone provided that immediate and long-term deflections based on cracked section analysis are acceptable and provided that concrete covers are increased by 50% if member exposed to earth, weather, or corrosive environment	$0.45f'_c$	(a) $0.5\lambda\sqrt{f'_c}$ in precompressed tensile zone, but may be exceeded provided that adequate deflection, crack control, and fatigue resistance are ensured (b) $0.25\lambda\sqrt{f'_c}$ in precompressed tensile zone exposed to corrosive environment

*The CSA Code used the factor λ to account for low-density concrete ($\lambda = 1.00$ for normal density, 0.85 for semidense, and 0.75 for structural low-density concretes).

centroid of the transformed section (at the c.g.i. level) and the curvature, ϕ , where

$$\epsilon_{cen} = \frac{N - N_o}{E_c A_{trans}} \quad (6-1)$$

$$\phi = \frac{M - M_o}{E_c I_{trans}} \quad (6-2)$$

Sec. 6.5 Calculation of Stresses in the Concrete

where N = applied axial load

N_o = decompression force

E_c = concrete modulus

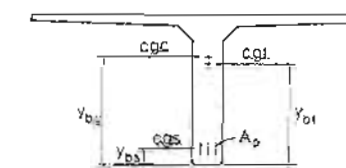
A_{trans} = transformed area of section

M = applied moment

M_o = decompression moment

I_{trans} = moment of inertia of transformed section taken about c.g.c.

The section properties of A_{trans} and I_{trans} can be calculated using the procedures of Section 5.11(d). For a section with just one significant area of reinforcement, these procedures are summarized in Fig. 6-3.



$$n = E_p/E_c \text{ for long-term } n = E_{p,eff}/E_{c,eff}$$

$$A_{trans} = A_{gross} + (n-1) A_p$$

$$y_{bt} = (A_{gross} y_{bs} + (n-1) A_p y_{bs}) / A_{trans}$$

$$I_{trans} = I_{gross} + A_{gross} (y_{bs} - y_{bt})^2 + (n-1) A_p (y_{bt} - y_{bs})^2$$

Figure 6-3 Calculation of transformed section properties.

The decompression actions, N_o and M_o , account for the influence of prestressing. If a section is subjected to an axial tension of N_o and a positive moment of M_o , the concrete strains will be zero over the complete section. In determining the concrete stresses under long-term action, creep of the concrete is accounted for by using an effective modulus for the concrete, $E_{c,eff}$, while relaxation of the prestressing steel is accounted for by using an effective modulus, $E_{p,eff}$, when determining the transformed section properties. The effect of shrinkage is accounted for by modifying the decompression actions, N_o and M_o (see the definitions of N_o and M_o in Section 5.11). The resulting short-term and long-term response predictions are illustrated in Fig. 6-4.

Once ϵ_{cen} and ϕ are determined, the distribution of total concrete strains across the section can be drawn (see Fig. 6-5). The strains, ϵ_{cf} , caused by stress, are found by subtracting the shrinkage (and thermal strains if present) from the total concrete strains, as shown in Fig. 6-5. All that remains is then to multiply the strains caused by stress by the appropriate concrete modulus to determine the stresses (i.e., $f_c = E_c \epsilon_{cf}$).

If the tendons are not bonded to the surrounding concrete, the strain in the tendon will not be directly related to the strain in the surrounding concrete. One conservative approach

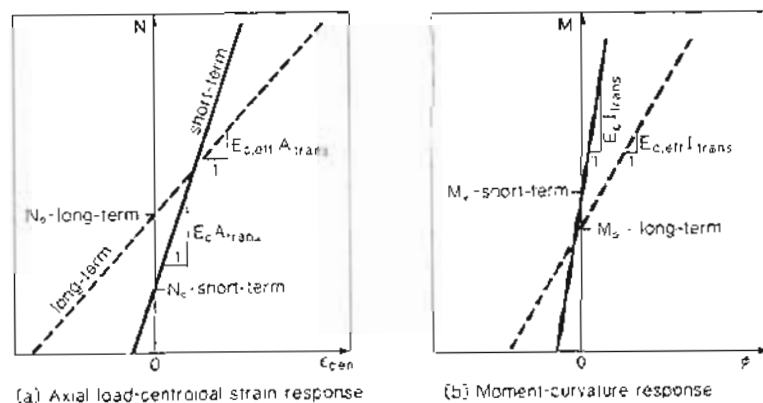


Figure 6-4 Short-term and long-term elastic responses.

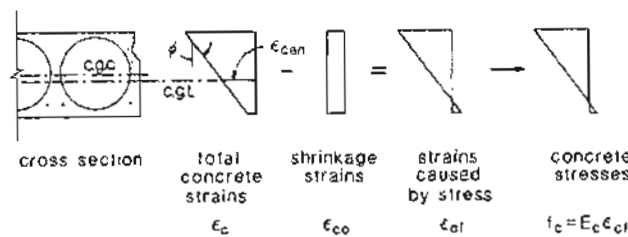


Figure 6-5 Determining concrete stresses from total concrete strains.

is to assume that the strain in the prestressing tendon remains equal to $\Delta\epsilon_p$ throughout the service life of the member. Thus it is assumed that for long-term loading the stress in the unbonded tendon is equal to $E_{p,eff} \Delta\epsilon_p$. The consequence of the assumption that the strain in the prestressing tendon remains constant is that for unbonded tendons the area of the tendon is neglected when calculating transformed section properties (of course, any reinforcing bars or bonded prestressing tendons are still included in the transformed section). If the ducts containing the unbonded tendons form a significant part of the cross section, the lack of concrete in these areas should be properly accounted for in determining the transformed section properties.

It is important to recognize that in post-tensioned construction the tendons are unbonded during the stressing stage, and hence the procedures for unbonded tendons must be used in determining the stresses at this stage.

(b) "Force-in-the-Tendon" Approach

The strain compatibility approach determines the total concrete strains due to prestressing, external loads, creep, relaxation, shrinkage, and thermal effects at any stage in the life of the member. An alternative approach is to separately determine the self-equilibrating stresses due to prestressing and then to add the stresses due to external actions.

The self-equilibrating forces due to prestressing consist of a tensile force, P , in the tendon and an equal and opposite compressive force, P_e , in the concrete acting at the same locations (see Fig. 6-6). Thus if the force in the tendon is known, the magnitude and location of the force resulting from the concrete stresses is known. The concrete stresses are equivalent to a compressive force of P_e acting at the centroid of the concrete together with a moment of $P_e e$ acting about the centroidal axis of the concrete, where e is the distance from the center of the tendon to the centroid of the concrete (see Fig. 6-6). In this figure S_t and S_b are the section moduli for calculating flexural stresses on the top and bottom faces.

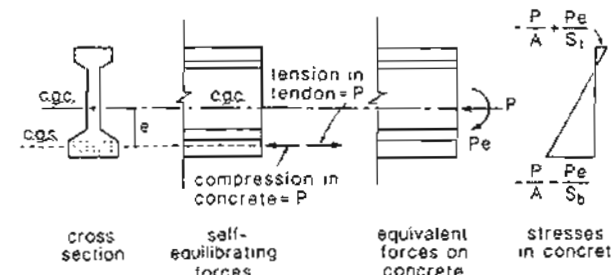


Figure 6-6 Self-equilibrating stresses due to prestressing.

The first step in this approach is to estimate the prestressing force in the tendon. For post-tensioned members the initial prestressing force, $P_i = A_p f_{p,i}$, depends upon the specific details of the post-tensioning operation, such as initial jacking force, stressing sequence, and friction losses. For standard pretensioned members, a reduction in tendon force between jacking and transfer is typically assumed to be 10% for stress-relieved strand and 7.5% for low-relaxation strand (Ref. 6-3).

To estimate the final prestressing force, $P_f = A_p f_{p,f}$, in the tendon after all losses have occurred, it is necessary to account for the influence of creep, shrinkage, and relaxation on the tendon force. Table 6-3 gives suggested values of long-term losses and the values of $f_{p,i}$ and $f_{p,f}$ for the design of standard precast, pretensioned members. The long-term loss values in Table 6-3 are based on a study by Zia, Preston, Scott, and Workman (Ref. 6-4).

If the force in the tendon has been estimated, the stresses in the concrete due to the prestressing can be calculated. These self-equilibrating prestressing stresses are added to the stresses due to external loads to find the total concrete stresses (see Fig. 6-7). It is important to recognize that when calculating the self-equilibrating concrete stresses by this "force-in-the-tendon" approach, the tendon area must be neglected in determining

Table 6-3 Values of f_{pu} and f_{pf} for precast pretensioned members.

Strand Type $f_{pu} = 270 \text{ ksi}$ (1860 MPa)	$f_{p,des}$	f_{pt} ksi (MPa)	Long-Term Losses ksi (MPa)	f_{pf} ksi (MPa)
Stress-relieved	$0.7f_{pu}$	170 (1172)	35 (240)	135 (932)
Low-relaxation	$0.75f_{pu}$	187 (1290)	30 (210)	157 (1080)

the section properties. When calculating the concrete stresses due to external loads the transformed area of the tendon may be accounted for if the tendon is bonded to the concrete (see Fig. 6-7).

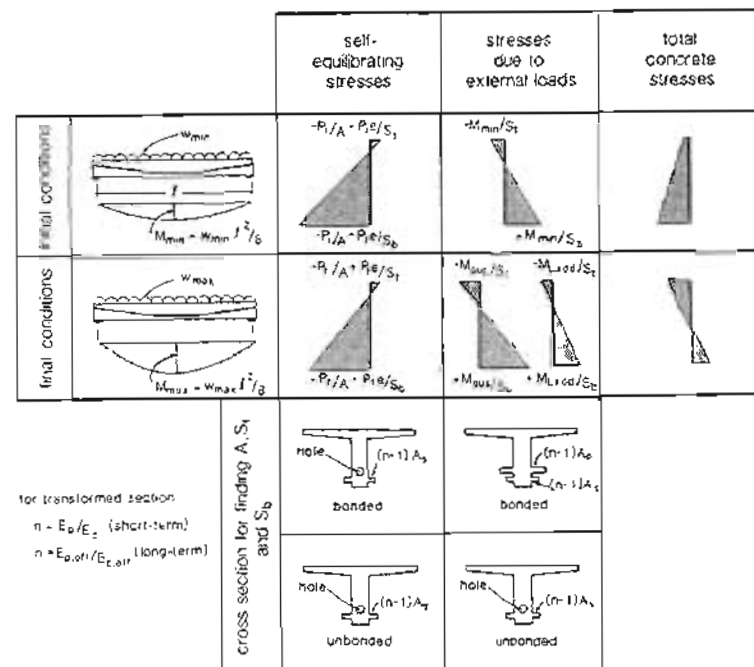


Figure 6-7 Calculating concrete stresses by the "force-in-the-tendon" approach.

An additional point to note is that the transformed section properties used for short-term loads are different than those used for long-term loads. Thus in determining the stresses due to external loads, we should distinguish between sustained loads (dead load plus sustained live loads) and short-term applied loads.

To simplify the calculation of stresses, the gross section properties are often used in determining both the self-equilibrating stresses due to prestress and the stresses due to external loads. This procedure can be unconservative for unbonded, post-tensioned construction if the area of the ducts forms a significant portion of the cross section. For bonded construction, using the gross section properties will be conservative. However, as shown in Fig. 6-8, the gross section modulus may be substantially less than the transformed section modulus for standard precast stemmed deck elements.

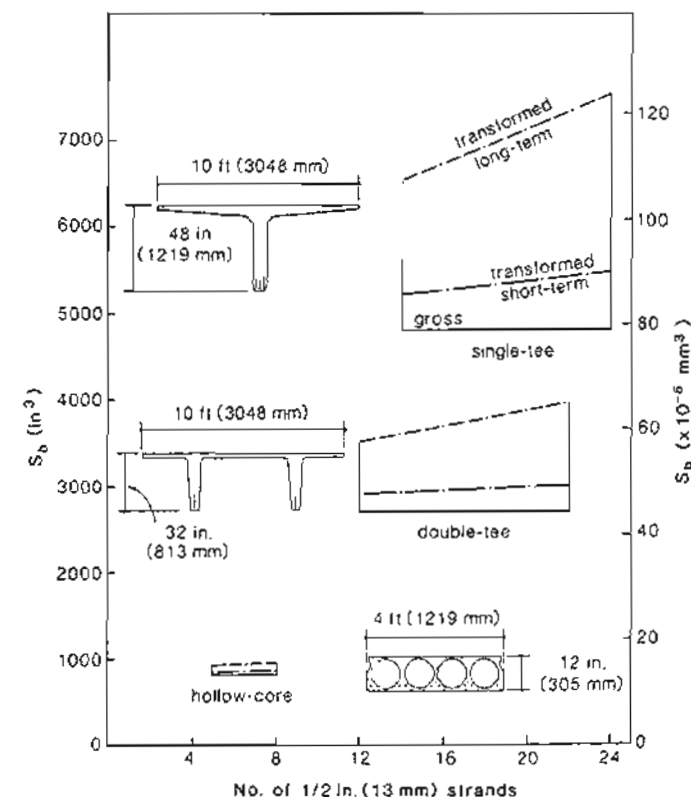


Figure 6-8 Benefits of using transformed section. (n - 1) assumed to be 5.5 for short term, 22 for long term.

Because the traditional estimates of stresses in the tendon given in Table 6-3 were intended primarily for calculations assuming gross section properties, care must be exercised in using these values in calculations using transformed section properties. The values of $f_{p,f}$ in Table 6-3 are appropriate estimates of the stress in the tendon when the dead-load moment is acting, and hence in calculating concrete stresses due to the dead load, it is not appropriate to use the transformed section properties. Use of the transformed section properties for dead load would imply a further increase in tendon stress due to dead load.

6.6 EXAMPLE OF CALCULATING STRESSES IN THE CONCRETE

A PCI 8ST36 single tee contains fourteen 1/2 in. (13 mm) diameter low-relaxation strands and spans 80 ft (24.4 m). The strands have an eccentricity of 10.29 in. (261 mm) at the ends and have been depressed at midspan to an eccentricity of 22.51 in. (572 mm). The beams are being used for a floor system, which is to be designed for a specified live load of 40 psf (19 kN/m²) and a superimposed dead load of 10 psf (0.48 kN/m²). The concrete strength at transfer, f'_{ct} , is 3500 psi (24 MPa) and the minimum specified 28-day strength, f'_c , is 5000 psi (34.5 MPa); normal-density concrete. The prestressing steel is tensioned to 0.75 $f_{p,u}$ in the tensioning bed. Check if the tensile stress limits given in Table 6-2 are satisfied under full service load.

In investigating the stresses in pretensioned beams that have a single harping point at midspan, it is typical to find that the section located at 40% along the span is somewhat more critical than the section at midspan. Hence in this example we will check the stresses at 0.4 ℓ . The cross-sectional properties at this location are described in Fig. 6-9.

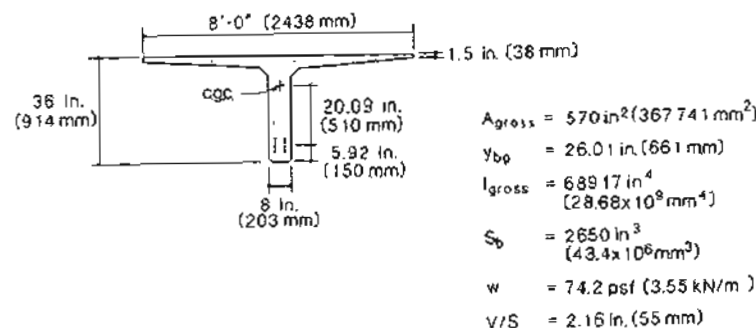


Figure 6-9 Cross-sectional properties of single tee at 0.4 ℓ .

At 0.4 ℓ , the total dead-load moment is 518 ft-kips (702 kNm) and the live-load moment is 307 ft-kips (416 kNm).

In order to satisfy the concrete stress limit given in Table 6-2, the tensile stress in the bottom fiber of the beam should not exceed $6\sqrt{f'_c} = 6\sqrt{5000} = 424$ psi (2.93 MPa).

(a) "Force-in-the-Tendon" Approach Using Gross Section Properties

From Table 6-3 the stress in the tendon after all losses is assumed to be 157 ksi (1080 MPa). Hence

$$\begin{aligned} P_f &= 14 \times 0.153 \times 157 \\ &= 336 \text{ kips (1496 kN)} \end{aligned}$$

From the expression in Fig. 6-7, the tensile stress in the bottom fiber is

$$\begin{aligned} f_b &= -\frac{P_f}{A} - \frac{P_f e}{S_b} + \frac{M_{max}}{S_b} \\ &= -\frac{336 \times 10^3}{570} - \frac{336 \times 10^3 \times 20.09}{2650} + \frac{(518 + 307) \times 10^3 \times 12}{2650} \\ &= -589 - 2547 + 3736 \\ &= +600 \text{ psi (4.14 MPa)} \end{aligned}$$

Hence according to these calculations, more prestressing steel would be required in the beam to satisfy the stress limits.

(b) "Force-in-the-Tendon" Approach Using Transformed Section Properties

In using the transformed section approach, different cross-sectional properties must be used in calculating the different stress components (see Fig. 6-7). The self-equilibrating stresses due to prestress and the stresses due to dead load should be calculated using the net transformed section, which does not include the prestressing steel. The stresses due to live loads are calculated using the transformed section properties distinguishing between long-term loads and short-term loads.

For short-term loading,

$$\begin{aligned} E_c &= 57,000\sqrt{5000} \\ &= 4030 \text{ ksi (27787 MPa)} \end{aligned}$$

and

$$E_p = 29,000 \text{ ksi (200,000 MPa)}$$

Hence

$$\begin{aligned} n - 1 &= \frac{29,000}{4030} - 1 \\ &= 6.20 \end{aligned}$$

For long-term loading, loads are first applied when the concrete strength is 3500 psi (34.5 MPa). Assume a creep coefficient of 2.40.

$$\begin{aligned} E_{c,eff} &= \frac{E_c}{1 + \phi(t, t_i)} \\ &= \frac{57,000\sqrt{3500}}{1 + 2.4} \\ &= 992 \text{ ksi (6840 MPa)} \end{aligned}$$

and assuming that the relaxation loss in the prestressing strand is 3%,

$$\begin{aligned}E_{p,eff} &= 0.97 E_p \\&= 28,130 \text{ ksi (194,000 MPa)}$$

Hence

$$\begin{aligned}n - 1 &= \frac{28,130}{992} - 1 \\&= 27.36\end{aligned}$$

The resulting section properties are given in Table 6-4.

Table 6-4 Sectional properties for single-tee member.

	Gross	Net	Transformed	
			Short-term (n - 1) = 6.20	Long-term (n - 1) = 27.36
$A, \text{ in}^2$ (mm^2)	570 (367,741)	568 (366,451)	583 (376,128)	629 (405,806)
$y_b, \text{ in.}$ (mm)	26.01 (661)	26.09 (663)	25.53 (649)	24.14 (613)
$S_b, \text{ in}^3$ (mm^3)	2650 (43.4×10^6)	2609 (42.8×10^6)	2902 (47.6×10^6)	3744 (61.4×10^6)

Assuming that 30% of the live load is sustained, the long-term live-load moment on the section is $0.3 \times 307 = 92$ ft-kips (325 kNm) while the additional short-term live-load moment will be $0.7 \times 307 = 215$ ft-kips (291 kNm). Hence the calculated tensile stress in the bottom fiber is

$$\begin{aligned}f_b &= -\frac{P_f}{A_n} - \frac{P_f \epsilon}{S_{bn}} + \frac{M_{dead}}{S_{bn}} + \frac{0.3M_L}{S_{btxc}} + \frac{0.7M_L}{S_{bt}} \\&= -\frac{336 \times 10^3}{568} - \frac{336 \times 10^3 \times (26.09 - 5.92)}{2609} + \frac{518 \times 10^3 \times 12}{2609} \\&\quad + \frac{92 \times 10^3 \times 12}{3744} + \frac{215 \times 10^3 \times 12}{2902} \\&= -592 - 2598 + 2383 + 295 + 889 \\&= +377 \text{ psi (2.60 MPa)}$$

Hence these more accurate calculations show that the tensile stress in the bottom fiber is less than the code limit of 424 psi (2.93 MPa).

(c) Strain Compatibility Approach

We will first calculate the stresses in the concrete due to long-term loads which consist of the dead load plus 30% of the live load. These calculations are summarized below. It is assumed that the concrete shrinkage strain is -0.48×10^{-3} .

$$\Delta \epsilon_p = \frac{0.75 \times 270}{29,000} = 6.98 \times 10^{-3}$$

From Eq. (5-35),

$$\begin{aligned}N_o &= E_{p,eff} \Delta \epsilon_p A_p - E_{c,eff} \epsilon_{co} A_c \\&= 28,130 \times 6.98 \times 10^{-3} \times 14 \times 0.153 - 992 \times (-0.48 \times 10^{-3}) \times 568 \\&= 421 + 270 = +691 \text{ kips (3074 kN)}$$

From Eq. (5-36),

$$\begin{aligned}M_o &= E_{p,eff} \Delta \epsilon_p A_p (y_{bt} - y_{bs}) + E_{c,eff} \epsilon_{co} A_c (y_{bg} - y_{bt}) \\&= 421 \times (24.14 - 5.92) - 270 \times (26.09 - 24.14) \\&= 7671 - 527 = +7145 \text{ in.-kips (807 kNm)}$$

From Eq. (6-1),

$$\begin{aligned}\epsilon_{cen} &= \frac{N - N_o}{E_{c,eff} I_{trans}} \\&= \frac{0 - 691}{992 \times 629} \\&= -1.107 \times 10^{-3}\end{aligned}$$

From Eq. (6-2),

$$\begin{aligned}\phi &= \frac{M - M_o}{E_{c,eff} I_{trans}} \\&= \frac{(518 + 92) \times 12 - 7145}{992 \times 90,364} \\&= +1.95 \times 10^{-6} \text{ rad/in. (+76.8} \times 10^{-6} \text{ rad/m)}$$

The total concrete strain in the bottom fiber due to long-term loads is thus

$$\begin{aligned}\epsilon_c &= \epsilon_{cen} - \phi y \\&= -1.107 \times 10^{-3} - 1.95 \times 10^{-6} \times (-24.14) \\&= 1.060 \times 10^{-3}\end{aligned}$$

As the concrete shrinkage strain is -0.48×10^{-3} , the strain in the bottom fiber due to stress is

$$\begin{aligned}\epsilon_{cf} &= \epsilon_c - \epsilon_{co} \\&= -1.060 \times 10^{-3} - (-0.48 \times 10^{-3}) = -0.580 \times 10^{-3}\end{aligned}$$

Hence the stress in the bottom fiber due to sustained loads is $-0.580 \times 10^{-3} \times 992 = -575$ psi (3.97 MPa). The remaining 70% of the live load is considered to be applied as a short-term loading. This will increase the stress in the bottom fiber by $215 \times 10^3 \times 12 / 2902 = 889$ psi (6.13 MPa). Hence the total stress in the bottom fiber is $(-575) + 889 = +314$ psi (2.17 MPa).

While this approach requires more calculations, it does not depend on an assumed stress level in the tendon and hence gives the most accurate estimate of the tensile stress in the concrete.

6.7 CONTROL OF CRACK WIDTHS

Crack widths need only be investigated in partially prestressed concrete members and in non-prestressed concrete members. The crack width limits implied in the ACI Code (Ref. 6-1) are summarized in Table 6-5 for non-prestressed members. Also shown are the corresponding limits for partially prestressed members given in the CSA Code (Ref. 6-2).

Table 6-5 Code limits on z and corresponding average crack widths. Data from Refs. 6-1, 6-2, and 6-3

Type Exposure	Non-Prestressed		Partially Prestressed	
	Interior	Exterior	Interior	Exterior
Maximum z , kips/in. (kN/mm)	175 (30)	145 (25)	317 (20)	88 (15)
Corresponding w_{max} , in. (mm)	0.016 (0.40)	0.013 (0.33)	0.011 (0.27)	0.008 (0.20)

In comparing the crack width limits above with the CEB-FIP (Ref. 6-6) recommended crack width limits of Table 3-17, it is important to recognize that CEB-FIP is referring to crack widths calculated at what they call the "frequent load level," which means the dead load plus the frequently occurring live load, while the ACI and CSA Codes check crack control for the full service load.

For a partially prestressed member the average crack width under specified loading can be calculated using the procedures described in Sections 5.15 and 5.16. That is, the average crack width, w_m , is calculated by multiplying the average calculated concrete tensile strain at the extreme tension fiber, ϵ_{cf} , by the average crack spacing, s_m . The maximum crack width is then assumed to be $1.7w_m$.

In lieu of directly calculating crack widths in prestressed members, the ACI Code permits checking crack control by calculating a crack control parameter, z , where

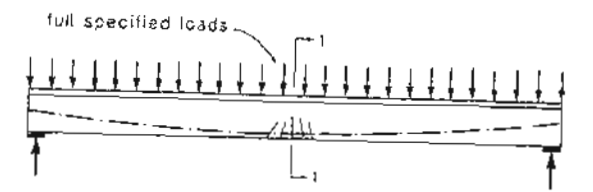
$$z = f_s \sqrt[3]{d_c A} \quad \text{ksi and in.} \quad (6-3)$$

$$z = f_s \sqrt{d_c A} \times 10^{-3} \quad \text{MPa and mm}$$

The terms d_c and A are defined in Fig. 6-10. The calculated value of z should not exceed the limits given in Table 6-5.

6.8 CAMBER AND DEFLECTIONS

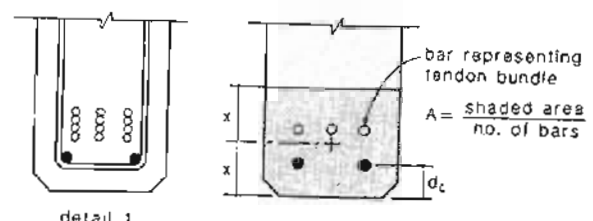
The ACI Code requires that the deflections of prestressed concrete beams due to both "short-term" live loads and "long-term" dead loads and sustained live loads be calculated. In calculating long-term camber and deflections, creep and shrinkage of the concrete and relaxation of the steel are to be taken into account. Further, for partially prestressed members the reduction in stiffness caused by cracking is to be considered. The computed deflections are not to exceed the limits given in Table 6-6.



(a) Single tee with moment M at midspan under specified loads



(b) Calculation of I_s



(c) Definition of A and d_c

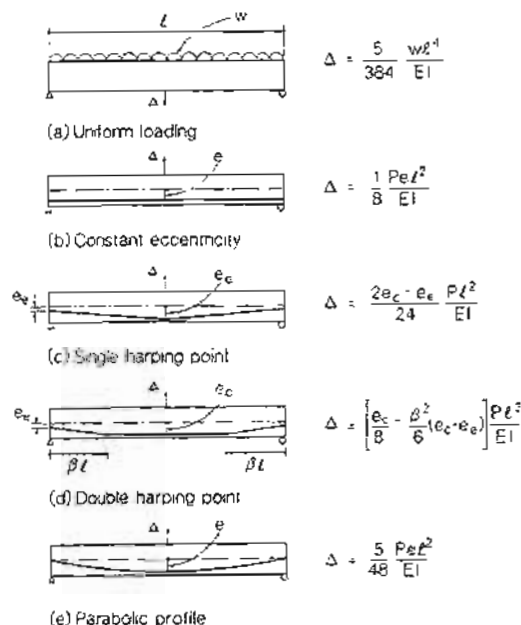
Figure 6-10 Parameters for calculating z .

For partially prestressed concrete members the deflections can be computed from the calculated moment-curvature response using the procedures explained in Sections 5.13 and 5.14. The deflections of members that remain uncracked under service loads can be calculated in a more straightforward manner.

If the strain compatibility approach is being used, the curvature can be found from Eq. (6-2). If the "force-in-the-tendon" approach is being used, the curvature of the beam can be found by superimposing the curvature due to the applied moment, M , and the curvature resulting from the eccentric prestress. In determining the resulting deflections, the expressions given in Fig. 6-11 are useful.

Table 6-6 Maximum permissible computed deflections. From Ref. 6-1.

Type of Member	Deflection to Be Considered	Deflection Limitation
Roof member	Immediate deflection due to specified live load	$\ell/180$
Floor member	Immediate deflection due to specified live load	$\ell/360$
Roof or floor supporting or attached to nonstructural element likely to be damaged by large deflection	Sum of long-term deflection due to all sustained loads that occurs after attachment of nonstructural element and immediate deflection due to additional live load	$\ell/480$
Roof or floor supporting or attached to nonstructural element not likely to be damaged by large deflection		$\ell/240$

Figure 6-11 Expressions for deflections due to uniform load, w , and camber due to tendon force, P .

6.9 DESIGN FOR FLEXURAL STRENGTH AND DUCTILITY

The ACI Code utilizes a partial safety factor approach in which factors are applied to both the loads and the resistances. The flexural strength requirement is that the design strength of the member must be equal to or greater than the required moment strength, that is, $\phi M_n \geq M_u$, where M_n is the nominal flexural strength of the section, $\phi = 0.90$ and M_u is the factored moment due to external loads. Thus for a simply supported beam carrying a uniformly distributed live load, w_L , and having a uniformly distributed dead load, w_D , the factored moment at midspan is

$$M_f = \frac{(1.40w_D + 1.70w_L)\ell^2}{8} \quad (6-4)$$

The nominal flexural strength is computed assuming that the member dimensions and details along with the material properties are as indicated on the structural drawings. The nominal flexural strength, M_n , can be determined using the plane-sections analysis procedures described in Chapter 5. That is, M_n would be the highest moment obtained from a full response prediction.

Rather than determining M_n from the complete moment-curvature response, we can assume that the maximum moment resistance will occur when the top fiber reaches a compressive strain of -0.003. The equivalent rectangular stress-block factors corresponding to this assumed strain are given by the ACI Code as

$$\alpha_1 = 0.85 \quad (6-5)$$

and

$$\begin{aligned} \beta_1 &= 0.85 \quad (\text{for } f'_c \leq 4000 \text{ psi}) \\ &= 0.85 - (f'_c - 4000)0.00005 \geq 0.65 \quad (\text{for } f'_c > 4000 \text{ psi}) \end{aligned} \quad (6-6)$$

The resulting plane-sections analysis for determining M_n is illustrated in Fig. 6-12.

The strain compatibility approach described above is suitable for bonded tendons. Bonded tendons exhibit large stress increases in regions of high moment (particularly at crack locations), while unbonded tendons have stresses which are averaged out over the total length between anchorages (see Fig. 6-13). An iterative analysis procedure that takes account of the uniformity of the force in unbonded tendons along the length of a member is described in Sections 5.20 and 5.21.

In lieu of determining f_{ps} from a strain compatibility analysis, the ACI Code gives the following approximate expressions for the prestressing steel stress at the maximum moment:

(a) For Members with Bonded Tendons

$$f_{ps} = f_{pu} \left(1 - \frac{\gamma_p}{\beta_1} \left[\rho_p \frac{f_{pu}}{f'_c} + \frac{d}{d_p} (\omega - \omega') \right] \right) \quad (6-7)$$

where γ_p = factor accounting for the shape of the stress-strain relationship of the prestressing steel.

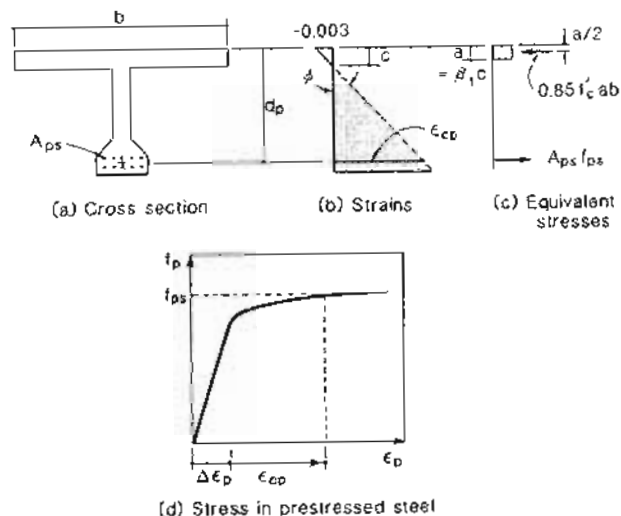


Figure 6-12 Strain compatibility analysis for beam with bonded tendons.

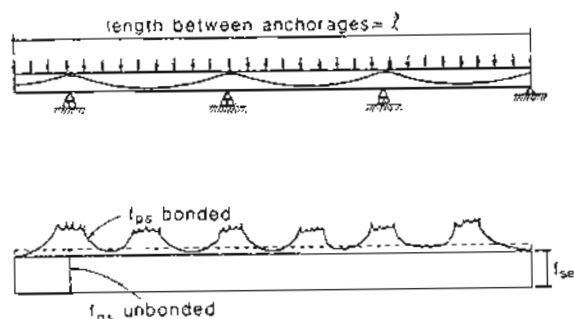


Figure 6-13 Tendon stress variation for unbonded and bonded tendons.

- $\gamma_p = 0.4$ for $f_{py}/f_{pu} \geq 0.85$ (stress-relieved strand)
- $\gamma_p = 0.28$ for $f_{py}/f_{pu} \geq 0.90$ (low-relaxation strand)
- $\rho_p = \text{ratio of prestressed reinforcement} = A_{ps}/bd_p$
- d = distance from extreme compression fiber to centroid of non-prestressed reinforcement
- d_p = distance from extreme compression fiber to centroid of prestressed reinforcement

$$\omega = \rho f_y/f'_c, \text{ where } \rho \text{ is the ratio of non-prestressed reinforcement}$$

(i.e., $\rho = A_s/bd$)

$$\omega' = \rho' f_y/f'_c, \text{ where } \rho' \text{ is the ratio of compression reinforcement}$$

(i.e., $\rho' = A'_s/bd$)

Due to the empirical nature of Eq. (6-7), it is restricted to members in which the effective stress, f_{se} , in the prestressed reinforcement after all losses is not less than $0.5 f_{pu}$. In addition, if compression reinforcement is accounted for in Eq. (6-7) (i.e., $\omega' > 0$), the term inside the square brackets must not be taken greater than 0.17. Since Eq. (6-7) assumes that the compression reinforcement is yielding, then the distance, d' , from the extreme compression fiber to the centroid of the compression steel must be limited. If d' is greater than $0.15d_p$, then ω' is taken as zero.

Applying Eq. (6-7) to the single-tear beam investigated in Section 5.9 gives

$$f_{ps} = 270 \left(1 - \frac{0.28}{0.80} \left[\frac{2.142}{96 \times 28} \cdot \frac{270}{5} + 10 \right] \right)$$

$$= 266 \text{ ksi (1834 MPa)}$$

With this value of f_{ps} we have

$$a = \frac{2.142 \times 266}{0.85 \times 5 \times 96} = 1.40 \text{ in. (35 mm)}$$

$$M_n = 2.142 \times 266 \left(28 - \frac{1.40}{2} \right)$$

$$= 15,555 \text{ in.-kips (1758 kNm)}$$

This estimate of the flexural strength of the tee-beam is virtually identical to that calculated in Section 5.9.

(b) For Members with Unbonded Tendons

Based on the work of Mattock, Yamazaki, and Kattula (Ref. 6-7) the ACI Code gives the following expression for evaluating the stress, f_{ps} , in unbonded prestressing tendons in members with span-to-depth ratios of 35 or less:

$$f_{ps} = f_{se} + 10,000 + \frac{f'_c}{100 \rho_p} \quad \text{psi} \quad (6-8a)$$

but not greater than f_{py} nor $f_{se} + 60,000$ psi.

$$f_{ps} = f_{se} + 69 + \frac{f'_c}{14,500 \rho_p} \quad \text{MPa} \quad (6-8b)$$

but not greater than f_{py} nor $f_{se} + 414$ MPa.

For members with larger span-to-depth ratios, the following expressions are used:

$$f_{ps} = f_{se} + 10,000 + \frac{f'_c}{300 \rho_p} \quad \text{psi} \quad (6-9a)$$

but not greater than f_{py} nor $f_{sc} + 30,000$ psi.

$$f_{ps} = f_{sc} + 69 + \frac{f'_c}{43,500 \rho_p} \quad \text{MPa} \quad (6-9b)$$

but not greater than f_{py} nor $f_{sc} + 207$ MPa. Both Eqs. (6-8) and (6-9) are restricted to members in which the effective stress, f_{sc} , in the unbonded tendons after all losses is not less than $0.5f_{pu}$.

For the unbonded rectangular beam investigated in Section 5.21, the span-to-depth ratio is 108 in./12 in. = 9.0. Applying Eq. (6-8) to this member gives a predicted stress increase equal to $10,000 + f'_c/100 \rho_p$, where

$$\begin{aligned} \rho_p &= \frac{A_{ps}}{bd_p} \\ &= \frac{4 \times 0.08}{6 \times 8.30} = 0.00643 \end{aligned}$$

Hence

$$\begin{aligned} \Delta f_{ps} &= 10,000 + \frac{4930}{100 \times 0.00643} \\ &= 17,667 \text{ psi} = 17.7 \text{ ksi (122 MPa)} \end{aligned}$$

Recall that the stress increase determined by Janney, Hognestad, and McHenry (Ref. 5-17) from strain measurements was 37.4 ksi (538 MPa).

As well as providing adequate flexural capacity, we must ensure that the member has sufficient ductility to provide warning of impending failure and to provide the ability to absorb considerable energy prior to collapse. As shown in Fig. 6-14, the member will have a ductile response if it possesses adequate postcracking capacity and if the steel "yields" prior to crushing of the concrete. To ensure adequate postcracking capacity, the ACI Code requires that $\phi M_n \geq 1.2M_{cr}$. This check is usually applied only at the critical section (e.g., at midspan of a simply supported beam). To satisfy this limit it may sometimes be necessary to add a small amount of non-prestressed reinforcement. This requirement may be waived if the flexural and shear strengths provided are at least twice the required strengths.

To ensure "yield" of the reinforcement, the ACI Code limits the reinforcement index as follows:

1. For a member with prestressing steel only:

$$\omega_p \leq 0.36\beta_1 \quad (6-10)$$

where ω_p is the reinforcement index for prestressing steel, equal to $\rho_p f_{ps}/f'_c = A_{ps} f_{ps}/(bd_p f'_c)$.

2. For a member containing prestressing reinforcement, tension reinforcing bars, and compression reinforcement:

$$\omega_p + (\omega - \omega') \frac{d}{d_p} \leq 0.36\beta_1 \quad (6-11)$$

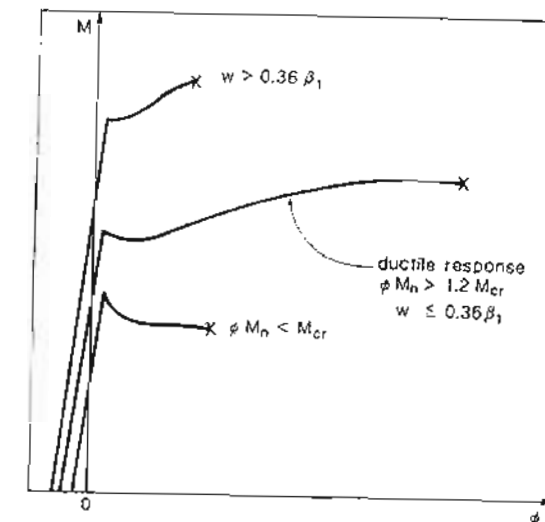


Figure 6-14 Flexural ductility requirements for member with only prestressed reinforcement.

where ω is the reinforcement index for non-prestressed tension steel, equal to $\rho f_y/f'_c = A_s f_y/(bd f'_c)$ and ω' is the reinforcement index for non-prestressed compression steel, equal to $\rho' f_y/f'_c = A'_s f_y/(bd f'_c)$.

3. For a flanged section:

$$\omega_{pw} + (\omega_w - \omega'_w) \frac{d}{d_p} \geq 0.36 \quad (6-12)$$

where ω_{pw} , ω_w , ω'_w are the reinforcement indices as computed for ω_p , ω , and ω' , with b taken as the web width and the reinforcement area is the area required to develop the compressive strength of the web only.

If reinforcement in excess of that given by Eqs. (6-10) to (6-12) is provided, the design moment strength shall not exceed the moment strength based on the compression portion of the moment couple. That is, a rectangular section of width, b , containing only prestressing steel in the tension zone with $\omega_p > 0.36\beta_1$, would have a design strength of

$$\phi M_n = \phi 0.85 f'_c ab(d_p - \frac{a}{2}) \quad (6-13)$$

In addition to the requirements above, beams and one-way slabs containing unbonded tendons must contain a minimum area, A_s , of bonded reinforcement given by

$$A_s = 0.004A \quad (6-14)$$

where A is the area of the cross section that is between the centroid of the cross section and the extreme tension fiber. This minimum area of bonded reinforcement must be uniformly distributed over the precompressed tension zone and placed as close as is practical to the extreme tension fiber. The minimum amounts of bonded reinforcement required in two-way flat plates are described in Chapter 11.

6.10 THE DESIGN PROCESS

The designer of a prestressed concrete beam must determine the cross-sectional dimensions, the material properties, the tendon profile, the required prestressing force, the required area of reinforcing bars, and the specific details of how this reinforcement will be placed.

The designer must ensure that the stress limits are not violated, that the deflections are within acceptable limits, and that the member has adequate strength. Further discussion on how these various design constraints can be satisfied is given below.

(a) Choice of Cross Section

Usually, the type of prestressed concrete member and the sequence of construction have been chosen as part of the initial conceptual design. In this regard, Fig. 6-15 is useful in deciding on the appropriate type and size of standard precast, pretensioned elements.

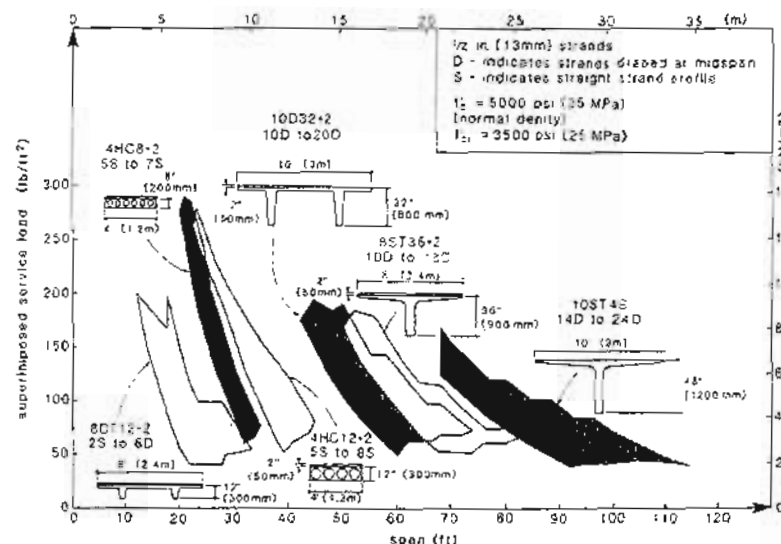


Figure 6-15 Span and load ranges for standard deck elements.

Sec. 6.10 The Design Process

After the type of element has been selected, it is usual practice to choose the overall member depth based on the typical span-to-depth ratios listed in Fig. 6-16. After a preliminary choice of cross section has been made, the dead load of the member can be calculated and we can then proceed to investigate the design limits.

Type of element	Live load psi (kN/m ²)	Span/depth, E/h ratio
	<dead load	40
	50 (2.4) 100 (4.8)	40-50 32-42
	50 (2.4) 100 (4.8)	20-30 18-28
	50 (2.4) 100 (4.8)	23-32 19-24
	<dead load	20
	<dead load	30
	highway loading	18

Figure 6-16 Typical span-to-depth ratios for simply supported prestressed concrete members.

(b) Satisfying Stress Limits

The limits on the tensile stress in the tendon, given in Table 6-1, are satisfied by choosing a conservative upper limit for the stress induced in the strand during tensioning.

In order to check the concrete stress limits given in Table 6-2, it is necessary to investigate various stages in the life of the beam. Thus if we are considering the stresses at midspan of a simply supported beam, it is necessary to consider at least the following two stages:

1. The initial stage when the prestress force has its highest value, P_i , the young concrete still has a relatively low strength, f'_c , and the moment is at its lowest value, M_{min} . At this stage we are concerned with limiting the tensile stress on the top face of the beam and limiting the compressive stresses on the bottom face.
2. The final stage when the prestress force has its lowest value, P_f , the concrete has reached a compressive strength of at least f'_c , and the moment is at its highest value, M_{max} . At this stage we are concerned about limiting the tensile stress on the bottom face and limiting the compressive stress on the top face.

In determining values of prestressing force and eccentricity that will satisfy the stress limits, it is important to realize that it is the concrete tensile stress limits which are usually critical. To understand how these tensile stress limits may be satisfied, it is helpful to consider the case where no tension is permitted in the concrete.

Figure 6-17 illustrates the initial and final conditions for the stresses in the concrete for situations which just meet the requirement that there be no tension in the concrete. The initial low moment, M_{min} , is resisted by an internal couple consisting of the tensile force, P_i , in the tendon balanced by an equal compressive force in the concrete. For the condition of zero tension on the top face, the resultant compressive force in the concrete must be located at the bottom kern point (i.e., a distance $k_b = S_t/A$ from the centroid). Hence to avoid tension on the top face of the beam.

$$P_i \leq \frac{M_{min}}{e - k_b} \quad (6-15)$$

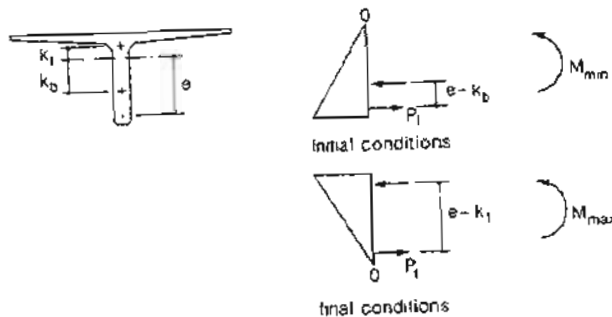


Figure 6-17 Conditions with zero tension in concrete.

Under the final conditions (see Fig. 6-17) the large moment at midspan, M_{max} , is resisted by an internal couple consisting of the tensile force, P_f , in the tendon and the balancing compressive force, P_f , in the concrete. For the condition of zero tension on the bottom face, the compressive force in the concrete must be located at the top kern point (i.e., a distance of $k_t = S_b/A$ from the centroid). Hence to avoid tension on the bottom

face of the beam,

$$P_f \geq \frac{M_{max}}{e + k_t} \quad (6-16)$$

The distance, $e + k_t$, in Eq. (6-16) is the lever arm of the internal couple (see Fig. 6-17). The larger this lever arm, the smaller is the required value of the prestressing force, and hence the more efficient is the section. Figure 6-18 gives approximate values of $e + k_t$ for typical prestressed concrete sections. These values are useful in preliminary design.

Cross section shape	$e + k_t$	$k_t + k_b$
	0.50 h	0.33 h
	0.47 h	0.33 h
	0.58 h	0.49 h
	0.70 h	0.43 h
	0.76 h	0.48 h
	0.64 h	0.51 h
	0.82 h	0.56 h

Figure 6-18 Approximate values of flexural lever arms for preliminary service load design.

Equations (6-15) and (6-16) can be rearranged to give

$$P_f(k_t + k_b) \geq M_{max} - \frac{P_f}{P_i} M_{min} \quad (6-17)$$

The term $k_t + k_b$ is the distance the compressive force in the concrete can move, as the moment increases, without producing tension in the concrete and hence is a measure of the variation in moment that can be tolerated. Values of $k_t + k_b$ for typical prestressed concrete sections are given in Fig. 6-18.

It is often the case that the critical stress limit at midspan of a simply supported beam is the limit on the tensile stress on the bottom face under the final conditions. To satisfy this limit it is economical to use the largest possible eccentricity that can be accommodated within the cross section. With the midspan eccentricity chosen, the minimum required prestressing force could be estimated from Eq. (6-16). Figure 6-19 illustrates how the conditions are modified if small tensile stresses are permitted in the concrete. With tension in the concrete the internal lever arm can be smaller under the initial conditions and larger under the final conditions, thus permitting a larger range of moments. The condition that the tensile stress on the bottom face does not exceed f_b can be written as

$$\frac{M_{max}}{S_b} - \frac{P_f}{A} - \frac{P_f e}{S_b} \leq f_b \quad (6-18)$$

which can be rearranged to give

$$P_f \geq \frac{M_{max} - S_b f_b}{e + k_t} \quad (6-19)$$

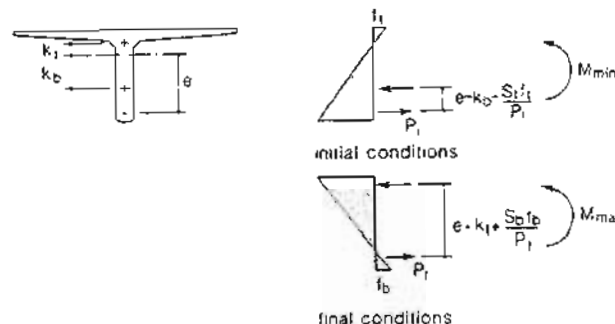


Figure 6-19 Limiting tensile stresses in concrete.

Equation (6-19) can be used to calculate the required prestressing force once a trial cross section and eccentricity have been chosen.

After satisfying the stress limits at midspan, the designer must then consider the stress conditions at other locations within the span. Toward the ends of the beam the main concern is that the tensile stresses at the top face will be excessive. The condition that the tensile stress at the top face does not exceed f_t can be written as

$$\frac{P_f e}{S_t} - \frac{P_f}{A} - \frac{M_{min}}{S_t} \leq f_t \quad (6-20)$$

which can be rearranged to give

$$e \leq k_b + \frac{M_{min} + S_t f_t}{P_f} \quad (6-21)$$

Equation (6-21) can be used to calculate the maximum eccentricities permitted along the span if it is desired to limit the tensile stresses on the top face to f_t . Larger eccentricities can be used if appropriate crack control reinforcement is provided (see Fig. 6-2).

Figure 6-20 illustrates the range of tendon eccentricities corresponding to the stress limits. It can be seen that the use of straight tendons with constant eccentricity from end to end of the beam may cause the stress limits to be exceeded. For post-tensioned tendons a parabolic profile will efficiently satisfy the stress limits both at midspan and at the supports. For pretensioned tendons it may be necessary to use a single harping point at midspan or double harping points at about the third-points of the span to obtain a satisfactory tendon profile.

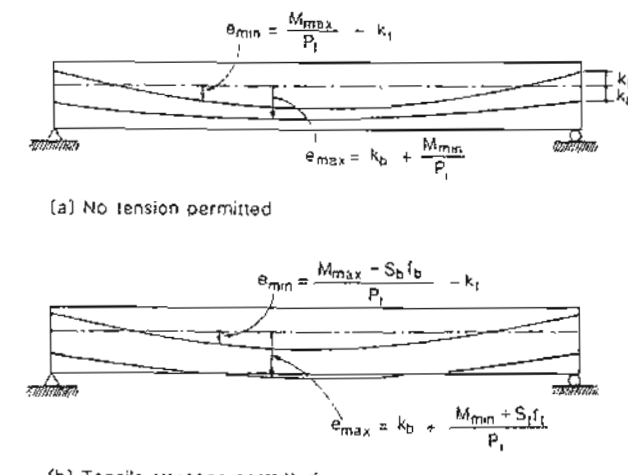


Figure 6-20 Range of tendon eccentricities corresponding to stress limits.

(c) Satisfying Deflection Limits

Prestressing of a simply supported beam causes an upward camber while dead loads and live loads cause a downward deflection. The prestressing force and tendon profile can be chosen so that under one particular level of gravity loading the upward deflection due to prestress cancels out the downward deflection due to the loads. If, for example, it was desired to have zero deflection under uniform dead load, w_d , for a simply supported,

pretensioned beam with a single harping point, zero end eccentricity, and a span ℓ , the final prestressing force, P_f , and midspan eccentricity, e , would, from Fig. 6-11, need to satisfy

$$P_f e = \frac{5}{32} w_d \ell^2 \quad (6-22)$$

For a post-tensioned beam with a parabolic profile the requirement would be

$$P_f e = \frac{w_d \ell^2}{8} \quad (6-23)$$

For this case, the parabolically varying curvatures due to the final prestressing force cancel out the curvatures due to external load all along the span and hence the beam remains straight. The external load for which the beam remains straight is spoken of as the "balanced load."

(d) Satisfying Strength Requirements

Figure 6-21 illustrates the manner in which the flexural strength requirements for a simple span beam can be checked. The nominal flexural resistance, M_n , of the beam is provided by a couple consisting of a tensile force provided by the reinforcement (both prestressed and non-prestressed) and the compressive force in the concrete near the top face of the beam. The lever arm of this couple, jd , is a measure of the flexural efficiency of the section. For efficient sections such as single tees and double tees, jd is about 0.9 h . For such sections, an approximate expression useful in the preliminary choice of reinforcement is

$$\phi M_n = \phi (A_{ps} 0.95 f_{pv} + A_s f_y) 0.9h \quad (6-24)$$

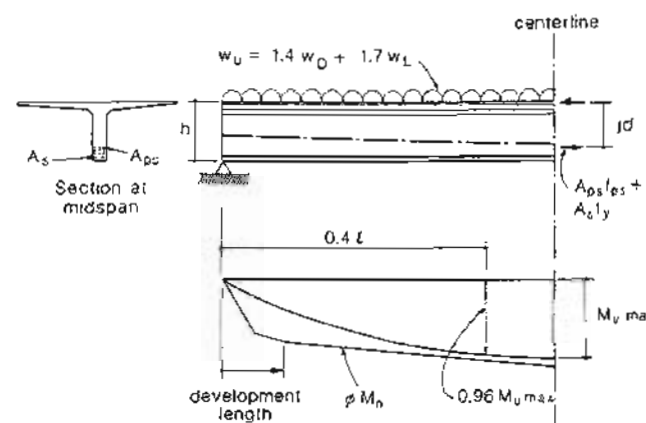


Figure 6-21 Checking that ϕM_n exceeds M_n

In investigating the flexural strength requirements of pretensioned beams which have a single harping point at midspan, it is typical to find that the section located about 40% of the way along the span is somewhat more critical than the section at midspan (see Fig. 6-21).

(e) Sequence of Design

The design of prestressed concrete beams, like most design problems, is an iterative procedure, the first step of which involves an initial estimate of the required cross section and the required prestressing. These initial estimates then enable a detailed check of the design to be made. The sequence of operations in this preliminary design process is illustrated in Fig. 6-22. The entire design procedure is illustrated in the examples given later in this chapter.

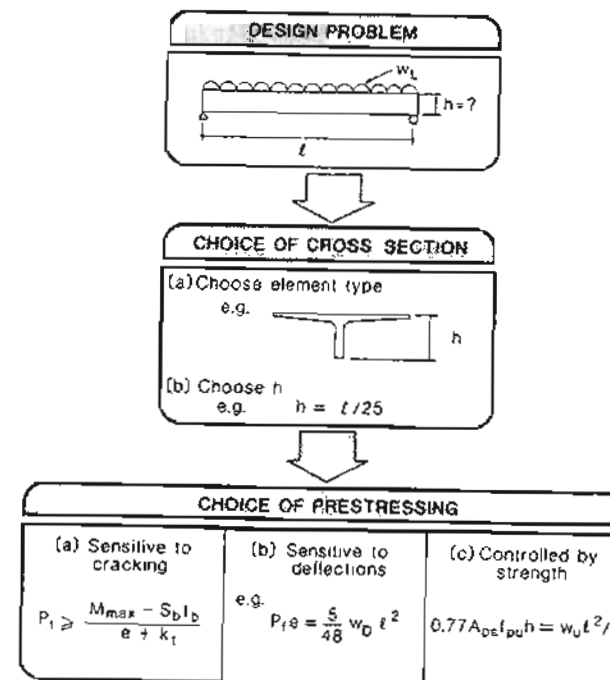


Figure 6-22 Guide to preliminary design.

6.11 ADDITIONAL CONSIDERATIONS FOR COMPOSITE CONSTRUCTION

In the design of all prestressed concrete members it is necessary to consider the different stages in the life of a member (see Fig. 6-1). For noncomposite members, concrete stresses are usually checked for just two stages, the initial stage and the final stage (see Fig. 6-19). For composite construction it is necessary to check at least the following three stages (see Fig. 6-23):

(a) Stage 1 — Initial conditions at transfer

At this stage the prestress force has its highest value, P_i , the concrete has a relatively low strength, f'_c , and the external moment is low, being caused only by the self-weight of the girder.

The stress on the top face of the girder is

$$f_t = -\frac{P_i}{A_g} + \frac{P_i e_g}{S_{tg}} - \frac{M_{dg}}{S_{tg}} \quad (6-25)$$

The stress on the bottom fiber of the girder is

$$f_b = -\frac{P_i}{A_g} - \frac{P_i e_g}{S_{bg}} + \frac{M_{dg}}{S_{bg}} \quad (6-26)$$

where A_g , e_g , S_{tg} , and S_{bg} refer to section properties of the girder alone and M_{dg} is the moment due to self-weight of the girder.

These calculated stresses must satisfy the initial stress limits for the girder concrete.

(b) Stage 2 — Conditions at time of placing wet concrete on girder

For the usual case where the girder is not propped during construction the girder alone must carry its own weight plus the weight of the wet concrete. At this stage, which is some time after prestress transfer, the concrete strength will have reached f'_c while the prestressing force will lie between the initial force, P_i , and the final force, P_f . As a simplification, the prestressing force is conservatively taken as P_f . The concrete stresses at this stage can therefore be calculated as

$$f_t = -\frac{P_f}{A_g} + \frac{P_f e_g}{S_{tg}} - \frac{M_{dg} + M_{ds}}{S_{tg}} \quad (6-27)$$

$$f_b = -\frac{P_f}{A_g} - \frac{P_f e_g}{S_{bg}} + \frac{M_{dg} + M_{ds}}{S_{bg}} \quad (6-28)$$

where M_{ds} is the moment caused by the dead load of the wet concrete and associated formwork. These calculated stresses must satisfy the final stress limits for the girder concrete (e.g., see Table 6-2).

(c) Stage 3 — Final conditions

The hardening of the cast-in-place concrete results in a composite section that will resist all future loading as a unit. Because the precast concrete girder was strained when the

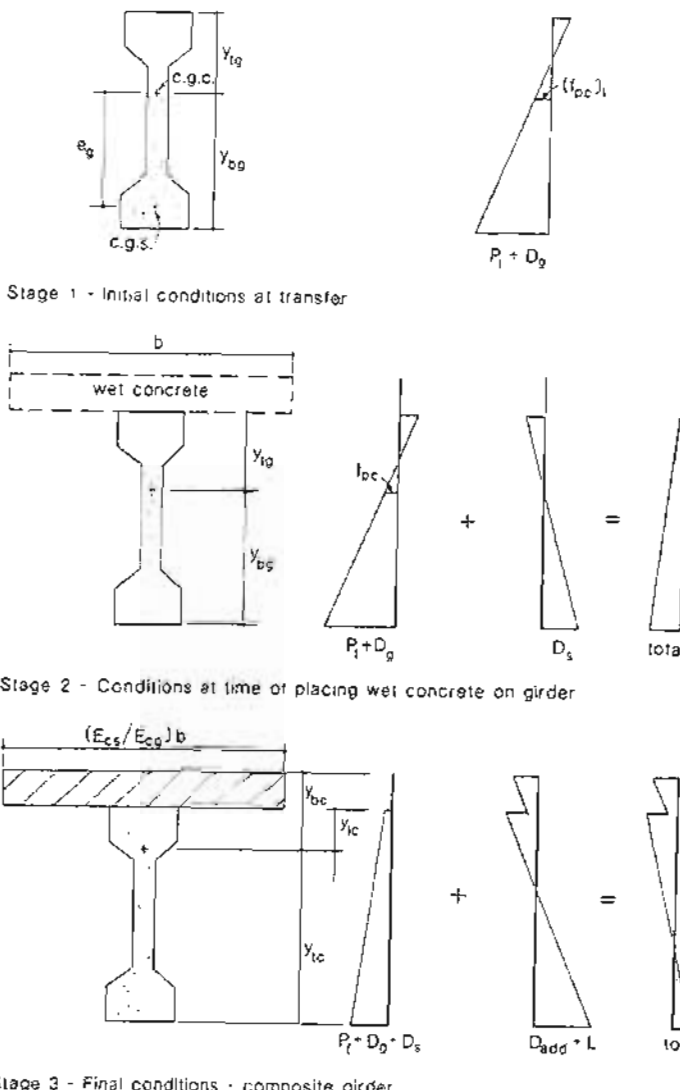


Figure 6-23 Calculation of concrete stresses for composite girder.

cast-in-place concrete was joined to it, there will be a strain discontinuity at the interface of the two concretes, which must be taken into account when predicting the response of the composite girder.

The actual behavior of a composite girder is rather complex, in that with time there will be a redistribution of stresses between the precast concrete and the cast-in-place concrete due to creep and differential shrinkage. Methods for predicting this complex response are discussed in Section 5.17.

For design purposes a simple procedure is typically used to predict the concrete stresses. It is assumed that the stresses on the girder due to prestress (P_f), self-weight of the girder (D_g), and weight of the cast-in-place concrete (D_s) remain unchanged from those calculated in Stage 2. The stresses due to the additional dead load (D_{add}) and the live load (L) are assumed to be resisted by the composite section, with the final stresses being found by summing these two sets of stresses (see Fig. 6-23). In computing the stresses in the composite section the cast-in-place concrete with an elastic modulus of E_{cs} is transformed to an equivalently stiff area of precast concrete, having an elastic modulus of E_{cg} .

The stress at the top face of the composite section, f_{ts} , is

$$f_{ts} = \frac{M_{da} + M_L}{S_{tc}} \cdot \frac{E_{cs}}{E_{cg}} \quad (6-29)$$

where M_{da} is the moment due to additional dead load applied after the cast-in-place concrete hardens, M_L is the live-load moment, and S_{tc} is the section modulus of the composite transformed section.

The stress at the top face of the precast girder is

$$f_{tg} = -\frac{P_f}{A_g} + \frac{P_f e_g}{S_{tg}} - \frac{M_{dg} + M_{ds}}{S_{tg}} - \frac{M_{da} + M_L}{S_{tc}} \quad (6-30)$$

The stress in the bottom face of the precast girder is

$$f_{bg} = -\frac{P_f}{A_g} - \frac{P_f e_g}{S_{bg}} + \frac{M_{dg} + M_{ds}}{S_{bg}} + \frac{M_{da} + M_L}{S_{tc}} \quad (6-31)$$

where S_{tc} and S_{tc} are the section moduli of the composite transformed section for calculating flexural stresses at the interface of the two concretes and at the bottom face, respectively. These calculated stresses must satisfy the final stress limits for the two different concretes. It is useful to recognize that the need to control the tensile stress on the bottom fiber, Eq. (6-31), often governs the choice of the prestressing force.

In addition to investigating the stresses at the three stages listed above, it is necessary to satisfy the strength requirements at both Stage 2 and Stage 3. In checking the flexural strength of the composite section for the final conditions (Stage 3) it is conventional to ignore the strain discontinuity at the interface, but of course to account for the actual strength of the cast-in-place concrete in calculating the depth of the compression zone. In checking the shear strength, the full depth of the composite member is used.

The deflections for composite members can be estimated using the multipliers given in Table 5-10. An example of the design of a composite bridge girder is given in Chapter 13.

6.12 EXAMPLE DESIGN OF DOUBLE-TEE FLOOR MEMBER

The untopped double-tee floor member shown in Fig. 6-24, spans 46 ft (14.0 m) in an office building and carries a service live load of 50 psf (2.4 kN/m²) as well as a superimposed dead load of 15 psf (0.72 kN/m²). The concrete strength at transfer, f'_{ct} , is 3500 psi (24.1 MPa), and the minimum specified 28-day strength is 5000 psi (34.5 MPa) (normal-weight concrete). The prestressing steel is 1/2 in. (13 mm) diameter low-relaxation strand, with an ultimate strength, $f_{pu} = 270$ ksi (1860 MPa), which will be tensioned to $0.75 f_{pu}$ in the pretensioning bed. Design the double tee following the conventional practice of using only prestressing strand for longitudinal reinforcement in the stems.

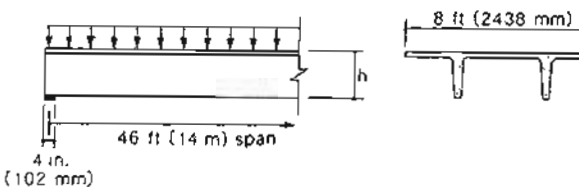


Figure 6-24 Double-tee floor member.

Step 1: Choose depth.

From Fig. 6-16 the span-to-depth ratio should be in the range 20 to 30. A 24 in. (610 mm) deep section would have a span-to-depth ratio of 23. Hence choose a 24 in. (610 mm) deep PCI double tee as shown in Fig. 6-25.

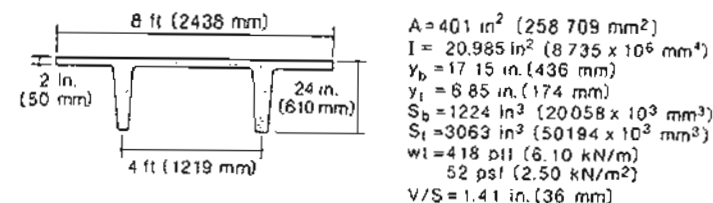


Figure 6-25 Cross section of PCI double tee.

Step 2: Choose prestressing.

We will use the approximate expressions given in Fig. 6-22 to estimate the required amount of prestressing. To use these expressions we will need the maximum service-load moment, M_{max} , and the required moment strength, M_n , at midspan.

$$\begin{aligned}\text{member self-weight} &= 418 \text{ lb/ft (6.10 kN/m)} \\ \text{superimposed dead load} &= 15 \text{ psf} \times 8.0 \text{ ft} \\ &= 120 \text{ lb/ft (1.75 kN/m)} \\ \text{live load} &= 50 \text{ psf} \times 8.0 \text{ ft} \\ &= 400 \text{ lb/ft (5.84 kN/m)}\end{aligned}$$

Maximum service-load moment at midspan:

$$\begin{aligned}M_{max} &= (0.418 + 0.120 + 0.400) \frac{46^2}{8} \\ &= 248 \text{ ft-kips (336 kNm)}\end{aligned}$$

Required moment strength at midspan:

$$\begin{aligned}M_n &= [1.4(0.418 + 0.120) + 1.7 \times 0.400] \frac{46^2}{8} \\ &= 379 \text{ ft-kips (514 kNm)}\end{aligned}$$

From Fig. 6-18 for this double-tee member, $c + k_t$ is about $0.70h = 0.70 \times 24 = 16.8$ in. (427 mm). Hence in order to satisfy the bottom fiber tensile stress limit of $6\sqrt{f'_c} = 6\sqrt{5000} = 424$ psi (3.20 MPa) (see Table 6-2), the required prestressing force from Eq. (6-19) is

$$\begin{aligned}P_f &\geq \frac{M_{max} - S_b f_b}{c + k_t} \\ &\geq \frac{248 \times 12 - 1224 \times 0.424}{16.8} \\ &\geq 146 \text{ kips (651 kN)}\end{aligned}$$

From Table 6-3 the stress in the low-relaxation strands after losses will be about 157 ksi (1080 MPa). Hence the area of strands must satisfy

$$\begin{aligned}A_{ps} &\geq \frac{146}{157} \\ &\geq 0.93 \text{ in}^2 (588 \text{ mm}^2)\end{aligned}$$

From Eq. (6-24), ϕM_n will be about

$$\phi M_n = 0.77 A_{ps} f_{pu} h$$

Hence to satisfy the strength requirement at midspan.

$$0.77 A_{ps} f_{pu} h \geq 379 \text{ ft-kips (514 kNm)}$$

Hence

$$\begin{aligned}A_{ps} &\geq \frac{379 \times 12}{0.77 \times 270 \times 24} \\ &\geq 0.91 \text{ in}^2 (588 \text{ mm}^2)\end{aligned}$$

These preliminary calculations demonstrate that for this case the stress limit is slightly more critical than the strength limit. We will choose a total of six 1/2 in. (13 mm) strands with $A_{ps} = 6 \times 0.153 = 0.92 \text{ in}^2 (592 \text{ mm}^2)$.

Step 3: Choose the tendon profile.

At midspan we will use the maximum possible eccentricity, but at the ends of the member we will reduce the eccentricity to limit the tensile stress on the top face of the beam to $6\sqrt{f'_c} = 6\sqrt{3500} = 355$ psi (2.45 MPa) (see Table 6-2). At the end face of the beam the stress in the prestressing tendon is zero. We will investigate the stress conditions 50 strand diameters from this end face, where the full prestressing force is assumed to be developed in the tendons. To control the tensile stress on the top face, the eccentricity must satisfy Eq. (6-21). Hence

$$e \leq k_b + \frac{M_{max} + S_t f_t}{P_i}$$

where $k_b = S_t/A = 3063/401 = 7.64$ in. (194 mm)

M_{min} = member self-weight moment 25 in. (635 mm) from end face, that is,

$$\begin{aligned}&23 \text{ in. from bearing centerline} \\ &= 0.418 \times 46/2 \times 23 - 0.418 \times 23^2/2 \\ &= 111 \text{ in.-kips (12 kNm)}\end{aligned}$$

$$\begin{aligned}P_i &= A_p f_p \\ &= 0.92 \times 187 \\ &= 172 \text{ kips (765 kN)}\end{aligned}$$

Hence

$$\begin{aligned}e &\leq 7.64 + \frac{111 + 3063 \times 0.355}{172} \\ &\leq 14.6 \text{ in. (371 mm)}\end{aligned}$$

This large value on the upper limit on e indicates that the stress limits at the end of the beam will not be critical. A convenient strand pattern that will easily satisfy this limit is illustrated in Fig. 6-26.

Having completed the preliminary design, we can now check in detail all of the conditions that the member must satisfy.

Step 4: Check the concrete stresses at service loads.

The stresses will be checked at three sections along the length of the member: at midspan, at $0.4L$, and at a location 50 strand diameters from the end of the member, where the full prestress force is first developed.

The stresses will be checked for two conditions: the initial condition when only the self-weight of the member acts, $w = 418 \text{ plf (6.10 kN/m)}$, and the prestress force is at its highest value; and the final conditions when the full service loads are acting, $w = 938 \text{ lb/ft (13.7 kN/m)}$, and all prestress losses have occurred.

The stresses will be calculated using the "force-in-the-tendon" approach and using the gross cross-sectional properties given in Fig. 6-25. The stresses calculated using these

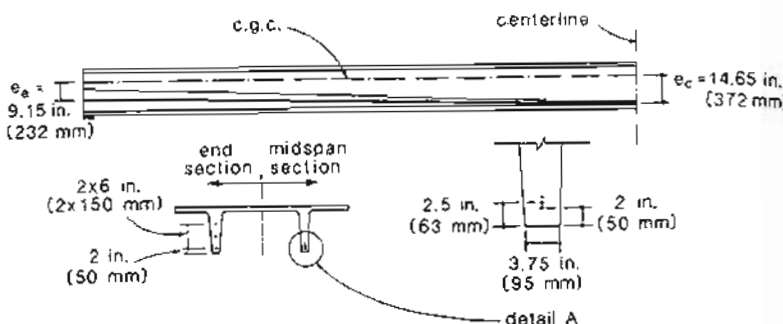


Figure 6-26 Strand profile.

assumptions are listed in Table 6-7. It can be seen that the calculated stresses all satisfy the stress limits. The highest calculated tensile stress occurs at the bottom fiber at the section 0.4 ℓ from the support where the stress is 381 psi (2.63 MPa), which is below the tensile stress limit of 424 psi (2.92 MPa). Hence it can be assumed that the member remains uncracked under service loads.

Table 6-7 Concrete stresses at service loads (psi units).

		50 strand diameters from end ($e = 9.64$ in.)		At 0.4 ℓ ($e = 13.56$ in.)		At midspan ($e = 14.63$ in.)	
		$M_{min} = 111$ in.-kips		$M_{min} = 1247$ in.-kips		$M_{min} = 1327$ in.-kips	
		$M_{max} = 248$ in.-kips		$M_{max} = 2858$ in.-kips		$M_{max} = 2977$ in.-kips	
		Top	Bottom	Top	Bottom	Top	Bottom
Initial condition	$-P_i/A$	-429	-429	-429	-429	-429	-429
Tensile limit $= +177$ psi	$\pm P_{tc}/S$	+541	-1355	+761	-1906	+823	-2059
Compressive limit $= -2100$ psi	$\mp M_{min}/S$	-36	+91	-416	+1041	-435	+1084
	Total	+76	-1693	-84	-1294	-39	-1404
Final condition	$-P_f/A$	-359	-359	-359	-359	-359	-359
Tensile limit $= +424$ psi	$\pm P_{tc}/S$	+453	-1134	+637	-1595	+689	-1724
Compressive limit $= -2250$ psi	$\mp M_{max}/S$	-81	+203	-933	+2335	.972	+2432
	Total	+13	-1290	-653	+381	-642	+349

Step 5: Check the flexural capacities.

The flexural capacity may be critical either at midspan or at 0.4 ℓ (see Fig. 6-21). The effective depth, d_p , of the prestressing tendon at each of these locations is shown in Fig. 6-27.

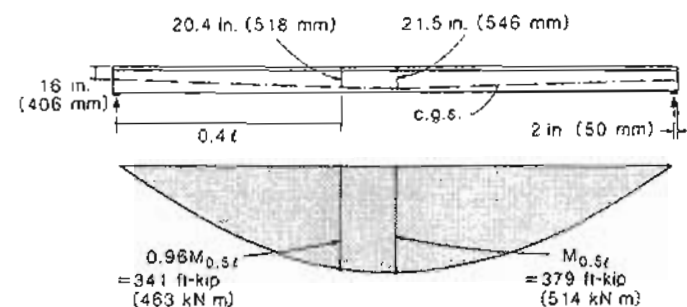


Figure 6-27 Effective depth of prestressing tendon.

(a) At 0.4 ℓ . For this section with only prestressed reinforcement Eq. (6-7) simplifies to

$$f_{ps} = f_{pu} \left(1 - \frac{\gamma_p}{\beta_1} \rho_p \frac{f_{pu}}{f'_c} \right)$$

$$= 270 \left(1 - \frac{0.28}{0.80} \times \frac{0.92}{96 \times 20.4} \times \frac{270}{5} \right)$$

$$= 268 \text{ ksi (1846 MPa)}$$

The equivalent rectangular stress-block depth is

$$a = \frac{A_{ps} f_{ps}}{0.85 f'_c b} = \frac{0.92 \times 268}{0.85 \times 5 \times 96} = 0.60 \text{ in. (15 mm)}$$

Note that $\omega_p = A_{ps} f_{ps} / (bd_p f'_c) = 0.92 \times 268 / (96 \times 20.4 \times 5) = 0.025$, which is less than the ACI Code limit of $0.36\beta_1 = 0.36 \times 0.80 = 0.288$, ensuring that the prestressing steel will "yield" prior to concrete crushing.

The design flexural strength is

$$\phi M_n = \phi A_{ps} f_{ps} (d_p - \frac{a}{2})$$

$$= 0.9 \times 0.92 \times 268 (20.4 - \frac{0.60}{2})$$

$$= 4460 \text{ in.-kips}$$

$$= 372 \text{ ft-kips (504 kNm)}$$

Since $\phi M_n > M_u$, (see Fig. 6-27), the flexural capacity at this section is adequate.

(b) At midspan. At midspan $f_p = 268$ ksi (1846 MPa), $a = 0.60$ in. (15 mm), and $\phi M_n = 392$ ft-kips (532 kNm) which is greater than M_u (see Fig. 6-27). Therefore, the capacity is adequate.

Step 6: Check the reserve of strength after cracking.

The concrete is assumed to crack when the tensile stress reaches the modulus of rupture, $f_r = 7.5\sqrt{f'_c} = 7.5\sqrt{5000} = 530$ psi (3.66 MPa). Under the final conditions, the tensile stress in the bottom fiber at midspan is 349 psi (2.41 MPa). Hence to cause cracking at this location an additional tensile stress of $530 - 349 = 181$ psi (1.25 MPa) is required. This additional tensile stress would be caused by an additional moment of $S_b \times 0.181 = 222$ in.-kips (15 kNm). Thus the cracking moment at midspan will be $2977 + 222 = 3199$ in.-kips (361 kNm). Hence

$$\frac{\phi M_n}{M_{cr}} = \frac{392 \times 12}{3199} = 1.47 > 1.20$$

Hence an adequate reserve of strength exists after cracking.

Step 7: Check the deflections.

Since the member will not crack at service loads, the deflections can be calculated assuming an elastic, uncracked response. We will assume that the partitions used in this office building are "likely to be damaged by large deflections" (see Table 6-6).

(a) *Immediate deflection due to live load.* For this short-term loading,

$$E_c = 57,000\sqrt{f'_c} = 57,000\sqrt{5000} = 4031 \text{ ksi (27,800 MPa)}$$

Hence, from Fig. 6-11,

$$\begin{aligned}\Delta_L &= \frac{5}{384} \frac{wt^4}{EI} \\ &= \frac{5 \times 0.400 \times 46^4 \times 12^3}{384 \times 4031 \times 20,985} \\ &= 0.48 \text{ in. (12 mm)}\end{aligned}$$

The ACI Code limits this immediate deflection to

$$\frac{\ell}{360} = \frac{46 \times 12}{360} = 1.53 \text{ in. (39 mm)}$$

Hence the immediate deflection due to live load is well below the limit.

(b) *Check deflections likely to damage partitions.* To calculate the deflection that will affect the attached partitions, we must first estimate the deflection of the member at the time the partitions were attached. In these calculations, we will use the suggested multipliers given in Table 5-10.

The modulus of the concrete at the time of release of the prestress is

$$\begin{aligned}E_c &= 57,000\sqrt{f'_c} = 57,000\sqrt{3500} \\ &= 3372 \text{ ksi (23,251 MPa)}\end{aligned}$$

The elastic deflection due to member self-weight is

$$\begin{aligned}\Delta &= \frac{5}{384} \frac{wt^4}{EI} \\ &= \frac{5 \times 0.418 \times 46^4 \times 12^3}{384 \times 3372 \times 20,985} \\ &= 0.60 \text{ in. (15 mm)}\end{aligned}$$

The elastic camber (upward deflection taken as negative quantity) due to initial prestress (see Fig. 6-11) is

$$\begin{aligned}\Delta &= -\left(\frac{2e_c + e_t}{24}\right) \frac{P_i \ell^2}{EI} \\ &\approx -\left(\frac{2 \times 14.65 + 9.15}{24}\right) \frac{172 \times 46^2 \times 12^2}{3372 \times 20,985} = -1.19 \text{ in. (-30 mm)}\end{aligned}$$

Applying the multipliers from Table 5-10, the net deflection at the time of erection is

$$\begin{aligned}\Delta &= 1.85 \times 0.60 - 1.80 \times 1.19 \\ &= -1.03 \text{ in. (-26 mm) upward}\end{aligned}$$

We will now calculate the long-term deflections due to self-weight, prestress, superimposed dead load, and sustained live load (assumed to be 30% of the specified live load). The elastic deflection due to the superimposed dead load and the sustained live load is

$$\begin{aligned}\Delta &= \frac{5}{384} \frac{wt^4}{EI} \\ &= \frac{5 \times (0.120 + 0.30 \times 0.400)46^4 \times 12^3}{384 \times 3372 \times 20,985} \\ &= 0.34 \text{ in. (9 mm)}\end{aligned}$$

Applying the multipliers from Table 5-10, the total long-term deflection is

$$\begin{aligned}\Delta &= 2.70 \times 0.60 - 2.45 \times 1.19 + 3.00 \times 0.34 \\ &= -0.28 \text{ in. (-7 mm)}\end{aligned}$$

Hence the long-term deflection that occurs after the attachment of the partitions is a downward deflection, from 1.03 in. upward to 0.28 in. upward. Thus

$$\begin{aligned}\Delta &= -0.28 - (-1.03) \\ &= 0.75 \text{ in. (19 mm) downward}\end{aligned}$$

The additional immediate deflection due to the rest of the live load is

$$\Delta = 0.70 \times 0.48 = 0.34 \text{ in. (9 mm) downward}$$

Hence the total downward deflection likely to damage the partitions is

$$\Delta = 0.75 + 0.34 = 1.09 \text{ in. (28 mm)}$$

For partitions sensitive to deflections, the ACI Code limits this total deflection (see Table 6-6) to

$$\frac{l}{480} = \frac{46 \times 12}{480} = 1.15 \text{ in. (29 mm)}$$

Therefore, the deflection control is satisfactory.

Rather than using the deflection multiplier from the *PCI Design Handbook* (Ref. 6-3) (i.e., those given in Table 5-10), the long-term deflections could have been calculated using appropriate creep coefficients. This alternative procedure is demonstrated in the example in Section 6.13.

6.13 EXAMPLE DESIGN OF POST-TENSIONED, ONE-WAY FLOOR SLAB

The one-way, simply supported floor slab shown in Fig. 6-28 is post-tensioned with unbonded, low-relaxation, 0.6 in. (15 mm) diameter tendons in 0.75 in. (19 mm) diameter plastic sheaths. The floor slab supports a specified live load of 50 psf (2.4 kN/m²) and a superimposed dead load of 10 psf (0.5 kN/m²). The partitions supported by the floor slab are "likely to be damaged by large deflections." The slab will be post-tensioned when the concrete is 7 days old and has reached a strength of 3500 psi (24 MPa). The specified 28-day strength of the normal-weight concrete is 4500 psi (31 MPa). Design the floor slab to satisfy the ACI Code requirements.

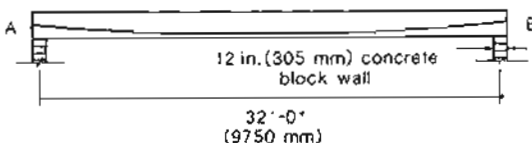


Figure 6-28 Post-tensioned, one-way floor slab.

Step 1: Choose the slab thickness.

From Fig. 6-16 the typical span-to-depth ratio for such slabs is 40. Hence we will choose a slab thickness of 10 in. (254 mm).

Step 2: Select the tendon profile.

For this uniformly loaded slab choose a parabolic tendon profile with zero eccentricity at the supports and the maximum possible eccentricity at midspan. From Table 3-16 the required concrete cover is 3/4 in. (19 mm), and hence the maximum possible eccentricity is

$$e = \frac{10}{2} - 0.75 - \frac{0.75}{2} = 3.88 \text{ in. (98 mm)}$$

Step 3: Estimate the stresses in the tendon.

Each tendon will be stressed from just one end, with the other end being a dead-end anchorage. Every second tendon will be stressed from end A and the alternate tendons will be stressed from end B. After anchoring, the stress in the tendons must not exceed $0.70 f_{py}$ at the anchorages (see Table 6-1). Hence the tendons will be jacked to a stress of $0.75 f_{py}$ and then anchored. Information from the post-tensioning supplier indicates that the friction coefficients appropriate for the tendon are $\mu = 0.06$ and $K = 0.0006$ per foot (0.002 per meter). The anchorage set will be taken as 0.25 in. (6 mm).

The total intended angular change of the tendon profile from one end to the other end is

$$\alpha = \frac{2 \times 2 \times 3.88}{16 \times 12} = 0.081 \text{ rad}$$

When the tendon is stressed from end A, the force in the tendon at end B can be found from Eq. (2-3) as

$$\begin{aligned} P_B &= P_A e^{-(\mu \alpha + K z)} \\ &= P_A e^{-(0.06 \cdot 0.081 + 0.0006 \cdot 32)} \\ &\approx 0.976 P_A \end{aligned}$$

It is common practice in estimating friction losses in unbonded post-tensioned slabs to assume a loss of 7.5% of the prestressing force per 100 ft length of tendon (or 2.5% per 10 m length of tendon). It can be seen that for this case, this would be a reasonable estimate.

The stress variation along the tendon prior to anchoring is shown in Fig. 6-29. It can be seen that the average stress in the strand is 200 ksi (1379 MPa), corresponding to an elongation of

$$\begin{aligned} \Delta &= \frac{200 \times 32 \times 12}{29,000} \\ &\approx 2.65 \text{ in. (67 mm)} \end{aligned}$$

Due to anchorage set, the elongation of the tendon will decrease by 0.25 in. (6 mm), which will result in a decrease in the average stress in the tendon of $(0.25/2.65) \times 200 \approx 19$ ksi (130 MPa). Because the tendon is now slipping back, the friction forces are reversed and the stresses in the tendon will be as shown in Fig. 6-29.

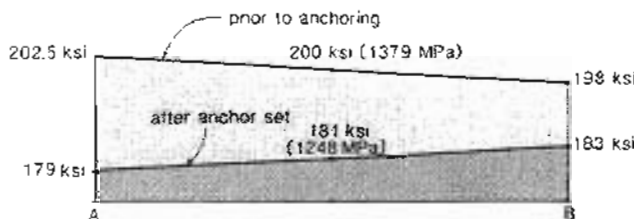


Figure 6-29 Variation of tendon stress along span for tendon stressed from end A.

It is noted that after anchoring, the highest stress occurs at the dead-end anchor, where the stress is 183 ksi (1262 MPa), which is less than the limiting stress of $0.70f_{pu} = 189$ ksi (1303 MPa). Because of the stressing operation (alternate ends stressed) the average stress of two adjacent tendons has a constant value of 181 ksi (1248 MPa) from end A to end B.

This average tendon stress will be reduced over time by creep, shrinkage, and relaxation. We will estimate the resulting long-term loss to be 30 ksi (207 MPa), so that the final stress in the tendon after all losses will be $181 - 30 = 151$ ksi (1041 MPa).

Step 4: Choose the tendon spacing.

Since the slab is "deflection sensitive" we will choose a prestressing amount such that even after all prestressing losses, 90% of the self-weight of the slab, that is, $0.9 \times (10/12) \times 150 = 112.5$ psf (5.4 kN/m²), will be "balanced" by the prestressing. Hence from Eq. (6-23) for a 1 ft wide strip,

$$\begin{aligned} P_f &= \frac{w_d l^2}{8e} \\ &= \frac{0.1125 \times 32^2}{8 \times 3.88/12} \\ &= 44.5 \text{ kips/ft (650 kN/m)} \end{aligned}$$

After losses, each tendon will have a force of $0.215 \times 151 = 32.5$ kips (144 kN), and hence using a spacing of 8 in. (200 mm) will provide 48.8 kips/ft (711 kN/m) of tendon force and $0.323 \text{ in}^2/\text{ft}$ ($684 \text{ mm}^2/\text{m}$) of tendon area.

Step 5: Check the concrete stresses.

We will determine the concrete stresses using the "force-in-the-tendon" approach, assuming gross-section properties. For a 1 ft wide strip, $A = 120 \text{ in}^2$ (77420 mm^2) and $S_b = 200 \text{ in}^3$ ($3.28 \times 10^6 \text{ mm}^3$).

(a) Initial conditions. The self-weight moment at midspan is

$$\begin{aligned} M_{min} &= \frac{0.125 \times 32^2}{8} \\ &= 16.0 \text{ ft-kips (21.7 kNm)} \end{aligned}$$

The initial prestressing force per foot width is

$$\begin{aligned} P_i &= \frac{12}{8} \times 0.215 \times 181 \\ &= 58.4 \text{ kips (260 kN)} \end{aligned}$$

Hence the stress in the bottom fiber at midspan is

$$\begin{aligned} f_b &= -\frac{58.4 \times 10^3}{120} - \frac{58.4 \times 10^3 \times 3.88}{200} + \frac{16.0 \times 10^3 \times 12}{200} \\ &= -487 - 1133 + 960 \\ &= -660 \text{ psi (-4.55 MPa)} \end{aligned}$$

The stress in the top fiber at midspan is

$$\begin{aligned} f_t &= -487 + 1133 - 960 \\ &= 314 \text{ psi (-2.17 MPa)} \end{aligned}$$

Both of these calculated stresses are within the concrete stress limits given for the initial conditions in Table 6-2.

(b) Final conditions. The total moment at midspan is

$$\begin{aligned} M_{max} &= \frac{(0.125 + 0.010 + 0.050) \times 32^2}{8} \\ &= 23.7 \text{ ft-kips (32.1 kNm)} \end{aligned}$$

The final prestressing force is 48.8 kips per foot width of slab (711 kN per meter).

Hence the stress in the bottom fiber at midspan is

$$\begin{aligned} f_b &= -\frac{48.8 \times 10^3}{120} - \frac{48.8 \times 10^3 \times 3.88}{200} + \frac{23.7 \times 10^3 \times 12}{200} \\ &= -407 - 947 + 1422 \\ &= +68 \text{ psi (0.47 MPa)} \end{aligned}$$

The stress in the top fiber at midspan is

$$\begin{aligned} f_t &= -407 + 947 - 1422 \\ &= -882 \text{ psi (-6.08 MPa)} \end{aligned}$$

Both of these calculated stresses are within the calculated stress limits for the final conditions given in Table 6-2 [i.e., 402 psi (2.78 MPa) tension and 2025 psi (13.97 MPa) compression].

Step 6: Calculate the minimum bonded reinforcement required.

The ACI Code requires that one-way slabs post-tensioned with unbonded tendons contain a minimum amount of bonded reinforcement for crack control. The required amount of reinforcing bars is

$$\begin{aligned} A_s &= 0.004A \\ &= 0.004 \times \frac{10}{2} \times 12 \\ &= 0.24 \text{ in}^2/\text{ft} (508 \text{ mm}^2/\text{m}) \end{aligned}$$

Hence choose #4 bars, $f_y = 60 \text{ ksi}$ (414 MPa) at 8 in. (203 mm) centers, resulting in 0.30 in²/ft width (635 mm²/meter width).

Step 7: Check the flexural capacity.

The required moment at midspan for a 1 ft wide strip is

$$\begin{aligned} M_f &= \frac{w_f \ell^3}{8} \\ &= \frac{[1.4 \times (0.125 + 0.010) + 1.7 \times 0.050] \times 32^2}{8} \\ &= 35.1 \text{ ft-kips (47.6 kNm)} \end{aligned}$$

For this slab the span-to-depth ratio is $32 \times 12 / 10 = 38.4$, and hence the stress in the unbonded tendons at ultimate from Eq. (6-9) and Fig. 6-30 is

$$\begin{aligned} f_{ps} &= f_{sc} + 10,000 + \frac{f'_c}{300\rho_p} \\ &= 151,000 + 10,000 + \frac{4500}{300 \times 0.215 / (8 \times 8.88)} \\ &= 166 \text{ ksi (1144 MPa)} \end{aligned}$$

but

$$f_{ps} \leq f_{py} = 0.90 \times 270 = 243 \text{ ksi (1676 MPa)}$$

and

$$f_{ps} \leq f_{sc} + 30,000 = 151 + 30 = 181 \text{ ksi (1248 MPa)}$$

Hence

$$f_{ps} = 166 \text{ ksi (1144 MPa)}$$

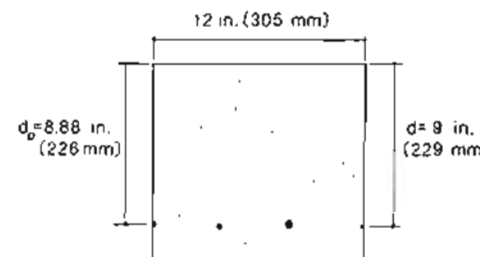


Figure 6-30 Cross section for 1 ft wide strip.

The reinforcement indices for this slab are

$$\begin{aligned} \omega_p &= \frac{A_{ps}}{bd_p} \frac{f_{ps}}{f'_c} = \frac{(12/8) \times 0.215}{12 \times 8.88} \times \frac{166}{4.5} = 0.112 \\ \omega &= \frac{A_s}{bd} \frac{f_y}{f'_c} = \frac{(12/8) \times 0.20}{12 \times 9} \frac{60}{4.5} = 0.037 \end{aligned}$$

Hence

$$\omega_p + \frac{d}{d_p} \omega = 0.112 + \frac{9}{8.88} \times 0.037 = 0.150$$

Since $0.36\beta_1 = 0.36 \times 0.825 = 0.297 > 0.150$ the section is not overreinforced.

The required equivalent, rectangular stress-block depth is

$$\begin{aligned} a &= \frac{0.323 \times 166 + 0.30 \times 60}{0.85 \times 4.5 \times 12} \\ &= 1.56 \text{ in. (40 mm)} \end{aligned}$$

Hence the design flexural strength for a 1 ft wide strip is

$$\begin{aligned} \phi M_n &= 0.9 \left[A_{ps} f_{ps} \left(d_p - \frac{a}{2} \right) + A_s f_y \left(d - \frac{a}{2} \right) \right] \\ &= 0.9 \left[0.323 \times 166 \left(8.88 - \frac{1.56}{2} \right) + 0.30 \times 60 \left(9 - \frac{1.56}{2} \right) \right] \\ &= 524 \text{ in.-kips} = 43.7 \text{ ft-kips (59.2 kNm)} \end{aligned}$$

As 43.7 ft-kips > 35.1 ft-kips, the flexural capacity of the section is adequate.

Step 8: Check the reserve of strength after cracking.

To ensure ductility, we must ensure that ϕM_n exceeds $1.2M_{cr}$. The concrete is assumed to crack when the tensile stress reaches the modulus of rupture, $f_r = 7.5\sqrt{f'_c} = 7.5\sqrt{4500} = 503$ psi (3.47 MPa). The moment required to cause this tensile stress can be calculated from

$$503 = -407 - 947 + \frac{M_{cr}}{200}$$

Hence $M_{cr} = 371$ in.-kips (41.9 kNm). Thus $\phi M_n/M_{cr} = 524/371 = 1.41$. Therefore there is adequate postcracking capacity.

Step 9: Check the deflections.

We must check that the deflections satisfy the limits given in Table 6-6. As the tensile stresses under service loads remain below the cracking stress, we can use the uncracked section properties when calculating deflections.

(a) *Immediate deflection due to live load.*

$$\Delta_L = \frac{5}{384} \frac{w\ell^4}{E_c I_g}$$

where

$$E_c = 57,000\sqrt{4500} = 3824 \text{ ksi (26370 MPa)}$$

$$I_g = \frac{12 \times 10^3}{12} = 1000 \text{ in}^4 (416 \times 10^6 \text{ mm}^4)$$

Hence

$$\begin{aligned}\Delta_L &= \frac{5 \times 0.050 \times 32^4 \times 12^3}{384 \times 3824 \times 1000} \\ &= 0.31 \text{ in. (8 mm)}\end{aligned}$$

This is less than the specified limit of $\ell/360 = 32 \times 12/360 = 1.07$ in. (27 mm), hence O.K.

(b) *Check deflection likely to damage partitions.* We will assume that the partitions are attached when the concrete is 28 days old. Further, we will assume that 30% of the live load is sustained.

To calculate the deflection that will affect the attached partitions, we must first estimate the deflection of the slab at the time the partitions were attached. The modulus of the concrete at 7 days is

$$\begin{aligned}E_c &= 57,000\sqrt{f'_{c7}} = 57,000\sqrt{3500} \\ &= 3372 \text{ ksi (23250 MPa)}\end{aligned}$$

The immediate deflection due to member self-weight applied at 7 days is

$$\begin{aligned}\Delta &= \frac{5}{384} \frac{w\ell^4}{E_c I_g} \\ &= \frac{5 \times 0.125 \times 32^4 \times 12^3}{384 \times 3372 \times 1000} \\ &= 0.87 \text{ in. (22 mm) downward}\end{aligned}$$

while the immediate camber due to the initial prestress, from Fig. 6-11, is

$$\begin{aligned}\Delta &= \frac{5}{48} \frac{P_i c \ell^2}{E_c I_g} \\ &= \frac{5 \times 58.4 \times 3.88 \times 32^2 \times 12^2}{48 \times 3372 \times 1000} \\ &= 1.03 \text{ in. (26 mm) upward.}\end{aligned}$$

The immediate deflection due to the superimposed dead load 10 psf (0.5 kN/m²) and the sustained live load $0.3 \times 50 = 15$ psf (0.72 kN/m²), applied at 28 days, is

$$\begin{aligned}\Delta &= \frac{5}{384} \frac{w\ell^4}{E_c I_g} \\ &= \frac{5 \times (0.010 + 0.015) \times 32^4 \times 12^3}{384 \times 3824 \times 1000} \\ &= 0.15 \text{ in. (4 mm) downward}\end{aligned}$$

while the immediate deflection due to the application of the remainder of the live load that is, $0.7 \times 50 = 35$ psf (1.67 kN/m²) is

$$\Delta = 0.7 \times 0.31 = 0.22 \text{ in. (6 mm) downward.}$$

For this relatively thick slab having a volume/surface ratio of 5 in. (127 mm), the creep coefficients can be calculated from Eq. (3-10) as

$$\begin{aligned}\phi(28, 7) &= 0.32 \\ \phi(10,000, 7) &= 1.95 \\ \phi(10,000, 28) &= 1.66\end{aligned}$$

Hence the downward deflection due to dead load and live load, which will occur after the partitions are attached is

$$\begin{aligned}\Delta &= (1.95 - 0.32) \times 0.87 + 1.66 \times 0.15 + 0.22 \\ &= 1.89 \text{ in. (48 mm)}\end{aligned}$$

If the prestressing force remained constant with time, the upward deflection due to prestress that would occur after 28 days is

$$\begin{aligned}\Delta &= (1.95 - 0.32) \times 1.03 \\ &= 1.68 \text{ in. (43 mm)}\end{aligned}$$

Because the prestressing force decreases with time (from 58.4 kips at 7 days to about 48.8 kips at 10,000 days), the upward deflection due to the prestress will be somewhat smaller than the value above. While it would be possible to estimate this decrease using

the adjusted effective modulus of Eq. (3-15), we will here use the simple, conservative assumption that the upward deflection due to prestress that occurs after 28 days is

$$\Delta = \frac{48.8}{58.4} \times 1.68 = 1.40 \text{ in. (36 mm)}$$

The deflection that may damage the partitions is thus,

$$\Delta = 1.89 - 1.40 = 0.49 \text{ in. (12 mm) downward.}$$

This is less than the limit given in Table 6-6 of $\ell/480 = 32 \times 12/480 = 0.80 \text{ in. (20 mm)}$.

Hence the design is satisfactory.

References

- 6-1 ACI Committee 318, "Building Code Requirements for Reinforced Concrete (ACI 318-89) and Commentary – ACI 318 R-89," American Concrete Institute, Detroit, 1989, 353 pp.
- 6-2 CSA Committee A23.3, *Design of Concrete Structures for Buildings*, CAN3-A23.3-M84, Canadian Standards Association, Rexdale, Canada, 1984, 281 pp.
- 6-3 Prestressed Concrete Institute, *PCI Design Handbook: Precast and Prestressed Concrete*, 3rd ed., PCI, Chicago, 1985.
- 6-4 Zia, P., Preston, H.K., Scott, N.L. and Workman, E.B., "Estimating Prestress Losses," *Concrete International: Design and Construction*, Vol. 1, No. 6, June 1979, pp. 32–38.
- 6-5 Gergely, P., and Lutz, L.A., "Maximum Crack Width in Reinforced Concrete Flexural Members," *Causes, Mechanism, and Control of Cracking in Concrete*, SP-20, American Concrete Institute, Detroit, 1968, pp. 87–117.
- 6-6 CEB-FIP, *Model Code for Concrete Structures: CEB-FIP International Recommendations*, 3rd ed., Comité Euro-International du Béton, Paris, 1978, 348 pp.
- 6-7 Mantock, Alan H., Yarnazaki, Jun, and Katula, Basil T., "Comparative Study of Prestressed Concrete Beams with and without Bond," *ACI Journal*, Vol. 68, No. 2, Feb. 1971, pp. 116–125.

Demonstration Problems

- 6-1 A simply supported tee-beam spans 70 ft (21 m). Using the simplified code approaches for f_p at flexural capacity, compare the nominal flexural strengths at midspan for the precast, pretensioned and the cast-in-place, post-tensioned beams shown in Fig. 6-31. The strands are 1/2 in. (13 mm) in diameter [$f_{pu} = 270 \text{ ksi (1860 MPa)}$]. The concrete strength for both beams is 5000 psi (35 MPa) and the yield stress of the reinforcing bars is 60 ksi (400 MPa).

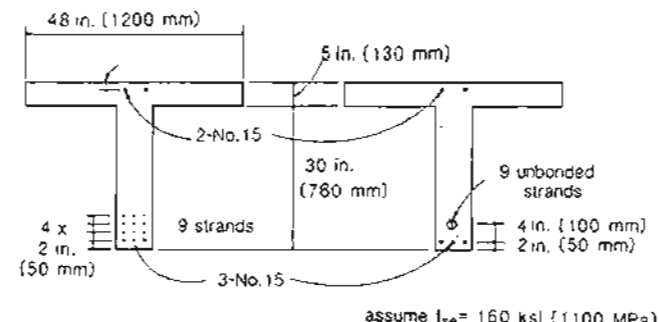


Figure 6-31 Details of pretensioned and post-tensioned beams.

- 6-2 A post-tensioned beam of rectangular cross section is to carry a service load of 600 pif (8.75 kN/m) in addition to its own weight over a simply supported span of 25 ft (8 m). The

width of the beam is to be 8 in. (200 mm) and the concrete strength is to be 5000 psi (35 MPa). Design the beam.

- 6-3 An untopped hollow-core, simply supported floor slab system spans 36 ft (11 m) in a hotel corridor area. The service live load is 100 psf (4.8 kN/m²) and the additional dead load is 10 psf (0.5 kN/m²). The normal-density concrete has $f'_{ci} = 3500$ psi (25 MPa) and $f'_c = 5000$ psi (35 MPa). Low-relaxation 1/2 in. (13 mm) diameter strand ($f_{pu} = 270$ ksi (1860 MPa)) is to be used. Assume that transfer of the prestress occurs after 1 day of steam curing. A preliminary cross section with a span-to-depth ratio of 37 is given in Fig. 6-32. Design the floor slab.

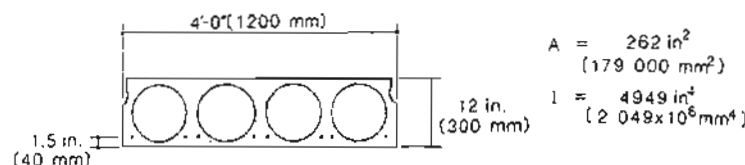


Figure 6-32 Hollow-core floor slabs.

- 6-4 A post-tensioned girder for an apartment building is used to span 40 ft (12.2 m) with two 12 ft (3.65 m) cantilevers as shown in Fig. 6-33. A preliminary design has resulted in a cross section and tendon profile as shown. The prestressing force is to be supplied by stress-relieved 1/2 in. (13 mm) diameter strands with $f_{pu} = 270$ ksi (1860 MPa). In addition to its self-weight the beam carries dead load from a precast concrete slab of 600 plf (8.75 kN/m), an additional dead load of 100 plf (1.5 kN/m), and a service live load of 500 plf (7.3 kN/m). The post-tensioning is applied in two stages. An initial, low stress is applied to the tendon when only the self-weight of the girder is acting. Then after the additional dead loads are applied, the stress in the tendon is increased. The normal-weight concrete at the time of initial stressing is 5000 psi (35 MPa) at an age of 14 days. The concrete strength at 28 days is 6000 psi (40 MPa).

- (a) Choose the number of strands such that the ultimate strength requirements are met at sections B and C.
- (b) Consider the initial stage of prestressing with the prestressing force at $0.4A_{ps}f_{pu}$ and check the initial conditions at sections B and C with only the self-weight of the beam acting. If necessary, adjust the level of prestress. Ignore prestress losses due to friction.
- (c) Consider the final stage after 30 years with an effective tendon force of $0.6A_{ps}f_{pu}$ with all service loads acting and check the stresses at sections B and C. Ignore prestress losses due to friction.

- 6-5 A light industrial warehouse has a 24 × 24 ft (7.32 × 7.32 m) framing grid with double tees supported on ledger beams spanning between the columns (see Fig. 6-34). The floor carries a specified live load of 100 psf (4.79 kN/m²) and a superimposed dead load of 10 psf (0.48 kN/m²). The precast, pretensioned, inverted tee has a concrete strength at transfer, $f'_{ci} = 4000$ psi (27.58 MPa), and a specified 28-day strength of 6000 psi (41.37 MPa). The precast beam is steam cured for 1 day. The cast-in-place concrete topping has a specified 28-day strength of 3000 psi (20.69 MPa). The prestressing steel is 1/2 in. (13 mm) diameter

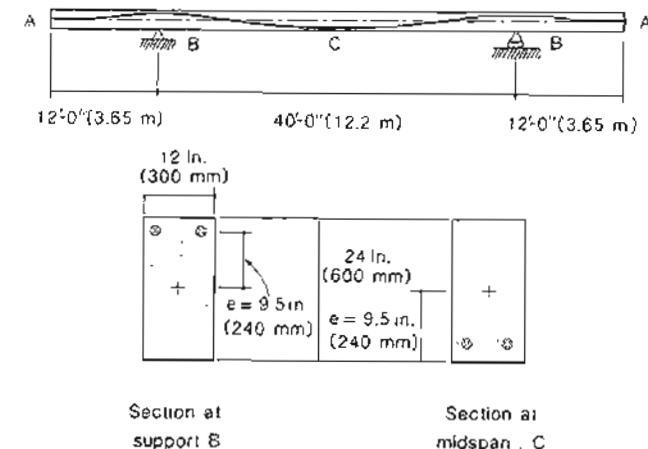


Figure 6-33 Post-tensioned girder

low-relaxation strand with $f_{pu} = 270$ ksi (1860 MPa), which will be tensioned to $0.75f_{pu}$ in the pretensioning bed. Non-prestressed reinforcement with $f_y = 60$ ksi (414 MPa) will be used. As is usual practice for these types of members, the ledger beam will not be propped during construction. Design the ledger beam for flexure.

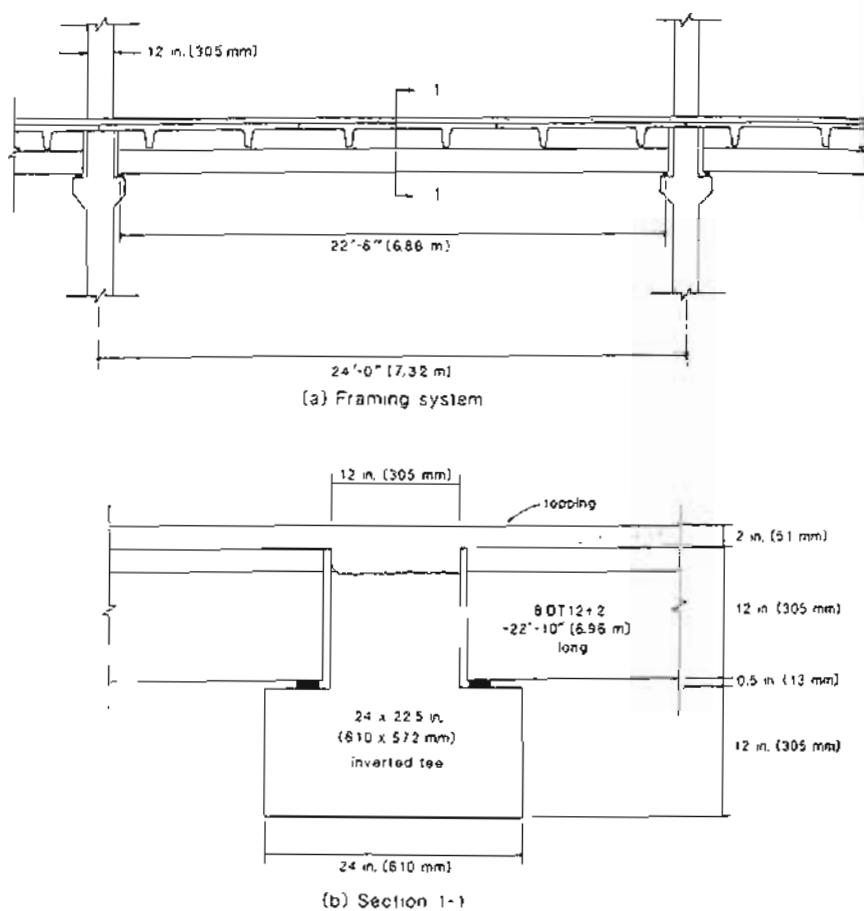


Figure 6-34 Structural framing of industrial warehouse.

Members Subjected to Shear

During the next decade it is hoped that the design regulations for shear strength can be integrated, simplified and given a physical significance so that designers can approach unusual design problems in a rational manner.

ACI-ASCE Shear Committee, 1973

7.1 INTRODUCTION

In treating the behavior and design of flexural members in Chapters 5 and 6 we restricted our attention to only longitudinal strains and their corresponding longitudinal stresses. In reality all flexural members will also be subjected to shear stresses and these shear stresses may result in diagonal cracks (see Fig. 7-1). Unless appropriate amounts of properly detailed web and longitudinal reinforcement have been provided, these diagonal cracks can result in the premature failure of the member. Such failures are called shear failures. The behavior of beams in shear, and design procedures for avoiding shear failures are discussed in this chapter.

7.2 DIAGONAL CRACKING

A crack will form in concrete when the principal tensile stress at some location reaches the cracking strength of the concrete. The crack will form normal to the direction of the principal tensile stress. For members subjected to pure axial tension or to pure flexure the principal tensile stresses are parallel with the longitudinal axis of the member and hence cracks due to these actions will be perpendicular to the member axis. If a cross section of a

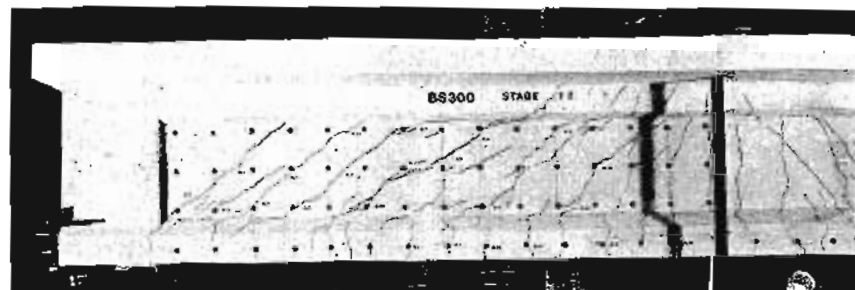


Figure 7-1 Diagonal cracks in pretensioned I-girder. From Vrana (Ref. 7-1).

member is subjected to shear stresses, the principal tensile stress directions are inclined to the longitudinal axis of the member. Hence if a crack forms at a location where significant shear stresses exist, the crack will be inclined to the member axis. Such cracks are called diagonal cracks.

Figure 7-2 shows a typical prestressed concrete beam subjected to shear. The shear force carried by the concrete will be equal to the applied shear force V , minus the vertical component of the force in the inclined tension, V_p . At the centroid of this beam the concrete will be subjected to a shear stress, v , and a longitudinal compressive stress, f_{pc} , due to the prestress. The resulting principal tensile stress can be determined from the Mohr's circle of stress in Fig. 7-2 as

$$f_1 = \sqrt{v^2 + (\frac{f_{pc}}{2})^2} - \frac{f_{pc}}{2} \quad (7-1)$$

If the concrete cracks when f_1 reaches the cracking stress, f_{cr} , then the shear stress that will cause diagonal cracking can be found by rearranging Eq. (7-1) as

$$v_{cr} = f_{cr} \sqrt{1 + \frac{f_{pc}}{f_{cr}}} \quad (7-2)$$

The inclined cracks will form parallel to the principal compressive stress direction. The inclination of these cracks can be found from the Mohr's circle (Fig. 7-2) as

$$\tan 2\theta = \frac{2v}{f_{pc}} \quad (7-3)$$

Note that in these equations the compressive stress, f_{pc} , is taken as a positive quantity. As the axial compressive stress increases the shear stress required to cause cracking will increase and the inclination of the cracks to the longitudinal axis will decrease (see Fig. 7-3).

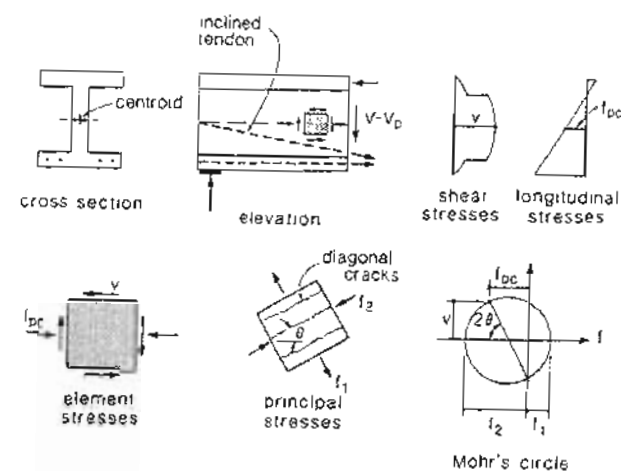


Figure 7-2 Diagonal cracking in web of prestressed beam.

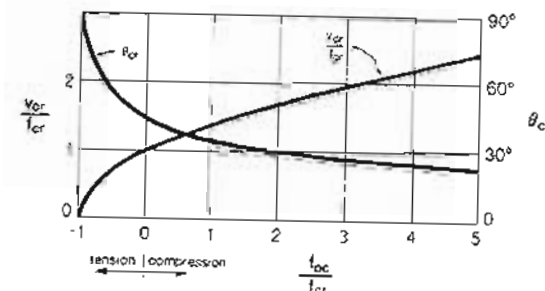


Figure 7-3 Variations of cracking shear stress and crack inclination with axial stress

The ACI Code (Ref. 7-2) recommends that the principal tensile stress at web-shear cracking be taken as $4\sqrt{f'_c}$ psi ($0.33\sqrt{f'_c}$ MPa). In lieu of calculating the shear to cause web-shear cracking, V_{cw} , from Eq. (7-2), the ACI Code permits the use of the following approximate expression:

$$V_{cw} = (3.5\sqrt{f'_c} + 0.3f_{pc})b_w d + V_p \quad \text{psi units} \quad (7-4a)$$

$$V_{cw} = (0.29\sqrt{f'_c} + 0.3f_{pc})b_w d + V_p \quad \text{MPa units} \quad (7-4b)$$

Because of concern with the applicability of these empirical equations to beams made from high-strength concrete, the current version of the ACI Code (Ref. 7-2) requires that

the values of $\sqrt{f'_c}$ used in all shear design equations be limited to 100 psi for the equations in psi units, and to 8.3 MPa for the equations in MPa units. This limit can be waived if additional web reinforcement is provided.

In the discussion above, we have assumed that the diagonal cracks form in the web near the centroid of the member in concrete that has not been cracked previously. Such cracks are called web-shear cracks. Diagonal cracks can also develop as extensions of previously existing flexural cracks. This second type of inclined cracking is called flexure-shear cracking (see Fig. 7-4). Predicting the shear at which existing flexural cracks will develop into flexure-shear cracks is a complex problem which has received considerable attention over the years.

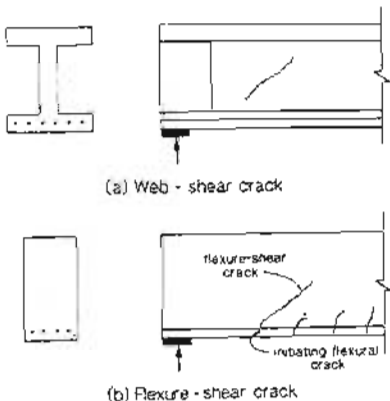


Figure 7-4 Types of diagonal cracking.

If the longitudinal flexural stresses at different sections of a beam are known, then the shear stresses can be determined from equilibrium considerations. In 1902, Mörsch (Ref. 7-3) used such an approach to derive the shear stress distribution for a reinforced concrete beam containing flexural cracks (see Fig. 7-5). Mörsch predicted that the shear stress would reach its maximum value at the neutral axis and would then remain constant from the neutral axis down to the flexural steel. The value of this maximum shear stress would be

$$v = \frac{V}{b_w jd} \quad (7-5)$$

where b_w is the web width and jd is the flexural lever arm. Note that Mörsch's predicted shear stress distribution implies that high shear stresses are transmitted across the flexural cracks. In fact, for typical percentages of reinforcement Mörsch's shear stress distribution predicts that only about 30% of the total shear is carried in the uncracked compression zone.

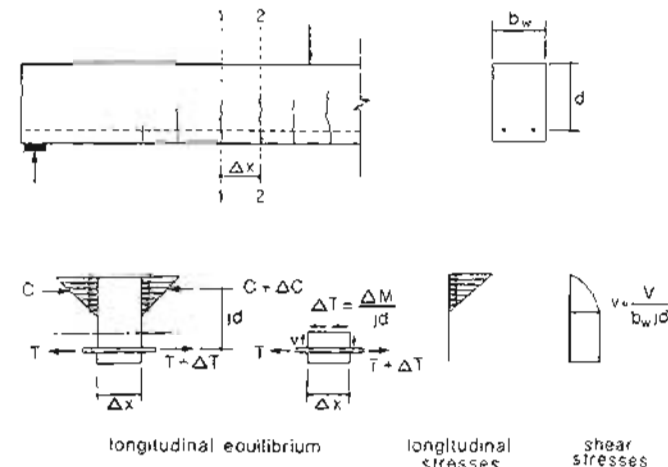


Figure 7-5 Determining shear stress distribution in a reinforced concrete beam containing flexural cracks.

In the 1950s, researchers such as Zwoyer and Siess (Ref. 7-4), Bresler and Pister (Ref. 7-5), Guralnick (Ref. 7-6), and Walther (Ref. 7-7) studied the stress conditions in the concrete above flexural cracks in order to develop expressions for the shear capacity of members containing flexure-shear cracks. They typically assumed that all of the shear would be carried in the flexural compression zone and hence believed that the actual shear stress distribution was significantly different from that shown in Fig. 7-5. The uncertainty about the actual distribution of shear stresses over the section caused engineers to refer to the traditional shear stress of Eq. (7-5) as the "nominal" shear stress.

Since Eq. (7-5) was regarded as only a nominal indicator of shear intensity, the 1963 ACI Code (Ref. 7-8) decided to simplify this shear stress equation to

$$v = \frac{V}{b_w d} \quad (7-6)$$

where d is the distance from the extreme compression fiber to the centroid of the tension reinforcement.

Based on a review of the available research by the ACI-ASCE Shear Committee (Ref. 7-9) the 1963 ACI Code gave the following empirical expression for the nominal shear stress at the flexure-shear cracking load of a reinforced concrete beam:

$$v_{cr} = 1.9\sqrt{f'_c} + 2500\rho_w \frac{Vd}{M} \quad \text{psi} \\ \leq 3.5\sqrt{f'_c} \quad (7-7a)$$

In SI units these expressions are

$$\begin{aligned} v_{cr} &= 0.16\sqrt{f'_c} + 17\rho_w \frac{Vd}{M} \quad \text{MPa} \\ &\leq 0.29\sqrt{f'_c} \end{aligned} \quad (7-7b)$$

where ρ_w is the ratio of non-prestressed reinforcement to the shear area $b_w d$ (i.e., $\rho_w = A_s/b_w d$) and Vd/M is the indicator of shear-to-moment ratio at the section being considered.

As can be seen in Fig. 7-6, the nominal shear stress at flexure-shear cracking is predicted to decrease as the moment-to-shear ratio increases, going from $3.5\sqrt{f'_c}$ psi ($0.29\sqrt{f'_c}$ MPa) for zero moment to $1.9\sqrt{f'_c}$ psi ($0.16\sqrt{f'_c}$ MPa) for very high moments. It can also be seen in Fig. 7-6 that there is considerable scatter in the observed values of shear stresses at flexure-shear cracking.

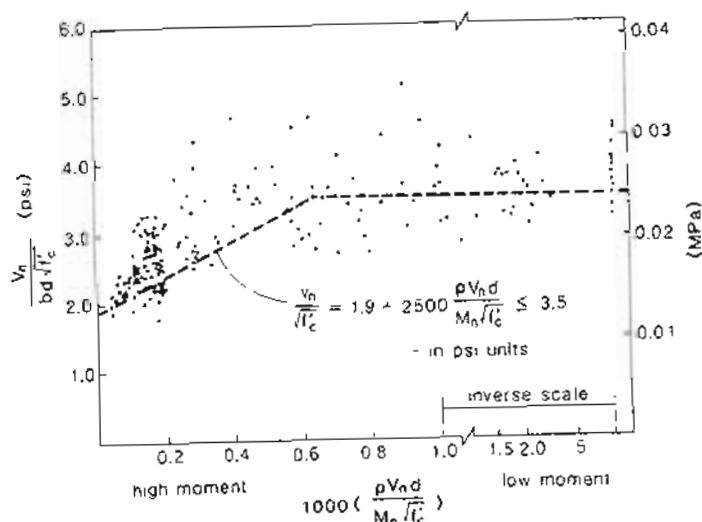


Figure 7-6 ACI Code expression for flexure-shear cracking of reinforced concrete beams. Adapted from Ref. 7-9.

As a simplification to Eq. (7-7) the ACI Code permits the shear at flexure-shear cracking for reinforced concrete beams to be taken as

$$V_c = 2\sqrt{f'_c} b_w d \quad \text{psi} \quad (7-8a)$$

$$V_c = 0.17\sqrt{f'_c} b_w d \quad \text{MPa} \quad (7-8b)$$

In 1964, Kani (Ref. 7-10) suggested a "comb" model for idealizing the load-carrying mechanisms of reinforced concrete beams, cracked in flexure and subjected to shear. In this analogy (see Fig. 7-7), the uncracked concrete is represented by the backbone of the comb and the concrete between the flexural cracks is represented by the teeth of the comb. Bond forces in the reinforcement are resisted by bending action in the cantilevered teeth. When the bending moment in a cantilevered tooth becomes large enough to "break off" the tooth at its base, diagonal cracking is considered to have occurred.

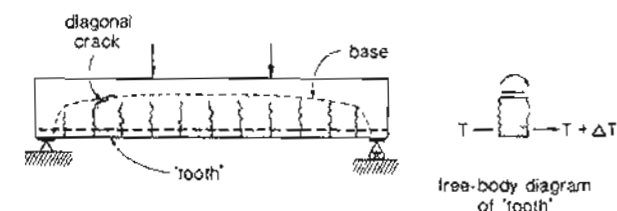


Figure 7-7 Kani's comb model for cracked beams subjected to shear.

Kani's analogy can help us to understand several aspects of the shear behavior of members without web reinforcement. Slender beams that do not contain stirrups can fail in an abrupt manner immediately after the occurrence of diagonal cracks. On the other hand, beams with low span-to-depth ratios can often tolerate significant increases in load after the formation of diagonal cracks. In such members the backbone of the comb forms a robust tied arch that can continue to carry load even after the teeth have failed. The comb analogy also emphasizes the importance of bond on the shear transfer mechanisms. According to Kani's model a beam reinforced only with an unbonded tendon will not develop flexure-shear cracks. Because larger beams have longer teeth the comb model predicts that such beams will fail at lower shear stresses (Ref. 7-11).

Kani's model assumes that no shear stresses are transmitted across the flexural cracks. In the 1960s a number of investigations were conducted to determine how much shear was transmitted across the flexural cracks. The investigators were surprised to find that even quite close to failure the compression zone carried only about 25% of the total shear (see Fig. 7-8). The remainder of the shear is carried across the flexural crack by what Fenwick and Paulay (Ref. 7-13) called "aggregate interlock" and by dowel forces in the flexural reinforcing bars. Thus it was found that Mörsch's predicted distribution was fairly accurate after all.

The ACI Code (Ref. 7-2) suggests that the shear to cause flexure-shear cracks in prestressed concrete members can be found by adding $0.6\sqrt{f'_c} b_w d$, where f'_c is in psi ($0.05\sqrt{f'_c} b_w d$, where f'_c is in MPa) to the shear that exists when flexural cracks first form

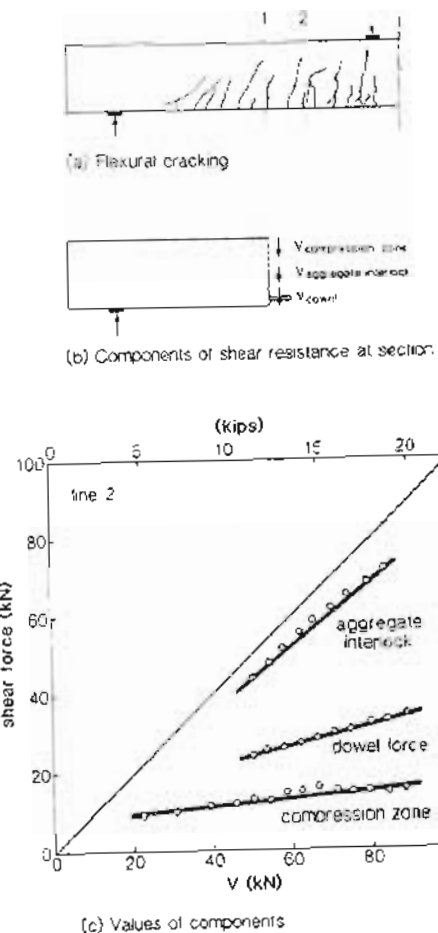


Figure 7-8 Experimentally determined components of shear resistance at cracked section. Adapted from Taylor (Ref. 7-12).

at the section being considered. For noncomposite beams the resulting expression is

$$V_{ci} = 0.6 \sqrt{f'_c} b_w d + \frac{V}{M} M_{cr} \quad \text{psi} \quad (7-9a)$$

$$V_{ci} = 0.05 \sqrt{f'_c} b_w d + \frac{V}{M} M_{cr} \quad \text{MPa} \quad (7-9b)$$

where V/M is the shear-to-moment ratio at the section under consideration and M_{cr} is the moment required to cause flexural cracking at the section. Flexure cracking is assumed to

occur when the tensile stress reaches $6\sqrt{f'_c}$ psi ($0.5\sqrt{f'_c}$ MPa). However, V_{ci} need not be taken as less than $1.7\sqrt{f'_c} b_w d$ (psi) or $0.14\sqrt{f'_c} b_w d$ (MPa).

The ACI Code requires that in calculating web-shear cracking, Eq. (7-4), and flexure-shear cracking, Eq. (7-9), the term d be taken as the distance from the extreme compression fiber to the centroid of the prestressed reinforcement or as 0.8 times the overall depth of the beam, if this term is larger.

7.3 EXAMPLE OF ESTIMATING DIAGONAL CRACKING SHEARS

The floor beam shown in Fig. 7-9 is a PCI standard single tee (10ST36) with strands depressed at midspan. The beam spans 60 ft (18.3 m) and is subjected to a uniformly distributed load. Estimate the load at which diagonal cracking will occur using the ACI Code expressions.

The prestressing steel consists of twelve 1/2 in. (12.7 mm) diameter low-relaxation strands with eccentricities of 14.95 in. (380 mm) at the ends and 24.03 in. (610 mm) at midspan. Assume that the stress in the strands after all losses is 152 ksi (1046 MPa).

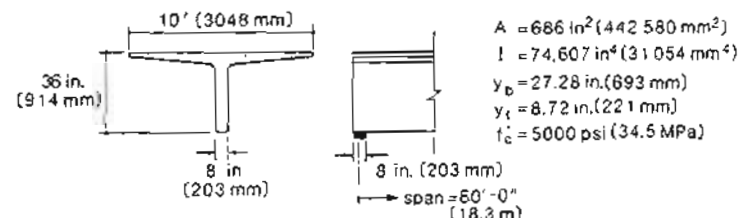


Figure 7-9 Details of cross section.

In order to determine the magnitude of the uniformly distributed load, w , which will cause diagonal cracking, it is necessary to calculate the shears to cause web-shear cracking and flexure-shear cracking at different sections along the length of the beam. For example, for the section that is at the end of the strands' transfer length (i.e., 50 strand diameters from the end of the beam), the calculations are as follows:

(a) Web-Shear Cracking

The shear to cause web-shear cracking is given by Eq. (7-4) as follows:

$$V_{cw} = \left(3.5 \sqrt{f'_c} + 0.3 f_{pc} \right) b_w d + V_p$$

where

$$f_{pc} = \frac{P}{A} = \frac{12 \times 0.153 \times 152}{686} \\ = 407 \text{ psi (2.80 MPa)}$$

and

$$\begin{aligned} d &= y_t + e \text{ but not less than } 0.8h \\ &= 8.72 + 15.57 < 0.8 \times 36 \\ &= 24.29 < 28.80 \end{aligned}$$

Hence

$$d = 28.8 \text{ in. (732 mm)}$$

The vertical component, V_p , of the prestressing force is

$$\begin{aligned} V_p &\approx 12 \times 0.153 \times 152 \times \frac{24.03 - 14.95}{30.33 \times 12} \\ &= 6.96 \text{ kips (30.9 kN)} \end{aligned}$$

Hence

$$\begin{aligned} V_{cw} &= (3.5\sqrt{5000} + 0.3 \times 407) \times 8 \times 28.8 + 6960 \\ &= 92.1 \text{ kips (410 kN)} \end{aligned}$$

The uniformly distributed load, w , required to cause a shear of 92.1 kips (410 kN) at a location 28.25 ft (8.61 m) from midspan of the beam is

$$\begin{aligned} w &= \frac{92.1}{28.25} \\ &= 3.26 \text{ kips/ft (47.6 kN/m)} \end{aligned}$$

(b) Flexure-Shear Cracking

The shear to cause flexure-shear cracking is given by Eq. (7-9) as

$$V_{cr} = 0.6\sqrt{f'_c b_w d} + \frac{V}{M} M_{cr}$$

The moment-to-shear ratio at a distance of 1.75 ft (0.53 m) from the center of the support is

$$\begin{aligned} \frac{M}{V} &= \frac{30w \times 1.75 - w \times 1.75^2/2}{30w - 1.75w} \\ &= 1.80 \text{ ft} = 21.7 \text{ in. (550 mm)} \end{aligned}$$

The prestressing causes a compressive stress on the bottom fiber of the beam equal to

$$\begin{aligned} \frac{P}{A} + \frac{Pey_b}{I} &= \frac{279}{686} + \frac{279 \times 15.57 \times 27.28}{74607} \\ &= 1.995 \text{ ksi (13.7 MPa)} \end{aligned}$$

Flexural cracking is assumed to occur when the stress on the bottom fiber of the beam reaches $6\sqrt{f'_c} = 424$ psi (2.93 MPa). Hence the moment required to cause cracking is

$$\begin{aligned} M_{cr} &= (1.995 + 0.424) \times \frac{74607}{27.28} \\ &= 6616 \text{ in.-kips (748 kNm)} \end{aligned}$$

Hence

$$\begin{aligned} V_{cr} &= 0.6\sqrt{5000} \times 8 \times 28.8 + \frac{6616 \times 1000}{21.7} \\ &= 315 \text{ kips (1400 kN)} \end{aligned}$$

The uniformly distributed load, w , required to cause this shear is

$$\begin{aligned} w &= \frac{315}{28.25} \\ &= 11.2 \text{ kips/ft (163 kN/m)} \end{aligned}$$

Repeating the calculations above for a number of different locations along the length of the beam, we obtain the values given in Table 7-1 and plotted in Fig. 7-10.

Table 7-1 Checking sections for diagonal cracking.

x ft (m)	d in. (mm)	P kips (kN)	V_p kips (kN)	f'_{pc} psi (MPa)	V_{cr} kips (kN)	w kips/ft (kN/m)	Web-Shear Cracking		Flexure-Shear Cracking			
							M/V in. (mm)	e in. (mm)	M_{cr} in.-kips (kNm)	V_{cr} kips (kN)	w^* kips/ft (kN/m)	
0.33	28.8	89.3	2.23	130	68.2	2.30	3.98	15.15	2869	731	24.6	
(0.10)	(731)	(397)	(9.91)	(0.90)	(304)	(33.6)	(101)	(385)	(324)	(3250)	(360)	
1.75	28.8	279	6.96	407	92.1	3.26	21.7	15.57	6616	315	11.2	
(0.53)	(731)	(1241)	(30.9)	(2.80)	(410)	(47.6)	(1550)	(1396)	(748)	(1400)	(163)	
6.00	28.8	279	6.96	407	92.1	3.84	81.0	16.85	6973	95.9	4.0	
(1.83)	(731)	(1241)	(30.9)	(2.80)	(410)	(56.0)	(2057)	(428)	(788)	(426)	(58.3)	
12.00	28.8	279	6.96	407	92.1	5.12	192	18.64	7473	48.7	2.71	
(3.66)	(731)	(1241)	(30.9)	(2.80)	(410)	(74.7)	(4877)	(473)	(8441)	(217)	(39.5)	
15.00	28.8	279	6.96	407	92.1	6.14	270	19.54	7724	38.4	2.56	
(4.57)	(731)	(1241)	(30.9)	(2.80)	(410)	(89.6)	(6858)	(496)	(873)	(171)	(37.4)	
18.00	29.2	279	6.96	407	93.3	7.78	378	20.44	7975	31.0	2.58	
(5.49)	(741)	(1241)	(30.9)	(2.80)	(415)	(114)	(9601)	(519)	(901)	(138)	(37.7)	
24.00	31.0	279	6.96	407	98.6	16.4	864	22.23	8474	29.8	4.97	
(7.32)	(786)	(1241)	(30.9)	(2.80)	(439)	(240)	(21946)	(565)	(957)	(133)	(72.5)	
30.00	32.8	279	6.96	407	104.0	∞	∞	24.03	8976	31.5	∞	
(9.15)	(832)	(1241)	(30.9)	(2.80)	(462)	∞	∞	(610)	(1014)	(140)	∞	

It can be seen that diagonal cracking will first occur either as web-shear cracking near the support or as flexure-shear cracking near the quarter-point of the span. For this particular beam web-shear cracking is predicted to occur when the uniformly distributed load reaches 2.30 kips/ft (33.6 kN/m).

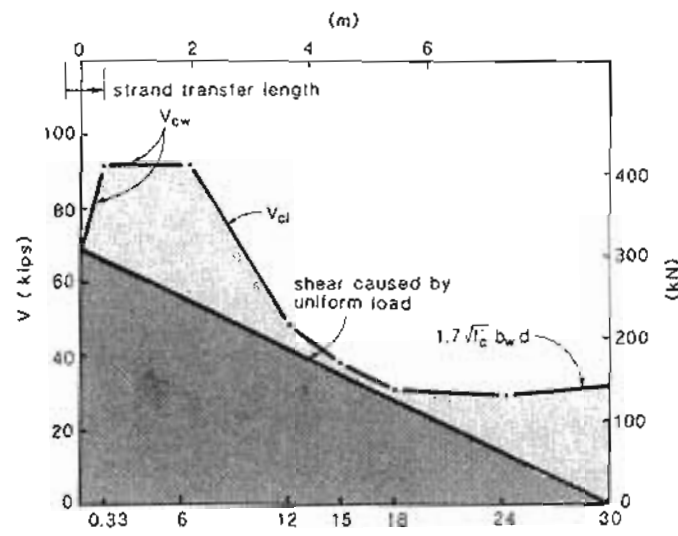
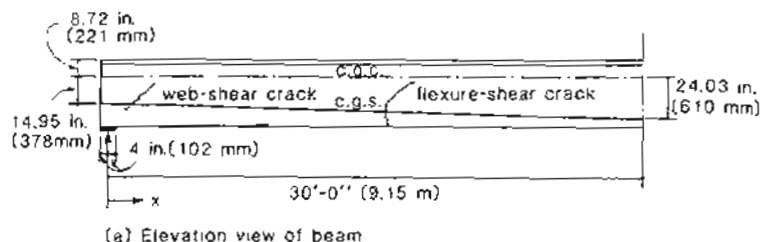


Figure 7-10 Diagonal cracking of uniformly loaded beam.

7.4 BEHAVIOR AFTER DIAGONAL CRACKING

Prior to cracking of the concrete, the shear in the web of a beam is carried by a set of diagonal compressive stresses in one direction complemented by a set of diagonal tensile stresses at 90° to the compressive stresses. Figure 7-11 shows the trajectories of these principal stresses for a reinforced concrete T-beam subjected to uniform load.

When diagonal cracks form, the ability of the concrete to transmit principal tensile stresses is severely reduced and unless appropriate reinforcement is present, failure may result. With appropriate reinforcement a new system of internal stresses can develop after

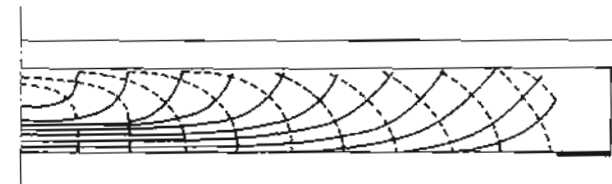


Figure 7-11 Reinforced concrete T-beam subjected to uniform load. Adapted from Mörsch (Ref. 7-14).

cracking which will enable the member to continue to carry shear. Figure 7-12 compares possible stress fields in the web of a reinforced concrete beam before and after cracking. Before cracking the principal tensile and compressive stresses play an equal role in resisting the shear (i.e., $f_1 = f_2 = v$). After cracking, if the tensile stresses in the concrete go to zero (i.e., $f_1 = 0$) and if the principal compressive stresses in the concrete remain inclined at 45°, then these compressive stresses must double in value to carry the same shear (i.e., $f_2 = 2v$). Assuming no tension in the concrete, longitudinal reinforcement in tension is required to balance the longitudinal component of the diagonal compression and web reinforcement in tension is required to balance the transverse component of the diagonal compression.

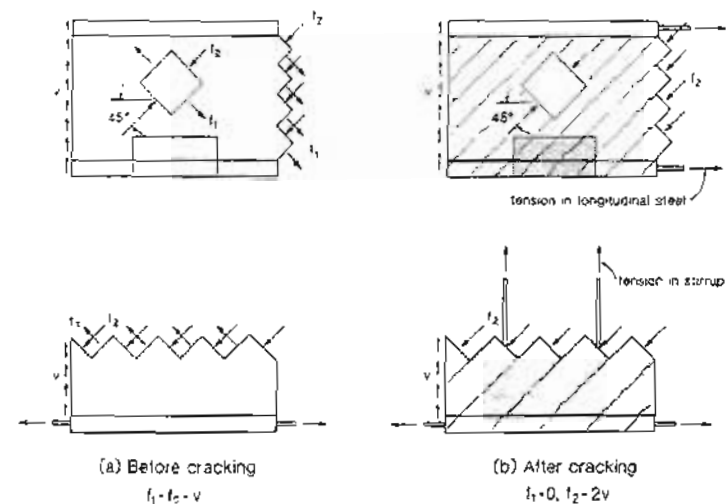


Figure 7-12 Stress fields resisting shear before and after cracking in a reinforced concrete beam.

Two early tests by Mörsch illustrate well the behavior of beams after diagonal cracking. The two simply supported T-beams were subjected to increasing levels of uniformly distributed loading. The only significant difference between the two beams was that one beam contained stirrups while the other did not. As can be seen in Fig. 7-13, the initial behavior of the two beams was very similar. In both beams flexural cracks developed at midspan at a load of about 8 tons and by 20 tons, flexural cracks had developed over most of the span. In the beam without stirrups a flexure-shear crack had developed at a load of about 20 tons with a shear failure occurring shortly thereafter. The beam containing stirrups continued to carry load after flexure-shear cracks had formed. At a load of about 36 tons, new diagonal cracks inclined at a flatter angle formed. The beam finally failed in flexure at midspan at a load of 42 tons.

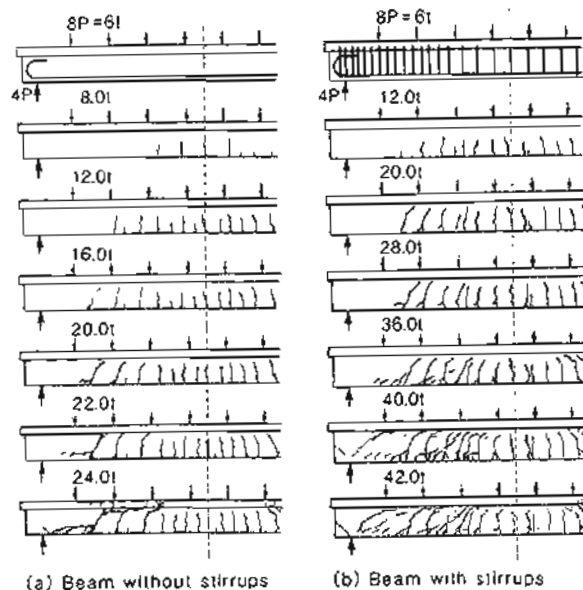


Figure 7-13 Tests of simply supported T-beams subjected to uniformly distributed loads. Adapted from Mörsch (Ref. 7-14).

The objective of shear design is to avoid premature brittle shear failures such as that displayed by the beam without stirrups described above. We wish to design members so that their shear capacity is high enough to ensure a ductile flexural failure of the type exhibited by the beam with stirrups.

Some design models for shear will be briefly reviewed in the following sections.

7.5 THE 45° TRUSS MODEL

In 1899 Ritter (Ref. 7-15) explained the flow of forces in a cracked reinforced concrete beam in terms of a truss model (see Fig. 7-14). The diagonal compressive stresses in the concrete act as the diagonal members of the truss while the stirrups act as vertical tension members. The bottom chord of the truss consists of the longitudinal tension reinforcement while the flexural compression zone of the beam acts as the top chord.

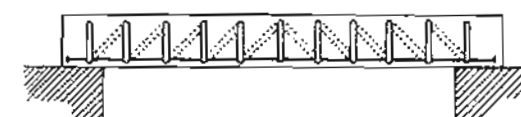


Figure 7-14 Ritter's original drawing of the truss analogy for shear. Adapted from Ref. 7-15.

In his classic 1902 text, Mörsch (Ref. 7-3) explained the truss model in more detail. He made it clear that the compression diagonals do not have to go from the top of one stirrup to the bottom of the next stirrup (see Fig. 7-15a). Later editions of his text (Ref. 7-14) made it clear that rather than having discrete diagonal compressive struts there was a continuous field of diagonal compression resisting the shear (see Fig. 7-15b).

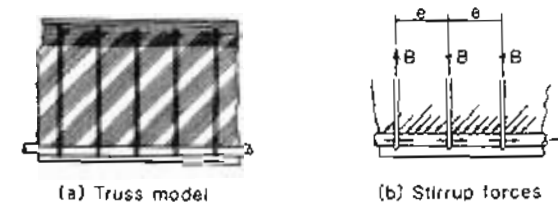


Figure 7-15 Mörtsch's truss model. Adapted from Refs. 7-3 and 7-14.

Both Ritter and Mörsch neglected the tensile stresses in the cracked concrete and assumed that after cracking the diagonal compression stresses would remain at 45°. The equilibrium conditions used by Ritter and Mörsch are summarized in Fig. 7-16. If the shear stresses are assumed to be uniformly distributed over an effective shear area b_w wide and jd deep (see Fig. 7-16a), then the required magnitude of the principal compressive stresses can be found from the free-body diagram in Fig. 7-16b. As the total diagonal compressive force $f_2 \cdot b_w \cdot jd / \sqrt{2}$ must equal $\sqrt{2} V$, the principal compressive stress is given by

$$f_2 = \frac{2V}{b_w jd} \quad (7-10)$$

The longitudinal component of the diagonal compressive force will equal V (see Fig. 7-16b). This force must be counteracted by an equal tensile force, N_v , in the longitudinal reinforcement caused by the shear. Hence the tensile force in the longitudinal reinforcement caused by the shear is given by

$$N_v = V \quad (7-11)$$

From the free-body diagram shown in Fig. 7-16c, it can be seen that the diagonal compressive force, $f_z \cdot b_{ws}/\sqrt{2}$, has a vertical component of $f_z \cdot b_{ws}/2$, which must be balanced by the tensile force in the stirrup, $A_v f_v$. Substituting for f_z from Eq. (7-10) gives

$$\frac{A_v f_v}{s} = \frac{V}{jd} \quad (7-12)$$

where A_v is the cross-sectional area of the stirrup legs, s is the stirrup spacing, f_v is the tensile stress in the stirrups.

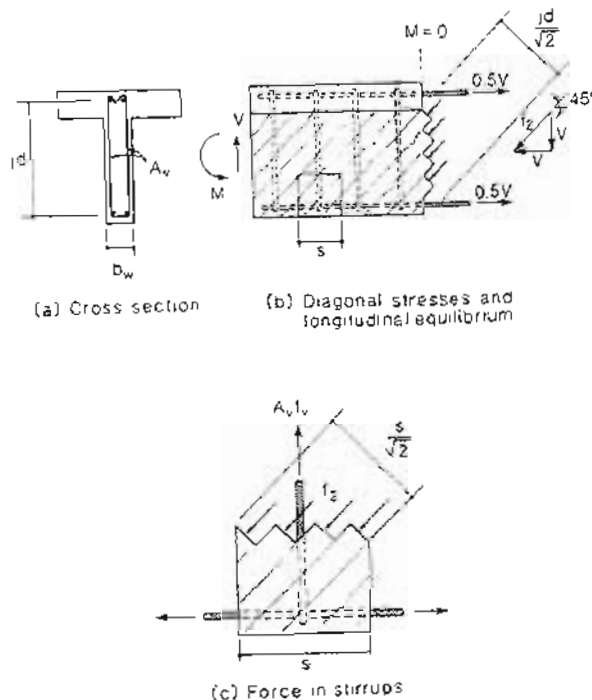


Figure 7-16 Equilibrium considerations for 45° truss

At the time that these equations were developed, design was based upon limiting the stresses at working loads. Stirrup areas and spacings were chosen so that the stirrup stresses given by Eq. (7-12) remained below permissible values. The additional tensile stress in the longitudinal reinforcement caused by shear was checked using Eq. (7-11) while the concrete compressive stress in the web was checked by Eq. (7-10).

In discussing the choice of the angle of inclination of the diagonal compressive stresses, Mörsch in 1922 (Ref. 7-14) made the following statement:

We have to comment with regards to practical application that it is absolutely impossible to mathematically determine the slope of the secondary inclined cracks according to which one can design the stirrups. For practical purposes one has to make a possibly unfavourable assumption for the slope θ and therefore, with $\tan 2\theta = \infty$, we arrive at our usual calculation for stirrups which presumes $\theta = 45^\circ$. Originally this was derived from the initial shear cracks which actually exhibit this slope.

The "secondary inclined cracks" mentioned by Mörsch are the flatter cracks shown in Fig. 7-13b which formed late in the life of the beam. If the stirrups were designed for this flatter slope, fewer stirrups could be used. While Mörsch obviously recognized that the choice of 45° was conservative, he could not see any practical way to determine the slope.

7.6 TRADITIONAL ACI APPROACH

Between 1904 and 1922 several hundred reinforced concrete beams were tested by Talbot and his co-workers at the University of Illinois and by Moritz and Withey at the University of Wisconsin [this work was summarized by Hognestad (Ref. 7-16)]. These early American tests demonstrated that the stirrup stresses were considerably lower than those predicted by the 45° truss model (see Fig. 7-17).

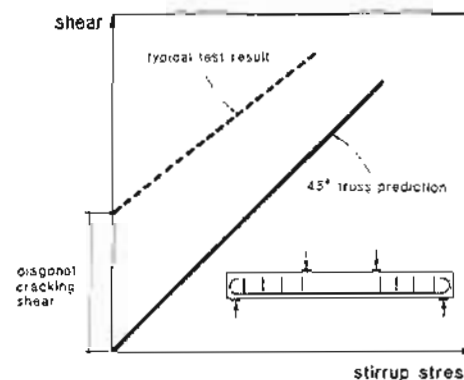


Figure 7-17 Variation of stirrup stress with applied shear.

It is interesting to note that Richart (Ref. 7-17), who conducted many of the early shear tests at the University of Illinois, concluded that the assumption of 45° for the direction of principal compression might be the cause of the discrepancy between the predicted stirrup strains and the smaller measured stirrup strains. He pointed out that decreasing θ to 40° would decrease the predicted stirrup stresses by about 20%.

The conservatism of the 45° truss model is due to the neglect of tensile stresses in the concrete and the choice of 45° for the compressive strut inclination. The 45° truss model predicts that a beam without any transverse reinforcement, such as that shown in Fig. 7-13a, would have zero shear strength. As we have seen, such a beam will not fail in shear until diagonal cracks have formed.

In order to account for the contribution of the tensile stresses in the concrete the first ACI Code in 1910 (Ref. 7-18) stated: "In calculating web reinforcement the concrete shall be considered to carry 40 psi, the remainder to be provided for by means of web reinforcement in tension." As the typical concrete compressive strength in those days was 2000 psi (14 MPa) this working stress code permitted a concrete tensile stress at working loads of 0.02 f'_c (i.e., about 0.04 f'_c at ultimate).

Since this first ACI Code, it has become accepted North American design practice to allocate part of the shear resistance of a beam to concrete in tension, the "concrete contribution," and the remainder to the web reinforcement, the "steel contribution." In the format of the 1989 ACI Code (Ref. 7-2), stirrups must be chosen such that the design shear strength, ϕV_n , is greater than the factored shear, V_u , where the nominal shear strength, V_n , is given by

$$V_n = V_c + V_s \quad (7-13)$$

The concrete contribution, V_c , is taken as the shear at the commencement of diagonal cracking. Typically, for non-prestressed members, V_c is calculated from Eq. (7-8). For prestressed concrete members, V_c can be taken as the smaller of V_{cu} , Eq. (7-4), or V_{ci} , Eq. (7-9). This approach was based primarily on research conducted at the University of Illinois, which is summarized by MacGregor, Sozen, and Siess in Ref. 7-19.

It was seen in Section 7.3 that the determination of V_{cu} and V_c for a practical beam involves considerable calculation. Consequently, the ACI Code gives a more simple expression for V_c which can be used for prestressed concrete members if the effective prestress force exceeds 40% of the flexural strength of the flexural reinforcement. The background for this simplified expression is given by MacGregor and Hanson in Ref. 7-20. The expression is

$$V_c = \left(0.6\sqrt{f'_c} + 700 \frac{V_u d_p}{M_u} \right) b_w d \quad \text{psi} \quad (7-14a)$$

but

$$2\sqrt{f'_c} b_w d \leq V_c \leq 5\sqrt{f'_c} b_w d$$

$$V_c = \left(0.05\sqrt{f'_c} + 4.8 \frac{V_u d_p}{M_u} \right) b_w d \quad \text{MPa} \quad (7-14b)$$

but

$$0.17\sqrt{f'_c} b_w d \leq V_c \leq 0.42\sqrt{f'_c} b_w d$$

In applying Eq. (7-14), the term $V_u d_p/M_u$ shall not be taken as greater than 1.0.

As can be seen from Fig. 7-10, for pretensioned members the diagonal cracking load becomes smaller near the end of the beam due to the reduction in stress in the strands over the transfer length. To account for this reduction, the ACI Code requires that in the transfer length the value of V_c calculated by Eq. (7-14) not exceed V_{cu} given by Eq. (7-4).

The 45° truss equations are used to calculate the steel contribution, V_s . Hence for a beam containing stirrups perpendicular to its axis,

$$V_s = \frac{A_s f_y d}{s} \quad (7-15)$$

To avoid diagonal crushing of the concrete under the factored shear and to limit diagonal cracking at service loads, the steel contribution is limited to

$$V_s \leq 8\sqrt{f'_c} b_w d \quad \text{psi} \quad (7-16a)$$

$$V_s \leq 0.67\sqrt{f'_c} b_w d \quad \text{MPa} \quad (7-16b)$$

In the traditional ACI approach, stirrups are needed only if the required shear strength exceeds V_c . As a consequence, many non-prestressed and prestressed beams constructed in North America contain no stirrups. Beams that do not contain web reinforcement may fail in a relatively brittle manner immediately after the formation of the first diagonal crack. As a consequence, the shear capacity of such members can be substantially reduced by factors such as repeated loading which propagates existing cracks and lowers the "apparent" tensile strength of the concrete; tensile stresses caused by the restraint of shrinkage strains, thermal strains, or creep strains; stress concentrations due to discontinuities such as web openings, termination of flexural reinforcement, or local deviations in tendon profiles.

The 1955 shear failures of the roof beams (see Fig. 7-18) in warehouses used by the U.S. Air Force dramatically illustrated the unsafe nature of the ACI shear design provisions existing then. The beams failed under dead load only, at a shear stress of less than 75 psi (0.5 MPa) while the ACI Code permitted a working shear stress of 90 psi (0.62 MPa), which would correspond to a failure shear stress of about 160 psi (1.10 MPa). The investigation of these failures by Elstner and Hognestad (Ref. 7-21) led to the following recommendations for changes to North American design practice:

1. A minimum amount of web reinforcement should be provided.
2. Flexural reinforcement should be sufficiently extended beyond the points of contraflexure.
3. Tension caused by restraint should be taken into account.

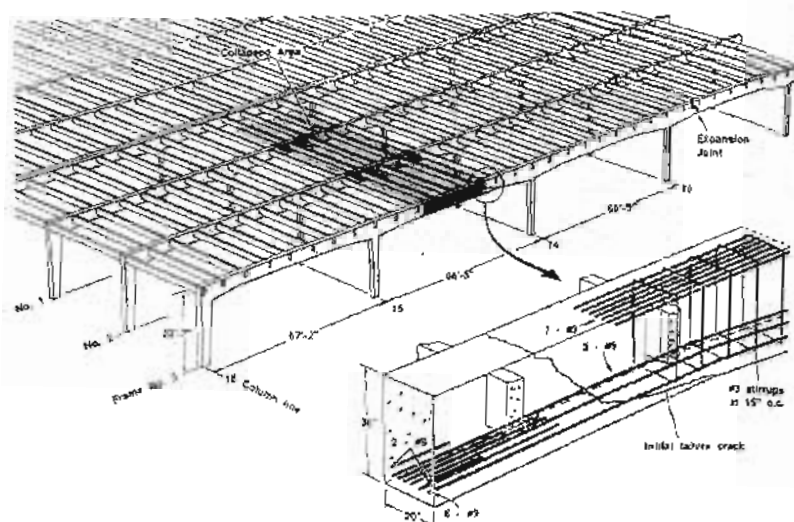


Figure 7-18 Shear failure of roof beams in Air Force warehouse, Wilkins Air Force Depot, Shelby, Ohio.

The current ACI Code (Ref. 7-2) requires a minimum amount of web reinforcement in all flexural members where the factored shear force, V_u , exceeds $\phi V_c/2$. Further, the commentary to this code (Ref. 7-2) recommends that some web reinforcement be used in all thin-webbed post-tensioned members even if V_u is less than $\phi V_c/2$. The minimum amount required by this code is

$$A_c = 50 \frac{b_{w,s}}{f} \quad \text{psi and in.} \quad (7-17a)$$

$$A_v = 0.35 \frac{b_{av} s}{f_u} \quad \text{MPa and mm} \quad (7-17b)$$

In terms of the 45° truss model, this amount of web reinforcement could resist a shear stress of 50 psi (0.35 MPa). For prestressed beams with an effective prestress force not less than 40% of the tensile strength of the flexural reinforcement, the ACI Code permits the minimum amount of shear reinforcement to be calculated by the following equation:

$$A_4 = \frac{A_{p_s}}{80} \frac{f_{pu}}{f_u} \frac{s}{d} \sqrt{\frac{d}{b_m}} \quad (7-18)$$

In addition to requiring a minimum amount of web reinforcement, the ACI Code sets limits on the maximum spacing of the stirrups. The stirrup design requirements are summarized in Fig. 7-19.

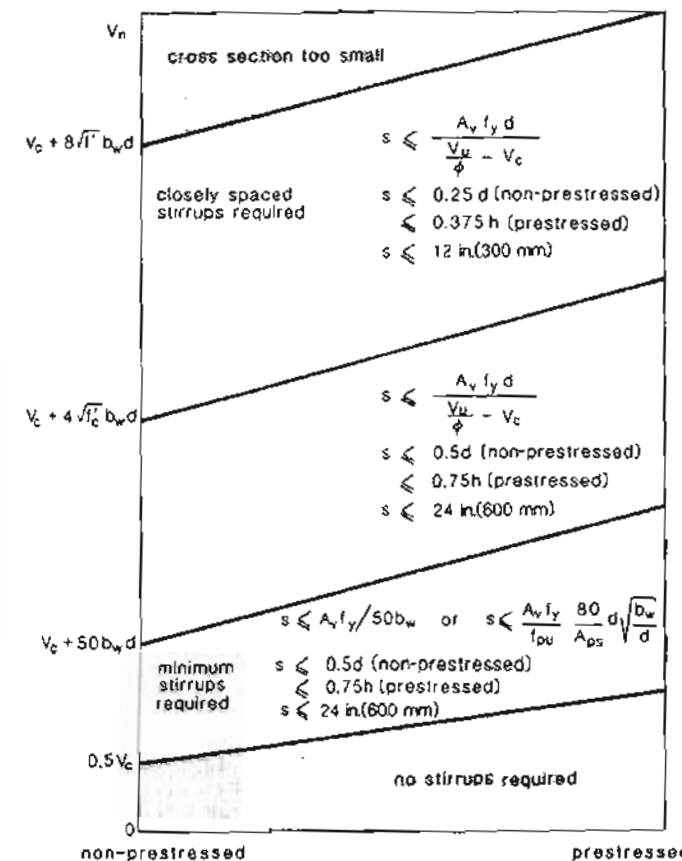


Figure 7-19 Startup design requirements of ACI Code.

If for high-strength concrete members it is desired to use a value of $\sqrt{f'_c}$ higher than 100 psi (8.3 MPa) then the amount of minimum reinforcement must be increased by a factor equal to $f'_c/5000$ psi ($f'_c/35$ MPa) but this factor need not exceed 3.

The most serious deficiency of the ACI shear design practice of the 1950s was the neglect of the role played by the longitudinal reinforcement. The Air Force warehouse beams would not have collapsed if they had contained sufficient longitudinal reinforcement. The truss analogy predicts that in order to resist shear, a beam needs both stirrups and longitudinal reinforcement. Richart in 1927 observed that the measured stresses in the longitudinal reinforcement were considerably higher than those calculated by considering only the influence of moment. Unfortunately, it was not clearly identified that the increase in stress in the longitudinal reinforcement was due to shear. After 1963 the ACI Code, rather than specifying the additional amount of longitudinal reinforcement required for shear, gave rules for the extension of flexural reinforcement (e.g., "reinforcement shall extend beyond the point at which it is no longer required to resist flexure for a distance equal to the effective depth of the member").

Because of concern that the ACI approach may be unconservative for beams with low amounts of longitudinal reinforcement, the ACI-ASCE committee on shear and diagonal tension (Ref. 7-22) recommended that V_c should be taken as a function of the percentage of longitudinal reinforcement. However, this recommendation was not incorporated into the ACI Code because there was concern with complexity and it was believed that the minimum shear reinforcement requirements would prevent unconservative designs.

The ACI equations and the truss model imply that as the shear is increased more stirrups are required. For a simply supported beam subjected to a uniform load it would thus appear that the amount of shear reinforcement would have to keep increasing up to the face of the support, where the shear is a maximum. However, experiments on such beams have shown that the maximum stirrup stresses do not occur at the face of the support (see Fig. 7-20). To recognize the beneficial influence of direct supports, the ACI Code permits regions close to such supports to be designed for the shear that exists at distance d from the face of the support for non-prestressed members and for the shear that exists at a distance of $h/2$ from the face of the support for prestressed members.

7.7 DESIGN EXAMPLE USING ACI SHEAR PROVISIONS

Design the stirrups for the PCI Standard single-tee beam described in Section 7.3. Assume that the member carried a service live load of 75 psf (3.6 kN/m^2) as well as a superimposed dead load of 15 psf (0.72 kN/m^2). The self-weight of the normal-density 10ST36 is 715 lb/ft (10.4 kN/m).

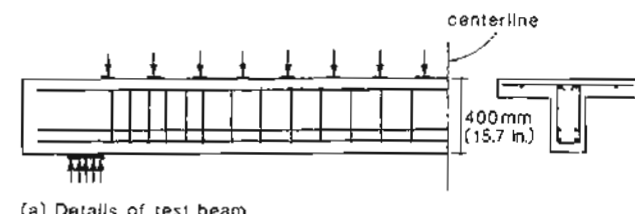
Step 1: Determine the required shear strengths.

The uniformly distributed factored load, w_u , is

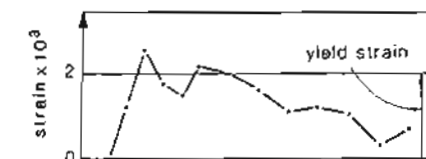
$$\begin{aligned} w_u &= 1.4(0.715 + 0.015 \times 10) + 1.7(0.075 \times 10) \\ &= 2.49 \text{ kips/ft (36.3 kN/m)} \end{aligned}$$

Hence the shear at $h/2$ from the face of the support is

$$\begin{aligned} V_u &= 2.49(30 - 0.33 - 1.50) \\ &= 70.1 \text{ kips (312 kN)} \end{aligned}$$



(a) Details of test beam



(b) Observed stirrup strains near failure load

Figure 7-20 Observed variation of stirrup strains along length of uniformly loaded beam. Adapted from Mailhot (Ref. 7-23).

Hence the required nominal shear strength near the support is

$$\begin{aligned} V_n &= \frac{V_u}{\phi} \\ &= \frac{70.1}{0.85} \\ &= 82.5 \text{ kips (367 kN)} \end{aligned}$$

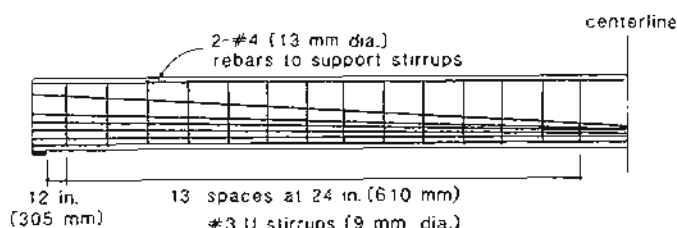
Step 2: Determine the concrete contribution, V_c .

The concrete contribution, V_c , is taken as equal to the diagonal cracking shear. The shears required to cause diagonal cracking at various locations along the beam have been calculated in Section 7.3 and are summarized in Fig. 7-21.

Step 3: Determine the required steel contributions, V_s .

The required steel contribution, V_s , is $V_u/\phi - V_c$. As can be seen from Fig. 7-21, V_u/ϕ exceeds V_c near the end of the beam and in a region near the quarter-point of the span. The maximum value of V_s required occurs at the face of the support and has a value of

$$\begin{aligned} V_s &= \frac{V_u}{\phi} - V_c \\ &= 82.5 - 68.2 \\ &= 14.3 \text{ kips (64 kN)} \end{aligned}$$



(a) Reinforcement details

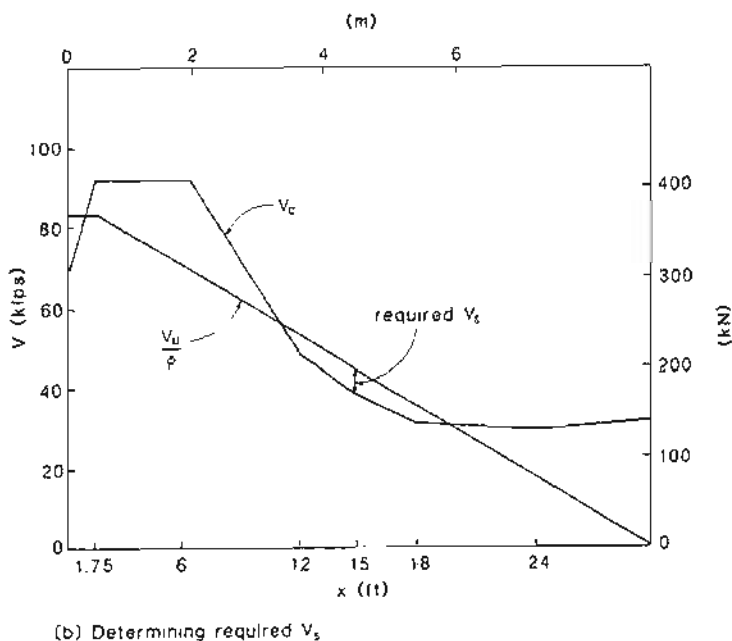


Figure 7-21 Design of stirrups by ACI method.

As we will use #3 double-legged stirrups with $f_y = 60$ ksi (414 MPa), the maximum stirrup spacing at this location, from Eq. (7-15) is:

$$s = \frac{A_v f_y d}{V_s}$$

$$= \frac{0.22 \times 60 \times 28.8}{14.3}$$

$$= 26.6 \text{ in. (675 mm)}$$

Step 4: Determine the minimum shear reinforcement.

From Fig. 7-19,

$$s \leq \frac{A_v f_y}{50 b_w} = \frac{2 \times 0.11 \times 60,000}{50 \times 8}$$

$$= 33 \text{ in. (838 mm)}$$

or

$$s \leq \frac{A_v f_y}{f_{pu}} \cdot \frac{80}{A_{ps}} d \sqrt{\frac{b_w}{d}}$$

$$= \frac{2 \times 0.11 \times 60,000}{270,000} \times \frac{80}{12 \times 0.153} \times 28.8 \sqrt{\frac{8}{28.8}}$$

$$= 32 \text{ in. (821 mm)}$$

but

$$s \leq 0.75 h = 0.75 \times 36$$

$$= 27 \text{ in. (686 mm)}$$

and

$$s \leq 24 \text{ in. (610 mm)}$$

Hence a stirrup spacing of 24 in. (610 mm) will satisfy both the minimum shear reinforcement requirements and the spacing limits of the ACI Code.

Step 5: Choose the stirrup arrangement.

For a stirrup spacing of 24 in. (610 mm), V_s will be

$$V_s = \frac{A_v f_y d}{s}$$

$$= \frac{2 \times 0.11 \times 60 \times 28.8}{24}$$

$$= 15.8 \text{ kips (71 kN)}$$

Hence a uniform spacing of 24 in. (610 mm) will also satisfy the strength requirements. The chosen stirrup arrangement is shown in Fig. 7-21. As is usual practice, the first stirrup has been placed at $s/2$ from the face of the support.

7.8 VARIABLE-ANGLE TRUSS MODELS

The ACI Code modified Mörsch's 45° truss model by adding a "concrete contribution" to compensate for the conservative nature of this model. Alternatively, Mörsch's model can be made more accurate by accounting for the fact that θ is typically less than 45°. Figure 7-22 summarizes the equilibrium conditions for the variable-angle truss model.

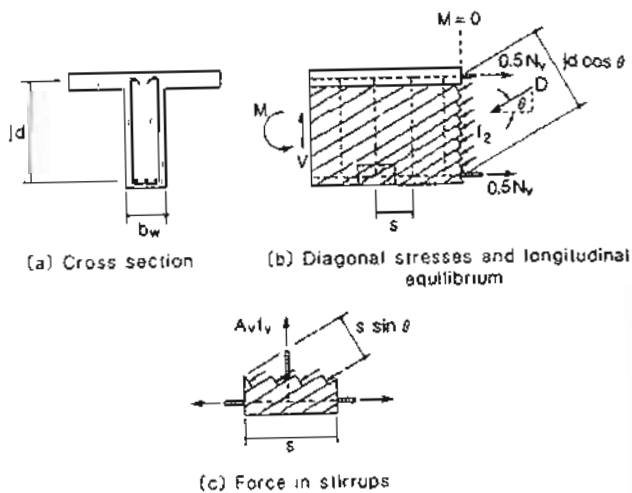


Figure 7-22 Equilibrium conditions for variable-angle truss.

The required magnitude of the principal compressive stresses, f_2 , can be found from the free-body diagram shown in Fig. 7-22b. Equilibrium requires that the resultant D of the diagonal stresses must equal $V/\sin \theta$. As D must equal $f_2 b_w j d \cos \theta$, the principal compressive stress is

$$f_2 = \frac{V}{b_w j d} \frac{1}{\sin \theta \cos \theta} \quad (7-19)$$

$$= \frac{V}{b_w j d} (\tan \theta + \cot \theta)$$

The longitudinal component of the diagonal compressive force will equal $V \cot \theta$ (see Fig. 7-22b). This force must be counteracted by an equal tensile force, N_v , in the longitudinal reinforcement. Hence the tensile force in the longitudinal reinforcement due to shear is

$$N_v = V \cot \theta \quad (7-20)$$

From the free-body diagram shown in Fig. 7-22c it can be seen that the diagonal compressive force, $f_2 b_w s \sin \theta$, has an outward thrust of $f_2 b_w s \sin^2 \theta$, which must be counteracted by the tensile force, $A_v f_r$, in the stirrup. Substituting for f_2 from Eq. (7-19) gives

$$\frac{A_v f_r}{s} = \frac{V}{j d} \tan \theta \quad (7-21)$$

The equilibrium equations above are not sufficient to find the stresses in a beam caused by a given shear. There are four unknowns (i.e., the principal compressive stress, the tensile force in the longitudinal reinforcement, the stress in the stirrups, and the inclination, θ , of the principal compressive stresses), but there are only three equilibrium equations. The fact that there are four unknowns and three equations caused Mörsch to believe that it was impossible to determine the slope θ mathematically.

In 1964, Kupfer (Ref. 7-24) developed a procedure for determining the angle θ using minimum energy principles. In this derivation he assumed that the reinforcement and the concrete were linearly elastic and hence was able to predict the angle, θ , for the cracked elastic range. To minimize the energy in a load-carrying system the stiffer elements must carry more load. For typical reinforced concrete beams the longitudinal reinforcement is much stiffer than the stirrups, and hence the value of θ for minimum energy is less than 45°.

In the traditional truss model the failure shear of a beam is determined from equilibrium equation (7-21) by assuming that at failure the stirrups yield (i.e., $f_r = f_y$) and by assuming that $\theta = 45^\circ$. Rather than assuming that $\theta = 45^\circ$, we could assume a compressive stress, f_2 , in the concrete at failure and then find V and θ by solving the two simultaneous equations (7-19) and (7-21). Alternatively, we could assume that at failure both the longitudinal reinforcement and the stirrups yield and then use Eqs. (7-20) and (7-21) to determine V and θ . These approaches which consider the mechanisms of failure, are referred to as plasticity methods. Summaries of these methods are given by Nielsen (Ref. 7-25) and by Thürliann et al. (Ref. 7-26).

In predicting the shear strength of beams using variable-angle truss models it is necessary to use an "effective" concrete compressive strength less than the cylinder crushing strength. A value of $0.6 f'_c$ is frequently recommended (e.g., Refs. 7-26 and 7-27). Additionally, it has been recommended (Ref. 7-26) that $\tan \theta$ not be taken less than 0.5 (i.e., $\theta \geq 27^\circ$). The variable-angle truss model was introduced into the 1978 CEB-FIP Code (Ref. 7-28). In using this code, the designer can choose θ between 31° and 59°. Additionally, for lightly loaded beams there is a small concrete contribution.

In the derivations of the truss equations we have considered a length of beam over which the shear remains constant (see Fig. 7-22). Some additional considerations are necessary when the shear force varies along the length of the member. Fig. 7-23a shows a cantilever beam subjected to uniformly distributed load. The internal flow of forces in this beam can be approximated using the truss model shown in Fig. 7-23b. By solving the statics of the truss the stirrup forces along the length of the beam can be found (see Fig. 7-23c). It can be seen that the force in a stirrup at a certain location is not directly related to the shear at that location. The stirrup force, $A_v f_r$, given by Eq. (7-21) equals $V \cdot s \tan \theta / (j d)$. As can be seen from Fig. 7-23c, the "correct" stirrup force is obtained

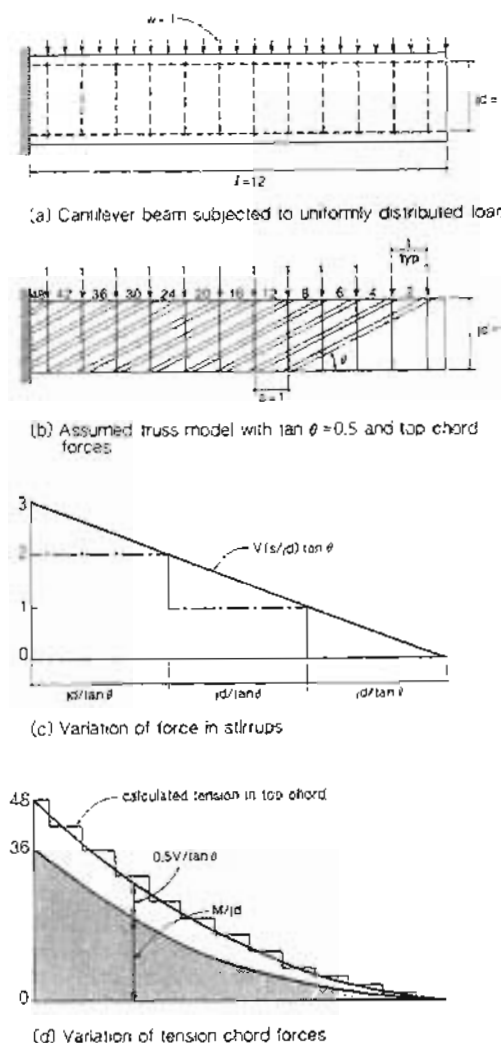


Figure 7-23 Internal forces in uniformly loaded beam.

from this expression if the shear used. V_s is the lowest value of shear within the length $jd \cot \theta$. Designing for this lowest shear has become known as the "staggering concept" for shear design (Refs. 7-23, 7-29, 7-30 and 7-31).

Figure 7-24 illustrates the staggering concept for shear design. The stirrups between A and B in this figure must resist a force equal to the difference between the upward support reaction and the downward uniform load. This difference in force equals the shear at section B. Hence the stirrups between sections A and B are designed to resist the lowest shear within this length.

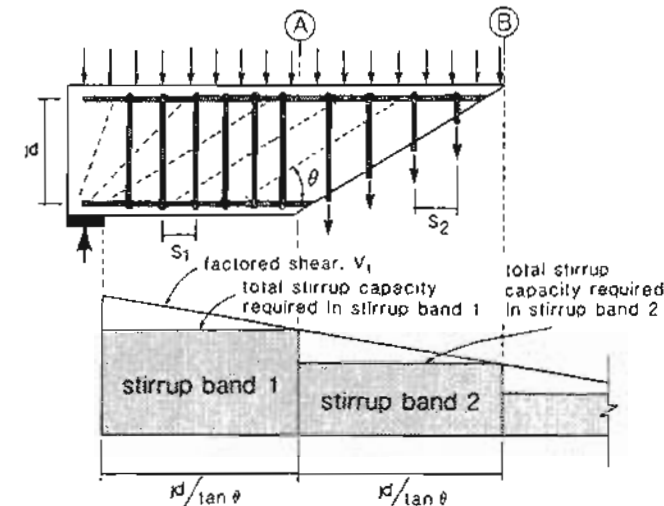
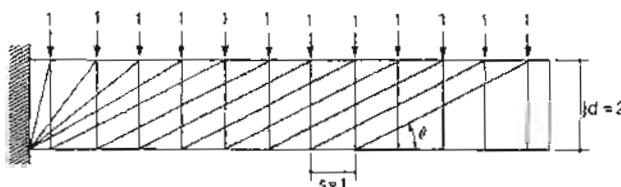
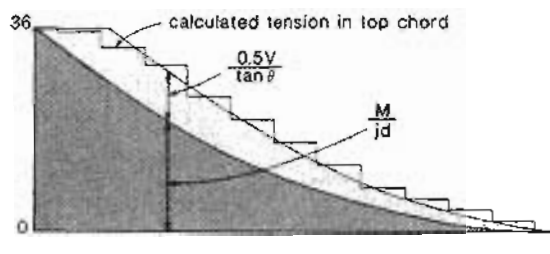


Figure 7-24 The staggering concept for shear design.

Shear causes tension, not only in the stirrups, but also in the longitudinal reinforcement. Fig. 7-23d gives the calculated tension in the top chord of the truss. It can be seen that this tension exceeds that due to flexure, M/jd , by an amount equal to about $0.5V \cot \theta$.

The truss model shown in Fig. 7-23b assumes that the shear stresses at the support are uniformly distributed over the depth of the beam. If the top longitudinal steel begins to yield the shear stress distribution will change so that more of the shear is carried in the flexural compression zone of the beam. The truss model shown in Fig. 7-25a will more accurately model the internal flow of forces for this situation. The fanning of the diagonal compressive struts near the support will reduce the tension in the top chord in this region. The tension in the top chord at the support now equals that due to moment alone, M/jd (see Fig. 7-25b).

Constructing the truss model for the simple cantilever shown in Fig. 7-23 was a straightforward task. However, in many practical situations more thought is required before a suitable truss can be developed. Figure 7-26a shows a simply supported beam subjected to uniform load. A possible truss model, which approximates the flow of internal forces, is shown in Fig. 7-26b. Analyzing this truss is complicated by the fact that it is internally

(a) Assumed truss model with $\tan \theta = 0.5$ 

(b) Variation of tension chord forces

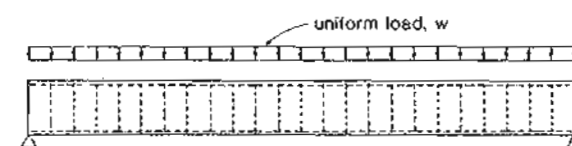
Figure 7-25 Effect of fanning of diagonal compressive stresses on tensile forces in longitudinal reinforcement.

statically indeterminate. A simpler, statically determinate truss model can be developed using the procedures recommended by Marti (Ref. 7-27). In this truss (see Fig. 7-26c), each vertical member represents the group of stirrups within a length of $jd \cot \theta$. The force in each vertical member is thus equal to the total stirrup force within the length $jd \cot \theta$. In a similar fashion each diagonal member of the simplified truss represents a zone of diagonal compression. From the equilibrium conditions given in Fig. 7-22b, the compressive stress in the concrete, f_2 , can be related to the diagonal force, D , as

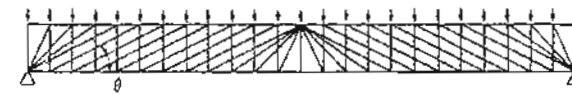
$$f_2 = \frac{D}{b_w jd \cos \theta} \quad (7-22)$$

7.9 COMPRESSION FIELD THEORY

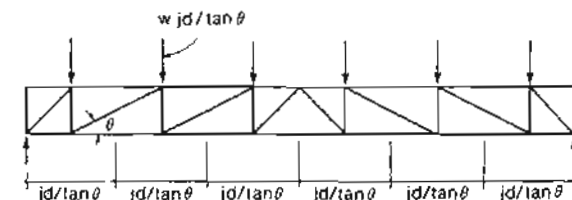
Before the equilibrium equations of the variable-angle truss model can be used to design a member for shear, the inclination, θ , of the diagonal compressive struts must be known. In 1929, Wagner (Ref. 7-32) treated an analogous problem in studying the postbuckling shear



(a) Simply supported beam subjected to uniform load



(b) Detailed truss model of beam



(c) Truss model used for design

Figure 7-26 Development of truss model for design

resistance of thin-webbed metal girders. He assumed that after buckling, the thin webs would not resist compression and that the shear would be carried by a field of diagonal tension (see Fig. 7-27).

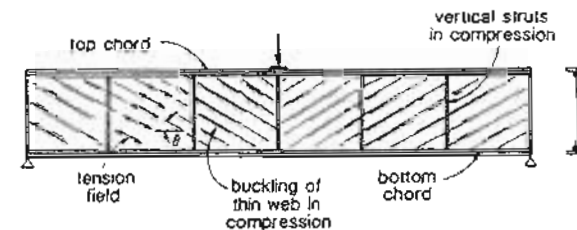


Figure 7-27 Tension fields in thin-webbed metal girder subjected to shear.

To determine the angle of inclination of the diagonal tension, Wagner considered the deformations of the system. He assumed that the angle of inclination of the diagonal tensile stresses would coincide with the angle of inclination of the principal tensile strains. This approach became known as the tension field theory.

Applying Wagner's approach to reinforced concrete, and assuming that after cracking the concrete carries no tension and that the shear is carried by a field of diagonal compression, results in the following expression for the angle of inclination of the diagonal compression

$$\tan^2 \theta = \frac{\epsilon_x - \epsilon_2}{\epsilon_t - \epsilon_2} \quad (7-23)$$

where ϵ_x = longitudinal strain of web, tension positive

ϵ_t = transverse strain, tension positive

ϵ_2 = principal compressive strain, negative quantity

For a given value of θ , Eq. (7-23) can be regarded as a compatibility condition relating the three strains, ϵ_2 , ϵ_x and ϵ_t .

If strains in three directions are known, the strain in any other direction can be found from geometry. The Mohr's circle of strains shown in Fig. 7-28 elegantly summarizes the transformations involved. For cracked concrete these compatibility relationships are expressed in terms of the "average" strains. That is, strains measured over base lengths long enough to include several cracks (see Fig. 7-28a).

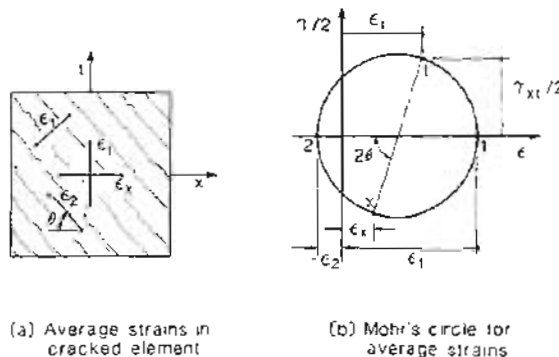


Figure 7-28 Compatibility conditions for cracked web element.

Note that from the Mohr's circle, the principal tensile strain in the web is

$$\epsilon_1 = \epsilon_x + \epsilon_t - \epsilon_2 \quad (7-24)$$

and the shear strain in the web is

$$\gamma_{xy} = 2(\epsilon_x - \epsilon_2) \cot \theta \quad (7-25)$$

The physical significance of Eq. (7-23) can be appreciated if Fig. 7-29a and b are compared. For low crack inclinations (i.e., low θ), the web reinforcement will be highly strained while for steep crack inclinations (i.e., high θ), the longitudinal reinforcement will be highly strained.

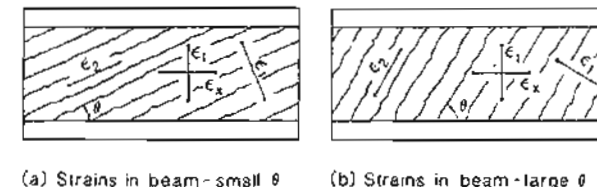


Figure 7-29 Influence of θ on reinforcement strains.

If we consider a symmetrically reinforced, longitudinally prestressed concrete beam subjected to shear, we can see that for a given level of shear, V , there are a total of five unknowns: the stress in the longitudinal bars, f_z ; the stress in the longitudinal prestressing tendons, f_p ; the stress in the stirrups, f_v ; the diagonal compressive stress in the concrete, f_2 ; and the inclination, θ , of these diagonal compressive stresses. To find these five unknowns we have three equilibrium equations, two compatibility equations, and the constitutive relationships for the materials linking the stresses and the strains (see Fig. 7-30). By using the equilibrium, compatibility, and stress-strain relationships, the complete load-deformation response of a member subjected to shear can be determined. This approach has become known as the compression field theory (Refs. 7-29, 7-33 and 7-34).

The compressive stress-strain relationship for concrete is usually defined from the response of a standard concrete cylinder. As described in Section 3.3, this relationship may be described by a parabola or by the more complex expression of Eq. (3-1). In either case, the stress peaks at a stress of f'_c when the corresponding strain is ϵ'_c . In formulating stress-strain relationships for the cracked concrete in the web of a beam subjected to shear, it must be appreciated that the strain conditions to which this concrete is subjected differ from those in a cylinder test. As shown in Fig. 7-31, concrete in a cylinder test is subjected to only small tensile strains due to the Poisson's effect. On the other hand, in the diagonally cracked web the concrete is subjected to very substantial tensile strains. In addition, the compressive stress, f_2 , may need to be transmitted across previously formed cracks. Because of these influences the concrete in a diagonally cracked web is weaker and softer than the concrete in a cylinder.

To investigate the stress-strain characteristics of diagonally cracked concrete, Vecchio and Collins (Ref. 7-35) tested reinforced concrete elements in pure shear (see Fig. 7-32). Based on these tests, they found that the principal compressive stress in the concrete, f_2 , is a function not only of the principal compressive strain, ϵ_2 , but also of the coexisting principal

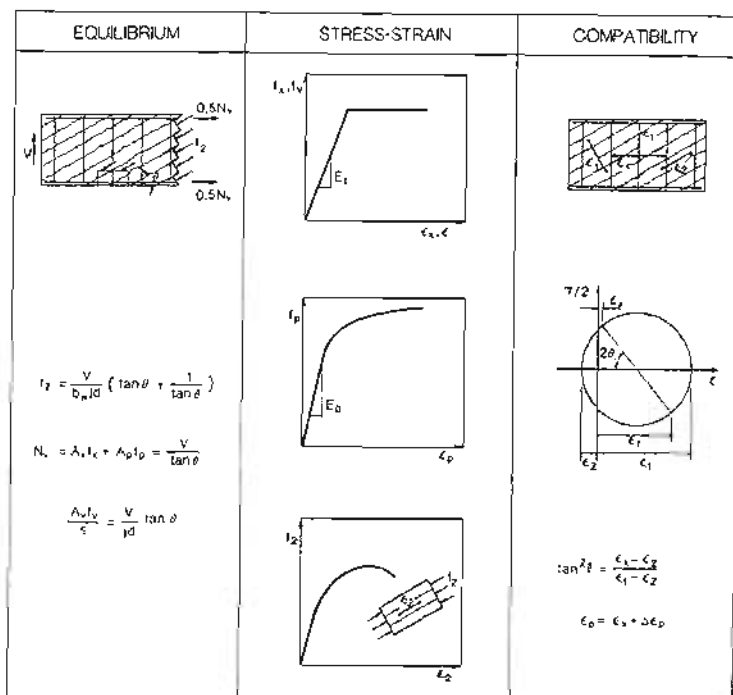


Figure 7-30 Compression field theory for prestressed beam subjected to shear.

tensile strain, ϵ_1 . They suggested (Ref. 7-36) the following stress-strain relationship

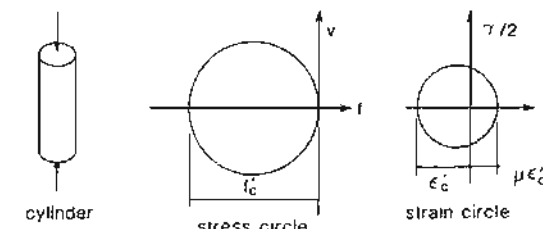
$$f_2 = f_{2\max} \left[2 \left(\frac{\epsilon_1}{\epsilon'_c} \right) - \left(\frac{\epsilon_1}{\epsilon'_c} \right)^2 \right] \quad (7-26)$$

where

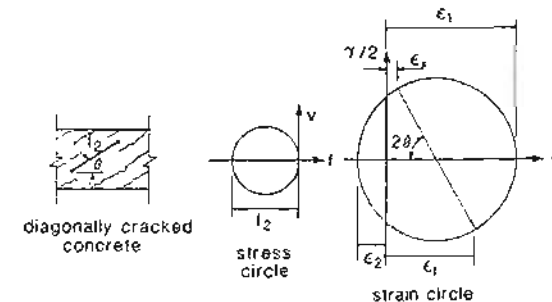
$$\frac{f_{2\max}}{f'_c} = \frac{1}{0.8 + 170\epsilon_1} \leq 1.0$$

Note that increasing ϵ_1 will reduce $f_{2\max}/f'_c$. This relationship is illustrated in Fig. 7-33.

By using the equilibrium conditions, the compatibility conditions, and the appropriate stress-strain relationships for reinforcement and for diagonally cracked concrete it is possible to predict not only the strength but the load-deformation response of members loaded in shear. However, because the compression field theory neglects the contribution of tensile stresses in the cracked concrete, it overestimates deformations and gives conservative estimates of strength. The modified compression field theory, explained in Section 7.10, accounts for the influence of tension in the concrete.



(a) Stress and strain conditions for a concrete cylinder



(b) Stress and strain conditions for diagonally cracked web

Figure 7-31 Comparison of conditions in a cylinder and in diagonally cracked concrete.

7.10 THE MODIFIED COMPRESSION FIELD THEORY

Figure 7-34 illustrates the stress field in the web of a non-prestressed beam before and after cracking. Prior to cracking, the shear is carried equally by diagonal tensile and diagonal compressive stresses acting at 45°. After diagonal cracks form the tensile stresses in the concrete are substantially reduced. In the compression field theory it is assumed that the principal tensile stress, f_1 , equals zero after the concrete has cracked. On the other hand, the modified compression field theory accounts for the contribution of the tensile stresses in the concrete between the cracks (see Fig. 7-34c).

The equilibrium conditions for the modified compression field theory will be introduced using the symmetrical cross section subjected to pure shear shown in Fig. 7-35. The total area of longitudinal prestressing tendons in the section is A_{pt} and the total area of non-prestressed reinforcement is A_{sr} . The shear on this section will be resisted by the diagonal compressive stresses, f_2 , together with the diagonal tensile stresses, f_1 . It should



Figure 7-32 Reinforced concrete element failing in shear. From Vecchio and Collins (Ref. 7-35).

be recognized that the tensile stresses in the diagonally cracked concrete vary in magnitude from zero at the crack locations to peak values between the cracks (see Fig. 7-35b). As the equilibrium equations are obtained by integrating the stresses over the cross section it is appropriate to use the average value of the tensile stresses when formulating these equilibrium expressions.

From the Mohr's stress circle shown in Fig. 7-35c, the following relationship for the principal compressive stress, f_2 , can be derived:

$$f_2 = (\tan \theta + \cot \theta) v - f_1 \quad (7-27)$$

where

$$v = \frac{V}{b_w j d} \quad (7-5)$$

The diagonal compressive stresses push apart the flanges of the beam while the diagonal tensile stresses pull them together (see Fig. 7-35). The unbalanced component must be carried by tension in the web reinforcement. This equilibrium requirement can be expressed as

$$A_u f_v = (f_2 \sin^2 \theta - f_1 \cos^2 \theta) b_w s$$

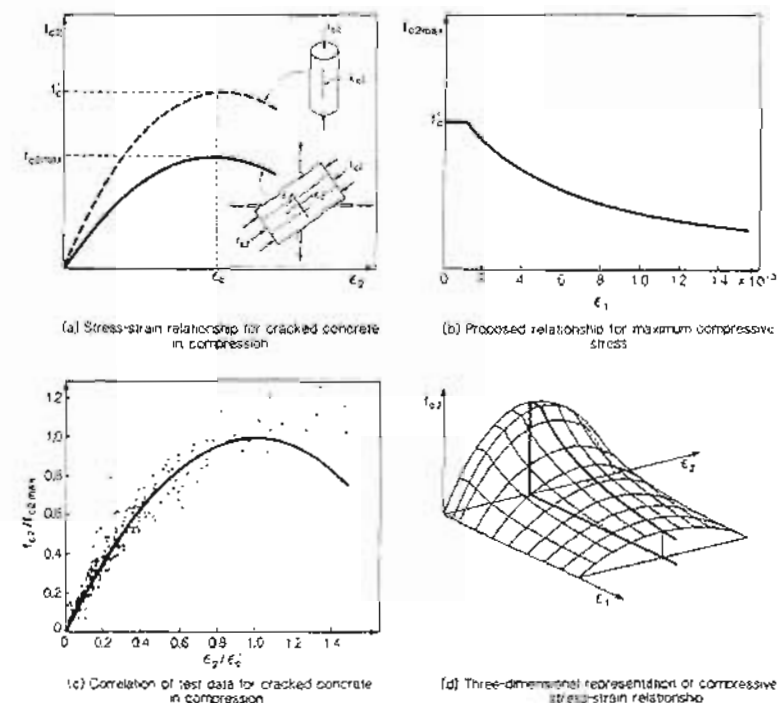


Figure 7-33 Compressive stress-strain relationship for cracked concrete.

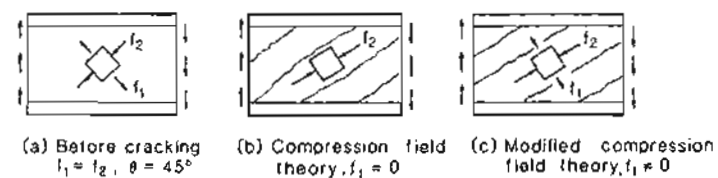


Figure 7-34 Stress fields in web of reinforced concrete beam.

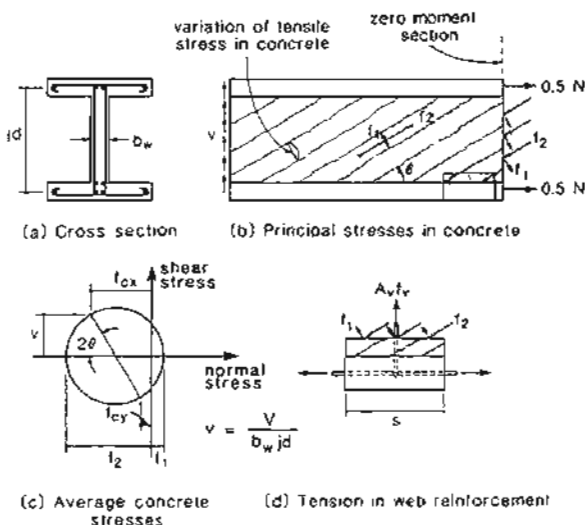


Figure 7-35 Equilibrium conditions of modified compression field theory.

where f_{cr} is the average stress in the stirrups. Substituting for f_2 from Eq. (7-27) gives

$$V = f_1 b_w j d \cot \theta + \frac{A_v f_v}{s} j d \cot \theta \quad (7-28)$$

Equation (7-28) expresses the shear resistance of a member as the sum of a concrete contribution, which depends on tensile stresses in the concrete, and a steel contribution, which depends on tensile stresses in the stirrups. That is, it has the same form as the ACI shear equation $V_c + V_s$.

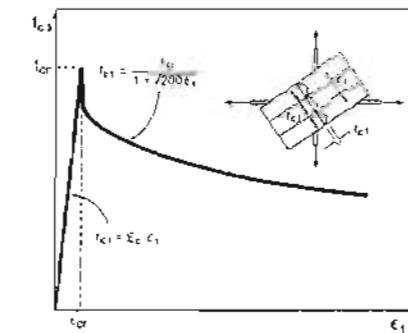
If the axial load on the member is zero, the unbalanced longitudinal component of the diagonal concrete stresses must be equilibrated by tensile stresses in the longitudinal reinforcement. This longitudinal equilibrium requirement can be expressed as

$$A_{sx} f_t + A_{px} f_p = (f_2 \cos^2 \theta - f_1 \sin^2 \theta) b_w j d$$

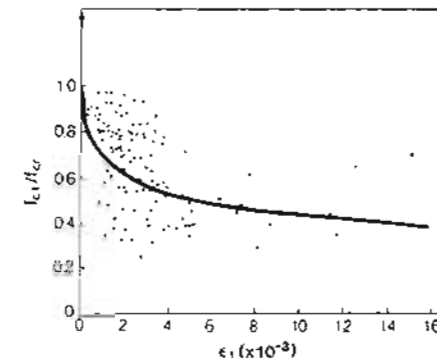
where f_t and f_p are the average stresses in the longitudinal reinforcing bars and longitudinal prestressing steel. Substituting for f_2 from Eq. (7-27) gives

$$A_{sx} f_t + A_{px} f_p = V \cot \theta - f_1 b_w j d \quad (7-29)$$

Based on their tests of reinforced concrete panels in pure shear, Vecchio and Collins (Ref. 7-36) recommended the average tensile stress vs. average tensile strain relationship illustrated in Fig. 7-36



(a) Average stress-strain relationship for cracked concrete in tension



(b) Correlation of test data for cracked concrete in tension

Figure 7-36 Tensile stress-strain relationship for diagonally cracked concrete.

To be consistent with the expression used in Section 4.10, it is recommended that the following relationships be used

$$\text{if } \epsilon_1 \leq \epsilon_{cr} \text{ then } f_1 = E_c \epsilon_1 \quad (7-30)$$

$$\epsilon_1 > \epsilon_{cr} \text{ then } f_1 = \frac{\alpha_1 \alpha_2 f_{cr}}{1 + \sqrt{500\epsilon_1}} \quad (7-31)$$

where α_1 and α_2 are factors accounting for the bond characteristics of the reinforcement and the type of loading (see Section 4.10).

In the treatment above we have considered average stresses and average strains and have not dealt with local variations. The stresses that occur at a crack location will differ from the calculated average values (see Fig. 7-37). At a crack the tensile stress in the concrete goes to zero, while the tensile stresses in the reinforcement become larger. The shear capacity of the member may be limited by the ability of the member to transmit forces across the crack.

At low shear values, tension is transmitted across the crack by local increases in reinforcement stresses. At a certain shear force the stress in the web reinforcement will just reach yield at the crack locations. At higher shear forces transmitting tension across the crack will require local shear stresses, v_{ci} , on the crack surface (see Fig. 7-37c).

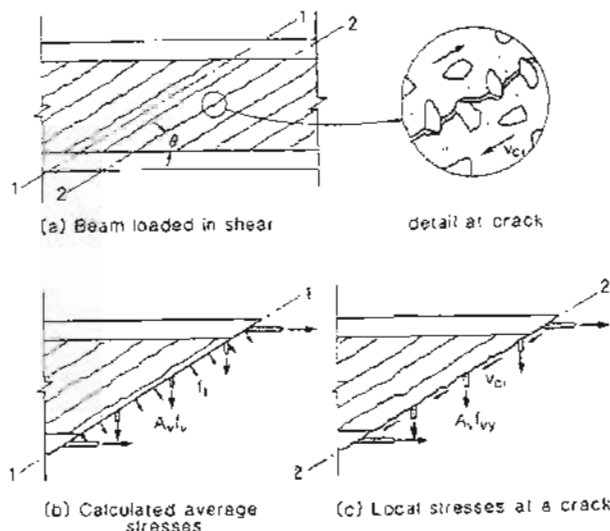


Figure 7-37 Transmitting forces across cracks.

The ability of the crack interface to transmit these shear stresses will depend on the crack width, w . It is suggested that the limiting value of v_{ci} be taken as

$$v_{ci} = \frac{2.16\sqrt{f'_c}}{0.3 + \frac{24w}{a+0.63}} \quad \text{psi and in} \quad (7-32a)$$

$$v_{ci} = \frac{0.18\sqrt{f'_c}}{0.3 + \frac{24w}{a+16}} \quad \text{MPa and mm} \quad (7-32b)$$

where a is the maximum aggregate size. The expression above has been simplified from the expressions developed by Vecchio and Collins (Ref. 7-36) using the experimental data of Walraven (Ref. 7-37). In the expression above the beneficial effects of local compressive stresses across the crack have been ignored.

The two sets of stresses shown in Fig. 7-37b and c must be statically equivalent. The requirement that the two sets of stresses produce the same vertical force is

$$A_v f_v \left(\frac{jd}{s \tan \theta} \right) + f_1 \frac{b_w jd}{\sin \theta} \cos \theta = A_v f_{vy} \left(\frac{jd}{s \tan \theta} \right) + v_{ci} b_w jd$$

and hence, to maintain this equality, f_1 must be limited to

$$f_1 = v_{ci} \tan \theta + \frac{A_v}{sb_w} (f_{vy} - f_v) \quad (7-33)$$

where v_{ci} is given by Eq. (7-32).

The crack width, w , to be used in Eq. (7-32) can be taken as the product of the principal tensile strain, ϵ_1 , and the average spacing of the diagonal cracks. Thus

$$w = \epsilon_1 s_{m\theta} \quad (7-34)$$

The spacing of the inclined cracks will depend upon the crack control characteristics of both the longitudinal and the transverse reinforcement. It is suggested that this spacing be taken as

$$s_{m\theta} = 1 / \left(\frac{\sin \theta}{s_{mx}} + \frac{\cos \theta}{s_{mv}} \right) \quad (7-35)$$

where s_{mx} and s_{mv} are the crack spacings indicative of the crack control characteristics of the longitudinal and transverse reinforcement, respectively (see Fig. 7-38). Thus s_{mx} is the average crack spacing that would result if the member was subjected to longitudinal tension while s_{mv} is the average crack spacing that would result if the member was subjected to a transverse tension.

These crack spacings can be estimated from the CEB-FTP Code (Ref. 7-28) crack spacing expression, Eq. (4-23). The CEB expression was intended to calculate crack spacings on the surface of the member. For use in Eq. (7-32) it is crack spacings in the shear area of the beam that are of interest. To account for the fact that crack spacings become larger as the distance from the reinforcement increases, the maximum distance from the reinforcement, instead of the cover distance c , will be used (see Fig. 7-39). Thus, for the uniform tensile straining (i.e., $k_2 = 0.25$), Eq. (4-23) becomes

$$s_{mx} = 2 \left(c_x + \frac{s_x}{10} \right) + 0.25 k_1 \frac{d_{bx}}{\rho_x} \quad (7-36)$$

$$s_{mv} = 2 \left(c_v + \frac{s_v}{10} \right) + 0.25 k_1 \frac{d_{bv}}{\rho_v} \quad (7-37)$$

where $\rho_v = A_v/(b_w s)$ and $\rho_x = (A_{sx} + A_{px})/A_c$, and k_1 is 0.4 for deformed bars or 0.8 for plain bars or bonded strands.

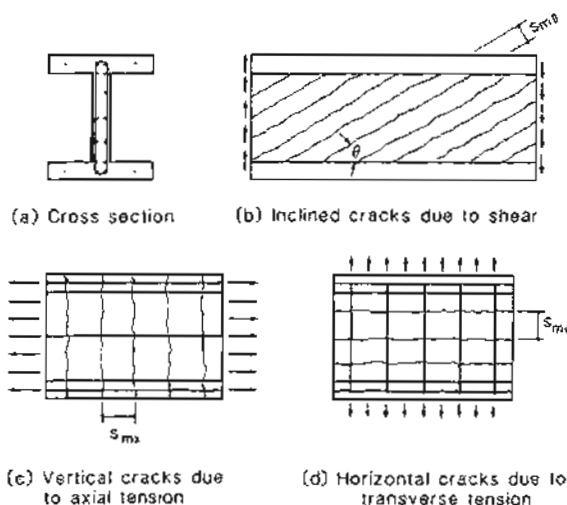


Figure 7-38 Spacing of inclined cracks.

Yielding of the longitudinal reinforcement at a crack may also limit the magnitude of concrete tension that can be transmitted. The requirement that the two sets of stresses in Fig. 7-37 produce the same horizontal force will be satisfied if

$$A_{sx} f_y + A_{px} f_p \geq A_{sx} f_{sx} + A_{px} f_{px} + f_1 b_w j d \\ + \left[f_1 - \frac{A_v}{b_w s} (f_{vy} - f_t) \right] b_w j d \cot^2 \theta \quad (7-38)$$

All of the relationships needed to predict the response of a beam loaded in shear have been discussed above. A suitable solution technique for using these relationships is as follows:

- Step 1: Choose a value of ϵ_1 at which to perform the calculations.
- Step 2: Estimate θ .
- Step 3: Calculate w from Eqs. (7-34), (7-35), (7-36), and (7-37).
- Step 4: Estimate f_v .
- Step 5: Calculate f_t from Eqs. (7-31) and (7-33) and take the smaller value.
- Step 6: Calculate V from Eq. (7-28).
- Step 7: Calculate f_2 from Eq. (7-27).
- Step 8: Calculate f_{2max} from Eq. (7-26).
- Step 9: Check that $f_2 \leq f_{2max}$.
If $f_2 > f_{2max}$, solution is not possible. Return to Step 1 and choose a smaller ϵ_1 .

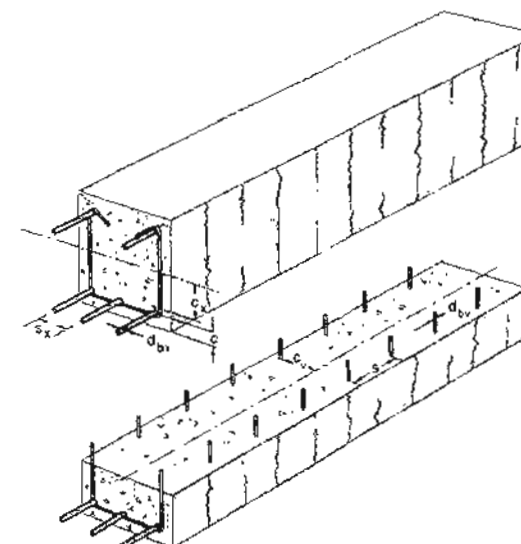


Figure 7-39 Parameters influencing crack spacing.

Step 10: Calculate $c_2 = c'_c \left(1 - \sqrt{1 - f_2/f_{2max}} \right) \dots$ from Eq. (7-26).

Step 11: Calculate ϵ_x and ϵ_t from Eqs. (7-23) and (7-24) as

$$\epsilon_x = \frac{\epsilon_1 \tan^2 \theta + \epsilon_2}{1 + \tan^2 \theta} \\ \epsilon_t = \frac{\epsilon_1 + \epsilon_2 \tan^2 \theta}{1 + \tan^2 \theta}$$

Step 12: Calculate $f_v = E_v \epsilon_t \leq f_{vy}$.

Step 13: Check estimate of f_v . If necessary, revise estimate and return to Step 5.

Step 14: Calculate $f_{v,x} = E_v \epsilon_x \leq f_v$ and $f_p = E_p(\epsilon_x + \Delta \epsilon_p) \leq f_{py}$.

Step 15: Calculate the axial force on the member.

$$N = A_{sx} f_{sx} + A_{px} f_p - \frac{V}{\tan \theta} + f_1 b_w j d - f_c (A_c - b_w j d)$$

where f_c is the axial compressive stress in the concrete areas outside the web.

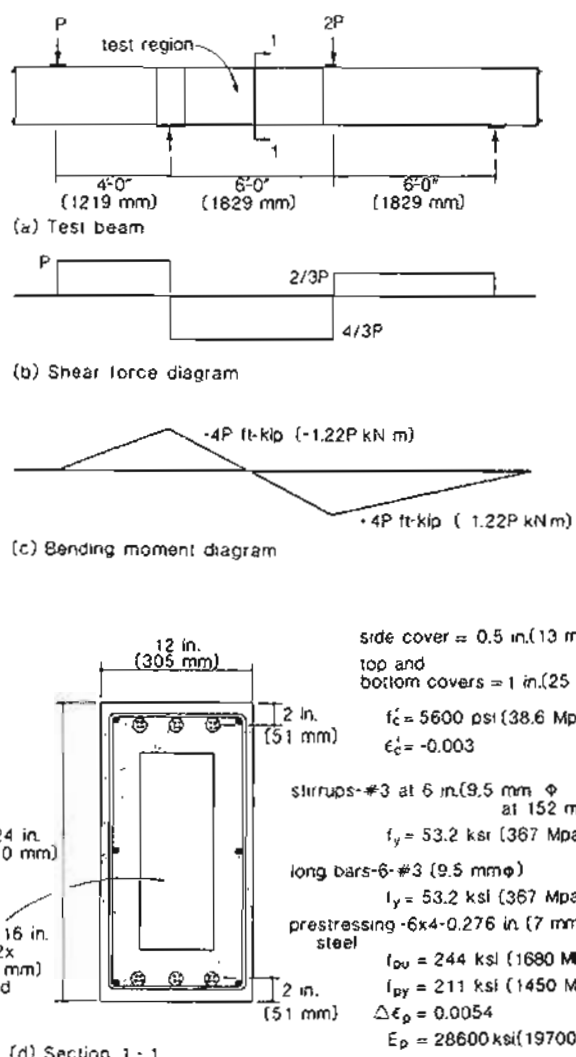


Figure 7-40 Details of beam CF1 tested by Arbesman and Conte (Ref. 7-38).

If ϵ_x is tensile then $f_c = 0$, otherwise,

$$f_c = f'_c \left[2 \left(\frac{\epsilon_x}{\epsilon'_c} \right) - \left(\frac{\epsilon_x}{\epsilon'_c} \right)^2 \right]$$

Step 16: Check the axial load. If N is not equal to the desired value (usually zero), make a new estimate of θ and return to Step 2. Increasing θ increases N .

Step 17: Check that the longitudinal reinforcement can carry stresses across the crack, using Eq. (7-38). If this requirement is not satisfied, we must lower f_t and return to Step 6.

To obtain the complete response of the beam, these calculations are repeated for a range of values of ϵ_1 starting from the cracking strain ($\epsilon_1 \approx 0.1 \times 10^{-3}$) and increasing ϵ_1 until the shear has reached its maximum value. A short computer program called SHEAR, based on the calculation procedure above, is described in Appendix B.

7.11 EXAMPLE OF PREDICTING RESPONSE IN SHEAR

In order to illustrate the procedure that can be used to predict the load-deformation response of a prestressed concrete member subjected to shear, we will consider the member described in Fig. 7-40. This symmetrically reinforced post-tensioned box beam was loaded so that a point of zero moment occurred midway along the test length. We wish to determine the relationship between the applied shear and the strains in the stirrups.

To determine the complete shear force-stirrup strain response, we will determine the shears and stirrup strains that correspond to various values of the principal tensile strain, ϵ_1 . The procedure is described in Section 7.10.

The response of this beam at the location of zero moment can be determined using program SHEAR described in Appendix B. In using this program we must input the crack spacing parameters s_{mx} and s_{my} . As the longitudinal reinforcement consists of both bonded wires ($k_1 = 0.8$) and deformed bars ($k_1 = 0.4$) it is appropriate to use a weighted average for k_1 when calculating s_{mx} . Thus

$$k_1 = \frac{0.4 \times 0.66 + 0.8 \times 1.436}{0.66 + 1.436} = 0.67$$

Hence

$$s_{mx} = 2 \left(5.05 + \frac{2.5}{10} \right) + \frac{0.25 \times 0.67 \times 0.375}{(0.66 + 1.436)/192} = 16.3 \text{ in. (414 mm)}$$

The crack-control parameter in the y -direction is

$$s_{my} = 2 \left(2.125 + \frac{6}{10} \right) + \frac{0.25 \times 0.4 \times 0.375}{0.22/(6 \times 6)} = 11.6 \text{ in. (295 mm)}$$

The results obtained by using program SHEAR are given in Table 7-2.

Table 7-2 Summary of shear response predictions for beam CF1 using the modified compression field theory

$\epsilon_1 \times 10^3$	θ	$\epsilon_t \times 10^3$	$\epsilon_z \times 10^3$	$\gamma \times 10^3$	f_2 ksi (MPa)	$f_{2\max}$ ksi (MPa)	f_1 psi (MPa)	w in. (mm)	V kips (kN)	Comments
0.01	10.5	0	-0.30	0.11	1.10 (7.6) (38.6)	5.60 (3.6) (38.6)	37 (0.3) (2.1)	0.000 (0) (0.03)	24.3 (108) (339)	
0.08	25.2	0	-0.30	0.36	1.35 (9.3) (38.6)	5.60 (3.6) (38.6)	299 (2.1) (1.1)	0.001 (0.03) (0.36)	76.2 (339)	Cracking
0.5	23.7	0.35	-0.26	0.67	1.42 (9.8) (38.6)	5.60 (3.6) (38.6)	200 (1.4) (1.1)	0.005 (0.13) (0.36)	71.5 (318)	
1.0	24.6	0.75	-0.21	1.11	1.60 (11.0) (38.6)	5.60 (3.6) (38.6)	176 (1.2) (1.1)	0.010 (0.25) (0.36)	80.5 (358)	
1.5	25.4	1.13	-0.15	1.57	1.79 (12.3) (38.6)	5.60 (3.6) (38.6)	161 (1.1) (1.1)	0.014 (0.36) (0.36)	91.0 (405)	
2.0	26.1	1.49	-0.10	2.06	1.99 (13.7) (37.6)	5.46 (3.7) (37.6)	150 (1.0) (1.0)	0.019 (0.48) (0.48)	101.4 (451)	
2.5	26.3	1.87	-0.06	2.56	2.11 (14.5) (35.6)	5.17 (3.5) (35.6)	110 (0.8) (0.8)	0.024 (0.61) (0.61)	105.7 (470)	Stirrups yield and crack slipping
3.0	25.7	2.30	-0.04	2.93	2.15 (14.8) (33.9)	4.91 (3.3) (33.9)	96 (0.7) (0.7)	0.029 (0.74) (0.74)	105.1 (468)	
4.0	24.8	3.15	-0.01	3.70	2.21 (15.3) (30.8)	4.47 (2.6) (30.8)	76 (0.5) (0.5)	0.038 (0.97) (0.97)	104.4 (464)	
6.0	23.9	4.84	.07	5.26	2.26 (15.6) (26.1)	3.78 (2.4) (26.1)	54 (0.4) (0.4)	0.058 (1.47) (1.47)	102.8 (457)	
8.0	23.4	6.52	0.13	6.82	3.28 (15.7) (22.6)	3.28 (2.0) (22.6)	42 (0.3) (0.3)	0.077 (1.96) (1.96)	101.7 (452)	
10.0	23.2	8.20	0.17	8.41	2.29 (15.8) (20.0)	2.90 (2.0) (20.0)	35 (0.2) (0.2)	0.097 (2.46) (2.46)	100.9 (449)	
14.0	23.1	11.48	0.12	11.84	2.26 (15.6) (16.2)	2.35 (2.0) (16.2)	26 (0.2) (0.2)	0.135 (3.43) (3.43)	98.8 (439)	Concrete crushing

Figure 7-41 compares the predicted and measured stirrup strains for this beam. Note that for shears less than the diagonal cracking shear the stirrup strains are negligibly small, a phenomenon correctly predicted by the modified compression field theory. The growth in stirrup strain after diagonal cracking is predicted well by the theory. Also shown in Fig. 7-41 is the response predicted using the compression field theory, which can be obtained by inputting a value of zero for the cracking strength of the concrete.

It can be seen from Fig. 7-41 that by accounting for the tensile stresses in the cracked concrete, we have more accurately predicted the response of the prestressed concrete member. As can be seen from Table 7-2, after cracking, the principal tensile stress, f_1 , in the concrete decreases with increasing values of ϵ_1 . For this example, the ability of the crack to transmit shear limited f_1 at higher values of ϵ_1 .

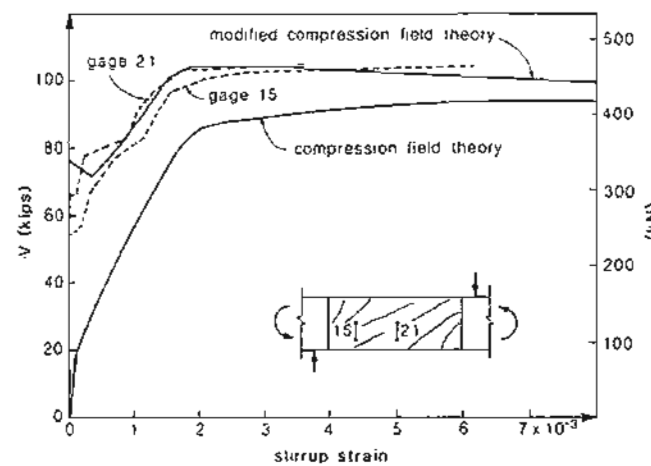


Figure 7-41 Comparison of measured stirrup strains and predicted stirrup strains for beam CF1.

It is interesting to note that for this prestressed concrete member, the inclination, θ , of the principal compressive stresses starts at zero when the shear is zero (i.e., the principal compressive stresses due to prestressing are longitudinal). As shear is increased, the principal compressive stresses become more steeply inclined reaching a maximum of about 26° as the stirrups yield. The very flat inclination of the diagonal compressive stresses means that the diagonal cracks form at small angles as can be seen in Fig. 7-42.

In predicting the response of beam CF1 shown above, it was assumed that the member was subjected to pure shear. While the moment was zero at a section midway along the test length (see Fig. 7-40), other sections in the test length were subjected to significant flexure. The presence of flexure reduced somewhat the shear capacity of the beam, and hence failure was initiated in the higher moment regions.

Under the combined action of shear and moment, the longitudinal strains vary over the depth of the beam (see Fig. 7-43). Vecchio and Collins (Ref. 7-39) have shown how it is possible to perform a detailed analysis of a cross section subjected to combined shear and moment. By considering two adjacent cross sections they are able to calculate the distribution of shear stresses over the cross section. In this analysis, the biaxial stresses and strains and the manner in which they vary over the height of the beam are considered. It is found that the inclination, θ , of the principal compressive stress changes over the height of the beam, becoming larger near the flexural tension face and smaller near the flexural compression face (see Fig. 7-43a).

The detailed, dual-section analysis is very time consuming. It is possible to greatly reduce the computation time if the following simplifications are adopted:

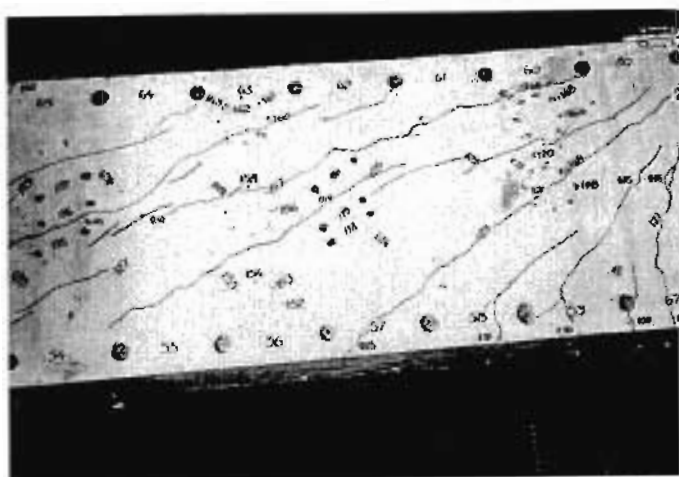


Figure 7-42 Crack pattern near failure load of prestressed beam CF1.

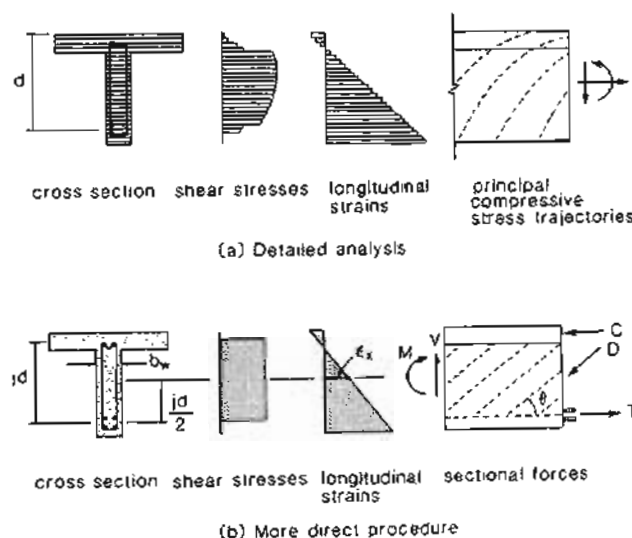


Figure 7-43 Influence of moment on shear response.

1. The redistribution of shear stresses that occurs at higher moments is ignored. That is, the shear stress is assumed to be given by Eq. (7-5) (see Fig. 7-43b).

2. The biaxial stresses and strains are considered at just one level of the web. The longitudinal strain at this location, ϵ_x , is used to calculate θ , which is then assumed to remain constant over the depth of the web (see Fig. 7-43b).

With this simplified procedure a suitable solution technique for analyzing a section subjected to combined shear and moment is as follows:

Steps 1 through 13: Identical to the steps for pure shear given in Section 7.10.

Step 14: Using a plane-sections analysis with the strain at the chosen level set to the ϵ_x value calculated in Step 11, find the strain distribution that corresponds to the desired moment and then determine the corresponding axial load, N_p .

Step 15: Calculate the axial force on the member, allowing for the influence of the longitudinal compressive stresses in the concrete over area $b_w d$ caused by the shear

$$N = N_p - V \cot \theta$$

Step 16: Check whether N equals the desired axial load on the member. If it does not, make a new estimate of θ and return to Step 3. Increasing θ increases N .

The procedure above has been incorporated into program RESPONSE (described in Appendix A), which can be used to predict the response of sections subjected to combined shear, moment, and axial load.

Before this procedure can be used, a decision must be made as to where in the web ϵ_x will be calculated. As an increase in ϵ_x decreases the shear capacity, it would be conservative to use the highest value of ϵ_x . However, members with web reinforcement have a considerable capacity for redistribution, which results in the shear stresses being transferred from the most highly strained portions of the cross section to the less highly strained portions. Because of this redistribution, it is reasonable to use the longitudinal strain at mid-depth of the web as ϵ_x . Members that do not contain web reinforcement have less capacity for redistribution and hence, for such members the highest longitudinal strain in the web should be used as ϵ_x .

Figure 7-44 compares the shear-moment interaction diagram for beam CF1 obtained from program RESPONSE with that obtained from the more detailed dual-section analysis. Note that even though ϵ_x was taken as the longitudinal strain at mid-depth of the web, the failure envelope predicted by program RESPONSE is more conservative than that given by the dual-section analysis. Also shown in Fig. 7-44 is the shear stress distribution at one point on the failure envelope predicted by the dual-section analysis. The significant redistribution of shear stresses across the section that has occurred, can be seen.

Flexure reduces the shear capacity of beam CF1 because it increases the longitudinal strain, ϵ_x . As this strain increases, shear capacity decreases. Recognizing the key role played by the longitudinal strain enables us to develop a simple method of accounting for the influence of flexure on shear capacity.

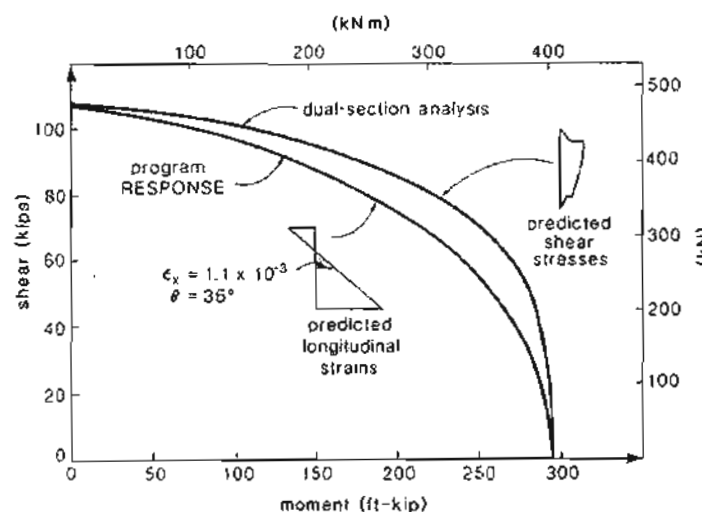


Figure 7-44 Shear-moment interaction diagrams for beam CF1 predicted by program RESPONSE and by a dual-section analysis.

For the non-prestressed section shown in Fig. 7-45 the applied moment, if acting alone, would cause a tensile strain in the reinforcement of

$$\epsilon_r = \frac{M}{jdA_sE_s} \quad (7-39)$$

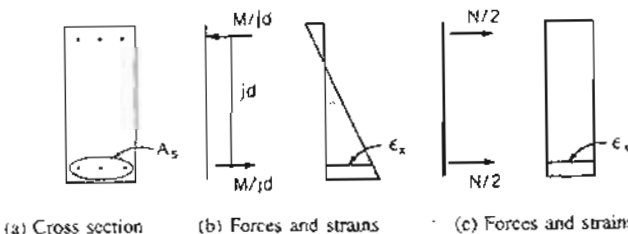


Figure 7-45 Comparison of forces and strains due to moment and tension.

If the section was subjected to a pure axial tension, the tensile strain in the reinforcement would be

$$\epsilon_x = \frac{0.5N}{A_sE_s} \quad (7-40)$$

Sec. 7.12 Design Using Modified Compression Field Theory

Comparing Eqs. (7-39) and (7-40) we see that to produce the same longitudinal strain with an axial force as with a moment, the magnitude of the axial force must be

$$N = \frac{2M}{jd} \quad (7-41)$$

Thus, if beam CF1 is subjected to a moment of 200 ft-kips (271 kNm) it will have the same shear capacity as if it was subjected to an axial tension of

$$N = \frac{2 \times 200 \times 12}{20} = 240 \text{ kips (1068 kN)}$$

If beam CF1 is analyzed using program SHEAR, for combined shear and axial tension, with a constant axial tension of 240 kips (1068 kN) it will be found that the shear capacity is predicted to be 75.0 kips (334 kN). It can be seen from Fig. 7-44 that this predicted shear capacity agrees well with the shear capacity predicted by program RESPONSE for the case of beam CF1 subjected to a moment of 200 ft-kips (271 kNm).

7.12 DESIGN USING MODIFIED COMPRESSION FIELD THEORY

The modified compression field theory was presented in the previous sections as an analysis method capable of predicting the response of a particular section of a prestressed concrete member when that section was subjected to combined shear, axial load, and moment. With the aid of a suitable computer program, such as program RESPONSE or SHEAR, this method can be used to evaluate the suitability of a chosen section and hence can be used to design sections for shear.

By making some simplifying assumptions it is possible to rearrange the basic equations of the modified compression field theory so that they can be used in a more direct fashion to design a section subjected to combined shear, axial load, and flexure.

Typically, before design for shear commences, the cross-sectional dimensions, pre-stressing and material strengths have all been chosen to satisfy other design considerations. Shear design then reduces to checking that the cross-sectional dimensions are adequate and finding the required amounts of web reinforcement and additional longitudinal reinforcement that will ensure that the required shear strength of the section can be developed.

The nominal shear resistance of a section can be expressed as

$$V_n = V_c + V_s + V_p \quad (7-42)$$

where V_c is the nominal shear strength provided by tensile stresses in the concrete, V_s is the nominal shear strength provided by tensile stresses in the web reinforcement, and V_p is the nominal shear strength provided by the component in the direction of the applied shear, of the force in the longitudinal prestressing tendons.

The shear resisted by tensile stresses in the concrete can be expressed as

$$V_c = \beta \sqrt{f'_c b_w jd} \quad (7-43)$$

where jd equals the flexural lever arm, which need not be taken less than $0.9d$. For prestressed members, d need not be taken less than $0.8h$. The factor β depends on the average tensile stresses in the cracked concrete. Assuming that the cracking stress, f_{cr} , equals $4\sqrt{f'_c}$ psi ($0.33\sqrt{f'_c}$ MPa) Eqs. (7-28) and (7-31) can be rearranged to give

$$\beta = \frac{\alpha_1 \alpha_2 4 \cot \theta}{1 + \sqrt{500 \epsilon_1}} \quad \text{psi} \quad (7-44a)$$

$$\beta = \frac{\alpha_1 \alpha_2 0.33 \cot \theta}{1 + \sqrt{500 \epsilon_1}} \quad \text{MPa} \quad (7-44b)$$

If the crack widths are too wide, the average tension in the concrete will be limited by the mechanisms that transmit the forces across the cracks. In particular, the shear stress on the crack, v_{ci} , will become critical. To avoid such "crack slipping" failures, β must be limited to

$$\beta \leq \frac{2.16}{0.3 + \frac{24 \epsilon_1 s_{mb}}{a + 0.63}} \quad \text{psi and in.} \quad (7-45a)$$

$$\beta \leq \frac{0.18}{0.3 + \frac{24 \epsilon_1 s_{mb}}{a + 16}} \quad \text{MPa and mm} \quad (7-45b)$$

Equation (7-45) was derived from Eqs. (7-28), (7-32), (7-33), and (7-34). It was assumed that the stirrups would be yielding at failure ($f_u = f_{vy}$).

It can be seen from both of the above expressions for β that as the tensile straining of the concrete increases (i.e., ϵ_1 increases), the shear that can be resisted by tensile stresses in the concrete, V_c , decreases. The value of the principal tensile strain, ϵ_1 , will depend on the magnitude of the longitudinal tensile straining, ϵ_x , the inclination, θ , of the principal stresses, and the magnitude of the principal compressive strain, ϵ_2 , in the concrete. From Eqs. (7-23) and (7-24), ϵ_1 is

$$\epsilon_1 = \epsilon_x + (\epsilon_x - \epsilon_2) \cot^2 \theta \quad (7-46)$$

The strain ϵ_2 depends upon the magnitude of the principal compressive stress, f_2 . This stress can be estimated conservatively from Eq. (7-27) as

$$f_2 = (\tan \theta + \cot \theta)v \quad (7-47)$$

Assuming that the strain, ϵ'_c , at which the concrete reaches its peak stress is -0.002 , we can rearrange Eq. (7-26) to give

$$\epsilon_2 = -0.002 \left(1 - \sqrt{1 - f_2/f_{2max}} \right) \quad (7-48)$$

where

$$f_{2max} = \frac{f'_c}{0.8 + 170 \epsilon_1} \quad (7-49)$$

If we substitute the expression for ϵ_2 given by Eq. (7-48) into Eq. (7-46) and in addition, substitute the expressions for f_2 and f_{2max} from Eqs. (7-47) and (7-49) we obtain the following quadratic equation for ϵ_1

$$\epsilon_1 = \epsilon_7 + \left[\epsilon_1 + 0.002 \left(1 - \sqrt{1 - \frac{v}{f'_c} (\tan \theta + \cot \theta)(0.8 + 170 \epsilon_1)} \right) \right] \cot^2 \theta \quad (7-50)$$

Thus, if ϵ_7 , θ , and v/f'_c are known, the strain, ϵ_1 , can be found by solving Eq. (7-50). With ϵ_1 known, the β factor can be calculated from Eqs. (7-44) and (7-45) provided that the crack spacing, s_{mb} , the maximum aggregate size, a , and the tension-stiffening factors, $\alpha_1 \alpha_2$, are known.

To simplify the calculations we will assume that for members with web reinforcement, the crack spacing, s_{mb} , equals 12 in. (305 mm), that $\alpha_1 \alpha_2$ equals unity, and that a equals 0.75 in. (19 mm). For the values of v/f'_c , ϵ_7 , and θ given in Table 7-3, the values of β calculated from the approach above are listed. In using this table, the nominal shear stress on the concrete is computed as

$$v = \frac{V_n - V_p}{b_v jd} \quad (7-51)$$

Table 7-3 Values of θ and β , psi units*, for members with web reinforcement.

Shear Stress, v/f'_c	Longitudinal Strain $\epsilon_x \times 1000$									
	0	0.25	0.50	0.75	1.00	1.50	2.00	2.50	3.00	5.00
≤ 0.050	θ	28°	31°	34°	36°	38°	41°	43°	45°	46°
	β	3.24	3.70	3.01	2.62	2.33	1.95	1.72	1.54	1.39
0.075	θ	28°	30°	30°	34°	36°	40°	42°	43°	36°
	β	4.86	3.37	2.48	2.37	2.15	1.90	1.65	1.44	1.23
0.100	θ	22°	26°	30°	34°	36°	38°	38°	38°	55°
	β	2.71	2.42	2.31	2.27	2.08	1.72	1.39	1.16	1.00
0.125	θ	23°	27°	31°	34°	36°	36°	36°	36°	55°
	β	2.40	2.33	2.29	2.16	2.00	1.52	1.23	1.03	0.88
0.150	θ	25°	28°	31°	34°	34°	34°	34°	35°	55°
	β	2.53	2.25	2.13	2.06	1.73	1.30	1.04	0.83	0.77
0.175	θ	26°	29°	32°	32°	32°	34°	36°	38°	54°
	β	2.34	2.19	2.11	1.69	1.40	1.01	0.94	0.91	0.88
0.200	θ	27°	30°	33°	34°	34°	37°	39°	41°	53°
	β	2.16	2.13	2.09	1.82	1.52	1.08	1.11	1.04	0.99
0.225	θ	28°	31°	34°	34°	34°	37°	39°	42°	44°
	β	1.97	2.07	2.08	1.67	1.35	1.29	1.17	1.16	1.09
0.250	θ	30°	32°	34°	35°	36°	39°	42°	45°	49°
	β	2.26	2.00	1.87	1.63	1.45	1.37	1.32	1.28	1.24

*For β values in MPa units, divide the values given in the table by 12.

The shear resisted by tensile stresses in the web reinforcement can be determined from Eq. (7-28) as

$$V_s = \frac{A_s f_y j d \cot \theta}{s} \quad (7-52)$$

It can be seen from Eq. (7-52) that for a given quantity of stirrups, the lower the value of θ , the higher the value of V_s . However, for a given value of ϵ_x , lower values of θ will result in higher values of ϵ_1 [see Eq. (7-50)], and hence lower values of V_c .

The θ values given in Table 7-3 have been chosen to ensure that, for highly stressed members, the compressive stress in the concrete, f_2 , does not exceed the crushing strength, f_{2max} and that the strain in the web reinforcement, ϵ_{yv} , is at least equal to 0.002. Within the possible range of values of θ , the values given in the table will result in close to the minimum amount of shear reinforcement.

To be conservative, the longitudinal strain, ϵ_x , will be taken at the level of the flexural tension reinforcement. This strain will depend upon the magnitude of the flexural moment, the axial tension (see Fig. 7-45) and the shear (see Fig. 7-23) as well as the amount of non-prestressed and prestressed longitudinal reinforcement. It may be computed as

$$\epsilon_x = \frac{\frac{M_u}{Jd} + 0.5N_u + 0.5V_u \cot \theta - A_{ps}f_{sc}}{E_s A_s + E_p A_{ps}} \quad (7-53)$$

Equation (7-53) neglects the stiffness of the concrete when calculating strain. While this is reasonable for tensile strains, it will not be appropriate for compressive strains. Hence, if ϵ_x given by Eq. (7-53) is negative, the value will be overestimated. In this case it will be conservative to take ϵ_x as equal to zero.

Because the amount of longitudinal reinforcement provided must be sufficient to avoid yielding of the reinforcement, a simple, conservative procedure for calculating ϵ_x is to estimate the concrete strain associated with yielding of the reinforcement. That is,

$$\epsilon_x \leq \frac{f_y}{E_s} \quad (7-54)$$

and

$$\epsilon_x \leq \frac{f_{py} - f_{sc}}{E_p} \quad (7-55)$$

Carrying part of the shear by tensile stresses in the concrete reduces the required amount of web reinforcement but increases the stresses in the longitudinal reinforcement at a crack [see Fig. 7-37c and Eq. (7-38)].

The force in the longitudinal reinforcement at a crack caused by shear can be determined from Eq. (7-38). Substituting for the average reinforcement force $A_{sx}f_{sx} + A_{px}f_{ps}$ from Eq. (7-29) and assuming the stirrups are yielding ($f_u = f_{vy}$) enables Eq. (7-38) to be written as

$$A_{sx}f_y + A_{px}f_{ps} \geq V \cot \theta + f_1 b_w j d \cot^2 \theta \quad (7-56)$$

But from Eq. (7-28)

$$V_c = f_1 b_w j d \cot \theta \quad (7-57)$$

Hence Eq. (7-56) can be written as

$$A_{sx}f_y + A_{px}f_{ps} \geq V_c \cot \theta + V_c \cot \theta \quad (7-58)$$

For the symmetrically reinforced member considered in deriving Eq. (7-38)

$$V = V_c + V_s$$

Thus Eq. (7-58) can be expressed as

$$A_{sx}f_y + A_{px}f_{ps} \geq (2V_c + V_s) \cot \theta \quad (7-59)$$

Considering only the reinforcement on the flexural tension side of the member enables Eq. (7-59) to be written as

$$A_s f_y + A_{ps} f_{ps} \geq (V_c + 0.5V_s) \cot \theta \quad (7-60)$$

But, from Eq. (7-42),

$$V_c + 0.5V_s = V_n - 0.5V_s - V_p$$

Hence the force in the longitudinal tension reinforcement caused by shear can be expressed as

$$A_s f_y + A_{ps} f_{ps} \geq \left(\frac{V_n}{\phi} - 0.5V_s - V_p \right) \cot \theta \quad (7-61)$$

Thus to avoid yielding of the longitudinal reinforcement, for combined loading the reinforcement on the flexural tension face must be proportioned so that

$$A_s f_y + A_{ps} f_{ps} \geq \frac{M_u}{\phi j d} + 0.5 \frac{N_u}{\phi} + \left(\frac{V_n}{\phi} - 0.5V_s - V_p \right) \cot \theta \quad (7-62)$$

Thus the shear design of a member containing web reinforcement consists of the following steps:

Step 1: Calculate the nominal shear stress, v , from Eq. (7-51) and divide by the concrete strength, f'_c , to obtain the shear stress ratio, v/f'_c . If this ratio is higher than 0.25 the section is too small, or the concrete is too weak.

Step 2: Calculate the longitudinal strain, ϵ_x , either directly from Eqs. (7-54) and (7-55) or by trial and error from Eq. (7-53), where an estimate of θ will be required.

Step 3: Using the calculated values of v/f'_c and ϵ_x determine θ and β from Table 7-3. Linear interpolation can be used or the values given for the next higher value of ϵ_x and the next higher value of v/f'_c can be taken.

Step 4: Calculate the required value of V_s from Eqs. (7-42) and (7-43) as

$$V_s = \frac{V_u}{\phi} - V_p - \beta \sqrt{f'_c b_w d} \quad (7-63)$$

Step 5: Calculate the required spacing of stirrups from Eq. (7-52) as

$$s \leq \frac{A_v f_y d \cot \theta}{V_s} \quad (7-64)$$

Step 6: Check yielding of the longitudinal reinforcement using Eq. (7-62). If needed, either add more longitudinal reinforcement or revise the values of θ and β using the values for a higher ϵ_y . These values will reduce the amount of longitudinal reinforcement but increase the amount of stirrups required.

Because the procedure above was based on the assumption that the member contained enough reinforcement to ensure reasonable crack control, irrespective of the crack direction, it is not appropriate to use this procedure for members that do not contain web reinforcement. Such members may have crack spacings, s_{mx} , considerably greater than the assumed value of 12 in. (305 mm). As can be seen from Eq. (7-37), if there is no web reinforcement (i.e., $\rho_v = 0$) the crack spacing becomes infinity.

If s_{mx} equals infinity then Eq. (7-35) becomes

$$s_{mx} = \frac{s_{mx}}{\sin \theta} \quad (7-65)$$

where s_{mx} is the spacing of vertical cracks (see Fig. 7-38).

For members without web reinforcement, the nominal shear resistance can be expressed as

$$V_n = V_c + V_p \quad (7-66)$$

Assuming that the crack spacing is given by Eq. (7-65), that $\alpha_1 \alpha_2$ equals unity, and that the maximum aggregate size, a , equals 0.75 in. (19 mm), the values for β can be obtained from Eqs. (7-44), (7-45), and (7-50). These values are listed in Table 7-4. The values of θ given in the table are those that result in the highest value of β .

The crack spacing, s_{mx} , will be mainly influenced by the maximum distance from the reinforcement, c_z [see Eq. (7-36) and Fig. 7-39]. Rather than calculating s_{mx} from Eq. (7-36) we can determine it from the simple expressions given in Fig. 7-46. From this figure and from Table 7-4 it can be seen that as beams without web reinforcement become deeper, the shear stress required to cause failure becomes smaller.

Convincing evidence of the reduction in shear stress capacity that occurs as members become larger was provided by an extensive experimental program conducted in Japan by Shioya, Iguro, Nojiri, Akiyama, and Okada (Refs. 7-40 and 7-41). In this program, 13 beams having effective depths, d , ranging from 4 in. (100 mm) to 118 in. (3000 mm) were uniformly loaded until failure. As shown in Fig. 7-47, the shear stress required to cause failure decreased as d increased and decreased as the maximum aggregate size decreased. The largest beam in this series weighed nearly 500 tons and would have failed in shear under its own weight. The member was tested "upside down" by pressurizing a water-filled rubber bag between the specimen and a stronger reaction beam (see Fig. 7-48).

Table 7-4 Values of θ and β , psi units*, for members without web reinforcement.

Spacing Parameter s_{mx}	θ	Longitudinal Strain $\epsilon_x \times 1000$									
		0	0.25	0.50	0.75	1.00	1.50	2.00	2.50	3.00	5.00
≤ 5 in.	θ	27°	30°	32°	33°	34°	36°	38°	39°	40°	43°
≤ 125 mm	β	4.89	3.74	3.19	2.81	2.55	2.19	1.95	1.77	1.63	1.27
10 in.	θ	30°	34°	37°	39°	41°	43°	45°	47°	48°	52°
250 mm	β	4.65	3.40	2.83	2.46	2.21	1.87	1.64	1.48	1.35	1.03
15 in.	θ	32°	37°	41°	43°	45°	48°	50°	52°	53°	58°
380 mm	β	4.47	3.15	2.59	2.23	1.99	1.67	1.45	1.30	1.17	0.87
25 in.	θ	35°	42°	46°	49°	51°	54°	57°	59°	61°	65°
630 mm	β	4.24	2.82	2.27	1.90	1.70	1.39	1.19	1.05	0.94	0.67
50 in.	θ	38°	48°	53°	57°	60°	64°	66°	69°	70°	75°
1270 mm	β	3.70	2.39	1.82	1.50	1.28	1.01	0.84	0.72	0.63	0.41
100 in.	θ	42°	56°	62°	66°	69°	73°	75°	77°	78°	81°
2540 mm	β	3.55	1.87	1.35	1.06	0.88	0.65	0.52	0.43	0.37	0.23
200 in.	θ	46°	64°	71°	74°	77°	80°	82°	83°	84°	85°
5080 mm	β	3.19	1.39	0.90	0.66	0.53	0.37	0.29	0.23	0.20	0.12

*For β values in MPa units, divide the values in the table by 12.

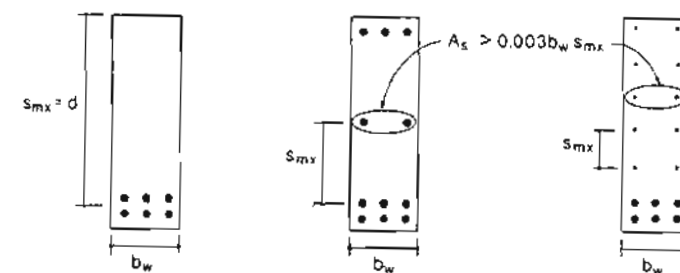


Figure 7-46 Values of crack spacing parameter, s_{mx} .

It is interesting to note that the beams described in Fig. 7-47 contained about the same percentage of longitudinal reinforcement as the roof beams of the Air Force warehouse described in Fig. 7-18. The warehouse beams had an effective depth of about 34 in. (850 mm) and failed at a shear stress of about $1.2\sqrt{f'_c}$ ($0.10\sqrt{f'_c}$ MPa). This shear stress level is consistent with the failure stresses observed for beams about 3 ft (1000 mm) deep in the tests of Shioya et al. Thus it seems likely that the size effect in shear played an important role in the Air Force warehouse collapse.

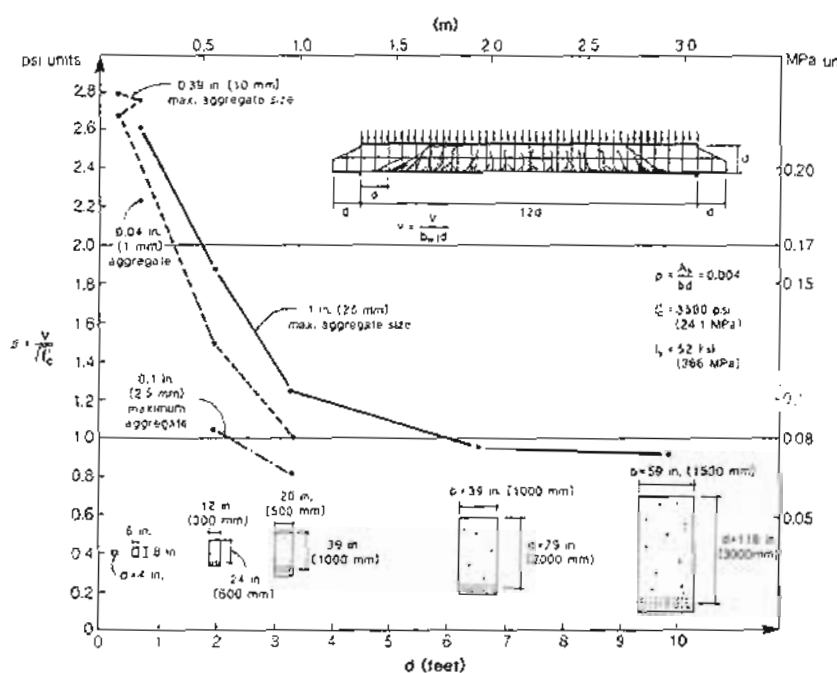


Figure 7-47 Shear stress at failure, on section at distance d from support for series of beams with different depths and different aggregate sizes. Results from Shioya (Ref. 7-41).

The β values in Table 7-4 were derived for a maximum aggregate size of 0.75 in. (19 mm). However, the tabulated values can be used for other aggregate sizes by the use of an equivalent spacing parameter, s_{mz} . From Eqs. (7-45) and (7-65) β is a function of the parameter $24\epsilon_x s_{mz}/(a + 0.63)$. Hence the values in the table can be used for aggregate sizes other than 0.75 in. (19 mm) if we use an equivalent spacing parameter of

$$s_{mzc} = s_{mz} \frac{1.38}{a + 0.63} \quad \text{in.} \quad (7-67a)$$

$$s_{mzc} = s_{mz} \frac{35}{a + 16} \quad \text{mm} \quad (7-67b)$$

Thus the largest beam shown in Fig. 7-47, which had a maximum aggregate size of 1.00 in. (25 mm) and an effective depth of 118 in. (3000 mm) would have an equivalent



Figure 7-48 Large beam failing in shear. Failure crack between S and X. Photograph courtesy of Shimizu Corporation.

crack spacing of

$$s_{mzc} = 118 \times \frac{1.38}{1.00 + 0.63} = 100 \text{ in. (2540 mm)}$$

Hence the strength of this large beam could be predicted using the θ and β values given for a crack spacing of 100 in. (2540 mm) in Table 7-4. For example, for ϵ_x equals 0.50×10^{-3} , the θ and β values would be 62° and 1.35. As there is no web reinforcement,

$$\begin{aligned} V &= V_c = \beta \sqrt{f_c b_w d} \\ &= \beta \sqrt{3500} \times 59 \times 0.9 \times 118 \\ &= 371\beta = 501 \text{ kips (2230 kN)} \end{aligned}$$

If ϵ_x equals 0.50×10^{-3} then, from Eq. (7-53), with A_s equal to 28.3 in^2 (18240 mm^2)

$$0.50 \times 10^{-3} = \frac{\frac{M}{100} + 0.5 \times 501 \times \cot 62^\circ}{29,000 \times 28.3}$$

Hence $M = 29,380 \text{ in.-kips} = 2450 \text{ ft-kips (3320 kNm)}$.

Repeating the calculations above for different values of ϵ_x we obtain the different combinations of shear and moment that are predicted to cause failure. For high values of ϵ_x , yielding of the longitudinal reinforcement will govern the failure and hence the moment values will be found from Eq. (7-62). The predicted shear-moment interaction diagram is shown in Fig. 7-49.

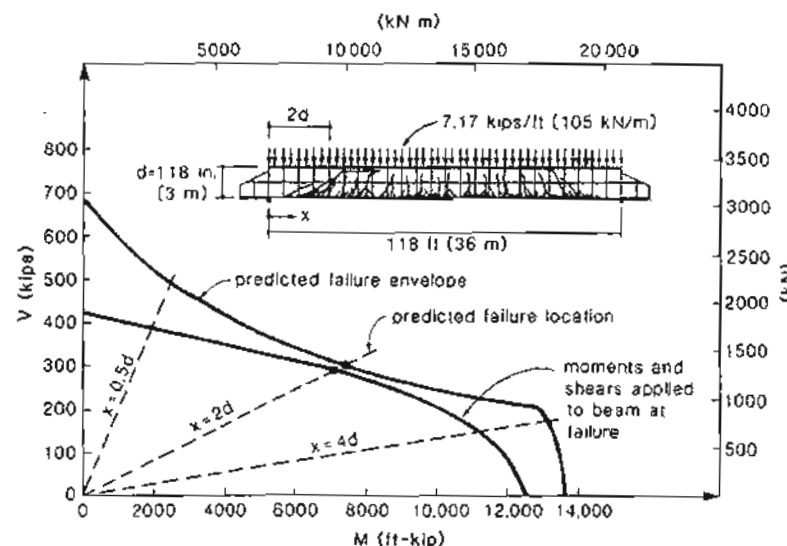


Figure 7-49 Shear-moment interaction diagram showing predicted failure location.

When a uniformly distributed load is applied to a simply supported beam, different sections along the span are subjected to different combinations of shear and moment. Thus the section at the support has the highest shear but no moment, while the section at midspan has the highest moment but no shear. For the large beam reported by Shioya et al. (Ref. 7-40), Fig. 7-49 shows both the predicted failure envelope and the moments and shears applied to different sections of the beam at failure. It can be seen that if the loads were increased by about 4% the loading envelope would touch the failure envelope at a point corresponding to a location in the span which is $2d$ from the support. In the experiment, the failure crack extended from a location about d from the support to a location about $3d$ from the support. Thus, in the experiment, failure occurred at about the location predicted, and at a load that was 96% of the predicted failure load.

7.13 DESIGN EXAMPLE USING MODIFIED COMPRESSION FIELD THEORY

As an example of the use of the modified compression field theory (MCFT), we will redesign the PCI standard single tee described in Sections 7.3 and 7.7.

Step 1: Choose the sections where stirrups will be designed.

The modified compression field theory can be used to calculate the required stirrups at a particular section, given the shear and moment acting at that section. However, a shear failure caused by yielding of the stirrups involves yielding this reinforcement over a length of beam of about $jd \cot \theta$ (see Figs. 7-37 and 7-24). Hence a calculation for one section can be taken as representing a length of beam $jd \cot \theta$ long, with the calculated section being in the middle of this length. Thus, the first section we will check is $0.5jd \cot \theta$ from the face of the support. Additional sections will then be checked at about every $jd \cot \theta$ along the length of the beam.

For the purpose of choosing the design sections, we need to make a conservative estimate of θ (that is, a high value). For this prestressed beam, ϵ_x will probably be close to zero near the support. From Table 7-3 choose θ equal to 30° . Thus $jd \cot \theta$ will equal $0.72 \times 36 \times \cot 30^\circ = 45$ in. = 3.75 ft (1140 mm). Thus the first section we will check will be 22.5 in. (572 mm) from the face of the support. That is, $(22.5 + 4)/12 = 2.21$ ft (673 mm) from the center of the support.

The sections we will check are summarized in Table 7-5. Also given in this table are the factored shear forces, V_u , and the factored moments, M_u , at these sections.

Table 7-5 Design of single tee by modified compression field method.

No.	x ft m	V_u kips kN	M_u ft-kips kN	$d - \frac{b}{2}$ in. mm	jd in. mm	$\frac{x}{jd}$	θ deg	$\epsilon_x \times 10^3$ psi MPa	β	V_c kips kN	s in. mm	f_p^* ksi MPa
1	2.21	69.2	159	23.9	25.9	0.072	28	0	4.86	71.2	198	111
	0.67	308	216	607	658			0.405	317	5025	764	
2	5.96	59.9	401	25.1	25.9	0.061	28	0	4.86	71.2	∞	167
	1.82	266	544	638	658			0.405	317	1154		
3	9.71	50.5	608	26.2	26.2	0.050	36	0.63	2.62	38.8	34.9	200
	2.96	225	824	665	665			0.218	173	886	1382	
4	13.46	41.2	780	27.3	27.3	0.038	43	1.61	1.72	26.6	25.9	227
	4.10	183	1058	693	693			0.143	118	658	1565	
5	17.21	31.8	917	28.4	28.4	0.027	45	2.34	1.54	24.7	63.9	247
	5.24	141	1243	721	721			0.128	110	1622	1702	
6	20.96	22.5	1019	29.6	29.6	0.017	46	2.72	1.39	23.3	∞	256
	6.39	100	1382	752	752			0.116	104		1766	
7	24.71	13.2	1086	30.7	30.7	0.007	46	2.85	1.39	24.1	∞	257
	7.53	59	1472	780	780			0.116	107		1772	
8	28.46	3.8	1118	31.8	31.8	0	46	2.72	1.39	25.0	∞	255
	8.67	17	1516	808	808			0.116	111		1758	
9	30.00	0	1121	32.3	32.3	0	46	2.58	1.39	25.4	∞	252
	9.14	1520	820	820				0.116	113		1738	

*Stress required in strands.

Step 2: Determine values of $(d - \frac{a}{2})$ and jd .

In this beam the distance from the extreme compression fiber to the centroid of the prestressed reinforcement varies along the length as shown in Fig. 7-10.

The effective shear depth, jd , can be taken as the flexural lever arm, $d - \frac{a}{2}$, but need not be taken as less than $0.9d$ nor $0.72h$. A conservative estimate of the depth of compression, a , can be obtained by assuming that the strands are stressed to their ultimate stress of 270 ksi (1860 MPa). Thus

$$a = \frac{12 \times 0.153 \times 270}{0.85 \times 5 \times 120} = 0.97 \text{ m. (25 mm)}$$

The values of the flexural lever arm, $(d - \frac{a}{2})$, calculated using this value of a are listed in Table 7-5. Also given are the values of jd .

Step 3: Design the stirrups.

For the first section,

$$\begin{aligned} \frac{v}{f'_c} &= \frac{V_u/0.85 - V_p}{b_w j d f'_c} \\ &= \frac{69.2/0.85 - 6.96}{8 \times 25.9 \times 5} \\ &= 0.072 \end{aligned}$$

From Table 7-3, and assuming that ϵ_x is zero, choose θ equal to 28° . While interpolation could be used when choosing values from Table 7-3, it is more convenient to take the value from the next higher row and the next higher column.

From Eq. (7-53),

$$\begin{aligned} \epsilon_x &= \frac{159 \times 12/25.9 + 0.5 \times 69.2 \cot 28^\circ - 12 \times 0.153 \times 152}{29.000 \times 12 \times 0.153} \\ &\approx -2.64 \times 10^{-3} \end{aligned}$$

Because Eq. (7-53) neglects the stiffness of the concrete it will overestimate compressive strains. Hence ϵ_x will actually be between zero and -2.64×10^{-3} . Thus we will use the column for ϵ_x equal to zero when using Table 7-3. Hence our choice of θ equal to 28° was appropriate.

From Table 7-3, with ϵ_x equal to zero and v/f'_c equal to 0.075 we find that β equals 4.86. Hence, from Eq. (7-43)

$$\begin{aligned} V_c &= 4.86 \sqrt{5000} \times 8 \times 25.9 \\ &= 71.2 \text{ kips (317 kN)} \end{aligned}$$

Thus

$$\begin{aligned} V_s &= V_u/\phi - V_c - V_f \\ &= 69.2/0.85 - 71.2 - 6.96 \\ &= 3.25 \text{ kips (14 kN)} \end{aligned}$$

That is, only a small quantity of stirrups is required near the support. We will use #3 double-legged stirrups, with $f_y = 60$ ksi (414 MPa). Hence, from Eq. (7-52),

$$\begin{aligned} s &\leq \frac{0.22 \times 60 \times 25.9 \cot 28^\circ}{3.25} \\ &\leq 198 \text{ in. (3025 mm)} \end{aligned}$$

Hence the stirrups at this section will be governed by maximum spacing requirements.

Repeating the calculations above for the other sections, we obtain the required stirrup spacings listed in Table 7-5.

Figure 7-50 illustrates the amount of stirrups required at different locations in the span. It is of interest that no stirrups are required for sections more than about 20 ft (6 m) from the support and that the sections requiring the most stirrups are located about 13 ft (4 m) from the support. These predictions agree very closely with those made by the ACI method (see Fig. 7-21).

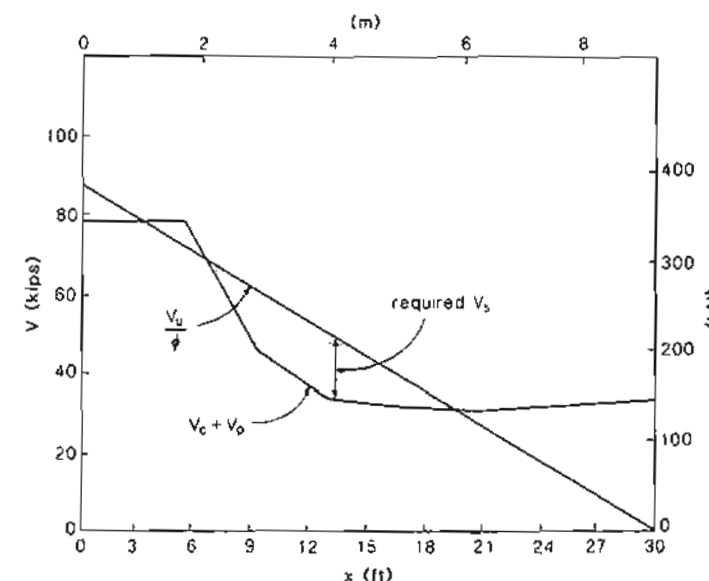


Figure 7-50 Design of stirrups by modified compression field theory.

To satisfy minimum shear reinforcement requirements

$$\begin{aligned} s &\leq \frac{A_v f_y}{50 b_w} = \frac{2 \times 0.11 \times 60,000}{50 \times 8} \\ &\leq 33 \text{ in. (838 mm)} \end{aligned}$$

To satisfy spacing requirements

$$\begin{aligned}s &\leq 0.75h = 0.75 \times 36 \\&\leq 27 \text{ in. (686 mm)} \\&\text{but } s \leq 24 \text{ in. (610 mm)}\end{aligned}$$

Hence a stirrup spacing of 24 in. (610 mm) will satisfy strength, minimum reinforcement and maximum spacing requirements. Thus the stirrup arrangement shown in Fig. 7-21a will be used.

Step 4: Design the longitudinal reinforcement.

The longitudinal reinforcement must be capable of resisting the moment and the axial tension caused by the shear. The tensile force that will be required in the reinforcement on the flexural tension side of the member is given by Eq. (7-62) as

$$A_{ps} f_{ps} = \frac{M_u}{\phi J d} + \left(\frac{V_u}{\phi} - 0.5V_s - V_p \right) \cot \theta$$

Because we are providing more stirrups than are required, we will determine the actual value of V_s at each section since an increase in V_s will decrease the required force in the longitudinal steel. At the first section, where θ equals 28° ,

$$\begin{aligned}V_s &= \frac{0.22 \times 60 \times 25.9 \times \cot 28^\circ}{24} \\&= 26.8 \text{ kips (119 kN)}$$

Thus

$$\begin{aligned}A_{ps} f_{ps} &= \frac{159 \times 12/0.9}{23.9} + \left(\frac{69.2}{0.85} - 0.5 \times 26.8 - 6.96 \right) \cot 28^\circ \\&= 89 + 115 = 204 \text{ kips (905 kN)}$$

Hence the tensile stress required in the strands is

$$f_{ps} = \frac{204}{12 \times 0.153} = 111 \text{ ksi (765 MPa)}$$

Repeating these calculations for the other sections we obtain the required stresses listed in Table 7-5. From these values it can be seen that the longitudinal reinforcement is most highly stressed at section 7.

From Eq. (6-7) we can develop at this location, at least the following stress in the strands:

$$\begin{aligned}f_{ps} &= 270 \left(1 - \frac{0.28}{0.80} \cdot \frac{12 \times 0.153 \times 270}{120 \times 31.2 \times 5} \right) \\&= 267 \text{ ksi (1844 MPa)}$$

As the strands can provide a stress of 267 ksi (1844 MPa), while the required stress is 259 ksi (1788 MPa), the longitudinal reinforcement in the central region of the beam is adequate.

Figure 7-51 compares the required tensile force in the reinforcement at different locations along the span with the tensile force that can be provided by the pretensioned strands. Note that in the middle third of the beam, the shear causes only a very small increase in longitudinal tension. However, near the support it is the shear that is causing most of the tension in the longitudinal reinforcement. From Fig. 7-51, it can be seen that the strands alone will not be capable of providing all of the tension required at the face of the support. At this location, where the moment is very small, the required tension is

$$T = \left(\frac{V_u}{\phi} - 0.5V_s - V_p \right) \cot \theta \quad (7-68)$$

While Eq. (7-68) was derived from Eq. (7-62) it can also be determined on the basis of the free-body diagram shown in Fig. 7-52 by taking moments about point O. Thus

$$\begin{aligned}T &= \left(\frac{73.9}{0.85} - 0.5 \times 26.8 - 2.23 \right) \cot 28^\circ \\&= 134.1 \text{ kips (597 kN)}$$

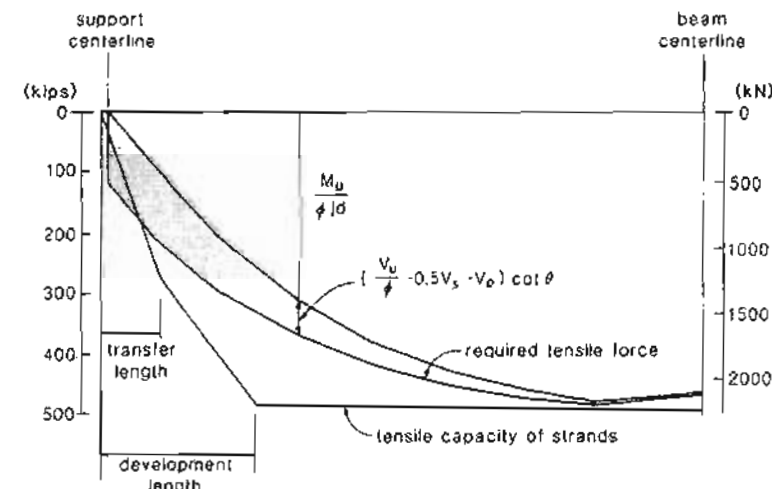


Figure 7-51 Comparison of required tensile force in reinforcement with tensile capacity of strands.

Hence the tensile stress required in the strands at this location is $134.1/(12 \times 0.153) = 73.0$ ksi (503 MPa). As this location is just 8 in. (203 mm) from the free end of the beam (see Fig. 7-9), the tensile stress the strand can resist will be limited by its bond strength. The ACI Code (Ref. 7-2) suggests that the stress in the strand can be assumed to vary linearly from zero at the free end to the effective prestress, f_{se} , over a distance of 50 strand diameters. Hence the stress that the strand can resist at the inner edge of the bearing area is

$$f_{ps} = \frac{8}{50 \times 0.5} \times 152 \\ = 48.6 \text{ ksi (335 MPa)}$$

Therefore the strands can resist a tensile force of $48.6 \times 12 \times 0.153 = 89.2$ kips (397 kN), which is 44.9 kips (200 kN) less than the required force. If two #6 bars, welded to an embedded anchor plate, are provided at the support, the additional tension that can be resisted will be $2 \times 0.44 \times 60 = 52.8$ kips (235 kN), which will cover the deficiency.

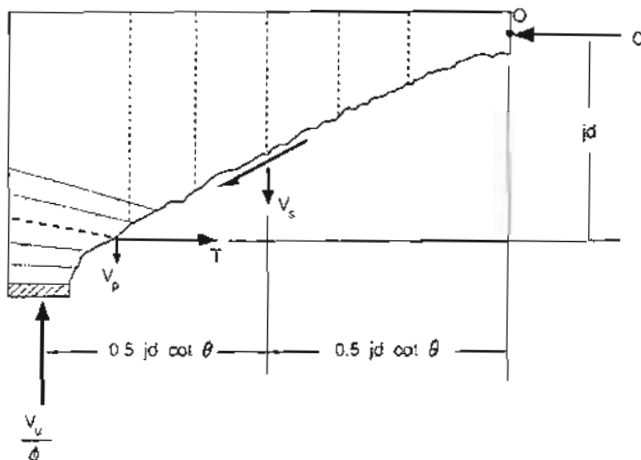


Figure 7-52 Free-body diagram of end region of beam.

It is a serious deficiency of the current ACI shear design provisions that they ignore the fact that shear causes high tension in the longitudinal reinforcement at the face of a support.

References

- 7-1 Vrana, J., "The Behaviour and Repair of Prestressed Bridge Girders in Shear," Project Report No. G83-9, Department of Civil Engineering and Applied Mechanics, McGill University, Montreal, Aug. 1983, 87 pp.
- 7-2 ACI Committee 318, "Building Code Requirements for Reinforced Concrete (ACI 318-89) and Commentary - ACI 318 R-89," American Concrete Institute, Detroit, 1989, 353 pp.
- 7-3 Mörsch, E., *Concrete-Steel Construction*, McGraw-Hill Book Company, New York, 1909, 368 pp. (English translation by E.P. Goodrich of 3rd ed. of *Der Eisenbetonbau*, 1st ed., 1902.)
- 7-4 Zwoyer, E.M., and Siess, C.P., "Ultimate Strength in Shear of Simply-Supported Prestressed Concrete Beams without Web Reinforcement," *ACI Journal, Proceedings* Vol. 51, Oct. 1954, pp. 181-200.
- 7-5 Bresler, B., and Pister, K.S., "Strength of Concrete under Combined Stresses," *ACI Journal, Proceedings* Vol. 55, No. 3, Sept. 1958, pp. 321-345.
- 7-6 Guralnick, S.A., "Shear Strength of Reinforced Concrete Beams," *Journal of the Structural Division, ASCE*, Vol. 85, No. ST1, Jan. 1959, pp. 1-42.
- 7-7 Walther, R., "Calculation of the Shear Strength of Reinforced and Prestressed Concrete Beams by the Shear Failure Theory," Translation 110, Cement and Concrete Association from *Beton und Stahlbetonbau*, Vol. 57, No. 11, Nov. 1962, pp. 261-271.
- 7-8 ACI Committee 318, *Building Code Requirements for Reinforced Concrete*, 1963 ed., American Concrete Institute, Detroit, 1963, 144 pp.
- 7-9 ACI-ASCE Committee 326, "Shear and Diagonal Tension," *ACI Journal*, Vol. 59, Jan., Feb., and Mar. 1962, pp. 1-30, 277-344, and 352-396.
- 7-10 Kani, G.N.J., "The Riddle of Shear Failure and Its Solution," *ACI Journal*, Vol. 61, Apr. 1964, pp. 441-467.
- 7-11 Kani, G.N.J., "How Safe Are Our Large Concrete Beams," *ACI Journal*, Vol. 64, Mar. 1967, pp. 128-141.
- 7-12 Taylor, H.P.J., "Investigation of Forces Carried across Cracks in Reinforced Concrete Beams in Shear by Interlock of Aggregate," TRA 42.447, Cement and Concrete Association, London, 1970, 22 pp.
- 7-13 Fenwick, R.C., and Poulet, T., "Mechanisms of Shear Resistance of Concrete Beams," *Journal of the Structural Division, ASCE*, Vol. 94, No. ST10, Oct. 1968, pp. 2235-2350.
- 7-14 Mörsch, E., *Der Eisenbetonbau* (Reinforced Concrete Construction), Verlag von Konrad Wittwer, Stuttgart, West Germany, 1922, 460 pp. (quote is from page 128).
- 7-15 Ritter, W., *Die Bauweise Hennebique* (Construction Techniques of Hennebique), Schweizerische Bauzeitung, Zurich, Feb. 1899.
- 7-16 Hognestad, E., "What Do We Know about Diagonal Tension and Web Reinforcement in Concrete," *University of Illinois Engineering Experiment Station, Circular Series*, No. 64, 1952, 47 pp.
- 7-17 Richart, F.E., "An Investigation of Web Stresses in Reinforced Concrete Beams," *Bulletin No. 166, Engineering Experiment Station, University of Illinois*, Urbana, Ill., 1927, 106 pp.
- 7-18 NACU, "Standard No. 4: Standard Building Regulations for Reinforced Concrete," *Proceedings, National Association of Cement Users*, Vol. 6, Feb. 1910, pp. 349-361.

- 7-19 MacGregor, J.G., Sozen, M.A., and Siess, C.P. "Strength of Concrete Beams with Web Reinforcement." *ACI Journal*, Vol. 62, No. 12, Dec. 1965, pp. 1503-1519.
- 7-20 MacGregor, J.G., and Hanson, J.M. "Proposed Changes in Shear Provisions for Reinforced and Prestressed Concrete Beams," *ACI Journal*, Vol. 66, No. 4, Apr. 1969, pp. 276-288.
- 7-21 Elstner, R.C., and Hognestad, E. "Laboratory Investigation of Rigid Frame Failure," *ACI Journal*, Vol. 53, No. 1, Jan. 1957, pp. 637-668.
- 7-22 ACI-ASCE Committee 426, "Shear Strength of Reinforced Concrete Members," *Journal of the Structural Division, ASCE*, Vol. 99, No. ST6, June 1973, pp. 1091-1187.
- 7-23 Mailhot, G. "Experiments on the Staggering Concept for Shear Design," Project Report No. G84-5, Department of Civil Engineering and Applied Mechanics, McGill University, Mar. 1985, 96 pp.
- 7-24 Kupfer, H. "Erweiterung der Mörsch'schen Fachwerk analogie mit Hilfe des Prinzips vom minimum Formänderungsarbeit" (Extension to the Truss-Analogy of Mörsch using the Principle of Minimum Potential Energy), *CEB Bulletin d'Information*, No. 40, Jan. 1964.
- 7-25 Nielsen, M.P. *Limit Analysis and Concrete Plasticity*, Prentice-Hall Inc., Englewood Cliffs, N.J., 1984, 420 pp.
- 7-26 Thürlemann, B., Marti, P., Pralong, J., Ritz, P., and Zimmerli, B. *Anwendung der Plastizitätstheorie Stahlbeton* (Application of the Theory of Plasticity to Reinforced Concrete), Institut für Baustatik und Konstruktion, Eidgenössische Technische Hochschule, Zürich, Apr. 1983, 252 pp.
- 7-27 Marti, Peter. "Basic Tools of Reinforced Concrete Beam Design," *ACI Journal*, Vol. 82, No. 1, Jan.-Feb. 1985, pp. 46-56.
- 7-28 CEB-FIP. *Model Code for Concrete Structures: CEB-FIP International Recommendations*, 3rd ed., Comité Euro-International du Béton, Paris, 1978, 348 pp.
- 7-29 Collins, M.P., and Mitchell, D., "Shear and Torsion Design of Prestressed and Non-Prestressed Concrete Beams," *PCI Journal*, Vol. 25, No. 5, Sept.-Oct. 1980, pp. 32-100; Discussion and Closure, *PCI Journal*, Vol. 26, No. 6, Nov.-Dec. 1981, pp. 96-118.
- 7-30 Hsu, T.T.C., "Is the Staggering Concept of Shear Design Safe?" *ACI Journal*, Vol. 79, No. 6, Nov.-Dec. 1982, pp. 435-443; Discussion and Closure, *ACI Journal*, Vol. 80, No. 5, Sept.-Oct. 1983, pp. 445-454.
- 7-31 Marti, Peter, "Staggered Shear Design of Simply Supported Concrete Beams," *ACI Journal*, Vol. 83, No. 1, Jan.-Feb. 1986, pp. 36-42.
- 7-32 Wagner, H. "Ebene Blechwandträger mit sehr dünnem Stegblech" (Metal Beams with Very Thin Webs), *Zeitschrift für Flugtechnik und Motorluftschiffahrt*, Vol. 20, Nos. 8 to 12, 1929.
- 7-33 Mitchell, D., and Collins, M.P., "Diagonal Compression Field Theory - A Rational Model for Structural Concrete in Pure Torsion," *ACI Journal*, Vol. 71, Aug. 1974, pp. 396-408.
- 7-34 Collins, M.P., "Towards a Rational Theory for RC Members in Shear," *Journal of the Structural Division, ASCE*, Vol. 104, Apr. 1978, pp. 649-666.
- 7-35 Vecchio, F., and Collins, M.P., "The Response of Reinforced Concrete to In-Plane Shear and Normal Stresses," Publication No. 82-03, Department of Civil Engineering, University of Toronto, Mar. 1982, 332 pp.
- 7-36 Vecchio, F.J., and Collins, M.P., "The Modified Compression Field Theory for Reinforced Concrete Elements Subjected to Shear," *ACI Journal*, Vol. 83, No. 2, Mar.-Apr. 1986, pp. 219-231.

- 7-37 Walraven, Joost C., "Fundamental Analysis of Aggregate Interlock," *Journal of the Structural Division, ASCE*, Vol. 107, No. ST11, Nov. 1981, pp. 2245-2270.
- 7-38 Arbesman, B., and Conte, D.F., "The Design and Testing to Failure of a Prestressed Concrete Beam Loaded in Flexure and Shear," B.A.Sc. thesis, Department of Civil Engineering, University of Toronto, 1973, 176 pp.
- 7-39 Vecchio, F.J., and Collins, M.P., "Predicting the Response of Reinforced Concrete Beams Subjected to Shear Using the Modified Compression Field Theory," *ACI Structural Journal*, Vol. 85, No. 4, May-June 1988, pp. 258-268.
- 7-40 Shioya, T., Iguro, M., Nojiri, Y., Akiyama, H., and Okada, T., "Shear Strength of Large Reinforced Concrete Beams," *Fracture Mechanics: Application to Concrete*, SP-118, American Concrete Institute, Detroit, 1989, 309 pp.
- 7-41 Shioya, T., "Shear Properties of Large Reinforced Concrete Member," Special Report of Institute of Technology, Shimizu Corporation, No. 25, Feb. 1989, 198 pp.

Demonstration Problems

- 7-1 Estimate the load at which diagonal cracking will occur for the single-tie beam described in Section 7.3 using the simplified expression, Eq. (7-14), for diagonal cracking shear.
- 7-2 Investigate whether the shear capacity of the hollow-core slab system described in Prob. 6-3 is adequate. Assume that the slabs contain eight 1/2 in. (13 mm) strands and do not contain any shear reinforcement. Use the modified compression field design method.
- 7-3 It is proposed to build a new railway bridge across a river valley as a series of simply supported box girders each spanning 140 ft (43 m), center to center of bearings. The bearings are 24 in. (600 mm) long. As shown in Fig. 7-53, the post-tensioned box girder supports two railway tracks, two walkways, and a substantial quantity of ballast in addition to its own weight. The loadings are as follows:
- Live loads:**
- train — 6 kips/ft (88 kN/m) each track, including impact
 - walkway — 0.3 kips/ft (4.4 kN/m) each walkway
- Dead loads:**
- superimposed ballast and hardware — 9.5 kips/ft (139 kN/m)
 - self-weight of box girder — 19.7 kips/ft (288 kN/m)
- A preliminary design has resulted in a choice of 18 tendons each containing twelve 0.6 in. (15 mm) diameter, 270 ksi ($f_{pu} = 1860$ MPa) low-relaxation strands with the strands post-tensioned to $0.7f_{pu}$. Ten of these tendons are located at mid-depth of the bottom flange and are straight from end to end of the beam. Eight of the tendons are located in the webs of the box girder and have parabolic profiles. At midspan the centroid of these eight tendons is 7 in. (180 mm) from the bottom face, while at the supports the centroid of these eight tendons is 24 in. (600 mm) from the top face of the box girder. Design the startups and the longitudinal reinforcement required for shear and moment using the modified compression field approach described in Section 7.12. Use a load factor of 1.3 for both dead loads and live loads. The concrete compressive strength is 5000 psi (34.5 MPa).
- 7-4 The pretensioned bridge I-girder in Fig. 7-54 contains twenty-eight 1/2 in. (13 mm) diameter, 270 ksi ($f_{pu} = 1860$ MPa) low-relaxation strands. The effective stress, f_{se} , in these strands after allowing for all losses is 164 ksi (1130 MPa). The precasting plant wishes to use straight strands to simplify manufacturing of the beam. They propose blanketing a number of the

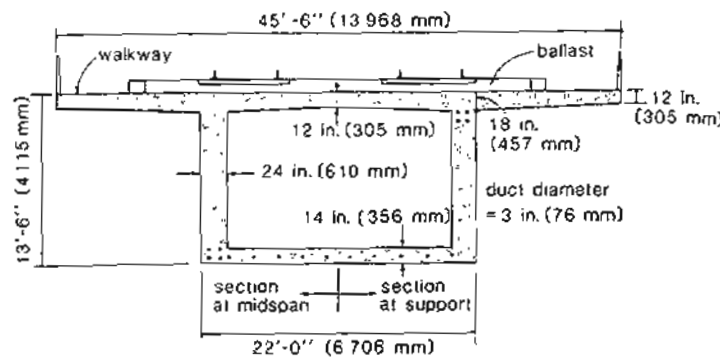


Figure 7-53 Box-girder railway bridge.

strands at the ends of the beam to minimize cracking of the beam on the top face near the supports.

Under the factored loading the factored shear, V_u , at the face of the support is 237 kips (1053 kN). The compressive strength of the concrete is 6000 psi (41.4 MPa). Using the design approach based on the modified compression field theory, design the stirrups near the end of the beam. Estimate the maximum percentage of the strands that could be blanketed without causing an anchorage problem at the support.

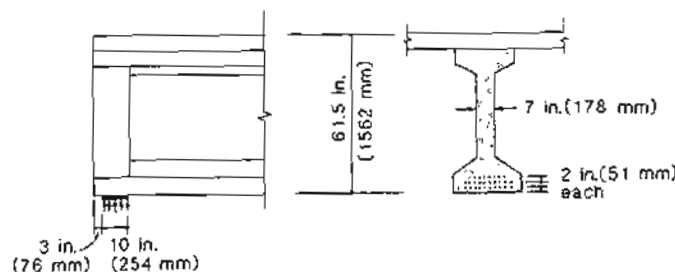


Figure 7-54 Pretensioned bridge girder.

7.5 The floor system of a low-rise industrial building consists of untopped 10 ft (3048 mm) wide T-beams spanning 65 ft (19.8 m). The moment-shear interaction diagram for the T-beam that

has uniform properties along its length is shown in Fig 7-55. Note that for this unsymmetrically reinforced section the maximum shear capacity does not occur at zero moment. Estimate the uniform superimposed load required to collapse the floor. Where along the length of the span will the failure occur? The self-weight of the T-beam is 1020 lb/ft (14.9 kN/m).

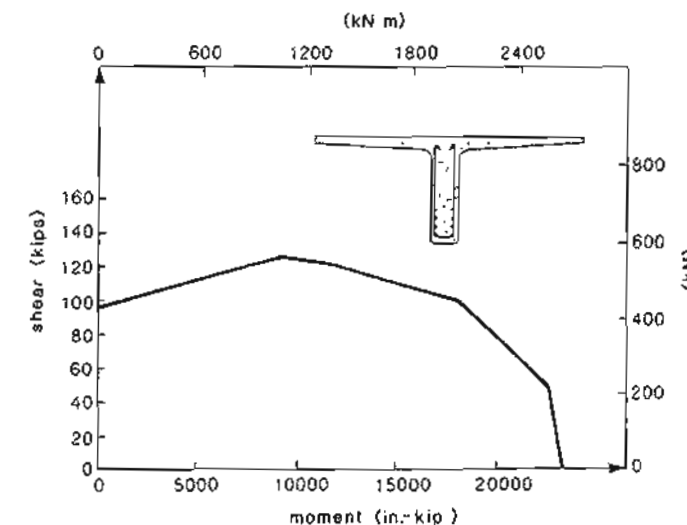


Figure 7-55 Shear-moment interaction diagram for T-beam.

7.6 Figure 7-44 shows the moment-shear interaction diagram for beam CF1. Using either program SHEAR or program RESPONSE calculate the shear capacity of beam CF1 for a range of values of axial load assuming in each case that the moment is zero. Use the results to plot a shear force-axial load interaction diagram.

7.7 Beam CF1 contained #3 (9.5 mm diameter) stirrups at 6 in. (152 mm) centers. Using either program SHEAR or program RESPONSE, calculate how the shear capacity of CF1 would change as the stirrup spacing was changed from 1 in. (25 mm) to 24 in. (600 mm). Make a plot showing how the shear capacity changes with change in the amount of stirrups ($A_s f_v/s$). Also show on this plot the shear strengths predicted by the ACI Code.

7.8 Use program RESPONSE to predict the response of the single-tear beam described in Figs. 7-21a and 7-9. Considering the section located at the quarter-point of the span, calculate the superimposed load that will cause diagonal cracks 0.02 in. (0.5 mm) wide.

7.9 For beam CF1 estimate the strain in the stirrups when the shear equals 100 kips (445 kN) and 50 kips (222 kN). Use the relationship

$$V = \beta \sqrt{f_c b_w d} + \frac{A_s f_v j d \cot \theta}{s}$$

to calculate f_v , taking θ and β from Table 7-3. Compare the results with those in Fig. 7-41.

Design for Torsion

If torsion is a dominant design factor in a large concrete member, it is wise to resort to prestressing ...

Henry J. Cowan, 1968

8.1 INTRODUCTION

Eccentrically loaded beams, members curved in plan, and members of space frames will be subjected to torsion. For most prestressed concrete members the torsional effects will be insignificant. However, for a number of prestressed concrete members such as those shown in Fig. 8-1, torsional effects may govern the design.

This chapter will concentrate on explaining torsion design procedures based on the compression field theory (Ref. 8-1). The ACI Code (Ref. 8-2) does not contain provisions for the design of prestressed concrete members subjected to torsion. The background to the ACI torsion provisions for non-prestressed members and the way in which these provisions can be extended to prestressed concrete has been explained by Hsu (Ref. 8-3).

8.2 THIN-WALLED TUBES IN TORSION

To introduce the problem, we will first review the behavior of thin-walled tubes in torsion. For these simple members the shear stresses caused by torsion can be determined using only equilibrium relationships. Figure 8-2 shows a thin-walled tube, with a varying wall thickness, subjected to pure torsion. Because the wall of the tube is thin, it is assumed that

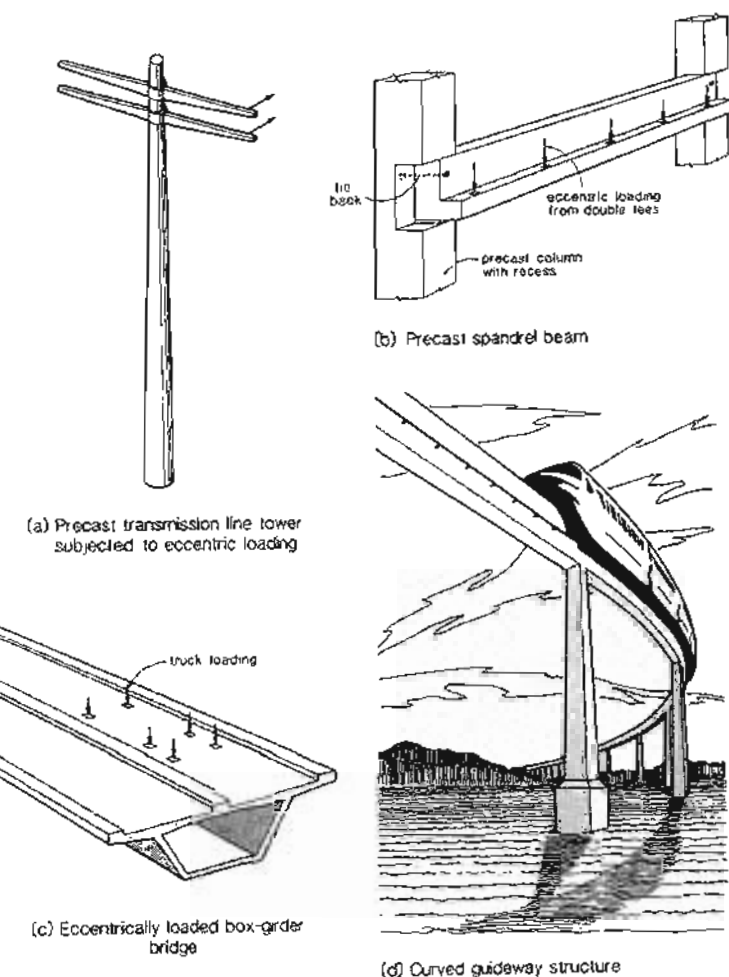


Figure 8-1 Examples of prestressed concrete structures with significant torsion.

the shear stresses are constant across the wall thickness. If we consider the equilibrium in the longitudinal direction of the small element shown in Fig. 8-2, we conclude that the shear stress times the wall thickness (τt) must remain constant around the section. The

shear stress times the wall thickness is called the shear flow, q (i.e., $q = vt$). The turning effect about the x -axis exerted by the shear stresses acting on the small length of perimeter, dp in length, is

$$dT = q h_p dp \quad (8-1)$$

where h_p is the "lever arm" of the force qdp . Integrating around the circumference of the tube gives

$$\begin{aligned} T &= q \int_p h_p dp \\ &= q 2A_o \end{aligned} \quad (8-2)$$

where A_o is the area enclosed by the centerline of the tube, which corresponds to the area enclosed by the shear flow. Thus the shear stress caused by torsion is

$$v = \frac{T}{2A_o t} \quad (8-3)$$

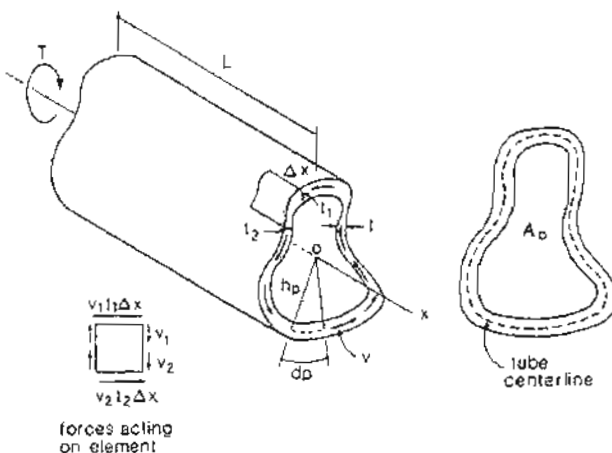


Figure 8-2 Thin-walled tube subjected to pure torsion.

The torsional stiffness of the thin-walled tube can be found by using the principle of virtual work. The external work done by the applied torque acting through the torsional rotation, θ , is equated to the internal work done by the shear stresses acting through the

shear strains, γ . Hence

$$\begin{aligned} T\theta &= \int_V v\gamma dV \\ &= L \int_p \frac{T}{2A_o t} \gamma t dp \end{aligned} \quad (8-4)$$

If the wall thickness remains constant around the perimeter, the twist (i.e., the torsional rotation per unit length) can be determined from Eq. (8-4) as

$$\psi = \frac{\theta}{L} = \frac{\gamma p_o}{2A_o} \quad (8-5)$$

where p_o is the perimeter of A_o . For an elastic member, where $\gamma = T/(2A_o t G)$, Eq. (8-5) becomes

$$\psi = \frac{Tp_o}{4A_o^2 t G} \quad (8-6)$$

Conventionally, we define the torsional stiffness, GK , as the torsion divided by the twist, and thus

$$GK = G \frac{4A_o^2 t}{p_o} \quad (8-7)$$

8.3 TORSIONAL RESPONSE PRIOR TO CRACKING

Diagonal torsional cracks will occur when the principal tensile stress reaches the cracking strength of the concrete, f_{cr} . Equations (7-2) and (7-3) can be used to determine the shear stress to cause diagonal cracking in the prestressed concrete and to determine the inclination of these cracks.

For a thin-walled tube the torsional shear stress, v , can be found from the applied torsion, T , using Eq. (8-3). For other sections this relationship can be determined from elastic theory (Saint-Venant, Ref. 8-4) or from plastic theory (Nadai, Ref. 8-5). Rather than using these relatively complex procedures, an approximate procedure based on the concept that most of the torsion is resisted by the high shear stresses near the outer perimeter of the section may be used. In this approach the actual cross section is represented by an equivalent thin-walled tube having the same external dimensions as the actual cross section but having a wall thickness, t_c , of

$$t_c = \frac{3}{4} \frac{A_c}{p_c} \quad (8-8)$$

where A_c is the area enclosed by the outside perimeter of the concrete cross section and p_c is the outside perimeter of concrete cross section.

While the area enclosed by the shear flow path, A_o , could be calculated from the external dimensions and wall thickness of the equivalent tube, it is a reasonable approximation to take A_o as 2/3 of A_c . Hence, from Eqs. (8-3) and (8-8),

$$v = \frac{Tp_c}{A_c^2} \quad (8-9)$$

The torsional stress in a solid rectangular section calculated using Eq. (8-9) is compared with that calculated from the elastic theory and the plastic theory in Fig. 8-3. Also shown in Fig. 8-3 is the torsional stress function for rectangular beams suggested by Zia and McGee (Ref. 8-6), who developed this function based on a study of the reported cracking torques for 218 rectangular beams.

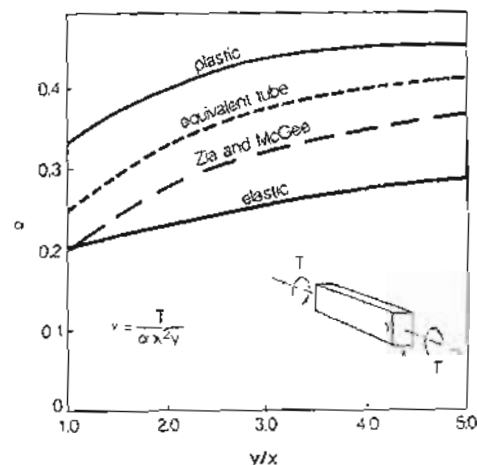


Figure 8-3 Comparison of different methods for determining maximum torsional shear stress.

Based on Eqs. (8-9) and (7-2) and assuming that f_{cr} equals $4\sqrt{f'_c}$ psi ($0.33\sqrt{f'_c}$ MPa), the cracking torsion of a prestressed concrete member is

$$T_{cr} = \frac{A_c^2}{P_c} 4\sqrt{f'_c} \sqrt{1 + \frac{f_{pc}}{4\sqrt{f'_c}}} \quad \text{psi} \quad (8-10a)$$

In SI units this expression is

$$T_{cr} = \frac{A_c^2}{P_c} 0.33\sqrt{f'_c} \sqrt{1 + \frac{f_{pc}}{0.33\sqrt{f'_c}}} \quad \text{MPa} \quad (8-10b)$$

8.4 EXAMPLE OF CALCULATING PRE-CRACKING RESPONSE

Figure 8-4 shows the measured torque-twist responses of three prestressed concrete beams (Ref. 8-7). The significant difference among these three solid, rectangular beams was the level of prestress (see Fig. 8-4). Note how an increase in the amount of prestressing increases the torsion at which cracks form. Also note the very substantial reduction in torsional stiffness that occurs after cracking. Estimate the cracking torques and the twists at cracking using the equivalent tube analysis.

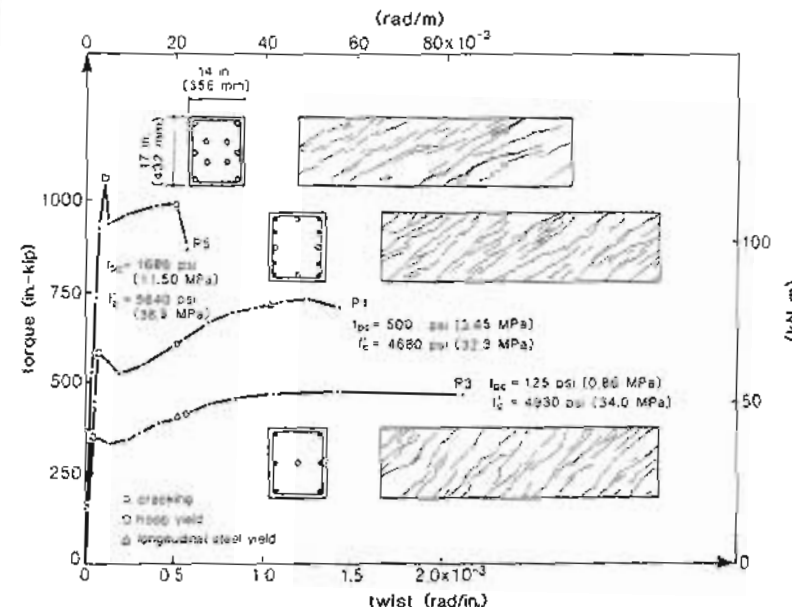


Figure 8-4 Torsional response of three prestressed concrete beams. Adapted from Ref. 8-7.

From Eq. (8-10), T_{cr} for member P3 is

$$\begin{aligned} T_{cr} &= \frac{(14 \times 17)^2}{2(14 + 17)} 4\sqrt{4930} \sqrt{1 + \frac{125}{4\sqrt{4930}}} \\ &= 308 \text{ in.-kips (34.9 kNm)} \end{aligned}$$

Similarly, the predicted cracking torques for members P1 and P5 are 420 in.-kips (48 kNm) and 703 in.-kips (79 kNm), respectively.

The equivalent tube thickness for all three beams can be found from Eq. (8-8) as

$$t_c = \frac{3}{4} \frac{14 \times 17}{2(14 + 17)} \\ = 2.9 \text{ in. (73 mm)}$$

The area enclosed by the shear stress and the perimeter of the shear flow path for this thin-walled tube are

$$A_o = (14 - 2.9)(17 - 2.9) = 157 \text{ in}^2 (101 \times 10^3 \text{ mm}^2)$$

and $p_o = 2(14 - 2.9 + 17 - 2.9) = 50.4 \text{ in. (1280 mm)}$

If we assume that the shear modulus of the concrete is equal to $0.5E_c$, then, from Eq. (8-6), the twist at torsional cracking for beam P3 is

$$\psi = \frac{308 \times 10^3 \times 50.4}{4 \times 157^2 \times 0.5 \times 57,000 \sqrt{4930} \times 2.9} \\ = 27.1 \times 10^{-6} \text{ rad/in. (1.07} \times 10^{-3} \text{ rad/m)}$$

Similarly, the twists at cracking for members P1 and P5 are 38.0×10^{-6} rad/in. (1.49×10^{-3} rad/m) and 57.9×10^{-6} rad/in. (2.28×10^{-3} rad/m), respectively.

8.5 TORSIONAL RESPONSE AFTER CRACKING

After cracking of the concrete, torsion is resisted by diagonal concrete compressive stresses that spiral around the beam at an angle θ (see Fig. 8-5). The tangential component of these diagonal compressive stresses provides the shear flow, q , needed to equilibrate the torsion, where

$$q = \frac{T}{2A_\theta} \quad (8-11)$$

If tensile stresses in the cracked concrete are neglected, the normal component, $q \cot \theta$ per unit length, of the diagonal compressive stresses results in a longitudinal compressive force which must be balanced by a tensile force, N_v , in the longitudinal reinforcement. Thus

$$N_v = A_t f_t + A_p f_p = \frac{T p_o \cot \theta}{2A_o} \quad (8-12)$$

An examination of the equilibrium of the corner element shown in Fig. 8-5 indicates that the tensile force in each leg of the hoop is

$$A_t f_t = q s \tan \theta$$

Hence

$$\frac{A_t f_t}{s} = \frac{T}{2A_\theta} \tan \theta \quad (8-13)$$

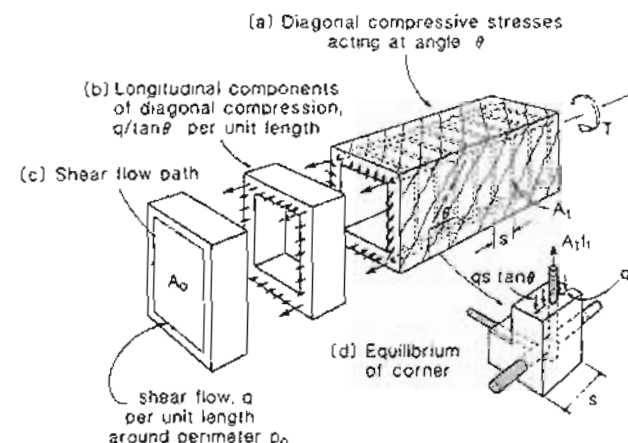


Figure 8-5 Equilibrium conditions for cracked beam in torsion.

Figure 8-6 illustrates why not all of the concrete is effective in providing diagonal compressive stresses to resist the torsion. Compressive stresses in the concrete cover need to curve inward toward the reinforcement at the corners. This changing direction of the compressive stresses produces tensile stresses perpendicular to the plane of the stirrups. At higher loads these tensile stresses may cause the concrete to split along the plane of weakness formed by the stirrups. Because of the potential for spalling of the concrete cover, it is assumed that the effective outer surface of the concrete coincides with the hoop centerline.

If the deformed shape of the twisted beam shown in Fig. 8-7 is examined, it can be seen that the walls of the beam are curved. Because of this curvature the diagonal compressive strains will be a maximum at the surface and will decrease linearly from the surface becoming tensile below a certain distance, t_d . Thus in torsion, as in flexure, we have a depth of compression below which the concrete, being in tension, is ineffective. The cover concrete spalls off and the inner concrete goes into tension; hence we are left with a tube of effective concrete, t_d thick, which lies just inside the hoop centerline.

The diagonal concrete stresses will vary in magnitude over the thickness of the effective concrete tube. As in flexure, we can replace this actual stress distribution by a uniform stress of magnitude $a_1 f'_c$ acting over a depth $a_o = \beta_1 t_d$. The centerline dimensions of the resulting tube of uniformly stressed concrete of thickness a_o will define the path of the shear flow, q . Examination of Fig. 8-7 shows that A_o for a rectangular section with

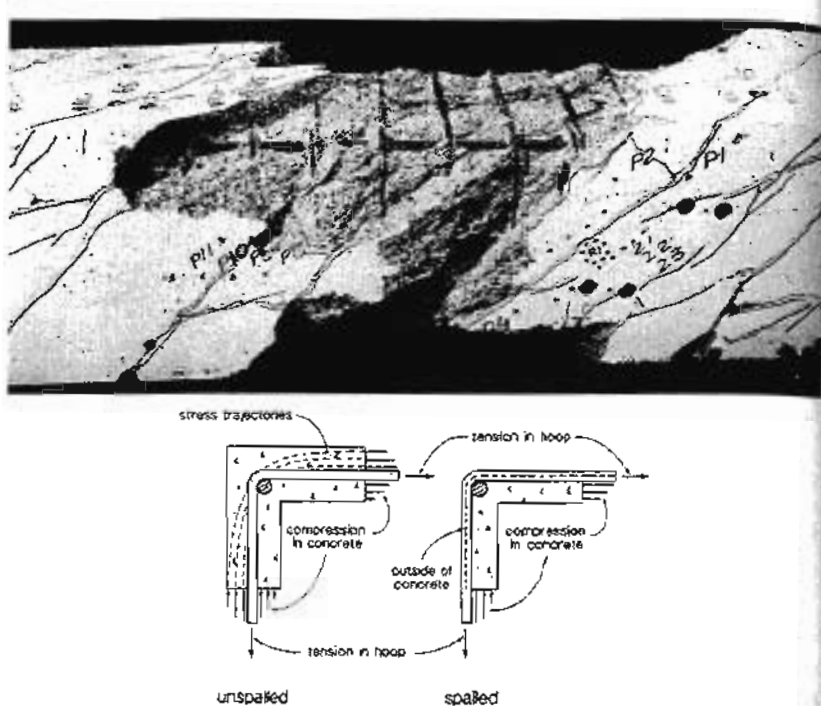


Figure 8-6 Spalling of the concrete cover due to torsion. Adapted from Ref. 8-8.

spalled dimensions of $b_h \times h_h$ is

$$\begin{aligned} A_o &= (b_h - a_o)(h_h - a_o) \\ &= b_h h_h - \frac{a_o}{2}(2b_h + 2h_h) + a_o^2 \\ &\approx A_{oh} - \frac{a_o}{2} p_h \end{aligned} \quad (8-14)$$

and

$$\begin{aligned} p_o &= 2(b_h - a_o + h_h - a_o) \\ &= 2(b_h + h_h) - 4a_o \\ &= p_h - 4a_o \end{aligned} \quad (8-15)$$

where A_{oh} is the area enclosed by the centerline of the hoop and p_h is the hoop centerline perimeter.

Equations (8-14) and (8-15) are appropriate for determining the torsional sectional parameters, A_o and p_o , for a wide variety of cross-sectional shapes (see Fig. 8-8).

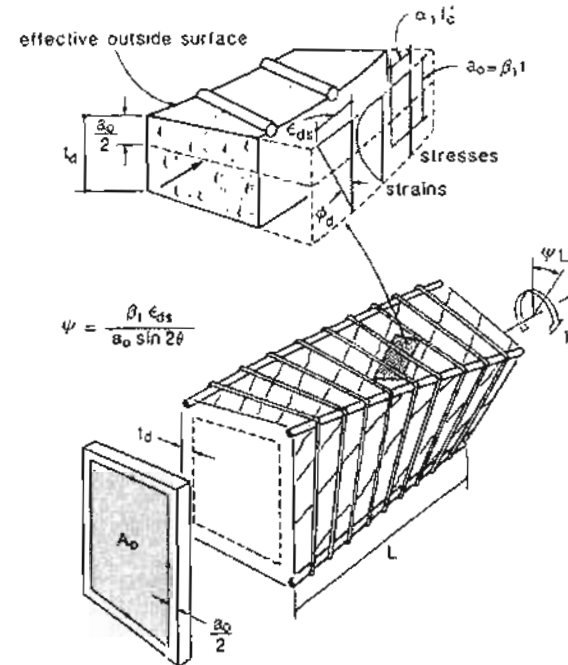


Figure 8-7 Effective wall thickness of a twisted beam.

The relationship between the uniform diagonal compressive stresses, $\alpha_1 f'_c$, and the shear flow, q , can be derived from the vertical equilibrium of the element shown in Fig. 8-9 as

$$q = \alpha_1 f'_c a_o \cos \theta \sin \theta \quad (8-16)$$

If both sides of Eq. (8-12) are divided by p_o and the resulting equation is added to Eq. (8-13), we have

$$\frac{A_l f_l + A_p f_p}{p_o} + \frac{A_l f_t}{s} = \frac{T}{2A_o} (\cot \theta + \tan \theta) \quad (8-17)$$

Substituting $T/2A_o$ by the expression for q in Eq. (8-16) then gives

$$\frac{A_l f_l + A_p f_p}{p_o} + \frac{A_l f_t}{s} = \alpha_1 f'_c a_o \quad (8-18)$$

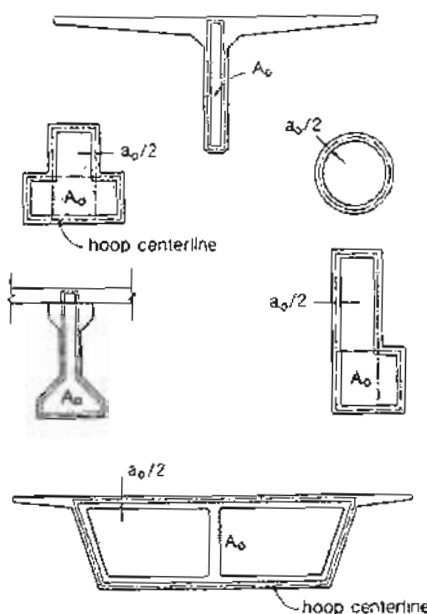


Figure 8-8 Area enclosed by shear flow for different cross sections.

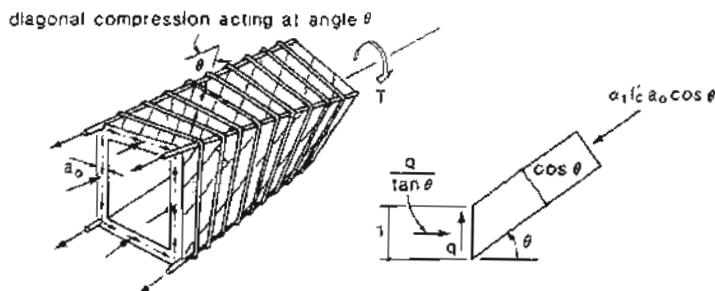


Figure 8-9 Relationship between shear flow and diagonal compressive stress.

Substituting from Eqs. (8-12), (8-13), and (8-14) results in a quadratic equation for a_o which, when solved gives

$$a_o = \frac{A_{oh}}{p_h} \left[1 - \sqrt{1 - \frac{T p_h}{\alpha_1 f'_c A_{oh}^2} (\tan \theta + \cot \theta)} \right] \quad (8-19)$$

In using this equation for the depth of compression in torsion we will assume that α_1 is 0.70. Note that it will not be possible to solve Eq. (8-19) if the term $T p_h / A_{oh}^2$ exceeds $0.5 \alpha_1 f'_c$. The term $T p_h / A_{oh}^2$, which will be called the nominal torsional shear stress, is a good indicator of the intensity of torsional loading on the cross section.

In order to have a consistent treatment for shear and torsion, the principal compressive stress due to torsion will be taken as

$$f_2 = \frac{T p_h}{A_{oh}^2} (\tan \theta + \cot \theta) \quad (8-20)$$

This compressive stress is not permitted to exceed f_{2max} , where f_{2max} is given by Eq. (7-26).

8.6 EXAMPLE OF CALCULATING TORSIONAL STRENGTH

In order to illustrate the use of the expressions for postcracking torsional response we will estimate the torsional capacity of beam P1 described in Fig. 8-4. This beam contained twelve 0.276 in. (7 mm) diameter wires with $f_{py} = 214$ ksi (1476 MPa) and $E_p = 28,600$ ksi (197 200 MPa), post-tensioned to 166 ksi (1145 MPa) ($\Delta \epsilon_p = 5.9 \times 10^{-3}$), as well as eight #3 reinforcing bars ($A_t = 8 \times 0.11 = 0.88$ in 2), with $f_y = 47.5$ ksi (328 MPa). The #3 hoops ($A_h = 0.11$ in 2 , $f_y = 47.5$ ksi) were spaced at 3.8 in. (96 mm). The clear concrete cover was 1/2 in. (13 mm).

Step 1: Determine the geometry of the hoop centerline.

The hoop centerline is located at a distance of $0.5 + 0.375/2 = 0.69$ in. (17 mm) from the outside surface of the concrete. Hence

$$A_{oh} = (14 - 2 \times 0.69)(17 - 2 \times 0.69) = 197 \text{ in}^2 \text{ (127 200 mm}^2\text{)}$$

and

$$p_h = 2(14 - 2 \times 0.69 + 17 - 2 \times 0.69) = 56.5 \text{ in. (1435 mm)}$$

Step 2: Estimate θ .

The equations in Section 8.5 are set up for convenient design rather than for convenient analysis. Analysis thus requires an iterative approach in which we first estimate the angle θ and then check the behavior of the member for this assumption. We will assume $\theta = 35^\circ$ as our first estimate.

Step 3: Estimate A_o .

As a first estimate, we will take A_o as $0.80 A_{sh}$.

$$A_o = 0.80 \times 197 = 158 \text{ in}^2 (102,000 \text{ mm}^2)$$

Step 4: Calculate the torsion assuming that the stirrups yield.

From Eq. (8-13),

$$\begin{aligned} T &= 2 \times 158 \times \frac{0.11 \times 47.5}{3.8} \cot 35^\circ \\ &= 621 \text{ in.-kips (70.1 kNm)} \end{aligned}$$

Step 5: Calculate a_o , A_o , and p_o .

From Eq. (8-19),

$$\begin{aligned} a_o &= \frac{197}{56.5} \left[1 - \sqrt{1 - \frac{621 \times 56.5}{0.7 \times 4.680 \times 197^2} (\tan 35^\circ + \cot 35^\circ)} \right] \\ &\approx 1.25 \text{ in. (32 mm)} \end{aligned}$$

From Eq. (8-14),

$$\begin{aligned} A_o &= 197 - 0.5 \times 1.25 \times 56.5 \\ &= 162 \text{ in}^2 (104,300 \text{ mm}^2) \end{aligned}$$

From Eq. (8-15),

$$\begin{aligned} p_o &= 56.5 - 4 \times 1.25 \\ &= 51.5 \text{ in. (1308 mm)} \end{aligned}$$

Step 6: Check A_o and if necessary, revise.

A_o was estimated to be $158 \text{ in}^2 (102,000 \text{ mm}^2)$ in Step 3 and calculated as $162 \text{ in}^2 (104,300 \text{ mm}^2)$ in Step 5. We need to revise the estimate of A_o and repeat Steps 4 and 5 until the calculated value agrees with the estimate. Convergence is reached for

$$\begin{aligned} A_o &= 161 \text{ in}^2 (103,900 \text{ mm}^2) \\ T &= 632 \text{ in.-kips (71.4 kNm)} \\ p_o &= 51.4 \text{ in. (1305 mm)} \end{aligned}$$

Step 7: Calculate the longitudinal strain, ϵ_x .

From Eq. (8-12),

$$\begin{aligned} N_v &= \frac{632 \times 51.4 \times \cot 35^\circ}{2 \times 161} \\ &= 144 \text{ kips (641 kN)} \end{aligned}$$

Sec. 8.6 Example of Calculating Torsional Strength

This tension would cause a longitudinal strain, ϵ_x , in the reinforcing bars of

$$\begin{aligned} \epsilon_x &= \frac{N_v - A_p E_p \Delta \epsilon_p}{A_t E_z + A_p E_p} \\ &= \frac{144 - 12 \times 0.0598 \times 28,600 \times 5.9 \times 10^{-3}}{8 \times 0.11 \times 29,000 + 12 \times 0.0598 \times 28,600} \\ &= 0.50 \times 10^{-3} \end{aligned} \quad (8-21)$$

Step 8: Check the diagonal crushing of concrete.

The principal compressive stress, f_2 , from Eq. (8-20) is

$$\begin{aligned} f_2 &= \frac{632 \times 56.5}{197^2} (\tan 35^\circ + \cot 35^\circ) \\ &= 1.96 \text{ ksi (13.5 MPa)} \end{aligned}$$

The principal tensile strain, ϵ_1 , from Eqs. (7-23) and (7-24) is

$$\epsilon_1 = \epsilon_x + \frac{\epsilon_2 - \epsilon_1}{\tan^2 \theta} \quad (8-22)$$

The principal compressive strain, ϵ_2 , varies over the effective wall thickness (see Fig. 8-7). In addition, θ and ϵ_1 will also vary across the wall thickness. For simplicity we will assume that θ remains constant across the wall thickness and that the value of ϵ_2 at mid-depth can be used to determine ϵ_1 from Eq. (8-22). At failure the principal compressive strain at the surface will be about -0.003 and hence, at mid-depth ϵ_2 will be about -0.0015 . Thus, from Eq. (8-22)

$$\begin{aligned} \epsilon_1 &= 0.50 \times 10^{-3} + \frac{0.50 \times 10^{-3} + 1.5 \times 10^{-3}}{\tan^2 35^\circ} \\ &= 4.58 \times 10^{-3} \end{aligned}$$

The limiting compressive stress, f_{2max} , from Eq. (7-26) is

$$\begin{aligned} f_{2max} &= \frac{4.680}{0.8 + 170 \times 4.58 \times 10^{-3}} \\ &= 2.96 \text{ ksi (20.4 MPa)} \end{aligned}$$

Step 9: Revise the estimate of θ .

As f_2 is less than f_{2max} , the beam can still resist more load. In other words, a lower value of θ can be used. Note that lowering θ will increase f_2 and reduce f_{2max} . The beam is predicted to fail when f_2 reaches f_{2max} .

Repeating Steps 2 to 9 we find that f_2 reaches f_{2max} when $\theta = 32.3^\circ$, $a_o = 1.47 \text{ in. (37 mm)}$, $A_o = 155.5 \text{ in}^2 (100,300 \text{ mm}^2)$, and $p_o = 50.6 \text{ in. (1285 mm)}$, corresponding to

a torque of 676 in.-kips (76.4 kNm). At failure, ϵ_x is predicted to be 1.15×10^{-3} and ϵ_1 is predicted to be 7.79×10^{-3} . The observed failure torque for beam P1 was 725 in.-kips (81.9 kNm).

Assuming that at failure $\epsilon_2 = -1.5 \times 10^{-3}$, the stirrup strains can be found from Eq. (7-24) as

$$\begin{aligned}\epsilon_1 &= \epsilon_1 - \epsilon_2 - 1.5 \times 10^{-3} \\ &= 7.79 \times 10^{-3} - 1.15 \times 10^{-3} - 1.5 \times 10^{-3} \\ &= 5.14 \times 10^{-3}\end{aligned}\quad (8-23)$$

which confirms that the stirrups are yielding at failure.

From Eq. (7-25) the shear strain at failure is

$$\begin{aligned}\gamma_{xy} &= 2 [1.15 \times 10^{-3} - (-1.5 \times 10^{-3})] \cot 32.3^\circ \\ &= 8.38 \times 10^{-3}\end{aligned}$$

Hence, from Eq. (8-5) the predicted twist at failure is

$$\psi = \frac{8.38 \times 10^{-3} \times 50.6}{2 \times 155.5} = 1.36 \times 10^{-3} \text{ rad/in. (} 53.7 \times 10^{-3} \text{ rad/m)}$$

The predicted torque and twist at failure agree well with the experimental values (see Fig. 8-4).

8.7 COMBINED TORSION AND FLEXURE

Under the combined action of torsion and moment the longitudinal strains and the inclination, θ , of the principal compressive stresses will vary over the depth of the beam. Onsongo (Ref. 8-9) has developed a version of the compression field theory that accounts for these variations. In this section a simpler procedure for predicting the strength of beams under combined torsion and flexure will be described.

In the analogous case of combined shear and flexure, the influence of flexure was accounted for by increasing the longitudinal strain, ϵ_x (see Eq. 7-53). For combined torsion and flexure we will use the procedure given in Section 8.6 for pure torsion, except that in calculating ϵ_x we will use

$$\epsilon_x = \frac{\frac{M}{jd} + 0.5 \frac{T p_o \cot \theta}{2 A_o} - A_{ps} f_{se}}{E_s A_s + E_p A_{ps}} \quad (8-24)$$

where A_s and A_{ps} are the areas of longitudinal reinforcement on the flexural tension side of the member.

In addition, we will check that the tension in the longitudinal reinforcement does not exceed the tensile capacity of the reinforcement. Thus

$$A_s f_y + A_{ps} f_{ps} \geq \frac{M}{jd} + 0.5 \frac{T p_o \cot \theta}{2 A_o} \quad (8-25)$$

To investigate the accuracy of the simple method outlined above, it was used to predict the torsion-flexure interaction relationship for a series of uniformly prestressed, box-girder beams which had been tested at the University of Toronto (Ref. 8-10). The concrete cylinder strength varied somewhat between the five beams of the test series, so in the calculations the average value of 5570 psi (38.4 MPa) was used.

The predicted interaction curve was determined in the following manner. For a chosen moment M the angle θ , which would result in either the concrete crushing ($f_2 = f_{2max}$) or the longitudinal reinforcement yielding was determined and the corresponding torsion was thus found.

For example, with a moment of 500 in.-kips (56.5 kNm) the procedure results in

$$\begin{aligned}\theta &= 28.6^\circ \\ T &\approx 466 \text{ in.-kips (52.7 kNm)} \\ a_o &= 1.12 \text{ in. (28.4 mm)} \\ A_o &= 155.4 - 0.5 \times 1.12 \times 50.5 = 127.2 \text{ in}^2 (82000 \text{ mm}^2) \\ p_o &= 50.5 - 4 \times 1.12 = 46.0 \text{ in. (1169 mm)} \\ \epsilon_x &= \frac{500}{13.6} + 0.5 \frac{466 \times 46.0 \times \cot 28.6^\circ}{2 \times 127.2} - 8 \times 0.0598 \times 166 \\ &= 0.99 \times 10^{-3} \\ \epsilon_1 &= 0.99 \times 10^{-3} + \frac{0.99 \times 10^{-3} + 1.5 \times 10^{-3}}{\tan^2 28.6^\circ} \\ &= 9.37 \times 10^{-3} \\ f_{2max} &= \frac{5.57}{0.8 + 170 \times 9.37 \times 10^{-3}} = 2.33 \text{ ksi (16.1 MPa)} \\ f_2 &= \frac{466 \times 50.5}{155.4^2} (\tan 28.6^\circ + \cot 28.6^\circ) \\ &= 2.32 \text{ ksi (16.0 MPa)}\end{aligned}$$

Thus it can be seen that at $\theta = 28.6^\circ$ the concrete is about to crush with $f_2 = f_{2max}$. At this stage, Eq. (8-25) is satisfied since

$$\begin{aligned}0.62 \times 52.6 + 0.11 \times 54.5 + 8 \times 0.0598 \times 230 &> \frac{500}{13.6} + 0.5 \frac{466 \times 46.0 \times \cot 28.6^\circ}{2 \times 127.2} \\ 148.6 &> 114.0 \text{ kips}\end{aligned}$$

Repeating these calculations for different values of moment enables the interaction diagram of Fig. 8-10 to be constructed. Note that for higher values of moment, yielding of the longitudinal reinforcement governs the failure.

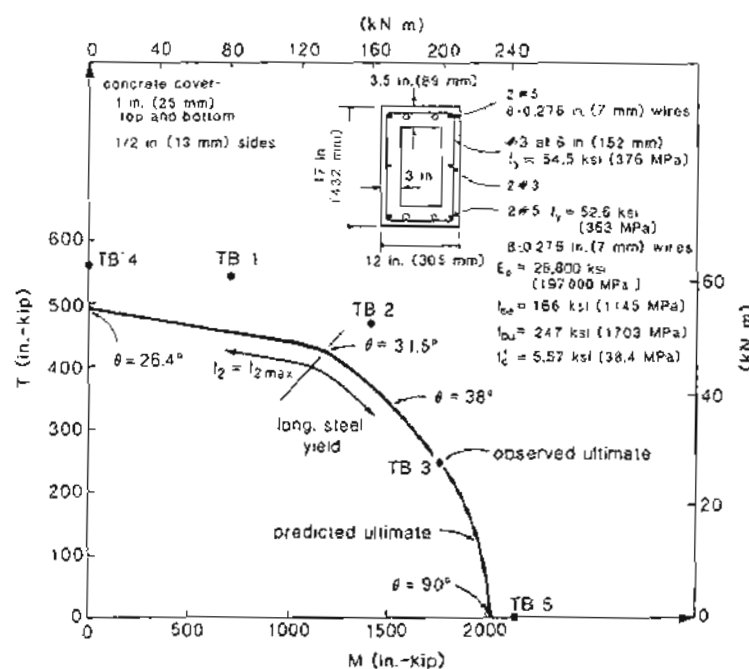


Figure 8-10 Torsion-flexure interaction for a series of prestressed concrete beams.

The theory predicts that as the ratio of torsion to moment decreases, the angle of inclination of the diagonal compression θ will increase. Predicted values of θ range from 26.4° for pure torsion to 90° for pure flexure. While these predicted values of θ will not necessarily coincide with the average inclination of the cracks (they will coincide with the inclination of cracks that form just prior to failure), this inclination will provide an indication of the value of θ . If the crack patterns for the five tested beams, which are shown in Fig. 8-11, are studied, it can be seen that the crack inclinations are in reasonable agreement with the predicted values of θ .

8.8 VARIABLE-ANGLE TRUSS MODEL FOR COMBINED TORSION, SHEAR, AND FLEXURE

A behavioral model, called the variable-angle space truss (Ref. 8-11), is capable of predicting the response of rectangular prestressed concrete beams in combined torsion, shear, and flexure and has been used (Ref. 8-12) as the basis for the computer-aided design of

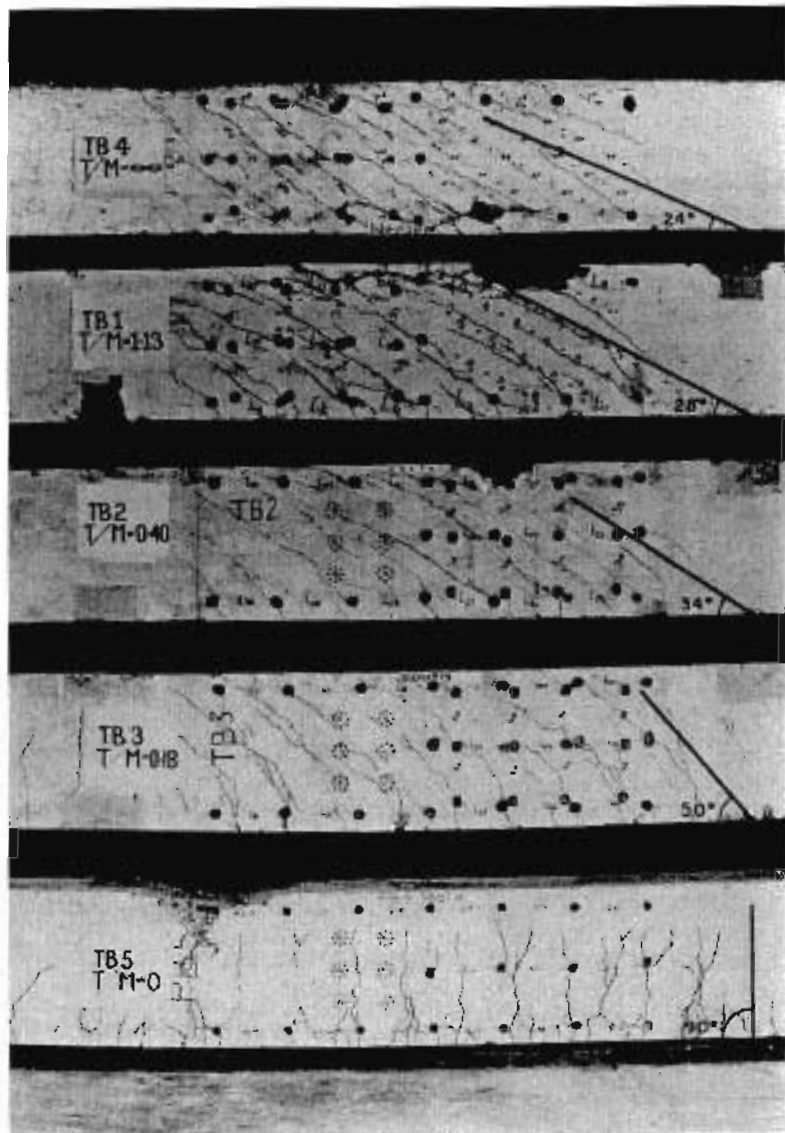
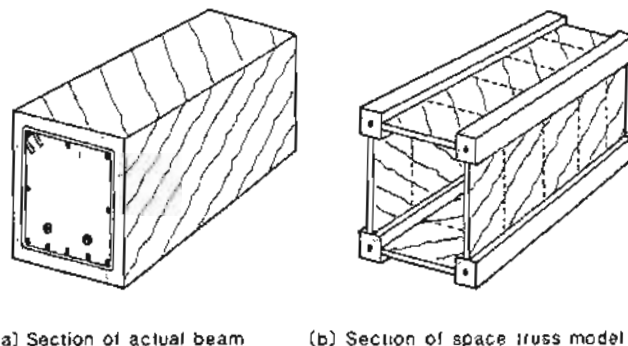


Figure 8-11 Crack patterns for five prestressed concrete beams, tested by Mardukhi (Ref. 8-10).

such members. In this model (see Fig. 8-12) the cross section is idealized by four parallel longitudinal chords, consisting of longitudinal prestressing steel and reinforcing bars as well as concrete. The chords are joined together by four walls, consisting of transverse reinforcement and diagonally cracked concrete. Moments and axial forces acting on the cross section are resisted by axial stresses in the chords, while shears and torsions acting on the cross section are resisted by shear flows in the walls. Due to the different shear flows and the different strain conditions in the chords adjacent to the walls, the angle of inclination of the principal compressive stress in each of the four walls will differ.



(a) Section of actual beam (b) Section of space truss model

Figure 8-12 Variable-angle space truss model for prestressed concrete beam subjected to torsion, shear, and moment. Adapted from Ref. 8-11.

Figure 8-13 illustrates how the inclinations, θ , of the principal compressions in the four walls of the truss change with the ratios of loading applied. It can be seen that for pure torsion the diagonal stresses spiral around the member at a constant angle, while for zero torsion the diagonal stresses in the two side walls are parallel. It is interesting to note that on the side where the shear stresses due to torsion and shear add (the left side), the angle θ is not greatly influenced by the loading ratio.

8.9 DESIGN APPROACH FOR COMBINED TORSION, SHEAR, AND FLEXURE

Section 7.12 presented a design procedure for members subjected to shear and flexure. In this section we will extend this procedure to include the additional effects of torsion. This design method does not explicitly consider the way in which the conditions will vary from one side of the beam to the other, but rather, it concentrates on the side of the beam where the shear and torsional stresses are additive.

From Eqs. (7-51) and (8-20) the nominal shear stress is

$$\tau = \frac{V_u - V_p}{b_w j d} + \frac{T_n p_h}{A_{sh}^2} \quad (8-26)$$

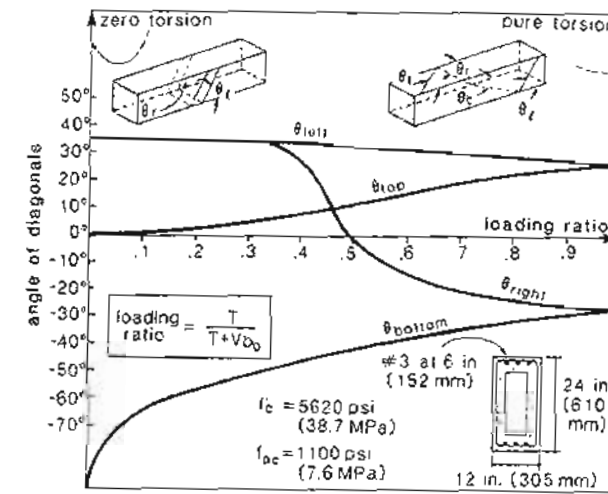


Figure 8-13 Influence of loading ratios on inclination of principal compressive stresses for prestressed concrete box girder subjected to torsion, shear and moment ($M/Vd = 3.0$). Adapted from Ref. 8-11.

This equation will be accurate for hollow box girders but will be somewhat conservative for solid sections, where significant redistribution of the shear stresses is possible. For such sections, a more appropriate expression for the nominal shear stress is

$$\tau = \sqrt{\left(\frac{V_u - V_p}{b_w j d}\right)^2 + \left(\frac{T_n p_h}{A_{sh}^2}\right)^2} \quad (8-27)$$

As was the case for shear, the angle θ will be chosen from Table 7-3 and will thus depend on the values of τ/f'_c and ϵ_x . The longitudinal strain, ϵ_x , is computed from

$$\epsilon_x = \frac{\frac{M_u}{j d} + 0.5 N_u + 0.5 N_v - A_{ps} f_{sc}}{E_s A_s + E_p A_{ps}} \quad (8-28)$$

where the equivalent longitudinal tension due to shear and torsion is given by

$$N_e = \text{col} \theta \sqrt{(V_u - V_p)^2 + \left(\frac{T_n p_h}{2 A_c}\right)^2} \quad (8-29)$$

This equation assumes that the equivalent longitudinal tension for combined shear and torsion is the square root of the sum of the squares of the individually calculated

tensions for shear and for torsion. The tensions are not simply additive because on one face of the member the torsion and shear stresses counteract, reducing the total longitudinal force required.

The required amount of transverse reinforcement is assumed to be the sum of the amount required for shear and the amount required for torsion. The required amount of transverse reinforcement for torsion is determined from Eq. (8-13) as

$$T_n = \frac{A_t f_y}{s} 2 A_o \cot \theta \quad (8-30)$$

The required amount of transverse reinforcement for shear is found from Eqs. (7-42), (7-43), and (7-52) as

$$V_n = \beta \sqrt{f'_c b_w j d} + \frac{A_v f_y}{s} j d \cot \theta + V_p \quad (8-31)$$

where β is found from Table 7-3.

To avoid yielding of the longitudinal reinforcement, the reinforcement on the flexural tension face must be proportioned so that

$$A_s f_y + A_{ps} f_{ps} \geq \frac{M_u}{\phi j d} + 0.5 \frac{N_u}{\phi} + \cot \theta \sqrt{\left(\frac{V_u}{\phi} - 0.5 V_s - V_p \right)^2 + \left(\frac{0.5 T_u p_o}{\phi 2 A_o} \right)^2} \quad (8-32)$$

Further details of this design approach are explained in Section 8.12 where a design example is given.

8.10 DETAILING CONSIDERATIONS

In order to properly detail beams subjected to torsion, it is necessary to understand the functions of the concrete and the reinforcement and to recognize the possibility of spalling of the concrete cover. A diagonally cracked beam subjected to torsion is idealized in Fig. 8-14, where the functions of the concrete and the reinforcement can be visualized more clearly. The function of the concrete is to provide the diagonal compression required to resist the torsion, the function of the longitudinal reinforcement is to hold the beam together in the longitudinal direction, and the function of the transverse reinforcement is to hold the beam together in the transverse direction.

Because the longitudinal reinforcement acts as a tension tie between the ends of the beam, care must be taken to provide adequate end anchorage and appropriate splice details if splicing is required. As pointed out by Jirsa (Ref. 8-14), a common error in detailing cast-in-place spandrel beams is to provide inadequate end anchorage for the bottom longitudinal steel (see Fig. 8-15a).

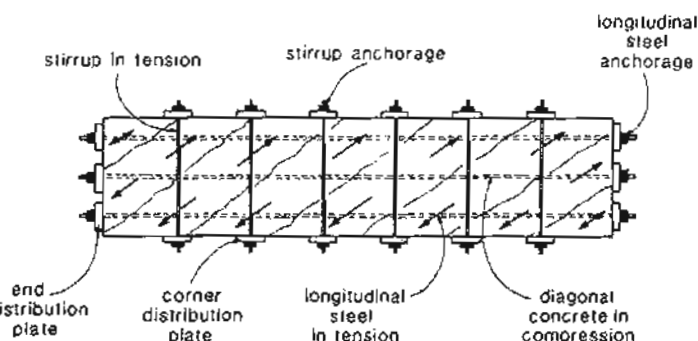


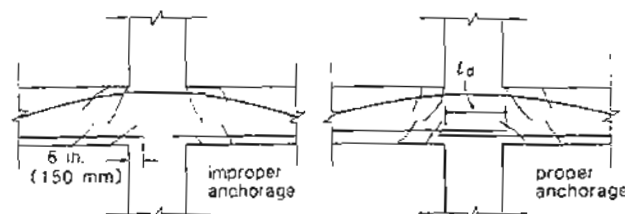
Figure 8-14 Idealized functions of the concrete and reinforcement. Adapted from Ref. 8-13.

The transverse reinforcement acts as ties between the corners of the beam and must be provided in all sides of the beam. Because at higher torsions the concrete cover may spall, lap-spliced stirrups and stirrups anchored with 90° bends will be rendered ineffective (see Fig. 8-15b).

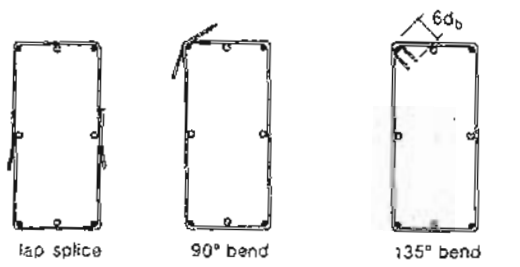
The idealized corner distribution plates shown in Fig. 8-14 enable the concentrated stirrup tensions to be distributed along the length of the beam, balancing the outward thrust of the concrete. In an actual beam, the longitudinal corner bars act as the corner distribution plates. If large stirrup spacings together with small corner bars are used, then a premature corner push-out failure may occur between the stirrups (see Fig. 8-15c). The CSA Code (Ref. 8-15) requires a minimum corner bar diameter of $s/16$ to prevent corner push-out and also limits the spacing of transverse torsion reinforcement to $p_h/(8 \tan \theta)$, in order to ensure reasonable uniformity in the distribution of diagonal compressive stresses along the length of the beam.

8.11 REDISTRIBUTION OF TORSION IN STATICALLY INDETERMINATE STRUCTURES

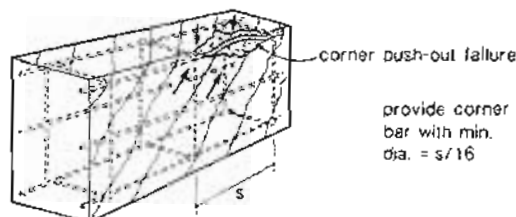
In many statically indeterminate structures the magnitude of the torsion that will occur in a particular member will depend upon the torsional stiffness of this member. When a member cracks in torsion there is a dramatic loss in torsional stiffness (see Fig. 8-4). The reduction in torsional stiffness after cracking is much more severe than the loss in flexural stiffness caused by flexural cracking. Examples of structures in which the torsion arises only because members must twist to maintain compatibility are shown in Fig. 8-16. In such cases, called compatibility torsion, the magnitude of the torsion will be proportional to the torsional stiffness. A conventional analysis using gross stiffness values (i.e., assuming elastic, uncracked behavior) would overestimate the magnitudes of the torsions in the members.



(a) Anchorage of bottom bars in spandrel beam



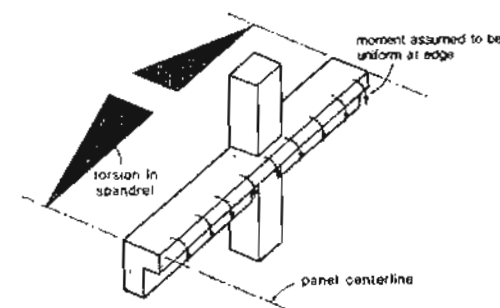
(b) Anchorage of transverse reinforcement



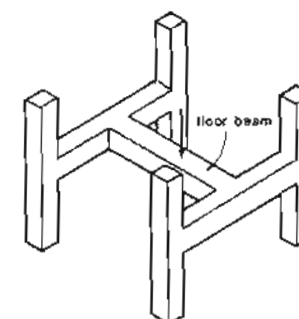
(c) Corner support for diagonal struts

Figure 8-15 Detailing of torsion reinforcement.

Figure 8-17 demonstrates the manner in which the measured torsion in a spandrel beam deviates from that predicted using gross stiffness values. The gross torsional stiffness for the spandrel beam shown in Fig. 8-17 can be calculated from the equivalent tube method as follows:



(a) Torsion in spandrel beam due to imposed rotation from cast-in-place slab



(b) Torsion in spandrel beams due to imposed rotation from floor beam

Figure 8-16 Example of compatibility torsion.

From Eq. (8-8),

$$t_c = \frac{3.17 \times 17}{4 \cdot 4 \times 17} = 3.19 \text{ in. (81 mm)}$$

$$A_o = (17 - 3.19)^2 = 191 \text{ in}^2 (123 \times 10^3 \text{ mm}^2)$$

$$p_o = 4(17 - 3.19) = 55.2 \text{ in. (1403 mm)}$$

From Eq. (8-7),

$$GK = \frac{0.5 \times 57000 \sqrt{3500} \times 4 \times 191^2 \times 3.19}{55.2} \\ \approx 14.2 \times 10^6 \text{ kip-in}^2 (4) \times 10^3 \text{ kNm}^2$$

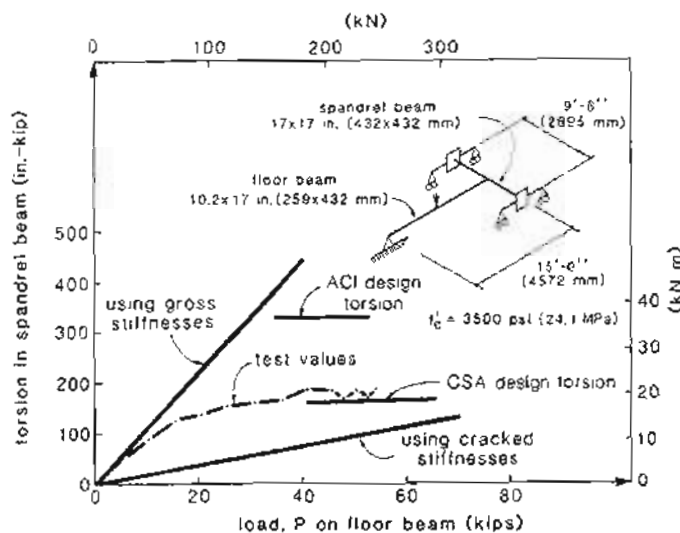


Figure 8-17 Relationship between torsion in spandrel and load on floor beam
Adapted from Ref. 8-16.

The use of this torsional stiffness together with the gross flexural stiffnesses ($EI = E_c b h^3 / 12$) results in the predicted relationship between torsion and load labeled "gross stiffness" in Fig. 8-17.

An estimate of the torsional stiffness after cracking can be obtained from the thin-walled tube expression of Eq. (8-7). After the concrete cracks, it is principally the deformation of the reinforcement which governs the stiffness. An appropriate expression for this stiffness is

$$GK_{cr} = \left(\frac{E_s}{2} \right) \frac{4A_s^2}{p_o} \sqrt{\left(\frac{A_t}{s} \right) \frac{A_t + A_p}{p_o}} \quad (8-33)$$

In using this expression A_o can be approximated as $0.85A_{oh}$ and p_o as $0.9p_h$.

The spandrel beam shown in Fig. 8-17 contained #2 hoops at 6 in. (152 mm) centers, with dimensions of 16 x 16 in. (406 x 406 mm). The longitudinal reinforcement had a total area of 1.20 in² (780 mm²). Hence, from Eq. (8-33) we have

$$\begin{aligned} GK_{cr} &= \frac{29000 \times 4 \times (0.85 \times 16)^2}{2 \times 4 \times 0.9 \times 16} \sqrt{\frac{0.05 \times 1.20}{6 \times 4 \times 0.9 \times 16}} \\ &= 628 \times 10^3 \text{ kip-in}^2 (1.80 \times 10^3 \text{ kNm}^2) \end{aligned}$$

Note that after cracking of the concrete, the torsional stiffness drops to about 4% of the stiffness prior to cracking. The use of this postcracking torsional stiffness together with the

postcracking flexural stiffnesses results in the relationship between torsion and applied load labeled "cracked stiffnesses" in Fig. 8-17. As expected, at low loads the observed torsion in the spandrel is close to the values predicted using gross stiffness values. However, after significant cracking has occurred the torsion is closer to the values predicted using cracked stiffness values. Note that because of the decreasing torsional stiffness, the observed torsion in the spandrel beam remains relatively constant even as the load on the floor beam is increased.

In recognizing the reduction of torsional moment that will occur after cracking for members subjected to compatibility torsion, the CSA Code (Ref. 8-15) permits such members to be designed for a maximum torsion of $0.67T_{cr}$ where T_{cr} is given by Eq. (8-10). Thus

$$T_u = \phi 0.67 \frac{A_c^2}{p_c} 4\sqrt{f'_c} \sqrt{1 + \frac{f_{pc}}{4\sqrt{f'_c}}} \quad \text{psi} \quad (8-34a)$$

or

$$T_u = \phi 0.67 \frac{A_c^2}{p_c} 0.33 \sqrt{f'_c} \sqrt{1 + \frac{f_{pc}}{0.33\sqrt{f'_c}}} \quad \text{MPa} \quad (8-34b)$$

For the spandrel beam shown in Fig. 8-17 this would give

$$\begin{aligned} T_u &\approx 0.85 \times 0.67 \times \frac{17^4}{4 \times 17} \times 4\sqrt{3500} \\ &= 165 \text{ in.-kips (18.7 kNm)} \end{aligned}$$

As can be seen from Fig. 8-17, this is a reasonable estimate of the torsion in the spandrel after cracking for this case of compatibility torsion. Of course, if the torsion is required by equilibrium, this reduction will not occur.

The ACI Code (Ref. 8-2) also permits the torsion in statically indeterminate structures to be reduced. For non-prestressed members it suggests a torsion of

$$T_u = \phi (4\sqrt{f'_c} \sum x^2 y / 3) \quad (8-35)$$

$$= 0.85 \times 4\sqrt{3500} \times 17^3 / 3$$

$$= 329 \text{ in.-kips (37.2 kNm)}$$

It can be seen from Fig. 8-17 that the ACI Code expression overestimates the torsion in the member.

8.12 DESIGN OF GUIDEWAY GIRDER FOR TORSION, SHEAR, AND MOMENT

Analysis of a guideway girder has shown that the critical section shown in Fig. 8-18 is subjected to the following factored loads: $T_u = 185 \text{ ft-kips (251 kNm)}$, $V_u = 150 \text{ kips (667 kN)}$, and a negative moment, $M_u = 3200 \text{ ft-kips (4340 kNm)}$.

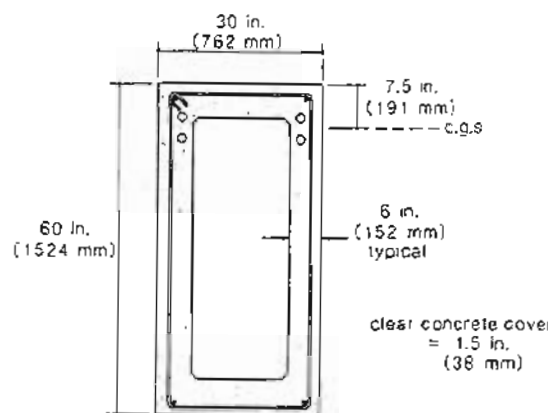


Figure 8-18 Cross section of post-tensioned guideway girder.

At this section, which is near a support, the prestressing tendon profile is essentially horizontal (i.e., $V_p = 0$). The girder has been post-tensioned with a total of thirty-two 1/2 in. (13 mm) diameter, low-relaxation strands located in four 2 in. (50 mm) diameter ducts as shown. The tendons have an ultimate strength of 270 ksi (1860 MPa) and were post-tensioned so that $\Delta\epsilon_p = 5.7 \times 10^{-3}$. The effective stress in the tendons after losses, f_{se} , is 157 ksi (1080 MPa). The 28-day concrete strength is specified as 6000 psi (41.4 MPa). Design the required amounts of transverse and longitudinal reinforcement at this section using 60 ksi (414 MPa) steel.

Step 1: Determine the cross-sectional parameters.

The required cross-sectional parameters for the shear and torsion design are b_w , jd , A_{oh} , and p_h .

The presence of post-tensioning ducts in the web of a beam can result in a reduced effective web width (Ref. 8-17). The CSA Code (Ref. 8-15) requires that in determining the effective web width, the diameter of ungrouted ducts or one-half the diameter of grouted ducts be subtracted from the web width. Thus

$$\begin{aligned} b_w &= 2 \times 6 - 2 \times 0.5 \times 2 \\ &= 10 \text{ in. (254 mm)} \end{aligned}$$

The effective shear depth, jd , can be assumed to be $0.9d$ but need not be taken less than $0.72h$. Hence

$$\begin{aligned} jd &= 0.9 \times (60 - 7.5) \\ &= 47.25 \text{ in. (1200 mm)} \end{aligned}$$

The area enclosed by the hoop centerline, assuming #4 (13 mm diameter) hoops, is

$$\begin{aligned} A_{oh} &= (30 - 2 \times 1.5 - 0.5)(60 - 2 \times 1.5 - 0.5) \\ &= 26.5 \times 56.5 \\ &= 1497 \text{ in}^2 (966 \times 10^3 \text{ mm}^2) \end{aligned}$$

The perimeter of the hoop centerline is

$$\begin{aligned} p_h &= 2 \times (26.5 + 56.5) \\ &= 166 \text{ in. (4216 mm)} \end{aligned}$$

Step 2: Choose the value of θ .

The angle θ will be chosen from Table 7-3 using the values of v/f'_c and ϵ_x . From Eq. (8-26)

$$\begin{aligned} v &= \frac{(150/0.85) - 0}{10 \times 47.25} + \frac{(185/0.85) \times 12 \times 166}{1497^2} \\ &\approx 0.373 + 0.193 = 0.566 \text{ ksi (3.91 MPa)} \end{aligned}$$

Hence

$$\frac{v}{f'_c} = \frac{0.566}{6} = 0.094$$

The longitudinal strain, ϵ_x , is found from Eq. (8-28) and (8-29). In using Eq. (8-29) it is appropriate to approximate A_s as $0.85A_{oh}$ and p_o as $0.9p_h$. Hence

$$\begin{aligned} N_v &= \cot \theta \sqrt{150^2 + \left(\frac{185 \times 12 \times 0.9 \times 166}{2 \times 0.85 \times 1497} \right)^2} \\ &= 198.7 \cot \theta \end{aligned}$$

Assuming that a #8 bar (25 mm diameter) is placed in each corner of the hoops

$$\begin{aligned} \epsilon_x &= \frac{\frac{3200 \times 12}{47.25} + 0.5 \times 198.7 \cot \theta - 32 \times 0.153 \times 157}{29000 \times 2 \times 0.79 + 29000 \times 32 \times 0.153} \\ &= 0.234 \times 10^{-3} + 0.529 \times 10^{-3} \cot \theta \end{aligned}$$

From Table 7-3, for a value of v/f'_c of 0.100 and ϵ_x equal to 1×10^{-3} , θ is given as 36° , with a corresponding β value of 2.08. For θ equal to 36°

$$\begin{aligned} \epsilon_x &= 0.234 \times 10^{-3} + 0.529 \times 10^{-3} \cot 36^\circ \\ &= 0.962 \times 10^{-3} \end{aligned}$$

Hence use $\theta = 36^\circ$.

Step 3: Determine spacing of hoops.

From Eq. (8-31)

$$\frac{150,000}{0.85} = 2.08\sqrt{6000} \times 10 \times 47.25 + \frac{A_v}{s} \times 60,000 \times 47.25 \times \cot 36^\circ$$

$$176,470 = 76,127 + 3,902,000 \times \frac{A_v}{s}$$

Hence the amount of transverse reinforcement required for shear is

$$\frac{A_v}{s} = 0.0257 \text{ in}^2/\text{in.} (0.65 \text{ mm}^2/\text{mm})$$

Before calculating the amount of transverse reinforcement required for torsion we will make a more precise determination of the area enclosed by the shear flow, A_o . From Eq. (8-19)

$$a_o = \frac{1497}{166} \left[1 - \sqrt{1 - \frac{185 \times 12 \times 166(\tan 36^\circ + \cot 36^\circ)}{0.85 \times 0.7 \times 6 \times 1497^2}} \right]$$

$$= 0.45 \text{ in. (11 mm)}$$

From Eq. (8-14)

$$A_o = 1497 - 0.5 \times 0.45 \times 166 = 1460 \text{ in}^2 (942,000 \text{ mm}^2)$$

From Eq. (8-15)

$$p_o = 166 - 4 \times 0.45 = 164.2 \text{ in. (4170 mm)}$$

From Eq. (8-30)

$$\frac{185,000 \times 12}{0.85} = \frac{A_t}{s} \times 60,000 \times 2 \times 1460 \times \cot 36^\circ$$

$$\frac{A_t}{s} = 0.0108 \text{ in}^2/\text{in.} (0.28 \text{ mm}^2/\text{mm})$$

In adding together the required amounts of transverse reinforcement for shear and torsion, recall that A_v is the area of two legs, while A_t is the area of one leg. Hence the required amount of reinforcement on one side of the girder is

$$0.5 \frac{A_v}{s} + \frac{A_t}{s} = 0.5 \times 0.0257 + 0.0108 = 0.0237 \text{ in}^2/\text{in.} (0.60 \text{ mm}^2/\text{mm})$$

Hence, for #4 (13 mm diameter) hoops the maximum spacing, s , which can be used is

$$s = \frac{0.20}{0.0237} \approx 8.44 \text{ in. (214 mm)}$$

Therefore, choose $s = 8$ in. (203 mm).

Step 4: Check the longitudinal reinforcement.

From Eq. (8-32) the required tensile capacity of the longitudinal reinforcement is

$$A_s f_y + A_{ps} f_{ps}$$

$$\geq \frac{3200 \times 12}{0.9 \times 47.25} + \cot 36^\circ \sqrt{\left[\frac{150}{0.85} - 0.5(176.5 - 76.1) \right]^2 + \left(\frac{0.5 \times 185 \times 12 \times 164.2}{0.85 \times 2 \times 1460} \right)^2}$$

$$\geq 903 + 201 = 1104 \text{ kips (4910 kN)}$$

Thus, for the longitudinal reinforcement on the tension face

$$2 \times 0.79 \times 60 + 32 \times 0.153 \times f_{ps} \geq 1104$$

Therefore

$$f_{ps} \geq 206 \text{ ksi (1420 MPa)}$$

As the low-relaxation strands can develop a stress at ultimate considerably higher than 206 ksi (1420 MPa) [see Eq. (6-7)], the tensile capacity of the longitudinal reinforcement is adequate.

While no additional longitudinal reinforcement is required for strength, we will provide #4 (13 mm diameter) bars at 12 in. (305 mm) spacing around the perimeter of the hoops. This additional reinforcement will assist in controlling diagonal cracks.

References

- 8-1 Collins, M.P., and Mitchell, D., "Shear and Torsion Design of Prestressed and Non-Prestressed Concrete Beams," *PCI Journal*, Vol. 25, No. 5, Sept.-Oct. 1980, pp. 32-100; Discussion and Closure, *PCI Journal*, Vol. 26, No. 6, Nov.-Dec. 1981, pp. 96-118.
- 8-2 ACI Committee 318, "Building Code Requirements for Reinforced Concrete (ACI 318-89) and Commentary - ACI 318 R-89," American Concrete Institute, Detroit, 1989, 353 pp.
- 8-3 Hsu, T.T.C., *Torsion of Reinforced Concrete*, Van Nostrand Reinhold, New York, 1984, 516 pp.
- 8-4 de Saint-Venant "Mémoires présentés par divers savants à l'Académie des Sciences de l'Institut Impérial de France," Vol. 14 (Second Series), 1856.
- 8-5 Nadai, A., *Theory of Flow and Fracture of Solids*, McGraw-Hill Book Company, New York, 1950.
- 8-6 Zia, P., and McGee, W.D., "Torsion Design of Prestressed Concrete," *PCI Journal*, Vol. 19, No. 2, Mar.-Apr. 1974, pp. 46-65.
- 8-7 Mitchell, D., and Collins, M.P., "Influence of Prestressing on Torsional Response of Concrete Beams," *PCI Journal*, Vol. 23, No. 3, May-June 1978, pp. 54-73.
- 8-8 Mitchell, D., and Collins, M.P., "Diagonal Compression Field Theory - A Rational Model for Structural Concrete in Pure Torsion," *ACI Journal*, Vol. 71, Aug. 1974, pp. 396-408.
- 8-9 Onsongo, W.M., "The Diagonal Compression Field Theory for Reinforced Concrete Beams Subjected to Combined Torsion, Flexure and Axial Load," Ph.D. thesis, Department of Civil Engineering, University of Toronto, 1978, 246 pp.
- 8-10 Mardukhi, J., "The Behaviour of Uniformly Prestressed Concrete Box Beams in Combined Torsion and Bending," M.A.Sc. thesis, Department of Civil Engineering, University of Toronto, Toronto, 1973, 73 pp.
- 8-11 Rabbat, B., and Collins, M.P., "A Variable Angle Space Truss Model for Structural Concrete Members Subjected to Complex Loading," *Douglas McHenry International Symposium on Concrete and Concrete Structures*, SP-55, American Concrete Institute, Detroit, 1978, pp. 547-587.
- 8-12 Rabbat, B., and Collins, M.P., "The Computer Aided Design of Structural Concrete Sections Subjected to Combined Loading," *Computers and Structures*, Vol. 7, No. 2, Apr. 1977, pp. 229-236.
- 8-13 Mitchell, D., and Collins, M.P., "Detailing for Torsion," *ACI Journal*, Vol. 73, No. 9, Sept. 1976, pp. 506-511.
- 8-14 Jirsa, J.O., "Torsion in Floor Slab Structures," *Analysis of Structural Systems for Torsion*, SP-35, American Concrete Institute, Detroit, 1973, pp. 265-292.
- 8-15 CSA Committee A23.3, *Design of Concrete Structures for Buildings*, CAN3-A23.3-M84, Canadian Standards Association, Rexdale, Canada, 1984, 281 pp.
- 8-16 Collins, M.P., and Lampert, P., "Redistribution of Moments at Cracking — The Key to Simpler Torsion Design?" *Analysis of Structural Systems for Torsion*, SP-35, American Concrete Institute, Detroit, 1973, pp. 343-383.
- 8-17 Campbell, T.J., Bachelor, B. de V., and Chithruymondh, L., "Web Crushing in Concrete Girders with Prestressing Ducts in the Web," *PCI Journal*, Vol. 24, No. 5, Sept.-Oct. 1979, pp. 70-88.

Demonstration Problems

- 8-1 Estimate the cracking torque and the corresponding twist for the members having the cross sections shown in Fig. 8-19. The compressive strength of the concrete is 5000 psi (34.5 MPa) and the sections are uniformly prestressed with f_{py} equal to 500 psi (3.45 MPa).

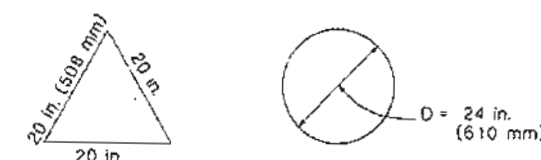


Figure 8-19 Cross sections of members subjected to torsion.

- 8-2 Determine the pure torsional capacity of specimen P3 described in Fig. 8-4. The beam contained three 0.276 in. (7 mm) diameter wires ($f_{py} = 214$ ksi or 1476 MPa) post-tensioned to 166 ksi (1145 MPa) (i.e., $\Delta\epsilon_p = 5.9 \times 10^{-3}$) as well as six #3 (9.5 mm diameter) reinforcing bars with f_y of 47.5 ksi (328 MPa). The #3 hoops were spaced at 3.8 in. (96 mm). The concrete strength was 4930 psi (34.0 MPa) and the clear concrete cover was 1/2 in. (13 mm).
- 8-3 Redesign the guideway girder described in Section 8.12 assuming that the cross section is solid rather than hollow. Comment on the influence of the added concrete.
- 8-4 The hollow guideway girder described in Section 8.12 is subjected to a factored axial tension of 700 kN in addition to the specified values of torsion, shear, and moment. How will this axial tension affect the design of the section?
- 8-5 Comment on how prestressing influences the magnitude of torsion in cast-in-place spandrel beams.
- 8-6 In Section 8.7 a procedure was explained for calculating the torsion-flexure interaction curve for prestressed concrete beams. The resulting interaction curve for a symmetrically prestressed box girder is shown in Fig. 8-10. Calculate the torsion-positive-flexure interaction curve for this box girder if the top two tendons, each containing four 0.276 in. (4.7 mm) diameter wires were removed. Note that ϵ_x must be calculated at the level of the top and the bottom reinforcement since the larger of the two values will govern the behavior. Further, yielding of the longitudinal reinforcement may occur on either the top or the bottom face. Comment on the influence of the unsymmetrical reinforcement on the shape of the interaction diagram.

Design of Disturbed Regions

The inadequate and inconsistent treatment of disturbed regions using so-called "detailing," "past experience," or "good practice" has been one of the main reasons for the poor performance and even failure of structures.

Schlach, Schäfer, and Jennewein, 1987

9.1 INTRODUCTION

In the previous chapters we have discussed the response of prestressed concrete members to sectional forces such as axial load, moment, shear, and torsion. The methods described in these chapters were based on traditional engineering beam theory, which assumes that plane sections remain plane and does not address the problem of how the forces were introduced into the member. However, in regions near discontinuities, such as those shown in Fig. 9-1, these assumptions do not apply and hence it is necessary to use design procedures that more closely approximate the actual flow of the forces. Such zones adjacent to abrupt changes in cross-sectional dimensions or cross-sectional forces will be referred to as disturbed regions.

An example of a disturbed region is given in Fig. 9-2, which shows a concrete member subjected to an axial compressive force, P , where the force, P has been applied over a small bearing area. Some distance away from the point of load application the stresses will be uniform and uniaxial [i.e., $f_x = P/(bh)$ and $f_y = 0$] and in these regions the assumption that plane sections remain plane will be appropriate. Closer to the applied load the distribution of stresses in the member is more complex. The dispersion of the high local stresses under the bearing plate causes transverse tensile stresses, f_y , which may crack the concrete. Longitudinal cracks may form in a zone behind the bearing plate.

called the bursting zone, or on the end face of the member in an area called the spalling zone (see Fig. 9-2b).

The region in which the stress field is disturbed by the high local end stresses will, according to Saint-Venant's principle, extend over a length of the beam about equal, in this case, to the depth of the beam. The design of this disturbed region requires procedures which more accurately model the flow of the stresses. The techniques used in designing such regions are discussed in this chapter.

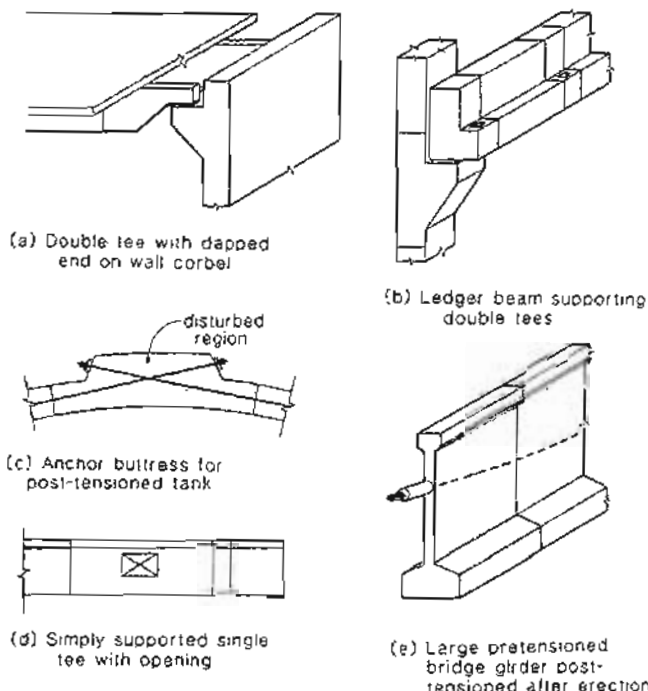


Figure 9-1 Examples of disturbed regions in prestressed concrete construction.

9.2 BEHAVIOR PRIOR TO CRACKING — ELASTIC ANALYSIS

Prior to cracking, the flow of stresses in disturbed regions can be understood with the aid of elastic analysis. Elastic analysis is an excellent tool for predicting where and when the first significant cracking of the concrete will occur. After cracking, there will be a

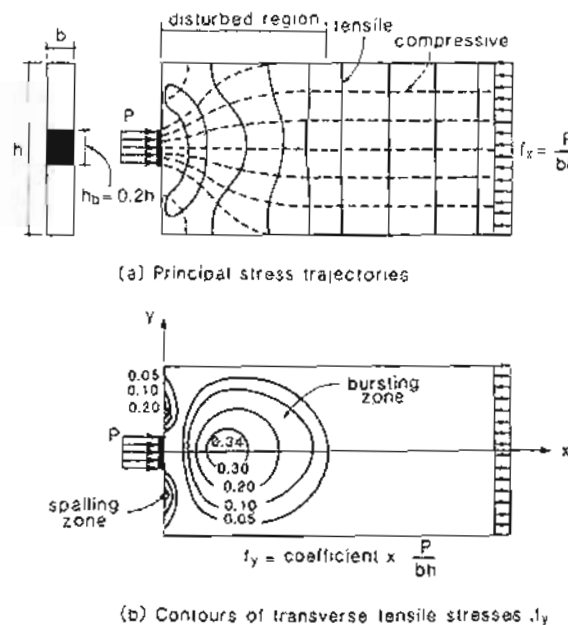


Figure 9-2 Example of disturbed region.

significant redistribution of the internal stresses and this redistribution cannot be predicted by traditional elastic analysis. Nevertheless, the results of an elastic analysis can be used to guide the engineer as to where reinforcement is required and what amount will be needed.

An example of the use of elastic analysis in the design of disturbed regions is illustrated in Fig. 9-3, which shows a wall containing a doorway and supporting a large vertical load (Ref. 9-1). In this design, the engineers have placed the main tensile reinforcement in a pattern that resembles that formed by the calculated principal tensile stress trajectories. The area of tensile reinforcement has been chosen so that it can carry the tensile force calculated by integrating the tensile stresses in the surrounding concrete. In addition to the tensile reinforcement, compression reinforcement has been provided in those areas where the calculations show very high compressive stresses in the concrete. This compression reinforcement has been enclosed in column ties to restrain it against buckling. As well as the main tension and compression reinforcement, the engineers have provided a well-distributed array of vertical and horizontal bars that will help to control the cracking of the concrete and will improve the ductility of the wall.

Traditionally, the end anchorage zones of post-tensioned members have been designed using the results of elastic analyses (Ref. 9-2). Thus the amount of reinforcement required to control bursting stresses has been determined from elastic stress distributions such as those

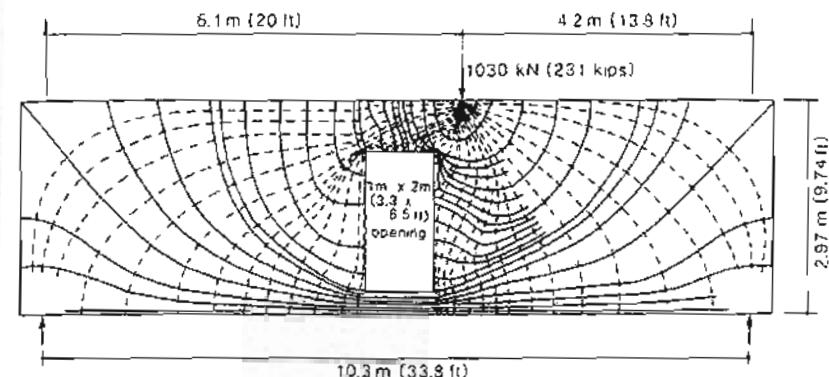


Figure 9-3 Design of a deep beam containing an opening. Adapted from Zelkler and Thiel (Ref. 9-1).

shown in Fig. 9-4. The amount of transverse reinforcement is chosen so that it is capable of carrying the tensile force obtained by integrating the tensile stress distribution. Usually, the stress in the reinforcement is limited to one-half the yield stress and the reinforcement is uniformly distributed over the zone of significant tensile stresses. A simple expression recommended by Leonhardt (Ref. 9-4) to conservatively estimate the total transverse tensile

force, T , obtained by integrating the bursting stresses, is

$$T = 0.3P \left(1 - \frac{h_b}{h} \right) \quad (9-1)$$

where P = maximum prestressing force due to post-tensioning operation

h_b = depth of bearing plate

h = depth of member.

Equation (9-1) is appropriate for relatively small bearing areas, with h_b/h less than 0.2. For larger bearing areas a more accurate estimate of the total transverse tensile force is obtained by replacing the coefficient 0.3 in Eq. (9-1) with 0.25. Thus for h_b/h greater than 0.2, use

$$T = 0.25P \left(1 - \frac{h_b}{h} \right) \quad (9-2)$$

Equation (9-2) was proposed by Morsch in 1924 (Ref. 9-5).

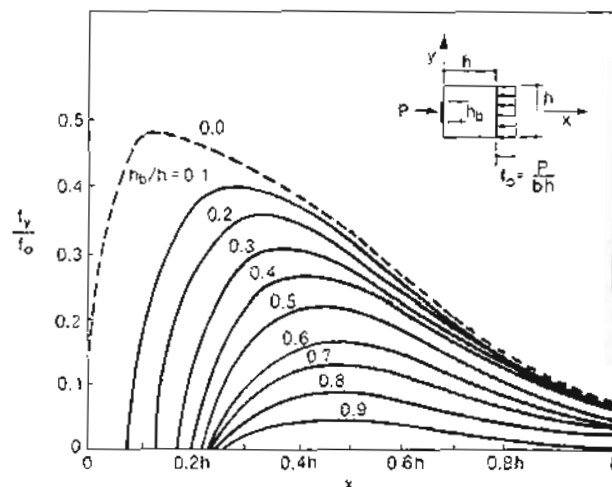


Figure 9-4 Transverse tensile stress distributions in bursting zones. Adapted from Iyengar (Ref. 9-3)

In the spalling zone the calculated tensile stresses are very high but they act over only a very small area (see Fig. 9-2b) and hence the resulting tensile force is very small.

The contours of transverse tensile stresses for different anchorage configurations are given in Fig. 9-5. Note that if the force is transmitted by bond (e.g., pretensioned strand) rather than by a bearing plate at the end of the member, there are no significant spalling

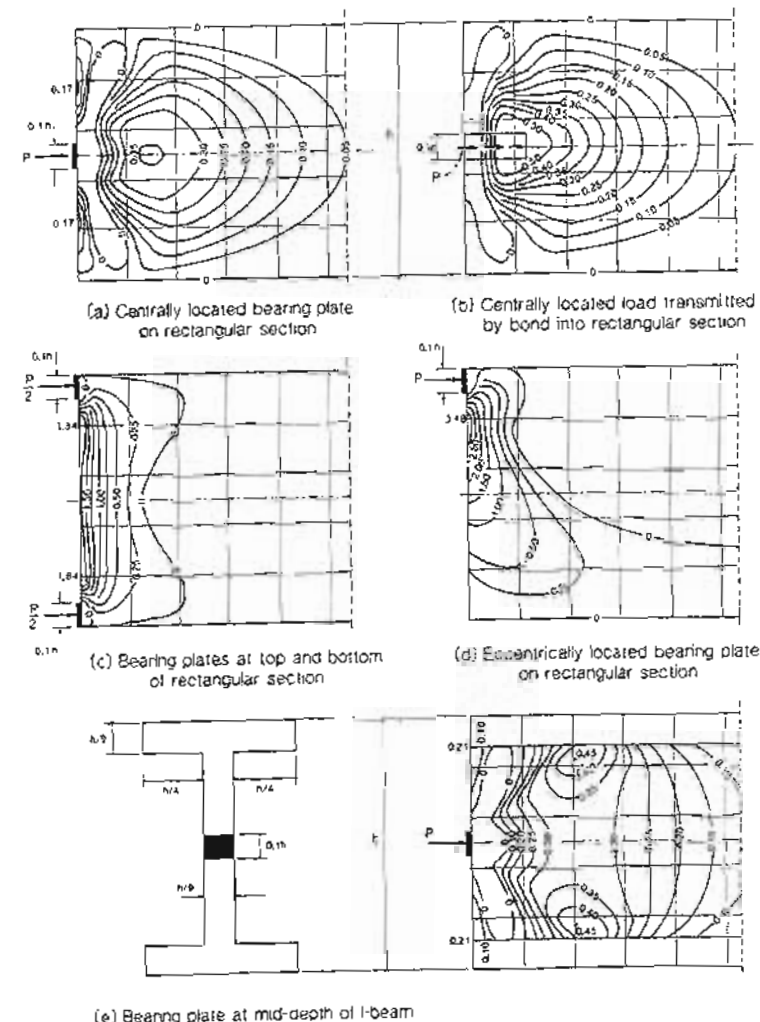


Figure 9-5 Contours of significant tensile stresses in y -direction for different anchorage configurations. Adapted from Kammenhuber and Schneider (Ref. 9-6).

stresses. For bearing plates located near the top and bottom of the member, significant tensions occur between the bearing plates over a relatively short length of the member. For the I-beam shown in Fig. 9-5c, a greater degree of dispersion is required because a large percentage of the compressive force must find its way into the top and bottom flanges. Because of this, large transverse tensile stresses occur across the entire web.

The influence of the support reaction on the tensile stress distributions and the resulting tensile forces, T , is illustrated in Fig. 9-6. As can be seen from Fig. 9-6b, with a relatively small support reaction the resultant tensile force in the spalling zone above the tendon is about $0.022P$. An increase in the support reaction (Fig. 9-6c) reduces this tensile force resultant. Positioning the anchor at mid-depth of the section results in smaller tensile forces in the spalling regions but larger tensile forces in the bursting regions.

Figure 9-7 illustrates how elastic analysis can be used to gain insight into the behavior of deep beams. For span-to-depth ratios of about 4 and greater, the plane-sections theory for flexure applies. Hence for a plain concrete slender beam the neutral axis is at mid-depth of the section, the flexural lever arm is two-thirds of h , and the section modulus is $bh^2/8$. As the maximum moment at midspan is $w\ell^2/8$, the maximum tensile stress, f_t , at midspan for the case of $h = \ell/4$ is

$$\begin{aligned} f_t &= \frac{w\ell^2/8}{b(\ell/4)^2/6} \\ &= 12w/b \end{aligned}$$

and the tensile stress resultant, T , is

$$\begin{aligned} T &= \frac{w\ell^2/8}{\frac{2}{3}(\ell/4)} \\ &= 0.75w\ell \end{aligned}$$

As the beam becomes deeper the stress distribution becomes nonlinear with the tensile stresses concentrating toward the bottom of the beam. As the span-to-depth ratio decreases, the stresses at midspan deviate more and more from those predicted by plane sections theory. Once again the amount of reinforcement required to carry the tensile force obtained by integrating the tensile stresses can be determined. It is important to recognize that the stress distribution for the very deep beam shown in Fig. 9-7 corresponds to that shown for the end anchorage zone region in Fig. 9-5c.

9.3 EXAMPLE DESIGN OF ANCHORAGE ZONE REINFORCEMENT USING ELASTIC ANALYSIS

The end anchor region of a post-tensioned beam is shown in Fig. 9-8. Each tendon consists of fourteen 1/2 in. (13 mm) diameter low-relaxation strands with an ultimate stress of 270 ksi (1860 MPa). During jacking the maximum stress reached in the strands is $0.75f_{pu}$. The concrete strength at the time of jacking is 5000 psi (34.5 MPa). Design the required end anchorage reinforcement using reinforcing bars with a yield stress of 60 ksi (414 MPa).

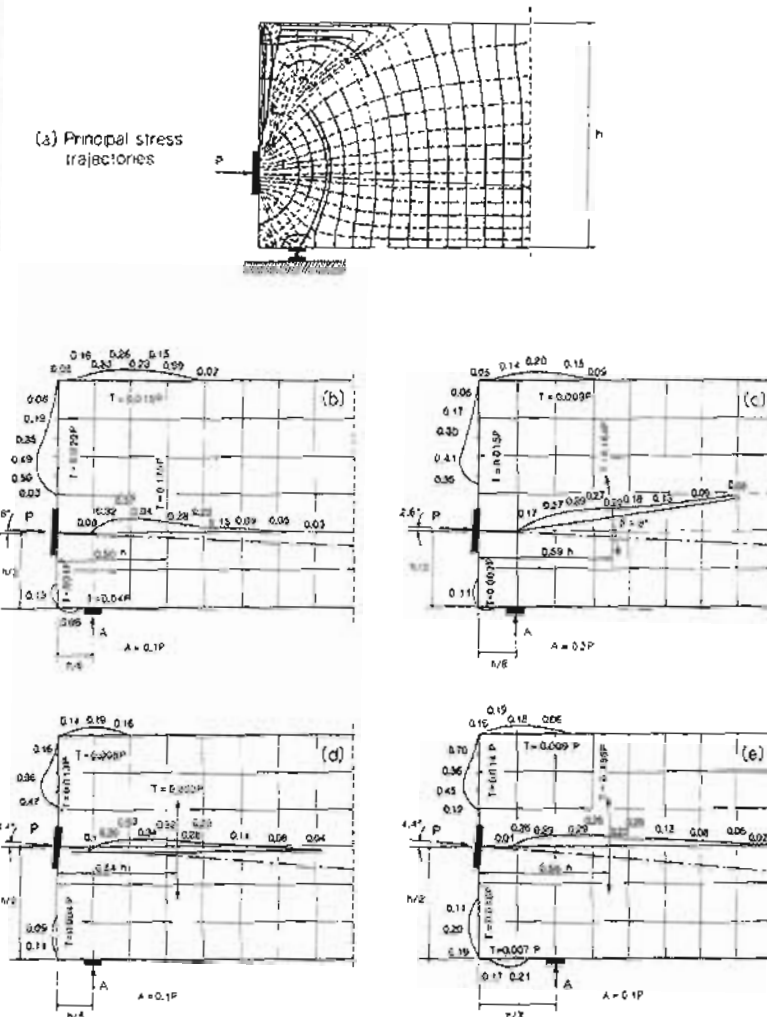


Figure 9-6 Influence of magnitude and position of support reaction and location and inclination of post-tensioning anchors on tensile stresses and tensile stress resultants. Adapted from Sarginus (Ref. 9-7), and Mehlhorn (Ref. 9-8).

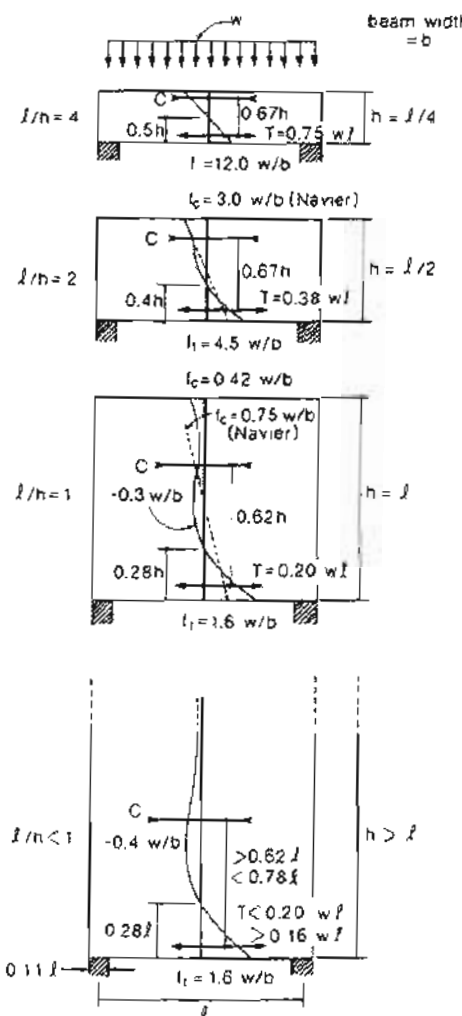


Figure 9-7 Longitudinal stresses at midspan in uniformly loaded, simply supported beams with different depths. Adapted from Leonhardt and Walther (Ref. 9-9).

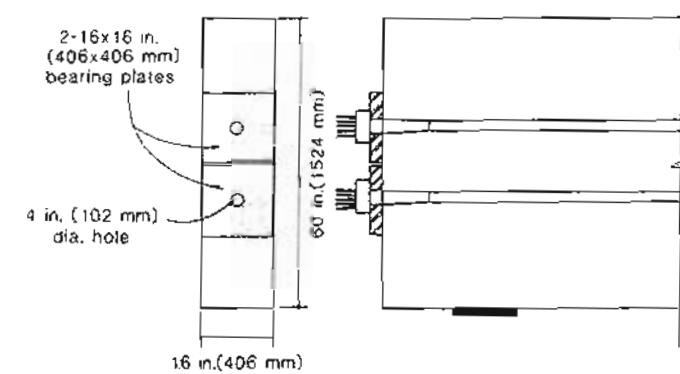


Figure 9-8 Details of anchor region.

Step 1: Check the bearing stress under the anchor plates. Force applied to each anchor plate during jacking

$$P = 14 \times 0.153 \times 0.75 \times 270 = 434 \text{ kips (1929 kN)}$$

Net bearing area of each plate

$$A = 16 \times 16 - \frac{\pi \times 4^2}{4} = 243 \text{ in}^2 (157 \times 10^3 \text{ mm}^2)$$

$$\frac{P}{A} = \frac{434}{243} = 1.79 \text{ ksi (12.3 MPa)}$$

As this temporary service load stress is only $0.36 f'_c$, it will be acceptable.

Step 2: Determine the transverse tensile force.

Due to the positioning of the two bearing plates, we will treat this case as a single force P of $2 \times 434 = 868$ kips (3860 kN) acting over a bearing area 16 in. (406 mm) wide and 32 in. (812 mm) deep. Hence, from Eq. (9-2),

$$T = 0.25 \times 868 \left(1 - \frac{32}{60}\right)$$

$$= 101 \text{ kips (450 kN)}$$

It can be seen from Fig. 9-4 that for the case of $h_b/h = 0.53$, the transverse tensile bursting stresses will start at a distance of about $0.22 \times 60 = 13$ in. (335 mm) from the end face and will die out at about 60 in. (1524 mm) from the end face.

Step 3: Choose the transverse reinforcement.

In order to keep the stress in the reinforcement below $0.5f_y = 0.5 \times 60 = 30$ ksi (207 MPa), the minimum area required is

$$A_s = \frac{101}{30} = 3.37 \text{ in}^2 (2170 \text{ mm}^2)$$

Hence the number of #3 (9.5 mm diameter) closed stirrups required is $3.37/(2 \times 0.11) = 15.3$ stirrups. We will use 16 stirrups with the first stirrup at 12 in. (305 mm) from the end face and the remaining stirrups spaced at 3.5 in. (89 mm).

In order to control spalling we will provide reinforcement to resist a tensile force of $0.02P = 0.02 \times 868 = 17.36$ kips (77.2 kN). Hence the minimum number of #4 (13 mm diameter) bars working at 30 ksi is $17.36/(0.20 \times 30) = 2.89$. Hence use four #4 bars. Additionally, we will provide eight #3 U-bars to control potential vertical splitting cracks on the end face. The reinforcing details are summarized in Fig. 9-9.

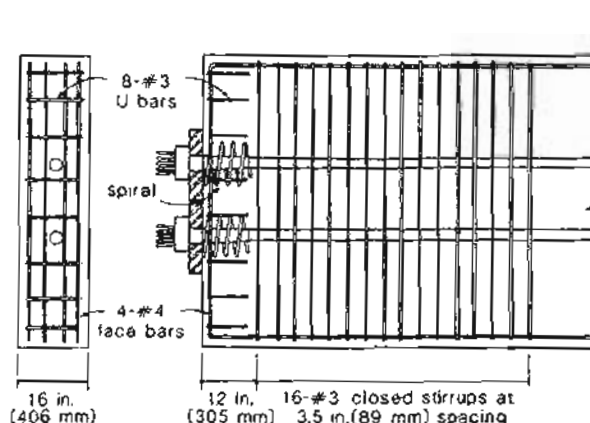


Figure 9-9 Reinforcement details of anchorage zone.

9.4 DEEP BEAM ANALOGY FOR DESIGN OF END ZONES

Estimating the transverse tensile forces using elastic analysis is a time-consuming process if a standard solution is not available. A simpler approach for estimating the tensile forces is to consider the end zones as deep beams subjected to the bearing stresses on the free end and subjected to the statically equivalent, linearly distributed stresses on the other end. The "depth" of the equivalent deep beam is taken as the length of the disturbed zone. This approach to the design of end zones was proposed by Magnel (Ref. 9-10) and was further developed by Gergely and Sozen (Ref. 9-11). The steps used in this approach are illustrated in Fig. 9-10 and are as follows:

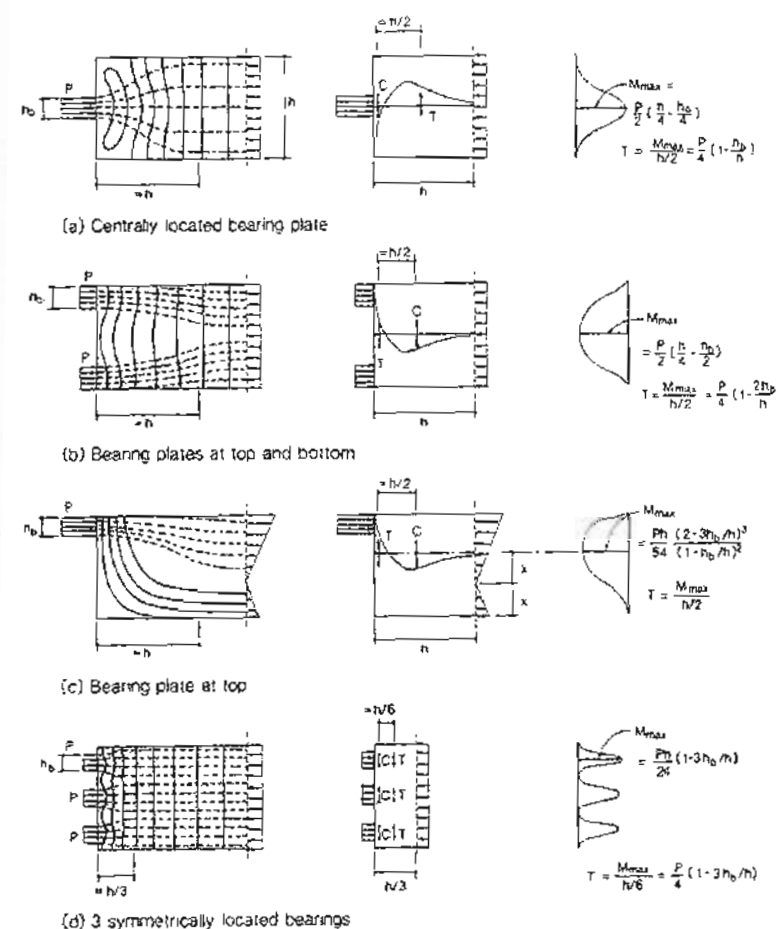


Figure 9-10 Application of deep beam analogy to anchorage zones of rectangular beams

1. Calculate the linearly distributed stresses on a face removed from the disturbed region.
2. Estimate the length of the disturbed zone. In this regard Saint-Venant's principle is useful. This states that the stresses caused by a self-equilibrating stress system die out over a distance about equal to the extent of the self-equilibrating system (see Fig. 9-11).

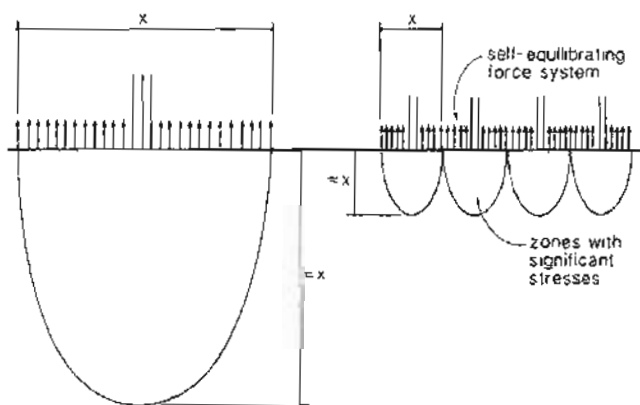


Figure 9-11 Saint-Venant's principle.

3. Treating the disturbed region as a deep beam with its depth equal to the length of the disturbed zone, compute the moments that this deep beam must resist.
4. Determine the flexural tensions caused by the moments using an estimated internal lever arm, typically taken as one-half of the length of the disturbed region (see Fig. 9-10).
5. Calculate the amount of reinforcement required to provide this flexural tension and place the reinforcement in the zones where this flexural tension will occur.

For the particular case of the rectangular beam loaded by a centrally located bearing plate shown in Fig. 9-10a, the tensile force calculated by the deep beam analogy is the same as that given by Eq. (9-2).

9.5 BEHAVIOR AFTER CRACKING

In the design of disturbed regions we must choose appropriate reinforcement to control cracking and provide the required load paths. While elastic analysis is capable of predicting where concrete cracking may occur, it can only give an approximate estimate of the flow of stresses after cracking because of the significant change in stiffnesses that will occur with the spread of cracking.

Nonlinear finite element analysis is a powerful tool capable of investigating the response of disturbed regions after cracking. The use of finite element techniques to predict the postcracking response of reinforced concrete was pioneered by Ngo and Scordelis (Ref. 9-12) in 1967. Since that time, considerable advances have been made, some of which are summarized in the ASCE state-of-the-art report (Ref. 9-13). A critical feature of these techniques is the relationship between stresses and strains in the cracked concrete

The stress-strain characteristics for cracked concrete used in the modified compression field theory (see Section 7.10) have been used as the basis for a number of nonlinear finite element computer programs (e.g., Refs. 9-14, 9-15, and 9-16).

Figure 9-12 summarizes the results of nonlinear finite element analyses of end anchorage regions having different arrangements of transverse reinforcement. Each of the specimens contained 10 double-legged stirrups with a total yield force of 10.7 kips (47.5 kN). It can be seen from Fig. 9-12 that from elastic analysis the total transverse tensile force to be resisted is 0.24 times the prestressing force. In order to keep the force in the stirrups below one-half of the yield force, the applied prestressing force, P , should satisfy

$$P < \frac{0.5 \times 10.7}{0.24} = 22.3 \text{ kips (99 kN)}$$

Thus the area of transverse reinforcement provided would be appropriate for a prestressing force of about 22.3 kips (99 kN).

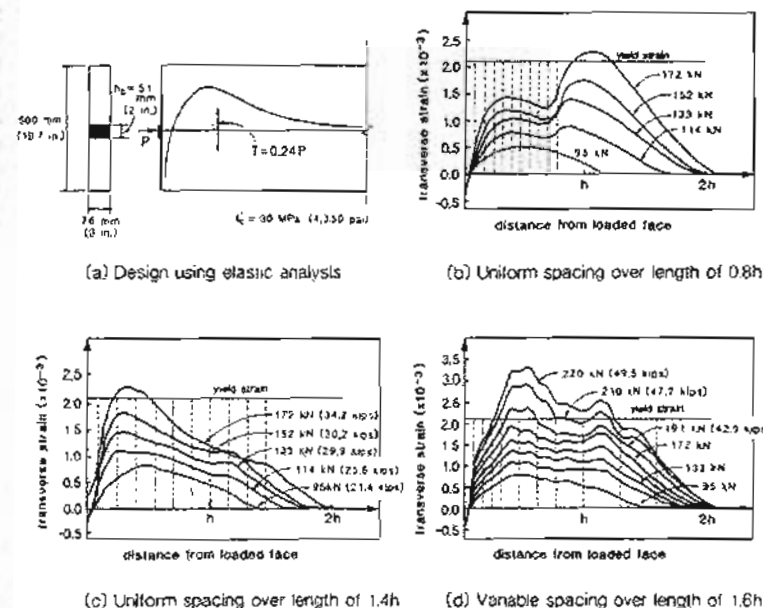


Figure 9-12 Predicted transverse tensile strains in end regions for different stirrup arrangements. All specimens contain the same number of stirrups. Adapted from Adegbie and Collins (Ref. 9-14).

The arrangement of stirrups shown in Fig. 9-12b corresponds to the traditional design approach of uniformly spacing the stirrups in the region where the elastic analysis predicts

- high tensile stresses. In the finite element analysis the cracking stress of the concrete was assumed to be 130 psi (0.9 MPa) and this resulted in a predicted cracking load, P_c , of 21.4 kips (95 kN). Just after cracking, the predicted transverse tensile strain distribution matches the shape of the elastic stress distribution reasonably well. However, as the load is increased, considerable tensile straining occurs in the region beyond the reinforced zone. Failure was predicted to take place in this region at a load of about 38.7 kips (172 kN). In this analysis it was assumed that the concrete immediately under the bearing plate was well confined and hence an enhanced concrete strength was used for the element behind the bearing plate.

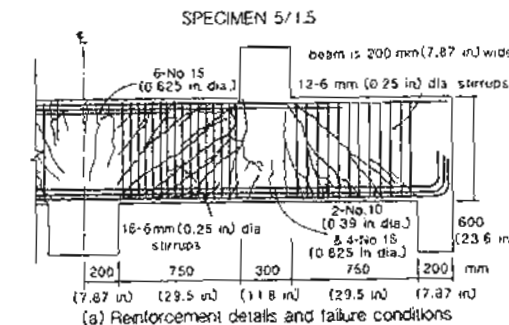
It is evident from Fig. 9-12b that after cracking, the concrete compressive stresses disperse at a shallower angle, resulting in a need for transverse reinforcement farther down the beam. Figure 9-12c and d shows the influence of distributing the 10 stirrups over a longer length. As can be seen, the pattern of Fig. 9-12d results in the largest predicted failure load and more efficiently utilizes the reinforcement since most of the bars yield at ultimate.

Figure 9-13 summarizes the results of a nonlinear finite element analysis of a two-span deep beam. The disturbed regions of this statically indeterminate structure, which was tested by Rogowsky, MacGregor, and Ong (Ref. 9-17), underwent considerable redistribution of stresses after cracking. It can be seen that high compressive stresses flow directly between the loading columns and the central supporting column and that the severe diagonal cracking in this region causes very high principal tensile strains. Failure was predicted to occur due to crushing of the concrete after yielding of the stirrups at a load of 200 kips (890 kN). The experimentally determined failure load was 193 kips (858 kN). Because of the very high principal tensile strains (max. $\epsilon_1 \approx 0.0063$) the concrete was predicted to crush at a stress of only $0.53 f'_c$ [see Eq. (7-26)].

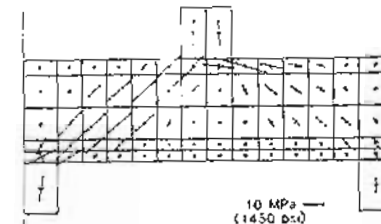
9.6 STRUT AND TIE MODELS

By definition, disturbed regions are characterized by a complex flow of internal stresses. While elastic analysis can accurately model the flow of stresses prior to cracking, it cannot predict the redistribution of stresses that will occur after cracking of the concrete. Inelastic finite element models are capable of predicting the stress flows in disturbed regions for all levels of loading up to failure. While these models are suitable for special investigative studies and for calibrating simpler design approaches, they are too time-consuming for use in everyday design.

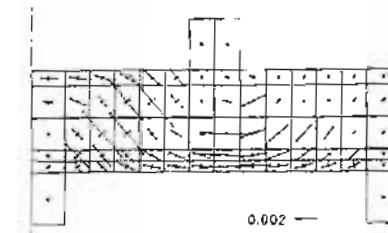
Considerable insight into the flow of forces in disturbed regions can be gained by the use of simple strut and tie models. Cracked reinforced concrete carries load principally by compressive stresses in the concrete and tensile stresses in the reinforcement. After significant cracking has occurred, the principal compressive stress trajectories in the concrete tend towards straight lines and hence can be approximated by straight compressive struts. The internal flow of forces in disturbed regions such as those shown in Fig. 9-14 can be modeled using concrete compressive struts to represent the concrete in uniaxial compression, tension ties to model the principal reinforcement and nodal zones which represent



(a) Reinforcement details and failure conditions



(b) Predicted principal stresses



(c) Predicted principal strains

Figure 9-13 Nonlinear finite element analysis of continuous deep beam.
Adapted from Cook and Mitchell (Ref. 9-15).

the regions of concrete subjected to multidirectional stresses where the struts and the ties meet.

The concept of using uniaxially stressed truss members to model the complex stress flow in cracked reinforced concrete was used by the pioneers of reinforced concrete design

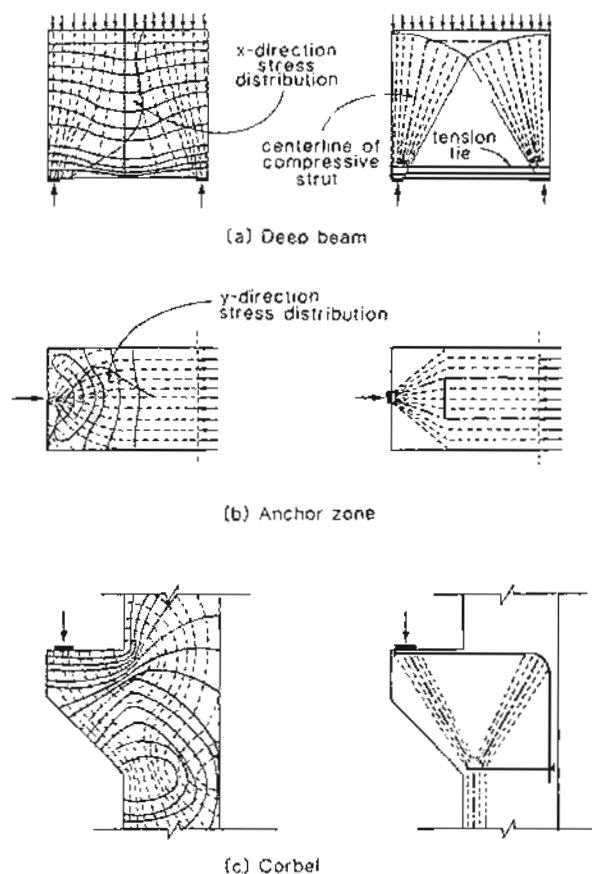


Figure 9-14 Elastic stress trajectories and strut and tie modeling of stress flows in disturbed regions.

(e.g., Ref. 9-18). More recently, significant advances have been made in this approach. A comprehensive study of elastic stress fields in disturbed regions and the way in which these elastic stress flows can be represented by detailed strut and tie models, is given by Schlaich, Schäfer and Jennewein (Ref. 9-19). Marti (Ref. 9-20) has pointed out the importance of considering the actual dimensions of the compressive struts and tension ties in formulating the strut and tie models. The finite member dimensions mean that the "truss joint" becomes a "nodal zone" with finite dimensions. A simple design approach

for disturbed regions based upon a strut and tie model was developed for the Canadian Concrete Code (Refs. 9-21 and 9-22). This model, which gives some consideration to compatibility conditions in addition to the usual equilibrium conditions, will be described below in the context of ACI load factors and ϕ factors (Ref. 9-23).

In designing a disturbed region such as the deep beam shown in Fig. 9-15, the first step is to sketch the flow of forces in the region and locate the nodal zones. The nodal zones must be made large enough to ensure that the nodal zone stresses remain below permissible limits. Concrete compressive stresses in the nodal zones should not exceed $0.85\phi f'_c$ in nodal zones bounded by compressive struts and bearing areas, $0.75\phi f'_c$ in nodal zones anchoring one tension tie, and $0.60\phi f'_c$ in nodal zones anchoring tension ties in more than one direction. In these nodal zone stress limits, the strength reduction factor, ϕ , is taken as that for bearing on concrete, that is, $\phi = 0.70$.

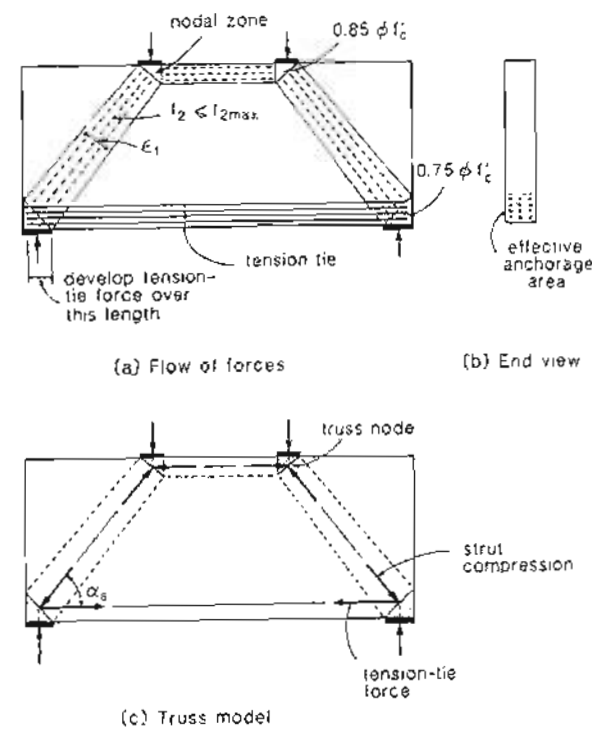


Figure 9-15 Strut and tie model for a deep beam.

The next step is to determine the geometry of the truss model. The nodes of the truss are located at the points of intersection of the forces meeting at the nodal zones (see Fig. 9-15c). With the geometry of the truss model determined, the forces in the struts and the ties of the truss due to factored loads can be found from statics (for statically indeterminate trusses an estimate of the relative stiffnesses of the members is required).

After determining the forces, the required area of tension-tie reinforcement is calculated. In determining the area of tension-tie reinforcement required, the strength reduction factor for axial tension (i.e., $\phi = 0.90$) is used. Hence to resist a tension, N_u , due to factored loads, the area of reinforcement in the tension tie must satisfy

$$\phi(A_s f_y + A_{ps} f_{ps}) \geq N_u \quad (9-3)$$

The tension-tie reinforcement must be anchored so that it can transfer the required tension to the nodal zone of the truss. Additionally, the tension-tie reinforcement must be uniformly distributed over an area of concrete at least equal to the tension-tie force divided by the nodal zone stress limit (see Fig. 9-15b).

The dimensions of the strut must be large enough to ensure that

$$\phi A_c f_{2max} \geq N_u \quad (9-4)$$

where N_u is the calculated axial compression in the strut due to factored loads, ϕ is the strength reduction factor for axial compression (i.e., $\phi = 0.70$), A_c is the effective cross-sectional area of the strut, and f_{2max} is the effective compressive strength of the concrete.

The effective cross-sectional area of a compressive strut is calculated by considering both the available concrete area and the anchorage conditions at the ends of the strut. The manner in which the anchorage conditions influence the effective cross-sectional area of the strut is illustrated in Fig. 9-16. In the case illustrated in Fig. 9-16a, the width of the strut is influenced by the stiffness of the bar anchoring the strut. In Fig. 9-16b the effective width of the compressive strut depends on the length of the bearing plate and the height over which the tension-tie reinforcement is distributed. Figure 9-16c illustrates the effective width of a strut anchored by a bearing plate and another compressive strut.

The concrete compressive stress in the struts must not exceed the crushing strength of the cracked concrete, f_{2max} , given by

$$f_{2max} = \frac{f'_c}{0.8 + 170\epsilon_1} \leq 0.85f'_c \quad (9-5)$$

The value of principal tensile strain, ϵ_1 , which is required in calculating f_{2max} , is determined by considering the strain conditions of the concrete and the reinforcement in the vicinity of the strut. If a tension tie crosses a compressive strut, the required tensile straining will reduce the capacity of the concrete to resist compressive stresses. Assuming that the principal compressive strain in the strut at failure is 0.002 and that the tensile strain in the tie is ϵ_s , the principal tensile strain required by compatibility (see Eq. 7-46) is

$$\epsilon_1 = \epsilon_s + (\epsilon_s + 0.002) \cot^2 \alpha_s \quad (9-6)$$

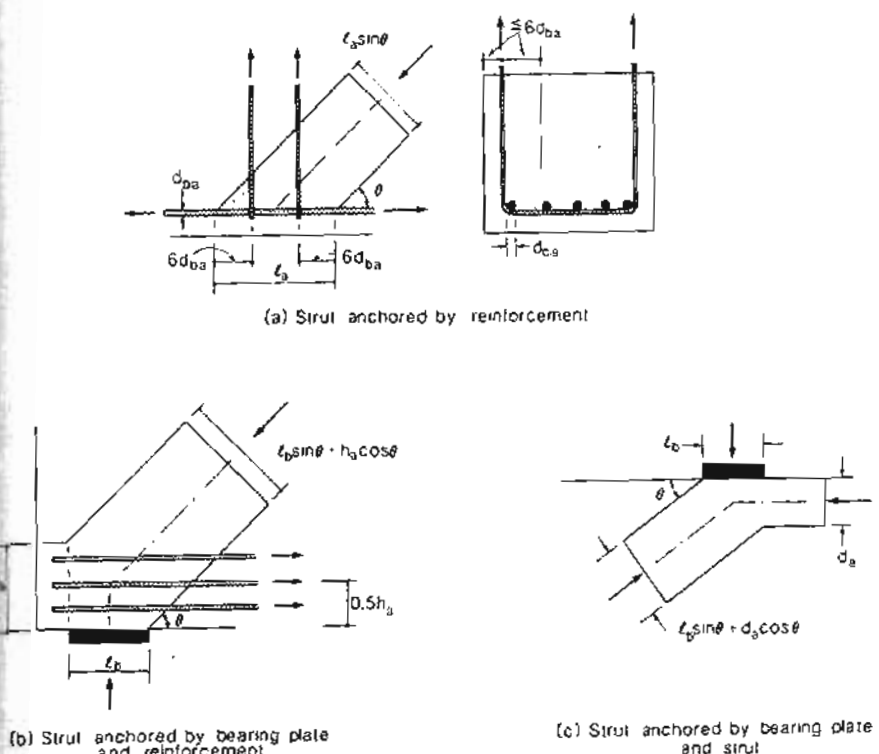


Figure 9-16 Influence of anchorage conditions on effective cross-sectional area of strut.

where α_s is the smallest angle between the tie and the strut (see Fig. 9-15) and ϵ_s is the tensile strain of the tension-tie reinforcement (i.e., $\epsilon_s \leq 0.002$ for $f_y = 60$ ksi (414 MPa)).

Figure 9-17 illustrates the manner in which f_{2max} changes as α_s changes. Reducing α_s results in larger values of ϵ_1 and hence lower values of the crushing strength f_{2max} . In the limit, no compressive stresses would be permitted in a strut that is superimposed on a tension tie (i.e., $\alpha_s = 0$), a situation that violates compatibility. Since the geometry and hence the statics of the truss depends on the sizes of the members, design using the strut and tie model typically involves trial and error.

If the compressive strut contains reinforcing bars that are parallel to the strut and that are enclosed by ties to restrain the bars against buckling (see Fig. 9-3), the design of the

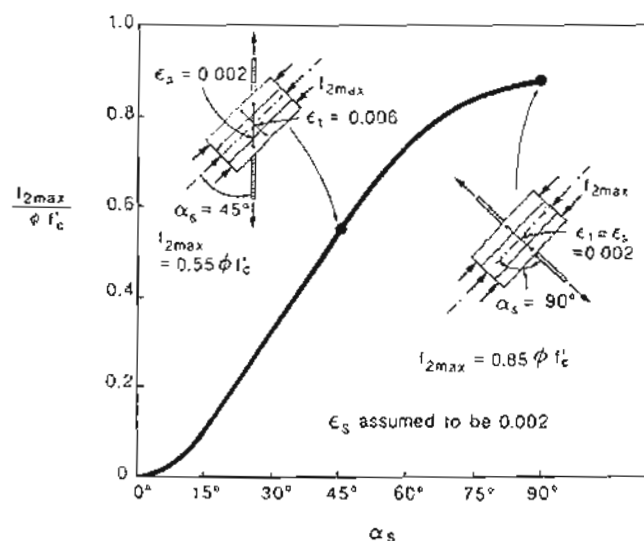


Figure 9-17 Crushing strength of compressive strut as a function of the orientation of the tension tie passing through the strut.

reinforced strut can be checked by using the following equation

$$\phi (A_c f_{2max} + A_s f_y) \geq N_u \quad (9-1)$$

In addition to the primary tension-tie reinforcement, disturbed regions usually require minimum amounts of uniformly distributed, secondary reinforcement to control crack widths and ensure ductility. For example, the ACI Code (Ref. 9-23) requires well-distributed transverse and longitudinal reinforcing bars in deep beams with volumetric ratios of at least 0.0025 for the longitudinal reinforcement and 0.0015 for the transverse reinforcement.

An example of the use of the strut and tie model is illustrated in Fig. 9-18, which shows how the shear strength of a simply supported reinforced concrete beam loaded with two point loads changes as the "shear span" (defined as the distance from the support to the load) changes. It can be seen that a beam can resist a very high shear force if the shear is caused by a load that is close to the support. For this series of beams, which was tested by Kani (Ref. 9-24), the shear strength was reduced by a factor of about 6 as the shear-span-to-depth ratio (a/d) increased from 1 to 7. As the beams contained a large amount of longitudinal reinforcement, flexural failures at midspan did not become critical until a shear-span-to-depth ratio of about 9.

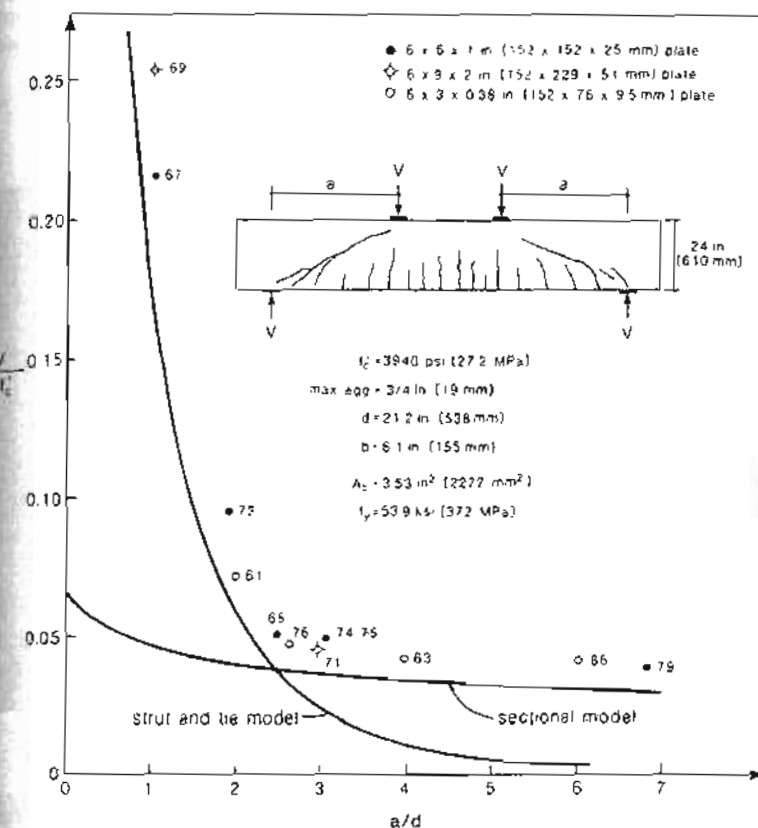


Figure 9-18 Predicted and observed strengths of a series of reinforced concrete beams tested by Kani

Examination of the experimental results shown in Fig. 9-18 and of the observed failure conditions of the beams shown in Fig. 9-19 reveals that two different load-carrying mechanisms govern the behavior of these beams. Beams with shear-span-to-depth ratios less than about 2.5 carry the load by strut-and-tie action of the type illustrated in Fig. 9-15. In this range, the strength of the beams decreases rapidly as the shear span increases. Further, the strength is strongly influenced by details such as the size of the bearing plates

supporting the beam. Failure of the beams involves crushing of the concrete. Beams with shear-span-to-depth ratios greater than about 2.5 are governed by conditions away from the disturbed regions adjacent to the supports and the loads. The response of these beams can be predicted by the sectional models explained in Chapter 7. In this range, the strength of the beams is not influenced by details such as the size of the bearing plates and the strength decreases by only a small amount as the shear span increases.

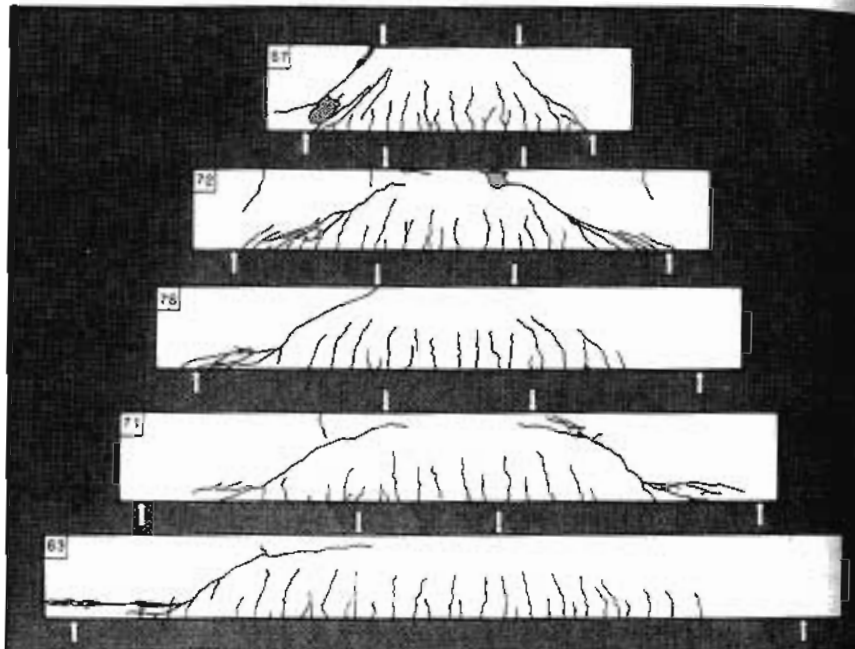


Figure 9-19 Typical failure conditions of beams tested by Kani.

To clarify the details of the calculations involved in determining the predicted capacities shown in Fig. 9-18 we will give the calculations for the case of a shear-span-to-depth ratio of 2 and a bearing plate length of 6 in. (152 mm).

For the strut and tie model shown in Fig. 9-15

$$\tan \alpha_s = \frac{h - 0.5h_u - 0.5d_u}{a} \quad (9-8)$$

where h is the overall height of the beam, $0.5h_u$ is the distance from the bottom face of the beam to the centroid of the tension-tie reinforcement (see Fig. 9-16b), d_u is the depth of the top horizontal compression strut (see Fig. 9-16c), and a is the shear span

If we estimate that d_u will be 3 in. (76 mm), then

$$\begin{aligned} \tan \alpha_s &= \frac{24 - (24 - 21.2) - 0.5 \times 3}{2 \times 21.2} \\ &= 0.465 \\ \text{hence } \alpha_s &= 24.9^\circ \end{aligned}$$

From the equilibrium conditions for the truss shown in Fig. 9-15c we can conclude that the tension, T , in the horizontal tie must equal the compression, C , in the horizontal strut and that these two forces are related to the applied loads, V (see Fig. 9-18), by

$$C = T = V \cot \theta \quad (9-9)$$

The capacity of the top horizontal strut can be found from Eq. (9-4) as

$$\begin{aligned} C &= 1.0 \times 6.1 \times 3.0 \times 0.85 \times 3.94 \\ &= 61.3 \text{ kips (273 kN)} \end{aligned}$$

Because we wish to compare our predictions with experimental results, we take a value of 1.0 for the strength reduction factors.

Hence, from Eq. (9-9)

$$V = 61.3 \times 0.465 = 28.5 \text{ kips (127 kN)}$$

The compressive force, D , in the diagonal struts is

$$\begin{aligned} D &= \frac{V}{\sin \alpha_s} \\ &= \frac{28.5}{\sin 24.9^\circ} = 67.7 \text{ kips (301 kN)} \end{aligned} \quad (9-10)$$

The top ends of the diagonal struts are not crossed by tension ties and hence $f_{2,max}$ at these locations can be taken equal to 0.85 f_c. From Eq. (9-4) and Fig. 9-16c the capacity of the struts at these locations is

$$\begin{aligned} \delta A_c f_{2,max} &= 1.0 \times 6.1 \times (6 \sin 24.9^\circ + 3 \cos 24.9^\circ) 0.85 \times 3.94 \\ &= 107.2 \text{ kips (477 kN)} \end{aligned}$$

The bottom ends of the diagonal struts are crossed by the tension tie and hence it is necessary to determine $f_{2,max}$ from Eqs. (9-5) and (9-6). The tensile strain, ϵ_s , in the tie is

$$\epsilon_s = \frac{61.3}{3.53 \times 29,000} = 0.60 \times 10^{-3}$$

Since the tension-tie reinforcing bars crossing the strut are being developed in this region, the strain in these bars will decrease from 0.60×10^{-3} to zero. Hence the strain, ϵ_1 , at the center of the strut will be taken as $0.5 \times 0.60 \times 10^{-3} = 0.30 \times 10^{-3}$. Thus Eq. (9-6) gives

$$\begin{aligned}\epsilon_1 &= 0.30 \times 10^{-3} + (0.30 \times 10^{-3} + 2.0 \times 10^{-3}) \cot^2 24.9^\circ \\ &= 10.97 \times 10^{-3}\end{aligned}$$

From Eq. (9-5)

$$f_{2max} = \frac{3.94}{0.8 + 170 \times 10.97 \times 10^{-3}} = 1.48 \text{ ksi (10.2 MPa)}$$

From Eq. (9-4) and Fig. 9-16b the capacity of the struts at these locations is

$$\begin{aligned}\phi A_c f_{2max} &= 1.0 \times 6.1 \times (6 \sin 24.9^\circ + 2 \times 2.80 \cos 24.9^\circ) \times 1.48 \\ &= 68.7 \text{ kips (305 kN)}\end{aligned}$$

As the capacity of the strut slightly exceeds the calculated compressive force in the strut, the loads could still be increased by a small amount. That is, our estimate of d_a was a little low. It will be found that the diagonal struts are predicted to fail when d_a equals 3.04 in. (77 mm) and V equals 28.7 kips (128 kN).

Hence

$$\frac{V}{bd f'_c} = \frac{28.7}{6.1 \times 21.2 \times 3.94} = 0.056$$

As these beams did not contain any web reinforcement, their shear strength, according to the sectional model of Section 7.12, is strongly influenced by the crack spacing parameter, s_{max} (see Table 7-4). In calculating s_{max} from Eq. (7-36) we will take c_x as the maximum distance away from the reinforcement or from the flexural compression zone of the beam. The depth of the compression zone can be calculated from the traditional working stress design expression for the depth of the neutral axis, kd . Namely,

$$kd = \left[\sqrt{(n\rho)^2 + 2n\rho} - n\rho \right] d \quad (9-11)$$

where n is the modular ratio, E_s/E_c , and ρ is the reinforcement ratio. For these beams,

$$n\rho = \frac{29,000,000}{57,000\sqrt{3940}} \frac{3.53}{6.1 \times 21.2} = 0.221$$

Hence

$$\begin{aligned}kd &= \left[\sqrt{(0.221)^2 + 2 \times 0.221} - 0.221 \right] \times 21.2 \\ &= 10.2 \text{ in. (259 mm)}\end{aligned}$$

While the arrangement of the flexural reinforcement varied somewhat from beam to beam, most of the beams contained four #8 bars (25 mm diameter) arranged in two layers, and one #6 bar (19 mm diameter) placed between the other two layers. The top of the

upper layer of #8 bars was about 4.4 in. (112 mm) from the bottom of the beam. Hence the distance from the top of the reinforcement to the bottom of the flexural compression zone was $24 - 4.4 - 10.2 = 9.4$ in. (239 mm).

Thus Eq. (7-36) gives

$$\begin{aligned}s_{max} &= 2 \left(\frac{9.4}{2} + \frac{4}{10} \right) + 0.25 \times 0.40 \times \frac{1.0}{3.53/(6.1 \times 21.2)} \\ &= 13.9 \text{ in. (353 mm)}\end{aligned}$$

Thus the β values can be found by interpolating between the values listed for 10 in. (250 mm) and 15 in. (380 mm) in Table 7-4.

As there is no web reinforcement

$$\begin{aligned}V &= V_c = \beta \sqrt{f'_c b_w jd} \\ &= \beta \sqrt{3940 \times 6.1 \times 0.9 \times 21.2} \\ &= 7.31\beta \text{ kips}\end{aligned}$$

To find β from Table 7-4 we must still calculate ϵ_x from Eq. (7-53). The section $0.5jd/\cot\theta$ away from the load will be used in evaluating ϵ_x . At this location the moment is

$$M = V(a - 0.5jd \cot\theta)$$

Hence, from Eq. (7-53)

$$\begin{aligned}\epsilon_x &= \frac{\frac{Va}{jd} - 0.5V \cot\theta + 0.5V \cot\theta}{E_s A_s} \\ \epsilon_x &= \frac{Va/jd}{E_s A_s} \\ &= \frac{V \times 2 \times 21.2 / (0.9 \times 21.2)}{29,000 \times 3.53} \\ &= \frac{V}{46,100}\end{aligned} \quad (9-12)$$

Thus, if we estimate that V equals 20 kips (89 kN), ϵ_x will be calculated as 0.43×10^{-3} . Interpolating from Table 7-4 we will find that β equals 2.80, which corresponds to

$$V = 2.80 \times 7.31 = 20.5 \text{ kips (91 kN)}$$

The estimated and the calculated values of V converge for $V = 20.3$ kips (90 kN). Hence

$$\frac{V}{bd f'_c} = \frac{20.3}{6.1 \times 21.2 \times 3.94} = 0.040$$

Repeating the calculations above for different shear spans we obtain the two lines plotted in Fig. 9-18 which show the predicted variation of shear strength with shear span. It can be seen that by using both the strut and tie model and the sectional model, the trend of the experimental data can be predicted very well.

Some further examples of strut and tie models are illustrated in Fig. 9-20. The need for well-distributed transverse and longitudinal reinforcement in deep beams in addition to the primary tension-tie reinforcement is made clear by the refined truss model shown in Fig. 9-20b. The power of strut and tie models is demonstrated by the ability to follow the flow of stresses around openings (see Fig. 9-20c and f).

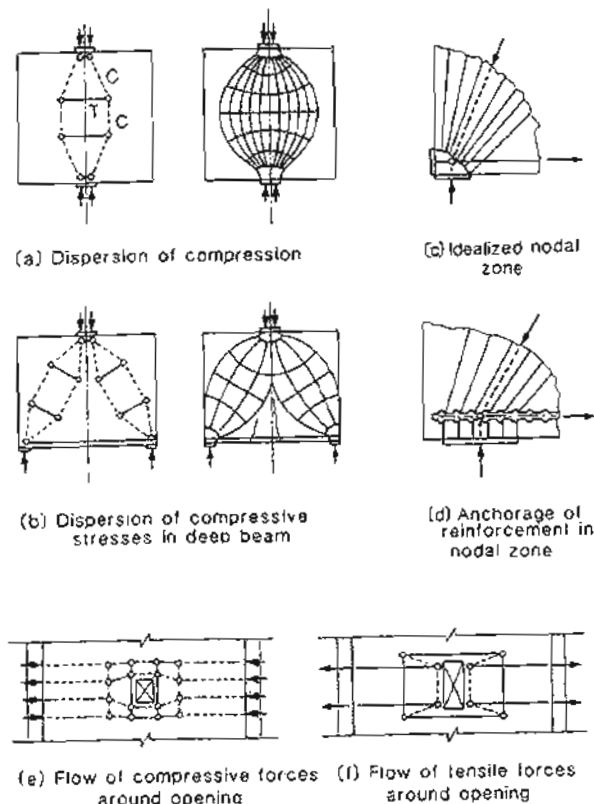


Figure 9-20 Strut and tie models of some stress flows. Adapted from Schlaich, Schäfer and Jennewein (Ref. 9-19).

The predicted and observed behavior of a reinforced concrete corbel are compared in Fig. 9-21. The analysis of the double-sided corbel using a strut and tie model is illustrated in Fig. 9-21b. In the test, the horizontal force was 20% of the vertical force acting on the corbel. Using the measured material properties (all strength reduction factors are taken as 1.0) the main tension tie can supply a force of $A_s f_y = 79.8$ kips (355 kN). If we assume that the yield force of the tension tie will govern the corbel failure, then from the statics of the truss the predicted failure loads are 91.7 kips (408 kN) vertically and 18.3 kips (81.6 kN) horizontally. The fanning compression strut has its maximum stress in the nodal zone at the top of the corbel. The nodal zone stress under the 1.97 in. (50 mm) wide by 11.8 in. (300 mm) long bearing plate is $91.7/(1.97 \times 11.8) = 3.94$ ksi (27.2 MPa). The nodal zone stress limit is $0.75 f'_c = 0.75 \times 5.86$ ksi = 4.40 ksi (30.3 MPa). Hence it is predicted that yielding of the main tension tie will initiate the failure of the corbel, followed closely by crushing of the concrete in the top nodal zone. The actual reinforcement details for this corbel are shown in Fig. 9-21c. As can be seen, additional closed horizontal ties, having an area of at least 50% of A_s and distributed within the top two-thirds of the corbel, have been provided in accordance with the ACI Code (Ref. 9-23) detailing requirements for brackets and corbels. In the analysis using the simplified strut and tie model, this additional reinforcement was neglected. Failure occurred in the specimen at a vertical load of 113 kips (502 kN) by concrete crushing under the bearing plate after large strains were recorded in the main tension tie and after the occurrence of severe spalling of the concrete cover surrounding the bearing plate (see Fig. 9-21c and d).

Figure 9-21c illustrates the principal stresses and principal strains in the concrete predicted by a nonlinear finite element analysis. In the modeling of this corbel, stiff truss elements were used to simulate the presence of the steel loading block attached to the top of the steel bearing plate. The two elements in the top row surrounding the bearing area were given thicknesses of 11.8 in. (300 mm) to simulate the spalling of the 1 in. (25 mm) of concrete outside the bearing plate. As can be seen from Fig. 9-21c, the mesh also simulated the likely concrete spalling zones outside the bearing plate. All of the reinforcement in the corbel and column was modeled in the finite element analysis. As can be seen, the predicted flow of concrete compressive stresses is somewhat different from that assumed in the simple strut and tie model. Due to the presence of the additional horizontal reinforcement and due to the vertical cracking in the corbel, the compressive stresses are more curved toward the outer surface of the corbel and become more concentrated as they funnel into the column. The nonlinear analysis predicts failure to occur at a vertical load of 101 kips (450 kN) by yielding of the main tension-tie reinforcement. The large tensile strains predicted are evident in Fig. 9-21c.

Additional examples of strut and tie models for corbels and ledge supports are given in Fig. 9-22. The strength of these disturbed regions depends critically on the anchorage details of the tension-tie reinforcement (Ref. 9-25). Often some form of mechanical anchorage is required to develop the required tensile force. A structural steel angle welded to the main tension-tie reinforcement will enable the yield strength of the tie to be developed and will also act as a bearing surface and will armor the outer corner of the bracket or corbel.

In the ledger beams shown in Fig. 9-22b and c, the hanger steel transmits the vertical component from the inclined compression struts toward the top of the beam. As can be

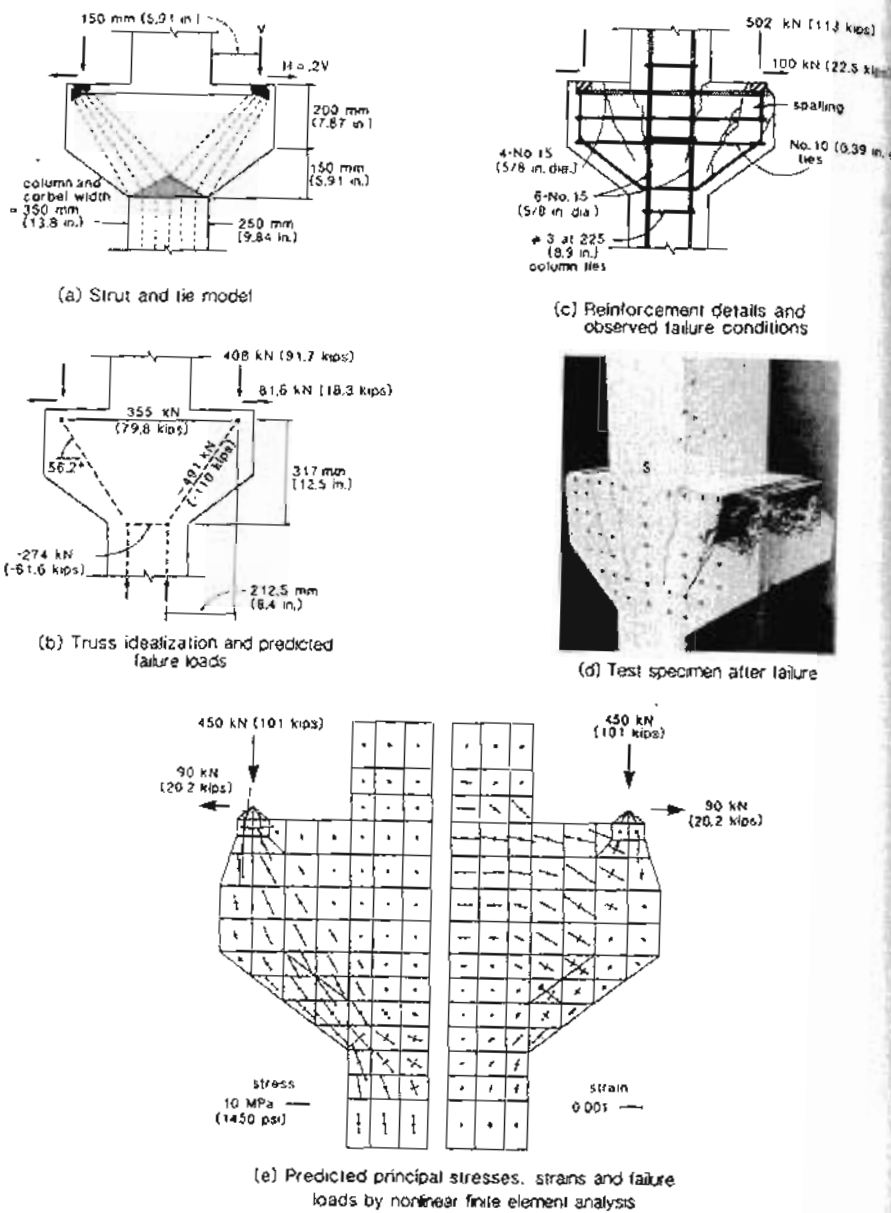


Figure 9-21 Predicted and observed behavior of reinforced concrete corbel.
Adapted from Ref. 9-15.

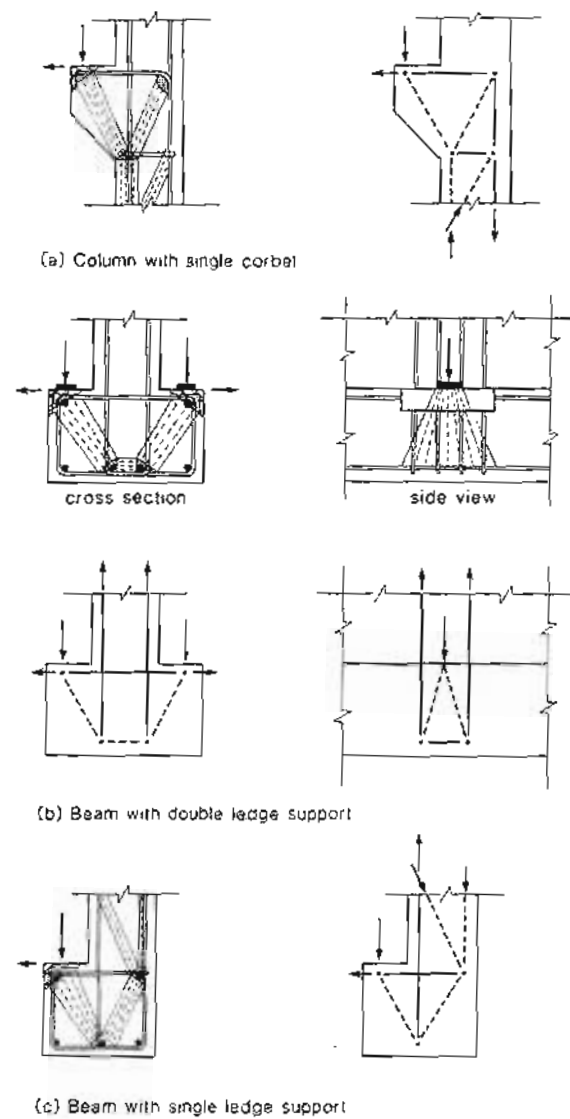


Figure 9-22 Strut and tie models and truss idealization for corbels and ledge supports.

seen, this hanger steel can be spread over a short length of the ledger beam and should be provided in addition to the shear and torsion reinforcement required in the ledger beam.

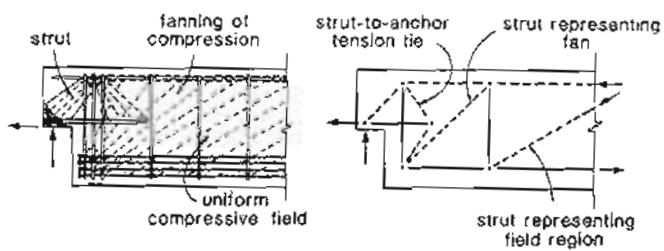
Figure 9-23 illustrates the application of a strut and tie model to a beam with a dapped end. In the beam shown, a vertical tension tie with significant capacity is required to "lift" the force from the bottom of the full-depth section to the top of the beam. From the top of the beam, the force can be delivered directly to the support by a diagonal compressive strut. The horizontal component from this diagonal strut needs to be equilibrated by a horizontal tension tie. The tension in this tie will be transmitted into the member by bond stresses acting over some length of the tie and hence the bar should be extended beyond the vertical tie for a distance of at least 1.7 times the development length (see Ref. 9-15). In this strut and tie model the node at the inner end of this tension tie is placed halfway along the anchorage length of the bar. The anchorage of the horizontal tension tie at the bottom of the full-depth section requires careful detailing in order that the large tensile forces required can be developed. Guidance on the detailing of precast prestressed members with dapped ends has been provided by Mattock and Theryo (Ref. 9-26).

Figure 9-24 illustrates the strut and tie models and truss idealizations for some deep beams. The simply supported deep beam is easily modeled with a statically determinate truss as shown in Fig. 9-24a. The design must ensure that premature failure due to inadequate tension-tie reinforcement, insufficient anchorage of tension ties, crushing of bearing areas, and crushing of compressive struts does not occur. The contribution of the small amount of uniformly distributed reinforcement required by the Code (Ref. 9-23) is usually neglected in designing deep beams using a simple strut and tie model.

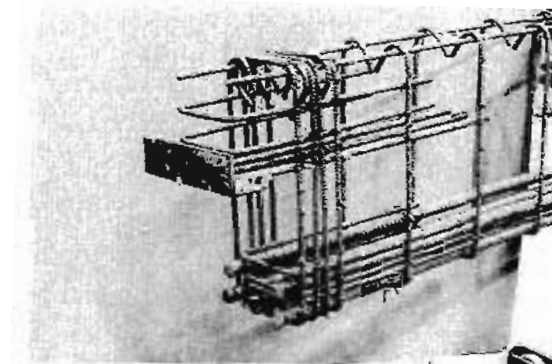
Strut and tie models and the resulting statically indeterminate truss idealizations for continuous deep beams are shown in Fig. 9-24b and c. In order to solve for the truss member forces, it is necessary to account for the relative stiffness of the members. As the span-to-depth ratio is increased, not all of the load is transmitted by compressive struts that travel directly to the supports. The fanning out of the compressive stresses may cause significant tensile stresses in the vertical stirrups. As the beam becomes even more shallow, a uniform compressive field could develop between the fanning regions near the supports and loading points.

Figure 9-25 illustrates strut and tie models and truss idealizations for anchorage zones of prestressed concrete beams. The design of these zones using the strut and tie model proceeds as follows:

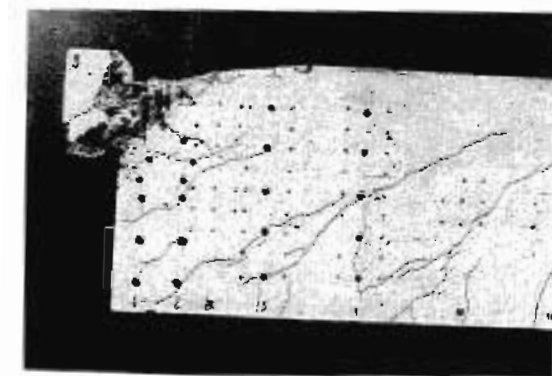
1. Check the stress in the nodal zones under the bearing plates.
2. Calculate the linearly distributed stresses on a face removed from the disturbed region.
3. Represent the flow of forces between the applied end loads and the linearly distributed stresses by a strut and tie model as shown in Fig. 9-25.
4. Solve the statics of the truss to determine the required tension-tie forces.
5. Calculate the required amount of reinforcement and detail the reinforcement to ensure that the assumed flow of forces is possible.



(a) Strut and tie model



(b) Reinforcing cage



(c) Observed failure conditions

Figure 9-23 Strut and tie model and truss idealization for beams with dapped ends and beams with opening in web. Adapted from Ref. 9-15.

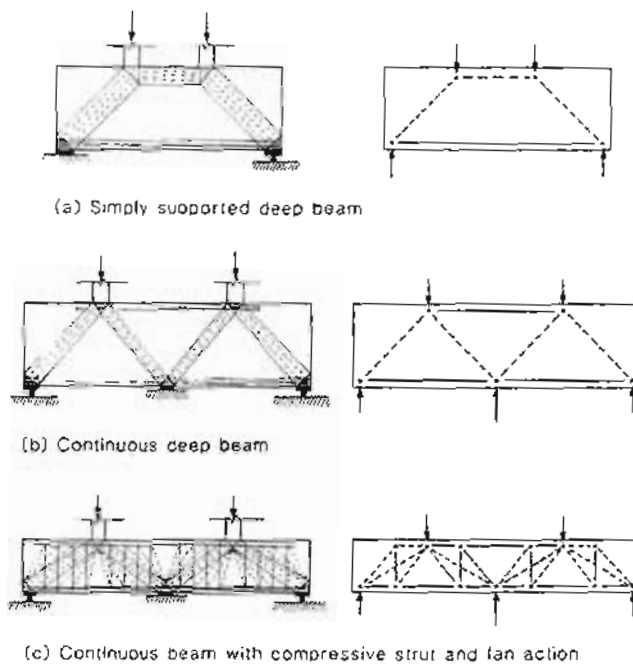


Figure 9-24 Strut and tie models and truss idealizations for deep beams.

9.7 EXAMPLE DESIGN OF ANCHORAGE ZONE USING STRUT AND TIE MODEL

The end anchor region of a post-tensioned 1-beam is shown in Fig. 9-26. Each tendon consists of four 1/2 in. (13 mm) diameter low-relaxation strands with an ultimate stress of 270 ksi (1860 MPa). During jacking, the maximum stress reached in the strands is $0.75f_{pu}$. The concrete strength at the time of jacking is 5000 psi (34.5 MPa).

Design the required end anchorage reinforcement.

Step 1: Determine the factored loads.

The ACI Code requires that "post-tensioning anchorage zones shall be designed to develop the guaranteed ultimate tensile strength of prestressing tendons using a strength reduction factor, ϕ , of 0.90 for concrete." Hence for each tendon,

$$P = 4 \times 0.153 \times 270 = 165 \text{ kips (735 kN)}$$

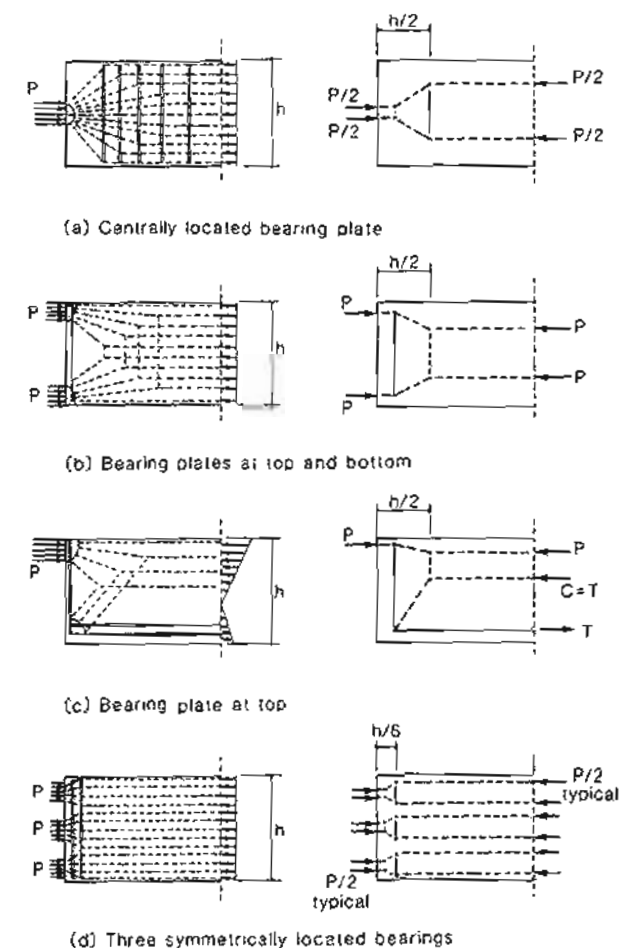


Figure 9-25 Strut and tie models and truss idealizations for anchorage zones.

Step 2: Check the bearing stress under the anchorage plates.

Net bearing area of each plate:

$$\begin{aligned} A &= 7 \times 7 - \pi \times \frac{2^2}{4} \\ &= 45.9 \text{ in}^2 (29600 \text{ mm}^2) \end{aligned}$$

$$\text{bearing stress} = \frac{165}{45.9} = 3.60 \text{ ksi (24.8 MPa)}$$

$$\text{permissible nodal zone stress limit} = 0.85\phi f'$$

$$\begin{aligned} &= 0.85 + 0.90 \times 5 \\ &= 3.83 \text{ ksi (26.4 MPa)} \end{aligned}$$

Hence the bearing stress is acceptable.

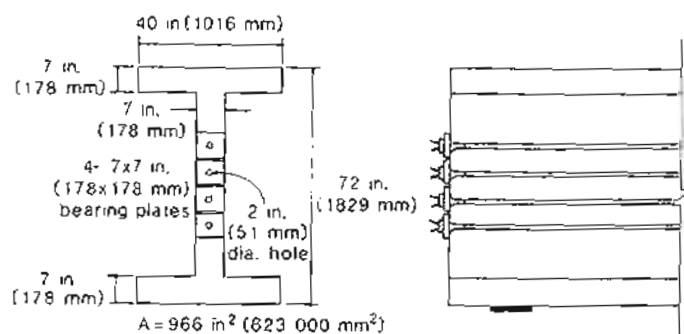


Figure 9-26 Details of anchorage region in post-tensioned I-beam.

Step 3: Calculate the stress distribution outside the disturbed region.

Outside the disturbed region, the stresses will be uniform. If each tendon is at its ultimate tensile strength, this uniform compressive stress will be

$$f_c = \frac{4 \times 165}{966} = 0.683 \text{ ksi (4.71 MPa)}$$

This uniform stress will result in a compressive force of 191 kips (851 kN) in each flange and 277 kips (1233 kN) in the web.

Step 4: Draw the strut and tie model.

The flow of the compressive stresses out across the web and into the flanges can be modeled by the strut and tie model shown in Fig. 9-27. The total bearing force of 660 kips

(2936 kN) acting over the 28 in. (711 mm) high bearing area has been subdivided into two forces which flow into the flanges and two forces which flow into the web. That is, the bearing area has been subdivided into four areas in proportion to the four forces required (see Fig. 9-27a).

Step 5: Determine the forces in the tension ties by statics.

The forces in the tension ties are given in Table 9-1.

Table 9-1

Member	CD	DE	GH
Force, kips (kN)	126.7 (564)	173.9 (772)	39.4 (175)

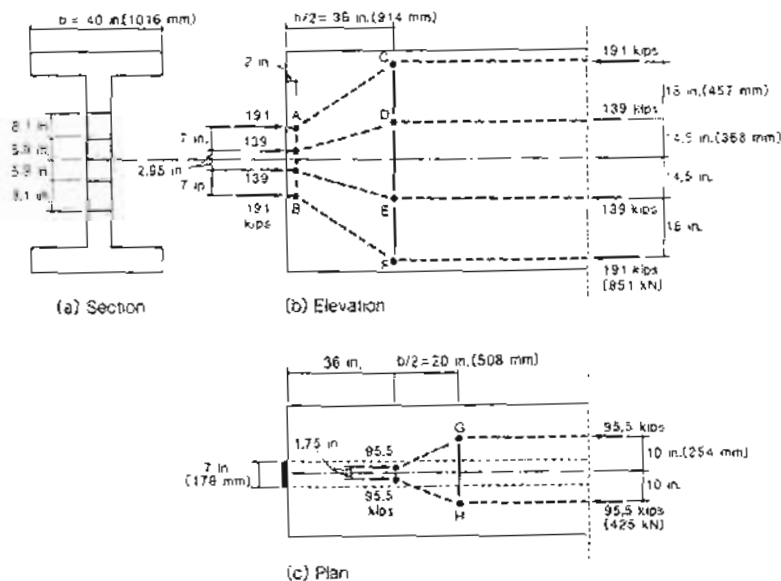


Figure 9-27 Strut and tie models showing dispersion of stresses into web and into flange.

Step 6: Detail the reinforcement.

If #4 (13 mm diameter) closed stirrups with $f_y = 60 \text{ ksi (414 MPa)}$ are used, each stirrup has a factored tensile resistance of $0.9 \times 60 \times 0.40 = 21.6 \text{ kips (96 kN)}$. Hence

$173.9/21.6 = 8.1$ stirrups are required in the web. As shown in Fig. 9-28, use nine #4 closed stirrups spaced at 9 in. (229 mm). The stirrup at the end face is intended to control potential spalling cracks. It can resist 21.6 kips (96 kN), which is $0.033P$ and therefore exceeds the suggested minimum of $0.02P$.

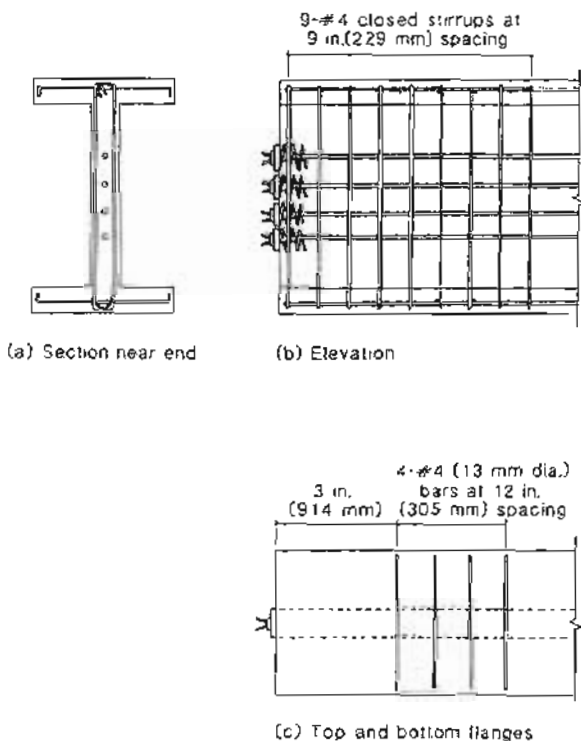


Figure 9-28 Reinforcement details of anchorage zone.

With a single #4 "stirrup" leg in each flange, the factored resistance is $0.9 \times 60 \times 0.20 = 10.8$ kips (48 kN). Hence $39.4/10.8 = 3.6$ such stirrups are required. Use four #4 stirrups spaced at 12 in. (305 mm) as shown in Fig. 9-28. It should be noted that only the reinforcement required for dispersion of the prestressing force into the cross section has been determined in this example.

9.8 EXAMPLE DESIGN OF CORBEL USING STRUT AND TIE MODEL

Figure 9-29 shows a corbel projecting from a 14 x 14 in. (356 x 356 mm) column which supports a precast girder. The corbel is subjected to a dead load of 18 kips (80 kN) and a live load of 22 kips (98 kN). We will design the corbel using a strut and tie model. A concrete strength of 5000 psi (34.5 MPa) and a reinforcement yield strength of 60 ksi (414 MPa) will be used.

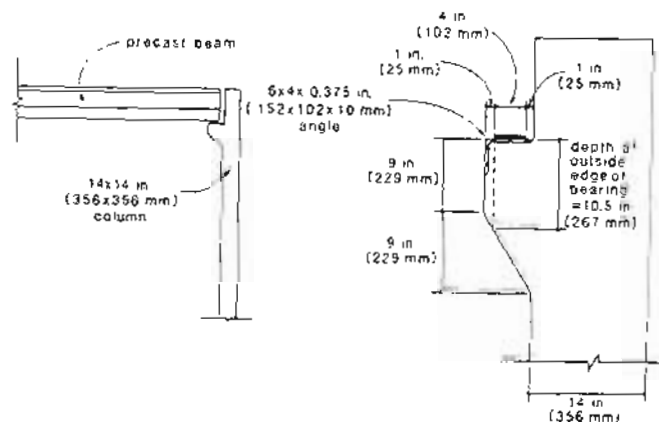


Figure 9-29 Corbel geometry.

Step 1: Determine the factored loads.

The vertical factored load is

$$\begin{aligned} V_u &= 1.4D + 1.7L \\ &= 1.4 \times 18 + 1.7 \times 22 \\ &= 62.6 \text{ kips (278 kN)} \end{aligned}$$

The ACI Code (Ref. 9-23) requires the tension on the corbel resulting from creep, shrinkage, or temperature change to be treated as a live load. This tension is assumed to be 8 kips (35.6 kN). Hence the horizontal factored load is

$$\begin{aligned} N_{uc} &= 1.7T \\ &= 1.7 \times 8 \\ &= 13.6 \text{ kips (60.5 kN)} \end{aligned}$$

The ACI Code requires that N_{uc} shall not be taken less than $0.2V_c = 0.2 \times 62.6 = 12.5$ kips (56 kN). Hence use $N_{uc} = 13.6$ kips.

Step 2: Determine the bearing plate dimensions.

In order to provide a means of anchoring the main tension-tie reinforcement and in order to armor the corner of the corbel against spalling of the concrete cover, we will use a structural steel angle as shown in Fig. 9-29. Choose a $12 \times 4 \times 1/2$ in. ($305 \times 102 \times 13$ mm) bearing pad.

The bearing stress is

$$\frac{62.6}{12 \times 4} = 1.30 \text{ ksi (9 MPa)}$$

Since this is less than $0.75\phi f'_c = 0.75 \times 0.70 \times 5 = 2.63$ ksi (18 MPa), the bearing size is adequate.

Step 3: Choose the corbel dimensions.

Choose an overall corbel depth at the column face of 18 in. (457 mm). This dimension will be revised if an excessive amount of reinforcement is required.

Choose a depth at the free end of the corbel to satisfy the ACI Code requirement that the depth at the outside of the bearing area is at least one-half of the depth at the column face. The dimensions chosen for the corbel are summarized in Fig. 9-29.

Step 4: Determine the geometry of the strut and tie model.

To allow for load eccentricities and erection tolerances, consider the vertical load to be placed 1 in. (25 mm) toward the edge of the corbel from the center of the bearing plate. The assumed compressive strut, tension tie, and nodal zone model for the corbel is shown in Fig. 9-30a. To clarify the geometry of the assumed truss, a separate line drawing of the truss is given in Fig. 9-30b.

Nodes A and B are located at the intersections of the centerlines of the tension ties. Node C is located at the intersection of the centerline of the upper tension tie and the line of action of the resultant applied load. Node D is located at the intersection of the centerline of the lower tension tie and the centerline of the vertical compressive strut below the corbel. The location of this strut centerline is found by calculating the strut width a .

The compressive force in this vertical strut, N_c , can be found by taking moments about Node A:

$$62.6 \times 15.99 + 13.6 \times 17.38 = N_c \left(11.75 - \frac{a}{2} \right)$$

As the stress on the nodal zone at D is to be limited to $0.75\phi f'_c = 0.75 \times 0.70 \times 5 = 2.63$ ksi (18.1 MPa) we can relate a and N_c as follows:

$$a = \frac{N_c}{2.63 \times 14}$$

We can determine the depth, a , and the force, N_c , by solving these two equations. Hence

$$N_c = 122.7 \text{ kips (546 kN)}$$

$$a = 3.33 \text{ in. (85 mm)}$$

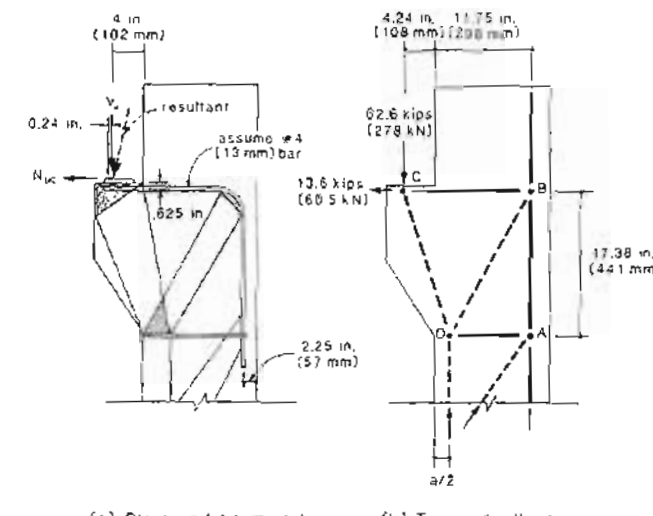


Figure 9-30 Determination of truss model.

This fixes the geometry of the truss shown in Fig. 9-30b and means that member CD has a horizontal projection of $4.24 + 3.33/2 = 5.91$ in. (150 mm), while member BD has a horizontal projection of 10.1 in. (256 mm).

Step 5: Determine the forces in the truss by statics.

The forces in the other important members of the truss are given in Table 9-2.

Table 9-2

Member	CD	CB	BD	BA	DA
Force*, kips (kN)	-66.1 (-294)	+34.9 (+155)	-69.4 (-309)	+60.0 (+267)	+13.6 (+60)

*Positive indicates tension, negative compression.

Step 6: Design the tension ties.

The area of reinforcement required for tension tie CB is

$$A_s = \frac{N}{\phi f_y} = \frac{34.9}{0.9 \times 60} = 0.65 \text{ in}^2 (417 \text{ mm}^2)$$

Hence use four #4 (13 mm diameter) bars.

Although tie BA has a larger tension, it must be appreciated that the longitudinal reinforcement in the column will have been designed to resist this longitudinal tensile

force. Hence continue the four #4 bars for a sufficient distance down the column to develop these bars fully.

The area of reinforcement required for tension tie DA is

$$A_s = \frac{13.6}{0.9 \times 60} = 0.25 \text{ in}^2 (162 \text{ mm}^2)$$

Hence use two #3 (10 mm diameter) additional column ties at location DA.

Step 7: Design the nodal zones.

The width a of nodal zone D was chosen in Step 4 to satisfy the stress limits on this nodal zone. To anchor tension tie CB, weld the four #4 bars to the horizontal leg of the steel angle.

To satisfy the nodal zone stress limit, the tension-tie reinforcement must engage an effective depth of concrete at least equal to

$$\frac{34.9}{0.75 \times 0.70 \times 5.0 \times 14} = 0.95 \text{ in. (24 mm)}$$

As the vertical leg of the steel angle will engage 4 in. (102 mm) of concrete, this limit is easily satisfied.

Step 8: Check the compressive struts.

Strut BD is subjected to the highest compressive force and is anchored at both ends by reinforcement. Hence we will check this strut first.

Based on Fig. 9-16a we will assume that the strut bearing area at end B extends 6 bar diameters from the joint in both the horizontal and vertical directions. The angle BDA is equal to the arc tangent of $10.1/17.38$ which is 30.2° . Hence, from the expression in Fig. 9-16b, the width of strut BD is

$$6 \times 0.5 \sin 30.2^\circ + 6 \times 0.5 \cos 30.2^\circ = 4.10 \text{ in. (104 mm)}$$

As there are four #4 (13 mm diameter) bars across the 14 in. (356 mm) thickness of the column and each bar can engage a tributary area of concrete extending up to six bar diameters from each side of the bar (see Fig. 9-16a), all 14 in. (356 mm) of the thickness will be effective. Hence the effective area of the strut is

$$A_e = 4.10 \times 14 = 57.4 \text{ in}^2 (37000 \text{ mm}^2)$$

If the longitudinal reinforcement in the column at location BA consists of three #9 (29 mm diameter) bars, the tensile strain in tie BA at B will be

$$\epsilon_s = \frac{60}{(3 \times 1.0 + 4 \times 0.20) \times 29.000} = 0.54 \times 10^{-3}$$

Hence, from Eq. (9-6)

$$\begin{aligned}\epsilon_1 &= 0.54 \times 10^{-3} + (0.54 \times 10^{-3} + 2.0 \times 10^{-3}) \cot^2 30.2^\circ \\ &= 8.04 \times 10^{-3}\end{aligned}$$

Eq. (9-5) thus gives

$$f_{2max} = \frac{5.0}{0.8 + 170 \times 8.04 \times 10^{-3}} = 2.31 \text{ ksi}$$

The capacity of strut BD, from Eq. (9-4) is

$$\begin{aligned}\phi A_e f_{2max} &= 0.70 \times 57.4 \times 2.31 \\ &= 92.8 \text{ kips (413 kN)}\end{aligned}$$

As this capacity exceeds the compression in the strut due to factored loads, which is 69.4 kips (309 kN), strut BD is satisfactory.

As strut CD is less critical than BD, it too will be satisfactory.

Step 9: Check the minimum reinforcement requirements.

According to the ACI Code, the area, A_{st} , of the primary, tensile-tie reinforcement must satisfy

$$\begin{aligned}A_{st} &\geq 0.04 \frac{f'_c bd}{f_y} \\ &= 0.04 \times \frac{5}{60} \times 14 \times 17.38 \\ &= 0.81 \text{ in}^2 (523 \text{ mm}^2)\end{aligned}$$

We will accept the four #4 bars (13 mm diameter) as being satisfactory since they provide an area equal to 99% of the specified minimum.

In addition, the code requires closed stirrups or ties parallel to A_s to be uniformly distributed with 2/3 of the effective depth adjacent to A_s . The area of these ties must exceed $0.5(A_s - A_n)$, where A_n is the area of reinforcement resisting the tensile force, N_{uc} . Hence the area required is

$$0.5 \left(0.80 - \frac{13.6}{0.9 \times 60} \right) = 0.27 \text{ in}^2 (177 \text{ mm}^2)$$

Hence provide two #3 (10 mm diameter) closed stirrups. The details of the corbel are summarized in Fig. 9-31.

9.9 EXAMPLE DESIGN OF DEEP BEAM USING STRUT AND TIE MODEL

Figure 9-32 shows a deep beam that is laterally supported at the top by a floor slab (not shown). The beam acts as a transfer girder to carry the two vertical factored loads which have been increased to account for the self-weight of the beam and the uniform loading from the floor slab.

A concrete strength of 4000 psi (27.6 MPa) and a reinforcement yield strength of 60 ksi (414 MPa) will be used.

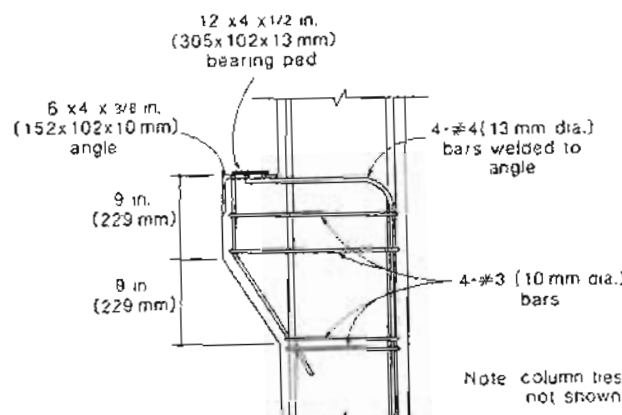


Figure 9-31 Reinforcement details for corbel.

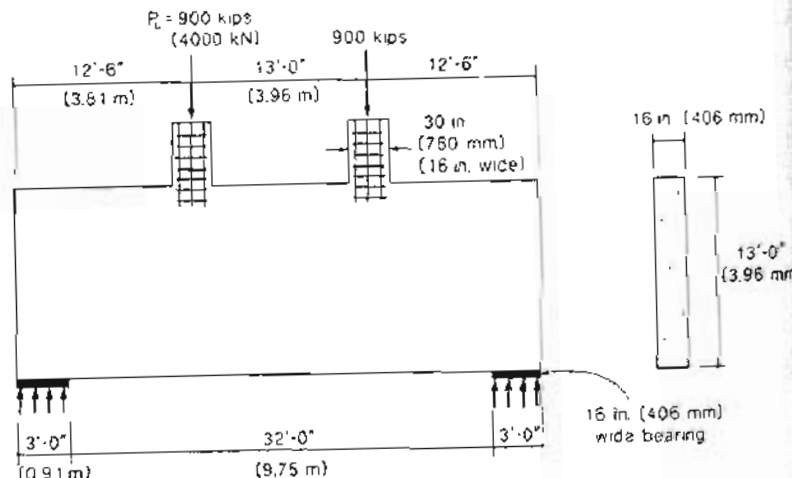


Figure 9-32 Transfer girder

Step 1: Check the bearing stresses at the supports.

At the support, the bearing stress is

$$\frac{900}{16 \times 36} = 1.56 \text{ ksi (10.8 MPa)}$$

The permissible stress (see Fig. 9-15) for this nodal zone anchoring a tension tie is

$$\begin{aligned} 0.75\phi f'_c &= 0.75 \times 0.70 \times 4 \\ &= 2.10 \text{ ksi (14.5 MPa)} \end{aligned}$$

Hence the bearing area is sufficient.

Step 2: Estimate the geometry of the strut and tie model.

Figure 9-33 shows the strut and tie model of the transfer girder.

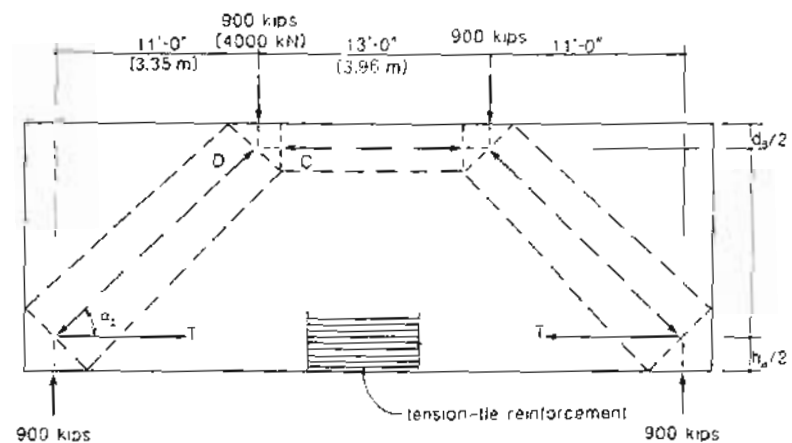


Figure 9-33 Strut and tie model of transfer girder.

Before the forces in the struts and tie can be calculated, it is necessary to estimate the height, h_a , over which the tension-tie reinforcement will be distributed (see Fig. 9-16b) and the depth, d_a , of the top compressive strut (see Fig. 9-16c).

Between the two point loads, the external moment on the beam is resisted by a couple consisting of compression in the top strut and tension in the tie. While the compressive force, C , in the strut must equal the tension force, T , in the tie, the permissible nodal zone stress ($0.75\phi f'_c$) at the ends of the tension tie is lower than the permissible stress ($0.85\phi f'_c$)

at the ends of the compressive strut (see Fig. 9-15a) and hence the minimum size of h_a is larger than d_a by a factor of $0.85/0.75 = 1.133$. Equating the external and internal moments gives

$$\begin{aligned} 900 \times 11 \times 12 &= C \times (13 \times 12 - 0.5d_a - 0.5 \times 1.133d_a) \\ &= 0.7 \times 0.85 \times 4 \times 16d_a(156 - 1.067d_a) \end{aligned}$$

Hence, to satisfy the stress limits, the minimum value of d_a is 23.9 in. (607 mm). As a first trial we will take d_a as 25 in. (635 mm) and h_a as 29 in. (737 mm). For these dimensions

$$\tan \alpha_s = \frac{13 \times 12 - 0.5 \times 25 - 0.5 \times 29}{11 \times 12} = 0.977$$

Hence $\alpha_s = 44.3^\circ$.

Step 3: Determine the forces in the struts and ties.

From statics,

$$\begin{aligned} D \sin \alpha_s &= 900 \\ D &= 900 / \sin 44.3^\circ = 1289 \text{ kips (5730 kN)} \\ T &= D \cos \alpha_s \\ &= 1289 \cos 44.3^\circ = 923 \text{ kips (4100 kN)} \\ C &= T = 923 \text{ kips (4100 kN)} \end{aligned}$$

Step 4: Choose the reinforcement for the tension tie.

From Eq. (9-3),

$$A_s \geq \frac{923}{0.90 \times 60} = 17.1 \text{ in}^2 (11030 \text{ mm}^2)$$

We will choose a bar size such that the reinforcement can be developed at the inner edge of the bearing (see Fig. 9-15a). That is, the tension development length of the bar must be less than $36 - 1.5 = 34.5$ in. (876 mm). From Table 3-12 it can be seen that a #8 (25 mm diameter) bar is the largest that can be used. Hence use twenty-four #8 bars having a total area of 19.0 in^2 (12230 mm^2) distributed as shown in Fig. 9-34.

Step 5: Check the capacities of the struts.

The horizontal compressive strut is not crossed by a tension tie and hence $f_{2max} = 0.85f'_c$. Thus, from Eq. (9-4) the capacity of the strut is

$$\begin{aligned} \phi A_c f_{2max} &= 0.70 \times 16 \times 25 \times 0.85 \times 4 \\ &= 952 \text{ kips (4230 kN)} \end{aligned}$$

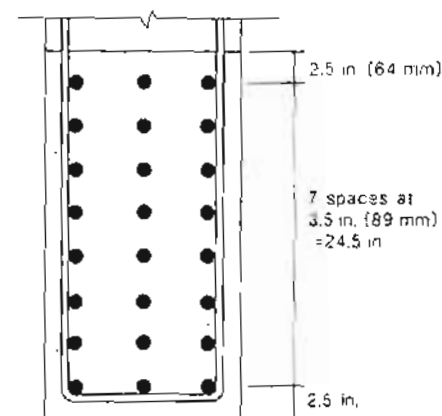


Figure 9-34 Arrangement of tension-tie reinforcement.

As this exceeds the required compression of 923 kips (4100 kN) the strut has adequate capacity.

Since the conditions at the top and bottom ends of the diagonal struts differ, it is necessary to check the compressive capacity at both ends. At the top these struts are not crossed by tension ties and hence $f_{2max} = 0.85f'_c$. From Eq. (9-4) and from Fig. 9-16c, the capacity of the strut is

$$\begin{aligned} \phi A_c f_{2max} &= 0.70 \times 16 \times (30 \sin 44.3^\circ + 25 \cos 44.3^\circ) 0.85 \times 4 \\ &= 1479 \text{ kips (6580 kN)} \end{aligned}$$

The bottom of these struts is crossed by the tension tie and hence it is necessary to determine f_{2max} from Eqs. (9-5) and (9-6). The tensile strain, ϵ_t , in the tie is

$$\epsilon_t = \frac{923}{18.96 \times 29,000} = 1.68 \times 10^{-3}$$

Since the tension-tie reinforcing bars are being developed in this region, the strain in these bars will decrease from 1.68×10^{-3} to zero at their ends. Hence, at the center of the strut, the strain, ϵ_s , will be taken as $0.5 \times 1.68 \times 10^{-3} = 0.84 \times 10^{-3}$ and thus, Eq. (9-6) gives

$$\begin{aligned} \epsilon_s &= 0.84 \times 10^{-3} + (0.84 \times 10^{-3} + 2.00 \times 10^{-3}) \cot^2 44.3^\circ \\ &= 3.82 \times 10^{-3} \end{aligned}$$

From Eq. (9-5)

$$f_{2,max} = \frac{4.0}{0.8 + 170 \times 3.82 \times 10^{-3}} = 2.76 \text{ ksi (19.0 MPa)}$$

From Eq. (9-4) and Fig. 9-16b, the capacity of the strut is

$$\phi A_c f_{2,max} = 0.70 \times 16 \times (36 \sin 44.3^\circ + 29.5 \cos 44.3^\circ) \times 2.76 = 1430 \text{ kips (6360 kN)}$$

Hence the conditions at the bottom of the strut are somewhat more critical. As the capacity of the strut exceeds the required compression of 1289 kips (5730 kN), the capacities of the diagonal struts are adequate.

Step 6: Calculate the minimum reinforcement required for crack control.

The ACI Code (Ref. 9-23) requires uniformly distributed reinforcement in both the vertical and horizontal directions with minimum volumetric ratios of 0.0015 and 0.0025 respectively. We will use pairs of #4 (13 mm diameter) bars having an area of $2 \times 0.20 = 0.40 \text{ in}^2 (258 \text{ mm}^2)$. Hence the required spacing of the vertical reinforcement is

$$s < \frac{0.40}{0.0015 \times 16} = 16.7 \text{ in. (423 mm)} \\ < 18 \text{ in. (457 mm)} \\ < d/5 = (13 \times 12 - 0.5 \times 29.5)/5 = 141.3/5 = 28.3 \text{ in. (718 mm)}$$

Hence, to satisfy the vertical steel requirement, provide pairs of #4 (13 mm diameter) bars at 16 in. (406 mm) spacing.

The required spacing of the horizontal reinforcement is

$$s < \frac{0.40}{0.0025 \times 16} = 10.0 \text{ in. (254 mm)} \\ < 18 \text{ in. (457 mm)} \\ < d/3 = 141.3/3 = 47.1 \text{ in. (1196 mm)}$$

Hence, to satisfy the requirement for uniformly distributed horizontal reinforcement, provide pairs of #4 (13 mm diameter) bars at 10 in. (254 mm) spacing.

Step 7: Summarize the design.

The reinforcement details for the deep beam are shown in Fig. 9-35. Horizontal U-shaped bars have been added as shown in order to provide some restraint against vertical splitting at the ends of the beam.

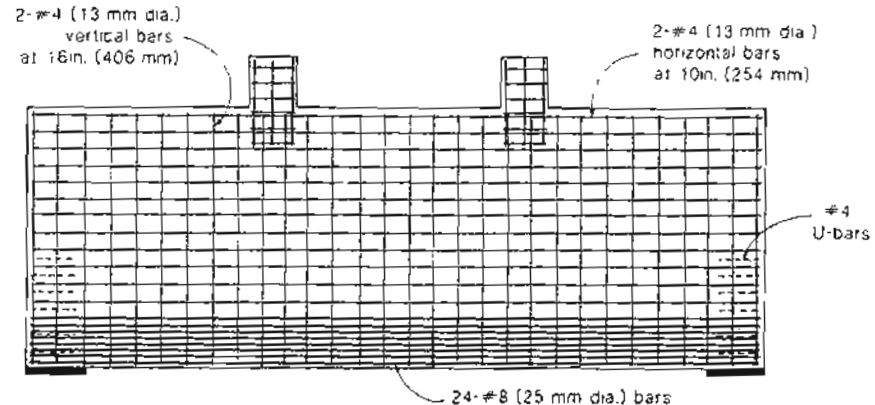


Figure 9-35 Reinforcement details of deep beam

9.10 EXAMPLE DESIGN OF POST-TENSIONED DEEP BEAM

The deep beam described in Section 9.9 will be redesigned with an alternative solution using post-tensioning.

Step 1: Choose the degree of post-tensioning.

One possible method of design is to provide a relatively small amount of post-tensioning such that $\phi A_{ps} f_{ps}$ is greater than or equal to the tension-tie force, N_u . This method would require tensile straining, ϵ_s , of the prestressing steel to attain a stress f_{ps} . The required tensile straining would result in a reduced compressive strength of the compressive struts in the vicinity of the tension tie as demonstrated in the non-prestressed solution given in Section 9.9.

Another approach is to provide a larger area of post-tensioning such that $\phi A_{ps} f_{ps}$ is greater than or equal to the tension-tie force, N_u . Since the post-tensioned steel is capable of carrying the necessary tension-tie force without additional tensile straining (i.e., $\epsilon_s = 0$), then the compressive struts in the vicinity of the tension tie can carry a compressive stress of $\phi 0.85 f'_c$. Similarly, the nodal zones at the bearing areas can also carry a compressive stress of $\phi 0.85 f'_c$. We will use this approach to design the deep beam.

Step 2: Check the bearing stresses at the supports.

In checking the bearing stresses at the supports we will need to account for the presence of the post-tensioning ducts over the bearing area. Since the ducts will be grouted, we will deduct one-half of their diameter from the thickness of the beam. If it is assumed

that pairs of 1.75 in. (44 mm) diameter grouted ducts are used, then the bearing stress at the support is

$$\frac{900}{(16 - 2 \times 0.5 \times 1.75) \times 36} = 1.75 \text{ ksi (12.1 MPa)}$$

The permissible stress for this nodal zone anchoring a post-tensioned tension tie is

$$\begin{aligned} 0.85\phi f'_c &= 0.85 \times 0.70 \times 4 \\ &= 2.38 \text{ ksi (16.4 MPa)} \end{aligned}$$

Hence the bearing capacity is sufficient.

Step 3: Estimate the geometry of the strut and tie model.

In the strut and tie model shown in Fig. 9-33 the permissible compressive stresses over the depth h_a and over the depth d_a are both $0.85\phi f'_c$ and hence, since $C = T$ then $d_a = h_a$. Equating the external and internal moments gives

$$\begin{aligned} 900 \times 11 \times 12 &= C \times (13 \times 12 - d_a) \\ &= 0.70 \times 0.85 \times 4 \times 16d_a(156 - d_a) \end{aligned}$$

Hence to satisfy the stress limits, the minimum value of d_a is 23.6 in. (599 mm). We will use the same strut and tie geometry as used in the non-prestressed concrete solution (see Section 9.9).

Step 4: Determine the forces in the struts and ties.

As determined in Section 9.9, $D = 1289$ kips (5730 kN) and $T = C = 923$ kips (4100 kN).

Step 5: Choose the reinforcement for the tension tie.

We will use high-strength, deformed prestressing bars with an ultimate strength, f_{pu} , of 150 ksi (1030 MPa). Assuming a stress in the prestressing steel of $f_{st} = 0.6f_{pu} = 0.6 \times 150 = 90$ ksi (620 MPa), the required area of prestressing steel, from Eq. (9-3) is

$$\begin{aligned} A_{ps} &\geq \frac{923}{0.90 \times 90} \\ &\approx 11.40 \text{ in}^2 (7350 \text{ mm}^2) \end{aligned}$$

From Table 3-6 we will choose eight 1 3/8 in. (36 mm) diameter threaded bars with 7 × 7.5 × 1.75 in. (178 × 191 × 44 mm) end-anchor plates (see Fig. 2-16) as shown in Fig. 9-36.

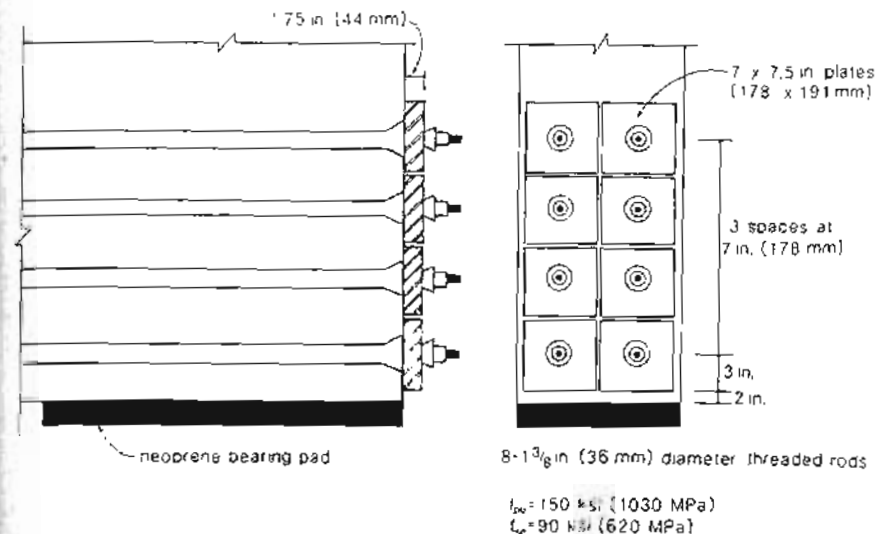


Figure 9-36 Post-tensioning details for deep beam.

Step 6: Check the capacities of the struts.

Since the additional strain, ϵ_c , required in the tension tie is zero, a higher stress of $0.85\phi f'_c$ is permitted in the bottom region of the diagonal compressive strut and hence the strut capacities are adequate (see Section 9.9).

Step 7: Calculate the minimum reinforcement for crack control.

The same uniformly distributed reinforcement provided in the non-prestressed solution (see Section 9.9) will be used in this post-tensioned deep beam.

Step 8: Summarize the post-tensioned solution.

The advantages of using post-tensioning are as follows:

1. The performance at service loads is improved with smaller deflections and no tensile stresses in the concrete at the bottom fiber.
2. The anchorage plates provide excellent anchorage of the tension tie at the outer face of the nodal zone above the supports.
3. The post-tensioning can be carried out in stages as the load is incrementally increased during construction (see Section 12.5) and hence deflections of the beam can be minimized.

9.11 SPECIAL CONSIDERATIONS FOR BEARING AREAS

In post-tensioned construction, use is often made of the ability of confined concrete to resist high bearing stresses. As discussed in Section 3.12, lateral confinement greatly increases the ability of concrete to resist compression. This confinement can be provided either by lateral reinforcement or by the presence of surrounding unloaded concrete.

The beneficial effect of surrounding unloaded concrete is accounted for by the following expression for the bearing stress:

$$f_{\text{bearing}} = 0.85 \phi f'_c \sqrt{\frac{A_2}{A_1}} \quad (9-13)$$

where

$$\sqrt{\frac{A_2}{A_1}} \leq 2.0$$

where A_1 is the net loaded area and A_2 is the maximum area of the portion of the supporting surface that is geometrically similar to and concentric with the loaded area (see Fig. 9-37). The amplification factor, $\sqrt{A_2/A_1}$, which was based on experimental studies by Hawkins (Ref. 9-27), is also recommended by the CEB-FIP Model Code (Ref. 9-28) except that in the CEB-FIP Code an upper limit of 3.3 is used rather than 2.0.

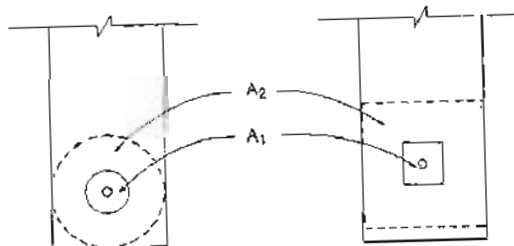


Figure 9-37 Definition of A_2 for determining permissible bearing stress.

Most post-tensioned systems incorporate spiral reinforcement behind the bearing area to confine the concrete and hence improve its bearing capacity (see Fig. 9-38). This special reinforcement, which is typically used for multi-strand anchorages, enables bearing stresses considerably higher than those given by Eq. (9-13) to be resisted safely. An estimate of the magnitude of the beneficial effect of this confining reinforcement can be obtained by using Eq. (3-22). A comprehensive study by Stone and Breen (Ref. 9-29) has shown that spiral reinforcement can increase the bearing capacity by more than 200%.

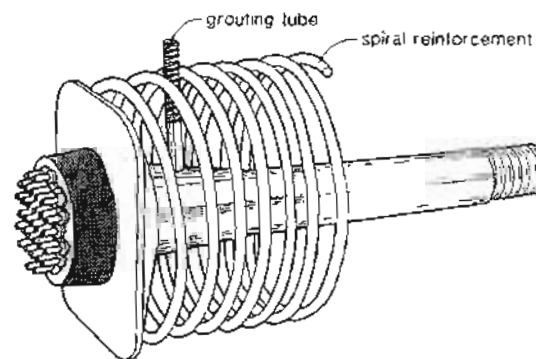


Figure 9-38 Typical spiral reinforcement to confine bearing area of post-tensioning anchorage.

9.12 SPECIAL CONSIDERATIONS WHERE TENDONS CHANGE DIRECTION

It is important to recognize that if a tendon deviates from a straight line, then radial stresses are induced between the tendon and the surrounding concrete. Thus, as can be seen in Fig. 9-39a, a tendon curving with a radius of R pushes against the concrete with a force of P/R per unit length, where P is the tension in the tendon. A "kink" in the tendon (see Fig. 9-39b) causes a force of $P\alpha$, where α is the angular deviation (in radians) of the tendon at the kink.

Even if a post-tensioned tendon is intended to be straight there will be small deviations from the intended straight line which will introduce transverse stresses in the concrete. Because these transverse stresses may crack the concrete as shown for the beam in Fig. 9-40, it is good practice to provide a minimum amount of transverse reinforcement in the webs of all post-tensioned beams.

The local radial force that a curved tendon imposes on the concrete has a tendency to split the concrete in the plane of the tendon. Walls or webs containing large, steeply curved tendons may require local reinforcement to control such potential splitting (see Fig. 9-41). The required amount of such reinforcement can be estimated using the strut and tie model shown in Fig. 9-41b.

Intermediate anchorages are often required in post-tensioned construction. Relatively large deviations in the tendon profile usually occur at these locations (see Fig. 9-42). Significant amounts of transverse reinforcement will be required at these locations to control potential cracking and to tie the tendon back into the concrete.

Particular care is needed in identifying regions of potential cracking in curved concrete structures. For example, a circular tank prestressed with tendons located at midthickness of the wall would seem to be subjected to only axial compressive stresses. However,

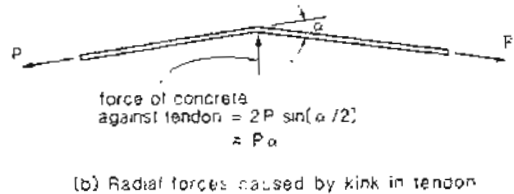
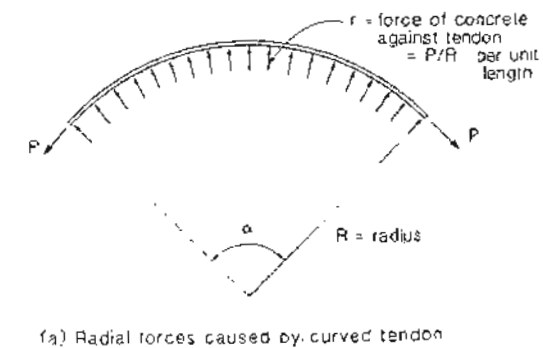


Figure 9-38 Radial forces caused by change in direction of tendon.

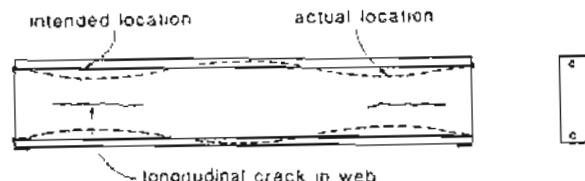


Figure 9-40 Unintended curvature due to tendon wobble, causing longitudinal cracks in web of beam.

Closer examination of the equilibrium of this structure reveals that because the inward radial forces imposed by the tendons are localized, while the outward radial forces of the concrete are distributed, local tensile stresses will be caused in the concrete. As shown in

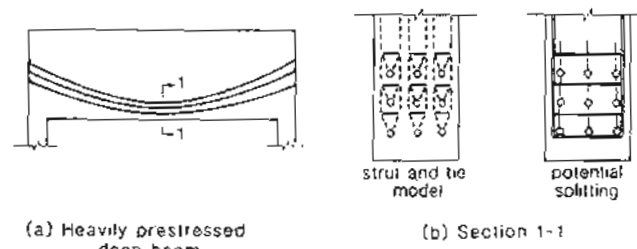
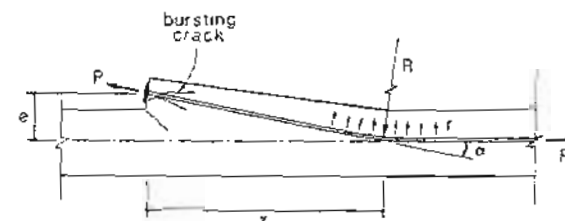


Figure 9-41 Curvature of tendons causing vertical splitting.



$$\text{total outward thrust from radial force, } r = Pa = P \frac{\theta}{x}$$

Figure 9-42 Radial forces at intermediate anchorage.

Fig. 9-43a, transverse tensions of magnitude $P/2R$ per unit length are required to equilibrate the curving compressive stresses in the outer half of the wall of the tank. These tensions will tend to cause vertical splitting cracks as shown in Fig. 9-43b. Locating the tendons closer to the outer face of the wall would decrease these tensions, while moving the tendons closer to the inner face would increase them. Transverse reinforcement through the thickness of the wall will control the splitting cracks that may result from these tensions. In addition, vertical reinforcement may be required to control horizontal cracks on the inner face resulting from dispersion of the inward radial compression (see Fig. 9-43b).

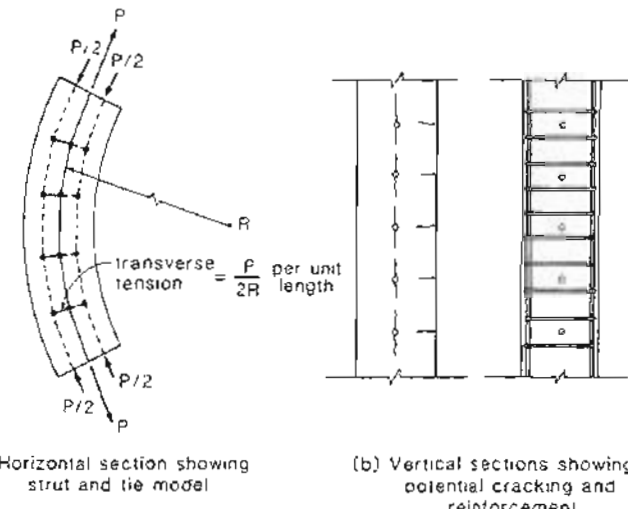


Figure 9-43 Circular tank prestressed with tendons located at midthickness of wall.

9.13 SHEAR TRANSFER ACROSS PLANES OF WEAKNESS — THE SHEAR FRICTION CONCEPT

There are many situations in prestressed concrete structures where it is necessary to transfer shear across planes of weakness such as interfaces between concretes cast at different times or interfaces between steel attachments and concrete. Examples of such situations are given in Fig. 9-44.

The shear-friction concept, introduced by Anderson in 1960 (Ref. 9-30), provides a simple but powerful design model to investigate situations such as those shown in Fig. 9-44. The basis of this model is explained in Fig. 9-45. Because the interface is rough, shear will cause not only a shear displacement but also a widening of the crack. This crack opening will cause tension in the reinforcement crossing the crack balanced by compressive stresses in concrete across the crack (see Fig. 9-45b). The shear stresses on the concrete face are assumed to be related to the compressive stresses on the face by a coefficient of friction μ . The maximum capacity is assumed to be reached when the reinforcement crossing the crack yields leading to a shear resistance of

$$V_n = A_{rf} f_y \mu \quad (9-14)$$

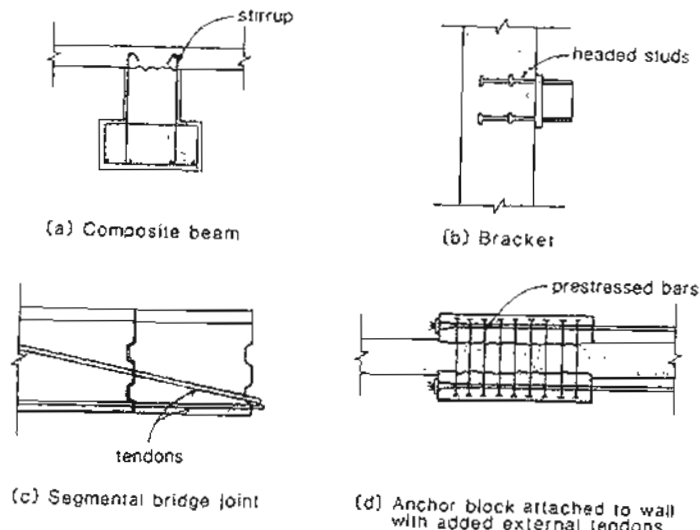


Figure 9-44 Examples where shear friction design is appropriate.

The ACI Code sets an upper limit for V_n as the smaller of $0.2 f'_c A_c$ and $800 A_c$ lb, where A_c is the area of the concrete section, in in^2 , resisting shear transfer. Values of the coefficient of friction specified by the ACI Code are given in Table 9-3.

Table 9-3 Values of coefficients of friction.

Crack Interface Conditions	Recommended μ^*
Concrete placed monolithically	1.4λ
Concrete placed against hardened concrete roughened to an amplitude of $1/4$ in. (6 mm)	1.0λ
Concrete placed against hardened concrete not intentionally roughened	0.6λ
Concrete anchored to structural steel by headed studs or reinforcing bars	0.7λ

*Where λ is 1.0 for normal-weight concrete, 0.85 for sand-lightweight concrete, and 0.75 for all-lightweight concrete.

Experimental and analytical studies have been conducted by among others, Fenwick and Paulay (Ref. 9-31), Mattock (Ref. 9-32), Shaikh (Ref. 9-33), Vecchio and Collins (Ref. 9-34), and Walraven, Frenay, and Pruijssers (Ref. 9-35) on the ability of cracked surfaces to transmit shear. These studies have shown that the relationship between the compressive stress across the crack and the shear which can be transmitted across the

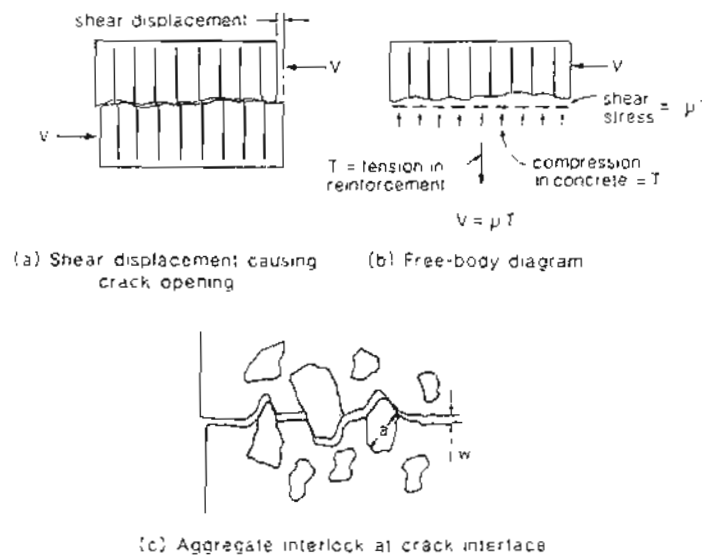


Figure 9-45 Shear friction concept.

crack is more complex than the shear friction model assumes. Figure 9-46 compares the form of this relationship predicted by a number of investigators. It can be seen that most of these investigators conclude that cracked surfaces are capable of transmitting shear stresses even when the compressive stress across the crack is zero. The relationship suggested by Vecchio and Collins illustrates the influence of crack width on the ability of cracked surfaces to transmit shear. It can be seen that the shear friction values of the ACI Code are conservative, particularly for small values of compressive stress.

9.14 DESIGN OF SHEAR INTERFACES OF COMPOSITE BEAMS

Figure 9-47 illustrates the determination of the longitudinal shear stress at a shear interface between precast and cast-in-place concrete. The average factored horizontal shear stress, v_n , between the maximum-moment section and the adjacent zero-moment section can be expressed as

$$v_n = \frac{C}{b_v l_{sh}} \quad (9-15)$$

where C = total force to be transmitted across the shear plane

b_v = width of shear interface

l_{sh} = distance between the maximum-moment section and the adjacent zero-moment section

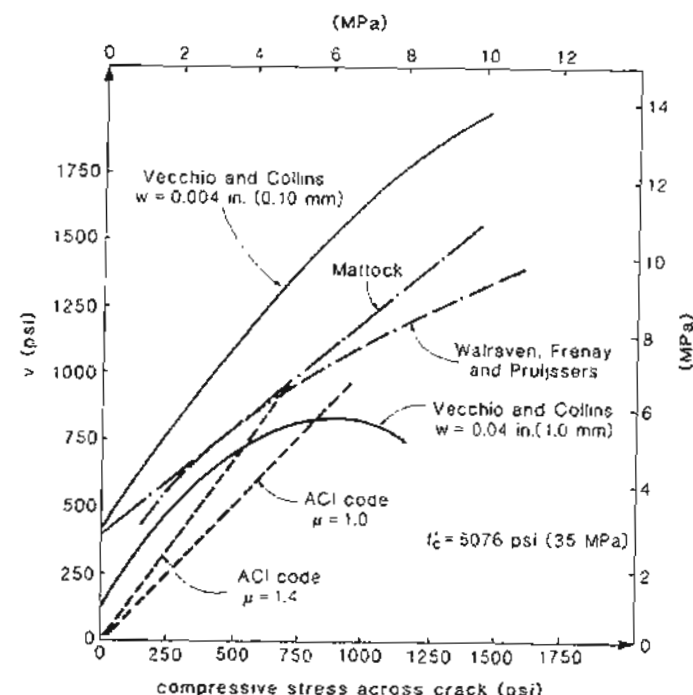


Figure 9-46 Comparison of suggested relationships between shear stress that can be transmitted across the crack and compressive stress across the crack.

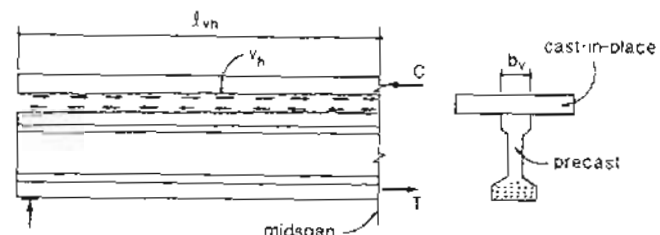


Figure 9-47 Investigating longitudinal shear at interface of composite members.

Care must be taken during construction to ensure that all interface surfaces are clean and free of laitance. The ACI Code (Ref. 9-23) limits v_n to 80 psi (0.55 MPa) for surfaces that are intentionally roughened or contain minimum ties across the interface. If minimum ties are present and the contact surface is intentionally roughened to a full amplitude of 1/4 in. (6 mm), then v_n is limited to 350 psi (2.41 MPa). If the factored shear stress exceeds 350 psi (2.41 MPa), then the total area of shear reinforcement crossing the shear interface is determined by the shear friction expression given in Eq. (9-14).

References

- 9-1 Zellerer, E., and Thiel, H. "Über das Kraftfeld einer Stahlbetonwand mit einer Türöffnung unter unsymmetrisch wirkender Einzellast" (Concerning the Stressfield of a Reinforced Concrete Wall with a Door Opening Subjected to an Unsymmetrically Acting Concentrated Load). *Beton und Stahlbetonbau*, Vol. 51, No. 12, Dec. 1956, pp. 267-274.
- 9-2 Guyon, Y., *Béton précontrainte - Etude théorique et expérimentale*. Editions Eyrolles, Paris, 1951. Also available as *Prestressed Concrete*, John Wiley & Sons Inc., New York, 1960.
- 9-3 Iyengar, K.T.S.R., "Two-Dimensional Theories of Anchorage Zone Stresses in Post-Tensioned Prestressed Beams." *ACI Journal*, Vol. 59, No. 10, Oct. 1962, pp. 1443-1446.
- 9-4 Leonhardt, F. *Prestressed Concrete - Design and Construction*, English translation, 2nd ed., Wilhelm Ernst und Sohn, Berlin, 1964, 677 pp.
- 9-5 Mörsch, E., "Über die Berechnung der Gelenkguader" (Design of Joints). *Beton und Eisen*, No. 12, 1924, pp. 156-161.
- 9-6 Kammerhuber, J., and Schneider, J., *Arbeitsunterlagen für die Berechnung vorgespannter Konstruktionen* (Notes on the Design of Prestressed Concrete Construction), RA Verlag, Rapperswil, Switzerland, 1974, 197 pp.
- 9-7 Sargious, M., "Beitrag zur Ermittlung der Hauptzugspannungen am Endauflager vorgespannter Betonbalken" (Determination of Tension Forces in the End Region of Concrete Beams). Doctoral dissertation, Technical University of Stuttgart, Stuttgart, West Germany, 1960.
- 9-8 Mehlhorn, G., "Massivbau-Grundlagen II" (Principles of Structures II), Institut für Massivbau, Technische Hochschule, Darmstadt, West Germany, Winter semester, 1980/81.
- 9-9 Leonhardt, F., and Walther, R., "Wandartiger Träger" (Deep Beams). Bulletin No. 178, Deutscher Ausschuss für Stahlbeton, Wilhelm Ernst und Sohn, Berlin, 1966, 159 pp.
- 9-10 Magnel, G., *Prestressed Concrete*, 3rd ed., McGraw-Hill Book Company, New York, 1954, 345 pp.
- 9-11 Gergely, P., and Sozen, M.A., "Design of Anchorage Zone Reinforcement in Prestressed Concrete Beams." *PCI Journal*, Vol. 12, No. 2, Apr. 1967, pp. 63-75.
- 9-12 Ngo, D., and Scordelis, A.C., "Finite Element Analysis of Reinforced Concrete Beams." *ACI Journal*, Vol. 64, No. 3, Mar. 1967, pp. 152-163.
- 9-13 ASCE Task Force, *State-of-the-Art Report on Finite Element Analysis of Reinforced Concrete*, American Society of Civil Engineers, New York, 1981, 545 pp.
- 9-14 Adegbie, L.N., and Collins, M.P., "A Finite Element Model for Studying Reinforced Concrete Detailing Problems," Publication No. 86-12, Department of Civil Engineering, University of Toronto, Oct. 1986, 267 pp.
- 9-15 Cook, W.D., and Mitchell, D., "Studies of Disturbed Regions near Discontinuities in Reinforced Concrete Members." *ACI Structural Journal*, Vol. 85, No. 2, Mar.-Apr. 1988, pp. 206-216.
- 9-16 Vecchio, F.J., "Nonlinear Finite Element Analysis of Reinforced Concrete Membranes." *ACI Structural Journal*, Vol. 86, No. 1, Jan.-Feb. 1989, pp. 26-35.
- 9-17 Rogowsky, D.M., MacGregor, J.G., and Ong, S.Y., "Tensile of Reinforced Concrete Deep Beams." *ACI Journal*, Vol. 83, No. 4, July-Aug. 1986, pp. 614-623.

- 9-18 Mörsch, E., "Concrete-Steel Construction", McGraw-Hill Book Company, New York, 1909, 368 pp. (English translation by E.P. Goodrich, from third edition of *Der Eisenbetonbau*, first edition, 1902.)
- 9-19 Schlaich, J., Schafer, K., and Jennewein, M., "Towards a Consistent Design of Reinforced Concrete Structures," *PCI Journal*, Vol. 32, No. 3, May-June 1987, pp. 74-150.
- 9-20 Marti, P., "Basic Tools of Reinforced Concrete Beam Design," *ACI Journal*, Vol. 82, No. 1, Jan.-Feb. 1985, pp. 46-56.
- 9-21 CSA Committee A23.3, *Design of Concrete Structures for Buildings*, CAN3-A23.3-M84, Canadian Standards Association, Rexdale, Canada, 1984, 281 pp.
- 9-22 Collins, M.P., and Mitchell, D., "A Rational Approach to Shear Design - The 1984 Canadian Code Provisions," *ACI Journal*, Vol. 83, No. 6, Nov.-Dec. 1986, pp. 925-933.
- 9-23 ACI Committee 318, "Building Code Requirements for Reinforced Concrete (ACI 318-89) and Commentary - ACI 318 R-89," American Concrete Institute, Detroit, 1989, 353 pp.
- 9-24 Karl, M.W., Huggins, M.W., and Wittkopp, R.R., *Karl on Shear in Reinforced Concrete*, Department of Civil Engineering, University of Toronto, Toronto, 1979, 225 pp.
- 9-25 Mattock, A.H., Chen, K.C., and Soongswang, K., "The Behavior of Reinforced Concrete Corbels," *PCI Journal*, Vol. 21, No. 2, Mar.-Apr. 1976, pp. 52-77.
- 9-26 Mattock, A.H., and Theryo, T.S., "Strength of Precast Prestressed Concrete Members with Dapped Ends," *PCI Journal*, Vol. 31, No. 5, Sept.-Oct. 1986, pp. 58-75.
- 9-27 Hawkins, N.M., "The Bearing Strength of Concrete for Strip Loadings," *Magazine of Concrete Research*, Vol. 22, No. 71, June 1970, pp. 87-98.
- 9-28 CEB-FIP, *Model Code for Concrete Structures*, CEB-FIP International Recommendations, 3rd ed., Comité Euro-International du Béton, Paris, 1978, 348 pp.
- 9-29 Stone, W.C., and Breen, J.E., "Behavior of Post-Tensioned Girder Anchorage Zones," *PCI Journal*, Vol. 29, No. 1, Jan.-Feb. 1984, pp. 64-109.
- 9-30 Anderson, A.R., "Composite Designs in Precast and Cast-in-Place Concrete," *Progressive Architecture*, Sept. 1960, pp. 172-179.
- 9-31 Fenwick, R.C., and Paulay, T., "Mechanisms of Shear Resistance of Concrete Beams," *Journal of the Structural Division, ASCE*, Vol. 94, ST10, Oct. 1968, pp. 2235-2350.
- 9-32 Mattock, A.H., "Design Proposals for Reinforced Concrete Corbels," *PCI Journal*, Vol. 21, No. 3, May-June 1976, pp. 18-42.
- 9-33 Shaikh, A.F., "Proposed Revisions to Shear Friction Provisions," *PCI Journal*, Vol. 23, No. 2, Mar.-Apr. 1978, pp. 12-21.
- 9-34 Vecchio, F.J., and Collins, M.P., "The Modified Compression Field Theory for Reinforced Concrete Elements Subjected to Shear," *ACI Journal*, Vol. 83, No. 2, Mar.-Apr. 1986, pp. 219-231.
- 9-35 Walraven, J., Frenay, J., and Pruijssers, A., "Influence of Concrete Strength and Load History on the Shear Friction Capacity of Concrete Members," *PCI Journal*, Vol. 32, No. 1, Jan.-Feb. 1987, pp. 66-84.

Demonstration Problems

- 9-1 Using strut and tie models, compute the required tension-tie forces for the four different anchorage zones shown in Fig. 9-25. Assume that h_0/h_i is 0.10. Compare the required tension-tie forces with those obtained from the application of the deep beam analogy shown in Fig. 9-10.
- 9-2 Choose the bearing details and design the corbel shown in Fig. 9-48. The specified 28-day concrete strength is 5000 psi (34.5 MPa) and the yield stress of the reinforcement is 60 ksi (414 MPa) the corbel is subjected to the vertical and horizontal factored loads as shown. Prepare a drawing of the resulting reinforcement.

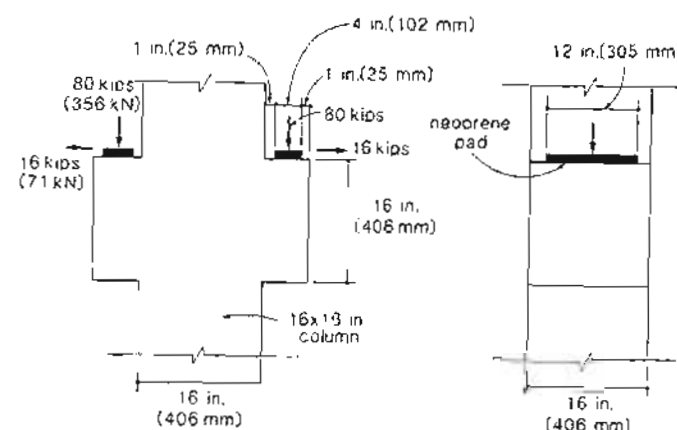


Figure 9-48 Rectangular corbel.

- 9-3 Using a strut and tie model, design the bottom ledge of the spandrel beam shown in Fig. 9-49. Also design the additional hanger reinforcement required to transfer the force from the ledge into the spandrel beam. The 20 in. (500 mm) deep double tees are simply supported and span 32 ft (10 m). The service live load is 50 psf (2.4 kN/m²) and the superimposed dead load is 15 psf (0.72 kN/m²).
- 9-4 A circular prestressed concrete containment structure for a nuclear power plant similar to that shown in Fig. 1-18 has an internal diameter of 80 ft (24.4 m) and a wall thickness of 30 in. (762 mm). Choose the circumferential post-tensioning such that under an internal overpressure of 70 psi (0.48 MPa), a residual compression of 50 psi (0.35 MPa) still exists in the wall. Sketch a suitable tendon layout and investigate whether transverse reinforcement through the thickness of the wall is required. Assume that when the structure is post-tensioned, the concrete strength is 3500 psi (24.1 MPa).
- 9-5 The circular containment structure described in Prob. 9-4 has four buttresses to anchor the circumferential tendons. Each tendon travels 180° around the tank and hence half of the

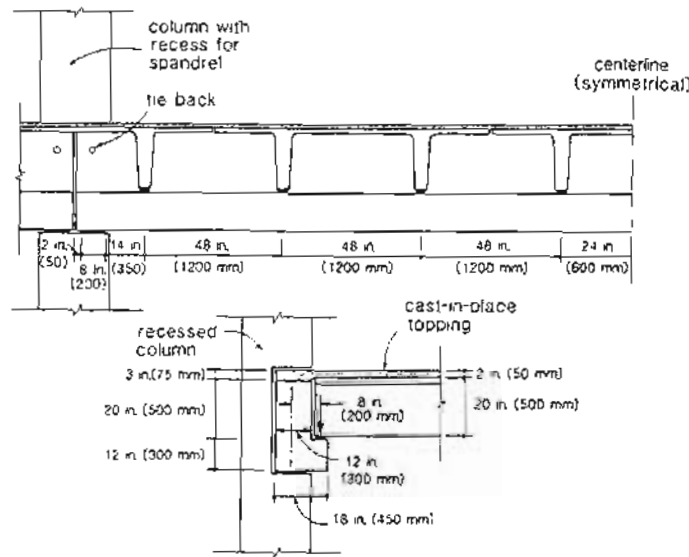


Figure 9-49 Framing of double tees and spandrel beam.

tendons are anchored at each buttress (see Fig. 1-18). For the tendon arrangement chosen in the solution to Prob. 9-4 choose appropriate dimensions for the buttress and design appropriate reinforcement for this buttress.

- 9-6 The deck of a box-spandrel bridge is transversely post-tensioned with 1 1/4 in. (32 mm) diameter Dwyidag bars having an area of 1.25 in^2 (804 mm^2) spaced at every 20 in. (508 mm) along the length of the bridge as shown in Fig. 9-50. Check the size of the bearing plate and calculate the amount of longitudinal reinforcement required to control potential transverse splitting of the concrete. Assume that the concrete strength when the bars are post-tensioned is 5000 psi (35 MPa).

- 9-7 Using a strut and tie model, design the reinforcement for the wall with an opening shown in Fig. 9-51. Assume that $f'_c = 3500 \text{ psi}$ (24.1 MPa).

- 9-8 Using a strut and tie model design the reinforcement for the deep beam with an opening shown in Fig. 9-3a. Assume that the factored load applied to the wall is 350 kips (1590 kN) and that the wall is 14 in. (356 mm) thick. Use $f'_c = 4000 \text{ psi}$ (27.6 MPa) and $f_{yv} = 60 \text{ ksi}$ (414 MPa).

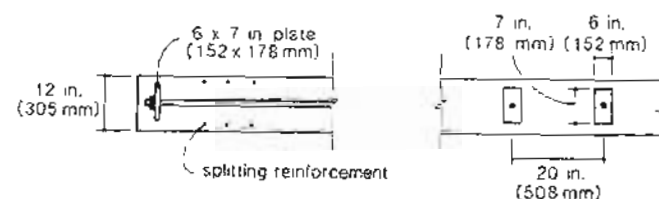


Figure 9-50 Anchorage details for transverse post-tensioning.

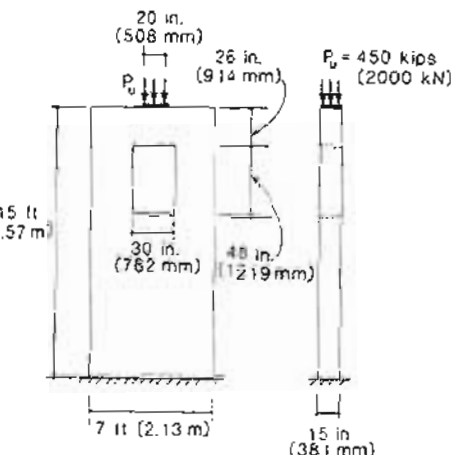


Figure 9-51 Wall containing opening.

Statically Indeterminate Structures

Except in special cases ... the statically indeterminate reactions for a beam supported at more than two points are altered by prestressing.

Gustave Magnel, 1954

10.1 INTRODUCTION

The stress resultants (moments, axial loads, shears, etc.) at the different locations within a statically indeterminate structure cannot be determined from statics alone. Element stiffnesses and geometric compatibility must also be considered.

Because the actions in statically indeterminate structures are affected by geometric considerations, actions can be caused by imposed deformations as well as by imposed loads. Thus for the two-span bridge shown in Fig. 10-1, bending moments can be caused not only by the weight of a truck, but also by settlement of one of the supports. The moments due to settlement shown in Fig. 10-1b occur because the statically indeterminate structure is not free to follow the imposed deformation. It is restrained by its stiffness. We will call these actions resulting from the restraint of imposed deformations "restraint actions."

In examining whether the truck is likely to cause the bridge to fail, we compare the moments caused by the truck with the flexural strength of the bridge section. In examining whether the settlement is likely to cause the bridge to fail, we should compare the required deformations with the ability of the bridge to deform. Because of the nonlinear nature of the load-deformation response of reinforced and prestressed concrete sections, it is not appropriate to treat these two different types of actions in the same manner.

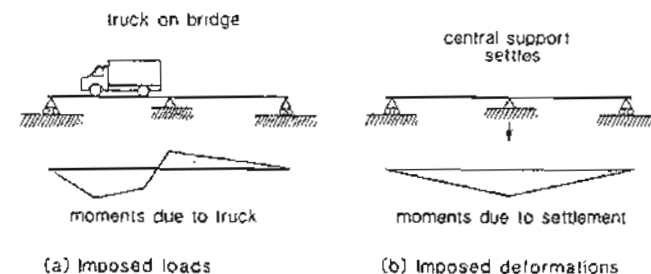


Figure 10-1 Actions due to imposed loads and imposed deformations.

To stress the importance of distinguishing between different stresses that might occur in prestressed concrete structures, Leonhardt (Ref. 10-1) quotes the definitions for three types of stress given in earlier German codes. These three types of stress are described in Fig. 10-2.

type	load stresses	restraint stresses	eigenstresses
definition	Stresses caused by external loads (dead loads, live loads, etc.)	Stresses caused by restraint of deformation. Only occurs in statically indeterminate structures.	Self-equilibrating stresses. At each section they sum to zero. They cause no bearing reactions.
example	 moments	 moments	 moments = 0
			Note that the cause of the eigenstresses may also cause restraint stresses.

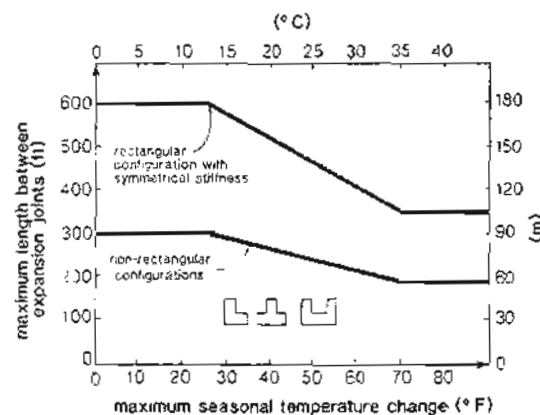
Figure 10-2 Three different types of stress.

In this chapter we will review how restraint actions in statically indeterminate prestressed concrete structures can be calculated, how they change with time, and how they are influenced by the sequence of construction. We will also discuss how these actions should be treated in the design of prestressed concrete structures.

10.2 RESTRAINT ACTIONS IN PRESTRESSED CONCRETE STRUCTURES

Restraint actions in prestressed concrete structures can be caused by volume changes of the concrete due to temperature changes or shrinkage, or they may be caused by deformations resulting from the prestress.

In non-prestressed concrete buildings, restraint actions due to volume changes are usually controlled by providing "expansion joints," which serve to subdivide the structure. These joints are often located by "rules of thumb." One set of such rules, which comes from Ref. 10-2 and is quoted in the *PCI Design Handbook* (Ref. 10-3), is given in Fig. 10-3.



Modification factors:

- For heated buildings with hinged-column bases, use length specified.
- For air-conditioned as well as heated buildings increase allowable length by 15 percent.
- For unheated buildings, decrease the allowable length by 33 percent.
- For fixed-column bases, decrease the allowable length by 15 percent.
- For eccentric stiffness against lateral displacement decrease the allowable length by 25 percent.

Figure 10-3 Recommended maximum length between expansion joints.
Adapted from Ref. 10-3. See Fig. 3-19 for seasonal temperature changes.

While rules such as those given in Fig. 10-3 can be used as a guide in the design of prestressed concrete structures, it will often be appropriate to make more detailed evaluations of volume change effects. In making these evaluations of volume change effects, we should recognize that in typical structures it is the shortening of the beams which causes significant restraint actions. As the beams shorten they try to drag the columns with them (see Fig. 10-4). Thus restraint forces are reduced if stiff vertical elements are placed close to the center of stiffness of the structure, or if the stiffness of vertical elements is reduced.

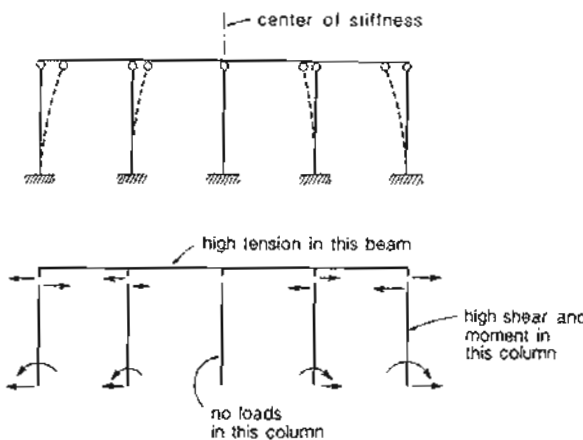


Figure 10-4 Restraint actions caused by shortening of beams.

We have seen that a typical prestressed concrete member is deformed even when no external loads are acting and that these axial and flexural deformations increase with time (see Figs. 4-8 and 5-21). In a statically indeterminate structure these deformations due to prestress will typically be restrained, giving rise to restraint actions.

Thus if the beams of the multistory frame shown in Fig. 10-5 are post-tensioned, they will all try to shorten. However, the foundation will prevent the base of the columns from moving in along with the beams. Hence restraint forces from the foundation will bend the ground-level columns and will cause an axial tensile force in the second-floor beams.

Post-tensioning of the two-span beam shown in Fig. 10-6 with a straight, eccentric tendon would cause the beam to try to lift off the center support. The restraint forces required to hold the beam on the support would cause shears and moments in the beam. These restraint moments, M_r , are often referred to as "secondary moments." It is characteristic of restraint moment diagrams that they vary linearly between supports. This is because the restraint forces causing these moments arise only at the supports.

10.3 CALCULATION OF DEFORMATIONS

Because restraint moments arise from the restraint of deformations, it is appropriate to review procedures for calculating deformations. The curvature of a member due to prestressing can either be calculated from the strain compatibility approach or from the "force-in-tendon" approach reviewed in Section 6.5. For post-tensioned members, the latter approach is often more convenient.

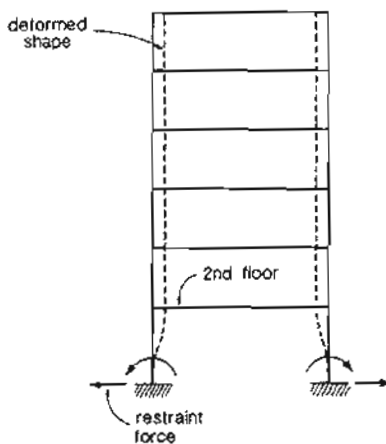


Figure 10-5 Restraint forces caused by post-tensioning of beams.

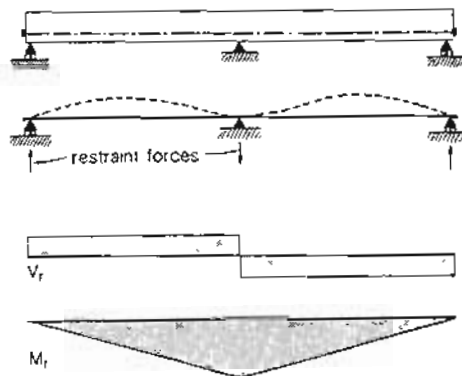


Figure 10-6 Restraint actions caused by post-tensioning two-span beam.

When a statically determinate beam is post-tensioned, the tension force P in the tendon must be balanced by an equal compressive force P on the concrete. If the concrete remains elastic and uncracked, this force P at an eccentricity of e will result in the concrete strain distribution described in Fig. 10-7.

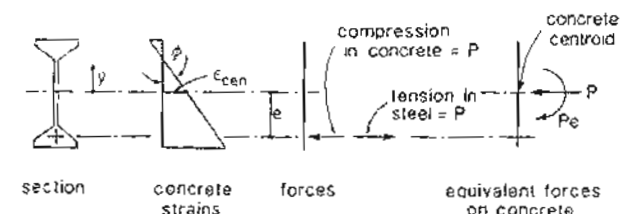


Figure 10-7 Concrete strains due to prestressing.

The strain at the concrete centroid due to the prestressing is thus

$$\epsilon_{cen} = -\frac{P}{E_c A_c} \quad (10-1)$$

where A_c is the area of concrete. The curvature due to prestressing is

$$\phi = \frac{Pe}{E_c I_c} \quad (10-2)$$

where I_c is the second moment of area of the concrete section about the centroid of the concrete area, and e is the eccentricity of the prestressing tendon from the centroid of the concrete.

The moment-area procedures that can be used to calculate the deflections of beams from the known curvatures have been discussed in Sections 5.13 and 5.14. In calculating the deflections of frames it is sometimes more convenient to use procedures based on the principle of virtual work.

The principle of virtual work states that if for a particular structure we have a force system in which the external forces are in equilibrium with the internal stresses and we have a displacement system in which the external displacements are compatible with the internal strains, then the external work done by the external forces moving through the external displacements will be equal to the internal work done by the stresses moving through the strains.

For our purposes the displacement system we will use will be the actual sectional strains (ϵ_{cen}, ϕ) and their resulting displacements, while the force system will consist of a unit external force at the location and in the sense of the external displacement we wish to find, combined with sectional actions that are in equilibrium with this unit force. We will explain the procedure by means of an example.

10.4 USE OF VIRTUAL WORK TO CALCULATE DEFLECTION

As an example of the use of the principle of virtual work, we will derive an expression for the horizontal deflection of support D of the frame shown in Fig. 10-8 when the frictionless

tendon is stressed to a force of P . The external work done by the external forces of Fig. 10-9a is equal to $1^* \times \Delta = \Delta$. Note 9d acting through the external displacements of Fig. 10-9a is equal to $1^* \times \Delta = \Delta$. Note that the forces and stresses associated with the force system have been identified by an asterisk.

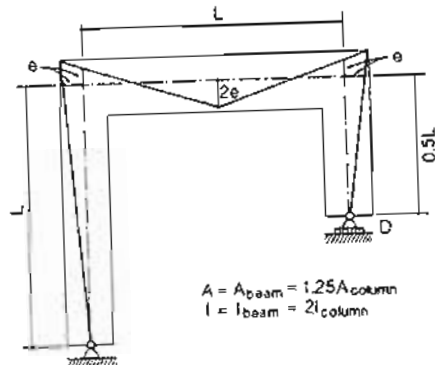


Figure 10-8 Post-tensioning frame.

The internal work done when the stresses σ^* , associated with the force system, act through the strains, ϵ , associated with the displacement system could be found by evaluating the integral $\int_v \sigma^* \epsilon dv$ over the volume. For structures consisting of linear elements, the internal work is more conveniently evaluated by integrating the product of the sectional actions times the sectional displacements along the length. That is,

$$\text{Internal work} = \int_L M^* \phi dx + \int_L N^* \epsilon_{cen} dx \quad (10-3)$$

In a more general situation the expression for the internal work could be expanded to include all six possible stress resultants times the corresponding six strain resultants.

Evaluating the integrals of Eq. (10-3) is analogous to finding the volume of a solid, whose plan is given by the M^* or N^* diagram and whose elevation is given by the ϕ or ϵ_{cen} diagram. Figure 10-10 is useful in evaluating these volume integrals. Thus, in our example we evaluate the internal work by calculating the relevant volume integrals, piece by piece, around the frame: first column AB, then beam BC, then column CD. Note that the $M^* \phi$ integral for beam BC is evaluated first for the left half of the beam and then for the $M^* \phi$ integral for beam BC is evaluated first for the left half of the beam and then for

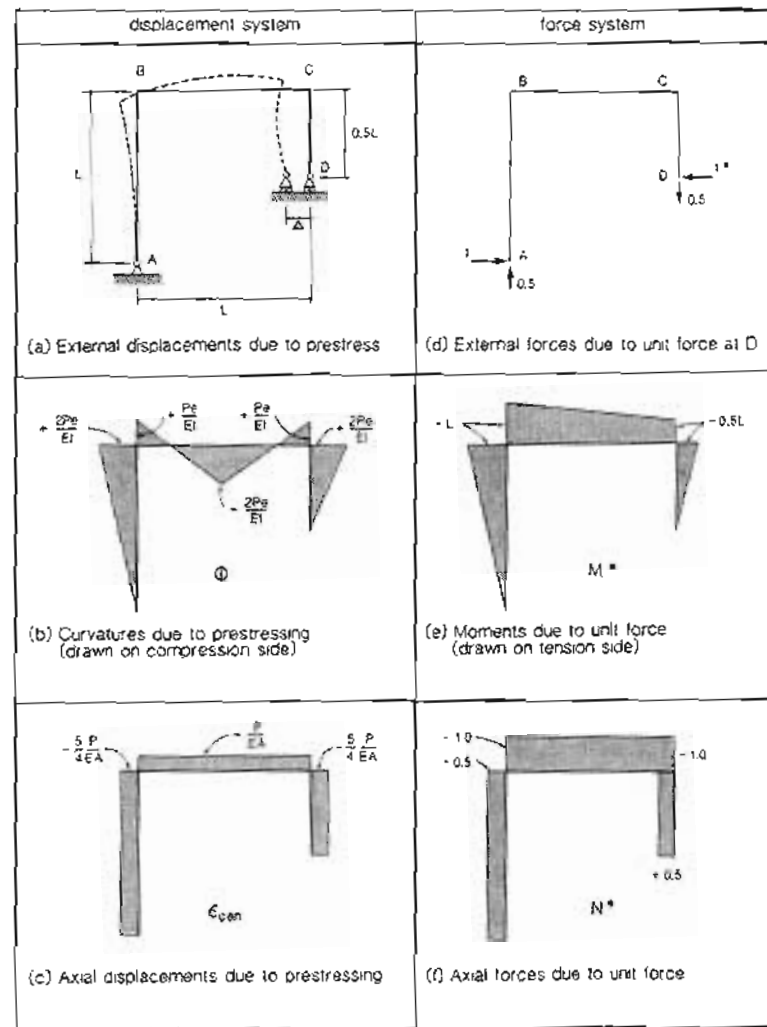


Figure 10-9 Application of principle of virtual work to a prestressed frame.

the right half using the expression in box 12 of Fig. 10-10. Hence

$$\begin{aligned}\Delta &= \int_L M^* \phi \, dx + \int_L N^* \epsilon_{con} \, dx \\ &= \frac{1}{3} \cdot L \left(-L \frac{2P_c}{EI} + \frac{1}{6} \cdot \frac{L}{2} \left[-L \left(2 \frac{P_c}{EI} - \frac{2Pe}{EI} \right) - 0.75L \left(\frac{P_c}{EI} - 2 \frac{Pe}{EI} \right) \right] \right. \\ &\quad \left. + \frac{1}{6} \cdot \frac{L}{2} \left[-0.75L \left(-2 \frac{Pe}{EI} + \frac{Pe}{EI} \right) - 0.5L \left(-\frac{2Pe}{EI} + 2 \frac{Pe}{EI} \right) \right] \right. \\ &\quad \left. + \frac{1}{3} \cdot \frac{L}{2} (-0.5L) \frac{2Pe}{EI} + L(-0.5) \left(-\frac{5}{4} \frac{P}{EA} \right) + L(-1.0) \left(-\frac{P}{EA} \right) \right. \\ &\quad \left. + \frac{L}{2} (+0.5) \left(-\frac{5}{4} \frac{P}{EA} \right) \right] \\ &= \frac{PeL^2}{EI} \left(-\frac{2}{3} - \frac{1}{6} + \frac{1}{6} - \frac{3}{48} + \frac{1}{4} + \frac{1}{4} - \frac{3}{48} + \frac{1}{12} - \frac{1}{12} - \frac{1}{6} \right) \\ &\quad + \frac{PL}{EA} \left(+\frac{5}{8} + 1 - \frac{5}{16} \right) = -\frac{22 PeL^2}{48 EI} + \frac{63 PL}{48 EA}\end{aligned}$$

The negative sign on the calculated deflection term indicates that this component causes a deflection in a direction opposite to that of the unit force.

10.5 CALCULATION OF RESTRAINT ACTIONS – FLEXIBILITY APPROACH

In the flexibility approach to determining actions in a statically indeterminate structure, we first release redundant forces and make the structure statically determinate. Then we use the compatibility requirements at the releases and the calculated flexibility of the structure to determine the magnitude of the redundant forces.

As an example of the flexibility approach, let us consider the two-span beam shown in Fig. 10-11 and let us calculate the restraint actions caused when the straight, eccentric tendon in this beam is post-tensioned to a tension of P .

To make the two-span beam statically determinate, we will remove the middle support at C. With this support gone the beam would deflect upward due to the curvature caused by the prestress. The curvature for this beam of constant cross section would depend only on the eccentricity, e , and hence the curvature diagram would look like the shaded eccentricity diagram shown in Fig. 10-11.

From the moment-area theorem the displacement at the released central support (see Fig. 10-12) would be

$$\Delta_{ca} = L \frac{Pe}{EI} \frac{L}{2} = \frac{PeL^2}{2EI}$$

The next step of the procedure is to calculate the flexibility of the released structure. That is, how much deflection is caused by a unit value of the released redundant force?

plan	1	2	3
elevation	4	$\frac{Lae}{2}$	$\frac{La(a+b)}{2}$
	5	$\frac{Lae}{3}$	$\frac{La(2a+b)}{8}$
	6	$\frac{Lae}{2}$	$\frac{La(a+2b)}{6}$
	7	$\frac{Lae}{6}$	12
	8	$\frac{La(2c+d)}{6}$	$\frac{La(3c+d) - La(d+2a)}{6}$
	9		
	10	$\frac{La(c+d)}{2}$	
	11	$\frac{La(2c+d)}{6}$	
	12		
	13	$\frac{La(c+2d)}{6}$	$\frac{La(c+2d) + La(2d+e)}{6}$
	14	$\frac{La(c+d)}{6}$	
	15		

Figure 10-10 Common volume integrals.

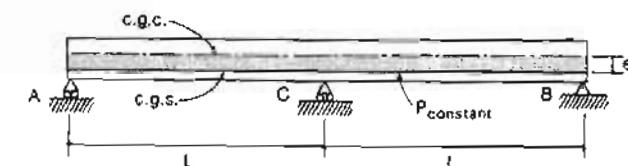


Figure 10-11 Two-span, post-tensioned beam. Eccentricity of tendon shaded.

It can be seen from Fig. 10-13 that a unit load at location C will cause a deflection at C of

$$\Delta_{c1} = \frac{1}{2} L \frac{L}{2EI} \frac{2}{3} L = \frac{L^3}{6EI}$$



Figure 10-12 Deflection at released support.

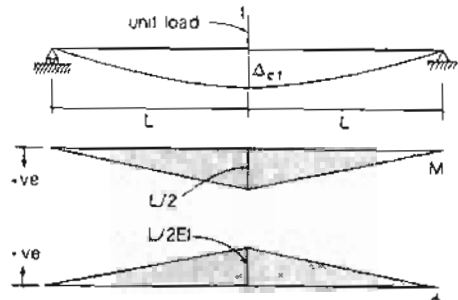


Figure 10-13 Flexibility of released structure.

The compatibility requirement is that the deflection at C must be zero. Thus, for a redundant force of X ,

$$\Delta_{co} = X \Delta_{cl}$$

Hence

$$X = \frac{\Delta_{co}}{\Delta_{cl}} = \frac{P_e L^2}{2EI} \frac{6EI}{L^3} = \frac{3P_e}{L}$$

Knowing the redundant forces, we can calculate the restraint actions (see Fig. 10-14). Note that in this case, the restraint moment, or so-called "secondary moment," has a magnitude 50% larger than the term P_e , which is sometimes referred to as the "primary moment."

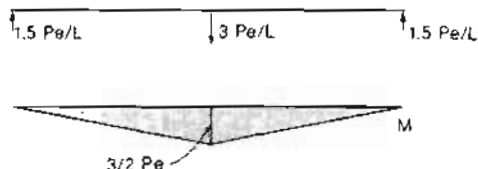


Figure 10-14 Restraint actions due to prestressing.

As a second example of finding restraint actions by the flexibility approach, a fixed-ended beam with a harped tendon is considered in Fig. 10-15. Note that because restraint

moments are caused by forces acting at supports (or joints), the restraint moment diagram is always linear between supports (or joints).

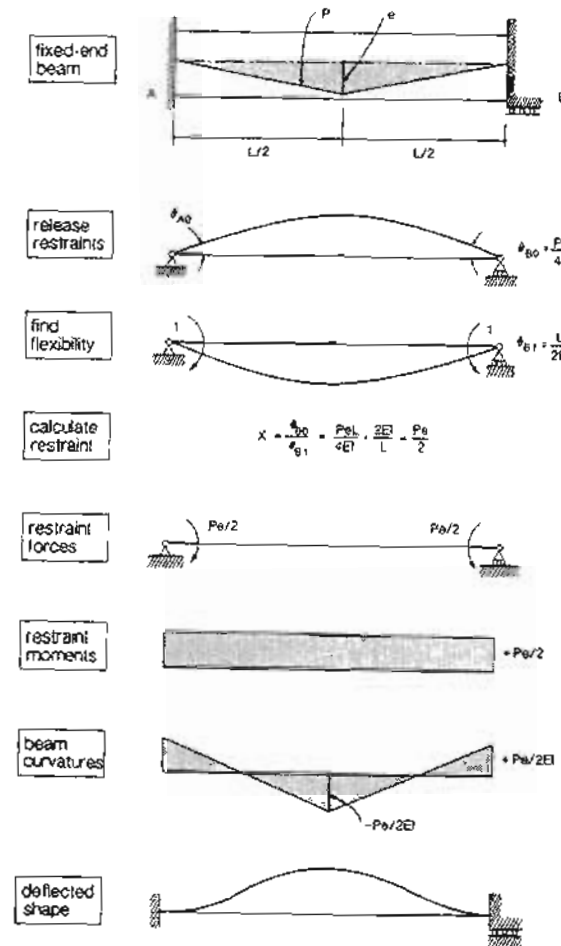


Figure 10-15 Calculation of restraint moments caused by prestressing a fixed-ended beam.

10.6 FINDING RESTRAINT ACTIONS BY MOMENT DISTRIBUTION

The well-known moment distribution method, developed by Hardy Cross (Ref. 10-4), may be summarized as follows. We first lock the joints against displacement and thus make the structure geometrically determinate. For this condition, the end actions developed on the members are calculated (fixed-end moments). Each joint is then successively released and relocked, in turn, as often as is required, until each joint has displaced to its equilibrium condition (i.e., statics are satisfied). As each joint is released, the unbalanced action at the joint is distributed between the members meeting at the joint in proportion to their relative resistances to rotation (distribution factors). As an action is applied to the near end of a member, an action is also induced at the far end of the member (carry-over factor). Figure 10-16 gives some useful information on flexural stiffnesses and carry-over factors.

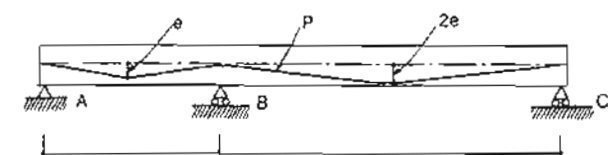
boundary conditions	A 	A 	A 	A 	A 	A 
K _{AB}	$\frac{4EI}{L}$	$\frac{2EI}{L}$	0	$\frac{EI}{L}$	$\frac{2EI}{L}$	$\frac{6EI}{L}$
carry-over factor	0.5	0	0	-1.0	-	-

Figure 10-16 Stiffnesses and carry-over factors for members with uniform EI.

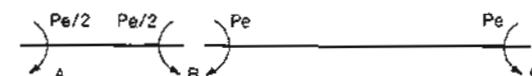
As an example of finding restraint moments using moment distribution, let us calculate the restraint moments produced when the two-span beam, shown in Fig. 10-17a, is post-tensioned. First, we find the moments required at the ends of each beam segment to hold these ends against rotation. In this case these fixed-end moments, shown in Fig. 10-17b, can be found from the expression in Fig. 10-15. Next, we find the relative stiffnesses of members BA and BC. As we will first release, and leave released, joints A and C, both BA and BC will be members unrestrained against rotation at their far ends. Hence the distribution factors can be found from the ratio of stiffnesses as follows:

$$K_{BA} : K_{BC} = \frac{3EI}{L} : \frac{3EI}{2L} = 2 : 1 = \frac{2}{3} : \frac{1}{3}$$

We can now proceed to perform the moment distribution (see Fig. 10-18). Note that we have used the sign convention that a clockwise couple applied to the end of a member is positive. Knowing the restraint couples applied to the ends of the members, we can calculate the restraint reactions and the restraint shears and restraint moments along the length of the beam (see Fig. 10-19).



(a) Geometry



(b) Fixed-end moments

Figure 10-17 Two-span, post-tensioned beam.

	AB	BA	BC	CB
FEM's	$\frac{Pe}{2}$	$-\frac{Pe}{2}$	$+Pe$	$-Pe$
release A and C	$-\frac{Pe}{2}$	$-\frac{Pe}{4}$	$-\frac{Pe}{2}$	$+Pe$
release B	0	$-\frac{Pe}{2}$	$-\frac{Pe}{4}$	0
		$\frac{5Pe}{4}$	$+\frac{5Pe}{4}$	

Figure 10-18 Moment distribution for two-span continuous beam.

10.7 CALCULATION OF FIXED-END MOMENTS DUE TO PRESTRESS

To use the moment distribution method we need to know the moments required to hold the ends of the members against rotation (i.e., the fixed-end moments). While these can be calculated from first principles (see Fig. 10-15), a more direct approach is frequently possible.

If the tendon force P_e and the member stiffness, EI , are constant along the span, the free curvatures of the beam due to prestress are directly proportional to the tendon eccentricity, e . That is, the curvatures causing rotation of the beam when the ends are released are given by a diagram showing the eccentricity (see Fig. 10-20).

The final curvature diagram for the beam is obtained by adding to the free curvatures the curvatures caused by the two end-restraint moments, M_A and M_B . As these added

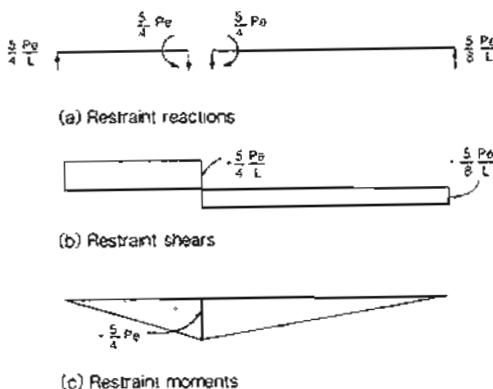


Figure 10-19 Restraint actions due to prestressing.

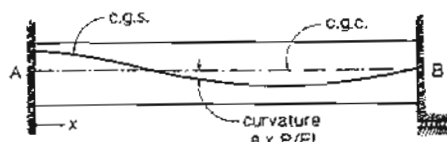


Figure 10-20 Diagram showing free curvatures due to prestress.

curvatures will vary linearly from end to end of the beam, the final curvature diagram can be obtained by a linear shift of the base line of the free curvature diagram (see Fig. 10-21).

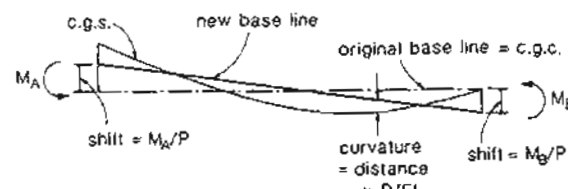


Figure 10-21 Final curvatures due to prestress and end-restraint moments.

For a fixed-ended beam, the final curvature diagram must satisfy two requirements:

- As the change in slope from end A to end B is zero, the area under the curvature diagram must be zero. That is, the area above the new base line must equal the area under the new base line.
- As the deviation of end A from a tangent drawn at end B is zero, the first moment of area of the curvature diagram about end A must be zero. That is, the centroid of the area above the base line must be at the same location as the centroid of the area below the base line.

Two diagrams that satisfy the conditions above for harped and parabolic tendon profiles are given in Fig. 10-22.

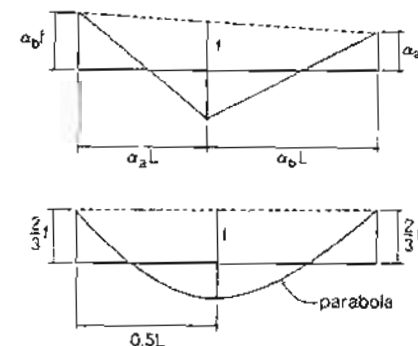


Figure 10-22 Fixed-end curvature diagrams.

Using our knowledge of the required properties of the final curvature diagram, the needed shift in the base line, and hence the required fixed-end moments, can often be determined by inspection. Figure 10-23 gives three examples of finding the fixed-end moments by this procedure.

10.8 EXAMPLE OF FINDING RESTRAINT MOMENTS

The tendon profile for a three-span, post-tensioned bridge is shown in Fig. 10-24. Determine the restraint moments produced when the tendons are stressed to a force (assumed to be constant along the length) of 5000 kips (22 240 kN).

In calculating the restraint moments we can replace the actual tendon profile by the equivalent profile shown in Fig. 10-25. Fixed-end moments calculated using this equivalent profile will not be significantly different from those calculated from the actual profile.

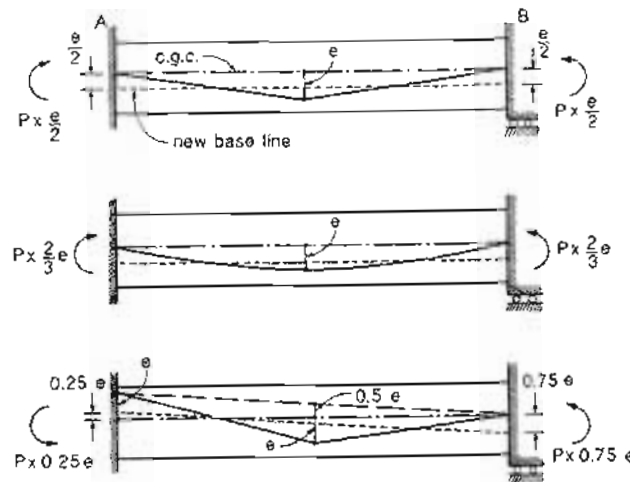


Figure 10-23 Finding fixed-end moments by required shift in base line. Note that the fixed-end moment direction is from the new base line position toward the old base line position.

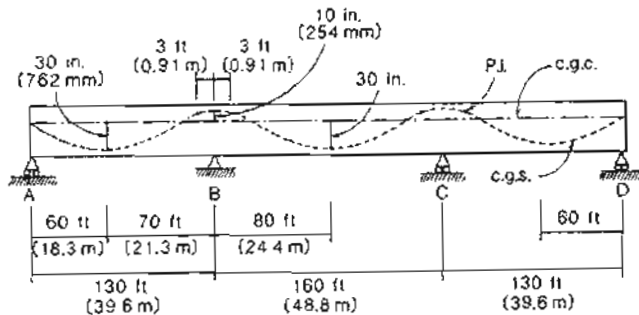


Figure 10-24 Three-span, post-tensioned bridge.

For span AB the distance down from the top of the tendon at B to the point of inflection is given from Eq. (2-1) as

$$h_2 = \frac{\beta}{\lambda} (e_1 + e_2) = \frac{3}{70} (30 + 10) = 1.71 \text{ in. (44 mm)}$$

Sec. 10.8 Example of Finding Restraint Moments

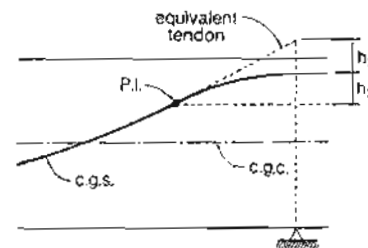


Figure 10-25 Equivalent tendon profile.

The distance up from the low point of the parabola to the tendon location at midspan is

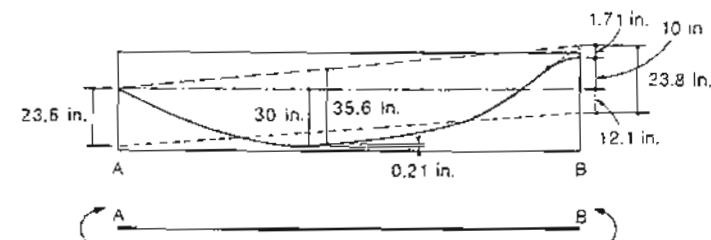
$$y = (30 + 10 - 1.71) \left(\frac{5}{67} \right)^2 = 0.21 \text{ in. (5 mm)}$$

The drape of the equivalent parabola at midspan is thus

$$\begin{aligned} f &= \frac{1}{2}(10 + 1.71) + 30 - 0.21 = 35.6 \text{ in. (905 mm)} \\ \frac{2}{3}f &= 23.8 \text{ in. (604 mm)} \end{aligned}$$

As shown in Fig. 10-26, the required base line shift at B is

$$23.8 - 10 - 1.71 = 12.1 \text{ in. (307 mm)}$$



$$5000 \times 23.8 / 12 = 9917 \text{ ft-kip} \quad (13446 \text{ kN m})$$

$$5000 \times 12.1 / 12 = 5042 \text{ ft-kip} \quad (6836 \text{ kN m})$$

Figure 10-26 Calculation of fixed-end moments for span AB.

For span BC.

$$h_2 = \frac{3}{80} (30 + 10) = 1.5 \text{ in. (38 mm)}$$

$$f = 1.5 + 10 + 30 = 41.5 \text{ in. (1054 mm)}$$

$$\frac{2}{3} f = 27.7 \text{ in. (703 mm)}$$

$$27.7 - 1.5 - 10 = 16.2 \text{ in. (411 mm)} \quad (\text{see Fig. 10-27})$$

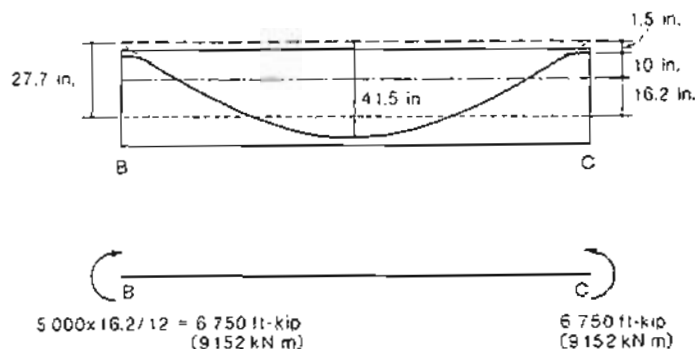


Figure 10-27 Calculation of fixed-end moments for span BC.

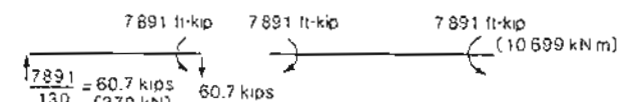
In the distribution we will release A and D first, then B and C simultaneously. The relative stiffnesses of BA and BC are thus

$$K_{BA} : K_{BC} = \frac{3EI}{L} : \frac{2EI}{L} = \frac{3}{130} : \frac{2}{160} = 0.649 : 0.351$$

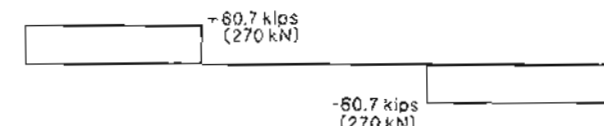
The moment distribution can now be performed (see Fig. 10-28). The restraint actions are shown in Fig. 10-29.

	AB	BA	BC
FEM's		0.649	0.351
release A and D	+ 9917	- 5042	+ 6750
release B and C	- 9917	- 4959	
	0	+ 2110	+ 1141
		- 7891	+ 7891 ft-kip

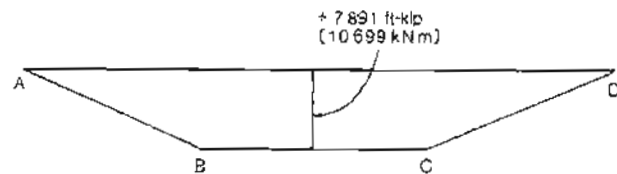
Figure 10-28 Moment distribution for three-span bridge.



(a) Restraint reactions



(b) Restraint shears



(c) Restraint moments

Figure 10-29 Restraint actions in three-span bridge.

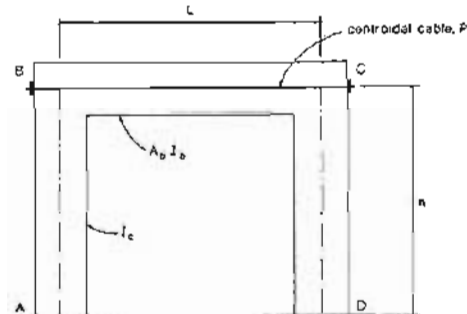
10.9 RESTRAINT OF AXIAL DEFORMATIONS

As we have already discussed, significant restraint actions can arise because the axial shortening of horizontal members is restrained by the flexural stiffness of vertical members. Thus when the beam of the portal frame shown in Fig. 10-30a is post-tensioned, the columns will resist the resulting shortening of the beam.

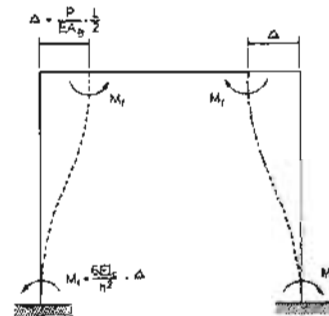
The restraint actions caused by the restraint of axial deformation can be calculated using moment distribution. First, we calculate the fixed-end moments that would be required if the full "free" axial deformation of the members occurred (see Fig. 10-30b). We then perform a moment distribution and calculate the restraint forces produced by these fixed-end moments (see Fig. 10-30c). The tension in the beam caused by the outward pull of the columns will actually reduce somewhat the axial shortening of this member, Δ . Hence we could correct the calculated restraint actions (they will be reduced) to allow for this effect.

10.10 EXAMPLE INVOLVING RESTRAINT OF AXIAL DEFORMATION

A four-span, post-tensioned guideway girder has a solid rectangular cross section 60 in. (1.52 m) wide and 78 in. (1.98 m) deep. The girder is supported by columns cast integrally with the girder, as shown in Fig. 10-31.



(a) Details of frame



(b) Fixed-end moments due to axial deformation

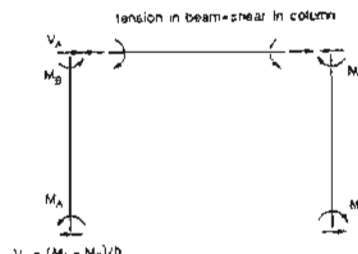


Figure 10-30 Portal frame with post-tensioned beam.

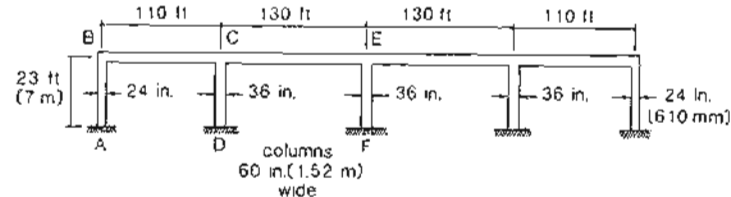


Figure 10-31 Four-span, post-tensioned guideway structure.

The tendon profile in the guideway girder is as shown in Fig. 10-32. The tendons are post-tensioned in such a manner that the average force in each span after tensioning is 4500 kips (20 000 kN). Calculate the restraint actions caused by the prestressing. Assume that E_c at the time of post-tensioning is 4000 ksi (27 600 MPa).

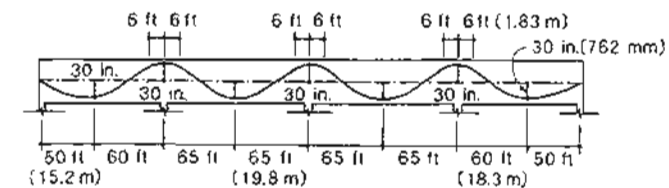


Figure 10-32 Tendon profile in guideway girder.

Step 1: Calculate the fixed-end moments.

For beam BC (see Fig. 10-33).

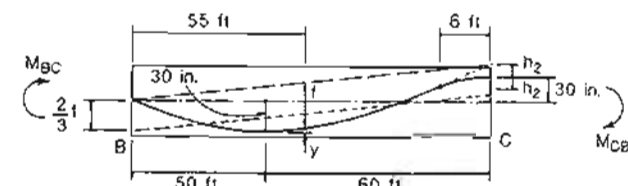


Figure 10-33 Determining fixed-end moments for beam BC.

$$h_2 = \frac{6}{60}(30 + 30) = 6 \text{ in. (152 mm)}$$

$$y = (30 + 30 - 6) \left(\frac{5}{54} \right)^2 = 0.5 \text{ in. (12 mm)}$$

$$f = (30 - 0.5) + \frac{30 + 6}{2} = 47.5 \text{ in. (1207 mm)}$$

$$\frac{2}{3}f = 31.7 \text{ in. (804 mm)}$$

Therefore,

$$M_{BC} = 4500 \times \frac{31.7}{12} = 11,888 \text{ ft-kips (16,120 kNm)}$$

$$M_{CB} = 4500 \times \frac{30 + 6 - 31.7}{12} = 1613 \text{ ft-kips (2186 kNm)}$$

For beam CE (see Fig. 10-34),

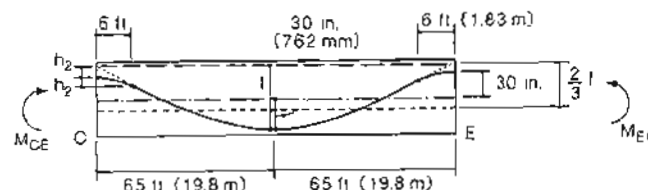


Figure 10-34 Determining fixed-end moments for beam CE.

$$h_2 = \frac{6}{65}(30 + 30) = 5.5 \text{ in. (141 mm)}$$

$$f = 30 + 30 + 5.5 = 65.5 \text{ in. (1664 mm)}$$

$$\frac{2}{3}f = 43.7 \text{ in. (1109 mm)}$$

Therefore,

$$M_{CE} = M_{EC} = 4500 \times \frac{43.7 - 30 - 5.5}{12} = 3075 \text{ ft-kips (4169 kNm)}$$

For column AB (see Figs. 10-35 and 10-30).

$$\Delta_B = \frac{4500 \times (240 \times 12)}{60 \times 78 \times 4000} = 0.69 \text{ in. (18 mm)}$$

$$I_{BA} = \frac{60 \times 24^3}{12} = 69,120 \text{ in}^4 (28.8 \times 10^9 \text{ mm}^4)$$

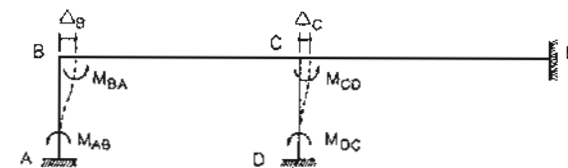


Figure 10-35 Determining fixed-end moments in columns.

Therefore,

$$M_{BA} = M_{AB} = \frac{6EI}{h^2} \Delta = \frac{6 \times 4000 \times 69,120}{(23 \times 12)^2} \times 0.69 \\ = 15,026 \text{ in.-kips} = 1252 \text{ ft-kips (1698 kNm)}$$

For column DC,

$$\Delta_C = 0.69 \times \frac{130}{240} = 0.37 \text{ in. (9 mm)}$$

$$I_{CD} = \frac{60 \times 36^3}{12} = 233,280 \text{ in}^4 (97.1 \times 10^9 \text{ mm}^4)$$

$$M_{CD} = M_{DC} = \frac{6EI}{L^2} \Delta = \frac{6 \times 4000 \times 233,280}{(23 \times 12)^2} \times 0.37 \\ = 27.194 \text{ in.-kips} = 2266 \text{ ft-kips (3072 kNm)}$$

Note that these column moments are based on the assumption that the beam will shorten the full amount. In fact the columns will restrain the shortening of the beams and hence the Δ values will be somewhat smaller and so the resulting fixed-end moments will be a little smaller than those calculated.

Step 2: Calculate the distribution factors.

$$I_{beam} = \frac{60 \times 78^3}{12} = 2,372,760 \text{ in}^4 (988 \times 10^9 \text{ mm}^4)$$

$$K_{BA} : K_{BC} = \frac{4EI}{L} : \frac{4EI}{L} = \frac{69,120}{23} : \frac{2,372,760}{110} = 0.122 : 0.878$$

$$K_{CB} : K_{CD} : K_{CE} = \frac{2,372,760}{110} : \frac{233,280}{23} : \frac{2,372,760}{130} = 0.432 : 0.203 : 0.365$$

Step 3: Perform the moment distribution.

The calculations are summarized in Fig. 10-36. Recall that the fixed-end moments due to axial restraint are somewhat in error and hence great precision in the distribution calculations is not warranted.

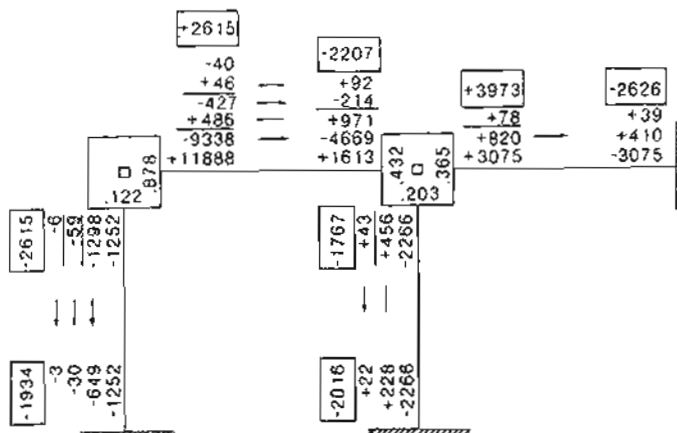


Figure 10-36 Moment distribution.

Step 4: Determine the restraint actions.

Figure 10-37 shows the restraint moments determined from the moment distribution, while Fig. 10-38 shows the resulting reactions, shears, and axial loads.

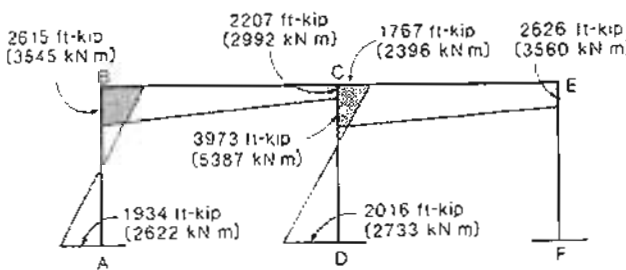


Figure 10-37 Restraint moments due to prestressing. Moments plotted on tension side.

Discussion of results:

Note that the axial tension in beam CE is 362 kips (1610 kN). This tension will reduce the shortening of beam CE by about 8%. A second iteration using reduced values for the beam shortenings would give somewhat more "accurate" answers but is usually not required.

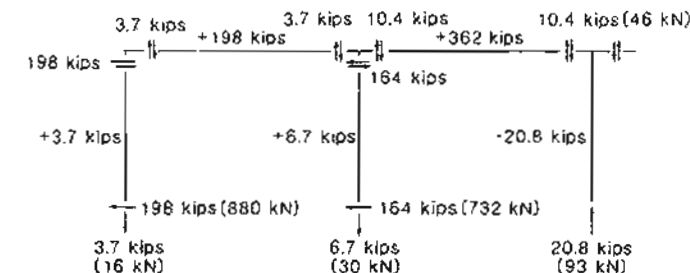


Figure 10-38 Restraint reactions, shear and axial load due to prestressing.

More important, note that the calculated restraint actions are based on the assumption that the structure remains uncracked and elastic. On this basis we have calculated that the moment in the column at B is 2615 ft-kips (3545 kNm).

Assuming that the cracking stress of the concrete was 530 psi (3.7 MPa), the moment required to crack the non-prestressed column would be

$$M_{cr} = \frac{60 \times 24^3}{6} \times 0.530 = 3053 \text{ in.-kips} = 254 \text{ ft-kips (345 kNm)}$$

Thus the column will certainly crack when the beam is prestressed. Once the column cracks its flexural stiffness, EI , will be substantially reduced and hence the restraint moments will be significantly reduced.

To investigate the likely state of the column after the beam has been prestressed, we can assume that while the calculated restraint moments in Fig. 10-37 are too high, the corresponding calculated curvatures are reasonably accurate. This is because the column is subjected to an imposed deformation, not an imposed load.

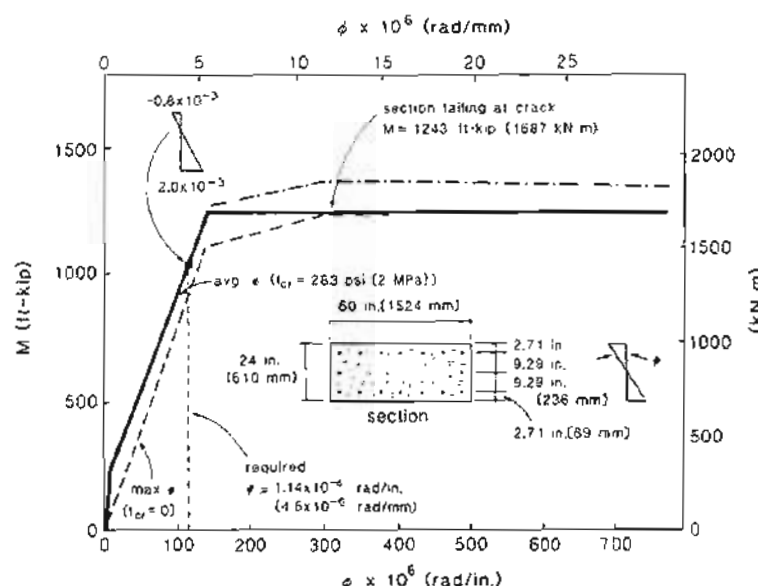
The calculated curvature in column AB at end B is

$$\phi = \frac{M}{EI} = \frac{2615 \times 12}{4000 \times 69,120} = 0.1135 \times 10^{-3} \text{ rad/in. (} 4.5 \times 10^{-6} \text{ rad/mm)}$$

If the column is reinforced with sixteen #11 (35 mm diameter) bars in the manner shown in Fig. 10-39 and if $f'_c = 5000$ psi (34.5 MPa) and $f_y = 60$ ksi (414 MPa), then the calculated $M-\phi$ response of the column section (using program RESPONSE) will be as shown in Fig. 10-39.

As can be seen, such a column would fail at a moment of only 1243 ft-kips (1687 kNm). However, the restraint actions will not cause the column to fail, for the column can tolerate the maximum imposed curvature of 0.1135×10^{-3} rad/in. (4.5×10^{-6} rad/mm). Prestressing the beam will, however, severely crack the column. If the average crack spacing is 10 in. (254 mm), the average crack width in the column when the strain on the tensile face is 2.0×10^{-3} (see Fig. 10-39) would be

$$w_m = 10 \times 2.0 \times 10^{-3} = 0.020 \text{ in. (} 0.51 \text{ mm)}$$

Figure 10-39 Calculated M - ϕ response of column.

These cracks would probably be unacceptably wide, particularly when it is recognized that the crack widths will increase with time due to creep and shrinkage of the concrete.

Adding additional reinforcement will not solve the problem. To alleviate the restraint actions, we need to make the end columns more flexible either by reducing their cross section or by introducing hinges at one or both ends. If hinges are introduced we must check that the resistance of the frame to lateral forces is still adequate.

10.11 FINDING RESTRAINT ACTIONS USING STANDARD COMPUTER PROGRAMS

We have seen that restraint actions in relatively simple structures can be calculated using moment distribution. However, for more complex structures analysis for restraint effects is more conveniently conducted by using standard frame analysis programs. In most standard frame analysis programs the restraint actions can be entered as the end actions on each member required to restrain the ends of the member against deformation (fixed-end actions). Examples of such fixed-end actions are shown in Fig. 10-40. The fixed-end actions for other tendon profiles can be determined using the procedures of Section 10.7.

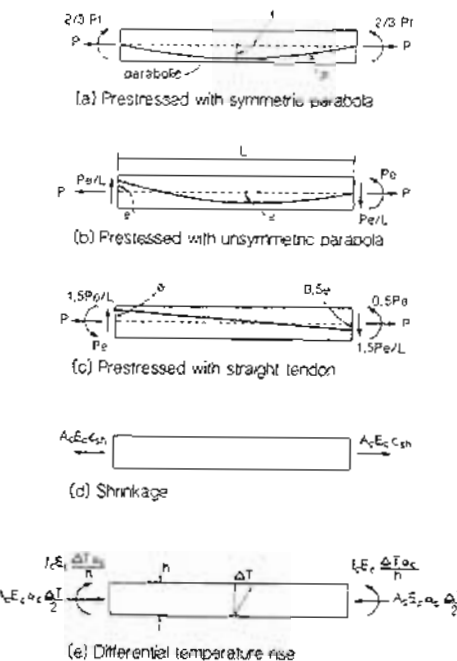


Figure 10-40 Examples of fixed-end actions.

10.12 CALCULATING RESTRAINT ACTIONS USING ELASTIC PLANE-FRAME PROGRAM

The beams of the six-story frame shown in Fig. 10-41 are post-tensioned with straight, centroidal tendons. Calculate the axial restraint actions that arise in each beam as the beams are post-tensioned one by one, to a tendon force of 288 kips (1280 kN).

The rectangular beams are 12 in. (305 mm) wide by 24 in. (610 mm) deep, while the rectangular columns are 24 × 48 in. (610 × 1220 mm). The concrete modulus, E_c , is 5000 ksi (34 500 MPa).

We first perform the calculations assuming that the structure has all been constructed and then the floor beams are post-tensioned one by one. The resulting axial restraint actions in the beams are shown in Table 10-1. Each column in this table shows the axial forces in the various floor beams, caused by post-tensioning one particular floor. Note that as each floor is post-tensioned, the attempt to pull together the columns at a particular floor level causes compression in the floors immediately above and below the floor in question and restraint tension in the floor being post-tensioned. When all six floors have been post-tensioned, the resulting restraint actions consist of a high tension in the second-floor beam

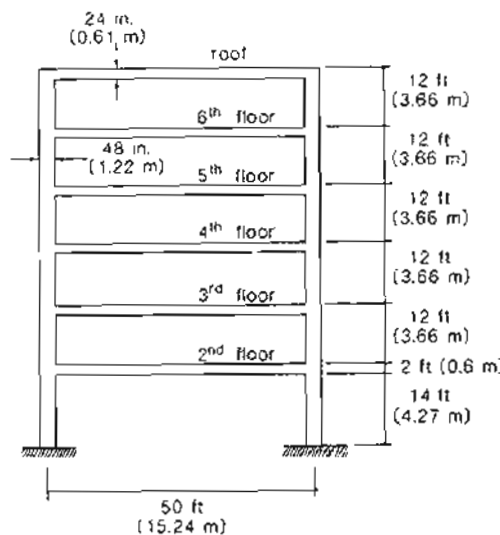


Figure 10-41 Six-story frame.

and compression in the third- and fourth-floor beams. At this stage the deformed shape of the structure will be as shown in Fig. 10-42. Once again the calculated restraint actions are based on the assumption that the frame remains uncracked.

Table 10-1 Axial forces (kips) in beams from post-tensioning completed structure, floor by floor. Tension positive.

Force in Beam on	Floor Being Post-Tensioned						Total Action
	2nd fl.	3rd fl.	4th fl.	5th fl.	6th fl.	Roof	
2nd floor	121.1	-62.1	4.0	4.8	0.3	-0.3	67.7
3rd floor	-62.1	102.5	-61.2	5.5	5.1	-0.4	-10.6
4th floor	4.0	-61.2	102.3	-61.2	5.8	4.3	-6.0
5th floor	4.8	5.5	-61.2	101.2	-64.2	13.9	0
6th floor	0.3	5.1	5.8	-64.2	91.6	-38.2	0.4
Roof	-0.3	-0.4	4.3	13.9	-38.2	20.8	0

The predicted 6227 in.-kips (704 kNm) restraint moment in the ground-floor column will exceed the cracking moment of the column and hence the stiffness of the column and the resulting restraint actions would be reduced.

What would happen to the calculated restraint actions if we assume that the frame was built and stressed in a number of stages? That is, we first build the ground-floor

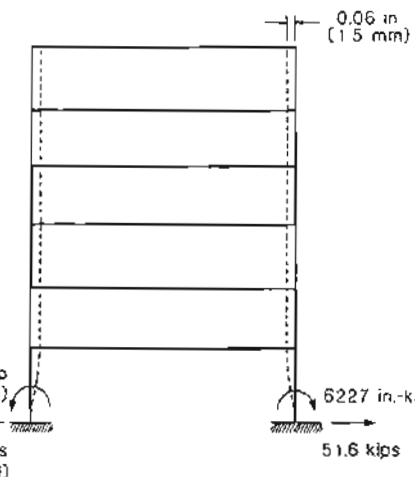


Figure 10-42 Deflected shape of frame.

columns and second-floor beam. Then after post-tensioning the second-floor beam, we build the second-floor columns, the third-floor beam, and stress this third-floor beam. We continue this sequence until finally we build the sixth-floor columns, the roof beam, and stress the roof beam. The calculated restraint actions in the beams of the frame constructed and post-tensioned in this stage-by-stage manner are shown in Table 10-2.

It can be seen from Tables 10-1 and 10-2 that the calculated restraint actions are very strongly affected by the sequence of construction. When the whole frame was post-tensioned after construction, the highest restraint actions occurred near the base of the structure while, when the structure was post-tensioned stage by stage, the highest restraint action occurred near the roof.

Table 10-2 Axial forces (kips) in beams when structure post-tensioned stage by stage.

Force in Beam on	Floor Being Post-Tensioned						Total Action
	2nd fl.	3rd fl.	4th fl.	5th fl.	6th fl.	Roof	
2nd floor	31.3	-41.8	12.5	4.4	-0.3	-0.3	5.8
3rd floor	-	21.8	-38.2	13.8	4.3	-0.4	1.3
4th floor	-	-	20.9	-38.2	13.9	4.3	0.9
5th floor	-	-	-	20.8	-38.2	13.9	-3.5
6th floor	-	-	-	-	20.8	-38.2	-17.4
Roof	-	-	-	-	-	20.8	20.8

The restraint actions shown in Table 10-2 will change in value with time due to creep of the concrete. An estimate of the change in value due to creep is given in the section below.

10.13 INFLUENCE OF CREEP ON RESTRAINT ACTIONS

In those situations where the structure or a component of the structure is subjected to a fixed deformation (e.g., settlement of a support, shrinkage of a beam, thermal expansion of one member), the resulting restraint actions will be directly proportional to the stiffness of the structure. As creep of the concrete will reduce the stiffness, it will reduce the restraint actions in these cases.

As an example of the strong influence of concrete creep, consider the restrained portal frame shown in Fig. 10-43 which was subjected to severe thermal loading by Vecchio (Ref. 10-5). The water inside this frame was heated to about 195°F (90°C) over a period of 2 1/2 hours and then held at this temperature for about a day. Prior to applying the thermal loading, the two tie rods joining the feet of the frame were preloaded to a total load of 5.2 kips (23 kN). The manner in which this restraint force changed during the application of the thermal loading is shown in Fig. 10-44. Note that as the thermal gradient was increased, the restraint force increased by about 3.4 kips (15 kN). However, this increase in restraint force decreased to about 1.1 kips (5 kN) after about 18 hours. That is, the creep of the concrete reduced the thermal restraint force by a factor of 3 after less than 1 day. This substantial reduction has been helped by the fact that at high temperatures concrete creeps at a much faster rate.

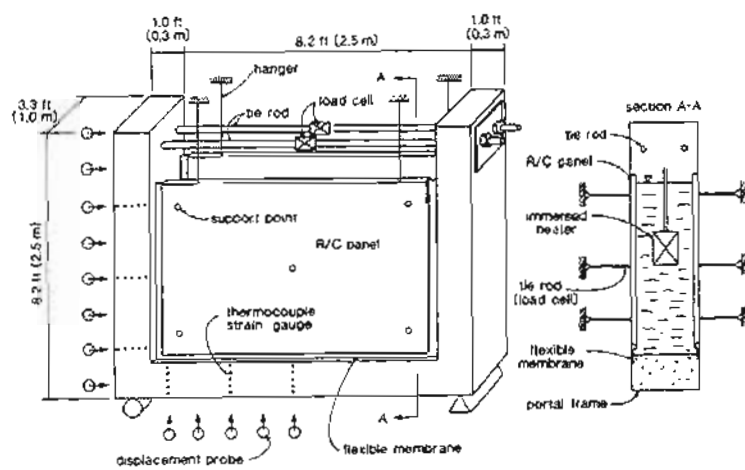


Figure 10-43 Restained reinforced concrete portal frame with inside of frame subjected to hot water. Adapted from Vecchio and Sato (Ref. 10-5).

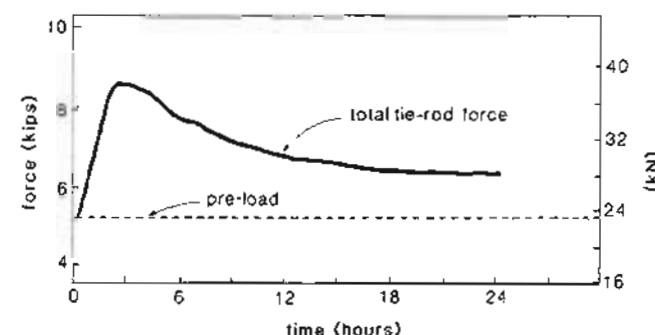


Figure 10-44 Variation of restraint force. Adapted from Vecchio and Sato (Ref. 10-5).

Thus when calculating the restraint actions that arise from support settlements, concrete shrinkage, or thermal loading, it is appropriate to use an effective modulus for the concrete, $E_{c,\text{eff}}$, which makes allowance for the creep of the concrete (see Section 3.6).

As the concrete creeps, the deformations due to the prestress increase. Thus prestressing does not subject the structure to fixed deformations. What is fixed is the strain difference between the prestressing tendon and the surrounding concrete.

If the restraint moments that are caused by post-tensioning the two-span beam shown in Fig. 10-11 are recalculated assuming that E_c is reduced by a factor of say 3, we still obtain the same values for the restraint actions (Fig. 10-14). The beam is only one-third as stiff, but the deflection due to prestress is three times as large. That is, a uniform reduction in concrete stiffness throughout the structure will not affect the restraint moments due to prestress.

Creep will affect the values of restraint actions due to prestress when there is a nonuniform change of stiffness or when there is a change in statical system after the application of some or all of the prestress. Cracking of parts of a structure will also affect the values of restraint actions because of the nonuniform change in stiffness. Thus cracking of the columns of the guideway structure of Section 10.10 will substantially reduce the restraint moments due to prestressing.

The manner in which creep influences restraint actions will be further illustrated by considering the two precast, pretensioned beams shown in Fig. 10-45, which, after erection, were joined together by a cast-in-place joint. If the initial rotation at support B due to the prestress was θ_{B0} and if the creep coefficient at time t was $\phi(t, t_i)$, then if the support at B had remained pinned, its rotation at time t would have increased by $\phi(t, t_i)\theta_{B0}$.

A unit value of the restraint moment (labeled X in Fig. 10-45) would cause the beam initially to rotate back through an angle of θ_{B1} . If this unit moment was held constant over time, then at time t the rotation due to the unit moment would be $[1 + \phi(t, t_i)]\theta_{B1}$.

Because the restraint moment in our case starts at zero and then increases slowly with time, the rotation due to a moment that reaches a value of unity by time t would be

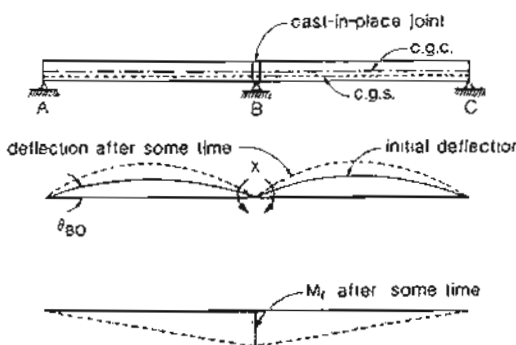


Figure 10-45 Restraint actions due to creep of prestress deformations.

$$(1 + \chi\phi(t, t_i)\theta_{B1})$$

where χ is given in Table 3-4.

The value of the restraint moment at time t , $X(t)$, required to hold the end of the beam against an increase in rotation is thus

$$X(t) = \frac{\phi(t, t_i)\theta_{B0}}{1 + \chi\phi(t, t_i)\theta_{B1}} \quad (10-4)$$

If the structure had been made in one operation and then post-tensioned with a continuous tendon, the restraint moment at B, which we will call X_{el} , could have been found from the flexibility approach as

$$X_{el} = \frac{\theta_{B0}}{\theta_{B1}} \quad (10-5)$$

Substituting from Eq. (10-5) into Eq. (10-4) gives

$$X(t) = \frac{\phi(t, t_i)}{1 + \chi\phi(t, t_i)} X_{el} \quad (10-6)$$

If the two beams contain straight tendons with a constant eccentricity of e and a prestressing force of P , the elastic value of the restraint moment, X_{el} , at B would be $1.5Pe$. Thus if $\phi(t, t_i)$ was 2.0 and χ was 0.8, the restraint action would be

$$X(t) = \frac{2.0}{1 + 0.8 \times 2.0} \times 1.5Pe = 1.15Pe$$

We should recognize that joining the two beams together will cause moments at B to arise, not only from the restraint of prestress deformations, but also from the restraint of deformations due to external loads. For example, the dead-load moment at support B if the structure were constructed in one operation would be $wL^2/8$. Again, Eq. (10-6) can

be used to estimate how the dead-load moment at B will grow once the two members are joined together. Thus

$$X(t) = \frac{2.0}{1 + 0.8 \times 2.0} \times \frac{wL^2}{8} = 0.096wL^2$$

Equation (10-6) was derived for the case where the initial value of the restraint was zero. If there is some initial value of the restraint, X_i , Eq. (10-6) can be generalized as

$$X(t) = X_i + \frac{\phi(t, t_i)}{1 + \chi\phi(t, t_i)} (X_{el} - X_i) \quad (10-7)$$

Equation (10-7) can be applied not only to the single redundant system of Fig. 10-45 but also to systems with multiple redundants, provided that we can assume that the creep characteristics of the total system are reasonably uniform and that the creep starts at about the same time.

For example, the value of the restraint tension in the second-floor beam of the six-story frame of Section 10.12, built stage by stage after, say, five years, can be estimated using Eq. (10-7). If we approximate the creep characteristics for the total frame by assuming $f'_c = 5000$ psi (35 MPa), a volume-to-surface ratio, $v/s = 6$ in. (150 mm) and $t_i = 30$ days, then from Eq. (3-10),

$$\phi(1825, 30) = 3.5 \times 0.66 \times 0.82 \left(1.58 - \frac{70}{120} \right) 30^{-0.118} \frac{1825^{0.6}}{10 + 1825^{0.6}} \\ = 1.14$$

Take $\chi = 0.80$. From Eq. (10-7) restraint tension after 5 years is

$$X(1825) = 5.8 + \frac{1.14}{1 + 0.8 \times 1.14} (67.7 - 5.8) \\ = 42.7 \text{ kips (190 kN)}$$

Thus creep has caused the restraint action to go from the initial value of 5.8 kips (26 kN), given in Table 10-2, toward the "elastic" value of 67.7 kips (301 kN), given in Table 10-1. Hence schemes that seek to greatly relieve restraint actions by changing the sequence of construction may only be postponing the problem.

10.14 EXAMPLE DESIGN OF A STATICALLY INDETERMINATE STRUCTURE

The one-way, two-span floor slab for an assembly hall is post-tensioned with bonded tendons (see Fig. 10-46). Each tendon consists of four 1/2 in. (13 mm) diameter, low-relaxation strands having $f_{pu} = 270$ ksi (1860 MPa) in an oval duct 3/4 in. (20 mm) high. The floor slab supports a specified live load of 100 psf (4.8 kN/m²) and a superimposed dead load of 10 psf (0.5 kN/m²). The slab will be post-tensioned when the concrete is 7 days old and has reached a strength of 3500 psi (24 MPa). The specified 28-day strength of the normal-density concrete is 4500 psi (31 MPa). Design the floor slab to satisfy the ACI Code requirements (Ref. 10-6).

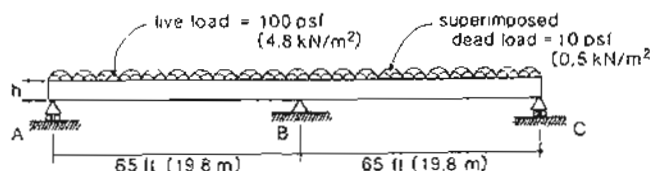


Figure 10-46 Continuous, one-way floor slab for an assembly hall.

Step 1: Choose the slab thickness.

Span-to-depth ratios of continuous one-way post-tensioned slabs typically vary from 40 to 50. For this relatively heavily loaded slab we will choose an overall slab thickness of 20 in. (508 mm). This results in a slab self-weight of 250 psf (12 kN/m²).

Step 2: Select the tendon profile.

For this uniformly loaded slab choose a tendon profile consisting of a series of parabolic segments. To maximize the flexural capacity, place the tendon as high as possible over the central support, B, and as low as possible in the spans. From Table 3-16 the required concrete cover is 3/4 in. (20 mm) and hence the maximum possible eccentricity from Fig. 10-47 is

$$\begin{aligned} e &= 10 - \frac{3}{4} - \frac{3}{4} + \frac{1}{4} \\ &= 8.75 \text{ in. (222 mm)} \end{aligned}$$

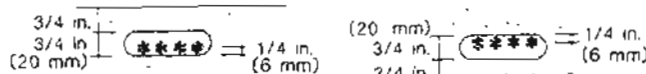


Figure 10-47 Determination of maximum eccentricity.

Because the maximum positive moment in the span will occur at a location somewhat closer to the simply supported end, we will locate the low point, D, of the tendon at 30 ft (9.1 m) from the simple support.

If the point of inflection of the tendon is located 2 ft (0.6 m) from support B, then the radius of curvature of the tendon as it passes over the support (see Fig. 2-23) will be

$$\begin{aligned} R &= \frac{\lambda \ell^2}{2(e_1 + e_2)} \\ &= \frac{35 \times 2}{2(8.75 + 8.75)/12} \\ &= 24 \text{ ft (7.3 m)} \end{aligned}$$

which is acceptable, and

$$\begin{aligned} h_2 &= \frac{j}{\lambda}(e_1 + e_2) \\ &= \frac{2}{35}(8.75 + 8.75) \\ &= 1 \text{ in. (25 mm)} \end{aligned}$$

The resulting tendon profile is summarized in Fig. 10-48.

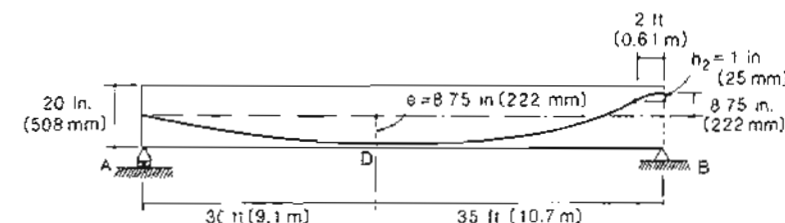


Figure 10-48 Tendon profile.

Step 3: Estimate the stresses in the tendons.

Each tendon will be stressed from just one end, with the other end being a dead-end anchorage. Every second tendon will be stressed from end A and the alternate tendons will be stressed from end C. The tendons will be jacked to a stress of $0.75 f_{pu}$ and then anchored. Information from the post-tensioning supplier indicates that the friction coefficients appropriate for the tendon are $\mu = 0.20$ and $K = 0.0006$ per ft (0.0020 per m). The anchorage set is 1/4 in. (6 mm). The resulting stresses in the tendon can be determined using the procedures explained in Sections 2.9 and 2.10. The calculations for tendons stressed from end A are summarized in Fig. 10-49. Note that after anchoring, the stress at the anchor is 181 ksi (1248 MPa), which is less than the limiting stress of $0.70 f_{pu} = 189$ ksi (1302 MPa). Tendons stressed from end B will have a tendon stress variation which is the mirror image of that shown in Fig. 10-49. Hence for the purpose of checking concrete stresses the average tendon stress at location D will be $(186+177)/2 = 182$ ksi (1254 MPa).

In calculating restraint moments and deflections due to prestress, it is sufficiently accurate to use the average tendon force in the span. From the stress variation shown in Fig. 10-49, the average tendon stress will be 182 ksi (1254 MPa).

The tendon stresses will be reduced with time due to creep, shrinkage and relaxation. We will estimate the resulting long-term loss in tendon stress to be 30 ksi (200 MPa).

Step 4: Choose the tendon spacing.

We will choose a prestressing amount such that 90% of the self-weight of the slab will be balanced by the prestressing even after prestressing losses have occurred. The

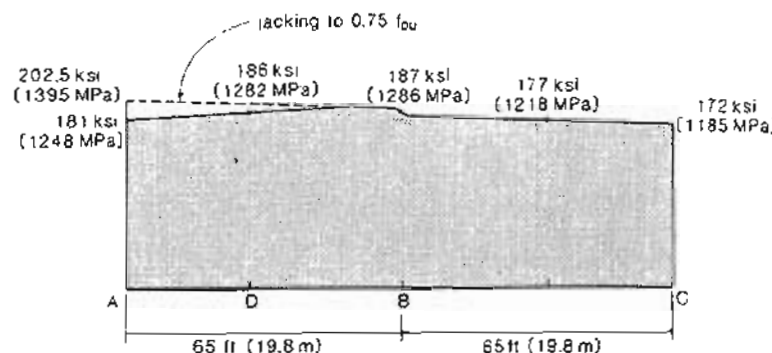


Figure 10-49 Stress variation in tendons stressed from end A.

drape, f , at midspan (see Fig. 10-50) is equal to

$$f = 0.5(8.75 + 1) + 8.75 - (8.75 + 8.75 - 1) \times \left(\frac{2.5}{33}\right)^2 = 13.53 \text{ in. (344 mm)}$$

Using the concept of the equivalent tendon profile (see Fig. 10-25) an approximate expression for the required prestressing force with a midspan drape of 13.53 in. (344 mm) to balance 90% of the self-weight is

$$\begin{aligned} P &= \frac{0.9w_D l^2}{8f} \\ &= \frac{0.9 \times 0.250 \times 65^2}{8 \times 13.53/12} \\ &= 105.4 \text{ kips/ft width (1538 kN/m width)} \end{aligned}$$

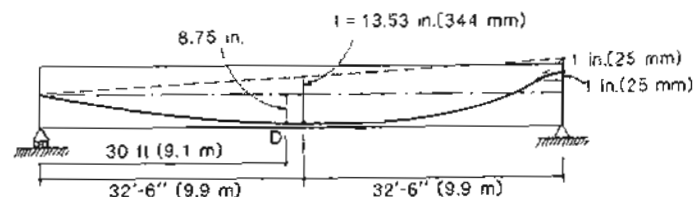


Figure 10-50 Determining tendon drape at midspan.

After losses, each tendon will have an average force of $4 \times 0.153 \times (182 - 30) = 93 \text{ kips (414 kN)}$. Hence using a tendon spacing of 10 in. (254 mm) will provide 112 kips/ft width (1629 kN/m width) of slab.

Step 5: Determine the service load moments.

Since we will check the concrete stresses at locations B and D, we need to calculate the maximum and minimum moments that can occur at these locations. In these calculations we must consider the possibility that the live load may be on only one span. Figure 10-51 gives the moment diagrams due to dead and live loads.

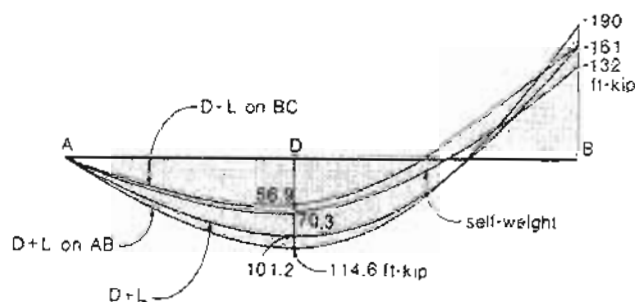


Figure 10-51 Service moments due to dead and live loads for 1 ft width of slab.

Post-tensioning of this two-span slab will cause restraint moments. The magnitude of these moments can be calculated using the methods explained in Sections 10.6 and 10.7. The initial prestressing force is $4 \times 0.153 \times 182 \times 12/10 = 134 \text{ kips/ft width (1951 kN/m width) of slab}$. After losses this force will drop to 112 kips/ft width. The calculated restraint moments for these two levels of prestress force are shown in Fig. 10-52.

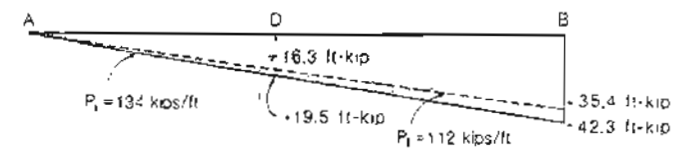


Figure 10-52 Restraint moments for 1 ft width of slab due to initial and final prestressing.

Step 6: Check the concrete stresses.

We will determine the concrete stresses using the force-in-the-tendon approach. Although the average tendon force was used to calculate the restraint moments, we will use the more accurate estimate of the local tendon stress when calculating concrete stresses. Thus the initial tendon force at location B is $4 \times 0.153 \times 187 \times 12/10 = 137 \text{ kips/ft (2004 kN/m)}$, while the final force will be $4 \times 0.153 \times 157 \times 12/10 = 115 \text{ kips/ft (1683 kN/m)}$.

At D the initial prestressing force is $4 \times 0.153 \times 182 \times 12/10 = 134$ kips/ft (1951 kN/m) and the final force will be 112 kips/ft (1629 kN/m).

In calculating the concrete stresses we must determine the maximum and minimum moments due to the combined effect of the restraint moments and the dead and live-load moments. For the initial conditions it is the minimum moment that is of interest while for the final conditions it is the maximum moment that is of interest. The maximum final moment at location D is $114.6 + 16.3 = 130.9$ ft-kips/ft (582 kNm/m), while the minimum initial moment is $56.9 + 19.5 = 76.4$ ft-kips/ft (340 kNm/m). At B the "maximum" negative final moment is $190 - 35.4 = 154.6$ ft-kips/ft (688 kNm/m), while the "minimum" initial moment is $132 - 42.3 = 89.7$ ft-kips/ft (399 kNm/m).

A summary of the stress checks is presented in Table 10-3. It can be seen that the stresses satisfy the stress limits at all locations except that the tensile stress on the top face of the slab at location B exceeds the limit of $6\sqrt{f'_c}$ psi. The ACI Code permits the extreme fiber stress in tension to go up to $12\sqrt{f'_c}$ psi provided that cracking is accounted for in checking deflections and provided that the minimum concrete cover is increased by 50% if the member is exposed to earth, weather, or corrosive environments.

Table 10-3 Concrete stresses at service loads.

		At D		At B	
		Top	Bottom	Top	Bottom
Initial condition	$-P_i/A$	-558	-558	-571	-571
Tensile limit = +177 psi (+1.22 MPa)	$\pm P_i \epsilon/S$	+1466	-1466	-1498	+1498
Compressive limit = -2100 psi (-14.5 MPa)	$\pm M_{min}/S$	-1146	+1146	+1346	-1346
	Total, psi (MPa)	-238 (-1.64)	-878 (-6.05)	-723 (-4.99)	-419 (-2.89)
Final condition	$-P_f/A$	-467	-467	-479	-479
Tensile limit = +402 psi (+2.78 MPa)	$\pm P_f \epsilon/S$	+1225	-1225	-1255	+1258
Compressive limit = -2025 psi (-13.96 MPa)	$\mp M_{max}/S$	-1964	+1964	+2319	-2319
	Total, psi (MPa)	-1206 (-8.32)	-272 (+1.88)	+582 (+4.01)	-1540 (-10.62)

Step 7: Check the flexural capacity.

The design moment strength of the slab, ϕM_n , must not be less than the factored moment, M_u . In calculating M_u , the ACI Code requires that restraint moments due to prestress be included with a load factor of 1.0. It is conventional to use the restraint moments associated with the "final" prestressing force (i.e., the force after all losses have occurred) in these calculations.

(a) At location B

$$\begin{aligned} M_u &= 1.4(132 + 5) + 1.7 \times (190 - 132 - 5) - 1.0 \times 35.4 \\ &= 246 \text{ ft-kips/ft (1094 kNm/m)} \end{aligned}$$

Using Eq. (6-7) for determining the stress in the prestressing steel at nominal strength gives

$$\begin{aligned} f_{ps} &= f_{psn} \left(1 - \frac{\gamma_p}{\beta_1} \rho_p \frac{f_{psn}}{f'_c} \right) \\ &= 270 \left(1 - \frac{0.28}{0.825} \times \frac{4 \times 0.153}{10 \times 18.75} \times \frac{270}{4.5} \right) \\ &= 252 \text{ ksi (1738 MPa)} \end{aligned}$$

The equivalent rectangular stress-block depth is

$$a = \frac{A_{ps} f_{ps}}{0.85 f'_c b} = \frac{4 \times 0.153 \times (12/10) \times 252}{0.85 \times 4.5 \times 12} = 4.03 \text{ in. (102 mm)}$$

Hence the design strength is

$$\begin{aligned} \phi M_n &= \phi A_{ps} f_{ps} (d - \frac{a}{2}) \\ &= 0.9 \times 4 \times 0.153 \times \left(\frac{12}{10} \right) \times 252 \left(18.75 - \frac{4.03}{2} \right) \\ &= 2787 \text{ in.-kips/ft} \\ &= 232 \text{ ft-kips/ft (1033 kNm/m)} \end{aligned}$$

As 232 is less than 246, the flexural strength at B needs to be increased by at least 14 ft-kips/ft. For ease of placement use #4 (13 mm) bars at a spacing of 10 in. With this additional reinforcement we have $f_{ps} = 251$ ksi (1729 MPa), $a = 4.33$ in. (110 mm), and $\phi M_n = 247$ ft-kips/ft (1100 kNm/m). Therefore, the capacity is adequate. We must check that the section is not over-reinforced. From Eq. (6-11),

$$\omega_p + (\omega - \omega') \frac{d}{d_p} = \frac{4 \times 0.153}{10 \times 18.75} \times \frac{251}{4.5} + \frac{0.20}{10 \times 19} \times \frac{60}{4.5} \times \frac{19}{18.75} = 0.196$$

Since this index is less than the ACI Code limit of $0.36\beta_1 = 0.36 \times 0.825 = 0.297$, the section is not over-reinforced.

(b) At location D

$$\begin{aligned} M_u &= 1.4(70.3 + 4.0) + 1.7(114.6 - 70.3 - 4.0) + 1.0 \times 16.3 \\ &= 189 \text{ ft-kips/ft (840 kNm/m)} \end{aligned}$$

The section, with only prestressing steel has a design strength, ϕM_n , of 232 ft-kips/ft (1033 kNm/m) and hence no additional reinforcement is required.

Step 8: Check the reserve of strength after cracking.

The ACI Code requires that ϕM_n exceeds $1.2M_{cr}$ where M_{cr} is calculated on the basis of the modulus of rupture

$$\begin{aligned} f_r &= 7.5\sqrt{f'_c} \\ &= 7.5\sqrt{4500} \\ &= 503 \text{ psi (3.47 MPa)} \end{aligned}$$

The moment to cause a tensile stress of 503 psi (3.47 MPa) on the top surface at B can be calculated from the stresses given in Table 10-3 as

$$503 = -479 - 1258 + \frac{M_{cr}}{12 \times 20^3/6}$$

Hence

$$M_{cr} = 1792 \text{ in.-kips/ft} = 149 \text{ ft-kips/ft (664 kNm/m)}$$

Thus, at B,

$$\frac{\phi M_n}{M_{cr}} = \frac{247}{149} = 1.66 > 1.20$$

Hence post-cracking capacity is adequate.

Similarly, at D,

$$\frac{\phi M_n}{M_{cr}} = \frac{232}{146} = 1.59 > 1.20$$

Step 9: Check the deflections at service loads.

Although some cracking is predicted to occur at support B under full service loading, we will first estimate the deflections by neglecting the influence of this cracking. As there are no partitions in this assembly hall, only the immediate deflection due to live load needs to be checked.

For a two-span continuous beam, the maximum deflection due to loading one span is

$$\Delta = \frac{1.6w\ell^4}{185EI} = \frac{1.6 \times 0.100 \times 64^4 \times 12^3}{185 \times 3824 \times 12 \times 20^3/12} = 0.82 \text{ in. (21 mm)}$$

As the maximum permissible deflection for live load is $\ell/360 = 65 \times 12/360 = 2.17 \text{ in. (55 mm)}$ the deflection due to live load will not be critical. Cracking over the support will cause a local reduction in stiffness, but as the midspan deflections are influenced mainly by the stiffness in the span, cracking only over the support will cause no more than a 15% increase in midspan deflections.

10.15 INFLUENCE OF RESTRAINT MOMENTS ON LOAD DISTRIBUTION AT ULTIMATE

A number of engineers have argued that while it is appropriate to include the restraint moments due to prestress when checking service load conditions, these "secondary" moments should be ignored when checking overload capacity ("ultimate loads"). It is contended that once the member has cracked, the calculated restraint moments have no relation to reality.

Figure 10-53 illustrates the manner in which the support moment for the two-span, continuous slab, designed in Section 10.14, increases as the uniform load on the slab increases. Three predicted relationships are shown in the figure: an elastic analysis including the prestress restraint moments, an elastic analysis neglecting these restraint moments, and a nonlinear analysis which accounts for the influence of concrete cracking and material nonlinearities. This nonlinear analysis was performed using the computer program TEMPEST, developed by Vecchio (Ref. 10-7).

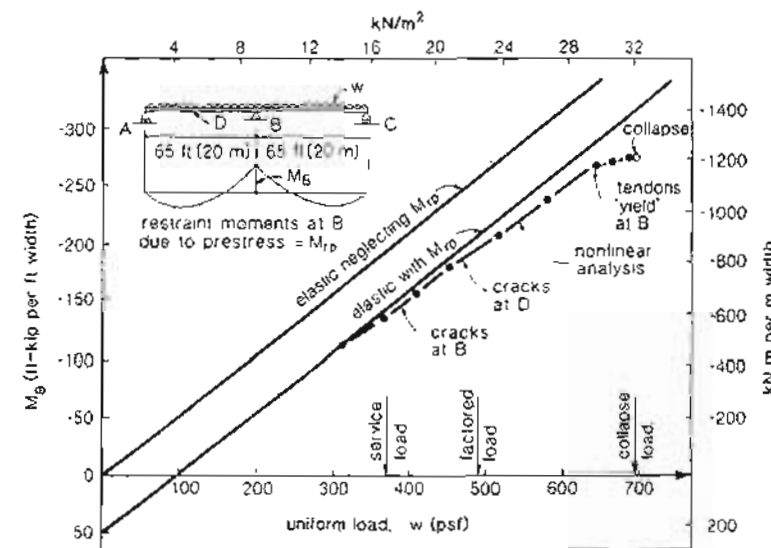


Figure 10-53 Predicted magnitude for the moment at support B.

From Fig. 10-53 it can be seen that including the influence of restraint moments resulted in an elastic analysis which gave values closer to those of the more sophisticated, nonlinear analysis. Figure 10-53 also shows that considerable redistribution can occur prior to failure. That is, the moment over the support may increase at a slower rate, while the moment in the span increases at a faster rate. The ACI Code permits allowance to be made

for such redistribution. Thus the one-way slab considered could be designed for a support moment which is reduced by

$$20 \left[1 - \frac{\omega_p + \frac{d}{d_p}(\omega - \omega')}{0.36\beta_1} \right] \text{ percent} = 6.8\%$$

provided that an appropriate increase is made in the corresponding moments in the span. Note that a redistribution of considerably more than 6.8% would be required to reduce the elastic moments, calculated ignoring restraint, to the "nonlinear" values.

It is true that an elastic analysis based on uncracked stiffness values can lead to unrealistically high values of restraint moments, particularly for those cases involving the restraint of axial deformations (see Section 10.10). However, this deficiency in the elastic analysis does not justify neglecting the presence of restraint actions. Such a neglect would violate the code limitations on allowable amounts of redistribution. To obtain more realistic estimates of the restraint moments, either a nonlinear analysis can be performed, or the flexural stiffnesses of the members can be reduced to allow for cracking.

References

- 10-1 Leonhardt, F., *Prestressed Concrete - Design and Construction*, English translation 2nd ed., Wilhelm Ernst und Sohn, Berlin, 1964, 677 pp.
- 10-2 Standing Committee on Structural Engineering of the Federal Construction Council, Building Research Advisory Board, Division of Engineering, "Expansion Joints in Buildings," Technical Report No. 65, National Research Council, National Academy of Science, Washington, D.C., 1974.
- 10-3 Prestressed Concrete Institute, *PCI Design Handbook: Precast and Prestressed Concrete*, 3rd ed., PCI, Chicago, 1985.
- 10-4 Cross, Hardy, "Analysis of Continuous Frames by Distributing Fixed-End Moments," *Transactions of the American Society of Civil Engineers*, Paper No. 1793, May 1930, 10 pp.
- 10-5 Vecchio, F.J., and Sato, J.A., "Thermal Gradient Effects in Reinforced Concrete Frame Structures," *ACI Structural Journal*, Vol. 87, No. 3, May-June 1990, pp. 262-275.
- 10-6 ACI Committee 318, "Building Code Requirements for Reinforced Concrete (ACI 318-89) and Commentary - ACI 318 R-89," American Concrete Institute, Detroit, 1989, 353 pp.
- 10-7 Vecchio, P.J., "Nonlinear Analysis of RC Frames Subjected to Thermal and Mechanical Loads," *ACI Structural Journal*, Vol. 84, No. 6, Nov.-Dec. 1987, pp. 492-501.

Demonstration Problems

- 10-1 The cast-in-place concrete frame shown in Fig. 10-54 is composed of rectangular members 10×20 in. (254×508 mm) in cross section. When the three frictionless tendons are post-tensioned to a force of 200 kips (890 kN), what will be the values of the restraint actions induced at the supports? What will be the horizontal deflection of point A due to stressing of the tendons? Assume that $E_c = 4000$ ksi (27600 MPa).

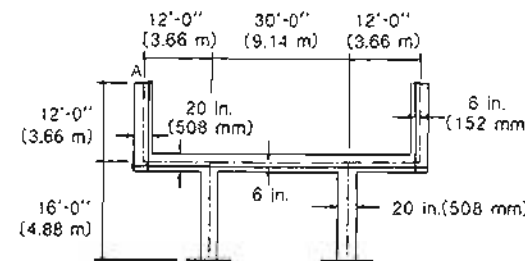


Figure 10-54 Cast-in-place, post-tensioned frame

- 10-2 Determine the fixed-end moments caused by post-tensioning the four members shown in Fig. 10-55.

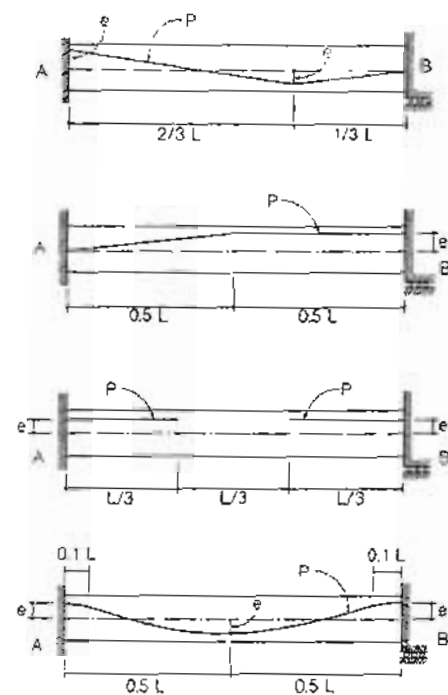


Figure 10-55 Fixed-ended beams.

- 10-3 A post-tensioned, one-way floor slab is described in Fig. 10-56. Ignoring frictional effects, calculate the restraint moments due to prestress. Express the moments in terms of the tendon force, P .

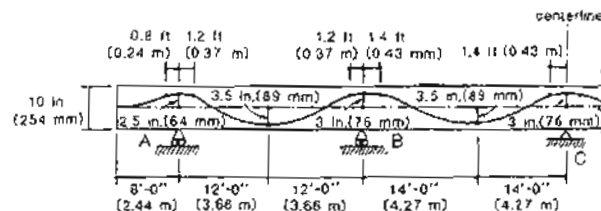


Figure 10-56 Post-tensioned, one-way floor slab.

- 10-4 A two-span, guideway structure is described in Fig. 10-57. Ignoring frictional effects, calculate the restraint moments in terms of the tendon force, P . Ignore the width of the support at 2.0.

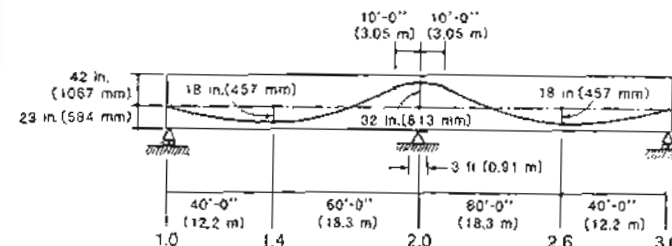


Figure 10-57 Post-tensioned guideway structures

- 10-5 The cross section of the guideway described in Fig. 10-57 is such that $A = 31 \text{ ft}^2 (2.88 \text{ m}^2)$ and $I = 81 \text{ ft}^4 (0.70 \text{ m}^4)$. Ignoring frictional effects, find the minimum tendon force required to ensure that when a train weighing 1.23 kips/ft (18 kN/m) crosses the structure, the tensile stresses at 1.4 and 2.0, do not exceed 150 psi (1.0 MPa). In calculating the external moments at 2.0 allow for the fact that the support at 2.0 is 3 ft (0.91 m) wide. Assume that concrete weighs 150 lb/ft³ (24 kN/m³). Suggest how the tendon profile could be improved.

- 10-6 A different construction scheme for the guideway structure described in Fig. 10-57 is being investigated. It is proposed to first cast and stress span 1-2. After coupling the tendons at 2, it is then proposed to cast and stress span 2-3. Ignoring friction effects, calculate the restraint moments due to prestress at location 2.0 immediately after construction is complete. Assuming that the average age of the concrete at coupling of the spans is 10 days, that $v/s = 6.89 \text{ in. (175 mm)}$ and that $f'_c = 5000 \text{ psi (35 MPa)}$, estimate the restraint moment at 2.0 three years after construction.

- 10-7 A post-tensioned prestressed concrete portal frame is made from rectangular members with 12 × 24 in. (305 × 610 mm) cross sections. To reduce restraint actions, support D is allowed to move horizontally during the prestressing operation. After post-tensioning (which occurs 20 days after casting) support D is fixed against horizontal movement (i.e., it becomes a pin similar to A) (see Fig. 10-58).

- (a) What is the moment at B due to prestressing immediately after post-tensioning?
(b) Estimate the restraint moment at B due to prestressing 5 years after construction.

- 10-8 The two-span bridge shown in Fig. 10-59 is post-tensioned by continuous tendons stressed from both ends. The tendons are jacked to 80% f_{pu} , released to 60%, re-jacked to 70%, and anchored. Anchorage set is 0.25 in. (6 mm), $\mu = 0.2$ and $K = 0.001/\text{ft (0.003/m)}$. Choose 3 tendon profile and the area of tendons so that the given stress limits are satisfied.

- 10-9 Recalculate the restraint moments due to prestress in the guideway girder structure of Section 10-10, except to allow for reductions in flexural stiffness caused by cracking use $I = 0.5bh^3/12$. Comment on the results.

- 10-10 Investigate the influence of changing the tendon profile in the guideway girder of Section 10-10 on the restraint moments. Lift the eccentricity at B to 20 in. (508 mm).

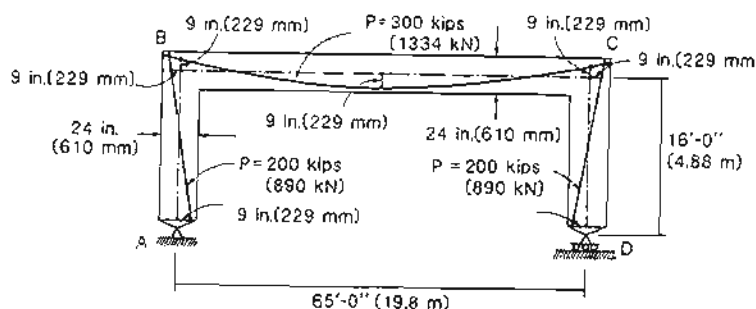
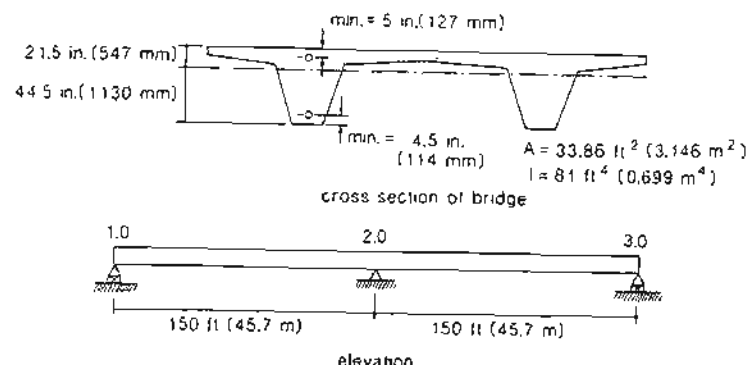


Figure 10-58 Post-tensioned portal frame.



	D.L. + L.L. Moments	Prestress
t = 0	6048 ft-kip (8200 kN m)	-14,235 ft-kip (-19,300 kN m)
t = ∞	10,473 ft-kip (14,200 kN m)	-18,439 ft-kip (-25,000 kN m)

$f_{pu} = 270 \text{ ksi (1860 MPa)}$
 $f_c = 5000 \text{ psi (34.5 MPa)}$
 Allowable tension:
 top fiber = 0
 bottom fiber = 200 psi (1.5 MPa)
 Allowable compression:
 ≈ 2000 psi (15 MPa)

Figure 10-59 Two-span, post-tensioned bridge.

Post-Tensioned Slabs

Tools available to the average engineer in thinking about slabs are the limitations imposed by statics upon the total moments, principles of symmetry and asymmetry and mental pictures of the deflected slab. . . . It is consoling to realize that there is considerable evidence that if these statical limitations are met, the assumed distribution of the moments need not conform precisely to results of mathematical theory.

Hardy Cross, 1929

11.1 INTRODUCTION

Post-tensioned concrete slabs are widely used for the floor systems of office buildings, parking garages, shopping centers, and residential buildings. The popularity of this type of construction is due to the economic savings that result from reduced slab thicknesses, longer spans, and reduced construction time due to the earlier removal of formwork. In addition, the use of post-tensioning enables the engineer to control deflections and cracking at service loads.

Examples of different types of post-tensioned slabs are given in Fig. 11-1. One-way slabs (see Fig. 11-1a) are slabs which are supported such that under load they curve in predominantly one direction and hence are designed as beam strips in this direction. These one-way slabs usually span 20 to 30 ft (6 to 9 m) and have span-to-depth ratios of about 45.

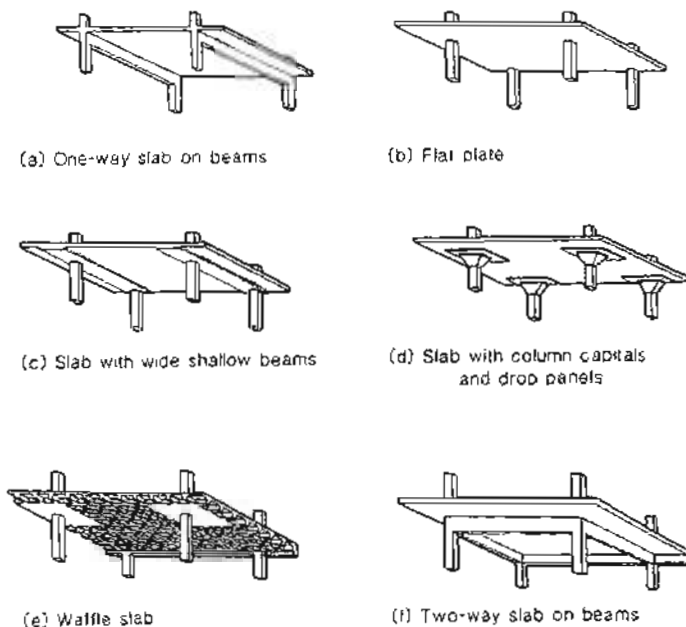


Figure 11-1 Types of post-tensioned slabs.

For spans of 24 to 40 ft (7 to 12 m) and live loads up to about 100 psf (5 kN/m^2) flat plate structures (see Fig. 11-1b) or slabs containing wide shallow beams (see Fig. 11-1c) are commonly used. For flat plate structures, span-to-depth ratios of about 45 are typical. For larger spans or larger live loads flat slabs with column capitals and/or drop panels (see Fig. 11-1d), waffle slabs (see Fig. 11-1e), or two-way slabs supported on beams (see Fig. 11-1f) are used. Slabs with drop panels can have span-to-depth ratios of about 55, while waffle slabs have span-to-total-depth ratios of about 35.

Floor slabs of buildings are relatively thin and the tendons are usually post-tensioned over several spans. The use of bonded tendons with corrugated sheaths having a circular cross section results in a large reduction in eccentricity as well as large frictional losses. The use of sheaths having an oval-shaped cross section enables bonded construction to be used without sacrificing as much of the eccentricity. The influence of tendon type on the available eccentricity is illustrated in Fig. 11-2. It can be seen that in order to attain the same eccentricities, larger slab thicknesses are required when bonded tendons are used.

In North America most post-tensioned slabs are prestressed using unbonded monostrand tendons consisting of a grease-coated, seven-wire strand encased in a plastic tube (see Fig. 2-12b). The small, lightweight stressing jacks used with these monostrand tendons

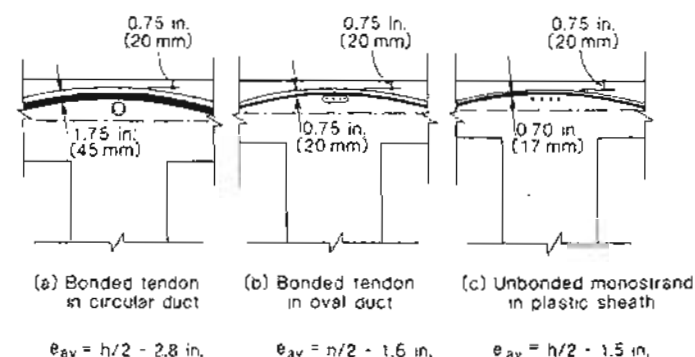


Figure 11-2 Effect of tendon type on eccentricity. Adapted from Ref. 11-1.

(see Fig. 2-18) permit the stressing operation to be carried out by one person. The simplicity of the stressing operation combined with the elimination of grouting enables unbonded post-tensioned slabs to be constructed more economically.

The design of a post-tensioned slab must ensure that concrete stresses will not be excessive at service loads, that adequate strength is provided to resist factored loads, and that the deflections of the slab remain within acceptable limits.

Two-way post-tensioned slabs are an efficient structural system which, being highly redundant, have many different ways of carrying the load. Because the structure is highly redundant, the designer has considerable freedom in proportioning and distributing the prestressing steel and the non-prestressed reinforcement.

Aspects of slab behavior that the designer must consider are discussed in the sections below. An appropriate design sequence is illustrated in the design example given in Section 11.12.

11.2 FACTORS INFLUENCING CHOICE OF SLAB THICKNESS

In choosing the slab thickness the designer must consider deflection control, shear resistance, fire resistance, and corrosion protection for the reinforcement.

While it is required to calculate deflections (see Section 11.11), at the preliminary design stage it is usual to calculate a minimum thickness for deflection control based on traditional span-to-depth ratios. Table 11-1 gives suggested span-to-depth ratios which have resulted in economical post-tensioned slabs that displayed satisfactory structural performance.

The deflection-control characteristics of post-tensioning enables very thin slabs to be used. Unless drop panels or column capitals are used, the load-carrying capacity of such thin two-way slabs will typically be governed by the punching shear resistance around the

Table 11-1 Span-to-depth ratios suggested by the Post-Tensioning Institute (Ref. 11-2).

One-way slab	48
Two-way slab	45
Two-way slab with drop panel (minimum drop panel at least $\frac{1}{6}$ each way)	50
Two-way slab with two-way beams	35
Waffle (5×5 grid)	35
Beams $b \geq h/3$	20
Beams $b \geq 3h$	30

columns. Hence in the design it is wise to check whether the slab thickness has adequate shear capacity. Procedures for checking the shear capacity are described in Section 11.10.

The fire resistance of a slab depends upon the concrete aggregate type, the overall thickness of the slab, the concrete cover over the reinforcement, and the restraint to thermal expansion. A summary of the requirements for fire resistance is given in the *Post-Tensioning Manual* (Ref. 11-3) and in Ref. 11-2. A comprehensive discussion of the fire resistance of post-tensioned structures is given by Gustafsson in Ref. 11-4. Fire endurance of a floor slab can be determined by subjecting a slab to the standard fire exposure (Ref. 11-5). Usually, the fire endurance of a post-tensioned slab is governed either by the temperature of the unexposed surface rising by an average of 250°F (140°C) or by the temperature of the tendons reaching 800°F (427°C). The time required to reach the critical temperature rise in the unexposed surface of a slab is controlled by the thickness of the slab and the thermal conductivity of the concrete. Minimum recommended slab thicknesses are given in Table 11-2.

Table 11-2 Required slab thickness in in. (mm) for different fire endurances.

Aggregate Type	Fire Endurance				
	1 hr	1 1/2 hr	2 hr	3 hr	4 hr
Siliceous	3 1/2 (89)	4 1/4 (108)	5 (127)	6 1/4 (159)	7 (178)
Carbonate	3 1/4 (83)	4 1/8 (105)	4 5/8 (117)	5 3/4 (146)	6 5/8 (168)
Lightweight	2 5/8 (67)	3 1/4 (830)	3 3/4 (951)	4 5/8 (1171)	5 1/4 (133)

For unrestrained slabs the values of minimum cover given in Table 11-3 are based on estimating the time required for the temperature of the tendon to reach about 800°F (427°C). At this temperature the tendon has lost about one-half of its tensile strength and hence it is assumed that an unrestrained slab would collapse. Heating of the slab causes the slab to try to expand, pushing against the surrounding structure. The restraint of this thermal expansion will induce compressive stresses into the slab which will increase

Sec. 11.3 Corrosion Protection of Unbonded Tendons

the slab's flexural strength. This enhancement of strength is referred to as compressive membrane action. Compressive membrane action will be induced by the restraint offered by the columns and/or the restraint offered by regions of the slab unaffected by the fire.

Recognizing the beneficial effects of restraint, the Post-Tensioning Institute (Ref. 11-3) recommends the use of the concrete cover values listed in Table 11-3. It is usually assumed, when using Table 11-3, that a two-way slab with several spans in each direction is restrained against thermal expansion.

Table 11-3 Minimum concrete cover in in. (mm) over post-tensioned tendons in concrete slabs*, suggested by the Post-Tensioning Institute. From Ref. 11-3.

Restraint	Aggregate Type	Fire Endurance				
		1 hr	1 1/2 hr	2 hr	3 hr	4 hr
Unrestrained	Siliceous	3/4 (19)	1 1/4 (32)	1 1/2 (38)	2 1/8 (54)	—
	Carbonate	3/4 (19)	1 1/16 (27)	1 3/8 (35)	1 7/8 (48)	—
	Lightweight	3/4 (19)	1 (25)	1 1/4 (32)	1 5/8 (41)	—
Restrained	Siliceous	3/4 (19)	3/4 (19)	3/4 (19)	1 (25)	1 1/4 (32)
	Carbonate	3/4 (19)	3/4 (19)	3/4 (19)	1 (25)	1 1/4 (32)
	Lightweight	3/4 (19)	3/4 (19)	3/4 (19)	3/4 (19)	1 (25)

*For bonded tendons cover is measured to the surface of the tendon.

For unbonded tendons cover is measured to the surface of the duct.

Cover is measured from fire-exposed surface of slab (i.e., usually bottom of slab).

As indicated in Section 3.19, the minimum clear concrete cover for slabs is 3/4 in. (20 mm) for concrete not exposed to weather or in contact with the ground and 1 in. (25 mm) for concrete exposed to earth or weather. For concrete exposed to corrosive environments, such as those caused by de-icing chemicals or sea water, the ACI Code (Ref. 11-6) recommends that "the amount of concrete protection shall be suitably increased and denseness and non-porosity of the protecting concrete shall be considered or other protection shall be provided." The ACI Commentary (Ref. 11-6) suggests that for corrosive environments, the minimum clear concrete cover for slabs should be 2 in. (50 mm).

11.3 CORROSION PROTECTION OF UNBONDED TENDONS

Because post-tensioned slabs are usually prestressed with unbonded single-strand tendons the designer must carefully consider the corrosion protection of these tendons. Some

structures in which the corrosion protection of the strands was inadequate have required substantial repairs. Examples of such problems have been given by Schupack (Ref. 11-7) and by Aalami and Swanson (Ref. 11-8).

To avoid corrosion, water and corrosion-inducing chemicals must be prevented from reaching the prestressing strands and destroying the passivity of the steel (see Section 3.19). The three barriers that protect the steel are the concrete cover, the plastic sheath, and the grease. The ACI Code (Ref. 11-6) requires that both the concrete cover and the concrete quality be increased as the environment becomes more corrosive. One aspect of the concrete barrier that is sometimes overlooked is the protection of the end anchorage. Schupack (Ref. 11-7) reports that "poor end anchor protection is a predominant cause of tendon failures." Careful filling of the anchorage pocket with high-quality grout that provides the specified concrete cover is required.

There have been significant improvements in unbonded tendon technology that improve the effectiveness of the second and third barriers to corrosion. Early tendons consisted of paper-wrapped strands that were filled with grease. Plastic sheaths were introduced in the 1960s. Although pushed-through sheaths (tendon and grease are pushed into the plastic sheath) and heat-sealed sheaths (sheath is heat sealed over the grease) were significant improvements over the paper-wrapped sheaths, they did not always provide a tightly packed system capable of keeping water out of the sheath. Extruded plastic sheaths, which are produced by extruding the plastic sheathing over the grease-covered strand, were introduced in 1970 and provide the best means of producing a watertight system. In 1985 the Post-Tensioning Institute provided specifications (Ref. 11-9) for unbonded single-strand tendons. These specifications addressed details for anchorages, couplers, sheathing, corrosion-protective coatings, and installation of tendons. In corrosive environments, these recommendations require that the sheathing be "connected to all stressing, intermediate, and fixed anchorages in a watertight fashion, thus providing a complete encapsulation of the prestressing steel" (see Fig. 2-18). The ACI Code (Ref. 11-6) requires that unbonded strands be protected against corrosion in accordance with the Post-Tensioning Institute's recommendations. Schupack (Ref. 11-7) recommends that for corrosive environments, consideration be given to a system involving total encapsulation. The main feature of this system is the continuous plastic covering of all metal components in order to electrically insulate the tendon and hardware. Because workmanship is a key factor in providing adequate corrosion protection, the Post-Tensioning Institute gives recommended field procedures (Ref. 11-10) for unbonded single-strand tendons that should be followed carefully.

Further aspects of corrosion protection for parking garages are discussed in Chapter 12 and aspects of evaluation and rehabilitation of corrosion-damaged structures are treated in Chapter 15.

11.4 LOAD BALANCING

Load balancing is a useful concept in understanding the manner in which two-way post-tensioned slabs respond to load. This concept enables the engineer to make an appropriate choice of tendon profile, prestressing amounts and tendon distribution.

As discussed in Section 9.12, a tendon curving with a radius of R pushes against the concrete with a radial force of P/R per unit length, where P is the tension in the tendon. For the typical tendon profile shown in Fig. 11-3 the radius of the tendon near midspan can be determined from the parabolic geometry as $\ell_1^2/8f_1$ (see Fig. 2-23). Therefore, in the concave-upward portion of the profile in Fig. 11-3, an effective upward load of $w = 8Pf_1/\ell_1^2$ per tendon acts on the concrete. In the concave downward portion of the tendon profile, near the column lines, a more intense downward load will act. If 90% of the tendon length is curving upward while 10% curves downward, the downward force per unit length will be nine times higher than the upward force per unit length (i.e., $9w$). Because prestressing is a self-equilibrating system, the total vertical load on the concrete caused by the prestressing tendons sums to zero.

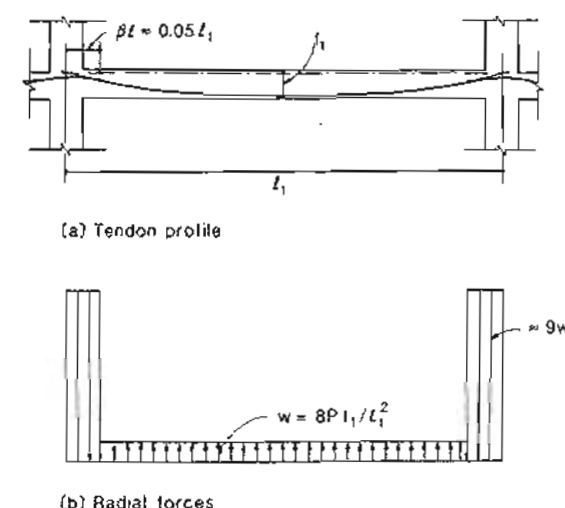


Figure 11-3 Typical tendon profile.

To illustrate the load-balancing concept for two-way post-tensioned slabs, we will consider an interior square panel of a flat plate structure containing uniformly spaced tendons in the two directions (see Fig. 11-4). It will be assumed that the tendons curve upward over 90% of the span length (see Fig. 11-3) and the drape and tendon force is such that the tendons in each direction produce an upward loading of w per unit area in the portion of the span where they curve upward.

Figure 11-5 illustrates the loads on the concrete resulting from the uniformly distributed tendons. The E-W tendons cause an upward force of w per unit area over 90% of the span where they curve upward and a downward force of $9w$ per unit area over the remaining 10% of the span (see Fig. 11-5b). The N-S tendons produce a similar effect.

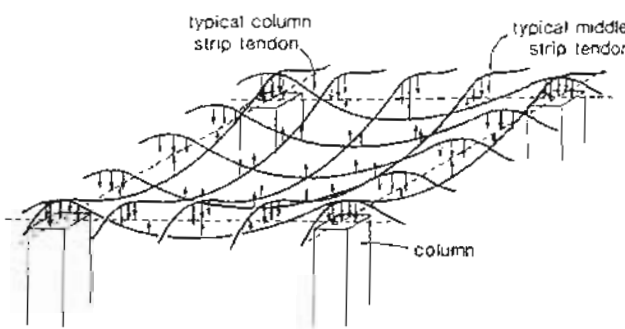


Figure 11-4 Radial forces acting on the concrete for a uniform tendon distribution.

Summing the loadings on the concrete from both sets of tendons results in the loads per unit area shown in Fig. 11-5d. If the dead load of the slab also happens to equal w per unit area, the net effect of the prestressing tendons and the dead load of the slab is as shown in Fig. 11-5e. It can be seen that the net result is an upward load of w per unit area in the large central portion of the slab where both sets of tendons curve upward and an intense downward load of $19w$ per unit area in the small corner regions of the slab where both sets of tendons curve downward. The resulting forces in the different areas of the slab are shown in Fig. 11-5f, where it can be determined that the total downward force equals the self-weight of the slab, $w\ell^2$.

If rather than using uniformly spaced tendons, the tendons are concentrated near the column lines, a better "balance" of the dead load of the slab will be achieved. Figure 11-6a illustrates a tendon distribution in which 25% of the tendons are placed in the middle strips (the middle 50% of the panel) while the remaining 75% of the tendons are concentrated in the column strips.

It can be seen from Fig. 11-6e that this distribution of tendons results in the central portion of the slab being "balanced" with no net upward or downward loading. It can be appreciated from Fig. 11-6e and f that the deflections of a slab, post-tensioned in this manner, will be very small.

Irrespective of the arrangement of tendons, the total prestressing force required to balance a uniform downward load of w is

$$P_1 = \frac{w\ell^2}{8f_1} \quad \text{for direction 1} \quad (11-1)$$

$$P_2 = \frac{w\ell^2}{8f_2} \quad \text{for direction 2} \quad (11-2)$$

where P_1, P_2 = average prestressing force per unit width of slab for tendons in the 1 and 2 directions, respectively

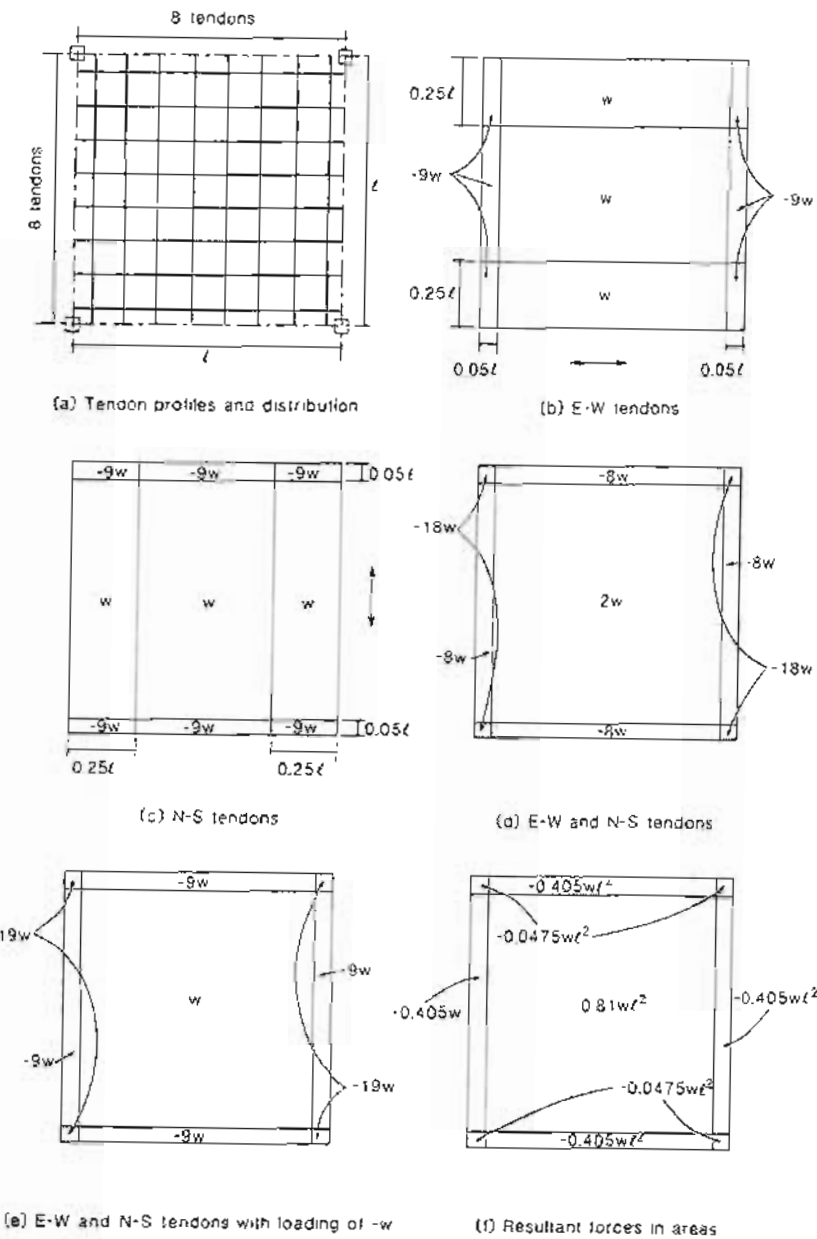


Figure 11-5 Load balancing in a two-way slab with uniformly distributed tendons

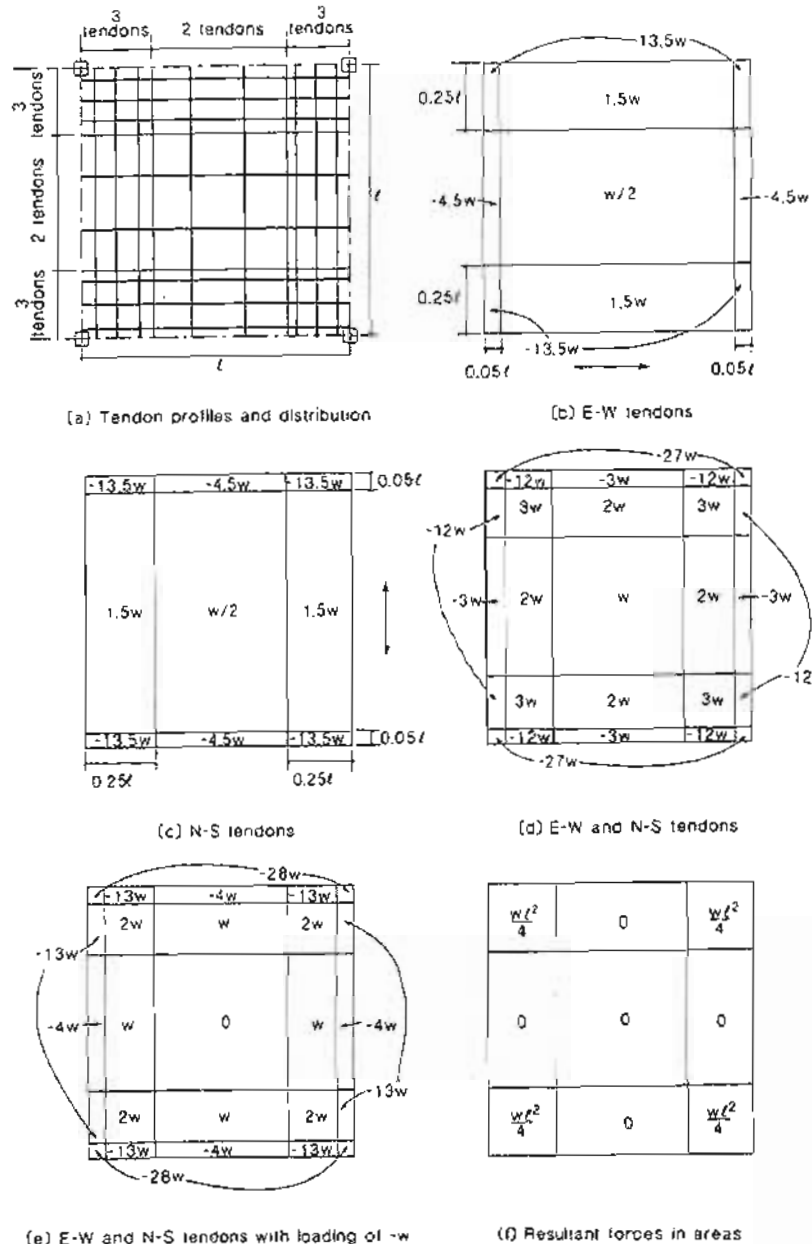


Figure 11-6 Load balancing in a two-way slab with 75% of the tendons concentrated in the column strips.

f_1, f_2 = equivalent drape of the tendon in the 1 and 2 directions, respectively
 ℓ_1, ℓ_2 = span in the 1 and 2 directions, respectively

11.5 DISTRIBUTION OF TENDONS IN TWO-WAY SLABS

As discussed in Section 11.4, a more uniform load balancing is achieved if the tendons are concentrated in the column strips. Figure 11-7 illustrates the construction of a post-tensioned slab containing tendons concentrated in the column strips.

As can be seen from Fig. 11-8, there are many different tendon distributions possible. It is possible, for example, to concentrate all of the tendons in bands running along column lines. Such bands would act as prestressed concrete beams supporting the edges of each slab panel. The interior of each panel would then need to be reinforced as a two-way slab supported on beams (see Fig. 11-8a).

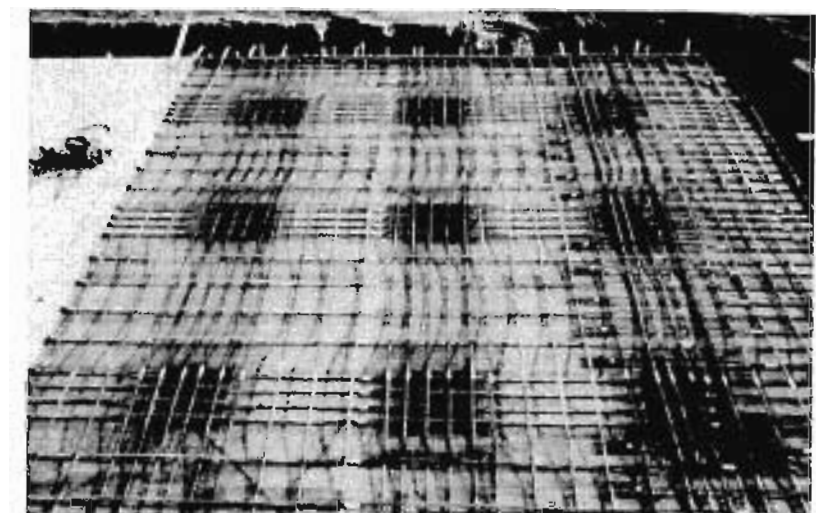


Figure 11-7 Tendon distribution showing concentration of tendons in column strips. Photograph courtesy of VSL International Ltd. (Ref. 11-1).

An alternative solution would be to use banded tendons in one direction and uniformly distributed tendons in the other direction (see Fig. 11-8b). In this solution the slab acts as a one-way slab in the direction of the uniformly distributed tendons supported by the "prestressed concrete beams" formed by the tendon bands. The tendon layout of Fig. 11-8b can achieve uniform load balancing and has the additional advantage of making the tendons simple to place. Excellent performance at both service load and at ultimate load levels of slabs designed in this manner has been observed in tests conducted by Burns, Hemakom, and Winter (see Ref. 11-2).

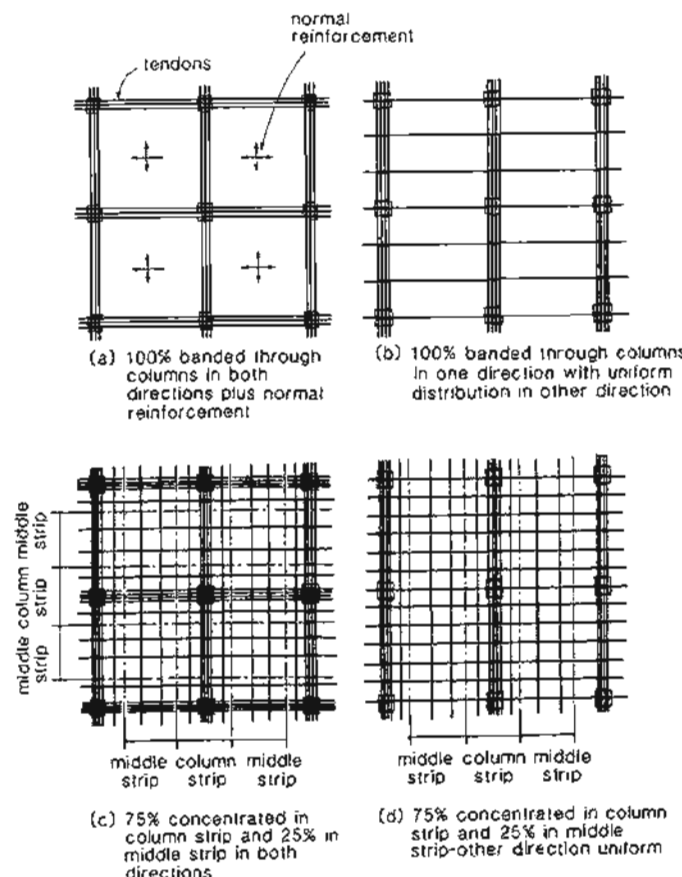


Figure 11-8 Examples of tendon distributions.

A more traditional tendon layout is shown in Figs. 11-8c and 11-7. This layout attempts to more closely match the elastic distribution of moments shown in Fig. 11-9. Recommended distributions for this layout include (1) placing 65 to 75% of the tendons in the "column strip," with the remainder being placed in the "middle strip" (Refs. 11-11 and 11-12), or (2) placing 50% of the tendons directly over the columns and the remainder uniformly distributed between the columns (Ref. 11-1).

The advantages of using tendons concentrated or banded in the column strip region rather than using uniform distributions of tendons in the two directions include:

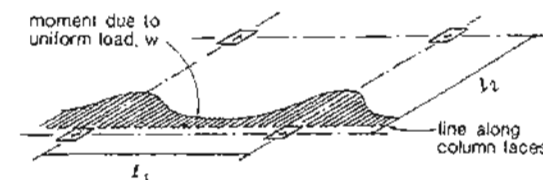


Figure 11-9 Elastic distribution of moments along column line.

1. A more uniform load-balancing effect is achieved.
2. The distribution more closely resembles the distribution of moments in the slab.
3. Concentration of tendons in the immediate column region increases the punching shear strength of the slab.
4. Tendons concentrated in a region through the column and immediately around the column result in an increase in moment-transfer strength of the slab-column connection.
5. Banding tendons in one or more directions facilitates placement of the tendons, whereas a uniform tendon distribution in both directions would require "weaving" of the tendons to obtain the required tendon profiles.

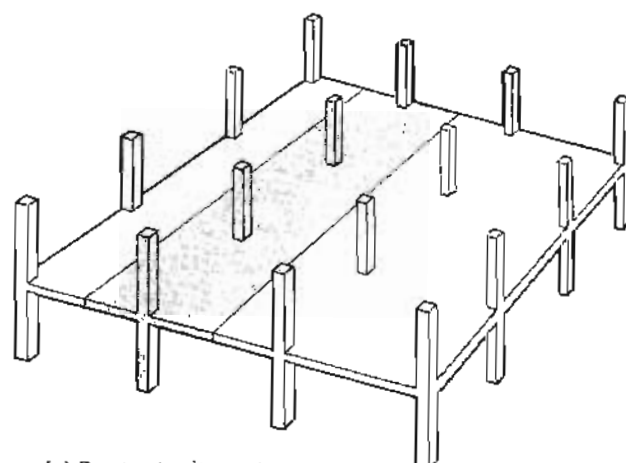
11.6 ANALYSIS USING THE EQUIVALENT FRAME METHOD

Before the flexural stresses at service load level or the flexural capacity under factored loads can be checked, it is necessary to determine the moments at critical sections in the slab caused by loading. The equivalent frame method is the most popular method in North America for the analysis of two-way slabs (see Ref. 11-6). This approach involves performing elastic analyses of "equivalent" two-dimensional frames composed of the slab strips connected to the columns above and below the slab being designed (see Fig. 11-10). This method is used for analyzing two-way post-tensioned slabs for service conditions as well as for ultimate conditions. A variety of frame analysis computer programs can be used to perform the analyses. The equivalent frame method is used to design a wide variety of two-way post-tensioned slabs, including flat plates, slabs supported on beams, flat slabs, and waffle slabs.

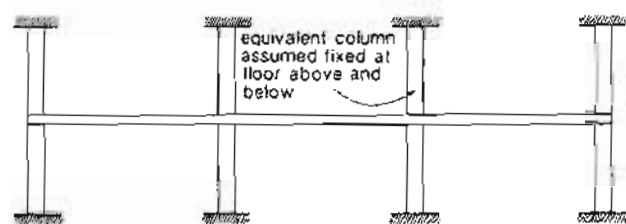
The steps used in the analysis are summarized below.

Step 1: Divide the slab into design strips.

Divide the slab into a series of design strips in the two principal directions of the structure. The width of each design strip is a function of both the center-to-center span, ℓ_1 , in the direction of the design strip, and the center-to-center span, ℓ_2 , perpendicular to the design strip as illustrated in Fig. 11-11.



(a) Design strip in structure



(b) Idealized two-dimensional frame for design strip

Figure 11-10 Equivalent frame idealization.

Step 2: Calculate the stiffnesses of equivalent frame members.

The stiffnesses of the slabs and the columns are then determined as illustrated in Fig. 11-12. The stiffnesses of the columns are then reduced to account for the twisting of the slab as shown in Fig. 11-13.

The equivalent column stiffness, K_{ec} , is determined from

$$\frac{1}{K_{ec}} = \frac{1}{\sum K_c} + \frac{1}{K_t} \quad (11-3)$$

where $\sum K_c$ is the sum of flexural stiffnesses of columns at the joint, and K_t is the torsional stiffness of the assumed torsional members attached to the column and perpendicular to

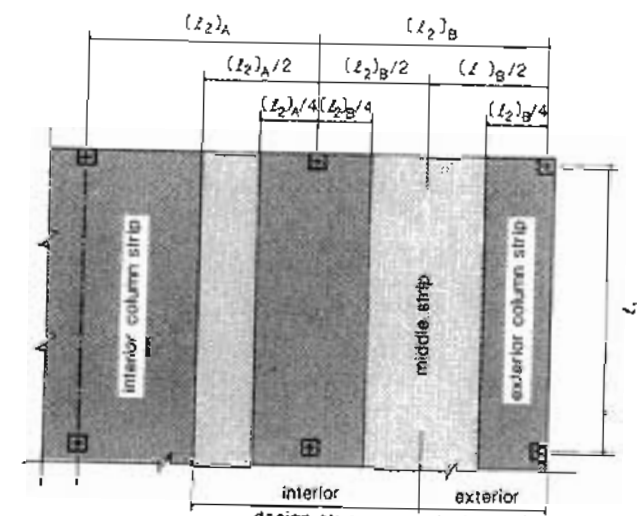
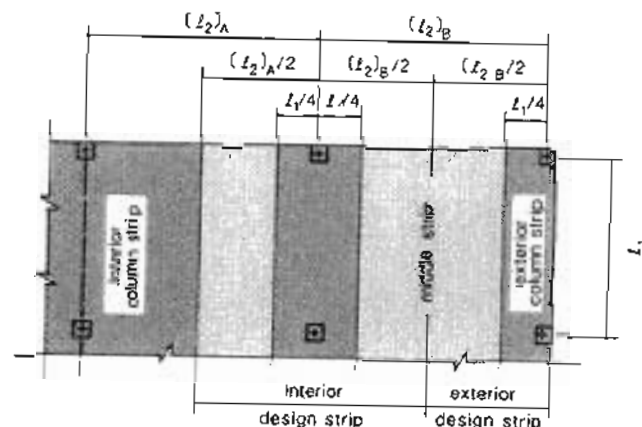
(a) Column strip for $l_2 \leq l_1$ (b) Column strip for $l_2 > l_1$

Figure 11-11 Definition of design strip.

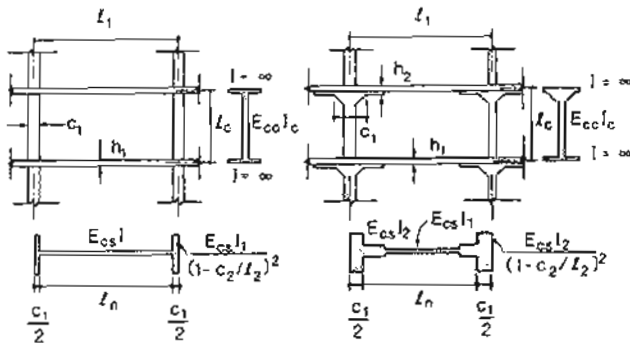


Figure 11-12 Determining the slab and column stiffnesses.

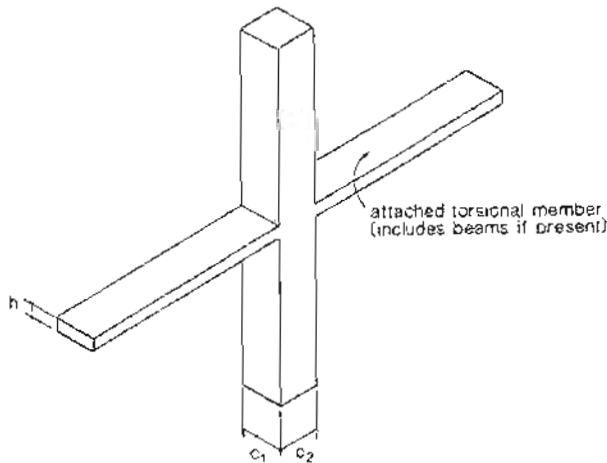


Figure 11-13 Column with attached torsional members.

the direction in which moments are being calculated. If torsional cracking is ignored,

$$K_t = \frac{\sum 9E_{cs}C}{L_2(1 - c_2/L_2)^3} \quad (11-4)$$

where

$$C = \frac{(1 - 0.63x/y)x^3y}{3} \quad (11-5)$$

and x and y are equal to h and c_1 for the case of a slab without beams.

Step 3: Analyze equivalent frames.

For different design strips determine the fixed-end moments due to the final prestressing after all losses. The final prestressing force can be approximated by assuming a lump sum loss. The equivalent frame is then analyzed to find the restraint moments. Perform separate analyses of the equivalent frame subjected to (1) slab dead loading, (2) additional dead loading, and (3) live loading.

It is important to recognize that the frame analyses may require different equivalent frames due to the sequence of construction. During the post-tensioning operation the columns above the slab may or may not offer restraint depending on whether the slab above has been constructed. Hence the equivalent frame used in determining the effects of prestressing and the slab dead load immediately after stressing may be different than the frame used to determine the moments due to the other loading effects as shown in Fig. 11-14.

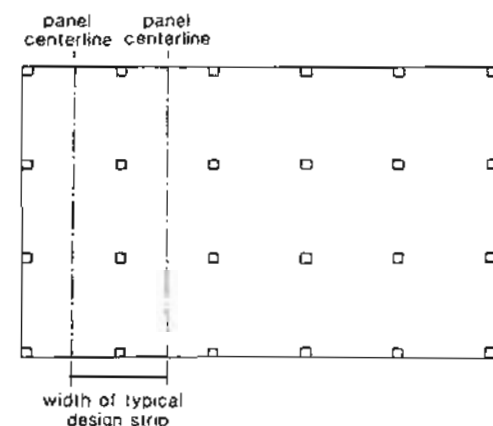
As discussed in Section 10.13, while the sequence of construction greatly influences the initial moments in a statically indeterminate structure, creep considerably reduces the influence of sequence of construction. Hence it is customary to neglect the influence of the sequence of construction when determining the moments in two-way floor slabs. For these structures the stresses under initial conditions are typically not critical. The moments calculated from the equivalent frame method are then used in checking the stresses in the slab at service loads and in checking the required flexural capacities of the slab.

11.7 STRESS CHECKS AND CONTROL OF CRACKING

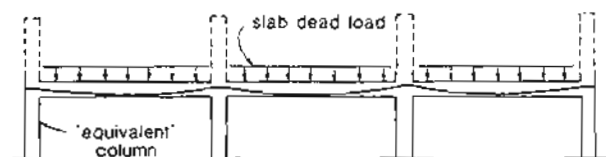
The ACI Code (Ref. 11-6) ensures crack control by limiting concrete tensile stresses to $6\sqrt{f'_c}$ psi ($0.5\sqrt{f'_c}$ in MPa) and by providing minimum amounts of bonded non-prestressed reinforcement. The stresses at service load level are determined using the moments calculated from the equivalent frame analysis. The moments used in calculating the stresses are the average moments across the entire width of the design strip. That is, no attempt is made to account for the actual distribution of moments across the design strip width (see Fig. 11-9). The ACI Code requirements for bonded reinforcement are summarized in Table 11-4.

The bonded reinforcement required in negative moment regions must be placed within a zone in the slab bounded by lines that are 1.5 times the slab thickness from the face of the column. At least 4 bars must be provided in each direction and the spacing of this bonded reinforcement must not exceed 12 in. (305 mm). These bars shall extend for at least one-sixth of the clear span from the faces of the support. The bonded reinforcement that may be required in the positive moment regions must have a minimum length of one-third of the clear span and must be centered in the positive moment area.

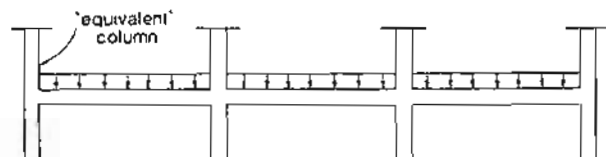
Figure 11-15 illustrates the bonded reinforcement required in the negative moment region of an 8 in. (203 mm) thick flat plate post-tensioned with unbonded tendons supported



(a) Design strip in a typical floor of multistory building



(b) Equivalent frame for prestressing and slab dead load



(c) Equivalent frame for additional dead load and live load

Figure 11-14 Equivalent frames for analysis

Table 11-4 Minimum amounts of bonded non-prestressed reinforcement required by the ACI Code (Ref. 11-6)

Type of Tendon	Bonded	Unbonded*
Beams and one-way slabs	0	0.004A
Flat Plates		
Negative moment regions	0	0.00075hℓ
positive moment regions	0	$N_c/(0.5f_y)$

*h, slab thickness; ℓ, span in direction of reinforcement; A, area of cross section subjected to tensile stress. N_c , tensile force in concrete under dead and live loads.

[†]Computed tensile stress $\leq 2\sqrt{f'_c}$.

on 24 in. (610 mm) square columns spaced at 27 ft (8.2 m) centers. From Table 11-4.

$$\begin{aligned}
 A_s &= 0.00075h\ell \\
 &= 0.00075 \times 8 \times 27 \times 12 \\
 &= 1.94 \text{ in}^2 (1254 \text{ mm}^2)
 \end{aligned}$$

Therefore, use ten #4 (13 mm diameter) top bars in both directions as shown.

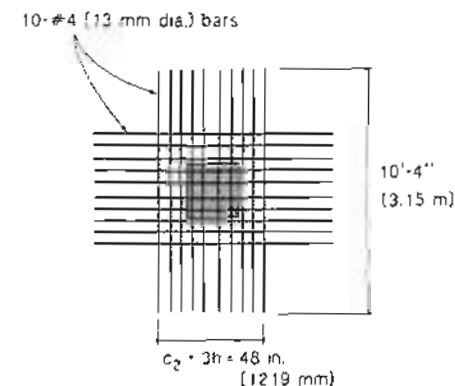


Figure 11-15 Example of amount and distribution of bonded top reinforcement in slab at interior column.

11.8 SPECIAL CONSIDERATIONS FOR EDGE AND CORNER PANELS

Figure 11-16 illustrates a situation with 100% of the tendons in one direction passing through the columns. Due to the distance required for the spreading of the compressive stresses from the anchorage regions, there are edge zones that are not prestressed. In these zones bonded reinforcement should be placed perpendicular to the free edge.

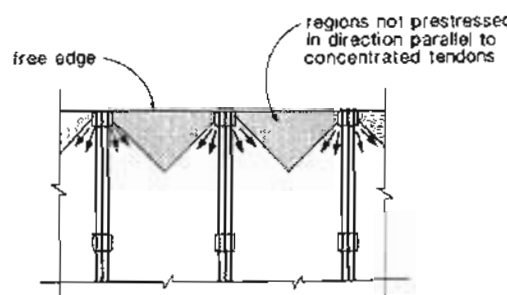


Figure 11-16 Non-prestressed regions in two-way slab with highly concentrated tendons.

The recommended practice in Switzerland (Ref. 11-1) requires a minimum amount of bonded bottom non-prestressed reinforcement perpendicular to the edge in all end spans. The required reinforcement ratio is

$$\rho_s = 0.0015 - 0.5\rho_p \quad (11-6)$$

but not less than 0.0005

where ρ_s is the reinforcement ratio based on the average effective depth, d , measured to the non-prestressed reinforcement ($\rho_s = A_s/bd$) and ρ_p is the reinforcement ratio for the prestressing steel based on the effective depth, d_p , measured to the prestressing steel ($\rho_p = A_{ps}/bd_p$). The resulting layout of this bottom bonded reinforcement is shown in Fig. 11-17.

11.9 INVESTIGATION OF THE FLEXURAL CAPACITY OF SLABS

The flexural capacity of slabs is usually investigated by comparing the factored moments, M_d , determined from the equivalent frame analysis, with the design flexural strengths, ϕM_n , computed using the procedures of Section 6.9. Once again no consideration is given to the manner in which these moments are distributed across the width of the design strip.

Since two-way slabs have a high degree of static indeterminacy there will be considerable redistribution of moments prior to flexural failure of the slab. The ACI Code

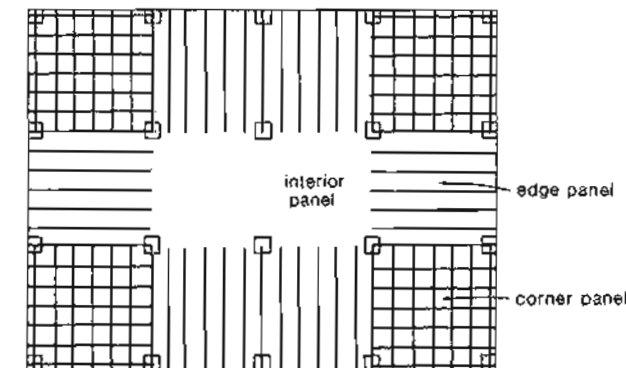


Figure 11-17 Required bottom reinforcement for edge panels. From Ref. 11-1.

permits some allowance to be made for this redistribution of moments. The negative moments calculated from the equivalent frame analysis can be decreased or increased such that

$$\text{percentage change in moment} = 20 \left[1 - \frac{\omega_p + \frac{d_p}{d}(\omega - \omega')}{0.36\beta_1} \right] \quad (11-7)$$

However, redistribution is not permitted if the amount calculated by Eq. (11-7) is less than 6.7%

Rather than estimating the flexural capacity of slabs from the elastic equivalent frame analysis together with limited redistribution, use can be made of yield line theory. Yield line theory is a simple but powerful approach for estimating the loads at which a flexural failure mechanism will form. It is based on the concept that flexural failure of a slab will not occur until flexural yielding of the slab sections has extended over a large enough region of the slab so that a failure mechanism can form. A comprehensive treatment of yield line theory is given by Park and Gamble (Ref. 11-13), while a summary of useful expressions is given by Ritz et al. (Ref. 11-1).

Figure 11-18 illustrates yield line mechanisms that need to be investigated for a typical two-way slab structure. The "yield" moments are assumed to be equal to the design flexural strength. A conservative assumption is made that the negative moment yield lines pass through the centerlines of the columns instead of along lines joining the column faces.

If the yield line mechanism for an interior span is considered (see Fig. 11-18a), then for a virtual displacement of 1 at midspan the external work can be equated to the internal work as

$$\frac{w_f \ell_1 \ell_2}{2} = \frac{4m_p \ell_2}{\ell_1} + \frac{4m_n \ell_1}{\ell_1}$$

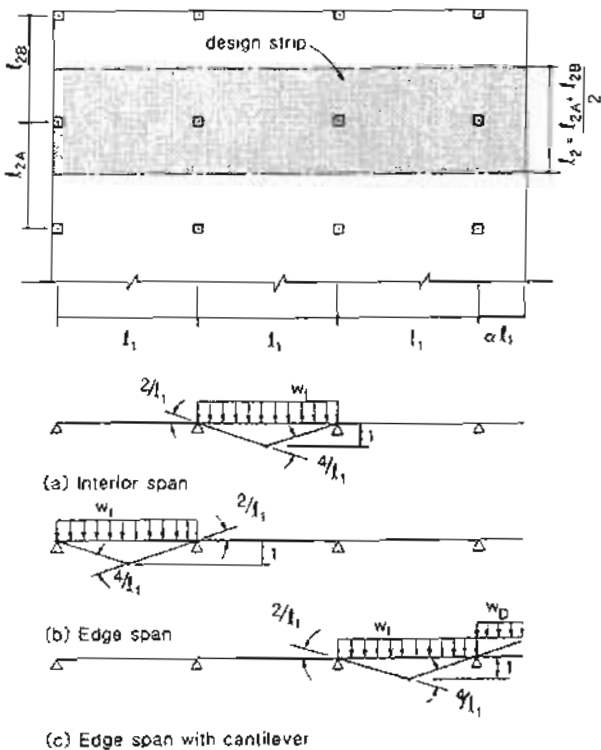


Figure 11-18 Yield line analysis of two-way slab.

and hence

$$w_f = \frac{8}{l_1^2} (m_p + m_n) \quad (11-8)$$

where w_f = factored uniformly distributed load

l_1 = center-to-center span between columns

l_2 = design strip width (see Fig. 11-18)

m_n = negative "yield" moment per unit width of slab

m_p = positive "yield" moment per unit width of slab.

The yield line mechanism for an edge span (Fig. 11-18b) results in

$$w_f = \frac{8}{l_1^2} (m_p + \frac{m_n}{2}) \quad (11-9)$$

The factored loading on an edge span with a cantilever of length αl_1 (see Fig. 11-18c), assuming that only the service dead load, w_d , acts on the cantilever, is

$$w_f = \frac{8}{l_1^2} (m_p + \frac{m_n}{2}) + 2w_d\alpha^2 \quad (11-10)$$

In determining the positive and negative moment resistances per unit length, m_p and m_n , the prestressing tendons and the reinforcing bars are treated as if they were uniformly distributed across the design strip, irrespective of their actual distribution.

Since the yield line approach gives an upper bound solution, the designer must be careful that another mechanism giving a lower loading does not exist. Figure 11-19 illustrates other possible mechanisms consisting of local fanning yield lines around the columns. If the column were a point support, then the factored loading on the slab to cause a fanning yield line mechanism to form would be

$$w_f = \frac{2\pi}{l_1^2} (m_p + m_n) \quad (11-11)$$

The load required to cause this fanning mechanism increases rapidly as the column dimensions increase. Ritz et al. (Ref. 11-1) suggest that if the column dimension is greater than about $0.06l_1$, this fanning mechanism will not be critical.

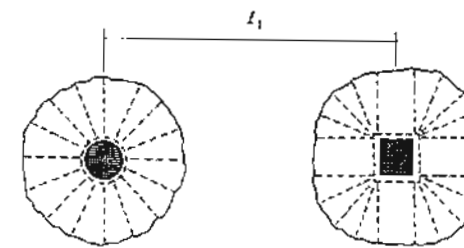


Figure 11-19 Fan yield line mechanisms.

11-10 SHEAR DESIGN OF SLABS

Due to their inherent ductility in flexure, two-way slabs display considerable ability in redistributing high local loads and in finding alternative ways of carrying the load. Further, the beneficial effects of compressive membrane action, usually neglected in the design, give the slabs an ability to resist surprisingly large overloads. A test on a two-way slab

and beam floor system by Ockleston (Ref. 11-14) demonstrated just how large this reserve of strength can be. The floor had been designed by the working stress method for a service live load of 70 psf (3.35 kN/m^2). A superimposed load of more than 10 times this load was required to fail the floor. Vecchio and Collins (Ref. 11-15) report an incident in which a flat slab designed for 125 psf (6.0 kN/m^2) supported a load of nearly 900 psf (43.1 kN/m^2) prior to collapse.

The load-carrying ability of a two-way slab will typically be governed by shear rather than flexure. Because slabs usually do not contain shear reinforcement, they will fail in a relatively brittle manner if local shear stresses become high enough to cause significant diagonal cracking.

As shown in Fig. 11-20, such shear failures can occur either by a failure plane occurring across the entire slab width (i.e., a wide-beam shear failure) or by a localized shear failure around a column. For interior columns such localized failures are usually called punching shear failures. For edge and corner columns the shear failures are more complex due to the combined effect of shear and moment transferred from the slab to the column.

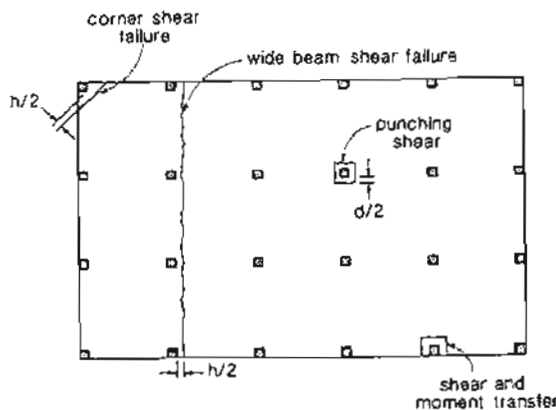


Figure 11-20 Types of shear failures.

The nominal shear strength for a wide-beam shear failure can be conservatively estimated using the one-way beam shear provisions as

$$\begin{aligned} V_c &= 2\sqrt{f'_c} b_w d & \text{psi} \\ V_c &= 0.17\sqrt{f'_c} b_w d & \text{MPa} \end{aligned} \quad (11-12)$$

where b_w is the length of the shear failure plane and d is the distance from extreme compression fiber to centroid of tension reinforcement but need not be less than $0.8h$. The design shear strength, ϕV_c , should exceed the factored shear at a section $h/2$ from the face of the column. Hawkins and Mitchell (Ref. 11-16) recommend that the same conservative approach be taken in checking the corner shear failure shown in Fig. 11-20.

In checking the punching shear capacity around interior columns in two-way prestressed concrete slabs, the ACI Code (Ref. 11-6) recommends that the nominal shear strength be taken as

$$V_c = (\beta_p \sqrt{f'_c} + 0.3 f_{pc}) b_o d + V_p \quad (11-13)$$

where β_p = smaller of 3.5 (0.29 in MPa units) or $\alpha_s d/b_o + 1.5$ ($\alpha_s d/b_o + 0.13$ in MPa units)

$\alpha_s = 40$ (3.33 in MPa units) for interior columns, 30 (2.50 in MPa units) for edge columns, and 20 (1.67 in MPa units) for corner columns

b_o = minimum perimeter of the critical section around the column which need not approach closer than $d/2$ to the face of the column

f_{pc} = average value of P/A for the two directions but P/A must be greater than 125 psi (0.86 MPa) in each direction and cannot be taken as greater than 500 psi (3.45 MPa). If f_{pc} is less than 125 psi (0.86 MPa) Eq. (11-14) should be used.

f'_c = specified compressive strength of the concrete but shall not be taken greater than 5000 psi (34.5 MPa)

V_p = vertical component of all effective prestress forces crossing the critical section

For exterior columns where any portion of the column cross section is closer than 4 times the slab thickness from the free edge, the nominal shear capacity shall be taken as

$$V_c = \left(2 + \frac{4}{\beta_c} \right) \sqrt{f'_c} b_o d$$

but

$$V_c \leq \left(\frac{\alpha_s d}{b_o} + 2 \right) \sqrt{f'_c} b_o d$$

and

$$V_c \leq 4\sqrt{f'_c} b_o d \quad \text{psi} \quad (11-14a)$$

$$V_c = \left(0.17 + \frac{0.33}{\beta_c} \right) \sqrt{f'_c} b_o d$$

but

$$V_c \leq \left(\frac{\alpha_s d}{b_o} + 0.17 \right) \sqrt{f'_c} b_o d$$

and

$$V_c \leq 0.33\sqrt{f'_c} b_o d \quad \text{MPa} \quad (11-14b)$$

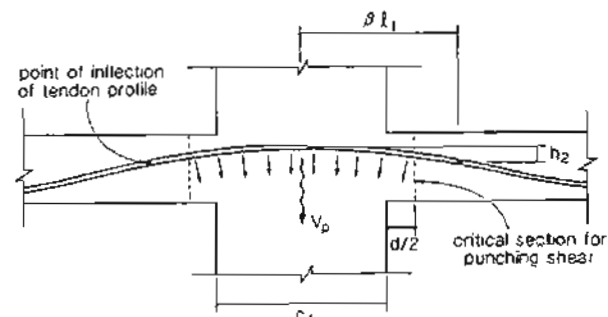
where β_c is the ratio of long to short sides of column.

Figure 11-21 illustrates the manner in which the vertical component of prestressing, V_p , can be calculated. It can be seen from Fig. 11-21b that the vertical component of the

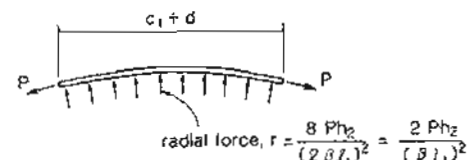
prestressing force crossing the critical section must be balanced by the radial forces, r , acting on the tendon. Hence the contribution of one tendon to V_p is

$$V_p = \frac{2Ph_2}{(\beta l_1)^2} (c_1 + d) \quad (11-15)$$

The total V_p is found by summing the contributions for all tendons in both directions crossing the critical section. Note that small changes in the actual tendon profile will significantly affect the value of V_p . It is therefore prudent to evaluate V_p conservatively.



(a) Tendon profile through column region



(b) Free-body diagram of tendon

Figure 11-21 Determination of V_p .

If the connection between the slab and the column is required to transmit moment in addition to the shear, its ability to transmit shear will be reduced. The ACI Code (Ref. 11-6) contains procedures to investigate these moment-transfer effects.

The ACI Code assumes that a fraction of the unbalanced moment, $\gamma_f M_{u1}$, is transmitted by flexural stresses in a slab width between lines that are $1.5h$ outside opposite faces of the column (see Fig. 11-22).

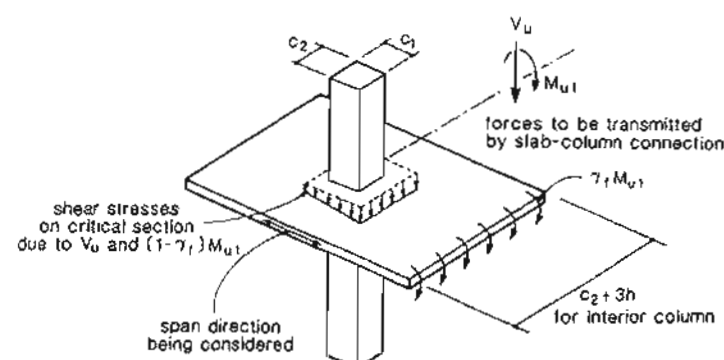


Figure 11-22 Shear and moment transfer in slab-column connections.

The fraction of the unbalanced moment, $\gamma_f M_{u1}$, not transferred by flexure, is considered to be transferred by a linear variation of shear stresses around the critical section. The resulting shear stress distribution around the critical section is obtained by summing the uniform shear stress due to the shear force, V_f , and the linearly varying shear stress due to the moment, $\gamma_f M_{u1}$ (see Fig. 11-23). If there are moments transferred in the two orthogonal directions (directions 1 and 2) the maximum shear stress can be written as

$$v_u = \frac{V_u}{A} + \frac{\gamma_{u1} M_{u1} e_1}{J_1} + \frac{\gamma_{u2} M_{u2} e_2}{J_2} \quad (11-16)$$

where the terms in this equation are defined for rectangular columns in Fig. 11-24. Note that the moments, M_{u1} and M_{u2} , are the moments about the centroidal axes of the critical section. For a circular interior column of diameter, D , the term J/e is $(D+d)^2d + d^3/3$.

The ACI Code (Ref. 11-6) requires that the calculated maximum shear stress due to factored shear and moment, v_u , not exceed the permissible shear stress resistance, v_c , where

$$v_c = \frac{\phi V_c}{b_s d} \quad (11-17)$$

where V_c is determined using Eq. (11-13) or (11-14).

Hawkins (Ref. 11-17) has recommended that reinforcing bars detailed to act as torsional reinforcement be provided in post-tensioned slabs at the exterior column-slab connections whenever the calculated upward shear stress on the exterior edge of the critical section exceeds $2\sqrt{f'_c}$ psi ($0.17\sqrt{f'_c}$ in MPa units). Such reinforcement is illustrated in Fig. 11-25.

The shear strength of slab-column connections can be increased by using column capitals, drop panels, or appropriately detailed shear reinforcement. The nominal shear

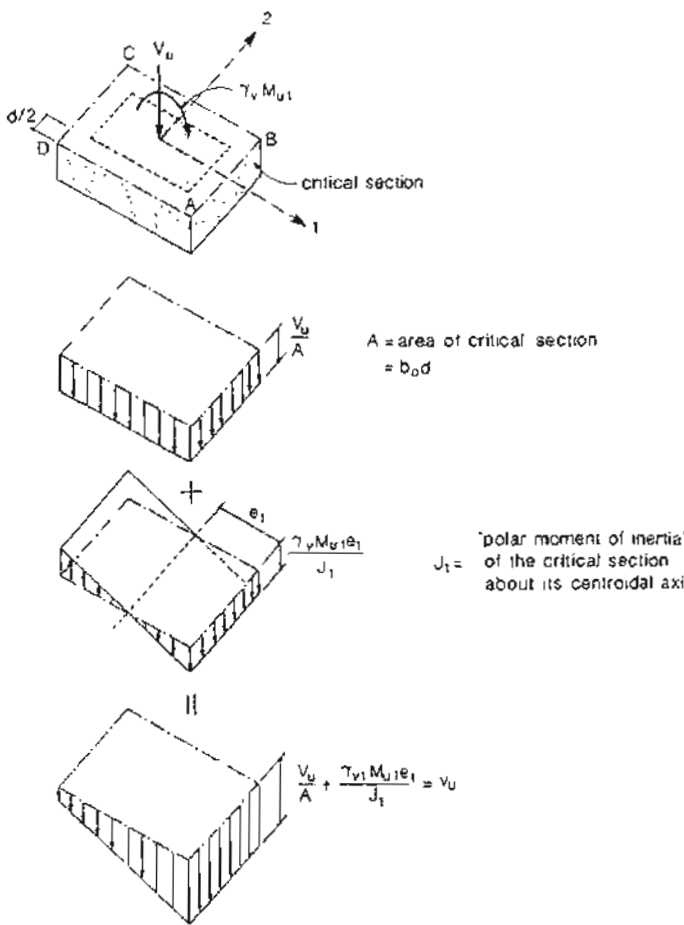


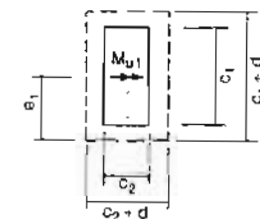
Figure 11-23 Shear stress distribution due to V_u and $\gamma_v M_{u1}$ for interior column.

strength, V_n , of slabs containing shear reinforcement is computed as $V_c + V_s$, where

$$\begin{aligned} V_n &= V_c + V_s \\ &= 2\sqrt{f'_c b_o d} + \frac{A_v f_y d}{s} \leq 6\sqrt{f'_c b_o d} \quad \text{psi} \quad (11-18) \\ V_n &= 0.17\sqrt{f'_c b_o d} + \frac{A_v f_y d}{s} \leq 0.5\sqrt{f'_c b_o d} \quad \text{MPa} \end{aligned}$$

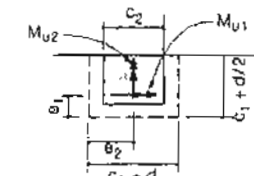
(a) Interior column

$$\begin{aligned} A &= 2d(c_1 + c_2 + 2d) \\ e_1 &= (c_1 + d)/2 \\ J_1 &= [(c_1 + d)d^3/6 + (c_1 + d)^3d/6 \\ &\quad + d(c_2 + d)(c_1 + d)^2/2] \\ \gamma_v &= 1 - \frac{1}{1 + \frac{2}{3}\sqrt{\frac{c_1 + d}{c_2 + d}}} \end{aligned}$$



(b) Edge column

$$\begin{aligned} A &= d(2c_1 + c_2 + 2d) \\ e_1 &= (c_1 + d/2)^2/(2c_1 + c_2 + 2d) \\ e_2 &= (c_2 + d)/2 \\ J_1 &= [(c_1 + d/2)d^3 + (c_1 + d/2)^3d]/6 \\ &\quad + (c_2 + d)d[e_1]^2 + 2(c_1 + d/2)d[(c_1 + d/2)/2 - e_1]^2 \\ J_2 &= [(c_2 + d)d^3 + (c_2 + d)^3d]/12 + 2(c_1 + d/2)d[e_2]^2 \\ \gamma_{v1} &= 1 - \frac{1}{1 + \frac{2}{3}\sqrt{\frac{c_1 + d/2}{c_2 + d}}} \\ \gamma_{v2} &= 1 - \frac{1}{1 + \frac{2}{3}\sqrt{\frac{c_2 + d}{c_1 + d/2}}} \end{aligned}$$



(c) Corner column

$$\begin{aligned} A &= d(c_1 + c_2 + d) \\ e_1 &= (c_1 + d/2)^2/[2(c_1 + c_2 + d)] \\ J_1 &= [(c_1 + d/2)d^3 + (c_1 + d/2)^3d]/12 \\ &\quad + (c_2 + d/2)d[e_1]^2 + (c_1 + d/2)d[(c_1 - d/2)/2 - e_1]^2 \\ \gamma_v &= 1 - \frac{1}{1 + \frac{2}{3}\sqrt{\frac{c_1 + d/2}{c_2 + d/2}}} \end{aligned}$$

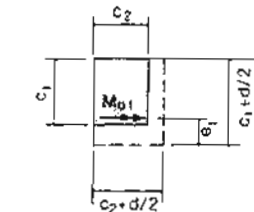


Figure 11-24 Parameters used in determining shear stresses for rectangular columns.

Because shear resistance often controls the design, it is wise to conduct a preliminary check of shear capacity during the early stages of the design process. In many cases the designer wishes to avoid the use of column capitals, drop panels, or shear reinforcement in the slab. In this case the shear capacity will be influenced primarily by the slab thickness and the column dimensions. At this preliminary stage of design the unbalanced moments

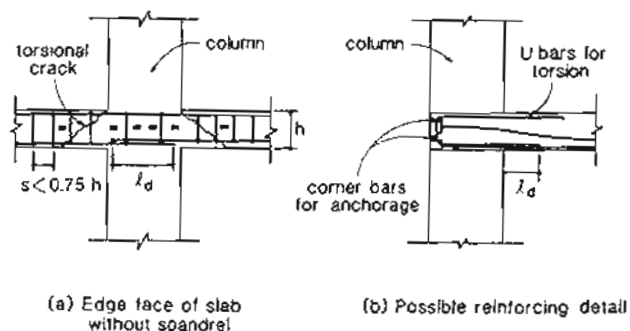


Figure 11-25 Torsional reinforcement in slab at exterior column connection.

which must be transferred by the slab-column connection will not be known. Simmonds (Ref. 11-18) recommends that to account approximately for the detrimental effect of moment transfer, the shear stress from shear acting above be multiplied by 1.2 for interior columns, 1.6 for edge columns, and 2.0 for corner columns.

11.11 ESTIMATION OF DEFLECTIONS OF SLABS

As discussed in Chapter 6, the ACI Code (Ref. 11-6) requires that the deflections of all prestressed concrete structures be investigated both for immediate deflections due to live load and for long-term deflections due to sustained loads. A significant portion of the gravity load deflection of the slab will be counteracted by the upward deflection due to prestress. Hence in calculating long-term deflections only that sustained load in excess of that balanced by the prestress needs to be considered.

The accurate calculation of the deflections of two-way post-tensioned slabs is a complex operation involving considerations of the boundary conditions, loading patterns and history, the change of stiffness due to local cracking, loss of prestress, and creep. For design purposes it is usually adequate to use simple, approximate, conservative expressions to estimate the deflections. If calculations show that deflections may be critical, a more detailed study can be made.

Figure 11-26a shows the deflected shape of a typical panel of a two-way slab. As can be seen, the deflection at the midpoint of the panel can be estimated by adding together the deflections of two orthogonal beam strips. In estimating the deflections of these beam strips, the expressions given in Fig. 11-26b are useful. For example, the maximum deflection of the interior panel in a 3-bay by 3-bay two-way slab with equal spans, subjected to a live

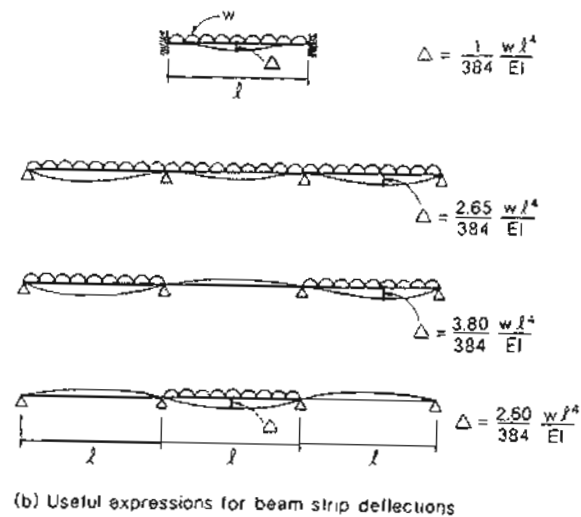
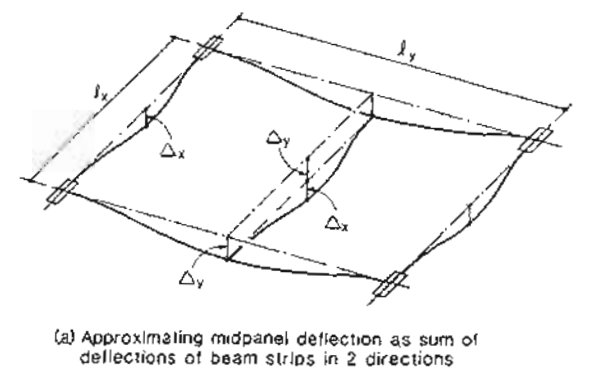


Figure 11-26 Estimating slab deflections.

load of w only on this interior panel is

$$\begin{aligned}\Delta &= \left(\frac{2.60 + 2.60}{384} \right) \frac{w l \times l^4}{E \times l \times h^3 / 12} \\ &= 0.163 \frac{w l^4}{E h^3}\end{aligned}\quad (11-19)$$

The expressions given in Fig. 11-26b can also be applied without undue loss of accuracy to slabs with more than three bays.

The use of gross stiffness values in the expression above is justifiable only if the tensile stresses in the concrete remain below the cracking stress. Scanlon and Murray (Ref. 11-19) suggest that in order to account for the effects of restrained shrinkage stresses the modulus of rupture should be reduced to $4\sqrt{f'_c}$ psi ($0.33\sqrt{f'_c}$ MPa). If cracking is predicted to occur, then the effective moment of inertia may be used to estimate the influence of cracking on the deflection.

11.12 EXAMPLE DESIGN OF POST-TENSIONED FLAT PLATE

The design of the flat plate floor system for the condominium office building described in Fig. 11-27 will be used to illustrate the steps in the design of such a structure.

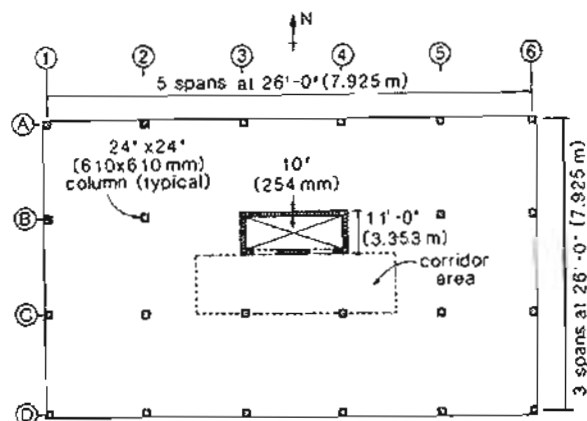


Figure 11-27 Typical floor plan – condominium office building.

Design Data :

Loads : live load = 50 psf (2.4 kN/m^2) (office loading)
 100 psf (4.8 kN/m^2) (corridor loading)
 additional = 25 psf (1.2 kN/m^2) (partitions, services, floor finishes)
 dead load = 50 psf (2.4 kN/m^2) (corridor with terrazzo floor and services)

Fire rating : 2 hr

Story height : 12 ft (3.658 m)

Materials: concrete: normal-density, $f'_c = 5000 \text{ psi}$ (34.5 MPa) for all structural components
 reinforcing bars: $f_y = 60 \text{ ksi}$ (414 MPa)

Sec. 11.12 Example Design of Post-Tensioned Flat Plate

prestressing: 0.6 in. (15 mm) diameter, unbonded, low-relaxation strand, $f_{pu} = 270 \text{ ksi}$ (1860 MPa)
 3/4 in. (19 mm) diameter greased plastic sheath

Step 1: Estimate the slab thickness.

Typical span-to-depth ratio for continuous prestressed floor slabs = 45 (see Table 11-1).

Therefore, thickness = $\ell/45 = 26 \times 12/45 = 6.9 \text{ in. (176 mm)}$.

Assuming concrete with siliceous aggregate, minimum h for 2 hr fire rating = 5 in. (127 mm) (see Table 11-2).

Try $h = 7 \text{ in. (178 mm)}$.

Step 2: Make a preliminary check of the punching shear.

(a) Check interior column B2. Check the direct shear capacity of column B2. Increase V_u by about 20% to account for the increase in tributary area and moment transfer.

Self-weight of slab = $(7/12) \times 150 = 87.5 \text{ psf (4.19 kN/m}^2)$

$$w_u = 1.4 \times (87.5 + 25) + 1.7 \times 50 = 242.5 \text{ psf (11.6 kN/m}^2)$$

$$V_u = 1.20 \times 26 \times 26 \times 0.2425 = 196.7 \text{ kips (875 kN)}$$

Assume that $d = 0.8h = 0.8 \times 7 = 5.60 \text{ in. (142 mm)}$.

$$\text{Hence } b_p = 4 \times (24 + 5.60) = 118.4 \text{ in. (3007 mm)}$$

Assuming an average prestress of 250 psi (1.72 MPa) and neglecting V_p , Eq. (11-13) gives

$$\beta_p = \frac{40 \times 5.60}{118.4} + 1.5 = 3.39$$

$$\phi V_c = 0.85(3.39\sqrt{5000} + 0.3 \times 250)118.4 \times 5.6 \\ = 177.4 \text{ kips (789 kN)}$$

Since ϕV_c is less than V_u the slab thickness needs to be increased.

(b) Check the exterior column B1. Increase V_u by about 50% to account for increase in shear stress due to moment transfer and decrease in tributary area.

$$V_u = 1.50 \times 26 \times 13 \times 0.2425 = 122.9 \text{ kips (547 kN)}$$

$$b_p = 24 + 5.6 + 2(24 + \frac{5.6}{2}) = 83.2 \text{ in. (2113 mm)}$$

From Eq. (11-14), for this square edge column,

$$\phi V_c = 0.85 \times 4\sqrt{5000} \times 83.2 \times 5.6 = 112.0 \text{ kips (498 kN)}$$

$$\leq \left(\frac{30 \times 5.6}{83.2} + 2 \right) \sqrt{5000} \times 83.2 \times 5.6 = 132.4 \text{ kips (589 kN)}$$

Hence $\phi V_c = 112.0 \text{ kips (498 kN)}$. Since $\phi V_c < V_u$, the slab thickness is inadequate.

(c) Revise the slab thickness. For $h = 8$ in. (203 mm), $w_u = 260.0$ psf (12.4 kN/m 2). Hence for exterior column B1.

$$V_u = 1.50 \times 26 \times 13 \times 0.260 = 131.8 \text{ kips (586 kN)}$$

$$d = 0.8 \times 8 = 6.4 \text{ in. (163 mm)}$$

$$b_o = 24 + 6.4 + 2(24 + \frac{6.4}{2}) = 84.8 \text{ in. (2154 mm)}$$

$$\phi V_c = 0.85 \times 4\sqrt{5000} \times 84.8 \times 6.4 = 130.5 \text{ kips (580 kN)}$$

As this is 99% of the estimated required strength, use a slab thickness of 8 in. (203 mm).

Step 3: Determine the load to be balanced.

Practical design experience has shown that if the superimposed service loads are less than the self-weight of the slab, then an economical design satisfying serviceability and ultimate requirements will be achieved if the load balanced by the prestressing, after all losses have occurred, is between 80 and 100% of the slab self-weight. Self-weight of slab = 100 psf (4.8 MPa). For this slab choose the prestressing such that 90% of the self-weight is balanced [i.e., $w_{balanced}$ = 90 psf (4.3 kN/m 2)].

Step 4: Philosophy for choosing tendon profiles.

The upward force provided by the prestressing is a function of the tendon force, the tendon drape, and the span length [see Eqs. (11-1) and (11-2)]. The philosophy of load balancing when applied to this structure offers two different possibilities for choosing the profile and the prestressing forces. To achieve a uniform load-balancing effect we must either use less than the maximum possible drape in interior spans or use extra tendons in the exterior spans (see Fig. 11-28).

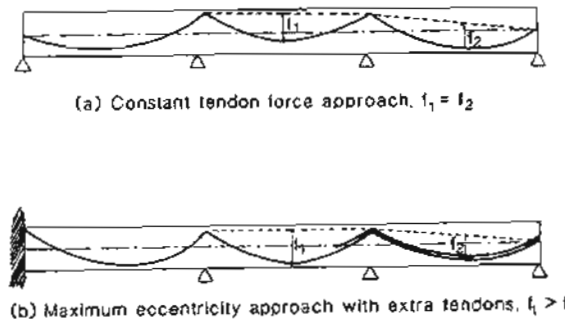


Figure 11-28 Different approaches in choosing tendon profiles and prestressing force.

We will use the "maximum eccentricity" scheme with extra end span tendons, 33 ft (10.1 m) long, in the E-W direction to reduce the total amount of prestressing required. We will use the "constant tendon force" scheme with varying eccentricities in the N-S direction.

Step 5: Determine the maximum eccentricities.

In the column regions place the tendons in the short direction of the structure (N-S direction) below those in the long direction. Minimum clear cover for 2 hr fire rating = 3/4 in. (19 mm) from Table 11-3.

Assume that a top mat of #4 (13 mm diameter) bars will be used to satisfy the minimum bonded reinforcement requirements. As can be seen from Fig. 11-29, the maximum eccentricities that can be obtained at the columns are:

$$\text{In E-W direction, } e = 4 - 3/4 - 1/2 - 3/8 = 2.375 \text{ in. (60 mm)}$$

$$\text{In N-S direction, } e = 4 - 3/4 - 1/2 - 3/4 - 3/8 = 1.625 \text{ in. (41 mm)}$$

At midspan it is possible to use the same maximum eccentricity in the two directions (see Fig. 11-29); thus

$$e = 4 - 3/4 - 3/8 = 2.875 \text{ in. (73 mm)}$$

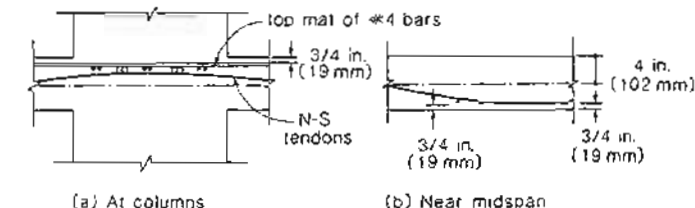


Figure 11-29 Determining maximum tendon eccentricity.

Step 6: Determine the tendon profiles and prestressing forces.

(a) E-W direction. We will choose the location of the point of inflection so that it coincides with the critical section for punching shear (see Fig. 11-21). That is,

$$\beta l_1 = \frac{c_1}{2} + \frac{d}{2} = \frac{c_1}{2} + \frac{0.8h}{2} = \frac{24}{2} + 0.8 \times \frac{8}{2} = 15.2 \text{ in. (386 mm)}$$

Thus $\beta = 15.2/(26 \times 12) = 0.0487$.

For a typical interior span the drape, f , of the equivalent tendon profile, is 5.762 in. (146 mm) (see Fig. 11-30a) and hence the tendon force required to balance 90% of the slab self-weight is

$$P = \frac{0.090 \times 26^2}{8 \times 5.762/12} = 15.84 \text{ kips/ft (231 kN/m)}$$

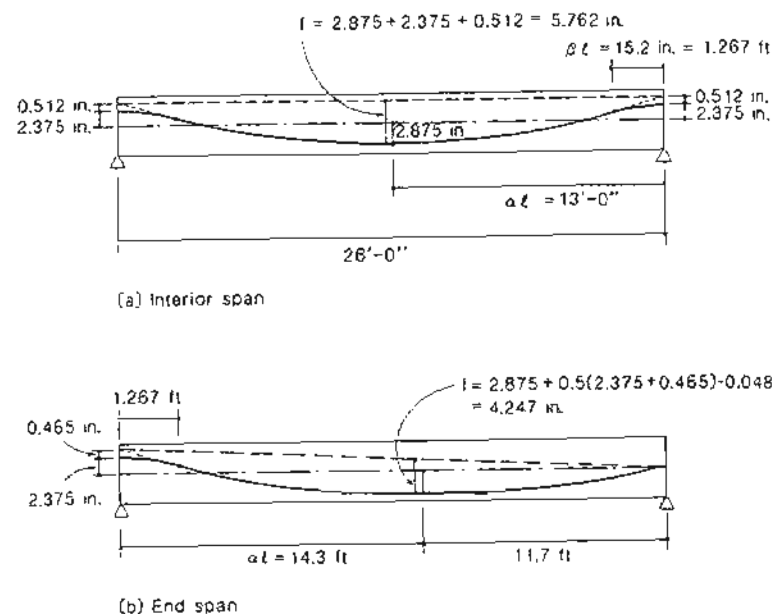


Figure 11-30 Tendon profiles in E-W direction.

For the end spans the low point of the profile will be set at 0.45ℓ from the edge. The drape, f , of the equivalent tendon profile (see Fig. 11-30b) is 4.247 in. (108 mm). Hence the tendon force in this end span to balance 90% of the self-weight is

$$P = \frac{0.090 \times 26^2}{8 \times 4.247/12} = 21.5 \text{ kips/ft (314 kN/m)}$$

(b) N-S direction. It is desired to use the same tendon force for all spans in the N-S direction. Using the maximum eccentricities in the end span, we will determine the tendon force required to balance the dead load in this span. For this span the drape of the equivalent tendon profile is 3.846 in. (98 mm) (see Fig. 11-31a). Hence the tendon force required to balance 90% of slab self-weight is

$$P = \frac{0.090 \times 26^2}{8 \times 3.846/12} = 23.7 \text{ kips/ft (346 kN/m)}$$

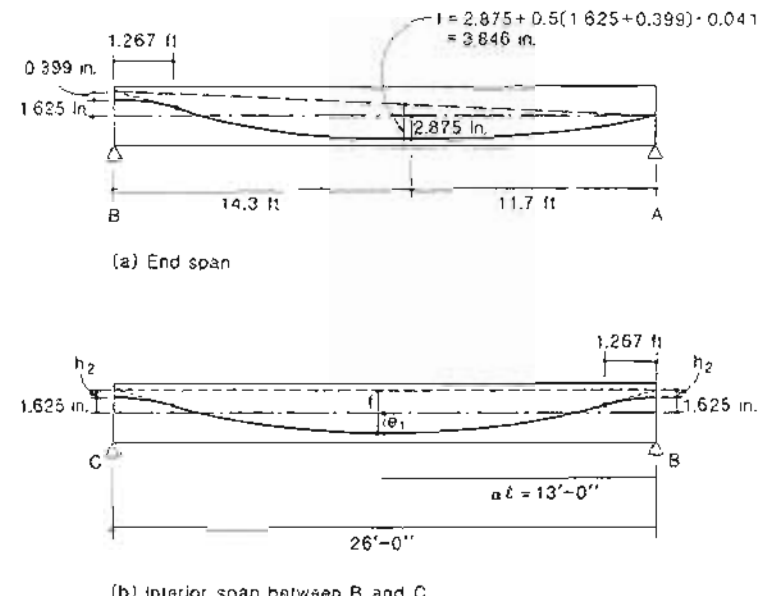


Figure 11-31 Tendon profiles in N-S direction.

Since the tendon force will be kept constant in the N-S direction, the drape of the tendon in the interior span between lines B and C is 3.846 in. (98 mm)

With the point of inflection located at 1.267 ft (386 mm) from the center of the support, then from Eq. (2-1),

$$h_2 = \frac{1.267}{13}(e_1 + 1.625)$$

and

$$f = e_1 + 1.625 + h_2$$

Hence

$$3.846 = e_1 + 1.625 + \frac{1.267}{13}(e_1 + 1.625)$$

Therefore,

$$e_1 = 1.879 \text{ in. (48 mm)}$$

and

$$h_2 = 0.342 \text{ in. (8.7 mm)}$$

The radius of curvature, R , of the tendons should not be less than about 8 ft (2.4 m). In the regions over the supports the radius of curvature is given by

$$R = \frac{(\beta\ell)^2}{2h_2}$$

The smallest radius of curvature in the profiles selected above occurs over the supports in the interior span in the E-W direction and is

$$R = \frac{(1.267)^2}{2 \times 0.512/12} = 18.8 \text{ ft (5.73 m)}$$

Hence the profiles above are satisfactory.

Step 7: Estimate the prestress losses.

(a) *Friction losses and anchorage set losses.* For unbonded tendons in floor slabs it is accurate enough to use an approximate friction loss estimate of 7.5% of the prestressing force per 100 ft (30.5 m) length of tendon. All tendons will be stressed from just one end with the other end being a dead-end anchorage. However, to make the friction losses more uniform, every second tendon will be stressed at one end of the structure while the remaining tendons will be stressed from the opposite end.

The tendons are stressed to $0.75f_{pu}$ and then anchored. The anchorage set is assumed to be 1/4 in. (6 mm). Loss of prestressing stress per foot due to friction is

$$\Delta f_p = 0.00075 \times 0.75 \times 270 = 0.152 \text{ ksi/ft} = 3.44 \text{ MPa/m}$$

Hence, from Eq. (2-7) the length affected by anchorage set is

$$\ell_{set} = \sqrt{\frac{0.25 \times 29,000}{0.152/12}} = 757 \text{ in.} = 63 \text{ ft (19.2 m)}$$

In view of the small variation in stresses along the tendons (see Fig. 11-32), the average stress in each tendon will be used for the calculations

(b) *Elastic shortening loss.* The highest prestressing force is in the N-S direction where a force of about 23.7 kips/ft (346 kN/m) is required. This corresponds to a compressive stress in the concrete of 247 psi (1.70 MPa). Assuming that the slab is post-tensioned when the concrete is 4 days old and has a compressive strength of 3000 psi (20.7 MPa), the elastic strain in the concrete corresponding to a stress of 247 psi (1.70 MPa) is -0.08×10^{-3} .

If the tendons were all post-tensioned simultaneously, the stress in the tendons would not be affected by the elastic shortening of the concrete. However, in our case the tendons will be stressed one at a time. The last tendon to be stressed will not be influenced by elastic shortening, while the first tendon stressed will suffer a loss due to the stressing of subsequent tendons of about $29,000 \times 0.08 \times 10^{-3} = 2.32 \text{ ksi (16 MPa)}$. Hence the average elastic shortening loss in the tendons will be about 1.2 ksi (8 MPa).

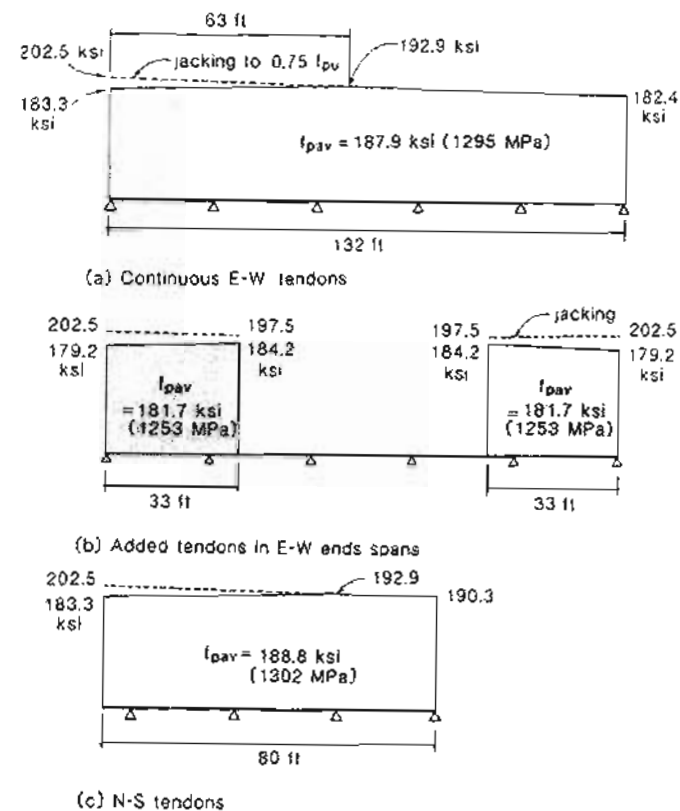


Figure 11-32 Average stresses in tendons after anchoring.

(c) *Loss due to restraint.* As discussed in Chapter 10, the flexural stiffness of the column restrains somewhat the axial shortening of the floor slabs. If the columns are stiff and the slab has a large number of spans, the resulting loss of axial compression in the floor slabs can be significant, particularly for the second-level floor slab (see Fig. 10-42).

In the E-W direction the axial compressive strain in the slab due to prestressing is about -0.08×10^{-3} in the end spans and -0.05×10^{-3} in the interior spans. Hence the slab would tend to move inward by the amounts shown in Fig. 11-33.

If the edge column were fully fixed against rotation at its top and bottom, the force required to move it 0.048 in. (1.2 mm) would be

$$H = \frac{12EI}{\ell^3} \Delta \quad (11-20)$$

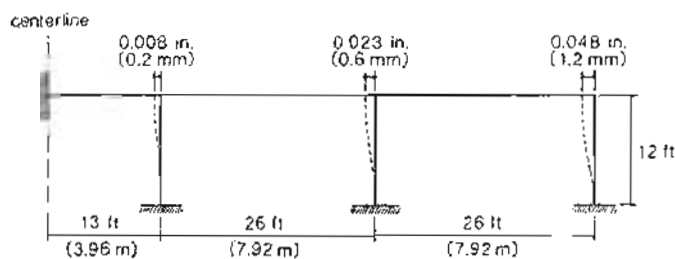


Figure 11-33 First-story columns restraining axial shortening of slabs.

where H = horizontal restraining force

L = height of column

EI = flexural stiffness of column.

Hence if the edge column remained uncracked, the restraining force would be

$$H = \left(\frac{12 \times 57\sqrt{3000} \times 24^4 / 12}{(12 \times 12)^3} \right) \times 0.048 = 16.7 \text{ kips (74 kN)}$$

The actual restraining force will be much less because the column will crack in flexure, reducing its stiffness, and also because the ends of the column are not fully fixed against rotation. These two effects will reduce the restraint force to about 1/4 of the above value. This means that the restraint force for this slab level will be about 0.7% of the prestressing force and can be neglected.

(d) *Long-term losses.* From Eq. (3-29) the relaxation loss after 30 years for an initial stress of 189 ksi (1303 MPa) is about 2.7%, which corresponds to a loss of 5.2 ksi (36 MPa) and a long-term effective modulus of 28,200 ksi (195,600 MPa).

From Eq. (3-19) the shrinkage strain after 30 years if the relative humidity is 70% can be estimated as -0.38×10^{-3} , which would correspond to a loss of about $28,200 \times 0.38 \times 10^{-3} = 10.7$ ksi (74 MPa).

The creep coefficient after 30 years for the concrete first loaded at an age of 4 days can be estimated from Eq. (3-10) as 2.2, which corresponds to a creep strain of $2.2 \times 0.08 \times 10^{-3}$. Hence the loss in tendon stress due to creep will be about $28,200 \times 2.2 \times 0.08 \times 10^{-3} = 5$ ksi (34 MPa).

The total long-term losses are thus $5.2 + 10.7 + 5.0 = 20.9$ ksi (144 MPa).

(e) *Resulting stresses in tendons.* Table 11-5 summarizes the resulting stresses in the tendons immediately after anchoring when only the friction and elastic shortening losses have occurred and the final stresses, f_{sc} , after all losses have occurred. Note that it is common practice to assume that f_{sc} for such structures is $0.6f_{pu} = 0.6 \times 270 = 162$ ksi (1117 MPa).

Table 11-5 Stresses in tendons.

Tendon	Stress after Anchoring ksi (MPa)	Stress after All Losses f_{sc} , ksi (MPa)	Tendon Force after All Losses, kips (kN)
Continuous E-W	187.9 (1295)	167.0 (1151)	35.9 (160)
Extra tendons E-W	181.7 (1253)	160.8 (1109)	34.6 (154)
N-S	188.8 (1302)	167.9 (1158)	36.1 (161)

Also given in Table 11-5 is the tendon force based on a tendon area of 0.215 in^2 (140 mm^2) (see Table 3-6).

Step 8: Determine the number and distribution of tendons.

Table 11-6 summarizes the choice of the number and distribution of the tendons. In distributing the E-W tendons it was decided to concentrate about 70 to 75% of the tendons in the column strips. All of the N-S tendons are concentrated in the column strips. Note that the resulting average compressive stress in the slab varies from 173 psi (1.19 MPa) to 260 psi (1.79 MPa). Typical levels of prestress range from about 125 psi (0.86 MPa) to about 500 psi (3.4 MPa) (Refs. 11-1 and 11-11).

Table 11-6 Number and distribution of tendons.

Span	Total Force Required	Column Strip		No. of Strands in Mid. Strip	Total P kips	P/A psi (MPa)
		No. of Strands in Column	No. of Strands outside Column			
E-W interior spans	$15.84 \times 26 = 411.8$ kips	5	4	3	430.8 (1916)	173 (1.19)
E-W end spans	$21.5 \times 26 = 559$ kips	5	4	3 + 2 extra	569.2 (2532)	228 (1.57)
N-S spans	$23.7 \times 26 = 616$ kips	10	8	0	649.8 (2890)	260 (1.79)

Step 9: Determine the equivalent frame properties.

The analyses will be carried out using the equivalent frame method described in Section 11.5.

(a) *Equivalent column stiffness, K_{eq} .* The equivalent frame method idealizes the columns as flexural members with uniform flexural stiffness over the clear height of the column and with infinite stiffness assumed over the thickness of the slabs. This results in a nonprismatic member. An approximate method suggested by Rice and Hoffman in

Ref. 11-20 gives the column stiffness, K_c , as

$$K_c = \frac{4E_c I}{l - 2h} \quad (11-21)$$

where E_c = modulus of elasticity for column concrete

I = column moment of inertia

ℓ = story height (center to center of slabs)

and h = slab thickness.

The equivalent column (stiffness = K_{ec}) is assumed to consist of the actual columns above and below the slab plus an attached torsional member transverse to the direction in which moments are being determined and bounded by the lateral panel centerlines.

The calculations of these effective column stiffnesses using Eqs. (11-3), (11-4), (11-5), and (11-21) are summarized in Table 11-7.

Table 11-7 Determination of K_{ec} for typical column in interior design strip.

I in 4	K_c	C	K_t	K_{ec}
$\frac{\pi d^4}{32}$ $= 27,648$	$\frac{4E_c \times 27,648}{(72 \times 12) - 3 \times 8}$ $= 864E_c$	$(1 - 0.63 \times \frac{8}{24}) \frac{8^3 \times 24}{3}$ $= 3236$	$\frac{2 \times 9 E_{cs} \times 3,736}{26 \times 12(1 - 34/36 \times 12/24)}$ $= 237E_{cs}$	$208E_c$

(b) *Slab stiffness, K_s .* The equivalent frame method idealizes the slabs as beams having uniform flexural stiffness along the clear span and having an increased flexural stiffness from the face of each column to the center of each column. Reference 11-20 suggests a simplified approach for estimating K_s as

$$K_s = \frac{4E_{cs} I}{l_1 + c_1/2} \quad (11-22)$$

where E_{cs} = modulus of elasticity of slab concrete

I = moment of inertia of slab bounded by panel centerlines

l_1 = center-to-center span between columns in direction in which moments are being determined

c_1 = column dimension in direction in which moments are determined

For a typical 26 ft (7.92 m) wide interior design strip.

$$K_s = \frac{4E_{cs} \times 26 \times 12 \times 8^3 / 12}{26 \times 12 - 24/2} = 177E_{cs}$$

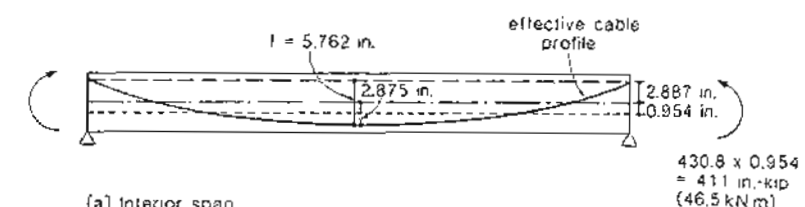
(c) *Distribution factors.* The distribution factor for moment distribution at each joint

$$\frac{K_s}{\sum K_s + K_c}$$

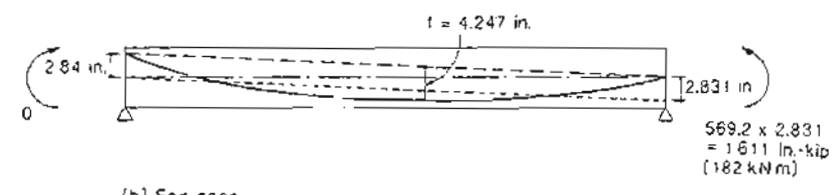
The carry-over factors are all taken as 0.5.

Step 10: Determine the fixed-end moments due to prestressing.

The calculations of the fixed-end moments due to prestressing for the E-W spans are summarized in Fig. 11-34. The calculations of the fixed-end moments due to prestressing for the N-S spans are summarized in Fig. 11-35.

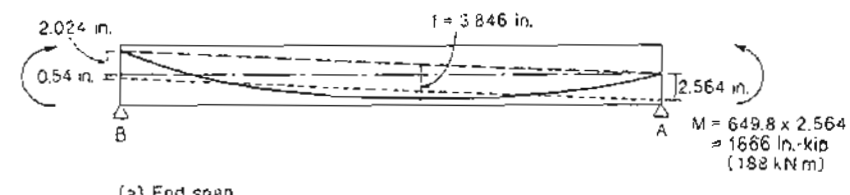


(a) Interior span

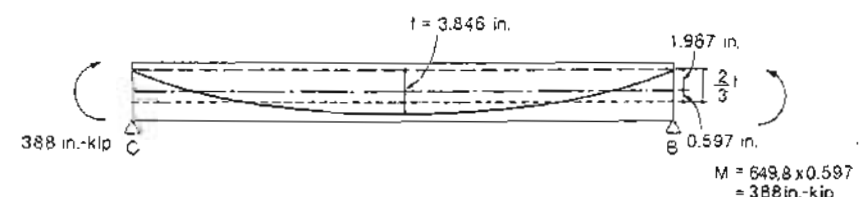


(b) End span

Figure 11-34 Fixed-end moments due to prestress for E-W spans.



(a) End span



(b) Interior span

Figure 11-35 Fixed-end moments due to prestress in N-S spans.

Step 11: Analyze the equivalent frames.

To demonstrate the analysis procedures we will analyze the equivalent frames centered on column line B and column line 2. We will calculate the moments in the slab due to the restraint of prestressing deformations, due to dead load and due to live load.

Since the live load acting on the slab is less than 75% of the dead load, then pattern live loading need not be taken into account (Ref. 11-6).

The moment distributions for these two equivalent frames are summarized in Figs. 11-36 and 11-37.

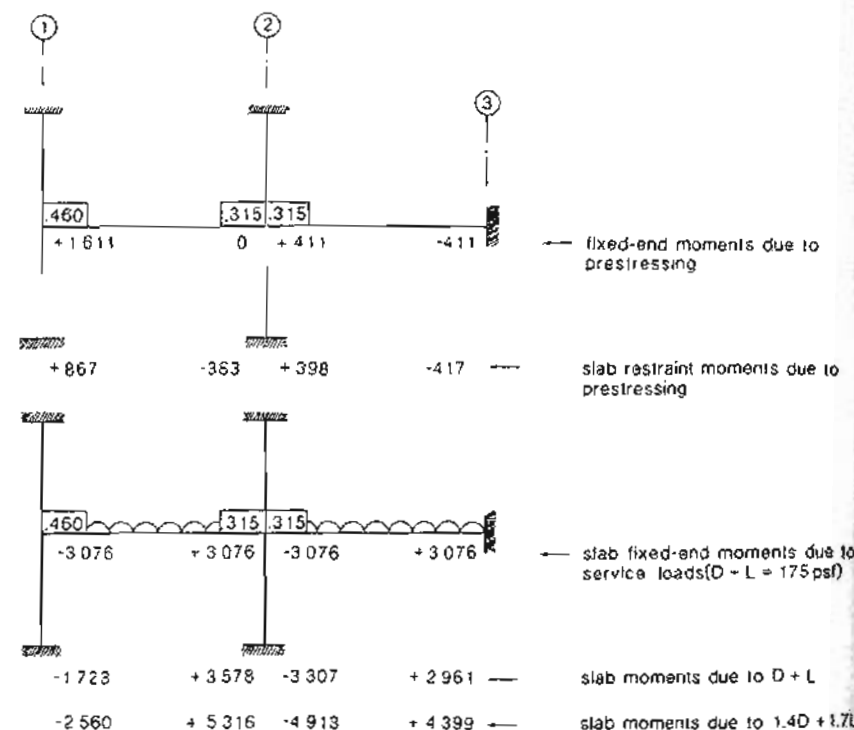


Figure 11-36 Moments (in.-kips) in slabs from equivalent frame analysis for 26 ft wide E-W design strip on column line B.

Step 12: Determine the moments under service loads and under factored loads.

By combining the frame analysis results summarized in Figs. 11-36 and 11-37, the moments at critical sections of the slab under specified loads and under factored loads are obtained (see Figs. 11-38 and 11-39).

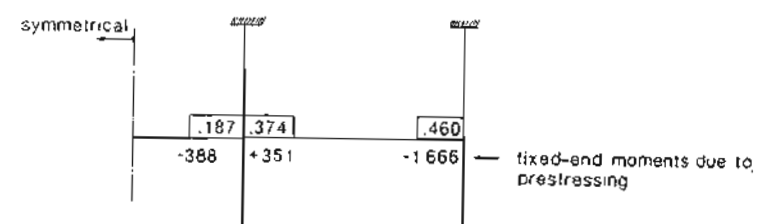


Figure 11-37 Moments (in.-kips) in slabs from equivalent frame analysis for 26 ft wide design strip on column line 2.

Step 13: Check the stresses under service loads.

The stress calculations are summarized in Table 11-8.

When calculating stress at the face of a column, the eccentricity of the tendon at this location needs to be determined. This eccentricity is the eccentricity at the center of the column minus $h_2(0.5c/\beta\ell)^2$ (see Fig. 11-21).

It can be seen that none of the stresses exceed the ACI Code tensile stress limit of $6\sqrt{5000} = 424$ psi (2.93 MPa).

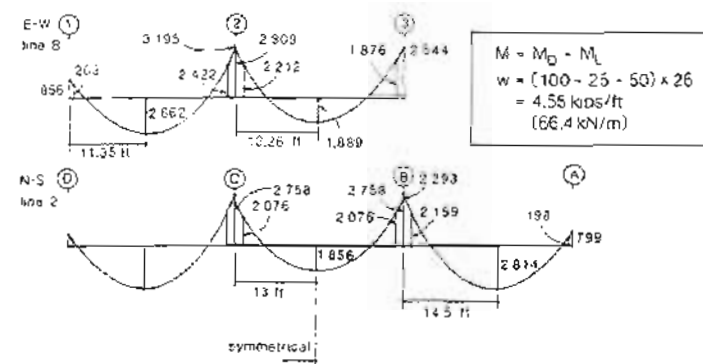


Figure 11-38 Moments under service loads.

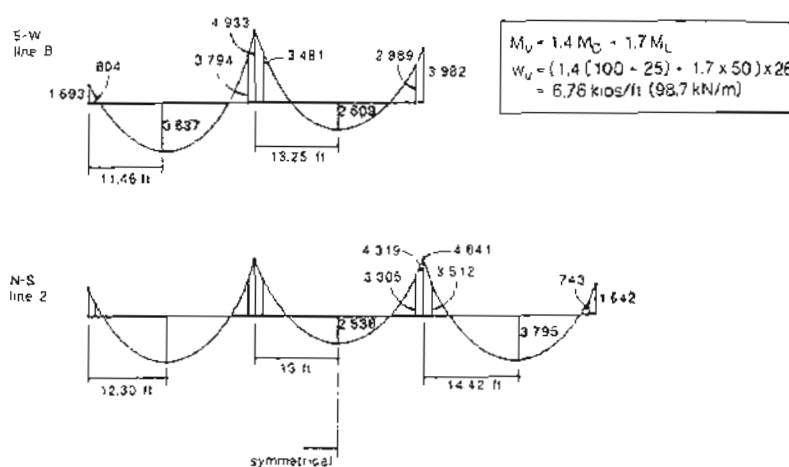


Figure 11-39 Moments under factored loads.

Step 14: Provide crack-control reinforcement.

As none of the calculated tensile stresses on the bottom face of the slab exceed $2\sqrt{5000} = 141 \text{ psi}$ (0.98 MPa), bonded reinforcement is not required in the positive moment areas.

Table 11-8 Stresses at service loads.

Design Strip	Location	Stress calculations				
		$-\frac{P}{A}$	$-\frac{P_s}{S}$	$+\frac{M}{S}$	$f, \text{ psi}$	
E-W	Top face at B2	-228	$-\frac{460.8 \times 10^3 \times 2.085}{3328}$	$+\frac{2422 \times 10^3}{3328}$	+143	+0.99
	Top face at B3	-173	$-\frac{460.8 \times 10^3 \times 2.085}{3328}$	$+\frac{1876 \times 10^3}{3328}$	+125	+0.86
	Bot. face span 1-2	-228	$-\frac{460.8 \times 10^3 \times 2.575}{3328}$	$+\frac{2062 \times 10^3}{3328}$	+80	+0.55
	Bot. face span 2-3	-173	$-\frac{460.8 \times 10^3 \times 2.875}{3328}$	$+\frac{1849.8 \times 10^3}{3328}$	+25	+0.18
N-S	Top face at B2	-260	$-\frac{649.8 \times 10^3 \times 1.776}{3328}$	$+\frac{3159.6 \times 10^3}{3328}$	+120	+0.83
	Bot. face span A-B	-260	$-\frac{649.8 \times 10^3 \times 2.875}{3328}$	$+\frac{2415 \times 10^3}{3328}$	+24	+0.17
	Bot. face span B-C	-260	$-\frac{649.8 \times 10^3 \times 1.876}{3328}$	$+\frac{1956 \times 10^3}{3328}$	-69	-0.48

In the negative moment areas near the columns, the area of bonded reinforcement required in each direction is

$$A_s = 0.00075 h f$$

$$= 0.00075 \times 8 \times 26 \times 12 = 1.87 \text{ in}^2 (1208 \text{ mm}^2)$$

Hence use ten #4 (13 mm diameter) bars located over a width of $24 + 2 \times 1.5 \times 8 = 48 \text{ in}$. (1219 mm).

We will provide bottom reinforcing bars perpendicular to all free edges as shown in Fig. 11-17. In the E-W direction the reinforcement ratio, ρ_s , required from Eq. (11-6) is

$$\rho_s = 0.0015 - 0.5 \rho_p$$

$$= 0.0015 - \frac{0.5 \times 16 \times 0.215}{26 \times 12 \times 0.8 \times 8}$$

$$= 0.00064 \text{ but not less than } 0.0005$$

Hence the minimum area of bottom reinforcement having an effective depth d equal to 7 in. (178 mm) is

$$A_s = \rho_s b d$$

$$= 0.00064 \times 26 \times 12 \times 7$$

$$= 1.39 \text{ in}^2 (900 \text{ mm}^2)$$

Hence provide eight #4 (13 mm diameter) bottom bars uniformly distributed across the 26 ft (7.92 m) width of the design strip. Use the same reinforcement in the N-S direction.

Step 15: Check the flexural strength requirements.

In order to satisfy the flexural strength requirements of the ACI Code the design flexural strength ϕM_n must be greater than or equal to the factored moment M_u . In computing ϕM_n we will take account of the presence of the bonded reinforcing bars.

The flexural strength calculations are summarized in Table 11-9. A detailed illustration of the calculations involved is given in Step 7 of the example in Section 6.13. From Table 11-9 it can be seen that the flexural strength of the slab is adequate at all locations.

Table 11-9 Flexural strength checks.

Design Strip	Location	$A_{ps}^{(1)}$ in. ²	A_s m ²	$d_p^{(3)}$ in.	$d^{(3)}$ in.	$f_{ps}^{(4)}$ ksi	$\frac{c_e}{d}$ $\times \frac{d}{d_y}$	ϕM_n in.-kips (kNm)	M_u in.-kips (kNm)
E-W	M'' at face column B2	3.44	2.00	6.085	6.50	184.7	0.0795	3988 (4511)	3794 (429)
	M'' at face wall B3	2.58	2.00	6.056	6.50	189.2	0.0645	3237 (366)	2989 (338)
	Max. M^* span 1-2	3.44	1.60	6.875	6.50	185.9	0.0686	4335 (489)	3637 (411)
	Max. M^* span 2-3	3.58	—	6.875	—	190.9	0.0458	2965 (335)	2609 (295)
N-S	M'' at face span A-B	3.87	2.00	5.376	7.00	185.1	0.0998	3985 (450)	3512 (397)
	Max. M^* span A-B	3.87	1.60	6.875	7.00	187.1	0.0765	4857 (549)	3795 (429)
	Max. M^* span B-C	3.87	—	5.879	—	185.8	0.0784	3629 (410)	2536 (287)

⁽¹⁾See Table 11-6.⁽²⁾ $d_p = 4 + e$ (see Table 11-8).⁽³⁾N-S reinforcing bars are outermost bars.⁽⁴⁾Values of f_{se} for individual tendons given in Table 11-5.⁽⁵⁾Less than limit of $0.36\beta_1 = 0.36 \times 0.80 = 0.288$.**Step 16:** Check the shear and moment-transfer strength requirements.

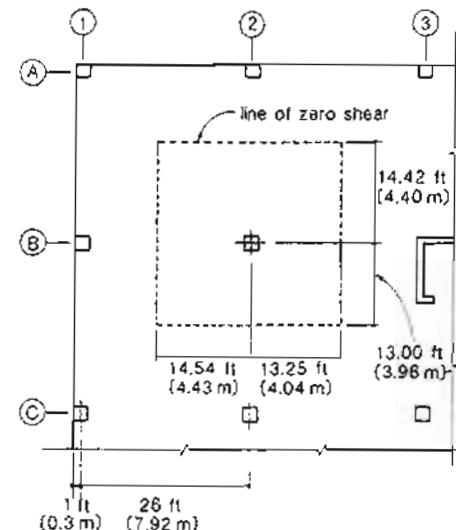
(a) *Critical interior column.* Column B2 has the largest direct shear, V_u , and a significant moment to be transferred. The tributary area for shear for this column can be estimated from the locations of maximum moments shown in Fig. 11-39. This tributary area, shown in Fig. 11-40, is

$$A = (14.54 + 13.25) \times (14.42 + 13.00) \\ = 762 \text{ ft}^2 (70.8 \text{ m}^2)$$

This tributary area is 13% greater than the tributary area assuming zero shear along panel centerlines. We will use an effective depth, $d = 0.8h = 6.4$ in. (163 mm), for calculating

the shear resistance. Hence the factored shear force acting on the critical shear periphery is

$$V_u = [1.4(100 + 25) - 1.7 \times 50] \left[762 - \left(\frac{24 + 6.4}{12} \right)^2 \right] \\ = 196.5 \text{ kips (874 kN)}$$

**Figure 11-40** Tributary area for column B2

The vertical component of prestressing can be found by summing the contributions of the tendons passing through the critical section in the two directions. There are five tendons passing through the 30.4 in. (772 mm) wide critical section in the E-W direction and 10 tendons in the N-S direction. Hence, from Eq. (11-15),

$$V_p = \frac{2 \times 5 \times 35.9 \times 0.465}{(1.267 \times 12)^2} \times 30.4 + \frac{2 \times 10 \times 36.1 \times 0.399}{(1.267 \times 12)^2} \times 30.4 \\ = 22.0 + 37.9 \\ = 59.9 \text{ kips (266 kN)}$$

The unequal moments on each side of the column shown in Fig. 11-39 cause biaxial bending of the column and the transfer of the moments in two directions as shown in Fig. 11-41.

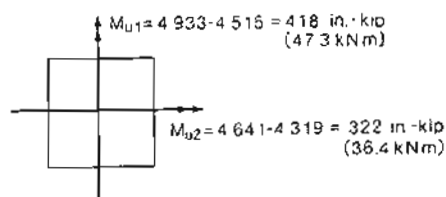


Figure 11-41 Moments transferred to column B2.

The terms required to calculate the factored shear stress, from Fig. 11-24, are

$$\begin{aligned} A &= 2 \times 6.4(24 + 24 + 2 \times 6.4) \\ &= 778 \text{ in}^2 (502,000 \text{ mm}^2) \\ e_1 = e_2 &= \frac{24 + 6.4}{2} = 15.2 \text{ in. (386 mm)} \\ J_1 = J_2 &= (24 + 6.4) \times \frac{6.4^3}{6} + (24 + 6.4)^3 \times \frac{6.4}{6} + \frac{6.4(24 + 6.4)(24 + 6.4)^2}{2} \\ &= 121,198 \text{ in}^4 (50.4 \times 10^9 \text{ mm}^4) \\ \gamma_{e1} = \gamma_{e2} &= 1 - \frac{1}{1 + \frac{2}{3} \sqrt{\frac{24+6.4}{24+6.4}}} = 0.40 \end{aligned}$$

From Eq. (11-16) the maximum shear stress due to V_u , M_{u1} , and M_{u2} is

$$\begin{aligned} v_u &= \frac{196.5 \times 10^3}{778} + \frac{0.4 \times 418 \times 10^3 \times 15.2}{121,198} + \frac{0.40 \times 322 \times 10^3 \times 15.2}{121,198} \\ &= 253 + 21 + 16 \\ &= 290 \text{ psi (2.00 MPa)} \end{aligned}$$

The permissible shear stress can be found from Eqs. (11-13) and (11-17). From Table 11-6, the average f_{pc} in the two directions is $(228 + 260)/2 = 244$ psi. Hence the permissible shear stress is

$$v_c = \phi \left(\beta_p \sqrt{f'_c} + 0.3 f_{pc} + \frac{V_p}{b_o d} \right)$$

where

$$\beta_p = \alpha_s(d/b_o) + 1.5 = 40(6.4/(4 \times 30.4)) + 1.5 = 3.61$$

Hence

$$\begin{aligned} v_c &= 0.85 \left(3.5 \sqrt{5000} + 0.3 \times 244 + \frac{59,900}{4 \times 30.4 \times 6.4} \right) \\ &= 338 \text{ psi (2.33 MPa)} \end{aligned}$$

Since the permissible shear stress is greater than the factored shear stress, the shear strength requirements are satisfied. The portion of the unbalanced moment transferred by flexure is 0.60 times the unbalanced moments. Hence in the E-W direction the required factored moment resistance is $0.60 \times 418 = 251$ in.-kips (28 kNm). This moment must be resisted in a slab of width $24 + 3 \times 8 = 48$ in. (1219 mm). In this width there are five tendons passing through the column plus one tendon on each side of the column. In addition there are ten #4 (13 mm diameter) bars in this width. As determined previously, the stress in the prestressing, f_{ps} , at ultimate is 184.7 ksi (1274 MPa). The equivalent rectangular stress-block depth is

$$\begin{aligned} a &= \frac{7 \times 0.215 \times 184.7 + 2.00 \times 60}{0.85 \times 5 \times 48} \\ &= 1.95 \text{ in. (49.6 mm)} \end{aligned}$$

The design flexural strength of this part of the slab is

$$\begin{aligned} \phi M_n &= 0.9 \left[7 \times 0.215 \times 184.7 \left(6.085 - \frac{1.95}{2} \right) + 2 \times 60 \left(6.50 - \frac{1.95}{2} \right) \right] \\ &= 1875 \text{ in.-kips (212 kNm)} \end{aligned}$$

Hence there is no difficulty in transferring the unbalanced moment by flexure.

(b) Critical exterior column. Column B1 has a tributary area (see Fig. 11-40) of about $(27 - 14.54) \times 26 = 324 \text{ ft}^2 (30 \text{ m}^2)$. Hence the factored shear force acting on the critical shear periphery is

$$\begin{aligned} V_u &= 260 \times \left[324 - \frac{(24 + 6.4/2)(24 + 6.4)}{12} \right] \\ &= 82.7 \text{ kips (368 kN)} \end{aligned}$$

We will neglect the vertical component of prestressing.

The moment to be transferred in the E-W direction as determined from Fig. 11-39 is 1693 in.-kips (191 kNm) (see Fig. 11-42).

The terms required to calculate the factored shear stress, from Fig. 11-24, are

$$\begin{aligned} A &= 6.4(2 \times 24 + 24 + 2 \times 6.4) \\ &= 542.7 \text{ in}^2 (350,140 \text{ mm}^2) \\ e_1 &= \frac{(24 + 6.4/2)^2}{2 \times 24 + 24 + 2 \times 6.4} \\ &= 8.72 \text{ in. (222 mm)} \\ J_1 &= \frac{(24 + 6.4/2) \times 6.4^3 + (24 + 6.4/2)^3 \times 6.4}{6} + (24 + 6.4) \times 6.4 \times 8.72^2 \\ &\quad + 2 \left(24 + \frac{6.4}{2} \right) \times 6.4 \times \left(\frac{24 + 6.4/2}{2} - 8.72 \right)^2 \\ &= 45,739 \text{ in}^4 (19.04 \times 10^9 \text{ mm}^4) \\ \gamma_{e1} &= 1 - \frac{1}{1 + \frac{2}{3} \sqrt{\frac{24+6.4/2}{24+6.4}}} = 0.387 \end{aligned}$$

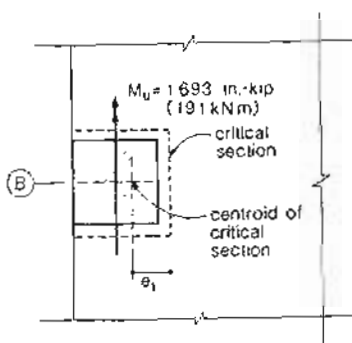


Figure 11-42 Moment transferred to edge column B1.

The value of the moment, M_u , at the centroid of the critical section can be found from M_u at the column centerline minus the shear times the distance from the column centerline to the centroid of the critical section = 6.48 in. (165 mm). Hence

$$M_u = 1693 - 82.7 \times 6.48 = 1157 \text{ in.-kips (131 kNm)}$$

From Eq. (11-16) the maximum shear stress due to V_u and M_u is

$$\begin{aligned} v_u &= \frac{82.7 \times 10^3}{542.7} + \frac{0.387 \times 1157 \times 10^3 \times 8.72}{45.739} \\ &= 152 + 85 = 237 \text{ psi (1.64 MPa)} \end{aligned}$$

The additional small moment acting in the N-S direction has been neglected in the calculations above.

For this edge column the ACI Code requires that the beneficial effects of prestressing be neglected and hence, from Eqs. (11-14) and (11-17), the permissible shear stress, v_c , is

$$\begin{aligned} v_c &= \phi \left(2 + \frac{4}{\beta_c} \right) \sqrt{f'_c} = 0.85 \left(2 + \frac{4}{1} \right) \sqrt{5000} = 424 \text{ psi (2.93 MPa)} \\ &\leq \phi \left(\frac{\alpha_s d}{b_o} + 2 \right) \sqrt{f'_c} = 0.85 \left(\frac{30 \times 6.4}{24 + 6.4 + 2(24 + 6.4/2)} + 2 \right) \sqrt{5000} \\ &= 256 \text{ psi (1.77 MPa)} \\ &\leq \phi 4 \sqrt{f'_c} = 0.85 \times 4 \sqrt{5000} = 240 \text{ psi (1.66 MPa)} \end{aligned}$$

Hence $v_c = 240 \text{ psi (1.66 MPa)}$ and the shear resistance is satisfactory.

The portion of the unbalanced moment transferred by moment in the slab is $(1 - 0.387) \times 1157 \text{ in.-kips} = 709 \text{ in.-kips (80 kNm)}$. As calculated previously, the design

flexural strength of the slab over a width of $24 + 3 \times 8 = 48 \text{ in. (1219 mm)}$ is 1875 in.-kips (212 kNm). Therefore, the moment-transfer requirements are satisfied.

(c) *Corner column.* As shown in Fig. 11-20, the one-way beam shear provisions can be used to determine the shear resistance at the corner of the slab. The geometry of the critical section is shown in Fig. 11-43.

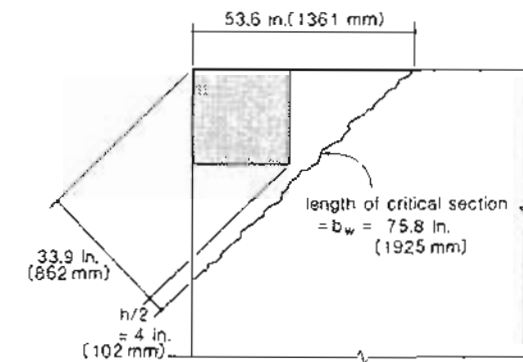


Figure 11-43 Critical shear section for corner column.

The factored shear force acting on the critical section (see Figs. 11-40 and 11-43) is

$$\begin{aligned} V_u &= 260 [(27 - 14.54) \times (27 - 14.42) - 0.5(53.6/12)^2] \\ &= 38.2 \text{ kips (170 kN)} \end{aligned}$$

The design shear strength is

$$\begin{aligned} \phi V_c &= \phi 2 \sqrt{f'_c} b_w d \\ &= 0.85 \times 2 \sqrt{5000} \times 75.8 \times 6.4 \\ &= 58.3 \text{ kips (259 kN)} \end{aligned}$$

Therefore, adequate shear resistance is provided.

Step 17: Investigate structural integrity requirements.

The ACI Code (Ref. 11-6) requires that two-way slabs without beams contain at least two bottom bars in each direction which are either continuous, spliced (splice length equal to $1.3\ell_d$) or anchored at the supports.

These bars must pass through the column and should be placed within the column core. These bottom bars are intended to provide some minimum level of "structural

integrity" by enabling the slab to hang from the supports after an initial failure occurs. Due to punching shear failures, the top bars tend to rip out of the top surface of the slab and hence are considered ineffective (Refs. 11-16 and 11-21). Mitchell and Cook (Ref. 11-21) recommend that draped prestressing steel, passing through the columns or supports, be considered as effective in assessing the structural integrity requirements. Since at least two draped tendons pass through the columns in each direction, the structural integrity requirements can be considered satisfied.

Step 18: Estimate the deflections.

The maximum deflection of the floor slab will occur in one of the corner panels. The instantaneous live load deflection for a corner panel due to pattern live load can be approximated from Fig. 11-26 as

$$\Delta = \frac{3.80 w t^4}{384 EI} + \frac{3.80 w t^4}{384 EI}$$

$$= 2 \left[\frac{3.80 \times 50 \times 26 \times 26^3 \times 12^3}{384 \times 57.000 \sqrt{5000} \times 26 \times 12 \times 8^3 / 12} \right]$$

$$= 0.38 \text{ in. (9.6 mm)}$$

This is less than the limit of $t/360 = 0.87$ in. (22 mm) and hence is satisfactory.

The total dead load is 125 psf (6.0 kN/m^2) and the prestressing has been chosen to balance 90 psf (4.3 kN/m^2). We will assume that 30% of the live load is sustained (i.e., $0.30 \times 50 = 15 \text{ psf}$). Hence, from Fig. 11-26, a uniform loading of $125 - 90 + 15 = 50 \text{ psf}$ (2.4 kN/m^2) will cause a deflection in the corner panel equal to

$$\Delta = 2 \times \frac{2.65 w t^4}{384 EI} = \frac{2.65}{3.80} \times \frac{50}{50} \times 0.38 = 0.27 \text{ in. (6.7 mm)}$$

The creep deflection due to this sustained load can be approximated by assuming a creep factor of 2.0 (Refs. 11-1 and 11-2). Therefore, a creep deflection of about $2.0 \times 0.27 = 0.54$ in. (13.7 mm) is expected.

The sum of the creep deflection and the deflection due to non-sustained live load is $0.54 + 0.7 \times 0.38 = 0.81$ in. (20.5 mm), which corresponds to a deflection of $t/385$. The deflection limit is $t/360$ for floors attached to nonstructural elements likely to be damaged by large deflections. Hence the deflection limits are satisfied.

Step 19: Summarize design.

Figure 11-44 shows the tendon layout for the slab and Fig. 11-45 shows the layout of the reinforcing bars.

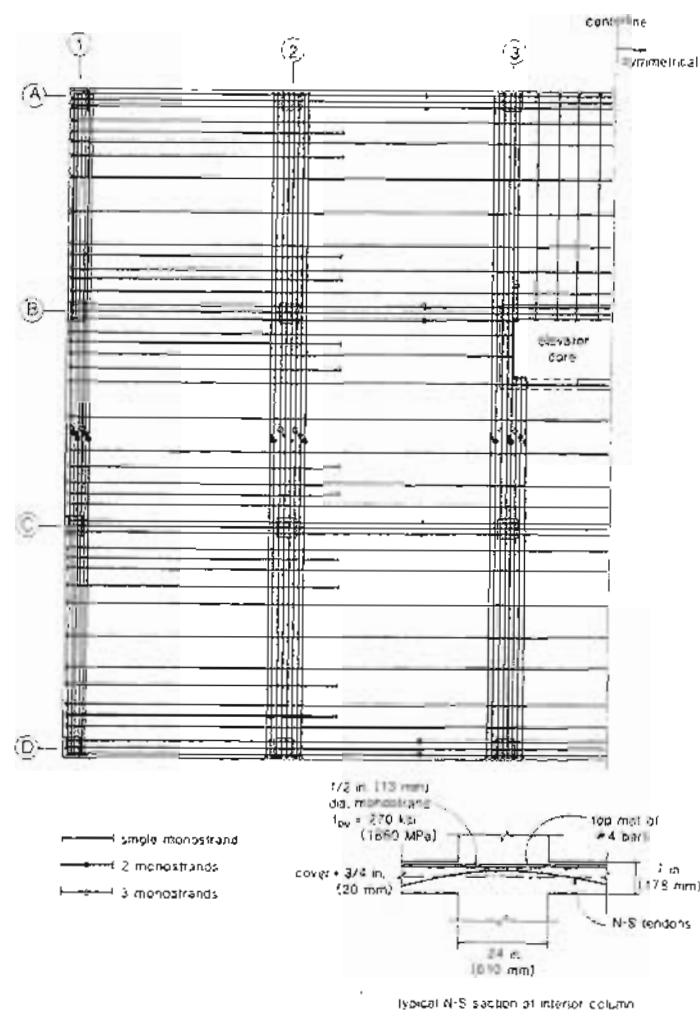


Figure 11-44 Tendon layout

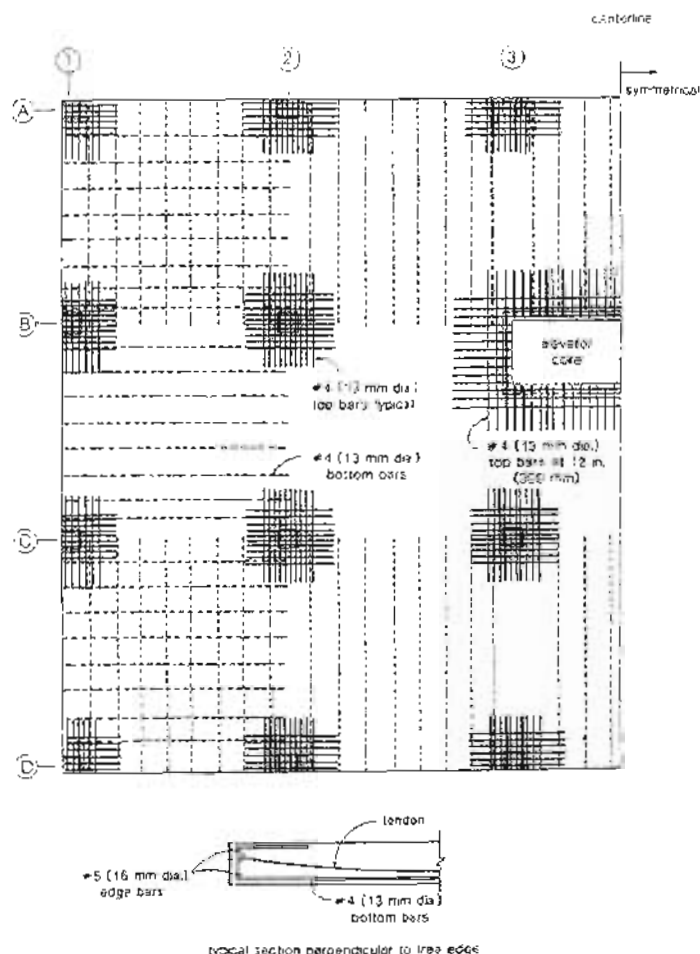


Figure 11-45 Reinforcing bar layout.

References

- 11-1 Ritz, P., Matt, P., Tellenbach, Ch., Schiub, P., and Aeberhard, H.U., *Post-Tensioned Concrete In Building Construction - Post-Tensioned Slabs*, Losinger Ltd., Berne, Switzerland, 1981, 41 pp.
- 11-2 Post-Tensioning Institute, *Design of Post-Tensioned Slabs*, Post-Tensioning Institute, Glenview, Ill., 1977, 52 pp.
- 11-3 Post-Tensioning Institute, *Post-Tensioning Manual*, Post-Tensioning Institute, Glenview, Ill., 1976, 288 pp.
- 11-4 Gustafson, A.H., *Fire Resistance of Post-Tensioned Structures*, Post-Tensioning Division, Prestressed Concrete Institute, Chicago, 1972.
- 11-5 American Society for Testing and Materials, "Standard Methods of Fire Tests of Building Construction and Materials," ASTM E119-88, ASTM, Philadelphia, 1989.
- 11-6 ACI Committee 318, "Building Code Requirements for Reinforced Concrete (ACI 318-89) and Commentary - ACI 318 R-89," American Concrete Institute, Detroit, 1989, 353 pp.
- 11-7 Schupack, M., "Unbonded Performance," *Civil Engineering*, Vol. 59, No. 10, Oct. 1989, pp. 75-77.
- 11-8 Aalami, B.O., and Swanson, D.T., "Innovative Rehabilitation of a Parking Structure," *Concrete International: Design and Construction*, Vol. 10, No. 2, Feb. 1988, pp. 30-35.
- 11-9 Post-Tensioning Institute, "Specification for Unbonded Strand Tendons," *PCI Journal*, Vol. 30, No. 2, Mar.-Apr. 1985, pp. 22-39.
- 11-10 Post-Tensioning Institute, "Field Procedures for Unbonded Single Strand Tendons," Post-Tensioning Institute, Phoenix, Ariz., 1989, 41 pp.
- 11-11 ACI-ASCE Committee 423, "Tentative Recommendations for Prestressed Concrete Flat Plates," *ACI Journal*, Feb. 1974, pp. 61-71.
- 11-12 ACI-ASCE Committee 423, "Recommendations for Concrete Members Prestressed with Unbonded Tendons," *Concrete International: Design and Construction*, Vol. 5, No. 7, July 1983, pp. 61-76.
- 11-13 Park, R., and Gamble, W.L., *Reinforced Concrete Slabs*, John Wiley & Sons Inc., New York, 1980, 618 pp.
- 11-14 Ockleston, A.J., "Load Tests on a Three Storey Reinforced Concrete Building in Johannesburg," *Structural Engineer*, London, Vol. 33, No. 10, Oct. 1955, pp. 304-322.
- 11-15 Vecchio, F.J., and Collins, M.P., "Investigating the Collapse of a Warehouse," *Concrete International: Design and Construction*, Vol. 12, No. 3, Mar. 1990, pp. 72-78.
- 11-16 Hawkins, N.M., and Mitchell, D., "Progressive Collapse of Flat Plate Structures," *ACI Journal*, Vol. 76, No. 7, July 1979, pp. 775-808.
- 11-17 Hawkins, N.M., "Lateral Load Resistance of Unbonded, Post-Tensioned Flat Plate Construction," *PCI Journal*, Vol. 26, No. 1, Jan.-Feb. 1981, pp. 94-116.
- 11-18 Simmonds, S.H., "Chapter 3 - Slabs," *Concrete Design Handbook*, Canadian Portland Cement Association, Ottawa, 1985.
- 11-19 Scanlon, A., and Murray, D.W., "Practical Calculation of Two-Way Slab Deflections," *Concrete International: Design and Construction*, Vol. 4, No. 11, Nov. 1982, pp. 43-50.

- 11-20 Rice, P.E., and Hoffman, E.S., *Structural Design Guide to the ACI Building Code*, Van Nostrand Reinhold, New York, 1985, 477 pp.
- 11-21 Mitchell, D., and Cook, W.D., "Preventing Progressive Collapse of Slab Structures," *Journal of Structural Engineering, ASCE*, Vol. 110, No. 7, July 1984, pp. 1513-1532.

Demonstration Problems

- 11-1 The post-tensioned slab designed in Section 11.12 is subjected to a uniformly distributed overload applied on the bay between column lines 2 and 3 (see Fig. 11-27). Use yield line theory to estimate the superimposed load to cause flexural failure of the floor slab.
- 11-2 A post-tensioned, flat plate floor structure has columns spaced at 25 ft (7.5 m) centers in the N-S direction and at 30 ft (9.0 m) centers in the E-W direction. The columns are 28 × 28 in. (700 × 700 mm) square; the slab is 9 in. (225 mm) thick and is constructed with normal-weight concrete. The post-tensioning consists of 0.6 in. (15 mm) diameter unbonded low-relaxation strands in 3/4 in. (20 mm) greased ducts. Assume that the stress in the tendons after all prestress losses is 162 ksi (1117 MPa). The minimum clear cover for the reinforcement is 34 in. (20 mm). Choose appropriate tendon profiles and tendon spacings so that the self-weight of the slab is balanced by the prestressing for (a) a typical corner panel and (b) a typical interior panel.
- 11-3 For the floor slab designed in Prob. 11-2, check the punching shear capacity of the interior columns by the simplified procedure which increases the tributary area by 20% to account for the detrimental effects of moment transfer. The superimposed dead load on the floor is 15 psf (0.7 kN/m²), while the live load is 50 psf (2.4 kN/m²).
- 11-4 If the connection between the slab and the column is required to transmit moment, its ability to transmit shear will be reduced. For the slab-interior column connection of the structure described in Prob. 11-2, prepare a plot of the shear vs. moment-transfer interaction (i.e., V_s vs. M_{u1}). Assume that the moment is transferred about only one axis.

Buildings

If a builder has built a house for a man and has not made his work sound, and the house which he has built has fallen down and so caused the death of the householder, that builder shall be put to death.

Code of Hammurabi, c. 1770 B.C.

12.1 INTRODUCTION

About 80% of the precast, prestressed concrete components and about 60% of the post-tensioning steel produced in North America are used in the construction of buildings. Building construction is one of North America's largest industries, constituting about 10% of total economic activity. Within this large market, the prestressed concrete industry is an important component whose market share is growing rapidly (see Fig. 1-5).

Many aspects of the design of prestressed concrete buildings have already been covered in this text. Further, an extensive treatment of the use of prestressed concrete in building construction is given in the *PCI Design Handbook* (Ref. 12-1). This chapter will summarize some important considerations in the design of buildings using precast, pretensioned components or cast-in-place, post-tensioned construction.

12.2 TYPICAL FRAMING OF PRECAST CONCRETE BUILDINGS

Precast concrete components are capable of providing the floor system, the vertical load-carrying system, the lateral load-resisting system, and the enclosure for building structures. Typically, the floor system will consist of hollow-core slabs spanning up to about 35 ft

(11 m) or double tees spanning up to about 70 ft (21 m) or single tees spanning up to about 100 ft (30 m) (see Fig. 6-15). For many buildings, load-bearing walls are an efficient means of carrying both vertical and lateral loads. However, where large open spaces are required, a beam-and-column framing system can be used. Precast concrete exterior wall panels are capable of both enclosing the building and providing the architectural finish.

The framing system shown in Fig. 12-1 is commonly used for apartment buildings and hotels which have a large number of interior walls. The use of precast concrete walls and hollow-core slabs results in construction rates of up to two floors per week. A cast-in-place topping containing reinforcement is sometimes used in order to help tie the building together.

The precast concrete beam-column framing system shown in Fig. 12-2 provides the large open spaces required in office buildings. With a double-tee floor system, relatively large column spacings can be used. The precast spandrel beams provide a ledge support for the double tees and can also support the enclosure of the building. In the structure shown in Fig. 12-2 the spandrels and interior inverted-tee beams are supported by corbels projecting from the multistory precast columns.

Figure 12-3 illustrates the structural system for a precast single-story industrial building. The roof members are double tees which are supported around the perimeter by ledges built into the load-bearing wall panels. Inverted-tee beams provide the support for the double-tee roof members in the interior of the building.

12.3 STRUCTURAL INTEGRITY OF PRECAST CONCRETE BUILDINGS

Cast-in-place reinforced concrete structures possess inherent continuity that enables them to carry a given load via a number of different load paths. This redundancy gives them a high degree of protection against the likely spread of local damage and the ability to absorb considerable energy prior to collapse. Cast-in-place reinforced concrete structures thus possess considerable "structural integrity" and hence have a low probability of suffering a progressive collapse.

Buildings constructed with precast components are basically statically determinate and the joints between the components are significant discontinuities in the structure. The lack of alternative load paths together with the presence of potential weak links at the connections means that special care is required to achieve adequate structural integrity. If a structure possesses a significant ability to resist lateral loads, it will typically also possess a significant ability to resist progressive collapse. Hence one of the critical decisions in the design of a precast concrete building is the manner in which the lateral loads will be resisted.

The primary lateral load-resisting system typically consists of either shear walls or moment-resisting frames. In either case the floor systems must be designed to act as horizontal diaphragms transmitting the lateral loads to the walls or frames.

Figure 12-4 illustrates the manner in which the lateral forces can be transferred through the floor diaphragms. It can be seen that the precast concrete floor components must be appropriately tied together in order that the floor can act as a horizontal diaphragm.

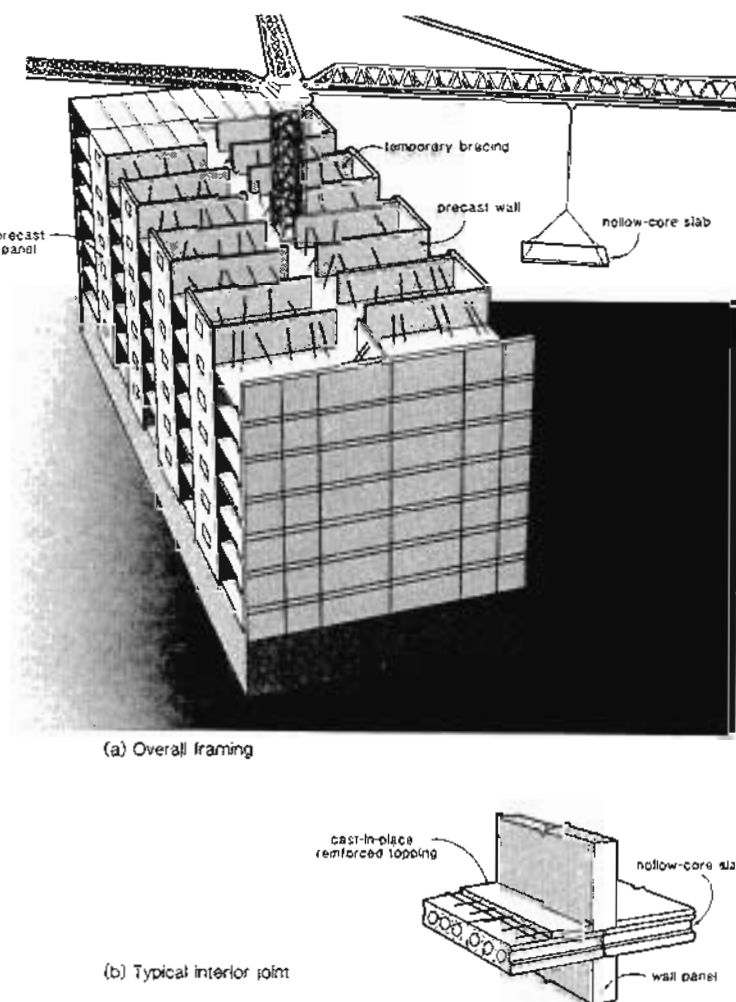
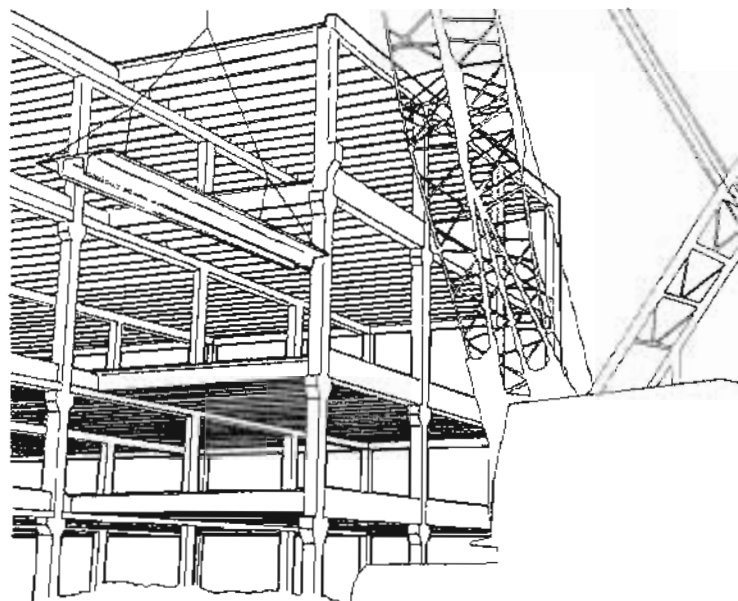
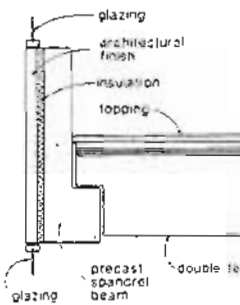


Figure 12-1 Framing of precast concrete apartment buildings

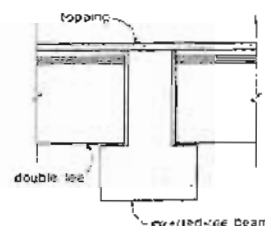
If double tees are used for the floor system, then the flange tips may be connected as shown in Fig. 12-5a in order to transmit the chord tension force, T , and the shear between elements. The shear across the interior support may be transmitted by the welded plate details shown in Fig. 12-5b



(a) Overall framing

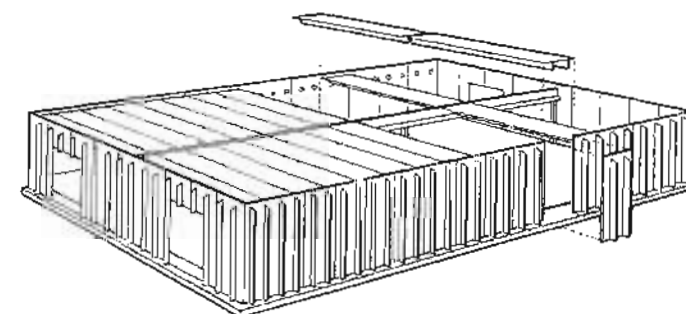


(b) Typical exterior framing

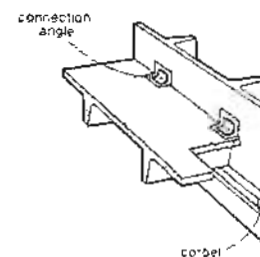


(c) Typical interior connection

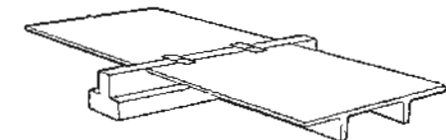
Figure 12-2 Framing details for precast office building.



(a) Double-tee roof and bearing wall members



(b) Connection of double-tee roof member with bearing wall panel



(c) Double-tee members supported by inverted-tee beam

Figure 12-3 Framing of single-story industrial building.

In untopped hollow-core slabs, grout keys can transmit shear stresses of about 80 psi (0.55 MPa) (Ref. 12-1). Some suggested reinforcement details for connecting untopped hollow-core slabs are shown in Fig. 12-6. Alternatively, a reinforced, cast-in-place topping can be used to ensure diaphragm action. The reinforcement in the topping required to resist shear can be designed using the shear friction concept explained in Chapter 9.

In precast concrete construction, the use of moment-resisting, beam-column connections is typically avoided because such connections require complex details which are difficult and costly to fabricate. For precast concrete beam-column structures, the lateral load resistance can usually be provided by the shear walls that will exist in the structure. Again, it is important to design the floor system so that it can transmit the applied lateral forces to the load-resisting shear walls (see Fig. 12-7).

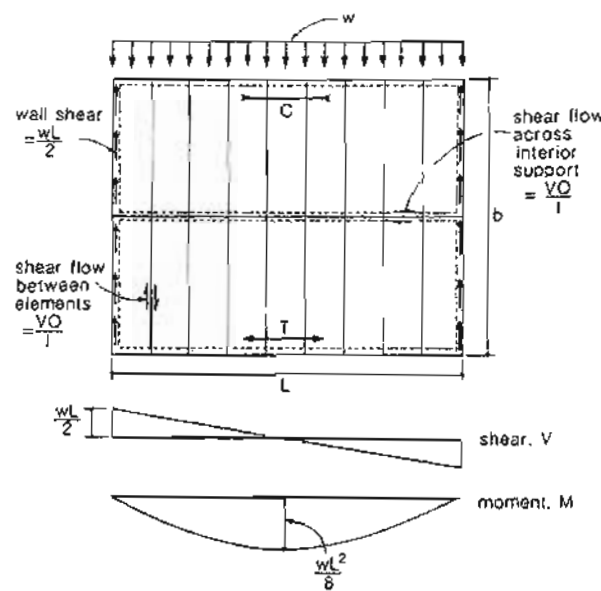


Figure 12-4 Transfer of lateral forces through floor diaphragm.

In addition to carefully following the flow of lateral forces through the horizontal diaphragm, the engineer must consider the manner in which the vertical elements will transmit the load from the floor down to the foundation. As shown in Fig. 12-8, the precast wall panels of multistory buildings need to be tied together in order to transmit the flexural tension (the "chord force") and to provide shear friction reinforcement across the wall-to-floor connections. For low-rise structures, wall panels can either be tied together to form a single shear wall (see Fig. 12-9a), or the panels can be designed to act as individual cantilevers (see Fig. 12-9b). Spencer and Tong (Ref. 12-3) have demonstrated that superior seismic performance will be obtained with the panels detailed to act as separate cantilevers.

The trend toward the use of large panel construction in North America has focused attention on ways of providing structural integrity in order to prevent progressive collapse. Figure 12-10 illustrates the way in which structural integrity in the form of alternate load paths can be provided in precast concrete wall panel structures. The provision of continuous reinforcement across joints of elements enables tie forces to develop, therefore permitting an alternate load path to form. Figure 12-10a illustrates the secondary defence mechanism that prevents the spread of collapse after the loss of a load-bearing wall panel. A simple model utilizing equilibrium and compatibility can be used to determine the amount of horizontal ties required to resist the notional removal of any panel in the structure. The

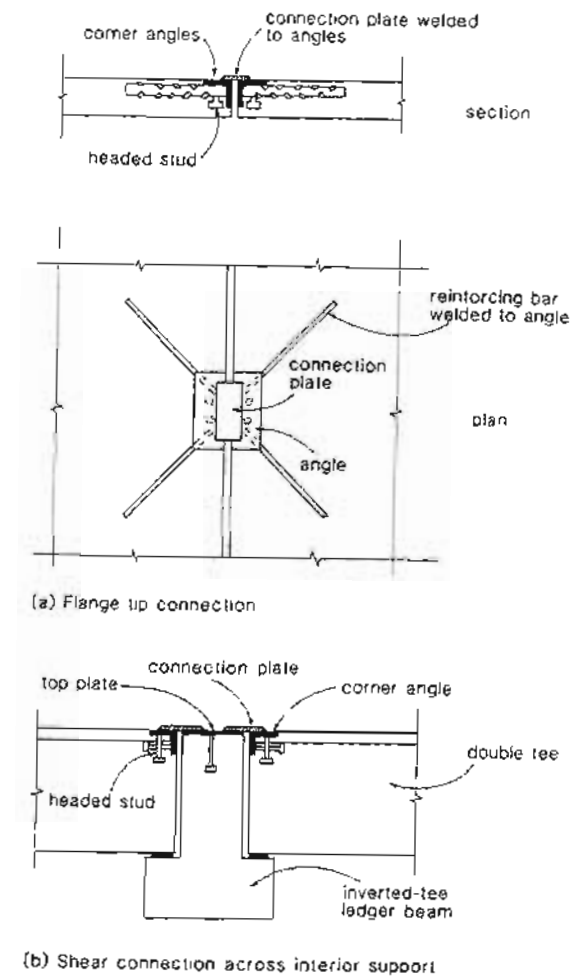


Figure 12-5 Diaphragm connections for untopped double tees. Adapted from Ref. 12-1.

vertical ties shown in Fig. 12-10b provide the shear connection between the horizontal joints and thus ensure that the wall panels above a failed element act as a unit.

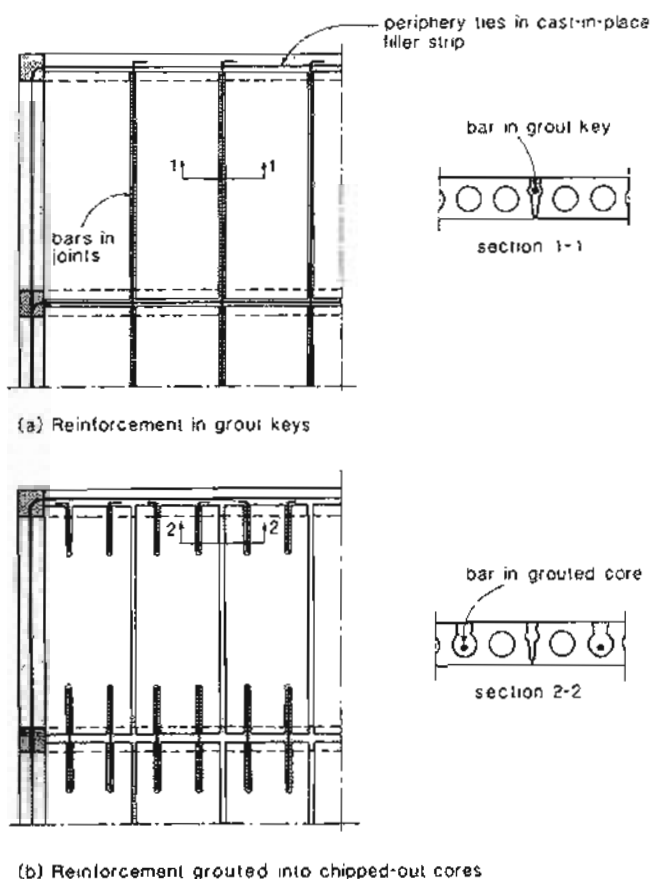


Figure 12-6 Diaphragm connections for untopped hollow-core slabs. Adapted from Vambergky (Ref. 12-2).

Figure 12-10c illustrates the role of longitudinal ties that are placed over the supports in the span direction. These longitudinal ties permit a secondary defense mechanism to be set up in the form of a suspension system. In the event of a support failure, this suspension system can prevent the failure from progressing to the floor below.

Wall returns or the inclusion of internal reinforced columns at the ends of some walls provide strong points that add stability in the event of a local failure (see Fig. 12-10d). The

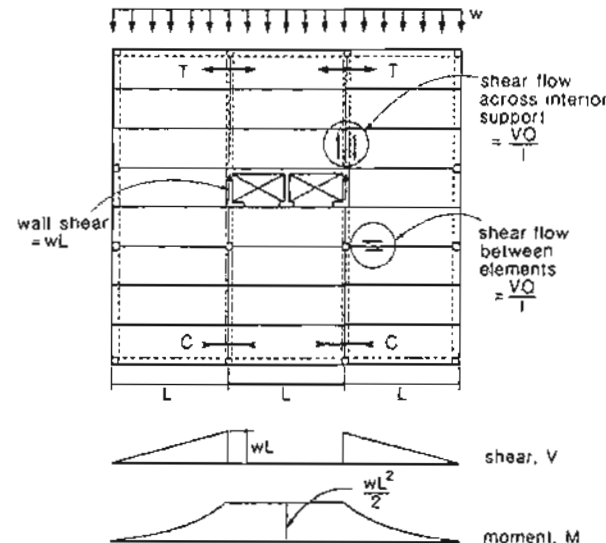


Figure 12-7 Transfer of lateral forces by diaphragm to shear core.

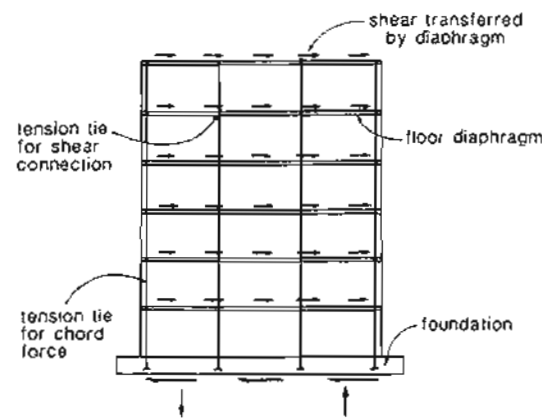
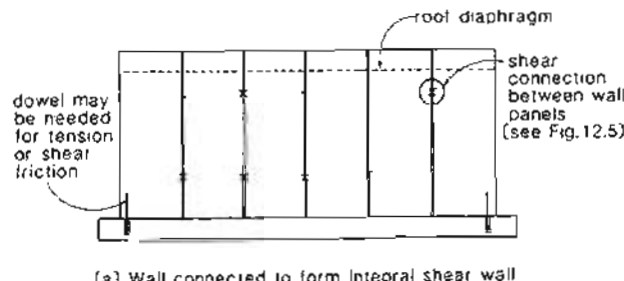
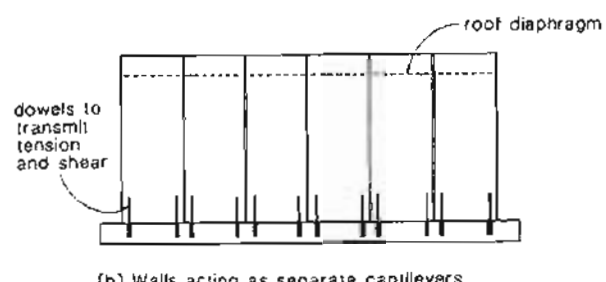


Figure 12-8 Transfer of lateral forces through shear wall



(a) Wall connected to form integral shear wall



(b) Walls acting as separate cantilevers

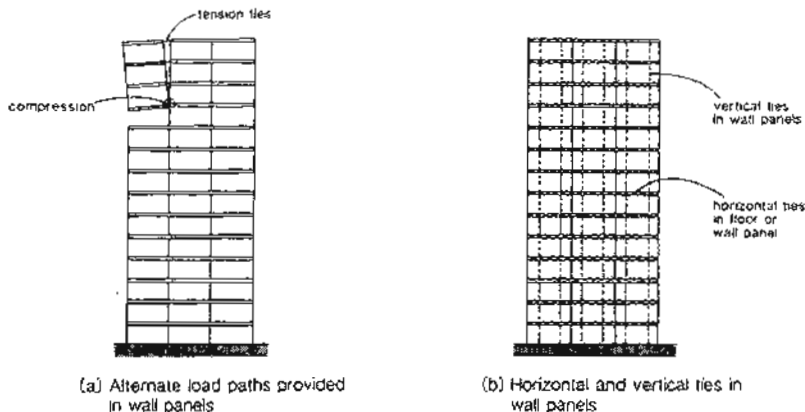
Figure 12-9 Reinforcement required in shear wall of one-story precast structure.

continuous peripheral ties in the floor slab provide tension ties necessary for diaphragm action and also provide a resisting mechanism for the corner region of the slab in the event of loss of support at the corners of the building.

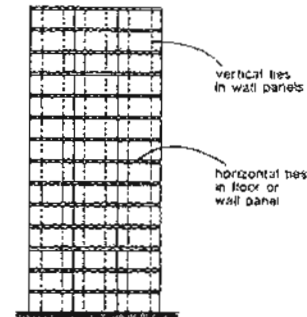
12.4 PARKING STRUCTURES

Most parking garage structures are open structures exposed to the environment and hence are subjected to many cycles of wetting and drying, expansion and contraction, and in northern climates, freezing and thawing. Further, many of these structures are subjected to de-icing salts or sea-water spray. Because of this severe environment, significant deterioration of many non-prestressed reinforced concrete parking structures has occurred.

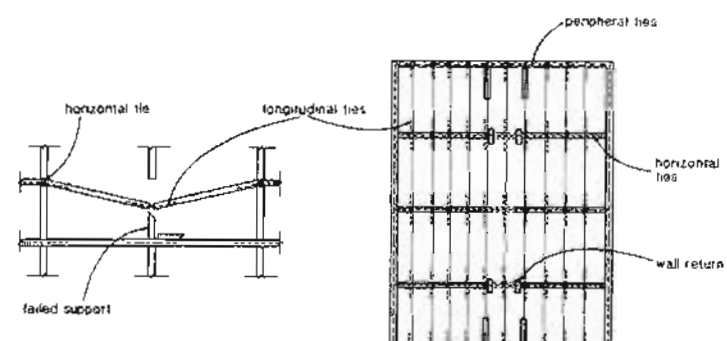
While significant deterioration problems have occurred in non-prestressed concrete parking garages, a detailed field survey of 39 precast, prestressed concrete parking structures (Ref. 12-5) revealed that "in general, the overall condition of the structures surveyed was excellent." The high-quality, low-permeability concrete typically used in prestressed concrete construction, together with the superior crack control obtained by appropriate prestressing, result in structures that are less susceptible to corrosion problems. Of course,



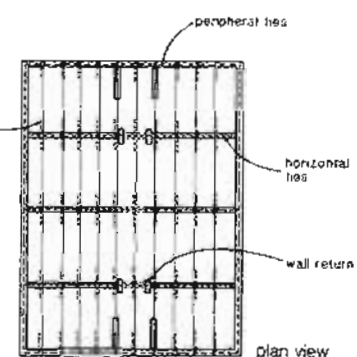
(a) Alternate load paths provided in wall panels



(b) Horizontal and vertical ties in wall panels



(c) Alternate load paths provided in floor members



(d) Ties in floor systems

Figure 12-10 Tie reinforcement requirements to achieve structural integrity in large panel structures. Adapted from Fintel, Schultz, and Iqbal (Ref. 12-4).

careful design, detailing, and strict control of construction quality is essential to achieve durable prestressed concrete parking garages. In this section we summarize a few of the important aspects of the design of prestressed concrete parking garages.

The efficient utilization of parking space requires large bays with a minimum of obstructions. Figure 12-11 illustrates the large open spaces that can be achieved using precast, pretensioned double tees. The flat ceilings that result from the use of hollow-core slabs as parking decks make it simpler to achieve the high level of lighting now required in public parking structures (see Fig. 12-12).

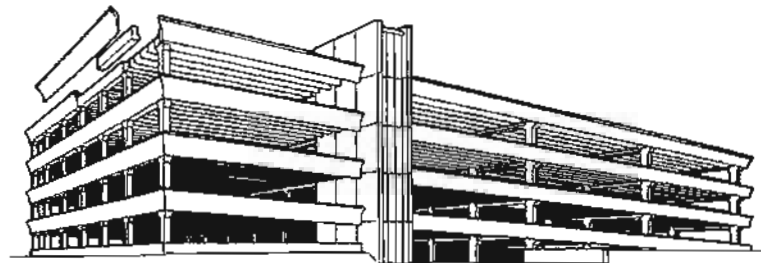


Figure 12-11 Precast pretensioned double-tee parking structure.

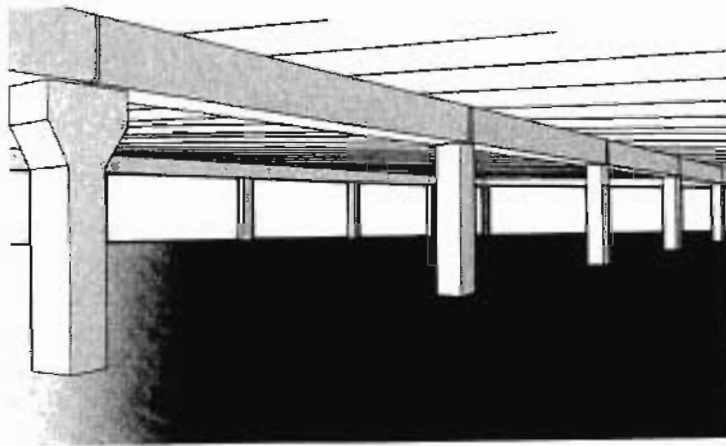
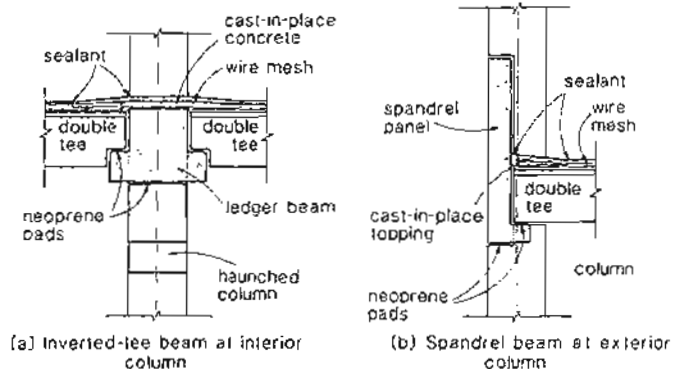


Figure 12-12 Hollow-core slab, parking deck.

A precast concrete parking structure is described by Ellenzweig, Ravindra, Hagen, and Vitelli (Ref. 12-6) who demonstrate that it is possible "to dispel the usual dreary image of this building type."

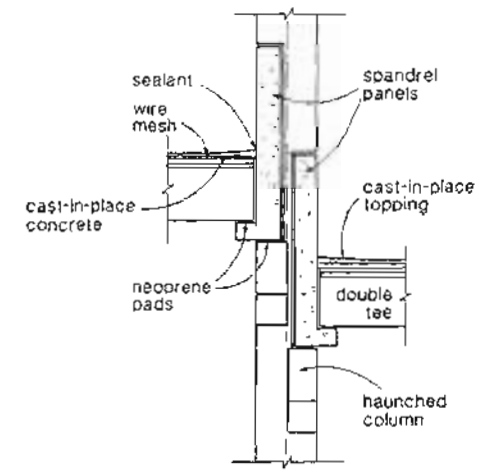
In one typical system (Ref. 12-7) 10 ft (3 m) wide by 28 in. (700 mm) deep double tees span 60 ft (18 m) onto spandrel and inverted-tee beams. A reinforced concrete topping is used to tie the double-tee members together. The supporting beams span 30 ft (9 m)

between precast multistory columns with corbel seats. Typical connection details for such a structural system are shown in Fig. 12-13. Figure 12-14 shows the connection details for a hollow-core slab framing system.



(a) Inverted-tee beam at interior column

(b) Spandrel beam at exterior column



(c) Interior spandrels supporting ramps

Figure 12-13 Connection details for a double-tee parking structure. Adapted from Ward (Ref. 12-7).

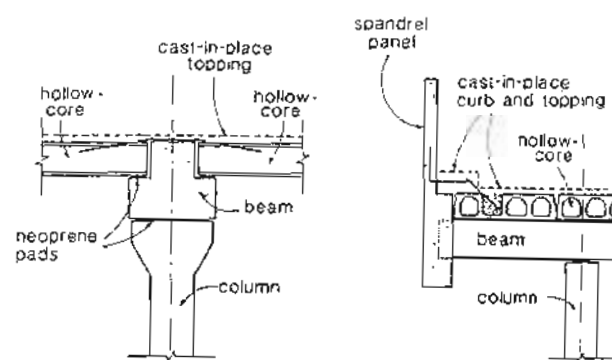


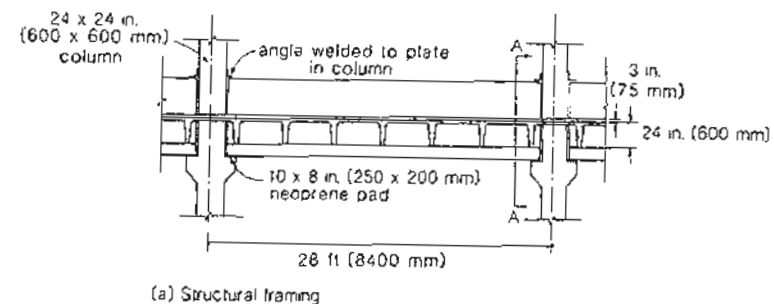
Figure 12-14 Connection details for a hollow-core slab parking structure.
Adapted from Ward (Ref. 12-7).

Prestressed concrete spandrel beams not only serve to support the parking deck but can also serve as safety barriers. These elements are typically designed to resist a concentrated factored "bumper load" of about 11 kips (50 kN) (Ref. 12-6). An example of a parking garage spandrel beam is given in Fig. 12-15. The eccentric loads that the stems of the double tees apply to the bottom ledge of the spandrel beam cause significant torsion in the spandrel beam. This torsion requires appropriate reinforcement in the spandrel beams and appropriate connections at the column face which can restrain the rotation at the ends of the spandrel beams. The reinforcing bars welded to the corner angles shown in Fig. 12-15c prevent local failures at these end connections. The additional hanger reinforcement in Fig. 12-15c has been provided to transmit the high local loads from the stem of the double tees to the web of the spandrel.

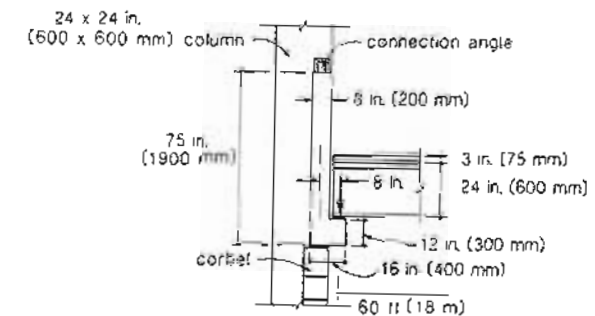
Figure 12-16 illustrates the structural layout for a post-tensioned eight-story parking structure. The typical floor slab was 8 in. (200 mm) thick and is designed for a live load of 40 psf (2 kN/m^2). The slabs are post-tensioned with 0.6 in. (15 mm) diameter unbonded monostrands. This 273 ft (83.3 m) long open structure was constructed without any expansion joints in the slabs.

Because the deterioration of existing concrete parking structures is such a significant problem, a large number of studies have been conducted recently to find out how such problems can be avoided for future parking garages. While some of the special details differ somewhat, there is general agreement on what is required to produce durable parking structures. Some of the recommendations given in Refs. 12-1, 12-5, 12-7, 12-10, 12-11, 12-12, 12-13, and 12-14 are summarized below:

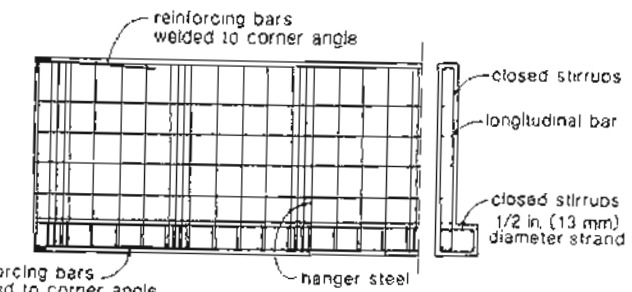
1. **Drainage.** – Positive drainage to ensure good runoff and prevent ponding is essential. A minimum slope of 1 to 2% is recommended. Drains should have a minimum diameter of 8 in. (200 mm) and be designed to be easily cleaned. Drainage should



(a) Structural framing



(b) Section A-A



(c) Spandrel reinforcement details

Figure 12-15 Details of precast pretensioned parking garage spandrel beam.
Adapted from Ref. 12-8.

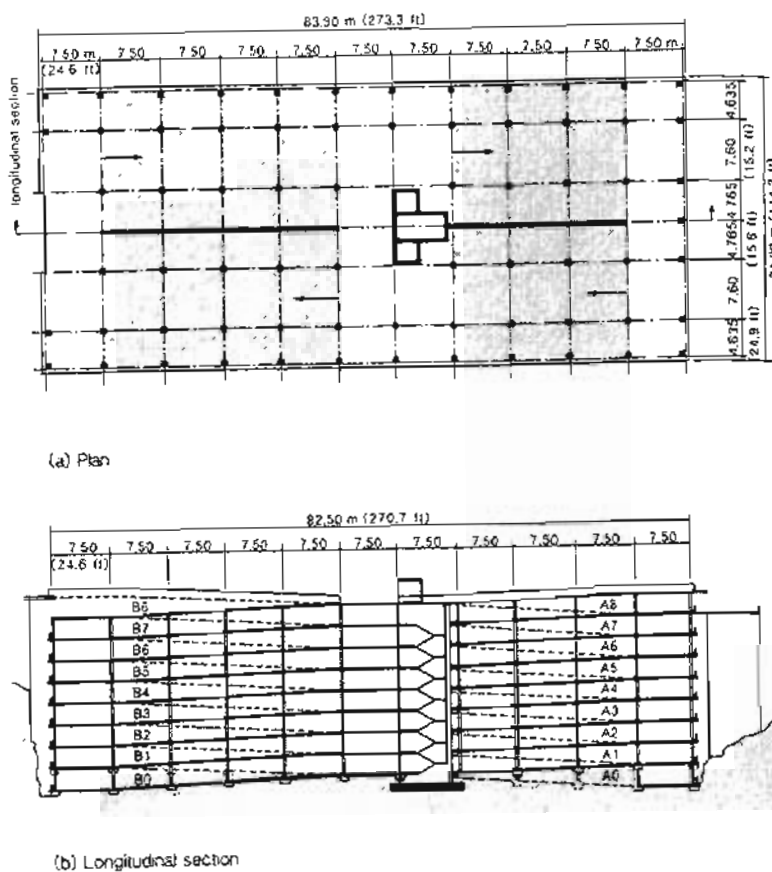


Figure 12-16 Structural layout of 950-car cast-in-place, post-tensioned parking structure. Adapted from Ritz et al. (Ref. 12-9).

take water away from all joints, columns, and spandrel beams to prevent leakage and corrosion of connections.

- Concrete quality. — Concrete in the parking decks, whether for cast-in-place post-tensioned slabs or for topping over precast units, must have low permeability (water/cement ratio of less than 0.40 to 0.45), must be resistant to freeze-thaw deterioration (minimum air entrainment of 4 to 6%), must be made from sound, durable aggregates, and must have high alkalinity for good corrosion protection. A minimum

Sec. 12.4 Parking Structures

cement content of 600 to 700 lb/yd³ (360 to 415 kg/m³) is recommended. Mechanized screeds may be required to level off the low-slump concrete. Overfinishing of the surface may raise the water/cement ratio and reduce the air content in the surface concrete and hence must be avoided. A minimum period of 3 days of moist curing should be provided for all cast-in-place concrete.

- Concrete cover. — Concrete cover over top reinforcing bars and post-tensioning ducts should be a minimum of 1.5 to 2 in. (40 to 50 mm). This requirement may be relaxed for the small wires of welded wire fabric, which do not have as high a corrosion potential. A cover of at least 2 1/2 times the wire diameter must be provided. Care needs to be taken to account for the effect of camber in choosing a topping thickness and ensuring adequate concrete cover. The application of penetrating sealant such as linseed oil or proprietary products reduces the water and chloride ion penetration and hence can reduce the potential for corrosion of the reinforcement.
- Crack Control. — Good practice for crack control is to design the prestressing such that cracking at service loads is eliminated wherever possible and to provide sealed control joints where cracking cannot be avoided. Cracking is usually due to the restraint to creep, shrinkage, and thermal movement, and hence the overall layout of the structure will influence the potential for cracking. For example, stiff vertical elements such as shear walls should be located in the center of buildings. Since expansion joints frequently cause problems in parking structures, they should be avoided wherever possible. Symmetrical structures less than 300 ft (90 m) in length can usually be designed without such joints. Bearing pads used at the supports of pretensioned members serve to relieve the buildup of restraint forces.

A minimum average axial compression due to prestress of 200 psi (1.4 MPa) for post-tensioned slabs and 170 psi (1.2 MPa) for precast floor elements is recommended. Since the reinforced cast-in-place topping over pretensioned deck units is not prestressed and further, since its function is to transfer force across the discontinuities between the precast units, cracking of this topping will occur at these discontinuities. To control this cracking, a series of control joints should be tooled into the topping above all joints in the precast members below. After cleaning the joint a good-quality joint sealant is applied.

For column-supported garages a liberal use of column ties and stirrups is recommended to control any diagonal cracking that may arise due to the restraint of cyclic thermal movements, with particular attention being paid to very short columns.

- Corrosion protection of hardware. — Rusting of exposed steel hardware in the corrosive environment of a parking garage causes unsightly staining and can lead to the failure of connections. Because of this, all steel hardware should be hot-dipped galvanized and all field-welded connections should be coated with a zinc-rich paint. Such steel hardware should be located so that it can be easily maintained.
- Maintenance. — A regular maintenance program is of critical importance in extending the life of a parking structure. It is appropriate for the designer to provide the owner with a detailed maintenance manual. Such a manual should specify the need for regular inspection (to check for leaks, rust, and damaged joints), regular unclogging

of drains, regular painting of exposed steel work, regular sweeping of decks, and regular washing down of the structure.

12.5 SPECIAL APPLICATIONS OF POST-TENSIONING TO BUILDING STRUCTURES

The use of post-tensioning enables the engineer to provide economical solutions to some difficult design and construction problems encountered in building structures. Figure 12-17 illustrates the application of stage post-tensioning to a transfer girder at the base of a 12-story building. First, scaffolding is erected to support the weight of the transfer girder. After placement of the reinforcing bars and post-tensioning sheaths, the concrete for the transfer girder is cast. When the concrete reaches sufficient strength, the first stage of post-tensioning, force P_1 , is applied (see Fig. 12-17a). At this stage the concrete stresses must be within the code stress limits computed for the initial concrete strength. The prestressing force, P_1 , is chosen to balance the weight of the first three floors and thus permits these floors to be constructed without exceeding the stress limits in the concrete of the transfer girder (see Fig. 12-17b). The prestressing force for stage 2 of the post-tensioning operation is chosen to balance the weight of floors 3 to 6 without exceeding the stress limits (see Fig. 12-17c and d). This process of stage post-tensioning is repeated until the structure is completed. After all of the stages are completed, the tendons can be re-tensioned to regain losses that have occurred due to shrinkage, elastic shortening, creep, and relaxation of the prestressing steel. Slater (Ref. 12-15) has found that prestressing losses may be reduced by about 15 ksi (100 MPa) by this re-tensioning operation.

Figure 12-18 illustrates the use of four transfer girders to support the 34-story, 2 Bloor Street East office tower in Toronto. The transfer girders span across the existing subway structure and were constructed using the stage post-tensioning technique (Ref. 12-15). The largest girders are 109 ft (33 m) long, 10 ft (3 m) wide, and 20 ft (6 m) deep. Each transfer girder is post-tensioned with 49 tendons, each consisting of 19 strands of 0.6 in. (15 mm) diameter. The total prestressing force on each girder, after all losses, is 33,500 kips (149,000 kN). The transfer girders had five stages of post-tensioning, at floors 1, 7, 14, 21, and 27. Monostrand jacks were used in order to give better control of the post-tensioning operation and to reduce the jacking space required.

Figure 12-19 shows the application of post-tensioned segmental construction to an office tower. The central core wall, together with the eight large exterior columns, provide a column-free interior. A total of 44 Vierendeel trusses 75 ft 7 in. (23 m) long by 16 ft 8 in. (5.08 m) deep provide the long-span framing members between the columns, as shown in Fig. 12-19b and c. Each Vierendeel truss is one story deep and supports two floors. These trusses were made of precast segments that were match-cast in a precasting yard. The segments were assembled on scaffolding and then post-tensioned, as shown in Fig. 12-19c. In floors 6 to 13, the post-tensioning in each Vierendeel truss consisted of four tendons, each with 66 wires of 0.276 in. (7 mm) diameter with f_{pu} equal to 255 ksi (1760 MPa). After post-tensioning, the ducts were grouted and the columns were cast around the embedded ends of the top and bottom chords of the Vierendeel truss. The truss and column frames were designed to take 25% of the earthquake loads (Ref. 12-17).

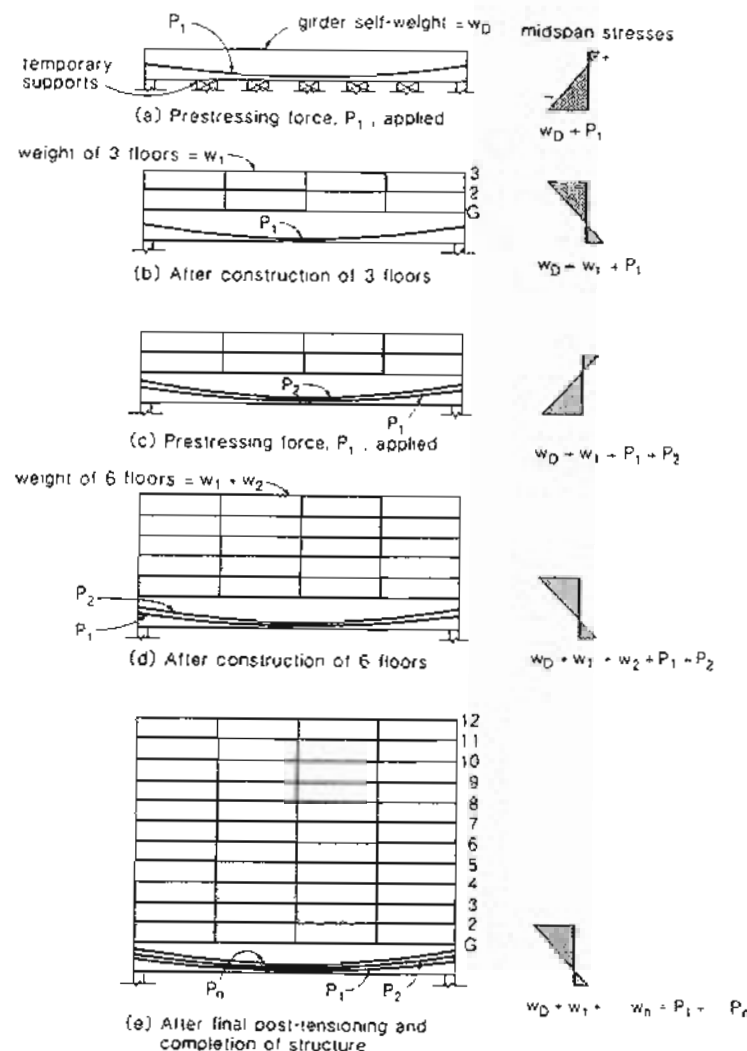


Figure 12-17 Stage post-tensioning of a transfer girder supporting a 12-story structure. Adapted from Slater (Ref. 12-15).

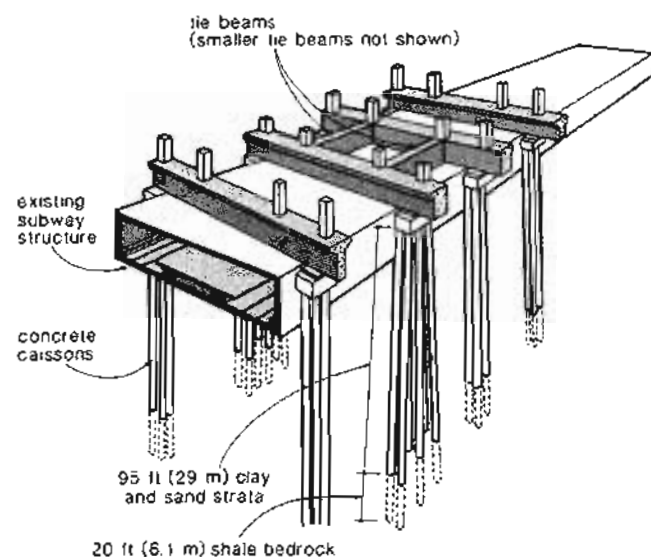


Figure 12-18 Stage post-tensioned transfer girder used for 2 Bloor East Office Building in Toronto. Adapted from Slater (Ref. 12-15).

Post-tensioning provides a useful means of providing tension-tie forces in buildings with inclined columns. Figure 12-20 illustrates the structural framing of the 19-story Manulife Centre in Toronto. As can be seen, the exterior columns slope inward near the base from the fifth and sixth floors. Multi-strand post-tensioning was used to resist the outward thrusts at the locations where the columns changed direction. Multi-strand tendons provide the tension-tie forces in the two principal directions of the building (Ref. 12-15). The first stage of post-tensioning was carried out when the construction reached the fifth and sixth floors. The second and third stages were carried out when the construction reached floors 12 and 17, respectively. Total post-tensioning forces of 9000 kips (40,000 kN) and 3800 kips (17,000 kN) were applied in the short and long building directions, respectively. The tensioning operation was carried out using monostrand jacks to minimize the space and handling requirements.

12.6 POST-TENSIONED FOUNDATIONS

In special circumstances post-tensioning provides an efficient solution to difficult foundation problems. The main application in building foundations is for mats or rafts (see Figs. 12-21 and 12-22). An excellent review of the design considerations for post-tensioned foundations

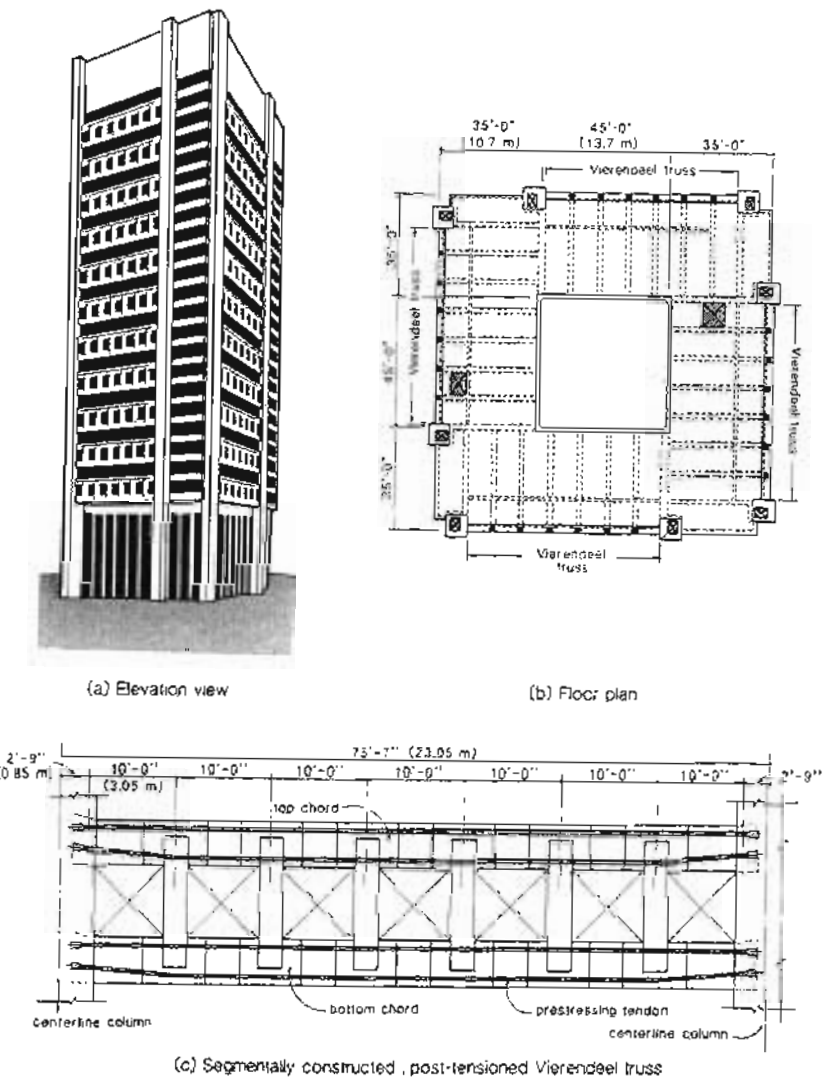


Figure 12-19 Structural framing of the 28-story International Aviation Organization Headquarters in Montreal. Adapted from Martynowicz and McMillan (Ref. 12-16).

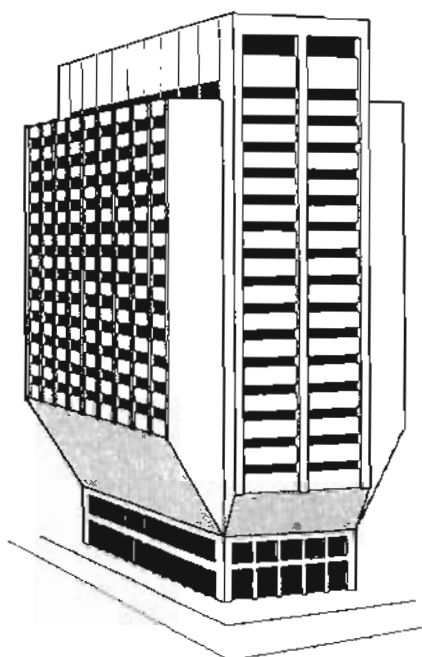


Figure 12-20 The 19-story Manulife Centre in Toronto with inclined columns.

is given by Aeberhard, Ganz, Marti, and Schuler (Ref. 12-18). The advantages in using post-tensioned foundation mats include the following:

1. By means of load balancing, post-tensioning can achieve more uniform soil pressure distributions, reducing differential settlement.
2. Post-tensioning enables a thinner mat to be used, reducing excavation costs.
3. Post-tensioning reduces concrete cracking, improving water tightness and durability.

Figure 12-23 demonstrates the manner in which the interaction between the foundation mat and the soil can be modeled. The stiffness of the soil is represented by a grid of springs having stiffnesses $k_s A$ where k_s is the subgrade modulus having units of kips/ ft^3 (kN/m^3) and A is the tributary area of each spring in ft^2 (m^2). The modulus of subgrade reaction, k_s , can vary from about 100 kips/ ft^3 ($16000 \text{ kN}/\text{m}^3$) for soft clay to 1500 kips/ ft^3 ($10 \times 10^6 \text{ kN}/\text{m}^3$) for dense gravel. Figure 12-23b illustrates the variation of soil pressure that would be predicted if the foundation mat were not prestressed.

When the mat is post-tensioned with the tendon profile shown, it will tend to "lift up" at the columns and "push down" between the columns, resulting in the changes in

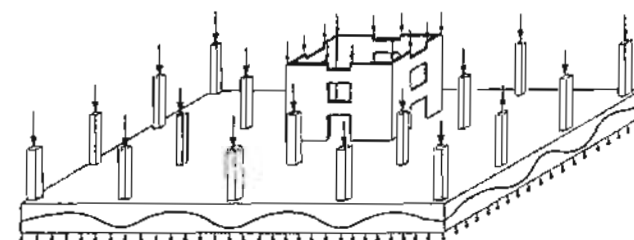


Figure 12-21 Post-tensioned foundation mat.

the soil pressure shown in Fig. 12-23c. The soil pressure due to the combined action of the column loads and the prestressing is shown in Fig. 12-23d.

When designing a post-tensioned foundation mat, careful attention must be given to the influence of the restraint caused by the friction between the mat and the subgrade. When the mat is post-tensioned it will attempt to shorten (see Fig. 12-24a). This shortening will be restrained by the friction, which will cause a substantial tension in the mat (see Fig. 12-24c). The result will be that the concrete compressive stresses will be substantially smaller at the center of the mat than at the free edges. While the subgrade friction will reduce the average concrete compressive stresses caused by the post-tensioning, it will not reduce the beneficial "load-balancing" effects of the prestress described in Fig. 12-23.

Often the foundation mat is post-tensioned in several stages as the dead weight of the supported superstructure increases. In these cases the shortening of the mat will be restrained not only by the subgrade friction but also by the superstructure. Methods for calculating the resulting restraint actions have been described in Chapter 10.



Figure 12-22 Post-tensioned foundation slab for five-story parking structure in Cupertino, California. From *VSL Newsletter*, Jan. 1989.

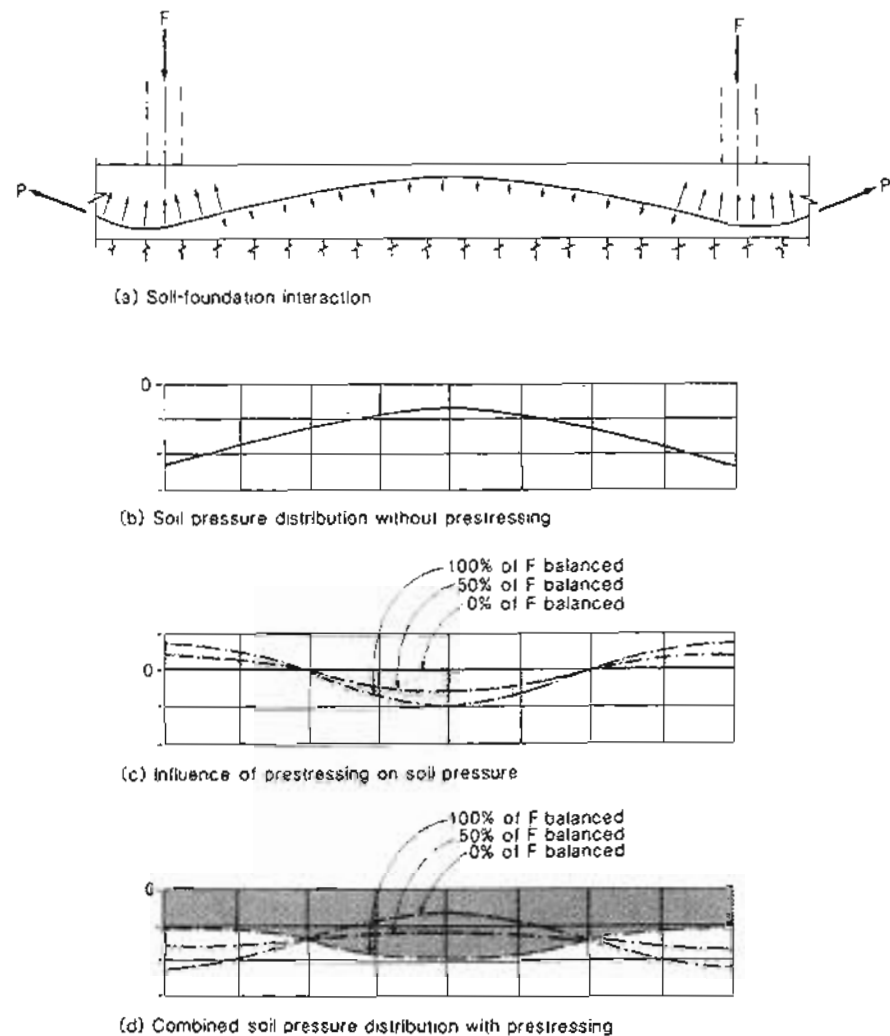


Figure 12-23 Effect of prestressing a mat foundation. Adapted from Ref. 12-18.

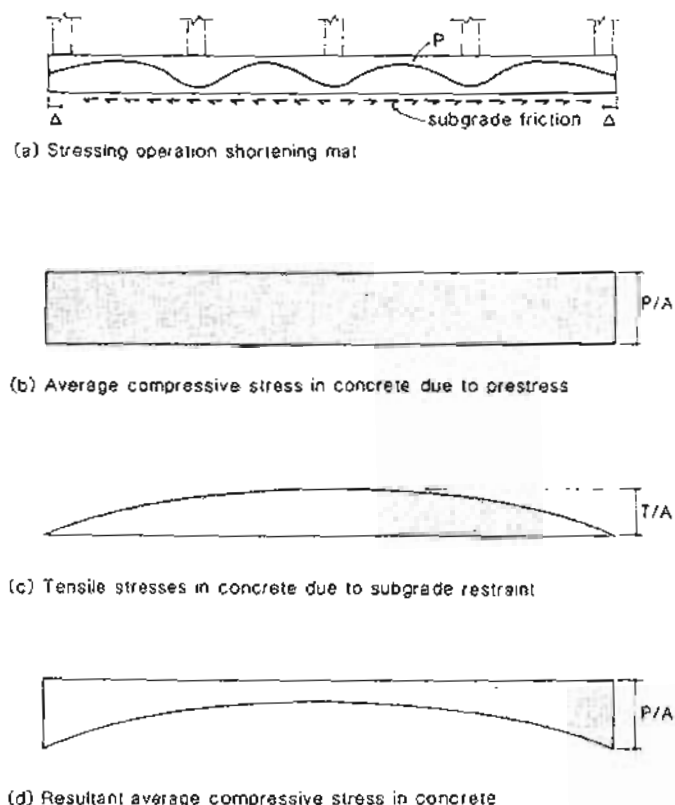


Figure 12-24 Loss of compressive stress due to subgrade friction.

References

- 12-1 Prestressed Concrete Institute. *PCI Design Handbook: Precast and Prestressed Concrete*, 3d ed., PCI, Chicago, 1985.
- 12-2 Vambergky, J.N.J.A., "FIP Recommendations on Multi-story Buildings," *Proceedings of the FIP/CP/CPCI Symposia*, Calgary, Vol. 3, Aug. 1984, pp. 99-106.
- 12-3 Spencer, R.A., and Tong, W.K.T., "Design of a One-Storey Concrete Building for Earthquake Loading," *Proceedings of the Eighth World Conference on Earthquake Engineering*, San Francisco, 1984, Vol. 5, pp. 653-660.
- 12-4 Fintel, M., Schultz, D.M. and Iqbal, M., "Design and Construction of Large-Panel Concrete Structures: Report 2 - Philosophy of Structural Response to Normal and Abnormal Loads," Portland Cement Association, Skokie, Ill., Aug. 1975, 133 pp.
- 12-5 The Consulting Engineers Group Inc., "Survey of Precast Prestressed Concrete Parking Structures," Report on Research Project No. 7, Prestressed Concrete Institute, Chicago, 1986, 73 pp.
- 12-6 Ellenzweig, H., Ravindra, M.V., Hagen, H.W., and Vuelli, R.J., "Blue Cross and Blue Shield Parking Facility," *PCI Journal*, Vol. 35, No. 1, Jan.-Feb. 1990, pp. 26-36.
- 12-7 Ward, D.L., "Prestressed Concrete Garage Construction in Canada," *Proceedings of the FIP/CP/CPCI Symposia*, Calgary, Vol. 3, Aug. 1984, pp. 163-171.
- 12-8 Collins, M.P., and Mitchell, D., "Shear and Torsion Design of Prestressed and Non-Prestressed Concrete Beams," *PCI Journal*, Vol. 25, No. 5, Sept.-Oct. 1980, pp. 32-100.
- 12-9 Ritz, P., Matt, P., Tellernbach, Ch., Schlub, P., and Aeberhard, H.U., *Post-Tensioned Concrete in Building Construction - Post-Tensioned Slabs*, Losinger Ltd., Berne, Switzerland, 1981, 41 pp.
- 12-10 Monroe, D.C., "The Prestressed Advantage for Durable Parking Structures," *Proceedings of the FIP/CP/CPCI Symposia*, Calgary, Vol. 3, Aug. 1984, pp. 172-178.
- 12-11 MacGregor, J.G., Saatcioglu, M., and Cumming, S., "Chapter 1 - General," *Concrete Design Handbook*, Canadian Portland Cement Association, Ottawa, 1984, pp. 1-1 to 1-59.
- 12-12 PCI Committee on Parking Structures, "Recommended Practice for Design, Manufacture, Erection and Maintenance of Precast, Prestressed Concrete Parking Structures," Prestressed Concrete Institute, Chicago, 1986.
- 12-13 Chrest, A.P., "Designing Concrete Parking Structures for Long-Term Durability," *Concrete International: Design and Construction*, Vol. 10, No. 11, Nov. 1988, pp. 45-46.
- 12-14 Falconer, D.W., "Tips for Post-Tensioning," *Concrete International: Design and Construction*, Vol. 10, No. 2, Feb. 1988, pp. 36-39.
- 12-15 Slater, W.M., "Stage Post-Tensioning - A Versatile and Economic Construction Technique," *PCI Journal*, Vol. 20, No. 1, Jan.-Feb. 1975, pp. 14-27.
- 12-16 Martynowicz, A., and McMillan, C.B., "Large Precast Prestressed Vierendeel Trusses Highlight Multistory Building," *PCI Journal*, Vol. 20, No. 6, Nov.-Dec. 1975, pp. 50-65.
- 12-17 Prestressed Concrete Institute, *PCI Manual for Structural Design of Architectural Precast Concrete*, PCI, Chicago, 1977, pp. 10-8 to 10-15.
- 12-18 Aeberhard, H.U., Ganz, H.R., Marti, P., and Schuler, W., *Post-Tensioned Concrete in Building Construction - Post-Tensioned Foundations*, VSL International Ltd., Berne, Switzerland, June, 1988, 24 pp.

Bridges

The uncertainty as to the magnitude of the effect of impact on bridges has for many years been a stumbling-block in the path of systemization of bridge designing. . . . The impact formula for highway bridges . . . $I = 100/(L + 150)$ was established to fit the author's practice. Its correctness is not likely to be ever determined by experiment

J.A.L. Waddell, 1899

13.1 INTRODUCTION

Bridges are the purest expression of the art and science of structural engineering. As well as ensuring that the bridge can safely fulfil its function, the engineer must carefully consider the impact of the bridge on its surrounding environment. The successful bridge will be economical both in terms of initial cost and in terms of maintenance costs over its long life, functional, and aesthetically pleasing.

Because prestressed concrete bridges can be economical, durable, and elegant, they constitute an increasingly large share of the total bridge market. Approximately 50% of bridges are now constructed of prestressed concrete. In North America there are over 600,000 bridges, with a total replacement value of about 250 billion dollars.

Information on the structural behavior of prestressed concrete which is needed in the design of a prestressed concrete bridge has been covered in the earlier chapters of this text. In this chapter we will deal with some of the additional special considerations involved in bridge design.

13.2 TYPES OF PRESTRESSED CONCRETE BRIDGES

While there are many different forms of prestressed concrete bridges, some of the types more common in North America are shown in Fig. 13-1 along with their typical span ranges. The most common form of prestressed concrete bridge in the small- to medium-span range consists of precast, pretensioned standard I-girders with a cast-in-place deck slab (see Figs. 1-9 and 1-10). For somewhat longer spans the precast concrete I-girders can be made continuous by using reinforcement over the supports in the cast-in-place deck slab. Longer spans can be achieved by post-tensioning the precast girders to form continuous spans. By splicing together individual precast beams, spans of up to 160 ft (50 m) have been achieved (see Fig. 13-2).

Post-tensioned, voided-slab bridges are an alternative form of prestressed concrete bridge which has been widely used in the small- to medium-span range. They are particularly suitable for highway interchange bridges, which are typically curved in plan and have limited headroom (see Fig. 13-3).

In recent years, box-girder bridges have become increasingly popular for medium- to long-span bridges. This is due to their efficient structural form, the existence of ingenious construction techniques, and their elegant appearance. The cross section of a box girder has excellent torsional resistance and can efficiently carry large positive and negative moments. With the use of transverse post-tensioning the cantilevering portions of the top flange can be lengthened considerably. Clean simple lines and single-cell construction minimize formwork costs. By changing the cross section along the span, box-girder bridges can be used for very large spans (see Fig. 13-4). An excellent summary of the design of box-girder bridges is given by Schlaich and Scheef (Ref. 13-1).

Arch bridges are particularly suited to long spans across valleys with solid rock walls, as shown in Fig. 13-1. Innovative construction techniques incorporating traveling formwork have made this traditional form of construction competitive once again.

Cable-stayed bridges offer an economical solution where very long spans are required. For example, the East Huntington Bridge, which is a precast, prestressed concrete, cable-stayed bridge, was chosen over a steel alternative design because the concrete bridge could be built for 70% of the cost of the steel bridge (Ref. 13-2). The segmentally precast girder, which was constructed from 8000 psi (55 MPa) concrete, has a slender, graceful appearance with a span-to-depth ratio of 180 (see Fig. 1-12). It is interesting to note that if a two-tower, symmetrical configuration had been used the structural system of the East Huntington Bridge would be capable of spanning 1600 ft (500 m) (Ref. 13-2).

13.3 ECONOMIC CONSIDERATIONS

In the conceptual design phase for a bridge, the engineer needs to appreciate the economics of bridge construction. Figure 13-5 summarizes the cost breakdown for a number of post-tensioned concrete bridges. It can be seen that the in-place cost of the prestressing steel in the superstructure is only 11% of the total project cost, while the concrete in the superstructure accounts for only 6%. Design refinements resulting in small reductions in the quantities of these materials will not significantly change the project cost.

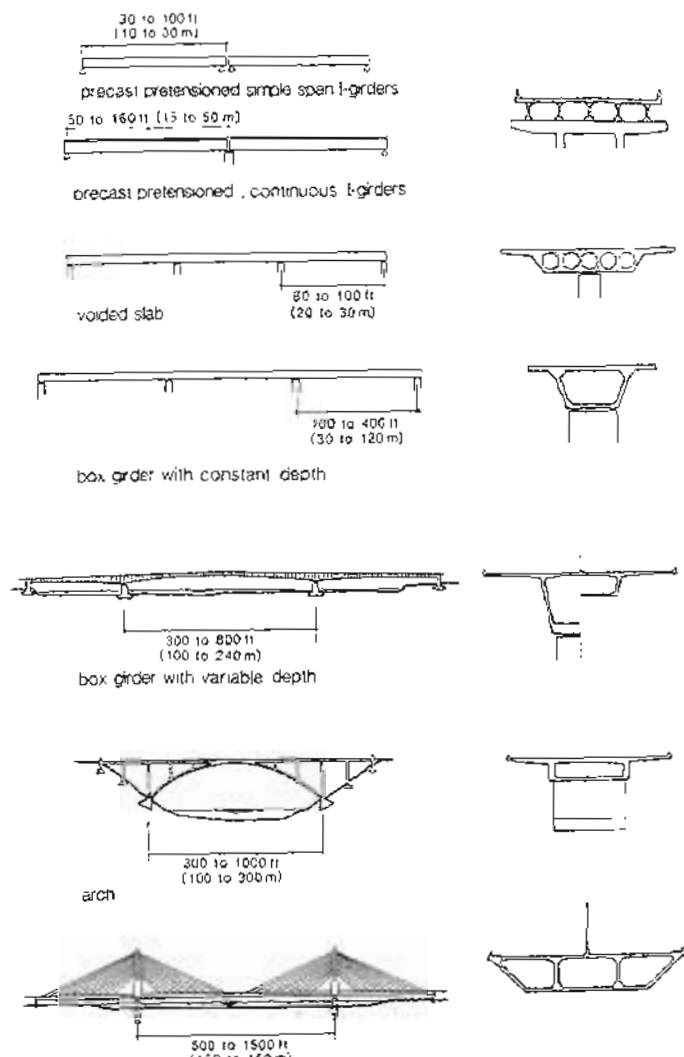


Figure 13-1 Approximate span ranges of different bridge types.



Figure 13-2 Workers positioning the yet-to-be spliced end of a precast I-girder on temporary tubular steel scaffolding. Photograph courtesy of CPCI.

Figure 13-6 provides a guide for estimating the quantities of materials required in the superstructure of a typical highway box-girder bridge. It should be appreciated that the concrete volumes and the prestressing steel quantities are significantly influenced by construction requirements, and hence significant variations for different construction schemes are to be expected. The percentage of reinforcing bars, on the other hand, is relatively constant since the majority of this reinforcement is controlled by minimum reinforcement requirements. For box-girder railway bridges the material quantities increase by about one-third.

Because labor costs have increased much faster than material costs (see Fig. 13-7) it has become increasingly important to develop construction methods that minimize the amount of labor required. In the 1930s the total labor required to construct a large concrete bridge was about 50 hr/yd³ (40 hr/m³) of concrete. By the 1980s this had been reduced to about 13 hr/yd³ (10 hr/m³), and some particularly efficient construction techniques require only about 5 hr/yd³ (4 hr/m³).

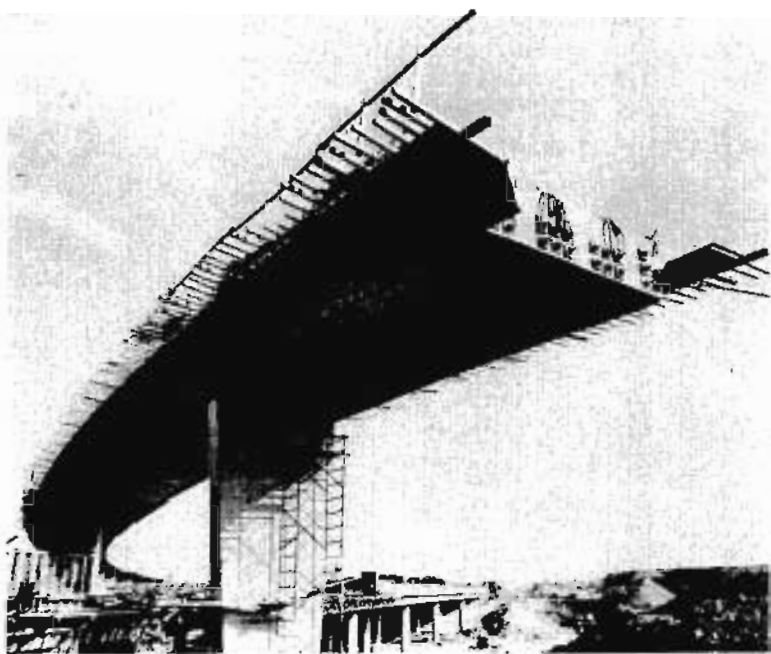


Figure 13-3 Post-tensioned voided-slab highway interchange bridge under construction. Photograph courtesy of Ministry of Transportation, Ontario.



Figure 13-4 Gateway Bridge in Brisbane, Australia. Box-girder bridge with a main span of 850 ft (260 m). Photograph courtesy of VSL International Ltd.

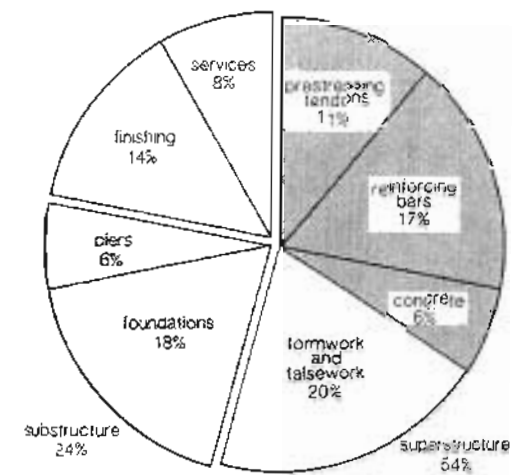


Figure 13-5 Cost breakdown for typical post-tensioned concrete bridges. Adapted from Schlaich and Scheff (Ref. 13-1)

13.4 SPECIAL CONSTRUCTION TECHNIQUES

Over the past 30 years a number of innovative construction techniques have been developed which have significantly reduced the costs involved in bridge construction. Some of the more significant of these recently developed techniques, most of which are applicable to long-span bridges, are summarized in Fig. 13-8.

The balanced cantilever construction method developed by the firm of Dyckerhoff and Widmann (Ref. 13-3) eliminates the need for falsework by using traveling formwork supported from previously constructed portions of the bridge (see Fig. 13-8a). Beginning at a pier, two traveling forms proceed outward into the adjacent spans, typically in steps of 8 to 16 ft (2.5 to 5 m). After each segment has been cast, post-tensioned tendons are used to tie the segment to the existing structure. The Burlington Skyway Bridge shown in Fig. 1-11 was constructed using this technique (Ref. 13-4).

A launching truss can be used to make the cantilever construction method more versatile. For cast-in-place segmental construction the launching truss is used to support the traveling formwork and to transport the construction materials. For precast segmental construction the launching truss is used to place the segments. The truss can also be used to stabilize the cantilevers during construction. The use of launching trusses becomes more economical if they can be reused for several different bridges. Figure 13-9 shows the two launching trusses used in constructing the Credit River Bridge. Each of these trusses had previously been used to construct different bridges. Some details of the Credit River Bridge

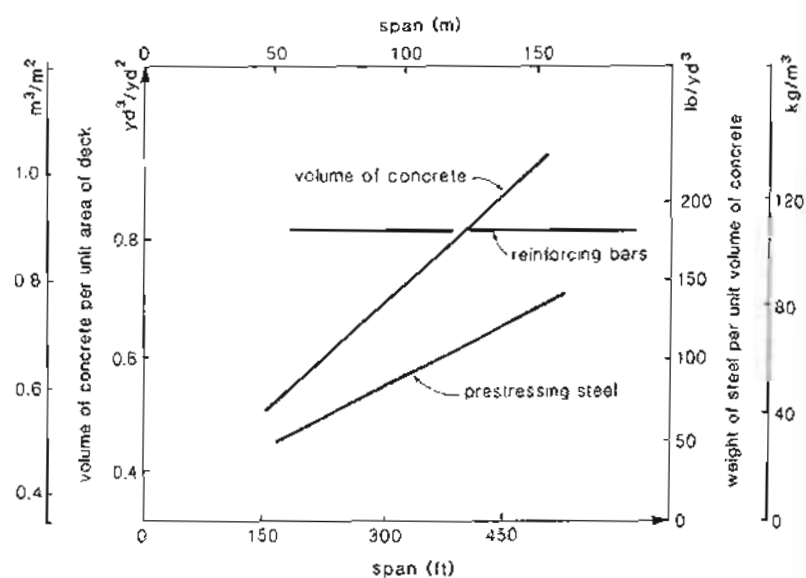


Figure 13-6 Average quantities in superstructures for typical highway box-girder bridges. Adapted from Schlaich and Scheef (Ref. 13-1).

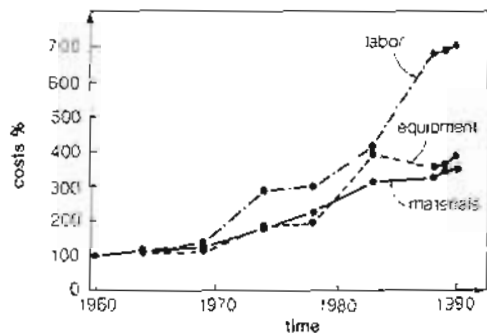
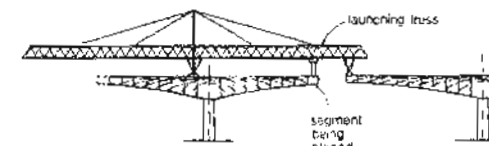


Figure 13-7 Growth of construction costs. Based on data from Means' *Building Construction Cost Data*.



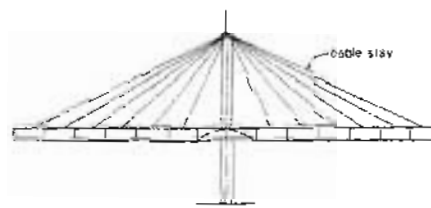
(a) Cast-in-place balanced cantilever construction



(b) Cantilever construction using precast segments and launching truss



(c) Incremental launching method



(d) Segmental construction of cable-stayed bridge

Figure 13-8 Recent construction methods.

are given in Fig. 13-10. In this bridge, shear keys recessed toward the inner faces of the webs were used to aid in transmitting shear between the segments.

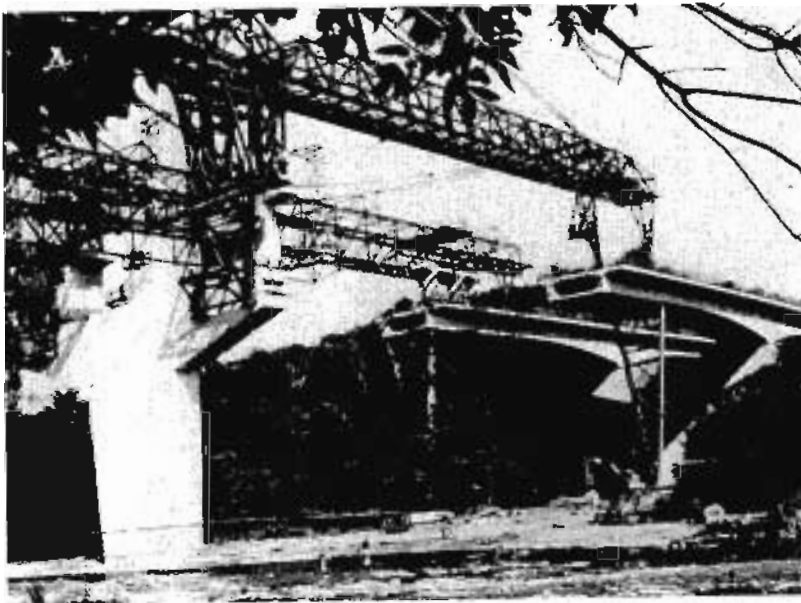


Figure 13-9 Erection of precast segments of Credit River Bridge using two launching trusses. Photograph courtesy of R. Skelton.

13.5 LOADS

While the primary purpose of a bridge is to safely support the traffic crossing over it, the dominant loading for many bridges is, in fact, the self-weight of the bridge. In addition to the traffic loads and the dead loads, the bridge must be capable of withstanding safely environmental loads such as wind pressures, water pressures, thermal variations, seismic forces, and ice forces. The design must investigate the safety of the bridge not only in its final configuration but also in its various construction stages (see Fig. 13-8).

The vast majority of North American highway bridges have been designed using the traffic loads specified by the American Association of State Highway and Transportation Officials (AASHTO) in their *Standard Specifications for Highway Bridges* (Ref. 13-6). As shown in Fig. 13-11, AASHTO represents traffic loading either by a single truck load or by lane loading consisting of uniform loading together with a concentrated load.

The AASHTO traffic loading models were based on studies made in the early 1940s. Since this time the nature of truck traffic has changed substantially. The three-axle AASHTO design truck (HS 20-44) has a total weight of only 72 kips (320 kN). However, modern highway trucks may weigh more than 145 kips (650 kN). This is partially compensated for by using a significantly increased load factor for live loads and their

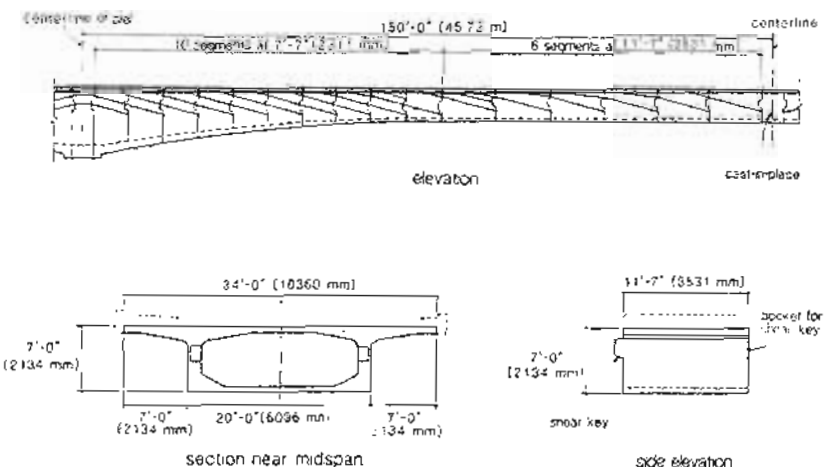


Figure 13-10 Details of Credit River Bridge. Adapted from Skelton (Ref. 13-3).

associated impact loads. For example, one typical factored load combination is

$$1.3 \left[D + \frac{5}{3}(L + I) \right] \quad (13-1)$$

The *Ontario Highway Bridge Design Code* (OHBDC, Ref. 13-7) specifies vehicle loads that are directly related to the legal loads on the highways. The five-axle OHBD truck (see Fig. 13-12), with a gross weight of 700 kN (157 kips), is an upper bound representation of modern heavy trucks based on maximum observed loads from extensive vehicle surveys (Refs. 13-8 and 13-9). With this heavy design truck the Ontario code uses a load factor of 1.3 for live loads and impact loads.

Since highway traffic consists of a large number of light vehicles and a comparatively small number of heavy vehicles, the *Ontario Highway Bridge Design Code* specifies two loading conditions to be considered separately. These are: (1) the OHBD truck, shown in Fig. 13-12, and (2) the OHBD lane load, which consists of an OHBD truck with each axle load reduced to 70% of the values shown in Fig. 13-12 combined with a uniformly distributed load of magnitude q , as given in Fig. 13-13.

When more than one lane is loaded, the live loads are reduced in view of the improbability of all lanes having their maximum loading at the same time. Because of this, AASHTO recommends the reductions in load intensity given in Table 13-1.

Roughness of the riding surface will cause a dynamic variation in the axle loads. To allow for these dynamic effects AASHTO has traditionally applied an impact factor, I , to

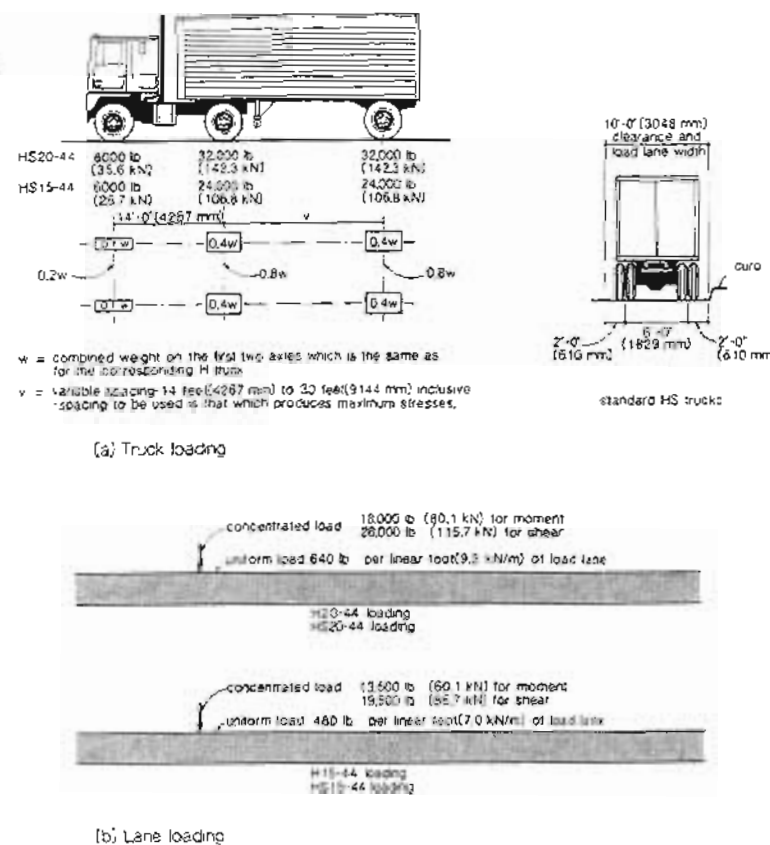


Figure 13-11 AASHTO loading. Adapted from Ref. 13-6.

Table 13-1 Reduction in load intensity for multilane loading.

Number of Loaded Lanes	% of Live Load to Be Used
1 or 2	100
3	90
4 or more	75

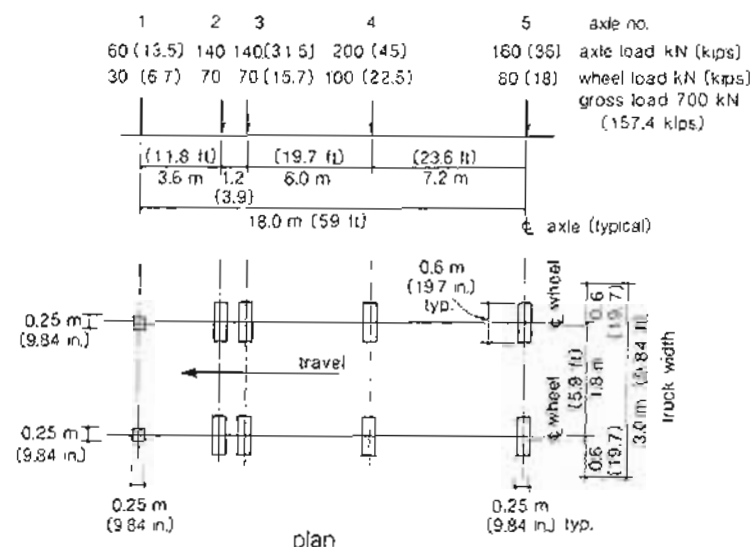


Figure 13-12 The OHBD truck load. From Ref. 13-7.

the specified truck loads. For more than 60 years this equation has been

$$I = \frac{50}{L + 125} \quad (13-2)$$

where I is the impact factor, not to exceed 0.30, and L is the span length in feet for computing moments, or length of the loaded portion of span from point under consideration to the far reaction for computing shear. A similar formulation, but with different coefficients, was proposed by Waddell in 1899 (Ref. 13-10).

The OHBD code uses the term "dynamic load allowance" in lieu of the more traditional impact factor. For spans greater than 22 m (72 ft) in length, the dynamic load allowance for two or more axle loads is made a function of the first flexural frequency of the bridge, as shown in Fig. 13-14. It is interesting to note that AASHTO would give an impact factor of 0.25 for a span of 75 ft and a factor of 0.20 for a span of 125 ft (38 m). In the range 2 to 5 Hz, the dynamic load allowance of the OHBD code is increased to account for the dynamic amplifications due to the interaction between the vehicle and the bridge when their natural frequencies are similar.

The formulation for the impact factor given in the OHBD Code was "based primarily on the results of full-scale bridge testing" (Ref. 13-11). The new approach was stated to be "a first step in trying to relate the dynamic design process to some of the most significant parameters" (Ref. 13-11).

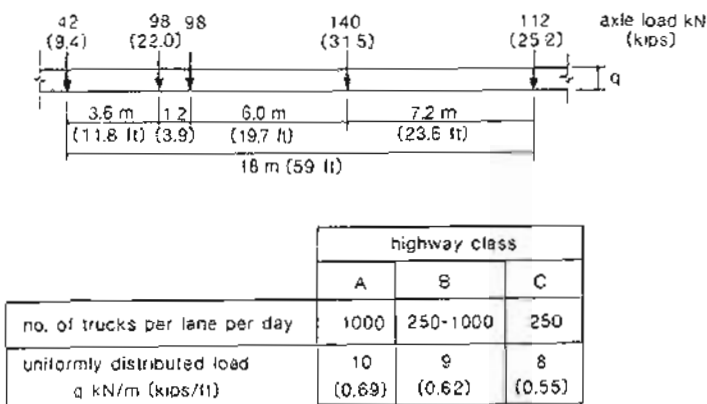


Figure 13-13 The OHBD lane load. From Ref. 13-7.

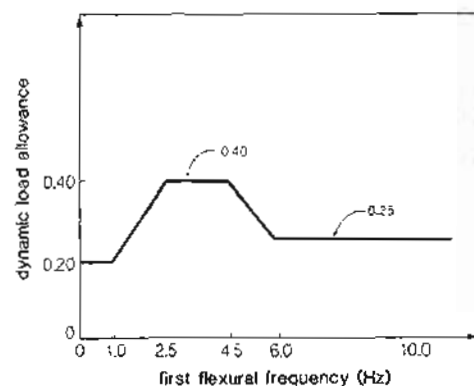


Figure 13-14 Dynamic load allowance for truck loads on spans greater than 72 ft (22 m). From Ref. 13-8

13.6 ANALYSIS

In current practice, the manner in which the applied loads are distributed among the elements of the bridge is determined on the basis of elastic analysis or by using approximate

expressions developed from such analyses. Because the wheel loads from trucks are concentrated over a small area, one important analysis problem is to decide what width of bridge will participate in resisting the wheel loads. Thus, in designing the girders for the composite slab-on-girder bridge shown in Fig. 13-15, we must decide how much of the wheel load needs to be carried by each longitudinal girder or stringer. If the girder spacing were about equal to the lane width, each girder may have to carry the total truck load.

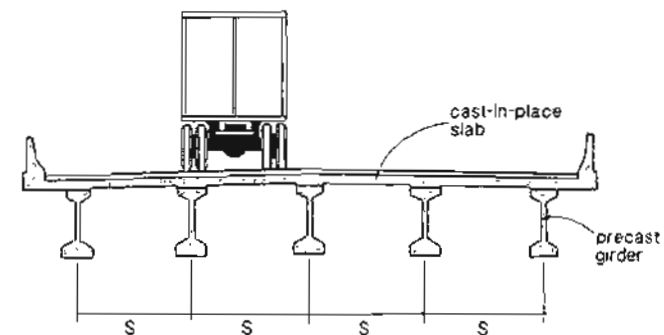


Figure 13-15 Truck on slab-on-girder bridge

The AASHTO Code (Ref. 13-6) relates the load on each stringer to the truck wheel load, the spacing of the stringers, the type of bridge construction and the number of traffic lanes. Thus each interior girder of a bridge like that shown in Fig. 13-15 is assumed to carry the wheel load times $S/5.5$, where S is the spacing in feet. Thus, if the girders were spaced at 11 ft, each girder would have to be capable of carrying the total truck load (i.e., the two lines of wheel loads).

Usually, separate structural analyses of a bridge are conducted for the transverse and the longitudinal directions of the bridge. Thus for the box girder shown in Fig. 13-16, the section is checked for the moments and axial loads in the transverse direction. In a separate analysis, the longitudinal response of the girder is then checked, assuming in this case that the cross section is rigid.

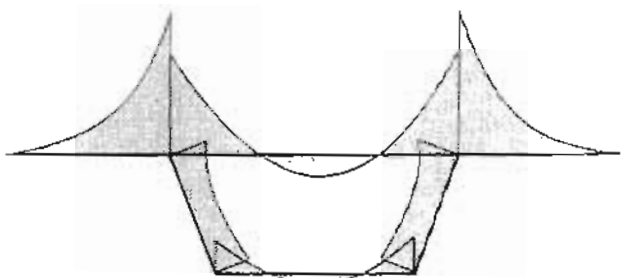
In the transverse direction, the design is typically dominated by the dead-load moments or the moments due to uniform live loads. The moments due to concentrated wheel loads "spread out" along a considerable length of the bridge and hence their "demand" on the section is reduced.

To estimate the moments caused by a concentrated load, a "dispersion angle" of 45° is sometimes assumed. If this assumption is used, the calculated moments caused by a point load acting on a cantilever slab are as shown in Fig. 13-17. Note that for the simplified distribution, the transverse moment per unit length of the slab is given by

$$m = \frac{PL}{2L} = 0.5P \quad (13-3)$$



(a) Cross section of box-girder bridges



(b) Transverse moments due to dead loads

Figure 13-16 Analysis of bridge in transverse direction.

Thus increasing the "span" of the cantilever slab does not increase the required flexural strength per unit length. The actual distribution of these transverse moments will depend strongly on the specific details of the cantilever. Methods for more accurately estimating these distributions have been given by Bakht (Ref. 13-12).

13.7 MEMBRANE ACTION IN DECK SLABS

The deck slabs must be designed to carry the dead loads and truck loads to the supporting girders. In assessing the structural capacity of deck slabs in composite beam-slab bridges traditional elastic analysis techniques lead to very conservative results. In the elastic analysis of slabs it is assumed that the bending of the slab causes no change in length of the slab. Thus when uniform load is applied to the two-span, elastic beam shown in Fig. 13-18a, the centroidal axis of the beam remains the same length. Thus the roller supports shown at A and C will not move due to application of the uniform load.

When uniform load is applied to the reinforced concrete beam shown in Fig. 13-18b, the centroidal axis will become longer. Cracking of the concrete at sections D and

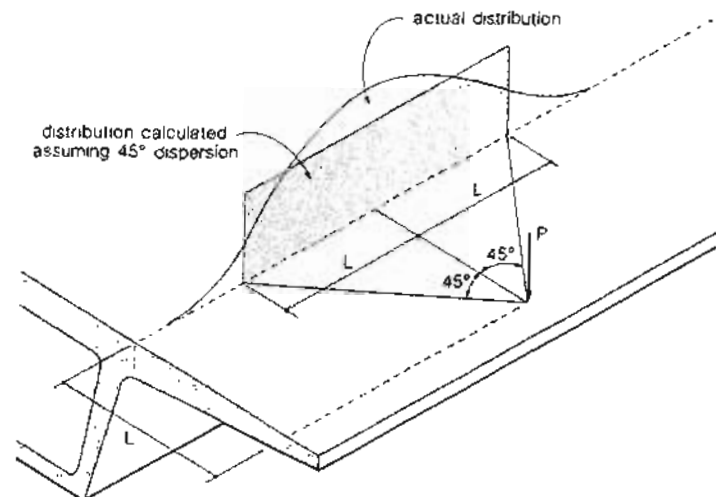
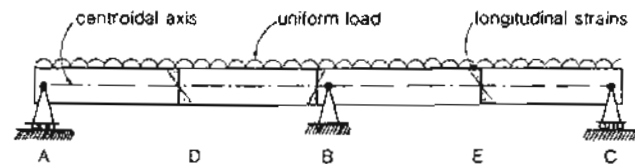
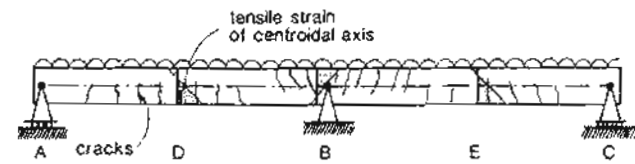


Figure 13-17 Transverse moments caused by point load on cantilever slab.



(a) Elastic beam on three supports - no elongation



(b) Reinforced concrete beam on three supports - beam becomes longer

Figure 13-18 Influence of flexure on elongation of centroidal axis.

E will result in large tensile strains on the bottom surface and much smaller compressive strains on the top surface. As a result, the axis at mid-depth will be subjected to a tensile strain. Cracking of the concrete at B will cause large tensile strains on the top surface and smaller compressive strains on the bottom surface. Once again the axis at mid-depth will be subjected to a tensile strain. Integrating these centroidal tensile strains along the length of the beam gives the magnitude of the outward movement of the rollers at both A and C.

In an actual structure a reinforced concrete flexural member is not free to elongate but will have to push against the surrounding, supporting structure. As a result of the restraint of these axial elongations, axial compression will develop in the member. This axial compression will substantially increase the flexural strength of the reinforced concrete member (see Fig. 13-19). The large increase in carrying capacity of the reinforced concrete member caused by the restraint of axial elongations is called "membrane action" or "arching action." Insight into just how significant this effect can be was provided by Ockleston (Ref. 13-13). Ockleston tested to failure a two-way beam and slab floor system in a reinforced concrete building. The floor had been designed for a live load of 70 psf. It actually took over 700 psf to fail the floor.

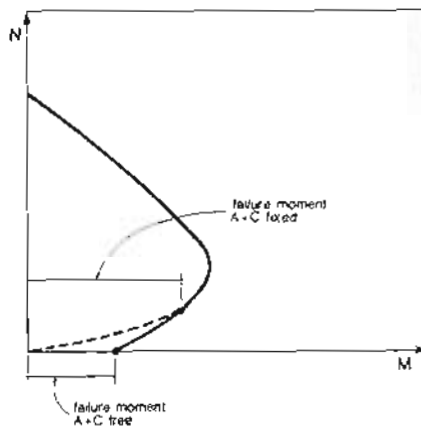


Figure 13-19 Influence of restraint on flexural capacity.

The *Ontario Highway Bridge Design Code* (Ref. 13-7) recognizes the beneficial effects of compressive membrane forces on the performance of reinforced concrete slabs in composite beam-slab bridges. Based primarily upon the work of Baichelor and Hewitt (Refs. 13-14 and 13-15), the code permits deck slabs to be designed by what is called the "empirical method." In this method the flexural and shear capacity of the slab does not have to be investigated provided that the following conditions are met:

1. An area of reinforcement at least equal to 0.003 times the slab area is provided near each face of the slab in each direction.

Sec. 13.9 Example Design of Precast Bridge Girder

625

2. The spacing of the bars required by condition (1) does not exceed 12 in. (300 mm).
3. The span length of the slab perpendicular to the direction of traffic does not exceed 12 ft (3.7 m).
4. The span length-to-thickness ratio of the slab does not exceed 15.
5. The slab thickness is not less than 9 in. (225 mm).
6. The girders of the bridge are tied together by diaphragms at the support lines.
7. Edge stiffening of the slab is provided by an integral reinforced section of slab and curb or some other effective means.

13.8 DIMENSIONING AND DETAILING

In the dimensioning and detailing phase of the design, the response of the individual elements of the bridge to their calculated stress resultants is investigated, the dimensions of each element are checked, the required amounts of reinforcing bars and prestressing tendons are determined, and the specific details of how this reinforcement will be placed are decided upon. Much of this text has been devoted to explaining the procedures used in this phase of the design.

While the longitudinal design of the bridge is very similar to the design of beams, the transverse design, particularly of box-girder bridges, does involve some additional considerations. Figure 13-20 summarizes some of the reinforcement details for a box-girder bridge. Schlaich and Scheel (Ref. 13-11) recommend that the transverse tendons in the deck slab of such a bridge be placed with a spacing of less than 20 in. (500 mm). Further, they recommend that the tendons be placed as high as possible over the webs, using the smallest possible radius, and as low as possible midway between the webs. The level of prestress should be chosen so that the transverse bending of the webs due to gravity loads and prestressing is minimized.

13.9 EXAMPLE DESIGN OF PRECAST BRIDGE GIRDER

The composite beam-and-slab two-lane highway bridge described in Fig. 13-21 is to be designed to resist HS 20-44 loading (Ref. 13-6). The design of an interior girder is described in the steps given below.

Step 1: Choose the girder depth.

From Fig. 6-16 the span-to-depth ratio should be about 18. A 54 in. (1372 mm) deep girder would have a span-to-depth ratio of $82 \times 12/54 = 18.2$. Hence choose the section shown in Fig. 13-21.

Step 2: Determine the loads on the girder.

(a) Dead Loads. The dead loads are determined as shown in Table 13-2. The cross-sectional area of the precast girder is 685 in^2 ($442\,000 \text{ mm}^2$).

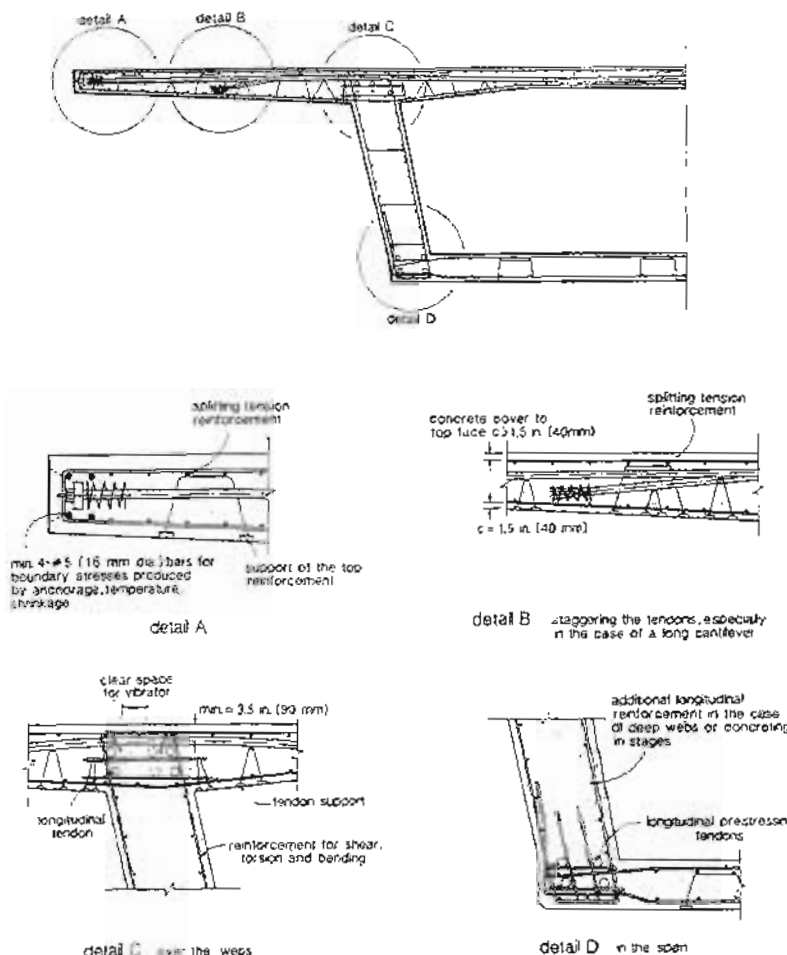


Figure 13-20 Details of reinforcement in box-girder bridge. Adapted from Schlaich and Scheel (Ref. 13-1).

(b) Live Loads. The fraction of wheel load applied to each girder is determined from Table I 3.1(B) of AASHTO (Ref. 13-6);

$$\frac{\text{girder spacing (ft)}}{5.5} = \frac{8.2}{5.5} = 1.491$$

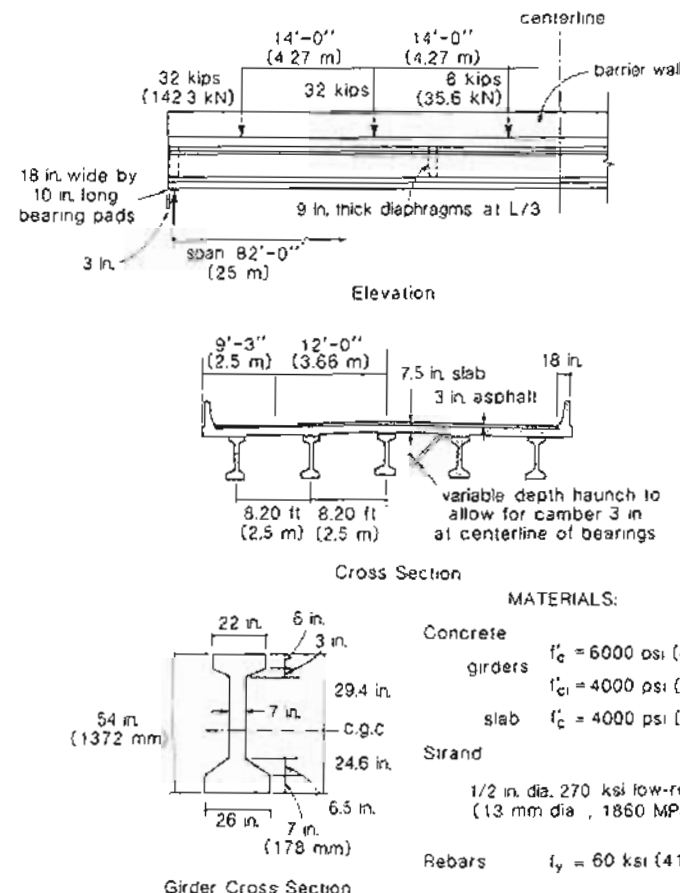


Figure 13-21 Design example – composite beam-slab highway bridge.

Therefore, fraction of truck load applied to each girder:

$$\frac{1}{2} \times 1.491 = 0.745$$

Table 13-2 Determination of dead loads.

Dead loads supported by naked girder:		
Girder	$685 \times 150/144$	= 0.714 kips/ft (10.42 kN/m)
Slab	$12 \times 8.20 \times 7.5$	= 738
Haunch	22×3	= .66
	$804 \times 150/144$	= 0.838 kips/ft (12.23 kN/m)
Diaphragms at 1/3 points	$0.75 \times 3.66 \times 7.5 \times 0.150$	= 3.09 kips (13.75 kN)
Dead loads supported by composite section:		
3 in. asphalt	$37.5 \times 0.25 \times 150$	= 1406 lb/ft
Barrier walls	$322.5 \times 2 \times 150/144$	= 672 lb/ft
Rails (approx.)	$.58$	lb/ft
Each composite girder takes	$2136/5$	= 0.427 kips/ft (6.23 kN/m)

Impact allowance for truck load moments from Eq. (13-2):

$$I = \frac{50}{L + 125}$$

$$= \frac{50}{82 + 125}$$

$$= 24.2\%$$

Note that for shear, I is a function of position along the span. The maximum moments and shears at different locations along the girder that result from the application of the HS 20 loading are shown in Table 13-3. As is customary in bridge design, the moments and shears have been calculated at tenth-points along the span.

Step 3: Choose the prestressing.

The area of prestressing required will be controlled either by the concrete stress limits at service loads or by the sectional strength requirement under factored loads. In order to choose the amount of prestressing we will use an approach analogous to that used in Fig. 6-22.

For the final condition, the AASHTO Code permits a concrete tensile stress of $6\sqrt{f_c}$ psi ($0.5\sqrt{f_c}$ MPa) in the precompressed tension zone. However, if the member were subjected to severe corrosive conditions, this allowable tensile stress is halved. We will use Eq. (6-31) to calculate the minimum value of P_f to ensure that the tension in the bottom fiber of the beam does not exceed the limit of $6\sqrt{6000} = 465$ psi (3.21 MPa).

We will assume that at midspan the centroid of the pretensioned strands will be 4 in. (102 mm) above the bottom face of the girder. Hence, from Fig. 13-21, the eccentricity of prestressing in the precast girder, $e_g = 24.6 - 4.0 = 20.6$ in. (523 mm). The moment of inertia of the precast girder alone is $242,930 \text{ in}^4$ and hence the section modulus to the bottom fiber is 9875 in^3 ($162 \times 10^6 \text{ mm}^3$). The dimensions needed to calculate the section properties of the transformed composite cross section are given in Fig. 13-22. Note

Table 13-3 Calculated moments and shears for bridge girder at tenth-points along span.*

		Distance from Support					
		0	0.1L	0.2L	0.3L	0.4L	0.5L
Service loads, M_s ft-kips	Girder self-weight, M_{dg}	0	716	384	504	576	600
	DL on naked girder, $M_{dg} + M_{ds}$	0	495	886	1172	1336	1388
	DL on composite, M_{du}	0	129	230	301	345	359
	Total DL	0	624	1116	1473	1681	1747
	$LL + I$	0	430	750	961	1063	1107
V_{ax} , kips	Total DL	84.2	68.0	51.7	35.5	16.2	0
	$I, \%$	24.2	25.2	26.2	27.4	28.7	30
	$LL + I$	59.0	52.8	46.5	40.1	33.6	27.0
Factored loads, M_u ft-kips	$1.3[D + \frac{1}{3}(L + I)]$	0	1743	3076	3997	4488	4670
V_u , kips	$1.3[D + \frac{1}{3}(L + I)]$	237	203	168	133	94	59

* 1 kip = 4448 kN, 1 ft-kip = 1.356 kNm

that for simplicity it has been assumed that the haunch has a depth of 1.5 in. (38 mm). In transforming the cast-in-place concrete into equivalently stiff precast concrete it was assumed that the ratio of the moduli of the cast-in-place concrete to the precast concrete was $\sqrt{4000/6000} = 0.816$. The calculated moment of inertia of the transformed composite section is $635,800 \text{ in}^4$ and hence the $S_{bc} = 15,470 \text{ in}^3$ ($254 \times 10^6 \text{ mm}^3$).

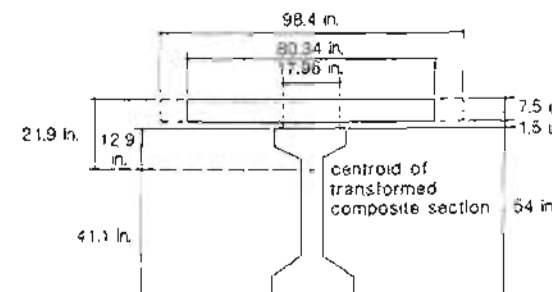


Figure 13-22 Composite cross section transformed to girder concrete.

Hence, from Eq. (6-31) and Table 13-3 the limit on the bottom fiber tensile stress under final conditions can be expressed as

$$f_{b,f} = -\frac{P_f}{685} - \frac{P_f \times 20.6}{9875} + \frac{1388 \times 12}{9875} + \frac{(359 + 1107) \times 12}{15,470} \leq 0.465 \text{ ksi}$$

Solving this equation gives $P_f \geq 665$ kips (2959 kN). The low-relaxation strands are stressed in the pretensioning bed to $0.75 f_{pu} = 0.75 \times 270 = 203$ ksi (1396 MPa) and the stress in the strands after all losses is assumed to be 164 ksi (1130 MPa) or about $0.6 f_{pu}$. Therefore, the minimum area of strands is

$$A_{ps} \geq \frac{665}{164} = 4.06 \text{ in}^2 (2626 \text{ mm}^2)$$

In order to satisfy the strength requirements the approximate expression for flexural strength, from Eq. (6-24), recognizing that the AASHTO capacity reduction factor for flexural strength is 1.0, is

$$1.0 \times A_{ps} \times 0.95 f_{pu} \times 0.9 h \geq M_u$$

Hence

$$A_{ps} \geq \frac{4670 \times 12}{0.95 \times 270 \times 0.9 \times 63} = 3.85 \text{ in}^2 (2486 \text{ mm}^2)$$

The preliminary calculations above demonstrate that for this case the concrete stress limit is a little more critical than the strength limit. We will choose a total of $28 - 1/2$ in. (13 mm) strands, giving $A_{ps} = 28 \times 0.153 = 4.28 \text{ in}^2 (2761 \text{ mm}^2)$.

Step 4: Choose the tendon profile.

For this size of girder hold-down points at the third-points of the span will provide a practical tendon profile. We will choose to drape 10 of the 28 strands, with the other 18 strands remaining straight. The strand pattern is described in Fig. 13-23 and the resulting tendon profile is shown in Fig. 13-24.

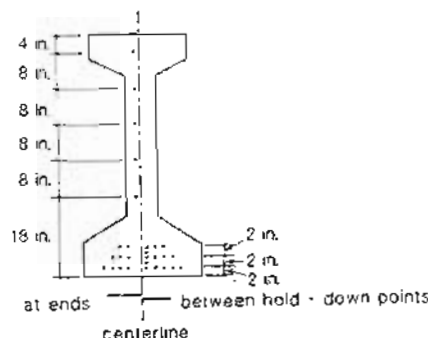


Figure 13-23 Strand pattern in bridge girder.

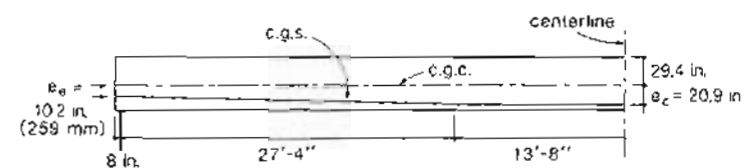


Figure 13-24 Tendon profile in bridge girder.

Step 5: Check the concrete stresses at service loads. The stresses in the concrete at service loads will be calculated using the equations given in Section 6.11. The stresses are calculated at three stages in the life of the beam: at transfer, at placing of the concrete for the deck slab, and for the final conditions when the beam acts as a composite member. These calculations are summarized in Table 13-4

Table 13-4 Calculated concrete stresses at service loads.

	Distance from Support Centerline					
	17 in.*	0.1L	0.2L	0.3L	0.4L	0.5L
(a) Initial conditions						
P_t , kips	801	801	801	801	801	801
e_g , in.	10.7	13.6	16.7	19.9	30.9	20.9
M_{dg} , ft-kips	41	216	384	504	576	600
f_t , ksi	-0.192	-0.165	-0.108	+ 0.026	+ 0.020	-0.015
f_b , ksi	-1.987	-2.010	-2.057	-2.171	-2.165	-2.136
(b) Conditions at time of placing deck concrete						
P_f , kips	703	703	703	703	703	703
$M_{dg} + M_{ds}$, ft-kips	93	495	886	1172	1336	1388
f_t , ksi	-0.251	-0.588	-0.892	-1.035	-1.188	-1.264
f_b , ksi	-1.675	-1.393	-1.139	-1.019	-0.891	-0.828
(c) Final conditions						
$M_{dg} + M_c$, ft-kips	106	559	980	1262	1408	1466
f_t , ksi	-0.036	-0.189	-0.331	-0.426	-0.475	-0.495
$f_{t,f}$, ksi	-0.277	-0.724	-1.131	-1.342	-1.531	-1.621
f_{bg} , ksi	-1.593	-0.959	-0.379	-0.040	+0.201	+0.309

* 50 strand diameters from end of girder

In calculating the prestressing force, P_t , for the initial conditions it was assumed that the stress in the low-relaxation strands was 187 ksi (1290 MPa), as suggested in Table 6-3. In calculating the prestressing force, P_f , detailed calculations of the loss due to creep,

shrinkage, and relaxation indicated that the stress in the strands after all losses was about 164 ksi (1130 MPa).

It can be seen from Table 13-4 that at transfer tensile stresses only occur on the top face of the girder, near the third-point of the span. Because these tensile stresses are very small, it will not be necessary to provide additional reinforcement for crack control. As the strength of the girder concrete at the time of transfer is 4000 psi (27.6 MPa), the highest compressive stress permitted by AASHTO for this pretensioned member is $0.60 \times 4 = 2.40$ ksi (16.5 MPa). Hence the highest calculated compressive stress of 2.171 ksi (15.0 MPa) is permissible.

At the time of placing the deck concrete, no tensile stresses are predicted to occur in the concrete and the compressive stresses are less than the permitted level of $0.40f'_c = 2.40$ ksi (16.5 MPa). Under full service loads a maximum tensile concrete stress of 0.309 ksi (2.13 MPa) is predicted to occur on the bottom face of the girder at midspan. The maximum concrete tensile stress permitted by AASHTO for this case is $6\sqrt{6000} = 0.465$ ksi (3.20 MPa) and hence the calculated stress levels are acceptable.

Step 6: Check the flexural capacity at midspan.

From Table 13-3 the factored moment, M_u , at midspan is 4670 ft-kips (6330 kNm). In determining the flexural capacity we will use the ACI code (Ref. 13-16) approach. The effective depth d_p , at midspan for this composite section is $7.5 + 1.5 + 29.4 + 20.9 = 59.3$ in. (1506 mm) (see Figs. 13-22 and 13-24). For this section with only prestressed reinforcement Eq. (6-7) simplifies to

$$\begin{aligned} f_{p_e} &= f_{p_u} \left(1 - \frac{\gamma_p}{\beta_1} \rho_p \frac{f_{p_u}}{f'_c} \right) \\ &= 270 \left(1 - \frac{0.28}{0.85} \times \frac{28 \times 0.153}{8.2 \times 12 \times 59.3} \times \frac{270}{4} \right) \\ &= 266 \text{ ksi (1830 MPa)} \end{aligned}$$

The equivalent rectangular stress-block depth is

$$\begin{aligned} a &= \frac{A_{ps} f_{p_u}}{0.85 f'_c b} = \frac{28 \times 0.153 \times 266}{0.85 \times 4 \times 8.2 \times 12} \\ &= 3.41 \text{ in. (87 mm)} \end{aligned}$$

Note that

$$\omega_p = \frac{A_{ps} f_{p_u}}{bd_p f'_c} = \frac{28 \times 0.153 \times 266}{8.2 \times 12 \times 59.3 \times 4} = 0.049$$

which is less than the upper limit of 0.30, ensuring that the prestressing steel will "yield" prior to concrete crushing.

The design flexural strength can be calculated using the AASHTO capacity reduction factor of 1.0 for flexure as

$$\begin{aligned} \phi M_u &= \phi A_{ps} f_{p_u} (d_p - \frac{a}{2}) \\ &= 1.0 \times 28 \times 0.153 \times \frac{266(59.3 - 3.41/2)}{12} \\ &= 5469 \text{ ft-kips (7416 kNm)} \end{aligned}$$

Since this capacity exceeds the required flexural capacity of 4670 ft-kips (6330 kNm), the flexural capacity is adequate at midspan.

Step 7: Check the reserve of strength after cracking.

The concrete is assumed to crack when the tensile stress reaches $7.5\sqrt{f'_c} = 7.5\sqrt{6000} = 0.581$ ksi (4.0 MPa). Under the final conditions the tensile stress on the bottom fiber at midspan is 0.309 ksi (2.13 MPa). Hence to cause cracking at this location an additional tensile stress of $0.581 - 0.309 = 0.272$ ksi (1.86 MPa) is required. This additional tensile stress would be caused by an additional moment of

$$S_{bc} \times 0.272 = 15,470 \times 0.272 = 4208 \text{ in.-kips} = 351 \text{ ft-kips (475 kNm)}$$

Hence the cracking moment at midspan would be $1388 + 1466 + 351 = 3205$ ft-kips (4346 kNm). Hence

$$\frac{\phi M_u}{M_{cr}} = \frac{5469}{3205} = 1.71 > 1.20$$

Hence an adequate reserve of strength exists after cracking.

Step 8: Shear design at tenth-points of span.

We will design the stirrups for the bridge girder using the modified compression field approach explained in Section 7.12. In addition, we will use this same approach to check the capacity of the longitudinal reinforcement at different locations along the span. In applying this design approach we will use the capacity reduction factors of the AASHTO Code (i.e., $\phi = 1.0$ for factory-produced precast prestressed concrete members and $\phi = 0.90$ for shear).

In the middle third of the span the tendon has a constant eccentricity (see Fig. 13-24) and hence the vertical component of the prestress force, V_p , is zero. Outside of this region,

$$\begin{aligned} V_p &= 28 \times 0.153 \times 164 \times \frac{20.9 - 10.2}{28 \times 12} \\ &= 22.4 \text{ kips (99.5 kN)} \end{aligned}$$

In Step 6 the value of jd at midspan was calculated to be $d_p - a/2 = 59.3 - 3.41/2 = 57.6$ in. (1460 mm). The jd values for the other locations listed in Table 13-5 were calculated by subtracting 3.41/2 in. from the appropriate values of d_p .

The values of θ and β were chosen from Table 7-3 based on the values of v/f'_c and c_x . For example, at the section at 0.2L from the support, Eq. (7-51) gives

$$\begin{aligned} \frac{v}{f'_c} &= \frac{(168/0.9) - 22.4}{7 \times 53.4 \times 6} \\ &= 0.073 \end{aligned}$$

while Eq. (7-53) gives

$$\begin{aligned} c_x &= \frac{(3076 \times 12/53.4) + 0.5 \times 168 \cot \theta - 28 \times 0.153 \times 164}{29,000 \times 28 \times 0.153} \\ &= -0.091 \times 10^{-3} + 0.676 \times 10^{-3} \cot \theta \end{aligned}$$

Table 13-5 Shear design of bridge girder.

	Distance from Support Centerline					
	6.5 in.	0.1L	0.2L	0.3L	0.4L	0.5L
V_u , kips	215	203	168	133	94	59
M_u , ft-kips	1116	1743	3076	3997	4488	4670
V_p , kips	22.4	22.4	22.4	22.4	0	0
jd , in.	49.2	50.3	53.4	56.6	57.6	57.6
v/f'_c	0.105	0.096	0.073	0.053	0.043	0.027
θ , deg.	23	22	36	42	45	43
$\epsilon_x \times 1000$	0	0	0.84	1.77	2.25	2.41
β	2.40	2.71	2.15	1.65	1.54	1.54
V_c , kips	64.0	73.9	62.3	50.6	48.1	48.1
V_t , kips	152.5	129.3	102.0	74.8	56.3	17.5
s , in.	18.2	23.1	17.3	20.2	24.6	79.0
f_{ps} required, ksi	141	177	198	221	236	240

From Table 7-3, for $v/f'_c = 0.075$ and $\epsilon_x = 1 \times 10^{-3}$, θ is given as 36° with a corresponding β value of 2.15. For θ equal to 36°

$$\begin{aligned}\epsilon_x &= -0.091 \times 10^{-3} + 0.676 \times 10^{-3} \cot 36^\circ \\ &\approx 0.84 \times 10^{-3}\end{aligned}$$

As this calculated value of ϵ_x is less than 1×10^{-3} the θ and β values chosen are satisfactory.

From Eq. (7-43)

$$\begin{aligned}V_c &= 2.15\sqrt{6000} \times 7 \times 53.4 \\ &\approx 62.3 \text{ kips (277 kN)}\end{aligned}$$

Hence, from Eq. (7-63).

$$\begin{aligned}V_t &= \frac{168}{0.9} - 22.4 - 62.3 \\ &= 102.0 \text{ kips (454 kN)}\end{aligned}$$

If #4 (13 mm diameter) double-legged stirrups, with $f_y = 60$ ksi (414 MPa), are used, then from Eq. (7-52), the required spacing at $0.2L$ is

$$\begin{aligned}s &= \frac{2 \times 0.20 \times 60 \times 53.4 \times \cot 36^\circ}{102.0} \\ &= 17.3 \text{ in. (439 mm)}$$

The required spacings at the other tenth-points are given in Table 13-5.

The longitudinal reinforcement must be capable of resisting the tension caused by the moment and the shear. Thus, at $0.2L$ Eq. (7-62) gives

$$28 \times 0.153 f_{ps} \geq \frac{3076 \times 12}{1.0 \times 53.4} + \left(\frac{168}{0.9} - 0.5 \times 102.0 - 22.4 \right) \cot 36^\circ$$

Hence

$$f_{ps} \geq 198 \text{ ksi (1360 MPa)}$$

In Step 6 we already determined that f_{ps} can reach a value of 266 ksi (1830 MPa) at midspan. The calculated value of f_{ps} from Eq. (6-7) will only change slightly at the tenth-points due to the change in d_y . Thus, at $0.2L$, f_{ps} can reach a value of 265 ksi (1825 MPa). Hence the tensile capacity of the longitudinal reinforcement at $0.2L$ and at the other tenth-points (see Table 13-5) is adequate.

Step 9: Shear design near the support.

As discussed in Section 7.13, failure caused by yielding of the stirrups involves yielding this reinforcement over a length of the beam of $jd \cot \theta$. Thus, in designing the stirrups near the support, we will use the section located at $0.5jd \cot \theta$ from the face of the support.

From Table 13-5 it can be seen that, near the support, jd will be about 49 in. (1250 mm) and θ will be about 23° . Hence $0.5jd \cot \theta$ is about 58 in. (1470 mm) and so, the section we will check is $58 + 5 = 63$ in. (1600 mm) from the support centerline. The shear and moment at this location can be found by interpolating between the values given in Table 13-3. The stirrup spacing and f_{ps} required at this section are shown in Table 13-5.

At the inner edge of the bearing, which is 13 in. (330 mm) from the end of the girder, the stress in the prestressing strands will be $164 \times 13/25 = 85.3$ ksi (588 MPa). At this location the required tension in the longitudinal reinforcement can be found from Eq. (7-68) as

$$\begin{aligned}T &= \left(\frac{V_u}{\phi} - 0.5V_s - V_p \right) \cot \theta \\ &= \left(\frac{237}{0.9} - 0.5 \times 152.5 - 22.4 \times \frac{13}{25} \right) \cot 23^\circ \\ &\approx 413.3 \text{ kips (1840 kN)}\end{aligned}$$

While the tensile force of 413.3 kips is required, the strands are only capable of providing a force of $28 \times 0.153 \times 85.3 = 365.4$ kips (1625 kN) resulting in a deficiency of 47.9 kips (213 kN). If four #4 (13 mm diameter) bars are provided at the support, the additional tension that can be resisted will be $4 \times 0.20 \times 60 = 48$ kips (214 kN), which will cover the deficiency. To ensure development of this steel in the short distance from the end of the bars to the inner edge of the bearing, provide the #4 bars in the form of two "hairpins".

Step 10: Finalize the reinforcement details.

The AASHTO Code requires that a minimum amount of web reinforcement be provided such that $A_g f_y / (b_w s)$ is at least 50 psi (0.35 MPa). This requirement limits the maximum stirrup spacing for our beam to 68 in. (1740 mm). In addition, AASHTO requires that the spacing of the stirrups not exceed three-quarters of the depth of the beam, or 24 in. (610 mm).

The stirrups not only act as shear reinforcement for the web of the girder but also provide reinforcement across the girder-slab interface to resist horizontal shear and ensure composite action. The AASHTO Code states that full transfer of horizontal shear forces

may be assumed when contact surfaces are clean and intentionally roughened and when minimum vertical ties with an area of at least 0.22 in²/ft are provided. To satisfy this requirement with #4 (13 mm diameter) double-legged stirrups, the spacing of the stirrups must not exceed 21 in. (550 mm). In addition, the spacing of these ties must not exceed four times the slab thickness, or 24 in. (610 mm).

The chosen stirrup layout is summarized in Fig. 13-25.

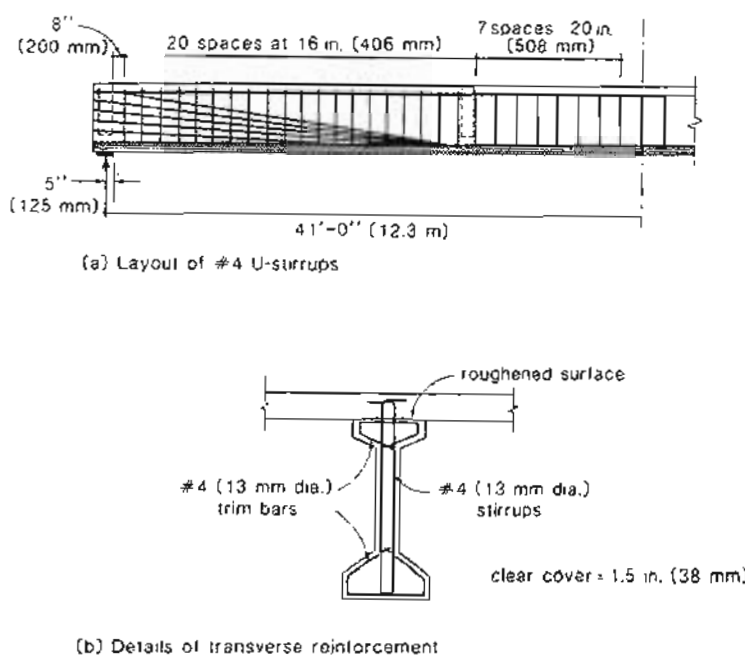


Figure 13-25 Details of transverse reinforcement.

Step 11: Check the deflections.

While the AASHTO Code does not require the deflection of prestressed concrete bridges to be checked, it is good practice to estimate the deflection of the bridge and to consider the consequences of these deflections.

The stress calculations in Step 5 have indicated that the girder will not crack under service loads and hence deflections can be calculated assuming uncracked response.

(a) *Immediate deflection due to live load and impact.* The total truck weight is 72 kips (320 kN) and the impact allowance is 24.2%. Each girder takes 74.5% of the truck load.

Hence the total truck load, including impact, on each girder is $0.745 \times 1.242 \times 72 = 66.6$ kips (296 kN). We can conservatively estimate the maximum girder deflection due to this truck load by taking it as a concentrated load applied at midspan of the girder. Hence

$$\Delta_L = \frac{PL^3}{48EI}$$

$$= \frac{66.6 \times (82 \times 12)^3}{48 \times 57\sqrt{6000} \times 635,800}$$

$$= 0.47 \text{ in. (12 mm)}$$

This deflection corresponds to 1/2090 of the span, which is significantly less than the limit of 1/1000 given for steel bridges with pedestrian traffic. Hence live-load deflections will cause no problems.

(b) *Long-term deflections.* The long-term deflection can be estimated by using the factors given in Table 5-10.

The elastic deflection due to girder self-weight at release of prestress is

$$\Delta = \frac{5}{384} \frac{wL^4}{EI}$$

$$= \frac{5}{384} \frac{0.714(82 \times 12)^4}{57\sqrt{4000} \times 242.930 \times 12}$$

$$= 0.83 \text{ in. (21 mm) downward}$$

The elastic camber due to prestress at time of release can be determined from Fig. 6-11 as

$$\Delta = \left[\frac{\frac{e_c}{8}}{\frac{e_c}{8} - \frac{e_i}{6}} - \frac{e_i^2}{6}(e_c - e_i) \right] \frac{PL^3}{EI}$$

$$= \left[\frac{20.9}{8} - \frac{0.333^2}{6}(20.9 - 10.2) \right] \frac{801(82 \times 12)^3}{57\sqrt{4000} \times 242.930}$$

$$= 2.14 \text{ in. (54 mm) upward}$$

Thus at release there will be a net upward deflection of $2.14 - 0.83 = 1.31$ in. (33 mm).

The elastic deflection due to the weight of composite topping and diaphragms is

$$\Delta = \frac{5}{384} \frac{wL^4}{EI}$$

$$= \frac{5}{384} \frac{0.913(82 \times 12)^4}{57\sqrt{6000} \times 242.930 \times 12}$$

$$= 0.87 \text{ in. (22 mm) downward}$$

The elastic deflection due to superimposed dead load acting on the composite girder is

$$\Delta = \frac{5}{384} \frac{0.427(82 \times 12)^4}{57\sqrt{6000} \times 635,800 \times 12}$$

$$= 0.15 \text{ in. (4 mm) downward}$$

Using the multipliers in Table 5-10 the net upward deflection at the time the topping is cast is

$$\Delta = 1.80 \times 2.14 - 1.85 \times 0.83 \\ = 2.32 \text{ in. (59 mm) upward}$$

Hence the 3 in. (75 mm) launch to allow for camber is appropriate.

The net long-term upward deflection, using the multipliers in Table 5-10, is

$$\Delta = 2.20 \times 2.14 - 2.4 \times 0.83 - 2.30 \times 0.87 - 3.00 \times 0.15 \\ = 0.27 \text{ in. (7 mm) upward}$$

Thus after construction has been completed the center of the bridge will creep downward an amount equal to $2.32 - 0.27 = 2.05$ in. (52 mm). This deflection corresponds to 1/480 of the span, which should be acceptable.

References

- 13-1 Schlaich, J., and Scheff, H., "Concrete Box Girder Bridges," *Structural Engineering Documents*, International Association for Bridge and Structural Engineering, Zurich, 1982, 108 pp.
- 13-2 Grant, A., "Design and Construction of the East Huntington Bridge," *PCI Journal*, Vol. 32, No. 1, Jan.-Feb. 1987, pp. 20-29.
- 13-3 Dywidag Systems International, "Prestressed Concrete Bridges," Dywidag Report No. 7, Dickerhoff and Widmann AG, Munich, West Germany.
- 13-4 Bassi, K.G., Lin, W.L., and Holowka, M., "Design and Construction of the Burlington Skyway," Report from the Ontario Ministry of Transportation and Communications, Structural Office, Toronto, Sept. 1985, 29 pp.
- 13-5 Skelton, R., "Recent Segmental Concrete Bridge Construction in Ontario," *Proceedings of the Canadian Structural Concrete Conference*, Toronto, 1981, pp. 285-323.
- 13-6 American Association of State Highway and Transportation Officials, *Standard Specifications for Highway Bridges*, 14th ed., AASHTO, Washington, 1989.
- 13-7 Ontario Ministry of Transportation and Communications, *Ontario Highway Bridge Design Code*, OHBDC, Ontario Ministry of Transportation and Communications, Toronto, 1983, 357 pp.
- 13-8 Ontario Ministry of Transportation and Communications, *Ontario Highway Bridge Design Code Commentary*, OHBDC, Ontario Ministry of Transportation and Communications, Toronto, 1983, 279 pp.
- 13-9 Csagoly, P.F., and Dorton, R.A., "Proposed Ontario Bridge Design Load," Research Report 186, Research and Development Division, Ontario Ministry of Transportation and Communications, Downsview, Ontario, 1973.
- 13-10 Waddell, J.A.L., *De Pontibus. A Pocket-Book for Bridge Engineers*, John Wiley & Sons, Inc., New York, 1899, 403 pp.
- 13-11 Dorton, R.A., and Csagoly, P.F., "The Development of the Ontario Bridge Code," report published by the Ontario Ministry of Transportation and Communications, Toronto, Oct. 1977, 67 pp.
- 13-12 Bakht, B., "Simplified Analysis of Edge Stiffened Cantilever Slabs," *Journal of the Structural Division, ASCE*, Vol. 107, No. ST3, Mar. 1981, pp. 535-550.
- 13-13 Ockleston, A.J., "Load Tests on a Three Storey Reinforced Concrete Building in Johannesburg," *Structural Engineer*, Vol. 33, No. 10, Oct. 1955, pp. 304-322.
- 13-14 Batchelor, B. de V., and Hewitt, B.E., "An Investigation of the Ultimate Strength of Deck Slabs of Composite Steel/Concrete Bridges," Reports OJT and CRP, Project Q50, Queen's University, Kingston, Canada, 1972.
- 13-15 Hewitt, B.E., and Batchelor, B. de V., "Punching Shear Strength of Restrained Slabs," *Journal of the Structural Division, ASCE*, Vol. 101, No. ST9, Sept. 1975, pp. 1837-1853.
- 13-16 ACI Committee 318, "Building Code Requirements for Reinforced Concrete (ACI 318-89) and Commentary - ACI 318 R-89," American Concrete Institute, Detroit, 1989, 353 pp.
- 13-17 Collins, M.P., and Mitchell, D., "Evaluating Existing Bridge Structures Using the Modified Compression Field Theory," *Strength Evaluation of Existing Concrete Bridges*, SP-88, American Concrete Institute, Detroit, 1983, pp. 109-141.

Design of Complex Structures

... the basics apply to the most sophisticated structures.

Ben C. Gerwick, Jr., 1988

14.1 INTRODUCTION

Determining the response of a structure to applied loads involves two interrelated tasks: determining the sectional forces at various locations throughout the structure caused by the applied loads (structural analysis), and determining the response of the local section to the sectional forces (sectional analysis).

For a simple building frame such as that shown in Fig. 14-1, the sectional forces (i.e., the axial loads, the moments, and the shears) can be determined using a plane-frame computer program. The designer must then compute the amount of longitudinal and transverse reinforcement required at each section to ensure that the member strength under the applied combinations of factored loads is adequate. In addition, service load performance must be checked. The sectional analysis procedures required to perform these evaluations have been given in Chapters 4 through 7.

For more complex frames such as that shown in Fig. 14-2, a space-frame model may be required to determine the sectional forces. The three-dimensional analysis gives the values of six sectional forces at each section. These are the axial load, N_z , the vertical shear, V_y , the lateral shear, V_z , the torsion, T , the lateral bending moment, M_y , and the vertical bending moment, M_z . The variable-angle truss model, explained in Chapter 8, may be used to determine the reinforcement needed in a section subjected to all six sectional forces and to evaluate the response at service loads.

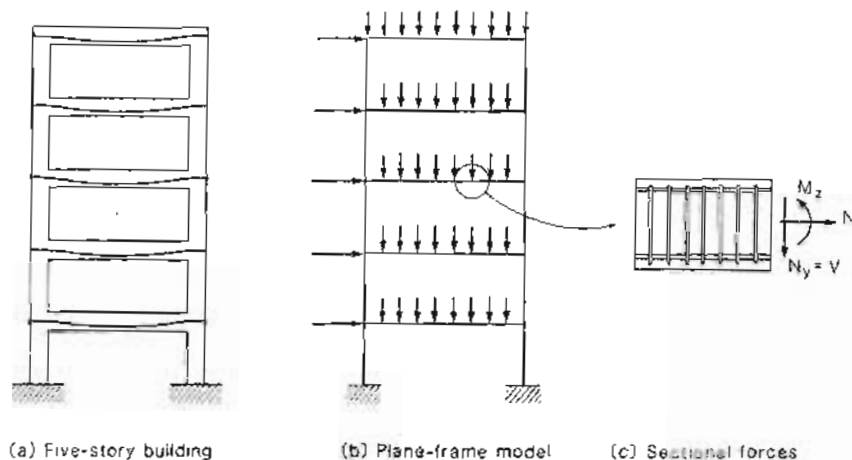
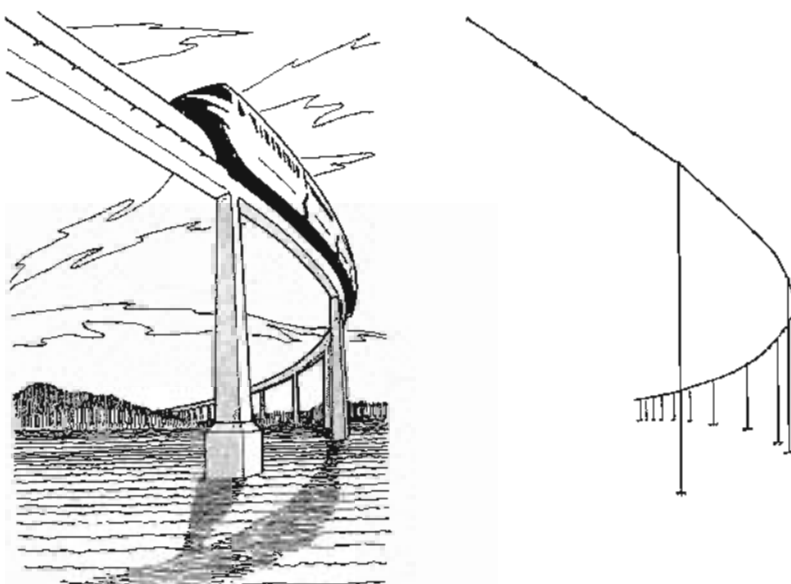


Figure 14-1 Determining sectional forces using plane-frame analysis.

In the design of complex prestressed concrete structures such as that shown in Fig. 14-3 it must be verified that at each location the sectional forces caused by the factored loads do not exceed the sectional resistances. Usually, the sectional forces at the different locations for the different load cases are determined by integrating the stresses obtained from an elastic finite element analysis (see Fig. 14-3b). The sectional forces for these structures, made up of plates and shells, are more complex than those of simple frame structures. The loading demand placed on a particular location of the structure can be expressed in terms of eight stress resultants, that is, three membrane forces (N_x , N_y , and V_{xy}), three moments (M_x , M_y , and T_{xy}), and two out-of-plane shear forces (V_{xz} and V_{yz}). Note that these stress resultants have been obtained by integrating the stresses over the thickness of the element. While they represent the stress resultants at a location in the structure, they are typically expressed in terms of forces per unit width (e.g., $N_x = 15$ kips/ft). The manner in which the sectional design procedures can be extended to cover these more complex loading situations will be discussed in this chapter.

14.2 LINEAR VS. NONLINEAR ANALYSIS

It must be appreciated that even for simple structures the design assumptions currently used are somewhat paradoxical. The structural analysis typically assumes that all sections



(a) Curved guideway structure

(b) Space-frame model

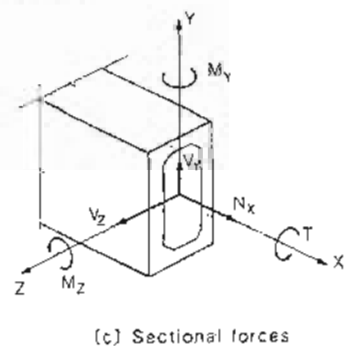
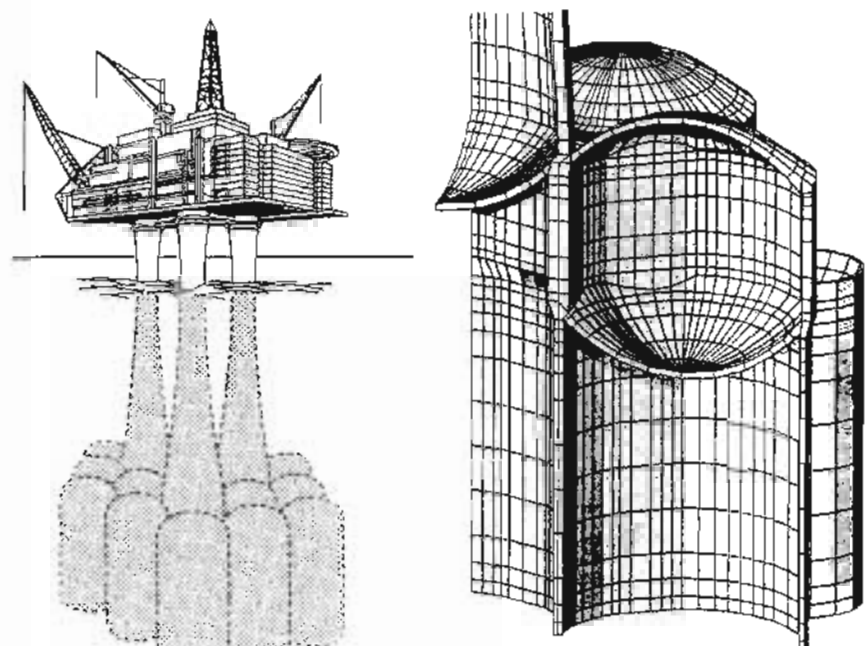


Figure 14-2 Determining sectional forces using space-frame analysis.

are linearly elastic and uncracked, whereas the sectional analysis typically assumes that the section is cracked and that its response is nonlinear.

In determining the sectional forces in a structure it is conventional to carry out an analysis assuming that the concrete is uncracked and linear elastic. It is recognized that this



(a) Offshore Platform

(b) Finite Element Model

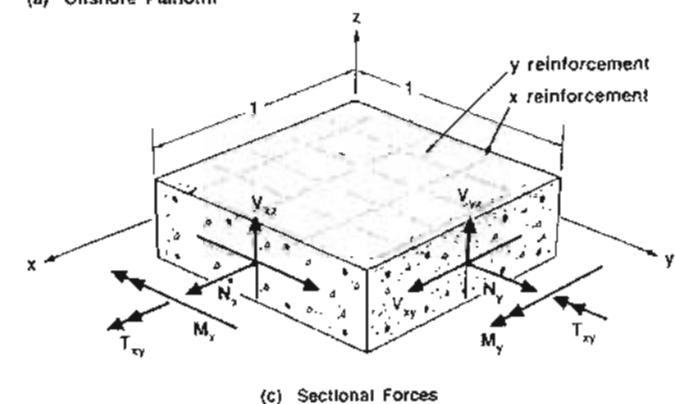


Figure 14-3 Determining sectional forces using finite element analysis

is an approximate procedure and that cracking of the concrete and material nonlinearities may result in significant redistribution of the stresses. Some of these nonlinear aspects have already been discussed in Chapter 8. For example, the significant drop in torsional stiffness after cracking results in considerable redistribution of the sectional forces (see Fig. 8-17). In addition, in Chapter 10, the need to distinguish between imposed loads and imposed deformations was discussed. Thus for a two-span continuous bridge subjected to an extremely heavy truck, the moments predicted by an elastic analysis are probably reasonably accurate, but the deflections predicted by an elastic analysis are probably too small. On the other hand, if the central support of this bridge settles (see Fig. 10-1) by 4 in. (100 mm), a traditional elastic analysis of this case would overestimate the moments caused by the support settlement but would estimate reasonably well the distribution of curvatures along the bridge caused by the settlement. An example showing how adjustments can be made to the elastic analysis to account for these effects is given in Section 10.10. In the elastic analysis of frames it is assumed that bending causes no change in length of the centroidal axis. In fact, when a cracked concrete beam bends, the tension face elongates much more than the compression face contracts, resulting in an elongation of the centroidal axis of the beam. The surrounding structure will typically restrain this elongation, causing axial compression in the beam. This compression will typically strengthen the beam, resulting in much higher failure loads than those predicted by elastic analyses. This phenomenon is known as "membrane action" or "arching action" (see Section 13.7).

In spite of the inconsistencies involved in combining a linear elastic structural analysis with a nonlinear sectional analysis, this remains the standard procedure for designing reinforced concrete structures. However, with the development of nonlinear analysis techniques it is now possible to conduct a consistent analysis of the complete load-deformation response of a structure. Because such analyses are still very expensive, they are employed only in special circumstances. An excellent summary of the development of nonlinear finite element analysis of reinforced concrete structures is provided in Ref. 14-1.

In the remaining sections of this chapter we will concentrate on explaining the nonlinear sectional analysis procedures.

14.3 TYPES OF ELEMENTS

Sectional analysis models can be classified by identifying whether the calculations involve consideration of uniaxial, biaxial, or triaxial strains. Such a classification is presented in Fig. 14-4 and is discussed below. Figure 14-4a shows the simple case of a reinforced concrete beam subjected to axial load only. As discussed in Chapter 4, the response of this element can be predicted by assuming that the only significant strains are those in the axial direction and that these strains are uniform over the complete section.

The response of reinforced concrete beam elements subjected to combined flexure and axial load can be predicted by considering only the axial strains and by assuming that these strains vary linearly over the depth of the element (see Fig. 14-4b). The assumption of a linear strain variation for members subjected to bending, which is equivalent to assuming that plane sections remain plane, was first suggested by Hooke in 1678 and still forms the basis of engineering beam theory. The plane-sections theory is described in Chapter 5.

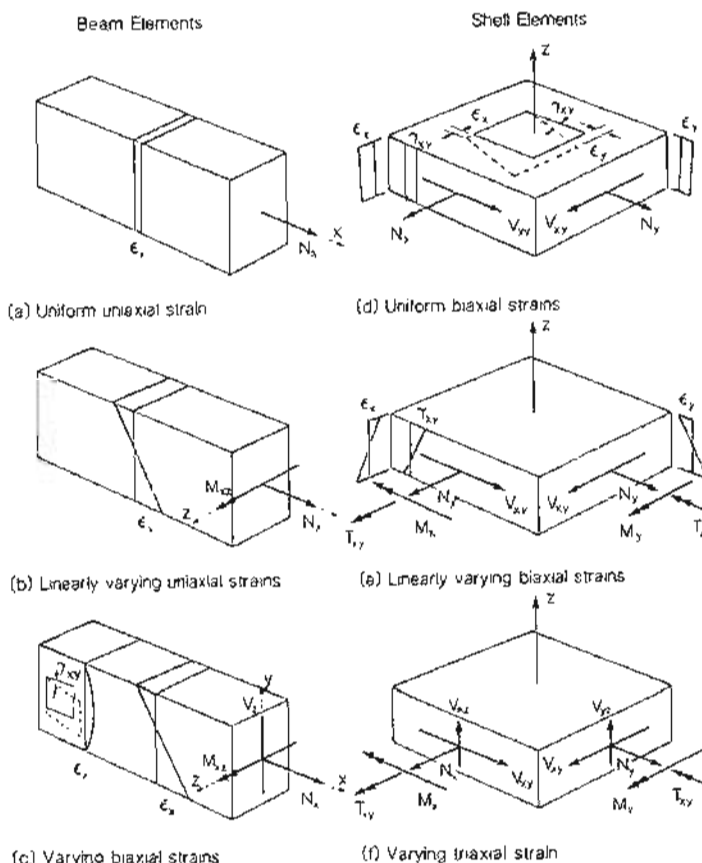


Figure 14-4 Elements with significant uniaxial, biaxial or triaxial strains.

When a beam is subjected to shear (Fig. 14-4c), the strains and stresses in the y -direction can no longer be ignored, and hence predicting the response of such an element involves dealing with biaxial strains and stresses. Rather than directly dealing with this biaxial problem, reinforced concrete building codes (e.g., Ref. 14-2) typically neglect the influence of shear on flexural response and rely upon restrictive, empirical equations for

predicting shear strength. The compression field theory described in Chapter 7 accounts directly for the biaxial strains and stresses that occur in a beam subjected to shear.

A shell element subjected to only the three membrane forces, N_x , N_y , and V_{xy} , can be referred to as a membrane element (see Fig. 14-4d). The response of such an element can be predicted by considering only the in-plane strains ϵ_x , ϵ_y , and γ_{xy} , and assuming that these strains are constant over the thickness of the element. This type of element will be described further in Section 14.4.

The response of shell elements subjected to the three membrane forces, N_x , N_y , and V_{xy} , and the three moments, M_x , M_y , and T_{xy} , can also be predicted by considering only the three in-plane strains ϵ_x , ϵ_y , and γ_{xy} , except now these three strains are assumed to vary linearly over the thickness of the element (see Fig. 14-4e). With this assumption, which can be regarded as a generalization of Hooke's plane-sections assumption for beams, the strains within the element can be described in terms of just six strain variables (e.g., the values of ϵ_x , ϵ_y , and γ_{xy} on the top face and on the bottom face of the element). For a given choice of these six strain variables the stresses in the concrete and the reinforcement can be determined. Integrating the stresses over the thickness of the element gives the six stress resultants, N_x , N_y , V_{xy} , M_x , M_y , and T_{xy} . This type of element will be described further in Section 14.6.

When a shell element is subjected to out-of-plane shears, V_x and V_{yy} , the out-of-plane strains, ϵ_z , γ_{xz} , and γ_{yz} , can no longer be ignored and hence predicting the response of such an element involves dealing with triaxial strains and stresses. If the in-plane strains are still assumed to vary linearly over the thickness of the element, then these strains are still defined by just six variables. Unfortunately, for every integration point within the element three more strain variables, ϵ_z , γ_{xz} , and γ_{yz} , remain to be defined. These three strains can be determined from three stress conditions. The out-of-plane shear stresses can be assumed to be uniformly distributed over the effective thickness of the element, which defines the shear stresses on the x and y planes, and the resultant axial stresses on the z plane can be assumed to be zero. Rather than dealing with these triaxial strains and stresses designers of complex concrete structures have typically ignored the influence of the out-of-plane stresses on the in-plane stresses and have used modified versions of traditional empirical equations for the shear strength of beams to evaluate out-of-plane shear capacity. Some further information on this type of element will be given in Section 14.6.

14.4 MEMBRANE ELEMENTS

The fundamental problem for a reinforced concrete membrane element, such as that shown in Fig. 14-4d, is to determine how the three in-plane stress resultants N_x , N_y , and V_{xy} , are related to the three in-plane strains ϵ_x , ϵ_y , and γ_{xy} . Figure 14-5 summarizes how these relationships can be determined using the modified compression field theory proposed by Vecchio and Collins (Ref. 14-3). In this method, the response of a cracked reinforced concrete element is determined by separately considering the response of the reinforcement and the response of the cracked concrete. The average strains in the reinforcement and the average strains in the cracked concrete are assumed to be identical. The stress in the

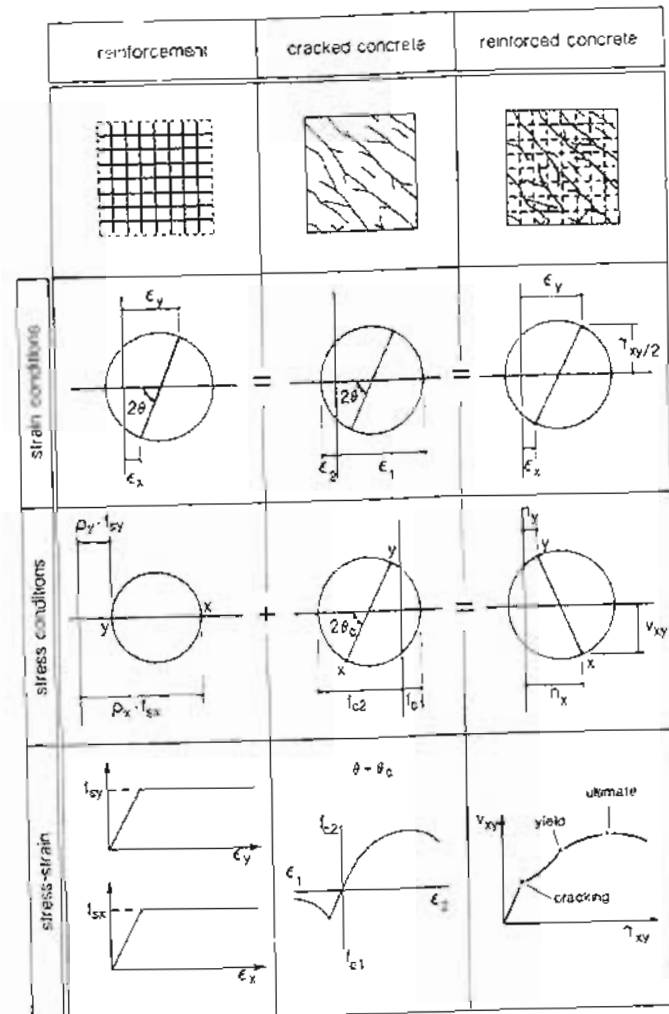


Figure 14-5 Predicting the response of membrane elements using the modified compression field theory.

x -reinforcement is found from the stress-strain relationship for the reinforcement and from the value of ϵ_x while the stress in the y -reinforcement is found from the strain ϵ_y . For the cracked concrete it is assumed that the directions of the principal stresses coincide with the directions of the principal strains. The principal compressive stress in the concrete, f_2 , is found from the values of both the principal compressive strain, ϵ_2 , and the principal tensile strain, ϵ_1 as follows:

$$f_2 = \beta f'_c \left[2 \left(\frac{\epsilon_2}{\epsilon'_c} \right) - \left(\frac{\epsilon_2}{\epsilon'_c} \right)^2 \right] \quad (14-1)$$

where β is the modification factor to account for the influence of principal tensile strains, ϵ_1 , given as

$$\beta = \frac{1}{0.8 - 0.34(\epsilon_1/\epsilon'_c)} \leq 1.00 \quad (14-2)$$

where ϵ'_c is the strain in a concrete cylinder at the peak stress, f'_c . Note that since ϵ'_c is a negative quantity (about -0.002 for short-term loading), increasing ϵ_1 decreases f_2 (see Fig. 7-33). Note that in Eq. (14-1) the β factor has been applied to a parabolic stress-strain curve for concrete. As discussed in Section 3.3, this simple parabola is accurate for concrete strengths less than about 6000 psi (41 MPa). For higher concrete strengths the more complex Eq. (3-1) should be used.

The average principal tensile stress in the concrete, f_1 , is found from the principal tensile strain ϵ_1 using the following expressions from Chapter 4.

$$\text{if } \epsilon_1 \leq \epsilon_{cy} \text{ then } f_1 = E_c \epsilon_1 \quad (14-3)$$

$$\text{if } \epsilon_1 > \epsilon_{cy} \text{ then } f_1 = \frac{\alpha_1 \alpha_2 f_{cr}}{1 + \sqrt{500 \epsilon_1}} \quad (14-4)$$

where α_1 = a factor accounting for the bond characteristics of the reinforcement

$\alpha_1 = 1.0$ for deformed reinforcing bars

$\alpha_1 = 0.7$ for plain bars, wires, or bonded strands

$\alpha_1 = 0$ for unbonded reinforcement

α_2 = a factor accounting for sustained or repeated loading

$\alpha_2 = 1.0$ for short-term monotonic loading

$\alpha_2 = 0.7$ for sustained and/or repeated loads

Knowing the stresses in the reinforcement and in the concrete, the resultant forces on the x - and y -faces can be calculated.

While finding the three in-plane stress resultants that correspond to a given set of three in-plane strains is a relatively simple and direct procedure, the problem of finding the strains given the applied loads is considerably more difficult. We may, for example, wish to calculate the maximum value of V_{xy} that a particular element can resist given that both N_x and N_y are zero. We could solve this problem by first selecting a value of γ_{xy} at which to perform the calculations. By trial and error we could then find the corresponding values of ϵ_x and ϵ_y that would result in values of zero for N_x and N_y .

Having found a valid strain state (i.e., one that satisfies our given stress conditions) we have one point on the shear force-shear strain response diagram (see Fig. 14-5). Repeating

the calculations for different values of γ_{xy} we would find the complete load-deformation response and hence could determine the resistance or maximum load-carrying capacity of the element.

While accounting for tensile stresses in the concrete between the cracks is appropriate in estimating deformations, it must be recognized that the capacity of an element may be limited by its ability to transmit forces across the cracks. This capacity may be governed by yielding of the reinforcement at a crack or by sliding along the crack interface. At cracks there is no tensile stress in the concrete while the tensile stresses in the reinforcement are greater than their average values. Figure 14-6 compares the average stresses that occur between the cracks (plane 1-1) with the local stresses that occur at a crack (plane 2-2). Since the states of stress on these two parallel planes must both balance the same external loads, they must be statically equivalent. That is, they must produce the same resultant force perpendicular to the plane and the same resultant force parallel to the plane. Equilibrium perpendicular to the plane will be satisfied if

$$f_1 = \rho_x(f_{sx,cr} - f_{sx}) \sin^2 \theta + \rho_y(f_{sy,cr} - f_{sy}) \cos^2 \theta \quad (14-5)$$

where ρ_x and ρ_y are the reinforcement ratios, f_{sx} and f_{sy} are the average steel stresses while $f_{sx,cr}$ and $f_{sy,cr}$ are the reinforcement stresses at the crack. Thus the average tension that can be carried by the concrete is limited by the ability of the reinforcement to increase its stress at a crack. If, for example, the average stress in both the x - and y -reinforcement reach their yield stress it will not be possible to transmit any tension through the cracked concrete (i.e., $f_1 = 0$).

In order to satisfy equilibrium parallel to the plane the shear stress on the crack, v_{cr} , must equal

$$v_{cr} = [\rho_x(f_{sx,cr} - f_{sx}) - \rho_y(f_{sy,cr} - f_{sy})] \sin \theta \cos \theta \quad (14-6)$$

The ability of the concrete to transmit shear across the crack is a function of the crack width, w .

In Chapter 7 it is suggested that v_{cr} be limited to

$$v_{cr} = \frac{-2.16 \sqrt{f'_c}}{0.3 + \frac{w}{a + 0.63}} \quad \text{psi and in.} \quad (14-7a)$$

$$v_{cr} = \frac{-0.18 \sqrt{f'_c}}{0.3 + \frac{w}{a + 16}} \quad \text{MPa and mm} \quad (14-7b)$$

where

$$w = \epsilon_1 s_{int} \quad (14-8)$$

and s_{int} is the average crack spacing (see Fig. 7-38). Hence, for large values of principal tensile strain, ϵ_1 , the shear that can be transmitted across the crack will be low.

The procedures above for predicting the response of membrane elements have been incorporated into program MEMBRANE, which is described in Appendix C. Further, these

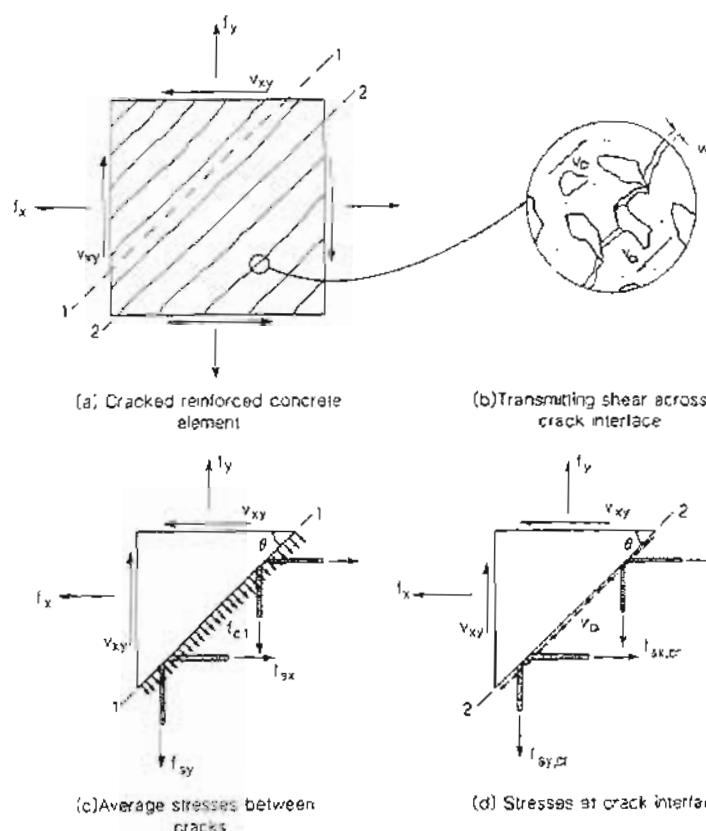


Figure 14-6 Local stresses at a crack.

procedures have been used as the basis of a number of nonlinear finite element programs for predicting the response of "two-dimensional" reinforced concrete structures. FIELDS (Ref. 14-4) and TRIX (Ref. 14-5) are examples of such programs. Example applications of nonlinear finite element analyses are given in Section 9.5.

14.5 EXAMPLE OF CALCULATING STRESSES IN A MEMBRANE ELEMENT

As part of a load test on a structure the strains in a 8 in. (203 mm) thick reinforced concrete wall were measured (see Fig. 14-7). It was found that due to the short-term load, the strains

determined from a strain rosette were:

$$\epsilon_x = 0.96 \times 10^{-3}$$

$$\epsilon_y = 4.59 \times 10^{-3}$$

$$\epsilon_1 = 6.50 \times 10^{-3}$$

$$\epsilon_2 = -0.95 \times 10^{-3}$$

$$\theta = 30.4^\circ$$

At this location the reinforcement in the x -direction consisted of #5 (15 mm diameter) bars at 4 in. (102 mm) spacing on both faces, while the reinforcement in the y -direction consisted of #5 bars at 8 in. (203 mm) spacing on both faces.

The concrete cylinder strength was 3500 psi (24 MPa) and the maximum aggregate size was 3/4 in. (19 mm). The yield stress of the reinforcement was 60 ksi (414 MPa). Estimate the sectional forces at this location of the structure.

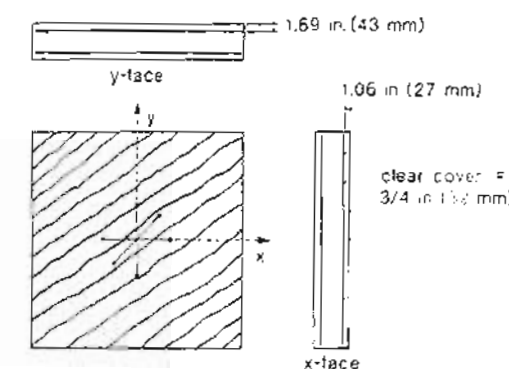


Figure 14-7 Strain measurements on cracked, reinforced concrete element

Step 1: Calculate the stresses in the reinforcing bars.

For the x -direction reinforcement.

$$f_{sx} = E_s \epsilon_x \leq f_y$$

$$= 29,000 \times 0.96 \times 10^{-3}$$

$$= 27.8 \text{ ksi (192 MPa)}$$

For the y -direction reinforcement,

$$\begin{aligned} f_{yy} &= E_s \epsilon_r \leq f_y \\ &\approx 29,000 \times 4.59 \times 10^{-3} \\ &= 133 \text{ ksi} \end{aligned}$$

Hence

$$f_{yy} = 60 \text{ ksi (414 MPa)}$$

Step 2: Calculate the contribution of reinforcement to the sectional forces.

The x -direction reinforcement only influences the axial force N_x . Hence the contribution of the x -direction reinforcement over a length of 1 ft is

$$\begin{aligned} N_{sx} &= 2 \times 0.31 \times \frac{12}{4} \times 27.8 \\ &= 51.7 \text{ kips/ft (755 kN/m)} \end{aligned}$$

The contribution of the y -direction reinforcement is

$$\begin{aligned} N_{sy} &= 2 \times 0.31 \times \frac{12}{8} \times 60 \\ &= 55.8 \text{ kips/ft (755 kN/m)} \end{aligned}$$

Step 3: Calculate the principal compressive stress in concrete.

From Table 3-3 the strain, ϵ'_c , corresponding to f'_c of 3500 psi (24 MPa) is -1.91×10^{-3} . Since we are dealing with a short-term load, we may assume that all of the measured strains were caused by stress. From Eq. (14-2),

$$\begin{aligned} J &= \frac{1}{0.8 - 0.34(\epsilon_1/\epsilon'_c)} \leq 1.00 \\ &= \frac{1}{0.8 - 0.34[6.5/(-1.91)]} \\ &= 0.51 \end{aligned}$$

From Eq. (14-1) the principal compressive stress in the concrete is

$$\begin{aligned} f_c &= \beta f'_c \left[2 \left(\frac{\epsilon_2}{\epsilon'_c} \right) - \left(\frac{\epsilon_2}{\epsilon'_c} \right)^2 \right] \\ &= 0.51 \times 3.5 \left[2 \left(\frac{-0.95}{-1.91} \right) - \left(\frac{-0.95}{-1.91} \right)^2 \right] \\ &= 1.33 \text{ ksi (9.2 MPa)} \end{aligned}$$

Sec. 14.5 Example of Calculating Stresses in a Membrane Element

Step 4: Calculate the principal tensile stress in concrete.

From Eq. (5-16) the cracking stress of the concrete can be estimated as

$$\begin{aligned} f_{cr} &= 4\lambda\sqrt{f'_c} \\ &= 4 \times 1.0\sqrt{3500} \\ &= 237 \text{ psi (1.63 MPa)} \end{aligned}$$

The average principal tensile stress in the cracked concrete ($\epsilon_1 > \epsilon_{cr}$) can be determined from Eq. (14-4) as

$$\begin{aligned} f_1 &= \frac{\alpha_1 \alpha_2 f_{cr}}{1 + \sqrt{500 \epsilon_1}} \\ &= \frac{1.0 \times 1.0 \times 0.237}{1 + \sqrt{500 \times 6.5 \times 10^{-3}}} \\ &= 0.085 \text{ ksi (0.58 MPa)} \end{aligned}$$

Step 5: Check the transmission of tension across cracks.

The reinforcement ratios in the x - and y -directions are:

$$\begin{aligned} \rho_x &= \frac{2 \times 0.31}{4 \times 8} = 0.0194 \\ \rho_y &= \frac{2 \times 0.31}{8 \times 8} = 0.0097 \end{aligned}$$

If the average tensile stress in the concrete is 0.085 ksi (0.58 MPa), the stresses in the reinforcement at the crack must satisfy Eq. (14-5) and hence

$$\begin{aligned} f_1 &= \rho_x(f_{sx,cr} - f_{sy}) \sin^2 \theta + \rho_y(f_{sy,cr} - f_{sx}) \cos^2 \theta \\ 0.085 &= 0.0194(f_{sx,cr} - 27.8) \sin^2 30.4^\circ + 0.0097(f_{sy,cr} - 60) \cos^2 30.4^\circ \end{aligned}$$

As the y -direction reinforcement is already yielding, it will not be capable of increasing its stress at the crack (i.e., $f_{sy,cr} = 60$ ksi). The stress in the x -reinforcement at the crack must thus be

$$\begin{aligned} f_{sx,cr} &= \frac{0.085}{0.0194 \sin^2 30.4^\circ} + 27.8 \\ &= 44.9 \text{ ksi (310 MPa)} \end{aligned}$$

The shear stress on a crack can be found from Eq. (14-6) as

$$\begin{aligned} v_{cr} &= [\rho_{sx}(f_{sx,cr} - f_{sx}) - \rho_{sy}(f_{sy,cr} - f_{sy})] \sin \theta \cos \theta \\ &= [0.0194(44.9 - 27.8) - 0.0097(60 - 60)] \sin 30.4^\circ \cos 30.4^\circ \\ &= 0.145 \text{ ksi (1 MPa)} \end{aligned} \quad (14-9)$$

In order to determine the ability of the crack to transmit this shear we must first calculate the crack width, w . The crack spacing in the x -direction, s_{max} , can be estimated from Eq. (14-23) as

$$\begin{aligned}s_{max} &= 2 \left(c + \frac{s}{10} \right) + k_1 k_2 \frac{d_b}{\rho_{eff}} \\&= 2 \left(2.63 + \frac{4}{10} \right) + 0.4 \times 0.25 \times \frac{0.625}{0.0194} \\&= 9.28 \text{ in. (236 mm)}$$

Because we are interested in the crack width in the interior of the wall rather than on the surface of the wall, we have taken c as the distance from the center of the wall to the surface of the bar.

Similarly

$$\begin{aligned}s_{min} &= 2 \left(2.0 + \frac{8}{10} \right) + 0.4 \times 0.25 \times \frac{0.625}{0.0097} \\&= 12.04 \text{ in. (306 mm)}$$

From Eq. (7-35) the spacing of the cracks at an angle of 30.4° is

$$\begin{aligned}s_{avg} &= 1 / \left(\frac{\sin \theta}{s_{max}} + \frac{\cos \theta}{s_{min}} \right) \\&= 1 / \left(\frac{\sin 30.4^\circ}{9.28} + \frac{\cos 30.4^\circ}{12.04} \right) \\&= 7.93 \text{ in. (201 mm)}$$

Hence the crack width from Eq. (14-8) is

$$\begin{aligned}w &= \epsilon s_{avg} \\&= 6.5 \times 10^{-5} \times 7.93 \\&= 0.052 \text{ in. (1.3 mm)}$$

Hence, from Eq. (14-7) the maximum shear stress that can be transmitted across the crack is

$$\begin{aligned}\tau_{cr} &= \frac{2.16 \sqrt{f_c}}{0.3 + \frac{24w}{a+0.63}} \\&= \frac{2.16 \sqrt{3500}}{0.3 + \frac{24 \times 0.052}{0.75 + 0.63}} \\&= 106 \text{ psi} \\&= 0.106 \text{ ksi (0.73 MPa)}$$

Hence the previously calculated shear stress of 0.145 ksi (1 MPa) cannot be transmitted across the crack. In order to limit the shear stress transmitted across the crack to 0.106 ksi

(0.73 MPa), the maximum stress in the x -reinforcement at the crack can be determined by rearranging Eq. (14-6) to give

$$\begin{aligned}f_{x,y,cr} &= \left[\frac{v_{cr}}{\sin \theta \cos \theta} + \mu_{xy} (f_{x,y,cr} - f_{xy}) \right] \frac{1}{\rho_{sx}} + f_{sx} \\&= \left[\frac{0.106}{\sin 30.4^\circ \cos 30.4^\circ} + 0.0097(60 - 60) \right] \frac{1}{0.0194} + 27.8 \\&= 40.3 \text{ ksi (278 MPa)}$$

Hence, from Eq. (14-5) the tension in the concrete is limited to

$$\begin{aligned}f_t &= \rho_x (f_{x,t,cr} - f_{xt}) \sin^2 \theta + \rho_y (f_{y,t,cr} - f_{yt}) \cos^2 \theta \\&= 0.0194(40.3 - 27.8) \sin^2 30.4^\circ + 0.0097(60 - 60) \cos^2 30.4^\circ \\&= 0.062 \text{ ksi (0.43 MPa)}$$

Step 6: Calculate the contribution of the concrete to the sectional forces.

Knowing the magnitudes and directions of the principal concrete stresses on the x - and y -faces, from the Mohr's circle for concrete stress shown in Fig. 14-8, we obtain

$$\begin{aligned}c_{cr} &= \frac{1.33 + 0.062}{2} \sin 60.8^\circ \\&= 0.608 \text{ ksi (4.2 MPa)}$$

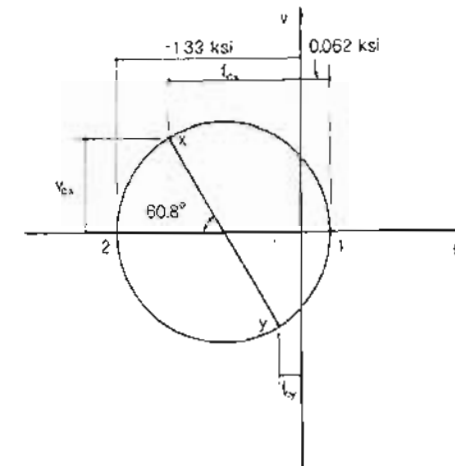


Figure 14-8 Mohr's circle for concrete stresses.

$$\begin{aligned} f_{cx} &= \frac{-1.33 + 0.062}{2} - \frac{0.608}{\tan 60.8^\circ} \\ &= -0.634 - 0.340 \\ &= -0.974 \text{ ksi } (-6.72 \text{ MPa}) \end{aligned}$$

$$\begin{aligned} f_{cy} &= -0.634 + 0.340 \\ &= -0.294 \text{ ksi } (-2.03 \text{ MPa}) \end{aligned}$$

Hence

$$N_{cx} = -0.974 \times 8 \times 12 = -93.5 \text{ kips/ft } (-1365 \text{ kN/m})$$

$$N_{cy} = -0.294 \times 8 \times 12 = -28.2 \text{ kips/ft } (-412 \text{ kN/m})$$

$$V_{xy} = -0.608 \times 8 \times 12 = -58.4 \text{ kips/ft } (-852 \text{ kN/m})$$

Step 7: Sum the concrete and reinforcement contributions.

$$\begin{aligned} N_x &= N_{cx} + N_{sx} \\ &= -93.5 + 51.7 \\ &= -41.8 \text{ kips/ft } (-610 \text{ kN/m}) \end{aligned}$$

$$\begin{aligned} N_y &= N_{cy} + N_{sy} \\ &= -28.2 + 55.8 \\ &= 27.6 \text{ kips/ft } (403 \text{ kN/m}) \end{aligned}$$

$$\begin{aligned} V_{xy} &= V_{sxy} \\ &= -58.4 \text{ kips/ft } (-852 \text{ kN/m}) \end{aligned}$$

These calculated sectional forces are summarized in Fig. 14-9.

The calculations above can be checked using program MEMBRANE, which is described in Appendix C. If the axial loads shown in Fig. 14-9 are specified and c_1 is set equal to 6.50×10^{-3} it will be found that the program predicts the shear to be 58.3 kips/ft (851 kN/m). Further, it will be found that this is the maximum shear force that the section can resist at the specified axial forces. The principal tensile strain can be increased to 10×10^{-3} , by which point the shear has decreased to 57.3 kips/ft (836 kN/m) and the concrete crushes. Just prior to failure the crack width is predicted to be 0.080 in. (2.0 mm).

14.6 SHELL ELEMENTS

It has already been mentioned that a shell element not subjected to out-of-plane shears can be analyzed considering only the in-plane biaxial strains, which can be assumed to vary

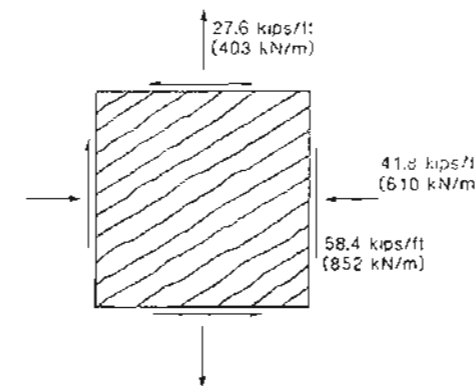


Figure 14-9 Sectional forces acting on membrane element.

linearly over the thickness of the element (see Fig. 14-4e). Conceptually, we subdivide the element into layers and assume that in each layer the strains and stresses are uniform. That is, each layer is a membrane element. As discussed previously, it is assumed that the strains (ϵ_x , ϵ_y , and γ_{xy}) vary linearly over the thickness of the element (see Fig. 14-10).

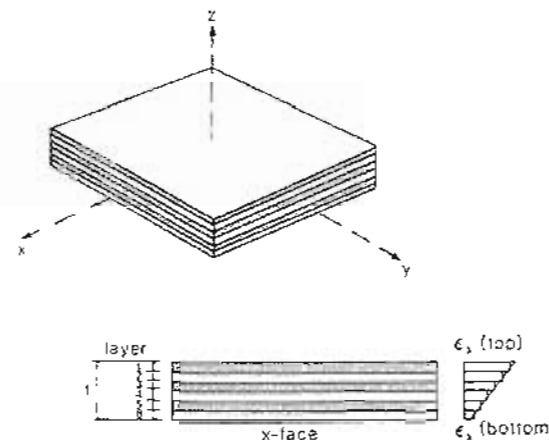


Figure 14-10 Layered shell element.

We have seen that if we know the six strain variables, we can directly calculate the six sectional forces. If, on the other hand, we know the six sectional forces and wish to find the corresponding six strain variables, then trial and error is required. Finding the six unknown variables by trial and error for this nonlinear system is not a trivial task. However, by appropriate numerical techniques efficient analysis and automatic design programs for shell elements using the layered approach have been developed [e.g., programs CONDIM and SEP (Refs. 14-6 and 14-7)].

Figure 14-11 shows the University of Toronto's shell element testing machine. This equipment is capable of applying the eight sectional forces shown in Fig. 14-4f to large reinforced concrete specimens. Figure 14-12 compares the observed and predicted response of a series of shell elements subjected to combined membrane shear and bending moment. It can be seen that the interaction between the two loadings is predicted well by the layered shell model. Shell elements subjected to significant quantities of all eight stress resultants commonly occur in offshore platforms. When the out-of-plane stresses and strains cannot be neglected, the problem becomes triaxial.

Currently, designers of offshore structures use rational models, similar to those described above, to evaluate the response of reinforced concrete to the three membrane forces and the three bending moments. However, in treating the out-of-plane shears, empirical procedures developed for simpler beam elements are used. These "equivalent beam" procedures can result in large amounts of awkward-to-place shear reinforcement being required, particularly in regions where significant membrane tension coexists with significant out-of-plane shear.

The traditional $V_c + V_s$ (concrete contribution plus reinforcement contribution) beam shear design rules were derived for uniaxial bar-like members (e.g. beams and columns) in which the in-plane reinforcement, the membrane forces, and the principal out-of-plane shear are all traveling in the longitudinal direction. The manner in which these procedures should be applied when calculating the required amount of stirrup reinforcement in a shell element is a matter of some debate.

Program SHELL474 (Refs. 14-8 and 14-9) is capable of predicting the response of shell elements subjected to out-of-plane shear. The assumption of linear variation of the in-plane strains is retained, which enables the three in-plane strains at any point in the element still to be defined by the same six variables. An additional three strains are required to define the strain completely at a given point. These three additional variables are determined from three stress conditions. The out-of-plane shear stresses are assumed to be uniformly distributed over the thickness of the element, which is analogous to the constant shear flow assumption for the sectional analysis of beams. Additionally, the resultant normal stress on planes parallel to the midplane of the element is assumed to be zero.

In the model, the principal concrete stresses, f_1 , f_2 , f_3 , are determined from the principal concrete strains, ϵ_1 , ϵ_2 , ϵ_3 , by triaxial stress-strain relationships which are generalizations of the modified compression field theory. For example, if ϵ_1 and ϵ_2 are tensile while ϵ_3 is compressive, the principal compressive stress f_{c3} is calculated from ϵ_3 by using

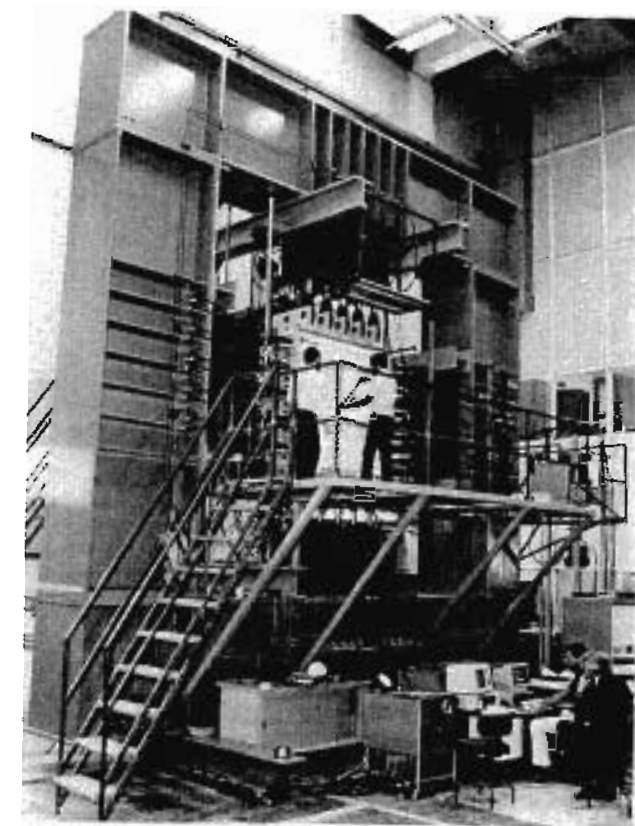


Figure 14-11 University of Toronto's shell element tester.

the parabolic uniaxial stress-strain relationship of Eq. (14-1), except that now

$$\beta = 1 / \left(0.8 + 0.34 \sqrt{\left(\frac{\epsilon_1}{\epsilon'_c} \right)^2 + \left(\frac{\epsilon_2}{\epsilon'_c} \right)^2} \right) \quad (14-11)$$

Figure 14-13 compares the observed and predicted responses of a series of shell elements subjected to combined membrane shear, V_{xy} , and out-of-plane shear, V_{yz} and V_{xz} . Note that for some situations the addition of in-plane shear actually increases the

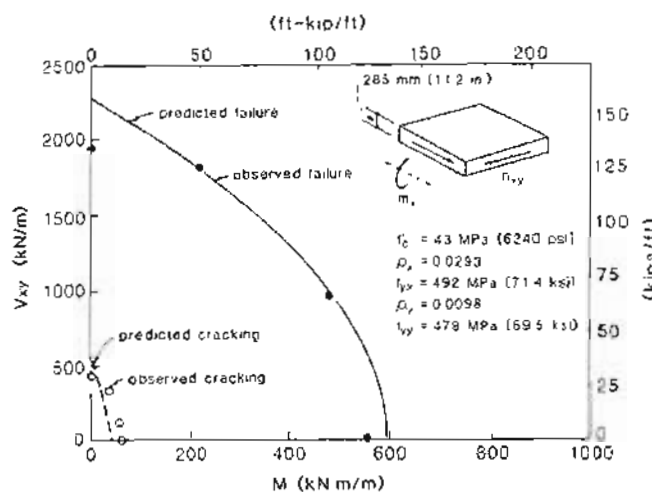


Figure 14-12 Membrane shear-bending moment interaction diagram. Adapted from Kirschner and Collins (Ref. 14-7).

out-of-plane shear capacity. Program SHELL474 correctly predicts this phenomenon while the equivalent beam approach fails to account for this.

The procedures described above have been incorporated into the Canadian code for concrete offshore structures, CSA S474 (Ref. 14-10).

14.7 TESTS OF COMPLEX STRUCTURES

As discussed earlier in this chapter, the current state-of-the-art in the design of complex prestressed concrete structures consists of combining a linear elastic structural analysis with a nonlinear sectional analysis to determine the response of the local section to the sectional loads. Tests to failure of complex structures (usually scale models) provide insight into the actual behavior of complex structures.

In the design of the buoyancy tanks of offshore concrete platforms the load-carrying capacity of the upper domes (see Fig. 14-3) is often controlled by the high values of moments and shears which occur at the junction of the cylinder and the dome. As can be seen from Fig. 14-14, these high moments and shears predicted by elastic theory are concentrated at the junction and die out quickly away from this location. A test on a large prestressed concrete shell structure was carried out by Reineck, Reibnagl, Reinke, and Koch (Ref. 14-12) to investigate the actual distribution of these edge actions at the

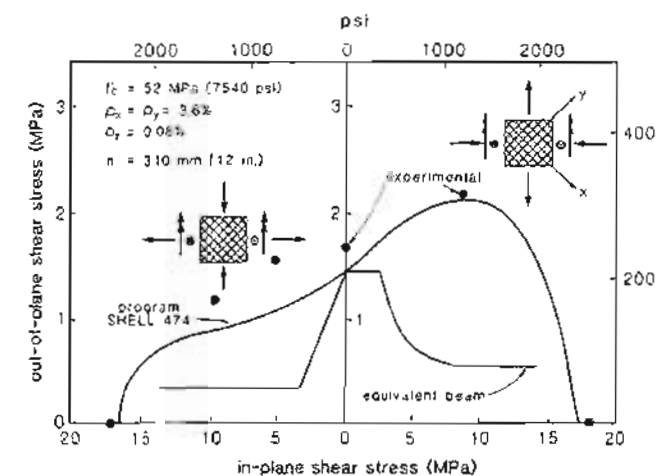


Figure 14-13 Out-of-plane shear vs. in-plane shear interaction diagram. Adapted from Adebar (Ref. 14-9).

failure load of the shell. They simulated the dome by a truncated cone and replaced the large uniform hydrostatic pressure by a concentrated load applied on a compression ring (see Fig. 14-15).

Because of the considerable redistribution of actions that occurred between first cracking and failure, it was found that the amount of reinforcement could be substantially reduced from that calculated using the values of the actions predicted by elastic theory.

Another example of a test of a complex structure is the loading to failure of a 1/14-scale model of a prestressed concrete containment structure for a CANDU nuclear power plant by Rizkalla, Simmonds, and MacGregor (Ref. 14-13). The prototype structure is illustrated in Fig. 14-18. Details of the test structure are given in Fig. 14-16.

The purpose of the concrete containment structure is to prevent the release of radioactive materials into the atmosphere in the event of an accident. The design specifications for these structures require that the concrete on the inside faces remain free of tensile stresses under a specified accident pressure. To reduce the possibility of an explosive failure, water rather than air was used to apply the internal pressure during the test. The first crack developed at an internal pressure of 30 psi (0.21 MPa) on the inside face of the dome. Meridional and circumferential cracks occurred at 40 psi (0.28 MPa). At an internal pressure of 80 psi (0.55 MPa), leakage through the cracks in the walls, caused by the failure of several seams in the plastic liner, prevented additional loading. After a stronger liner was installed, the pressure was further increased. Outward bulging of the cylindrical walls was

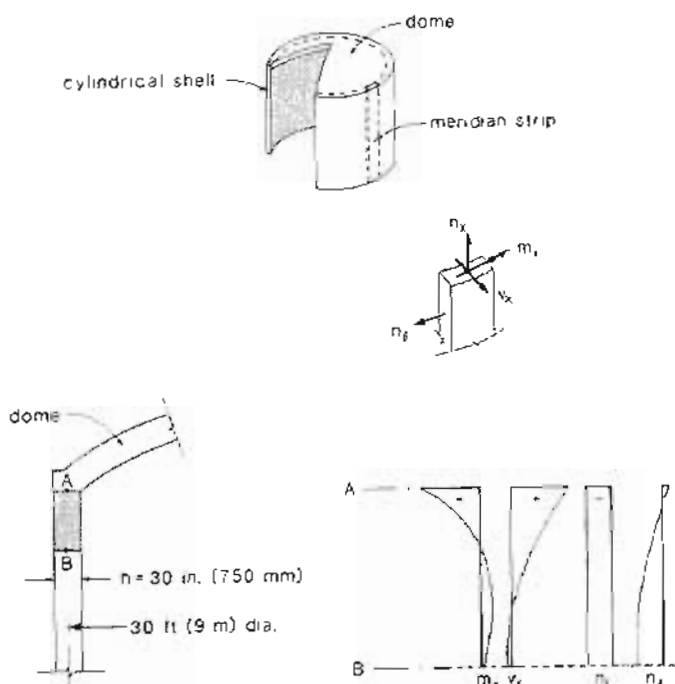


Figure 14-14 Edge moments and shears near junction of dome and cylinder.
Adapted from Reineck (Ref. 14-11).

noticeable above 80 psi (0.55 MPa), with the buttresses also bulging outward. There was a marked increase in deformation at about 110 psi (0.76 MPa) associated with widespread yielding of the reinforcement. Failure occurred at a pressure of 159.5 psi (1.10 MPa) due to rupture of three circumferential tendons and one vertical tendon at midheight near a buttress (see Fig. 14-17).

Figure 14-18 demonstrates the considerable ductility displayed by the structure prior to failure and also illustrates that the deflections at failure were approaching the wall thickness of the structure. The four buttresses that were used to anchor the circumferential tendons (see Fig. 14-18) had a localized stiffening effect on the wall of the structure. Thus while the wall bulged outward by 2.5 in. (64 mm) at maximum pressure, the buttresses bulged outward only 1.25 in. (32 mm). The outward bending of the buttresses resulted in cracks adjacent to most of the tendon anchorages. Final failure seems to have been initiated at these locations.

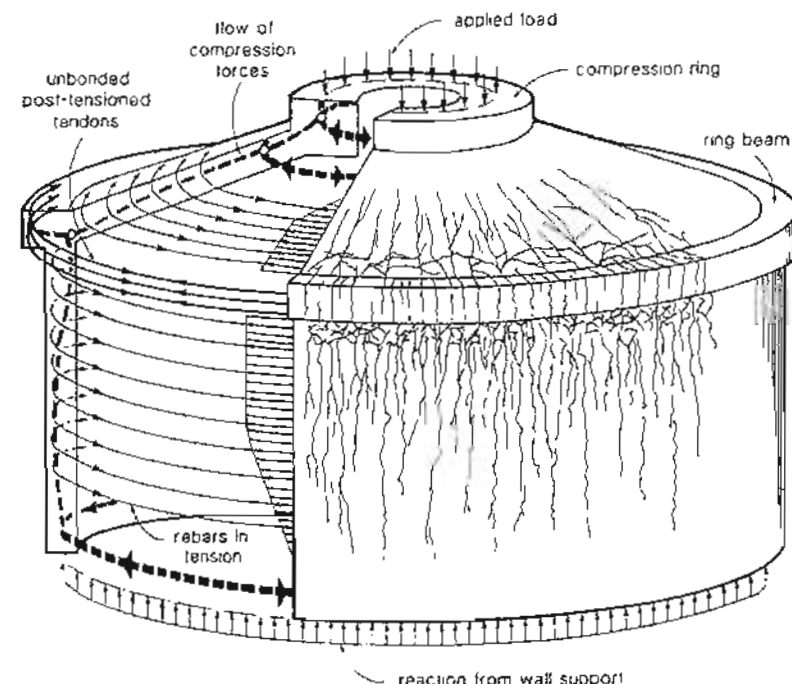


Figure 14-15 Test of complex shell structure. Adapted from Reineck (Ref. 14-11).

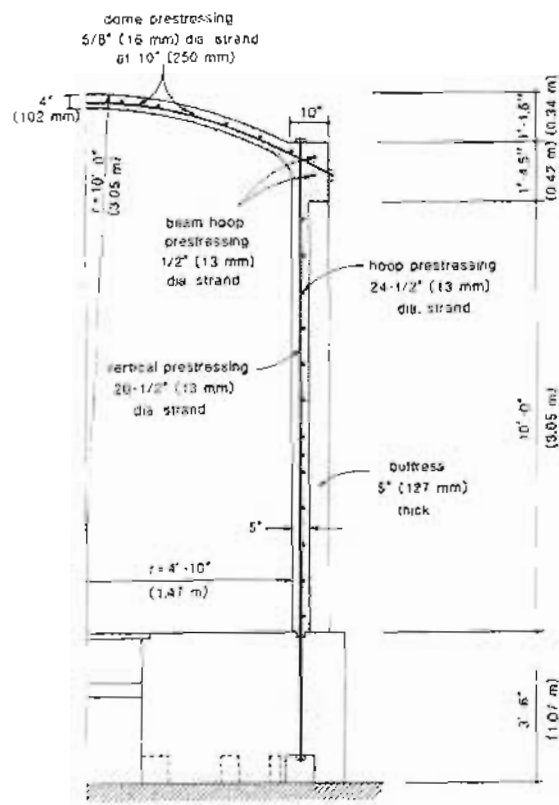


Figure 14-16 Vertical section through test structure. Adapted from Rickalla, Simmonds, and MacGregor (Ref. 14-13).



Figure 14-17 Failure of prestressed concrete containment structure. Photographs courtesy of James G. MacGregor.

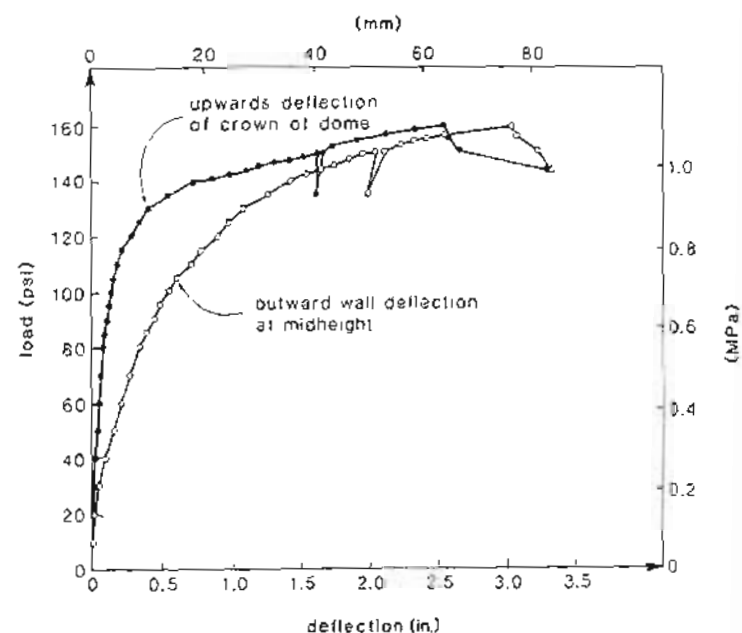


Figure 14-18 Load-deflection response of prestressed concrete containment structure. Adapted from Ref. 14-13.

References

- 14-1 ASCE Task Committee on Finite Element Analysis. *Finite Element Analysis of Reinforced Concrete*. American Society of Civil Engineers, New York, 1982. 345 pp.
- 14-2 ACI Committee 318. "Building Code Requirements for Reinforced Concrete (ACI 318-89) and Commentary - ACI 318 R-89." American Concrete Institute, Detroit, 1989. 353 pp.
- 14-3 Vecchio, F.J., and Collins, M.P., "The Modified Compression Field Theory for Reinforced Concrete Elements Subjected to Shear," *ACI Journal*, Vol. 83, No. 2, Mar.-Apr. 1986, pp. 219-231.
- 14-4 Cook, William D., and Mitchell, Denis, "Studies of Disturbed Regions near Discontinuities in Reinforced Concrete Members," *ACI Structural Journal*, Vol. 85, No. 2, Mar.-Apr. 1988, pp. 206-216.
- 14-5 Vecchio, Frank J., "Nonlinear Finite Element Analysis of Reinforced Concrete Membranes," *ACI Structural Journal*, Vol. 86, No. 1, Jan.-Feb. 1989, pp. 26-35.
- 14-6 Fiskvatin, A., and Grosch, H., "Design of Reinforced Concrete Shells in Offshore Structures by the Computer Programme CONDIM," *Journal of the Nordic Concrete Federation*, 2-4, 1982, pp. 106-110.
- 14-7 Kirschner, U., and Collins, M.P., *Investigating the Behaviour of Reinforced Concrete Shell Elements*, Publication No. 86-9, Department of Civil Engineering, University of Toronto, Sept. 1986, 209 pp.
- 14-8 Collins, Michael P., Adebar, Perry, and Kirschner, Uwe, "SHELL474 - A Computer Program to Determine the Sectional Resistance of Concrete Structures in Accordance with CSA Standard S474-M89," Canadian Standards Association, Rexdale, Canada, Apr. 1989, 32 pp. plus appendices.
- 14-9 Adebar, Perry E., "Shear Design of Concrete Offshore Structures," Ph.D. thesis, Department of Civil Engineering, University of Toronto, 1989, 197 pp. plus appendices.
- 14-10 Canadian Standards Association Committee S474, "Preliminary Standard S474-M1989 Concrete Structures. Part IV of the Code for the Design, Construction, and Installation of Fixed Offshore Structures," CSA, Rexdale, Canada, Aug. 1989, 39 pp.
- 14-11 Reineck, K.-H., "Versuche an Stahlbeton-Schalen für Offshore-Bauten" (Tests for a Reinforced Concrete Offshore Structure), *Institutbericht 1979-1987*, Institut für Massivbau, Universität Stuttgart, Stuttgart, West Germany, 1988, pp. 4.20-4.23.
- 14-12 Reineck, K.-H., Reibnagl, T., Reinke, H.-G., and Koch, R., "Test on a Complex Reinforced Concrete Shell Structure," *Institut für Massivbau, Universität Stuttgart*, Stuttgart, West Germany, Sept. 1983.
- 14-13 Rizkalla, Sami H., Simmonds, Sydney H., and MacGregor, James G., "Prestressed Concrete Containment Model," *Journal of Structural Engineering*, Vol. 11, No. 4, Apr. 1984, pp. 730-743.

Evaluation and Rehabilitation

To assess an existing concrete structure ... requires the highest degree of professional integrity, expertise and knowledge from the assessing engineer. ...

CEB Task Group "Diagnosis and Assessment of Concrete Structures," 1989

15.1 INTRODUCTION

There is an increase in the number of concrete structures which either exhibit signs of deterioration or have become functionally obsolete. Hence the assessment of such structures is becoming an increasingly important responsibility for structural design engineers. As shown in Fig. 15-1, the three main stages in the evaluation and rehabilitation of a structure involve examination, diagnosis, and design of remedial measures.

The first stage of a structural assessment is to carry out a detailed examination in order to establish the facts about the structure's current condition. This stage involves collecting all existing information about the structure, surveying the structure for signs of distress, and conducting appropriate physical and chemical tests. Most of these tests require specialized equipment and expert interpretation.

The diagnostic stage involves developing an understanding of the way in which the structure behaves. If the structure is in distress, the prime concern is to understand the deficiencies that have resulted in this distress and to predict the future consequences of these deficiencies. The more sophisticated response models described in the earlier chapters of this book are well suited to this task.

In prescribing a remedy for a structure in distress the engineer must assess the future needs of the structure, must minimize disruptions to the use of the structure during repair, must satisfy local authorities having legal jurisdiction, must address safety aspects, and at

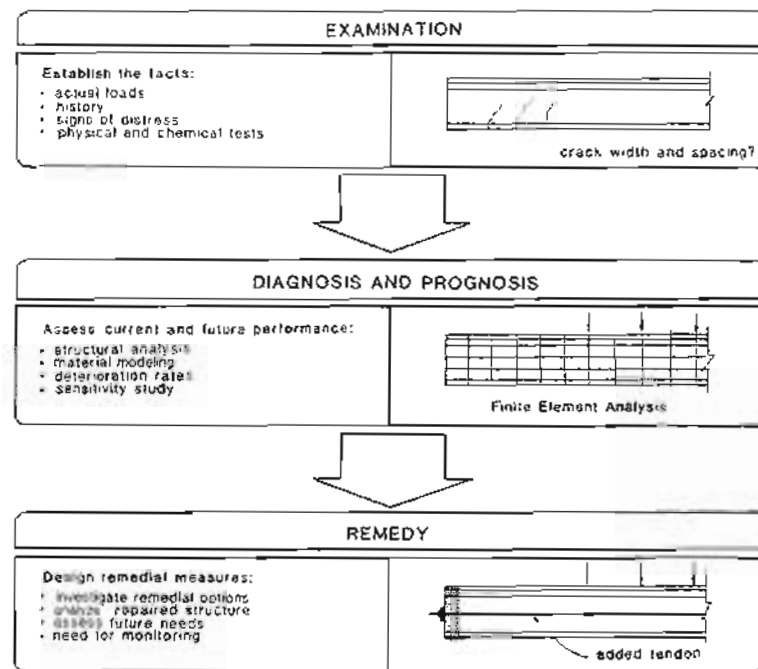


Figure 15-1 Guide to evaluation and rehabilitation.

the same time must provide a practical, economical solution. In arriving at a solution that satisfies the criteria above, the engineer will often find it appropriate to consider the use of post-tensioning.

In this chapter a guide to interpreting some of the key symptoms of distress is given. In addition, some aspects of both physical and chemical testing, which are of particular importance to the structural engineer, will be summarized. The applicability of rational behavioral models for both evaluating structures and designing remedial measures will be illustrated by a number of examples.

15.2 SYMPTOMS OF DISTRESS

Typical symptoms of distress for reinforced concrete structures include concrete cracking, spalling and delamination of the concrete, corrosion of reinforcement, and excessive deflections. For reinforced concrete structures the most evident sign of distress is cracking of the concrete. It must be recognized that many cracks are to be expected in non-prestressed

concrete structures under full service loading. One of the prime reasons for prestressing a concrete structure is to greatly reduce the amount of cracking that occurs under service loads. Since cracks form perpendicular to the direction of principal tension in the concrete, they indicate the direction of principal compressive stresses and hence can help the engineer to understand the flow of forces in a structure. In addition, the width and spacing of the cracks provide means of estimating the principal tensile strains in the concrete (see Section 4.13).

Figure 15-2 illustrates some examples of crack patterns caused by external loads. Although the idealized load cases of pure tension, pure flexure, pure shear, and pure torsion rarely occur in practice, it is useful to be able to recognize the uniform crack patterns associated with these loads. Figure 15-2f illustrates the cracking pattern of the more typical loading case of combined bending and shear, where the inclination of the cracks changes along the length of the beam as the moment-to-shear ratio changes. Concentrated loads or reactions cause cracks that fan out from the load or reaction (see Fig. 15-2g and h).

It is important to realize that except for the simple cases of pure axial load and pure flexure, after cracking, the direction of principal compressive stresses typically changes as the load is increased. The initial crack directions are not significantly influenced by the reinforcement and usually correspond closely to the directions predicted using a linear elastic analysis that neglects the presence of reinforcement. After first cracking, the compressive stress trajectories are strongly influenced by the amount and direction of the reinforcement. Typically, reinforced concrete structures contain an orthogonal grid of reinforcement, and usually the amounts of reinforcement are different in the two directions. After cracking, the principal compressive stress trajectories and hence the direction of new cracks tend toward the direction of the stiffer reinforcement. This change in direction of the cracks is particularly significant in regions of a structure subjected to combined loading and containing reinforcement in only one direction (see Fig. 15-3).

The tensile stresses in the concrete that cause cracks will not necessarily be due to external loads applied to the structure. Shrinkage of the concrete and temperature changes will cause the concrete to change volume. If the structure subjected to these volume-change effects is restrained against deformation, stresses can arise in the concrete which may cause cracking. Methods for determining these restraint effects are given in Sections 4.5, 5.11, and 5.12 and in Chapter 10.

Figure 15-4 illustrates situations involving cracking caused by restraint of volume change. Figure 15-4a shows a beam restrained at each end by very stiff walls. To demonstrate the importance of restraint stresses, let us assume that these walls are so stiff that axial deformation of the beam is totally prevented. Let us further assume that the beam is subjected to a decrease of temperature of ΔT degrees. If the beam were unrestrained it would shorten by an amount $\alpha_c \Delta T L$, where L is the length of the beam and α_c is the coefficient of thermal expansion. Because the walls totally prevent the beam from changing length, they must pull on the beam with a force great enough to produce a lengthening of $\alpha_c \Delta T L$, which will counteract the unrestrained thermal shortening. If the beam is uncracked, this produces a concrete tensile stress of $\alpha_c \Delta T E_c$. Thus, for concrete with a tensile strength of, say, 300 psi (2.1 MPa), an elastic modulus, E_c , of 4000 ksi (27 600 MPa) and a coefficient of thermal expansion, α_c , of $6 \times 10^{-6}/^{\circ}\text{F}$ ($10 \times 10^{-6}/^{\circ}\text{C}$),

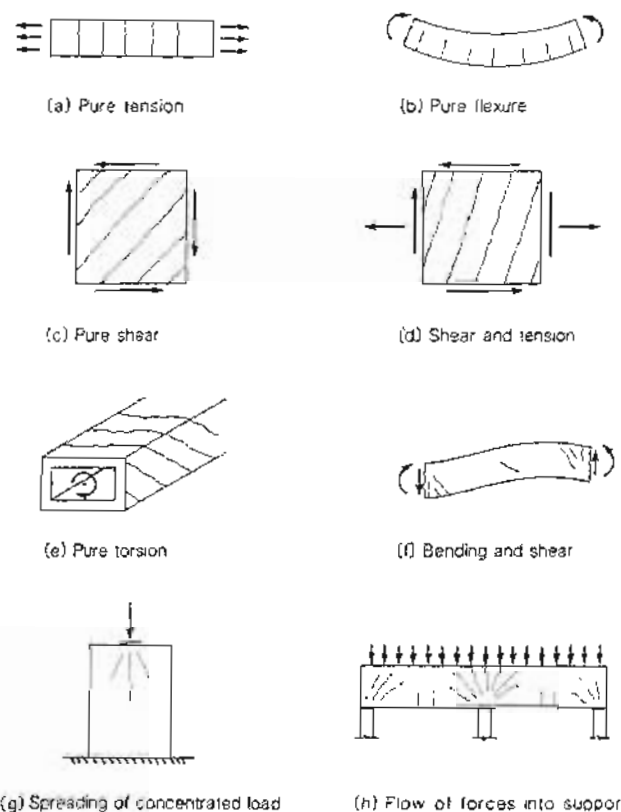
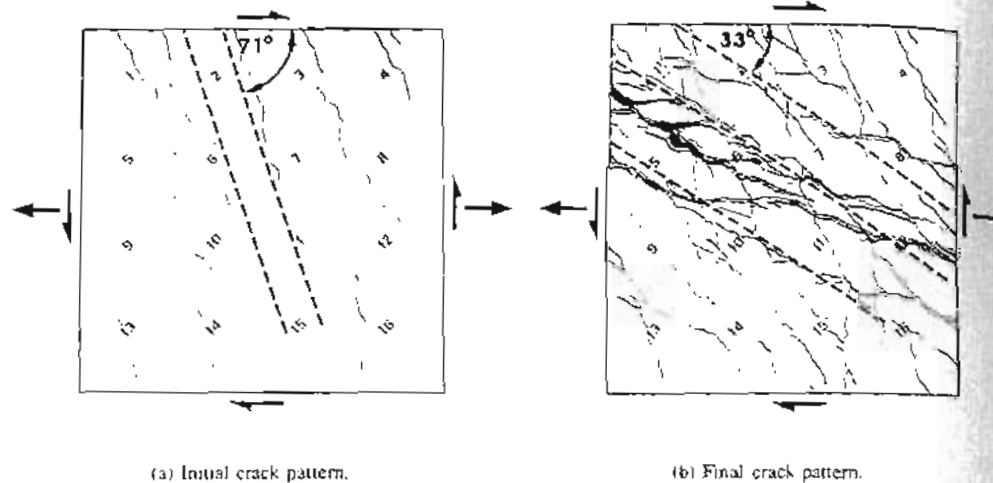


Figure 15-2 Examples of crack patterns indicating principal compressive stress trajectories caused by external loads.

cracking would occur when the temperature drops by only 12.5°F (6.9°C). Thus it is obvious that a concrete member, fully restrained against axial shortening, will crack due to small decreases in ambient temperature. Further, even if the temperature were maintained constant, the beam would crack due to the restraint of shrinkage of the concrete. After cracking, if the small tensile strains in the concrete between the cracks are neglected, the sum of the crack widths, $\sum w_i$, along the beam will be given by

$$\sum w_i = -(\alpha_c \Delta T + \epsilon_{s,i})L \quad (15-1)$$

This relationship is useful in the diagnosis of cracking patterns in members with significant



(a) Initial crack pattern.

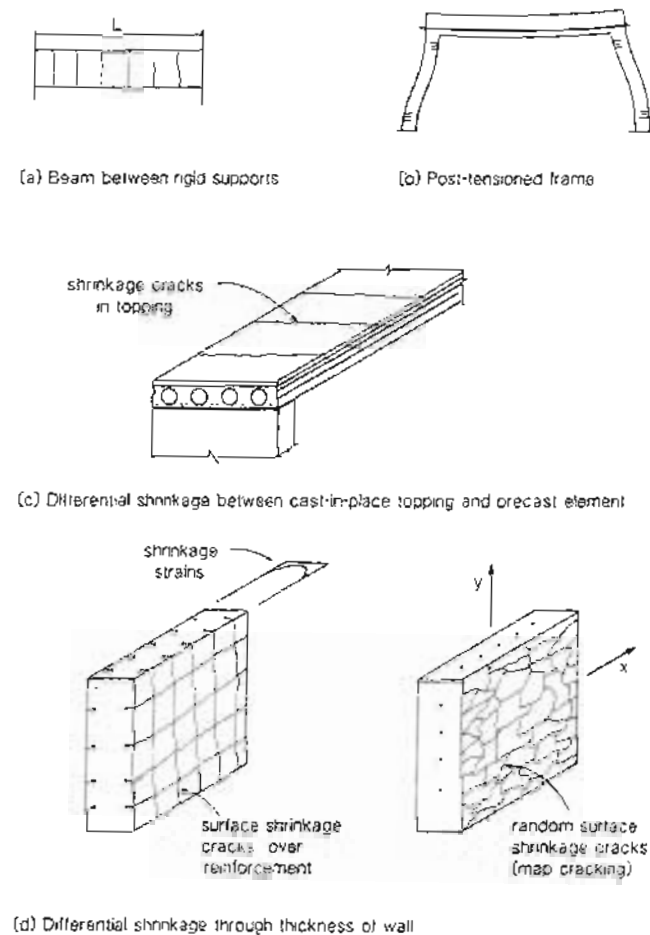
(b) Final crack pattern.

Figure 15-3 Change in direction of cracks in element subjected to combined shear and tension. Element contains reinforcement in only the horizontal direction. Adapted from Bhinde and Collins (Ref. 15-1).

restraint. Thus, if ΔT is about -50°F (-28°C) and c_{sh} is about -0.4×10^{-3} , then the sum of the widths of all of the cracks that occur in the member would be about $0.7 \times 10^{-3}L$.

A situation involving restraint stresses which is particularly relevant for post-tensioned construction is illustrated in Fig. 15-4b. When the beam is post-tensioned it will try to shorten; however, the foundation will restrain the bases of the columns, causing significant bending moments in the columns. The resulting crack pattern, with cracks forming on outside faces of the columns near their bases and on the inside faces near the tops of the columns, is typical of post-tensioned frames. These cracks will usually occur at the time of post-tensioning. Sometimes steps are taken to reduce these restraint effects, such as introducing temporary "hinges" or permitting lateral movement at the base during post-tensioning. Usually, the bases of the columns are fixed after post-tensioning. After the post-tensioning operation, the beam will continue to shorten due to creep and shrinkage and if this additional movement is now restrained, then restraint stresses will grow in the columns, causing the typical crack pattern to develop some time after post-tensioning. Methods for analyzing these effects are given in Section 10.13.

Another typical crack pattern caused by restraint of volume change is illustrated in Fig. 15-4c. Because the topping concrete will typically have a higher water/cement ratio than the precast concrete and because the precast concrete will already have experienced most of its shrinkage prior to application of the topping, there will be a significant differential shrinkage between the two concretes. The precast member restrains the shrinkage



(c) Differential shrinkage between cast-in-place topping and precast element

(d) Differential shrinkage through thickness of wall

Figure 15-4 Crack patterns caused by restraint of volumetric changes.

of the cast-in-place topping and the resulting restraint stresses will crack the concrete, particularly in regions of low moment (see Fig. 5-44).

Differential shrinkage also occurs through the thickness of most reinforced concrete elements, with the surface concrete shrinking at a faster rate than the interior concrete. This differential shrinkage will cause tensile stresses near the surface of the concrete which may result in surface shrinkage cracks (see Fig. 15-4d). Because the restrained shrinkage

stresses near the surface of the element have no preferred direction in the $x-y$ plane, the cracking pattern visible on the surface of the element will be determined by local stress concentrations and local defects in the concrete. The resulting pattern of random cracks is referred to as map cracking (see Fig. 15-4d). If reinforcing bars are located close to the surface, they will form a regular pattern of stress concentrations, resulting in an orthogonal pattern of cracks. The cracking patterns shown in Fig. 15-4d can also be caused by differential thermal strains or by any other differential volumetric strain, such as alkali-aggregate reaction (see Fig. 15-5). Methods for accounting for differential strains are discussed in Section 5.18.

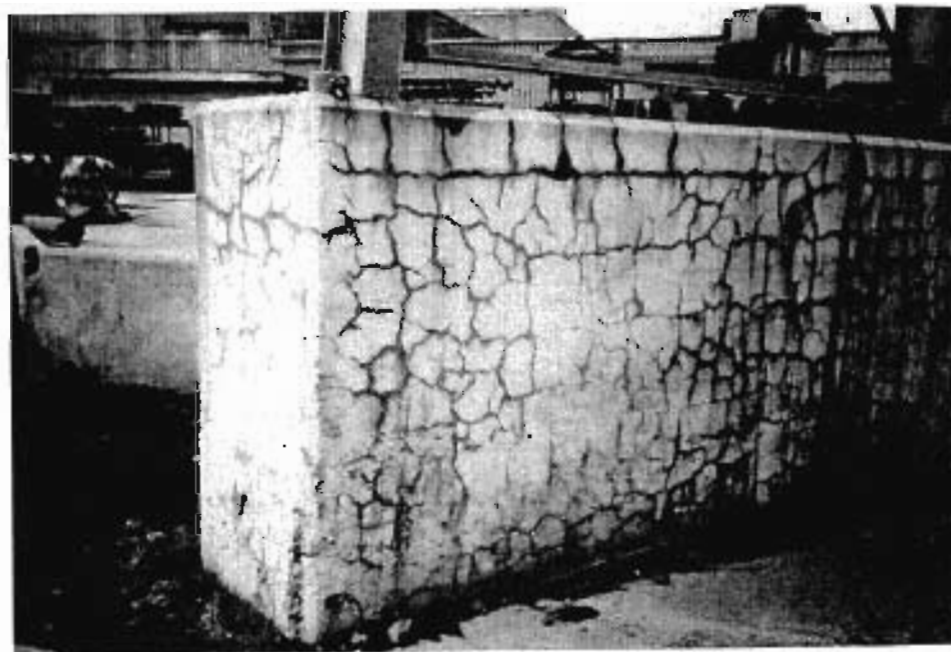
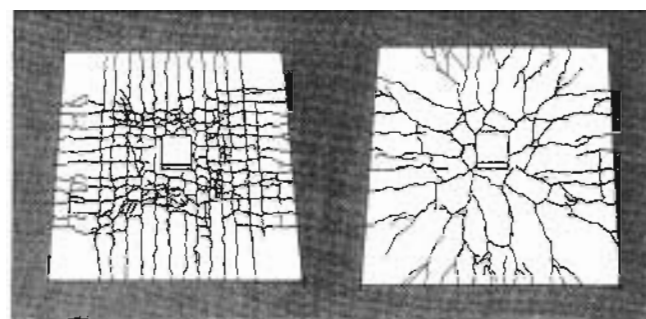


Figure 15-5 Map cracking in reinforced concrete wall. Photograph courtesy of George Ochrym.

There are many situations where the cracking pattern is strongly influenced by the detailing of the reinforcement. As a general rule, a small number of wide cracks indicates improperly detailed reinforcement or insufficient reinforcement to control cracking (see Figs. 4-25 and 4-26). The width of the cracks on the surface of the concrete is almost directly proportional to the concrete cover over the bar (see Fig. 4-12). Knowledge of this fact is useful in detecting misplaced reinforcing bars, particularly top reinforcing bars in

floor slabs, which, if not properly supported, can be displaced downward during concreting. The top reinforcing bars in floor slabs typically have only 3/4 in. (19 mm) of cover and hence act as crack initiators, giving rise to an orthogonal crack pattern around the column (see Fig. 15-6a). The crack pattern that results when the reinforcement has been misplaced significantly is shown in Fig. 15-6b. This pattern of radial and circumferential cracks is dictated by the column rather than by the reinforcing bars. In addition to changing the pattern, the increase in the concrete cover will result in considerably wider cracks. The presence of the "spider-web" pattern of radial and circumferential cracks around columns in flat plate or flat slab construction usually indicates significant reinforcement misplacement, which can have dangerous consequences, such as the premature punching failure of the slab. Such "spider-web" cracks were observed (Ref. 15-3) in the floor slab in a condominium structure prior to its collapse.



(a) 0.75 in (19 mm) cover (b) 2.5 in (64 mm) cover

Figure 15-6 Influence of reinforcing bar location on crack pattern in top surface of two-way slab around column. Adapted from Lee, Harns, and Mitchell (Ref. 15-2).

Figure 15-7 illustrates a number of additional situations where detailing of the reinforcement influences the crack patterns. Cracks are likely to form at locations where significant amounts of reinforcement are terminated (see Fig. 15-7a and c). In a beam containing an insufficient amount of stirrups, an extension of a flexure-shear crack may develop and run along the longitudinal reinforcing bars (see Figs. 15-7a and 7-13a). Such a crack indicates that shear failure may be imminent. If the longitudinal reinforcement is not appropriately anchored at the support, an inclined crack may develop over the support, which may cause a premature failure of the beam (see Fig. 15-7a and b). Support failures may also occur in corbeils and ledge supports if the tie-back reinforcement is not capable of transferring the tension from the beam to the support (see Fig. 15-7b). Near a negative moment support, longitudinal splitting cracks will sometimes occur directly above the longitudinal reinforcement. The diagonal compressive stresses caused by the shear push

outward against the reinforcing bars as shown in Fig. 7-15b. This outward thrust combined with the bond stresses may split the concrete cover above the bar (see Fig. 3-39a). If such cracks are present, it will be necessary to investigate the anchorage details of the longitudinal reinforcement and the increased risk of corrosion of the steel. Anchorage zones of post-tensioned tendons typically contain cracks caused by spreading of the highly concentrated compressive stresses in the concrete behind the anchor blocks (see Section 9.2). If significant cracking is observed in an anchor zone, the details of the reinforcement provided in this region must be investigated. In the situation illustrated in Fig. 15-7d, the anchorage zone cracking has been aggravated by the placement of the anchor blocks on the interface between the slab and the beam band.

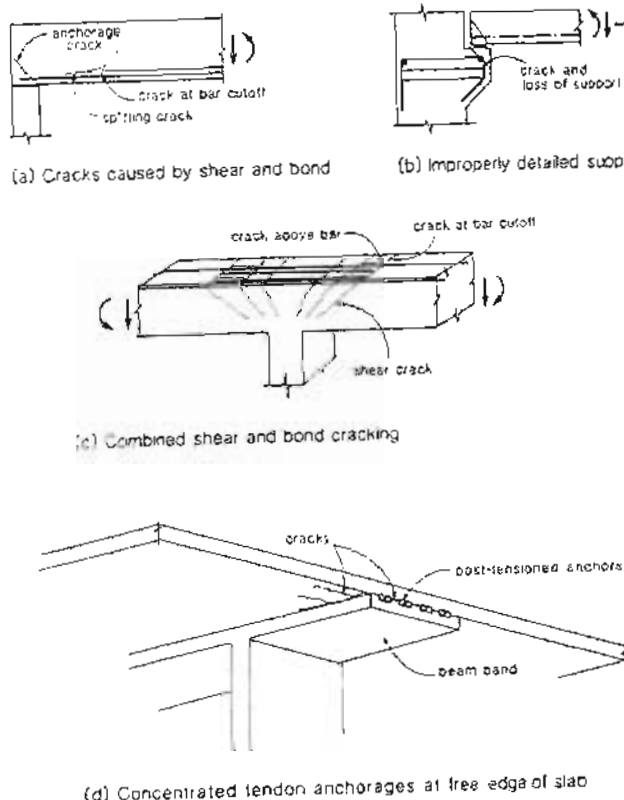


Figure 15-7 Cracking influenced by reinforcement details.

Sec 15.3 Testing Techniques

In addition to the pattern of cracking, it is also important to examine the specific details of individual cracks. Cracks less than about 0.004 in. (0.10 mm) are difficult to see and are not normally a cause for concern. Crack widths above 0.020 in. (0.50 mm) are clearly visible and may indicate serious problems. Crack widths can be measured with a simple comparator that consists of a series of lines of different thicknesses. A quick check to see if the crack width exceeds 0.020 in. (0.50 mm) is to attempt to insert a standard 0.5 mm lead from a mechanical pencil into the crack.

Spalling and delamination are caused by tensile stresses which are perpendicular to the concrete surface. These stresses can result from corrosion of reinforcement, freezing of water in internal voids, alkali-aggregate reaction, splitting caused by curved reinforcement (see Section 9.12), splitting caused by curving compressive stresses (see Fig. 3-6) or splitting caused by impact forces. Figure 15-8 illustrates delamination of the wall of a water tank caused by freeze-thaw damage. The layer of reinforcement forms a plane of weakness that splits when significant tensions are produced transverse to the plane of the wall. The presence of lap splices aggravates this problem.

As discussed in Section 3.19, corrosion of reinforcement usually poses the greatest threat to the durability of a reinforced concrete structure. Unfortunately, the symptoms of corrosion are not usually evident until a significant amount of corrosion has already occurred. Typical symptoms include spalling or delamination of the concrete or staining of the concrete. Figure 15-9 shows corrosion damage to a 1/2 in. (13 mm) diameter seven-wire strand which had been used as an unbonded tendon in the floor slab of an office building. Some methods for determining susceptibility to corrosion are discussed in Section 15.3.

Large deformations are often the first indication of significant distress of reinforced concrete structures. The engineer must determine whether these deformations are caused by excessive imposed loads, deterioration of stiffness of the structure, or change in the support conditions of the structure.

15.3 TESTING TECHNIQUES

The technology for determining the characteristics of in-situ concrete has developed considerably in the last few years, with a number of new testing techniques now becoming practical. The CEB state-of-the-art report "Diagnosis and Assessment of Concrete Structures" (Ref. 15-5) provides a review of these techniques. A brief summary of some aspects important to a structural engineer is given below.

Figure 15-10 categorizes a number of important physical and chemical tests according to the structural property being evaluated. Since the compressive strength of concrete is used as the prime indicator of concrete quality, test methods for estimating in-situ compressive strength are of particular importance.

The most reliable method for estimating in-situ compressive strength is to test core samples taken from the structure (Ref. 15-6). Unfortunately, this test method is expensive and the core sample needs to be relatively large in order to obtain reliable results, with a 4 in. (102 mm) core diameter being common.

The Schmidt Rebound Hammer (Ref. 15-7) provides a practical and inexpensive way of surveying large areas of in-situ concrete to investigate concrete uniformity and

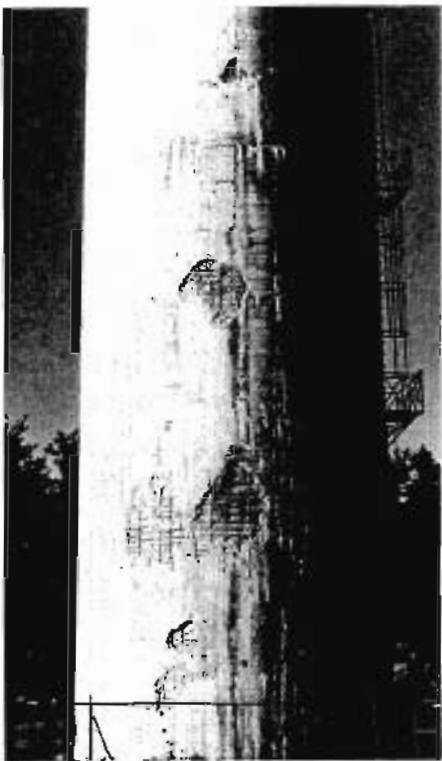


Figure 15-8 Delamination on the external face of a concrete water tank.
Courtesy of Grieve, Slater, and Rothenburg (Ref. 15-4).

to identify possible critical zones where core samples could be taken. This hand-held instrument, which gives a measure of the hardness of the concrete surface, operates by measuring the rebound of a small spring-driven mass which impacts against a steel rod in contact with the concrete. A display on the side of the hammer records the percentage rebound of the mass, which is quoted as the rebound number. A rebound number above 40 indicates a hard surface, while a number below 20 usually indicates cracks and delamination near the surface. The rebound number can be used to estimate the concrete strength using an approximate calibration curve. More reliable estimates can be made if the technique is calibrated against strength tests on cores taken from the structure.

While the Schmidt hammer measures surface hardness, the Windsor probe (Ref. 15-8) measures penetration resistance in order to estimate in-situ compressive strength. The

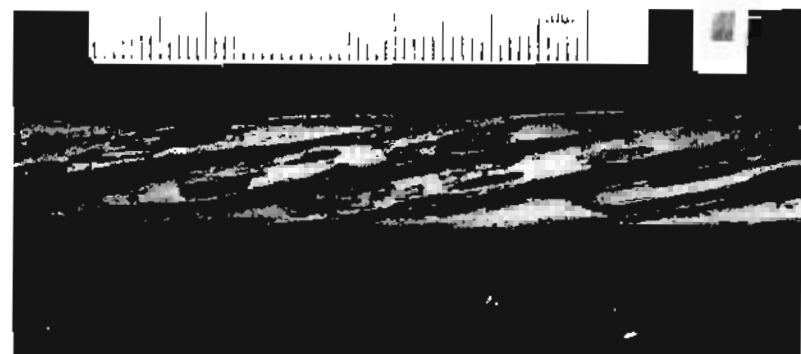


Figure 15-9 Corrosion of a 1/2 in. (13 mm) diameter strand. Photograph courtesy of Carnuthers and Wallace.

penetration of a steel probe, with a conically shaped end, is determined after firing the probe into the concrete with a standard explosive charge. The relationship between the penetration depth and the compressive strength of the concrete is a function of the hardness of the aggregate and hence this property must be determined before standard calibration charts can be used.

The pull-out test (Ref. 15-9), illustrated in Fig. 15-11a, involves drilling a hole into the existing concrete, under-reaming a larger-diameter hole at the bottom of the drilled shaft, inserting a bolt with an expanding ring insert into the shaft, and then determining the force required to pull out the bolt. While the pull-out resistance is a function of the tensile strength of the concrete, empirical relationships can be used to estimate the compressive strength of the concrete from the measured "tensile strength." A similar method for determining the tensile strength of the concrete is the internal-fracture test (Ref. 15-10) (see Fig. 15-11b). This method involves first drilling a hole into the concrete, inserting an expansion bolt, and then determining the force required to pull out the wedged anchor bolt. A simple method for determining the tensile strength of the concrete at its surface is the pull-off test (see Fig. 15-11c). In this test a circular disk is glued to the concrete surface using an epoxy resin and then the force required to pull off the disk is determined. Figure 15-11d illustrates the break-off test (Ref. 15-11), which is used to determine the tensile strength of the concrete in flexure. In this method the concrete is first cored to a predetermined depth with a special coring bit which also cuts a thicker ring at the surface. A hydraulic jacking device is inserted into one side of the top ring and used to determine the force required to break off the core.

As already mentioned, the Schmidt hammer is a convenient tool for determining the uniformity of the surface of large areas of concrete. The somewhat more expensive Windsor

PHYSICAL TESTS		CHEMICAL TESTS	
Compressive strength	- cores	Chemical composition	- cement content
- Schmidt hammer	- pull-out test	- aggregate/cement ratio	- water/cement ratio
- pull-out test	- break-off test	- cement type	- aggregate reactivity
- Windsor probe	- internal fracture		
Tensile strength	- pull-out test	Corrosion susceptibility	- chloride content
- break-off test	- ultrasonic pulse velocity	- chloride penetration	- carbonation depth
- internal fracture		- reinforcement potential	- concrete resistivity
Uniformity			
- Schmidt hammer			
- Windsor probe			
- ultrasonic pulse velocity			
Voids and delaminations	- chain drag test		
- ultrasonic pulse velocity			
Locating reinforcement	- cover meter		
- radiography			
Durability	- absorption		
- permeability			
- surface absorption			
- oxygen diffusion			
- carbon dioxide diffusion			
- air entrainment			
- aggregate type			

Figure 15-10 Guide to some physical and chemical tests for concrete.

probe enables the uniformity of not only the surface concrete but also the immediate subsurface concrete to be determined. Ultrasonic pulse velocity measurements (Ref. 15-12) enable an assessment of the uniformity of the concrete, including the presence of internal cracks and voids, to be evaluated. In its simplest form a transmitter of ultrasonic pulses is used on one side of a concrete member and a receiver on the other side. The time taken for the pulse to travel a known distance through the concrete enables the pulse velocity to be determined and these velocities are usually compared with the velocities measured on cores taken from the concrete. A pulse velocity exceeding 13,000 ft/sec (4 km/sec) indicates good-quality concrete, while a velocity below 10,000 ft/sec (3 km/sec) indicates a poor quality of concrete (Ref. 15-13).

The ultrasonic pulse velocity method can also be used to determine the quality of the concrete cover as illustrated in Fig. 15-12. The transit time taken for the pulse to travel from a transmitter to a number of receivers is plotted against the distances of these receivers from the transmitter. If these plotted readings lie on a straight line, it can be concluded that the cover concrete is of uniform quality (see Fig. 15-12b). Cracking of the

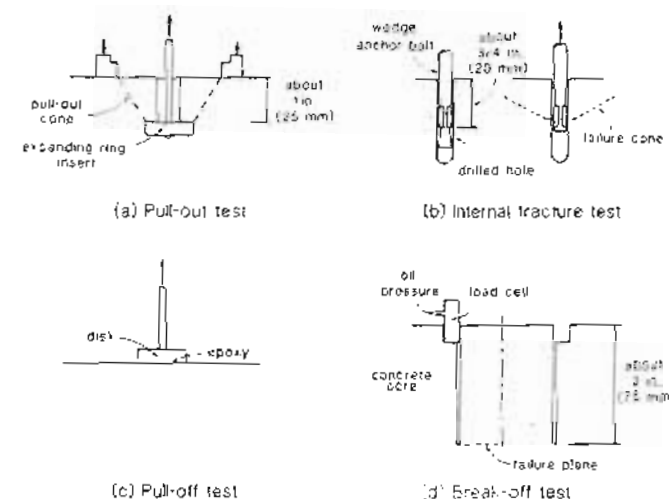


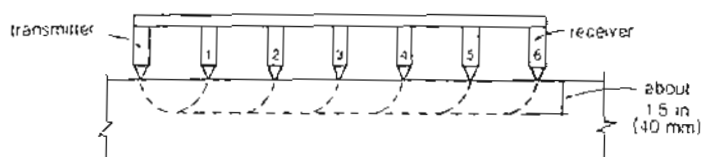
Figure 15-11 Some test methods for determining in-situ tensile strength.

cover concrete results in an offset of the plotted points, as shown in Fig. 15-12c. If the cover concrete is of poor quality (with many cracks or honeycombing), then the plot of the transit time versus distance will display a wide scatter, as shown in Fig. 15-12d.

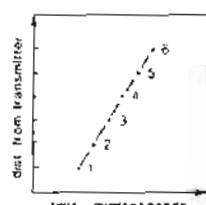
The results from the ultrasonic pulse velocity measurements can be used to map areas exhibiting delamination, which is important in assessing structures subjected to corrosive environments, such as bridge decks and decks of parking structures. This mapping can also be carried out using simpler techniques, such as hammer sounding or the chain-drag test. One method of quantifying the hammer sounding technique involves placing a hand-held instrument on the concrete surface to measure the reflected impact energy caused by the hammer impact.

In evaluating the condition of a concrete structure it is essential to know the amount and location of the reinforcement. For structures in corrosive environments it is of particular importance to determine the depth of concrete cover. An inexpensive method for determining the location and cover of reinforcement is to use a cover meter (Ref. 15-14). This technique measures the electromagnetic field caused by the size and distance of reinforcing steel and should be calibrated on-site by comparing readings with examples of covers measured to exposed reinforcement. Alternatively, gamma-rays or X-rays can be used to detect density variation within the concrete, enabling the location of reinforcement to be estimated (Ref. 15-15).

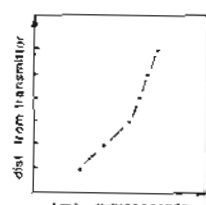
The durability of many concrete structures is governed by the rate of corrosion of the reinforcement and hence assessing durability involves estimating the parameters



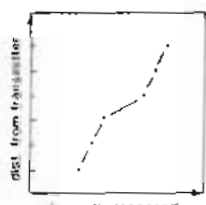
(a) Transmitter with six equally spaced receivers



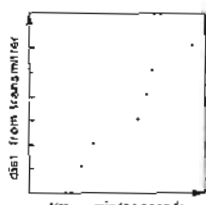
(b) Linear - uniform concrete



(c) Bilinear - weak surface layer



(d) Offset - cracked concrete



(e) Scatter - honeycombing or cracks

Figure 15-12 Determining uniformity of concrete in cover zone using the ultrasonic pulse velocity method. Adapted from Ref. 15-13.

that influence the rate of corrosion (see Fig. 3-48). Other common durability concerns include freeze-thaw resistance, alkali-aggregate reaction, and loss of surface concrete due to physical or chemical attack.

Useful tests to assess the durability of the concrete include determining the absorption (Ref. 15-16), the permeability (Ref. 15-17), oxygen diffusion (a measure of the rate of ingress of gases into the concrete), size and spacing of air voids (Ref. 15-18), and aggregate type. Chemical analyses permit the determination of the concrete constituents, such as cement content (Ref. 15-19), water/cement ratio (Ref. 15-20), and cement type

(Ref. 15-20). In order to assess the risk of corrosion of the reinforcement, samples of the concrete at the level of the reinforcement are tested for chloride content (Refs. 15-20 and 15-21). A typical chloride content distribution with depth for concrete exposed to salt water is given in Fig. 15-13. It is recommended (Ref. 15-23) that chloride contents below 0.4% of the weight of the cement pose a "low corrosion risk," whereas chloride contents greater than 1.0% pose a "high corrosion risk."

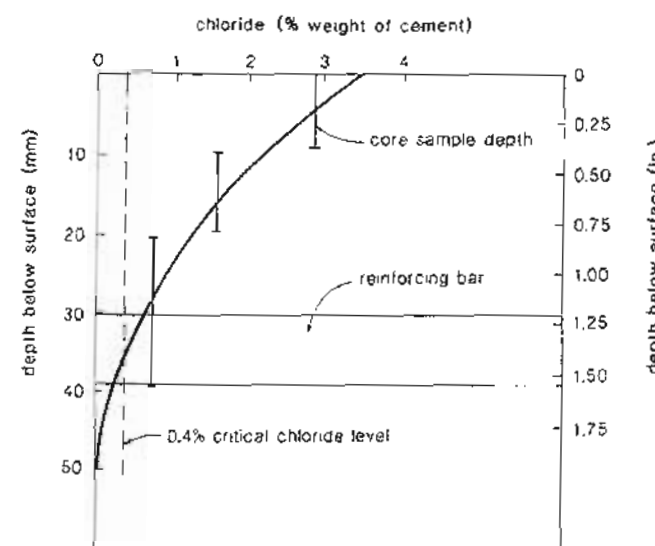


Figure 15-13 Variation of chloride content with depth from concrete surface exposed to marine conditions. Adapted from Browne and Geohagan (Ref. 15-22).

Simple chemical tests (Ref. 15-24) can be performed to determine the carbonation depth below the concrete surface. Carbonation results from the reaction of carbon dioxide from the atmosphere with the alkaline hydrated-cement compounds to form carbonates, thus reducing the pH below the level required for passivity. The carbonation depth is determined by coating the sides of a freshly drilled core sample with a solution of phenolphthalein in alcohol and water. The depth of carbonation stops at the level where the solution turns pink in the uncarbonated region of the core. Knowledge of the carbonation depth and the age of the concrete enables an assessment of the time required for the carbonation to reach the level of the reinforcement.

Figure 15-14 illustrates the manner in which the electrical potential between the surface of the concrete and the reinforcement can be measured (Ref. 15-25). One terminal of the voltmeter is connected to the reinforcement and then the reference electrode.

which is connected to the other terminal of the voltmeter, is moved around on the concrete surface. The potential differences recorded at different locations are then plotted to produce an equipotential contour map. According to Van Daveer (Ref. 15-26), regions with electrochemical potential readings that are algebraically greater than -200 mV have a 5% likelihood of corrosion, while those with readings algebraically less than -350 mV have a 95% likelihood of corrosion. Since corrosion is an electrochemical process (see Fig. 3-48), higher values for the resistivity of the cover concrete result in lower corrosion rates (Ref. 15-26). Browne and Geohegan (Ref. 15-22) suggest that for concrete resistivities greater than 20×10^3 ohm·cm, there is a low likelihood of corrosion, while for values less than 5×10^3 ohm·cm there is a high likelihood of corrosion.

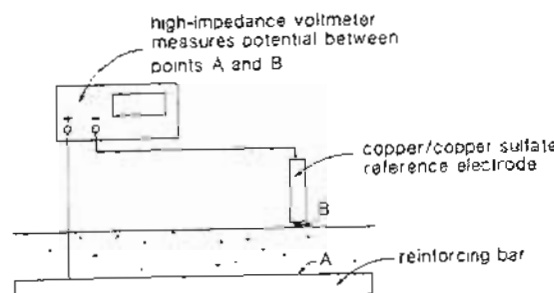


Figure 15-14 Determining areas susceptible to corrosion by mapping electrical potentials. Adapted from Ref. 15-20

15.4 ANALYTICAL ASSESSMENT

After a detailed inspection of the structure and after all information about the history of the structure (including structural drawings, specifications, shop drawings, and records of previous use) has been collected and after the appropriate physical and chemical tests have been performed, the engineer begins the formal process of analytically assessing the present state of the structure and its likely future performance. The first step in this process is to prepare detailed drawings summarizing all relevant information about the structure. It will often be necessary for the engineer to consult the technical literature for more specific information relevant to particular problems. For example, the information presented in Section 15.2 on interpreting crack patterns may not cover the specific case under investigation, and therefore it may be necessary to consult more detailed studies of crack formation such as those presented by Leonhardt (Ref. 15-27) or ACI Committee 224 (Ref. 15-28).

Before commencing detailed analytical modeling it is advisable to perform simple, approximate calculations to develop an understanding of the flow of forces through the

structure and to identify regions of the structure which may be critical. The information presented in Chapter 9 on the flow of forces in a structure can be supplemented by additional examples presented in the technical literature [e.g., Schlaich, Schäfer, and Jennewein (Ref. 15-29) and Park and Paulay (Ref. 15-30)].

In conducting an analytical assessment of an existing structure it is important to keep in mind the substantial differences that exist between designing a new structure and assessing an existing structure. The code design approaches for new structures are cast in a simple deterministic format in order to simplify and standardize the design tasks. Although the format of the code is deterministic, its goal is to appropriately account for variability in loads, load combinations, material properties, construction tolerances, reliability of analytical models, and the consequences of failure. While the code expressions account for a certain variability in the material properties, they do not account for gross defects such as corrosion of reinforcement, alkali-aggregate damage, splitting, spalling, or delamination. Similarly, these provisions assume that a new structure will be constructed according to the specifications and they do not account for serious errors in construction, such as gross misplacement of the reinforcement, serious deficiencies in placing or curing the concrete, and damage to immature concrete caused by premature removal of formwork.

When applying the code to the design of a new structure it is a simple matter to decide what material strengths to use. The structural engineer simply specifies the yield strength of the reinforcing bars and the cylinder compressive strength of the concrete and relies upon standard procedures to ensure that the materials used in construction conform to the design assumptions. In design the engineer assumes that the concrete has a uniform strength equal to the specified value and does not directly account for the variability that will occur in practice. The designer of a new structure usually assumes that all of the reinforcing bars will have the same yield strength, will have sufficient ductility, and will display a similar bilinear stress-strain relationship. In fact, reinforcing bars with the same specified yield strength can have widely differing properties.

In assessing an existing structure, particularly one showing symptoms of distress, it is not a simple matter to decide upon appropriate material properties to use in the analytical assessment. The engineer faces the following difficulties:

1. The tests to evaluate in-situ material properties are typically indirect and require expert interpretation.
2. Even for the sound material there will be a considerable variation of the measured properties at different locations in the structure.
3. The design equations use the 28-day strength of the concrete, which has been determined under a relatively fast rate of loading. In design we do not directly consider that the strength of the concrete will be reduced if loads are applied more slowly, but we also neglect the increase in concrete strength that will occur as the concrete matures after 28 days. In assessment, these features must be accounted for more directly.
4. It may be inappropriate to use material strengths higher than those specified in the original design because there will typically be only a small number of test results. Further, the design code approach has been calibrated against standard practice and contains many hidden reserves of strength. For example, a new properly constructed

structure will typically have material strengths considerably higher than those specified in the design.

5. Appropriate properties for deteriorated or damaged material must be estimated and a decision must be made concerning the areas affected by the defects and the likely future spreading of these areas.

Other significant differences between designing a new structure and assessing an existing structure are the consequences of conservative assumptions. In designing a new structure it is prudent to use the simple, conservative design equations of the code recognizing that the additional cost associated with the conservatism will be small and the limited design life is better applied to more critical issues, such as considering alternative structural configurations and designing for constructability. On the other hand, in assessing an existing structure there may be a very large cost associated with using the simple, conservative code equations and hence it may be appropriate to invest considerable engineering time in conducting more accurate assessments. After an analytical model has been developed to represent the structure, it should be used to perform sensitivity studies whose objectives are to explore the consequences of significant variations in measured material properties, assumed loading, and rates of deterioration.

Usually, it is appropriate to apply a number of different modeling techniques in the process of understanding how the structure behaves. Beginning with simple "back-of-the-envelope" calculations the engineer progressively refines the analytical model, first using a simple sectional analysis and perhaps progressing all the way to a nonlinear finite element analysis (see Chapter 14).

At the end of the analytical assessment the engineer should have developed an understanding of how the structure behaves, of why it is displaying symptoms of distress, and what the future life of the structure is likely to be. It is essential that the assessing engineer have a clear understanding of the fundamental principles governing the behavior of structures as well as intimate knowledge of the entire design process so that sound judgments can be made on matters influencing public safety.

15.5 REHABILITATION AND UPGRADING MEASURES

After the examination and diagnostic stages it may be necessary to rehabilitate or upgrade an existing structure. It is prudent for the engineer to investigate a number of different options for the rehabilitation or upgrading in order to choose the most cost-efficient and practical solution. This analysis stage involves an assessment of the future needs of the structure as well as the modeling of the existing structure with the design modifications. Once again it is important for the engineer to carry out a sensitivity study of the major parameters involved in the upgrading or repair. The rehabilitation or upgrading will require close construction supervision and possible adjustments during the construction stage. It is often decided to monitor the structure after any repairs or strengthening to ensure that the structural performance is acceptable. Some examples of different types of repairs are discussed below.

(a) Repair of Cracking Caused by Restraint of Deformations

Figure 15-15 illustrates the cracking observed in a parking structure reported by Horn and Kost (Ref. 15-31). The underground parking garage consists of a 5.5 in. (140 mm) thick one-way post-tensioned slab supported by post-tensioned beams. The continuous post-tensioned beams are spaced at 20 ft (6.1 m) centers. The signs of distress included an opening of the expansion joint of 1.5 to 2 in. (38 to 51 mm) and a large number of cracks varying in width from 0.125 in. (3.2 mm) up to almost 0.25 in. (6.4 mm). The observed pattern of major cracking is shown in Fig. 15-18b. Further inspection revealed that the cracks penetrated through the total thickness of the slab. This observation together with the pattern of cracking led to the conclusion that the cause of cracking was the restraint of axial deformation provided by the perimeter walls and shear walls. This restraint of axial deformation resulted in tensile forces developing in the slab due to the prestressing operation and due to shrinkage of the slab concrete.

A simple two-dimensional, linear-elastic analysis, with plate elements to represent the slab and truss elements to represent the axial stiffness of the beams, was carried out for the portion of the slab shown in Fig. 15-15c. The stiffness of the perimeter wall was modeled by equivalent spring elements and only the in-plane effects from the prestressing, shrinkage, and creep were modeled. Several analyses were carried out with different amounts of creep and shrinkage until the predicted displacement at the expansion joint was about 1.24 in. (31.5 mm). The cracking pattern predicted by this simple analysis (see Fig. 15-15c) together with the characteristic cracks through the slab thickness enabled the engineers to correctly diagnose that the major cracking was caused by the restraint of the slab. Since no corrosion had taken place in the prestressing steel, a simple repair, involving injecting the cracks with epoxy, was adopted. Some core samples were taken to ensure that the epoxy had adequately filled the cracks.

(b) Repair of Corrosion Damaged Structures

If a parking structure or a bridge has been estimated to have a short future life, the engineer will have to consider a number of different repair schemes. The possibilities include simply patching and sealing, patching together with placing a new waterproofing membrane, the removal of the delaminated concrete, and the placement of a high-performance (latex-modified concrete) overlay, hydro-demolition of the damaged concrete together with cathodic protection and the placement of a high-performance overlay, or total deck replacement. Figure 15-16 illustrates a qualitative guide to the relative costs of these various options.

Figure 15-17 shows the top surface of a parking structure that had experienced delaminations and significant depths of carbonation resulting in corrosion of the reinforcement. The hydro-demolition resulted in the removal of the top cover slab of the waffle floor system over significant regions of the multilevel garage. After inspection of the reinforcement it was necessary to replace those bars exhibiting significant corrosion (e.g., see Fig. 15-18). The floor was shored, waffle pans forms were installed, and a new concrete overlay and waterproofing membrane were placed.

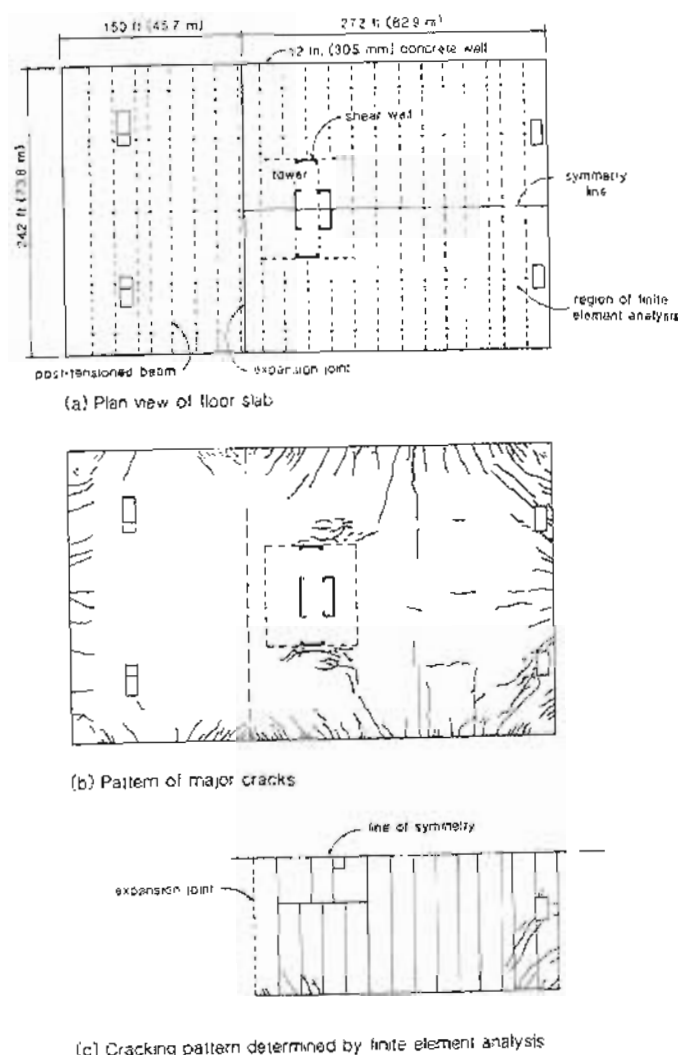


Figure 15-15 Observed cracking in a post-tensioned parking garage slab and predicted cracking patterns. Adapted from Horn and Kost (Ref. 15-31).

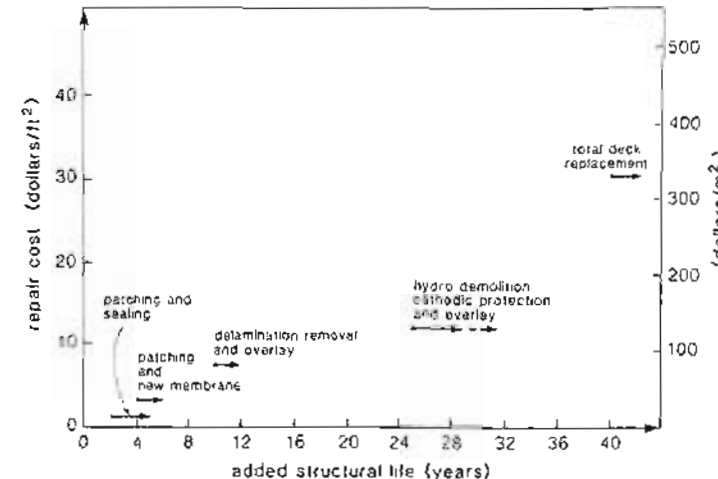


Figure 15-16 Relative costs of different repair methods for reinforced concrete parking structures. Adapted from Tighe and Van Volkinburg (Ref. 15-32).

(c) Applications of Non-Prestressed Reinforcement

A common method of increasing the strength and stiffness of an existing structural member is to add external reinforcement. Figure 15-19 shows the use of externally applied stirrups to a bridge that was judged to have an insufficient amount of shear reinforcement. The severe damage caused by the 1985 Mexican earthquake led to an unprecedented effort to both repair and strengthen existing reinforced concrete structures. Figure 15-20 illustrates some examples of the strengthening of columns by the addition of reinforced concrete to the existing reinforced column. The resulting strengthened column is not only stiffer and stronger but has the additional advantage of having greater ductility due to the addition of improved reinforcing details.

Figure 15-21 illustrates how columns in a precast concrete warehouse structure, located in a moderate seismic region, were strengthened for lateral load resistance. The one-story structure consisted of 24 in. (610 mm) double-tee roof members spanning 60 ft (18.3 m) with 10.5 ft (3.2 m) cantilever overhangs. The lateral load resistance for a typical 24 ft (7.3 m) wide bent consisted of a central 12 × 12 in. (305 × 305 mm) precast column and two 9 in. (229 mm) thick by 36 in. (914 mm) wide exterior precast columns. The repair method chosen (Ref. 15-34) involved encasing the central columns of the structure with reinforced concrete resulting in 24 × 24 in. (610 × 610 mm) columns as well as increasing the size of the column pedestal as shown in Fig. 15-21. This strengthening method increased the overall strength of the structure to lateral loads, greatly improved

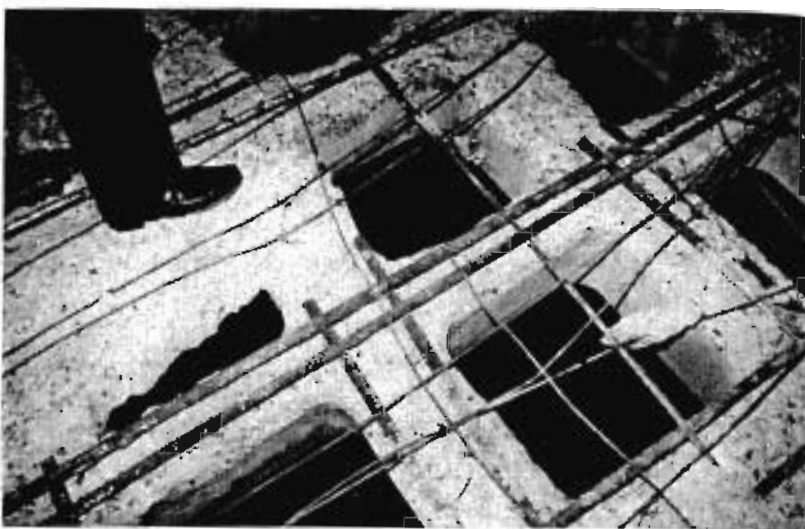


Figure 15-17 Top surface of a parking garage waffle slab after hydro-demolition.

the stiffness, thus reducing the drift and the $P\Delta$ effects, and increased the ductility by providing improved reinforcement details (closely spaced column ties as well as continuous reinforcement across the precast column connection). This localized strengthening scheme applied to the central columns resulted in a negligible loss in usable floor space, little disruption during construction, and minimized the additional restraints to thermal movements. The performance of a typical upgraded column was predicted (Ref. 15-34) using the techniques described in Chapter 5 and the computer program RESPONSE given in Appendix A.

(d) Applications of Post-Tensioning

Because post-tensioning enables structures to resist applied loads without significant deformations, it is a popular method for rehabilitation and upgrading. Construction details as well as examples of applying external tendons to bridges, tanks, and buildings are given in Ref. 15-35. Figure 15-22 shows how post-tensioning tendons have been applied externally to a bridge structure in order to actively control cracking and reduce displacements. An interesting example (Ref. 15-36) of the application of post-tensioning in the rehabilitation of a structure which had experienced distress is shown in Fig. 15-23. The five-level Pier 39 parking structure in San Francisco consists of 4.5 in. (114 mm) one-way post-tensioned slabs supported by 36 in. (914 mm) deep post-tensioned beams. Symptoms of distress included severe slab cracking at the roof level, water leakage, and breakage of



Figure 15-18 Severe corrosion of a bar in the top reinforcing mat of a waffle slab parking garage structure.

several of the unbonded post-tensioned strands in the beams due to corrosion. The rehabilitation consisted of replacing the slab tendons that displayed signs of corrosion and adding two external tendons per beam, each consisting of six 1/2 in. (13 mm) diameter strands. Saddles located at midspan and over the interior supports enabled a harped tendon profile to be achieved (see Fig. 15-23b). The application of external post-tensioning enabled the parking garage to remain in operation during rehabilitation.

Post-tensioning is also a useful technique for adding new parts to existing structures. Figure 15-24 shows a beam seat that has been added to an existing concrete column. The contact surface between the beam seat and the existing column was first roughened, then 1 in. (25.4 mm) diameter Dywidag threaded rods were epoxied into holes drilled into the large column, the concrete for the beam seat was placed, and the threaded bars were post-tensioned.

Post-tensioning also offers ideal solutions to difficult foundation problems. Figure 15-25 illustrates a method of increasing the strength of a foundation using precast segmental piles. This technique was used on a number of existing structures in Mexico City that were supported by floating foundations founded on a subsoil consisting of highly compressible

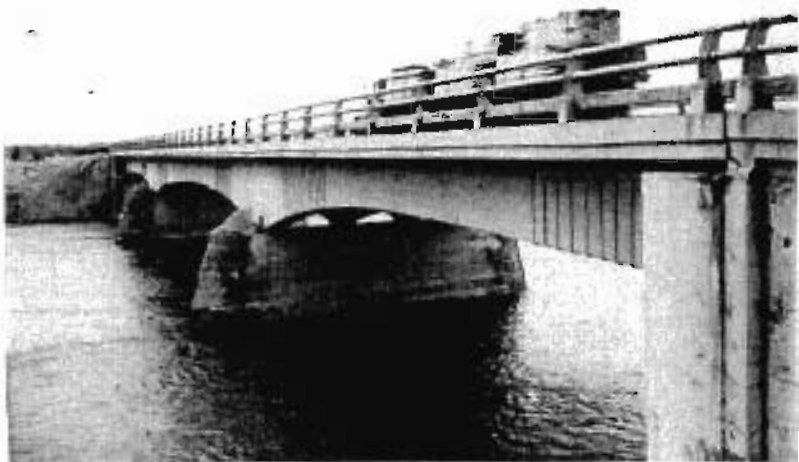
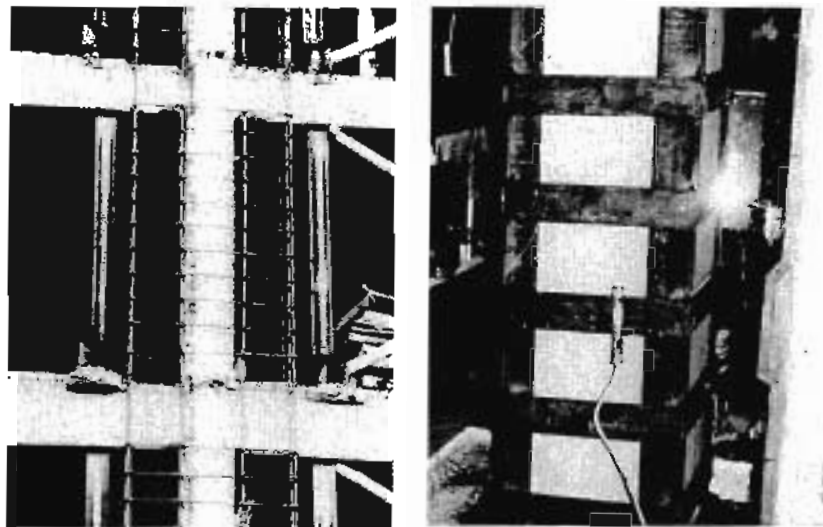


Figure 15-19 Bridge reinforced with additional stirrups.

clay. For the structure shown in Fig. 15-25, the foundation strengthening involved hydraulically pushing precast pile segments through holes created in the existing foundation by using a special jacking frame that reacted against the structure. To reach the stiffer sand layer, located about 65 ft (20 m) below the existing foundation, 20 segments, each 39 in. (1 m) long, were used. The "lead pile" segment contained the anchorage for six 1/2 in. (13 mm) diameter strands that protruded from the top of the segment. After hydraulically pushing the "lead pile" segment, the post-tensioning tendon was threaded through a central hole in the next segment, which was then pushed. This process was repeated for all 20 segments until the desired end bearing was achieved and then the tendon was post-tensioned. The resulting pile was then joined to the existing foundation by a reinforced concrete pile cap and a thickened foundation wall.

The 550 ft (168 m) high Montreal Olympic Tower is a post-tensioned structure which is inclined at an angle of about 35° degrees from the vertical and supports the removable roof structure over the Olympic Stadium (see Fig. 1-24). When the structure was built to a height of 302 ft (92 m), the construction was halted. Finite element analyses (see Fig. 1-24b) indicated that a maximum tensile stress of about 1480 psi (10.2 MPa) would result due to all permanent loads, prestressing, and live loads if the structure were completed as originally planned. The zone of predicted tensile stresses is in the region at the bottom of the front wall between the two front abutments as shown in Fig. 15-26. The two front abutments are 300 ft (91 m) apart and the distance between these abutments and the rear abutment is 500 ft (152 m). The tower is supported by thirty-six 3 × 3 ft (914 × 914 mm)



(a) Adding reinforced concrete.

(b) Welding steel angles and plates.

Figure 15-20 Examples of strengthening existing columns in Mexico City following the 1985 earthquake. Adapted from Mitchell, Dandurand, and Paultre (Ref. 15-33).

neoprene bearing pads at each of the two front abutments. Figure 15-26 also shows the two longitudinal stiffeners and the transverse stiffeners that support the domed roof for the Olympic swimming pool under the tower. To enable completion of this project a number of different solutions were examined, including providing a large column support between the front abutments and providing large post-tensioning tendons to be anchored on the exterior of the tower. The solution chosen involved a reduction of the weight of the upper part of the structure and the provision of post-tensioned tendons on the interior of the structure (see Fig. 15-27). Six 233.5 ft (71 m) long tendons (P1) each containing twenty-seven 0.6 in. (15 mm) diameter strands were post-tensioned between the vertically post-tensioned countersigns on the inside of the front wall. Three 47 ft (14 m) long tendons (P3) with 21 -0.6 in. (15 mm) diameter strands were post-tensioned between the two longitudinal stiffeners. Eight 117 ft (36 m) long tendons (P2) each with twenty-seven 0.6 in. (15 mm) diameter strands were post-tensioned between abutments constructed on both sides of the first transverse stiffener behind the front wall. Details of the post-tensioning anchorage in one of these abutments are given in Fig. 15-28. The abutments were connected to both sides of the existing wall by first roughening the contact surfaces and then post-tensioning the abutments through the wall using forty-five 1-3/8 in. (36 mm) diameter Dywidag threaded bars. The post-tensioning force through the thickness of the wall was chosen such that the shear friction capacity was sufficient to clamp the new abutment to the wall in order to resist the post-tensioning force from the main tendons (see Section 9.13). The structure

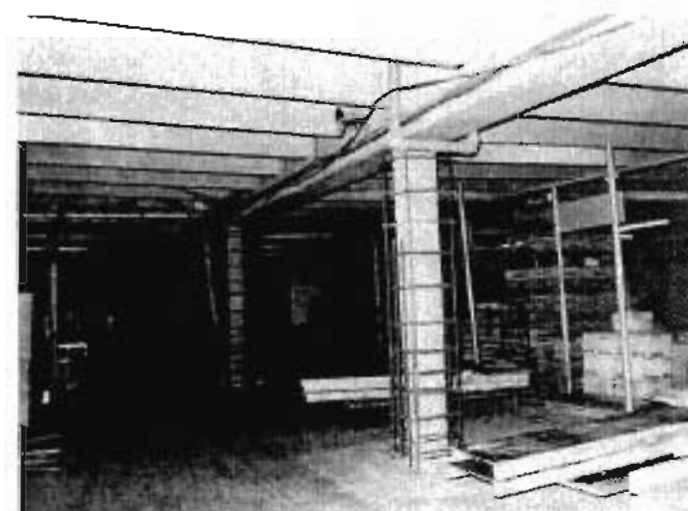


Figure 15-21 Upgrading the seismic resistance of a precast concrete warehouse structure by encasing the central precast columns in reinforced concrete. Adapted from Mitchell, Cook, Eyre, and Maurel (Ref. 15-34).

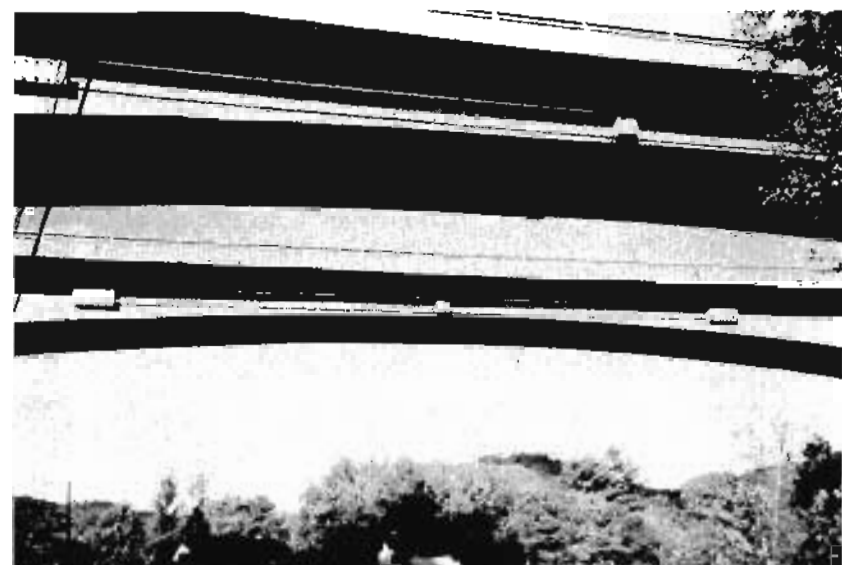
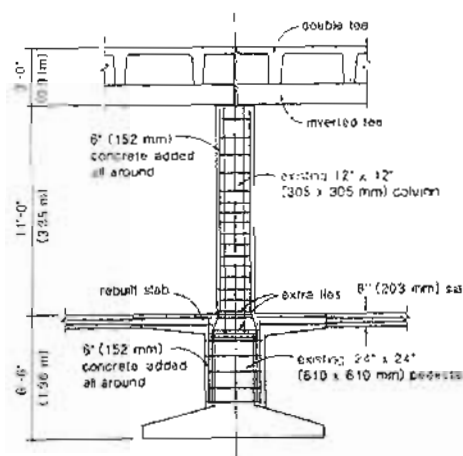


Figure 15-22 Post-tensioned tendons added to an existing bridge.

was completed after the post-tensioning and no cracking was observed in the region of the front wall.

The underpinning of Christ Church Cathedral in Montreal provides a dramatic example of the use of post-tensioning. This church, built in 1859, is a landmark example of Gothic architecture with load-bearing stone walls, a stone tower, a 220 ft (67 m) spire, a timber roof, and stained glass windows. As a part of a large redevelopment project it was decided to construct two underground retail levels and an additional level for a parking garage under the church. The original structure was supported by masonry spread footings on clay and glacial till. Bedrock is about 50 ft (15 m) below grade. The design constraints in choosing a solution for underpinning the 18,000 ton church included the following:

1. Minimize deflections to prevent damage to the masonry structure.
2. Enable the church to remain functional during construction.
3. Provide a maximum column-free space under the church.
4. Provide a structural system that would fit within the 4 to 7 ft (1.2 to 2 m) headroom in the church basement.



(a) End anchorages of external tendons.



(b) Saddles at midspan of beams.

Figure 15-23 Rehabilitation of parking structure through post-tensioning. From Aalami and Swanson (Ref. 15-36).

The solution reported by Dressel, Gallaccio, and Mavaddat (Ref. 15-37) involved the following construction sequence:

1. Twenty-three 36 in. (914 mm) diameter caissons were driven outside the existing masonry strip footings (see Fig. 15-29). An additional ten 26 in. (660 mm) diameter interior caissons were installed for additional support, eight of which were used to

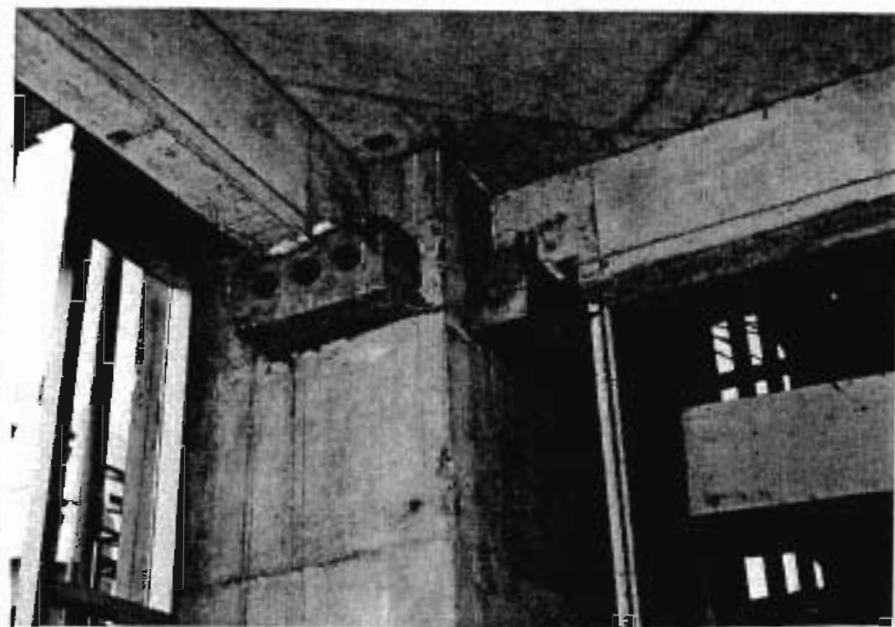


Figure 15-24 Beam seat connected to an existing reinforced concrete column for an expansion of an existing structure.

support the tower and spire. The caissons were socketed into bedrock, reinforced, and filled with concrete.

2. Access openings were made in the perimeter masonry walls.
3. The tendons and non-prestressed reinforcement were placed for the grid of longitudinal and transverse beams in the church basement. The primary 6 ft (1.8 m) deep (E-W) beams are T-shaped in cross section and span 82.5 ft (25.1 m) between the perimeter caissons (see Figs. 15-29 and 15-30). These primary beams support 4 ft (1.2 m) deep beams spanning in the N-S direction.
4. The 2800 yd^3 (2140 m^3) of concrete was pumped in stages into the formwork for the grid of beams. This operation was difficult because of the limited headroom.
5. After sufficient concrete strength was achieved, pairs of 1 in. (25.4 mm) diameter Dywidag bars at 3 ft (0.9 m) centers were post-tensioned transversely through the N-S secondary beams and through the existing masonry walls and piers in order to frictionally grip the masonry elements and permit transfer of the loads through the N-S girders to the primary E-W girders.
6. The N-S girders were post-tensioned and then the E-W girders were post-tensioned.

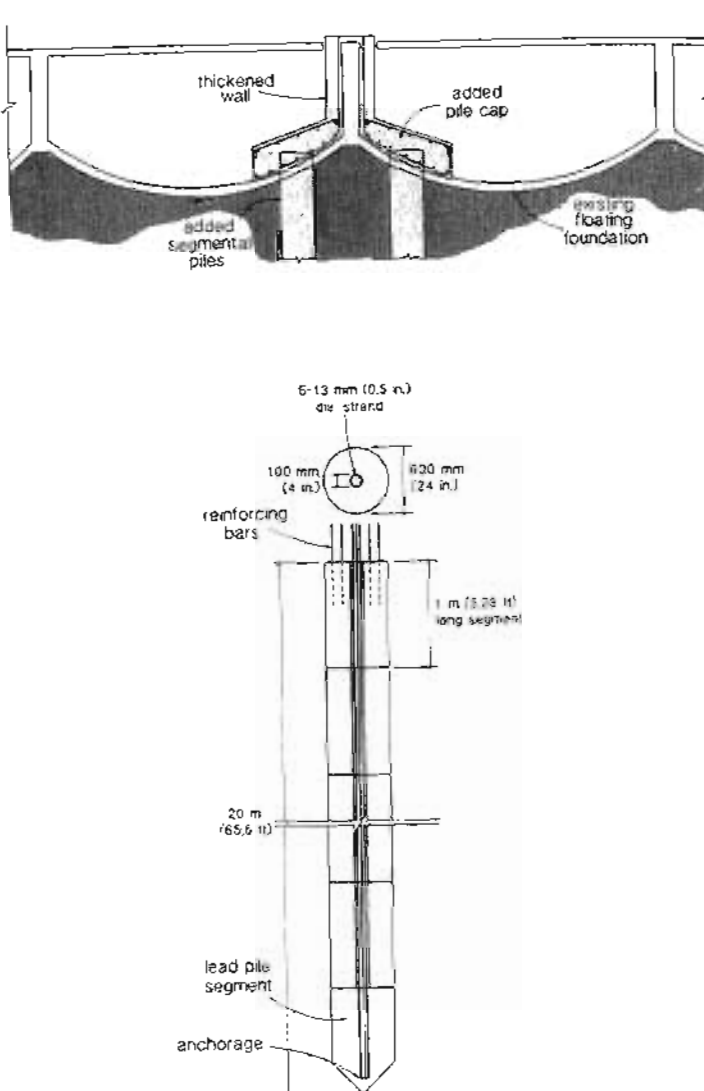


Figure 15-25 Post-tensioned segmental piles used to strengthen an existing floating foundation in Mexico City. Adapted from Mitchell, Dandurand, and Paultre (Ref. 15-33).

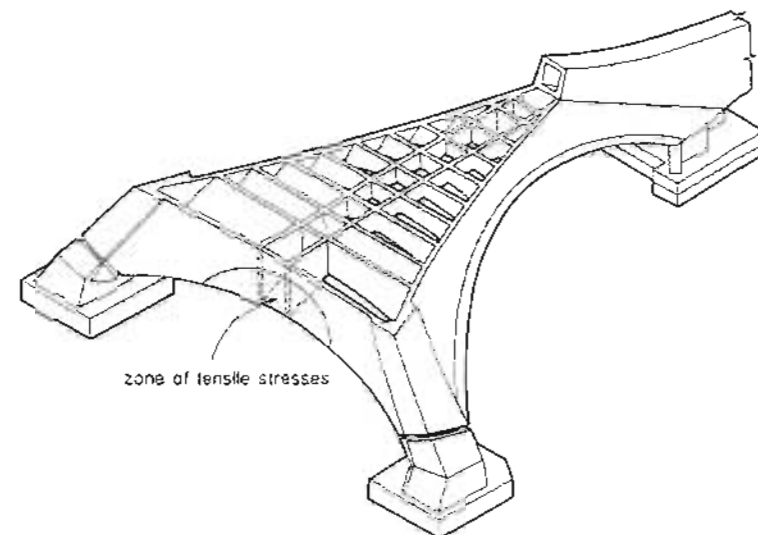


Figure 15-26 Predicted tensile stress region at the bottom of the front wall of the Olympic Tower. Courtesy of LAVALIN.

7. An 8 in. (203 mm) thick slab was placed between the beams after all the post-tensioning was completed in order to minimize the restraint during post-tensioning.
8. The soil under the church was excavated and the masonry footings were removed from the underside of the new foundation. As the excavation proceeded temporary bracing was added to the 50 ft (15 m) high caissons (see Fig. 15-31).
9. The deflections were closely monitored and provisions were made to either increase or decrease the post-tensioning, with the grouting of the post-tensioning ducts delayed for several weeks. The maximum vertical displacement measured was 0.2 in. (5 mm) and no damage was caused to the church.
10. The soil under the tower was carefully excavated and additional post-tensioned beams were constructed to underpin the existing foundations for the 3000 ton spire.
11. After completion of the underpinning the two levels of retail space and parking garage were constructed.

This project is an excellent example of how post-tensioning can be used to actively control load distribution and to resist large applied loads without significant deformation.

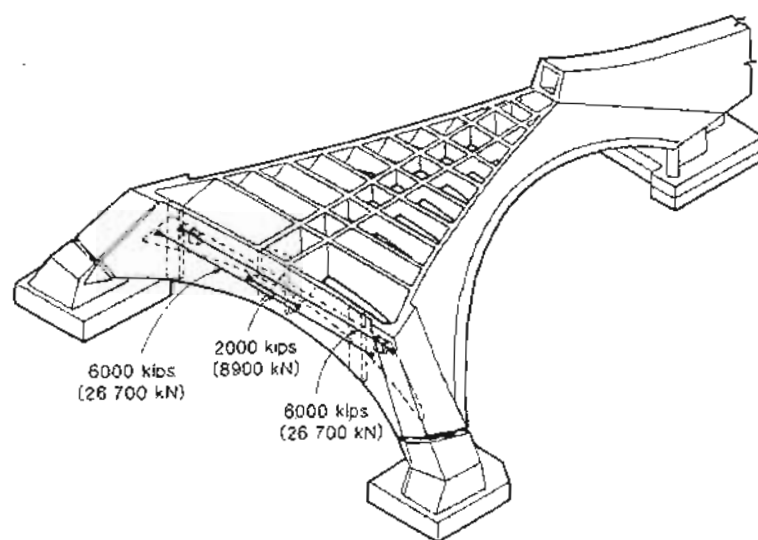


Figure 15-27 Additional post-tensioning tendons used to reduce tensile stresses at base of front wall. Courtesy of LAVALIN.

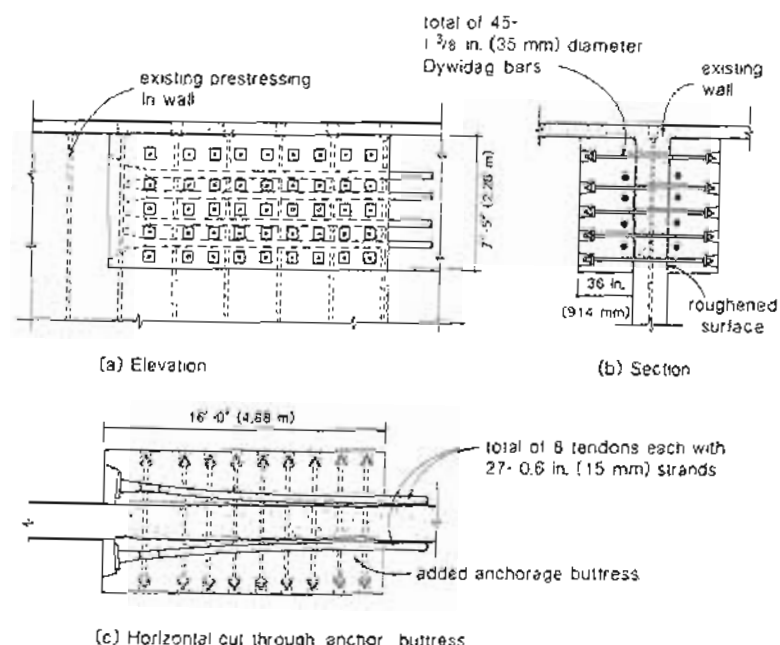


Figure 15-28 Attachment of stressing abutment to stiffener wall for anchorage of additional tendons. Courtesy of LAVALIN.

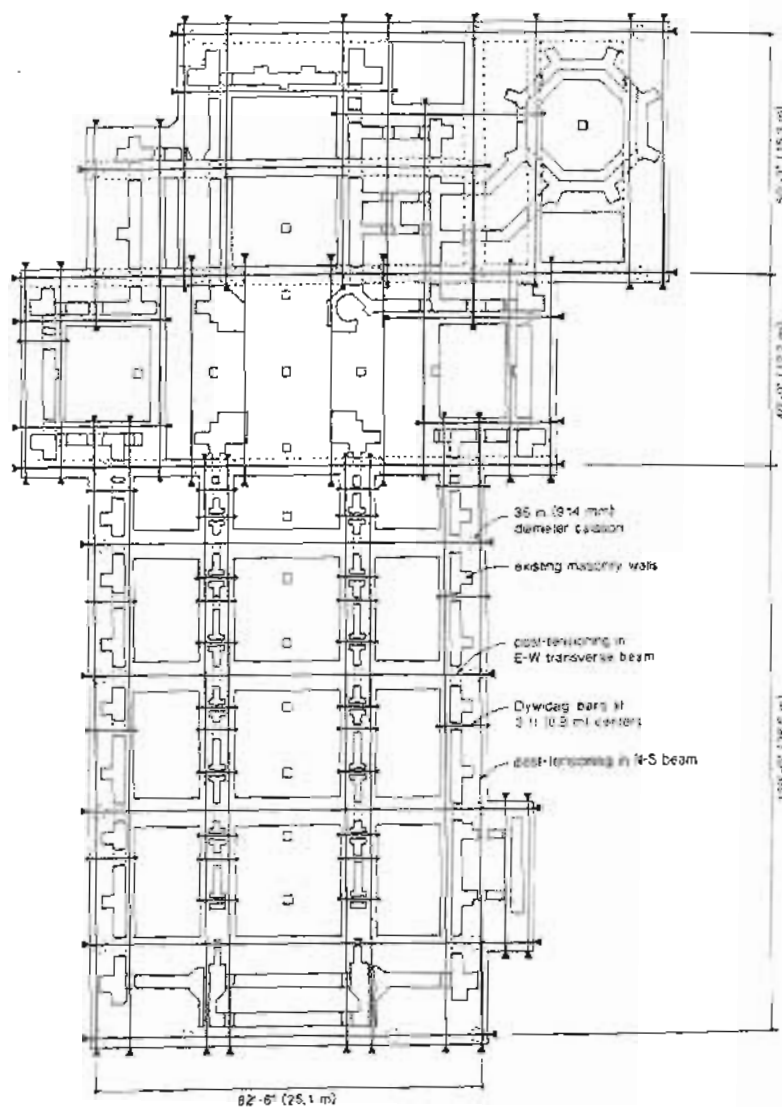


Figure 15-29 Plan view of post-tensioned grid of beams used to underpin Christ Church Cathedral. Information courtesy of Quinn Dressel Associates.

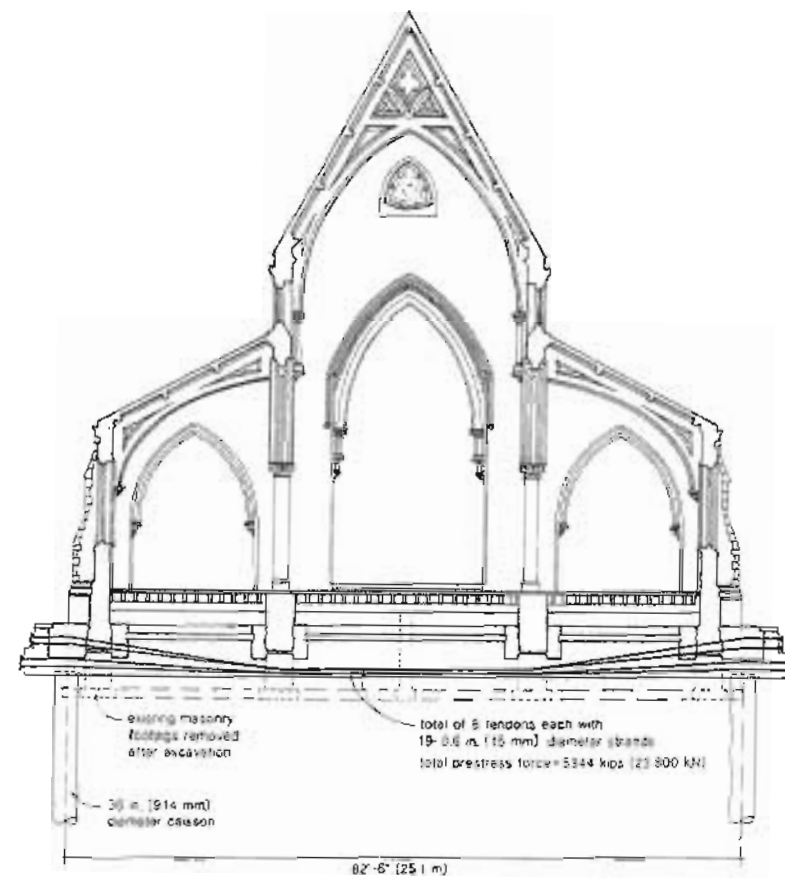


Figure 15-30 Typical post-tensioned primary girder used to underpin Christ Church Cathedral. Information courtesy of Quinn Dressel Associates.

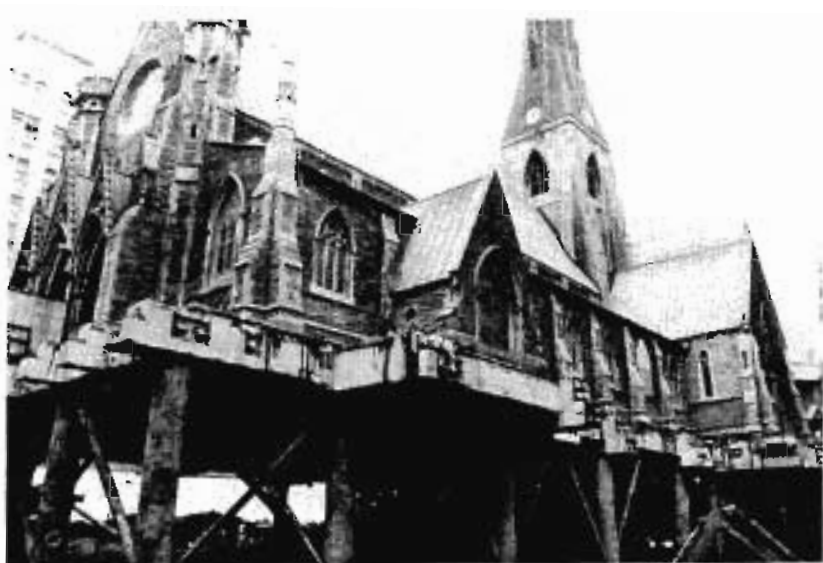


Figure 15-31 Underpinning of Christ Church Cathedral.

References

- 15-1 Bhide, S., and Collins, M.P., "Tension Influence on Shear Capacity of Members," *ACI Structural Journal*, Vol. 86, No. 5, Sept.-Oct. 1989, pp. 570-581.
- 15-2 Lee, Y.M., Mitchell, D., and Harris, P.J., "Lessons from Structural Performance - Slabs Containing Improperly Placed Reinforcing," *Concrete International: Design and Construction*, Vol. 1, No. 6, June 1979, pp. 45-53.
- 15-3 National Bureau of Standards, "Investigation of Construction Failure of Harbour Cay Condominium in Cocoa Beach, Florida," Report No. NBSIR 81-2374, U.S. Department of Commerce, National Bureau of Standards, Washington, D.C., Sept. 1981, 130 pp.
- 15-4 Grieve, R., Slater, W.M., and Rothenburg, L., "Deterioration and Repair of Above Ground Concrete Water Tanks in Ontario, Canada," report to Ontario Ministry of the Environment, Sept. 1987.
- 15-5 CEB General Task Group 19, "Diagnosis and Assessment of Concrete Structures - State-of-the-Art Report," *Bulletin d'Information No. 192*, Comité Euro-International du Béton, Lausanne, Switzerland, Jan. 1989, 120 pp.
- 15-6 American Society for Testing and Materials, "Standard Method of Obtaining and Testing Drilled Cores and Sawed Beams of Concrete," ASTM C42-87, ASTM, Philadelphia, 1988.
- 15-7 American Society for Testing and Materials, "Standard Test Method for Rebound Number of Hardened Concrete," ASTM C805-85, ASTM, Philadelphia, 1988.
- 15-8 American Society for Testing and Materials, "Standard Test Method for Penetration Resistance of Hardened Concrete," ASTM C803-82, ASTM, Philadelphia, 1988.
- 15-9 American Society for Testing and Materials, "Standard Test Method for Pullout Strength of Hardened Concrete," ASTM C900-87, ASTM, Philadelphia, 1988.
- 15-10 Chabowski, A.J., and Bryden-Smith, D.W., "A Simple Pull-Out Test to Assess the Strength of In-situ Concrete," Current Paper CP25/77, Building Research Establishment, London, June 1977.
- 15-11 Johansen, R., "In Situ Strength Evaluation of Concrete - The 'Break-Off' Method," *Concrete International: Design and Construction*, Vol. 1, No. 9, Sept. 1979, pp. 45-51.
- 15-12 American Society for Testing and Materials, "Standard Test Method for Pulse Velocity through Concrete," ASTM C597-83, ASTM, Philadelphia, 1988.
- 15-13 Taylor Woodrow Research Laboratories, "Marine Durability Survey of the Tongue Sands Tower," published for Concrete in the Oceans Management Committee by the Cement and Concrete Association, Wexham Springs, UK, 1980.
- 15-14 British Standards Institute, "Recommendations on the Use of Electromagnetic Covermeters," BS 1881 : Part 204, BSI, London, 1988.
- 15-15 British Standards Institute, "Recommendations for Radiography of Concrete," BS 1881 : Part 205, BSI, London, 1986.
- 15-16 American Society for Testing and Materials, "Standard Test Method for Specific Gravity, Absorption, and Voids in Hardened Concrete," ASTM C642-82, ASTM, Philadelphia, 1988.
- 15-17 Figg, J.W., "Methods of Measuring Air and Water Permeability of Concrete," *Magazine of Concrete Research*, Vol. 25, No. 85, Dec. 1973, pp. 213-219.
- 15-18 American Society for Testing and Materials, "Standard Practice for Microscopical Determination of Air-Void Content and Parameters of the Air-Void System in Hardened Concrete," ASTM C457-82a, ASTM, Philadelphia, 1988.

- 15-19 American Society for Testing and Materials, "Cement Content of Hardened Portland Cement Concrete," ASTM C85-66 (reapproved 1973), ASTM, Philadelphia, 1988.
- 15-20 British Standards Institute, "Analysis of Hardened Concrete," BS 1881, Part 6, BSI, London, 1971.
- 15-21 American Association of State Highway and Transportation Officials, "Sampling and Testing for Total Chloride Ion in Concrete Raw Materials," AASHTO T260-84, AASHTO, Washington, D.C., 1984.
- 15-22 Browne, R.D., and Geoghegan, M.P., "The Corrosion of Concrete Marine Structures: The Present Situation," *Society of Chemical Industry's Symposium "Corrosion of Steel Reinforcement in Concrete Construction,"* London, Feb. 1978.
- 15-23 Building Research Establishment, "The Durability of Steel in Concrete: Part 2 - Diagnosis and Assessment of Corrosion-Cracked Concrete," Digest 264, Building Research Establishment, London, Aug. 1982.
- 15-24 International Union of Testing and Research Laboratories on Materials and Structures, RILEM CPC-18, Paris.
- 15-25 American Society for Testing and Materials, "Standard Test Method for Half-Cell Potentials of Uncoated Reinforcing Steel in Concrete," ASTM C876-87, ASTM, Philadelphia, 1988.
- 15-26 Van Daveer, J.R., "Techniques for Evaluating Reinforced Concrete Bridge Decks," *ACI Journal*, Vol. 72, No. 12, Dec. 1975, pp. 697-704.
- 15-27 Leonhardt, F., "Crack Control in Concrete Structures," IABSE Surveys, No. S-4/77, International Association of Bridge and Structural Engineering, Zurich, 1977, 26 pp.
- 15-28 ACI Committee 234, "Control of Cracking in Concrete Structures," ACI 224R-80 (revised 1984), American Concrete Institute, Detroit, 1984.
- 15-29 Schlaich, J., Schäfer, K., and Jennewein, M., "Towards a Consistent Design of Reinforced Concrete Structures," *PCI Journal*, Vol. 32, No. 3, May-June 1987, pp. 74-150.
- 15-30 Park, R., and Paulay, T., *Reinforced Concrete Structures*, Wiley-Interscience, New York, 1975, 769 pp.
- 15-31 Hom, S., and Kost, G., "Investigation and Repair of Post-Tensioned Concrete Slabs - A Case History," *Concrete International: Design and Construction*, Vol. 5, No. 7, July 1983, pp. 44-49.
- 15-32 Tighe, M.R., and Van Volkinburg, D., "Parking Garage Crisis," *Civil Engineering*, Vol. 59, No. 9 Sept. 1989, pp. 70-73.
- 15-33 Mitchell, D., Dandurand, A., and Paultre, P., "Repair and Upgrading of Concrete Structures in Mexico City after the 1985 Earthquake," *Canadian Journal of Civil Engineering*, Vol. 15, No. 6, Dec. 1988, pp. 1052-1066.
- 15-34 Mitchell, D., Cook, W.D., Eyre, D.G., and Maurel, G., "Evaluation and Strengthening of Large Precast Concrete Warehouse Structure," *Journal of Performance of Constructed Facilities*, Vol. 4, No. 2, May 1990, pp. 70-87.
- 15-35 Aeberhard, H.U., Buerki, P., Gunz, H.R., Mari, P., Matt, P., and Sieber, T., "External Post-Tensioning," VSL International Ltd., Berne, Switzerland, 25 pp.
- 15-36 Aslam, B.O., and Swanson, D.T., "Innovative Rehabilitation of a Parking Structure," *Concrete International: Design and Construction*, Vol. 10, No. 2, Feb. 1988, pp. 30-35.
- 15-37 Dressel, D.J., Gallaccio, J., and Mavaddat, S., "The Church on Stilts," *Civil Engineering*, Vol. 59, No. 5, May 1989, pp. 72-74.

Appendix A

Computer Program RESPONSE

A.1 INTRODUCTION

Program RESPONSE can be used to determine the load-deformation response of a prestressed concrete cross section subject to moment, axial load, and shear. Because RESPONSE was written to be user friendly and to facilitate many different ways of analyzing concrete sections it is a relatively large program consisting of about 10,000 lines of code compiled using TURBO C (TM Borland).

RESPONSE is written for the IBM personal computer or compatibles. It was compiled to run with or without a mathematical coprocessor. However, the use of a machine with a coprocessor is strongly recommended. Due to the amount of computation involved, RESPONSE will crawl on a XT or PC, walk at a brisk pace on an AT, and sprint on a 386 machine.

RESPONSE graphics will run with a CGA, EGA, VGA, or Hercules graphics card (for more information see Section A.8.5).

Some of the input and display routines use modified Borland INT'L subroutines. Borland's permission to use these routines is gratefully acknowledged.

In this appendix, anything that the user must type to install or run the program is printed in *italics* and enclosed in double quotes (""). Do not type the quotation marks.

A.2 DISCLAIMER

Program RESPONSE was written to help students develop an understanding of the response of prestressed concrete. We do not claim that RESPONSE is appropriate for anything besides educational purposes – if you think it is, great, but it is your decision. No guarantees

or warranties are made for the correctness or accuracy of any of the answers obtained using RESPONSE. The developers and distributors of RESPONSE are not liable or responsible for any losses occurring to the user due to the use of results produced by the program.

A.3 INSTALLING RESPONSE

RESPONSE consists of the following program files: RESPONSE.EXE, RESPONSE.KIZ, RESPHELP.EXE, and RESPONSE.HLP. In addition, several sample data files are included with the program. These are ST59, ST510, ST517, CF1, BOX, BOXTEMP, PANEL-LT, and PANEL-ST. The distribution diskette is a 5.25 in., 1.2 megabyte, MS DOS format floppy diskette. If your particular computer does not have a 5.25 in. high-capacity floppy disk drive, you must use a system with the appropriate combination of input-output devices to transfer the necessary files to the storage medium that is appropriate to your system.

Program RESPONSE should be installed on a hard disk, however it can run off a floppy disk. For the program to run, all of the program files listed above must be stored in a single directory.

To install program RESPONSE on a hard drive, simply copy the program files (and the data files, if you wish) from the distribution disk to the directory of your choice on the hard drive. For example, if you wished to run program RESPONSE from a yet-to-be-created subdirectory called ANALYSIS in the root directory of drive C:, with the distribution disk in floppy drive A:, you might enter the following commands at the DOS prompt:

```
C:> "c"
C:> "cd \"
C:> "md analysis"
C:> "cd analysis"
C:> "copy a:r>.*"
C:> "copy a:st>."
C:> "copy a:c>."
C:> "copy a:b>."
C:> "copy a:p>."
C:> "response"
```

If necessary, consult your DOS manual for further details on creating subdirectories and copying files.

A.4 DEFINITION OF TERMS

In this appendix, the following terminology is used.

Cell	A cell is the place where a parameter for the cross-sectional data can be entered.
Active-Cell	The active cell is the cell which is currently highlighted. To change the active cell use the cursor keys. Note: Only the cells which contain input parameters can be activated.
Data-Editing Spreadsheet	The part of the screen which is used for creating new or editing old section data.
Section-Data	All the parameters used to define the section geometry, the material properties and thermal shrinkage and initial strains are referred to as section data.

A.5 HELP

Short explanatory help messages are available when data is entered. To get help on a specific parameter simply make the cell containing the parameter active and then press "F1". The screen now displays a help message which should clarify what the parameter is used for. To remove the help screen from the screen press "Esc".

A.6 TAKING A TEST DRIVE

In this section you will be taken on a series of short test drives to become familiar with the capabilities of the program. RESPONSE is an interactive, menu-driven program. Simply follow the instructions below and you will be introduced to the features of RESPONSE. The program has to be installed before you go for this spin.

A.6.1 Test Drive Part 1: Moment-Curvature Response

1. Start up the program by typing and entering "response".
2. Once the screen displays the response logo hit any key to continue.
3. The program now displays the data-editing spreadsheet. The main menu is displayed on the first two lines of the screen. The first line of the menu shows all the options that are available; the second line explains the option in a little more detail. If this is the first time you are running RESPONSE on your computer then the graphics card of your system has to be specified. To do this select "Configure" from the menu by pressing "c".
4. The configuration menu is now displayed. Select "Graphics_Driver" from the menu by pressing "g".
5. Now select the driver applicable to your system by pressing the first letter of the option. (For more information on which option to select, refer to Section A.8.5.)

6. To save the selected graphics driver permanently press "c" and then press "u" to select "Update".
7. Now that the graphics driver has been specified you can begin to use the program. For this test drive you will load a cross section created previously. Select the "Load" option by pressing the right cursor key until the option is highlighted and then press "Enter".
8. You are now asked to type in the name of the data file which you wish to load. Type and enter "sl59". This is the single-tee beam which is described in Section 5.9 of the text.
9. Once the file is loaded, the spreadsheet will display some of the data which describes the section. To browse through the remainder of the data file select "Edit" from the main menu by pressing "e".
10. The cursor is now in the data-editing spreadsheet and can be moved around using the cursor keys. Try this and you will notice that the cursor can only be moved to certain positions. In addition, there is now a bar displayed at the bottom of the screen indicating specific uses for designated function keys. Try to produce a plot of the section by pressing "F9".
11. If your screen now displays a cross-sectional plot the correct graphics driver is installed. If the program terminated, restart and either try a different graphics driver or specify no graphics.
The current plot shows most of the data describing the cross section. This plot can be displayed at any time during the editing of a cross section.
The current plot shows the concrete T-section comprised of five trapezoidal layers. Four of these layers are shaded with diagonal lines and the bottom of the stem is shaded solid. The different shadings are used to distinguish the portion of the section participating in tension stiffening. To the right of the concrete section the location of the prestressing tendons is indicated. Press any key to return to the data-editing spreadsheet.
12. The cross-section plot indicated that different types of concrete were used to represent the concrete section. These different types of concrete are defined near the top of the section data. To view the stress-strain curves for the different concrete types press "F8". The screen now displays the concrete stress-strain relationship for the first concrete type. Hit any key and the plot for the next concrete type will be displayed. If no more concrete types are specified then the data-editing spreadsheet will return.
13. Now let's change some of the dimensions of the cross sections to see what happens to the section. Find the line on the data-editing spreadsheet which reads "Number of Concrete Layers (1-20):" Change this number from 5 to "6".
14. The number of concrete layers described below this line has increased by one. Concrete layer number six was added to the existing five layers. Move the cursor down to concrete layer number six and you can see that the program used the following defaults. It was assumed that layer six starts at the height where layer number five stopped and layer number six was assumed to be as wide as layer number five. The height of the sixth layer was assumed to be the lesser of the height of layer number five or the distance remaining to the top of the section. For the current section the

- default height was 0. Now, to create a wider stem at the bottom of the section change the parameters describing layer number six to the following (to change data overwrite the existing value, press "Enter" and then use the cursor key to move to the next cell): $y = 0$, bottom width = 6, top width = 6, height = 6.
15. After adding layer number six let's look at the section again by pressing "F9". Layer number six is displayed at the bottom of the section and it is assumed to be of the same concrete type as the flange. Note that the layer was split into two because it interfered with the stem.
 16. To remove layer number six change the "Number of Concrete Layers" back to five by entering "5" as the number of concrete layers. Now if you press "F9" you should see the original T-section.
 17. At this point we will leave the data-editing spreadsheet and return to the main menu. Press "F10" to bring up the main menu.
 18. To help you become familiar with some of the analysis options the next steps will guide you through the procedure involved in calculating the moment-curvature response.
To perform an analysis on section sl59 select "Analyze" from the main menu by pressing "a".
To perform a flexural analysis select "Moment & Axial-Load" by pressing "m". Next select the "Constant-Axial-Load" option by pressing "c".
 19. Now the program prompts you for an axial load. Simply press "Enter" to accept the default value of zero axial load. The next prompt asks whether or not to account for tension stiffening. The default assumes that you do not. To account for tension stiffening you must press "y" and then press "Enter".
 20. From the next menu select "Full-Response" by pressing "f". At this stage RESPONSE begins to calculate points for the moment-curvature response. The top of the screen displays the following information: name of the section, axial load, the Concrete Model used, whether Tension Stiffening is accounted for, whether the material properties are factored or not, and the degree of convergence desired for the results.
The next two lines serve as headings for the data points being calculated below.
The last line on the screen displays a number that is constantly changing. This number determines how close the current iteration is to converging. The iteration is considered to have converged once the number is less than 1.
 21. Once the program has calculated several points press "F9". Now the Stresses and Strains plot is displayed for the last successfully calculated data point. Press any key to return to the calculations.
 22. The calculation of data points can be interrupted any time by pressing "Esc". Once you have pressed "Esc" the menu at the top displays "Continue Stop Plot". Press "p" to select "Plot" and the screen will display the moment-curvature response of the section for the points calculated so far. Press any key to return to the menu. Select "c" to continue the calculations.
 23. While the program continues calculating data points you can repeat steps 21 and 22 as often as you wish. Depending on the speed of your computer the calculation of

- the full response can take a while, so lets stop at this point by pressing "Esc" and then selecting "Stop" by pressing "s". Now the "View Save Finer Plot Quit" menu appears.
24. Select "View" from this menu by pressing "v". The program now displays all the data points calculated so far. Use the cursor keys to scroll through the data points. To plot the stress and strain distributions for the highlighted data point press "F9". Hit any key to return to the display of data points. To exit this option press "Esc".
 25. To save the data points calculated so far select "Save" by pressing "s". The program will now prompt you for a file name. Enter "Trial1". The file is saved to disk with the extension ".NM". Had the file TRIAL1.NM existed previously the program would have prompted you whether you wanted to overwrite it or not.
 26. Now you have produced part of a moment-curvature response and it is time to try one of the other options of the "Moment&Axial-Load" analysis option. To get to these options press "q" to select "Quit".
 27. If you are by now exhausted and wish to exit the test drive press "q" three times and then press "r" and then press "n". Otherwise continue to part two of this test drive.

A.6.2 Test Drive Part 2: Other Flexural Analyses

In this part of the test drive you will become acquainted with more of the analysis options of RESPONSE. You are expected to have completed Part 1 successfully and from now on you are expected to know how to select menu items, display graphs, and scroll through data records.

0. If you have exited the program after Part 1 start the program and load the section st59. Next select "Analyze" and then select "Moment & Axial-Load".
1. The next type of analysis you will perform is finding the moment and axial load required to produce a given linear strain distribution. This type of analysis is called "Two-Strain". Select "Two-Strain" and you will be prompted to specify the location and magnitude of two strains within the section. For this example we will select a strain at the lowest tendon which is just past rupture and a strain at the top which gives an axial load of zero.
2. At the first prompt enter "2." (the distance from the bottom to the first tendon) then enter "33.11". Next accept the default value of "36" by pressing "Enter" and then enter a strain of "-1.748" (you will calculate this strain later). Then select no tension stiffening, "N".
3. Now the screen displays the computed moments and curvatures and strains for the section. To view the stresses and strains acting on the section press "F9". Note that the plot on the left of the screen displays the strain caused by stress in the concrete and for the seven tendons (small rectangles). The lowest tendon is strained to 40.01 millistrain, implying that the tendon is ruptured (rupture strain for the tendon was specified as 40 millistrain). To return to the menu hit any key. Now the "Next Save View Quit" menu is activated. The option "Next" allows you to perform another "Two-Strain" analysis. The "Save" and "View" options work as outlined in Part 1. Select "Quit" to get back to the flexural analysis menu.

4. In step 2 you used a concrete strain of -1.748 millistrain at the top of the section to obtain zero axial load when the first tendon ruptures. This strain can be calculated using a different analysis routine. Select "Constant-Axial-Load" to calculate this strain. Choose an axial load of zero and do not account for tension stiffening. Now select "Specified-Strain".
5. This routine allows you to specify the axial load and one strain anywhere within the section. Choose a strain location of 2 in. from the bottom and then specify a strain of 33.11 millistrain (tendon rupture). Once you specify the strain the program begins to iterate until it finds the corresponding strain distribution and then it displays the result. Observe that the strain at the top is -1.748 millistrain, provided that the program is operating with the "high-strength" concrete model. Hit any key to return to the menu.
6. This same analysis routine can be used to find the point at which the section cracks at the bottom. To calculate the cracking moment select "Next" from the menu. Then specify 0 in. as the location of the strain and specify the cracking strain of 0.078 millistrain.
7. Once the program has converged on the answer it will display a cracking moment of 866 ft-kip. Hit any key to return to the menu and select "View". Now you can use the cursor keys to highlight a data record and then use the "F9" key to look at the stress distributions. Press "Esc" to return to the previous menu. Then select "Quit" to return to the flexural analysis menu.
8. Now that you have performed a few analyses you are developing a feel for the capacity of this particular section. One of the options of this program can be used to quickly determine estimates of the section capacities. To perform this analysis return to the main analysis menu by selecting "Quit". Now select "Rough-Capacities".
9. The Rough-Capacities option calculates the axial loads for two uniform strain distributions. The compressive capacity is assumed to occur when the section is subject to a uniform strain equivalent to ϵ'_c , and the tensile capacity is assumed to occur when the section is subject to a uniform tensile strain of 2 millistrains. The positive and negative flexural capacities are estimated to occur when the top and bottom strains respectively are equal to ϵ'_f . If no solution can be reached for an assumed value of ϵ'_f , then after 50 iterations the strain at the top or bottom will be assumed half of ϵ'_f . You will notice that in this example the positive moment capacity occurs at -1.0 millistrain ($\epsilon'_f/2$). The program will remember these capacities until you leave the analysis menu. To get back to the menu hit any key.
10. The next analysis type you will be exposed to is the "Fixed-M&N" analysis. Select "Moment & Axial-Load" again from the menu and then select "Fixed-M&N". This analysis is used to find the strain conditions for a given loading condition. To specify a compressive load of 100 kips enter "-100" as an axial load and then enter a moment of "950" ft-kip. Specify no tension stiffening and then you will see that the program begins to iterate on the answer. Once the answer has been found you can see that for the given loading the strain at the top of the section is -0.392 millistrain and the strain at the bottom of the section is 0.225 millistrain. Hit any key and you will get to the, by now familiar, "Next Save View Quit" menu. Using the "Next" option try

a few more load cases if you wish. Select "Quit" three times to return to the main menu.

11. You have now covered most of the flexural analysis features of the program and in the next part of the test drive you will be introduced to the shear analysis features of the program. Exit from the program by selecting "Quit" from the main menu. Select "Terminate" to confirm your choice and then press "n" (since you do not want to save changes at this stage). Now the program has terminated.

A.6.3 Test Drive Part 3: Shear and Axial Load Analysis

In this part of the test drive you will analyze a section under the influence of axial load and shear. The section which will be analyzed is a hollow prestressed rectangular beam. As before, follow the steps outlined below.

1. The next section that you want to work with is called CF1. To start the program type and enter "response CF1". Once the logo is displayed hit any key. You will notice that the program automatically loads the section called CF1. To see what this section looks like select "Edit" and then press "F9".
2. The section displayed looks like an I-section and not a hollow rectangular section as promised above. This is due to the fact that the program treats all sections as being singly symmetric, and for the purpose of shear and flexural analysis (for the axis of concern) an I-section and a hollow rectangular section are equivalent. The area of concrete used for the shear analysis is shown as a rectangle (dotted line). As before the arrangement of reinforcing bars and tendons is shown on either side of the cross section. Hit any key to return to the data-editing spreadsheet.
3. Press "F10" to activate the main menu. The previous analysis was carried out using the stress-strain relationship for high-strength concrete. At this point you will change the concrete model to the parabolic stress-strain relationship. The concrete model is specified under the "Configure" option. Press "l" for "Configure" and then press "c" for "Concrete-Model". Now select "Parabolic". After you make the selection the main menu is displayed again.
4. Select "Analyze" from the main menu and then select "Rough-Capacities". You will notice that the program calculates the axial and flexural capacities as before. In addition the shear at cracking and the shear at a principal tensile strain of 5 millistrain will be calculated. Once all these capacities have been calculated press any key.
5. Now to perform an analysis involving shear and axial load select "Shear & Axial-Load". The analysis options available at this stage are similar to those for flexural analyses. Since you have already tried an analysis involving "Constant-Axial-Load" in a previous test drive, please select "Ratio-dN/dV" now. This option is used to analyze sections where the magnitude of the axial load is related to the magnitude of the shear. To define the relation between axial load and shear, you have to specify the axial-load at zero shear, and then you need to specify the ratio dN/dV. For this example analysis specify an axial load at zero shear of "-100" and a ratio dN/dV of "-1". From the next menu select "Full-Response". Now the program calculates shears corresponding to certain values of principal strain. At any time

during these calculations you can interrupt the iteration as outlined in steps 21 and 22 of Section A.6.1. Once the calculations are complete hit any key to continue.

6. Select "Plot" to view the following plots: Shear vs. Principal Tensile Strain, Shear vs. Transverse Strain, Shear vs. Shear Strain, and Shear vs. Theta. To proceed from one plot to the next hit any key.
7. The next feature of the program you will try is the "Finer" option. This option was designed to allow you to specify how many points you want calculated. Select "Finer" and a default of 10 points will be displayed. Enter "/100" as the number of points to be calculated. Next the default for the maximum tensile strain will be displayed as 40 millistrain. Change this number to "6" and press Enter. Then the program will increment the principal tensile strain (ϵ_1) in increments not exceeding 0.06 up to a value of 6 millistrain. Once a few points have been calculated you can either interrupt this process or you can wait for the program to calculate all points. Then return to the menu.
8. Select "Quit" and then select "Fixed-N&V" from the menu. This option will be used to find the strain state for a specific combination of shear and axial load. Specify an axial load of "-100" and a shear force of "100". The program will now determine the biaxial strain state. For this load combination the angle "theta" is 23.00 and the principal tensile strain is 1.38 millistrain. Once the program has converged on the answer hit any key to return to the menu. Press "v" to view the results and then press "F9" to display the, by now familiar, stresses and strains plot. Press any key and a plot displaying the biaxial stresses and strains will appear. For more information on this plot, refer to Section A.11.4.
9. By now you have been introduced to the main features of the shear analysis routine. The remaining features are similar to those outlined in Parts 1 and 2.

A.6.4 Test Drive Part 4: Shear, Axial Load, and Moment

The remaining type of analysis considers the influence of moment, axial load, and shear on the section. In this portion of the test drive you will determine the full response for a section subject to a given ratio of moment to shear and a given ratio of shear to axial load. As before, follow the steps outlined below.

0. If you exited the program after the last portion of the test drive then follow the first three steps of Section A.6.3. Once you have loaded section CF1 and you have changed the concrete model to "Parabolic" then proceed with the next steps.
1. Select the "All-Loads" analysis and then select "Ratio-M&N&V". Now you have to specify the relationship between shear, axial load, and moment. For this type of analysis the shear is the independent load and the axial load and the moment are both functions of the shear.

$$\text{Axial Load} = (\text{axial load at zero shear}) + dN/dV \cdot \text{shear}$$

$$\text{Moment} = (\text{moment at zero shear}) + dM/dV \cdot \text{shear}$$
To analyze the section subject to a given load combination enter the following: Axial Load at zero shear = "-50", Ratio dN/dV = "-1", Moment at zero shear = "0", and Ratio dM/dV = "3" ft.

2. Select "Full-Response" and the program will slowly calculate data points. The numbers shown on the bottom line of the screen represent the progress of the iteration. The first number is an indicator for convergence on the axial load and the second number is an indicator for convergence on the moment. Notice that the axial load and the moment are related to the shear as specified by the above-mentioned relationship. Once RESPONSE has calculated several points press "Esc" and then select "Plot". You will now be able to see the following plots: Moment vs. Curvature, Moment vs. Principal Tensile Strain, Shear vs. Principal Tensile Strain, Shear vs. Transverse Strain, Shear vs. Shear Strain, Shear vs. Theta, Axial Load vs. Principal Tensile Strain, and Axial Load vs. Longitudinal Strain. To proceed from one plot to the next hit any key.
 3. You may now decide to "Continue" or to "Stop" the iterations.
 4. After returning to the "All-Loads" menu select "Fixed-N&M&V". Specify the following load combination: Axial Load = "-100", Moment = "100", and Shear = "100".
- After several iterations RESPONSE converges. Again, the numbers at the bottom of the screen are convergence indicators, this time for shear, axial load, and moment. The screen now displays that the specified loading causes a principal tensile strain (ϵ_1) of 1.45 millistrain and a longitudinal strain (ϵ_x) of -0.31 millistrain.
5. Now you have used two of the main features of the "All-Loads" option and hence have concluded this portion of the test drive.

A.6.5 Test Drive Part 5: Thermal Strains

By now you have explored many of the options available in RESPONSE. The next type of analysis you will perform is the flexural analysis of a section which is subject to nonuniform thermal strains. The file for this section is called BOXTEMP. The section and the temperature distribution are described in detail in Section 5.18 of the textbook. By now you are assumed to be quite familiar with the menus of RESPONSE and the instructions will become less detailed to avoid boring you with things you already know.

Follow the steps outlined below and you will become familiar with the features included in RESPONSE to deal with thermal strains.

1. Start the program by entering "response BOXTEMP". As discussed previously the program automatically loads the section. For this analysis you will again use the "High-Strength" concrete model so use the "Configure" option to change the concrete model.
2. To see what this section looks like select "Edit" and then press "F9". You will notice that this box girder is again displayed as an I-section. The geometry of this section could be described using four trapezoidal layers, however, the section is defined using 11 layers. The larger number of layers is necessary to accurately represent the thermal strain distribution on the section.

To see the distribution of thermal strains hit any key. Now the "Shrinkage Thermal and Initial Strains" plot is displayed on screen. You can see a distribution of thermal strains at the top of the section with a peak value of 0.348 millistrain. At the bottom of the section a small thermal strain is specified for both the concrete and the tendons.

Sec. A.6 Taking a Test Drive

3. Using the cursor keys scroll down the screen to display the thermal strains which were entered for each layer. The thermal strains are specified at the bottom, middle, and top of each layer.
4. To investigate the stress distribution across the section at a constant strain of zero millistrain you will perform a "Two-Strain" analysis. For this analysis specify a strain of "0.0" millistrain at the bottom of the section and a strain of "0.0" millistrain at the top of the section (120 in. from the bottom). Select no tension stiffening. Once the program displays the results press "F9" for a plot of the stresses and strains. On this plot you will notice that the top of the strains plot shows two lines. One line (yellow) for the imposed strain distribution (zero curvature and zero axial strain) and another line (blue) for the strains causing stress in the concrete.
5. Next you will try to find the moment at which the concrete near the top of the section cracks. To find the cracking strain of the concrete return to the data-editing spreadsheet and press "F8". From the information at the top of this plot you can see that the cracking strain is 0.073 millistrain. Now perform a "Moment & Axial Load" analysis for a constant axial load of zero and don't account for tension stiffening. Specify the strain at the top of the section (120 in. from the bottom) to be 0.07 millistrain (slightly less than cracking). Once the program has converged on the axial load press any key and select "View" and then press "F9".
6. You will notice that while the moment is 33,203 ft-kips, none of the concrete is in tension. The vertical line represents zero stress and tension is to the right of this line. So we will have to try another strain at the top of the section. Using the "Next" option specify a strain of 0.418 millistrain (0.348 + 0.07) at the top. Again use the "View" option to look at the stress distribution and you will notice that the top fiber of the section is not cracked, however, the area immediately below is cracked due to the influence of thermal strains. Hence, for this moment of 1451 ft-kips the section is cracked.
7. By trial and error you can find that the strain in the top fiber which just causes cracking is approximately 0.232 millistrain. If you perform the analysis with this top strain you will notice that the section first cracks at a location about one-eighth of the way down from the top of the section. Thus, for moments less than about 4130 ft-kips, the concrete will be cracked near the top of the section.

A.6.6 Test Drive Part 6: Entering New Sections

After completing the previous portions of the test drive you are familiar with the program's analysis features. All these analyses were performed on cross sections which were provided with the program. In this portion you will create a section from scratch. The section which you will create is described in Problem 5-11 of the text book.

Before a new section is entered it is very useful to make a dimensioned sketch of the cross section and to work out all the material properties in advance so the information can be entered continuously.

To create a new section data file follow the steps outlined below.

1. Select "New" from the main menu by typing "n". If a section is currently loaded and has been changed the question "Save current DATA file (Y/N)?" will appear.

Select "No" by typing "n" if you do not want to save the current section otherwise select "Yes" by typing "y" and then specify a file name for the section data.

2. Now the data-editing spreadsheet displays the section data header, and the cell containing the section name is active. Enter a descriptive name such as "Prob 5-11" for the section in this cell. Then move to the cell below and specify that you want to use U.S. Customary units by entering "u". Once you have specified the units, You will notice that the program automatically displays default values for most parameters.
3. Now edit the concrete properties to reflect the properties of the section. Change the following parameters: $f'_c = "7120"$, $c'_c = "0"$, (if "0" is entered the program will estimate c'_c), and $f_{cr} = "338"$. Once these three parameters have been changed press "F8" to view the material properties for the concrete.
4. Next change the number of tendon types from 0 to "1" and then change the Ramberg-Osgood parameters to $A = "0.02"$, $B = "103"$, and $C = "7.3"$. Also change E to "27850" and f_{pu} to "283".
5. Now enter a height of section of "18" in. and then specify a distance to moment axis of "9". Since this section will not be analyzed considering the effects of shear you don't have to change the "N".
6. The geometry of this section (Fig. 5-76 of the textbook) can be described using five trapezoids. You will be building up the section layer by layer so change the following parameters for the first layer: bottom width = "9", top width = "9", and height = "3".
- Now change the number of concrete layers to "2".
7. Change the top width of the second layer to "3" and change the height of the layer to "2". Then change the number of concrete layers to "3". Now change the height of the third layer to "8". Press "F9" and you will see the lower part of the section. Next change the number of concrete layers to "4". Change the height of the fourth layer to "2" and its top width to "9". Increase the number of concrete layers to "5" and change the height of the fifth layer to "3". Now that you have described the geometry of the section press "F9" to view the section and verify that you have entered the correct section geometry.
8. Finally you have to enter the tendon layers. Specify "3" tendon layers and change the parameters to those found in Table A-1.

Table A-1 Example tendon data.

Layer	y	Area	Prestain	Tendon Type
1	1.50	0.34	5.84	1
2	3.25	0.23	5.84	1
3	12.00	0.11	5.84	1

Now you have entered all the section properties and to make a final check, press "F9" once more

9. Before you analyze this section you should save it to a file. Select "Save" from the main menu and enter a file name which does not exceed eight characters. For

example "Prob5-11". The cross-section data are now saved in a file called Prob5-11 and can be loaded again later. To print this file select "Print" from the main menu. You will be given the option to print to a printer or to print the data to a file. Printing to a file creates an ASCII file with the extension .prn.

A.7 MENUS

RESPONSE is a menu-driven program. The menu tree for program RESPONSE is displayed in Fig. A-1. The menus are displayed in the top two rows of the screen. The first line displays the currently available options and the second line gives more details on the highlighted option.

All menu selections are made either by typing the first letter of an option or by highlighting the option and then pressing "Enter". Options can be highlighted and selected using the following keys:

Left	moves the cursor one option to the left
Right	moves the cursor one option to the right
Home	moves the cursor to the first option
End	moves the cursor to the last option
Space	moves the cursor one option to the right
Backspace	moves the cursor one option to the left
Enter	selects the currently highlighted option

Pushing the Esc key returns control to the previous menu.

A.8 CONFIGURE-OPTIONS

RESPONSE can be configured so that many of the options will be selected automatically every time the program runs. To specify which options you want to have, use the configure menu to select the options. If you want the options to be remembered the next time the program is run use the "Update" option to save your selections.

A.8.1 Concrete Model

RESPONSE can be run using two different stress-strain curves for the concrete. Both of these stress-strain curves are discussed in Section 3.3 of the textbook. Throughout the program the stress-strain relationship proposed by Thorenfeldt, Tomaszewicz, and Jensen is referred to as the "High-Strength Model" and the parabolic stress-strain curve is referred to as the "Parabolic-Model". When results are displayed or stored, the models are referred to as "High" and "Para" respectively.

To change the stress-strain relationship select "Configure" from the main menu, select "Concrete-Model" and then select either the "Parabolic-Model" or the "High-Strength-Model". When the parabolic stress-strain model is used the program will run somewhat faster because the computations of stresses and strains are simpler, particularly in cases involving shear.

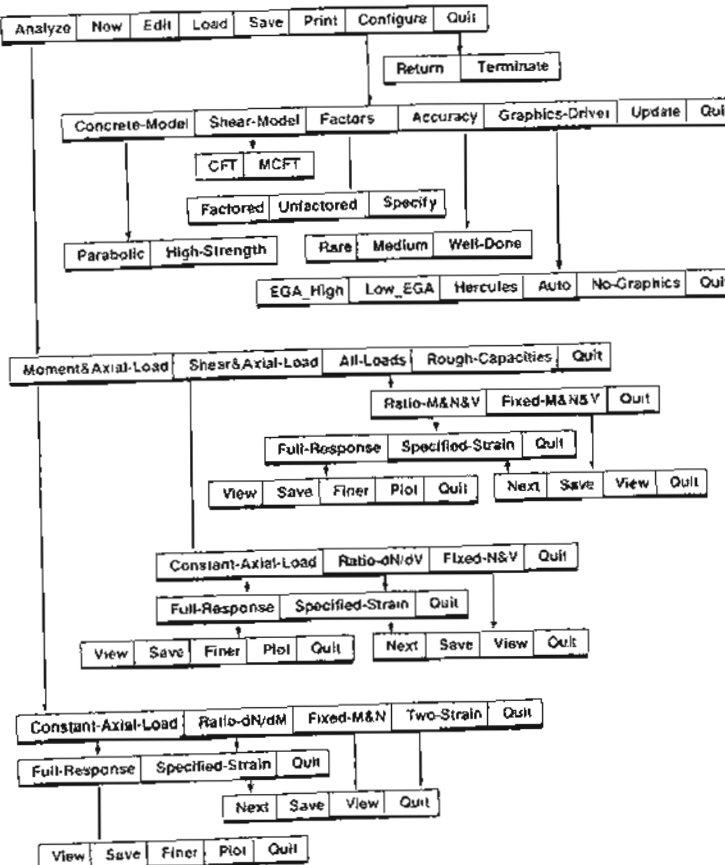


Figure A-1 Menu structure for program RESPONSE.

A.8.2 Shear Model

RESPONSE can be run using two different theories for shear analysis. The two models are the modified compression field theory (MCFT) and the compression field theory (CFT) described in Sections 7.9 and 7.10. When results are displayed or stored the theories are referred to as "MCFT" and "CFT".

To change the shear theory used for analysis select "Configure" from the main menu, select "Shear-Model" and then select either "MCFT" or "CFT".

Sec. A.8 Configure-Options

721

A.8.3 Factored

In the ACI code the design strength of a section is found by multiplying the nominal strength (i.e., the unfactored strength) by a strength reduction factor, ϕ . In the Canadian concrete design code the factored strength of a section is found by applying a material performance factor to each material and then calculating the strength using factored stress-strain curves for the materials. These material performance factors are: 0.60 for concrete, 0.85 for reinforcing steel, and 0.90 for prestressing steel and structural steel. The individual material factors can be changed using the "Specify" option, to accommodate other codes that use a factored-strength approach with different material factors.

To apply these factors to the individual material stress-strain curves select "Factored". To use no material factors select "Unfactored".

A.8.4 Accuracy

Response uses a number of different iteration routines to converge on the answer. To determine when the program has come sufficiently close to the answer the difference between the calculated result and the desired result are compared to a fraction of the axial capacity or the flexural capacity of the section.

There are three levels of convergence which can be specified: Rare, Medium, or Well-Done. The convergence limits used are specified in Table A-2.

Table A-2 Convergence limits.

Accuracy	Limit for Axial Load	Limit for Moment	Limit for Shear
Rare	$\pm \frac{\text{compressive capacity}}{200}$	$\pm \frac{\text{flexural capacity}}{300}$	$\pm \frac{\text{compressive capacity}}{400}$
Medium	$\pm \frac{\text{compressive capacity}}{1000}$	$\pm \frac{\text{flexural capacity}}{1000}$	$\pm \frac{\text{compressive capacity}}{1000}$
Well-Done	$\pm \frac{\text{compressive capacity}}{5000}$	$\pm \frac{\text{flexural capacity}}{5000}$	$\pm \frac{\text{compressive capacity}}{5000}$

A.8.5 Graphics Driver

RESPONSE can display several plots using a variety of graphics cards. To specify which graphic card your system has, select one of the following:

- EGA_High For high resolution EGA drivers and VGA drivers.
- Low_EGA For low resolution EGA drivers (some Compaq portables).
- Hercules For some Hercules drivers.
- Auto If none of the above drivers work or you can't find what you have then select this option. The program will try to match one of its drivers with your card. If this is unsuccessful you may not be able to display plots and the program will terminate when you try to display plots.
- No-Graphics If your computer is unable to display graphics select this option. With "No-Graphics" selected the program will not terminate unexpectedly because it can't communicate with your graphics card.

A.8.6 Update

Once you have selected all the configuration options and you want to save them so they can be used by the program at a later time simply select "Update". This option writes a small file called (RESPONSE.KIZ) containing all the settings.

A.9 DEFINING A CROSS SECTION

The following sections describe the parameters used to define a reinforced concrete section for analysis. Limits have been placed on parameters describing section geometry and material properties. The limitations on material properties were selected to allow reasonable material properties. These limitations were imposed to avoid problems with the display of very large force resultants and to provide a check on input data.

A.9.1 Units

Units can only be selected when a new section is entered. Once either Metric or U.S. Customary units has been specified, the units are fixed for the cross section and cannot be changed later. To select U.S. Customary units enter "u" and to select Metric units enter "m". Data is entered and displayed in the units specified in Table A-3.

Table A-3 Units used for input and output

Units System	Metric	U.S. Customary
Dimensions	millimeter [mm]	inches [in]
Stresses and Elastic Modulus	mega-pascals [MPa]	kips per square inch [ksi] ¹
Strains	millistrain	millistrain
Forces	kiloNewton [kN]	thousand pounds [kips]
Moments	kiloNewton-meters [kNm]	foot-kip [ft-kips]

¹Concrete stresses in U.S. Customary units are entered and displayed in pounds per square inch (psi).

Once the system of units has been specified, a default section will be displayed. This default section can be modified to a new cross section.

A.9.2 Number of Concrete Types

The program can use up to five different concrete types to model the response of a section. By default, it assumes that you have one type of concrete and it displays the parameters describing it. Typically, one concrete is used for the concrete which does not participate in tension stiffening and another type is used to represent the concrete which is close to the reinforcing steel. A third type of concrete could be used to model topping concrete for a composite section. Note: The shear analysis routines use the properties of the first concrete type.

There has to be at least one type of concrete specified. To facilitate error checking of subsequent parameters, the number of concrete types can not be reduced at a later stage. To increase the number of concrete types, simply enter the number of concrete types which you want to use for your section.

Sec. A.9 Defining a Cross Section

To change the parameters describing a concrete type, activate the cell containing the parameter and enter the new parameter. For each type of concrete enter the parameters defining the stress-strain relationship.

The parameter ϵ'_c refers to the strain when f_c reaches f'_c . If this strain is unknown, enter "0" and the program will estimate the strain based on the equations given in Chapter 3.

For the "Parabolic" concrete stress-strain model, the tangent modulus, E_{ct} , is estimated to be 1.1 times the secant modulus. Therefore the following equations are used to determine ϵ'_c : $E_t = 62,700\sqrt{f'_c}$, psi units, $E_c = 5200\sqrt{f'_c}$, MPa units, $\epsilon'_c = 2f'_c/E_{ct}$.

Tension Stiffening Factor refers to the product of the factor accounting for bond characteristics and the factor for the type of loading (see Section 4.10 of the text). Suggested values for this factor are obtained by pressing "F1" (for help).

A.9.3 Number of Reinforcing Bar Types

By default, the program assumes that the section contains no reinforcing bars. The program can use up to five different types of mild reinforcing steel. Each steel type is described by a trilinear stress-strain relationship described in Fig. A-2. Enter the number of reinforcing steels which you want to use for your section and then enter the parameters describing the stress-strain relationships. If you wish to ignore strain hardening of the reinforcement, enter the same value for f_u and f_y . Note: To facilitate error checking, the number of reinforcing bar types can only be increased.

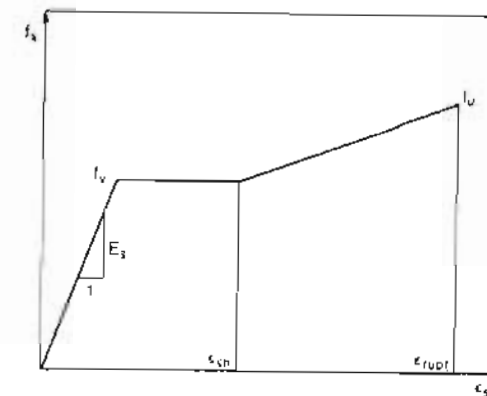


Figure A-2 Stress-strain relationship of reinforcing bar.

A.9.4 Number of Tendon Types

Again, by default, the program assumes that the section contains no prestressing tendons. The program can use up to five different types of prestressing steel. Prestressing steel types are defined using a modified Ramberg-Osgood curve for the stress-strain relationship as discussed in Section 3.14 of the text. To specify tendon types (prestressing steels) enter the number of different tendon types you want to consider for the section. Once one or more tendon types have been specified, the parameters describing the stress-strain curve(s) are displayed. These parameters can then be modified as described previously. Note: To facilitate error checking, the number of tendon types can only be increased.

A.9.5 Height and Moment Axis

Once all the material properties have been specified the section geometry can be entered. The program uses the total height of the section in a number of data checks. Because of this, the total height is another quantity which can only be increased. Therefore, the default height of a section is 2 [inches] or 50 [millimeters].

The distance from the bottom of the section to the moment axis is used to define the location about which moments are taken. In many cases, the moment axis is taken at half the height of the section or as the centroidal axis specified from the bottom of the section. If you do not know the location of the centroidal axis enter an initial estimate, which can be corrected after the program calculates the centroidal axis location.

A.9.6 Shear Information

If only analyses without the influence of shear are planned, it is not necessary to enter any information for shear calculations. Simply enter "n". If the influence of shear will be part of the analysis, enter "y" and specify the following information: the effective web width (b_w), the flexural lever arm (jd), the distance from the bottom of the section to the location where the uniaxial and biaxial strains are linked, the distance from the bottom of the section to the centroid of the effective shear area (b_wjd), the crack spacing parameter ($s_{m,r}$) as discussed in Section 7.10, and the maximum aggregate size.

If a reinforcing bar type was specified previously, the question "Stirrups Y/N ?" will be on screen. If no reinforcing bar types were specified, no stirrups can be entered. If your section has stirrups, enter "y" and specify the following information: crack spacing parameter ($s_{m,v}$) as discussed in Section 7.10, cross-sectional area of stirrups (A_s), stirrup spacing (s), and type of reinforcing used for the stirrups. Note: Strain hardening of stirrups will be ignored for the analysis even if it is specified for the reinforcing bar type.

A.9.7 Concrete Layers

The geometry of the cross section is defined by trapezoidal layers which can be combined to make up a large variety of cross sections. All sections are assumed to be symmetrical about a vertical plane and are displayed as such on the screen by pressing "F9". The numbers of layers used to model a cross section is determined by the minimum number of trapezoids required to define the cross-sectional geometry. Additional layers

may have to be used to differentiate between different concrete types. Note that because of the techniques used in the numerical integration (see Section A.12) it is not necessary to further subdivide the layers in an attempt to improve numerical accuracy. Each individual layer is defined using the following parameters: distance from the bottom of the section to the bottom of the layer, y , bottom width, top width and height (see Fig. A-3).

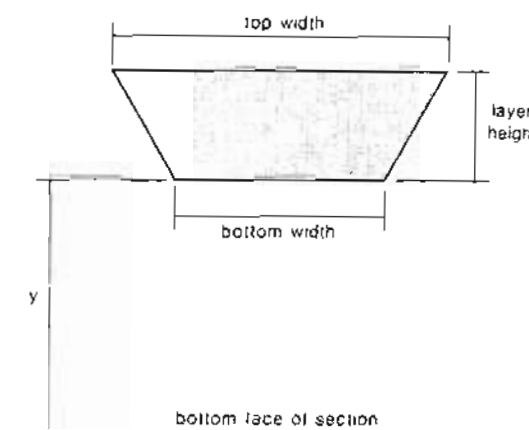


Figure A-3 Parameters defining a concrete layer.

The number of concrete layers used to describe a cross section is limited to 20. The number of concrete layers can be changed later, but a minimum of one layer has to be specified. Enter the number of concrete layers used and then modify the parameters for each layer to describe your section. At any time during this process you can press "F9" to see a plot of the cross section.

A.9.8 Reinforcing Bar Layers

If no reinforcing bar types were specified previously, no reinforcing bar layers can be entered. By default the number of reinforcing bar layers is zero. To specify reinforcing bar layers enter the number of layers you want to use (limited to a maximum of ten). Then define the location of each layer, the cross-sectional area of each layer, and the type of reinforcing bar used for each layer.

A.9.9 Tendon Layers

If no tendon types were specified previously, no tendon layers can be entered. By default the number of tendon layers is zero. To specify tendon layers enter the number of layers desired (limited to a maximum of ten). Define the location of each layer, the

cross-sectional area of each tendon layer, the strain difference between the concrete and the prestressing steel due to prestressing and the tendon type used for each layer.

A.9.10 Displaced Concrete

This option will account for the amount of concrete displaced by reinforcing bar and tendon layers. If you do not want to account for the displaced concrete enter "n", otherwise enter "y" and the concrete type replaced by each steel layer.

A.9.11 Thermal and Shrinkage Strains (Y/N)

If no thermal and shrinkage strains are to be accounted for then enter "n". To account for shrinkage or thermal strains enter "y" and then enter the shrinkage and thermal strains for the concrete, reinforcing bar and tendons. Note: Do not enter shrinkage strains if you are going to conduct a shear analysis.

A.9.12 Strain Discontinuities (Y/N)

Composite members, such as a precast beam with a cast-in-place topping, generally have a strain discontinuity at the interface between the component parts of the section. To account for this discontinuity, it is necessary to treat the total strain as the sum of the initial strains which existed when the final piece was placed and the additional strains occurring after the cross section had been completed (see Section 5.17). Note that for members with strain discontinuities the program reports the strains and curvatures associated with the additional strains and curvatures that occur after completion of the section rather than the total strains. For further details see the example given in Section 5.17 of the text.

If no strain discontinuities are present within the section then enter "n". To enter the strain discontinuities enter "y" and then enter the initial strains for the concrete, reinforcing bars, and tendons. Note: Do not enter strain discontinuities if you are going to conduct a shear analysis.

A.10 ANALYSIS OPTIONS

Once a section has been loaded or entered it can be analyzed. The many different analysis options (see Fig. A-1) can be divided into the following three categories:

1. Moment and Axial Load
 - Calculate moment-curvature relationships for given axial loads and/or axial-load-to-moment ratios.
 - Find the strain distribution for a given axial load and/or axial-load-to-moment ratio and a specific strain anywhere within the section.
 - Find the strains for given moment and axial load.
 - Find the axial load and moment for given strains.
2. Shear and Axial Load
 - Calculate shear force vs. strain relationships for given axial loads and/or axial-load-to-shear ratios.

Sec. A.10 Analysis Options

- Find the biaxial strain state for given axial load and/or axial-load-to-shear ratio with a specified principal strain.
- Find the biaxial strain state for given axial load and shear force.

3. All Loads

- Calculate axial load, shear, and moment vs. strain relationships of a variety of linear combinations of shear-to-axial-load and shear-to-moment ratios.
- Find the strain state due to applied moment, axial load and shear.

4. Rough Capacities

- Calculate estimates of the compressive and tensile capacities and the positive and negative moment capacities.
- Calculate estimates of the cracking shear force and the post-cracking shear strength.

The available analysis options are described in more detail in the sections below.

A.10.1 General

The three main types of analysis which can be performed with this program are:

1. Find load vs. deformation relationships.
2. Find one load and the strain distribution for a given load and a given strain (i.e., find the moment for a given axial load at which the bottom fiber cracks).
3. Find the strains for given loads.

Each of these analysis options has specific menus associated with it. These typical menus will be discussed here.

All analysis procedures can be interrupted by pressing "Esc" once. After the "Esc" key has been pressed either the "Continue-Stop" menu or the "Continue-Stop-Plot" menu will appear. Selecting "Continue" will result in a continuation of the current analysis. Selecting "Stop" will cause the program to stop the current analysis, save the successfully calculated points and then advance to the next menu. Selecting "Plot" will plot the load-deformation response from the points calculated so far. Note. The "Plot" option is only available for "Full-Response" type analysis.

A.10.1.1 Menu: "Full-Response Specified-Strain Quit"

The "Full-Response Specified-Strain Quit" menu appears after the axial load or the ratio between axial load and/or shear have been specified. The menu choices have the following consequences:

- Full-Response
 - Produces a full load-deformation response and ends up with a "View-Save-Finer-Plot-Quit" menu. For the generation of load vs. curvature response the program increments the curvature, starting from zero, until the specified loading (e.g., the axial load) can no longer be resisted or until the calculated load (e.g., the moment) passes its maximum value. Then the program decrements the curvature from zero until the given loading can no longer be resisted. Then

the program stores the curvature range for which it was successful. For the generation of load vs. deformation response when shear is present, the program increases the principal tensile strain from approximately 0 to 40 millistrain and stops when the specified load can no longer be resisted. Then the program stores the range of principal tensile strains for which it was successful.

c Specified-Strain

For moment and axial load analysis this option allows the user to specify a strain anywhere within the section. The program then finds the strain distribution under the given loading. For shear and axial load analysis, the user can specify the principal tensile strain and the biaxial strain state under the given loading will be calculated. After the strains have been found the program will display a "Next-Save-View-Quit" menu.

d Quit

Returns to the previous menu.

A.10.1.2 Menu: "View-Save-Finer-Plot-Quit"

If "Full-Response" was selected previously then the "View-Save-Finer-Plot-Quit" menu appears. Now the following options are available:

a View

The View option is used to look at the calculated points once the iteration is complete or after it has been interrupted. If no valid data points were calculated then this option will not respond. Simply press "v" to select "View" from the "View Save Finer Plot Quit" or the "Next Save View Menu" menu. Then the screen will display a heading similar to that shown during the iteration. The first fifteen data points are displayed on the screen and the remainder can be displayed using the "Down" or "PgDn" key. In addition, "Up" and "PgUp" can be used to scroll through the data. For every data point the strain and stress distribution across the section can be plotted by pressing "F9".

b Save

Save the current data to a file. The data files are saved with one of the following three extensions,

- 'NM' axial load and moment analysis
- 'NV' axial load and shear analysis
- 'NVM' axial load, shear, and moment analysis

c Finer

This option lets you refine the strain increment used to produce the full load vs. deformation response. Specify a number between 10 and 100 to select the number of points to be calculated. For a load vs. curvature response the number of points refers to the number of points between zero curvature and the maximum or minimum curvature. The program will then ask for the maximum positive curvature and the maximum negative curvature. For a load vs. principal tensile strain response the program asks for the maximum tensile strain.

Sec. A 10 Analysis Options

e Plot

Display plots of the calculated load-deformation curves.

f Quit

Returns to the previous menu. Warning: Any calculated points will be lost if they are not saved.

A.10.1.3 Menu: "Next-Save-View-Quit"

If "Specified-Strain" was selected previously then the "Next-Save-View-Quit" menu appears. This menu also appears if "Fixed-Loads" was selected previously. Now the following options are available:

g Next

This option asks for the next strain or the next load combination and then calculates the next point.

h Save

Saves the current data to a file.

i View

To look at all the successfully calculated points.

j Quit

Returns to the previous menu. Warning: Any calculated points will be lost if they have not been saved.

A.10.2 Moment&Axial-Load

The "Moment&Axial-Load" option has several analysis features which all use plane sections analysis. The moment and axial load option can be selected by first selecting "Analyze" from the main menu and then by selecting "Moment&Axial-Load" from the next menu.

Once "Moment&Axial-Load" has been selected the options outlined below are available.

A.10.2.1 Constant-Axial-Load

For a specified axial load the full moment-curvature response or the curvature and moment for a specified strain anywhere within the section can be calculated using this option.

To proceed with this analysis select "Constant-Axial-Load" from the menu and then specify the following:

1. Axial load.
2. Whether to account for tension stiffening or not.
3. Now the "Full-Response Specified-Strain Quit" menu will appear (refer to Section A.10.1.1). Select an option from the menu.
4. The iteration will now be displayed on screen.
5. Depending on your choice in the previous menu either the "View Save Finer Plot Quit" or the "Next Save View Quit" menu will appear (refer to Sections A.10.1.2 and A.10.1.3).

A.10.2.2 Ratio dN/dM

This analysis can be used to get the full response for a section loaded by an axial load which is a function of the moment. In addition, a moment and axial load pair satisfying the relationship described below can be calculated for a specified strain anywhere within the section. The relationship between moment and axial load is described by the following equation: axial load = (axial load at zero moment) + $dN/dM \times$ moment.

To proceed with this analysis select "dN/dM" from the menu and then specify the following:

1. Axial load when there is zero moment.
2. Ratio dN/dM.
3. Whether to account for tension stiffening or not.
4. Now the "Full-Response Specified-Strain Quit" menu will appear (refer to Section A.10.1.1). Select an option from the menu.
5. The iterations will now be displayed on screen.
6. Depending on your choice in the previous menu either the "View Save Finer Plot Quit" or the "Next Save View Quit" menu will appear (refer to Sections A.10.1.2 and A.10.1.3).

A.10.2.3 Fixed-M&N

This option is used to find the strain distribution across the section under a given moment and axial load.

To proceed with this analysis select "Fixed-M&N" from the menu and then specify the following:

1. Whether to account for tension stiffening or not.
2. Axial load.
3. Moment.
4. The iteration will now be displayed on screen.
5. Once the program has converged on the answer the "Next Save View Quit" menu will appear (refer to Section A.10.1.3).

A.10.2.4 Two-Strains

This option calculates the moment and axial load corresponding to a given strain distribution. The strain distribution is specified by entering two locations within the section and the strains at these locations.

To proceed with this analysis select "Two Strains" from the menu and then specify the following:

1. Enter the distance from the bottom of the section to the location where the first strain will be specified.
2. Enter the first strain.
3. Enter the distance from the bottom of the section to the location where the second strain will be specified.
4. Enter the second strain.
5. Specify whether to account for tension stiffening or not.

Sec. A 10 Analysis Options

6. Once the all the strains have been specified the program will display the moment and axial load corresponding to the strain distribution. Then the "Next Save View Quit" menu will appear (refer to Section A.10.1.3).

A.10.3 Shear&Axial-Load

The "Shear&Axial-Load" option has analysis features which are all based on the calculations described in Chapter 7. The analysis can be performed using either the compression field theory or the modified compression field theory (see Section A.8 for details on how to specify which theory to use).

Once "Shear&Axial-Load" has been selected the following options are available.

A.10.3.1 Constant-Axial-Load

For a specified axial load the full shear-deformation response or the shear force and the biaxial strain state for a specified principal tensile strain can be calculated using this option.

To proceed with this analysis select "Constant-Axial-Load" from the menu and then specify the following:

1. Axial load.
2. Now the "Full-Response Specified-Strain Quit" menu will appear (refer to Section A.10.1.1). Select an option from the menu.
3. The iteration will now be displayed on screen.
4. Depending on your choice in the previous menu either the "View Save Finer Plot Quit" or the "Next Save View Quit" menu will appear (refer to Sections A.10.1.2 and A.10.1.3).

A.10.3.2 Ratio dN/dV

This analysis can be used to get the full response for a section loaded by a shear force and an axial load which is a function of the shear force. In addition a shear and axial load pair satisfying the relationship described below can be calculated for a specified principal strain. The relationship between axial load and shear is described by the following equation: axial load = (axial load at zero shear) + $dN/dV \times$ shear.

To proceed with this analysis select "Ratio dN/dV" from the menu and then specify the following:

1. Axial Load when the shear is zero.
2. The ratio dN/dV.
3. Now the "Full-Response Specified-Strain Quit" menu will appear (refer to Section A.10.1.1). Select an option from the menu.
4. The iteration will now be displayed on screen.
5. Depending on your choice in the previous menu either the "View Save Finer Plot Quit" or the "Next Save View Quit" menu will appear (refer to Sections A.10.1.2 and A.10.1.3).

A.10.3.3 Fixed-N&V

This option is used to find the biaxial distribution for a given shear and axial load. The analytical method used for this analysis is a gradient approach which may run into convergence problems.

To proceed with this analysis select "Fixed-N&V" from the menu and then specify the following:

1. Axial load.
2. Shear force.
3. The iteration will now be displayed on screen.
4. Once the program has converged on the answer the "Next Save View Quit" menu will appear (refer to Section A.10.1.3).

A.10.4 All-Loads

This option enables the load-deformation response to be produced for a given ratio between shear and moment and between shear and axial load. In addition, the strain state for a given combination of loads can be found. Once "All-Loads" has been selected the following options are available.

A.10.4.1 Ratio-M&N&V

This analysis can be used to get the full response for a section loaded by a specific loading regime. Both the axial load and the moment are functions of the shear force.

$$\begin{aligned}\text{Axial Load} &= (\text{axial load at zero shear}) + dN/dV \cdot \text{shear} \\ \text{Moment} &= (\text{moment at zero shear}) + dM/dV \cdot \text{shear}\end{aligned}$$

To proceed with this analysis select "Ratio-M&N&V" from the menu and then specify the following:

1. Axial load when there is zero shear.
2. The axial-load-to-shear ratio.
3. Moment when there is zero shear.
4. The moment-to-shear ratio.
5. Whether to account for tension stiffening or not.
6. Now the "Full-Response Specified-Strain Quit" menu will appear (refer to Section A.10.1.1). Select an option from the menu.
7. The iteration will now be displayed on screen.
8. Depending on your choice in the previous menu either the "View Save Finer Plot Quit" or the "Next Save View Quit" menu will appear (refer to Sections A.10.1.2 and A.10.1.3).

A.10.4.2 Fixed-M&N&V

This analysis is used to find the strains corresponding to a specified axial load, moment and shear. To proceed with this analysis select "Fixed-M&N&V" from the menu and then specify the following:

1. Axial load.

2. Moment.
3. Shear.
4. The iteration will now be displayed on screen.
5. Once the program has converged on the answer the "Next Save View Quit" menu will appear (refer to Section A.10.1.3).

Note that if loads that are beyond the capacity of the section are specified, convergence will not be possible.

A.10.5 Rough Capacities

This option calculates estimates of the axial, moment and shear capacities for the current cross section. These estimates can be used to give the user a sense of the section capacity. In addition, the program uses these capacities to determine convergence criteria (see Section A.8.4).

The compressive capacity is defined as the axial load which causes a uniform strain of $\epsilon'_c(\max)$ across the section, $\epsilon'_c(\max)$ being the largest ϵ'_c of all the specified concrete types. The tensile capacity is defined as the axial load which causes a uniform strain of 2 millistrain across the section.

The rough moment capacities are calculated assuming no axial load is acting on the section. The moments are obtained by specifying a compressive strain at the top or bottom of the section. For the calculation of the positive moment capacity the compressive strain at the top face of the section is set to $\epsilon'_c(\max)$ and the program tries to find the strain distribution corresponding to zero axial load. If this solution cannot be reached then the specified strain is reduced by 50% and the process is repeated until a solution can be found. The resulting moment is then recorded. For the negative moment capacity, a similar procedure is used only now a compressive strain on the bottom face is specified.

If data for shear analysis were entered the shear capacity at cracking and at a principal tensile strain of 5 millistrain will be calculated. Since all shear calculations are based on type 1 concrete, the cracking strain ϵ_{cr} is calculated for concrete type 1. This strain is then used to calculate the cracking shear assuming zero axial load. The second shear capacity is calculated based on a principal tensile strain of 5 millistrain and zero axial load. If no solution can be found for this strain, the strain is reduced by 50% and the analysis is repeated until a solution can be obtained.

A.11 PLOTS

If RESPONSE can match one of its drivers to your graphics card (see Section A.8.5), the graphs described in the following sections can be displayed.

A.11.1 The Cross-Section Plot

The cross-section plot can be displayed, when section data is being edited or a new section is being entered, by pressing "F9". The section plot displays the section which will be analyzed by the program. The information given at the top of the screen is as follows:

Area	The area of the gross concrete cross section.
I _{xx}	The moment of inertia of the gross concrete cross section.
Height	The total height entered as a parameter.
Width	The maximum width of the section calculated from the concrete layers.
Distance to Centroid	The distance from the bottom of the cross section to the centroid of the gross concrete area.

The location and shape of the concrete layers is displayed in the center of the screen. The center of each layer displays the layer number. If a layer interferes with another layer, it is split in two and attached to the left and right of the first layer. The centroidal axis is displayed as a dashed line across the section. If information for shear calculations was entered, a rectangle showing the area $b_n \cdot jd$ will also be displayed. Below the concrete section a legend of concrete types is displayed and the concrete layers for the section are shaded according to their type. To the left of the concrete section the locations and type of reinforcing-bar layers are shown. To the right of the section the locations and type of tendon layers are indicated. To switch back to the data-editing screen hit any key. If shrinkage, thermal strains, or initial strains were specified, then a plot of these strains will appear first. (For more detail see Section A.11.2.)

A.11.2 The Shrinkage, Thermal, and Initial-Strains Plot

The Shrinkage, Thermal, and Initial-Strains Plot appears after the Cross-Section Plot if shrinkage and thermal strains or initial strains have been specified. The left half of the plot displays the shrinkage and thermal strains. A box is used to represent the height of the section and the sides of the box indicate the maximum and minimum strains. The strains for each concrete layer are displayed as a parabolic curve (using ten points per layer). The reinforcing bar strains are indicated by crosses and tendon strains by small rectangles. The right side of the screen is used to display initial strains using the same conventions as for the display of thermal strains. To return to the data-editing spreadsheet hit any key.

A.11.3 The Concrete Material Plot

The program can use up to five different types of concrete. The concrete type can be modeled using either the "Parabolic" or the "High-Strength" stress-strain relationship for concrete. While editing section data the stress-strain curve used for the concrete can be displayed by pressing "F8". The plot displays the number of the concrete type at the top of the screen. The concrete compressive strength and the tensile strength are displayed in the second line. The third line contains the strain at maximum concrete stress (ϵ'_c) and the elastic modulus of the concrete. If an ϵ'_c of zero was specified in the section data then the calculated value will be displayed (refer to Section A.9.2). In addition, the cracking strain is calculated and displayed with the tension-stiffening factor. Hit any key to display the next concrete type. If no further concrete types are specified, the program will return to the data-editing spreadsheet.

A.11.4 The Stresses and Strains Plot

The Stresses and Strains Plot can be used to display the strains and stresses across the section. This plot can be displayed during the calculation of a full response by pressing "F9". The plot is also available when previously-calculated data points are inspected using the "View" option. The first two lines of the display give the axial load and the moment acting on the section. In addition, the strain at the axis about which moments are taken and the curvature are displayed. The strains of the layers are shown in the box on the left of the screen. A yellow line is used to represent the linear strain distribution across the section (a function of the strain at the moment axis and the curvature). A blue line is used to represent the strains which cause stress in each concrete layer. If no shrinkage, thermal, or initial strains were specified for the concrete, the two lines will overlap. If it appears that the lines do not overlap when they should, it may be due to the resolution of your screen (different color pixels are located side by side). In addition, crosses are used to show the location and magnitude of strains due to stress, for reinforcing-bar layers. Similarly, tendon layers are represented by small rectangles.

The concrete stresses are displayed in a box to the right. The stress distribution across each layer is generated using ten points across the layer. The reinforcing bar and tendon stresses are displayed on the right of the screen.

If an analysis involving shear has been performed, another plot displaying the stresses and strains in the biaxially stressed web will appear if any key is pressed. This "Biaxial Stresses and Strains" plot displays the concrete stress state (on the left side of the screen) and the concrete strain state (on the right side of the screen). The stresses in the web reinforcing (stirrups) are displayed at the bottom of the screen.

A.11.5 The Load vs. Displacement Plots

To look at some of the load-deformation data generated by "Full-Response" analysis, several different load vs. deformation plots can be viewed. All of these plots define the horizontal (x -axis) and vertical (y -axis), and these axes are scaled to optimize the size of the plot on screen. These plots can be accessed during "Full-Response" iteration by pressing "Esc" and selecting "Plot". After the iterations, the "Plot" option can be selected from the menu.

A.12 NUMERICAL INTEGRATION

In determining the axial load and moment on the section, it is necessary to evaluate the following two integrals:

$$N_c = \int_{A_1} f_c(y) dA$$

$$M_c = \int_{A_1} f_c(u) \cdot y dA$$

Because these integrals cannot be evaluated in closed form, numerical integration is used. For the numerical integration, a parabolic stress distribution across each individual

layer is assumed. The shape of the parabolic distribution is determined from the calculated stresses at the bottom, middle, and top of the layer. This method of integration is very accurate for layers subject to compressive stresses (based on a "Parabolic" stress-strain relationship) over the depth of the layer. However, the approach can become inaccurate if the stresses are not compressive over the entire layer or if the "High-Strength" stress-strain relationship is used. Figure A-4 shows examples of the difference between the actual stress distributions and the parabolic distributions used in the numerical integration.

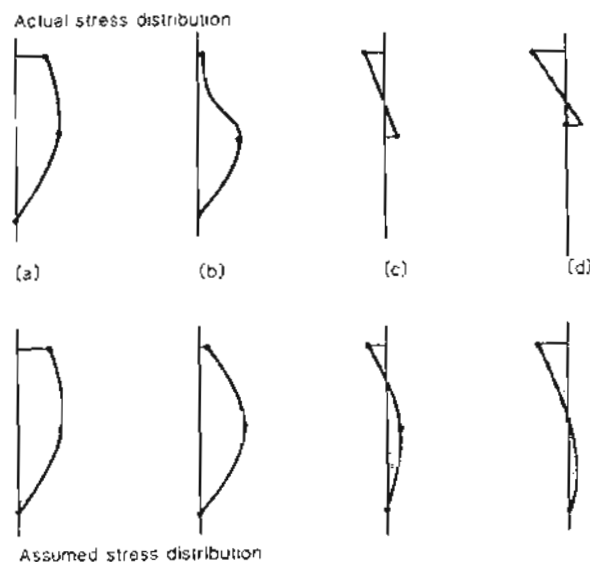


Figure A-4 Actual and assumed stress distributions across individual layers.

To determine if the integration is sufficiently accurate, the program uses the following procedure:

1. Calculate the stress at the top, middle, and bottom of the layer. Determine the parabolic stress distribution based on these three stresses.
2. Calculate the actual stresses at the fifth points within the layer and compare these to the stresses obtained from the parabolic stress distribution.
3. If the two sets of stresses do not agree within about 1% then split the layer into three equal sublayers.
4. Repeat steps 1, 2, and 3 for each sublayer.

This process, outlined in Figure A-5, is repeated up to eight times if necessary.

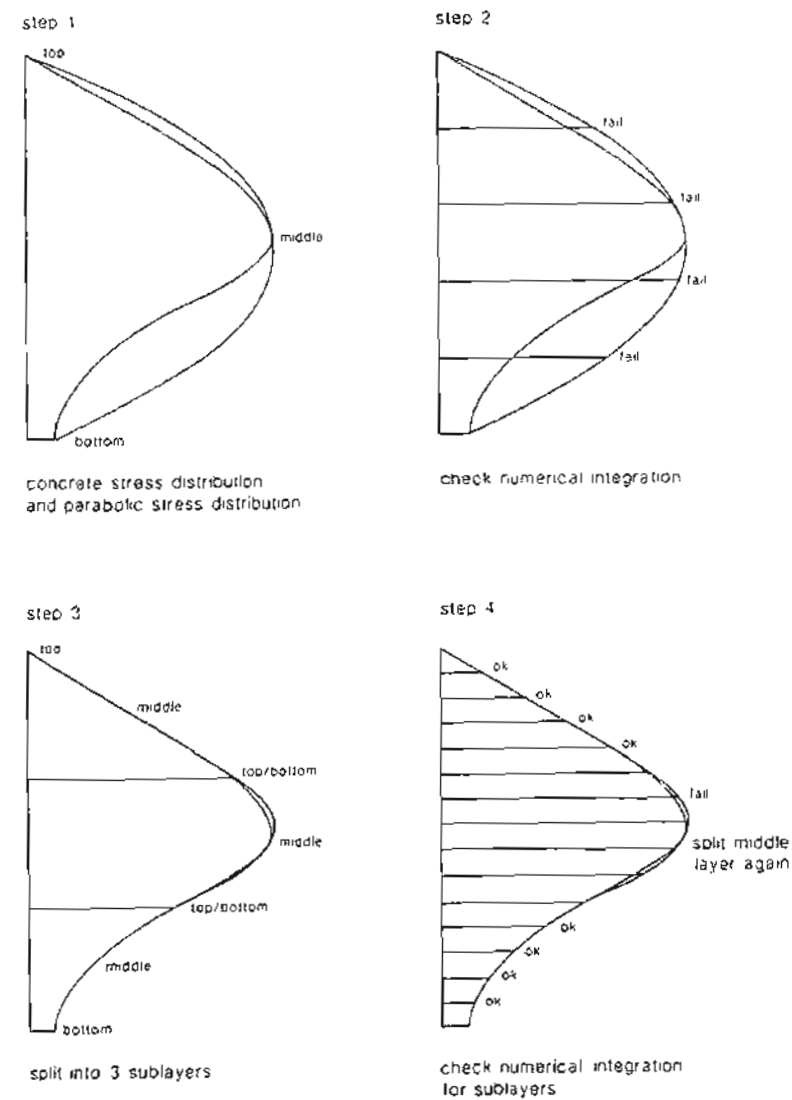


Figure A-5 Numerical integration check and automatic subdivision of layers.

Because of this automatic subdivision procedure, the number of layers used for the numerical integration does not have to be more than the minimum number of trapezoids necessary to describe the section geometry and material distribution. This algorithm is efficient because it increases the number of layers only where and when necessary.

A.13 ITERATION PROCEDURES

A.13.1 Iterating on One Strain Variable, Members with No Shear

For a specified axial load and a strain specified anywhere within the section (e.g., cracking strain at the bottom face), the corresponding moment is found using the following procedure:

1. Given the location of the specified strain select a location for a second strain and guess a second strain.
2. Calculate the stress resultants for the strain distribution defined by the specified strain and the second strain.
3. Increment the second strain by a small amount.
4. Calculate the axial stress resultant and the moment for the new strain distribution.
5. Compare the specified axial load to the new axial stress resultant obtained in step 4. If they are close enough then the moment obtained in step 4 is the moment corresponding to the specified axial-load and the specified strain. If they are not close enough proceed to step 6.
6. Find the rate of change of the axial stress resultant with respect to the second strain. Use this rate of change to make a new estimate of the second strain. Return to step 4.

The procedure above is a simplification of the actual algorithm used by the program. This algorithm is outlined in more detail in Ref. A-1.

Another single iteration algorithm is used to develop moment-curvature diagrams. The moments corresponding to a given axial load and specified curvatures are calculated. Then the curvature is incremented until the full response has been calculated. The procedure used to find the moment is similar to that outlined above. The difference is that the curvature is the fixed strain variable and the strain at the center is iterated on until the axial stress resultant converges to the specified axial load.

A third single-iteration algorithm is used to find the axial load corresponding to a given moment and a specified axial strain. This algorithm is used as a subroutine for calculations involving moment, axial load and shear. Again, the numerical procedure is similar to the one outlined above. The axial strain is fixed and the curvature is changed until the moment resultant converges on the given moment.

A.13.2 Iterating on Two Strain Variables, Members with No Shear

To determine the strain distribution corresponding to a given axial load and a given moment, the strain at the centroid and the curvature have to be found by iteration. This can

be achieved by two methods. The first method iterates on both variables simultaneously until the stress resultants have converged on the given loads. This approach is called the "Gradient" approach. Another approach called the "Two-Stage" algorithm is used when the "Gradient" approach runs into difficulties. The "Two-Stage" approach uses two nested single iterations to find the strain distribution.

A.13.2.1 The Gradient Approach

The "Gradient" approach starts with a guess of initial strains and then calculates the stress resultants and the stiffness of the section. Using these resultants and the stiffness a new estimate of the strains is calculated. This process is repeated until the resultants match the specified moment and axial load. This procedure can run into numerical difficulties when the given loads are close to those loads causing cracking of the section. Under these conditions the stiffness of the section changes suddenly from one iteration to the next. If this procedure has not converged after 20 attempts, the program then uses the "Two-Stage" approach. The gradient approach is outlined in more detail in Ref. A-1.

A.13.2.2 The Two-Stage Approach

The "Two-Stage" approach is more stable than the "Gradient" approach because only one variable is iterated on at a time. The iteration routine fixes the strain at the bottom of the section and finds the strain distribution for the given axial load using the routine described in Section A.13.1. The second iteration routine changes the bottom strain until the moment resultant converges to the given moment. If this method does not converge after 50 iterations a variant of the "Two-Stage" approach is used to iterate on the top strain. The "Two-Stage" algorithm is outlined in more detail in Ref. A-1.

A.13.3 Members with Shear

The analysis of a section subjected to combined moment, axial load, and shear requires the consideration of four strain variables (i.e., the longitudinal strain at the center of the web, ϵ_x , the curvature, ϕ , the principal tensile strain, ϵ_1 , and the angle of inclination of the principal compressive strain, θ). To solve this problem, the program uses the solution technique described below, which involves a series of nested iterations. More details are given in Ref. A-1. Also, see Appendix B of this text.

A.13.3.1 Algorithms for Shear and Axial Load

The algorithm, which assumes a curvature of zero (constant axial strain), cannot satisfy moment equilibrium. If moments are taken about the centroid of doubly symmetrical sections the moment resultant is zero. For unsymmetrical sections a non-zero moment will be required to keep the strain distribution constant across the section. This moment is recorded by the program. The algorithm used to solve for the principal tensile strain, ϵ_1 , the longitudinal strain, ϵ_x , and the inclination of the principal compressive stress, θ , consists of a series of nested iterations. The nested iteration procedure is outlined below using the assumptions of the MCFT adopted for the program. In this outline the equations for the parabolic concrete stress-strain relationship are used and a principal tensile strain larger than the cracking strain is assumed.

- Loop for iterating on the principal tensile strain, ϵ_1 .

Step 1: Guess a principal strain, ϵ_1 .

- Loop for iterating on θ .

Step I: Guess θ .

Step II: Calculate the crack width, w , and v_{ci} .

$$\begin{aligned} w &= \frac{\epsilon_1}{\left(\frac{\sin \theta}{s_{mx}} + \frac{\cos \theta}{s_{mv}}\right)} \\ v_{ci} &= \frac{2.16 \sqrt{f'_c}}{0.31 + \frac{24w}{a+0.63}} \quad \text{psi and in.} \\ v_{ci} &= \frac{0.179 \sqrt{f'_c}}{0.31 + \frac{24w}{a+16}} \quad \text{MPa and mm} \end{aligned}$$

where a is the maximum aggregate size.

- Loop for iterating on vertical equilibrium.

Step a: Guess the stress in the stirrups, f_v .

Step b: Calculate the principal tensile stress.

$$f_1 = \frac{\alpha_1 \alpha_2 f_{cr}}{1 + \sqrt{500 \epsilon_1}} \leq v_{ci} \tan \theta + \frac{A_v}{s b_u} (f_{v,y} - f_v)$$

Step c: Calculate shear stress resultant, V .

$$V = \left(\frac{A_v f_v}{s} + f_1 b_w \right) j d \cot \theta$$

Step d: Calculate the stress in the compressive strut.

$$f_2 = \left(\tan \theta + \frac{1}{\tan \theta} \right) \frac{V}{b_w j d} - f_1$$

Step e: Calculate the maximum compressive stress.

$$f_{2max} = f'_c \frac{1}{0.8 - 0.34 \epsilon_1 / \epsilon'_c} \leq f'_c$$

Step f: Check the compressive strut.

$$f_2 \leq f_{2max}$$

If the concrete crushes return to Step 1.

Step g: Calculate the strain in the compressive strut.

$$\epsilon_2 = \epsilon'_c \left(1 - \sqrt{1 - \frac{f_2}{f_{2max}}} \right)$$

Step h: Calculate the transverse and longitudinal strains.

$$\begin{aligned} \epsilon_x &= (\epsilon_1 \tan^2 \theta + \epsilon_2) / (1 + \tan^2 \theta) \\ \epsilon_t &= (\epsilon_1 + \epsilon_2 \tan^2 \theta) / (1 + \tan^2 \theta) \end{aligned}$$

Step i: Using the transverse strain, calculate the stress in the stirrup.

$$f_v = E_s \epsilon_t \leq f_{v,y}$$

Step j: If the stirrup stress is different from the guess in Step a return to Step a with a better estimate of the stirrup stress.

Step III: Calculate the axial force, N_v , on the section resulting from the concrete stresses in the effective shear area, $b_w j d$.

$$N_v = \frac{-V}{\tan \theta} + f_1 b_w d_c$$

Calculate the moment cause by N_v .

$$M_v = N_v y$$

where y is the distance between the center of the effective shear area and the moment axis.

Step IV: Using the plane-section procedures described in Chapter 5 find the stress resultants for the section corresponding to the longitudinal strain, ϵ_x , and a curvature, ϕ , of zero.

$$\begin{aligned} N_p &= f(\epsilon_x, \phi) = N_{gross} - N_{b_w j d} \\ M_p &= f(\epsilon_x, \phi) = M_{gross} - M_{b_w j d} \end{aligned}$$

Since the stresses acting on the concrete in the effective shear area have already been accounted for, the moments and axial resultant for the remainder of the cross section have to be calculated. This is done in two steps. First the resultants for the gross section, N_{gross} , and M_{gross} , are calculated. Then the concrete stress resultants, $N_{b_w Jd}$ and $M_{b_w Jd}$, for the effective shear area are subtracted. Note: The concrete in the effective shear area is assumed to be of Type I.

Step V: Calculate the axial resultant and moments

$$N = N_p + N_t$$

$$M = M_p + M_t$$

The technique of separating the section into a uniaxially stressed zone and a biaxially stressed zone is illustrated in Fig. A-6.

Step VI: Check whether the axial stress resultant is close enough to the axial load. If not, revise the estimate of θ and return to Step 1.

Step VII: Check that the reinforcement can carry the stresses across the crack. By limiting f_1 in Step b it is ensured that vertical equilibrium will be satisfied. Horizontal equilibrium is satisfied if

$$\sum_{i=1}^n (f_{v,i} - f_{v,i})A_{v,i} + \sum_{i=1}^m (f_{p,i} - f_{p,i})A_{p,i} \geq f_1 b_w J d + \left(f_1 - \frac{A_v}{b_w s} (f_{v,u} - f_v) \right) \frac{b_w J d}{\tan^2 \theta}$$

In this expression, the two summations on the left represent the reserve strength of the steel while the two terms on the right account for the additional demand placed on the longitudinal steel at the crack. If this check is not satisfied return to Step b and reduce the tensile stress.

Step 2: Check whether the shear stress resultant is close enough to the applied shear force. If it is not close enough return to Step 1 with a revised estimate of ϵ_1 .

These three nested iterations are performed by three algorithms: "Calculate-V", which performs Steps a through j; "Calculate-Angle", which performs Steps I through VII; and "Calculate-e1", which performs Steps 1 and 2. These three algorithms are described in more detail in Ref. A-1.

A.13.3.2 Algorithms for Shear, Axial Load, and Moment

To include moment equilibrium in the analysis, another iteration has to be introduced. This iteration changes the curvature, ϕ , at a specified center strain, ϵ_2 , until the moment stress resultant is close enough to the applied moment. To implement this procedure, the

algorithm described in Section A.13.3.1 has to be modified. Step V must be replaced by the Step V shown below and Step VII is omitted.

Step V: Using the iteration mentioned at the end of Section A.13.1, find the curvature corresponding to the longitudinal strain, ϵ_1 , and the applied moment. This iteration yields N_p , M , and ϕ where M is

$$M = M_{gross} - M_{b_w Jd} + M_t$$

This algorithm is called "Calculate-Angle&Curvature" and is described in more detail in Ref. A-1.

The analytical model used is illustrated in Fig. A-6.

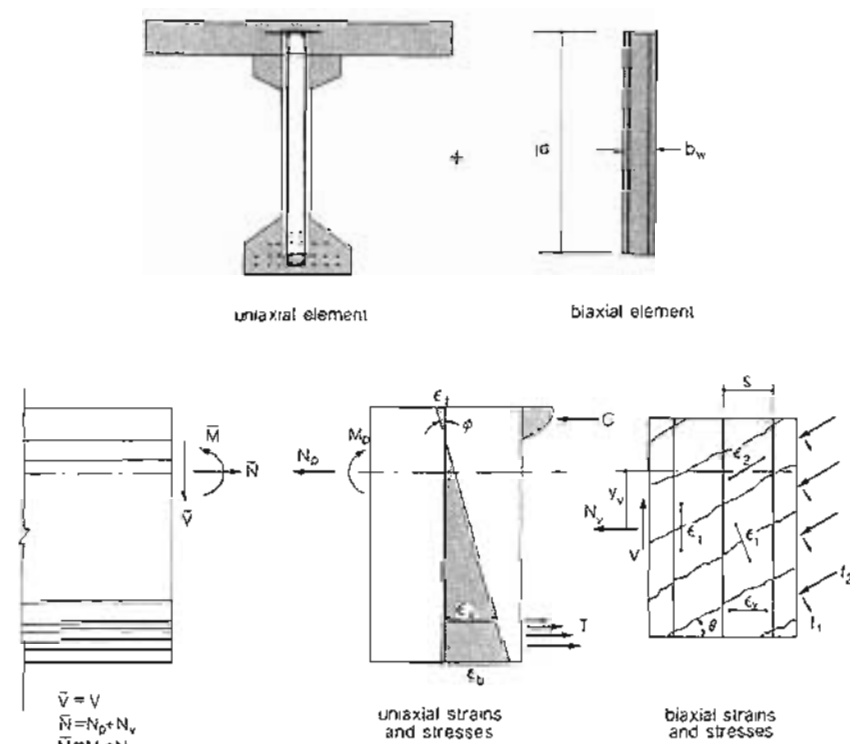


Figure A-6 Analytical model for N , M , and V .

A.13.4 Convergence Limits

The iterative algorithms described above are used to converge on stress resultants. To determine whether a stress resultant is close enough to the given loads, convergence limits have to be specified. Convergence limits used by the program are linked to the capacity of the section. In addition, the user can choose among three levels of accuracy, which have been provided to give the user some control over the limits used by the program. If answers do not have to be very exact, a lower accuracy can be used and fewer iterations will be required to perform calculations. This can translate into significant time savings on slow microcomputers (see Section A.8.4).

References

- A-1 Felber, Andreas J., "RESPONSE: A Program to Determine the Load-Deformation Response of Reinforced Concrete Sections", M.A.Sc. thesis, Department of Civil Engineering, University of Toronto, 1990, 148 pp.

Appendix B

Computer Program SHEAR

B.1 INTRODUCTION

Program SHEAR can be used to predict the load-deformation response of a prestressed concrete cross section subjected to shear or to shear combined with axial load. It is assumed that the longitudinal strains are uniform over the depth of the section and hence flexural effects are not considered.

Program SHEAR is a short (about 100 lines of BASIC), simple program whose main virtue is that it is easy to understand. The program follows exactly the 17-step solution technique described in Section 7.10. Program RESPONSE was built upon program SHEAR and uses the same basic solution technique. However the "easy-to-use" features of program RESPONSE and the many options available have made it "harder-to-understand."

The source code for program SHEAR is provided in a file called SHEAR.BAS on the diskette included. The executable file, SHEAR.EXE, which was compiled using Microsoft QuickBASIC (TM) version 4.5, is also provided.

B.2 EXAMPLE OF USING SHEAR

An example of using shear is given below. We have shown the data entered by the user in *italic* type enclosed in double quotes ("").

```
(C:\) "shear"
Name of beam? "CF1"
Web width in? "6"
Shear depth DV in? "20"
```

Total concrete area AC in²? "192"
 Cylinder strength of concrete FCP psi e.g. 3500? "5000"
 Peak strain × 1000 ECP e.g. -2.2? "-3"
 Cracking strength of concrete FCR psi? "300"
 Maximum aggregate size MAGG in e.g. 0.75? ".75"
 Tension stiffening factors e.g. 1.0, 0.7 or 0.49? "1"
 Total area of longitudinal rebars ASX in²? ".66"
 Yield strength of longitudinal rebars FYX ksi? "53.2"
 Area of longitudinal tendons APX in²? "1.436"
 Ultimate strength of tendons FPU ksi? "244"
 Modulus of tendons/1000 EP ksi e.g. 29? "28.6"
 Ram-Os parameters of tendon A, B, C eg. 0.025, 118, 10? ".017, 134, 10"
 Strain difference of tendon × 1000 DEP e.g. 6? "5.4"
 Area of stirrup legs AV in²? ".22"
 Spacing of stirrups S in? "6"
 Yield strength of stirrups FYV ksi? "53.2"
 Crack spacing controlled by long. reinf. SMX in? "16.3"
 Crack spacing controlled by stirrups SMV in? "11.6"

SHEAR RESPONSE OF MEMBER CF1

SECTION PROPERTIES

BV= 6 in DV= 20 in AC= 192 in² MAGG=.75 in
 FCP= 5600 psi ECP= -3 FCR= 300 psi TSF= 1
 ASX=.66 in² FYX= 53.2 ksi
 APX= 1.436 in² FPU= 244 ksi A=.017 B= 134 C= 10
 AV=.22 mm² FYV= 53.2 ksi
 SMX= 16.3 in SMV= 11.6 in

If axial load constant type 1 if N/V constant type 2? "1"

Axial load N kips? "0"

Axial Load N= 0 kips

Value of print.tens.str. × 1000 EI e.g. 2 Input 99 to change N. Input 100 to end? "

".08"

THETA= 25.18 N= 0.0 kip V= 76.1 kip

ET×1000= -0.00 EX×1000= -0.30 GAMMA×1000= 0.36

F1= 299 psi F2= 1349 psi F2MAX= 5600 psi

Crack spacing= 9.6 in Crack width= 0.001 in

Value of print.tens.str. × 1000 EI e.g. 2 Input 99 to change N. Input 100 to end?

We have now produced the data summarized in the second line of Table 7-2.

Appendix C

Computer Program MEMBRANE

C.1 INTRODUCTION

Program MEMBRANE is used to predict the load-deformation response of prestressed concrete elements subjected to in-plane shear or to in-plane shear and normal forces. The resulting state of strain and the associated concrete and steel stresses are determined.

Program MEMBRANE differs from program SHEAR in three main ways. Firstly, the input routine has been changed to allow the user to create, modify, and recall section files (files containing the characteristics of the element). Secondly, the user may include prestressing in both perpendicular in-plane directions, designated *x* and *y* in the program. Thirdly, normal loading in the *x*- and *y*-directions is specified as a constant (when shear = 0) plus a ratio of the shear.

The source code for the program, included on the disk provided is contained in file MEMBRANE.BAS. It is comprised of 326 lines of BASIC code: 140 lines for the input routine; 160 lines for the solution procedure; and 26 lines for the output routine. The solution procedure is based on the technique described in Section 7.10. A slight deviation from the 17-step solution technique was necessary to include the additional attributes of MEMBRANE. Descriptive variable names are used and the code is documented to help describe the solution procedure.

Two section files are also included on the floppy disk. EXAM14_5.MEM contains the section properties of the element in the example of Section 14.5, and SAMPLE.MEM contains the section properties of the element in the example to be described now.

C.2 EXAMPLE USING MEMBRANE

In this example, the user modifies an existing section file SAMPLE.MEM, changing existing material properties and the quantity of reinforcement. A loading state is specified and MEMBRANE is used to predict the response at five values of principal tensile strain.

A screen-by-screen description of the program's operation follows. Data to be entered by the user are shown in *italic* type and enclosed in double quotes ("").

Screen 1: The user chooses to retrieve file SAMPLE.MEM. The program displays the existing section properties of SAMPLE.MEM and the user chooses to modify the section properties.

Do You Wish to Retrieve an Existing Section File (Y or N)
? "y"

Enter Section Filename to be Retrieved (max. 8 + 3 characters)
" "sample.mem"

SECTION PROPERTIES

FCP = 4000 psi ECPx1000 = -2.22 FCR = 283 psi TSF = 1.00 MAgg = 0.75 in.
ASX = 2 in²/ft FSXYield = 60 ksi ASY = 1 in²/ft FSYYield = 60 ksi
APX = 0 in²/ft FPXULT = 0 ksi MODPX = 0 ksi DEPX = 0
AX = 0.000 BX = 0 CX = 0.0
APY = 1 in²/ft FPYULT = 270 ksi MODPY = 29 ksi DEPY = 6
AY = 0.025 BY = 118 CY = 10.0
THICK = 12 in. SMX = 9 in. SMY = 12 in.

Do You Wish to Modify Section Properties (Y or N)
? "y"

Screen 2: The program lists the concrete properties and the user chooses to change the cylinder compressive strength. The program changes the default peak strain and cracking strength [ECPx1000 = -2 x FCP/(57 x FCP⁵); FCR = 4 x FCP³] and the user changes the peak strain to -2 while accepting all other defaults.

INPUT SECTION DETAILS: STRIKING ENTER RETAINS DEFAULT

CONCRETE PROPERTIES

Cylinder Compressive Strength (psi):	FCP = 4000 ? "5000"
Peak Strain: ECPx1000 = -2.48 ? "-2"	
Cracking Strength of Concrete (psi):	FCR = 282.8 ?
Tension Stiffening Factor (e.g., 1, .7 or 49):	TSF = 1 ?
Maximum Aggregate Size (in.):	MAgg = .75 ?

Screen 3: The program displays updated section properties and lists the deformed bar properties. The user changes the area of steel in the *x*-direction to 3 in²/ft, the yield strength of the *x*-direction reinforcement to 58 ksi, and accepts all other defaults.

SECTION PROPERTIES

FCP = 3000 psi ECPx1000 = -2.00 FCR = 283 psi TSF = 1.00 MAgg = 0.75 in.

INPUT SECTION DETAILS: STRIKING ENTER RETAINS DEFAULT

Deformed Bar Characteristics

Area per foot of X-Reinforcement (sq.in./ft):	ASX = 2 ? "3"
Yield Strength of X-Reinforcement (ksi):	FSXYield = 60 ? "58"
Area per foot of Y-Reinforcement (sq.in./ft):	ASY = 1 ?
Yield Strength of Y-Reinforcement (ksi):	FSYYield = 60 ?

Screen 4: The program displays the updated section properties and lists the tendon characteristics. The user chooses to eliminate the prestressing steel in the *x*-direction. The program jumps down six lines to the next relevant question. The user increases the area of prestressing steel in the *y*-direction and accepts all other defaults.

SECTION PROPERTIES

FCP = 5000 psi ECPx1000 = -2.00 FCR = 283 psi TSF = 1.00 MAgg = 0.75 in.
ASX = 3 in²/ft FSXYield = 58 ksi ASY = 1 in²/ft FSYYield = 60 ksi

INPUT SECTION DETAILS: STRIKING ENTER RETAINS DEFAULT

Tendon Characteristics

Area per foot of X-Tendons (sq.in./ft): APX = 0 ?
Ultimate Strength of X-Tendons (ksi): FPXULT = 0
Modulus X-Tendons/1000 (ksi): MODPX = 0
Strain Difference of X-Tendons x 1000: DEPX = 0
Ram-Os Parameters of X-Tendons: AX = .000 BX = 0 CX = 0.0
Area per foot of Y-Tendons (sq.in./ft): APY = 1 ? "2"
Ultimate Strength of Y-Tendons (ksi): FPYULT = 270 ?
Modulus Y-Tendons/1000 (ksi): MODPY = 29 ?
Strain Difference of Y-Tendons x 1000: DEPY = 6 ?
Ram-Os Parameters of Y-Tendons: AY = -.025 ? BY = 118 ? CY = 10.0 ?

Screen 5: The program displays updated section properties and lists the crack-spacing parameters and thickness. The user changes SMX to 7 in. and SMY to 10 in.

SECTION PROPERTIES

FCP = 5000 psi ECPx1000 = -2.00 FCR = 283 psi TSF = 1.00 MAgg = 0.75 in.
ASX = 3 in²/ft FSXYield = 58 ksi ASY = 1 in²/ft FSYYield = 60 ksi
APX = 0 in²/ft FPXULT = 0 ksi MODPX = 0 DEPX = 0
AX = 0.000 BX = 0 CX = 0.0
APY = 2 in²/ft FPYULT = 270 ksi MODPY = 29 DEPY = 6
AY = 0.025 BY = 118 CY = 10.0

Crack-Spacing Parameters and Thickness

Thickness of Section: THICK = 12 ?
Crack Spacing Controlled by X-Reinforcement: SMX = 9 ? "7"
Crack Spacing Controlled by Y-Reinforcement: SMY = 12 ? "10"

Screen 6: The program displays the updated section properties. The user continues and saves the modified section properties in SAMPLEMD.MEM. The program saves the section properties and the user inputs the loading conditions. Note that the program does not save the loading conditions.

SECTION PROPERTIES

FCP = 5000 psi ECPx1000 = -2.00 FCR = 283 psi TSF = 1.00 MAgg = 0.75 in.
ASX = 3 in²/ft FSXYield = 58 ksi ASY = 1 in²/ft FSYYield = 60 ksi
APX = 0 in²/ft FPXULT = 0 ksi MODPX = 0 DEPX = 0
AX = 0.000 BX = 0 CX = 0.0
APY = 2 in²/ft FPYULT = 270 ksi MODPY = 29 DEPY = 6
AY = 0.025 BY = 118 CY = 10.0
THICK = 12 in. SMX = 7 in. SMY = 10 in.

HIT Enter to Continue. Type M to Modify Section Properties

?

To save MODIFIED section properties, Enter Desired Section Filename
(max. 8 + 3 characters) : Otherwise, just hit the Enter Key
? "samplemd.mem"

INPUT LOADING CONDITIONS

Force in X-Direction when Shear = 0, FXV0(kips/ft) ?
Ratio of (Incremental X-Dir. Force/Shear Force), RatioXX=dFX/dV ? ".2"
Force in Y-Direction when Shear = 0, FYV0(kips/ft) ? "100"
Ratio of (Incremental Y-Dir. Force/Shear Force), RatioYY=dFY/dV ? ".2"

Enter value of principal tensile strain, E1x1000 (e.g. 2) ? "1"
(Input 98 to change section properties, 99 to change loading state, 100 to end)

Sec. C.2 Example Using MEMBRANE

FX = 24.0 kips/ft		FY = 124.0 kips/ft		V = 120.1 kips/ft	
State of Strain		Average Steel Stresses		Concrete Stresses	
EXx1000	EYx1000	GAMMAX1000	FSX(ksi)	FSY(ksi)	F1(psi)
0.70	-0.13	1.15	20.41	-3.72	165.69
E1x1000	E2x1000	THETA(deg)	FPX(ksi)	FPY(ksi)	FCR(psi)
1.00	-0.42	63.03	0.00	169.87	282.84
MODPX = 0		MODPY = 29		DEPX = 0	
MODPY = 29		DEPY = 6		DEPY = 6	
Crack Spacing = 5.79 in.		Crack Width = 0.006 in.			

Enter value of principal tensile strain, E1x1000 (e.g. 2) ? "3"
(Input 98 to change section properties, 99 to change loading state, 100 to end)

FX = 37.0 kips/ft		FY = 137.0 kips/ft		V = 185.2 kips/ft	
State of Strain		Average Steel Stresses		Concrete Stresses	
EXx1000	EYx1000	GAMMAX1000	FSX(ksi)	FSY(ksi)	F1(psi)
1.71	0.41	3.64	49.69	11.99	127.13
E1x1000	E2x1000	THETA(deg)	FPX(ksi)	FPY(ksi)	FCR(psi)
3.00	-0.87	54.86	0.00	184.91	282.84
MODPX = 0		MODPY = 29		DEPX = 0	
DEPY = 6		DEPY = 6		DEPY = 6	
Crack Spacing = 5.73 in		Crack Width = 0.017 in.			

Enter value of principal tensile strain, E1x1000 (e.g. 2) ? "5"
(Input 98 to change section properties, 99 to change loading state, 100 to end)

FX = 40.9 kips/ft		FY = 140.9 kips/ft		V = 204.6 kips/ft	
State of Strain		Average Steel Stresses		Concrete Stresses	
EXx1000	EYx1000	GAMMAX1000	FSX(ksi)	FSY(ksi)	F1(psi)
2.74	0.71	6.24	58.00	20.66	109.58
E1x1000	E2x1000	THETA(deg)	FPX(ksi)	FPY(ksi)	FCR(psi)
5.00	-1.55	53.97	0.00	192.91	282.84
MODPX = 0		MODPY = 29		DEPX = 0	
DEPY = 6		DEPY = 6		DEPY = 6	
Shear on Crack Req'd for X-Dir. Equilibrium :		Crack Spacing = 5.74 in.		Crack Width = 0.029 in.	

Enter value of principal tensile strain, E1x1000 (e.g. 2) ? "6"
(Input 98 to change section properties, 99 to change loading state, 100 to end)

***** Concrete Crushing: Choose a smaller E1 *****
Enter value of principal tensile strain, E1x1000 (e.g. 2) ? "5.5"
(Input 98 to change section properties, 99 to change loading state, 100 to end)

$$F_x = 40.8 \text{ kips/ft} \quad F_y = 140.8 \text{ kips/ft} \quad V = 203.8 \text{ kips/ft}$$

$$F_y = 140.8 \text{ kips/ft} \quad V = 203.8 \text{ kips/ft}$$

$$= 203.8 \text{ kips/ft}$$

State of Strain			Average Steel Stresses		Concrete Stresses	
EXx1000	EYx1000	GAMMAx1000	FSX(ksi)	FSY(ksi)	F1(psi)	F2(psi)
2.95	0.70	7.00	58.00	20.18	106.40	2367.37
EIx1000 EEx1000 THETA(deg)			FPX(ksi)	FPY(ksi)	FCR(psi)	F2MAX(psi)
5.50	-1.86	53.92	0.00	192.47	282.84	2881.84
Shear on Crack Req'd for X-Dir. Equilibrium :			Crack Spacing = 5.74 in.		Crack Width = 0.032 in.	

Enter value of principal tensile strain, $E1 \times 1000$ (e.g. 2) ? "100"
(Input 98 to change section properties, 99 to change loading state, 100 to end)

Index

A

- Altimi, B.O., 528, 696
AASHTO, Standard Specifications for Highway Bridges.
 capacity reduction factors, 630, 632, 633
 composite action criteria, 635–6
 concrete stress limits, 628, 632
 deflection limits, 636
 loads, 616, 617, 618–9, 621
 surtup spacing limits, 635
 web reinforcement requirements, 635
Abelos, P.W., 22
Abrams, D.A., 97, 98
ACI 224R-80, 684
ACI 318-89: (*see also* Shear design, ACI traditional approach)
 anchorage zones, post-tensioning, 444
 bonded reinforcement limits, 277–8, 300, 539, 541
 camber and deflection limits, 270–2, 294, 296
 concrete cover, 111, 113, 527
 concrete cracking strength, 74
 concrete stiffness, 62
 corbel design, 449, 450, 453
 corrosion protection, 528
 crack control, 154–7, 159
 crack width limits, 270, 271
 development lengths, 98–100, 101, 102, 103, 104, 108
 flexural design, 258–304, 632
 equivalent stress-block factors, 273
 load and resistance factors, 273, 300–1
 flexural ductility,
 reinforcement limits, 276–8, 301, 515
 flexural stress estimates,
 bonded tendons, 273–5
 unbonded tendons, 275–6, 300
 flexure-shear cracking load, 315–7, 318–20
 load and resistance factors, 273, 300–1, 429, 430
 maximum flexural capacity, 238
 minimum reinforcement requirements, deep beams, 432, 442, 458
 moment redistribution allowance, 517–8, 542–3
 moment transfer at slab-column connections, 548–52
 nominal shear strength, 326–7, 331, 332
 postcracking reserve, 276, 294, 302, 516, 633
 restraint moments, 514
 shear friction, 467, 468, 469
 shear interface design, 470
 stress limits.

ACI 318-89 (*cont.*)
 concrete, 260, 298–9, 514, 539
 tendons, 49, 53, 258, 297–8
 structural integrity, flat plates, 575–6
 torsion design, 380, 405
 water/cement ratio, 111
 web-shear cracking, 311, 317–8, 319–20

ACI-ASCE Committee 426, 309, 313, 330

Adebar, P.E., 661

Adeghe, L.N., 425

Acberhard, H.U., 602

Aggregate interlock, 315, 316

Akiyama, H., 364

Allowable stresses: (*see also* Bearing stresses; Shear, cracking shear stress; Fatigue; Flexural design, design process)
 concrete, 258–9, 260, 298–9, 514, 539
 tendons, 49, 53, 258–9, 297–8

Anchorage, post-tensioning, 38, 42, 43 (*see also* Post-tensioning, systems)

Anchorage zones (*see* Disturbed regions)

Anderson, A.R., 466

Arbesman, B., 352

Arching action (membrane action), 624, 664

Axial load and flexure, 235–48
 interaction diagrams, 235–41
 moment-curvature response, 241–2, 243
 slender columns, 242–8

Axial loading, 124–67
 compatibility conditions, 124–6
 strain difference, $\Delta\varepsilon_y$, 125–6

crack control, 159–62

crack widths and spacing, 152–9
 Gergely-Lutz approach, 154–7, 159

elastic uncracked response, 137–42

equilibrium conditions, 126

influence of prestressing, 130–1, 132, 133

load-deformation response, 127–31

long-term response, 131–5, 142

short- vs. long-term response, 135–7

tension stiffening, 142–52
 average tensile stresses in concrete, 147–8

prestressed members, 150–2

B

Bakht, B., 622

Bars (*see* Reinforcement)

Batchelor, B. de V., 624

Bazant, Z.P., 70

Beam elements (*see* Complex structures)

Beams: (*see also* Flexural design; Flexure; Shear; Shear design; Statically indeterminate structures)
 with dapped ends, 442, 443
 deep beams, 415, 418, 420, 426, 427, 442–4, 453–61
 flexure, 168–242, 256–96
 influence of prestressing, 6, 8
 ledger beams, 413
 precast bridge girder design, 625–38
 shear, 309–79
 spandrel beams, 592, 593–5
 torsion, 380–411

Bearing stresses, 412–8, 462 (*see also* Disturbed regions; anchorage zones, strut and tie models, bearing areas; Nodal zones)

Beeby, A.W., 112, 114

Berggren, L., 105

Berlin Congress Hall collapse, 105

Bernoulli, Jacob, 170

Bhinde, S.B., 148, 672

Bischoff, P.H., 148, 150, 151

Blanketed strands, 29

Blanks, R.F., 75

Bond, reinforcement, 96–105, 106, 107, 108, 109
 deformed bars, 96–101, 102, 103, 104, 105
 development length, 97–101, 102, 103
 transfer length, 101–4, 106, 107

Bonded tendons (*see* Tendons, bonded)

Brackets, 439

Brandtzaeg, A., 79

Break-off test, 679, 680, 681

Breen, J.E., 462

Bresler, B., 313

Bridges, 8–9, 10, 11, 608–39
 analysis, 620–2, 623
 distribution of wheel loads, 621
 arch bridges, 609
 box-girder bridges, 609, 612
 Burlington Skyway, 11, 613
 cable-stayed bridges, 609
 codes (*see* AASHTO; OHBDC)
 construction techniques, 613, 615, 616, 617
 balanced cantilever, 613, 615
 launching truss, 613, 615
 Credit River Bridge, 613, 615, 616, 617
 deflections, 636–8
 design example, precast bridge girder, 625–38
 dimensioning and detailing, 625, 626
 East Huntington Bridge, 11, 609

economics, 609, 611, 613, 614
 Gateway Bridge, Brisbane, 612
 I-girder bridges, 609, 611
 loads, 616–20, 625–8, 629
 membrane action, deck slabs, 622–5
 span ranges, 609–10
 voided-slab bridges, 609, 612
 Walnut Lane Bridge, 19

Brown, R.L., 79

Browne, R.D., 683, 684

Bruce, R.N., 94

Building codes (*see* ACI 318-89; CEB-FIP Model Code; CSA A23.3-M84; FIP Recommendations; Hammurabi)

Buildings, 581–607 (*see also* Precast buildings; Parking structures; Post-tensioned foundations)
 special applications of post-tensioning, 598–600, 601, 602
 Burlington Skyway, 11, 613
 Burns, N.H., 533
 Buttresses, 13, 662, 664, 665

C

Camber, 201–8, 270–2, 283–4

Canadian Prestressed Concrete Institute (CPCI), 30

Carrasquillo, R.L., 63

CEB-FIP Model Code, 16
 crack spacing, 152–4, 155, 158, 210
 crack widths, 113–4, 152–4, 155, 158, 270
 development lengths, 100–1, 103, 104
 effective embedment zone, 153–4, 173
 fatigue of reinforcement, 93
 friction coefficients, 47, 49
 permissible bearing stress, 462

Celini, A., 208, 209

Centroidal axis:
 elongation in flexure, 622–4
 gross section, 169
 moments of area about, 192, 194
 transformed section, 191

Chain-drag test, 681

Christ Church Cathedral, Montreal, 14, 695–7, 699, 701–4

Clear, K.C., 111

CN Tower, 10, 17

Coefficients of friction, post-tensioning, 47–9, 53

Coefficient of thermal expansion:

concrete, 77
 reinforcement, 95

Collins, M.P., 146, 341, 344, 345, 346–7, 349, 355, 425, 467, 468, 469, 546, 616, 660, 672

Columns (*see* Axial load and flexure)

Compatibility torsion, 401, 403, 405

Complex structures, 640–67
 beam elements, 644–6
 finite element analysis, 641–4
 linear vs. nonlinear analysis, 641–2, 644
 membrane elements, 646–56, 657
 modified compression field theory, 646–56, 657

nonlinear sectional analysis, 644–60, 661

shell elements, 645, 646–60, 661
 shell elements with linearly varying strains, 645, 656–8
 layered shell elements, 645, 656–8
 shell elements with triaxial strains, 645, 658–60, 661
 out-of-plane shears, 658–60, 661
 program SHELL474, 658–60, 661
 shell element tester, 658, 659

space-frame models, 640, 642

testing, 660–6

variable-angle truss model, 640

Composite construction:
 flexural design, 213–21, 286–8
 shear interfaces, 468–70, 635–6

Compression field theory (*see* Shear)

Computer programs (*see* CONDM; FIELDS; MEMBRANE; RESPONSE; SEP; SHEAR; SHELL474; TEMPEST; TRIX)

Concrete, 57–80
 admixtures, 59
 age effect on response, 66
 aggregates, 59
 coefficient of thermal expansion, 77
 confinement, 79–80
 cover, 111–4
 cracking strength, 72–4
 double-punch test, 72, 74
 modulus of rupture, 72, 74
 split-cylinder test, 72, 74

creep, 67–72

cyclic loading, 65–6

cylinder strength, 61–7

effective stiffness, 67–72

fatigue, 65

high-strength, 59, 63–4, 329

web-shear cracking, 311–2

Concrete (*cont.*)
 hydration, 57–8, 60, 78
 lightweight, 59, 73, 79
 portland cement, 57–9, 60, 106, 115
 rate of loading, effect on response, 66–7
 shrinkage, 74–6
 sulfate attack, 115
 superplasticizers, 29, 59
 testing *in situ* (*see* Evaluation and rehabilitation of structures)
 thermal effects and properties, 76–8
 uniaxial compression, 61–5
 uniaxial tension, 72–4
 water, 58–9
 water/cement ratio, 59, 108, 111
 weight, 79
 CONDIM, computer program, 658
 Consideré, 143
 Construction stages, 213–21
 Conte, D.F., 352
 Cook, W.D., 427, 576, 694
 Corbels and ledge supports, 413, 426–9, 439–42, 449–53, 454
 Cordes, H., 210, 211
 Core testing, concrete, 679, 680
 Coming, L.H., 22
 Corrosion of reinforcement, 105–15 (*see also* Durability)
 Couplers, post-tensioning systems, 38, 43
 Cover meters, reinforced concrete, 681
 Cowan, H.J., 380
 Cracking:
 diagonal, 309
 flexure-shear, 312–7, 318–20
 web-shear, 311–2, 317–8, 319–20
 flexural, 172, 316–7
 patterns, 669–77
 microcracking, concrete, 61, 109
 torsional, 383
 Cracking strength, concrete (*see* Concrete)
 Credit River Bridge, 613, 615, 616, 617
 Creep of concrete, 67–72 (*see also* Long-term response)
 Crom, J.M., 19
 Cross, Hardy, 488, 523
 CSA A23.3-M84, 16
 concrete stress limits, 260
 crack width limits, 270
 design loads, compatibility torsion, 405
 detailing for torsion, 401, 402
 disturbed regions, design approach, 429
 effective web width, 406

CSA S474, Canadian code for concrete off-shore structures, 660
 Curvature diagrams, 202, 203, 205, 207
 Curvature friction losses, 47, 48
 Cyclic loading:
 concrete, 65–6
 reinforcement, 92–5, 96
 Cylinder strength, 61–7

D

Dakhil, F.H., 109, 111, 112
 Dandurand, A., 693, 698
 Dean, W.E., 32, 25
 Deep beams (*see* Disturbed regions)
 Deflections, 201–8, 270–2, 283–4, 294–6, 298, 302–4
 post-tensioned slabs, 552–4, 576
 prestressed bridges, 636–8
 statically indeterminate structures, 479–84, 485
 virtual work, 481–4, 485
 Deformed bars, 82, 84, 85
 ASTM standards, 84, 85
 bond characteristics, 96–101, 102, 103, 104, 105
 corrosion, 105–15
 fatigue, 92–3
 geometric properties, 84
 stress-strain response, 87, 88
 thermal properties, 96–7
 Design codes (*see* AASHTO; ACI 318-89; CEB-FIP Model Code; CSA A23.3-M84; CSA S474; FIP Recommendations; OHBDC)
 Design process, 15–6, 21, 278–85, 640–1
 Deterioration of structures (*see* Corrosion; Durability; Evaluation and rehabilitation of structures; Parking structures)
 Development length, 97–101, 102, 103
 Diagonal tension, 309, 311, 320, 321, 338–40, 343
 Disturbed regions, 412–75
 anchorage zones, 414–24, 426–9, 442, 444–8
 beams with dapped ends, 442, 443
 beams with web openings, 443
 bearing areas, 462–3
 bursting zone, 414
 corbels and ledge supports, 426–9, 439–42, 449–53, 454
 CSA A23.3-M84, 429

deep beam analogy, end zones, 422–4
 deep beams, 426–9, 432, 442, 444, 453–61
 elastic uncracked analysis, 415, 418, 420
 nonlinear finite element analysis, 426, 427
 detailing, beams with dapped ends, 442
 direction change, tendons, 463–6
 elastic uncracked analysis, 413–22
 end anchorage zones, 414–22
 deep beam, 414, 415, 418, 420
 nonlinear finite element analysis, 424, 425, 439, 440
 postcracking response, 424–59
 shear friction concept, 466
 shear interfaces, composite beams, 468–70
 spalling zone, 414
 strut and tie models, 426–59
 anchorage zones, 426–9, 442, 444–8
 beams, relationship to sectional model, 433, 436–8
 beams with dapped ends, 442, 443
 corbels and ledge supports, 426–9, 439–42, 449–53, 454
 crushing strength of cracked concrete, 430–2
 deep beams, 426–9, 453–61
 effective strut width, 430, 431
 reinforcement requirements, 430, 432, 438
 relationship to sectional model for shear, 433, 436–8
 Double-punch test, 72, 74
 Double-tear elements, 30, 31
 example design, 289–96
 flexural lever arm, 281
 sectional properties, 33
 span and load ranges, 278
 span-to-depth ratios, 279
 Draped tendons (*see* Tendons)
 Dressel, D.J., 696
 Ductility, 79
 Durability: (*see also* Grouting of ducts)
 concrete, 115
 corrosion, reinforcement, 105–15
 repair of corrosion damage, 687, 689, 690, 691
 symptoms, 677, 678, 679
 testing for corrosion, 680, 681–4
 unbonded tendons, 41, 527–8
 parking structures, 590–1, 594, 596–8
 Dyckerhoff and Widmann, 34, 39, 613

E

East Huntington Bridge, 11
 Effective embedment zone, 173 (*see also* Tension stiffening)
 Effective moment of inertia, 554
 Effective stiffness:
 concrete, 67–72
 prestressing, 90–2, 188
 Elastic shortening (*see* Loss of prestress)
 Elastic uncracked response:
 axial loading, 137–42
 disturbed regions, 413–22
 flexure, 190–201
 shear, 320–1
 torsion, 383–6
 Ellenzweig, H., 592
 El Shahawi, M., 154, 155
 Elstner, R.C., 327
 Engineering beam theory, limitations, 412 (*see also* Disturbed regions)
 Equivalent frame method, 535–9, 540, 563–4, 566–7, 568
 Evaluation and rehabilitation of structures, 668–706
 analytical assessment, 684–6
 applications of non-prestressed reinforcement, 689–90, 692, 693, 694
 applications of post-tensioning, 690–704
 additions to existing structures, 691, 697
 crack and deflection control, 690–1, 695, 696
 foundation problems, 691–2, 698
 underpinning existing structures, 695–7, 699, 701–4
 upgrading examples, 692–3, 695, 699, 700–4
 examination, 668, 669–84
 rehabilitation and upgrading measures, 686–705
 repair of corrosion damage, 687, 689, 690, 691
 repair of cracking, 687, 688
 symptoms of distress, 669–77
 corrosion of reinforcement, 677, 679
 crack patterns, 669–77
 individual cracks, 677
 large deformations, 677
 spalling and delamination, 677, 678
 testing, 677–84
 break-off test, 679, 680, 681

Evaluation and rehabilitation of structures
(*cont.*)
chain-drag test, 681
chemical composition, 680, 682
core testing, 679, 680
corrosion potential, 680, 683-4
cover meters, 681
durability factors, 680, 682-3
gamma- and x-rays, 681
internal fracture test, 679, 680, 681
pull-off test, 679, 680, 681
pull-out test, 679, 680, 681
Schmidt Rebound Hammer, 677-8, 680
ultrasonic pulse velocity, 680-1, 682
Windsor probe, 678-9, 679-80
Eyre, D.G., 694

F

Factored loads (*see ACI 318-89, load and resistance factors*)
Falkner, H., 161, 162
Fatigue:
concrete, 65-6
flexure, 227-9
fretting, 95, 229
Miner's rule, 227-8
reinforcement, 92-5, 96
Fenwick, R.C., 315, 467
FIELDS, computer program, 650
Finite element analysis: (*see also Complex structures*)
nonlinear, 424, 439, 440
program FIELDS, 650
program TRIX, 650
Fintel, M., 591
FIP Recommendations:
fatigue of prestressing, 94
fatigue resistance, flexure, 228
Flat plates 524, 541 (*see also Slabs; Post-tensioned slabs; ACI 318-89*)
design example, 554-78
Flat slabs, (*see Slabs; Post-tensioned slabs*)
Flexural design, 256-308 (*see also Axial load and flexure*)
ACI 318-89 method, 258-304
camber and deflections, 270-2, 283-4, 294-6
composite construction, 286-8
concrete stresses, calculation, 259-69

force-in-the-tendon approach, 263-6, 267-8, 271, 298-9
strain compatibility approach, 259-62, 268-9
crack width limits, 270, 271
design process, 278-85
choice of cross section, 278-9, 289, 296
deflection limits, 283-4, 294-6, 298, 302-4
design sequence, 285, 289-91
span-to-depth ratios, 279, 289, 296
strength requirements, 284-5, 293-4
stress limits, 279-83, 291-2, 297, 298-9
tendon profiles, 279-83, 291-2, 297
ductility,
bonded reinforcement limit, 277-78, 300
posttacking reserve, ACI, 276, 294, 302
reinforcement limits, ACI, 276-8, 301
equivalent stress-block factors, 273
flexural lever arm, 280-1, 284
general considerations, 256-8
life stages of member, 257, 279-80, 298-9
load and resistance factors, 273, 300-1
precast bridge girder, 632-3
strength, 273-8, 284-5, 293-4, 300-1
ACI stress estimate, bonded tendons, 273-5
ACI stress estimate, unbonded tendons, 275-6, 300
stress limits,
concrete, 258-9, 260
tendons, 258-9, 297-8
Flexure, 8, 168-255, 256-308 (*see also Flexural design; Axial load and flexure*)
camber, 201-8
compatibility conditions, 170
strain difference, $\Delta\epsilon_p$, 170
composite construction, 213-21
crack widths and spacing, 208-13
CEB-FIP Model Code, 210
curvature diagrams, 202, 203, 205, 207
deflections, 201-8
design (*see Flexural design*)
elastic uncracked response, 190-201
compatibility conditions, 191, 198
equilibrium conditions, 192-3, 196-7
long-term, 198-201
short- vs. long-term, 200-1
stress-strain relationships, 191-2
transformed section, 194-5, 196
equilibrium conditions, 171
fatigue resistance, 227-9

FIP Recommendations, 228
fretting, 229
influence of prestressing, 8
maximum capacity, ACI 318-89, 238
moment-curvature response, 171-201
layer-by-layer approach, 182-7
long-term, 187-90
stress-block approach, 177-82, 183
nonuniform thermal and shrinkage strains, 221-6
plane-sections hypothesis, 170
program RESPONSE (*see RESPONSE*)
section forces,
layer-by-layer approach, 173-5
stress-block approach, 175-7
tension stiffening, 172-3, 185-7
unbonded tendons, 229-35, 236
Flexure and axial load (*see Axial load and flexure*)
Floor slabs (*see Slabs*)
Floor systems, 11, 523-4 (*see also Slabs; Post-tensioned slabs*)
design example, double-tee floor member, 289-96
diaphragm action, 582-3, 585, 586, 587, 588, 589
precast concrete buildings, 581-2, 583, 584, 585
Fomerod, M., 22
45° truss model (*see Shear design; 45° truss model*)
Foundations (*see Post-tensioned foundations*)
Frames (*see also Statically indeterminate structures; Precast buildings; Complex structures*)
deflections, 481-4, 485
restraint actions, 478-9, 480, 495-502
effect of construction sequence, 503-6
frame analysis programs, 502-6, 640-1
torsion, 380
Freay, J., 467, 469
Fretting (*see Fatigue, fretting*)
Freysinet, Eugene, 1, 3-4, 18
Friction coefficients, post-tensioning, 47-9, 53
ACI, 47, 48
CEB-FIP Model Code, 47, 49

G

Gahiani, A.S., 109, 111, 112
Gallaccio, J., 696

Galtier Plaza, 13
Gamble, W.L., 543
Ganz, H.R., 602
Gateway Bridge, Brisbane, 612
Gaynor, R.D., 110
Geohegan, M.P., 683, 684
Gergely, P., 154-7, 159, 422
Germundson, T., 22
Gerwick, B.C., Jr., 109, 640
Ghali, A., 92
Gill, P.A.T., 144, 147
Girders (*see also Beams; Bridges; Disturbed regions; deep beams*)
bridge girders, 8-9, 10, 11, 30, 51-3, 609, 610, 611, 612, 614
stage post-tensioning, 598, 599, 600
Gopalaraman, V.S., 73
Goto, Y., 144
Grant, A., 11
Grieve, R., 678
Gross section:
properties, 194-5
in stress calculations, 265-6, 267
in structural analysis, 169
Grouping of ducts, 38, 41-2, 43
Gulliak, C., 13, 20
Guralnick, S.A., 313
Gustaferro, A.H., 526
Guyon, Y., 18

H

Hagen, H.W., 392
Hall, A.S., 124
Hammarabi, 581
Hanson, J.M., 93, 253
Harped tendons (*see Tendons*)
Harris, P.J., 675
Hawkins, N.M., 462, 549
Helgason, Th., 93
Hemakom, R., 533
Hewitt, B.E., 624
High-strength concrete (*see Concrete; high-strength*)
Hognestad, E., 229, 231, 235, 236, 276, 325, 327
Hollow-core elements, 31, 32
diaphragm action, 585, 588
flexural lever arm, 281
framing, 583, 592, 594
span and load ranges, 278

Hollow-core elements (*cont.*)
span-to-depth ratios, 279
structural integrity, 591

Hom, S., 687, 688
Hooke, Robert, 168, 170
Hoop reinforcement,
circumferential tendons, 15, 664
stirrups, 386–8, 390, 407, 408

Hoyer, E., 4, 104

Bulsbos, C.J., 93, 253

Humidity, relationship to:
creep coefficient, 68–9, 71–2

durability, 114

shrinkage, 74–6

Hwang, L.S., 154, 155

I

I-girders, 31 (*see also* Girders; Beams; Bridges)
design example, precast bridge girder, 623–38
flexural lever arm, 281
span-to-depth ratios, 279

Iguro, M., 364

Impact:

bridge loads, 608, 616–20, 628, 629
damage, 677

Inclined cracking, (*see* Cracking, diagonal)

Initial concrete strength, 258–60

Interaction diagrams:

axial load and moment, 235–41
shear-moment, 357–8, 367–8
torsion-flexure, 395–6

Internal fracture test, 679, 680, 681

International Aviation Organization Headquarters, Montreal, 601

Iqbal, M., 591

Iyengar, K.T.S.R., 416

J

Jaoney, J.R., 229, 231, 235, 236
Jennewein, M., 412, 428, 438, 685

Jensen, J.J., 61

Jirsa, J.O., 400

Joints: (*see also* Precast buildings, structural
integrity)

control joints, 597

expansion joints, 478, 597, 687

slab-column connections, 548–52, 570–5

Joists, 113 (*see also* Beams; Flexure; Flexural
design)

K

Kaar, P.H., 94, 101–2, 106, 107
Kammerhuber, J., 417
Kani, G.N.J., 315, 432, 433, 434
Kanula, B.T., 275
Kerr point, 280
Kirschner, U., 660
Koch, R., 660
Kollegger, J., 148
Kost, G., 687, 688
Kupfer, H., 335

L

La Fraugh, R.W., 101–2, 106, 107
Ledge supports (*see* Corbels and ledge sup-
ports)
Lee, Y.M., 675
Leonhardt, F., 22, 221, 415–6, 420, 477, 684
Lie, T.T., 78
Lightweight concrete (*see* Concrete, lightweight)
Lin, T.D., 78
Lin, T.Y., 22, 256
Load balancing, 528–33, 556–60
Loads. (*see also* ACI 318-89, load and resis-
tance factors; Impact)
AASHTO, 616, 617, 618–9, 621
bridge, 616–20, 615–8, 629
CSA A23.3, compatibility torsion, 405
OHBDC, 617, 619, 620
shear, cracking load, 315–7, 318–20
Loss of prestress:
creep and shrinkage, 3
friction loss calculations, 51–3
post-tensioning losses, 46–53, 560–3
anchorage set, 50–1, 53
curvature friction, 47, 48
elastic shortening, 560
friction coefficients, 47–9, 53
ACI, 47, 48
CEB-FIP, 47–9
wobble friction, 47, 48
pretensioning, elastic shortening, 27
Lu, F., 173, 177, 181, 182, 183
Lutz, L.A., 154–7, 159

M

McGee, W.D., 384
MacGregor, J.G., 326, 426, 427, 661, 664, 665
McHenry, D., 229, 231, 235, 236
McMillan, C.B., 601
Mailhot, G., 331
Magnel, G., 18–9, 422
Magura, D., 90
Maret, J.C., 15
Manulife Centre, Toronto, 600, 602
Mardukhi, J., 397
Marti, P., 338, 428, 602
Martin, L.D., 206
Martynowicz, A., 601
Mass, M.A., 101–2, 106, 107
Material properties, 57–123
Mausba, P., 148
Mattock, A.H., 88, 275, 442, 467, 469
Maurel, G., 694
Mavaddat, S., 696
Mechlhorn, G., 419
Mehta, P.K., 109
MEMBRANE, computer program, 649, 656,
users' manual, 747–52
Membrane elements (*see* Complex structures)
Mills, R.H., 60, 62
Miner, M.A., 227
Miner's rule, 227–8
Mitchell, D., 427, 576, 675, 693, 694, 698
Modified compression field theory (*see* Shear
Shear design; Complex structures)
Modulus of rupture, 72, 74
Moment-curvature (*see* Flexure; Axial load
and flexure)
Moment distribution, 488–502
Moment magnification, 242–8
Montreal Olympic Tower, 21, 692–4, 695,
699, 700–1
Moritz, E.A., 325
Mörsch, E., 143, 312, 313, 315, 321, 322,
323, 325, 334, 335, 416
Moselbi, O., 15
Murray, D.W., 554

N

Nadai, A., 383
Nathan, N.D., 247, 248
Navier, 170
Neutral axis, 155–6, 176, 178, 312, 418, 436

Ngo, D., 424

Nielsen, M.P., 335

Nilson, A.H., 62, 63

Nodal zones, strut and tie models, 426–30,
438, 439, 442, 446, 450, 451, 452, 455,
459–60, 461

Nojin, Y., 364

Nominal strength:
reinforcement, 81, 82, 85
shear strength, 326–7, 331, 332, 359, 364,
546, 547, 549–50
shear stress, 313–4, 361, 363
torsional shear stress, 391, 398–9
Nonlinear sectional analysis (*see* Complex
structures)

Nuclear containment structures, 10, 15, 16

O

Ochrym, G., 674
Ockleston, A.J., 546, 624
Offshore production platforms, 11–3, 18, 19,
20, 643, 660

Gulfaks C, 13, 20

OHBDC (Ontario Highway Bridge Design
Code):
"empirical method" of design, 624–5
loads, 617, 619, 620
low-relaxation steel, 90
membrane action, composite beam-slab
bridges, 624–5

Okada, T., 364

Ong, S.Y., 426, 427

Ono, K., 62

P

$P\Delta$ effect, 242–8
Park, R., 173, 177, 181, 182, 183, 543, 685

Parking structures, 9, 12, 590–8

durability, 590, 594, 596–8
precast connection details, 593–4
precast framing systems, 591–2
post-tensioning, 594, 596
precast spandrel beams, 594, 595

Paulay, T., 315, 467, 685

Paultre, P., 693, 698

Pauser, A., 223

Pauw, A., 62

PCA (Portland Cement Association), 229

PCI Design Handbook:
building construction, 581
expansion joints, 478
long-term cambers and deflections, 206
Pister, K.S., 313
Plane-secuons hypothesis, 170
Plasticity methods, 335
Point of inflection, tendon profiles, 44, 492, 510, 557, 559
Popovics, S., 61, 63
Portland cement (*see Concrete, portland cement*)
Post-tensioned foundations, 12, 14, 600, 602–6
Post-tensioned slabs, 12, 13, 32, 523–78
advantages, 523
analysis,
equivalent frame method, 535–9, 540, 563–4, 566–7, 568
sequence of construction and creep, 539
available eccentricity, 524, 525
control of cracking, 539, 541, 567–9
corrosion protection, 527–8
deflections, 552–4, 576
design examples,
flat plate, 554–78
one-way, simply supported, 296–304
one-way, two-span, 509–16
distribution of tendons, 2-way slabs, 533–5, 563
advantages of banding, 534–5
edge and corner panels, special considerations, 542, 543
fire resistance, 526–7
flexural capacity, 542–5, 570
yield line analysis, 543–5
load balancing, 528–33, 556–60
North American practice, 524–5
shear design, 545–52
exterior columns, 547, 555
interior columns (punching shear), 526, 546–52, 555
wide-beam shear capacity, 546
slab-column connections, 548–52, 570–5
slab thickness, 525–7, 555–6
span-to-depth ratios, 524, 525, 526
types, 523–4
Post-tensioning: (*see also Evaluation and rehabilitation of structures*)
losses (*see Loss of prestress*)
operations, 31–3, 34, 49–50
rehabilitation of structures, 690–704

special applications to buildings, 598–600, 601, 602
systems, 33–8, 39, 40, 41
anchorage, 38, 42, 43
BBR multi-wire, 38, 40
couplers, 38, 43
Dywidag threadbar, 34, 39
Freyssinet K-Range, 34, 36
monostrand, 38, 41
VSL multi-strand, 34, 37
Post-Tensioning Institute:
cover, post-tensioned slabs, 527
grouting specifications, 42
span-to-depth ratios, 526
unbonded single-strand tendons, 528
Post-Tensioning Manual:
fire-resistance requirements, 526
Precast buildings:
framing, 581–2, 583, 584, 585
structural integrity, 582–90, 591
floor systems, 582–3, 585, 586, 587, 588, 589
wall panels, 586–90, 591
Precast pretensioned elements, 9
standard shapes, 30–1, 32, 33
choosing, 278
Precasting operations, 29–31
Preload Company of N.Y., 10, 19, 22
Preston, H.K., 263
Prestressed concrete industry, growth, 6
Prestressed Concrete Institute (PCI), 22, 30
Prestressing losses (*see Loss of prestress*)
Prestressing steel (*see Tendons*)
Prestressing technology, 25–56
Pretensioning operations, 4–5, 27–30
Priestley, M.J.N., 173, 177, 181, 182, 183, 233
Principal of virtual work, 481–4, 485
Prujssers, A., 467, 469
Pull-off test, 679, 680, 681
Pull-out test, 679, 680, 681
Punching shear, 526, 546–52, 555

R

Rabba, B.G., 94, 95
Radius of curvature, tendons, 44–5, 47, 49, 95, 463, 510, 529, 560, 625
Ramberg-Osgood functions (*see Tendons*)
Rasheeduzzafar, 109, 111, 312
Ravindra, M.V., 592

Rehabilitation of structures (*see Evaluation and rehabilitation of structures*)
Reinbagnl, H.-G., 660
Reineck, K.-H., 660, 662, 663
Reinforcement: (*see also Deformed bars; Tendons; Welded wire fabric*)
types, 80–6
Reinforcement response, 87–105 (*see also Deformed bars; Tendons*)
Renke, H.-G., 660
Relaxation of prestressing (*see Tendons, relaxation*)
Repair of structures (*see Evaluation and rehabilitation of structures*)
RESPONSE, computer program, 175
construction stages, 219–21
crack widths, 211–3
long-term moment-curvature, 180–90
M-N interaction, 238–9
rehabilitation, 690
shear-moment interaction, 357–8
short-term moment-curvature, 182–5, 206–8
thermal strains, 224–6
users' manual, 707–46
Restraint actions, (*see Statically indeterminate structures*)
Richart, F.E., 79, 326, 330
Rigon, C., 95, 96
Ritter, W., 323
Ritz, P., 543, 545, 596
Rizkalla, S.H., 154, 155, 661, 664
Rogowski, D.M., 426, 427
Rosati, F.S., 148
Rothenburg, L., 678
Rowe, T.J., 78
Russell, H.G., 94

S

de Saint-Venant, 383, 413, 423–4
Sargious, M., 419
Sato, J.A., 506, 507
Scanlon, A., 554
Schäfer, K., 412, 428, 438, 685
Scheef, H., 609, 613, 625, 626
Schlaich, J., 412, 428, 438, 609, 613, 625, 626, 685
Schmidt Rebound Hammer, 677–8, 680
Schneider, J., 417
Schuler, W., 602
Schultz, D.M., 591

Schupack, M., 528
Scordelis, A.C., 424
Scott, N.L., 263
Seon, R.H., 144, 147
Secant modulus, concrete, 63
Secondary (restraint) moments, 479, 486, 517
(*see also Statically indeterminate structures, restraint actions*)
Second-order analysis, 244–5
Seismic design, 79
Shah, S.P., 73
Shaikh, A.F., 467
Shear, 309–79 (*see also Shear design; Shear friction concept; Shear interfaces*)
aggregate interlock, 315, 316
compression field theory, 338–43, 344, 345
cracking shear stress, 310, 311
diagonal cracking, 309–20
dual-section analysis, 355, 356, 358
elastic uncracked response, 320–1
flexure-shear cracking, 312–7, 318–20
ACI 318–8 cracking load, 315–7, 318–20
nominal shear stress, 313–4
Kani's comb model, 315
modified compression field theory, 343–74
program RESPONSE, 357–8
program SHEAR, 353–4, 359
postcracking response, 320–2
principal stress directions, 310, 311
web-shear cracking, 311–2, 317–8, 319–20
SHEAR, computer program, 353–4, 359,
users' manual, 745–6
Shear design, 323–38, 339, 359–74, 633–5
(*see also Shear*)
ACI traditional approach, 325–33
concrete contribution, 326–7, 331, 332
role of longitudinal reinforcement, 330, 374
steel contribution, 327, 331–2, 333
slipup design, 327–9, 332–3
45° truss model, 323–5
modified compression field theory, 359–74,
633–5
members with web reinforcement, 363–4, 368–74
members without web reinforcement, 364, 365
punching shear, 526, 547–9, 555
size effect, 364–6
slabs, 545–52
staggering concept, 335–7
variable-angle truss models, 334–8, 339

Shear friction concept (*see* Disturbed regions)
 Shear interfaces, 468–70, 635–6
 Shell elements (*see* Complex structures)
 SHELL474, computer program, 658–60, 661
 Shioya, T., 364–6, 367, 368
 Shorer, H., 22
 Shrinkage (*see* Concrete; *see also* Long-term response)
 Shrinkage stresses, 222
 Siess, C.P., 90, 313, 326
 Summonds, S.H., 552, 661, 664
 Single-tet elements, 30, 31
 analysis example, 182–90, 195–201, 204–8, 210–3, 213–21
 flexural lever arm, 281
 sectional properties, 33
 span and load ranges, 278
 span-to-depth ratios, 279
 Skelton, R., 616, 617
 SkyDome, 11, 17
 Slabs: (*see also* Post-tensioned slabs; Flexure; Flexural design)
 cover, 113
 span-to-depth ratios, 7–8, 9–10, 510
 standard precast elements, 30–1
 State, F.O., 63
 Slater, W.M., 598, 599, 600, 678
 Slender columns (*see* Axial load and flexure)
 Somes, N.F., 93
 Sozen, M.A., 90, 104, 326, 422
 Spacing limits:
 bonded reinforcement, 539, 541
 slab reinforcement, OHBDC “empirical method”, 625
 stirrups, 327, 329, 362, 371, 372, 401
 transverse tendons, bridges, 625
 web reinforcement, AASHTO, 635
 Span-to-depth ratios: (*see also* Post-tensioned slabs)
 beams, 418
 simply supported members, 279
 slabs, 7–8, 9–10, 510
 Spencer, R.A., 586
 Spiral reinforcement:
 post-tensioning anchorage zones, 462–3
 required cover, 113
 Splices:
 bridge segments, 611, 613
 effect on delamination, 677
 longitudinal reinforcement, 400–1
 Split-cylinder test, 72, 74
 Staggering concept (*see* Shear design)

Standard precast shapes (*see* Precast pretensioned elements)
 Statically indeterminate structures, 476–522
 deformations, 479–84, 485
 principle of virtual work, 481–4, 485
 design example, one-way floor slab, 509–16
 eigenstresses, 477
 expansion joints, 478
 influence of restraint moments at ultimate, 517–8
 load stresses, 477
 moment distribution, 488–502
 restraint actions, 478–518
 due to axial deformations, 478, 495–502
 due to post-tensioning, 479, 480, 491–5
 elastic uncracked assumption, implications, 501–2
 fixed-end moments due to prestress, 489–91, 492, 564–5
 flexibility approach, 484–7
 influence of creep, 506–9
 influence of construction sequence, 503–6
 standard computer programs, 502–6
 restraint stresses, 477
 torsion, 401–5
 Stocker, M.F., 104
 Stone, W.C., 462
 Strain difference, $\Delta\epsilon_p$, 125–6, 170
 Strain tempering (*see* Tendons)
 Stress-block factors, 175–82
 Stress relieving (*see* Tendons)
 Stress-strain response: (*see also* Tendons; Ramberg-Osgood functions)
 concrete,
 compression, 61–5
 tension, 72, 73
 reinforcement, 87–90
 Sulfate attack, concrete, 115
 Superplasticizers, 29, 59
 Swanson, D.T., 528, 696

T

Talbot, A.N., 325
 Tanks, 10, 14, 19, 413, 466
 Taylor, H.P.J., 316
 TEMPEST, computer program, 517
 Tendon profiles, 27–9, 42–6, 47, 279–83, 291–2, 297
 Tendons, 25–6, 80–105
 ASTM standards, 80–2

Tendons
 blanketed strands, 29
 bond, 101–5, 107, 108, 109
 bonded, 32, 35, 38, 41–2, 43 (*see also* Grouting of ducts)
 coefficient of thermal expansion, 95
 corrosion, 105–15
 CSA standards, 80, 81, 82
 deformed bars, 26
 draped, 27–9
 effective stiffness, 90–2, 188
 fatigue, 93–5, 96
 harped (*see* Tendons, draped)
 low-relaxation strand (*see* Tendons, strain tempering)
 profiles (*see* Tendon profiles)
 properties, standard tendons, 81
 Ramberg-Osgood functions, 88–9, 177, 188, 230
 relaxation, 90–2
 7-wire strand, 26, 80–1, 83, 85
 strain tempering, 80, 83, 85
 stress relieving, 80, 83, 85
 stress-strain response, 87–90
 systems, 33–4, 35
 thermal properties, 95–6, 97
 unbonded, 32, 35
 wires, 26
 Tensile strength:
 concrete, 1, 152, 229, 327, 679, 681
 tendons, 26, 82, 90, 95–6, 373, 526
 Tension stiffening:
 axial load, 142–52
 flexure, 172–3, 185–7
 Tepfers, R., 98
 Testing in-situ concrete (*see* Evaluation and rehabilitation of structures)
 Thermal properties:
 concrete, 76–8
 reinforcement, 95–6, 97
 Thermal strains, 131–2, 133–5
 Thermally-induced stresses, 222 (*see also* Flexure, nonuniform thermal and shrinkage strains)
 Theryo, T.S., 442
 Thiel, H., 415
 Thorenfeldt, E., 61
 Thormählen, U., 210, 211
 Thürlimann, B., 95, 96, 335
 Tide, R.H.R., 94, 228
 Tighe, M.R., 689

Time-dependent losses (*see* Loss of prestress; Creep of concrete; Tendons, relaxation; Concrete, shrinkage; Long-term response)
 Tomaszewicz, A., 61
 Tong, W.K.T., 586
 Torsion, 380–411
 ACI 318–89, 380, 403
 combined torsion and flexure, 394–6, 397
 interaction diagrams, 395–6
 combined torsion, shear, and flexure, 396–400
 design method, 398–400, 405–9
 compatibility torsion, 401, 403, 405
 CSA A23.3-M84,
 design loads, compatibility torsion, 405
 detailing, 401, 402
 detailing, 400–1, 402
 elastic uncracked response, 383–6
 cracking torsion, 384, 385
 equivalent-tube analysis, 383–4, 385–6
 postcracking response, 386–94
 effective wall thickness, 387–91
 equilibrium conditions, 386–7, 389–90
 principal compressive stress, 391
 statically indeterminate structures, 401–5
 compatibility torsion, 401, 403
 torsional stiffness, 401–5
 thin-walled tubes, 380–3
 shear stress, 382
 torsional stiffness, 382–3
 torsional stiffness, 382–3, 401–5
 variable-angle space truss, 396, 398, 399
 Torsion and flexure, 394–6, 397
 Torsion, shear and flexure, 396–400
 Towers:
 CN Tower, 10, 17
 Montreal Olympic, 21
 Transfer length (*see* Bond)
 Transformed section, 138–9, 191, 192, 193, 194–5, 196, 203–5, 215, 259–62, 264–6, 267–9, 288, 628–9
 Trevino, J., 92
 TRIX, computer program, 650
 Trost, H., 70, 210, 211
 Two-way slabs, 32, 524, 525, 526, 527, 546, 675
 deflections, 552–4
 load balancing, 528–35
 yield line analysis, 543–5

U

Ultrasonic pulse velocity test, 680–1, 682
 Unbonded tendons (*see* Tendons, unbonded)

V

Vambergky, J.N.J.A., 588
 Van Daveer, J.R., 684
 Van Horn, D.A., 94, 228, 253
 Van Vollenburg, D., 689
 Variable-angle truss models (*see* Shear design, variable-angle truss models)
 Vecchio, F.J., 146, 341, 344, 345, 346–7, 349, 355, 467, 468, 469, 506, 507, 517, 546, 646
 Virtual work, 481–4, 485
 Vitelli, R.J., 592
 Vitruvius, 57
 Vrana, J., 310
 VSL multi-strand post-tensioning system, 34, 37

W

Waddell, J.A.L., 608, 619
 Waffle slabs, 524, 526, 690, 691
 Wagner, H., 338–40
 Wall panels, 237–48, 255, 586–90
 Walnut Lane Bridge, 19
 Walraven, J.C., 349, 467, 469
 Walther, R., 313, 420
 Ward, D.L., 593, 594
 Warner, R.F., 65, 66, 93
 Water/cement ratio, 59, 108, 111

Web-shear cracks, 311–2, 317–8, 319–20
 Welded wire fabric, 82, 86
 Williams, A., 148, 59, 160
 Windsor probe, 678–9, 679–80
 Winter, V.C., 533
 Wilhey, M.O., 325
 Wobble effect, 47, 48, 49, 464
 Woodhead, R.W., 124
 Workman, E.B., 263

Y

Yamazaki, J., 275
 Yield line method, 543–5
 Yield stress: (*see also* Ramberg-Osgood functions)
 deformed bars, 82, 85
 tendons, 82, 87–8, 90, 238
 Young's modulus: (*see also* Stress-strain response; Secant modulus; Ramberg-Osgood functions)
 concrete, 69–70, 188, 215, 216, 218, 240, 260–1, 288, 295, 304, 507
 reinforcement, 50, 87, 131, 188, 196, 219, 240

Z

Z-factor, crack control, 270, 271
 Zellerer, E., 415
 Zia, P., 263, 384
 Zwoyer, E.M., 313